School of Earth and Planetary Science

The Geologic Record of Two Proterozoic Supercontinents within the Belt Basin Region of Western North America

Daniel Brennan
0000-0002-9221-6479

This thesis is presented for the Degree of
Doctor of Philosophy
of
Curtin University

August 2022

Declaration

To the best of my knowledge and belief this thesis contains no material previously published by any other person except where due acknowledgment has been made.

This thesis contains no material which has been accepted for the award of any other degree or diploma in any university.

I have obtained permission from the copyright owners to use any third-party copyright material reproduced in the thesis (e.g., questionnaires, artwork, unpublished letters), or to use any of my own published work (e.g., journal articles) in which the copyright is held by another party (e.g., publisher, co-author).

Signature:

Date: August 25, 2022

Acknowledgment of Country

I acknowledge that during my time at Curtin University, I lived and worked on the traditional lands of the Wadjuk people of the Nyungar Nation. The fieldwork conducted and geologic samples collected for this scientific inquiry are from the traditional lands of the Kalispel, Coeur d'Alene, and Nez Perce people. I wish to pay my deepest respects to the ancestors and community members, past, present, and emerging of these First Nation peoples. While I strove to honor the geologic significance of the North American study region, I acknowledge and appreciate that the value and meaning of these lands surpass metrics measurable by scientific inquiry.

Abstract

The cyclical amalgamation and dispersal of most of Earth's continents, a process known as the supercontinent cycle, has been operable for at least the last 1.8 billion years. Many consider the supercontinent cycle to be the first-order control on the non-uniform spatial and temporal distribution of Earth's resources, and to have played a governing role in the environmental and biologic evolutionary changes that facilitated life. Early attempts at reconstructing Precambrian supercontinents often relied upon simplified correlations of singular geologic entities such as paired rift margins. However, more recent attempts to reconstruct ancient supercontinent configurations require multidisciplinary studies considering an even broader set of geologic entities such as basement provinces, orogenic histories, basin histories, paired rift margins, plume events, global plate kinematics, and paleomagnetic data. As a result, reconstructions have become more detailed, but the compounding effect of regional tectonic disagreements is still evident in wildly variable proposed global paleogeographic configurations. The Belt Basin region of western Laurentia has long been recognized to contain a key, yet debated, geologic record of the timing and configurations of the first supercontinent Nuna (1.6–1.3 Ga; also called Columbia), and its successor Rodinia (0.9–0.7 Ga). This study addresses some of the most significant of the Proterozoic magmatic, stratigraphic and metamorphic tectonic debates in this region, including A) the origin of localized North American Magmatic Gap magmatism, B) the tectonostratigraphic framework of Proterozoic strata, and the occurrence, timing, source, and implications of allegedly non-Laurentian derived detrital zircon within these strata, and C) the tectonic implications of enigmatic ca. 1.3–1.0 Ga metamorphism reported in this region. By bolstering field observations with U/Pb geochronology (zircon, monazite, apatite), additional zircon isotopic data (Lu/Hf, O-), and metapelite phase equilibria modelling, the results of this study strengthened commonly advocated ties between southeastern Australia and the Belt Basin region (USA) within supercontinent Nuna. However, the results also identified discrepancies between the Belt Basin region and commonly favored conjugate blocks (southeastern Australia or South China) within popular "SWEAT" or "Missing-Link" Rodinia configurations. Consequently, this work supports the accuracy of recently proposed Nuna configurations but advocates the need for more work on Rodinia reconstructions.

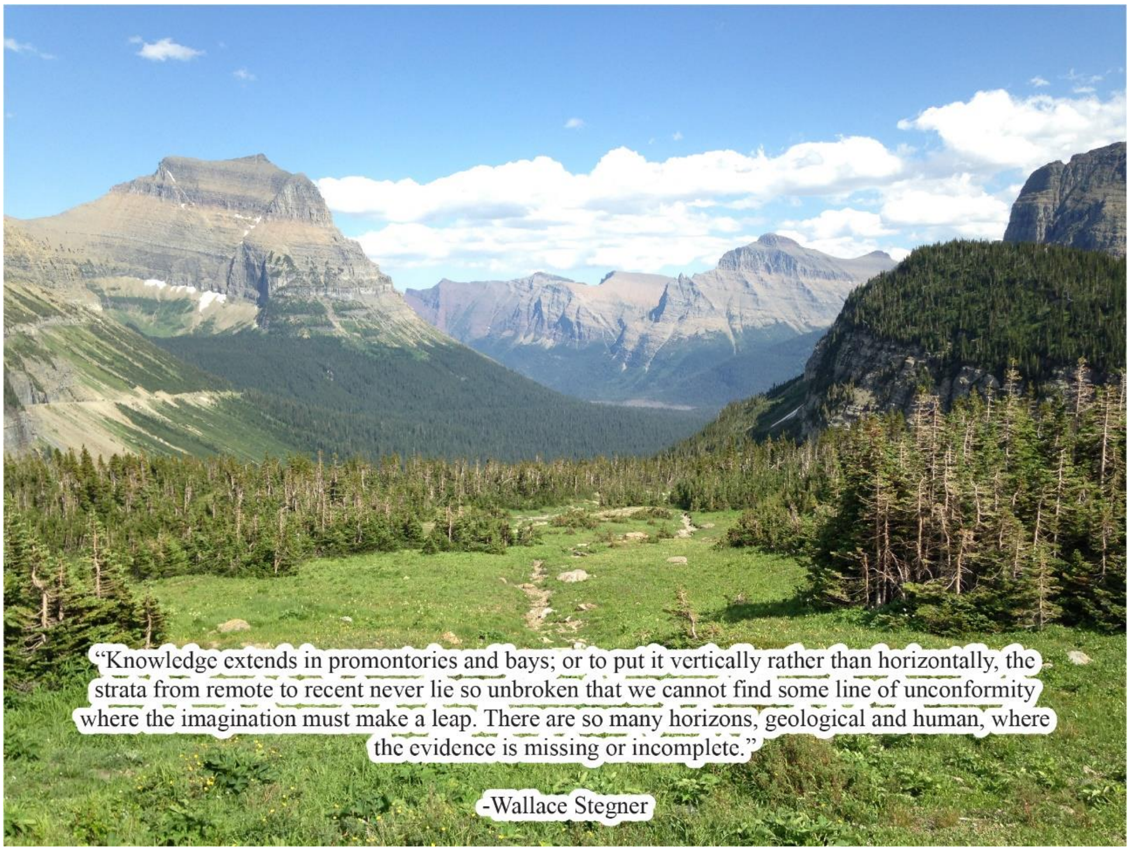
"Knowledge extends in promontories and bays; or to put it vertically rather than horizontally, the strata from remote to recent never lie so unbroken that we cannot find some line of unconformity where the imagination must make a leap. There are so many horizons, geological and human, where the evidence is missing or incomplete."
-Wallace Stegner

Author Acknowledgments

This document marks the culmination of a long personal and academic journey that spanned several relationships, continents, decades, and too many crappy student housing rentals. To paraphrase E. A., at times this journey did feel crooked, winding, lonesome, and dangerous…but man, did those hard times sure lead to some amazing views and fulfilling moments! I have gratitude for so many people who helped me find my path along the way. I would have been lost alone.

The first and perhaps the most important guides I had along the way were my parents. Mom and Dad, thank you. From encouraging my curiosity as a kid to answering those 3 A.M. stress-induced sleeplessness phone calls, your love, and unwavering reassurance that I am defined by far more than my failures or accolades did not go unappreciated. I could not have done this without you. To my sisters, cousins, aunts, and other family members… thank you for your support. However, it was perhaps your unassuming general disinterest in geology that always seemed to remind me when it was needed most that geology is not who I am, it is just something I enjoy doing.

To Professor Li, thanks for taking a chance on some kid you met in Leadore, Idaho. You taught me to be confident, and to think big and for myself. I feel that one of the greatest achievements of this PhD is the growth in our relationship. To live up to my philosophical reputation (or perhaps notoriety), of all the lessons I learned from you these past four years, those that extended beyond the topic of geologic reconstructions toward the topic of how to live a meaningful life, are probably the lessons I hope to have learned best in the end. To Tim, I appreciated your optimism and canny capacity to recognize "brilliance" when I was only seeing tribulation. Noreen, Brad, Luc, Sergei, Chris, Reed, Tom, Silvia, Vitor, Bryant, Ross, Adam, and those others that made time for me, when it was not compulsory and also your free allotment of it was usually in short supply, thank you. I could not have done this without you either.

Paul, Dave, Brian, Phil, Kent, Katherine, Scott, Lori… my time in Pocatello and Eau Claire was the foundation upon which this thesis was built. Your patience and dedication made sure it was a strong one. To Paul and Dave especially, I liked geology at UWEC, but I fell in love with it at ISU. You were both a big part of that. It is perhaps your opinion of my work that I value first and foremost. Thank you for always giving it to me with thoughtfulness and blunt honesty.

Lastly, to my friends, mates, and "broffice" siblings… you know who you are. Thank you for unpretentiously satisfying the requirement of my favourite quote… "No man is a failure who has friends" when I feared I was. Sorry, it was a more frequent occurrence than probably desired. When we catch up years from now, it is the "life" we fit in the all too short gaps between "work" that we will reminisce, laugh, and probably cry about. It is because of you all that I even had a life, thanks for making it a good one.

Publications during the course of this thesis

Peer-reviewed journal articles:

Brennan, D.T., Link, P.K., Li, Z.X., Martin, L., Johnson, T., Evans, N.J., and Li, J., 2022, Closing the "North American Magmatic" Gap: Crustal evolution of the Clearwater Block from multi-isotope and trace element zircon data: Precambrian Research, v. 369, p. 106533, doi:10.1016/j.precamres.2021.106533.
Corrigendum: https://doi.org/10.1016/j.precamres.2022.106871

Brennan, D.T., Brian Mahoney, J., Li, Z.X., Link, P.K., Evans, N.J., and Johnson, T.E., 2021, Detrital zircon U–Pb and Hf signatures of Paleo-Mesoproterozoic strata in the Priest River region, northwestern USA: A record of Laurentia assembly and Nuna tenure: Precambrian Research, v. 367, p. 106445, doi:10.1016/j.precamres.2021.106445.
Corrigendum: https://doi.org/10.1016/j.precamres.2022.106870

Brennan, D.T., Li, Z., Rankenburg, K., Evans, N., Link, P.K., Nordsvan, A.R., Kirkland, C.L., Mahoney, J.B., Johnson, T., and McDonald, B.J., 2021, Recalibrating Rodinian rifting in the northwestern United States: Geology, v. 49, no 6., 617–622, doi:10.1130/G48435.1

Brennan, D.T., Mitchell, R.N., Spencer, C.J., Murphy, J.B., and Li, Z., 2021, A tectonic model for the Transcontinental Arch: Progressive migration of a Laurentian drainage divide during the Neoproterozoic-Cambrian Sauk Transgression: Terra Nova, p. 1–11, doi:10.1111/ter.12528.

Conference presentations:

Brennan, D.T., Link, P.K., Li, Z.X., Martin, L., Johnson, T., Evans, N.J., and Li, J., 2022, Closing the "North American Magmatic" Gap: Crustal evolution of the Clearwater Block from multi-isotope and trace element zircon data, Geological Society of Australia Earth Sciences Student Symposium – Western Australia, Perth, 25 November 2021.
Awarded Best Talk of Conference

Brennan, D. T., Li, Z.-X., Link, P.K., and Johnson, T., 2021, Detrital zircon record of Proterozoic strata in the Priest River region of western Laurentia: Evaluating "SWEAT" relationships for supercontinents Nuna and Rodinia, Australian Earth Sciences Convention, Virtual, 9–12 February 2021.
Awarded Best Student Talk, Honorable Mention

Brennan, D.T., 2021, Reconciling Paleogeographic Reconstructions with the record of Rodinian Rifting in the Northwestern United States, International Geoscience Programme 648 Virtual Seminar Series, 6 May 2021.

Brennan, D.T., Li, Zheng-Xiang, Nordsvan, A., Link, P.K., Mahoney, J.B, Yao, W., and Parker, S.D. 2019, Detrital Zircon U/Pb and Lu/Hf Analyses Of The Buffalo Hump Formation And Underlying Deer Trail Group: Insights into the Proterozoic Tectonostratigraphic Record of Western Laurentia, Geological Society of America Abstracts with Programs, Vol. 51, No. 5, Phoenix Arizona, 22–25 September 2019.

Non Peer-Reviewed Science Outreach Articles:

Brennan, D.T., July–August 2021, A short hike on the edge of Ancient North America: Out There Outdoors Magazine, p. 20–21.

Brennan, D.T., August 2020, When the Mountains Were Made: A New Geological Discovery, Idaho Magazine, p. 9–17.

TABLE OF CONTENTS

Chapter 1: Introduction

1.1. The Supercontinent Cycle

One of the paradoxes of living on a tectonically active planet is that the same geologic processes responsible for exposing ancient rocks making them available for study also commonly obscures their original nature (Fig. 1.1). Consequently, there is regularly a correlation between the ambiguity in our understanding of tectonic events and their antiquity. During the late 20th and into the 21st century, the development of analytical methods to measure a variety of geochemical and isotopic systems within rocks and minerals, revolutionized the field of geology (e.g., Holmes, 1946; Goldschmidt, 1954; Stacey and Kramers, 1975; Frost et al., 2001; Hawkesworth and Kemp, 2006). Not only do geochemical and isotopic methods facilitate absolute dating of geologic and tectonic events, they can also be utilized as tracers/recorders of geologic and tectonic processes in situations where the original context has been obscured by younger events (e.g., Faure, 1977). When combined with field methods, the advent of geochemical and isotopic analytical methods has opened entirely new frontiers in the study of Earth systems.

Fig. 1.1: Panoramic photograph (looking northeast) of Belt Supergroup strata in Glacier National Park, Montana USA. The striking exposures of these Mesoproterozoic rocks results mostly from Late Cretaceous thrusting and uplift, followed by Pleistocene glacial incision. While these processes exposed these rocks for study, they also contributed to regional debates over particular stratigraphic correlations for decades. Photography by Brennan in 2018.

Prior to the availability of robust isotopic analytical methods, limited outcrop exposure, extensive tectonic over-printing, and the lack of absolute chronologic constraints made interpreting the geologic record of Precambrian rock assemblages particularly troublesome. As such, our knowledge of the 88% of earth's history that constitutes the Precambrian has only recently begun to be comparable with our knowledge of younger Phanerozoic events. However, 20th century advancements in our understanding of geochemical and isotopic systems within rocks and minerals have gradually revealed that Earth's geosphere has an ancient and geologically active past.

Congruent with the proliferation of geochemical and isotopic studies was a growing scientific acceptance of plate tectonic theory (e.g., MeKenzie and Parker, 1967; Dewey and Horsfield, 1970). Not only was this theory consistent with modern geologic phenomena, most notably it also offered a testable mechanism for the movement of earth's continents allowing evaluation of Wegner's (1912) assertion that most of Earth's continents may have once been assembled into a singular landmass or "supercontinent." Wegner (1912) called this landmass Pangea (derived from the ancient Greek 'pan' meaning all, and 'gaea' meaning land). It didn't take long before others proposed that similar geologic processes likely occurred deeper, in the pre-Pangea, geologic past.

In 1970, Valentine and Moores were the first to officially propose the occurrence of a pre-Pangea, late Precambrian supercontinent subsequently named Rodina (from the Russian word 'rodit' meaning 'to beget' or 'to give birth'; McMenamin and McMenamin, 1990). The origin of this name is particularly suitable, as it was within the nutrient rich extensive shallow seas that resulted from globally widespread rifting associated with the breakup of Rodinia, that the proliferation of lifeforms during the Neoproterozoic–Cambrian "explosion" took place (e.g., Marshall, 2006; Peters and Gaines, 2012; Brocks et al., 2017; Hoffman et al., 2017). The concept and configuration of this late Precambrian "Rodinia" supercontinent has been long debated since the early 1990's (e.g., Moores, 1991; Dalziel, 1991; Hoffman, 1991). These disagreements are often based on conflicting correlations of ca. 1300–1000 Ma "Grenville-age" orogens along which the supercontinent assembled and ca. 800–600 Ma rift margins that record subsequent supercontinent breakup.

In the late 1990's and early 2000's, the recognition of widespread ca. 2100–1800 Ma orogens led to the suggestion of the occurrence of an even older, pre-Rodinia supercontinent called "Nuna" (an Inuktitut term meaning "the land" or "all land", Hoffman, 1997) and/or "Columbia" (Rogers and Santosh, 2002; Zhao et al., 2002). As expected, the configuration of this Paleo-Mesoproterozoic supercontinent has also attracted much attention and debate within the geologic community. In particular, many geologic models favour similar configurations for both Rodinia and Nuna (e.g., Cawood and Hawkesworth, 2014; Li et al., 2019 and references within). This has raised discussions on whether they should be considered fully separate individual supercontinents (e.g., Condie et al., 2002) and consequently highlights the relatively poor understanding of the breakup and ensuing assembly processes of Earth's allegedly first and second supercontinents.

Despite intensive debate on the details, it has nonetheless generally been accepted that the assembly and subsequent dispersal of most of Earth's continents into supercontinents was a recurrent process for at least the past 1.8 billion years (Fig. 1.2; Condie, 2002; Nance et al., 2014; Evans et al., 2016; Li et al., 2019; Mitchell et al., 2021). The widespread recognition of long-term global cyclicity in tectonic processes is perhaps one of the most important developments in our understanding of the Earth since the acceptance of plate tectonic theory itself. Although it is now known that the supercontinent cycle was one of the first-order controls on the unequal spatial and temporal distribution of earth resources (e.g. Cawood and Hawkesworth, 2014) , the drivers and mechanisms of tectonic cyclicity associated with these processes have many unanswered questions. For example, some argue that mantle-convection patterns are the predominate control on the style and evolution of Earth's tectonic cyclicity (Li et al., 2019), while others advocate that surficial erosion driven changes in subduction patterns are the primary first order control (Sobolev and Brown, 2019). An important first step in addressing these ongoing disagreements is the establishment of reliable, accurate and testable paleogeographic tectonic framework reconstructions throughout Earth's history.

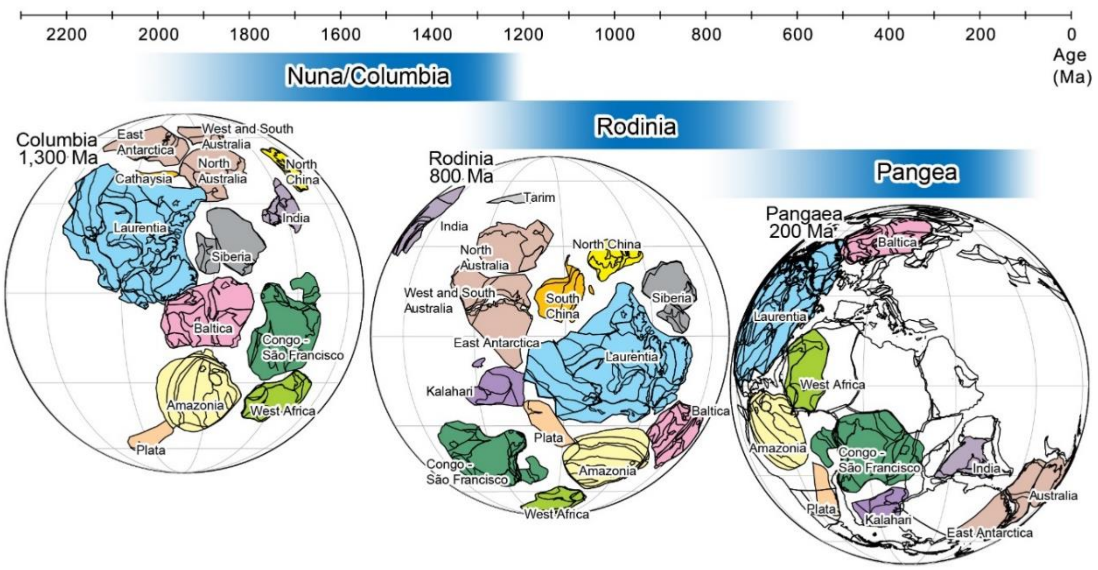

Fig. 1.2: Timeline of supercontinents through time with paleogeographic reconstructions of Nuna at ca. 1300 Ma (also called Columbia), Rodinia at ca. 800 Ma, and Pangea at ca. 200 Ma (from Mitchell et al., 2021).

1.2. A multidisciplinary approach to evaluating Precambrian supercontinent tectonics

Early attempts at Precambrian global paleogeographic tectonic reconstructions often relied heavily on correlation of singular geologic entities such as paired rift margins (e.g., Eisbacher, 1985). However, as Precambrian datasets grew, the correlation of multiple geologic entities such as paired rift margins and paleomagnetic data (Bell and Jefferson, 1987); and paired rift margins, paleomagnetic data, and orogenic histories (Dalziel, 1991; Moores, 1991; Hoffman, 1991) quickly became commonplace. More recently, it is generally accepted that robust paleogeographic reconstructions must be consistent with even broader set of geologic entities such as basement provinces, orogenic histories, basin histories, paired rift margins, plume events, global plate kinematic models, and paleomagnetic data (Fig. 1.3; e.g., Li et al., 2008). As such, the increasing consideration of multiple complementary datasets has aided in the generation of more detailed (e.g., Merdith et al., 2021) and hopefully more accurate reconstructions. However, these more detailed reconstructions have also highlighted how even minor disagreements and/or varying interpretations of what some may consider regional geologic discrepancies can be compounded into significant disagreements between global paleogeographic tectonic reconstructions. For example, disagreements on the Neoproterozoic geologic history of South China has led it to be placed centrally (Li et al., 2008), on the periphery (Wang et al., 2020), or perhaps even completely removed from Rodinia (Park et al., 2021).

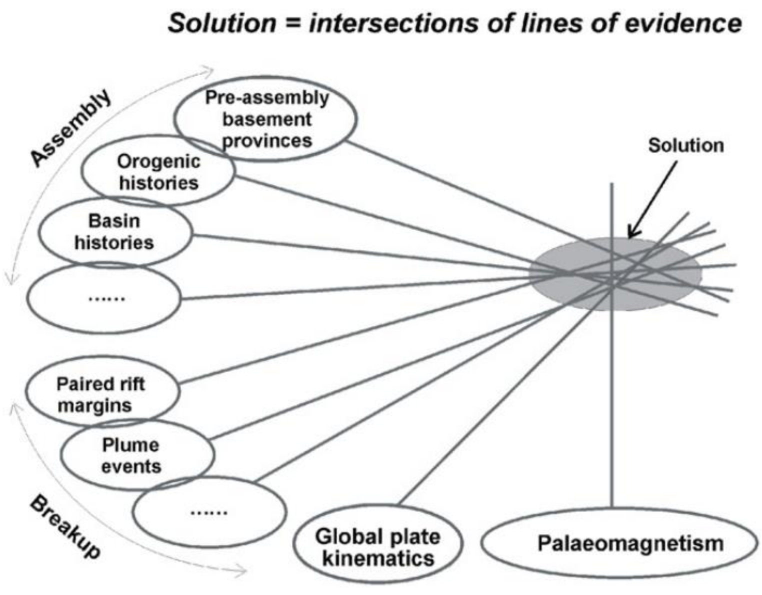

Fig 1.3: A schematic diagram illustrating the importance of a multidisciplinary approach to reconstructing and evaluating palaeography (from Li et al., 2008). Note how when only a single line of geologic evidence is considered, there are often many non-unique solutions.

Consequently, regions where Precambrian basement, orogenic, basin, rift, and/or plume geologic records are present in close proximity often warrant detailed study, as robust tectonic models of these regions are a prerequisite for accurate and testable global paleogeographic tectonic models. Comparison of the tectonic records of these regions allows them to be linked in the past with other currently far afield regions containing similar histories, thus acting as geologic "piercing points." As a result, solving global-scale tectonic and paleogeographic disagreements is impossible as long as notable regional geologic debates persist.

1.3. The Belt basin region – A critical Nuna and Rodina piercing point

As discussed, "Nuna" is a term in Inuktitut (the language of the indigenous people of the North American Arctic region) meaning "the land," or "all land," and Hoffman (1997) deserves credit for its first use to describe the Paleoproterozoic assembly of Laurentia and Baltica. Zhao et al. (2002) presented an extensive overview of global ca. 2100–1800 Ma orogens, and demonstrated that most other major Archean cratonic blocks such as those of North China, Australia, Siberia, India, South Africa, West Africa, and South America assembled along ca. 2000–1800 Ma orogens, suggesting synchronicity with Laurentia and Baltica's assembly. Following Rogers and Santosh (2002), Zhao et al. (2002) correlate these widespread ca. 2100–1800 Ma collisional orogens to reflect the assembly of a Paleo-Mesoproterozoic supercontinent they call Columbia. The Columbia name was first proposed by Rogers and Santosh (2002) who state that "the key evidence for its existence is the relationship between eastern India and the Columbia region of North America" (pg. 5). However, within the same Gondwana research volume, Meert (2002) presents the first paleomagnetic constraints for the Columbia Paleoproterozoic supercontinent, and in slight disagreement with the ca. 2100–1800 Ma assembly of Columbia advocated by Rogers and Santosh (2002), Meert notes that Paleomagnetic constraints suggest supercontinent assembly occurred primarily between ca. 1770–1500 Ma.

Consequently, an enduring controversy over the past two decades is not only whether the "Nuna" or "Columbia" name is better suited for the potential supercontinent that assembled in the late Paleoproterozoic (e.g., Meert, 2012), but if this supercontinent assembled coevally with widespread ca. 2000–1800 Ma "Trans-

Hudson" age orogens (e.g., Zhao et al., 2002), or if final assembly occurred later, probably after ca. 1800 Ma but prior to ca. 1500 Ma (e.g., Meert, 2002). In regards to the first (nomenclature) controversy, various arguments have been made recently to support both names. Harrison and St.-Onge (2022) note that the meaning of "Nuna" being "the land," or "all land," (in Inuktitut) is a more appropriate supercontinent name as it is akin to the meaning of Pangea (derived from the ancient Greek 'pan' meaning all, and 'gaea' meaning land). A sentiment shared by this author, and reflected by the preferred usage throughout this work. While others (e.g., Wang et al., 2021) suggest that the name Columbia, based off the "Columbia" region of western North America (namely Washington State) is more appropriate as it was the name used by the authors that first attempted global-scale reconstructions of this purported supercontinent (e.g., Rogers and Santosh, 2002; Zhao et al., 2002). While, naming preferences between myself and Rogers and Santosh (2002) differ, I do concur that the "Columbia" (which essentially comprises the western portion of Belt basin) region of western North American is critically understudied considering its long-recognized importance for global scale paleogeographic reconstructions (Fig. 1.4).

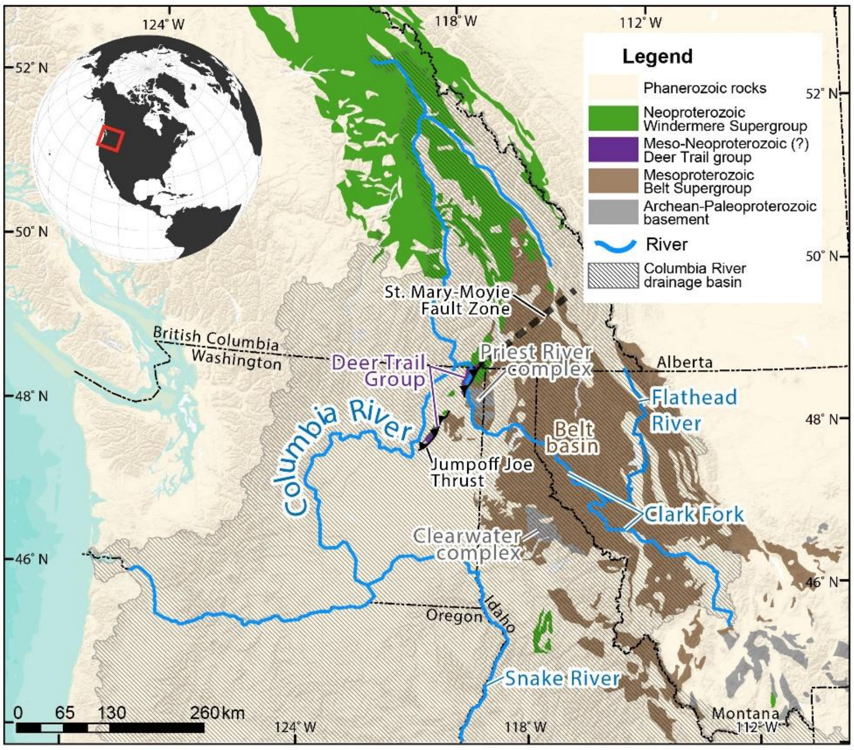

Fig. 1.4: Simplified geologic map of the northwestern United States, and southwestern Canada. The main Proterozoic tectonostratigraphic packages of this region, within the Columbia River drainage basin, consists of the extensive Mesoproterozoic Belt Supergroup (shown in brown), and Neoproterozoic Windermere Supergroup strata (and its correlatives, shown in green) which have both be integral in development of early Rodinia and Nuna paleographic reconstructions (e.g., Bell and Jefferson, 1982; Rogers and Santosh, 2002).

In fact, a growing body of paleomagnetic, geochronologic, and sedimentary provenance data has made the original "eastern India and the Columbia region of North America" correlation of Rogers and Santosh (2002) fall out of favor. Instead most recent models suggests links between the eastern margin of the North Australian craton (NAC) and the northwestern margin of Laurentia during assembly of supercontinent Nuna based on shared provenance, metamorphic and magmatic histories (Thorkelson et al., 2001; Ross and Villeneuve, 2003; Pisarevksy et al., 2014; Nordsvan et al., 2018; Pourteau et al., 2018; Volante et al., 2020, 2022). A lesser constrained southwest Laurentia-Mawson continent (Gawler Craton of South Australia and the Terre Adelie Craton of East Antarctica; Payne et al., 2009) connection is also suggested for this time (Mulder et al., 2015; Verbaas et al., 2018; Goodge et al., 2017). Based on similarities between crustal provinces in the Cathaysia Block of South China and southern Laurentia, Li et al. (1995), Yao et al. (2017) and others instead have proposed that the Cathaysia Block was between western Laurentia and Australia during Nuna time.

However, paleomagnetic constraints have demonstrated that the proposed Australia-Laurentia connection within Nuna could not have persisted uninterrupted during evolution to the subsequent supercontinent, Rodinia. Paleomagnetic constraints advocate that Australia and Laurentia separated between ca. 1300 and 1200 Ma (Pisarevsky et al., 2003; Kirscher et al., 2020), which suggests the occurrence of a complete Wilson cycle along the western Laurentia margin during the Nuna to Rodinia transition (Betts and Giles, 2006). However, a regional geologic record of this purported event is historically poorly recognized in western Laurentia.

The ensuing configuration of continents west of Laurentia within the supercontinent Rodinia (at ca. 1000 Ma) is an enduring (and perhaps endearing) controversy. Several original models are over 20 years old and continue to be revised and favoured by recent publications without a clear scientific consensus (see Fig. 1.5). Some of these leading models include a southwest U.S.–East Antarctic connection (SWEAT; Moores, 1991, Hoffman, 1991; Dalziel, 1991; Merdith et al., 2017; Zhao et al., 2018), possibly with a Rodinia-forming Grenville-age (Sibao) orogeny between (the Laurentia-connected) Cathayasia and the incoming Yangtze blocks of South China (Missing-Link; Li et al., 1995; Li et al., 2013), or with Australia located along the southwestern U.S. (AUSWUS; Karlstrom, 1999; Eyester et al., 2020) or Mexico (AUSMEX; Wingate et al., 2002). Completely different western Laurentia conjugates such as Tarim (Wen et al., 2017; 2018; Jing et al., 2021), or the North China Craton

(Ding et al., 2021) have also been suggested. However, at least one early model, the Siberian Connection (Sears and Price, 2000), which suggests that Siberia was conjugate to western Laurentian within Rodinia has generally fallen out of favor due to its inconsistency with most paleomagnetic data (Li et al., 2008; Pisarevsky et al., 2021; Evans, 2021).

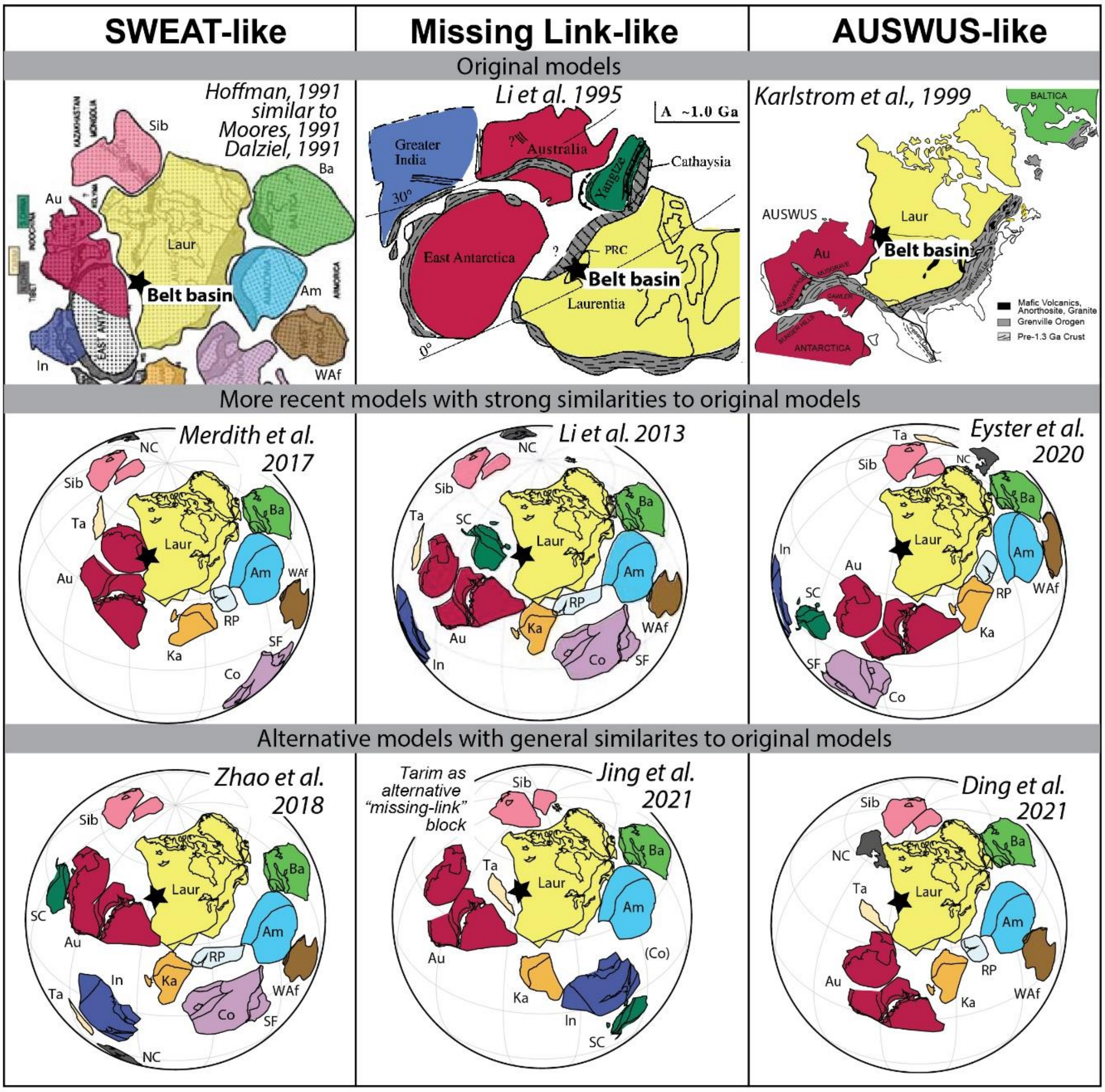

Fig. 1.5: Variable Rodinia reconstruction models including the original models (top row), more recently proposed "updated" interpretations that share strong similarities with the original models, and alternative recently proposed models that have general similarities with original models. The location of the Belt basin region, the focus of this study area, is indicated by the black star in each reconstruction. Note that in relation to the pertinent regions of this study, most of these models differ in the location of Australia/Antarctica (in dark red) relative to western Laurentia, and the occurrence (or not) of small intervening blocks between Laurentia and Australia/Antarctica. Figure adapted from Evans (2021 and references within). Abbreviations include: Am, Amazonia; Au, Australian cratons including Antarctic Mawsonland; Ba, Baltica; Co, Congo; In, India; Ka, Kalahari; Laur, Laurentia; NC, North China; RP, Rio Plata; SC, South China; SF, Sa˜o Francisco; Sib, Siberia; Ta, Tarim; WAf, West African craton.

1.4. Regional debates with global implications

Several unique and debated geologic records within the Belt basin of western Laurentia make this region a distinctive Laurentian piercing point for Precambrian paleogeography (Fig. 1.6). Addressing these regional debates will allow for the evaluation of many of the competing global models presented above, and thus have the potential to significantly influence our understanding of Proterozoic supercontinent processes.

Within the Priest River and Clearwater metamorphic complexes (Fig. 1.4) within the Belt Basin region, 2670 to 2650 Ma Neoarchean and 1880 to 1840 Ma Paleoproterozoic magmatic rocks of the Clearwater block are exposed (Vervoort et al., 2016). Interestingly, the ca. 1480–1380 Ma Belt Supergroup strata that overlie these basement rocks have long been known to lack detrital zircon ages consistent with this Laurentian basement and instead contain abundant ca. 1700–1500 Ma detrital zircon grains (Ross and Villeneuve, 2003; Lewis et al., 2010). Many of these grains have ages that fall within the ca. 1610–1490 Ma "North American Magmatic Gap" (NAMG), a time interval during which magmatism was rare in Laurentia, but common in Australia. Consequently, this relationship is often used to justify the proximal relationship of Australia with western Laurentia during the Mesoproterozoic (e.g., Ross and Villeneuve, 2003). However, the presence of NAMG-age magmatism in South China (Xu et al., 2019) has also brought into question the uniqueness of this interpretation.

In the Priest River complex (Fig. 1.4) , a thrust bounded ca. 1580 Ma granite (Evans and Fischer, 1986) represents one of the only ca. 1610–1490 Ma magmatic rocks in Laurentia. Its occurrence may negate the necessity of any non-Laurentian sources for the NAMG-age zircon grains in the Belt Supergroup. Within the Priest River complex, a thin coarse quartzite unit is either the basal unit of the Belt Supergroup, or is unconformably overlain by lower Belt Supergroup strata. Limited geochronology results suggest this unit lacks these unique ca. 1610–1490 Ma detrital zircon grains (Doughty et al., 1998).

Most of the metamorphism along western Laurentia is usually attributed to the late Mesozoic and younger Cordilleran orogeny (Dickinson, 2004). However, in the Clearwater complex, metasedimentary Belt Supergroup strata contain an enigmatic spread of pre-Cordilleran ca. 1380–1000 Ma Lu/Hf garnet ages (Zirakparvar et al., 2010; Nesheim et al., 2012). The older range of these garnets may correspond with ca.

1380–1350 Ma bimodal plutonism within the Belt Basin. This magmatism could be associated with the East Kootenay "orogeny" (McMechan and Price, 1982; Evans and Zartman, 1990; Doughty and Chamberlain, 1996; McFarlane and Pattison, 2000). The significance of the East Kootenay orogeny is contentious, but instead of an actual orogeny, it may represent a period of renewed subsidence along the western margin of Laurentia (in the Belt-Purcell basin) and potentially reflect the rifting of Australia from western Laurentia (Doughty and Chamberlain, 1996).

The tectonic context of the younger "Grenville" ca. 1150–1000 Ma metamorphic ages (Zirakparvar et al., 2010; Nesheim et al., 2012) are also debated. Some interpret a static thermal disturbance in the Belt region driven by magmatism at depth during this time interval (Doughty and Chamberlain, 2008). However, others advocate that the ca. 1100 Ma garnet growth requires crustal thickening (Zirakparvar et al., 2010) suggesting the presence of a Grenville-age orogen along western Laurentia during Rodinia assembly. Several global models propose either a ca. 1100 orogeny correlatable with the orogeny in the potentially adjacent South China (Sibao orogeny in the Missing-Link model, Li et al., 2008b) or a significant dextral transpressional margin (Wen et al., 2008, Mulder at al., 2018b) along western Laurentia that could account for this debated western Grenville-age orogenic event.

Along the northwestern edge of the Belt Basin, just west of the Priest River complex, the Buffalo Hump Formation and underlying Deer Trail Group strata crop out (Fig. 1.4). These rocks comprise the western-most exposures of Mesoproterozoic (and possibly Neoproterozoic) rocks in Laurentia. The entire Buffalo Hump Formation and Deer Trail Group were initially correlated with ca. 1470–1380 Ma Belt Supergroup to the east and across a significant thrust fault (the Jumpoff Joe Thrust), based on broad overall lithological similarities and the fact that they are overlain by the < 720 Ma Windermere Supergroup (Evans, 1987; Miller and Whipple, 1989). However, limited U-Pb analysis of detrital zircons from the Buffalo Hump Formation suggests a maximum depositional age of ca. 1100 Ma (Ross et al., 1992), indicating that it is too young to be part of the ca. 1380 Ma and older Belt Supergroup. This relationship requires either a significant unconformity between the Buffalo Hump Formation and the underlying allegedly Belt Supergroup correlative Deer Trail Group, or that the entire Deer Trail Group, which lacked any geochronologic constraints at the onset of this work, has also been miscorrelated.

The identification of ca. 1100 Ma detrital zircon grains within the Buffalo Hump Formation, and the relative absence of ca. 1100 Ma magmatism in western Laurentia, led Ross et al., (1992) to speculate that either: (a) The zircon grains were far-travelled or recycled, or (b) the grains record the former presence of Grenvillian orogenic activity within western Laurentia. However, the absence of a widespread Grenillian-orogenic belt in western Laurentia, and subsequent evidence for far-travelled Laurentia-sourced ca. 1100 Ma detrital zircon grains in northern and western Laurentia (e.g., Rainbird et al., 1992; Yonkee et al., 2014) tends to support the first hypothesis of Ross et al., (1992). Nevertheless, others (e.g., Yao et al., 2017) have continued to advocate that the necessity of a proximal, non-Laurentian source of ca. 1100 Ma zircon grains for the Buffalo Hump Formation requires South China, and its ca. 1100 Ma Sibao orogeny, adjacent to the Belt Basin region within Rodinia.

In the 30 years since Ross et al., (1992) published the first detrital zircon results from the western Belt Basin region, ca. 1100 Ma detrital zircon grains have been found to actually be quite common in the mostly Cryogenian and Ediacaran Windermere Supergroup and correlative strata along the western margin of Laurentia (e.g., Gehrels et al., 1995; Yonkee et al., 2014; Matthews et al., 2018; Box et al., 2020). Windermere Supergroup strata are generally younger than ca. 720 Ma, and record the onset of widespread rifting along western Laurentia associated with the breakup of Rodinia (e.g., Ross, 1991). Several occurrences of ca. 780–720 Ma, pre-Windermere Supergroup, strata within localized basins (Chuar, Pahrump, and Uinta groups) may record localized earlier rifting (e.g., Dehler et al., 2010). However, so far these ca. 780–720 Ma basins are only identified south of the Belt basin region, which has led to proposals (e.g. Haldari et al., 2021) that the Belt basin segment of the margin, specifically the St. Mary-Moyie fault zone (Fig. 1.4), reflects a notable Neoproterozoic boundary along the rift margin.

The St. Mary-Moyie fault zone (Fig. 1.4) roughly aligns with a basement structure called the Vulcan zone and was likely active during Mesoproterozoic Belt Supergroup deposition (e.g., McFarlane and Pattison, 2000). A segment of the St. Mary-Moyie Fault zone may also be reactivated as the Mesozoic thrust fault that currently separates exposures of Deer Trail Group strata, from Belt Supergroup rocks to the east (Miller and Whipple, 1989). Consequently, there are disagreements on if the exact timing, style, and number of Neoproterozoic rifting events differed for the segments south and north of the St. Mary Moyie structure, which has significant implications for Rodinia breakup processes in this region (e.g., Colpron et al., 2002; Lund et al., 2003; Hadlari et al., 2021).

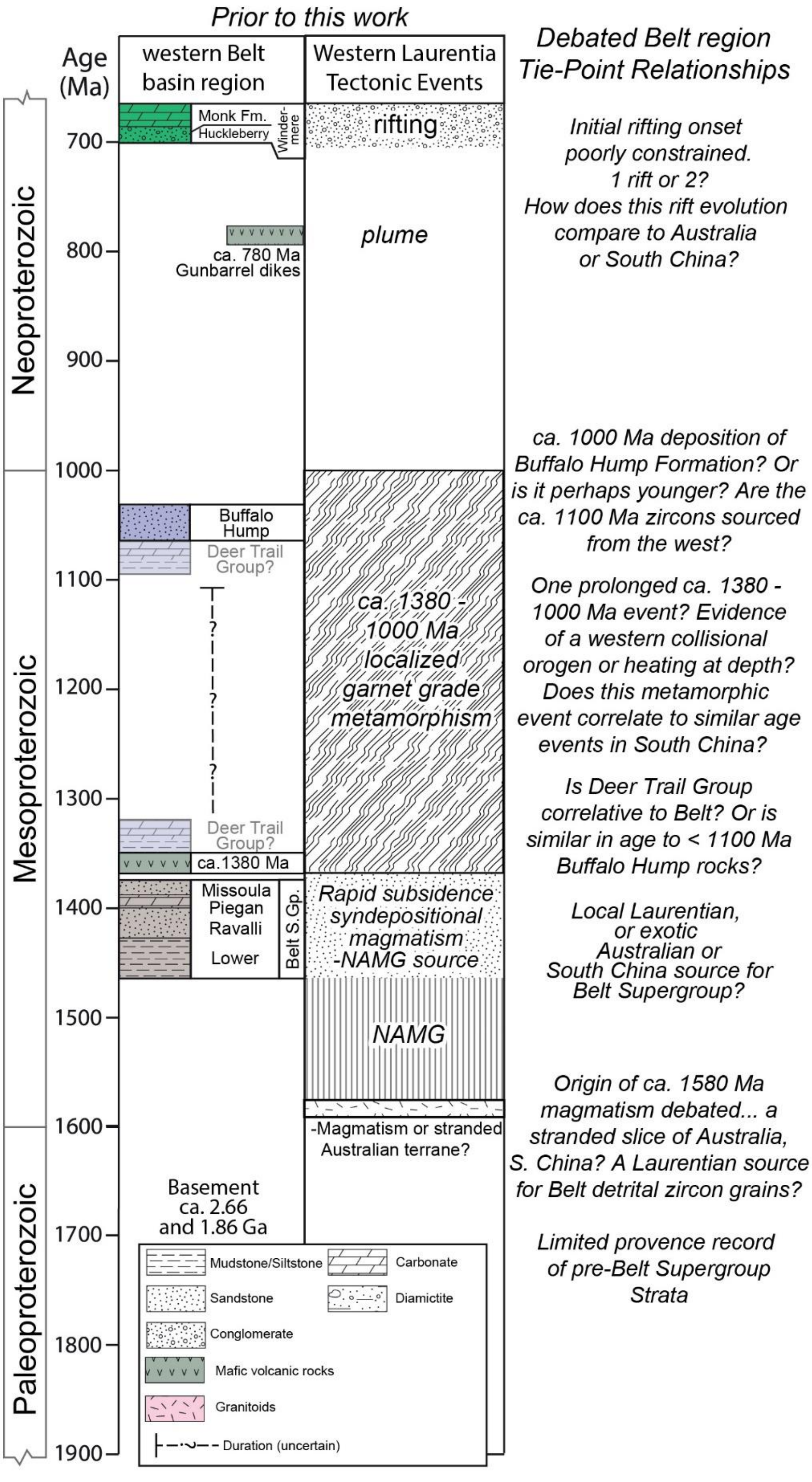

Fig. 1.6: Time-space diagram for the key debated Paleo–Neoproterozoic geologic and tectonic "tie-point" events of the western Belt basin region (northeastern Washington and northern Idaho, USA), prior to the onset of this work in 2018.

1.5. Research Objectives

The main objective of this work is to provide insights into several regional tectonic debates in the Proterozoic geologic history of the northwestern United States, notably along the western extent of the Mesoproterozoic Belt Basin (Fig. 1.6). Recalibrating the geologic record of this important Laurentian "piercing point" region allows evaluation of debated Nuna and Rodinia supercontinent tectonic reconstructions. Broken down into individual objectives, this task was accomplished through:

1) Investigation of the origin of ca. 1.58 Ga North American Magmatic Gap Magmatism (NAMG) within the Clearwater Block, and further characterization of the isotopic composition of the nearby Archean–Proterozoic magmatic rocks. These results provided insights into the Proterozoic tectonic history of the region, and the provenance of overlying sedimentary units.
2) Geochronology and metamorphic study to resolve the timing, conditions, and origin of Meso–Neoproterozoic (Grenville-age) metamorphic events previously reported in the Clearwater region, and evaluate their relationship to similar events reported elsewhere along the western extent of the Belt Basin, and in potentially conjugate blocks.
3) Determination of the age, stratigraphic framework, and provenance of the Paleoproterozoic to Neoproterozoic strata of northeast Washington and northern Idaho (USA). Link these sedimentary rocks to potential source regions either within and/or outside Laurentia and determine the likely tectonic mechanisms for their deposition and provenance signatures.

Finally, these findings were integrated with the available Laurentian and non-Laurentian data to evaluate Nuna and Rodinia models focusing on the evolution of the western Laurentian margin in comparison to proposed conjugate regions, such as southeastern Australia, East Antarctica and South China during this time interval.

1.6. Thesis Structure

This thesis is presented as a series of four published papers and a manuscript prepared for submission to a peer-reviewed journal. After peer review and publication, a data processing error was identified that affected the publications presented in Chapters 2 and 3. Corrigendum's to correct both publications were issued and Chapters 2 and 3 have been updated to reflect this correction and consequently vary slightly from their original published form. The text and figures of the published works (Chapters 2, 3, 5 and 6) and work currently in preparation for submission (Chapter 4) are reproduced in full and have been reformatted for consistency in the thesis. Thus, there is some unavoidable repetition between these chapters, particularly regarding the geological background and methods sections as each chapter is intended to read as standalone document.

Chapter 2: Closing the "North American Magmatic" Gap: Crustal evolution of the Clearwater Block from multi-isotope and trace element zircon data presents new U/Pb, Lu/Hf, O-, and trace element data from ca. 2.67 Ga, 1.86 Ga, and 1.58 Ga "North American Magmatic Gap" igneous rocks within the Clearwater Block. These data provide insights into the magmatic record of western Laurentian during the assembly of supercontinent Nuna. This data allows assessment of prior speculations that North American Magmatic Gap magmatism in the Clearwater Block may be associated with long recognized similar-age magmatism in the Gawler Craton of South Australia, or more recently identified similar-age magmatism in East Antarctica or the Hainan Island of South China.

Chapter 3: Detrital zircon U-Pb and Hf signatures of Paleo-Mesoproterozoic strata in the Priest River region, northwestern USA: A record of Laurentia assembly and Nuna Tenure investigates the provenance of the Paleoproterozoic Gold Cup Quartzite, Mesoproterozoic Belt Supergroup, and likely late Mesoproterozoic Deer Trail Group in the northwestern USA. This work provides the first laser-ablation split stream U/Pb and Lu/Hf data from detrital zircon grains within these sequences, and provides insights into the source and stratigraphic extent of North American Magmatic Gap detrital zircon grains recognized within these sequences.

Chapter 4: Grenville-age metamorphism within the Belt basin of western Laurentia examines the cryptic late Mesoproterozoic metamorphism reported within the Clearwater Complex. This work provides the first Pressure-Temperature-time constraints for this event based on U/Pb monazite and apatite geochronology, and thermocalc thermodynamic modelling.

Chapter 5: Recalibrating Rodinian rifting in the northwestern United States presents new detrital zircon U/Pb and Lu/Hf data from the Buffalo Hump Formation. The Buffalo Hump Formation was previously alleged to have a ca. 1.0 Ga depositional age. However, utilizing a rapid laser-ablation analysis methodology, a minor but significant ca. 760 Ma detrital zircon population was identified. This revised depositional age constraint has important ramifications for the occurrence of ca. 1.0 Ga (Grenvillian) tectonism in western Laurentia and the timing of Rodinian rifting.

Chapter 6: A tectonic model for the Transcontinental Arch: Progressive migration of a Laurentian drainage divide during the Neoproterozoic–Cambrian Sauk Transgression provides a new perspective on tectonic provenance models for ca. 1.1 Ga detrital zircon grains in western Laurentia. This new tectonic model is supported by two-dimensional quantitative comparison of a compilation of published U/Pb and Lu/Hf datasets from Neoproterozoic to early Paleozoic strata in western Laurentia, and potential eastern/southeastern Laurentian igneous sources.

Chapter 7: Synthesis and conclusions: The role of northwestern Laurentia in understanding global supercontinent processes. In this chapter the refined Proterozoic history of the Belt basin region of western Laurentia is synthesized, and the consistency of global Proterozoic supercontinent models with the regional geologic record of this key revised piercing point is assessed. In particular, this chapter summarizes how this work revises our understanding of:

1) The Paleoproterozoic history of western Laurentia and how it relates to Nuna assembly, in particular was there evidence of Nuna assembly by ca. 1.85 Ga, or was it a later ca. 1.65 Ga process?

2) The Mesoproterozoic history of western Laurentia and how it relates to the Nuna to Rodinia transition, specifically what evidence is there for a ca. 1.1 Ga "western Grenville" orogenic event?

3) The Neoproterozoic history of western Laurentia and how it relates to Rodinia breakup, in particular what is the timing and style of rifting in western Laurentia? How does it relate to other suggested conjugate blocks?

In answering these questions, Chapter 7 brings the work presented in the individual chapters together and presents a revised Proterozoic tectonic model for the Belt basin region of western Laurentia. This regional tectonic model is then used to evaluate the feasibility of inherently more speculative global tectonic reconstructions, and the implications are discussed. As always, all scientific knowledge is conjectural, and while this work answers some questions, it also raises many more. Consequently, an important part of this concluding chapter is to emphasize uncertainties with the tectonic models resulting from this work and to highlight questions for future investigation.

1.7. References

Geological Society of America reference style

Anderson, J.L., 1983, Proterozoic anorogenic granite plutonism of North America, in Medaris, L.G., Jr., Byers, C.W., Mickelson, D.M., and Shanks, W.C., eds., Proterozoic Geology; Selected Papers from an International Proterozoic Symposium: Geological Society of America Memoir 161, p. 133–154.

Bell, R.T., and Jefferson, C.W., 1987, An hypothesis for an Australian-Canadian connection in the Late Proterozoic and the birth of the Pacific Ocean: Pacific Rim congress 87. Proc. international congress, 1987, Gold Coast, Queensland, p. 39–50.

Betts, P.G., and Giles, D., 2006, The 1800-1100 Ma tectonic evolution of Australia: Precambrian Research, v. 144, p. 92–125, doi:10.1016/j.precamres.2005.11.006.

Bookstrom, A.A., Box, S.E., Cossette, P.M., Frost, T.P., Gillerman, V.S., King, G.R., and Zirakparvar, N.A., 2016, Geologic history of the Blackbird Co-Cu district in the Lemhi subbasin of the Belt-Purcell Basin: Geological Society of American Special Paper, v. 522, p. 185–219, doi:10.1130/2016.2522(08).

Box, S.E., Pritchard, C., Stephens, T.S., and O'Sullivan, P.B., 2020, Between the supercontinents -- Mesoproterozoic Deer Trail Group, an intermediate age unit between the Mesoproterozoic Belt-Purcell Supergroup and the Neoproterozoic

Windermere Supergroup in northeastern Washington, U.S.A.: Canadian Journal of Earth Sciences, v. 17, p. 1–17, doi:10.1139/cjes-2019-0188.

Brocks, J.J., Jarrett, A.J.M., Sirantoine, E., Hallmann, C., Hoshino, Y., and Liyanage, T., 2017, The rise of algae in Cryogenian oceans and the emergence of animals: Nature, v. 548, p. 578–581, doi:10.1038/nature23457.

Brown, M., Kirkland, C.L., and Johnson, T.E., 2020, Evolution of geodynamics since the Archean: Significant change at the dawn of the Phanerozoic: Geology, v. 48, p. 488–492, doi:10.1130/G47417.1.

Cawood, P.A., and Hawkesworth, C.J., 2014, Earth's middle age: Geology, v. 42, p. 503–506, doi:10.1130/G35402.1.

Colpron, M., Logan, J.M., and Mortensen, J.K., 2002, U-Pb zircon age constraint for late Neoproterozoic rifting and initiation of the lower Paleozoic passive margin of western Laurentia: Canadian Journal of Earth Sciences, v. 39, p. 133–143, doi:10.1139/e01-069.

Condie, K.C., 2002, The supercontinent cycle: Are there two patterns of cyclicity? Journal of African Earth Sciences, v. 35, p. 179–183, doi:10.1016/S0899-5362(02)00005-2.

Dalziel, I.W.D., 1991, Pacific margins of Laurentia and East Antarctica-Australia as a conjugate rift pair: evidence and implications for an Eocambrian supercontinent: Geology, v. 19, p. 598–601, doi:10.1130/0091-7613(1991)019<0598:PMOLAE>2.3.CO;2.

Dehler, C.M., Fanning, C.M., Link, P.K., Kingsbury, E.M., and Rybczynski, D., 2010, Maximum depositional age and provenance of the Uinta Mountain group and big cottonwood formation, northern Utah: Paleogeography of rifting western Laurentia: Bulletin of the Geological Society of America, v. 122, p. 1686–1699, doi:10.1130/B30094.1.

Dickinson, W.R., 2004, Evolution of the North American Cordillera: Annual Review of Earth and Planetary Sciences, v. 32, p. 13–45, doi:10.1146/annurev.earth.32.101802.120257.

Ding, J., Zhang, S., Evans, D.A.D., Yang, T., Li, H., Wu, H., and Chen, J., 2021, North China craton: The conjugate margin for northwestern Laurentia in Rodinia: Geology, v. 49, p. 773–778, doi:10.1130/G48521.1.

Doughty, P.T., and Chamberlain, K.R., 1996, Salmon River Arch revisited: new evidence for 1370 Ma rifting near the end of deposition in the Middle Proterozoic Belt basin: Canadian Journal of Earth Sciences, v. 33, p. 1037–1052, doi:10.1139/e96-079.

Eisbacher, G.H., 1981, Sedimentary tectonics and glacial record in the Windermere Supergroup, Mackenzie Mountains, northwestern Canada: Geological Survey of Canada Paper 80-27, 40 p.

Evans, J.G., 1987, Geology of the Stensgar Mountain quadrangle, Stevens County, Washington: U.S. Geological Survey Bulletin, v. 1679, p. 1–30.

Evans, K. V., and Zartman, R.E., 1990, U-Th-Pb and Rb-Sr geochronology of middle Proterozoic granite and augen gneiss, Salmon River Mountains, east-central Idaho: Bulletin of the Geological Society of America, v. 102, p. 63–73, doi:10.1130/0016-7606(1990)102<0063:UTPARS>2.3.CO;2.

Evans, D.A.D., Li, Z.X., and Murphy, J.B., 2016, Four-dimensional context of Earth's supercontinents, in Li, Z.X., et al., eds., Supercontinent Cycles Through Earth History: Geological Society [London] Special Publication 424, p. 1–14, https://doi .org/10.1144/SP424.12.

Eyster, A., Weiss, B.P., Karlstrom, K., and Macdonald, F.A., 2020, Paleomagnetism of the Chuar Group and evaluation of the late Tonian Laurentian apparent polar wander path with implications for the makeup and breakup of Rodinia: Bulletin of the Geological Society of America, v. 132, p. 710–738, doi:10.1130/B32012.1.

Faure, G., 1977, Principles of isotope geology. Wiley, New York.

Frost, B.R., Barnes, C.G., Collins, W.J., Arculus, R.J., Ellis, D.J., Frost, C.D., 2001, A geochemical classification for granitic rocks. Journal of Petrology, no. 42, p. 2033–2048.

Gehrels, G.E., Dickinson, W.R., Ross, G.M., Stewart, J.H., and Howell, D.G., 1995, Detrital zircon reference for Cambrian to Triassic miogeoclinal strata of western North America: Geology, v. 23, p. 831–834, doi:10.1130/0091-7613(1995)023<0831:DZRFCT>2.3.CO;2.

Goldschmidt, V.M., 1954. Geochemistry 78, LWW.

Goodge, J.W., Fanning, C.M., Fisher, C.M., Vervoort, J.D., and Fisher, C.M., 2017, Proterozoic crustal evolution of central East Antarctica: Age and isotopic evidence from glacial igneous clasts, and links with Australia and Laurentia: Precambrian Research, v. 299, p. 151–176, doi:10.1016/j.precamres.2017.07.026.

Hadlari, T., Arnott, R.W.C., Matthews, W.A., Poulton, T.P., Root, K., and Madronich, L.I., 2021, Provenance of the Incipient Passive Margin of NW Laurentia (Neoproterozoic): Detrital Zircon from Continental Slope and Basin Floor Deposits of the Windermere Supergroup , Southern Canadian Cordillera: Lithosphere, v. 2021, doi:10.2113/2021/8356327/5450477/8356327.pdf.

Harrison, C., and St-Onge, M.R., 2022, Geological history and supercontinent cycles of the Arctic: Geological Society of America Bulletin, p. 1–28, doi:10.1130/B36398.1/5600010/b36398.pdf.

Hawkesworth, C.J., and Kemp, A.I.S., 2006, Using hafnium and oxygen isotopes in zircons to unravel the record of crustal evolution: Chemical Geology, v. 226, p. 144–162, doi:10.1016/j.chemgeo.2005.09.018.

Hoffman, P.F., 1991, Did the breakup of Laurentia turn Gondwanaland inside out? Science, v. 252, p. 1409–1411.

Hoffman, P.F., 1997, Tectonic genealogy of North America, in van der Pluijm, B. A., and Mar- shak, S., eds., Earth Structure: An Introduction to Structural Geology and Tectonics: New York, McGraw-Hill, p. 459–464.

Hoffman, P.F. et al., 2017, Snowball Earth climate dynamics and Cryogenian geology - geobiology: Science Advances, v. 3

Holmes, A., 1946, An estimate of the age of the Earth: Nature, v. 157, no. 3995, p. 680-684.

Jing, X., Evans, D.A.D., Yang, Z., Tong, Y., Xu, Y., Wang, H., 2021, Inverted South China: a novel configuration for Rodinia and its breakup. Geology 49, p. 463-467. https://doi.org/10.1130/G47807.1.

Karlstrom, K.E., Harlan, S.S., Williams, M.L., McLelland, J., Geissman, J.W., and Ahall, K., 1999, Refining Rodinia: Geological evidence for the Australia–Western U.S. connection in the Proterozoic: GSA Today, v. 9, no. 10, p. 1–7.

Kirscher, U., Liu, Y., Li, Z.X., Mitchell, R.N., Pisarevsky, S.A., Denyszyn, S.W., and Nordsvan, A., 2019, Paleomagnetism of the Hart Dolerite (Kimberley, Western Australia) – A two-stage assembly of the supercontinent Nuna? Precambrian Research, doi:10.1016/j.precamres.2018.12.026.

Kirscher, U., Mitchell, R.N., Liu, Y., Nordsvan, A.R., Cox, G.M., Pisarevsky, S.A., Wang, C., Wu, L., Murphy, J.B., and Li, Z.-X., 2020, Paleomagnetic constraints on the duration of the Australia-Laurentia connection in the core of the Nuna supercontinent: Geology, v. XX, p. 1–6, doi:10.1130/g47823.1.

Lewis, R.S., Vervoort, J.D., Burmester, R.F., McClelland, W.C., and Chang, Z., 2007, Geochronological constraints on Mesoproterozoic and Neoproterozoic (?) high-grade metasedimentary rocks of north-central Idaho, U.S.A.: Sepm, v. 86, p. 37–53.

Lewis, R.S., Vervoort, J.D., Burmester, R.F., and Oswald, P.J., 2010, Detrital zircon analysis of Mesoproterozoic and Neoproterozoic metasedimentary rocks of north-central Idaho: implications for development of the Belt–Purcell basin: Canadian Journal of Earth Sciences, v. 47, p. 1383–1404, doi:10.1139/E10-049.

Li, Z.X., Zhang, L., and Powell, C.M., 1995, South China in Rodinia: Part of the missing link between Australia-East Antarctica and Laurentia? Geology, v. 23, p. 407–410, doi:10.1130/0091-7613(1995)023<0407:SCIRPO>2.3.CO;2.

Li, Z.X. et al., 2008, Assembly, configuration, and break-up history of Rodinia: A synthesis: Precambrian Research, v. 160, p. 179–210, doi:10.1016/j.precamres.2007.04.021.

Li, Z.X., Evans, D.A.D., and Halverson, G.P., 2013, Neoproterozoic glaciations in a revised global palaeogeography from the breakup of Rodinia to the assembly of Gondwanaland: Sedimentary Geology, v. 294, p. 219–232, doi:10.1016/j.sedgeo.2013.05.016.

Li, Z.X., Mitchell, R.N., Spencer, C.J., Ernst, R., Pisarevsky, S., Kirscher, U., and Murphy, J.B., 2019, Decoding Earth’s rhythms: Modulation of supercontinent cycles by longer superocean episodes: Precambrian Research, v. 323, p. 1–5, doi:10.1016/j.precamres.2019.01.009.

Lund, K., Aleinikoff, J.N., Evans, K. V., and Fanning, C.M., 2003, SHRIMP U-Pb geochronology of Neoproterozoic Windermere Supergroup, central Idaho: Implications for rifting of western Laurentia and synchroneity of Sturtian glacial deposits: Bulletin of the Geological Society of America, v. 115, p. 349–372, doi:10.1130/0016-7606(2003)115<0349:SUPGON>2.0.CO;2.

Matthews, W., Guest, B., and Madronich, L., 2018, Latest Neoproterozoic to Cambrian detrital zircon facies of western Laurentia: Geosphere, v. 14, p. 243–264, doi:10.1130/GES01544.1.

McFarlane, C.R., and Pattison, D.R., 2000, Geology of the Matthew Creek metamorphic zone, southeast British Columbia: a window into Middle Proterozoic metamorphism in the Purcell Basin: Canadian Journal of Earth Sciences, v. 37, p. 1073–1092, doi:10.1139/e00-018.

McFarlane, C.R.M., 2015, A geochronological framework for sedimentation and Mesoproterozoic tectono-magmatic activity in lower Belt–Purcell rocks exposed west of Kimberley, British Columbia: Canadian Journal of Earth Sciences, v. 52, p. 444–465, doi:10.1139/cjes-2014-0215.

McKenzie, D. P. and Parker, R. L., 1967, The North Pacific · an Example of Tectonics on a Sphere: Nature, v. 216, p. 1276–1280.

McMenamin, M. A. S., and McMenamin, D. L. S., 1990, The emergence of animals: The Cambrian break-through: New York, Columbia University Press, 217 p.

McMechan, M.E., and Price, R.A., 1982, Superimposed low-grade metamorphism in the Mount Fisher area, southeastern British Columbia—implications for the East Kootenay orogeny: Canadian Journal of Earth Sciences, v. 19, p. 476–489, doi:10.1139/e82-039.

McFarlane, C.R., and Pattison, D.R., 2000, Geology of the Matthew Creek metamorphic zone, southeast British Columbia: a window into Middle Proterozoic metamorphism in the Purcell Basin: Canadian Journal of Earth Sciences, v. 37, p. 1073–1092, doi:10.1139/e00-018.

Meert, J.G., 2002, Paleomagnetic Evidence for a Paleo-Mesoproterozoic Supercontinent Columbia: Gondwana Research, v. 5, p. 207–215, doi:10.1016/S1342-937X(05)70904-7.

Merdith, A.S. et al., 2021, Extending full-plate tectonic models into deep time: Linking the Neoproterozoic and the Phanerozoic: Earth-Science Reviews, v. 214, p. 103477, doi:10.1016/j.earscirev.2020.103477.

Moores, E.M., 1991, Southwest U. S.-East Antarctic (SWEAT) connection: A hypothesis: Geology, v. 19, p. 425–428.

Mulder, J.A., Halpin, J.A., and Daczko, N.R., 2015, Mesoproterozoic Tasmania: Witness to the East Antarctica-Laurentia connection within Nuna: Geology, v. 43, p. 759–762, doi:10.1130/G36850.1.

Mulder, J.A., Karlstrom, K.E., Halpin, J.A., Merdith, A.S., Spencer, C.J., Berry, R.F., and McDonald, B., 2018, Rodinian devil in disguise: Correlation of 1.25-1.10 Ga strata between Tasmania and Grand Canyon: Geology, v. 46, p. 991–994, doi:10.1130/G45225.1.

Nance, R.D., Murphy, J.B., and Santosh, M., 2014, The supercontinent cycle: A retrospective essay: Gondwana Research, v. 25, p. 4–29, doi:10.1016/j.gr.2012.12.026.

Nesheim, T.O., Vervoort, J.D., McClelland, W.C., Gilotti, J.A., and Lang, H.M., 2012, Mesoproterozoic syntectonic garnet within Belt Supergroup metamorphic tectonites: Evidence of Grenville-age metamorphism and deformation along northwest Laurentia: Lithos, v. 134–135, p. 91–107, doi:10.1016/j.lithos.2011.12.008.

Nordsvan, A.R., Collins, W.J., Li, Z., Spencer, C.J., Pourteau, A., Withnall, I.W., Betts, P.G., and Volante, S., 2018, Laurentian crust in northeast Australia : Implications for the assembly of the supercontinent Nuna: Geology, v. 46, p. 251–254, https:// doi .org /10 .1130 /G39980 .1.

Park, Y., Swanson-Hysell, N.L., Xian, H., Zhang, S., Condon, D.J., Fu, H., and Macdonald, F.A., 2021, A Consistently High-Latitude South China From 820 to 780 Ma: Implications for Exclusion From Rodinia and the Feasibility of Large-Scale True Polar Wander: Journal of Geophysical Research: Solid Earth, v. 126, p. 1–29, doi:10.1029/2020JB021541.

Payne, J.L., Hand, M., Barovich, K.M., Reid, A., and Evans, D.A.D., 2009, Correlations and reconstruction models for the 2500-1500 Ma evolution of the Mawson Continent: Geological Society, London, Special Publications, v. 323, p. 319–355, doi:10.1144/SP323.16.

Peters, S.E., and Gaines, R.R., 2012, Formation of the 'Great Unconformity' as a trigger for the Cambrian explosion: Nature, v. 484, p. 363–366, doi:10.1038/nature10969.

Pisarevsky, S.A., Wingate, M.T.D., and Harris, L., 2003, Late Mesoproterozoic (ca 1.2 Ga) palaeomagnetism of the Albany – Fraser orogen: no pre-Rodinia Australia–Laurentia connection: Geophys. J. Int., v. 155, p. 6–11.

Pisarevsky, S.A., Elming, S.Å., Pesonen, L.J., and Li, Z.X., 2014, Mesoproterozoic paleogeography: Supercontinent and beyond: Precambrian Research, v. 244, p. 207–225, doi:10.1016/j.precamres.2013.05.014.

Pourteau, A., Smit, M.A., Li, Z.-X., Collins, W.J., Nordsvan, A.R., Volante, S., and Li, J., 2018, 1.6 Ga crustal thickening along the final Nuna suture: Geology 46, 959–962. https:// doi.org/10.1130/G45198.1.

Ross, G.M., 1991, Tectonic setting of the Windermere Supergroup revisited: Geology, v. 19, p. 1125–1128, doi:10.1130/0091-7613(1991)019<1125:TSOTWS>2.3.CO;2.

Ross, Gerald M.; Parrish, Randall R.; Winston, D., 1992, Provenance and U-Pb geochronology of the Mesoproterozoic Belt Supergroup (northwestern United States): implications for the age of deposition and pre-Panthalassa plate reconstructions: Earth and Planetary Science Letters, v. 113, p. 57–76.

Ross, G.M., and Villeneuve, M., 2003, Provenance of the Mesoproterozoic (1.45 Ga) Belt basin (western North America): Another piece in the pre-Rodinia paleogeographic puzzle: Bulletin of the Geological Society of America, v. 115, p. 1191–1217, doi:10.1130/B25209.1.

Rogers, J.J.W., and Santosh, M., 2002, Configuration of Columbia, a Mesoproterozoic Supercontinent: Gondwana Research, v. 5, p. 5–22, doi:10.1016/S1342-937X(05)70883-2.

Sears, J.W., and Price, R.A., 2000, New look at the Siberian connection: No SWEAT: Geology, v. 28, p. 423–426.

Sobolev, S. V., and Brown, M., 2019, Surface erosion events controlled the evolution of plate tectonics on Earth: Nature, v. 570, p. 52–57, doi:10.1038/s41586-019-1258-4.

Stacey, J. S., and Kramers, J. D., 1975, Approximation of terrestrial lead isotope evolution by a two-stage model: Earth and Planetary Science Letters, v. 26, p. 207–221.

Sutton, J., 1963, Long term cycles in the evolution of continents. Nature, v. 198, p. 731–735.

Thorkelson, D.J., Mortensen, J.K., Creaser, R.A., Davidson, G.J., and Abbott, G.J., 2001, Early Proterozoic magmatism in Yukon, Canada: constraints on the evolution of northwestern Laurentia: Canadian Journal of Earth Sciences, v. 38, p. 1479–1494, doi:10.1139/cjes-38-10-1479.

Valentine, J.W., and Moores, E.M., 1970, Plate-tectonic regulation of faunal diversity and sea level: A model: Nature, v. 228, p. 657–659, doi: 10.1038/228657a0.

Verbaas, J., Thorkelson, D.J., Crowley, J., Davis, W.J., Foster, D.A., Gibson, H.D., Marshall, D.D., and Milidragovic, D., 2018, A sedimentary overlap assemblage links Australia to northwestern Laurentia at 1.6 Ga: Precambrian Research, v. 305, p. 19–39, doi:10.1016/j.precamres.2017.10.001.

Vervoort, J.D., Lewis, R.S., Fisher, C., Gaschnig, R.M., Jansen, A.C., and Brewer, R., 2016, Neoarchean and Paleoproterozoic crystalline basement rocks of north-central Idaho: Constraints on the formation of western Laurentia: Bulletin of the Geological Society of America, v. 128, p. 94–109, doi:10.1130/B31150.1.

Volante, S., Pourteau, A., Collins, W.J., Blereau, E., Li, Z.-X., Smit, M., Evans, N.J., Nordsvan, A.R., Spencer, C.J., McDonald, B.J., Li, J., Günter, C., 2020. Multiple P-T–d–t paths reveal the evolution of the final Nuna assembly in northeast Australia. Journal of Metamorphic Geology, no. 38, 593–627. https://doi.org/10.1111/jmg.12532.

Volante, S., Collins, W.J., Barrote, V., Nordsvan, A.R., Pourteau, A., Li, Z.X., Li, J., and Beams, S., 2022, Spatio–temporal evolution of Mesoproterozoic magmatism in NE Australia: A hybrid tectonic model for final Nuna assembly: Precambrian Research, v. 372, doi:10.1016/j.precamres.2022.106602.

Wang, C., Mitchell, R.N., Murphy, J.B., Peng, P., and Spencer, C.J., 2021, The role of megacontinents in the supercontinent cycle: Geology, doi:10.1130/g47988.1.

Wang, W., Cawood, P.A., Pandit, M.K., Xia, X., Raveggi, M., Zhao, J., Zheng, J., and Qi, L., 2020, Fragmentation of South China from greater India during the Rodinia-Gondwana transition: Geology, v. XX, p. 1–5, doi:10.1130/g48308.1.

Wegner, A., 1912, Die entstehung der kontinente. Geol. Rundschau 3, p. 276–292.

Wen, B., Evans, D.A.D., and Li, Y.X., 2017, Neoproterozoic paleogeography of the Tarim Block: An extended or alternative "missing-link" model for Rodinia? Earth and Planetary Science Letters, v. 458, p. 92–106, doi:10.1016/j.epsl.2016.10.030.

Wen, B., Evans, D.A.D., Wang, C., Li, Y.X., and Jing, X., 2018, A positive test for the Greater Tarim Block at the heart of Rodinia: Mega-dextral suturing of supercontinent assembly: Geology, v. 46, p. 687–690, doi:10.1130/G40254.1.

Wingate, M.T.D., Pisarevsky, S.A., and Evans, D.A.D., 2002, Rodinia connections between Australia and Laurentia: No SWEAT, no AUSWUS? Terra Nova, v. 14, p. 121–128, doi:10.1046/j.1365-3121.2002.00401.x.

Xu, Y.-J., Cawood, P.A., Zhang, H.-C., Zi, J.-W., Zhou, J.-B., Li, L.-X., and Du, Y.-S., 2019, The Mesoproterozoic Baoban Complex, South China: A missing fragment of western Laurentian lithosphere: GSA Bulletin, p. 1–15, doi:10.1130/b35380.1.

Zirakparvar, N.A., Vervoort, J.D., McClelland, W., and Lewis, R.S., 2010, Insights into the metamorphic evolution of the Belt–Purcell basin; evidence from Lu–Hf garnet geochronology: Canadian Journal of Earth Sciences, v. 47, p. 161–179, doi:10.1139/E10-001.

Zhao, G., Sun, M., Wilde, S.A., and Li, S., 2004, A Paleo-Mesoproterozoic supercontinent: Assembly, growth and breakup: Earth-Science Reviews, v. 67, p. 91–123, doi:10.1016/j.earscirev.2004.02.003.

Zhao, G., Wang, Y., Huang, B., Dong, Y., Li, S., Zhang, G., Yu, S., 2018, Geological reconstructions of the East Asian blocks: From the breakup of Rodinia to the assembly of Pangea. Earth-Science Reviews 186, p. 262–287

Chapter 2: Closing the "North American Magmatic" Gap: Crustal evolution of the Clearwater Block from multi-isotope and trace element zircon data

Abstract

Along the west-central margin of Laurentia, within the Priest River and Clearwater complexes, rare exposures of crystalline basement rocks of the Clearwater Block include "North American Magmatic Gap" (NAMG, ca. 1.61–1.49 Ga) ages. Elsewhere in this region, crystalline basement rocks are buried beneath thick deposits of the overlying Mesoproterozoic Belt Supergroup and younger sequences. The unique combination of magmatic basement ages and the detrital zircon components (which also include NAMG detrital ages) within the overlying Mesoproterozoic Belt Supergroup strata, has led researchers to identify the Clearwater Block region as a key tie-point for Proterozoic paleogeographic reconstructions. Some researchers even speculated that Proterozoic supercontinent events stranded exotic (possibly Australia, Antarctica or South China associated) basement terranes within the Clearwater Block. However, no comprehensive multi-isotopic data exist on the Neoarchean to Mesoproterozoic Clearwater Block crystalline basement leaving many of these speculations untested. We report new U–Pb, Lu–Hf and O isotopic data and trace element results of zircon grains for these rocks. Collectively, along with existing data these new results indicate a crustal evolution for the Clearwater Block that consists of: 1) ca. 2.67 Ga juvenile mantle-derived crustal growth as evident by mantle-like δ18O and slightly supra-chondritic (+4 to 0) εHf_t values, 2) ca. 1.87 to 1.83 Ga melting and metamorphism of this ca. 2.67 Ga crust as recorded by ca. 1.86 Ga samples containing zircon with low (<0.1) Th/U ratios and retention of mantle-like δ18O values, and similar-age ca. 1.87–1.83 Ga samples containing zircon with higher (>0.1) Th/U ratios, and 3) ca. 1.58 Ga "NAMG" magmatism that records mantle-like δ18O but sub-chondritic (-5.5 to -9.5) εHf_t values. We interpret the ca. 1.58 Ga NAMG magmatism to be consistent with (perhaps plume-driven) reworking of the Clearwater Block's ca. 2.67 Ga lower crustal reservoir. Consequently, these results support a Laurentian origin for NAMG-age magmatism within the Clearwater Block, but confirm the

necessity of non-Laurentian sources for juvenile (+εHf_t) NAMG-age detrital zircon grains in the overlying ca. 1.47 Ga lower Belt Supergroup strata, thus providing important constraints for western Laurentia's conjugate during the early Mesoproterozoic.

2.1. Introduction

The North American Magmatic Gap (NAMG) is an apparent tectono-magmatic lull from ca. 1.61 to 1.49 Ga within Laurentia (Van Schmus et al., 1993). This period of relative magmatic quiescence occurred after the culmination of the Paleoproterozoic Trans-Hudson (ca. 2.0–1.8 Ga) and Yavapai-Mazatzal-Mojave orogens (ca. 1.65 Ga), and prior to the start of extensive anorogenic magmatism within the Transcontinental Granite-Rhyolite Province at ca. 1.48 Ga (Ross and Villeneuve, 2003; Whitmeyer and Karlstrom, 2007). The NAMG coincides with the final assembly (at ca. 1.6 Ga; Thorkelson et al., 2001; Pourteau et al., 2018) and the following period of relative tectonic stability within the supercontinent Nuna (also called Columbia), and likely reflects Laurentia's central location within the supercontinent (Kirscher et al., 2021). Accordingly, the predominance of NAMG-age detrital zircon grains within western Laurentian strata such as the Mesoproterozoic, ca. 1.47–1.38 Ga Belt (Purcell in Canada) Supergroup (Fig. 2.1A; Ross et al., 1992; Ross and Villeneuve, 2003; Lewis et al., 2010; Box et al., 2020; Brennan et al., 2021), the ca. 1.49–1.44 Ga Hess Canyon Group in southwestern Laurentia (and correlative Trampas basin strata; Doe et al., 2012, 2013; Jones et al., 2015), and the ca. 1.46–1.42 Ga PR1 basin in northwestern Laurentia (Medig et al., 2014), is often interpreted to require non-Laurentian source terranes. Potential source terranes with evidence of NAMG-age magmatism include western Tasmania (Halpin et al., 2014; Mulder et al., 2015), Australia (Reid and Payne, 2017), Antarctica (Goodge et al., 2017) and/or parts of south China (Hainan Island with or without the Cathaysia Block; Li et al., 1995; Xu et al., 2019; Cawood et al., 2020). Consequently, these terranes are commonly located adjacent to western Laurentia within Nuna supercontinent reconstructions.

However, within the Priest River and Clearwater complexes in the northwestern United States of America, the westernmost pre-Belt Supergroup rocks of the Clearwater Block are exposed (Fig. 2.1B), including a small sliver of ca. 1.58 Ga (NAMG-age) granitic gneiss (the Laclede Gneiss; Evans and Fischer, 1986). The ca.

1.58 Ga Laclede Gneiss is the only NAMG-age granitoid in western North America. It has been interpreted as a (i) stranded block of a Proterozoic conjugate continent from Australia, Antarctica, or South China (Ross et al., 1992; Doughty et al., 1998; Goodge et al., 2017; Xu et al., 2019) or (ii) a remnant of a circum- Laurentian orogenesis during the assembly of supercontinent Nuna (Furlanetto et al., 2013). Others (Lewis et al., 2010; Rogers et al., 2018) have also suggested that the Laclede Gneiss might represent a Laurentian source for the ca. 1.7–1.5 Ga detrital zircon grains within parts of the Belt Supergroup, negating the necessity for a western, non- Laurentian source in paleographic reconstructions.

However, apart from U–Pb geochronology studies (Evans and Fischer, 1986; Doughty et al., 1998; Vervoort et al., 2016), Neoarchean–Paleoproterozoic Lu–Hf datasets, and some whole-rock geochemistry (Buddington et al., 2016), a multi-isotopic, integrated comparison of the Neoarchean–Mesoproterozoic Clearwater Block crystalline basement and overlying Paleoproterozoic–Mesoproterozoic strata does not exist. Consequently, many speculations about the Clearwater Block's paleogeographic importance remain untested. Here, we present the results of sensitive high-resolution ion microprobe (SHRIMP) U–Pb, secondary ionization mass spectrometry (Cameca SIMS 1280) δ18O, and laser-ablation inductively coupled mass spectrometry (LA-ICP-MS) Lu–Hf and trace element analyses for zircon from ca. 2.67, 1.86 and 1.58 Ga igneous rocks from the Clearwater Block. These new results, along with existing constraints (Evans and Fischer, 1986; Doughty et al., 1998; Lewis et al., 2010; Buddington et al., 2016; Vervoort et al., 2016), provide robust characterization of the westernmost exposed basement beneath the Mesoproterozoic Belt Basin. These rocks include a unique record of NAMG-age magmatism and allow evaluation of competing models for western Laurentia's assembly and supercontinent Nuna's configuration/evolution.

2.2. Geologic Background

2.2.1. The Priest River complex: American or Australian?

Along much of western North America, within the hinterland of the Cordilleran fold and thrust belt, Paleogene orogenic collapse and development of metamorphic core complexes have exhumed rare exposures of deeply buried crystalline basement beneath thick sequences of Mesoproterozoic to Mesozoic strata (e.g. Dickinson, 2004 and references therein). Within the Priest River complex, along the western extent of the Mesoproterozoic Belt Basin in northern Idaho and southern British Columbia (Fig. 2.1), granitic gneisses were among the first Precambrian rocks in the northwestern Cordillera to be dated by U–Pb geochronology (Clark, 1973; Evans and Fisher, 1986; Doughty et al., 1998). In part, these basement rocks drew early attention because of their sharp contrast with the surrounding extensive, siliciclastic and carbonate strata of the ca. 1.47–1.38 Ga Mesoproterozoic Belt (Purcell in Canada) Supergroup that had long been recognized for its economic and tectonic importance (Harrison, 1972; Ross et al., 1992).

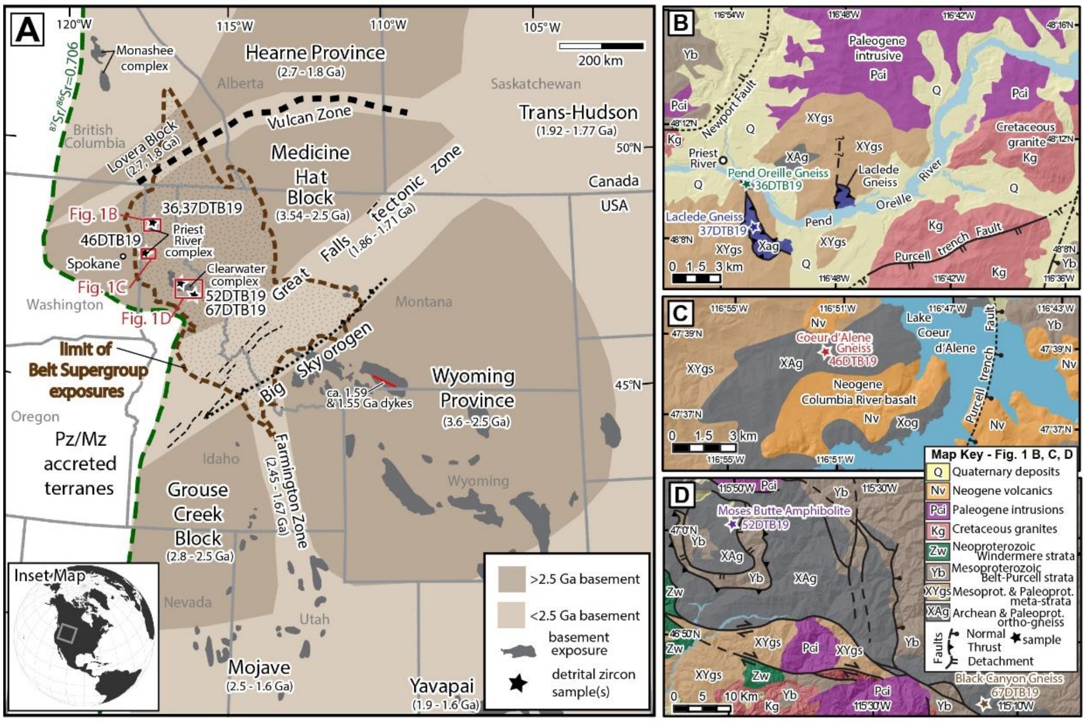

Fig. 2.1: A) Simplified tectonic map of western Laurentia (after Vervoort et al., 2016 and references within) showing the extent and general age of basement provinces, the limit of Belt Supergroup exposures, location of ca. 1.59 and 1.55 Ga mafic dykes in southern Montana (Tobacco Root Mountains; Rogers et al., 2018) and location of sampling areas. B) Geologic map of the northern extent of basement rock exposure within the Priest River complex where samples of the Pend Oreille Gneiss (36DTB19) and Laclede Gneiss (37DTB19) were collected. C) Geologic map of the southern extent of basement rock exposure within the Priest River complex where a sample of the Coeur d'Alene Gneiss (46DTB19) was collected. D) Geologic map of the southeastern extent of the Clearwater complex where a sample of the Moses Butte Amphibolite (52DTB19) and Black Canyon Gneiss (67DTB19) were collected. Geologic maps B, C, and D adapted from Lewis et al. (2012).

Early geochronological analyses on these basement exposures were characterized by analyses showing considerable U–Pb discordance (Table 1). Discordia regression calculations hinted that the western “Belt basement” within the Priest River complex consisted of Neoarchean orthogneiss (ca. 2650 ± 21 Ma) which was unconformably overlain by Belt or possibly pre-Belt strata (Doughty et al., 1998). In addition, the data suggested that the NAMG-age “Laclede Gneiss” (1576 ± 13 Ma by Evans and Fischer, 1986; ca. 1577 Ma by Doughty et al., 1998) was in fault contact with mylonitized lower Belt Supergroup equivalent strata (Doughty et al., 1998; Lewis et al., 2010; 2020; Fig. 2.1B, 2.1C). Based on the similarity of these ages to existing geochronological constraints for eastern Australia (notably the Gawler Craton), it was suggested that the basement rocks of the Priest River complex could be a remnant of eastern Australia left behind during late Proterozoic rifting (Ross et al., 1992; Doughty et al., 1998; Evans et al., 2000).

Within the Priest River complex, a thin (~300 m thick) quartzite (the Gold Cup Quartzite) unconformably overlies Neoarchean and Paleoproterozoic crystalline basement and is overlain by Mesoproterozoic Belt Supergroup strata (Doughty and Chamberlain, 2008; Buddington et al., 2016; Lewis et al., 2020). The Gold Cup Quartzite lacks detrital zircon grains younger than ca. 1.74 Ga, and records a Laurentian provenance (Brennan et al., 2021) suggesting deposition prior to the ca. 1.6 Ga final assembly of supercontinent Nuna (Nordsvan et al., 2018; Pourteau et al., 2018; Kirscher et al., 2019; Volante et al., 2020). Basin-wide studies of the overlying Belt Supergroup suggest that the Belt Basin received sediment from both Laurentian and disputed western non- Laurentian sources (e.g. Ross and Villeneuve, 2003). Within Belt Supergroup strata, a Laurentian signature is characterized by major age-peaks at ca. 2.7, 1.8–1.7, and 1.45 Ga, whereas a possible non- Laurentian signature is characterized as having a broad range of detrital zircon ages from ca. 1.9–1.4 Ga, including significant zircon grains with ages that fall within the ca. 1.61–1.49 Ga North American Magmatic Gap (Ross et al., 1992; Ross and Villeneuve, 2003; Box et al., 2020).

However, others (e.g. Lewis et al., 2010) have questioned if exotic sources are necessary to provide the NAMG-age zircon grains within Belt strata, citing the ca. 1.58 Ga Laclede Gneiss within the Priest River complex as a potential source. Rogers et al. (2018) also advocated that the ca. 1.59 Ga (1590 ± 3 Ma) Mammoth and ca. 1.55 Ga (1551 ± 5 Ma) Ramshorn Creek mafic dykes, located nearby in southern Montana, may have potentially eroded felsic equivalents that could have been additional Laurentian detrital zircon sources. Rogers et al., (2018) correlated the plume-related chemistry of the ca. 1.59 Ga Mammoth dykes to geochemically similar, coeval rocks in the Gawler Craton and Curnamona Province of southeastern Australia, which they consider connected as one single large igneous province (LIP) within Nuna.

2.2.2. The Clearwater Block: A Priest River and Clearwater complex connection

Approximately 150 km south/southeast of the the Priest River complex, pre-Belt Supergroup crystalline basement rocks are also exposed in the Clearwater complex (Fig. 2.1D; Reid et al., 1973; Doughty and Chamberlain, 2007; Vervoort et al., 2016). Early work on Clearwater complex crystalline basement rocks (Table 1) gave discordant geochronology results suggesting ca. 2.1–1.8 Ga crystallization ages (Reid et al., 1973). Follow-up geochronology (Doughty and Chamberlain, 2007) also showed significant Pb-loss, but supported the presence of ca. 1.8 Ga igneous (anorthosite) rocks within the Clearwater complex. Limited geochronology results from an amphibolite exposed within the granitic basement also hinted at the occurrence of ca. 1.59 Ga mafic magmatism based on the two oldest, slightly reverse discordant analyses out of six total analyses, with the younger four analyses suggesting ca. 1.38 Ga metamorphic growth (Doughty and Chamberlain, 2007). Overall, these results reflect the similar timing of pre-Beltian magmatism within the Priest River and Clearwater complexes.

Subsequent extensive geochronological study of the Priest River and Clearwater complexes by Vervoort et al. (2016) further solidified the similarity between the ages of basement rocks exposed within the complexes. Vervoort et al., (2016) dated 18 orthogneiss exposures across the Priest River (n = 2) and Clearwater (n = 16) complexes. All samples yielded ages that fall into two tightly defined age ranges of ca. 2.67 to 2.65, and 1.88 to 1.84 Ga, indicating two main periods of crustal formation beneath the western portion of the Belt Basin. Based on the similarity of these ages, Vervoort et al. (2016) suggested that the Priest River and Clearwater complexes expose crystalline basement of the same crustal block, which they named the Clearwater Block. The relationship between the Clearwater Block and the adjacent Medicine Hat Block to the east is not well known (Vervoort et al., 2016; Gifford et al., 2020).

Paleoproterozoic xenocrystic zircons within Phanerozoic plutonic rocks led Foster et al., (2006) to speculate that a separate ca. 2.4–1.5 Ga "Selway" terrane comprises the southern portion of the Clearwater Block. However, additional studies of the xenocrystic zircon cargo of Phanerozoic plutons (Gaschnig et al., 2013) and exposed basement rocks in the region (Vervoort et al., 2016) did not support this speculation. Consequently, Gaschnig et al. (2013) and Vervoort et al. (2016) refrained from delineating a separate terrane in the southern portion of the Clearwater Block. In addition, geophysical results do not support the interpretation of a separate terrane in the southern portion of the Clearwater Block (e.g. Bedrosian and Feucht, 2014).

2.2.3. Adjacent Laurentian basement framework

Western Laurentia is a complicated mosaic of igneous, metamorphic and sedimentary rocks that range in age from Archean to present and are the result of this region being at or near a continental margin periodically for the past 2.6 billion years (Hoffman, 1988; Whitmeyer and Karlstrom, 2007; Vervoort et al., 2016). East of the Clearwater Block, the Medicine Hat Block contains a mix of Archean (ca. 3.1–2.6 Ga) and Paleoproterozoic (ca. 1.81–1.75 Ga) crust (Gifford et al., 2018, 2020; Ross et al., 1991; Villeneuve et al., 1993). The Paleoproterozoic magmatism within the Medicine Hat block has an evolved Lu–Hf signature indicating reworking of the older Meso- to Neoarchean rocks (Gifford et al., 2020).

The Archean Wyoming Craton and Grouse Creek Block are separated from each other by the Farmington Zone and neighbor the Clearwater and Medicine Hat blocks to the south (Whitmeyer and Karlstrom, 2007; Mueller et al., 2011). The Wyoming Craton includes rocks as old as 3.6 Ga and detrital zircon ages as old as 4.0 Ga (Chamberlain et al., 2003; Mueller and Frost, 2006). The Grouse Creek Block in southcentral Idaho and northern Utah may also contain rocks as old as ca. 3.6 Ga preserved only as xenoliths within younger Snake River Plain volcanic rocks (Leeman et al., 1985), but has exposures of ca. 2.67–2.50 Ga felsic and ca. 1.85 Ga mafic magmatic rocks (Strickland et al., 2011; Link et al., 2017). The Farmington Zone contains ca. 2.45 Ga magmatism and ca. 1.67 Ga metamorphism, and likely records the final juxtaposition of the Wyoming Craton, Grouse Creek Block and Mojave Province (Mueller et al., 2011).

Paleoproterozoic (Trans-Hudson-age; ca. 1.9–1.7 Ga) suture/collisional zones separate the main Archean blocks of western Laurentia. The boundary between the Medicine Hat Block and the Wyoming Craton to the south (Mueller et al., 2002) is delineated by the broad Great Falls Tectonic Zone. The Great Falls Tectonic Zone records major ca. 1.86–1.73 Ga Paleoproterozoic convergent events including the Great Falls Orogeny and the more temporally and spatially restricted Big Sky Orogeny. Generally, Great Falls Tectonic Zone rocks indicate northwest-dipping subduction, closure of an intervening ocean and eventual amalgamation of the Medicine Hat Block to the Wyoming Craton (Gorman et al., 2002; Mueller et al., 2002; Foster et al., 2006; Condit et al., 2015; Gifford et al., 2014; 2018; 2020).

The Clearwater and Medicine Hat blocks are bordered to the north by the subsurface Vulcan structure. The Vulcan structure is likely another Trans-Hudson age feature that may reflect the collision of the southwestern margin of the ca. 2.7–1.8 Ga Hearne Province (the Lovera Block) with the northern margin of the Medicine Hat Block along a north-dipping subduction zone (Ross et al., 1991; Nieuwenhuis et al., 2014). However, differing geophysical interpretations have also resulted in Paleoproterozoic rift (Kanasewich et al., 1969), or south-dipping subduction/collision zone models (Eaton et al., 1999) for the Vulcan structure. North of the Lovera Block, limited geochronologic studies indicate ca. 2.24, 2.03 and 1.84 Ga basement rocks are exposed within the Monashee complex (Crowley et al., 1999).

Following the assembly of the main Archean blocks of western Laurentia during Trans-Hudson-age events, a long-lived accretionary boundary resulted in the addition of the ca. 1.84–1.70 Ga Mojave province, which comprises a mixture of juvenile and evolved components (suggesting the presence of crust as old as ca. 2.5 Ga; Wooden et al., 2012), and the juvenile ca. 1.90–1.70 and 1.65–1.60 Ga Yavapai and Mazatzal provinces along the southern/southwestern margin of Laurentia (Bowring and Karlstrom, 1990; Holland et al., 2020). Collectively, the Mojave-Yavapai-Mazatzal provinces may record progressive accretion of separate, predominantly juvenile arc systems (Whitmeyer and Karlstrom, 2007), or may represent an extensive arc-backarc system that developed along the Australia–Antarctica margin at ca. 1.8 Ga before their accretion to Laurentia at ca. 1.65 Ga (Gibson and Champion, 2019). Mueller et al. (2011) interpreted the ca. 1.67 Ga metamorphism within the Farmington Zone to record collision of Mojave-Yavapai provinces to the southern margin of the Wyoming craton.

2.3. Methods

2.3.1. Sample preparation

Samples were collected in the context of 1:100,000 scale geologic mapping of the Priest River and Clearwater complexes (Lewis et al., 2007; 2020). Petrographic thin sections were made by Wagner Petrographic, Utah USA. Zircon grains for isotopic analysis were separated from approximately 1 kg individual hand samples using standard techniques consisting of SEL-Frag fragmentation followed by Frantz magnetic and heavy liquid separation at Curtin University, Australia. Unknown zircon grains along with reference zircons OGC, 610, M257, 91500, and Z1 were mounted in epoxy resin within 6 mm of the center of 25 mm diameter disks and were polished to expose grain centers. Prior to analysis, all mounts were imaged in reflected and transmitted light on a Zeiss Axio Imager.M2m optical microscope and cathodoluminescence (CL) imaged using a MIRA3 variable-pressure field-emission scanning electron microscope (SEM) at the Microscopy and Microanalysis Facility at the John de Laeter Centre (JdLC), Curtin University for analysis targeting.

2.3.2. A threefold analytical approach: Measurement of U–Pb, $\delta^{18}O$, Lu–Hf, and trace element zircon values

U–Pb dating was carried out on the SHRIMP II at Curtin University. A 25 μm diameter spot size was used for all the analysed grains with a primary beam current of 2.5–3.0nA. Data for each spot were collected in sets of 6 scans through the mass range of $^{196}Zr^{2}O+$, $^{204}Pb+$, background, $^{206}Pb+$, $^{207}Pb+$, $^{208}Pb+$, $^{238}U+$, $^{248}ThO+$, $^{254}UO+$. The measured isotopic ratios were corrected for common Pb based on the measured ^{204}Pb and using the common Pb evolution curve of Stacey and Kramers (1975). U–Pb ages were normalized to the M257 zircon standard accepted value of 561.3 Ma (Nasdala et al., 2008). In addition to primary standard M257, secondary reference standard (OGC) analyses were interspersed between unknown analyses during each session (one standard every three to five unknowns). The weighted mean of 18 OCG analyses yielded a date of 3466.6 ± 3.1 (MSWD = 1.6) which is indistinguishable from accepted OGC reference age of 3465.4 ± 0.6 Ma (Stern et al., 2009). All isotopic measurements were reduced, processed and interpreted using SQUID II, and IsoplotR programs (Vermeesch, 2018; Bodorkos et al., 2020; Ludwig, 2003). All uncertainties reported within this text are at 2σ and include errors from U–Pb calibration based on the reproducibility of U–Pb standard measurements, counting statistics and the common-

Pb correction. Throughout the text, $^{207}Pb/^{206}Pb$ dates are used for all analyses besides sample 52DTB19 (Moses Butte Amphibolite). For sample 52DTB19, the $^{206}Pb/^{238}U$ and Concordia age values are also considered due to the ambiguity in the best isotopic ratio for dates between ca. 1.5 and 1.0 Ga (Ludwig, 1998), which is discussed further in the results.

Table 2.1

Existing and new results of studied Neoarchean–Mesoproterozoic magmatism within the Clearwater Block, western Laurentia.

Geologic Unit	Analysis method	Isotopic data	Values reported	Results	Reference
Pend Oreille Gneiss					
PR-93-747B	Dissolution TIMS	U-Pb (n = 3)	discordia upper intercept	2651 ± 21 Ma	Doughty et al., 1998
36DTB19	SIMS-SHRIMP	U-Pb (n = 20)	discordia intercept estimates	ca. 2.7 Ga crystallization, ca. 1.8 Ga metamorphism, or a possible paragneiss origin	this work
Black Canyon Gneiss					
08RAB025	LA-ICPMS	U-Pb (n = 20)	weighted mean of 20 ananlyses	2663 ± 8 Ma	Vervoort et al., (2016)
67DTB19	SHRIMP	U-Pb (n = 20)	weighted mean of 11 concordant analyses	2665 ± 4 Ma	this work
	SIMS	O- isotopes (n = 20)	weighted mean of 17 robust analyses	δ18O = 5.42 ± 0.08 ‰	this work
	LA-SS-ICPMS	Lu-Hf (n = 20)	three most concordant analyses	εHft = +3.5 to −0.5	this work
	LA-ICPMS	trace element abundances (n = 20)	abundances (ppm)	see Fig. 8A	this work
Coeur d'Alene Gneiss					
09RMG07, 07RMG22	LA-ICPMS	U-Pb (n = 20)	weighted mean of 20 ananlyses	1862 ± 3, 1867 ± 4 Ma	Vervoort et al., (2016)
67DTB19	SIMS-SHRIMP	U-Pb (n = 20)	weighted mean of 5 concordant analyses	1857 ± 5 Ma	this work
	SIMS	O- isotopes (n = 20)	weighted mean of 17 robust analyses	δ18O = 5.47 ± 0.07 ‰	this work
	LA-ICPMS	trace element abundances (n = 20)	abundances (ppm)	reported in supplementary	this work
Laclede Gneiss					
Not assigned	Dissolution TIMS	U-Pb (n = 3)	discordia upper intercept	ca. 1540 Ma	Clark, 1973
Not assigned	Dissolution TIMS	U-Pb (n = 4)	discordia upper intercept	1576 ± 13 Ma	Evans and Fischer, 1986
PR-93 –731	Dissolution TIMS	U-Pb (n = 3)	single most concordant analysis	1577.4 ± 2.3 Ma	Doughty et al., 1998
37DTB19	SIMS-SHRIMP	U-Pb (n = 24)	weighted mean of 22 concordant analyses	1581 ± 3 Ma	this work
	SIMS	O- isotopes (n = 20)	weighted mean of 17 robust analyses	δ18O = 5.15 ± 0.13 ‰	this work
	LA-SS-ICPMS	Lu-Hf (n = 20)	range of 18 analyses excluding 2 outliers	εHft = −5.5 to −9.7	this work
	LA-ICPMS	trace element abundances (n = 20)	abundances (ppm)	see Fig. 8B	this work
Moses Butte Amphibolite					
GM-01 –2	SIMS-SHRIMP	U-Pb (n = 6)	weighted mean of 2 oldest analyses weighted mean of 2 youngest analyses	1587 ± 9 Ma (crystallization) 1361 ± 13 Ma (metamorphic growth)	Doughty and Chamberlain, 2007
52DTB19	SIMS-SHRIMP	U-Pb (n = 27)	various metrics discussed in text	ca. 1417 to 1350 Ma metamorphic growth	this work
	SIMS	O- isotopes (n = 20)	weighted mean of 17 robust analyses	δ18O = 4.52 ± 0.31 ‰	this work
	LA-ICPMS	trace element abundances (n = 20)	abundances (ppm)	reported in supplementary	this work

Abbreviations: TIMS-Thermal Ionization Mass Spectroscopy, LA-Laser ablation, SS-Split stream, ICPMS-Iductively Coupled Plasma Mass spectrometry, SHRIMP-Sensitive High Resolution Ion Micro Probe, SIMS-Secondary Ionization Mass Spectroscopy.

After SHRIMP analysis, the sample mounts were thoroughly cleaned, and briefly repolished with a 3 µm diamond paste, prior to being coated with an approximately 30-nm-thick Au coating. Subsequent zircon oxygen isotopic compositions were measured using a Cameca IMS 1280 at the Centre for Microscopy, Characterization and Analysis (CMCA) facility at the University of Western Australia following procedures described by Hartnady et al., (2020). Oxygen analysis spots were placed within the same crystal domain as the SHRIMP analysis spots as identified by CL imaging but did not overlap and generally an approximately 10 µm gap or larger was left between analysis spots where feasible. Oxygen results were processed with a CMCA in-house excel macro. Oxygen isotope compositions are reported in the conventional delta notation; expressed as δ18O, reflecting the permil (‰) deviation in the (18O/16O) isotope ratio of the sample relative to average seawater (Vienna Standard Mean Ocean Water; VSMOW; Baertschi, 1976).

Instrumental drift and fractionation were determined through analysis of reference zircon 91,500 with OGC and M257 as secondary reference standards. During our first of two analytical runs, unknown samples 67DTB19, 46DTB19 and 37DTB19 were analysed with an approximately 20 µm diameter, 2.5nA, Cs+ ion-beam. During this run primary reference standard 91,500 (n = 14) yielded a δ18O weighted mean of 9.94 ± 0.08‰ (MSWD = 0.63) which is indistinguishable from the accepted value of 9.90 ± 0.30‰ (Wiedenbeck et al., 2004) and consequently did not require application of any drift correction. Secondary reference standards yielded δ18O weighted means of 5.68 ± 0.21‰ (OGC) and 13.99 ± 0.06‰ (M257) which are also indistinguishable from the accepted values of 5.88 ± 0.06‰ and 13.93 ± 0.22‰ (Nasdala et al., 2008; Petersson et al., 2019). $^{16}O^{1}H/^{16}O$ values were also monitored to evaluate secondary water update facilitated by radiation damage within the zircon (e.g. Liebmann et al., 2021). Reference standard $^{16}O^{1}H/^{16}O$ values ranged from 0.0006 to 0.0010. Only 5/60 analyses of the unknowns exceeded this range with no obvious effect on δ18O values. Nevertheless, these five analyses are disregarded due to their elevated $^{16}O^{1}H/^{16}O$ values recording possible alteration of their oxygen isotopic compositions.

Due to smaller zircon size, sample 46DTB19 was analysed during a separate run with a more targeted, approximately 10 µm diameter, 1.0nA, Cs+ ion-beam. Slight sample topology observed within the 91,500 reference material (and inability to polish further without removing the unknown grains) rendered it unfavourable as a primary standard (e.g. Kita et al., 2009), and consequently M257 was utilized as the primary reference standard. M257 yielded a δ18O weighted mean (n = 6) of 13.99 ± 0.12‰ (MSWD = 0.62) which is indistinguishable from the accepted value of 13.93 ± 0.22‰ (Nasdala et al., 2008) and consequently no drift correction was applied. Secondary reference standard OGC yielded a δ18O weighted mean of 5.86 ± 0.18‰ which is also indistinguishable from the accepted values of 5.88 ± 0.06‰ (Petersson et al., 2019). All unknown analyses (n = 8) fell within the $^{16}O^{1}H/^{16}O$ range given by the standards (0.0009 to 0.0013).

Final analysis consisted of measuring U–Pb, Lu–Hf, and trace element isotopes using laser ablation (single and) split-stream inductively coupled mass spectroscopy (LA-SS-ICP-MS) at the GeoHistory Facility in the John de Laeter Centre at Curtin University, Perth Australia across two analytical sessions. The first analysis session consisted of ablation with 38-µm analysis spot generated by a Resonetics RESOlution M50-A excimer laser. From this ablated material, U–Pb isotopes were measured on an Agilent 7700 s quadrupole ICP-MS for age determination, while Lu–Hf isotopes were simultaneously measured on a Nu Instruments NP II MC-ICP-MS. During this session, 38 µm analysis spots were placed over both the SHRIMP and SIMS analysis spots where possible.

Subsequently, during a second laser ablation analytical session (LA-ICP-MS), trace elements abundances were measured on an Agilent 8900 QQQ ICP-MS using a 20 µm spot generated by a Resonetics RESOlution M50-A excimer laser which was placed over the same zircon crystal domain as the prior analyses. Following analysis, data reduction was performed using the software Iolite v.3.6 (Paton et al., 2011). MudTank zircon standard was utilized as the primary standard for Lu–Hf results, while GJ-1 was utilized as a primary reference standard for the trace element results.

To evaluate the necessity of non-Laurentian sources for strata in the region, new trace element data from detrital zircon grains within overlying Paleoproterozoic Gold Cup Quartzite and Mesoproterozoic lower Belt Supergroup strata are reported. This analytical session also utilized a Resonetics RESOlution M50-A excimer laser paired with an Agilent 7700 s quadrupole and Nu Instruments NP II MC-ICP-MS at the GeoHistory Facility in the John de Laeter Centre at Curtin University for simultaneous measurement of U–Pb, Lu–Hf, and trace element abundances. Brennan et al. (2021) report the U–Pb and Lu–Hf results from this detrital zircon analytical session. Additional SHRIMP, SIMS, and LA-ICP-MS analytical details are included in the supplementary information.

2.4. Results

2.4.1. Sample 36DTB19 – Pend Oreille Gneiss

Within the core of the Priest River complex, the structurally lowest unit exposed is the Pend Oreille Gneiss (Lewis et al., 2020). Doughty et al., (1998) reported U–Pb (thermal ionization mass spectroscopy) data from five chemically abraded zircon grains from this unit that are variably discordant. Their discordia regression suggests a 2651 ± 21 Ma crystallization age, disturbed by an early Paleozoic (ca. 495 Ma) Pb-loss event.

To further evaluate this probable Neoarchean basement within the Priest River complex, sample 36DTB19 was collected from a heterogeneous migmatitic biotite gneiss outcrop of the Pend Oreille Gneiss in a similar location (Fig. 2.1B) to Doughty et al. (1998). The zircon grains separated from sample 36DTB19 show concentric zoning in CL imaging consistent with magmatic growth. Thin (<5 μm) metamorphic rims are present on some grains but their small size precluded analysis (Fig. 2.2A). Twenty SHRIMP U–Pb analytical results from these grains yielded complex (8% to 90%) discordant results with $^{207}Pb/^{206}Pb$ ages ranging from ca. 2824 Ma to 1634 Ma (Fig. 2.3). The extensive Pb-loss in this sample precluded calculation of a geologically meaningful weighted mean age. A range of Th/U ratios (approximately 0.7 to 0.007) and U (2350 to 350 ppm) abundances were measured (Fig. 2.4). More radiogenic (higher U) grains yielded younger $^{207}Pb/^{206}Pb$ ages. Due to the complexity of this sample, which is discussed further in section 5.1 and 5.2 of the discussion, we also present a more detailed concordia diagram and a thin section microphotograph (Fig. 2.5). The mineralogy observed within this sample (Fig. 2.5B) is relatively simple consisting of abundant lamellar twinned plagioclase, quartz, and biotite.

Fig. 2.2: Field photos of the sampled outcrops and cathodoluminescence (CL) images of representative zircon grains from the samples with analytical spots and results indicated. Labeled ages are based on $^{207}Pb/^{206}Pb$ ratios. Note the scale card in the field photos is approximately 8.5 by 5.4 cm and shows a cm scale bar on the top and inch scale bar on the bottom. Analytical spot key and zircon grain scale bar is in the bottom right.

2.4.2. Sample 67DTB19 – Black Canyon Gneiss

To compare the Archean isotopic composition of the Clearwater Block with the adjacent Medicine Hat Block and Wyoming Craton, the southern and easternmost exposure of Neoarchean Clearwater crust with a previously reported crystallization age of 2663 ± 8 Ma (Vervoort et al., 2016) was resampled from along Black Canyon near the southeastern extent of the Clearwater complex (Fig. 2.1D). The Black Canyon

Gneiss, sample 67DTB19, was collected from this Neoarchean biotite augen gneiss, and yielded zircon grains with concentric zoning in CL imaging consistent with magmatic growth (Fig. 2.2). Most grains also show bright (low U; e.g. Hanchar and Miller, 1993) overgrowths interpreted as metamorphic rims, which likely reflect late Mesozoic or younger metamorphism within the Clearwater complex (e.g. Doughty et al., 2007). Twenty analyses of the oscillatory zoned zircon cores yielded $^{207}Pb/^{206}Pb$ ages (21 to 0% discordant) ranging from ca. 2688 Ma to 2373 Ma (Fig. 2.3), with a relatively limited range of Th/U ratios (0.54 to 0.28; Fig. 2.4). Eleven of these twenty analyses overlap with concordia (within 2σ uncertainties) and yield a weighted mean age of 2665 ± 4 Ma (MSWD = 6.6) which is indistinguishable from the age reported by Vervoort et al. (2016). The relatively high MSWD value of the weighted mean age indicates that the calculated weighted mean uncertainty is likely an underestimation of the true imprecision (e.g. Spencer et al., 2016).

Sixteen robust analyses (2 rejected for elevated $^{16}O^{1}H/^{16}O$ values, another 2 rejected as outliers from the weighted mean calculation) of δ18O within the cores of these zircon give a weighted mean of 5.42 ± 0.08‰ (MSWD = 3.1; Fig. 2.6), which is indistinguishable from accepted 5.3 ± 0.6‰ δ18O value of mantle derived zircons (Valley et al., 1998; Valley, 2003). Eighteen of the twenty Lu–Hf measurements give εHf_t values from +4.2 to +0.2 when calculated using the preferred 2665 Ma crystallization age, indicating a Lu/Hf composition overlapping and slightly above CHUR (Chondritic Uniform Reservoir; Blichert-Toft et al., 1999; Bouiver et al., 2008). Two additional analyses give outlier εHf_t values at approximately +6.9 and +13.4 (Fig. 2.7).

2.4.3. Sample 46DTB19 – Coeur d'Alene Gneiss

To further evaluate the alleged (e.g. Doughty et al., 1998) southeastern Australian affinity of the basement rocks within the Priest River complex, the westernmost exposure of the late Paleoproterozoic Coeur d'Alene Gneiss, within the Priest River complex was sampled along the western shore of Lake Coeur d'Alene (Fig. 2.1C). Vervoort et al. (2016) sampled this same outcrop and report 1862 ± 3 and 1867 ± 4 Ma crystallization ages (LA-ICP-MS). The leucogranite lithology of the Coeur d'Alene Gneiss we sampled yielded zircon grains with poorly preserved and/or absent zoning, rather heterogenous mottled textures and small localized bright (in CL) patches (Fig. 2.2). Twenty analyses of the most uniform interior regions of these grains yielded $^{207}Pb/^{206}Pb$ ages from 1864 to 1694 Ma, with many of the analyses discordant and a plot along a Pb-loss line with an 1852 ± 13 Ma upper intercept and a ca. 155 Ma lower intercept (Fig. 2.3A). This lower intercept is similar to the timing of nearby late Jurassic terrane accretion (e.g. Schwartz et al., 2011). Five of the twenty total analyses overlap concordia within 2σ uncertainties and yield a weighted mean age of 1857 ± 5 Ma (MSWD = 0.9; Fig. 2.3B), which again is indistinguishable from the ages reported by Vervoort et al. (2016). The zircon grains from sample 46DTB19 yielded the highest U abundances (4472 to 1844 ppm) of all samples, with relatively consistent and low Th/U ratios (0.063 to 0.034; average of concordant grains = 0.051; Fig. 2.4).

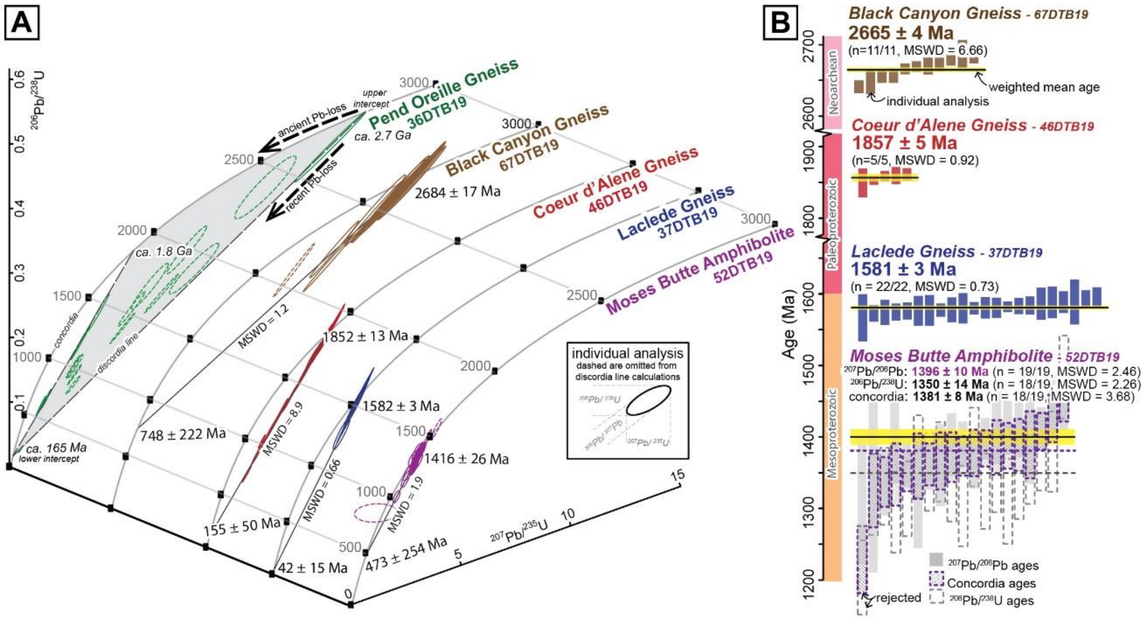

Fig. 2.3: A) Wetherill concordia diagram of SHRIMP U–Pb results for the sampled units. Dashed analyses are omitted from discordia calculations. B) Weighted Mean calculations for analyses that overlap with concordia. All uncertainties indicated at 2σ level. $^{207}Pb/^{206}Pb$ ratios are used for samples 67DTB19, 46DTB19, and 37DTB19. Initial plots and discordia regressions generated with ISOPLOTR (Vermeesch, 2018). MSWD – mean standard weighted deviation.

Seventeen robust analyses of δ18O from the same zircon domains as the SHRIMP analyses range from 4.54 to 5.61‰ and give a weighted mean of 5.47 ± 0.07‰ (MSWD = 3.1; Fig. 2.6), which is indistinguishable from the accepted 5.3 ± 0.6‰ δ18O value for mantle derived zircon (Valley et al., 1998; Valley, 2003). Interestingly, in addition to high U values, the average phosphorous (P), yttrium (Y), and lutetium (Lu) content of these grains (measured during LA-SS-ICP-MS analysis) is over twice that of samples 67DTB19 (Black Canyon Gneiss) and 37DTB19 (Laclede Gneiss). This suggests that the order of magnitude larger ablation volumes during LA-SS-ICP-MS analysis incorporated xenotime (YPO4), that was likely present within the zircon grains as either secondary overgrowth along fractures or inclusions. These contaminant phases were likely avoided during smaller volume U–Pb (SHRIMP) and δ18O (SIMS) analyses but contributed to the spurious (LA-SS-ICPMS) Lu–Hf measurements.

2.4.4. Sample 37DTB19 – Laclede Gneiss

Within the Priest River complex, a tabular body of megacrystic augen gneiss, the Laclede Gneiss, crops out over<9 km2 and lies in fault contact with surrounding metasedimentary strata of the lower Belt Supergroup (Clark, 1973; Doughty et al., 1998; Doughty and Chamberlain, 2008; Lewis et al., 2020). The Laclede augen gneiss is strongly foliated, with layering defined by biotite-rich and -poor zones, and contains conspicuous, subhedral to euhedral orthoclase megacrysts (3–6 cm in length) within a matrix of orthoclase (30–70%), plagioclase (5–35%), quartz (10–15%), biotite (3–7%), along with minor accessory minerals, such as apatite, zircon, epidote, and sphene (Clark, 1967). Prior geochronologic study of the Laclede Gneiss was on exposures north of the Oreille River and indicated disturbance in the U–Pb system resulting from recent Pb-loss (Evans and Fischer, 1986; Doughty et al., 1998). In an effort to minimize the likelihood of similar discordant results, a Laclede Gneiss sample was collected further from the nearby Cretaceous and Paleogene intrusions along the southeastern portion of the outcrop (Fig. 2.1B; Lewis et al., 2020).

This Laclede Gneiss sample yielded zircon grains that in CL imaging showed well-defined oscillatory zoning, with bright (low U) relatively homogenous metamorphic overgrowths (Fig. 2.2). Twenty-three SHRIMP analyses of the most uniform, oscillatory zoned interior regions of these grains yielded $^{207}Pb/^{206}Pb$ ages from 1595 to 1566 Ma (Fig. 2.3), with U values from 2800 to 220 ppm and Th/U values>0.24 consistent with magmatic crystallization (Fig. 2.4). Twenty-two of these analyses overlap concordia within 2σ uncertainties and yield a weighted mean age of 1581 ± 3 Ma (MSWD = 0.73). This weighted mean value is interpreted as the crystallization age and overlaps with the existing discordia-calculated upper-intercept age-constraint of 1576 ± 13 Ma (Fig. 2.3; Evans and Fischer, 1986). A single analysis on the metamorphic rims yielded a ca. 58 Ma ($^{206}Pb/^{238}U$) date, which falls between the crystallization age of the nearby 50 ± 6 Ma Paleogene pluton (Whitehouse et al., 1992) and ca. 64 Ma peak metamorphism with the Priest River complex (Stevens et al., 2015).

Twenty robust analyses of δ18O from the same zircon domains as the SHRIMP analyses give a weighted mean of 5.15 ± 0.13‰ (MSWD = 3.4; Fig. 2.6), which is also indistinguishable from accepted 5.3 ± 0.6‰ δ18O value of mantle-derived zircon (Valley et al., 1998; Valley, 2003). Seventeen Lu–Hf measurements give εHf_t values from -5.4 to -9.3, while three additional analyses give slight outlier εHf_t values of approximately -5.1, -4.5 and -4.2 (Fig. 2.7).

2.4.5. Sample 52DTB19 – Moses Butte Amphibolite

Doughty and Chamberlain (2007) reported six zircon analyses from a strongly lineated garnet-hornblende amphibolite collected near Moses Butte within the central portion of the Clearwater complex. Three of these analyses yielded concordant dates of 1520, 1589, and 1584 Ma, which they interpret to record a 1587 ± 9 Ma crystallization age of the mafic protolith. The additional three analyses yielded slightly discordant results suggesting 1361 ± 13 Ma metamorphism. To further evaluate the presence of NAMG-age magmatism within the Clearwater complex, we collected another sample (sample 52DTB19) of the Moses Butte Amphibolite.

Zircon grains recovered from this sample were sparse and small. Most grains showed very faint to absent zoning in CL imaging (Fig. 2.2). Only one recovered grain showed a faint oscillatory zoned core, with a smaller metamorphic overgrowth in CL imaging. Twenty of twenty-six individual SHRIMP U–Pb analyses yielded concordant ages. Nineteen concordant ages on the predominant zircon grains with faint to absent zoning showed Concordia ages from ca. 1440–1229 Ma (Fig. 2.3) with Th/ U ratios from 0.19 to 0.002 (Fig. 2.4). The single oscillatory zoned core yielded a concordant ca. 1546 Ma ($^{207}Pb/^{206}Pb$) age with the highest measured Th/U value within this sample of 0.22. The $^{207}Pb/^{206}Pb$ ratios from the nineteen grains with faint to absent zoning yield a 1396 ± 10 Ma (MSWD = 2.46) weighted mean age. Alternative weighted mean calculations based on Concordia ages suggest a 1381 ± 8 Ma (MSWD = 3.68, 1/19 analyses rejected) or 1350 ± 14 Ma (MSWD = 2.26, 1/19 analyses rejected) age using $^{206}Pb/^{238}U$ ratios. The MSWD values of these weighted mean ages suggest underestimated errors, or multiple ca. 1400–1350 Ma populations within in the dataset (e.g. Spencer et al., 2016).

Eight robust analyses of δ18O from the same zircon domains as the SHRIMP analyses range from 5.01 to 4.17‰ and give a weighted mean of 4.52 ± 0.31‰ (MSWD = 23; Fig. 2.6). This is lower than, but slightly overlapping with, the 5.3 ± 0.6‰ δ18O value of mantle derived zircon (Valley et al., 1998; Valley, 2003). It is also below the usual 5 to 17‰ value of metabasic metamorphic zircon (Cavosie et al., 2011). The tiny size of these grains precluded robust LA-ICP-MS analysis.

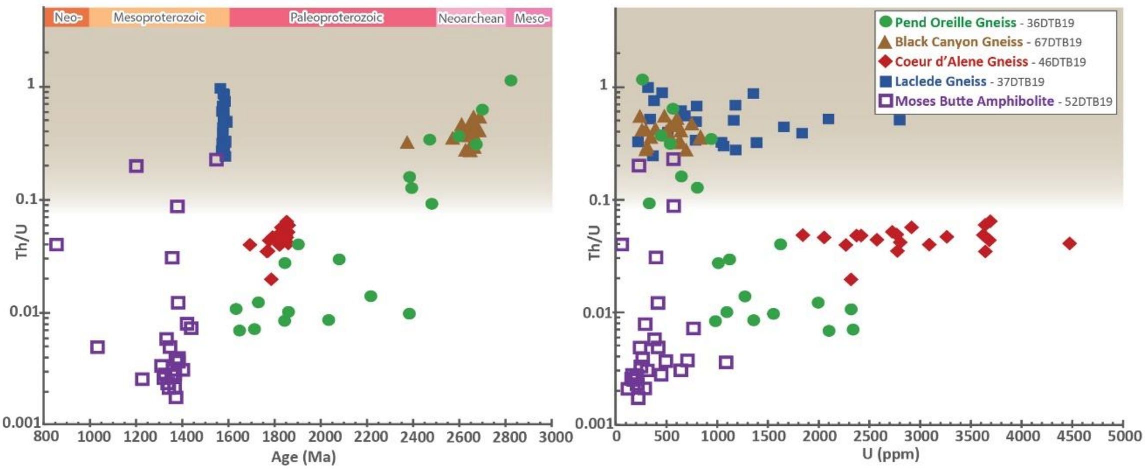

Fig. 2.4: Age (Ma) vs. Th/U (left) and U (ppm) vs. Th/U (right) scatterplots for individual SHRIMP U–Pb analyses. Background shading indicates a Th/U ratio of 0.1, which is the lower limit commonly found in igneous zircon (Yakymchuk et al., 2018). Note the vertical (Th/U) axis is logarithmic.

2.5. Discussion

2.5.1. Neoarchean growth of the Clearwater Block

The Neoarchean was a time of globally widespread continental growth as evident by the prevalence of ca. 2800–2500 Ma magmatic rocks within many other cratons (e.g. Slave, Yilgarn, Wyoming, etc.; Ivanic et al., 2012; Mole et al., 2019, 2021) as well similar age-peaks within the global detrital zircon record (e.g. Roberts and Spencer, 2015). The proposed mechanisms of crustal generation during the Archean are diverse but are generally placed into two end-member categories. These include modern plate tectonic style plume, rift or subduction processes (e.g. Frieman et al., 2021; Mole et al., 2021), and processes that do not require modern plate tectonics such as delamination, mafic reworking, and so-called “drip tectonics” (e.g. Johnson et al., 2014; B´edard, 2018; Mole et al., 2019). Our study of the Neoarchean crust within the Clearwater Block allows us to evaluate several of these potential mechanism for the generation of ca. 2670 Ma crust in this region.

Our sampling (sample 36DTB19) of the Neoarchean Pend Oreille Gneiss within the Priest River complex revealed more difficult to interpret U/Pb results than those reported by Doughty et al., (1998). When our results are viewed in Wetherill concordia space, they are consistent with an original ca. 2700 Ma crystallization event, and at least two Pb-loss events, one ancient at ca. 1800 Ma and one more recent in the latest Jurassic to early Cretaceous at ca. 165 Ma (Fig. 2.5A). The relationship between the Th/U ratio and the $^{207}Pb/^{206}Pb$ date of the individual zircon grains within sample 36DTB19, also suggests that the higher U grains, which likely experienced more radiation damage, were preferentially reset during these Pb-loss events (Fig. 2.4). This could indicate that the ca. 495 Ma discordia lower intercept (an age not commonly associated with metamorphism in this region) calculated by Doughty et al., (1998) for the Pend Oreille Gneiss is actually a mixing age between Paleoproterozoic and Cretaceous Pb-loss. However, given the complexity of the sampled gneiss outcrop (Fig. 2.2), it is also possible that our sample 36DTB19 represents a high-grade paragneiss phase containing ca. 2700 and 1800 Ma detrital zircon populations that experienced latest Jurassic to early Cretaceous Pb-loss. The lamellar twinned plagioclase feldspar, quartz, and biotite mineralogy observed within this sample is generally permissible with either a para- or orthogneiss interpretation (Fig. 2.5B).

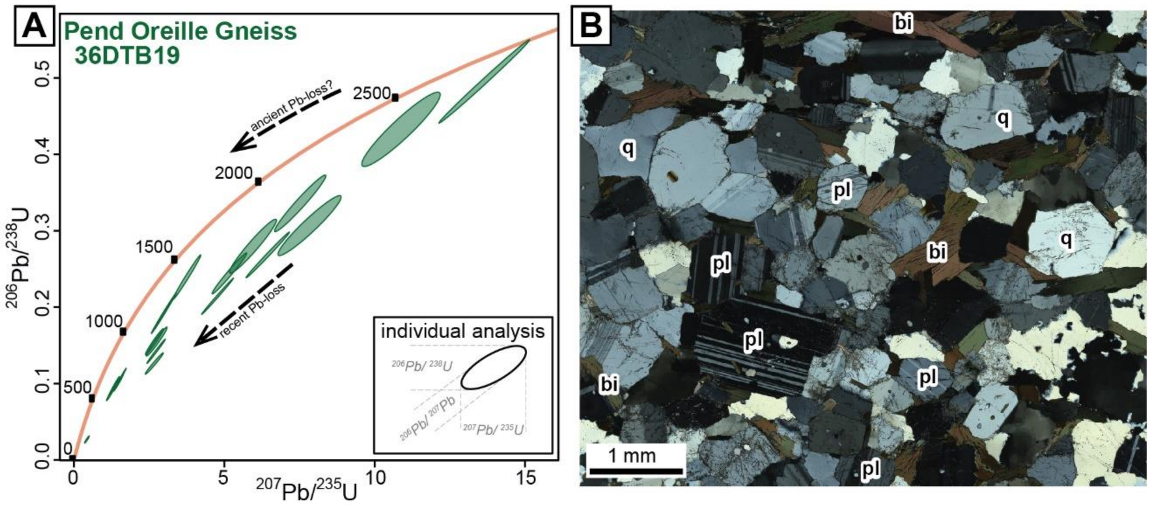

Fig. 2.5: A) Wetherill concordia diagram of SHRIMP U–Pb results for sample 36DTB19 indicating the complexity observed. B) A thin-section microphotograph of sample 36DTB19 in cross polarized light showing the main mineral modes of plagioclase (pl), quartz (q), and biotite (bi).

Within the ca. 2670 Ma Black Canyon Gneiss (sample 67DTB19), the augen texture (Fig. 2.2) and analytical results (Figs. 3, 4) are all consistent with a *meta*-igneous (orthogneiss) origin. The measured zircon δ18O value of 5.42 ± 0.08‰ from this sample indicates that the southwestern-most region of Archean crust within the

Clearwater Block did not undergo fractionation of O- isotopes since mantle extraction (Fig. 2.6). With some exceptions (e.g. Smithies et al., 2021), most Archean crust gives similar mantle-like δ18O values (Fig. 2.6; Spencer et al., 2014), indicating relatively limited intracrustal recycling of surface materials into magma by melting or contamination (Valley et al., 1998; 2003). The εHf$_t$ values of these same zircon grains range from +4.2 to +0.2, indicating an overall slightly supra-chondritic (above CHUR; Bouvier et al., 2008) Lu–Hf composition (Fig. 2.7). These εHf$_t$ values are approximately 3 εHf units below the value of the traditionally applied depleted mantle (DM) evolution line at ca. 2670 Ma. However, this traditional depleted mantle evolution line requires early (ca. 4560 Ma) widespread depletion of the mantle (e.g. Vervoort et al., 1996). If a later timing of widespread mantle depletion, such as widespread mantle extraction at ca. 3800 Ma (e.g. Vervoort and Kemp, 2016; Mole et al., 2021; Mulder et al., 2021) or the proposed new crust evolution curve (Dhuime et al., 2011) is accepted, then the εHf$_t$ values within the Black Canyon Gneiss are much closer (<2 εHf units) from overlapping the expected value of the mantle reservoir at ca. 2670 Ma (Fig. 2.7).

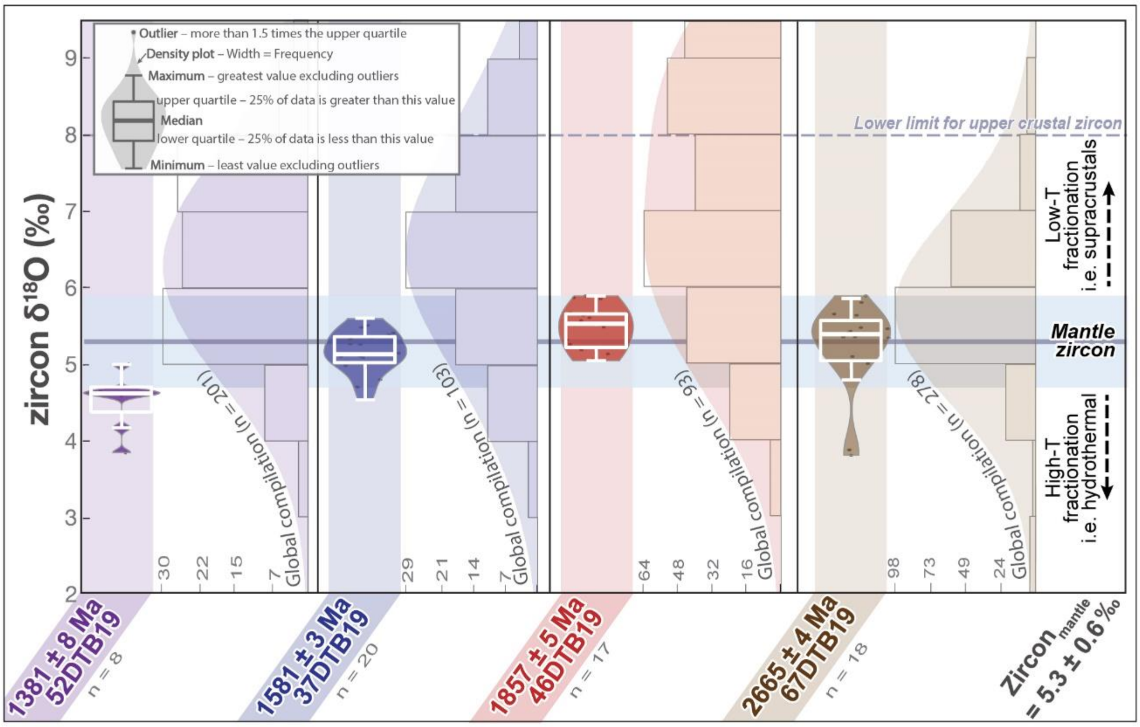

Fig. 2.6: SIMS δ18O results from the sampled units shown in violin plots. A violin plot includes both a box plot which indicates the min, max, median and quartiles of the dataset, and a mirrored density plot that shows the spread of the data. See explanation in the top left. On the vertical axis next to each sample's violin plot is a kernel density estimate plot of δ18O zircon values extracted from the global compilation of Spencer et al. (2014). The global compilation was filtered to include zircon with crystallization ages within 50 million years of each individual Clearwater Block sample, and is plotted with 1‰ bin and band widths. Range of mantle zircon δ18O values from Valley et al. (2008).

Consequently, our Lu–Hf data alone indicates that genesis of the Black Canyon Gneiss could have been derived directly from an only slightly depleted mantle reservoir at ca. 2670 Ma, or via reworking of older crust that was derived from a more depleted mantle reservoir during the Mesoarchean (ca. 3200–2800 Ma). The mantle-like δ18O values for the Black Canyon Gneiss (sample 67DTB19) indicate an absence of O- fractionation from mantle values by either tectonic or hydrothermal processes. The low (<0.3) Eu/Eu* [Chondrite normalized Eu/(Sm*Gd)^0.5] ratios from the Black Canyon Gneiss zircon grains (Fig. 2.8) also indicate considerable plagioclase fractionation, and minimal garnet fractionation within the melt during zircon crystallization. This is inconsistent with crystallization within thickened/hydrated continental crust, and suggests crystallization within shallower/drier crust (e.g. Lu et al., 2016; Tang et al., 2021). Based on these constraints alone, generation of the oldest crust within the Clearwater Block does not require crustal reworking of older Mesoarchean crust within a modern plate-tectonic style subduction setting. Consequently, we suggest that the Clearwater Block represents juvenile, mantle-derived, Neoarchean crustal growth.

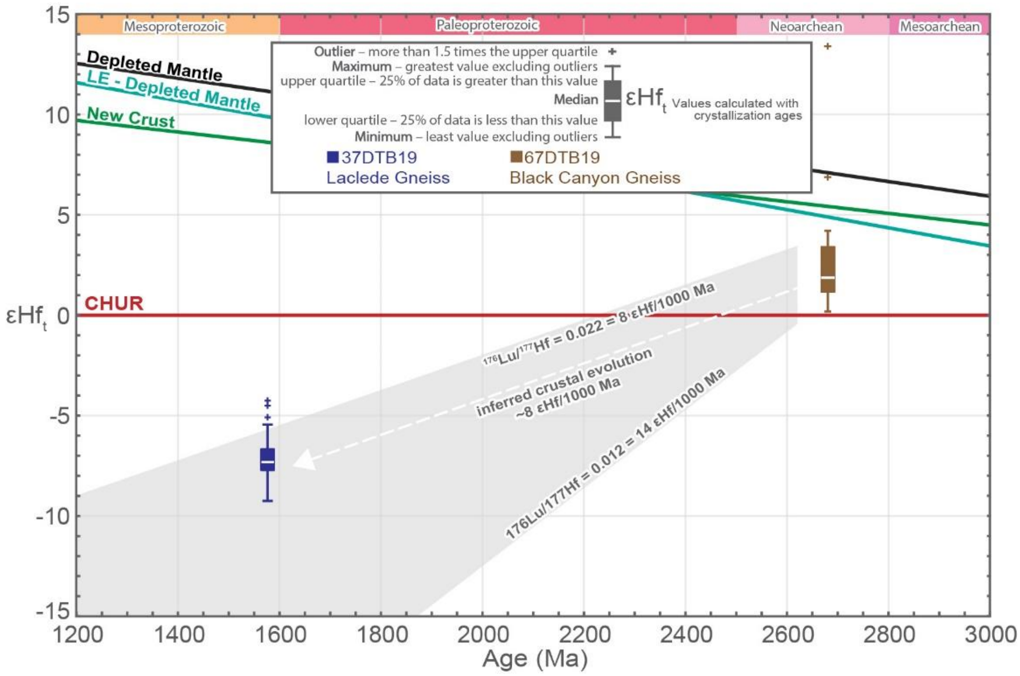

Fig. 2.7: εHf_t values vs. ($^{207}Pb/^{206}Pb$) Age plot for the Black Canyon Gneiss (67DTB19) and Laclede Gneiss (37DTB19). The colored box plots indicate the range of εHf_t values calculated for each gneiss based on the measured Lu/Hf, and the interpreted crystallization age of the sample. Here and in subsequent εHf_t vs. Age diagrams, we include three mantle evolution models including the classic Depleted Mantle (Bennett et al., 1993) assuming early mantle depletion at ca. 4560 Ma, the late extraction (LE) depleted mantle model (Vervoort et al., 2016; Fisher and Vervoort, 2018) assuming mantle depletion at ca. 3800 Ma, and the new crust model (Dhuime et al., 2011) which assumes Lu/Hf values of new juvenile crust is best represented by the average of oceanic arc values. CHUR–Chondritic Uniform Reservoir (Blichert-Toft et al., 1999; Bouvier et al., 2008).

However, the adjacent Medicine Hat Block contains both Mesoarchean rocks and locally preserves a sub-chondritic, Lu–Hf, and Sm–Nd, record of Neoarchean crustal growth reworking/recycling older Mesoarchean crust (Gifford et al., 2014; 2018; 2020). The thick deposits of Belt Supergroup strata between the Clearwater Block and the Medicine Hat Block prevent the detection of any clear geophysical or geological signature of either a suture/collisional zone or an Archean crustal continuity between the Clearwater and the Medicine Hat blocks (Bedrosian and Feucht, 2014; Gu et al., 2018). Consequently, it would be possible that the Clearwater Block was not associated with the Medicine Hat Block prior to the late Paleoproterozoic assembly of Laurentia via modern plate-tectonic subduction/collisional processes (Whitmeyer and Karlstrom, 2007; Weller and St-Onge, 2017; Wan et al., 2020). After ca. 1800 Ma, the continuity and similar provenance of strata across the Medicine Hat and Clearwater blocks indicate that they had achieved their near-current relative configuration (McMechan et al., 2021; Brennan et al., 2021). Consequently, we only advocate for the usage of a unified Medicine Hat-Clearwater Block (cf. Vervoort et al., 2016; Gifford et al., 2020) terminology for time after ca. 1800 Ma.

2.5.2. Paleoproterozoic Tectonism within the Priest River complex

As previously discussed, the Pend Oreille Gneiss (sample 36DTB19) within the Priest River complex records a composite ca. 2700, 1800, and 165 Ma tectonic history (Fig. 2.5). Within the nearby Coeur d'Alene Gneiss, zircons with low Th/U ratios (0.063 to 0.034), high U abundances (approximately 1800 to 4500 ppm) and rather heterogeneous mottled zircon textures (sample 46DTB19) yield a weighted mean age of 1857 ± 5 Ma and also record a similar timing of recent Pb-loss (ca. 155 Ma). Globally, high δ18O zircon values are common in ca. 1900–1800 Ma rocks (Fig. 2.6) due to widespread crustal reworking associated with Trans-Hudson age orogens (e.g. Spencer et al., 2014). However, the relatively robust δ18O isotopic results from the ca. 1860 Ma Coeur d'Alene Gneiss (sample 46DTB19) record similar mantle-like δ18O values to the ca. 2670 Ma Black Canyon Gneiss (sample 67DTB19). Consequently, we interpret the 1857 ± 5 Ma age for the Coeur d'Alene Gneiss (sample 46DTB19) to record the complete resetting of the U–Pb system of the existing ca. 2670 Ma crust within the Clearwater Block (Vervoort et al., 2016).

The proximity of the Priest River complex to the Vulcan structure suggests that the ca. 1860 Ma event recorded within the Coeur d'Alene Gneiss could be related to the collision of the Medicine Hat-Clearwater Block with the Lovera Block (the southwestern region of the Hearne Province) along the enigmatic Vulcan structure (Eaton et al., 1999; Nieuwenhuis et al., 2014). Tectonic models for the Vulcan structure include a Paleoproterozoic rift (Kanasewich et al., 1969), and a north- (Ross et al., 1991; Nieuwenhuis et al., 2014) or south-dipping (Eaton et al., 1999) subduction/collision zone. However, mantle-like δ18O isotopic values and the general absence of juvenile magmatism associated with this Paleoproterozoic tectonism within the Priest River complex or in the northern portion of the Medicine Hat Block (Gifford et al., 2020) are most consistent with the model of a north-dipping (away from the Medicine Hat-Clearwater Block) collisional zone within the Vulcan structure.

If our speculation that the ca. 1860 Ma tectonism within the Coeur d'Alene Gneiss reflects a collision (and perhaps collisions induced melting) along the Vulcan structure, it occurred coevally with magmatism within the ca. 1900–1700 Ma Great Falls Tectonic Zone (Mueller et al., 2002) but prior to the 1830–1800 Ma terminal phase of the Trans- Hudson orogeny (Corrigan et al., 2009). This is similar to the relative order of events indicated by geophysical cross cutting relationships (Nieuwenhuis et al., 2014). However, more extensive work is needed to evaluate the tectonic relationship of the ca. 1860–1830 Ma metamorphism and magmatism within the Priest River and Clearwater complexes (Buddington et al., 2016; Vervoort et al., 2016), with nearby similar late Paleoproterozoic events recorded in the Vulcan Structure, Great Falls Tectonic Zone, and Monashee Complex (e.g. Ross et al., 1991; Crowley, 1999; Mueller et al., 2002).

2.5.3. NAMG-age magmatism within the Clearwater Block

The results from sample 37DTB19 refine the crystallization age for the Laclede Gneiss from 1576 ± 13 Ma (Evans and Fischer, 1986) to 1581 ± 3 Ma. The Laclede Gneiss clearly falls within the ca. 1610 to 1490 Ma North American Magmatic Gap (Fig. 2.2; NAMG; Ross and Villeneuve, 2003). However, it does not overlap in age with the 1590 ± 5 and 1551 ± 5 Ma mafic dykes in southern Montana (Rogers et al., 2018). Of regional interest, it also confirms that the larger, augen gneiss outcrop south of the Pend Oreille River is correlative to the smaller dated bodies (Fig. 2.1B; Evans and Fischer, 1986; Doughty et al., 1998) on the northern side of the river as mapped (Lewis et al., 2020). The well-preserved oscillatory zoning, Th/U ratios above 0.2, absence of a U (ppm) vs. age trend (Fig. 2.4), and overall mineralogy including large K-spar augen (Fig. 2.2) indicates an igneous/magmatic origin for sample 37DTB19.

The new Lu–Hf and δ18O results also yield additional insights into the origin of this unique Laurentian magmatic event.

The εHf_t values of the Laclede Gneiss range from -5.1 to -9.3, which indicates an isotopically evolved signature consistent with recycling of Neoarchean or Paleoproterozoic crust. Although this sample records evolved Lu–Hf values, the δ18O results are consistent with mantle-like values signifying limited intracrustal recycling of surface materials into the magma by melting or contamination. These Lu–Hf and δ18O results indicate that ca. 1580 Ma magmatism within the Clearwater Block was unlikely subduction or arc-related as previously speculated (e.g. Furlanetto et al. 2013). The zircon trace element results from the Laclede Gneiss also show higher (>0.3) Eu/Eu* ratios than the nearby Neoarchean basement (Fig. 2.8). This higher Eu/Eu* ratio suggests limited plagioclase and signification garnet fractionation within the melt during zircon crystallization, and thus is consistent with derivation from thickened continental crust (e.g. Lu et al., 2016; Tang et al., 2021).

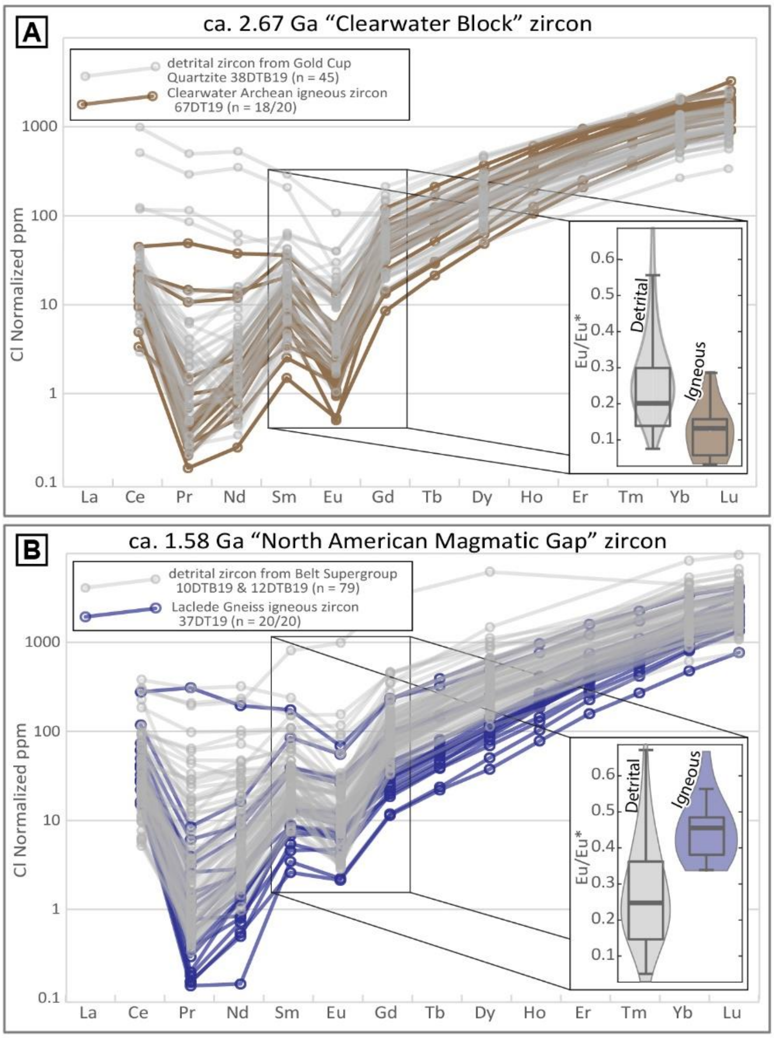

Fig. 2.8: A) Chondritic normalized trace element results for the ca. 2670 Ma (sample 67DTB19; shown in brown) igneous rocks of the Clearwater Block, and the same age (overlapping within 2σ error) detrital zircon grains from the overlying Gold Cup Quartzite (grey). B) Chondritic normalized trace element results for the ca. 1580 Ma (sample 37DTB19, shown in blue) igneous rocks of the Clearwater Block, and the same age (overlapping within 2σ error) detrital zircon grains from the overlying lower Belt Supergroup strata (grey). Inset charts highlight the Eu anomaly calculated as [Chondrite normalized Eu/(Sm*Gd)^0.5].

2.5.4. Crustal Evolution of the Clearwater Block

A Lu–Hf 'rewoking array' (e.g., Payne et al., 2016) fit through the 2670 and 1580 Ma Clearwater complex samples intersects with the main ca. 1860–1800 Ma detrital zircon population within the overlying Gold Cup Quartzite (Brennan et al., 2021; Figs. 2.7, 2.9). We interpret these Lu/Hf results to be consistent with a continuous crustal evolution trend recording limited input from a depleted mantle source, at least in the Priest River region, during the ca. 1860 and 1580 Ma events. The slope of this line yields an approximate 176Lu/177Hf = 0.022 evolution ratio that is higher than the generally suggested value for bulk felsic continental crust (176Lu/177Hf = 0.018 to 0.012) and results in a shallower εHf vs. time evolution. As mentioned, the available δ18O results from the igneous samples used to define this array are consistent with limited fractionation of O- isotopes from expected mantle values, indicating limited magmatic interaction with low temperature meteoric or high temperature hydrothermal water (Valley et al., 1998), suggesting that a subduction origin for these rocks is not required.

Consequently, the 176Lu/177Hf = 0.022 ratio suggested by the fit of a reworking array of both the igneous basement and proximally derived overlying detrital zircon samples is plausible given that lower continental (more mafic) crust generally yields higher 176Lu/177Hf values (0.025 to 0.017) than the often assumed values for the bulk or more-felsic upper continental crust (Payne et al., 2016; Spencer et al., 2020). Comparable 176Lu/177Hf ratios (e.g. 176Lu/177Hf = 0.022, Amelin et al., 1999; 176Lu/177Hf = 0.024, Næraa et al., 2012; 176Lu/177Hf = 0.022–0.020, Mole et al., 2019) have previously been calculated based on reworking arrays of other Archean provinces. This crustal evolution array suggests that the oldest, ca. 2670 Ma magmatism in the Clearwater Block represents the main crustal growth event within the block, and the subsequent events at ca. 1860 Ma and 1580 Ma likely reworked this Archean lower crustal reservoir, perhaps without the involvement of arc-magmatism. Given the plausibility of this crustal evolution model, the isotopic evidence does not require an Australian origin for the ca. 1580 Ma Laclede Gneiss as speculated by previous studies (e.g. Ross et al., 1992; Doughty et al., 1998).

2.5.5. Ca. 1.4 Ga metamorphism within the Clearwater complex

The results from the Moses Butte Amphibolite (sample 37DTB19) show no clear evidence for NAMG-age magmatism as most grains yielded textures, Th/U, and δ18O results consistent with metamorphic zircon growth in a hydrothermally affected environment (Figs. 2.3, 2.4, 2.6). A single grain showed an oscillatory zoned core (Fig. 2.2), which had the highest Th/U value of 0.22 and yielded a concordant ($^{207}Pb/^{206}Pb$) date of 1546 ± 17 Ma. This single grains supports speculations (Doughty and Chamberlain 2007), that the amphibolite's protolith may fall within the NAMG age interval and could be related to the nearby 1551 ± 5 Ma mafic dykes (Rogers et al., 2018). However, the remainder of the dates are interpreted to record metamorphic/hydrothermal zircon growth. The metamorphic event(s) recorded by these grains occurred between ca. 1416 and 1350 Ma, as determined by the oldest discordia upper-intercept age, and the youngest ($^{206}Pb/^{238}U$) weighted mean age. Magmatism (and associated metamorphism) of this age is well documented within the Belt Basin (Evans et al., 2001; Doughty and Chamberlain, 2008; Zirakparvar et al., 2010; Nesheim et al., 2012; McFarlane, 2015), which likely provided heat for the hydrothermal zircon growth documented here. This period of magmatism is correlated with rifting near the end of Belt Basin subsidence and is suggested to correspond to global events linked to the initial breakup of supercontinent Nuna/ Columbia (Ross and Villeneuve, 2003; Box et al., 2020; Brennan et al., 2021).

2.5.6. Constraints on detrital zircon provenance

In addition to providing insights into the genesis of Clearwater Block basement, our results allow evaluation of proposed detrital zircon provenance patterns for the overlying Paleo–Mesoproterozoic strata. In particular, within the Priest River complex, younger than ca. 1800 Ma coarse strata of the Gold Cup Quartzite overlie Clearwater Block Basement (Lewis et al., 2020). Detrital zircon U–Pb and Lu–Hf components from the Gold Cup Quartzite consist of two main age components. An older ca. 2670 Ma population with CHUR-like εHf_t values concentrated around +1, and younger ca. 1900–1750 Ma grains, with main age-peaks at ca. 1860 and 1800 Ma. These Paleoproterozoic zircon grains have a wide range of εHf_t values with the greatest density showing evolved εHf_t values between -4 and -8 (Fig. 2.9; Brennan et al., 2021). These isotopic results from the detrital zircon grains, including the trace element constraints for sample 67DTB19, are a good match for the basement rocks within the Clearwater Block and are consistent with our suggested crustal evolution trend. These similarities support prior interpretations that the Gold Cup Quartzite was sourced from proximal Laurentian basement sources primarily within the Clearwater and Medicine Hat Blocks (Doughty and Chamberlain, 2008; Buddington et al., 2016; Brennan et al., 2021).

In the Priest River region, finer-grained strata of the ca. 1480–1380 Ma Belt Supergroup overlie strata of the Gold Cup Quartzite. Brennan et al. (2021) sampled Prichard and Ravalli Group strata from the stratigraphically lower portion of the Belt Supergroup approximately 50 km to the west of the Priest River complex basement exposures. These samples contained a spread of ca. 1750–1470 Ma detrital zircon grains, including a significant portion of grains with ages within the ca. 1610–1490 Ma NAMG. These NAMG-age grains have predominately juvenile (+εHf_t) values. Consequently, the evolved εHf_t = -5.1 to -9.3 values within the ca. 1580 Ma Laclede Gneiss, make it a poor Lu–Hf match for the NAMG-age detrital grains within nearby Belt Supergroup strata (Fig. 2.9). In addition to the Lu–Hf mismatch, the trace element data from the Laclede Gneiss (sample 37DTB19) also match poorly with that of the detrital grains (Figs. 2.8, 2.9). Consequently, interpretations of an exotic source for these detrital grains (Ross and Villeneuve, 2003; Fanning et al., 2009; Box et al., 2020; Brennan et al., 2021) remains a valid hypothesis. Additionally, the non-Laurentian source for the similar, juvenile (+εHf_t) NAMG-age detrital zircon populations found in coeval ca. 1450 Ma Hess Canyon, Trampas basins in southwestern Laurentia also remains valid (Doe et al., 2012, 2013; Jones et al., 2015).

Southeastern Australia, notably the Gawler Craton, records widespread magmatism in pulses from ca. 1900 to 1500 Ma, which include: 1) the ca. 1850–1790 Ma Donington–Myola Suite (Fanning et al., 1988; Reid et al., 2008), 2) the ca. 1770–1740 Ma McGregor Volcanics and associated suites (Fanning et al., 1988), 3) the 1620–1605 Ma St Peter Suite (Swain et al., 2008), 4) the 1600–1575 Ma Gawler Range Volcanics–Hiltaba suite (Fanning et al., 2009), and 5) granites as young as ca. 1500 Ma in the Spilsby Suite (Fanning et al., 2009). The ca. 1620–1605 Ma St Peter Suite and ca. 1600–1575 Ma Hiltaba Suite and Gawler Range Volcanics show juvenile (+εHf_t) compositions (Swain et al., 2008; Reid and Payne, 2017) and are consequently a much better source match for the detrital zircon grains within Belt Supergroup strata than the Laclede Gneiss. Thermochronology (40Ar/39Ar) studies also indicate that the northern Gawler Craton was actively exhumed at ca. 1480–1440 Ma, the same time as the deposition of the lower Belt Supergroup strata in Laurentia (Reid and Forster, 2021).

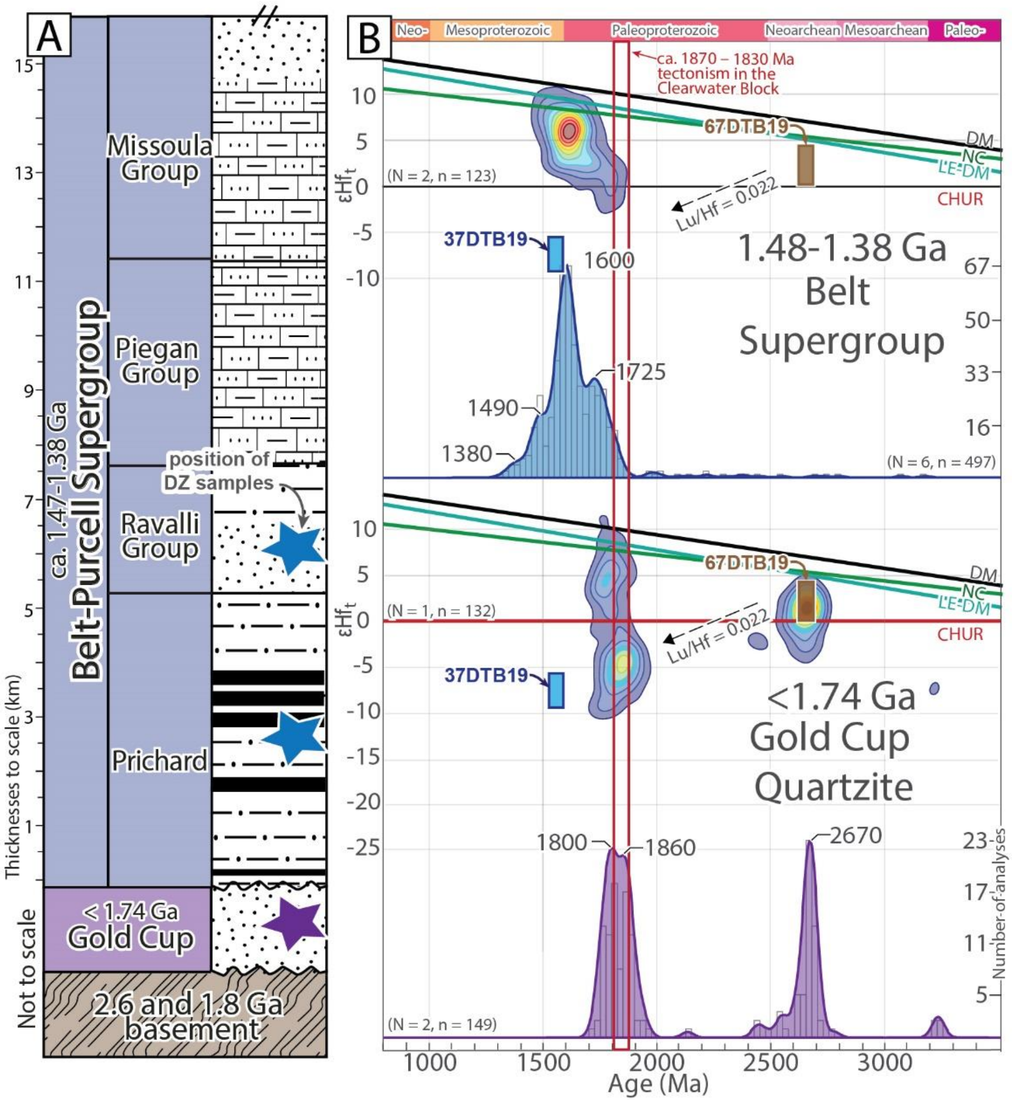

Fig. 2.9: Paleo–Mesoproterozoic stratigraphy and U–Pb/Lu–Hf detrital zircon results from the Priest River Region (Doughty and Chamberlain, 2008; Box et al., 2020; Lewis et al., 2020; Brennan et al., 2021) and the range of robust εHf_t values (samples 67DTB19 and 37DTB19) from the underlying ca. 2670 and 1580 Ma igneous basement. The red box indicates the age range (ca. 1.88–1.83 Ga) of Paleoproterozoic tectonism/magmatism within the Clearwater Block (Vervoort et al., 2016). Inferred crustal evolution line (Lu/Hf = 0.022) for the Clearwater Block indicated. We note that the main ca. 1860 Ma detrital zircon population within the Gold Cup Quartzite contains εHf_t values of -3 to -8, which are consistent with our suggested crustal evolution trend of the Clearwater Block. DM–Depleted Mantle, LE–Late Extraction, NC–New Crust, CHUR–Chondritic Uniform Reservoir. See Fig. 7 for explanation of mantle evolution lines.

2.5.7. Insights into the evolution and configuration of supercontinent Nuna

As previously discussed, with the exception of eastern Australia, notably the Gawler Craton, NAMG magmatism is relatively limited in the global geologic record (Figs. 2.10, 2.11). Thus, the Australian ca. 1600–1500 Ma magmatism is often considered a significant tie-point for locating eastern Australia-East Antarctica against western Laurentia during the early Mesoproterozoic (e.g. Goodge et al., 2017; Kirscher et al., 2019, 2021). In some reconstructions Hainan Island, including all or some of the Cathaysia Block of South China (cf. Yao et al., 2017; Xu et al., 2019; Cawood et al., 2020), is also placed in close proximity to western Laurentia in Nuna. Within southeastern Australia, NAMG-age magmatism is predominately juvenile (+εHf_t) and is episodic with two main pulses at ca. 1620–1575 Ma and ca. 1525 Ma, respectively (Fig. 2.10; Reid and Payne, 2017; Chapman et al., 2019; Hartnady et al., 2020). Granitic glacial clasts sampled from East Antarctica also contain a similar, two-pulsed magmatic record of NAMG-age magmatism (Goodge et al., 2017), consistent with East Antarctica being part of the Mawson continent together with the Gawler Craton for most of the Proterozoic (e.g., Payne et al., 2009). However, the ca. 1570 Ma magmatism in East Antarctica is more evolved than the mostly juvenile similar-age magmatism within the Gawler craton (Fig. 2.10). Compared to the East Antarctica constraints, the Laclede Gneiss (sample 37DTB19) is a slightly better age-match for Gawler craton NAMG magmatism but is not an ideal Lu–Hf match due to its more evolved composition.

The ca. 1551 ± 12 Ma felsic magmatism recently recognized within Hainan Island of south China (Xu et al., 2019) is perhaps the worst age-match for magmatism within the Gawler Craton and East Antarctica, as it falls between the two main pulses of magmatism. It is also ~ 30 Myr younger than the Laclede Gneiss but is similar to nearby 1551 ± 5 Ma mafic dykes in Laurentia (Rogers et al., 2018). Admittedly, the ca. 1550 Ma magmatism in Hainan Island does have the least evolved (most juvenile) Lu–Hf values, making it a slightly better Lu–Hf match for the Gawler Craton than other discussed ca. 1580–1550 Ma rocks (the Laclede Gneiss and East Antarctica glacial clasts). Interestingly, northeastern Australia (Mount Isa Inlier; Fig. 2.11B) also contains poorly studied ca. 1550–1500 Ma felsic magmatism (Page and Sun, 1998; Li et al., 2020) that appear to be a better age match with Hainan Island than the Gawler Craton. These ca. 1500 Ma granitoids in northern Australia likely provided the detrital zircon grains found within the ca. 1460–1400 Ma PR1 basin in northwestern Laurentia (Medig et al., 2014).

Genesis models for the prevalent NAMG-age magmatism in southeastern Australia are complex. However, the ca. 1600–1500 Ma magmatism has generally been associated with the final assembly of Australia and East Antarctica with western Laurentia to form Nuna (Betts et al., 2008; Payne et al., 2009; Kirscher et al., 2019). Most models emphasize mantle plume activity that may have modified subduction-related arc-magmatism, localized back-arc extension and/or continental collision orogenic processes (Betts et al., 2009; Payne et al., 2009; Forbes et al., 2011; Tiddy et al., 2020). Given the absence of a clear subduction-related isotopic signature in the Clearwater Block at this time, we suggest that a mantle plume, perhaps centered beneath southeastern Australia, supplied the heat to melt the (likely) adjacent Archean lower continental crust within the Clearwater Block (Fig. 2.11B), resulting in the generation of the evolved ca. 1580 Ma Laclede Gneiss. This proposed petrogenesis explains the predominantly juvenile NAMG magmatism in southeastern Australia, indicative of a location above the plume head, as well as the plume related geochemistry for the ca. 1590 Ma dykes in western Laurentia (Rogers et al., 2018) and our results for the Laclede Gneiss. This model is also consistent with paleomagnetic reconstructions of Nuna (Fig. 2.11B) which place the Gawler Craton adjacent to the Clearwater Block at ca. 1580 Ma (e.g. Kirscher et al., 2019, 2021; Pisarevsky et al., 2014).

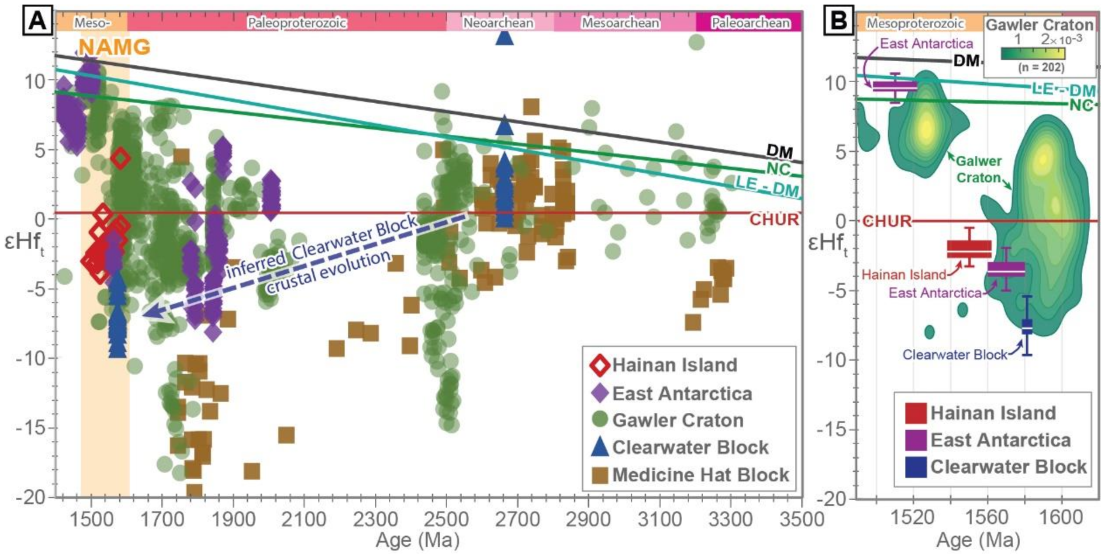

Fig. 2.10: A) Individual εHf$_t$ vs. $^{207}Pb/^{206}Pb$ ages for the Clearwater Block (including the inferred crustal evolution trend), Medicine Hat Block (Gifford et al., 2020) and the suggested Non-Laurentian conjugate blocks of Hainan Island (South China; Xu et al., 2019), East Antarctica (Goodge et al., 2017), and the Gawler Craton of southeastern Australia (Reid and Payne, 2017 and references therein; Hartnady et al., 2020). Inferred crustal evolution line (Lu/Hf = 0.022) for the Clearwater Block indicated. B) εHf$_t$ vs. $^{207}Pb/^{206}Pb$ values for ca. 1610–1490 Ma, North American Magmatic Gap magmatism. For comparison, the abundant magmatism of the Gawler Craton is plotted in a two-dimensional kernel density estimate plot with 1 εHf and 5 Ma bandwidths (Spencer et al., 2020) and individual NAMG-age granites sampled in Hainan Island (Xu et al., 2019), East Antarctica (Goodge et al., 2017) and the Clearwater Block (this work) shown in box and whisker plots, where the width of the box corresponds to the $^{207}Pb/^{206}Pb$ age uncertainty. Note that the evolved ca. 1580–1550 Ma magmatism in the Clearwater Block, East Antarctica, and Hainan Island are not a particularly good match for similar-age, juvenile magmatism within the Galwer Craton. DM–Depleted Mantle, LE–Late Extraction, NC–New Crust, CHUR–Chondritic Uniform Reservoir. See Fig. 2.7 for explanation of mantle evolution lines.

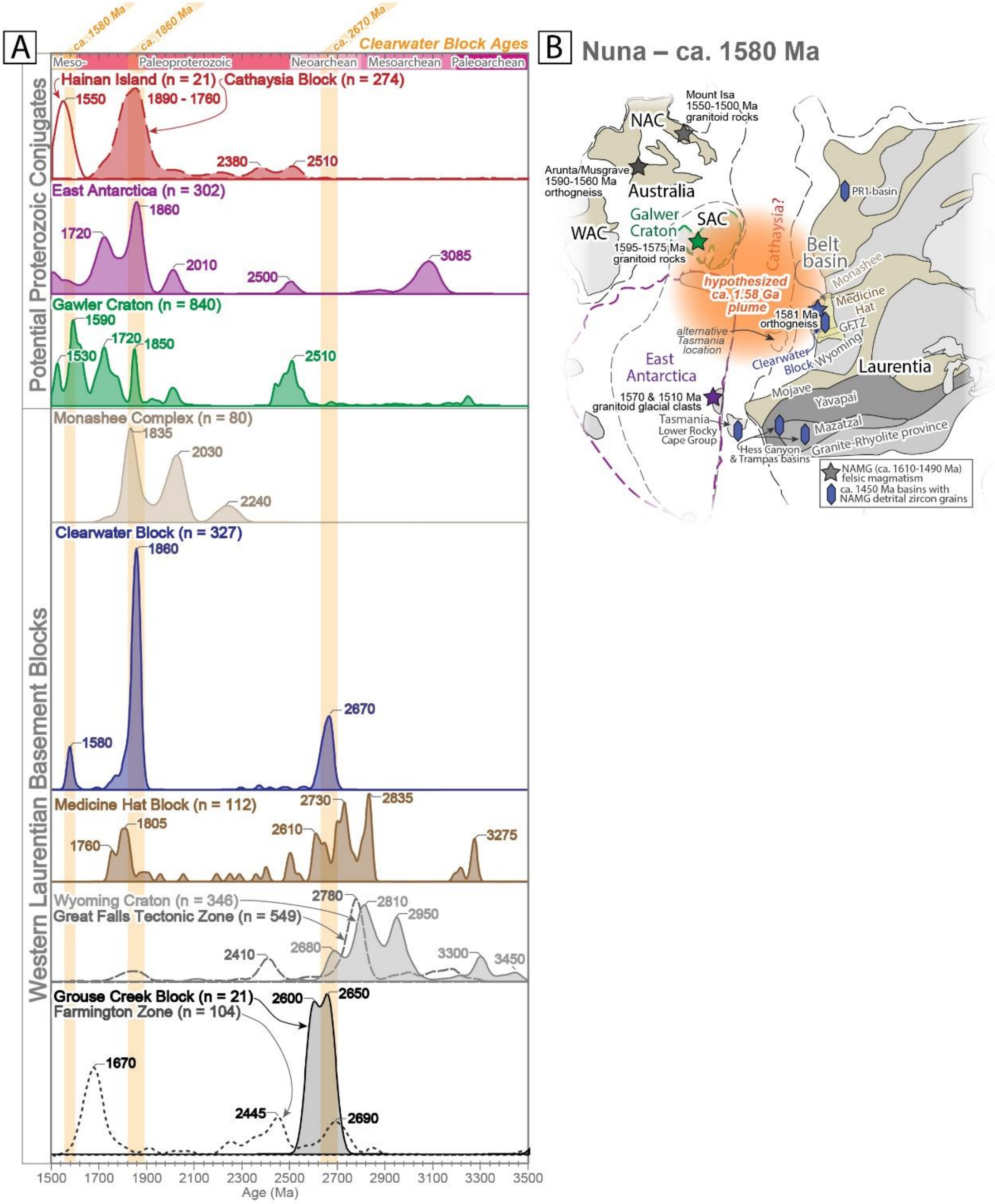

Fig. 2.11: A) Timing of Paleoarchean to early Mesoproterozoic magmatism for the main Archean blocks of western Laurentia and proposed conjugate blocks within Nuna shown in kernel density estimate plots with 25 Ma bandwidths. The main ca. 2670, 1860 and 1580 Ma ages of Clearwater Block magmatism are indicated in orange. Age peak labels are rounded to the nearest 5 Ma. Sources are compiled in the supplementary but include: Grouse Creek (Link et al., 2017); Farmington Zone (Mueller et al., 2011); Great Falls Tectonic Zone (Mueller et al., 2002; Foster et al., 2006; Gifford et al., 2018); Wyoming Craton (Frost and Fanning, 2006; Frost et al., 2006; 2017; Mueller et al., 2010); Medicine Hat Block (Gifford et al., 2020); Clearwater Block (Vervoort et al., 2016; this work); Monashee complex (Crowley et al., 1999); Gawler Craton (Reid and Payne, 2017 and references within; Hartnady et al., 2020); East Antarctica (Goodge and Fanning, 2016; Goodge et al., 2017); the Cathaysia Block of South China (Zhang et al., 2021 and references within); and Hainan Island of South China (Xu et al., 2019). B) Paleogeographic reconstruction of Nuna (after Goodge et al., 2017; Kirscher et al., 2019, 2021; Pisarevsky et al., 2014) with the extent of our proposed ca. 1580 Ma plume, NAMG-age (North American Magmatic Gap) felsic magmatism (indicated by star symbols), and Laurentian basins containing NAMG-age detrital zircon (indicated by tetragonal crystal symbol; for Hess Canyon and Trampas basins, see Doe et al., 2012; 2013; Jones et al., 2015, for PR1 basin see Medig et al., 2014) shown. A more detailed map of western Laurentia's basement framework is shown in Fig. 2.1A.

2.6. Conclusions

This work presents zircon U–Pb geochronological and comprehensive isotopic (Lu–Hf, δ18O, and trace element) study of Mesoproterozoic and older crystalline basement rocks within the Clearwater Block of western Laurentia, a key Proterozoic supercontinent tie-point that contains a unique record of NAMG-age magmatism. In addition to providing robust source terrane characterization for utilization by future provenance studies, the main findings from our study of the Clearwater Block crystalline basement are the following:

1) The juvenile Lu–Hf, mantle-like δ18O, and trace element results from the oldest, ca. 2670 Ma, granitic basement rocks indicate that Neoarchean crustal growth within the Clearwater Block did not involve significant reworking or assimilation of older crust, nor that it requires modern-style subduction processes. The isotopic record therefore does not necessitate that of the Clearwater Block was built onto the edge of the Mesoarchean Medicine Hat Block (or the Wyoming Craton either) in a modern plate-tectonic arc setting. Rather, we suggest that ca. 2670 Ma rocks within the Clearwater Block represent either juvenile crustal growth through direct mantle extraction without subduction-related processes, or remelting of an older Mesoarchean mafic lower crust.

2) The Neoarchean crust in the Priest River complex (northern Clearwater Block) was metamorphosed and melted (see Vervoort et al., 2016) during a ca. 1860 Ma event. We suggest this event likely records collision related to the assembly of Laurentia. Results from the Priest River complex are consistent with models involving north-dipping subduction within the Vulcan Structure.

3) The new 1581 ± 3 Ma crystallization age for the Laclede Gneiss supports prior assertions of NAMG-age magmatism within the Priest River complex based on discordia regression-age calculations (e.g. Evans and Fischer, 1986; Doughty et al., 1998). The evolved Lu–Hf, mantle-like δ18O, and trace element zircon values from the Laclede Gneiss are difficult to reconcile with a subduction or rift origin. Consequently, we favour a plume genesis, as is suggested for the nearby Laurentian 1590 ± 5 Mammoth dykes (Rogers et al., 2018). Similar-age magmatism in southeastern Australia also has plume-related genesis models (e.g. Reid and Payne 2017; Chapman et al., 2019). The proposed Lu–Hf 'reworking array' and O- isotope values from the Clearwater Block indicate that reworking of a nearby Neoarchean

lower continental crustal reservoir is the likely origin for the Laclede Gneiss. Consequently, we propose that the Laclede Gneiss is a crustal-derived, distal manifestation of a ca. 1580 Ma plume event beneath southeastern Australia.

4) The new geochronology and isotopic constraints from the Clearwater Block lend further support to interpretations (e.g. Brennan et al., 2021) that the overlying Gold Cup Quartzite and lower Belt Supergroup strata record a provenance shift from proximal Laurentian, to non-Laurentian sources sometime between ca. 1800 and 1480 Ma. This provenance shift likely corresponds to the final assembly of supercontinent Nuna/Columbia during this interval.

5) The Clearwater complex may contain NAMG-mafic magmatism. However, if present, the record of this event was overprinted by ca. 1410–1350 Ma hydrothermal metamorphism, likely associated with magmatism and rifting within the Mesoproterozoic Belt Basin.

2.7. References

Precambrian Research reference style

Amelin, Y., Lee, D.-C., Halliday, A.N., Pidgeon, R.T., 1999. Nature of the Earth's earliest crust from hafnium isotopes in single detrital zircons. Nature 399 (6733), 252–255. https://doi.org/10.1038/20426.

Baertschi, P., 1976. Absolute 18O content of standard mean ocean water. Earth Planet. Sci. Lett. 31 (3), 341–344. https://doi.org/10.1016/0012-821X(76)90115-1.

B´edard, J.H., 2018. Stagnant lids and mantle overturns: Implications for Archaean tectonics, magmagenesis, crustal growth, mantle evolution, and the start of plate tectonics. Geosci. Front. 9 (1), 19–49. https://doi.org/10.1016/j.gsf.2017.01.005.

Bedrosian, P.A., Feucht, D.W., 2014. Structure and tectonics of the northwestern United States from EarthScope USArray magnetotelluric data. Earth Planet. Sci. Lett. 402, 275–289. https://doi.org/10.1016/j.epsl.2013.07.035.

Bennett, V.C., Nutman, A.P., McCulloch, M.T., 1993. Nd isotopic evidence for transient, highly depleted mantle reservoirs in the early history of the Earth. Earth Planet. Sci. Lett. 119 (3), 299–317. https://doi.org/10.1016/0012-821X(93)90140-5.

Betts, P.G., Giles, D., Schaefer, B.F., 2008. Comparing 1800–1600 Ma accretionary and basin processes in Australia and Laurentia: Possible geographic connections in Columbia. Precambr. Res. 166 (1-4), 81–92. https://doi.org/10.1016/j.precamres.2007.03.007.

Betts, P.G., Giles, D., Foden, J., Schaefer, B.F., Mark, G., Pankhurst, M.J., Forbes, C.J., Williams, H.A., Chalmers, N.C., Hills, Q., 2009. Mesoproterozoic plume-modified orogenesis in eastern Precambrian Australia. Tectonics 28 (3), n/a–n/a. https://doi. org/10.1029/2008TC002325.

Blichert-Toft, J., Albar`ede, F., Rosing, M., Frei, R., Bridgwater, D., 1999. The Nd and Hf isotopic evolution of the mantle through the Archean Results from the Isua supracrustals, West Greenland, and from the Birimian terranes of West Africa. Geochim. et Cosmochim. Acta 63 (22), 3901–3914. https://doi.org/10.1016/S0016-7037(99)00183-0.

Brennan, D.T., Brian Mahoney, J., Li, Z.-X., Link, P.K., Evans, N.J., Johnson, T.E., 2021. Detrital zircon U-Pb and Hf signatures of Paleo-Mesoproterozoic strata in the Priest River region, northwestern USA: A record of Laurentia assembly and Nuna tenure. Precambr. Res. 367, 106445. https://doi.org/10.1016/j.precamres.2021.106445.

Bodorkos, S., Bowring, J.F., and Rayner, N.M., 2020, Squid3: Next-generation data processing software for Sensitive High Resolution Ion Micro Probe (SHRIMP). Geoscience Australia, Canberra. http://dx.doi.org/10.11636/133870.

Bouvier, A., Vervoort, J.D., Patchett, P.J., 2008. The Lu-Hf and Sm-Nd isotopic composition of CJUR: Constraints from unequilibrated chondrites and implications for the bulk composition of terrestrial planets. Earth Planetary Sci. 273, 48–57.

Bowring, S.A., Karlstrom, K.E., 1990. Growth, stabilization, and reactivation of Proterozoic lithosphere in the southwestern United States. Geology 18, 1203–1206. https://doi.org/10.1130/0091-7613(1990)018<1203:GSAROP>2.3.CO;2.

Box, S.E., Pritchard, C.J., Stephens, T.S., O'Sullivan, P.B., 2020. Between the supercontinents – Mesoproterozoic Deer Trail Group, an intermediate age unit between the Mesoproterozoic Belt-Purcell Supergroup and the Neoproterozoic Windermere Supergroup in northeastern Washington, U.S.A. Can. J. Earth Sci. 57 (12), 1411–1427. https://doi.org/10.1139/cjes-2019-0188.

Buddington, A.M., Wang, D., Doughty, P.T., 2016. Pre-Belt basement tour: Late Archean- Early Proterozoic rocks of the Cougar Gulch area, southern Priest River complex Idaho. GSA Field Guides 41, 265–284. https://doi.org/10.1130/2016.0041(09). Cavosie, A.J., Valley, J.W., Kita, N.T., Spicuzza, M.J., Ushikubo, T., Wilde, S.A., 2011. The origin of high δ18O zircons: marbles, megacrysts, and metamorphism. Contrib Mineral Petrol 162 (5), 961–974.

Cawood, P.A., Wang, W., Zhao, T., Xu, Y., Mulder, J.A., Pisarevsky, S.A., Zhang, L., Gan, C., He, H., Liu, H., Qi, L., Wang, Y., Yao, J., Zhao, G., Zhou, M.-F., Zi, J.-W., 2020. Deconstructing South China and consequences for reconstructing Nuna and Rodinia. Earth Sci. Rev. 204, 103169. https://doi.org/10.1016/j. earscirev.2020.103169.

Chamberlain, K.R., Frost, C.D., Frost, B.R., 2003. Early Archean to Mesoproterozoic evolution of the Wyoming Province: Archean origins to modern lithospheric architecture. Can. J. Earth Sci. 40 (10), 1357–1374. https://doi.org/10.1139/e03- 054.

Chapman, N.D., Ferguson, M., Meffre, S.J., Stepanov, A., Maas, R., Ehrig, K.J., 2019. Pb-isotopic constraints on the source of A-type Suites: Insights from the Hiltaba Suite - Gawler Range Volcanics Magmatic Event Gawler Craton, South Australia. Lithos 346-347, 105156. https://doi.org/10.1016/j.lithos.2019.105156.

Clark, S.H.B., 1973. Interpretation of a high-grade Precambrian terrane in Northern Idaho. Geol. Soc. Am. Bull. 84, 1999–2004. https://doi.org/10.1130/0016-7606 (1973)84<1999:IOAHPT>2.0.CO;2.

Condit, C.B., Mahan, K.H., Ault, A.K., Flowers, R.M., 2015. Foreland-directed propagation of high-grade tectonism in the deep roots of a paleoproterozoic collisional orogen SW montana, USA. Lithosphere 7, 625–645. https://doi.org/ 10.1130/L460.1.

Corrigan, D., Pehrsson, S., Wodicka, N., de Kemp, E., 2009. The Palaeoproterozoic Trans- Hudson Orogen: A prototype of modern accretionary processes. Geol. Soc. Spec. Pub. 327 (1), 457–479. https://doi.org/10.1144/SP327.19.

Crowley, J.L., 1999. U-Pb geochronologic constraints on paleoproterozoic tectonism in the Monashee complex, Canadian Cordillera: Elucidating an overprinted geologic history. Geol. Soc. Am. Bull. 111, 560–577. https://doi.org/10.1130/0016-7606 (1999)111<0560:UPGCOP>2.3.CO;2.

Dhuime, B., Hawkesworth, C., Cawood, P., 2011. When Continents Formed. Science v. 331, 155–156. https://doi.org/10.1126/science.1200643. Dickinson, W.R., 2004. Evolution of the North American Cordillera. Annu. Rev. Earth Planet. Sci. 32 (1), 13–45. https://doi.org/10.1146/annurev. earth.32.101802.120257.

Doe, M.F., Jones, J.V., Karlstrom, K.E., Thrane, K., Frei, D., Gehrels, G., Pecha, M., 2012. Basin formation near the end of the 1.60-1.45 Ga tectonic gap in southern Laurentia: Mesoproterozoic Hess Canyon Group of Arizona and implications for ca. 1.5 Ga supercontinent configurations. Lithosphere 4 (1), 77–88. https://doi.org/10.1130/ L160.110.1130/2012050.

Doe, M.F., Jones, J.V., Karlstrom, K.E., Dixon, B., Gehrels, G., Pecha, M., 2013. Using detrital zircon ages and Hf isotopes to identify 1.48-1.45Ga sedimentary basins and fingerprint sources of exotic 1.6-1.5Ga grains in southwestern Laurentia. Precambr. Res. 231, 409–421. https://doi.org/10.1016/j.precamres.2013.03.002.

Doughty, P.T., Chamberlain, K.R., 2007. Age of Paleoproterozoic Basement and Related Rocks in the Clearwater Complex, Northern Idaho, U.S.A.: Proterozoic Geology of Western North America and Siberia. In: Link, P.K., Lewis, R.S. (Eds.), Proterozoic Geology of Western North America and Siberia. SEPM (Society for Sedimentary Geology), pp. 9–35. https://doi.org/10.2110/pec.07.86.0009.

Doughty, P.T., Chamberlain, K.R., 2008. Protolith age and timing of Precambrian magmatic and metamorphic events in the Priest River complex, northern Rockies. Can. J. Earth Sci. 45 (1), 99–116. https://doi.org/10.1139/e07-067.

Doughty, P.T., Price, R.A., Parrish, R.R., 1998. Geology and U-Pb geochronology of Archean basement and Proterozoic cover in the Priest River complex, northwestern United States, and their implications for Cordilleran structure and Precambrian continent reconstructions. Can. J. Earth Sci. 35, 39–54. https://doi.org/10.1139/ cjes-35-1-39.

Doughty, P.T., Chamberlain, K.R., Foster, D.A., and Sha, G.S., 2007. Structural, metamorphic, and geochronologic constraints on the origin of the clearwater core complex, northern Idaho: Special Paper of the Geological Society of America, v. 433, p. 211–241, doi:10.1130/2007.2433(11).

Eaton, D.W., Ross, G.M., Clowes, R.M., 1999. Seismic-reflection and potential-field studies of the Vulcan structure, western Canada: A Paleoproterozoic Pyrenees? J. Geophys. Res. Solid Earth 104 (B10), 23255–23269.

Evans, K.V., Fischer, L.B., 1986. U-Pb geochronology of two augen gneiss terranes, Idaho-new data and tectonic implications two augen gneiss terranes, Idaho-new data and tectonic implications. Can. J. Earth Sci. 13 (10), 291–294. https://doi.org/10.1016/ 0148-9062(76)90561-1.

Evans, K.V., Aleinikoff, J.N., Obradovich, J.D., Fanning, C.M., 2000. SHRIMP U-Pb geochronology of volcanic rocks, Belt Supergroup, western Montana: evidence for rapid deposition of sedimentary strata. Can. J. Earth Sci. 37 (9), 1287–1300. https:// doi.org/10.1139/e00-036.

Fanning, C.M., Flint, R.B., Parker, A.J., Ludwig, K.R., Blissett, A.H., 1988. Refined Proterozoic evolution of Gawler craton, southern Australia through U-Pb zircon geochronology. Precambr. Res. 40, 363–380.

Fanning, C.M., Link, P.K., Woodhead, J., Hergt, J., 2009. Provenance of unique Meso-proterozoic sedimentary basins in Australia and North America: U-Pb and Lu-Hf isotopic data for detrital zircons and the implications for Rodinia reconstructions. Geological Society of London Fermor Meeting, Abstract, Edinburgh, United Kingdom, http://www.geos.ed.ac.uk/rodinia2009.

Fisher, C.M., Vervoort, J.D., 2018. Using the magmatic record to constrain the growth of continental crust—The Eoarchean zircon Hf record of Greenland. Earth Planet. Sci. Lett. 488, 79–91. https://doi.org/10.1016/j.epsl.2018.01.031.

Forbes, C.J., Giles, D., Hand, M., Betts, P.G., Suzuki, K., Chalmers, N., Dutch, R., 2011. Using P-T paths to interpret the tectonothermal setting ofprogrademetamorphism: an example from the northeastern Gawler Craton, South Australia. Precambr. Res. 185 (1-2), 65–85.

Foster, D.A., Mueller, P.A., Mogk, D.W., Wooden, J.L., Vogl, J.J., 2006. Proterozoic evolution of the western margin of the Wyoming craton: implications for the tectonic and magmatic evolution of the northern Rocky Mountains. Can. J. Earth Sci. 43 (10), 1601–1619. https://doi.org/10.1139/e06-052.

Frieman, B.M., Kelly, N.M., Kuiper, Y.D., Monecke, T., Kylander-Clark, A., Guitreau, M., 2021. Insight into Archean crustal growth and mantle evolution from multi-isotope U-Pb and Lu-Hf analysis of detrital zircon grains from the Abitibi and Pontiac subprovinces, Canada. Precambr. Res. 357, 106136. https://doi.org/10.1016/j.precamres.2021.106136.

Frost, C.D., Fanning, C.M., 2006. Archean geochronologi-cal framework of the Bighorn Mountains, Wyoming. Can. J. Earth Sci. 43 (10), 1399–1418. https://doi.org/10.1139/e06-051.

Frost, B.R., Frost, C.D., Cornia, M., Chamberlain, K.R., Kirkwood, R., 2006. The Teton - Wind River domain: A 2.68-2.67 Ga active margin in the western Wyoming Province. Can. J. Earth Sci. 43 (10), 1489–1510.

Frost, C.D., McLaughlin, J.F., Frost, B.R., Fanning, C.M., Swapp, S.M., Kruckenberg, S.C., Gonzalez, J., 2017. Hadean origins of paleoarchean continental crust in the central Wyoming province. Geol. Soc. Am. Bull. 129 (3-4), 259–280. https://doi.org/10.1130/B31555.110.1130/2016297.

Furlanetto, F., Thorkelson, D.J., Daniel Gibson, H., Marshall, D.D., Rainbird, R.H., Davis, W.J., Crowley, J.L., Vervoort, J.D., 2013. Late Paleoproterozoic terrane accretion in northwestern Canada and the case for circum-Columbian orogenesis. Precambr. Res. 224, 512–528. https://doi.org/10.1016/j.precamres.2012.10.010.

Gaschnig, R.M., Vervoort, J.D., Lewis, R.S., Tikoff, B., 2013. Probing for Proterozoic and Archean crust in the Northern U.S Cordillera with inherited zircon from the Idaho batholith. Geol. Soc. Am. Bull. 125 (1-2), 73–88. https://doi.org/10.1130/B30583.110.1130/2012273.

Gibson, G.M., Champion, D.C., 2019. Antipodean fugitive terranes in southern Laurentia: How Proterozoic Australia built the American West. Lithosphere 11, 551–559. https://doi.org/10.1130/l1072.1.

Gifford, J.N., Mueller, P.A., Foster, D.A., Mogk, D.W., 2014. Precambrian Crustal Evolution in the Great Falls Tectonic Zone: Insights from Xenoliths from the Montana Alkali Province. J. Geol. 122 (5), 531–548. https://doi.org/10.1086/677262.

Gifford, J.N., Mueller, P.A., Foster, D.A., Mogk, D.W., 2018. Extending the realm of Archean crust in the Great Falls tectonic zone: Evidence from the Little Rocky Mountains, Montana. Precambr. Res. 315, 264–281. https://doi.org/10.1016/j.precamres.2018.07.021.

Gifford, J., Malone, S., Mueller, P., 2020. The Medicine Hat Block and the Early Paleoproterozoic Assembly of Western Laurentia. Geosciences v. 10, 271. https://doi.org/10.3390/geosciences10070271.

Goodge, J.W., Fanning, C.M., 2016. Mesoarchean and Paleoproterozoic history of the Nimrod Complex, central Transantarctic Mountains, Antarctica: Stratigraphic revisions and relation to the Mawson Continent in East Gondwana. Precambr. Res. 285, 242–271. https://doi.org/10.1016/j.precamres.2016.09.001.

Goodge, J.W., Fanning, C.M., Fisher, C.M., Vervoort, J.D., Fisher, C.M., 2017. Proterozoic crustal evolution of central East Antarctica: Age and isotopic evidence from glacial igneous clasts, and links with Australia and Laurentia. Precambr. Res. 299, 151–176. https://doi.org/10.1016/j.precamres.2017.07.026.

Gorman, A.R., Clowes, R.M., Ellis, R.M., Henstock, T.J., Spence, G.D., Keller, G.R., Levander, A., Snelson, C.M., Burianyk, M.JA., Kanasewich, E.R., Asudeh, I., Hajnal, Z., Miller, K.C., 2002. Deep probe: Imaging the roots of western North America. Can. J. Earth Sci. 39 (3), 375–398. https://doi.org/10.1139/e01-064.

Gu, Y.J., Chen, Y., Dokht, R.M.H., Wang, R., 2018. Precambrian Tectonic Discontinuities in Western Laurentia: Broadband Seismological Perspectives on the Snowbird and Great Falls Tectonic Zones. Tectonics 37 (5), 1411–1434. https://doi.org/10.1029/ 2017TC004843.

Harrison, J.E., 1972. Precambrian Belt Basin of Northwestern United States: Its Geometry Sedimentation, and Copper Occurrences. Geol. Soc. 83 (5), 1215. https://doi.org/ 10.1130/0016-7606(1972)83[1215:PBBONU]2.0.CO;2.

Hanchar, J.M., Miller, C.F., 1993. Zircon zonation patterns as revealed by cathodoluminescence and backscattered electron images: Implications for interpretation of complex crustal histories. Chem. Geol. 110 (1-3), 1–13.

Halpin, J.A., Jensen, T., McGoldrick, P., Meffre, S., Berry, R.F., Everard, J.L., Calver, C. R., Thompson, J., Goemann, K., Whittaker, J.M., 2014. Authigenic monazite and detrital zircon dating from the Proterozoic Rocky Cape Group, Tasmania: Links to the Belt-Purcell Supergroup North America. Precambr. Res. 250, 50–67. https://doi. org/10.1016/j.precamres.2014.05.025.

Hartnady, M.I.H., Kirkland, C.L., Martin, L., Clark, C., Smithies, R.H., Spaggiari, C.V., 2020. Zircon oxygen and hafnium isotope decoupling during regional metamorphism: implications for the generation of low δ18O magmas. Contrib. Mineral. Petrol. 175, 1–17. https://doi.org/10.1007/s00410-019-1646-7.

Hoffman, P.F., 1988. United Plates of America, the Birth of a Craton: Early Proterozoic Assembly and Growth of Laurentia. Annu. Rev. Earth Planet. Sci. 16 (1), 543–603.

Holland, M.E., Grambling, T.A., Karlstrom, K.E., Jones, J.V., Nagotko, K.N., Daniel, C.G., 2020. Geochronologic and Hf-isotope framework of Proterozoic rocks from central New Mexico, USA: Formation of the Mazatzal crustal province in an extended continental margin arc. Precambr. Res. 347, 105820. https://doi.org/10.1016/j. precamres.2020.105820.

Ivanic, T.J., Van Kranendonk, M.J., Kirkland, C.L., Wyche, S., Wingate, M.T.D., Belousova, E.A., 2012. Zircon Lu-Hf isotopes and granite geochemistry of the Murchison Domain of the Yilgarn Craton: Evidence for reworking of Eoarchean crust during Meso-Neoarchean plume-driven magmatism. Lithos 148, 112–127. https:// doi.org/10.1016/j.lithos.2012.06.006.

Johnson, T.E., Brown, M., Kaus, B.J.P., VanTongeren, J.A., 2014. Delamination and recycling of archaean crust caused by gravitational instabilities. Nat. Geosci. 7 (1), 47–52. https://doi.org/10.1038/ngeo2019.

Jones, J.V., Daniel, C.G., Doe, M.F., 2015. Tectonic and sedimentary linkages between the Belt-Purcell basin and southwestern Laurentia during the Mesoproterozoic, ca. 1.60–1.40 Ga. Lithosphere 7 (4), 465–472. https://doi.org/10.1130/L438.1.

Kanasewich, E.R., Clowes, R.M., McCloughan, C.H., 1969. A buried Precambrian rift in western Canada. Tectonophysics 8 (4-6), 513–527.

Kirscher, U., Liu, Y., Li, Z.X., Mitchell, R.N., Pisarevsky, S.A., Denyszyn, S.W., Nordsvan, A., 2019. Paleomagnetism of the Hart Dolerite (Kimberley, Western Australia) – A two-stage assembly of the supercontinent Nuna? Precambr. Res. 329, 170–181. https://doi.org/10.1016/j.precamres.2018.12.026.

Kirscher, U., Mitchell, R.N., Liu, Y., Nordsvan, A.R., Cox, G.M., Pisarevsky, S.A., Wang, C., Wu, L., Murphy, J.B., Li, Z.-X., 2021. Paleomagnetic constraints on the duration of the Australia-Laurentia connection in the core of the Nuna supercontinent. Geology 49 (2), 174–179. https://doi.org/10.1130/g47823.1.

Kita, N.T., Ushikubo, T., Fu, B., Valley, J.W., 2009. High precision SIMS oxygen isotope analysis and the effect of sample topography. Chem. Geol. 264 (1-4), 43–57. https:// doi.org/10.1016/j.chemgeo.2009.02.012.

Leeman, W.P., Menzies, M.A., Matty, D.J., Embree, G.F., 1985. Strontium, neodymium and lead isotopic compositions of deep crustal xenoliths from the Snake River Plain: evidence for Archean basement. Earth Planet. Sci. Lett. 75 (4), 354–368. https://doi. org/10.1016/0012-821X(85)90179-7.

Lewis, R.S., Burmester, R.F., McFaddan, M.D., Kauffman, J.D., Doughty, P.T., Oakley, W. L., Frost, T.P., 2007. Geologic Map of the Headquarters 30 × 60 Minute Quadrangle Idaho. Idaho Geol. Surv. Digital Web Map 92.

Lewis, R.S., Link, P.K., Stanford, L., and Long, S.P., 2012, Geologic map of Idaho: Idaho Geological Survey Map M-9, scale 1:750,000.

Lewis, R.S., Vervoort, J.D., Burmester, R.F., Oswald, P.J., 2010. Detrital zircon analysis of Mesoproterozoic and Neoproterozoic metasedimentary rocks of north-central Idaho: implications for development of the Belt-Purcell basin. Can. J. Earth Sci. 47 (11), 1383–1404. https://doi.org/10.1139/E10-049.

Lewis, R.S., Burmester, R.F., Breckenridge, R.M., Mcfaddan, M.D., and Phillips, W.M., 2020, Geologic Map of the Sandpoint 30́ x 60́ Quadrangle, Idaho and Montana, and the Idaho Part of the Chewelah 30́ x 60́ Quadrangle: Idaho Geological Survey, Digital Web Map 183.

Li, J., Pourteau, A., Li, Z.X., Jourdan, F., Nordsvan, A.R., Collins, W.J., Volante, S., 2020. Heterogeneous Exhumation of the Mount Isa Orogen in NE Australia After 1.6 Ga Nuna Assembly: New High-Precision 40Ar/39Ar Thermochronological Constraints. Tectonics 39, 1–27. https://doi.org/10.1029/2020TC006129.

Li, Z.X., Zhang, L., Powell, C.M., 1995. South China in Rodinia: Part of the missing link between Australia-East Antarctica and Laurentia? Geology 23, 407–410. https://doi. org/10.1130/0091-7613(1995)023<0407:SCIRPO>2.3.CO;2.

Liebmann, J., Spencer, C.J., Kirkland, C.L., Xia, X.-P., Bourdet, J., 2021. Effect of water on δ18O in zircon. Chem. Geol. 574, 120243. https://doi.org/10.1016/j. chemgeo.2021.120243.

Link, P.K., Autenrieth-Durk, K.M., Cameron, A., Fanning, C.M., Vogl, J.J., and Foster, D. A., 2017, U-Pb zircon ages of the Wildhorse gneiss, Pioneer Mountains, south-central idaho, and tectonic implications: Geosphere, v. 13, p. 681–698, doi:10.1130/ GES01418.1.

Lu, Y.J., Loucks, R.R., Fiorentini, M., McCuaid, T.C., Evans, N.J., Yang, Z-M, Hou, Z-Q, Kirkland, C.L., Parra-Avila, L.A., Kobussen, A.., 2016, Zircon Compositions as a Pathfinder for Porphyry Cu ± Mo ± Au Deposits: Economic Geology Special Publication, v. 19, p. 329–347. Ludwig, K.R., 1998. On the treatment of concordant uranium-lead ages. Geochim. Cosmochim. Acta 62 (4), 665–676. https://doi.org/10.1016/S0016-7037(98)00059- 3.

Ludwig K. R., 2003, Isoplot Manual and Isoplotv4.15. Berkley Geochronology Center, Special Publication V. 4. McFarlane, C.R.M., Corfu, F., 2015. A geochronological framework for sedimentation and Mesoproterozoic tectono-magmatic activity in lower Belt-Purcell rocks exposed west of Kimberley. British Columbia: Canad. J. Earth Sci. 52 (7), 444–465. https:// doi.org/10.1139/cjes-2014-0215.

McMechan, M.E., Root, K.G., Simony, P.S., Pattison, D.R.M., 2021. Nailed to the craton: Stratigraphic continuity across the southeastern Canadian Cordillera with tectonic implications for ribbon continent models. Geology 49, 101–105. https://doi.org/ 10.1130/G48060.1.

Medig, K.P.R., Thorkelson, D.J., Davis, W.J., Rainbird, R.H., Gibson, H.D., Turner, E.C., Marshall, D.D., 2014. Pinning northeastern Australia to northwestern Laurentia inthe Mesoproterozoic. Precambr. Res. 249, 88–99. https://doi.org/10.1016/j. precamres.2014.04.018.

Mole, D.R., Kirkland, C.L., Fiorentini, M.L., Barnes, S.J., Cassidy, K.F., Isaac, C., Belousova, E.A., Hartnady, M., Thebaud, N., 2019. Time-space evolution of an Archean craton: A Hf-isotope window into continent formation. Earth Sci. Rev. 196, 102831. https://doi.org/10.1016/j.earscirev.2019.04.003.

Mole, D.R., Thurston, P.C., Marsh, J.H., Stern, R.A., Ayer, J.A., Martin, L.A.J., Lu, Y.J., 2021. The formation of Neoarchean continental crust in the south-east Superior Craton by two distinct geodynamic processes. Precambr. Res. 356, 106104. https://doi.org/10.1016/j.precamres.2021.106104.

Mueller, P.A., Frost, C.D., 2006. The Wyoming Province: A distinctive Archean craton in Laurentian North America. Can. J. Earth Sci. 43 (10), 1391–1397.

Mueller, P.A., Heatherington, A.L., Kelly, D.M., Wooden, J.L., Mogk, D.W., 2002. Paleoproterozoic crust within the Great Falls tectonic zone: Implications for the assembly of southern Laurentia. Geology 30, 127–130. https://doi.org/10.1136/jclinpath-2017-204981.

Mueller, P.A., Wooden, J.L., Mogk, D.W., Foster, D.A., 2011. Paleoproterozoic evolution of the Farmington zone: Implications for terrane accretion in southwestern Laurentia. Lithosphere 3 (6), 401–408. https://doi.org/10.1130/L161.110.1130/2011350.

Mulder, J.A., Halpin, J.A., Daczko, N.R., 2015. Mesoproterozoic Tasmania: Witness to the East Antarctica-Laurentia connection within Nuna. Geology 43 (9), 759–762. https://doi.org/10.1130/G36850.1.

Mulder, J.A., Nebel, O., Gardiner, N.J., Cawood, P.A., Wainwright, A.N., Ivanic, T.J., 2021. Crustal rejuvenation stabilised Earth’s first cratons. Nat. Commun. 12, 1–8. https://doi.org/10.1038/s41467-021-23805-6.

Næraa, T., Scherst´en, A., Rosing, M.T., Kemp, A.I.S., Hoffmann, J.E., Kokfelt, T.F., Whitehouse, M.J., 2012. Hafnium isotope evidence for a transition in the dynamics of continental growth 3.2 Gyr ago. Nature 485, 627–630. https://doi.org/10.1038/nature11140.

Nasdala, L., Hofmeister, W., Norberg, N., Martinson, J.M., Corfu, F., D¨orr, W., Kamo, S.L., Kennedy, A.K., Kronz, A., Reiners, P.W., Frei, D., Kosler, J., Wan, Y., G¨otze, J., H¨ager, T., Kr¨oner, A., Valley, J.W., 2008. Zircon M257 – a homogeneous natural reference material for the ion microprobe U-Pb analysis of zircon. Geostand. Geoanal. Res. 32 (3), 247–265.

Nesheim, T.O., Vervoort, J.D., McClelland, W.C., Gilotti, J.A., Lang, H.M., 2012. Mesoproterozoic syntectonic garnet within Belt Supergroup metamorphic tectonites: Evidence of Grenville-age metamorphism and deformation along northwest Laurentia. Lithos v. 134–135, 91–107. https://doi.org/10.1016/j. lithos.2011.12.008.

Nieuwenhuis, G., Unsworth, M.J., Pana, D., Craven, J., Bertrand, E., 2014. Three-dimensional resistivity structure of Southern Alberta, Canada: Implications for precambrian tectonics. Geophys. J. Int. 197, 838–859. https://doi.org/10.1093/gji/ggu068.

Nordsvan, A.R., Collins, W.J., Li, Z., Spencer, C.J., Pourteau, A., Withnall, I.W., Betts, P. G., and Volante, S., 2018, Laurentian crust in northeast Australia: Implications for the assembly of the supercontinent Nuna: Geology, p. 1–4.

Page, R.W., Sun, S.-S., 1998. Aspects of geochronology and crustal evolution in the Eastern Fold Belt. Mt Isa Inlier: Australian J. Earth Sci. 45 (3), 343–361. https://doi.org/10.1080/08120099808728396.

Paton, C., Hellstrom, J., Paul, B., Woodhead, J., Hergt, J., 2011. Iolite: freeware for the visualisation and processing of mass spectrometric data. J. Anal. Atomic Spectrometry 26 (12), 2508. https://doi.org/10.1039/c1ja10172b.

Payne, J.L., Hand, M., Barovich, K.M., Reid, A., Evans, D.A.D., 2009. Correlations and reconstruction models for the 2500–1500 Ma evolution of the Mawson Continent: Geological Society. London, Special Publications 323 (1), 319–355. https://doi.org/10.1144/SP323.16.

Payne, J.L., McInerney, D.J., Barovich, K.M., Kirkland, C.L., Pearson, N.J., Hand, M., 2016. Strengths and limitations of zircon Lu-Hf and O isotopes in modelling crustal growth. Lithos v. 248–251, 175–192. https://doi.org/10.1016/j.lithos.2015.12.015.

Petersson, A., Kemp, A.I.S., Hickman, A.H., Whitehouse, M.J., Martin, L., Gray, C.M., 2019. A new 3.59 Ga magmatic suite and a chondritic source to the east Pilbara Craton. Chem. Geol. 511, 51–70. https://doi.org/10.1016/j.chemgeo.2019.01.021.

Pisarevsky, S.A., Elming, S.Å., Pesonen, L.J., Li, Z.X., 2014. Mesoproterozoic paleogeography: Supercontinent and beyond. Precambr. Res. 244, 207–225. https://doi.org/10.1016/j.precamres.2013.05.014.

Pourteau, A., Smit, M.A., Li, Z.X., Collins, W.J., Nordsvan, A.R., Volante, S., Li, J., 2018. 1.6 Ga crustal thickening along the final Nuna suture. Geology 46, 959–962. https:// doi.org/10.1130/G45198.1.

Reid, A.J., Payne, J.L., 2017. Magmatic zircon Lu–Hf isotopic record of juvenile addition and crustal reworking in the Gawler Craton, Australia. Lithos v. 292–293, 294–306. https://doi.org/10.1016/j.lithos.2017.08.010.

Reid, A., Forster, M., 2021. Mesoproterozoic thermal evolution of the northern Gawler Craton from 40Ar/39Ar geochronology. Precambr. Res. 358, 106180. https://doi.org/10.1016/j.precamres.2021.106180.

Reid, R.R., Morrison, D.A., Greenwood, W.R., 1973. The Clearwater orogenic zone: A relict of Proterozoic orogeny in central and northern Idaho. Belt Symposium I: Idaho Bureau of Mines and Geology Special Publication 1, 10–56.

Reid, A., Hand, M., Jagodzinski, E., Kelsey, D., Pearson, N., 2008. Paleoproterozoic orogenesis in the southeastern Gawler Craton. South Australia: Australian J. Earth Sci. 55 (4), 449–471. https://doi.org/10.1080/08120090801888594.

Roberts, N.M.W., Spencer, C.J., 2015. The zircon archive of continent formation through time: Geological Society. London, Special Publications 389 (1), 197–225. https:// doi.org/10.1144/SP389.14.

Rogers, C., Kamo, S.L., S¨oderlund, U., Hamilton, M.A., Ernst, R.E., Cousens, B., Harlan, S. S., Wade, C.E., Thorkelson, D.J., 2018. Geochemistry and U-Pb geochronology of 1590 and 1550 Ma mafic dyke swarms of western Laurentia: Mantle plume magmatism shared with Australia. Lithos v. 314–315, 216–235. https://doi.org/10.1016/j.lithos.2018.06.002.

Ross, G.M., Villeneuve, M., 2003. Provenance of the Mesoproterozoic (1.45 Ga) Belt basin (western North America): Another piece in the pre-Rodinia paleogeographic puzzle. Geol. Soc. Am. Bull. 115 (10), 1191. https://doi.org/10.1130/B25209.110.1130/2003135.

Ross, G.M., Parrish, R.R., Villeneuve, M.E., Bowring, S.A., 1991. Geophysics and geochronology of the crystalline basement of the Alberta Basin, western Canada. Can. J. Earth Sci. 28 (4), 512–522.

Ross, G.M., Parrish, R.R., Winston, D., 1992. Provenance and U-Pb geochronology of the Mesoproterozoic Belt Supergroup (northwestern United States): implications for the age of deposition and pre-Panthalassa plate reconstructions. Earth Planet. Sci. Lett. 113, 57–76.

Schwartz, J.J., Snoke, A.W., Cordey, F., Johnson, K., Frost, C.D., Barnes, C.G., LaMaskin, T.A., Wooden, J.L., 2011. Late Jurassic magmatism, metamorphism, and deformation in the Blue Mountains Province, northeast Oregon. Geol. Soc. Am. Bull. 123 (9-10), 2083–2111. https://doi.org/10.1130/B30327.1.

Smithies, R.H., Lu, Y., Kirkland, C.L., Johnson, T.E., Mole, D.R., Champion, D.C., Martin, L., Jeon, H., Wingate, M.T.D., Johnson, S.P., 2021. Oxygen isotopes trace the origins of Earth ’ s earliest continental crust. Nature 592 (7852), 70–75.

Spencer, C.J., Cawood, P.A., Hawkesworth, C.J., Raub, T.D., Prave, A.R., Roberts, N.M. W., 2014. Proterozoic onset of crustal reworking and collisional tectonics: Reappraisal of the zircon oxygen isotope record. Geology 42 (5), 451–454. https://doi.org/10.1130/G35363.110.1130/2014158.

Spencer, C.J., Kirkland, C.L., Roberts, N.M.W., Evans, N.J., Liebmann, J., 2020. Strategies towards robust interpretations of in situ zircon Lu–Hf isotope analyses. Geosci. Front. https://doi.org/10.1016/j.gsf.2019.09.004.

Spencer, C.J., Kirkland, C.L., Taylor, R.J.M., 2016. Strategies towards statistically robust interpretations of in situ U-Pb zircon geochronology. Geosci. Front. 7 (4), 581–589. https://doi.org/10.1016/j.gsf.2015.11.006.

Stacey, J.S., Kramers, J.D., 1975. Approximation of terrestrial lead isotope evolution by a two-stage model. Earth Planet. Sci. Lett. 26 (2), 207–221.

Stern, R.A., Bodorkos, S., Kamo, S.L., Hickman, A.H., Corfu, F., 2009. Measurement of SIMS instrumental mass fractionation of Pb isotopes during zircon dating. Geostand. Geoanal. Res. 33, 145–168. https://doi.org/10.1111/j.1751-908X.2009.00023.x.

Stevens, L.M., Baldwin, J.A., Cottle, J.M., Kylander-Clark, A.R.C., 2015. Phase equilibria modelling and LASS monazite petrochronology: P-T-t constraints on the evolution of the Priest River core complex, northern Idaho. J. Metamorph. Geol. 33 (4), 385–411. https://doi.org/10.1111/jmg.12125.

Strickland, A., Miller, E.L., Wooden, J.L., 2011. The timing of tertiary metamorphism and deformation in the Albion-Raft River-Grouse Creek metamorphic core complex. Utah and Idaho: J. Geol. 119 (2), 185–206. https://doi.org/10.1086/658294.

Swain, G., Barovich, K., Hand, M., Ferris, G., Schwarz, M., 2008. Petrogenesis of the St Peter Suite, southern Australia: Arc magmatism and Proterozoic crustal growth of the South Australian Craton. Precambr. Res. 166 (1-4), 283–296. https://doi.org/10.1016/j.precamres.2007.07.028.

Tang, M., Ji, W.Q., Chu, X., Wu, A., Chen, C., 2021. Reconstructing crustal thickness evolution from europium anomalies in detrital zircons. Geology 49, 76–80. https://doi.org/10.1130/G47745.1.

Thorkelson, D.J., Mortensen, J.K., Creaser, R.A., Davidson, G.J., Abbott, G.J., 2001. Early Proterozoic magmatism in Yukon, Canada: constraints on the evolution of northwestern Laurentia. Can. J. Earth Sci. 38, 1479–1494. https://doi.org/10.1139/cjes-38-10-1479.

Tiddy, C.J., Betts, P.G., Neumann, M.R., Murphy, F.C., Stewart, J., Giles, D., Sawyer, M., Freeman, H., and Jourdan, F., 2020, Interpretation of a ca. 1600–1580 Ma metamorphic core complex in the northern Gawler Craton, Australia: Gondwana Research, v. 85, p. 263–290, doi:10.1016/j.gr.2020.04.008.

Valley, J.W., 2003. Oxygen Isotopes in Zircon. Rev. Mineral. Geochem. 53 (1), 343–385. https://doi.org/10.2113/0530343.

Valley, J.W., Kinny, P.D., Schulze, D.J., Spicuzza, M.J., 1998. Zircon megacrysts from kimberlite: oxygen isotope variability among mantle melts. Contrib. Mineral. Petrol. 133 (1-2), 1–11.

Van Schmus, W.R., Bickford, M.E., Sims, P.K., Anderson, R.R., Schearer, C.K., Treves, S. B., 1993. Proterozoic geology of the western Midcontinent basement. In: Reed, et al. (Eds.), Precambrian: Conterminous U.S., vol. C-2. Geological Society of North America, The Geology of North America, pp. 239–259.

Vermeesch, P., 2018. IsoplotR: A free and open toolbox for geochronology. Geosci. Front. 9 (5), 1479–1493. https://doi.org/10.1016/j.gsf.2018.04.001.

Vervoort, J.D., Kemp, A.I.S., 2016. Clarifying the zircon Hf isotope record of crust-mantle evolution. Chem. Geol. 425, 65–75. https://doi.org/10.1016/j.chemgeo.2016.01.023.

Vervoort, J.D., Patchett, P.J., Gehrels, G.E., Nutman, A.P., 1996. Constraints on early Earth differentiation from hafnium and neodymium isotopes. Nature 379 (6566), 624–627. https://doi.org/10.1038/379624a0.

Vervoort, J.D., Lewis, R.S., Fisher, C., Gaschnig, R.M., Jansen, A.C., Brewer, R., 2016. Neoarchean and Paleoproterozoic crystalline basement rocks of north-central Idaho: Constraints on the formation of western Laurentia. Geol. Soc. Am. Bull. 128, 94–109. https://doi.org/10.1130/B31150.1.

Villeneuve, M.E., Ross, G.M., Theriault, R.J., Milews, W.,Parrish, R.R., and Broome, J., 1993, Tectonic subdivision and U-Pb geochronology of the crystalline basement of the Alberta Basin, western Canada: Geological Survey of Canada Bulletin 447, p. 1–25.

Volante, S., Pourteau, A., Collins, W.J., Blereau, E., Li, Z.-X., Smit, M., Evans, N.J., Nordsvan, A.R., Spencer, C.J., McDonald, B.J., Li, J., Günter, C., 2020. Multiple P-T-Dd-t paths reveal the evolution of the final Nuna assembly in northeast Australia. J. Metamorph. Geol. 38 (6), 593–627. https://doi.org/10.1111/jmg.12532.

Wan, B., Yang, X., Tian, X., Yuan, H., Kirscher, U., and Mitchell, R.N., 2020, Seismological evidence for the earliest global subduction network at 2 Ga ago: Science Advances, v. 6, p. 1–10, doi:10.1126/sciadv.abc5491.

Weller, O.M., St-Onge, M.R., 2017. Record of modern-style plate tectonics in the Palaeoproterozoic Trans-Hudson orogen. Nat. Geosci. 10 (4), 305–311. https://doi.org/10.1038/ngeo2904.

Whitmeyer, S.J., Karlstrom, K.E., 2007. Tectonic model for the Proterozoic growth of North America. Geosphere 3, 220–259. https://doi.org/10.1130/GES00055.1.

Wiedenbeck, M., Hanchar, J.M., Peck, W.H., Sylvester, P., Valley, J., Whitehouse, M., Kronz, A., Morishita, Y., Nasdala, L., Fiebig, J., Franchi, I., Girard, J.-P., Greenwood, R.C., Hinton, R., Kita, N., Mason, P.R.D., Norman, M., Ogasawara, M., Piccoli, P.M., Rhede, D., Satoh, H., Schulz-Dobrick, B., Skår, O., Spicuzza, M.J., Terada, K., Tindle, A., Togashi, S., Vennemann, T., Xie, Q., Zheng, Y.-F., 2004. Further characterisation of the 91500 zircon crystal. Geostandards Geoanal. Res. 28 (1), 9–39. https://doi.org/10.1111/j.1751-908X.2004.tb01041.x.

Wooden, J.L., Barth, A.P., and Mueller, P.A., 2012, Crustal growth and tectonic evolution of the Mojave crustal province: Insights from hafnium isotope systematics in zircons: , p. 17–28, doi:10.1130/L218.1.

Xu, Y.-J., Cawood, P.A., Zhang, H.-C., Zi, J.-W., Zhou, J.-B., Li, L.-X., and Du, Y.-S., 2019, The Mesoproterozoic Baoban Complex, South China: A missing fragment of western Laurentian lithosphere: Geological Society of America Bulletin, p. 1–15, doi: 10.1130/b35380.1.

Yakymchuk, C., Kirkland, C.L., Clark, C., 2018. Th/U ratios in metamorphic zircon. J. Metamorphic Geol. 36 (6), 715–737. https://doi.org/10.1111/jmg.12307.

Yao, W., Li, Z.X., Li, W.X., Li, X.H., 2017. Proterozoic tectonics of Hainan Island in supercontinent cycles: New insights from geochronological and isotopic results. Precambrian Res. 290, 86–100. https://doi.org/10.1016/j.precamres.2017.01.001.

Zhang, A., Ma, L., Liu, H., Cai, Y., Chen, M., Fang, Q.i., 2021. Identification of two-phased late Paleoproterozoic magmatism in the Wuyishan Domain (SE China): Implications for the tectonic evolution of the Cathaysia Block. Precambrian Res. 355, 106093. https://doi.org/10.1016/j.precamres.2021.106093.

Zirakparvar, N.A., Vervoort, J.D., McClelland, W., Lewis, R.S., 2010. Insights into the metamorphic evolution of the Belt-Purcell basin; evidence from Lu–Hf garnet geochronology. Canad. J. Earth Sci. 47 (2), 161–179. https://doi.org/10.1139/E10-001.

Chapter 3: Detrital zircon U–Pb and Hf signatures of Paleo-Mesoproterozoic strata in the Priest River region, northwestern USA: A record of Laurentia assembly and Nuna tenure

Abstract

Rocks of the Gold Cup Quartzite, Belt Supergroup and Deer Trail Group crop out in the Priest River region of northeastern Washington and northern Idaho (USA). As these sequences represent the westernmost exposures of Paleoproterozoic–Mesoproterozoic strata between New Mexico (USA) and the northern Yukon (Canada), they are key to understanding the assembly of Laurentia and evaluating the duration and configuration of the supercontinent Nuna/Columbia. Here, we present detrital zircon U–Pb and Lu–Hf isotope data from these sequences. The results indicate that the <1.73 Ga Gold Cup Quartzite contains similar detrital zircon components to other widespread late Paleoproterozoic units that record final assembly of the main Archean blocks of western Laurentia; as such, they do not require any non-Laurentian source. Prominent ca. 1.7–1.5 Ga, isotopically juvenile zircon grains form the main component of the overlying ca. 1.47 Ga Lower Belt Supergroup. Some of these detrital zircon components lack a Laurentian source and are instead consistent with derivation from the Gawler Craton in southeastern Australia. The >1.38 Ga upper Belt Supergroup strata are structurally overlain by <1.3 Ga Deer Trail Group rocks that contain detrital zircon components consistent with mixed Laurentian sources. The paucity of any syndepositional volcanic detrital zircon in Deer Trail Group strata along with its fine siliciclastic and carbonate nature suggest deposition within a tectonically-quiescent basin coeval with breakup of Nuna.

3.1. Introduction

The cyclic amalgamation and dispersal of continents has punctuated Earth's history for at least the past two billion years in a process known as the supercontinent cycle (e.g. Li et al., 2019; Mitchell et al., 2021; Nance et al., 2014). Similarities in stratigraphy, sedimentary provenance and crustal evolution between western Laurentia (all directions expressed in modern-day coordinates), East Antarctica, and Australia have been used to argue that they were probably connected during most of the Proterozoic, a configuration referred to as the southwest-U.S.–East Antarctic, or SWEAT, connection (Moores, 1991).

Early models suggested the existence of a SWEAT-like connection from as early as 1.9 Ga, and that this configuration may have remained relatively stable until eventual breakup during the late Neoproterozoic (Moores, 1991; Dalziel, 1991; Hoffman, 1991). However, paleomagnetic-based paleogeographic reconstructions indicate that although a SWEAT-like configuration is permissible for most of the early Mesoproterozoic and Neoproterozoic, Australia and Laurentia appear to have been widely separated at ca. 1.25 Ga (Kirscher et al., 2019; Pisarevsky et al., 2014a,b; Kirscher et al., 2020). This suggests that some of the long recognized geological similarities between western Laurentia and Australia–East Antarctica (Moores, 1991; Bell and Jefferson, 1987) may instead provide evidence for the existence of two separate, but perhaps similarly configured, supercontinents—an older, predominately late Paleoproterozoic to Mesoproterozoic supercontinent called Nuna (or Columbia), and a younger, predominately Neoproterozoic, supercontinent called Rodinia (Zhao et al., 2002, 2004; Li et al., 2008a; Meert, 2012; Zhang et al., 2012; Kirscher et al., 2019; Li et al., 2019; Pisarevsky et al., 2014a; Kirscher et al., 2020). This SWEAT-like paleogeography during the late Paleoproterozoic to Mesoproterozoic between Australia, Antarctica and western Laurentia has been called a "proto-SWEAT" configuration (Fig. 3.1; Payne et al., 2009; Kirscher et al., 2019; 2020).

The main assembly of Laurentia occurred during ca. 1.92–1.77 Ga amalgamation of the Archean Rae, Slave, Hearne, Wyoming, Superior, and Medicine Hat cratons along the Trans-Hudson orogen and associated structures including the Great Falls Tectonic zone and Vulcan structure (Fig. 3.2A; Eaton et al., 1999; Mueller et al., 2002; Whitmeyer and Karlstrom, 2007). Similar-age ca. 2.1–1.8 Ga orogens also separate many Archean–Paleoproterozoic blocks in Australia, Siberia, North China, Antarctica, Africa and Baltica, which has led to suggestions that global assembly of Nuna occurred by ca. 1.8 Ga (Rogers and Santosh, 2002; Zhao et al., 2002). However, paleomagnetic (Pisarevsky et al., 2014b; Kirscher et al., 2019; 2020 and references therein) and geological (e.g. Betts et al., 2016; Furlanetto et al., 2013; Li et al., 2020; Nordsvan et al., 2018; Volante et al., 2020a; Volante et al., 2020b) constraints have suggested that an ocean existed between northern Australia and northwestern

Laurentia from ca. 1.8 to 1.6 Ga. Thus, whether Nuna assembly occurred at ca 1.8 Ga coeval with widespread Trans-Hudson events in Laurentia (e.g. Zhao et al., 2002), or rather involved a more protracted and complex, perhaps two-stage process, lasting from ca. 1.9 to 1.6 Ga (e.g. Kirscher et al., 2019), are debated. In the two-stage model, initial supercontinent amalgamation began with the assembly of a unified Laurentia–Baltica–Siberia landmass by ca. 1.8 Ga, but a final proto-SWEAT configured Nuna was not reached until ca. 1.6 Ga following closure of a small ocean between the Laurentia–Baltica–Siberia and Antarctica–Australia landmasses (Betts et al., 2016; Kirscher et al., 2019; Pourteau et al., 2018; Wang et al., 2020; Kirscher et al., 2020; Nordsvan et al., 2018).

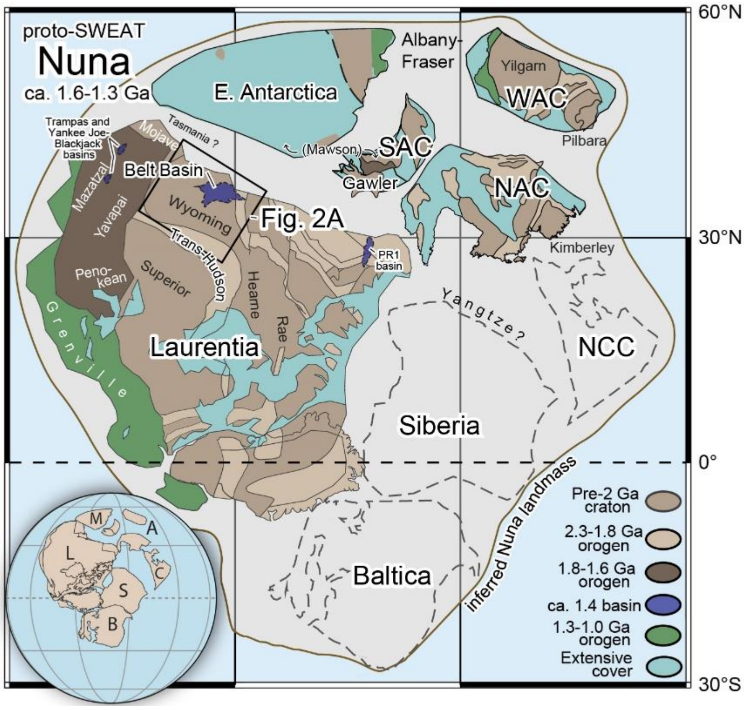

Fig. 3.1. Configuration of proto-SWEAT Nuna including its core constituents of Laurentia, Mawson (East Antarctica and Gawler Craton), Australia (NAC–North Australian craton, SAC–South Australia craton, WAC–West Australia craton), North China Craton (NCC), Siberia, and Baltica (adapted from Kirscher et al., 2020). The North China Craton, Siberia, and Baltica are not pertinent to this study and thus only outlines are shown. Paleomagnetic constraints (Kirscher et al., 2020 and references therein) suggest this configuration was stable (albeit underwent counterclockwise rotation) from ca. 1.6–1.3 Ga, and is shown here at ca. 1.3 paleolatitude. Extent of Fig. 3.2A, the Belt Basin, and generally coeval Trampas and Yankee–Joe Blackjack and PR1 basins (Doe et al., 2013; Jones et al., 2015) indicated. Additional abbreviations: L–Laurentia, M–Mawson, A–Australia, C–North China Craton, S–Siberia, B–Baltica.

Regional tectono-stratigraphic evaluation of the proposed two-stage model for Nuna assembly along the Laurentian margin has so far neglected an approximately 3000 km section of the margin (Fig. 3.1) between the PR1 Basin in northwestern Laurentia (Medig et al., 2014; Verbaas et al., 2018), and the Mojave province in southwestern Laurentia (Holland et al., 2015, 2018). The Priest River region (Fig. 3.2) contains one of the most complete records of the Neoarchean to Mesoproterozoic tectonic history of the west-central margin of Laurentia and thus offers a unique opportunity to evaluate the timing, duration and credibility of proposed relationships with Australia/Antarctica.

Here, we use existing U–Pb detrital zircon datasets and new U–Pb and Lu–Hf detrital zircon data from three unconformity-bounded sequences in the Priest River region of Laurentia, including the < 1.73 Ga Gold Cup Quartzite, the ca. 1.47–1.38 Belt Supergroup, and the < 1.3 Ga Deer Trail Group. These new data record changes in the provenance of western Laurentia stratigraphy, which can be related to the timing of amalgamation of Laurentia, and the timing of amalgamation then breakup of Nuna.

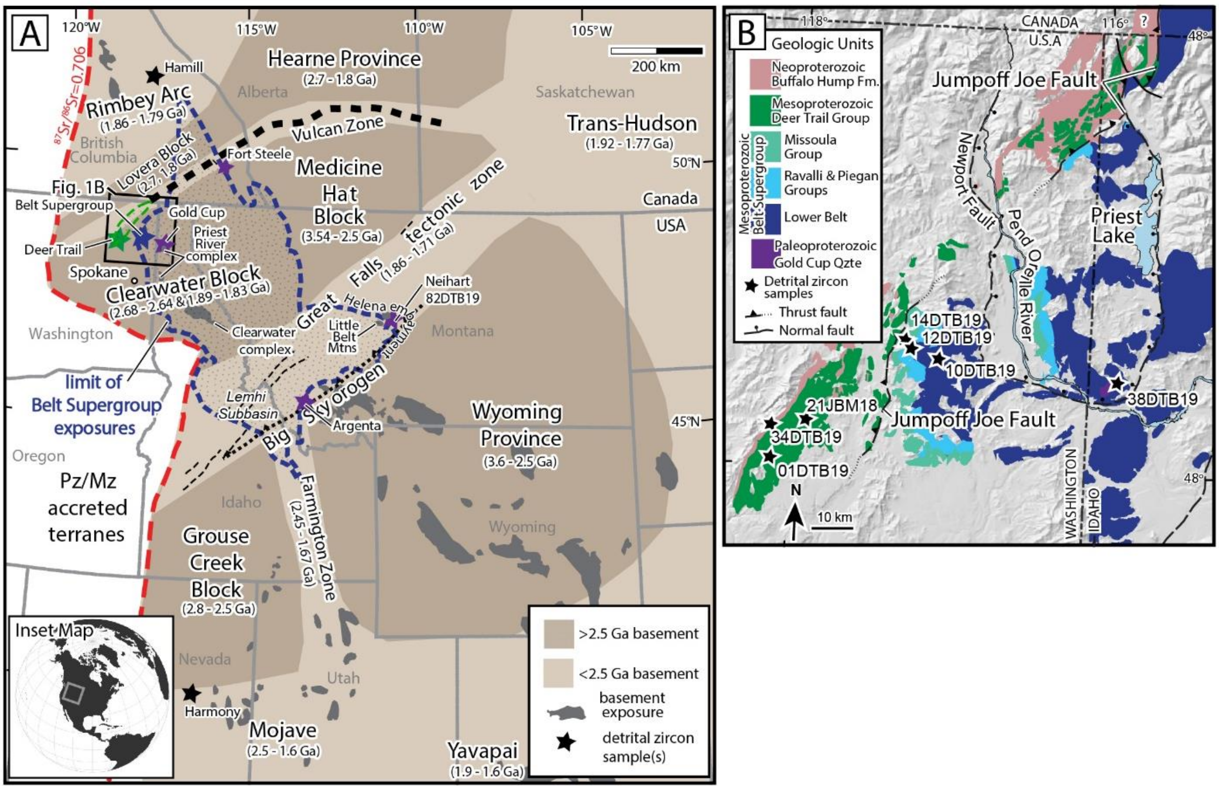

Fig. 3.2. A) General tectonic map of western Laurentia showing Laurentian basement terranes, the limit of Belt Supergroup exposures and geographic areas mentioned in text (after Foster et al., 2006; Whitmeyer and Karlstrom, 2007; Vervoort et al., 2016 and references therein). The extent of regional geologic map in Fig. 3.1B indicated. The 87Sr/86Sr < 0.706 line approximates the western edge of Laurentia generated during Neoproterozoic rifting (Armstrong et al., 1977; Elison et al., 1990). B) Geologic map of the Priest River region showing the extent of Proterozoic rocks and sample locations (map modified from Miller, 2001; Schuster, 2005 and Lewis et al., 2012).

3.2. Geological Setting

3.2.1. The Archean–Paleoproterozoic basement framework of western Laurentia

In the Priest River and Clearwater complexes (Fig. 3.2A) of northeastern Washington and northern Idaho (USA), exposures of ca. 2.67–2.61 and 1.88–1.84 Ga orthogneisses are considered to belong to the same Archean–Paleoproterozoic Clearwater Block (Vervoort et al., 2016). The Clearwater Block, which represents the westernmost exposures of Laurentian crust beneath the Belt Basin (Foster et al., 2006; Vervoort et al., 2016; Gifford et al., 2020), abuts, or is possibly an extension of, the Medicine Hat Block. The Medicine Hat Block is not exposed, but based on limited borehole and xenolith data is thought to be a mix of Archean (3.1–2.6 Ga) and Paleoproterozoic (ca. 1.81–1.75 Ga) crust (Gifford et al., 2018, 2020; Ross et al., 1991; Villeneuve et al., 1993). Highly evolved (εHf*t* = –8 to –23) ca. 1.8 Ga magmatism within the Medicine Hat Block suggests that the younger Paleoproterozoic period of crustal growth reworked an older Meso- to Neoarchean component (Gifford et al., 2020).

The Archean Wyoming Province and Grouse Creek Block are the southern neighbors of Clearwater and Medicine Hat blocks (Fig. 3.2A; Whitmeyer and Karlstrom, 2007). The Wyoming Province consists of temporally and geochemically distinct sub-provinces, including rocks as old as 3.6 Ga and detrital zircon ages as old as 4.0 Ga (Chamberlain et al., 2003; Mueller and Frost, 2006). The Grouse Creek Block in central Idaho contains ca. 2.67–2.50 felsic and ca. 1850 Ma mafic magmatic rocks (Link et al., 2017).

Paleoproterozoic (Trans-Hudson-age; ca. 1.9–1.7 Ga) suture/collisional zones separate the main Archean blocks of western Laurentia. The boundary between the Medicine Hat Block and the Wyoming Province to the south (Mueller et al., 2002) is delineated by the broad Great Falls Tectonic Zone, which records major ca. 1.86–1.73 Ga Paleoproterozoic convergent events including the Great Falls Orogeny and the more temporally and spatially restricted Big Sky Orogeny. Generally, Great Falls Tectonic Zone rocks indicate northwest-dipping subduction, closure of an intervening ocean and eventual amalgamation of the Medicine Hat Block to the Wyoming Province (Mueller et al., 2002; Cheney et al., 2004; Harms et al., 2004; Foster et al., 2006; Alcock et al., 2013; Condit et al., 2015; Gifford et al., 2014; 2018; 2020).

The Vulcan Zone is a Paleoproterozoic collisional belt that records north-dipping subduction between the Archean Medicine Hat–Clearwater block(s) and the southwestern Hearne Province (Eaton et al., 1999; Nieuwenhuis et al., 2014). The Loverna Block, which represents the most southwestern exposures of the Hearne Province, consists of ca. 2.71, 1.82, and 1.78 Ga rocks that are bordered to the north by the ca. 1.85–1.79 Ga Rimbey Arc (Ross et al., 1991).

The Farmington Zone in northeastern Utah contains primarily ca. 2.45 Ga *meta*-igneous rocks and < 2.42 Ga metasedimentary rocks that record upper amphibolite to granulite facies metamorphism at ca. 1.67 Ga (Link et al., 2017; Mueller et al., 2011; Nelson et al., 2011). Although the extent and tectonic significance of the Farmington Zone is uncertain, it likely: (i) separates the Archean Wyoming Province from the Grouse Creek Block to the west, and (ii) records the ca. 1.67 Ga collision of the predominantly late Paleoproterozoic Mojave province with the southern margin of the Grouse Creek–Wyoming provinces (Mueller et al., 2011).

Following assembly of the main Archean blocks of western Laurentia, a long-lived accretionary boundary resulted in the addition of the ca. 1.84–1.70 Ga Mojave province, which comprises a mixture of juvenile and evolved components, and the juvenile ca. 1.80–1.70 and 1.65–1.60 Ga Yavapai and Mazatzal provinces along the southern/ southwestern margin of Laurentia (Bowring and Karlstrom, 1990; Holland et al., 2020). The more evolved isotopic signatures of the Mojave province rocks suggest reworking of a Neoarchean crustal component, which may suggest an early association with East Antarctica (Holland et al., 2018; Wooden et al., 2013). Collectively, the Mojave–Yavapai–Mazatzal provinces may record progressive accretion of separate, predominantly juvenile arc systems (Whitmeyer and Karlstrom, 2007), or represent an extensive arc-backarc system that developed along the Australia–Antarctica margin at ca. 1.8 before their accretion to Laurentia after ca. 1.65 Ga (Gibson and Champion, 2019). Detrital zircon (U/Pb and Lu/Hf) data from the ca. 1.79–1.74 Ga Vishnu basin in the Mojave province shows similar detrital zircon ages with coeval Australia–Antarctica strata and igneous sources, supporting an early (ca. 1.8 Ga) Mojave–Australia–Antarctica connection (Holland et al., 2015, 2018). Additionally, recognition of ca. 1.6–1.5 Ga metavolcanic rocks is increasing in the southwestern U.S., including a preliminarily dated 1505 ± 6 Ma ash fall tuff within the Yankee Joe basin (Doe and Daniel, 2019), and the 1588 ± 7 Ma Blue Springs metarhyolite within the nearby Manzano group (Holland et al., 2020).

Several unconformity-bounded Paleo–Mesoproterozoic sequences (Fig. 3.3), including: 1) the Paleoproterozoic Gold Cup Quartzite (Doughty and Chamberlain, 2008); 2) the Mesoproterozoic (ca. 1.47–1.38 Ga) Belt Supergroup and; 3) the ca. <1.37 Ga Deer Trail Group (refined to <1.30 Ga by this work; Ross et al., 1992; Box et al., 2020) overlie basement rocks of the Clearwater Block in the Priest River region. Within the Priest River metamorphic complex, metamorphosed Belt Supergroup strata host a small (<3 km^2) tectonically interleaved slice of ca. 1.58 Ga orthogneiss (the Laclede Gneiss) whose petrogenesis is poorly understood but represents the only known ca. 1.6–1.5 Ga granitoid in western Laurentia. As such, the Laclede Gneiss is suggested to be a piece of Australia that was stranded during Nuna breakup (Doughty and Chamberlain, 1996, 2008; Lewis et al., 2010; Lewis et al., 2020).

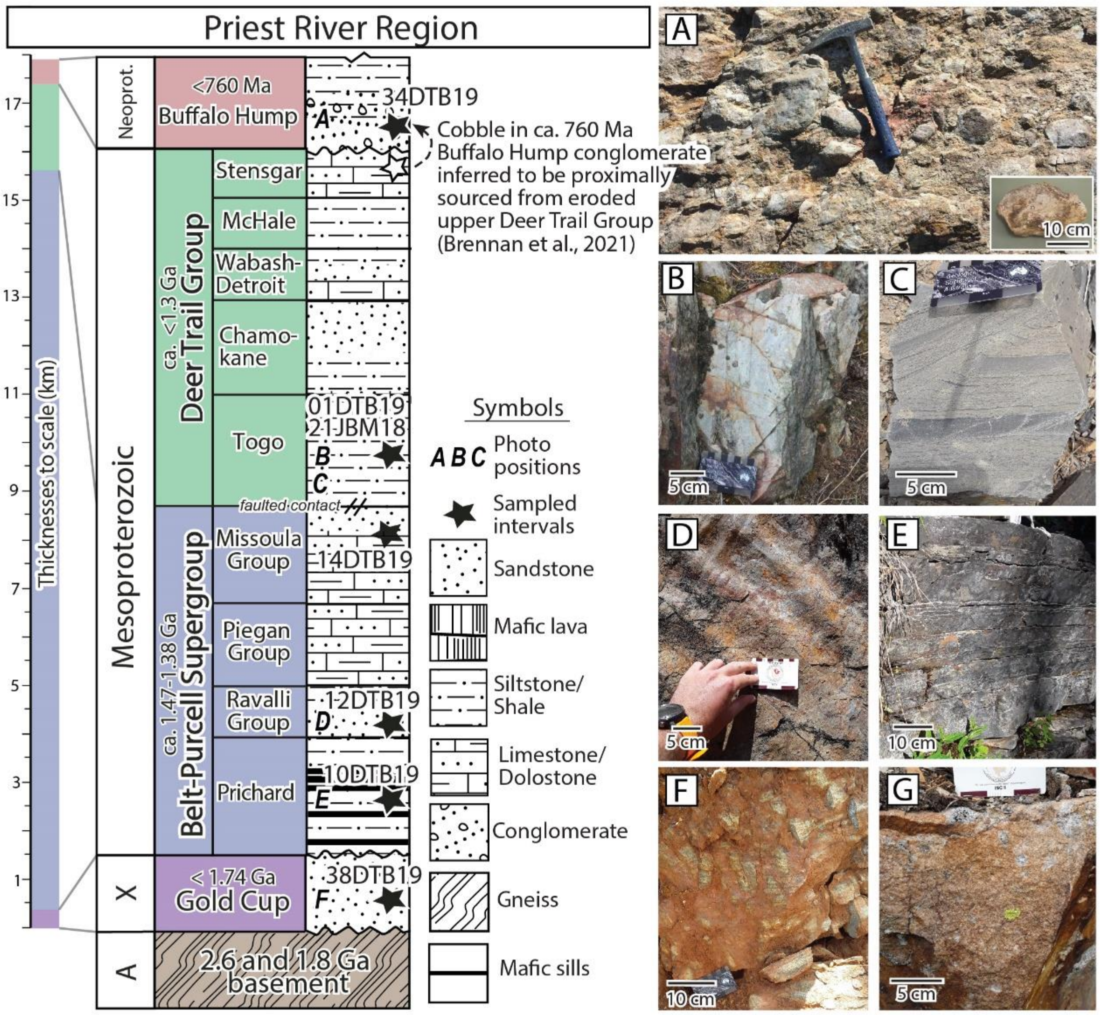

(Previous page) **Fig. 3.3.** Composite stratigraphic diagram of Paleo–Mesoproterozoic rocks from the Priest River region. Approximate stratigraphic thicknesses from Miller et al., (1999) and Lewis et al., (2020), and are only shown to scale on the far left of the diagram. Sampled and photographed intervals indicated. Field photographs include A) A conglomerate bed in the ca. 760 Ma Buffalo Hump Formation, and quartzite cobble (34DTB19) that has a likely eroded Deer Trail Group provenance (Brennan et al., 2021a), B) Fine-grained sandstone bed present in the Togo Formation (basal Deer Trail), C) Laminated mudstone showing soft-sediment deformation that is common in the Togo Formation, D) Ripples in Ravalli Group sandstones (Belt Supergroup), E) Laminated sandstones of the Prichard Formation (Lower Belt Supergroup), and F) Poorly exposed, but coarse-grained sandstone of the Gold Cup Formation. Photograph G is not from the Priest River region but rather shows coarse-grained to pebbly sandstone of the pre-Belt Supergroup Neihart Formation. The Neihart Formation crops out along the eastern edge of the Belt Basin, ~500 km east of the Priest River region (see Fig. 3.2A).

3.2.2. Proterozoic sequences in the Priest River region

3.2.2.1. Paleoproterozoic Gold Cup Quartzite and potential correlatives

An approximately 100 m-thick coarse pebbly quartzite (‘Quartzite of Gold Cup Mountain’, hereafter referred to as the Gold Cup Quartzite) unconformably overlies ca. 2.67 Ga Neoarchean and ca. 1.87 Ga Paleoproterozoic orthogneisses in the Priest River complex (Fig. 3.2B). Although its upper contact with the overlying lower Belt Supergroup equivalents is mylonitized, it is likely a tectonized unconformity (Fig. 3.3; Doughty et al., 1998; Doughty and Chamberlain, 2008; Lewis et al., 2010; Lewis et al., 2020). Doughty and Chamberlain (2008) analyzed 18 detrital zircon grains from the Gold Cup Quartzite and found ca. 2.65 Ga and ca. 1.8–1.93 age components. Based on these data, Doughty and Chamberlain (2008) favored correlation of the Gold Cup Quartzite with the Paleoproterozoic Neihart Formation that crops out along the eastern margin of the Belt Basin, consistent with the lithostratigraphic correlation proposed by Winston et al. (1989).

The ~ 300 m-thick Neihart Formation (the Neihart Quartzite) crops out in west-central Montana (Fig. 3.2A), and unconformably overlies ca. 1.87 Ga basement of the Great Falls Tectonic Zone (Mueller et al., 2002). The Neihart Formation was part of a widespread fluvial-nearshore sand sheet that was deposited prior to deposition of the Belt Supergroup (Freeman and Winston, 1987; Schieber, 1989). Detrital zircon provenance study indicated that the Neihart Formation contains primarily 1.9–1.7 Ga, and ca. 2.6 Ga detrital zircon components that do not support early correlations with lower Belt Supergroup strata from the main part of the basin further west (Mueller et al., 2016). Rather, these results suggest that deposition of the Neihart Formation occurred sometime after ca. 1.7 Ga, possibly during extensional collapse of the Great Falls Orogen, approximately 200 million years prior to onset of Belt Basin subsidence at ca. 1.47 Ga (Mueller et al., 2016).

Other possibly pre-Belt Supergroup quartzites crop out ~250 km southwest of the Little Belt Mountains, near Argenta Montana, where a ~150 m-thick mature quartzite (the quartzite of Argenta) is overlain by Cambrian strata in a shallow, west-dipping, angular unconformity (Sears et al., 2010). The base of the quartzite of Argenta is not exposed. Approximately 150 km southeast of the Priest River complex, along the western edge of the Clearwater complex, another suggested pre-Beltian quartzite, the Marble Creek Quartzite, unconformably overlies ca. 1.86 Ga orthogneiss and is overlain by Lower Belt Supergroup rocks in a likely faulted relationship (Baldwin et al., 2016).

In southeastern British Columbia, ~500 km northwest of the Little Belt Mountains, quartz arenite of the Fort Steele Formation occurs below Mesoproterozoic Belt Supergroup strata (Hoy, 1992; Ross and Villeneuve, 2003). However, the Fort Steele Formation is much thicker (>2000 m) than the other suggested pre-Belt Supergroup quartzites and shows a more varied composition. Generally, quartzite of the Fort Steele Formation fines upwards into deeper water facies siltstones and mudstones, possibly of the basal Belt Supergroup, and likely records an extensive fluvial system that flowed predominantly to the north-northwest (Hoy, 1992).

3*.2.2.2. Mesoproterozoic Belt–Purcell Supergroup*

The relatively fine-grained siliciclastic and carbonate rocks comprising the thick (up to 18 km) Mesoproterozoic (ca. 1.47–1.38 Ga) Belt Supergroup (known as the Purcell Supergroup in Canada) crop out over a large area (>200,000 km^2) throughout Montana, Idaho, eastern Washington, and southern British Columbia (Fig. 3.2A; Sears, 2007; Lonn et al., 2020; Mueller et al., 2016). The Belt Basin stratigraphy consists of the Lower Belt, Ravalli, Piegan, and Missoula groups (e.g. Link et al., 1993; Sears, 2007; Winston 2007; Fig. 3.3). In the Priest River region, the Lower Belt Group consists of the Prichard Formation, a >6 km-thick sequence of turbidities intruded by ca. 1469 Ma mafic sills that exhibit textures suggesting they were emplaced into unconsolidated sediments (Anderson and Davis, 1995; Sears et al., 1998; Schandl and Davis, 2000).

The Lower Belt Group grades upwards into the Ravalli Group, which shows different western and eastern facies. In the Priest River region, the western facies of the Ravalli Group consist of the Burke, Revett, and St. Regis formations (Lewis et al., 2020; Miller et al., 1999), which are generally fine-grained quartzites that extend eastward and represent a broad alluvial apron formed by massive sheet floods.

Overlying the Ravalli Group, the Piegan Group includes the Wallace and Helena formations. The Helena Formation consists of carbonates containing stromatolitic horizons. Sand-carbonate cycles that commonly include hummocky cross-stratification characterize the overlying Wallace Formation (Winston, 2007).

The stratigraphically highest, Missoula Group marks a return to dominantly siliciclastic facies with widespread fluvial-alluvial fan deposition (Sears, 2007). A localized 1401 ± 6 Ma tuff (the "Libby tuff"; all uncertainties given at 2σ) occurs ~1.7 km from the top of the Missoula Group, and constrains the depositional age of upper Belt Supergroup rocks to ca. 1.4 Ga (Evans et al., 2000). Strata in the southwestern part of the Belt Basin (in the Lemhi Subbasin of east-central Idaho), are termed the Lemhi Group and mostly contain Missoula Group equivalents (Winston et al., 1999; Link et al., 2007). In central Idaho (approximately 80 km west of Argenta, Montana; Fig. 3.2A), Lemhi Group rocks are intruded by ca. 1370 Ma granites and contain detrital zircon grains as young as ca. 1380 Ma (Doughty and Chamberlain 2008; Stewart et al., 2010; Link et al., 2016). Collectively, sedimentary features of Belt Supergroup rocks record their deposition within a vast, intracratonic, epeiric sea or lake. This sea may have opened to the ocean to the northwest, and likely experienced intermittent fluvial, playa, and lacustrine depositional systems (Winston, 2016; Winston and Link, 1993; Pratt, 2001).

Strata of the Lower Belt, Ravalli, and Piegan groups are interpreted to record provenance from both eastern (Laurentian) and western (non- Laurentian) sources (Ross and Villeneuve, 2003; Lewis et al., 2007). Specifically, these rocks contain ca. 1610–1490 Ma "North America Magmatic Gap" (NAMG) detrital zircons, which do not have igneous sources within Laurentia (e.g. Ross and Villeneuve, 2003). Consequently, these NAMG-grains are thought to record provenance from non-Laurentian terranes likely now located in Australia (Ross and Villeneuve, 2003; Fanning and Link, 2003) or possibly Antarctica or South China (e.g. Goodge et al., 2017; Xu et al., 2019; Li et al., 2008b).

Box et al. (2020) contended that NAMG zircon grains within the westernmost Missoula Group suggest a connection to a non-Laurentian source until at least ca. 1390 Ma. In rocks of the Missoula Group to the east of the Priest River Complex, NAMG zircon grains are absent and detrital populations comprise mostly juvenile (positive εHf*t*) ca. 1770–1640 Ma zircon grains interpreted to reflect sources from southwestern Laurentia (e.g. Ross and Villeneuve, 2003). Correlative strata in the Lemhi Subbasin contain similar age-populations, and paleocurrent indicators suggest a source to the south (Stewart et al., 2010; Link et al., 2016). The absence of NAMG grains in upper Belt Supergroup rocks, including the Missoula Group and Lemhi Group strata, is commonly interpreted to suggest a switch to sources in southern Laurentia and reorganization of drainage patterns associated with Nuna rifting (Ross and Villeneuve, 2003) and/or onset of the Picuris orogeny in southern Laurentia (Daniel et al., 2013).

Generally contemporaneous ca. 1.45 Ga Laurentian basin formation is noted ~1,500 km to the north of the Priest River region within the (1460–1420 Ma) PR1 basin (Medig et al., 2014) and ~1,000 km to the south of the Priest River region in the (1475–1450 Ma) Trampas and (1488–1436 Ma) Yankee Joe–Blackjack basins and correlatives (Doe et al., 2013; Daniel et al., 2013; Jones et al., 2015; Fig. 3.1). Collectively, Medig et al. (2014) interpreted the formation of these approximately contemporaneous basins to suggest a ca. 1.47–1.40 Ga period of Nuna extension, likely without full continental separation, along a north–south axis.

3.*2.2.3. Late Mesoproterozoic Deer Trail Group*

An estimated 2.5 km-thick package of argillite, siltite, quartzite and dolomite of the poorly-exposed Deer Trail Group consisting of the Togo, Chamokane, Wabash-Detroit, McHale, and Stensgar formations crops out in northeastern Washington State (Fig. 3.2B; Miller, 2000). The basal Togo Formation consists of >650 m of chiefly grey argillite, with a few coarser quartzose beds within the Togo Formation (Fig. 3.3B). Finer-grained intervals of the Togo Formation contain sub-millimeter- to 10 cm-thick bedding, sometimes graded and/or with erosional bases that range from wavy to parallel except where they are disturbed by soft-sediment deformation (Fig. 3.3C). Miller and Whipple (1989) reported syneresis cracks and fluid escape structures within this unit. The lower contact of the Togo Formation is faulted everywhere (Miller, 2000).

The Chamokane Creek Formation overlies the Togo Formation, and is perhaps the least exposed unit of the Deer Trail Group. The Chamokane Creek Formation is comprised of ~600 m of fine-grained sandstone interbedded with minor pale-grey/green argillite. Overlying the Chamokane Creek Formation is the Wabash-Detroit Formation, which is an approximately 400 m-thick, predominantly dolomitic unit with minor argillite and siltite. Overall, the Wabash-Detroit Formation bears an overall lithological similarity to the Togo Formation, but locally contains stromatolitic beds. The McHale Slate stratigraphically overlies the Wabash-Detroit Formation, and includes ~370 m of dark-grey, green and lavender-gray argillite and shale/slate. The McHale Slate also includes extensive soft-sediment deformation that may increase in abundance toward the northeast (Miller and Whipple, 1989).

The Stensgar Dolomite is the uppermost unit of the Deer Trail Group and consists of ~250 m of dolomite with sparse algal structures (Fig. 3.3), oolites, and nodular chert. Near the inferred top of the unit, Miller and Whipple (1989) reported probable salt casts. Evans (1987) identified no major unconformities within the Deer Trail Group but documented a significant unconformity beneath the (<760 Ma; Brennan et al., 2021a) overlying Buffalo Hump Formation that locally thins the underlying Stensgar Dolomite.

Deer Trail Group strata crop out only in the hanging-wall of the northwest-dipping Jumpoff Joe Fault (Fig. 3.2B; Miller, 2000). This fault was most recently active as a Mesozoic thrust fault. However, the absence of Deer Trail Group rocks in the footwall (to the east) of this fault, and the presence of reworked cobbles of the Deer Trail Group in the <760 Ma Buffalo Hump Formation strata, suggest that this Mesozoic thrust fault is a reactivated Neoproterozoic normal fault (Miller, 2000; Brennan et al., 2021a).

3*.2.2.3.1. Detrital zircon provenance.* Initially, the Deer Trail Group was correlated with the upper Piegan Group and lower Missoula Group of the Belt Supergroup, that only crop out east (in the footwall) of the Jumpoff Joe Fault based on similarities in sedimentary facies (Fig. 3.2B, 3; Miller and Whipple, 1989). However, subsequent detrital zircon provenance analysis (Box et al., 2020) suggested a 1364 ± 35 Ma maximum depositional age (MDA) for the lower Deer Trail Group (Togo Formation), indicating that the entire Deer Trail Group is likely younger than the upper Belt Supergroup. The remainder of the detrital zircon ages within the Deer Trail Group consist primarily of ca. 1.9 to 1.6 Ga and ca. 1.4 Ga age components (Box et al., 2020).

The ~500 m-thick, interbedded siltstone and coarse (locally conglomeratic) quartzite of the Buffalo Hump Formation unconformably overlies upper Deer Trail Group rocks (Fig. 3.3; Evans, 1987; Brennan et al., 2021a). Sandstones from the Buffalo Hump Formation are dominated by ca. 1.2–1.0 Ga detrital zircon grains (Box et al., 2020), but contain a small population of ca. 760 Ma detrital zircon grains, indicating deposition during rifting related to early Rodinia breakup (Brennan et al., 2021a). Quartzite cobbles from conglomerate channels within the Buffalo Hump Formation have a proximal upper Deer Trail Group source based on their large size and similarity of detrital zircon ages (Box et al., 2020; Brennan et al., 2021a). This suggests removal of an unknown thickness of Deer Trail Group strata during the late Tonian–Ediacaran breakup of Rodinia.

The late Tonian Buffalo Hump Formation is unconformably overlain by <720 Ma Windermere Supergroup correlative strata (Miller, 2000; Brennan et al., 2021a). Cryogenian and Ediacaran rocks of the Windermere Supergroup are widespread in this region of the Cordilleran margin (e.g. Lund et al., 2010; Yonkee et al., 2014; Brennan et al., 2020) and record "Snowball Earth" glacial intervals and poorly-dated rift-related magmatism (Lund and Cheney, 2016).

3.2.3 The East Kootenay event: Termination of Belt Supergroup deposition

A variety of geo- and thermochronometers applied to Belt Supergroup rocks from along the western extent of the Belt Basin record an enigmatic ca. 1.38–1.3 Ga tectono-thermal event, which is commonly associated with Pb–Zn–Ag and Co–Cu ± Au strata-hosted mineralization (Doughty and Chamberlain, 1996; McFarlane and Pattison, 2000; Zirakparvar et al., 2010; Nesheim et al., 2012; McFarlane and Corfu, 2015; Pattison and Seitz, 2012; Slack et al., 2020; Bookstrom et al., 2016). Early work in southern British Columbia suggested that Belt Supergroup strata must have undergone a period of tilting, gentle folding, erosion, and bimodal intrusion prior to deposition of unconformably overlying late Neoproterozoic and Cambrian strata. Some workers considered these observations to represent an East Kootenay "orogeny", reflecting a (oblique?) collision between Laurentia and a western terrane that terminated deposition of the Belt Supergroup at ca. 1.38–1.30 Ga (McFarlane and Corfu, 2015; McMechan and Price, 1982). Conversely, others have suggested that the ca. 1.38–1.30 Ga East Kootenay event was rather a period of basin rifting, renewed subsidence, and bimodal magmatism that shortly preceded the end of deposition within the Belt Basin (Doughty and Chamberlain, 1996; Pattison and Seitz, 2012).

3.3. Field relations and sample descriptions

To evaluate correlations and provenance interpretations of Paleo- to Mesoproterozoic strata in the Priest River region, existing detrital zircon U–Pb datasets were compiled and additional samples were collected from target stratigraphic intervals for further detrital zircon analysis (U–Pb and Lu–Hf isotopes; Table 1). The stratigraphically-lowest sampled interval was from the core of the Priest River

Complex (Lewis et al., 2020). This sample (38DTB19; Fig. 3.3F) was collected from poorly-exposed, coarse-grained, locally pebbly, Gold Cup Quartzite on the east side of Gold Cup Mountain. Here, the Gold Cup Quartzite overlies Archean igneous basement rocks and is approximately 120 m thick. In turn, a probable unconformity separates the Gold Cup Quartzite from overlying metamorphosed Lower Belt Supergroup strata (Miller et al., 1999; Doughty et al., 1999; Doughty and Chamberlain, 2008; Lewis et al., 2020). To evaluate the regional extent of potential pre-Belt Supergroup units, approximately 500 km east of the Priest River region within the Little Belt Mountains, a sample (82DTB19) of the Neihart Quartzite, a potentially Gold Cup Quartzite correlative (e.g. Doughty and Chamberlain, 2008; Lonn et al., 2020; Mueller et al., 2016), was collected from shallowly-dipping, coarse-grained to pebbly, thickly-bedded, cross-stratified quartzite (quartz arenite) (Fig. 3.3G).

West of the Newport Fault, a relatively intact stratigraphic section of Belt Supergroup rocks dips to the west and is offset by small-scale faults (Lewis et al., 2020). These rocks progress up section to the west (Miller, 2000), where upper Belt Supergroup rocks (or perhaps lowermost Deer Trail Group equivalent rocks; Box et al., 2020) are unconformably overlain by lower Paleozoic strata. In stratigraphic order, a fine-grained sandstone from the Lower Belt Supergroup (Prichard Formation; Fig. 3.3E; 10DTB19) was sampled. Approximately 8 km west of the Prichard Formation sample, medium-grained quartzite of the Revett Formation of the Ravalli Group, was sampled (Fig. 3.3D; 12DTB19). Approximately 3 km southwest of the Revett Formation sample, and ~800 m below the overlying sub-Cambrian unconformity that likely removed most Deer Trail Group strata here (Box et al., 2020; Brennan et al., 2021a), a fine-grained cross-laminated sandstone bed (sample 14DTB19) was sampled from within the predominately argillite sequence of the Snowslip Formation of the Missoula Group.

Deer Trail Group rocks are only mapped west (in the hanging wall) of the Jumpoff Joe Fault (Miller, 2000; Fig. 3.2B). Approximately 20 km southwest of the sampled Belt Supergroup section, an extensively faulted but relatively complete stratigraphic section of the Deer Trail Group is present. In this region, two samples (21JBM18 and 01DTB19; Fig. 3.3B) were collected (~15 km apart but broadly along strike) from the coarsest, medium-grained quartzite interval of the basal Deer Trail Group (Togo Formation) based off the mapping of Evans (1987) and Campbell and Raup (1964).

We also report new Lu–Hf detrital zircon data from a quartzite cobble within the ca. 760 Ma Buffalo Hump Formation that unconformably overlies upper Deer Trail Group. Brennan et al., (2021a) reported the U–Pb ages of the same detrital zircon grains from these cobbles (34DTB19) that are very similar in age to those in upper Deer Trail Group rocks (Box et al., 2020). This suggests that the cobbles were likely reworked from now eroded upper Deer Trail Group, probably during Neoproterozoic rifting (Brennan et al., 2021a).

Table 3.1

Paleo-Mesoproterozoic compiled and original detrital zircon samples from the Priest River region & potential Laurentian correlatives.

Geologic Unit	Sample number	Location		Analysis method	Isotopic data	Reference	Figure shown
		Latitude (°)	Longitude (°)				
Now eroded (?) Mesoproterozoic Deer Trail Group							
Buffalo Hump conglomerate	34DTB19	48.1312	−117.9977	LA-SS-ICPMS	U-Pb, Lu-Hf	Brennan et al. (2021a) ; this work	Fig. 7; Fig. 8A*; Fig. 9A
Mesoproterozoic Deer Trail Group							
Wabash-Detroit	07SB303A	48.1654	−117.9185	LA-ICPMS	U-Pb	Box et al. (2020)	Fig. 8A*
Wabash-Detroit	07SB302A	48.1596	−117.9264	LA-ICPMS	U-Pb	Box et al. (2020)	Fig. 8A*
Togo Formation	Togo3	48.1526	−117.9087	LA-ICPMS	U-Pb	Box et al. (2020)	Fig. 8A*
Togo Formation	01DTB19	48.0488	−118.0775	LA-SS-ICPMS	U-Pb, Lu-Hf	this work	Fig. 6, 8A*, Fig. 9A
Togo Formation	21JBM18	48.1619	−117.9272	LA-ICPMS	U-Pb	this work	Fig. 6, 8A*
Mesoproterozoic Belt Supergroup							
Snowslip	14DTB19	48.2713	−117.6567	LA-SS-ICPMS	U-Pb, Lu-Hf	this work	discussed in text
Snowslip	08SB203A	48.2740	−117.6573	LA-ICPMS	U-Pb	Box et al. (2020)	Fig. 8A*
Revett	12DTB19	48.2909	−117.6284	LA-SS-ICPMS	U-Pb, Lu-Hf	this work	Fig. 5, 8A*, Fig. 9B, 13*
Revett	07SB306A	48.1247	−117.5834	LA-ICPMS	U-Pb	Box et al. (2020)	Fig. 8A*
Prichard	10DTB19	48.2958	−117.5196	LA-SS-ICPMS	U-Pb, Lu-Hf	this work	Fig. 5, 8A*, Fig. 9B, 13*
Prichard	04RL213	47.4796	−116.2178	LA-ICPMS	U-Pb	Lewis et al., 2010	Fig. 8A*
Prichard	04RL175	48.3747	−116.1934	LA-ICPMS	U-Pb	Lewis et al., 2010	Fig. 8A*
Paleoproterozoic Quartzites							
Gold Cup Quartzite	GC-01-03	48.1772	−116.8646	SHRIMP	U-Pb	Doughty and Chamberlain (2008)	Fig. 8A*; Fig. 10*
Gold Cup Quartzite	38DTB19	48.1908	−116.7945	LA-SS-ICPMS	U-Pb, Lu-Hf	this work	Fig. 4; Fig. 8A*; Fig. 9; Fig. 10*, 11*
Neihart Formation	84DTB19	46.9077	−110.6898	LA-SS-ICPMS	U-Pb, Lu-Hf	this work	Fig. 4; Fig. 8A*; Fig. 9; Fig. 10*, 11*
Neihart Formation	VN-98-01	Stop 1-2 of Winston et al., 1989		SHRIMP	U-Pb	Ross and Villeneuve (2003)	Fig. 10*
Neihart Formation	NQ98-2	46.9130	−110.6983	SHRIMP	U-Pb	Mueller et al. (2016)	Fig. 10*
Quartzite of Argenta	07PL7	45.2977	−112.9126	LA-ICPMS	U-Pb	(Sears et al. (2010)	Fig. 10
Fort Steele Formation	RAR-98-FS	49.74088	−115.74255	SHRIMP	U-Pb	Ross and Villeneuve (2003)	Fig. 10

Note: All Locations converted to datum WGS84.
*data shown compiled with other correlative units
Abbreviations: LA-Laser ablation, SS-Split stream, ICPMS-Iductively Coupled Plasma Mass spectrometry, SHRIMP-Sensitive High Resolution Ion Micro Probe

3.4. Methods

3.4.1 Detrital zircon analysis

Samples for detrital zircon analysis were collected and separated using standard techniques (chipmunk, disc mill or SEL-Frag, Frantz magnetic and heavy liquid separation) at Curtin University, Australia or the University of Wisconsin-Eau Claire, USA. Zircon grains were mounted in epoxy resin, and hand polished to expose grain centers. Cathodoluminescence (CL) or backscatter electron (BSE) images were taken of all zircon grain mounts. All "DTB" samples were imaged using a MIRA3 variable-pressure field-emission scanning electron microscope (SEM) coupled to a CL detector and analyzed for U–Pb, and Lu–Hf isotopes using split-stream laser ablation inductively coupled mass spectroscopy (ICPMS) at the GEOHistory Facility in the John de Laeter Centre at Curtin University, Perth Australia. U–Pb isotopes were measured on an Agilent 7700 s quadrupole ICP-MS for age determination, whereas Lu–Hf isotopes were measured on a Nu Instruments Plasma II MC-ICP-MS to further constrain the provenance and character of the source terranes. Following analysis, data reduction was performed using Iolite v.3.6 software (Paton et al., 2011).

Backscattered electron (BSE) images of sample 21JBM18 were collected at University of Wisconsin – Eau Claire using a Hitachi S-3400 N Variable Pressure SEM and then analyzed for U–Pb isotopes at the University of Arizona Laserchron center with a Photon Machine Analyte G2 Excimer laser paired with a Thermo Element2 single-collector ICPMS. Following analysis, data reduction for 21JMB18 was performed with an Arizona Laserchron python decoding routine and an Excel spreadsheet (E2agecalc).

Detrital zircon age spectra are shown in kernel density estimate (KDE) plots generated with DensityPotter 8.5 (Vermeesch, 2012) with 25 Myr band and bin widths. Peak age labels were rounded to the nearest 5 Ma. For zircon grains with ages younger than 1500 Ma, the $^{206}Pb/^{238}U$ age was used, whereas for zircons older than 1500 Ma the $^{207}Pb/^{206}Pb$ age was used (Spencer et al., 2016). For samples, 10DTB19 and 12DTB19 which have depositional ages of ca. 1470 Ma, the $^{207}Pb/^{206}Pb$ ages are plotted. Only analyses with discordance (calculated as ($^{207}Pb/^{206}Pb$)–($^{238}U/^{206}Pb$))/($^{207}Pb/^{206}Pb$)) <10% to –5% are interpreted as robust and are included in the uni and bivariate KDE plots. Maximum depositional age constraints only use grains that met these criteria and also showed $^{206}Pb/^{207}Pb$ and $^{206}Pb/^{238}U$ ages that overlapped the concordia within 2σ uncertainties (e.g. Spencer et al., 2016). Maximum depositional ages are presented for samples 38DTB19 (Gold Cup Quartzite) and 10DTB19 (Prichard Formation) based on the youngest population with a mean square weighted deviation (MSWD) of ~1 (Coutts et al., 2019; Herriott et al., 2019). Concordia plots and ages were calculated with Isoplot 3.70 (Ludwig, 2008) and IsoplotR (Vermeesch, 2018). The $\varepsilon Hf_{(t)}$ values calculated for all data used the ^{176}Lu decay constant = 1.865 × 10–11 yr^{-1} proposed by Scherer et al. (2001). Chondritic values are after Bouvier et al. (2008): $^{176}Hf/^{177}Hf$ CHUR = 0.282785 and $^{176}Lu/^{177}Hf$ CHUR = 0.0336, where CHUR is the chondritic uniform reservoir. Depleted mantle values are after Griffin et al. (2002): $^{176}Hf/^{177}Hf$ = 0.28325 and $^{176}Lu/^{177}Hf$ = 0.0384.

Where possible, all published (U–Pb and Lu–Hf) data included were recalculated/reselected using the same criteria.

Bivariate kernel density estimates (2DKDEs) were employed to visualize U–Pb/Lu–Hf data distribution and density with 1 εHf_t and 45 Ma bandwidths using the methods and MATLAB code of Spencer et al., (2019). To further assess tectonostratigraphic correlations, and objectively evaluate the relative similarity between datasets, two-dimensional (U–Pb/Lu–Hf) statistical comparison of zircon density distributions utilizing the MATLAB program of Sundell and Saylor (2021) was also employed also using 1 εHf_t and 45 Ma bandwidths. See data repository for additional details.

3.5. Detrital Zircon U–Pb and Lu–Hf results

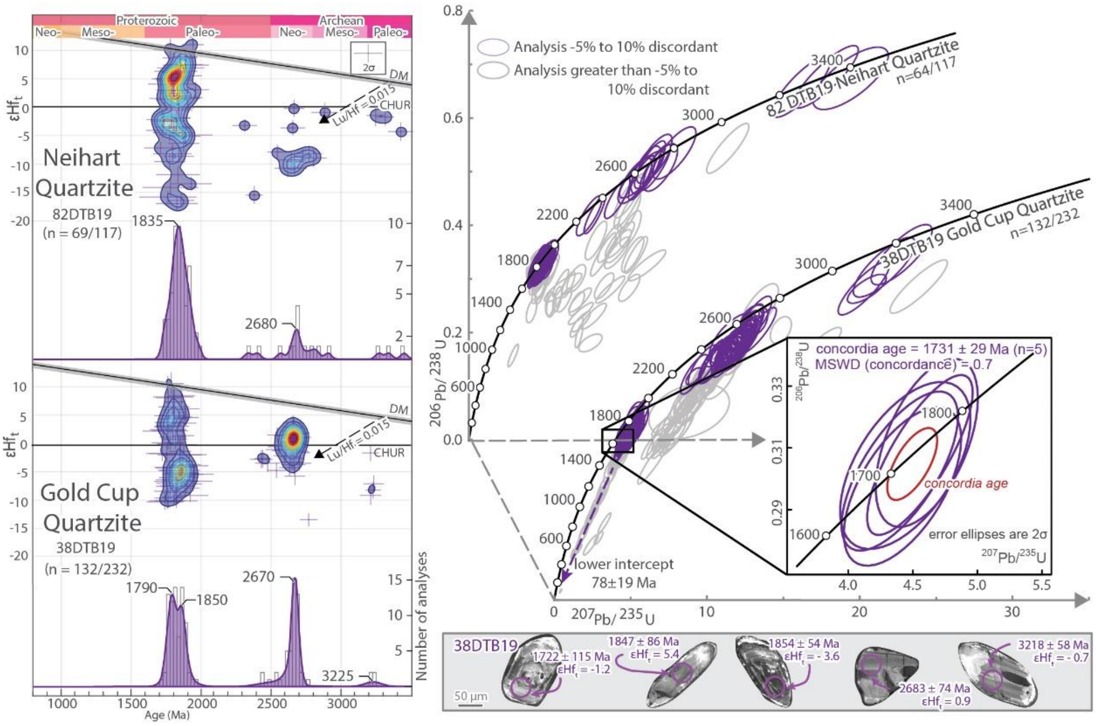

Fig. 3.4. Detrital zircon U–Pb/Lu–Hf for the Neihart Quartzite (82DTB19) and Gold Cup Quartzite (38DTB19) shown in KDE plots, and Wetherill concordia diagrams. In the Wetherill concordia diagram the purple analyses fit within our concordance limits and are reported in the KDE plots. The grey analyses are outside our concordance limits and are omitted from the KDE plots. The concordia inset shows the five youngest concordant analyses (purple) and their 1739 ± 30 Ma Concordia age (red) from sample 38DTB19. Representative zircon CL-images and individual analysis results are shown on the bottom right for sample 38DTB19. Approximate average crustal evolution (Lu/Hf = 0.015) indicated. Abbreviations: DM–depleted mantle, CHUR–chondritic uniform reservoir.

Detrital zircon grains (Fig. 3.4) from the Gold Cup Quartzite (38DTB19) and Neihart Quartzite (82DTB19) are similar in size, shape and appearance. Zircon grains from both samples are generally 80 to 250 μm long, with median aspect ratios (long axis/short axis) around ~1.85 but sometimes exceeding 3. In CL imaging grains from both samples show mostly concentric zoning, with some thin (<10 μm) bright metamorphic rims. U/Pb results show similar age-components with ca. 2.7–2.6 Ga and ca. 1.95–1.7 Ga grains common. Both samples lack zircon grains younger than ca. 1.7 Ga.

In the Gold Cup Quartzite, a ca. 2.67 Ga age-component yields a tight cluster of εHf*t* values from –2 to +3, indicating a CHUR-like Neoarchean source. The younger detrital component shows main age-peaks at 1850 and 1790 Ma and εHf_t values that mostly range from –10 to +10, suggesting similar-aged but isotopically discrete sources. Deposition of the Gold Cup Quartzite occurred after 1731 ± 29 Ma based on a Concordia age constrained by the five youngest concordant analyses with similar εHf*t* values that range from –0.9 to 3.9 (Fig. 3.4).

In the Neihart Quartzite, the ca. 2.68 Ga age-component exhibits εHf_t values ranging from –12 to 0. This is a greater variation in εHf_t than the similar-aged component in the Gold Cup Quartzite, which contain a tight cluster of εHf_t values ranging from –2 to +3. The ca. 1.95–1.7 Ga component in the Neihart Quartzite shows a main age-peak at 1835 Ma and contains a similar range of εHf_t values (approximately –17 to +9) to the temporally equivalent component in the Gold Cup Quartzite.

Detrital zircon grains from the Lower Belt Supergroup (Prichard Formation; 10DTB19), and Ravalli Group (Revett Formation; 12DTB19) are also similar in size, shape and appearance. Zircon grains from both samples are generally 40 to 90 μm long, with median aspect ratios (long axis/short axis) around ~1.9 but sometimes as high as 3, indicating preservation of elongate grains. In CL imaging grains from both samples show mostly faint concentric zoning. U–Pb zircon results show dominant ~1.8–1.5 Ga age-components that contain a significant number of grains with ages within the ca. 1.61–1.49 Ga North American Magmatic Gap ("NAMG"; Ross and Villeneuve, 2003). In the Prichard Formation (Fig. 3.5), the main 1610 Ma age-peak shows a tightly clustered range of εHf_t values between +4 and +9. It also contains two shoulder age-peaks, at ca. 1805 Ma and ca. 1500 Ma. The older ca. 1805 age-component shows more evolved εHf_t values concentrated between –6 to +3, whereas the younger ca. 1500 Ma age-peak shows juvenile εHf_t values (+6 to +10). A Concordia age of the six youngest (<ca. 1500 Ma) concordant analyses yields an age of 1472 ± 17 Ma (MSWD = 0.9), which overlaps within 2σ uncertainty with the 1468 ± 2 and 1469 ± 3 Ma age of mafic sills within the Prichard Formation that likely

intruded unconsolidated sediment and approximate the depositional age (Anderson and Davis, 1995; Sears et al., 1998). These six youngest concordant analyses have similar εHf$_t$ values from +5.3 to +9.8.

In the Ravalli Group sample (Fig. 3.5), the main age-components are at 1720 Ma and 1570 Ma. Both these age components contain mostly positive εHf$_t$ values. Detrital zircon grains from the Missoula Group (Snowslip Formation; 14DTB19) experienced significant Cretaceous lead loss and are mostly discordant precluding further interpretation.

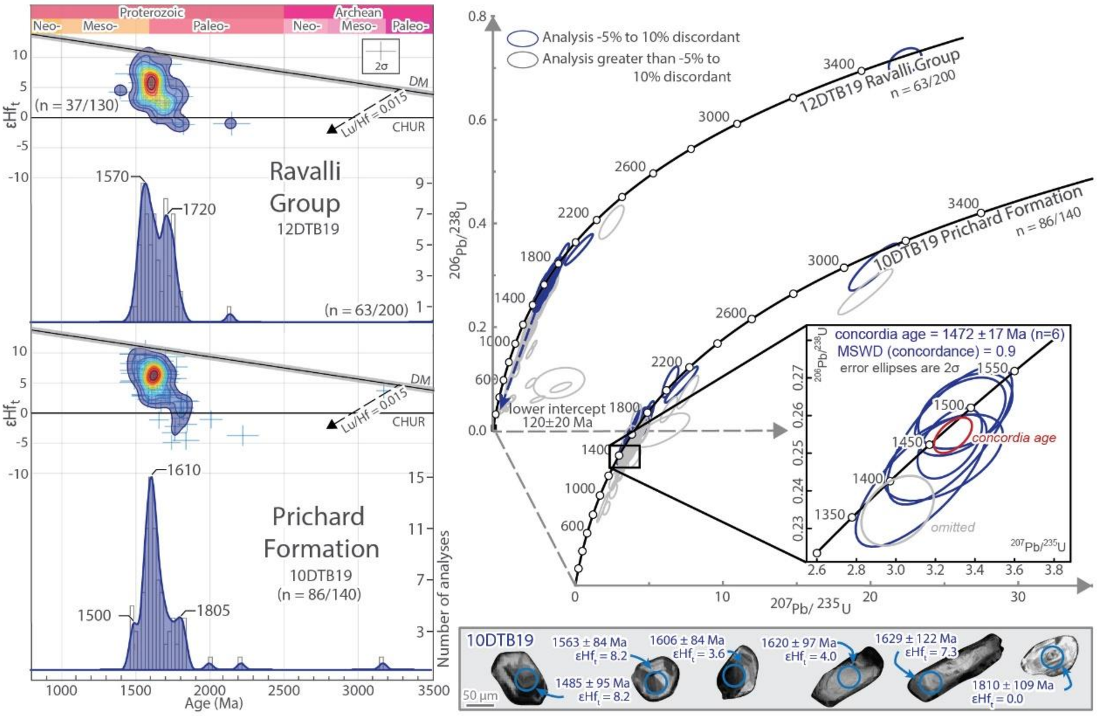

Fig. 3.5. Detrital zircon U–Pb/Lu–Hf for Belt Supergroup samples from the Prichard Formation (10DTB19) and Ravalli Group (12DTB19) shown in KDE plots, and Wetherill concordia diagrams. The concordia inset shows the five youngest concordant analyses (blue) and their 1486 ± 17 Ma Concordia age (red) from sample 10DTB19. In the Wetherill concordia diagram the blue analyses fit within our concordance limits and are reported in the KDE plots. The grey analyses are outside our concordance limits and are omitted from the KDE plots. Representative zircon CL-images and individual analysis results are shown on the bottom right for sample 10DTB19. Approximate average crustal evolution (Lu/Hf = 0.015) indicated. Abbreviations: DM–depleted mantle, CHUR–chondritic uniform reservoir.

Detrital zircon grains from the lower Deer Trail Group (Togo Formation; samples 01DTB19 and 21JBM18) are again similar in size, shape and appearance. Zircon grains from both samples are generally 30 to 80 μm long, with median aspect ratios (long axis/short axis) around 1.4, which indicates overall more equant zircon grains than observed within the Belt Supergroup and Gold Cup Quartzite samples. In CL imaging grains from sample 01DTB19 show mostly faint, darker, concentric zoning. Geochronology results from the Togo Formation indicate an absence of NAMG-age grains, and the presence of age-components younger than ca. 1380 Ma (Fig. 3.6). The Togo Formation samples both show broad-age components from ca. 1.9–1.6 Ga. Sample 21JBM18 shows a single 1710 Ma age-peak, which probably is the amalgamation of several age-populations. In sample 01DTB19, this broad ca. 1.9–1.6 Ga population suggests several discrete subpopulations (Fig. 3.6) with an older age-peak at ca. 1815 Ma characterized by more evolved εHf*t* values (–7 to +1), and two younger populations at ca. 1705 and 1660 Ma. These younger populations contain more CHUR-like/juvenile εHf_t values around +1 to +10. The next youngest main age-component at ~1450 Ma, is present in both samples. In sample 01DTB19, these grains show mostly juvenile εHf*t* values (+2 to +8). These main age-components are similar to Missoula and Lemhi Group samples from further east/southeast (e.g. Stewart et al., 2010; Link et al., 2016).

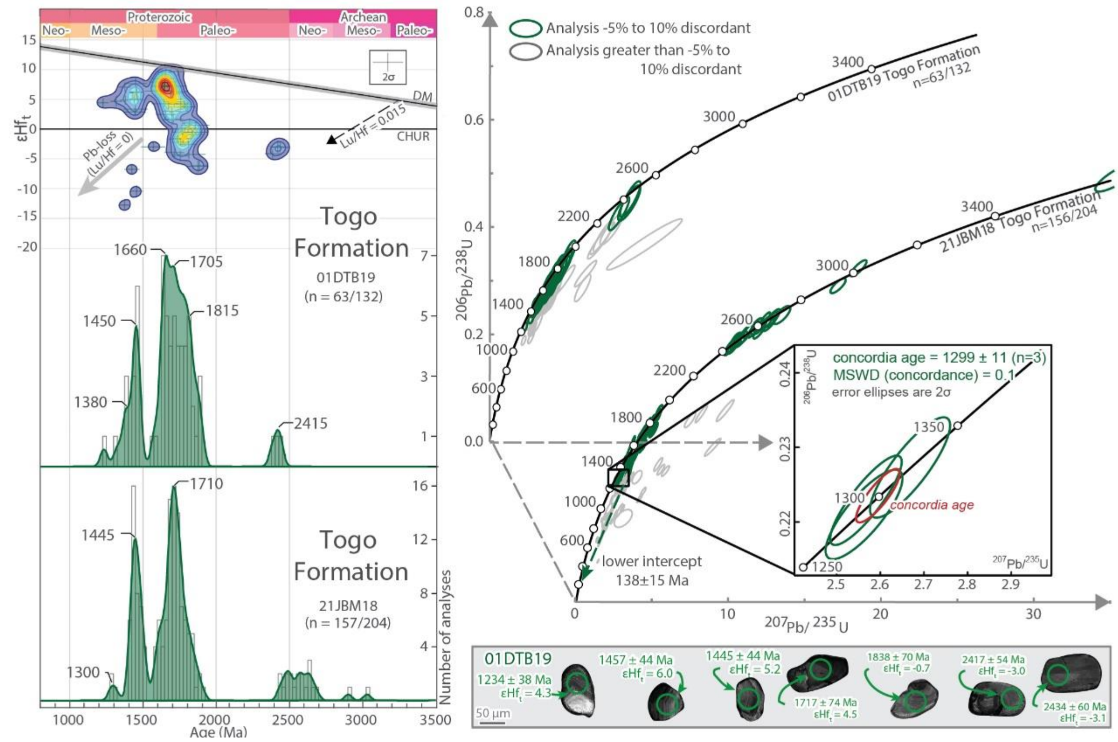

Fig. 3.6. Detrital zircon U–Pb/Lu–Hf results for Deer Trail Group samples from the Togo Formation (01DTB19 and 21JBM18) shown in KDE plots, and Wetherill concordia diagrams. In the Wetherill concordia diagram the green analyses fit within our concordance limits and are reported in the KDE plots. The grey analyses are outside our concordance limits and are omitted from the KDE plots. The concordia inset shows the three youngest concordant analyses (green) and their 1299 ± 12 Ma Concordia age (red) from sample 21JBM18, interpreted as the maximum depositional age of the Deer Trail Group. Representative zircon CL-images and individual analysis results are shown on the bottom right for sample 01DTB19. Approximate average crustal evolution (Lu/Hf = 0.015) indicated. Abbreviations: DM–depleted mantle, CHUR–chondritic uniform reservoir.

We favor a maximum depositional age of 1299 ± 12 Ma for the Deer Trail Group based on a Concordia age of the youngest three overlapping grains in sample 21JBM18 (Fig. 3.6), which was collected from near the base of the group. The other lower Deer Trail Group sample presented here (01DTB19) also contains grains that contain similar $^{206}Pb/^{238}U$ dates of 1324 ± 41 and a youngest single grain date of 1234 ± 38 Ma. A similar sample from the lower Deer Trail Group reported by Box et al., (2020) also contains a single concordant youngest grain at 1264 ± 29 Ma. Therefore, we interpret the Deer Trail Group to be younger than ca. 1.30 Ga.

The U–Pb results from the Buffalo Hump conglomerate cobble (34DTB19) that likely represents eroded upper Deer Trail Group also contain concordant grains with ($^{206}Pb/^{238}U$) crystallization dates of 1188 ± 34, and 1235 ± 39 Ma (Brennan et al., 2021a). These zircon grains are generally larger (lengths of 80 to 200 μm) than the grains found within the stratigraphically lower Deer Trail Group samples but also contain mostly lower aspect ratios (~1.4) and concentric zoning in CL-imaging. Here we present new Lu–Hf data from this cobble (Fig. 3.7) that complement the U-Pb data which indicates the presence of ca. 1.9–1.6 Ga and ca. 1.4 Ga age-components first reported by Brennan et al. (2021a). The ca. 1.9–1.6 Ga component shows a range of εHf*t* values (from –5 to +10) suggesting at least two discrete similar-age but different εHft populations. The youngest single grain analysis date of 1188 ± 34 Ma from the Buffalo Hump Cobble overlaps with the youngest concordant grains reported by Box et al., (2020) from the upper Deer Trail Group and yields a εHf_t value of +0.2.

Detrital zircons grains within all samples show varying levels of lead-loss. Generalized Discordia lines (calculated in IsoplotR; Vermeesch, 2018) for the Gold Cup Quartzite (38DT19), Belt Supergroup (12DTB19), and Deer Trail Group (21JBM19) samples yield lower intercepts from ca. 138 to 78 Ma. These Cretaceous ages likely reflect the timing of burial during the Sevier orogeny, and are generally consistent with peak metamorphism and magmatism within the Priest River Complex (Stevens et al., 2015, 2016).

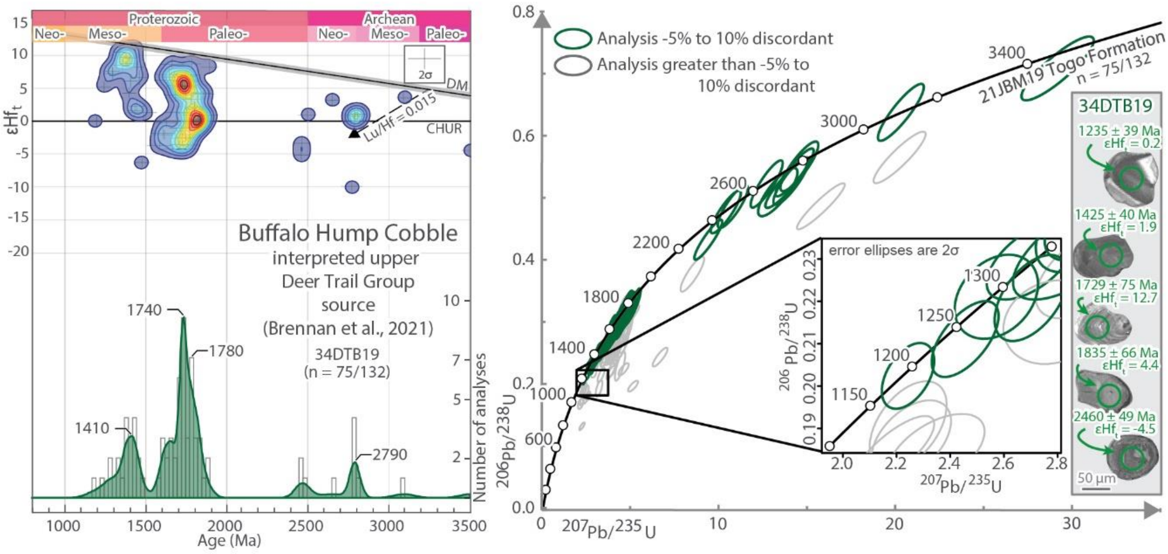

Fig. 3.7. Detrital zircon U–Pb/Lu–Hf results for the Buffalo Hump cobble (34DTB19) shown in a KDE plot and Wetherill concordia diagram. This cobble was collected from the <760 Ma Buffalo Hump Formation and was likely sourced from eroded upper Deer Trail Group (Brennan et al., 2021a). In the Wetherill concordia diagram the green analyses fit within our concordance limits and are reported in the KDE plot. The grey analyses are outside our concordance limits and are omitted from the KDE plot. The concordia inset shows youngest analyses that fit our concordance limits. Solid lines indicated the analyses overlapped with concordia. Representative zircon CL-images and individual analysis results are shown on the right. Approximate average crustal evolution (Lu/Hf = 0.015) indicated. Abbreviations: DM–depleted mantle, CHUR–chondritic uniform reservoir.

3.6. Discussion

3.6.1. The Gold Cup Quartzite: A record of Laurentia assembly prior to final Nuna amalgamation

The relatively high zircon grain aspect ratios within the Gold Cup and Neihart quartzite samples indicate the preservation of elongate grains, suggesting comparably low levels of mechanical abrasion during erosion and transport (e.g. Markwitz and Kirkland, 2018). The detrital zircon spectrum within these samples are dominated by relatively bimodal age distributions at ca. 2.8–2.5 and 1.95–1.7 Ga (Fig. 3.4). These ages are common in the Medicine Hat/Clearwater block, and the Great Falls Tectonic Zone (Fig. 3.8B; Gifford et al., 2020; Vervoort et al., 2016). The Lu–Hf crustal evolution trends suggest sourcing from predominately Meso- and Neoarchean crust that was reworked in the late Paleoproterozoic, but which also received broadly coeval juvenile mantle input. The Neihart quartzite sample (82DTB19) contains significantly evolved ca. 1.8 Ga grains with εHf$_t$ values that range from approximately –10 to –18 (Fig. 9A). Considering that juvenile ca. 1.9–1.6 Ga sources are widespread in Laurentian Trans-Hudson-age arcs and Yavapai–Mazatzal–Mojave terranes in southwestern Laurentia (e.g. Whitmeyer and Karlstrom, 2007), the most evolved grains within this age range may yield more unique provenance constraints. Many of these most evolved ca. 1.8 Ga grains yield εHf_t values similar to those in ca. 1.8 Ga rocks from the Medicine Hat Block (Fig. 3.9A; Gifford et al., 2020). Collectively, the zircon grain shape and U–Pb/Lu–Hf analytical results suggest a proximal provenance from the underlying Medicine Hat–Clearwater Block, and the Great Falls Tectonic Zone. Additional inputs from adjacent similar-age sources such as the Wyoming Craton, and poorly characterized (lacking Lu-Hf data) sources such as the Vulcan Structure, Hearne Province (Lovera Block), and the Rimbey Arc are also possible.

Sears et al. (2010) reported a detrital zircon sample (n = 95) from the Precambrian quartzite of Argenta, along the southern/southeastern margin of the Belt Basin. This sample also shows a bimodal age distribution, with broad peaks at ca. 2.8 to 2.5 and 2.0–1.7 Ga. Based on these ages Sears et al. (2010) favored a correlation to the Neihart Quartzite, an interpretation supported by our new data. The ca. 1.87 and ca. 2.59 Ga age-peaks in the quartzite of Argenta may reflect input from the Grouse Creek Block (Link et al., 2017; Fig. 3.2A). Comparable zircon ages are present in the Gold Cup and Neihart Quartzite, albeit less prevalent (Fig. 3.10).

A single sample in which detrital zircons were analyzed (n = 22) from a stratigraphic interval of the Fort Steele Formation that (probably conformably) underlies lower Belt Supergroup strata at the northern extent of the Belt Basin also shows ca. 1850 and 2.7–2.6 Ga age-peaks (Fig. 3.10; Ross and Villeneuve, 2003). However, the Fort Steele Formation is significantly thicker and contains finer-grained intervals than the Gold Cup and Neihart Quartzite. Additionally, the Fort Steele Formation contains a single concordant ca. 1635 Ma zircon grain, approximately 100 Myr younger than the youngest grains identified in the Gold Cup, Neihart, and Argenta units.

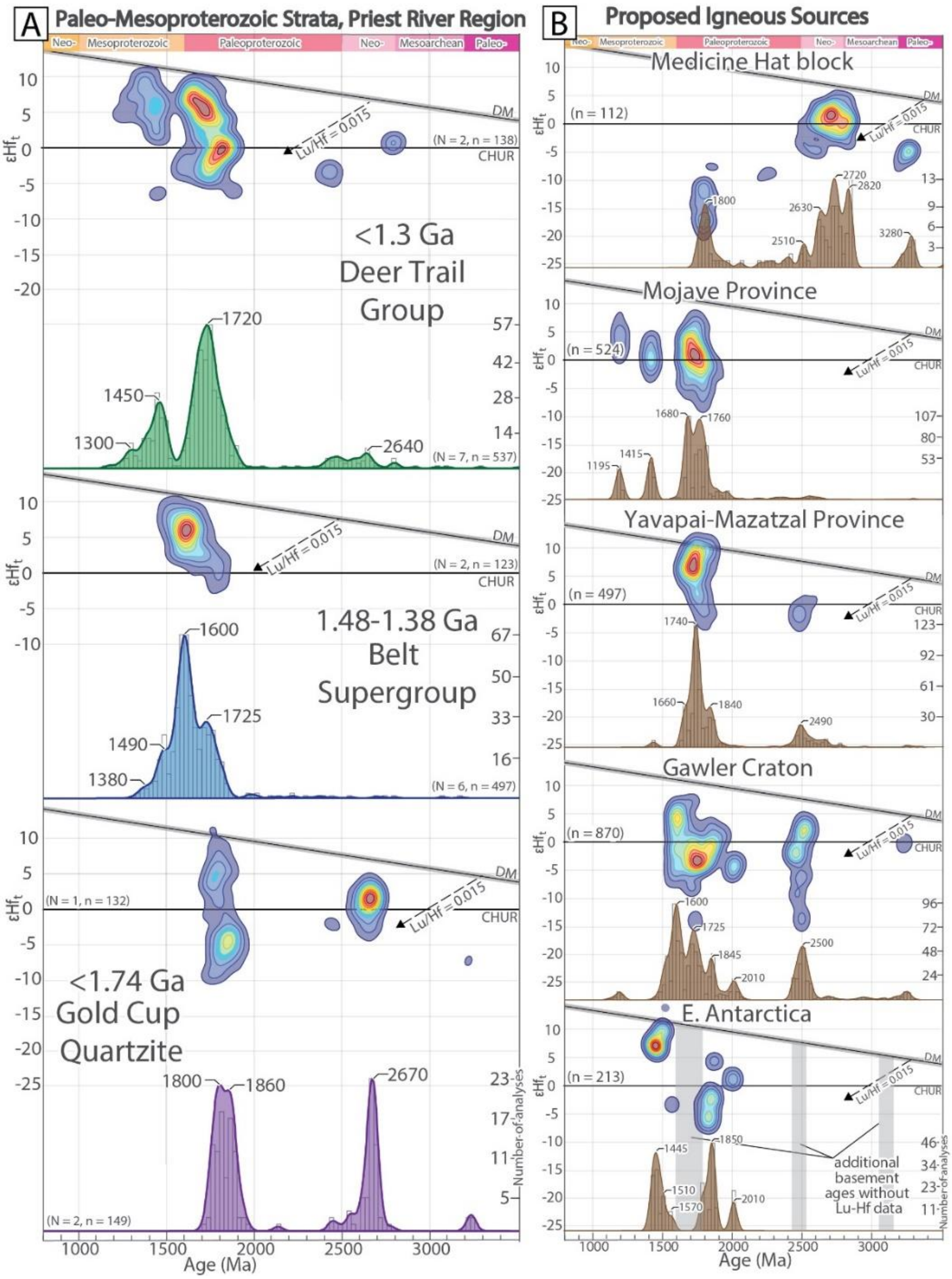

Fig. 3.8. A) Detrital zircon U–Pb and Lu–Hf data for Paleo–Mesoproterozoic strata from the Priest River region including our new U–Pb/Lu–Hf data and compiled U–Pb data. Average crustal evolution trends (Lu/Hf = 0.015) indicated. Data sources are in Table 1. B) Complied zircon U–Pb/Lu–Hf data for proposed igneous basement sources. Data source are in the supporting information, any omission of applicable data is non-intentional. Lu–Hf data is plotted using the bivariate kernel density estimate method of Spencer et al. (2020), note that warmer colors (red) indicate greater data density, while cooler colors (blue) indicate lesser data density. Abbreviations: DM–depleted mantle, CHUR–chondritic uniform reservoir, N = number of samples, n = total individual analyses.

Consequently, based on the lithologies and detrital zircon populations of these units, the Gold Cup, Neihart, and Argenta quartzites were likely deposited during a basin-forming event after ca. 1.74 Ga but prior to formation of the main Belt Basin at ca. 1.47 Ga. This period of Neihart–Gold Cup–Argenta sedimentation possibly occurred during final collision and post-collisional collapse of the Great Falls Orogen (e. g. Mueller et al., 2016) and other contemporaneous adjacent collisional zones (such as the Vulcan structure or the Rimbey Arc), and sourced detritus primarily from proximal Laurentian basement. Widespread sedimentation across the Medicine Hat–Clearwater Block and an inferred source from proximal basement rocks and bounding suture zones suggests that the Paleoproterozoic and Archean basement blocks in this region of Laurentia (e.g. Wyoming, Grouse Creek, Medicine Hat, Clearwater, and Hearne) were close to their current configuration by ca. 1.73 Ga. Importantly, in a broader context, these results indicate a widespread Laurentian provenance for the Priest River region between ca. 1.73–1.48 Ga.

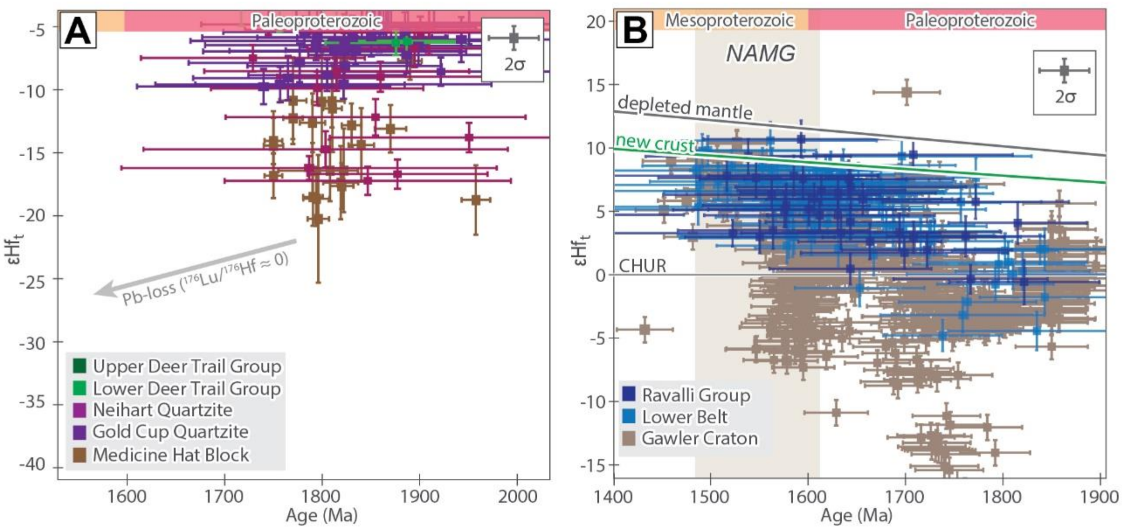

Fig. 3.9. A) U–Pb and Lu–Hf values for the most evolved ca. 1.8 Ga detrital zircon grains in the Gold Cup (dark purple; 38DTB19) and Neihart Quartzite (light purple; 84DTB19), lower Deer Trail Group (light green; Togo Formation; 01DTB19), upper Deer Trail Group (dark Green; Buffalo Hump cobble; 34DTB19), their likely Medicine Hat Block source (Gifford et al., 2018). B) U–Pb and Lu–Hf values for the ca. 1.9 to 1.45 Ga detrital zircon grains from the Lower Belt (light blue; 10DTB19; Prichard Formation), Ravalli Group (dark blue; 12DTB19; Revett Formation) and compilation of magmatic sources from the Gawler Craton of southeastern Australia (Reid and Payne, 2017; Hartnady et al., 2020).

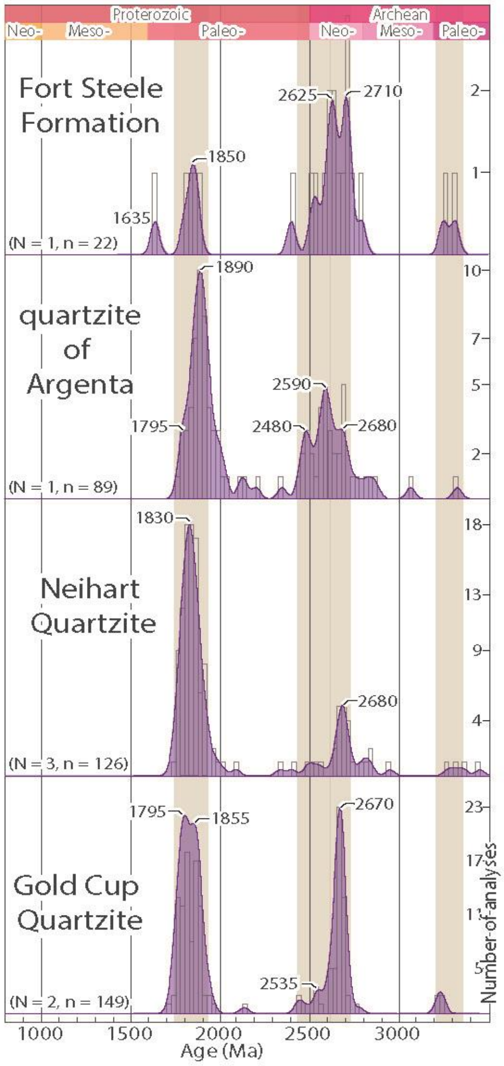

Fig. 3.10. Detrital zircon age-spectra for the Fort Steel Formation (Ross and Villeneuve, 2003), Quartzite of Argenta (Sears et al., 2010), Neihart Quartzite (Mueller et al., 2016; this study), and Gold Cup Quartzite (Doughty and Chamberlain, 2008; this study), and their main age-peaks highlighted indicated. These main age-peaks are consistent with proximal sourcing from the Medicine Hat Block and adjacent Paleoproterozoic collisional zones.

However, for this same general time interval, ca. 1.79–1.74 Ga strata in the Mojave province of southwestern Laurentia (e.g. Vishnu Schist), have been suggested to record a non-Laurentian, East Antarctica and Gawler Craton (southeastern Australia) provenance (Holland et al., 2015; 2018). During the Proterozoic, the East Antarctica and Gawler cratons were connected to form a larger continent called Mawson (Cawood and Korsch, 2008; Payne et al., 2009; Fig. 3.1). To evaluate Paleoproterozoic correlation of the Mawson Continent with Laurentia, statistical analysis of the detrital zircon U–Pb/Lu–Hf data from the Vishnu Schist, ca. 1.7 Ga southeastern Australian units, our studied Neihart–Gold Cup units and Mawson (combined East Antarctica-Gawler Craton) igneous sources was conducted. The statistical results (Fig. 3.11B) indicate that Mawson igneous sources show comparable similarity values with the ca. 1.7 Ga Gawler Craton strata and strata of the Vishnu basin in Mojave province. This similarity supports prior correlations of the Mojave province with the Mawson continent (Goodge et al., 2017; Goodge and Fanning, 2016;

Holland et al., 2015, 2018). However, the Gawler Craton igneous sources indicate a much weaker similarity with the Neihart–Gold Cup units. Notably, the presence of the CHUR-like (in regards to Lu–Hf) ca. 2.67 Ga populations within in the Neihart–Gold Cup, that are likely diagnostic of a Laurentian provenance, are not well represented in Mawson rocks.

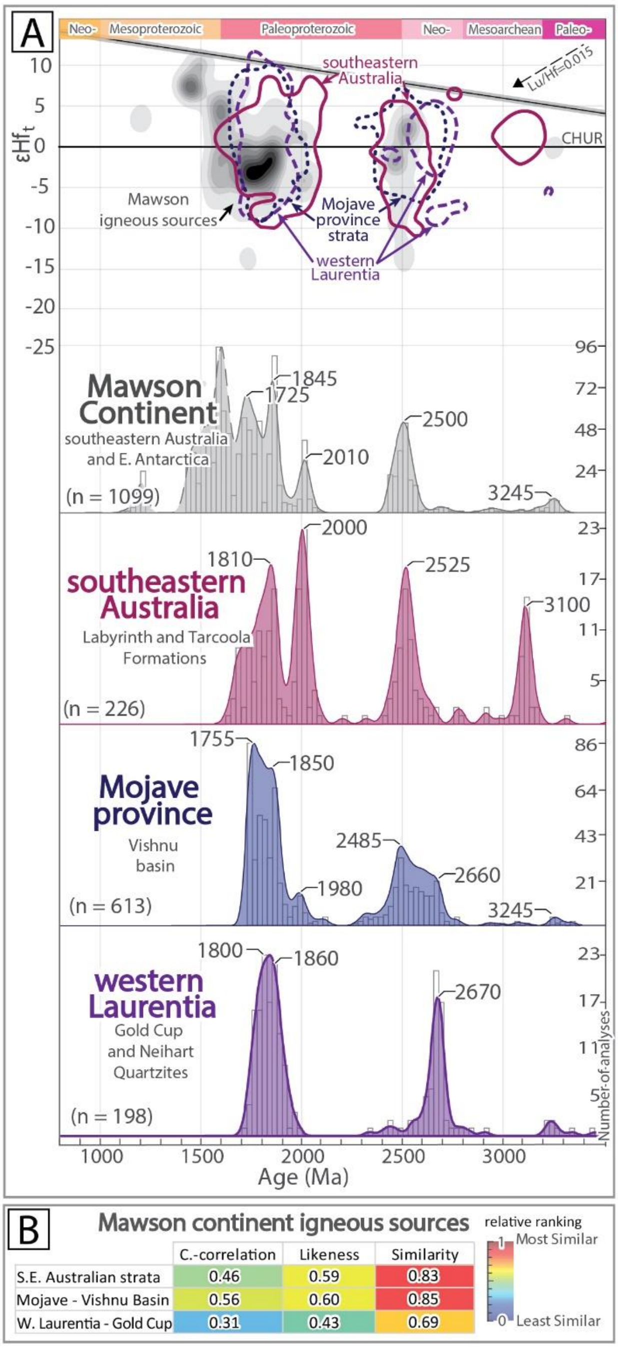

Fig. 3.11. A) U–Pb and Lu–Hf values for (bottom to top): < 1.73 Ga studied western Laurentian strata (Gold Cup, Neihart Quartzite), ca. 1.79 – 1.74 strata in southwestern Laurentia (Vishu basin strata; Holland et al., 2015, 2018; Wooden et al., 2013), ca. 1.7 Ga strata from the Gawler Craton (Howard et al., 2009, 2011; Szpunar et al., 2011), Mawson Continent (southeastern Australia and East Antarctica) igneous sources (Reid and Payne, 2017 and references within). B) Results of two-dimensional (Lu–Hf/U–Pb) statistical comparison (Sundell and Saylor, 2021) of the datasets, with a value of 1 indicating the most similar and 0 the least similar, between Mawson continent igneous sources, and southeastern Australian strata, strata of western Laurentia (Gold Cup and associated units) and southwestern Laurentia (strata of the Vishu basin). See Sundell and Saylor (2021) for further discussion of the Cross-correlation (C.-correlation), Likeness, and Similarity metrics. Please note that only zircon grains with both U–Pb and Lu–Hf values are included in the compilation and statistical comparison, any omission of applicable data is non-intentional.

Consequently, the U–Pb/Lu–Hf detrital zircon data from ca. 1.79–1.74 Ga Vishnu basin strata of the Mojave province are similar to coeval Australia–Antarctica strata and igneous sources. However, there is no evidence that the Priest River region and the surrounding main Archean blocks (Wyoming, Clearwater, Medicine Hat, Hearne, and Grouse Creek) of western Laurentia were exchanging sediments with Australia–Antarctica during the late Paleoproterozoic. As such, Paleoproterozoic strata in the main Archean blocks of western Laurentia do not support a final assembly of Nuna by ca. 1.8 Ga. Instead, we suggest that the Mojave province had an Australia–Antarctica origin and subsequently joined Laurentia during final Nuna assembly at ca. 1.65–1.6 Ga (Gibson and Champion, 2019). Alternatively, the assembly of Australia–Antarctica with Laurentia may have been a prolonged process that generally propagated from north to south along the western margin of Laurentia (modern coordinates) from ca. 1.75 to 1.6 Ga (c.f. Betts et al., 2011; Furlanetto et al., 2013; Kirscher et al., 2019; Pisarevsky et al., 2014a; Nordsvan et al., 2018).

3.6.2. NAMG-age magmatism within the Clearwater Block

The detrital zircon spectrum of the two analyzed Belt Supergroup samples (Prichard Formation and Ravalli Group) along with existing data (Fig. 3.5; 8A) compiled from the Priest River region, contain a large-proportion of grains that fall within the ca. 1610–1490 Ma NAMG, supporting a western non-Laurentian source. These samples were sourced primarily from juvenile (εHf_t = +5 to +7) ca. 1600 Ma and more evolved (εHf_t = –5 to +4) ca. 1720 Ma rocks. The only Laurentian sources, the ca. 1580 Ma Laclede Gneiss in the Priest River Complex (Evans and Fischer, 1986), and the recently identified 1588 ± 7 Ma *meta*-rhyolite (the Blue Springs metarhyolite) in the Mazatzal province of southwestern Laurentian (Holland et al., 2020) are localized and do not span the entire age-range present in Belt Supergroup strata. Although there is no Lu–Hf isotopic data available for the Blue Springs metarhyolite, the Laclede Gneiss has a relatively evolved εHf_t (approximately –6; Goodge et al., 2017). Thus, non-Laurentian sources are required to satisfy the range of detrital zircon ages (as previously noted; e.g. Ross and Villeneuve, 2003; Jones et al., 2015; Lewis et al., 2010) and Lu–Hf compositions identified within western Belt Supergroup rocks.

The Gawler Craton of southeastern Australia records widespread magmatism in pulses from ca. 1.9 to 1.5 Ga, which include: 1) the ca. 1850–1790 Ma Donington–Myola Suite (Fanning et al., 1988; Reid et al., 2008), 2) the ca. 1770–1740 Ma McGregor Volcanics and associated suites (Fanning et al., 1988), 3) the 1620–1605 Ma St Peter Suite (Swain et al., 2008), 4) the 1600–1575 Ma Gawler Range Volcanics–Hiltaba suite, and 5) granites as young as ca. 1500 Ma in the Spilsby Suite (Fanning et al., 2007). The ca. 1620–1605 Ma St Peter Suite and ca. 1600–1575 Ma Hiltaba Suite and Gawler Range Volcanics all show distinctly juvenile compositions with average εHf_t values up to +4 (Fig. 3.8B; Swain et al., 2008; Reid and Payne, 2017).

The juvenile, NAMG-age magmatism of the St. Peter Suite, and Hiltaba and Gawler Range Volcanics are predominately A-type, mantle-derived melts (Chapman et al., 2019) consistent with the U–Pb, and Lu–Hf results for NAMG zircons in the westernmost Belt Supergroup (Fig. 3.9B). Additionally, ($^{40}Ar/^{39}Ar$) thermochronology data records widespread exhumation of the Galwer Craton from ca. 1460–1415 (Reid and Forster, 2021), which is the same as the main timing of Belt Supergroup deposition. This strengthens interpretations of a Belt Supergroup–Gawler Craton connection similar to that proposed by Ross et al. (1992), Ross and Villeneuve (2003), Fanning et al. (2009) and Box et al. (2020), within a proto-SWEAT configured Nuna from at least ca. 1.5 to 1.4 Ga (Fig. 3.12B).

3.6.3. Provenance and age of the Deer Trail Group: A ca. 1.3–1.2 Ga sequence deposited after Nuna breakup but likely prior to Grenville-age tectonism

Upper Belt Supergroup strata (Missoula and Lemhi groups) are intruded by ca. 1370 Ma granites in east–central Idaho and lack detrital zircon grains younger than ca. 1380 Ma (Doughty and Chamberlain 2008; Stewart et al., 2010; Link et al., 2016). Thus, the 1299 ± 12 Ma maximum depositional age for the basal Deer Trail Group falsifies initial correlations of the Deer Trail Group to Piegan and lower Missoula group strata of the Belt Supergroup (Miller and Whipple, 1989). Furthermore, the ca. 80 Myr gap between depositional age constraints on the ca. 1.38 Ga upper Belt Supergroup rocks and the younger basal Deer Trail Group is similar in age and duration to the enigmatic East Kootenay tectono-thermal event. This may suggest that the East Kootenay event separated (or spanned) these two basin-forming intervals. Grenvillian (ca. 1.2–1.0 Ga) detrital zircons are common in nearby Neoproterozoic strata (e.g. Yonkee et al., 2014; Matthews et al., 2018; Box et al., 2020; Brennan et al., 2020; 2021a; 2021b) but are absent in the Deer Trail Group. Consequently, we suggest that deposition of the Deer Trail Group likely occurred prior to the ca. 1.1 Ga main collisional phase of Grenville orogeny in eastern/southeastern Laurentia (e.g. Tollo et al., 2004; Mulder et al., 2017). Alternatively, the Deer Trail Group could be a younger (<1.1 to 0.76 Ga) basin that was not fed by a Grenvillian-source but this is less likely given the relative abundance of Grenville-age detrital zircon grains in strata of this age.

The overall fine-grained siliciclastic and interbedded carbonate character of the Deer Trail Group stratigraphy is consistent with deposition in a shallow intracratonic basin or marine continental shelf depositional environment (Box et al., 2020). The prevalence of soft-sediment deformation may also signify slumping, perhaps influenced by seismically-induced slope instability (e.g. Bose et al., 2012; Pratt and Ponce, 2019; Pratt and Rule, 2021). The broad ca. 1.9–1.6 Ga and 1.45 Ga detrital zircon populations in the Deer Trail Group are similar in age to those found in the Missoula Group (and the correlative Lemhi Group) of the Belt Basin. However, the range of Lu–Hf values of the ca. 1.9–1.6 Ga detrital zircon grains within the Deer Trail Group are a poor match for any single basement source (Fig. 3.8). Consequently, to satisfy the range of ages and Lu–Hf values of the ca. 1.9 to 1.6 Ga zircon grains from Deer Trail Group strata, a mixed provenance from the Medicine Hat Block, Mojave province, and/or recycling from ca. 1.7 Ga Gold Cup/Neihart or ca. 1.4 Ga Lemhi Group strata is required (Figs. 3.8 and 3.12C).

The ca. 1.5–1.3 Ga grains within the Deer Trail Group samples contain εHf_t values mostly between 0 to +12, with a few grains containing evolved ($-\varepsilon Hf_t$) values. The ca. 1.5–1.3 Ga Laurentian midcontinent granite–rhyolite province in southwestern Laurentia contains sources of similar ages with mostly juvenile εHf_t values, consistent with crustal melts sourced from the late Paleoproterozoic juvenile Yavapai–Mazatzal–Mojave provinces they intrude (Bickford et al., 2015). Generally, the most evolved ca 1.45 Ga midcontinent granites intrude along the southeastern edge of the Superior province, in the midcontinent region (Bickford et al., 2015). However, the few detrital zircon grains with particularly evolved εHf_t values (below –5) within the Deer Trail Group, despite still being within our discordance filter, show a higher level of discordance (generally >5% discordant), suggesting these grains may not provide robust provenance constraints. Consequently, the Deer Trail Group detrital zircon components may indicate a mixed distal Laurentian and proximal recycled provenance. Notably, *syn*-depositional magmatism is limited or absent within the Deer Trail Group, and the fine-grained nature of these strata likely precludes significant proximal uplift.

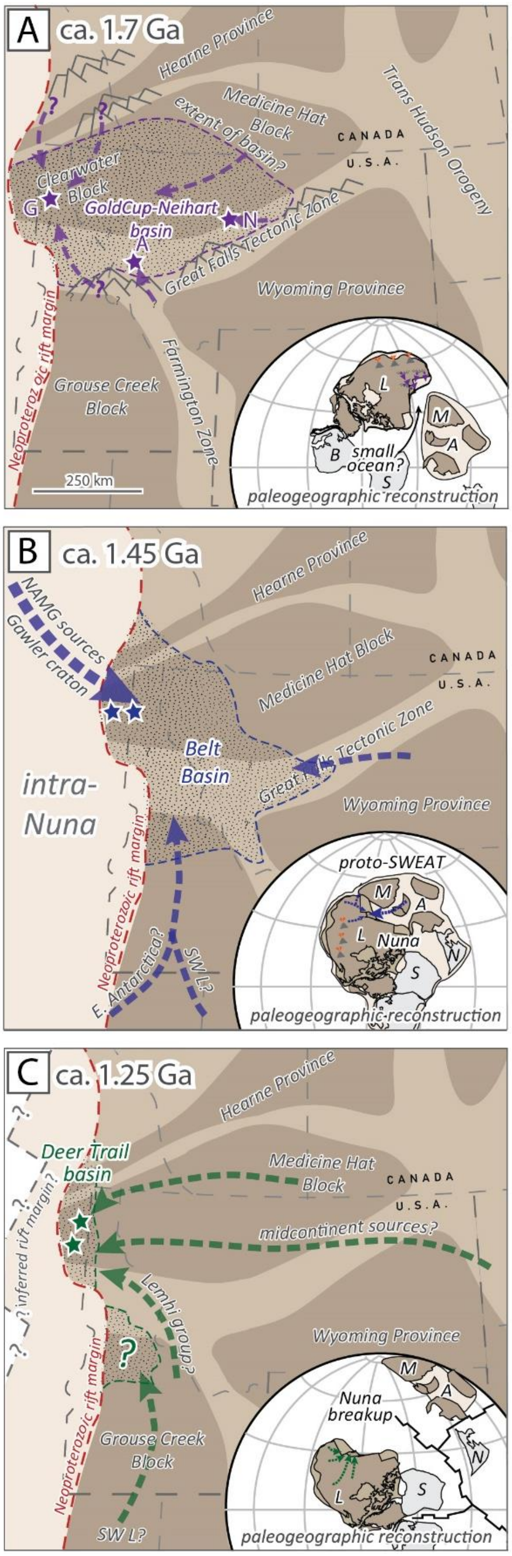

Fig. 3.12. Proposed sedimentary transfer systems (indicated by arrows) to the Priest River region during the A) early assembly, B) tenure, and C) breakup of Nuna with global paleogeographic reconstruction cartoons adopted from Kirscher et al. (2020). At ca. 1.7 Ga (A) during deposition of the Gold Cup Quartzite, and likely coeval Neihart Quartzite, Quartzite of Argenta, and perhaps Fort Steele Formation, proximal Paleoproterozoic suture zones (Great Falls Tectonic Zone; Vulcan Zone, Rimbey Arc) likely supplied sediment into a basin(s) that likely extended across most of the Medicine Hat–Clearwater Block. Abbreviations: A–Quartzite of Argenta, N–Neihart Quartzite, G–Gold Cup Quartzite, S– Fort Steele Formation. (B) At ca. 1.45 Ga during deposition of Belt Supergroup strata. Belt Supergroup strata in the Priest River region are characterized by NAMG detrital zircon populations consistent with sources from Australia–Antarctica, notably the Gawler craton. Belt strata along the eastern and southern extent of the basin, generally lack NAMG zircon grains, and contain ages reflecting southwestern Laurentia (SWL; e.g. Ross and Villeneuve, 2003; Ronemus et al., 2020) or perhaps E. Antarctica sources (Stewart et al., 2010; Link et al., 2016). (C) At ca 1.3 Ga during deposition of Deer Trail Group strata. These rocks generally indicate a mixed Laurentian provenance, and are consistent with depositional during the final interval of the ca. 1.38–1.30 Ga East Kootenay tectono-thermal event. We propose the East Kootenay orogeny recognized in this region, is consistent with Doughty and Chamberlain’s (2008) model of renewed rifting, and subsidence in the Priest River area. This event likely resulted in the end of Belt Supergroup deposition and shortly preceded deposition of the Deer Trail Group coeval with the proposed timing of widespread Nuna breakup (Pisarevsky et al., 2014a,b; Kirscher et al., 2020).

At first order, these stratigraphic observations are less consistent with collisional models for the ca. 1.38–1.30 Ga East Kootenay "orogeny" (McFarlane and Corfu, 2015; McMechan and Price, 1982). Instead, these stratigraphic constraints are more consistent with the East Kootenay "orogeny" as a period of basin rifting and renewed subsidence that marked the end of deposition within the Belt Basin (Doughty and Chamberlain, 2008). We suggest this event shortly preceded deposition of the Deer Trail Group coeval and was coeval with the proposed timing of widespread Nuna breakup at ca. 1.3 Ga (Pisarevsky et al., 2014b; Kirscher et al., 2020). If correct, this implies a late-rift to passive margin setting for deposition of the Deer Trail Group. However, given the relatively limited minimum depositional age-constraints, this is currently speculative. It is unclear how extensive the Deer Trail sequence may have been, although vestiges of its original extent may be present in central Idaho (Isakson, 2017; the "?" basin in Fig. 3.12C).

3.6.4. Smaller block within "proto-SWEAT" reconstructions

Various smaller crustal blocks, notably Hainan Island (with or without the entire Cathaysia Block; Li et al., 1995; 2008a; b; Xu et al., 2019; Yao et al., 2017) and Tasmania (Halpin et al., 2014; Mulder et al., 2015) are suggested to have occupied the region between western Laurentia and East Antarctica/Australia in a proto-SWEAT configured Nuna. The "Missing-Link" model proposes that the Cathaysia Block of South China was an extension of western Laurentia from ca. 1.8 Ga until Rodinia breakup (Li et al., 1995; 2008a). In particular, this model suggests that ca. 1.4 Ga juvenile granites on Hainan Island (Li et al., 2008b; Yao et al., 2017) represent a continuation of the A-type granitic province of southwestern Laurentia (e.g. Bickford et al., 2015). Additionally, the Baoban Complex metasedimentary rocks (including the generally coeval Shilu Group) that also contain NAMG-age detrital zircon age-components (Xu et al., 2019; Yao et al., 2017) are suggested correlatives to Belt Supergroup strata of western Laurentia. However, the Proterozoic configuration of South China, including whether Hainan Island was separate from or part of the Cathaysia or proto-Yangtze Block prior to the mid-Paleozoic is debated (c.f. Yao et al., 2017; Cawood et al., 2020; Liu et al., 2020; Xu et al., 2019). Consequently, Hainan Island may not be a reliable constraint for the location of the larger South China blocks.

On Hainan Island, the ca. 1.4 Ga paragneiss (the Gezhencun "succession") of the Baoban complex contains ca. 1.9–1.4 Ga detrital zircon grains, including some ca. 1.6–1.5 Ga NAMG grains. Based on limited Lu–Hf data ($n = 21$; Xu et al., 2019), these ca. 1.9–1.5 Ga detrital zircon grains show εHf$_t$ values less than +5 (Fig. 3.13A). Consequently, the juvenile (εHf$_t$ = +5 or greater) ca. 1.9 to 1.5 Ga grains that comprise approximately 50% of the total detrital zircon cargo in Belt Supergroup strata within the Priest River region are not recognized in coeval rocks on Hainan Island (Yao et al., 2017).

The identification of NAMG-age detrital zircon components in the lower–middle Rocky Cape Group of Tasmania led Halpin et al. (2014) and Mulder et al. (2015) to correlate the lower–middle Rocky Cape Group of Tasmania to the Belt Supergroup and Deer Trail Group of Laurentia. This interpretation has Tasmania located in a central position between western Laurentia and East Antarctica/southeastern Australia within Nuna (Halpin et al., 2014; Mulder et al., 2015). The juvenile (εHf*t* = +5 or greater) ca. 1.8 to 1.5 Ga grains that characterize Belt Supergroup strata in the Priest River region, and coeval strata in southwestern Laurentia (Doe et al., 2013) are present within the lower Rocky Cape Group (Fig. 3.13; Mulder et al., 2015), consistent with similar proposed Gawler Craton–East Antarctica (Mawson continent) sources. Consequently, Tasmania's proposed location adjacent to southwestern/western Laurentia (e.g. Halpin et al., 2014; Mulder et al., 2015; Fig. 3.1) at ca. 1.5 Ga is consistent with existing provenance constraints.

Statistical analysis of the detrital zircon (U–Pb/Lu–Hf) data from these ca. 1.45 Ga basins in Laurentia, Tasmania, Hainan Island and their proposed Gawler Craton source (Fig. 3.13B) allows objective evaluation of these proposed correlations. Overall, the statistical results indicate that the similarity of detrital zircon components in the Belt Basin and coeval southwestern Laurentian basins (Trampas, Yankee Joe-Blackjack basins) is the strongest as they consistently yield the greatest (closest to 1) comparison values (Fig. 3.13B). Thus, it is probable that the ca. 1.45 Ga Yankee-Joe Defiance Basin (Doe et al., 2013) in southwestern Laurentia and the Belt Basin, ~1500 km to the north, received sediment from a similar (non-Laurentian) source. This source was likely the Gawler Craton of southeastern Australia, and perhaps associated rocks in East Antarctica (Jones et al., 2015).

The next strongest statistical resemblance to the Belt Supergroup detrital zircon dataset is coeval strata of the lower Rocky Cape Group in Tasmania (Mulder et al., 2015). Gawler Craton igneous sources also generally show statistical similarity values (to the Belt Supergroup detrital zircon dataset) that are comparable to the values given by the Tasmanian strata (Fig. 3.13B). Consequently, the new data from the Belt

Supergroup is consistent with prior interpretations that Tasmania occupied a central position between western Laurentia and East Antarctica/southeastern Australia within Nuna (Halpin et al., 2014; Mulder et al., 2015). Based on the relatively limited detrital zircon Lu/Hf available from the Gezhencun succession of Hainan Island (Xu et al., 2019), the weakest correlation is between Belt Supergroup strata and coeval strata on Hainan Island. This weak statistical correlation likely reflects to the absence of juvenile (εHf_t = +5 or greater) ca. 1.6–1.5 Ga detrital zircon grains in the Hainan Island strata which are present in the Laurentian and Tasmanian strata, and the Galwer Craton igneous sources. Consequently, prior assertions of the correlation between Belt Supergroup rocks and coeval rocks on Hainan Island (e.g. Xu et al., 2019; Yao et al., 2017) are the least justified.

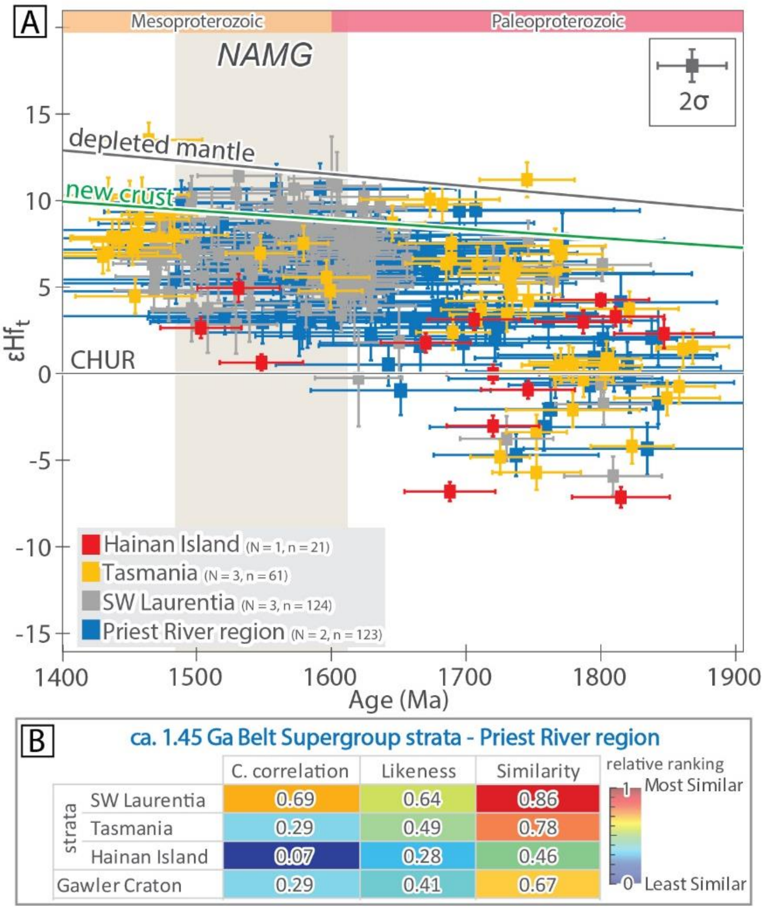

Fig. 3.13. A) Detrital zircon U–Pb and Lu–Hf data from ca. 1.45 Ga strata from Hainan Island, South China (the Gzehencun succession, Xu et al., 2019), Western Tasmania (lower Rocky Cape Group; Mulder et al., 2015), southwestern Laurentia (the Blackjack Formation and Defiance Quartzite; Doe et al., 2013), and Belt Supergroup strata of the Priest River region (Prichard and Revett formations). B) Results of two-dimensional (Lu–Hf/U–Pb) statistical comparison (Sundell and Saylor, 2021) of the datasets above, with a value of 1 indicating the most similar and 0 indicating the least similar between Belt Supergroup strata of the Priest River region, and strata of southwestern Laurentia, Tasmania, Hainan Island, and igneous sources within the Gawler Craton. See Sundell and Saylor (2021) for further discussion of the Cross-correlation (C.-correlation), Likeness, and Similarity metrics.

3.7. Conclusions

U–Pb and Lu–Hf detrital zircon provenance data from the (<1.73 Ga) Gold Cup Quartzite, (ca. 1.47–1.38 Ga) Belt Supergroup and overlying (<1.3 Ga) Deer Trail Group of the Priest River region (northern Idaho, and northeastern Washington state, USA) give insights into the regional tectonostratigraphy of western Laurentia, and yield important constraints on the assembly of western Laurentia and the evolution of supercontinent Nuna. Our major findings are the following:

1) The Gold Cup Quartzite, Neihart Quartzite, and the quartzite of Argenta show similar detrital zircon age spectra that suggests sourcing from proximal Neoarchean and Paleoproterozoic Laurentian basement. Such similarities, and the general absence of zircon grains younger than ca. 1.73 Ga within these units, suggest that assembly of the main Archean–Paleoproterozoic blocks of western Laurentia (Wyoming, Clearwater, Medicine Hat, Hearne, and Grouse Creek) was likely complete by ca. 1.73 Ga.

2) The Laurentian < 1.73–1.48 Ga, Gold Cup and Neihart quartzites do not have require non-Laurentian sources. Thereby, this data does not compel a proto-SWEAT configured Nuna by ca. 1.8 Ga as previously suggested (e.g. Rogers and Santosh, 2002; Zhao et al., 2002; Holland et al., 2018), and instead favors a protracted, perhaps two-stage assembly of Nuna from ca. 1.8 to 1.6 Ga (e.g. Kirscher et al., 2019).

3) Ca. 1.47 Ga strata in the western extent of the Belt Basin contain juvenile ca. 1610–1490 Ma "North American magmatic gap" zircon grains that lack a Laurentian source. The Gawler Craton contains igneous sources that span the required age and Lu–Hf compositions of these grains, and experienced active exhumation at ca. 1.47 Ga. Consequently, our new constraints are consistent with suggestions that southeastern Australia was a source of sediment for Belt Supergroup strata. This data supports proto-SWEAT reconstructions for Nuna that place the Gawler Craton of southeastern Australia adjacent to the Priest River region of Laurentia by at least ca. 1.47 Ga.

4) Deposition of the Deer Trail Group occurred after ca. 1.3 Ga, perhaps coeval with the end or latter part of the enigmatic East Kootenay tectono-magmatic event. The ages and range of Lu–Hf values recorded by the main detrital zircon components within the Deer Trail Group suggest a mixed provenance from several Laurentian sources, including the Mojave Province, Trans-Hudson Orogen, and perhaps the

Medicine Hat Block. Many of these grains could have been recycled from nearby older strata, such as the Lemhi Group of the Belt Basin. The fine-grained siliciclastic and carbonate lithology and the lack of significant *syn*-depositional magmatic detrital zircon components in Deer Trail Group strata are consistent with their deposition during a period of regional subsidence within the Priest River region that coincides with purported Nuna breakup at ca. 1.3 Ga (Kirscher et al., 2020).

Collectively, these new provenance constraints are most consistent with paleogeographic models that advocate widespread assembly of the main Archean blocks of western Laurentia from ca. 1.9 to 1.7 Ga, and indicate that the Priest River region does not record sedimentation from non-Laurentian source terranes until after ca. 1.5 Ga. Consequently, the Paleo–Mesoproterozoic tectonostratigraphic record of the Priest River region is consistent with models that indicate the main assembly of western Laurentia was a precursor to, and not necessarily synchronous with, the final assembly of a proto-SWEAT configured Nuna supercontinent.

3.8. References

Precambrian Research reference style

Alcock, J., Muller, P.D., Jercinovic, M.J., McFarlane, C., 2013. Monazite ages and pressure-temperature-time paths from anatectites in the southern Ruby Range, Montana, USA: Evidence for delamination, ultramafic magmatism, and rapid uplift at ca. 1780 Ma. Can. J. Earth Sci. 50 (11), 1069–1084. https://doi.org/10.1139/cjes-2013-0035.

Anderson, H.E., Davis, D.W., 1995. U-Pb geochronology of the Moyie sills, Purcell Supergroup, southeastern British Columbia: implications for the Mesoproterozoic geological history of the Purcell (Belt) basin. Can. J. Earth Sci. 32 (8), 1180–1193.

Armstrong, R.L., Taubeneck, W.H., Hales, P.O., 1977. Rb-Sr and K-Ar geochronometry of Mesozoic granitic rocks and their Sr isotopic composition, Oregon, Washington, and Idaho. Bull. Geol. Soc. Am. 88, 397–411. https://doi.org/10.1130/0016-7606(1977) 88<397:RAKGOM>2.0.CO;2.

Baldwin, J.A., Lewis, R.S., Vervoort, J.D., McDonald, C.D., 2016. Paleoproterozoic basement rocks in the western part of the Clearwater complex, Idaho. Geol. Soc. Am. Field Guide 41, 251–264. https://doi.org/10.1130/2016.0041(08).

Bell, R.T., and Jefferson, C.W., 1987, An hypothesis for an Australian-Canadian connection in the Late Proterozoic and the birth of the Pacific Ocean: Pacific Rim congress 87. Proc. international congress, 1987, Gold Coast, Queensland, p. 39–50.

Betts, P.G., Armit, R.J., Stewart, J., Aitken, A.R.A., Ailleres, L., Donchak, P., Hutton, L., Withnall, I., Giles, D., 2016. Australia and Nuna, 424. Geological Society Special Publication, pp. 47–81. https://doi.org/10.1144/SP424.2.

Betts, P.G., Giles, D., Aitken, A., 2011. Palaeoproterozoic accretion processes of Australia and comparisons with Laurentia. Int. Geol. Rev. 53 (11-12), 1357–1376. https://doi. org/10.1080/00206814.2010.527646.

Box, S.E., Pritchard, C.J., Stephens, T.S., O'Sullivan, P.B., 2020. Between the supercontinents – Mesoproterozoic Deer Trail Group, an intermediate age unit between the Mesoproterozoic Belt-Purcell Supergroup and the Neoproterozoic Windermere Supergroup in northeastern Washington, U.S.A. Can. J. Earth Sci. 57 (12), 1411–1427. https://doi.org/10.1139/cjes-2019-0188.

Brennan, D.T., Pearson, D.M., Link, P.K., and Chamberlain, K.R., 2020, Neoproterozoic Windermere Supergroup near Bayhorse, Idaho: late-stage Rodinian rifting was deflected west around the Belt basin. Tectonics, doi:10.1029/2020tc006145.

Brennan, D.T., Li, Z., Rankenburg, K., Evans, N., Link, P.K., Nordsvan, A.R., Kirkland, C. L., Mahoney, J.B., Johnson, T., Mcdonald, B.J., 2021a. Recalibrating Rodinian rifting in the northwestern United States. Geology. https://doi.org/10.1130/G48435.1/ 5230844/g48435.

Brennan, D.T., Mitchell, R.N., Spencer, C.J., Murphy, J.B., Li, Z.-X., 2021b. A tectonic model for the transcontinental arch: progressive migration of a Laurentian drainage divide during the Neoproterozoic-Cambrian Sauk Transgression. Terra Nova 33 (4), 430–440. https://doi.org/10.1111/ter.v33.410.1111/ter.12528.

Bickford, M.E., Van Schmus, W.R., Karlstrom, K.E., Mueller, P.A., Kamenov, G.D., 2015. Mesoproterozoic-trans-Laurentian magmatism: a synthesis of continent-wide age distributions, new SIMS U-Pb ages, zircon saturation temperatures, and Hf and Nd isotopic compositions. Precambr. Res. 265, 286–312. https://doi.org/10.1016/j. precamres.2014.11.024.

Bookstrom, A.A., Box, S.E., Cossette, P.M., Frost, T.P., Gillerman, V.S., King, G.R., and Zirakparvar, N.A., 2016, Geologic history of the Blackbird Co-Cu district in the Lemhi subbasin of the Belt-Purcell Basin, in MacLean, J.S., and Sears, J.W., eds., Belt Basin: Window to Mesoproterozoic Earth. Geol. Soc. Am. Special Paper 522, 185–219, doi:10.1130/2016.2522(08).

Bose, P.K., Eriksson, P.G., Sarkar, S., Wright, D.T., Samanta, P., Mukhopadhyay, S., Mandal, S., Banerjee, S., Altermann, W., 2012. Sedimentation patterns during the Precambrian: a unique record? Mar. Pet. Geol. 33 (1), 34–68. https://doi.org/ 10.1016/j.marpetgeo.2010.11.002.

Bouvier, A., Vervoort, J.D., Patchett, P.J., 2008. The Lu-Hf and Sm-Nd isotopic composition of CHUR: Constraints from unequilibrated chondrites and implications for the bulk composition of terrestrial planets. Earth Planet. Sci. Lett. 273 (1–2), 48–57. https://doi.org/10.1016/j.epsl.2008.06.010.

Campbell, A.B., and Raup, O.B., 1964, Preliminary geologic map of the Hunters quadrangle, Stevens and Ferry Counties, Washington: U.S. Geological Survey, Mineral Investigations Field Studies Map MF-276, 1:48,000 scale.

Cawood, P.A., and Korsch, R.J., 2008, Assembling Australia: Proterozoic building of a continent. Precambr. Res. 166, https://doi.org/10.1016/j.precamres.2008.08.006

Cawood, P.A., Wang, W., Zhao, T., Xu, Y., Mulder, J.A., Pisarevsky, S.A., Zhang, L., Gan, C., He, H., Liu, H., Qi, L., Wang, Y., Yao, J., Zhao, G., Zhou, M.-F., Zi, J.-W., 2020. Deconstructing South China and consequences for reconstructing Nuna and Rodinia. Earth Sci. Rev. 204, 103169. https://doi.org/10.1016/j. earscirev.2020.103169.

Chamberlain, K.R., Frost, C.D., Frost, B.R., 2003. Early Archean to Mesoproterozoic evolution of the Wyoming Province: archean origins to modern lithospheric architecture. Can. J. Earth Sci. 40 (10), 1357–1374. https://doi.org/10.1139/e03- 054.

Chapman, N.D., Ferguson, M., Meffre, S.J., Stepanov, A., Maas, R., Ehrig, K.J., 2019. Pb-isotopic constraints on the source of A-type Suites: Insights from the Hiltaba Suite - Gawler Range Volcanics Magmatic Event, Gawler Craton, South Australia. Lithos 346-347, 105156. https://doi.org/10.1016/j.lithos.2019.105156.

Cheney, J., Webb, A., Coath, C., McKeegan, K., 2004. Insitu ion microprobe 207Pb/206 dating of monazite from Precambrian metamorphic suites, Tobacco Root Mountains, Montana. Geological Society of America Special Paper 377, 151–179. https://doi. org/10.1130/0-8137-2377-9.151.

Condit, C.B., Mahan, K.H., Ault, A.K., Flowers, R.M., 2015. Foreland-directed propagation of high-grade tectonism in the deep roots of a Paleoproterozoic collisional orogeny, SW Montana, USA. Lithosphere 7, 625–645. https://doi.org/ 10.1130/L460.1.

Coutts, D.S., Matthews, W.A., Hubbard, S.M., 2019. Assessment of widely used methods to derive depositional ages from detrital zircon populations. Geosci. Front. 10 (4), 1421–1435. https://doi.org/10.1016/j.gsf.2018.11.002.

Daniel, C.G., Pfeifer, L.S., Jones, J. V., and McFarlane, C.M., 2013, Detrital zircon evidence for non-laurentian provenance, mesoproterozoic (ca. 1490-1450 ma) deposition and orogenesis in a reconstructed orogenic belt, northern new mexico, USA: Defining the picuris orogeny. GSA Bull. 125, 1423–1441, doi:10.1130/ B30804.1.

Dalziel, I.W.D., 1991. Pacific margins of Laurentia and East Antarctica-Australia as a conjugate rift pair: evidence and implications for an Eocambrian supercontinent. Geology 19, 598–601. https://doi.org/10.1130/0091-7613(1991)019<0598: PMOLAE>2.3.CO;2.

Doe, M.F., Daniel, C.G., 2019. Evidence for Mesoproterozoic ca. 1470-1444 Ma regional deformation of the Mazatzal Group and equivalent rocks in the type area of the Mazatzal orogeny, Tonto Basin, 55. GSA Field Guides, Arizona, pp. 237–272. https://doi.org/10.1130/2019.0055(10).

Doe, M.F., Jones, J.V., Karlstrom, K.E., Dixon, B., Gehrels, G., Pecha, M., 2013. Using detrital zircon ages and Hf isotopes to identify 1.48-1.45Ga sedimentary basins and fingerprint sources of exotic 1.6-1.5 Ga grains in southwestern Laurentia. Precambr. Res. 231, 409–421. https://doi.org/10.1016/j.precamres.2013.03.002.

Doughty, P.T., Chamberlain, K.R., 1996. Salmon River Arch revisited: new evidence for 1370 Ma rifting near the end of deposition in the Middle Proterozoic Belt basin. Can. J. Earth Sci. 33, 1037–1052. https://doi.org/10.1139/e96-079.

Doughty, P.T., Chamberlain, K.R., 2008. Protolith age and timing of Precambrian magmatic and metamorphic events in the Priest River complex, northern Rockies. Can. J. Earth Sci. 45 (1), 99–116. https://doi.org/10.1139/e07-067.

Doughty, P.T., Price, R.A., Parrish, R.R., 1998. Geology and U-Pb geochronology of Archean basement and Proterozoic cover in the Priest River complex, northwestern United States, and their implications for Cordilleran structure and Precambrian continent reconstructions. Canadian Journal of Earth Sciences 35, 39–54. https://doi.org/10.1139/cjes-35-1-39.

Eaton, D.W., Ross, G.M., Clowes, R.M., 1999. Seismic-reflection and potential-field studies of the Vulcan structure, western Canada: a Paleoproterozoic Pyrenees? J. Geophys. Res. Solid Earth 104 (B10), 23255–23269. https://doi.org/10.1029/ 1999JB900204.

Elison, M.W., Speed, R.C., Kistler, R.W., 1990. Geo- logic and isotopic constraints on the crustal structure of the northern Great Basin. Geological Society of America Bulletin 102, 1077–1092. https://doi.org/10.1130/0016-7606(1990)102<1077: GAICOT>2.3.CO;2.

Evans, J.G., 1987, Geology of the Stensgar Mountain Quadrangle, Stevens County, Washington: United States Geological Survey Bulletin 1679, 1:24,000 scale. doi:10.3133/b1679..

Evans, K.V., Aleinikoff, J.N., Obradovich, J.D., Fanning, C.M., 2000. SHRIMP U-Pb geochronology of volcanic rocks, Belt Supergroup, western Montana: evidence for rapid deposition of sedimentary strata. Can. J. Earth Sci. 37 (9), 1287–1300. https:// doi.org/10.1139/e00-036.

Fanning, C.M., Link, P.K., 2003. Detrital zircon provenance of the Mesoproterozoic Pandurra Formation, South Australia: gawler craton zircon population and implications for the Belt Supergroup. Geol. Soc. Am. Abstracts Programs 34 (7), 465.

Fanning, C.M., Flint, R.B., Parker, A.J., Ludwig, K.R., Blissett, A.H., 1988. Refined Proterozoic evolution of Gawler craton, southern Australia through U-Pb zircon geochronology. Precambr. Res. 40, 363–380.

Fanning, C.M., Link, P.K., Woodhead, J., Hergt, J., 2009, Provenance of unique Mesoproterozoic sedimentary basins in Australia and North America: U-Pb and Lu-Hf isotopic data for detrital zircons and the implications for Rodinia reconstructions. Geological Society of London Fermor Meeting, Abstract, Edinburgh, United Kingdom, http://www.geos.ed.ac.uk/rodinia2009.

Fanning, C.M., Reid, A.J., Teale, G., 2007. A geochronological framework for the Gawler Craton, South Australia. South Australia Geological Survey. Bulletin 55. https://sarigbasis.pir.sa.gov.au/WebtopEw/ws/samref/sarig1/image/DDD/BULL055.pdf.

Foster, D.A., Mueller, P.A., Mogk, D.W., Wooden, J.L., Vogl, J.J., 2006. Proterozoic evolution of the western margin of the Wyoming craton: Implications for the tectonic and magmatic evolution of the northern Rocky Mountains. Can. J. Earth Sci. 43 (10), 1601–1619. https://doi.org/10.1139/e06-052.

Freeman, W., Winston, D.W., 1987. A quartz arenite blanket at the base of, or below the middle Proterozoic Belt Supergroup? Montana and Idaho. Geol. Soc. Am. Abstracts Programs 19, no. 276.

Furlanetto, F., Thorkelson, D.J., Daniel Gibson, H., Marshall, D.D., Rainbird, R.H., Davis, W.J., Crowley, J.L., Vervoort, J.D., 2013. Late Paleoproterozoic terrane accretion in northwestern Canada and the case for circum-Columbian orogenesis. Precambr. Res. 224, 512–528. https://doi.org/10.1016/j.precamres.2012.10.010.

Gifford, J.N., Mueller, P.A., Foster, D.A., Mogk, D.W., 2014. Precambrian crustal evolution in the great falls tectonic zone: insights from xenoliths from the Montana Alkali Province. J. Geol. 122 (5), 531–548. https://doi.org/10.1086/677262.

Gifford, J.N., Mueller, P.A., Foster, D.A., Mogk, D.W., 2018. Extending the realm of Archean crust in the Great Falls tectonic zone: Evidence from the Little Rocky Mountains, Montana. Precambr. Res. 315, 264–281. https://doi.org/10.1016/j.precamres.2018.07.021.

Gibson, G.M., Champion, D.C., 2019. Antipodean fugitive terranes in southern Laurentia: How Proterozoic Australia built the American West. Lithosphere 11, 551–559. https://doi.org/10.1130/L1072.

Gifford, J., Malone, S., Mueller, P., 2020. The Medicine hat block and the early paleoproterozoic assembly of western laurentia. Geosciences v. 10, 271. https://doi.org/10.3390/geosciences10070271.

Goodge, J.W., Fanning, C.M., 2016. Mesoarchean and paleoproterozoic history of the nimrod complex, central transantarctic mountains, Antarctica: stratigraphicrevisions and relation to the Mawson Continent in East Gondwana. Precambr. Res. 285, 242–271. https://doi.org/10.1016/j.precamres.2016.09.001.

Goodge, J.W., Fanning, C.M., Fisher, C.M., Vervoort, J.D., Fisher, C.M., 2017. Proterozoic crustal evolution of central East Antarctica: Age and isotopic evidence from glacial igneous clasts, and links with Australia and Laurentia. Precambr. Res. 299, 151–176. https://doi.org/10.1016/j.precamres.2017.07.026.

Griffin, W., Wang, X., Jackson, S., Pearson, N., O'Reilly, S.Y., Xu, X., and Zhou, X., 2002, Zircon chemistry and magma mixing, SE China: In-situ analysis of Hf isotopes, Tonglu and Pingtan igneous complexes. Lithos v. 61, no. 3-4, p. 237–269, https://doi.org/10.1016/.

Halpin, J.A., Jensen, T., McGoldrick, P., Meffre, S., Berry, R.F., Everard, J.L., Calver, C. R., Thompson, J., Goemann, K., Whittaker, J.M., 2014. Authigenic monazite and detrital zircon dating from the Proterozoic Rocky Cape Group, Tasmania: links to the belt-purcell supergroup, North America. Precambrian Res. 250, 50–67. https://doi. org/10.1016/j.precamres.2014.05.025.

Harms, T.A., Brady, J.B., Burger, H.R., Cheney, J.T., 2004. Advances in the geology of the Tobacco Root Mountains, Montana, and their implications for the history of the northern Wyoming province. Geol. Soc. Am. Special Papers 377, 227–243. https:// doi.org/10.1130/0-8137-2377-9.227.

Hartnady, M.I.H., Kirkland, C.L., Dutch, R.A., Bodorkos, S., Jagodzinski, E.A., 2020. Evaluating zircon initial Hf isotopic composition using a combined SIMS–MC-LASS-ICP-MS approach: a case study from the Coompana Province in South Australia. Chem. Geol. 558, 119870. https://doi.org/10.1016/j.chemgeo.2020.119870.

Herriott, T.M., Crowley, J.L., Schmitz, M.D., Wartes, M.A., Gillis, R.J., 2019. Exploring the law of detrital zircon: LA-ICP-MS and CA-TIMS geochronology of Jurassic forearc strata, Cook Inlet, Alaska, USA. Geology 47, 1044–1048. https://doi.org/10.1130/ G46312.1.

Hoffman, P.F., 1991. Did the breakup of Laurentia turn Gondwanaland inside out? Science 252, 1409–1411.

Holland, M.E., Karlstrom, K.E., Doe, M.F., Gehrels, G.E., Pecha, M., Shufeldt, O.P., Begg, G., Griffin, W.L., Belousova, E., 2015. An imbricate midcrustal suture zone: The mojave-yavapai province boundary in grand canyon, arizona. Bulletin of the Geological Society of America 127, 1391–1410. https://doi.org/10.1130/B31232.1.

Holland, M.E., Karlstrom, K.E., Gehrels, G., Shufeldt, O.P., Begg, G., Griffin, W., Belousova, E., 2018. The Paleoproterozoic Vishnu basin in southwestern Laurentia: Implications for supercontinent reconstructions, crustal growth, and the origin of the Mojave crustal province. Precambr. Res. 308, 1–17. https://doi.org/10.1016/j. precamres.2018.02.001.

Holland, M.E., Grambling, T.A., Karlstrom, K.E., Jones, J.V., Nagotko, K.N., Daniel, C.G., 2020. Geochronologic and Hf-isotope framework of Proterozoic rocks from central New Mexico, USA: formation of the Mazatzal crustal province in an extended continental margin arc. Precambr. Res. 347, 105820. https://doi.org/10.1016/j. precamres.2020.105820.

Howard, K.E., Hand, M., Barovich, K.M., Payne, J.L., Belousova, E.A., 2011. U-Pb, Lu-Hf and Sm-Nd isotopic constraints on provenance and depositional timing of metasedimentary rocks in the western Gawler Craton: implications for Proterozoic reconstruction models. Precambr. Res. 184 (1-4), 43–62. https://doi.org/10.1016/j. precamres.2010.10.002.

Höy, T., 1992, Geology of the Purcell Supergroup in the Fernie West-Half Map Area, Southeastern British., 1992, Geology of the Purcell Supergroup in the Fernie West-Half Map Area, Southeastern British Columbia: British Columbia Mineral Resources Division Bulletin 84, 157 p..

Isakson, V.H., 2017, Geochronology of the tectonic, stratigraphic, and magmatic evolution of Neoproterozoic to early Paleozoic, North American Cordillera and Cryogenian glaciation [Ph.D. thesis]: Boise, Idaho, Boise State University, 657 p..

Howard, K.E., Hand, M., Barovich, K.M., Reid, A., Wade, B.P., Belousova, E.A., 2009. Detrital zircon ages: Improving interpretation via Nd and Hf isotopic data. Chemical Geology 262, 277–292. https://doi.org/10.1016/j.chemgeo.2009.01.029.

Jones, J.V., Daniel, C.G., Doe, M.F., 2015. Tectonic and sedimentary linkages between the Belt-Purcell basin and southwestern Laurentia during the Mesoproterozoic, ca. 1.60–1.40 Ga. Lithosphere 7 (4), 465–472. https://doi.org/10.1130/L438.1.

Kirscher, U., Liu, Y., Li, Z.X., Mitchell, R.N., Pisarevsky, S.A., Denyszyn, S.W., Nordsvan, A., 2019. Paleomagnetism of the Hart Dolerite (Kimberley, Western Australia) – A two-stage assembly of the supercontinent Nuna? Precambr. Res. 329, 170–181. https://doi.org/10.1016/j.precamres.2018.12.026.

Kirscher, U., Mitchell, R.N., Liu, Y., Nordsvan, A.R., Cox, G.M., Pisarevsky, S.A., Wang, C., Wu, L., Murphy, J.B., and Li, Z.-X., 2020, Paleomagnetic constraints on the duration of the Australia-Laurentia connection in the core of the Nuna supercontinent. Geology, p. 1–6, doi:10.1130/g47823.1.

Lewis, R.S., Vervoort, J.D., Burmester, R.F., McClelland, W.C., Chang, Z., 2007, Geochronological constraints on Mesoproterozoic and Neoproterozoic (?) high-grade metasedimentary rocks of north-central Idaho, U.S.A. Sepm, v. 86, p. 37–53.

Lewis, R.S., Burmester, R.F., Breckenridge, R.M., McFadden, M.D., Phillips, W.M., 2020, Geologic Map of the Sandpoint 30’ x 60’ Quadrangle, Idaho and Montana, and the Idaho Part of the Chewelah 30’ by 60’ Quadrangle: Idaho Geological Survey Digital Web Maps, DWM-189, 1:100,000 scale. https://www.idahogeology.org/produc t/dwm-189.

Li, J., Pourteau, A., Li, Z., Jourdan, F., Nordsvan, A.R., Collins, W.J., Volante, S., 2020. Heterogeneous exhumation of the Mount Isa orogen in NE Australia after 1.6 Ga Nuna assembly: new high-precision 40Ar/39Ar thermochronological constraints. Tectonics 1–27. https://doi.org/10.1029/2020tc006129.

Li, Z.X., Zhang, L., and Powell, C.M., 1995, South China in Rodinia: Part of the missing link between Australia-East Antarctica and Laurentia? Geology, v. 23, p. 407–410, doi:10.1130/0091-7613(1995)023<0407:SCIRPO>2.3.CO;2.

Li, Z.X. et al., 2008a, Assembly, configuration, and break-up history of Rodinia: a synthesis. Precambrian Res. 160, 179–210, doi:10.1016/j.precamres.2007.04.021.

Li, Z.X., Li, X.H., Li, W.X., Ding, S.J., 2008b. Was Cathaysia part of Proterozoic Laurentia? new data from Hainan Island, south China. Terra Nova, 20(2): 154-164. doi: 10.1111/j.1365-3121.2008.00802.x.

Lewis, R.S., Vervoort, J.D., Burmester, R.F., Oswald, P.J., 2010. Detrital zircon analysis of Mesoproterozoic and Neoproterozoic metasedimentary rocks of north-central Idaho: implications for development of the Belt–Purcell basin. Canadian Journal of Earth Sciences 47, 1383–1404. https://doi.org/10.1139/E10-049.

Li, Z.X., Mitchell, R.N., Spencer, C.J., Ernst, R., Pisarevsky, S., Kirscher, U., Murphy, J.B., 2019. Decoding Earth's rhythms: Modulation of supercontinent cycles by longer superocean episodes. Precambr. Res. 323, 1–5. https://doi.org/10.1016/j. precamres.2019.01.009.

Link, P.K., Fanning, C.M., Lund, K.I., Aleinikoff, J.N., 2007, Detrital-Zircon Populations and Provenance of Mesoproterozoic Strata of East-Central Idaho, U.S.A.: Correlation with Belt Supergroup of Southwest Montana: Proterozoic Geology of Western North America and Siberia, p. 101–128, doi:10.2110/pec.07.86.0101.

Link, P.K., Steel, T.D., Stewart, E.S., Sherwin, J.-A., Hess, L.R., McDonald, C., 2016. Detrital zircons in the Mesoproterozoic upper Belt Supergroup in the Pioneer, Beaverhead, and Lemhi Ranges, Montana and Idaho: The Big White arc. GSA Special Paper 522, 39–44. https://doi.org/10.1130/2016.2522(07).

Link, P.K., Autenrieth-Durk, K.M., Cameron, A., Fanning, C.M., Vogl, J.J., Foster, D.A., 2017. U-Pb zircon ages of the Wildhorse gneiss, Pioneer Mountains, south-central idaho, and tectonic implications. Geosphere 13 (3), 681–698. https://doi.org/ 10.1130/GES01418.1.

Liu, H., Zi, J.-W., Cawood, P.A., Cui, X., Zhang, L., 2020. Reconstructing South China in the Mesoproterozoic and its role in the Nuna and Rodinia supercontinents. Precambr. Res. 337, 105558. https://doi.org/10.1016/j.precamres.2019.105558.

Lonn, J.D., Burmester, R.F., Lewis, R.S. and McFaddan, M.D., 2020, The Mesoproterozoic Belt Supergroup, in Barth, S., ed., Geology of Montana: Montana Bureau of Mines and Geology Special Publication 122, v. 1, Chapter 1, p 1-38.

Ludwig, K.R., 2008, User's Manual for Isoplot 3.00: A Geochronological Toolkit for Microsoft Excel: Berkeley Geochronology Center Special Publication 4, 71 p.

Lund, K., Aleinikoff, J.N., Evans, K.V., duBray, E.A., Dewitt, E.H., Unruh, D.M., 2010. SHRIMP U-Pb dating of recurrent Cryogenian and Late Cambrian-Early Ordovician alkalic magmatism in central Idaho: Implications for Rodinian rift tectonics. Bulletin of the Geological Society of America 122, 430–453. https://doi.org/10.1130/ B26565.1.

Lund, K., and Cheney, E.R., 2016, Correlation of unconformity-bounded sequences of the Neo- proterozoic Windermere Supergroup in Idaho, Washington, and southern British Columbia, in Cheney, E.R., ed., The Geology of Washing- ton and Beyond: From Laurentia to Cascadia: Seattle, Washington, University of Washington Press, p. 28–42.

Markwitz, V., Kirkland, C.L., 2018. Source to sink zircon grain shape: Constraints on selective preservation and significance for Western Australian Proterozoic basin provenance. Geosci. Front. 9 (2), 415–430. https://doi.org/10.1016/j. gsf.2017.04.004.

Matthews, W., Guest, B., Madronich, L., 2018. Latest Neoproterozoic to Cambrian detrital zircon facies of western Laurentia. Geosphere 14, 243–264. https://doi.org/10.1130/GES01544.1.

McFarlane, C.RM., Pattison, D.RM., 2000. Geology of the Matthew Creek metamorphic zone, southeast British Columbia: a window into Middle Proterozoic metamorphism in the Purcell Basin. Can. J. Earth Sci. 37 (7), 1073–1092. https://doi.org/10.1139/ e00-018.

McFarlane, C.R.M., Corfu, F., 2015. A geochronological framework for sedimentation and Mesoproterozoic tectono-magmatic activity in lower Belt-Purcell rocks exposed west of Kimberley, British Columbia. Can. J. Earth Sci. 52 (7), 444–465. https://doi.org/10.1139/cjes-2014-0215.

Meert, J.G., 2012, What's in a name? The Columbia (Paleopangaea/Nuna) supercontinent. Gondwana Res. 21, 987–993, doi:10.1016/j.gr.2011.12.002.
McMechan, M.E., Price, R.A., 1982. Superimposed low-grade metamorphism in the Mount Fisher area, southeastern British Columbia—implications for the East Kootenay orogeny. Canadian Journal of Earth Sciences 19, 476–489. https://doi.org/10.1139/e82-039.

Medig, K.P.R., Thorkelson, D.J., Davis, W.J., Rainbird, R.H., Gibson, H.D., Turner, E.C., Marshall, D.D., 2014. Pinning northeastern Australia to northwestern Laurentia in the Mesoproterozoic. Precambr. Res. 249, 88–99. https://doi.org/10.1016/j.precamres.2014.04.018.

Mueller, P.A., Heatherington, A.L., Kelly, D.M., Wooden, J.L., Mogk, D.W., 2002. Paleoproterozoic crust within the Great Falls tectonic zone: Implications for the assembly of southern Laurentia. Geology 30, 127–130. https://doi.org/10.1136/jclinpath-2017-204981.

Mueller, P.A., Frost, C.D., 2006. The Wyoming Province: a distinctive Archean craton in Laurentian North America. Can. J. Earth Sci. 43 (10), 1391–1397. https://doi.org/10.1139/e06-075.

Mueller, P.A., Wooden, J.L., Mogk, D.W., Foster, D.A., 2011. Paleoproterozoic evolution of the Farmington zone: implications for terrane accretion in southwestern Laurentia. Lithosphere 3 (6), 401–408. https://doi.org/10.1130/L161.110.1130/2011350.

Mueller, P., Mogk, D., Wooden, J., Spake, D., 2016, U-Pb ages of zircons from the Lower Belt Supergroup and proximal crystalline basement: Implications for the early evolution of the Belt Basin. Geol. Soc. Am. Special Paper, 522, 1–21, doi:10.1130/2016.2522(11).

Mulder, J.A., Halpin, J.A., Daczko, N.R., 2015. Mesoproterozoic Tasmania: witness to the East Antarctica-Laurentia connection within Nuna. Geology 43 (9), 759–762. https://doi.org/10.1130/G36850.110.1130/2015259.

Mulder, J.A., Karlstrom, K.E., Fletcher, K., Heizler, M.T., Timmons, J.M., Crossey, L.J., Gehrels, G.E., Pecha, M., 2017. The syn-orogenic sedimentary record of the

Grenville Orogeny in southwest Laurentia. Precambr. Res. 294, 33–52. https://doi.org/10.1016/j.precamres.2017.03.006.

Miller, F.K., 2000, Geologic map of the Chewelah 30’X60’ quadrangle, Washington and Idaho, MF-2354: Reston, Virginia, U.S. Geological Survey, United States, scale 1:100,000..

Miller, F.K., Whipple, J.W., 1989, The Deer Trail Group—Is it part of the Belt Supergroup, in Joseph, N.L., ed., Geologic guidebook for Washington and adjacent areas: Washington Division of Geology and Earth Resources Information Circular 86, p. 1–21.

Miller, F.K., Burmester, R.F., Miller, D.M., Powell, R.E., and Derkey, P.D, 1999, Digital geologic map of the Sandpoint 1 x 2 degree quadrangle, Washington, Idaho and Montana: U.S. Geological Survey Open-File Report 99-144. p. 70. scale 1:250,000.

Mitchell, R.N., Zhang, N., Salminen, J., Liu, Y., Spencer, C.J., Steinberger, B., Murphy, J. B., Li, Z., 2021. The Supercontinent Cycle. Nature Reviews Earth and Environment 2, 358–374. https://doi.org/10.1038/s43017-021-00160-0.

Moores, E.M., 1991. Southwest U.S.-East Antarctic (SWEAT) connection: a hypothesis. Geology 19 (5), 425. https://doi.org/10.1130/0091-7613(1991)019<0425:SUSEAS>2.3.CO;2.

Nance, R.D., Murphy, J.B., Santosh, M., 2014. The supercontinent cycle: a retrospective essay. Gondwana Res. 25 (1), 4–29. https://doi.org/10.1016/j.gr.2012.12.026.

Nelson, S.T., Hart, G.L., and Frost, C.D., 2011, A reassessment of Mojavia and a new Cheyenne Belt alignment in the eastern Great Basin. Geosphere, v. 7, p. 513–527, doi:10.1130/GES00595.1.

Nesheim, T.O., Vervoort, J.D., McClelland, W.C., Gilotti, J.A., and Lang, H.M., 2012, Mesoproterozoic syntectonic garnet within Belt Supergroup metamorphic tectonites: Evidence of Grenville-age metamorphism and deformation along northwest Laurentia: Lithos, v. 134–135, p. 91–107, doi:10.1016/j.lithos.2011.12.008.

Nordsvan, A.R., Collins, W.J., Li, Z., Spencer, C.J., Pourteau, A., Withnall, I.W., Betts, P. G., and Volante, S., 2018, Laurentian crust in northeast Australia: Implications for the assembly of the supercontinent Nuna. Geology, p. 1–4. Paton, C.,

Hellstrom, J., Paul, B., Woodhead, J., Hergt, J., 2011. Iolite: Freeware for the visualisation and processing of mass spectrometric data. J. Anal. At. Spectrom. 26 (12), 2508–2518.

Pattison, D.R.M., Seitz, J.L.D., 2012. Stabilization of garnet in metamorphosed altered turbidites near the St. Eugene lead-zinc deposit, southeastern British Columbia: Equilibrium kinetic controls. Lithos 134–135, 221–235. https://doi.org/10.1016/j.lithos.2011.12.007.

Payne, J.L., Hand, M., Barovich, K.M., Reid, A., Evans, D.A.D., 2009. Correlations and reconstruction models for the 2500–1500 Ma evolution of the Mawson Continent. Geol. Soc. London Spec. Publ. 323 (1), 319–355. https://doi.org/10.1144/SP323.16.

Pisarevsky, S.A., Elming, S.Å., Pesonen, L.J., Li, Z.X., 2014a. Mesoproterozoic paleogeography: supercontinent and beyond. Precambr. Res. 244, 207–225. https://doi.org/10.1016/j.precamres.2013.05.014.

Pisarevsky, S.A., Wingate, M.T.D., Li, Z.X., Wang, X.C., Tohver, E., Kirkland, C.L., 2014b. Age and paleomagnetism of the 1210Ma Gnowangerup-Fraser dyke swarm, Western Australia, and implications for late Mesoproterozoic paleogeography. Precambr. Res. 246, 1–15. https://doi.org/10.1016/j.precamres.2014.02.011.

Pourteau, A., Smit, M.A., Li, Z.-X., Collins, W.J., Nordsvan, A.R., Volante, S., Li, J., 2018. 1.6 Ga crustal thickening along the final Nuna suture. Geology 46, 1–4. https://doi. org/10.1130/G45198.1.

Pratt, B.R., 2001, Oceanography, bathymetry and syndepositional tectonics of a Precambrian intracratonic basin: Integrating sediments, storms, earthquakes, and tsunamis in the Belt Supergroup (Helena Formation, ca. 1.45 Ga), Western North America. Sedimentary Geol. 141–142, 371–394, doi:10.1016/S0037-0738(01) 00083-5.

Pratt, B.R., Ponce, J.J., 2019, Sedimentation, earthquakes, and tsunamis in a shallow, muddy epeiric sea: Grinnell Formation (Belt Supergroup, ca. 1.45 Ga), western North America. GSA Bulle. 1–29, doi:10.1130/B35012.1.

Pratt, B.R., Rule, R.G., 2021. A Mesoproterozoic carbonate platform (lower Belt Supergroup of western North America): Sediments, facies, tides, tsunamis and earthquakes in a tectonically active intracratonic basin. Earth Sci. Rev. 217, 103626. https://doi.org/10.1016/j.earscirev.2021.103626.

Reid, A., Hand, M., Jagodzinski, E., Kelsey, D., Pearson, N., 2008. Paleoproterozoic orogenesis in the southeastern Gawler Craton, South Australia. Austral. J. Earth Sci. 55 (4), 449–471. https://doi.org/10.1080/08120090801888594. Reid, A., Forster, M., 2021. Mesoproterozoic thermal evolution of the northern Gawler Craton from 40Ar/39Ar geochronology. Precambr. Res. 358, 106180. https://doi. org/10.1016/j.precamres.2021.106180.

Reid, A.J., and Payne, J.L., 2017, Magmatic zircon Lu–Hf isotopic record of juvenile addition and crustal reworking in the Gawler Craton, Australia. Lithos 292–293, 294–306, doi:10.1016/j.lithos.2017.08.010.

Rogers, J.J.W., Santosh, M., 2002. Configuration of Columbia, a mesoproterozoic supercontinent. Gondwana Res. 5 (1), 5–22. https://doi.org/10.1016/S1342-937X (05)70883-2.

Ronemus, C.B., Orme, D.A., Campbell, S., Black, S.R., Cook, J., 2020. Mesoproterozoic–Early Cretaceous provenance and paleogeographic evolution of the Northern Rocky Mountains: Insights from the detrital zircon record of the Bridger Range, Montana, USA. GSA Bull 1–25. https://doi.org/10.1130/b35628.1.

Ross, G.M., Villeneuve, M., 2003. Provenance of the Mesoproterozoic (1.45 Ga) Belt basin (western North America): Another piece in the pre-Rodinia paleogeographic puzzle. Geol. Soc. Am. Bull. 115 (10), 1191. https://doi.org/10.1130/ B25209.110.1130/2003135.

Ross, G.M., Parrish, R.R., Villeneuve, M.E., Bowring, S.A., 1991, Geophysics and geochronology of the crystalline basement of the Alberta Basin, western Canada. Can. J. Earth Sci. 28, 512–522, doi:10.1139/e91-045.

Ross, G.M., Parrish, R.R., Winston, D., 1992. Provenance and U-Pb geochronology of the Mesoproterozoic Belt Supergroup (northwestern United States): implications for the age of deposition and pre-Panthalassa plate reconstructions. Earth Planet. Sci. Lett. 113, 57–76.

Sears, J.W., Chamberlain, K.R., Buckley, S.N., 1998. Structural and U-Pb geochronological evidence for 1.47 Ga rifting in the Belt basin, western Montana. Can. J. Earth Sci. 35 (4), 467–475. https://doi.org/10.1139/e97-121.

Schandl, E.S., and Davis, D.W., 2000, Geochronology of the Sullivan deposit: U-Pb and Pb-Pb ages of zircons and titanites: Chapter 8, in Lydon, J.W., H¨oy, T., Slack, J.F., and Knapp, M.E., eds., The Geological Environment of the Sullivan Deposit, British Columbia: Geological Association of Canada, Mineral Deposits Division Special Publication 1, p. 127–135..

Scherer, E., Münker, C., and Mezger, K., 2001, Calibration of the lutetium-hafnium clock. Science 293(5530), 683–687, https://doi.org/10.1126/science.1061372. Schieber, J., 1989, The origin of the Neihart Quartzite, a basal deposit of the mid-proterozoic belt supergroup, Montana, U.S.A. Geol. Magaz. 126, 271–281, doi: 10.1017/S0016756800022366.

Sears, J.W., 2007. Belt-Purcell Basin: Keystone of the Rocky Mountain fold-and-thrust belt, United States and Canada. Geol. Soc. Am. Special Paper 433, 147–166. https:// doi.org/10.1130/2007.2433(07).

Sears, J.W., Link, P.K., Balgord, E.A., Mahoney, J.B., 2010. Quartzite of Argenta, Beaverhead County, Montana, revisited: Definitive Evidence of Precambrian age indicates edge of Belt Basin. Northwest Geology 39, 41–48.

Slack, J.F., Neymark, L.A., Moscati, R.J., Lowers, H.A., Ransom, P.W., Hauser, R.L., Adams, D.T., 2020. Origin of Tin Mineralization in the Sullivan Pb-Zn-Ag Deposit, British Columbia: Constraints from Textures, Geochemistry, and LA-ICP-MS U-Pb. Geochronology of Cassiterite: Economic Geology 115, 1699–1724. https://doi.org/ 10.5382/econgeo.4761.

Spencer, C.J., Kirkland, C.L., Roberts, N.M.W., Evans, N.J., Liebmann, J., 2020. Strategies towards robust interpretations of in situ zircon Lu–Hf isotope analyses. Geoscience Frontiers. https://doi.org/10.1016/j.gsf.2019.09.004.

Spencer, C.J., Kirkland, C.L., Taylor, R.J.M., 2016. Strategies towards statistically robust interpretations of in situ U-Pb zircon geochronology. Geosci. Front. 7 (4), 581–589. https://doi.org/10.1016/j.gsf.2015.11.006.

Stewart, E.D., Link, P.K., Fanning, C.M., Frost, C.D., and McCurry, M., 2010, Paleogeographic implications of non-North American sediment in the Mesoproterozoic upper Belt Supergroup and Lemhi Group, Idaho and Montana, USA. Geology 38, 927–930, doi:10.1130/G31194.1.

Stevens, L.M., Baldwin, J.A., Cottle, J.M., Kylander-Clark, A.R.C., 2015. Phase equilibria modelling and LASS monazite petrochronology: P-T-t constraints on the evolution of the Priest River core complex, northern Idaho. Journal of Metamorphic Geology 33, 385–411. https://doi.org/10.1111/jmg.12125.

Stevens, L.M., Baldwin, J.A., Crowley, J.L., Fisher, C.M., Vervoort, J.D., 2016. Magmatism as a response to exhumation of the Priest River complex, northern Idaho: Constraints from zircon U–Pb geochronology and Hf isotopes. Lithos 262, 285–297. https://doi.org/10.1016/j.lithos.2016.07.006.

Sundell, K.E., Saylor, J.E., 2021. Two-dimensional quantitative comparison of density distributions in detrital geochronology and geochemistry. Geochem. Geophys. Geosyst. 22, 1–25. https://doi.org/10.1029/2020GC009559.

Swain, G., Barovich, K., Hand, M., Ferris, G., Schwarz, M., 2008. Petrogenesis of the St Peter Suite, southern Australia: arc magmatism and Proterozoic crustal growth of the South Australian Craton. Precambr. Res. 166 (1-4), 283–296. https://doi.org/ 10.1016/j.precamres.2007.07.028.

Szpunar, M., Hand, M., Barovich, K., Jagodzinski, E., Belousova, E., 2011. Isotopic and geochemical constraints on the Paleoproterozoic Hutchison Group, southern Australia: Implications for Paleoproterozoic continental reconstructions. Precambr. Res. 187 (1-2), 99–126. https://doi.org/10.1016/j.precamres.2011.02.006.

Tollo, R.P., Corriveau, L., McLelland, J., Bartholomew, M.J., 2004, Proterozoic tectonic evolution of the Grenville orogen in North America: An introduction, in Tollo, R.P., Corriveau, L., McLelland, J., and Bartholomew, M.J., eds., Proterozoic Tectonic Evolution of the Grenville Orogen in North America: Boulder, Colorado, Geol. Soc. Am. Memoir 197, p. 1–18.

Verbaas, J., Thorkelson, D.J., Crowley, J., Davis, W.J., Foster, D.A., Gibson, H.D., Marshall, D.D., Milidragovic, D., 2018. A sedimentary overlap assemblage links Australia to northwestern Laurentia at 1.6 Ga. Precambr. Res. 305, 19–39. https:// doi.org/10.1016/j.precamres.2017.10.001.

Vermeesch, P., 2012. On the visualisation of detrital age distributions. Chem. Geol. v. 312–313, 190–194. https://doi.org/10.1016/j.chemgeo.2012.04.021.

Vermeesch, P., 2018. IsoplotR: A free and open toolbox for geochronology. Geosci. Front. 9 (5), 1479–1493. https://doi.org/10.1016/j.gsf.2018.04.001.

Vervoort, J.D., Lewis, R.S., Fisher, C., Gaschnig, R.M., Jansen, A.C., Brewer, R., 2016. Neoarchean and Paleoproterozoic crystalline basement rocks of north-central Idaho: Constraints on the formation of western Laurentia. Bull. Geol. Soc. Am. 128, 94–109. https://doi.org/10.1130/B31150.1.

Villeneuve, M.E., Ross, G.M., Theriault, R.J., Milews, W., Parrish, R.R., and Broome, J., 1993, Tectonic subdivision and U-Pb geochronology of the crystalline basement of the Alberta Basin, western Canada. Geol. Geol. Survey Canada Bull. 447, p. 1–25..

Volante, S. et al., 2020a, Multiple P-T-d-t paths reveal the evolution of the final Nuna assembly in northeast Australia. J. Metamorphic Geol. 1–35, doi:10.1111/ jmg.12532.

Volante, S., Collins, W. J., Pourteau, A., Li, Z.-X., Li, J., and Nordsvan, A. R., 2020b, Structural evolution of a 1.6 Ga orogeny related to the final assembly of the supercontinent Nuna: Coupling of episodic and progressive deformation. Tectonics, no. 39, https:// doi.org/10.1029/2020TC006162..

Wang, C., Mitchell, R.N., Murphy, J.B., Peng, P., Spencer, C.J., 2020. The role of megacontinents in the supercontinent cycle. Geology 49, 402–406. https://doi.org/ 10.1130/g47988.1.

Whitmeyer, S.J., Karlstrom, K.E., 2007. Tectonic model for the Proterozoic growth of North America. Geosphere 3, 220–259. https://doi.org/10.1130/GES00055.1.

Winston, D., 2007, Revised stratigraphy and depositional history of the Helena and Wallace Formations, Mid-Proterozoic Piegan Group, Belt Supergroup, Montana and Idaho, U.S.A., in Link, P.K., and Lewis, R.S., eds., Proterozoic Geology of Western North America and Siberia, Society for Sedimentary Geology (SEPM) Special Publication 86, 65–100, , doi:10.2110/pec.07.86.0065.

Winston, D., 2016, Sheetflood sedimentology of the Mesoproterozoic Revett Formation, Belt Supergroup, northwestern Montana, USA: GSA Special Paper, v. 522, p. 1–56, doi:10.1130/2016.2522(01).

Winston, D., Link, P., 1993, Middle Proterozoic rocks of Montana, Idaho and eastern Washington: The Belt Supergroup, in Reed, Jr, J.C., Bickford, M.E., Houston, R.S., Link, P.K., Rankin, R.W., Sims, P.K., and VanSchmus, W.R., eds., Precambrian: Conterminous U.S.: Boulder, Colorado, Geological Society of America, The Geology of North America, v. C-2, p. 487–517..

Winston, D., Horodyski, R.J., Whipple, J.W., 1989. Middle Proterozoic Belt Supergroup, western Montana, in 28th International. In: Geological Congress, Field Trip Guidebook T334. American Geo-Belt Supergroup, western Montana American Geophysical Union, Washington, D.C Washington, D.C, p. 102.

Winston, D., Link, P.K., Hathaway, N., 1999, The Yellowjacket is not the Prichard and other heresies: Belt Supergroup correlations, structure and paleogeography, east-central Idaho: Guidebook to the Geology of Eastern Idaho, p. 3–20..

Wooden, J.L., Barth, A.P., and Mueller, P.A., 2013, Crustal growth and tectonic evolution of the Mojave crustal province: Insights from hafnium isotope systematics in zircons. Lithosphere 5, 17–28, doi:10.1130/L218.1.

Xu, Y.-J., Cawood, P.A., Zhang, H.-C., Zi, J.-W., Zhou, J.-B., Li, L.-X., Du, Y.-S., 2019. The Mesoproterozoic Baoban Complex, South China: A missing fragment of western Laurentian lithosphere. GSA Bulletin 1–15. https://doi.org/10.1130/b35380.1.

Yao, W., Li, Z.X., Li, W.X., Li, X.H., 2017. Proterozoic tectonics of Hainan Island in supercontinent cycles: New insights from geochronological and isotopic results. Precambr. Res. 290, 86–100. https://doi.org/10.1016/j.precamres.2017.01.001.

Yonkee, W.A., Dehler, C.D., Link, P.K., Balgord, E.A., Keeley, J.A., Hayes, D.S., Wells, M. L., Fanning, C.M., Johnston, S.M., 2014. Tectono-stratigraphic framework of Neoproterozoic to Cambrian strata, west-central U.S.: protracted rifting, glaciation, and evolution of the North American Cordilleran margin. Earth Sci. Rev. 136, 59–95. https://doi.org/10.1016/j.earscirev.2014.05.004.

Zhang, S., Li, Z.X., Evans, D.A.D., Wu, H., Li, H., Dong, J., 2012. Pre-Rodinia supercontinent Nuna shaping up: A global synthesis with new paleomagnetic results from North China. Earth Planet. Sci. Lett. 353–354, 145–155. https://doi.org/10.1016/j.epsl.2012.07.034.

Zhao, G., Cawood, P.A., Wilde, S.A., Sun, M., 2002. Review of global 2.1-1.8 Ga orogens: implications for a pre-Rodinia supercontinent. Earth Sci. Rev. 59 (1-4), 125–162. https://doi.org/10.1016/S0012-8252(02)00073-9.

Zhao, G., Sun, M., Wilde, S.A., Li, S., 2004. A Paleo-Mesoproterozoic supercontinent: assembly, growth and breakup. Earth Sci. Rev. 67 (1-2), 91–123. https://doi.org/10.1016/j.earscirev.2004.02.003.

Zirakparvar, N.A., Vervoort, J.D., McClelland, W., Lewis, R.S., 2010. Insights into the metamorphic evolution of the Belt-Purcell basin; evidence from Lu–Hf garnet geochronology.

Chapter 4: Grenville-age metamorphism within the Belt Basin of western Laurentia

Abstract

The presence or absence of ca. 1100–1000 Ma "Grenville-age" tectonism in western Laurentia is long debated and has significant implications for the assembly of supercontinent Rodinia. Recently, identification of ca. 1350–1020 Ma garnet-grade metamorphism within the Clearwater complex of the Belt Basin has renewed this debate. However, the tectonic implication of such cryptic metamorphic records is uncertain due to regional structural and thermal overprinting by younger Cordilleran processes. Here, we present new monazite and apatite U–Pb results from metapelites within the western region of the Clearwater complex. Although monazite ages overlap with existing garnet ages, some apatite records ca. 680 Ma ages associated with nearby rift-related magmatic rocks that formed during Rodinia breakup and indicate that locally Cordilleran conditions did not exceed ~450–550°C in the western Clearwater complex. Consequently, the mineral assemblages within these rocks most likely reflect the peak metamorphic event recorded by the youngest ca. 1100–1020 Ma garnet Lu–Hf and monazite U–Pb ages. Thermodynamic modeling of these assemblages indicates P/T conditions of 5–7.5 Kbar and 620–670°C, suggesting burial depths of at least ~17–22 km along a moderately-high average geothermal gradient of ~23–36°C/km. These ca. 1100–1020 Ma metamorphic conditions are difficult to satisfy with thermal upwelling/heating within the Belt Basin alone, and thus advocate for western tectonism and localized Grenville-age structural inversion and crustal thickening within the Belt Basin, likely along inherited structures. Consequently, global geologic models should account for ca. 1100–1020 Ma Grenville-age tectonism in continental blocks adjacent to the western margin of Laurentia within supercontinent Rodinia.

4.1. Introduction

The Mesoproterozoic Era (1600–1000 Ma) records the transition from Earth's first supercontinent Nuna (also called Columbia; ca. 1600–1300 Ma) to its successor, Rodinia (ca. 1100–800 Ma; e.g. Li et al., 2019). However, researchers have suggested that the global transition from Nuna to Rodinia may have significant geodynamic differences from the previous assembly of Nuna, and the ensuing Rodinia to Pangea supercontinent transition. Notably, the geologic record suggests evidence for a different style of plate tectonics associated with systemically higher thermobaric (temperature/pressure; T/P) conditions during metamorphism (Brown et al., 2020), a warmer upper mantle and the presence of hot, low and thin "Grenville-age" mountain belts (Spencer et al., 2021; Zhu et al., 2022), and/or the closure of "young" interior oceans, rather than older exterior oceans during this supercontinent transition (e.g. Li et al., 2019). Consequently, the Nuna to Rodinia supercontinent cycle is considered to be a perplexing geological time interval dubbed the "Boring Billion" (Cawood and Hawkesworth, 2014; Sobolev and Brown, 2019).

The ca. 1480–1380 Ma Belt Supergroup outcrops along the western margin of Laurentia and represents one of the largest Mesoproterozoic sedimentary sequences in the world, containing an immense thickness of strata (>15 km), covering >200,000 km^2 (Lonn et al., 2020). The monotonous lithology of Belt Supergroup stratigraphy records its deposition in an intracratonic rift basin near the center of the Nuna supercontinent landmass (Winston and Link, 1993; Box et al., 2020). Enigmatically, after deposition, despite paleogeographic models calling for globally widespread tectonism associated with the subsequent breakup of Nuna and assembly of Rodinia, most Belt Supergroup strata remained largely undisturbed for the next 1 billion years until the late Mesozoic Cordilleran (Sevier/Laramide) orogeny. Consequently, the general ca. 1300–900 Ma tectonic quiescence in this region, notably the absence of ca. 1100–1000 Ma Grenville-age tectonism, may indeed lend credence to the assertion that the Nuna to Rodinia transition was "boring", at least in this region.

Then again, isotopic studies along the western portion of the Belt Basin, particularly within strata recently buried deep within Cordilleran metamorphic core complexes (notably the Matthew Creek metamorphic zone and associated Priest River metamorphic complex, the Clearwater metamorphic core complex and the Bitteroot metamorphic core complex) have revealed a growing body of evidence for tectonism within this interval. This evidence includes indications of ca. 1115–1065 Ma Grenville-age metamorphism (e.g. Doughty and Chamberlain, 2008; Zirakparvar et al., 2010; Nesheim et al., 2012; Slack et al., 2020) that has notable implication for conflicting collisional (e.g. Li et al., 1995; 2013; Yao et al., 2017), transpressional (e.g. Merdith et al., 2020; Mulder et al., 2018) and/or apparently tectonically quiescent (e.g. Eyster et al., 2018) models of Rodinia assembly along western Laurentia (Fig. 4.1). However, interpretations of the importance of the Grenville-age isotopic ages within the Belt Basin, and consequently evaluation of proposed global geodynamic models are often in disagreement. Reaching a consensus on their importance is likely hampered by difficulties in separating the younger, Cordilleran record of metamorphism from the older, Grenville-age record. Some workers interpret the Grenville-age metamorphism to simply reflect static magmatic heating at depth (e.g. Doughty and Chamberlain, 2008; Slack et al., 2020), while others have suggested that the ages require tectonic thickening (Zirakparvar et al., 2010; Neishem et al., 2012).

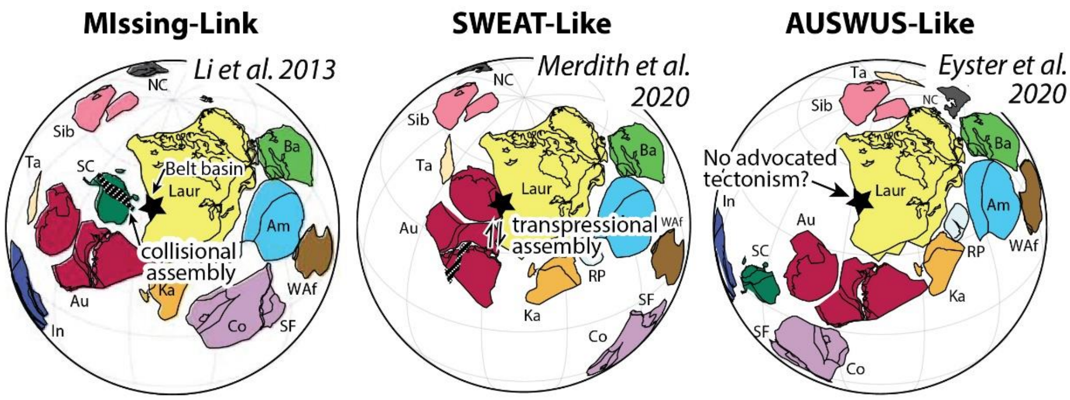

Fig. 4.1: Leading models with differing for Rodinia configurations and assembly mechanism. These models include: Missing-Link collisional (Li et al., 1995; 2013; Yao et al., 2017), SWEAT-like (Southwest U.S.–East Antarctica; Moores, 1991) transpressional (e.g. Mulder et al., 2018; Merdith et al., 2020) and/or apparently AUSWUS-like (Australia–Southwestern U.S.; Karlstrom et al., 1999) tectonically quiescent (e.g. Eyster et al., 2018) mechanism of Rodinia assembly along western Laurentia. Abbreviations include: Am, Amazonia; Au, Australian cratons including Antarctic Mawsonland; Ba, Baltica; Co, Congo; In, India; Ka, Kalahari; Laur, Laurentia; NC, North China; RP, Rio Plata; SC, South China; SF, Sao Francisco; Sib, Siberia; Ta, Tarim; WAf, West African craton.

Here, we present new laser-ablation inductively coupled mass spectroscopy (LA–ICPMS) monazite and apatite U–Pb geochronology, electron probe microanalysis (EPMA) of mineral compositions and phase equilibrium P–T modeling of metapelitic strata from the Clearwater complex. These rocks contain a record of ca. 1350–1000 Ma garnet growth under unknown conditions (Zirakparvar et al., 2010; Neishem et al., 2012), which is variably overprinted by younger ca. 130–55 Ma

Cordilleran metamorphism that reaches as high as lower granulite facies (Doughty et al., 2007). Collectively, our results were able to constrain a portion of the complex that was not buried deeply within the Cordilleran orogeny and thus preserves a critical record of amphibolite-grade Grenville-age metamorphism in this region. These results reveal important insights into the Nuna to Rodinia transition in western Laurentia, and provide additional constraints on evaluating global tectonic and metamorphic processes during the late Mesoproterozoic.

4.2. Geologic Overview

The North American Cordillera is a sinuous mountain belt that runs for ~6500 km along the western edge of Laurentia, from Alaska to Mexico. The orogen records prolonged subduction of oceanic lithosphere beneath western North America since the early Mesozoic. Along most of the Cordillera, Late Cretaceous to Paleogene overthickening of the orogenic wedge and/or changing subduction boundary conditions (e.g. flat slab subduction) resulted in the formation of metamorphic core complexes (Dickinson, 2004; Fig. 4.3). These core complexes expose rocks formerly buried deep within the hinterland of the Cordilleran orogen due to late Mesozoic or younger crustal thickening (e.g. Wernicke, 1981; Stevens et al., 2015; Howlett et al., 2021). Although the Cordillera is an archetypal natural laboratory to study modern orogenic processes, overprinting by Cordilleran processes commonly obscures the record of older events along the western margin of Laurentia. Unfortunately, the western margin of Laurentia occupies a critical, central, position along which most models advocate the final assembly of Proterozoic supercontinents Nuna and Rodinia occurred. As a result, difficulty in deciphering the regional pre-Cordilleran record of western Laurentia has made evaluation of conflicting global models challenging.

Following a tectonic lull during the ca. 1610–1490 Ma North American Magmatic Gap associated with final Nuna assembly (Ross and Villenavue, 2001; Brennan et al., 2022), juvenile terranes and arcs were accreted along most of the southern margin of Laurentia from ca. 1480–1350 Ma. Accretion was associated with widespread bimodal ‘A-type’ granite and anorthosite magmatism within the Granite-Rhyolite province (e.g. Bickford et al., 2015; Fig. 4.2). In southwestern Laurentia, magmatism was contemporaneous with the ca. 1460–1400 Ma Picuris orogeny (Karlstrom et al., 2001; Daniel et al., 2013) then, from ca. 1380–1320 Ma, development of an extensive backarc system (Mulder et al., 2017).

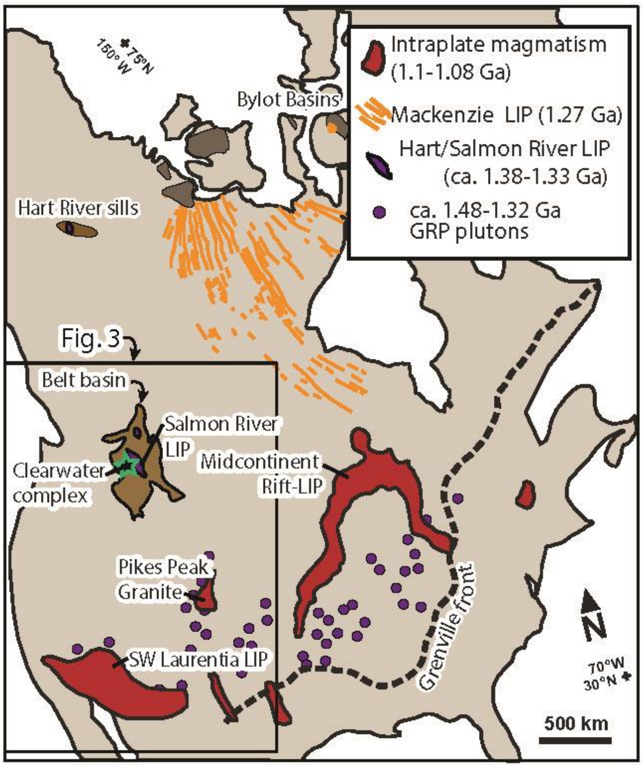

Fig. 4.2: Simplified geologic map of Laurentia (adapted from Greenman et al., 2021) indicating the relevant ca. 1480–1080 Ma geologic provinces including the ca. 1480–1380 Ma Belt basin, ca. 1480–1320 Ma Granite Rhyolite province, ca. 1380–1330 Ma Hart and Salmon River Large Igneous Provinces (LIP), ca. 1270 Mackenzie LIP and the ca. 1100–1080 Midcontinent Rift/LIP, Pikes Peak Batholith, Southwestern Laurentian LIP (SWLLIP), and Arctic Bylot Basins. The extent of the North American Cordillera shown in Fig. 4.3 is indicated.

The ca. 1470–1380 Ma Belt Basin is an extensive intracratonic basin that formed within the supercontinent Nuna, concurrent with the aforementioned more widespread tectonomagmatic activity in southern Laurentia, and contains over 15 km thick of shallow water and subaerially deposited strata, that record intermittent, localized syndepositional magmatism (Lonn et al., 2020 and references within). Following Belt Basin deposition, continental-arc magmatism occurred in southern Laurentia from ca. 1250–1230 Ma due to continued subduction beneath the southern margin of Laurentia that predated onset of the main episode of Grenvillian orogenesis.

Grenville-aged tectonism in southern Laurentia peaked at ca. 1140–1100 Ma (Mulder et al., 2017), broadly coeval with slab break-off and/or delamination beneath southern Laurentia (Mosher et al., 2008). Subsequent impingement of a mantle plume beneath the Laurentian midcontinent resulted in formation of the ~3000-km long Midcontinent Rift (Cannon and Hinze, 1992; Stein et al., 2015) and emplacement of ca. 1094–1080 Ma diabase dykes of the Southwestern Laurentian large igneous province (SWLLIP) (Bright et al., 2014). The record of magmatism at ca. 1080 Ma extends as far northwest as central Colorado, where the ca. 1115–1065 Ma Pikes Peak batholith intruded along crustal sutures within the Yavapai province, and likely records lithospheric delamination and/or plume activity (Guitreau et al., 2016). In northern Laurentia, intracratonic basins (the Bylot basins) developed from ca. 1090 Ma to 1050

Ma (Fig. 4.2; Gibson et al., 2019; Rainbird et al., 2020; Greenman et al., 2021). Collectively, the data are consistent with a widespread episode of thermal upwelling and localized extension across Laurentia around ca. 1120–1050 Ma, in a period otherwise dominated by Grenvillian orogenesis associated with assembly of Rodinia. Grenville-age (ca. 1300–1000 Ma) orogens are recognized on many continental blocks (such as Laurentia, South China, Australia, Kalahari and Baltica) and have long been known to reflect the widespread assembly of supercontinent Rodinia (e.g. Moores, 1991; Li et al., 2008; Mulder et al., 2017; Johansson et al., 2022).

The Clearwater complex is the central of three main core complexes that occur along the western edge of the Belt Basin, including the Priest River complex and associated Matthew Creek metamorphic zone ~150 km to the north, and the Bitterroot complex ~150 km to the southeast (Fig. 4.3). These complexes all record an enigmatic record of ca. 1400–1000 Ma tectonism, which is variably overprinted by younger Cordilleran processes, but is generally attributed to two main events. These two events consist of an older ca. 1380–1300 Ma East Kootenay "Orogeny" (McMechan and Price, 1982) and a younger poorly understood ca. 1115–1060 Ma Grenville-age event (e.g. Neishem et al., 2012).

The ca. 1380–1300 Ma East Kootenay tectono-magmatic event was contemporaneous with the final stages of tectonism and magmatism within the Granite-Rhyolite province in southern Laurentia, and largely records high-T, low-P regional metamorphism (McFarlane and Pattison, 2000; McFarlane, 2015) and bimodal magmatism within the Salmon River sills and associated Elk City Domain within the Belt Basin (Doughty and Chamberlain, 1996, 2008; Gaschnig et al., 2013). Consequently, the East Kootenay tectono-magmatic event has been interpreted as a period of either orogenic collapse (McMechan and Price, 1982; McFarlane, 2015) or volcanism and renewed subsidence near the end of deposition of the Belt Supergroup (Doughty and Chamberlain, 2010; McFarlane and Pattison, 2000; Pattison and Seitz, 2012). Some 1000 km further north, Verbaas et al., (2018) correlate the ca. 1380 Ma Hart River sills with the Salmon River sills, and suggests that the bimodal magmatic provinces may record rifting in western Laurentia. Ernst et al., (2008) considers the Hart River and Salmon River sills to comprise a single large igneous province (LIP) that may record rifting of Nuna. Recently, an ≥2.5 km thick package of fine-grained and carbonate rocks (the Deer Trail Group) has been shown to be younger than ca. 1300 and may record deposition during the final stages of this East Kootenay tectono-magmatic event (Box et al., 2020; Brennan et al., 2021b). Remnants of Deer Trail Group strata are likely present elsewhere along the western edge of the Belt Basin (Pearson and Link, 2021), suggesting that a substantial thickness of sedimentary rocks may have been removed from atop the Belt Basin prior to Rodinian rifting after ca. 760 Ma (Brennan et al., 2021a).

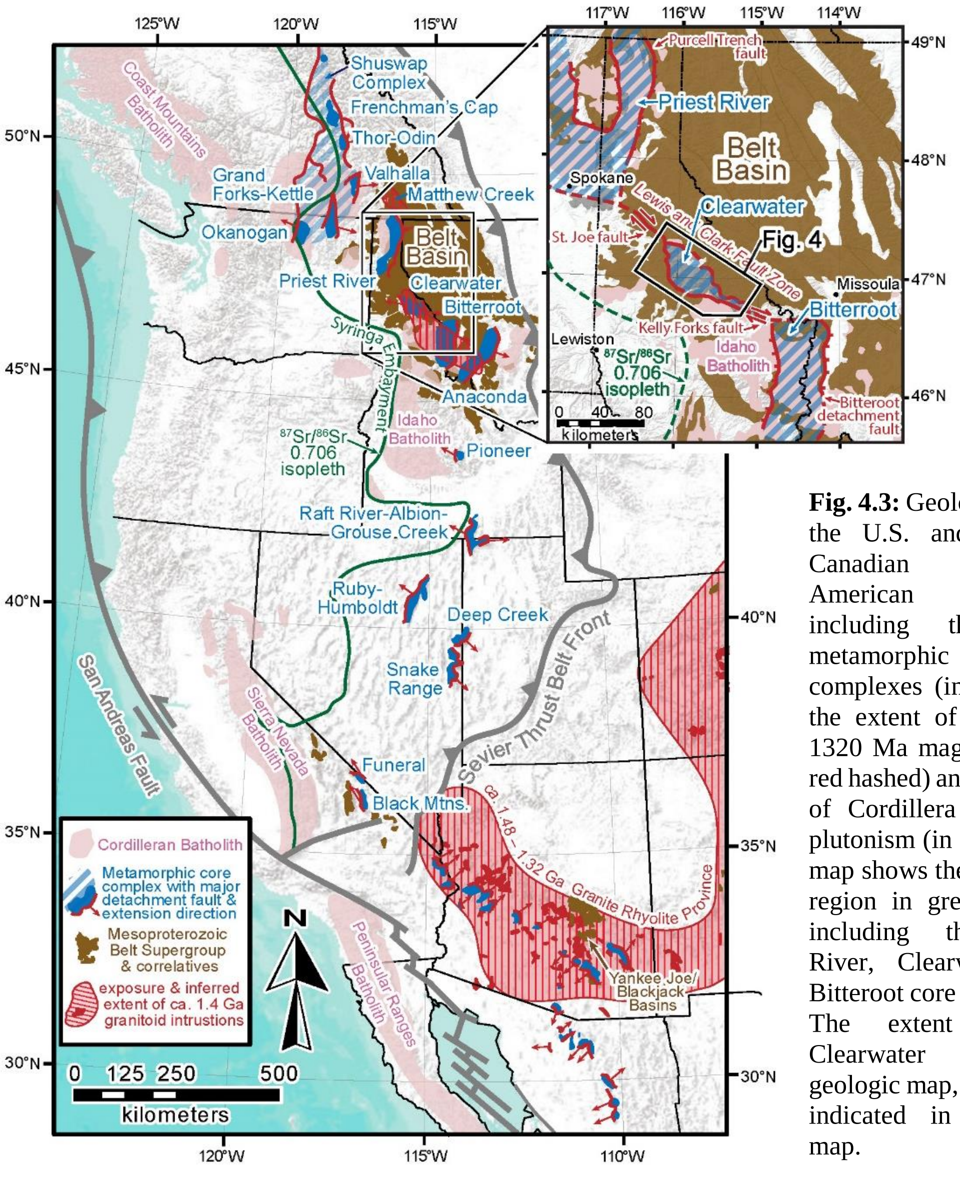

Fig. 4.3: Geologic map of the U.S. and southern Canadian North American Cordillera, including the major metamorphic core complexes (in blue) and the extent of ca. 1480–1320 Ma magmatism (in red hashed) and the extent of Cordillera associated plutonism (in pink). Inset map shows the Belt basin region in greater detail, including the Priest, River, Clearwater, and Bitteroot core complexes. The extent of the Clearwater regional geologic map, in Fig. 4, is indicated in the inset map.

The younger event is often attributed to ca. 1115–1060 Ma, Grenville-age, tectonothermal activity. This Grenville-age metamorphism has been suggested to simply reflect static magmatic heating at depth, perhaps suggesting a relation to coeval, deep (possibly plume related) magmatism within the Midcontinent Rift, and Southwest Laurentian Large Igneous Province (e.g. Doughty and Chamberlain, 2008; Slack et al., 2020). However, no magmatism of this age has been directly identified within the Belt Basin, while it is relatively widespread in these other coeval provinces. Others have instead suggested that the ca. 1100 Ma ages instead require tectonic thickening (Zirakparvar et al., 2010; Neishem et al., 2012), similar to the peak of Grenville orogenic burial in southern Laurentia at ca. 1140–1100 Ma (Mulder et al., 2017). Recently, the only suspected ca. 1100 Ma strata in this region, the Buffalo Hump Formation (e.g. Ross et al., 1992), was shown to contain ca. 760 Ma detrital zircon grains. These ages indicate that the Buffalo Hump Formation was actually deposited during Rodinia breakup, not assembly (Brennan et al., 2021a). Consequently, no magmatism or stratigraphy associated with this Grenville-age event within the Belt Basin is identified.

Most Belt Supergroup strata east of the Priest River, Clearwater and Bitterroot complexes record greenschist or lower-grade metamorphism and thus have not been examined by metamorphic studies. However, the enigmatic spread of ca. 1400–1000 Ma ages variably overprinted by younger ca. 130–50 Ma metamorphism recorded within the amphibolite-grade metamorphic assemblages of the within the Priest River, Clearwater and Bitterroot complexes have been investigated. In the Priest River and Bitteroot complexes, metamorphism has mostly been interpreted to relate to late Mesozoic and younger Cordilleran events, consistent with monazite U–Pb ages (Stevens et al., 2015; Aleinikoff et al., 2012). However, structures related to deposition of the Belt Supergroup and ca. 1380–1060 Ma U–Pb cassiterite (SnO2 ore; Slack, 2020), monazite (McFarlane, 2015) and xenotime (Aleinikoff et al., 2012) ages are known to occur.

Within the Priest River complex, Mesoproterozoic lower Belt Supergroup metapelitic rocks record peak metamorphic conditions of ~785–790 °C and ~9.6–10.3 kbar (constrained by phase equilibria modelling) between ca. 74 and 54 Ma as recorded by U–Pb monazite ages (Stevens et al., 2015). However, approximately 100 km north of the Priest River complex, in a similar structural position within the Cordilleran orogenic belt, lower Belt Supergroup strata in the Matthew Creek metamorphic zone (Fig. 3) are intruded by 1365 ± 5 and 1335 ± 5 Ma peraluminous granites and have an older, pre-Cordilleran metamorphic record. Lower Belt Supergroup metapelites in the Matthew Creek metamorphic zone contain layer-parallel foliation fabrics and peak metamorphic conditions of ~580–650 °C and ~3.5 kbar (also constrained by phase equilibria modelling) that occurred from ca. 1365–1335 Ma, as recorded by U–Pb monazite ages (McFarlane and Pattison, 2000; McFarlane, 2015). Some 10 km to the northeast, ca. 1468 Ma casserite hosted within metapelitic rocks of the lower Belt

Supergroup records thermal events (of unknown P/T conditions) at ca. 1380 and 1075 Ma (Slack, 2020).

Along the southern region of the Belt Basin, the Bitteroot complex records peak metamorphic conditions of ~700–750 °C and ~7–8 kbar (based on early garnet and amphibole composition thermobarometry methods; House et al., 1997) between ca. 64 and 56 Ma (Aleinikoff et al., 2012; Howlett et al., 2021). Monazite from Mesoproterozoic rocks in the Bitteroot complex generally record Cretaceous (ca. 110–92 Ma) U–Pb ages that are similar in age to the intrusion of nearby granites from the Idaho Batholith (Aleinikoff et al., 2012; Bookstrom et al., 2016). However, rocks in the Bitteroot complex also record evidence for pre-Cordilleran metamorphism, particularly within the Blackbird mineralized district that contains ca. 1370 Ma bimodal magmatism, ca. 1370–1320 Ma U–Pb xenotime ages, and ca. 1060 Ma hydrothermal xenotime ages (Aleinikoff et al., 2012). Mesoproterozoic metamorphism in this region is estimated to require pressures of 4–6 kbar (based on garnet thermobarometry methods) equating to ~14–20 km of burial (Doughty and Chamberlain, 2010; Bookstrom et al., 2016).

The Clearwater complex (Fig. 4.4) also records peak metamorphic conditions of ~700–750 °C and pressures as high as ~9 kbar (based on garnet thermobarometry methods) between ca. 82 and 64 Ma constrained by U–Pb ages of metamorphic zircon rims (Doughty et al., 2007). Doughty et al. (2007) only looked at the internal zone of the complex, which was likely buried the deepest in the Cordilleran orogeny, and suggests that the Clearwater complex experienced similar Cordilleran metamorphism as the previously described complexes to the north and south. However, early workers (Lang and Rice, 1985) recognized that metamorphism within the internal zone overprinted an early regional metamorphic event that is better preserved in the external (marginal) zones of the complex (Fig. 4.4; Doughty et al., 2007; Baldwin et al., 2016). Subsequent Lu–Hf garnet geochronology on metapelitic rocks primarily within these external zones revealed an enigmatic spread of ca. 1400–1000 Ma ages (Zirakparvar et al., 2010; Neishem et al., 2012) with no record of late Mesozoic to early Paleogene metamorphism (Doughty et al., 2007). These results suggest that the external zone of the Clearwater complex may contain a better preserved record of these Mesoproterozoic metamorphic events than amphibolite-grade regions to the north (Priest River complex and Matthew Creek metamorphic zone) or south (Bitterroot complex and Blackbird district).

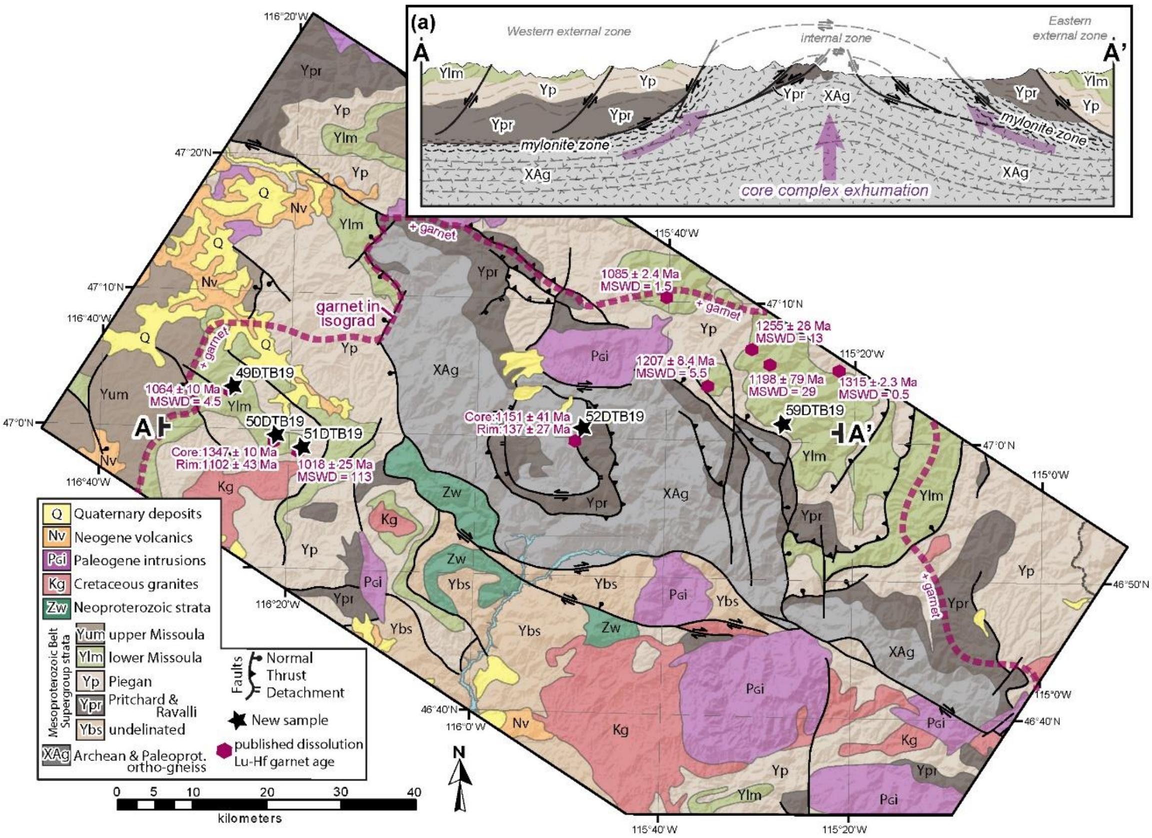

Fig 4.4: Geologic map of the Clearwater complex (modified from Lewis et al., 2012), including the published ca. 1350–1020 Ma garnet Lu–Hf ages in this region (Zirakparvar et al., 2010; Neishem et al., 2012), and the location of our samples along the western external region of the complex (49, 50, 51DTB19), center (52DTB19), and eastern external region (59DTB19). Schematic core complex cross section cartoon (A–A') after Doughty et al., (2007).

4.3. Methods

4.3.1 Mineralogy

From selected rock billets, Wagner Petrographic cut and polished (30 µm thick) thin sections for petrographic investigation. The thin sections were investigated using standard transmitted light microscopy and TESCAN integrated mineral analyzer (TIMA) at the John de Laeter Centre at Curtin University, Perth Australia. TIMA mapping of polished thin sections provided detailed X-ray and back-scattered electron (BSE) maps for mineralogical characterization, including quantification of mineral modes and the identification of accessory phases for subsequent dating. TIMA analyses used a 15mm working distance, a 2500eV beam intensity and a spot size of 50-µm. Full thin section photomicrographs were taken with a Zeiss Axio Imager 2 imaging system. A JEOL 8530F electron probe microanalyser (EPMA) at the Centre for Microscopy, Characterization and Analysis, University of Western Australia was used to measure semi-quantitative garnet mineral compositions. EPMA parameters included a 15kV accelerating voltage, 20 nA beam current, 100-ms dwell time and utilized natural and synthetic standards. Garnet formula were calculated stoichiometrically based on 12 oxygen following Droop (1987).

4.3.2 **Phase equilibrium modelling**

Material from the same hand sample as used for the thin sections was analyzed for bulk rock geochemistry by the Bureau Veritas Laboratory, in Perth, Western Australia using X-Ray Fluorescence (XRF). Isochemical *P–T* phase diagrams (pseudosections) were generated for the major element oxide compositions using THERMOCALC 3.50 (Holland and Powell, 2011) and the activity–composition models of White et al., (2014a, 2014b) within the MnO–Na_2O–CaO–K_2O–FeO–MgO–Al_2O_3–SiO_2–H_2O–TiO_2–O (MnNCKFMASHTO) system. Calculations used an Fe^{3+}/Fe^{2+} ratio of 0.2 (Johnson et al., 2021).

4.3.3 **Laser-ablation mass spectroscopy**

Monazite and apatite grains were targeted in-situ within the thin sections for measurement of U–Pb isotopes. During this analysis, material ablated by a Resonetics RESOlution SE 193nm laser incorporating a dual volume S155 sample cell was sent to an Agilent 8900 triple-quadrupole inductively coupled mass spectroscopy (LA-QQQ-ICPMS) which measured ^{202}Hg, ^{204}Pb (and ^{204}Hg), ^{206}Pb, ^{207}Pb, ^{208}Pb, ^{232}Th, and ^{238}U masses. All data was collected across two analytical sessions at the GeoHistory Facility in the John de Laeter Centre at Curtin University, Perth Australia. In Iolite 3.5, the monazite time-resolved mass spectra were reduced using the U_Pb_Geochronology4 data reduction scheme (Paton et al, 2011). Due to the presence of common-Pb bearing standards, apatite time-resolved mass spectra were reduced using VizualAge_UcomPbine reduction scheme (Chew et al., 2014 and references within). The VizualAge_UcomPbine reduction scheme applies a common-Pb correction to the primary standard before applying a drift correction to the unknowns; otherwise, no common (or non-radiogenic) Pb-correction was applied. Based on the long term-reproducibility of U-Pb standard analysis at the GeoHistory Facility an additional 2% error was propagated to individual analyses.

Due to the variable common-Pb content of apatite, the uncorrected U–Pb apatite data was plotted on Terra-Wasserburg Concordia diagrams (^{207}Pb/^{206}Pb vs. ^{238}U/^{206}Pb), and the apatite age was calculated as the lower Concordia intercept age of a free-regression Discordia line, with the common Pb-component represented by the y-intercept on the $^{207}Pb/^{206}Pb$ axis (Chew et al., 2011; Kirkland et al., 2018). This approach assumes that the U–Pb data are concordant and equivalent. To a lesser degree, monazite can also sometimes include a component of common Pb. Where a common-Pb component was apparent within some monazite analyses, a similar approach was employed which is covered further in the discussion. All data was calculated and plotted using IsoplotR (Vermeesch, 2018).

For monazite U–Pb analysis, monazite grains were targeted with a 10 µm laser spot. Monazite 44069 was utilized as the primary standard and gave a weighted mean age of 424.1 ± 4.6 Ma (mean square weighted deviation or MSWD = 0.02) which is the same as the accepted value (424.9 ± 0.4 Ma; Aleinikoff et al., 2006). Analysis of secondary reference standards, Manangotry (558 ± 3 Ma; Horstwood et al., 2003) and Stern (511.7 ± 1.2 Ma; Palin et al., 2013) gave weighted mean ages (562.4 ± 7.6, MSWD = 0.3; 509.9 ± 5.42, MSWD = 0.38) within uncertainty of accepted values. Only monazite U–Pb analyses that overlap Concordia within 2σ uncertainties are defined as concordant (e.g. Spencer et al., 2016).

Apatite U–Pb analyses used a 30 µm laser spot and data were calibrated against the Madagascar apatite standard, which gave a weighted $^{238}U/^{206}Pb$ mean age of 472.8 ± 5.1 Ma (MSWD = 0.06) which is the same as the published value (474.25 ± 0.85; Thomson et al., 2012). Secondary reference standards Forest Center–FC (1094 ± 34; Thomson et al., 2012) and McClure Mountain–MMC (523.5 ± 1.47 Ma; Schoene and Bowring, 2006), when treated as unknowns and allowed free regression on a discordia line in Tera-Wasserburg space yielded lower concordia intercept ages (1098.9 ± 34.2, MSWD = 0.39 and 522.8 ± 17.3, MSWD = 0.92, respectively), also consistent with published values.

4.4. Results

4.4.1 Field and petrographic observations

The metapelitic samples (49, 50, 51, and 59DTB19) were all collected from the Wallace Formation of the Belt Supergroup (Fig. 4.4; Lewis et al., 1999; 2001; 2005). To the north and east, where the Wallace Formation is only weakly metamorphosed, it consists mostly of fine sandstone and siltstone, commonly in graded couplets, with dolomite and carbonate intervals, and is overlain by at least 8 km of upper Belt Supergroup strata (Lonn et al., 2020). Approximately 250 km northeast of the study area within the Clearwater complex, a volcanic tuff from a similar stratigraphic position yielded a 1454 ± 9 Ma age, and a stratigraphically-higher rhyolitic lava an age of 1443 ± 7 Ma age (Evans et al., 2000), consistent with a ca. 1450 Ma depositional age for the protoliths of the metapelitic rocks discussed below.

Western extent of Clearwater Complex–Samples 49, 50, and 51DTB19

Sample 49DTB19 is a garnet–muscovite–staurolite–biotite–quartzofeldspathic schist with relict (4 to 20 mm thick) graded bedding (Fig. 4.5). This location was previously sampled (sample 05JV07) by Zirakparvar et al., (2010). They report a Lu–Hf garnet age of 1064 ± 10 (MSWD = 4.5) from this locality. In our collected sample (49DTB19), a foliation is mostly defined by alignment of feldspar and micas and is mostly subparallel to bedding. Staurolite porphroblasts are up to 4 cm long and may be twinned. Garnet forms small (mostly <1 mm) porphyroblasts containing apparently randomly-oriented inclusions (primarily quartz) that are preferentially concentrated in the cores of grains. There is no observed deflection in (i.e. wrapping of) the foliation around garnet or staurolite porphroblasts (Fig. 4.5A, inset i, inset ii; Fig. 4.6A). Monazite and apatite are present within the matrix but neither occur as inclusions within garnet, and neither garnet, monazite or apatite are found as inclusions within staurolite.

Sample 50DTB19 is a staurolite–muscovite–garnet–biotite–sillimanite–quartzofeldspathic schist from the same location of sample 08HL-04 of Neishem et al., (2012), who report similar lithologies and Lu–Hf garnet dissolution ages of 1347 ± 10 Ma (MSWD = 4.6; garnet cores) and 1102 ± 43 Ma (MSWD = 42; garnet rim). Sillimanite comprises both large prismatic porphyroblasts (up to 30 mm long; Fig. 4.5B, inset i), and as fibrolite (Fig. 4.5B, inset ii). The foliation is defined primarily by matrix micas, and sillimanite porphyroblasts. In thin section, thin veinlets filled primarily with K-feldspar crosscut the prismatic sillimanite porphyroblasts (Fig. 4.6B). Small, euhedral to subhedral staurolite crystals are found along the margins of sillimanite (Fig. 4.6B). Garnet grains within 50DTB19 are mostly euhedral, up to 3 mm in diameter, and are clearly wrapped by the foliation, locally exhibiting evidence for dissolution and quartz strain shadows. Garnet grains generally show an inclusion-rich (mostly quartz) core. Monazite grains occur within the matrix and as inclusions within garnet.

Sample 51DTB19 is a quartzofeldspathic muscovite–garnet–biotite–sillimanite schist. Sillimanite is present as small (up to 2 mm long) clusters of fibrolite that are preferentially alinged parallel a subtle foliation and are crosscut by K-feldspar (Fig. 4.6C). The mica- and quartz-defined foliation within this sample is less strongly developed and wraps large (≥5 mm in diameter) garnet porphyroblasts (Fig. 4.5Ci). This sample is from the same location as sample 05JV03 of Zirakparvar et al., (2010), who report similar lithologies and a Lu–Hf garnet dissolution age of 1018 ± 25 Ma (MSWD = 113). Based on the high MSWD of the Lu–Hf isochron including all five garnet fractions analysed, Zirakparvar et al., (2010) propose discrete Lu–Hf isochron model ages of 1024 ± 3 Ma (MSWD = 1.5) and 1081 ± 20 Ma (MSWD = 45) based on inclusion-richer and inclusion-poorer garnet fractions.

Core of Clearwater Complex–Sample 52DTB19

Sample 52DTB19 is a strongly-lineated mylonitic ilmenite- and apatite-bearing garnet amphibolite from the central portion of the Clearwater complex. In thin-section, interstitial quartz is abundant, suggesting alternation by hydrothermal fluids (Fig. 4.5D), and consequently this sample was not utilized for thermodynamic modelling, but was previously analyzed for zircon U/Pb and O- isotopes (Brennan et al., 2022), which we supplement with new apatite U/Pb results in this study.

Eastern extent of Clearwater Complex–Sample 59DTB19

Sample 59DTB19 is a quartzofeldspathic monazite- and apatite-bearing muscovite–garnet–biotite schist, collected along the eastern extent of the complex. Although no garnet ages are reported from this specific outcrop, 10 to 22 km to the north, Neishem et al., (2012) reports Lu–Hf garnet ages that range from ca. 1315 to 1085 Ma (see Fig. 4.4). In this sample, the foliation is mostly defined by quartz, feldspar and micas. Garnet grains have inclusion-rich (mostly quartz) cores and exhibit dissolution textures. Garnet grains locally show core/rim geometries and exhibit development of strain shadows that are filled with biotite, muscovite, and quartz (Fig. 4.5E inset i and ii; Fig. 4.6DE). Monazite and apatite grains are present within the matrix. A couple of monazite grains are also present as inclusions within garnet.

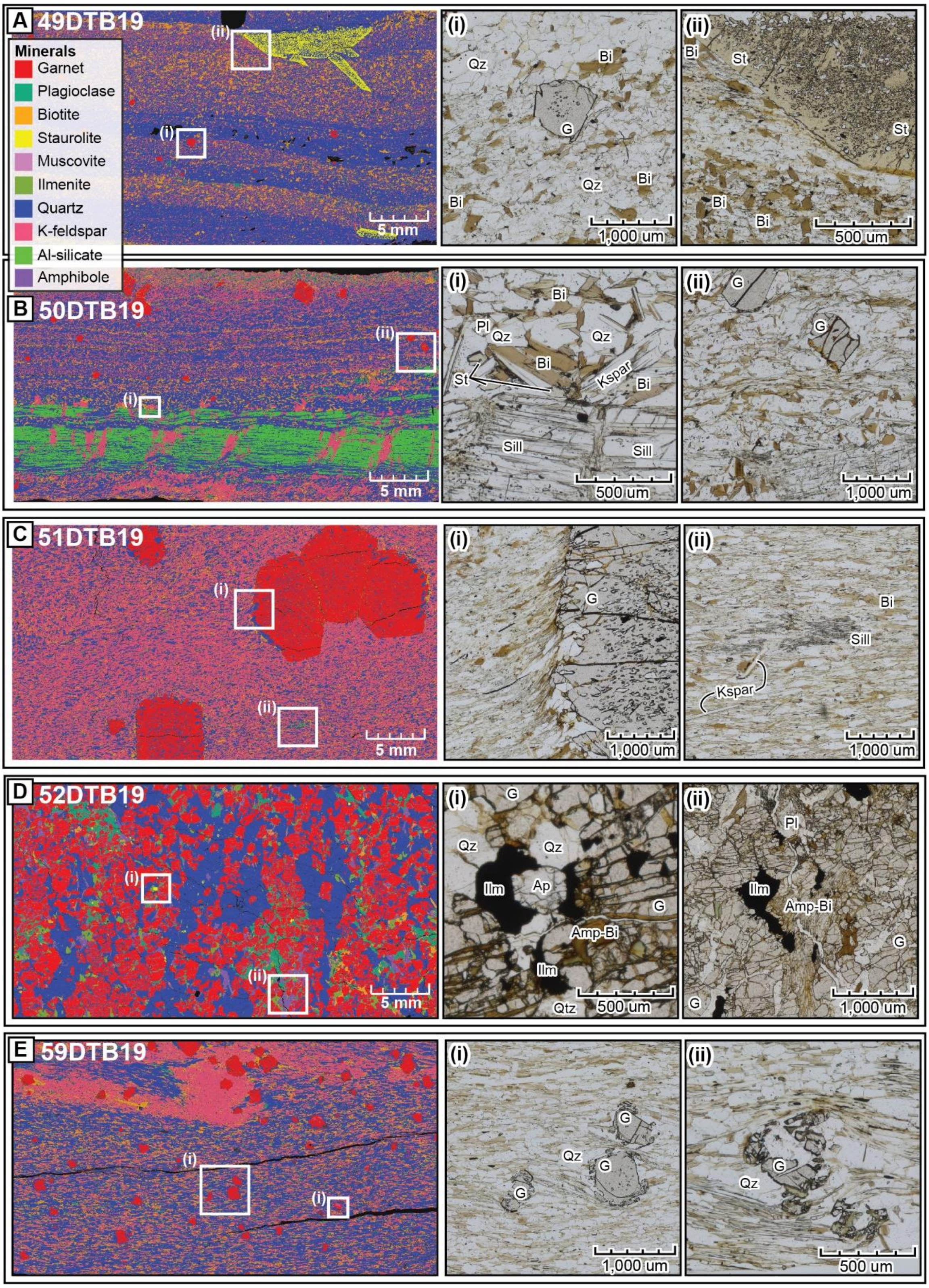

Fig. 4.5: Representative thin section mineralogy (produced by TESCAN integrated mineral analyzer; TIMA) and important mineralogical relationship highlighted inset boxes (i) and (ii). Mineral abbreviations from Whitney and Evans (2010).

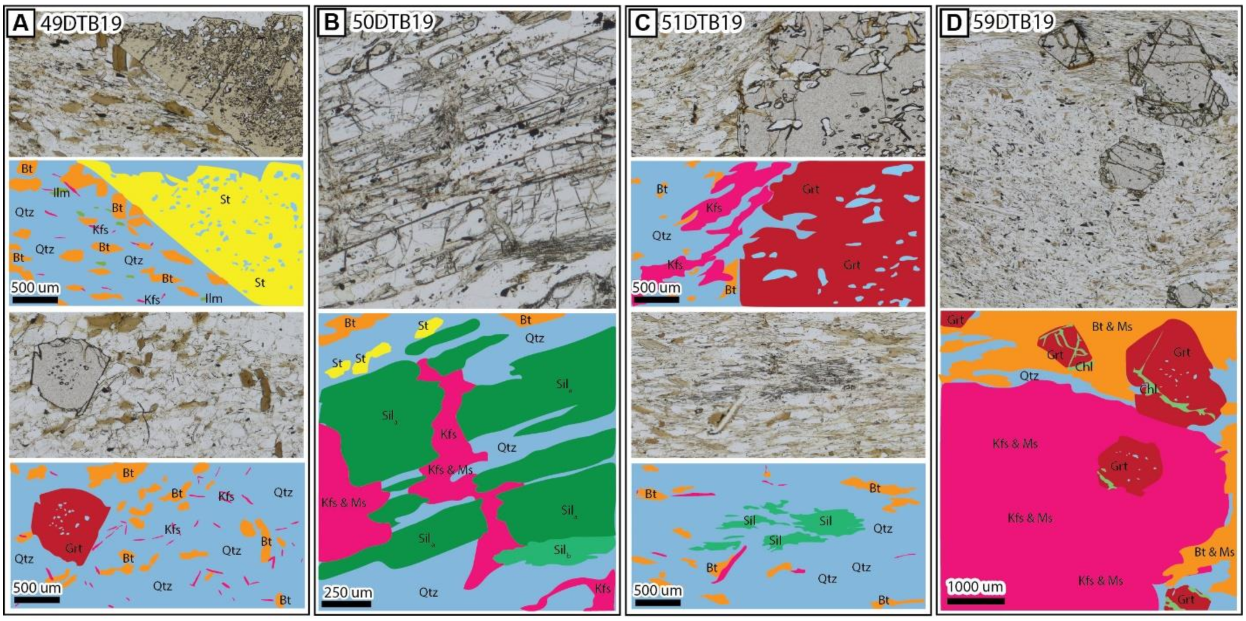

Fig. 4.6: Additional mineralogy of the metapelitic samples shown in plane polarized light microphotographs, and interpretative sketches. (A) Sample 49DTB19 garnet-muscovite-staurolite-biotite-quartzofeldspathic schist. (B) Sample 50DTB19 staurolite-muscovite-garnet-biotite-sillimanite-quartzofeldspathic schist, highlighting the two generations of sillimanite and their association, but non-cross cutting or inclusion, relationship with staurolite. (C) Sample 51DTB19 muscovite-garnet-biotite-sillimanite-quartzofeldspathic schist, showing the fibrolite sillimanite present, and large garnets. (D) Sample foliated monazite and apatite bearing muscovite-garnet-biotite-quartzofeldspathic schist, showing a large feldspar and muscovite-rich region that is perhaps a pseudomorph of an earlier higher-grade assemblage. Mineral abbreviations from Whitney and Evans (2010).

4.4.2 U–Pb Geochronology

Western extent of Clearwater Complex (samples 49, 50, and 51DTB19)

Monazite from the analyzed samples (Fig. 4.7A) yielded concordant U–Pb dates between ca. 1400 and 1060 Ma (Fig. 4.8). Apatite U–Pb results indicated younger dates, and generally fall into either a Cryogenian (ca. 676 Ma) or late Paleogene-early Eocene (ca. 58–54 Ma) population.

Monazite within sample 49DTB19 only occurs within the matrix. A free Discordia regression line fit through 15 analyses yields a 1074 ± 14 (MSWD = 0.6) age, with a $^{207}Pb/^{206}Pb$ common Pb upper intercept of ~0.9. Ten of the 15 analyses are concordant, and together yield a concordia age of 1087 ± 10 (MSWD = 1.9). A free Discordia regression line fit through 38 analyses of matrix apatite in sample 49DTB19 (Fig. 4.7B) yields a lower intercept age of 676 ± 13 Ma (MSWD = 2.8), and an upper $^{207}Pb/^{206}Pb$ common Pb intercept of ~0.9 (Fig. 4.9). Zirakparvar et al.,

(2010) report a 1064 ± 10 Ma (MSWD = 4.5) garnet Lu–Hf age for the same outcrop.

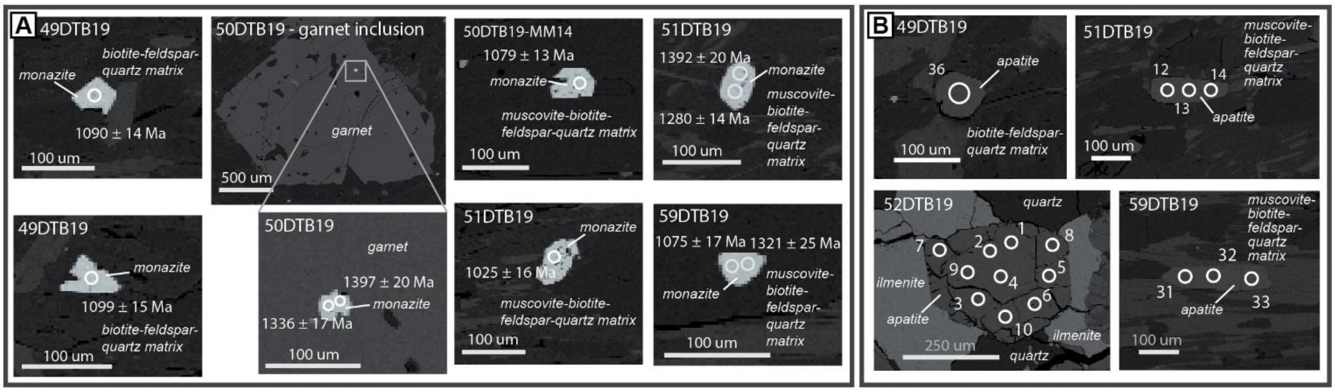

Fig. 4.7 (A) Representative back-scattered electron (BSE) images of U–Pb analyzed monazite with concordant ages labelled. Note that samples 50DTB19 (shown) and 51DTB19 contained monazite grains as inclusions within garnet that yielded older ca. 1365–1320 Ma ages. Of the limited monazite grains present in 59DTB19, a single grain able to fit two analyses spots yielded both ca. 1321 and 1075 Ma ages. (B) Representative back-scattered electron (BSE) images of U–Pb apatite grains with individual analyses spots indicated that correspond to the "Spot ID" within the supplementary tables. Note individual Pb-corrected apatite grain ages were not calculated and consequently not labelled here.

In sample 50DTB19, monazite occurs both in the matrix and as inclusions within garnet. Five of six monazite grains analyzed as inclusions within garnet show concordant dates (Fig. 4.7A; 4.8) that yield a concordia age of 1365 ± 17 Ma (MSWD = 0.1). Twenty-one analyses of matrix monazite yield 11 concordant dates ranging from 1358 ± 15 to 1060 ± 14 Ma (all individual spot ages reported as single spot concordia ages; Ludwig, 1998), the two youngest of which are 1079 ± 13 and 1060 ± 14 Ma. The two youngest concordant analyses, and the five youngest discordant grains with a common Pb anchor (of 0.9, e.g. Albarede and Martine, 1984) define a Discordia with an intercept age of 1056 ± 19 Ma (Fig. 4.8). Sample 50DTB19 does not contain any apatite. Neishem et al., (2012) microdrilled (rim and core zones) garnets from this same sampled outcrop and found Lu–Hf ages of 1347 ± 10 Ma (MWSD = 4.6; isochron from garnet cores) and 1102 ± 43 Ma (MSWD = 42; isochron from garnet rims).

Sample 51DTB19 contains monazite within the matrix and as inclusions within garnet (Fig. 4.7A). Seven of nine monazite grains were analyzed as inclusions within garnet yielded concordant dates that range from 1392 ± 20 to 1269 ± 19 Ma, and collectively give a concordia age of 1318 ± 14 Ma (MSWD = 0.3). A single inclusion monazite grain sufficiently large for two analytical spots yields different concordant ages (1392 ± 20 and 1280 ± 14 Ma; Fig. 4.7). Twenty-six of 30 concordant matrix monazite grains yield dates that range from 1379 ± 21 to 1007 ±

17 Ma. The three youngest monazite analyses yield a weighted mean age of 1021 ± 20 Ma (MSWD = 3.7; Fig. 4.8). For this location, Zirakparvar et al., (2010) reported a 1018 ± 25 Ma (MSWD = 113) Lu–Hf isochron age based on five garnet fractions (i.e. five fractions of a single garnet). Given the high MSWD, Zirakparvar et al., (2010) speculate their data may represent two stages of garnet growth at 1081 ± 20 (MSWD = 45, three garnet fractions) and 1024 ± 3 (MSWD = 1.4, two garnet fractions). Analyses of 32 matrix apatite grains (Fig. 4.7B) define a free Discordia regression with a lower intercept age of 56 ± 7 Ma (MSWD = 22), and an upper $^{207}Pb/^{206}Pb$ common Pb intercept of ~ 0.48 (Fig. 4.9). The high MSWD of the Discordia regression indicates complexity in the dataset, such as potentially multiple age-populations, which will be explored further in the discussion.

Core of Clearwater Complex (sample 52DTB19)

Sample 52DTB19 lacks monazite but contains abundant apatite (Fig. 4.7B). A free Discordia regression line fit through 91 apatite analyses yields a lower intercept age of 54 ± 2.7 Ma (MSWD = 1.3), and an upper $^{207}Pb/^{206}Pb$ common Pb intercept of ~ 0.50 (Fig. 4.9). Brennan et al., (2022) report zircon U–Pb and O-isotope data from this sample that indicate metamorphic/hydrothermal zircon growth at ca. 1396–1350 Ma.

Eastern extent of Clearwater Complex–Sample 59DTB19

Sample 59DTB19 contains rare, both garnet and matrix hosted, monazite (Fig. 4.7A). Six of eight concordant analyses give dates that fit into two age-populations, one at around 1337 Ma and another at around 1119 Ma (Fig. 4.8A). A single grain sufficiently large for two spot analyses yields concordant ages of ca. 1321 and 1075 Ma. The older two concordant analyses give dates of 1321 ± 25 and 1346 ± 19 Ma, that together define a concordia age of 1337 ± 30 Ma (MSWD = 1.2). The younger four concordant analyses dates range from 1150 ± 20 to 1075 ± 17 Ma, and give a concordia age of 1119 ± 18 Ma (MSWD = 0.5; Fig. 4.8). A discordia through 80 analyses of matrix apatite (Fig. 4.7B) define a lower intercept age of 58 ± 9 Ma (MSWD = 1.4), and an upper $^{207}Pb/^{206}Pb$ common Pb intercept of ~ 0.8 (Fig. 4.9).

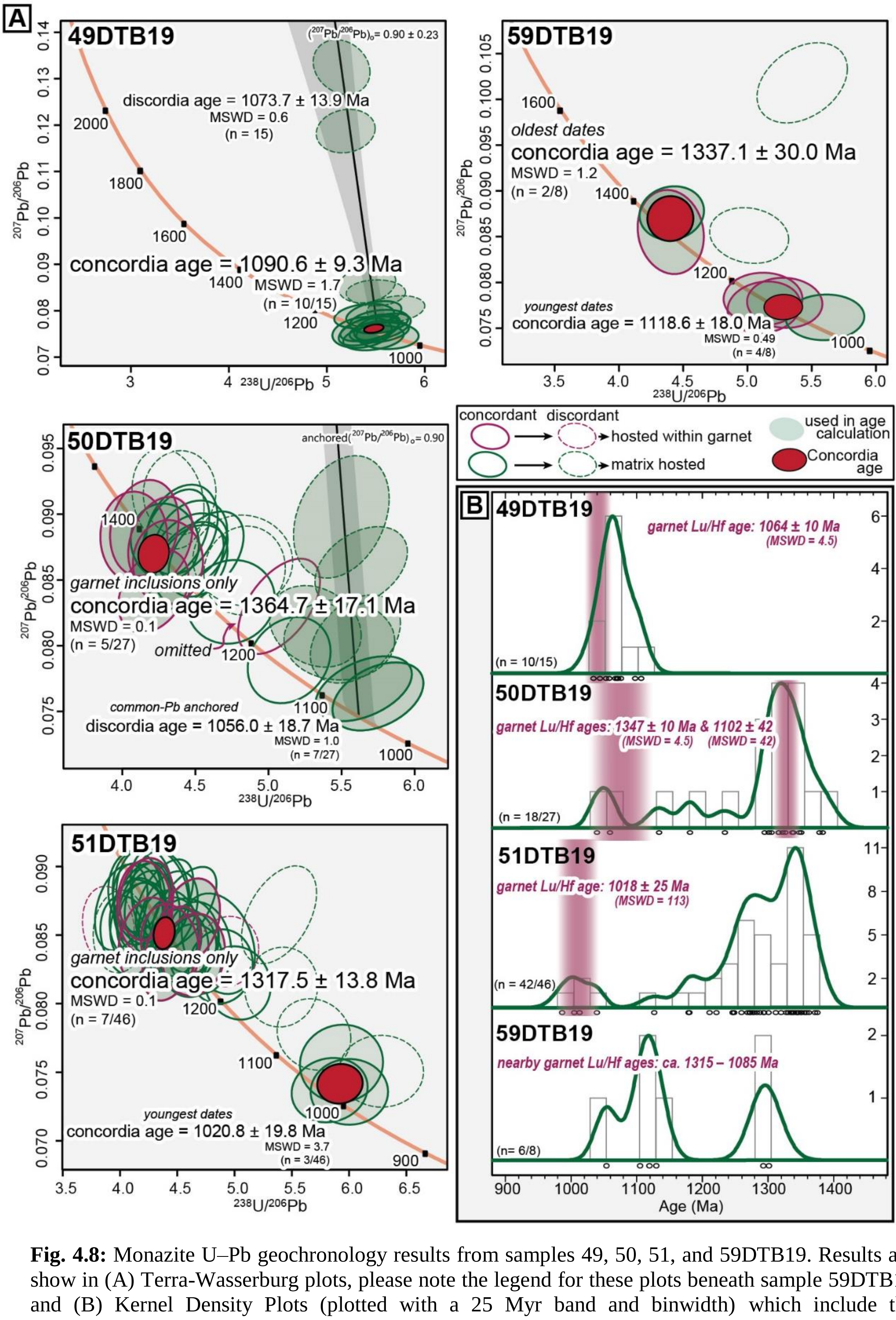

Fig. 4.8: Monazite U–Pb geochronology results from samples 49, 50, 51, and 59DTB19. Results are show in (A) Terra-Wasserburg plots, please note the legend for these plots beneath sample 59DTB19 and (B) Kernel Density Plots (plotted with a 25 Myr band and binwidth) which include the corresponding published garnet Lu–Hf dissolution ages (Zirakparvar et al., 2010; Neishem et al., 2012). Only analyses that overlap Concordia within 2σ uncertainties are plotted. Monazite grains hosted along cracks within garnet are plotted here as matrix hosted but are indicated in Appendix D4.4.

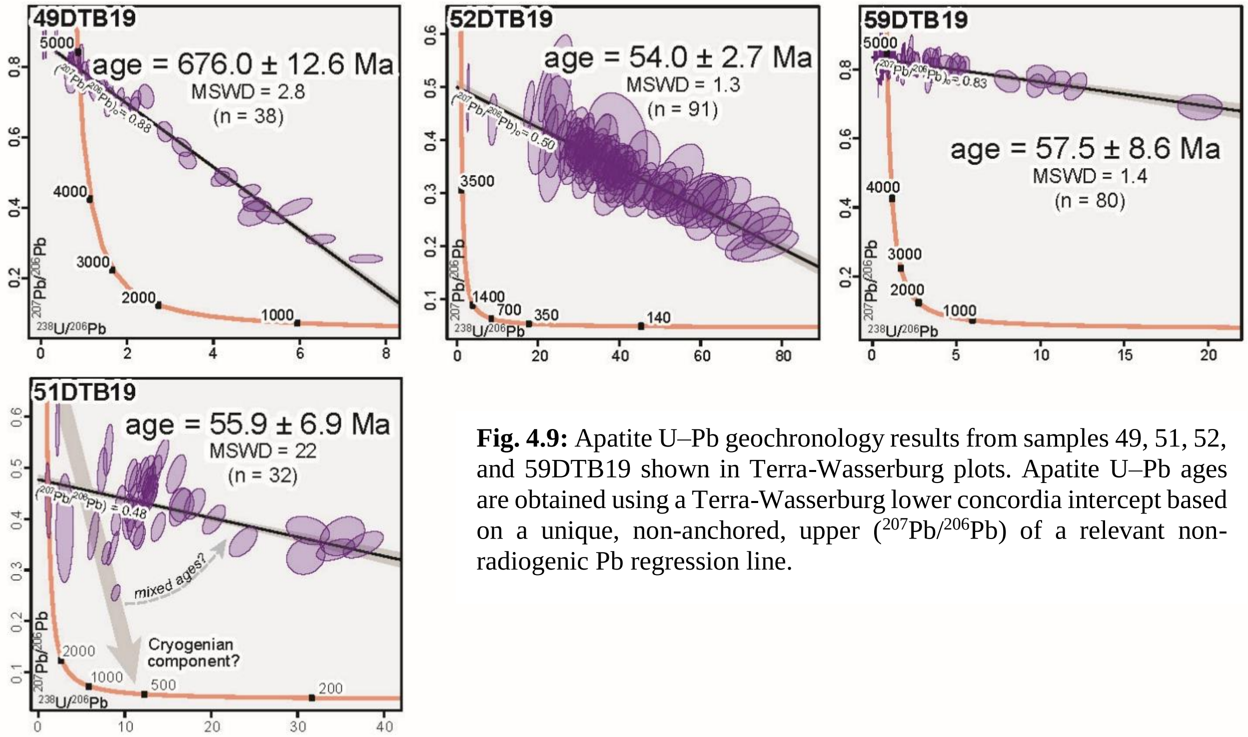

Fig. 4.9: Apatite U–Pb geochronology results from samples 49, 51, 52, and 59DTB19 shown in Terra-Wasserburg plots. Apatite U–Pb ages are obtained using a Terra-Wasserburg lower concordia intercept based on a unique, non-anchored, upper ($^{207}Pb/^{206}Pb$) of a relevant non-radiogenic Pb regression line.

4.4.3 Mineral Compositions and Phase Equilibrium Modelling

Pressure–temperature pseudosections for the four modelled samples are shown in Fig. 4.10, which the inferred peak assemblage fields are highlighted. For clarity, we show the stability of garnet (at P/T above the thick red line) and staurolite (at P/T above the thick yellow line).

Western extent of Clearwater Complex

The three samples collected along the western region of the Clearwater have similar major oxide bulk compositions and, consequently, similar calculated phase equilibria. None of the samples preserves evidence for partial melting, restricting peak metamorphic conditions to temperatures below the H_2O-saturated solidus (< or << 680 °C; Fig. 4.10).

Sample 49DTB19 contains an interpreted peak assemblage of garnet–muscovite–staurolite–biotite–plagioclase–ilmenite (+quartz, and H2O) , consistent with conditions of ~570–670 °C and 5.5–9.0 kbar. Garnet within this sample shows flat major element profiles with around 3 mol.% spessartine, 5 mol.% grossular (Ca_3Al_2), 11 mol.% pyrope, and 80% mol. almandine, and an Fe# = 89% (where Fe# = Fe^{2+}/[Fe^{2+} + Mg]; Fig. 4.11). As Ca is usually the slowest diffusing major cation (Carlson, 2006), we use the calculated 5 mol. grossular isopleth to more tightly constrain peak *P–T* conditions to 6.5–7.5 kbar, and 640–665 °C (Fig. 4.10).

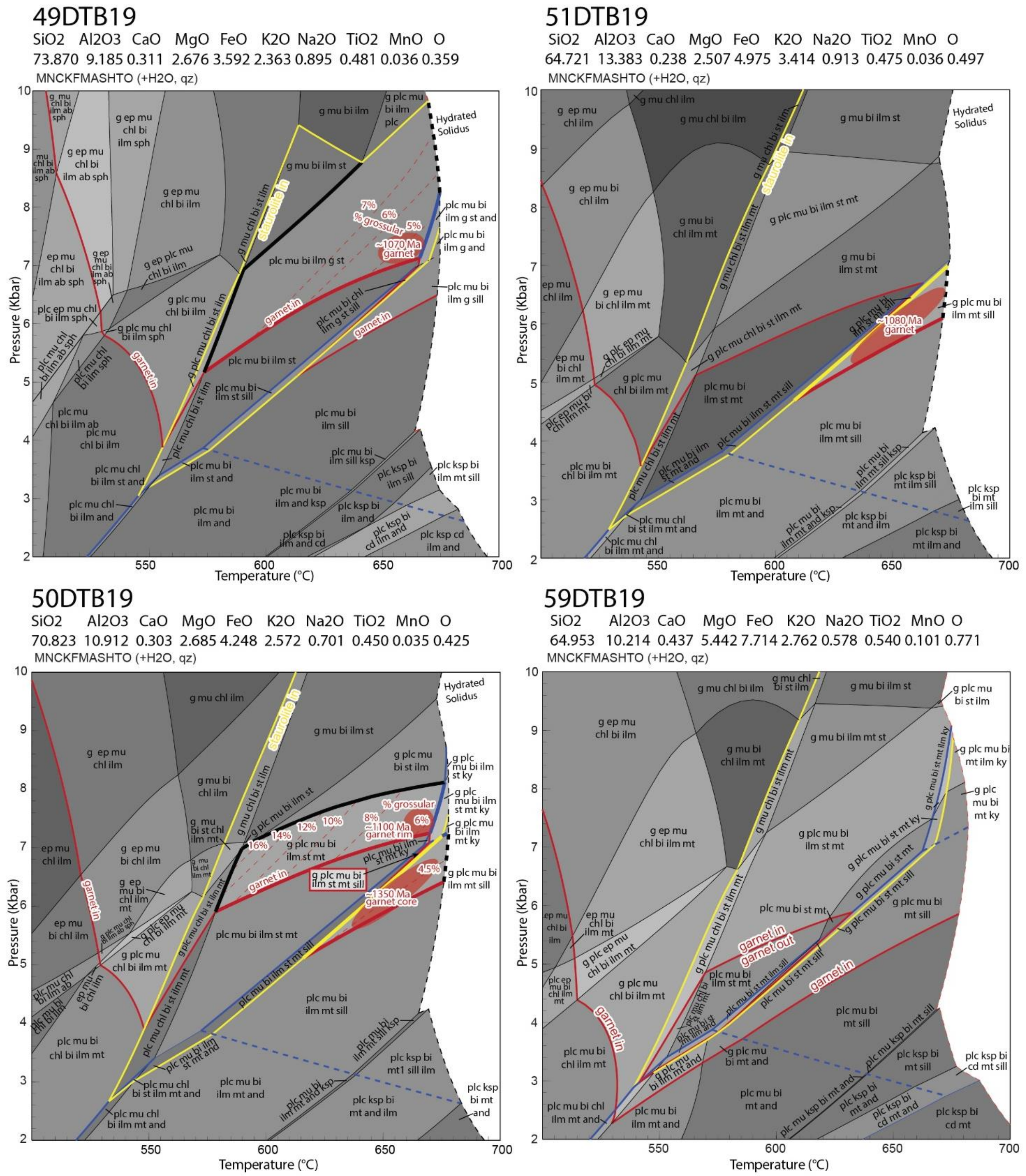

Fig. 4.10: Pressure–temperature pseudosections calculated for 49, 50, 51, and 59DTB19. The garnet-in isopleth is indicated in red, staurolite-in isopleth is indicated in yellow, and aluminosilicate triple point fields indicated in blue. Fields containing the observed mineral assemblages are highlighted with thick lines and the interpreted peak paragenesis is indicated by the red field. Please note for sample 50DTB19, the observed mineral assemblage falls within the narrow field labelled by the red box, while the stability field indicated by the garnet chemistry are shown in the red ovals. Mineral abbreviations from Whitney and Evans (2010). H2O and quartz (qz) were considered in excess for all calculations.

Sample 50DTB19 contains the interpreted peak assemblage garnet–muscovite–staurolite–biotite–plagioclase–ilmenite–sillimanite (+H2O and quartz; Fig. 4.5), which is predicted to be stable within a thin field from ~620 °C and 5 kbar, to ~680 °C and ~6.8 kbar (Fig. 4.10). The core of the garnets, dated at 1347 ± 10 Ma (Zirakparvar et al., 2010) show ~3–4.5% grossular (Fig. 4.11), which is broadly consistent with a modelled lower-pressure assemblage of garnet–muscovite–biotite–plagioclase–ilmenite–magnetite–sillimanite (+H2O and quartz) stable from ~620 °C and ~5.2 Kbar to ~680 °C and 7 Kbar (Fig. 4.10). The garnet rims, dated at 1102 ± 42 Ma (Zirakparvar et al., 2010), show a slight increase in percent grossular to perhaps as high as 9% grossular (Fig. 4.11). This compositional change in garnet is consistent with slightly higher-pressure garnet growth, and the assemblage of garnet–muscovite–staurolite–biotite–plagioclase–ilmenite–magnetite (+H2O and quartz), which is stable from ~6.8–7.8 Kbar and ~650–670 °C, indicating a very similar P/T condition to sample 49DTB19.

Sample 51DTB19 contains the interpreted peak assemblage garnet–muscovite–biotite–plagioclase–ilmenite–magnetite–sillimanite (+quartz, and H2O). The absence of staurolite is consistent with slightly lower pressure conditions than recorded within samples 49DTB19 and 50DTB19. Sillimanite and garnet are only predicted to be stable together in a small field between ~620 °C and 5 kbar to ~680 °C and ~6.8 kbar (Fig. 4.10).

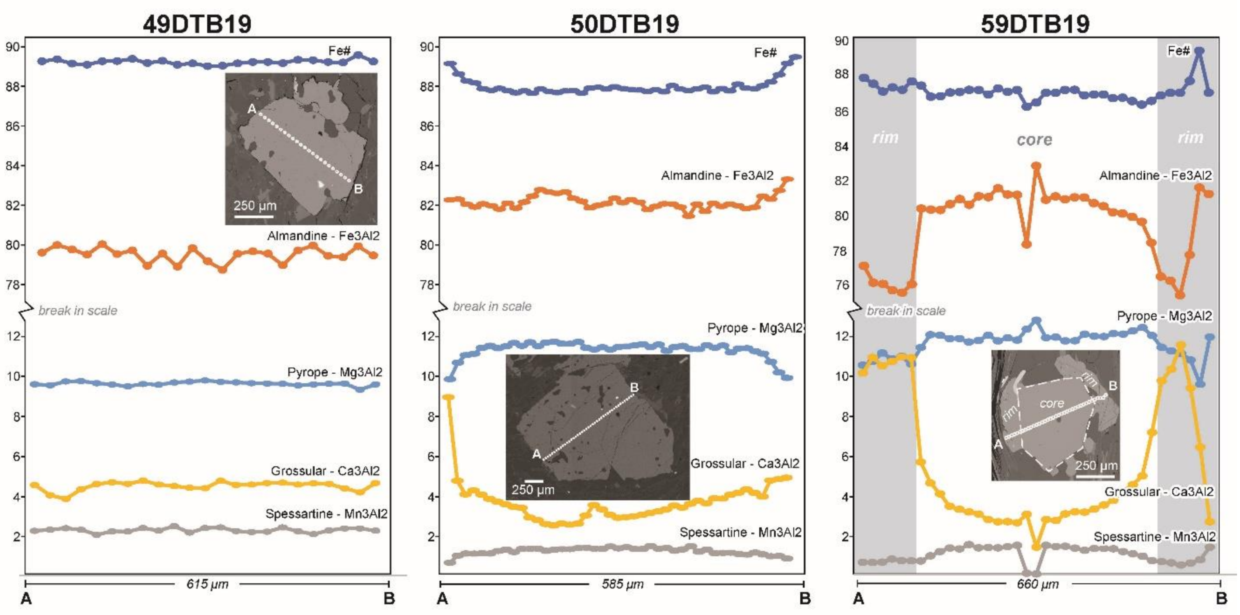

Fig. 4.11: Garnet compositional profiles of major elements for samples 49, 50, and 59DTB19 including back-scattered electron (BSE) images of analyzed traverses.

Eastern extent of Clearwater Complex

The calculated stability field for garnet in sample 59DTB19, from the eastern extent of the Clearwater complex, is significantly expanded compared to the other samples (Fig. 4.10), reflecting a threefold increase in the Mn content (e.g. White et al., 2014b). A small triangular garnet-absent field is also present related to the stability of staurolite and biotite at the expense of garnet and chlorite. Distinct rim and core domains (Fig. 4.11) suggest at least two stages of garnet growth. The preserved assemblage in this sample lacks staurolite, any aluminosilicate minerals, and contains significant potassium feldspar and muscovite agglomerates, that may have replaced an earlier higher-grade assemblage. Consequently, we interpret significant overprinting by lower (sub-garnet) grade metamorphism in this sample and do not assign a peak assemblage field.

4.5. Discussion

4.5.1 Chronological constraints on Metamorphism within the Clearwater region

Within the external regions (three samples from the western region, one from the eastern) of the Clearwater complex, the ages of 71 concordant monazite U–Pb analyses range from 1397 to 1007 Ma (Fig. 4.12), similar to the range of Lu–Hf garnet ages from the same rocks (1379 to 1018 Ma; Zirakparvar et al., 2010; Neishem et al., 2012). Lu–Hf dates from garnet are usually interpreted to represent its growth, which in metapelitic rocks generally requires pressures greater than 5 kbar, but can occur at temperatures as low as ~450 °C (Yakymchuk et al., 2017). Net diffusive gain or loss of Lu or Hf from garnet is thought to negligible at T < 800–900 °C (Smit et al., 2013; Bloch et al., 2020). Monazite in metapelitic rocks can also grow at temperatures as low as ~450 °C, and become closed to net diffusive gain or loss of U or Pb isotopes at T < 725 °C (Parrish, 1990) or higher (e.g. Cherniak, 2010). The U–Pb in apatite system is thought to have a much lower closure temperature of 450–550 °C, making it a valuable tool for constraining middle-T (mid-crustal) processes (Kirkland et al., 2018; Jepson et al., 2021).

The concordant monazite U–Pb analyses from the four studied samples indicate two age-peaks at 1352 Ma and 1083 Ma (Fig. 4.12), consistent with growth during the ca. 1380–1300 Ma East Kootenay and ca. 1115–1065 Ma Grenvillian tectono-thermal events (Zirakparvar et al., 2010; Neishem et al., 2014). On an individual sample basis, the northwestern most sample (49DTB19) records the strongest Grenville-age signature with a monazite U–Pb Concordia age of 1091 ± 9 Ma (MSWD = 1.7), slightly older than the 1064 ± 10 Ma (MSWD = 4.5) Lu–Hf garnet age (Zirakparvar et al., 2010; Fig. 4.8B). Interestingly, this is the only sample to contain a robust pre-Cordilleran U–Pb apatite age of 676 ± 13 Ma (MSWD = 2.8), contemporaneous with significant rift-related volcanism within the ca. 685–650 Ma Edwardsburg volcanics and Big Creek plutonic suite some 150 km to the south (Lund et al., 2003; 2010). Importantly, the absence of Phanerozoic ages indicates that this sample was largely unaffected by Cordilleran metamorphism (implying $T < 450$ °C).

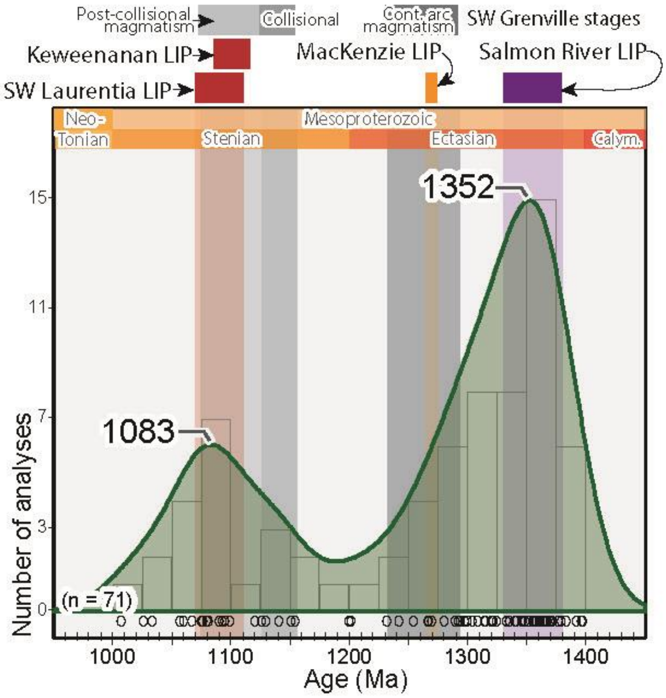

Fig. 4.12: All concordant monazite U–Pb ages from the Clearwater complex, plotted with a 25 Myr band and binwidth. The ages of corresponding southwestern Grenville stages (Mulder et al., 2017), and notable Laurentian Large Igneous Provinces (LIPS; Ernst et al., 2008 and references within) are indicated.

Sample 50DTB19 records a wider spread of monazite U–Pb dates, with five monazite grains armored as inclusions in garnet yielding a 1365 ± 17 Ma (MSWD = 0.1) concordia age, with the youngest seven grains defining a 1056 ± 19 Ma (MSWD = 1.0) discordia intercept age. These ages are in good agreement with the Lu–Hf garnet ages in rocks from the same outcrop, which records two stages of garnet growth at 1347 ± 10 Ma (garnet core, MSWD = 4.5) and 1102 ± 42 (garnet rim, MSWD = 42).

In sample 51DTB19, concordant U–Pb monazite ages between ca. 1400 and 1200 Ma are significantly older than the existing Lu–Hf garnet ages of ca. 1081–1024 Ma (Zirakparvar et al., 2010). Seven concordant monazite inclusions in garnet yield a 1318 ± 14 Ma concordia age (MSWD = 0.1), consistent with monazite (but not garnet) growth during the ca. 1380–1300 Ma East Kootenay tectono-thermal event. The youngest three concordant matrix monazite yield a 1021 ± 20 Ma concordia age that corresponds well with the Lu–Hf garnet age. Collectively, the data suggest this rock experienced lower-pressure conditions (under which garnet was not stable) during the East Kootenay event than during the Grenville age event.

The apatite U–Pb data from this sample yield an age of 56 ± 7 Ma (MSWD = 32; Fig. 4.8). The high MSWD of the Discordia regression suggests this sample contains more than one apatite age-population. The ~0.48 $^{207}Pb/^{206}Pb$ common-Pb intercept of this age is also much lower than predicted by common-Pb evolution models (Albarede and Juteau, 1984). Consequently, we suggest that apatite within sample 51DTB19 grew during partial breakdown (dissolution) of an older radiogenic Pb-bearing phase, likely a population of older Cryogenian apatite similar to the ca. 676 Ma apatite within nearby sample 49DTB19 (Fig. 4.9). The preservation of some likely Cryogenian apatite within this sample indicates that the Cordilleran processes this rocks experienced were within the U–Pb partial retention (or growth/dissolution) zone of apatite which is around 450–550 °C (Kirkland et al., 2018).

In the internal zone of the Clearwater complex, the Eocene 54 ± 2.7 Ma (MSWD = 1.3) apatite U–Pb age from sample 52DTB19 (Fig. 4.9) records cooling and exhumation of the Clearwater complex, and is contemporaneous with existing ca. 64–55 Ma metamorphic zircon rims and ca. 53 to 47 Ma $^{40}Ar/^{39}Ar$ mica ages (Doughty et al., 2007). These data indicate that rocks in the internal zone of the complex were buried deeper during Cordilleran processes than the external flanking zones (e.g. Lang and Rice, 1985; see Fig. 4.4). However, the internal zone does preserve a record of hydrothermal metamorphic zircon growth at ca. 1396–1350 Ma within this sample (Brennan et al., 2022). Apatite within sample 52DTB19 gave an upper $^{207}Pb/^{206}Pb$ common Pb intercept of ~0.50, which again is much lower than predicted by common-Pb evolution models (Albarede and Juteau, 1984). Consequently, it is likely that the apatite in this sample also grew during the breakdown/dissolution of an older unknown radiogenic Pb-bearing phase perhaps also apatite, consistent with Cordilleran conditions that exceeded the U–Pb partial retention zone of apatite (~550 °C; Kirkland et al., 2018).

Along the eastern flanking region of the Clearwater Complex, U–Pb monazite ages of 1337 ± 30 Ma and 1119 ± 18 Ma are present in sample 59DTB19 (Fig. 4.8). The apatite U–Pb results record a 58 ± 9 Ma (MSWD = 1.4) age (Fig. 4.9) that is also consistent with Cordilleran burial and Eocene core complex formation. No apatite record of an older Proterozoic component present in rocks further to the west (in samples 49DTB19 and likely 51DTB19) was found. Interestingly, the 58 ± 9 Ma U–Pb apatite age in sample 59DTB19 gives an upper $^{207}Pb/^{206}Pb$ common Pb intercept of ~0.83, which is similar to values predicted by common-Pb evolution models (Albarede and Juteau, 1984). Consequently, the apatite in this sample does not record breakdown/dissolution of an older common-Pb bearing phases, perhaps indicating that the Cyrogenian apatite growth present along the western external zone did not occur in the eastern zone.

4.5.2 Linking the timing and conditions of metamorphism

Integrating existing garnet Lu–Hf (Zirakparvar et al., 2010; Neishem et al., 2012) with U–Pb monazite and apatite data and phase equilibrium modelling allows the timing and conditions of metamorphism within the Clearwater region to be constrained, particularly along the western external zone of the complex. Along the western edge of the complex, monazite U–Pb ages (samples 49, 50, and 51DTB19) indicate that the rocks were affected by high-*T* processes during the older ca. 1380–1300 Ma East Kootenay tectono-thermal event. However, only one sample (50DTB19) records similar, ca. 1350 Ma, Lu–Hf garnet (core) ages (Neishem et al., 2012). While in these same three samples, younger ca. 1115–1065 Ma Grenville ages are ubiquitously recorded in monazite U–Pb and Lu–Hf garnet ages (Zirakparvar et al., 2010; Neishem et al., 2012). The presence of East Kootenay garnet ages in only one sample, while Grenville-age garnets are present in all samples, suggests that along the western, external, region of the Clearwater complex garnet did not grow in most rocks during the earlier Kootenay event, but was a common product of subsequent Grenville-age metamorphism. This relationship is consistent with higher pressures during the latter, Grenville-age event.

East Kootenay metamorphism

Determining metamorphic conditions for the older ca. 1380–1300 Ma East Kootenay tectonothermal event is difficult due to extensive overprinting by Grenvillian metamorphism. Near the northern extent of the Belt Basin, within the Matthew Creek metamorphic zone and nearby St. Eugene deposit, ca. 1350 Ma metamorphism of lower Belt Supergroup strata is constrained to ~580–650 °C and 3.0–4.0 kbar (McFarlane and Pattison, 2000) and 490–510 °C and 3.6–4.0 kbar (Pattison and Seitz, 2012), consistent with ‘warm’ average geothermal gradients of

≥35 °C/km (e.g. Tucker et al., 2015). These relatively low-*P* conditions identified within the northern extent of the Belt Basin, are consistent with our inference of limited garnet growth within the western Clearwater complex. The relatively low pressures, and warm geotherms are more characteristic of Buchan rather than Barrovian metamorphism (e.g. Pattison and Spear, 2018; Pattison and Goldsmith, 2022 and references within). Consequently, the P-T conditions of the East Kootenay event are broadly consistent with sedimentary burial and heating due to coeval bimodal intrusions into the Belt Basin at this time (Doughty and Chamberlain, 1996).

The scattering of older ca. 1400–1200 Ma Lu–Hf garnet ages further east in the Clearwater complex (Neishem et al., 2012), suggest that this event may be better preserved, or that pressures of East Kootenay metamorphism were greater, further to the east. In sample 50DTB19, the thermodynamic modeling and mineral assemblages suggest that ca. 1350 Ma garnet core growth requires conditions of at least 620 °C and ~5 kbar. However, only a few kilometers in either direction, there is no evidence for garnet growth at this time. Thus, we speculate that the localized garnet growth within the western portion of the Clearwater complex at ca. 1350 Ma could reflect localized higher T/P conditions from documented nearby ca. 1380–1330 Ma magmatism within the Belt Basin (e.g. Doughty and Chamberlain, 1996; Lewis et al., 2007; Pearson and Link, 2021).

Grenville-age metamorphism

Rocks in the western portion of the Clearwater complex mostly preserve ca. 1115–1065 Ma metamorphic ages and Barrovian metamorphic assemblages that provide robust *P–T* constraints. Sample 49DTB19, which preserves ca. 1090–1070 Ma U–Pb monazite and ca. 1060 Ma Lu–Hf garnet ages (Fig. 4.8B), has an assemblage consistent with peak metamorphic conditions of 6.5–7.5 kbar and 640–654°C (Fig. 4.9). Sample 50DTB19 records ca. 1100 Ma garnet Lu–Hf rim ages and ca. 1060 Ma monazite U–Pb ages (Fig. 4.7B), and also records similar metamorphic conditions of ~6.8–7.8 kbar and ~650–670°C (Fig. 4.9). Sample 51DTB19, contains ca. 1080–1020 Ma Lu–Hf garnet ages, ca. 1020 Ma U–Pb monazite ages (Fig. 4.7B) and a mineral assemblage that suggests metamorphic conditions of ~620–680 °C and ~5.0–6.8 kbar (Fig. 4.10). Collectively, these values suggest that the rocks along the western region of the Clearwater complex were buried to a depth of ~17–22 km or greater (assuming isostatic pressures and an average crustal density of 3.0–2.7 g/cm^3) around ca. 1080–

1020 Ma (Fig. 4.13). These results also imply a moderately-high average geothermal gradient (~23–36°C/km; e.g. Tucker et al., 2015).

In the central portion of the Clearwater complex, Doughty et al. (2007) assign peak metamorphic conditions of ~9–10 kbar and approximately 650°C at ca. 82–72 Ma, followed by a significant clockwise *P–T* path associated with core complex formation and exhumation from ca. 64 to 54 Ma (Fig. 4.13). These conditions suggest burial to a depth of ~31–38 km, along a geothermal gradient notably cooler (17–21°C/km) than recorded by the rocks in the western external zone of the complex. The well-defined 54 ± 3 Ma (MSWD = 1.3) and 58 ± 9 Ma (MSWD = 1.4) apatite U–Pb ages reported here in the central and eastern portions (samples 52 and 59DTB19; Fig. 4.9) of the complex are in good agreement with this Cordilleran *P–T*-t pathway, and support Clearwater core complex exhumation in the late Paleocene to early Eocene (Fig. 4.13).

The 676 ± 13 Ma (MSWD = 2.8) apatite U–Pb age within sample 49DTB19, and the over-dispersed 56 ± 7 Ma (MSWD = 22) age recorded in sample 51DTB19 (Fig. 4.9), which we interpret to record partial resetting/recrystallization of an older Cryogenian apatite population, indicates that the western external region likely did not exceed ~550°C (the apatite U/Pb partial retention zone) during Cordilleran orogenesis. As discussed, within these same samples the higher temperature Lu–Hf garnet or U–Pb monazite systems notably record no indication of this Cryogenian event, which is previously not identified regionally in other mid-temperature thermo-chronometers. Given that the Cryogenian apatite ages are the same as nearby (well-agreed upon) rift-related volcanism (the ca. 685–650 Ma Edwardsburg volcanics and Big Creek plutonic suite; Lund et al., 2003; 2010), which are not associated with any known super-greenschist facies metamorphism in this region, the Cryogenian apatite ages likely reflect a fluid-flow/thermal event associated Rodinian rifting. The absence of Cryogenian Lu–Hf garnet and U–Pb monazite ages indicate that this event did likely not result in re-equilibrium of the metamorphic assemblages from peak conditions at ca. 1115–1065 Ma (Fig. 4.13).

Interestingly, sample 49DTB19 contains the strongest signal of the ca. 1080 Ma Grenvillian event with complementary ca. 1090–1060 Ma U–Pb monazite and Lu–Hf garnet ages (Fig. 4.8), as well as the clearest ca. 676 Ma U–Pb apatite age of this Cryogenian rifting event (Fig. 4.9). Consequently, sample 49DTB19 is likely located proximal to a crustal/basin-scale structure that preferentially facilitated localized recording of these tectono-thermal events. The presence of Cryogenian apatite populations (samples 49 and 51DTB19) and/or more radiogenic than expected common-Pb values suggesting breakdown of an older apatite population (sample 52DTB19) along the central and western region of the complex, while no indication of an Cryogenian apatite population (or breakdown of an older more radiogenic population) in the eastern region of the complex (59DTB19; see Fig. 4.4 and 4.9) could also perhaps reflect a Proterozoic structure (with a Cryogenian history) between these two regions.

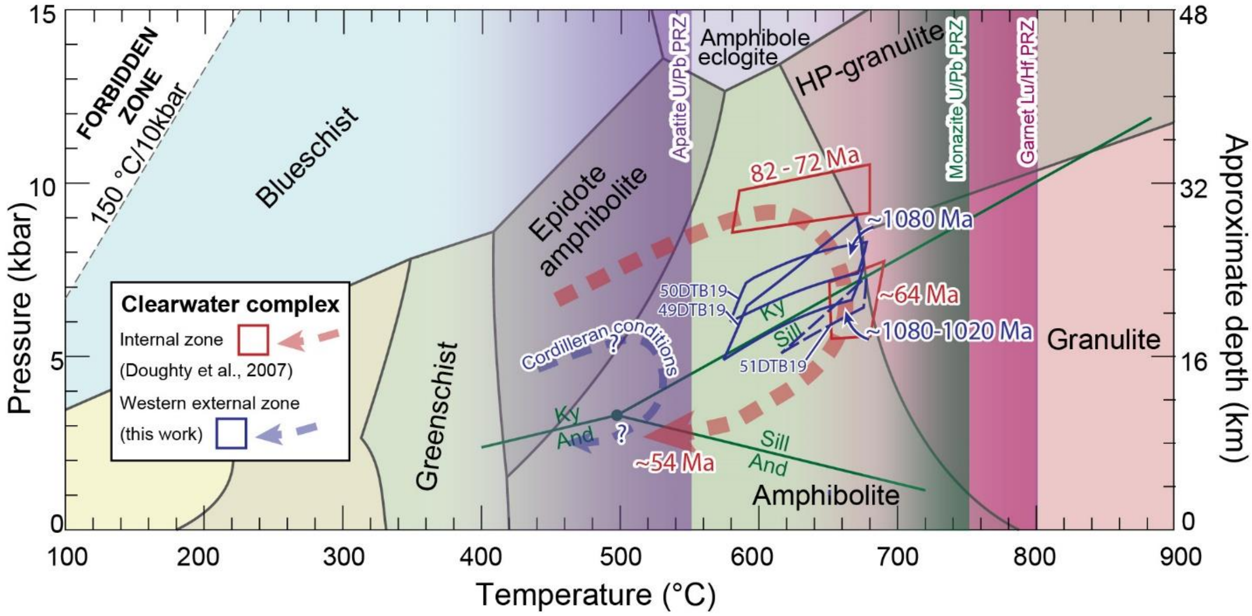

Fig. 4.13: Pressure–temperature–time pseudosection interpretations for the internal zone of the Clearwater complex (Doughty et al., 2007) that reflect Cordilleran conditions from ca. 82–54 Ma, and the western external zone (this work) that reflect the ca. 1080–1020 Ma "Grenvillian" conditions recorded in the corresponding samples.

4.5.3 A revised regional tectonic model

Rocks of the western Clearwater complex yield important new constraints that allow for a revised tectonic model for the Belt Basin region of western Laurentia during the Nuna to Rodinia transition. Insights into the absolute P/T conditions of ca. 1380–1300 Ma East Kootenay tectono-magmatic event in the studied region are limited due to overprinting by higher-grade ca. 1115–1065 Ma metamorphism. However, we note that the relatively extensive monazite growth, but only localized garnet crystallization identified during this event are consistent with high temperature, lower pressure, Buchan-style metamorphism similar to what workers (e.g. McFarlane and Pattison, 2000; Pattison and Seitz, 2012) identify coevally within similar rocks in the northern portion of the Belt Basin, and attribute to extension and magmatism within the basin.

From the investigated samples, the peak metamorphic event along the western extent of the Clearwater complex give more robust insights into the ca. 1115–1065 Ma Grenvillian event within the Belt Basin. Tectonic models for this event within the Belt Basin region must now account for burial of Belt Supergroup rocks to a depth of ~17–22 km or greater along a moderately-high average geothermal gradient (~23–36°C/km) at ca. 1100–1065 Ma. The most recent model to explain this period of Barrovian-style Grenville-age metamorphism within the Clearwater complex advocates for continental collision and crustal thickening mechanisms at ca. 1090–1070 Ma based primarily on Lu–Hf garnet ages, and the generalized metamorphic grade/fabric suggested by the accompanying mineral assemblages (Neishem et al., 2012). However, recent documentation of metamorphism of pelitic rocks to conditions of ~680–660°C and 5.5–10.5 kbar, within a deep intraplate rift-basin (Tucker et al., 2015) caution against the ubiquitous attribution of compressional tectonic thickening to explain medium-pressure metamorphism unless supported by other lines of regional geologic evidence.

The Stenian Period (ca. 1200–1000 Ma) is admittedly predominantly a time of orogenesis and crustal thickening across southern Laurentia, associated with development of the Grenville province (e.g. Mulder et al., 2017). However, during this period of generally widespread crustal thickening, there is a distinctive period of continent-wide mantle/thermal upwelling, intraplate volcanism, reactivation of crustal weaknesses, and extension from ca. 1110–1040 Ma within Laurentia. Manifestations of this event are found in the 1110–1085 Ma Midcontinent Rift (e.g. Swanson-Hysell et al., 2018), 1115–1078 Ma Pikes Peak batholith (Guitreau et al., 2016), 1094–1080 Ma Southwestern Laurentian Large Igneous Province (Timmons et al., 2001; Bright et al., 2014), and 1090–1040 Ma Bylot and correlative basins in northern Laurentia (Greenman et al., 2021; see Fig. 4.2). However, although located <500 km from the Grenville orogenic front, this period of mantle upwelling and extension within the Midcontinent rift was punctuated by localized ca. 1090–1030 Ma (Cannon et al., 1993; Cannon, 1994), and ca. 1010–980 Ma; Swanson-Hysell et al., 2019; Hodgin et al., 2022) structural basin inversion, associated with the Ottawan and Rigolet phases of the Grenville orogeny. This punctuated inversion of the Midcontinent Rift indicates that Grenville orogenic deformation propagated far into the Laurentian continental interior, often associated with inherited rift structures in regions weakened by recent thermal upwelling.

Consequently, the possibility of the ca. 1100–1065 Ma metamorphism within the Clearwater complex and Belt Basin to reflect similar processes (e.g. thermal upwelling and/or inversion of inherited structures) as is recognized coevally within the Midcontinent Rift is worth exploring. The work of various other geologists over the past couple of decades has demonstrated that significant syn-depositional, but commonly reactivated (with most reactivation generally attributed to Neoproterozoic rifting, and Mesozoic and younger Cordilleran deformation), crustal-scale faults break the Belt Basin up into segments with varying subsidence/exhumation histories (e.g. Winston, 1991; Sears, 2007; Lydon, 2010; Lonn et al., 2020 and references within). From north to south, the most significant of these crustal-scale structures consist of the St. Mary-Moyie and associated Rocky Mountain Trench fault-systems, the Showshoe fault and Jocko Line that border an intrabasin sydepositional high called the Central horst, and to the south, the Perry Line (Fig. 4.14A; Winston, 1986; Sears, 2007; Lydon, 2010). Some workers (e.g. Bookstrom, 2016) have suggested that the ca. 1380–1300 Ma East Kootenay and ca. 1115–1065 Ma Grenvillian events are generally pervasive along the western margin of the Belt Basin. However, alternatively we argue that it is only locally within the vicinity of these significant syn-depositional Belt Basin structures, that a clear record of ca. 1380–1330 Ma "East Kootenay" magmatism and metamorphism, and ca. 1115–1065 Ma "Grenville" metamorphism is identified.

In the northern region of the Belt Basin, adjacent to significant syndepositional structures of the northeast-southwest trending, St. Mary-Moyie Fault system, the Matthew Creek metamorphic zone and nearby world class Sullivan Pb-Zn-Ag deposit are present (Fig. 4.14A). Within the Matthew Creek metamorphic zone, sillimanite-grade amphibolite facies rock of the lower Belt Supergroup are of notably higher metamorphic grade than nearby greenschist facies Belt Basin rocks (McFarland and Pattison, 2000), and are intruded by the ca. 1365 Ma Hellroaring Creek and ca. 1335 Ma Matthew Creek stocks (Aleinikoff et al., 2015). These sillimanite-grade amphibolite facies rocks yield a spread of U–Pb monazite ages from ca. 1380–1000 Ma, with two distinct age-peaks at ca. 1350–1340 and 1080 Ma (Fig. 4.15; McFarlane, 2015). Associated with significant syn-depositional faults, casserite (tin-ore, SnO_2) from the nearby Sullivan SedEx deposit yields U–Pb ages with a major ca. 1470 Ma age-peak associated with the timing of mineralization, and two significant overprinting events at ca. 1380 and 1075 Ma that reflect dissolution-reprecipitation processes associated with localized thermal perturbations (Slack, 2020). Proterozoic structures of the St. Mary-Moyie Fault system also extend further southeast into the Priest River region, where rare ca. 1100 Ma metamorphic zircon rims are present (Doughty and Chamberlain, 2008).

The southernmost syn-depositional fault-system of the Belt Basin occurs along the east-west trending, down to the north, Perry Line (Fig. 4.14A; Winston, 1986; Link et al., 2007). The trend of the Perry Line extends west (e.g. Sims et al., 2004), into the Blackbird Co-Cu-Au district, where strata of the Lemhi Subgroup of the Belt Basin hosts Mesoproterozoic mineralization (Aleinikoff et al., 2012; Bookstrom et al., 2016). Ca. 1370 Ma diabase, diorite, and migmatites are also associated with the mineralized Belt Basin strata in the Blackbird district. Metamorphic barometry on these migmatites suggest initial pressures equivalent to ~14 km of burial, and subsequent pressure increases equivalent to ~20 km of burial (Doughty and Chamberlain, 2010). Monazite and xenotime U–Pb geochronology indicates that initial mineralization formed at ca. 1360 Ma, and experienced a subsequent Mesoproterozoic thermal event at ca. 1060 Ma (Fig. 4.15; Aleinikoff et al., 2012).

Within the central portion of the Belt Basin, the region investigated by this study, syndepositional basin-scale structures include a central horst block bounded to the north by the Snowshoe fault and to the south by the Jocko Line. Associated with the Snowshoe and Jocko syn-depositional structures are world-class Pb-Zn-Co-Ag deposits of the Coeur d'Alene and associated districts (e.g. Hobbs et al., 1965). The Jocko Line is of particular interest to this study, as it is a down to the south, significant syn-depositional Belt Basin fault that is an antecedent to the Lewis and Clark fault zone (Fig. 4.14; Winston, 1991; Sears, 2007). Notably, Lewis and Clark fault zone structures accommodated formation/exhumation of the Clearwater metamorphic complex during Cordilleran deformation (Doughty et al., 2007). As discussed, U–Pb monazite ages from the Clearwater complex contains distinct ca. 1380–1340 and 1080–1060 Ma bimodal age-peaks, that are similar to those found adjacent to other major syn-depositional Belt Basin structures (Fig. 4.15). Consequently, Grenville-age ca. 1080–1060 Ma metamorphism within the Belt Basin is associated with significant pre-existing crustal-scale structures. These structures were likely active in a normal-sense during the main ca. 1470–1380 Ma interval of

Belt Basin subsidence and were conduits for magmatism and mineralization during ca. 1370–1330 Ma East Kootenay metamorphism within the Belt Basin (Fig. 4.14A).

Importantly, the record of Grenville-age metamorphism is also associated with these major Belt Basin syn-depositional normal-fault structures. The sampled metapelitic units are from the Wallace Formation which occupies a middle-stratigraphic position of the Belt Supergroup, with an estimated ~9 km of underlying strata (Winston, 2016). The possibility that the sampled Wallace Formation is actually miscorrelated, lower Belt strata, is unlikely as the sampled unit contains consistent carbonate horizons absent in nearby lower Belt units, and also lacks the syn-depositional mafic sills common in nearby lower Belt strata (e.g. Lewis et al., 2001; 2005; 2007). Maximum thickness estimates for Belt Supergroup are generally ~20 km

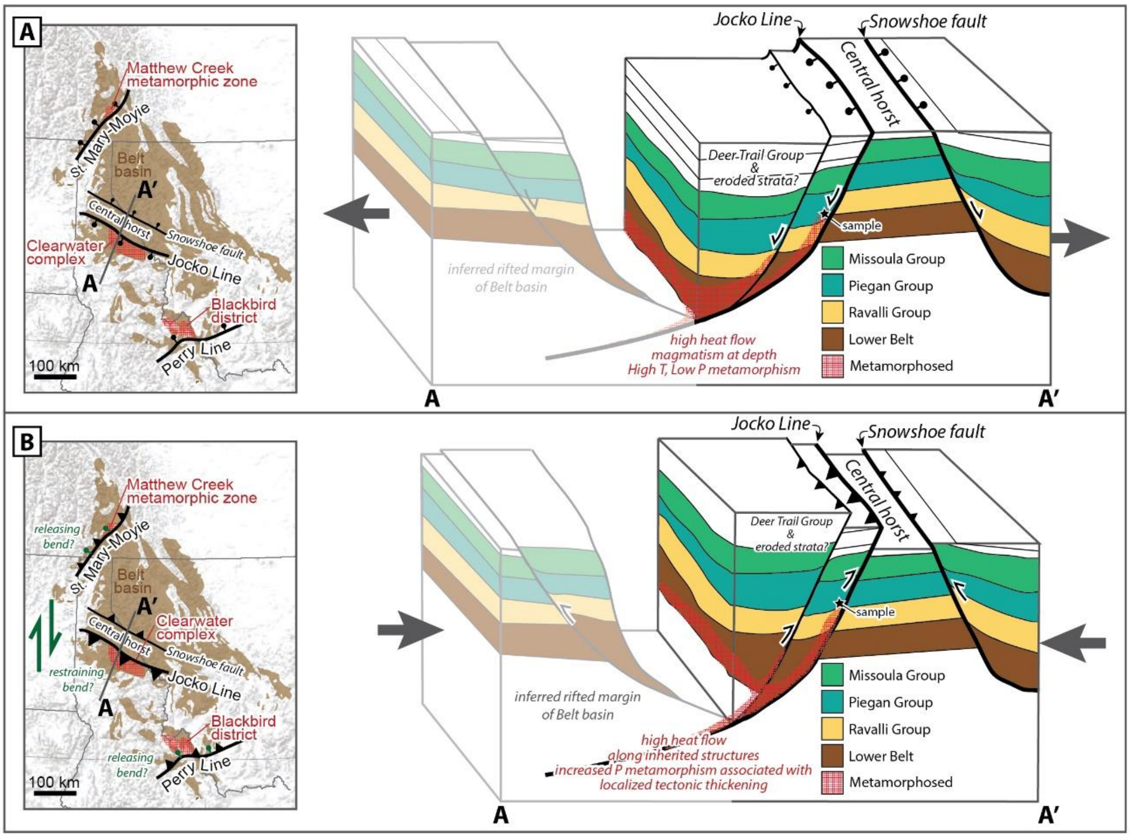

Fig 4.14: Generalized map (adapted from Sears, 2007 and Lonn et al., 2020), and schematic cross section cartoons of significant Belt basin syndepositional faults/fault zones at (A) the suggested occurrence of ca. 1380–1330 Ma East Kooteney, Buchan-style, metamorphism due to high heat flow, mineralization and magma intrusion into the Belt basin, and at (B) the suggested occurrence of ca. 1110–1060 Ma Grenville-age, Barrovian-style, metamorphism due to high heat flow and localized inversion of the Belt basin due to rejuvenation of inherited fault zones. Various mechanisms are worth investigating for this apparent Grenville-age tectonism, including a predominately compressional stress-field resulting in reverse-sense activation (shown by black faults) of inherited weaknesses, or an predominately transpressional stress-field resulting in some localized reverse sense, and perhaps some nominal or normal activation sense structures (alternative fault type shown in green) associated with restricting or releasing bends in the margin.

(Harrison, 1972) and re-correlation of the overlying Deer Trail Group strata (Box et al., 2020) may indicate at least another ~2.5 km (Miller and Whipple, 1989) of poorly preserved strata atop upper Belt strata. Consequently, at ca. 1080 Ma, the preserved stratigraphy can only account depositional burial of the Wallace Formation to depths of about 12–14 km, while the thermodynamic modelling results indicate pressures requiring at least 17–22 km of burial. It is possible that the stratigraphic thicknesses are underestimates due to subsequent erosion.

Nevertheless, the results presented in this work lend further support to earlier interpretations (Zirakparvar et al., 2010; Neishem et al., 2012) that Grenville-age tectonism in the Clearwater region of the Belt Basin requires a component of tectonic thickening or structural burial. Given the basin-wide association of this metamorphism with crustal-scale structures, and coeval timing to similar events elsewhere within Laurentia, we suggest this localized Grenville-age metamorphism within the Belt Basin was facilitated by enhanced heat flow and localized structural burial along inverted rift structures. This interpretation suggests that at ca. 1100–1020 Ma the Belt Basin experienced a period of mantle/thermal upwelling (e.g. Doughty and Chamberlain, 2008) and localized structural inversion (Fig. 4.14B), perhaps partially analogous/correlative to coeval processes recognized within the Midcontinent Rift and Southwest Laurentian large igneous province (e.g. Cannon, 1994; Bright et al., 2014; Swanson-Hysell, 2019; Hodgin et al., 2022). However, these processes in the Belt Basin differ notably from coeval Midcontinent and Southwest Laurentian processes. In particular, this time interval was amagmatic within the Belt Basin and there is no recognized associated sedimentation (Link et al., 1993; Brennan et al., 2021a; 2021b).

Identification of field-based relationships revealing this probable localized Grenville-age inversion of the western Belt Basin may be hampered by the fact that these same inherited structures were subsequently reactivated multiple times during Neoproterozoic rifting, and Mesozoic and younger Cordilleran orogenesis (e.g. Doughty et al., 2007; Lund et al., 2010; Bookstrom et al., 2016). During Neoproterozoic rifting the Belt Basin segment of the margin also experienced less subsidence and more exhumation than adjacent segments (Lund, 2008; Link et al., 2017; Brennan et al., 2020), which could have eroded a limited Grenville-age sedimentary record if it was ever present. However, as the geochronology and thermodynamic modeling results indicate, Grenville-age tectonism is indeed present in western Laurentia. The substantiation of this finding has significant implications for global models of supercontinent Rodinia formation.

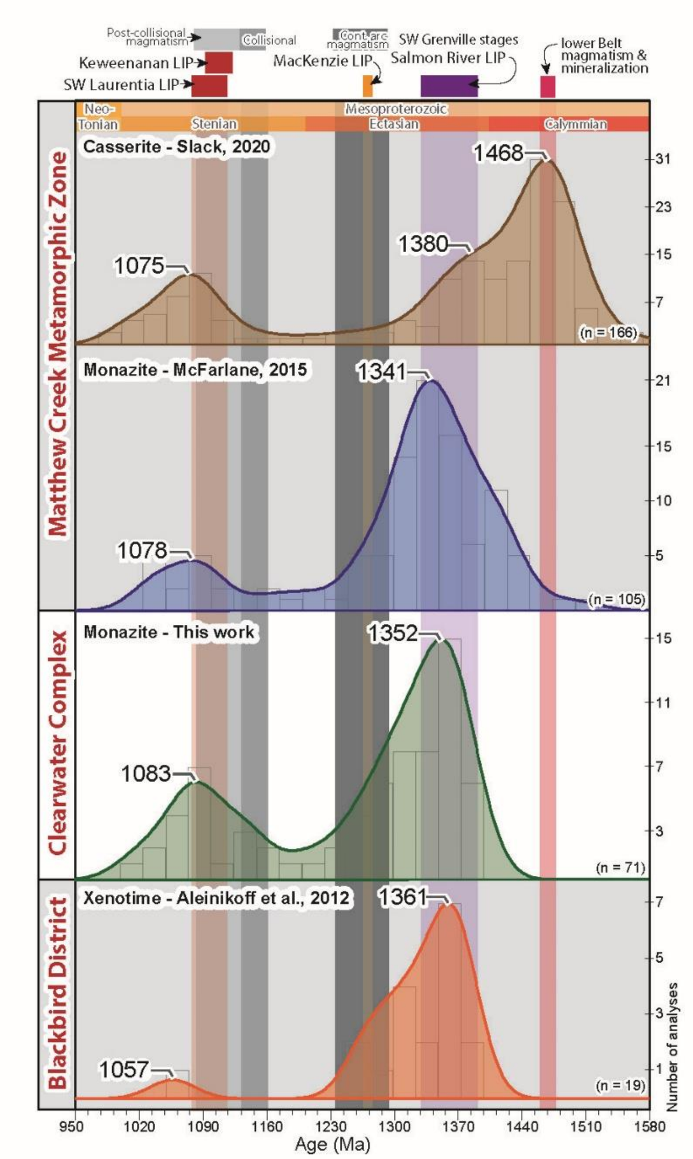

Fig. 4.15: Kernel Density U–Pb age spectra (plotted with 25 Myr band and binwidth) from amphibolite grade Belt Supergroup metapelites within the Matthew Creek metamorphic zone (Casserite, Slack, 2020; Monazite, McFarlane, 2015), the Clearwater complex (Monazite, this work), and the Blackbird district (Xenotime, Aleinikoff et al., 2012). The ages of corresponding southwestern Grenville stages (Mulder et al., 2017), lower Belt syndepositional mineralization, and notable Laurentian Large Igneous Provinces (LIPS; Ernst et al., 2008 and references within) are indicated. Note all three locations contain a bimodal age-distribution with 1380–1340, and 1080–1060 Ma age-peaks.

4.5.4 Global Implication of Grenville-age Barrovian metamorphism within the Belt Basin

Most paleographic reconstructions favor the assembly of continents along western Laurentia at ca. 1100–900 Ma associated with the greater amalgamation of supercontinent Rodinia (e.g. Li et al., 2008; Mulder et al., 2018; Merdith et al., 2020). Consequently, the presented evidence for ca. 1110–1020 Ma Barrovian metamorphism within the Belt Basin presents several new constraints to refine these global models.

Firstly, these results suggest that the onset of amalgamation of continents west of the Belt Basin region initiated around 1110 Ma, and concluded by ca. 1020 Ma. Given the absolute absence of recognized tectonism in the Belt Basin region from ca. 1020–780 Ma (e.g. Brennan et al., 2021a), we suggest this ca. 1020–780 Ma interval was the stable duration of Rodinia in this region. Notably, this timeframe is longer than suggested by most leading global models (e.g. Li et al., 2008; Merdith et al., 2020) that instead suggest the main amalgamation of Australia, Antarctica, western Laurentia, and perhaps South China occurred primarily between ca. 1040–900 Ma, and began breaking up around ca. 830–820 Ma. This discrepancy could indicate that the Belt Basin region only records the initial onset of this assembly process and lacks a record of the initial onset of breakup processes, or perhaps the absolute timing of these global models require refinement.

Importantly, the Clearwater region is ~1800 km from the nearest Grenville-orogenic front in southwest Laurentia (see Fig. 4.2). This distance is over three times further than the ~500 km from the Grenville orogenic front in eastern Laurentia and the reactivated/inverted structures of the Midcontinent Rift. Thus, it is doubtful that Grenville orogenic stresses in southern and eastern Laurentia could solely result in the far-field inversion of the Belt Basin, especially since the record of structural inversion appears concentrated more in the western extent of the basin. Consequently, Rodinia models with continental blocks exhibiting tectonism adjacent to western Laurentia at ca. 1110–1020 Ma should be favored over those that lack a satisfactory mechanism to account for the Grenville-age metamorphic record of the Clearwater complex.

One such model that provides a satisfactory Grenville-age mechanism is the "Missing-Link" model (Li et al., 1995). In this model, final Rodinia assembly may have occurred along the ca. 1040–900 Ma Sibao orogen in South China, which is suggested to have been located between western Laurentia and Australia/Antarctica (Fig. 4.16). Additionally, the "Missing-Link" model also has several other strengths. Notably, South China also provides a satisfactory Neoproterozoic plume and rifting record that could account for discrepancies in corresponding records of western Laurentia and eastern Australia (e.g. Li et al., 2008). However, the absence of any non-Laurentian derived Grenville-age sedimentation in (or along) the Belt region (see Brennan et al., 2021a; 2021b), contradicts a long-held prediction of this model (Li et al., 1995; 2002; 2008; Yao et al., 2017). Others have also utilized paleomagnetic constraints (Park et al., 2021; Chang et al., 2022), and the presence of moderately widespread ca. 950–830 Ma magmatism (Yao et al., 2019) in South China to instead argue that South China was located along the periphery, not center, of Rodinia. Based primarily on paleomagnetic data and broadly similar Neoproterozoic histories, alternative "Missing-Link" blocks with records of Grenville-age tectonism such as Tarim have also been proposed (Wen et al., 2017; 2018).

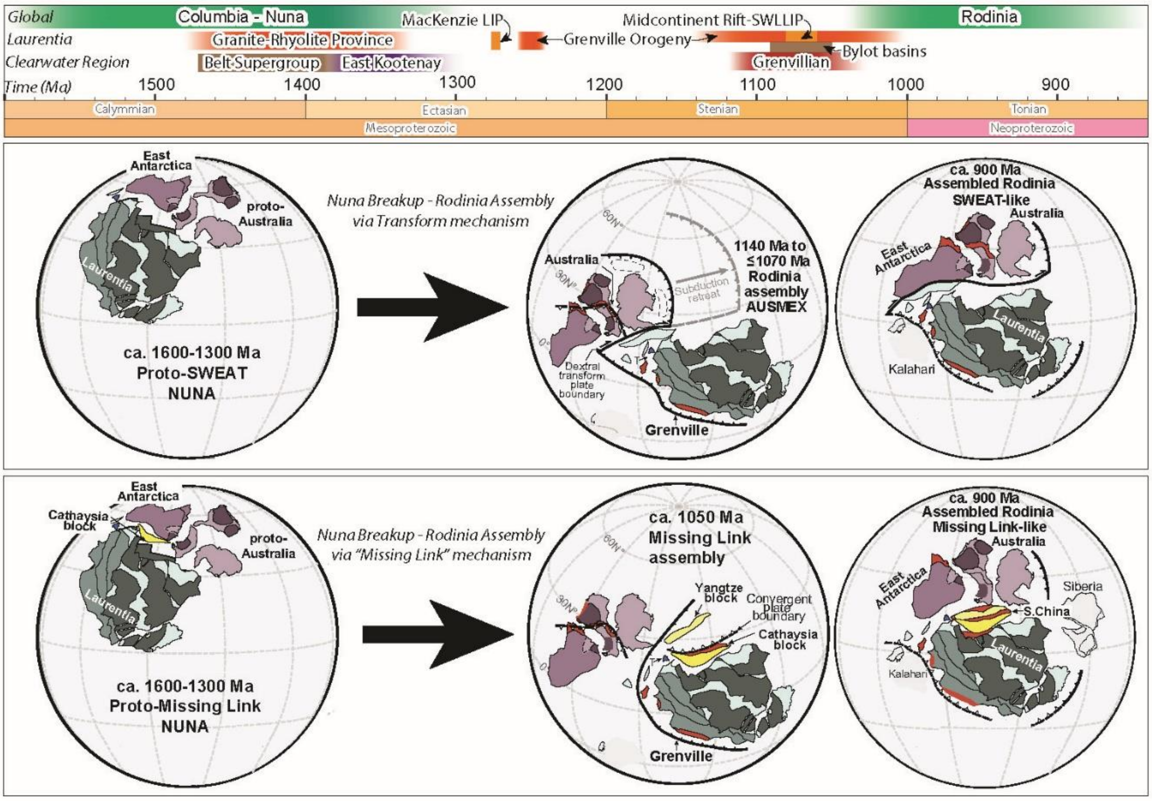

Fig. 4.16: Geologic timeline of the Nuna to Rodinia supercontinent transition, the relevant Laurentian-scale geologic events and local events within the Clearwater region. Below the timeline are two competing tectonic models for the Nuna to Rodinia transition along western Laurentia that could account for the ca. 1110–1020 Ma metamorphic record of the Clearwater complex. The upper model proposes a "SWEAT-like" (e.g. Moores, 1991) assembly of Rodinia along a large dextral transform boundary (after Mulder et al., 2018; Meredith et al., 2020). The lower "Missing-Link like" model proposes that the assembly of Rodinia occurred along the intervening Cathaysia and Yangtze blocks which contain a ca. 1100–900 Ma collisional (Sibao) orogen (after Li et al., 1995; 2008; 2013; Yao et al., 2017).

Alternative models besides the “Missing-Link” also warrant consideration. The most notable of which are those that advocate for the final assembly of western Laurentia and Australia/Antarctica along a dextral transpressional/transtensional boundary perhaps better recorded in smaller intervening blocks, such as Tasmania and the Western South Tasman Rise (Fig. 4.16). A strength of these models, is that Tasmania and the Western South Tasman Rise contain ca. 1300–1080 Ma metamorphism and provenance ties to western Laurentia (Halpin et al., 2014; Mulder et al., 2018; Merdith et al., 2020; Brown et al., 2022). It is also worth noting, that some alternative Missing-Link models, such as those that favor Tarim between western Laurentia and Australia/Antarctica (Wen et al., 2018) also advocate for dextral transpressional assembly of Rodinia along the western Laurentian margin.

In these models of transpressional Rodinia assembly, the observed ~6 km discrepancy between calculated burial depths and estimates for the thickness of overlying strata in the Clearwater region at ca. 1080 Ma, suggest that the Clearwater region (and the Jocko Line; see Fig. 4.14) could have acted as a localized restraining bend boundary along the western edge of the Belt Basin during this period (Fig. 4.14B; 4.16), consistent with the proposed dextral motion. If correct, based on the orientations of the Perry Line, and St. Mary-Moyie fault zones, the dextral assembly models predict these regions would have been predominantly releasing bends along the margin. This relationship may suggest nominal Grenville-age inversion and limited related Barrovian-style metamorphism, but perhaps still a record of thermal upwelling and/or subsidence, in these areas. Consequently, dextral transpressional models could explain why the ca. 1380–1330 Ma East Kooteney metamorphism along the Perry Line and St. Mary-Moyie Fault zone regions (Matthew Creek metamorphic zone and Blackbird district) appears to have a weaker Grenville-age overprint (e.g. Pattison and Seitz, 2012; Bookstrom et al.., 2016) compared to the Clearwater complex.

4.6 Conclusions

A key record to solving debates on the style and mechanism of the Nuna to Rodinia transition lies in the ca. 1100 Ma Grenville-age tectonic record of western Laurentia. Within the Clearwater complex of the Belt Basin in western Laurentia, existing Lu–Hf garnet geochronology (Zirakparvar et al., 2010; Neishem et al., 2012) and new monazite and apatite U–Pb results and Thermocalc (pressure-temperature) constraints from ca. 1450 Ma Belt Supergroup metapelitic strata record ca. 1350 and

1080 Ma metamorphism, and thus may contain a rare record of this supercontinent transition. However, variable overprinting by younger Mesozoic and Cordilleran orogenic processes has previously hindered interpretation of these older events. In the western external region of the Clearwater complex, metapelitic strata retain, or partially retain, Cryogenian apatite U–Pb ages associated with nearby rift-related magmatism during Rodinia breakup. These ages indicate that Cordilleran conditions did not exceed ~450–550°C (the U/Pb closure temperature of apatite) in this region. Consequently, the mineral assemblages within these rocks likely reflect an upper amphibolite grade, Barrovian-style, metamorphic event recorded by ca. 1100–1070 Ma garnet Lu–Hf and monazite U–Pb ages. Thermodynamic modeling of these metamorphic assemblages indicate they are consistent with pressures of 5–7.5 kbar and temperatures of 620–670°C, suggesting burial to a depth of ~17–22 km or greater around along a moderately-high average geothermal gradient of ~23–36°C/km.

These ca. 1100–1070 Ma metamorphic conditions are difficult to satisfy with static heating within the Belt Basin alone. Thus, these conditions advocate that thermal upwelling/heating and western tectonism facilitated rejuvenation of crustal-scale rift-structures which resulted in localized Grenville-age structural inversion, and crustal thickening within the Belt Basin. Manifestations of this critical period of thermal upwelling/heating, rejuvenation of crustal-scale structures, and sometimes localized structural rift inversion associated with Rodinia assembly may be recognized Laurentian-wide such as within the 1110–1085 Ma Midcontinent Rift (e.g. Swanson-Hysell et al., 2019), 1115–1078 Ma Pikes Peak batholith (Guitreau et al., 2016), 1094–1080 Ma Southwestern Laurentian Large Igneous Province (Timmons et al., 2001; Bright et al., 2014), and perhaps the 1090–1040 Ma Bylot and correlative basins in northern Laurentia (Greenman et al., 2021). Consequently, global geologic models must account for ca. 1100–1020 Ma Grenville-age tectonism in blocks adjacent to the western margin of Laurentia within supercontinent Rodinia. Future work should evaluate the viability of Grenville-age collisional or transpressional/transtensional settings along the western margin of Laurentia and alleged conjugates such as Australia/Antarctica, South China and/or Tarim.

4.7. References

Geological Society of American reference style

Anderson, J.L., 1983, Proterozoic anorogenic granite plutonism of North America. In: Medaris Jr., L.G., Byers, C.W., Mickelson, D.M., Shanks, W.C. (Eds.), Proterozoic Geology: Selected Papers from an International Proterozoic Symposium: Geological Society of America Memoir, 161, pp. 133–154.

Albarede, F., and Martine, J., 1984, Unscrambling the lead model ages: Geochimica et Cosmochimica Acta, v. 48, p. 207–212, doi:10.1016/0016-7037(84)90364-8.

Aleinikoff, J.N., Schenck, W.S., Plank, M.O., Srogi, L.A., Fanning, C.M., Kamo, S.L., and Bosbyshell, H., 2006, Deciphering igneous and metamorphic events in high-grade rocks of the Wilmington complex, Delaware: Morphology, cathodoluminescence and backscattered electron zoning, and SHRIMP U-Pb geochronology of zircon and monazite: Bulletin of the Geological Society of America, v. 118, p. 39–64, doi:10.1130/B25659.1.

Aleinikoff, J.N., Lack, J.F.S., Lund, K., Evans, K. V., Fanning, C.M., Mazdab, F.K., Wooden, J.L., and Pillers, R.M., 2012, Constraints on the timing of Co-Cu ± Au mineralization in the Blackbird district, Idaho, using SHRIMP U-Pb ages of monazite and xenotime plus zircon ages of related Mesoproterozoic orthogneisses and metasedimentary rocks: Economic Geology, v. 107, p. 1143–1175, doi:10.2113/econgeo.107.6.1143.

Allen, D.J., Braile, L.W., Hinze, W.J., Mariano, J., 1995, The Midcontinent rift system, U.S.A.: a major Proterozoic continental rift. In: Olsen, K.H. (Ed.), Continental Rifts: Evolution, Structure, Tectonics, Geotectonics. Elsevier, Netherlands, p. 373–407.

Baldwin, J.A., Lewis, R.S., Vervoort, J.D., and Mcdonie, C.D., 2016, Metamorphic history of the Belt Supergroup and underlying Paleoproterozoic basement rocks in the western part of the Clearwater complex, Idaho: The Geological Society of America FIeld Guide, v. 41, p. 251–264, doi:10.1130/2016.0041(08).

Bickford, M.E., Van Schmus, W.R., Karlstrom, K.E., Mueller, P.A., and Kamenov, G.D., 2015, Mesoproterozoic-trans-Laurentian magmatism: A synthesis of continent-wide age distributions, new SIMS U-Pb ages, zircon saturation temperatures, and Hf and Nd isotopic compositions: Precambrian Research, v. 265, p. 286–312, doi:10.1016/j.precamres.2014.11.024.

Bookstrom, A.A., Box, S.E., Cossette, P.M., Frost, T.P., Gillerman, V.S., King, G.R., and Zirakparvar, N.A., 2016, Geologic history of the Blackbird Co-Cu district in the Lemhi subbasin of the Belt-Purcell Basin: Geological Society of American Special Paper, v. 522, p. 185–219, doi:10.1130/2016.2522(08).

Box, S.E., Pritchard, C., Stephens, T.S., and O'Sullivan, P.B., 2020, Between the supercontinents -- Mesoproterozoic Deer Trail Group, an intermediate age unit between the Mesoproterozoic Belt-Purcell Supergroup and the Neoproterozoic

Windermere Supergroup in northeastern Washington, U.S.A.: Canadian Journal of Earth Sciences, v. 17, p. 1–17, doi:10.1139/cjes-2019-0188.

Bright, R.M., Amato, J.M., Denyszyn, S.W., and Ernst, R.E., 2014, U-Pb geochronology of 1.1 Ga diabase in the southwestern United States: Testing models for the origin of a post-Grenville large igneous province: Lithosphere, v. 6, p. 135–156, doi:10.1130/L335.1.

Brown, M., Kirkland, C.L., and Johnson, T.E., 2020, Evolution of geodynamics since the Archean: Significant change at the dawn of the Phanerozoic: Geology, v. 48, p. 488–492, doi:10.1130/G47417.1.

Brown, D. A., Simpson, A., Hand, M., Morrissey, L. J., Gilbert, S., Tamblyn, R., & Glorie, S., 2022, Laser-ablation Lu-Hf dating reveals Laurentian garnet in subducted rocks from southern Australia. Geology, v. 50, no. (7), p. 837–842. https://doi.org/10.1130/G49784.1

Bloch, E.M., Jollands, M.C., Devoir, A., Bouvier, A.S., Ibañez-Mejia, M., and Baumgartner, L.P., 2020, Multispecies diffusion of yttrium, rare earth elements and hafnium in garnet: Journal of Petrology, v. 61, doi:10.1093/petrology/egaa055.

Brennan, D.T., Pearson, D.M., Link, P.K., and Chamberlain, K.R., 2020, Neoproterozoic Windermere Supergroup near Bayhorse, Idaho: late-stage Rodinian rifting was deflected west around the Belt basin: Tectonics, doi:10.1029/2020tc006145.

Brennan, D.T., Li, Z., Rankenburg, K., Evans, N., Link, P.K., Nordsvan, A.R., Kirkland, C.L., Mahoney, J.B., Johnson, T., and Mcdonald, B.J., 2021a, Recalibrating Rodinian rifting in the northwestern United States: Geology, v. 49, p. 617–622, doi:10.1130/G48435.1/5230844/g48435.pdf.

Brennan, D.T., Mahoney, J.B., Li, Z.X., Link, P.K., Evans, N.J., and Johnson, T.E., 2021b, Detrital zircon U–Pb and Hf signatures of Paleo-Mesoproterozoic strata in the Priest River region, northwestern USA: A record of Laurentia assembly and Nuna tenure: Precambrian Research, v. 367, p. 106445, doi:10.1016/j.precamres.2021.106445.

Brennan, D.T., Link, P.K., Li, Z.-X., Martin, L., Johnson, T., Evans, N.J., and Li, J., 2022, Closing the “North American Magmatic” Gap: Crustal evolution of the Clearwater Block from multi-isotope and trace element zircon data: Precambrian Research, v. 369, p. 106533, doi:10.1016/j.precamres.2021.106533.

Brennan, D.T., Pearson, D.M., Link, P.K., and Chamberlain, K.R., 2020, Neoproterozoic Windermere Supergroup near Bayhorse, Idaho: late-stage Rodinian rifting was deflected west around the Belt basin: Tectonics, doi:10.1029/2020tc006145.

Cannon, W.F., and Hinze, W.J., 1992, Speculations on the origin of the North American Midcontinent rift: Tectonophysics, v. 213, p. 49–55, doi:10.1016/0040-1951(92)90251-Z.

Carlson, W.D., 2006, Rates of Fe, Mg, Mn, and Ca diffusion in garnet: American Mineralogist, v. 91, p. 1–11, doi:10.2138/am.2006.2043.

Cawood, P.A., and Hawkesworth, C.J., 2014, Earth's middle age: Geology, v. 42, p. 503–506, doi:10.1130/G35402.1.

Chang, L., Zhang, S., Li, H., Xian, H., and Wu, H., 2022, New Paleomagnetic Insights Into the Neoproterozoic Connection Between South China and India and Their Position in Rodinia: Geophysical Research Letters, p. 1–11, doi:10.1029/2022GL098348.

Cherniak, D.J., 2010, Diffusion in accessory minerals: Zircon, titanite, apatite, monazite and xenotime: Reviews in Mineralogy and Geochemistry, v. 72, p. 827–869, doi:10.2138/rmg.2010.72.18.

Chew, D.M., Sylvester, P.J., and Tubrett, M.N., 2011, U-Pb and Th-Pb dating of apatite by LA-ICPMS: Chemical Geology, v. 280, p. 200–216, doi:10.1016/j.chemgeo.2010.11.010.

Chew, D.M., Petrus, J.A., and Kamber, B.S., 2014, U-Pb LA-ICPMS dating using accessory mineral standards with variable common Pb: Chemical Geology, v. 363, p. 185–199, doi:10.1016/j.chemgeo.2013.11.006.

Dickinson, W.R., 2004, Evolution of the North American Cordillera: Annual Review of Earth and Planetary Sciences, v. 32, p. 13–45, doi:10.1146/annurev.earth.32.101802.120257.

Doughty, P.T., Chamberlain, K.R., Foster, D.A., and Sha, G.S., 2007, Structural, metamorphic, and geochronologic constraints on the origin of the clearwater core complex, northern Idaho: Special Paper of the Geological Society of America, v. 433, p. 211–241, doi:10.1130/2007.2433(11).

Doughty, P.T., and Chamberlain, K.R., 2008, Protolith age and timing of Precambrian magmatic and metamorphic events in the Priest River complex, northern Rockies: Canadian Journal of Earth Sciences, v. 45, p. 99–116, doi:10.1139/e07-067.

Doughty, P.T., and Chamberlain, K.R., 2010, Salmon River Arch revisited: new evidence for 1370 Ma rifting near the end of deposition in the Middle Proterozoic Belt basin: Canadian Journal of Earth Sciences, v. 33, p. 1037–1052, doi:10.1139/e96-079.

Droop, G. T. R., 1987, A general equation for estimating Fe 3+ concentrations in ferromagnesian silicates and oxides from microprobe analyses, using stoichiometric criteria: Mineralogical Magazine, v.51, p. 431–435. https://doi.org/10.1180/minmag.1987.051.361.10

Ernst, R.E., Wingate, M.T.D., Buchan, K.L., and Li, Z.X., 2008, Global record of 1600–700 Ma Large Igneous Provinces (LIPs): Implications for the reconstruction of the proposed Nuna (Columbia) and Rodinia supercontinents: Precambrian Research, v. 160, p. 159–178, doi:10.1016/j.precamres.2007.04.019.

Evans, K. V, Aleinikoff, J.N., Obradovich, J.D., and Fanning, C.M., 2000, SHRIMP U-Pb geochronology of volcanic rocks, Belt Supergroup, western Montana: evidence for rapid deposition of sedimentary strata: Canadian Journal of Earth Sciences, v. 37, p. 1287–1300, doi:10.1139/e00-036.

Eyster, A., Weiss, B.P., Karlstrom, K., and Macdonald, F.A., 2020, Paleomagnetism of the Chuar Group and evaluation of the late Tonian Laurentian apparent polar wander path with implications for the makeup and breakup of Rodinia: Bulletin of the Geological Society of America, v. 132, p. 710–738, doi:10.1130/B32012.1.

Gaschnig, R.M., Vervoort, J.D., Lewis, R.S., and Tikoff, B., 2013, Probing for Proterozoic and Archean crust in the Northern U.S. Cordillera with inherited zircon from the Idaho batholith: Bulletin of the Geological Society of America, v. 125, p. 73–88, doi:10.1130/B30583.1.

Gibson, T.M., Wörndle, S., Crockford, P.W., Hao Bui, T., Creaser, R.A., and Halverson, G.P., 2019, Radiogenic isotope chemostratigraphy reveals marine and nonmarine depositional environments in the late Mesoproterozoic Borden Basin, Arctic Canada: Bulletin of the Geological Society of America, v. 131, p. 1965–1978, doi:10.1130/B35060.1.

Greenman, J.W., Rooney, A.D., Patzke, M., Ielpi, A., and Halverson, G.P., 2021, Re-Os geochronology highlights widespread latest Mesoproterozoic (ca. 1090–1050 Ma) cratonic basin development on northern Laurentia: Geology, v. 49, p. 779–783, doi:10.1130/g48521.1.

Guitreau, M., Mukasa, S.B., Blichert-Toft, J., and Fahnestock, M.F., 2016, Pikes Peak batholith (Colorado, USA) revisited: A SIMS and LA-ICP-MS study of zircon U-Pb ages combined with solution Hf isotopic compositions: Precambrian Research, v. 280, p. 179–194, doi:10.1016/j.precamres.2016.05.001.

Halpin, J.A., Jensen, T., McGoldrick, P., Meffre, S., Berry, R.F., Everard, J.L., Calver, C.R., Thompson, J., Goemann, K., and Whittaker, J.M., 2014, Authigenic monazite and detrital zircon dating from the Proterozoic Rocky Cape Group, Tasmania: Links to the Belt-Purcell Supergroup, North America: Precambrian Research, v. 250, p. 50–67, doi:10.1016/j.precamres.2014.05.025.

Harrison, J.E., Griggs, A.B., and Wells, J.D., 1974, Tectonic features of the Precambrian Belt Basin and Their Influence on Post-Belt Structures: Geological Survey Professional Paper, v. 866.

Hobbs, S.W., Griggs, A.B., Wallace, R.E., and Campbell, A.B., 1965, Geology of the Coeur d'Alene District, Shoshone County, Idaho: U.S. Geological Survey Professional Paper 478, 139 p.

Holland, T.J.B., and Powell, R., 2011, An improved and extended internally consistent thermodynamic dataset for phases of petrological interest, involving a new equation of state for solids: Journal of Metamorphic Geology, v. 29, p. 333–383, doi:10.1111/j.1525-1314.2010.00923.x.

Horstwood, M.S.A., Foster, G.L., Parrish, R.R., Noble, S.R., and Nowell, G.M., 2003, Common-Pb corrected in situ U-Pb accessory mineral geochronology by LA-MC-ICP-

MS: Journal of Analytical Atomic Spectrometry, v. 18, p. 837–846, doi:10.1039/b304365g.

Horstwood, M.S.A. et al., 2016, Community-Derived Standards for LA-ICP-MS U-(Th-)Pb Geochronology–Uncertainty Propagation, Age Interpretation and Data Reporting: Geostandards and Geoanalytical Research, v. 40, p. 311–332, doi:10.1111/j.1751-908X.2016.00379.x.

House, M.A., Hodges, K. V., and Bowring, S.A., 1997, Petrological and geochronological constraints on regional metamorphism along the northern border of the Bitterroot batholith: Journal of Metamorphic Geology, v. 15, p. 753–764, doi:10.1111/j.1525-1314.1997.00052.x.

Howlett, C.J., Reynolds, A.N., and Laskowski, A.K., 2021, Magmatism and Extension in the Anaconda Metamorphic Core Complex of Western Montana and Relation to Regional Tectonics: Tectonics, v. 40, p. 1–31, doi:10.1029/2020TC006431.

Jepson, G., Carrapa, B., George, S.W.M., Triantafyllou, A., Egan, S.M., Constenius, K.N., Gehrels, G.E., and Ducea, M.N., 2021, Resolving mid- to upper-crustal exhumation through apatite petrochronology and thermochronology: Chemical Geology, v. 565, p. 120071, doi:10.1016/j.chemgeo.2021.120071.

Johnson, T., Yakymchuk, C., and Brown, M., 2021, Crustal melting and suprasolidus phase equilibria: From first principles to the state-of-the-art: Earth-Science Reviews, v. 221, p. 103778, doi:10.1016/j.earscirev.2021.103778.

Johansson, Å. et al., 2022, A geochronological review of magmatism along the external margin of Columbia and in the Grenville-age orogens forming the core of Rodinia: Precambrian Research, v. 371, doi:10.1016/j.precamres.2021.106463.

Karlstrom, K.E., Harlan, S.S., Williams, M.L., McLelland, J., Geissman, J.W., and Ahall, K., 1999, Refining Rodinia: Geological evidence for the Australia–Western U.S. connection in the Proterozoic: GSA Today, v. 9, no. 10, p. 1–7.

Kirkland, C.L., Yakymchuk, C., Szilas, K., Evans, N., Hollis, J., McDonald, B., and Gardiner, N.J., 2018, Apatite: a U-Pb thermochronometer or geochronometer? Lithos, v. 318–319, p. 143–157, doi:10.1016/j.lithos.2018.08.007.

Kirscher, U., Mitchell, R.N., Liu, Y., Nordsvan, A.R., Cox, G.M., Pisarevsky, S.A., Wang, C., Wu, L., Murphy, J.B., and Li, Z., 2020, Paleomagnetic constraints on the duration of the Australia-Laurentia connection in the core of the Nuna supercontinent: Geology, v. XX, p. 1–6, doi:10.1130/g47823.1.

Lang, H.M., and Rice, J.M., 1985, Metamorphism of pelitic rocks in the Snow Peak area, northern Idaho: sequence of events and regional implications.: Geological Society of America Bulletin, v. 96, p. 731–736, doi:10.1130/0016-7606(1985)96<731:MOPRIT>2.0.CO;2.

Lewis, R.S., Burmester, R.F., McFaddan, M.D., Derkey, P.D., and Oblad, J.R., 1999, Digital geologic map of the Wallace 1:100,000 quadrangle, Idaho, U.S. Geological Survey Open-File Report 99-390, scale 1:100,000.

Lewis, R.S., Burmester, R.F., Kauffman, J.D., and Frost, T.P., 2001, Geologic map of the St. Maries 30 × 60 minute quadrangle, Idaho: Idaho Geological Survey Geologic Map 28, scale 1:100,000.

Lewis, R.S., Bush, J.H., Burmester, R.F., Kauffman, J.D., Garwood, D.L., Myers, P.E., and Othberg, K.L., 2005, Geologic map of the Potlatch 30 × 60 minute quadrangle, Idaho: Idaho Geological Survey Geologic Map 41, scale 1:100,000.

Lewis, R.S., Burmester, R.F., McFaddan, M.D., Kauffman, J.D., Doughty, P.T., Oakley, W.L., and Frost, T.P., 2007, Geologic Map of the Headquarters 30 x 60 Minute Quadrangle, Idaho, Idaho Geological Survey, Digital Web Map DWM-92, 1:100,000.

Lister, G.S., and Davis, G.A., 1989, The origin of metamorphic core complexes and detachment faults formed during Tertiary continental extension in the northern Colorado River region, U.S.A.: Journal of Structural Geology, v. 11, p. 65–94, doi:10.1016/0191-8141(89)90036-9.

Li, Z. X., Mitchell, R. N., Spencer, C. J., Ernst, R., Pisarevsky, S., Kirscher, U., and Murphy, J. B., 2019, Decoding Earth's rhythms: modulation of supercontinent cycles by longer superocean episodes: Precambrian Research, doi:S0301926819300166.

Li, Z.X. et al., 2008, Assembly, configuration, and break-up history of Rodinia: A synthesis: Precambrian Research, v. 160, p. 179–210, doi:10.1016/j.precamres.2007.04.021.

Li, Z.X., Zhang, L., and Powell, C.M., 1995, South China in Rodinia: Part of the missing link between Australia-East Antarctica and Laurentia? Geology, v. 23, p. 407–410, doi:10.1130/0091-7613(1995)023<0407:SCIRPO>2.3.CO;2.

Link, P.K., Fanning, C.M., Lund, K.I., and Aleinikoff, J.N., 2007, Detrital zircons, correlation and provenance of Mesoproterozoic Belt Supergroup and correlative strata of east-central Idaho and southwest Montana, in Link, P.K., and Lewis, R.S., eds., Proterozoic Geology of Western North America and Siberia: SEPM (Society for Sedimentary Geology) Special Publication 86, p. 101–128, doi:10.2110/pec.07.86.0101.

Link, P.K., Todt, M.K., Pearson, D.M., and Thomas, R.C., 2017, 500–490 Ma detrital zircons in Upper Cambrian Worm Creek and correlative sandstones, Idaho, Montana, and Wyoming: Magmatism and tectonism within the passive margin: Lithosphere, v. 9, p. 1–17, doi:10.1130/L671.1.

Lonn, J.D., Burmester, R.F., Lewis, R.S., and McFaddan, M.D., 2020, The Mesoproterozoic Belt Supergroup: MBMG Special Publication 122: Geology of Montana, vol. 1: Geologic History

Ludwig, K.R., 1998, On the treatment of concordant uranium-lead ages: Geochimica et Cosmochimica Acta, v. 62, p. 665–676, doi:10.1016/S0016-7037(98)00059-3.

Lund, K., Aleinikoff, J.N., Evans, K. V., and Fanning, C.M., 2003, SHRIMP U-Pb geochronology of Neoproterozoic Windermere Supergroup, central Idaho: Implications for rifting of western Laurentia and synchroneity of Sturtian glacial deposits: Bulletin of the Geological Society of America, v. 115, p. 349–372, doi:10.1130/0016-7606(2003)115<0349:SUPGON>2.0.CO;2.

Lund, K., 2008, Geometry of the Neoproterozoic and Paleozoic rift margin of western Laurentia : Implications for mineral deposit settings: Geosphere, v. 4, p. 429–444, doi:10.1130/GES00121.1.

Lund, K., Aleinikoff, J.N., Evans, K. V., duBray, E.A., Dewitt, E.H., and Unruh, D.M., 2010, SHRIMP U-Pb dating of recurrent Cryogenian and Late Cambrian-Early Ordovician alkalic magmatism in central Idaho: Implications for Rodinian rift tectonics: Bulletin of the Geological Society of America, v. 122, p. 430–453, doi:10.1130/B26565.1.

Lydon, J.W., 2010, Tectonic Evolution of the Belt-Purcell Basin: Implications for the Metallogeny of the Purcell Anticlinorium: Geological Survey of Canada Open-File Report 6411, 40 p., https://doi .org/ 10.4095/261389.

McFarlane, C.R.M., 2015, A geochronological framework for sedimentation and Mesoproterozoic tectono-magmatic activity in lower Belt–Purcell rocks exposed west of Kimberley, British Columbia: Canadian Journal of Earth Sciences, v. 52, p. 444–465, doi:10.1139/cjes-2014-0215.

McFarlane, C.R., and Pattison, D.R., 2000, Geology of the Matthew Creek metamorphic zone, southeast British Columbia: a window into Middle Proterozoic metamorphism in the Purcell Basin: Canadian Journal of Earth Sciences, v. 37, p. 1073–1092, doi:10.1139/e00-018.

McMechan, M.E., and Price, R.A., 1982, Superimposed low-grade metamorphism in the Mount Fisher area, southeastern British Columbia—implications for the East Kootenay orogeny: Canadian Journal of Earth Sciences, v. 19, p. 476–489, doi:10.1139/e82-039.

Merdith, A.S. et al., 2020, Extending full-plate tectonic models into deep time: Linking the Neoproterozoic and the Phanerozoic: Earth-Science Reviews, v. 214, p. 103477, doi:10.1016/j.earscirev.2020.103477.

Miller, F.K., and Whipple, J.W., 1989, The Deer Trail Group—Is it part of the Belt Supergroup, in Joseph, N.L., ed., Geologic Guidebook for Washington and Adjacent Areas: Washington Division of Geology and Earth Resources Information Cir-cular 86, p. 1–21.

Moores, E.M., 1991, Southwest U. S.-East Antarctic (SWEAT) connection: A hypothesis: Geology, v. 19, p. 425–428.

Mosher, S., Levine, J.S.F., and Carlson, W.D., 2008, Mesoproterozoic plate tectonics: A collisional model for the Grenville-aged orogenic belt in the Llano uplift, central Texas: Geology, v. 36, p. 55–58, doi:10.1130/G24049A.1.

Mulder, J.A., Karlstrom, K.E., Fletcher, K., Heizler, M.T., Timmons, J.M., Crossey, L.J., Gehrels, G.E., and Pecha, M., 2017, The syn-orogenic sedimentary record of the Grenville Orogeny in southwest Laurentia: Precambrian Research, v. 294, p. 33–52, doi:10.1016/j.precamres.2017.03.006.

Mulder, J.A., Karlstrom, K.E., Halpin, J.A., Merdith, A.S., Spencer, C.J., Berry, R.F., and McDonald, B., 2018, Rodinian devil in disguise: Correlation of 1.25-1.10 Ga strata between Tasmania and Grand Canyon: Geology, v. 46, p. 991–994, doi:10.1130/G45225.1.

Nesheim, T.O., Vervoort, J.D., McClelland, W.C., Gilotti, J.A., and Lang, H.M., 2012, Mesoproterozoic syntectonic garnet within Belt Supergroup metamorphic tectonites: Evidence of Grenville-age metamorphism and deformation along northwest Laurentia: Lithos, v. 134–135, p. 91–107, doi:10.1016/j.lithos.2011.12.008.

Osborne, M.J., and Swarbrick, R.E., 1998, Mechanisms for generating overpressure in sedimentary basins: a reevaluation: reply: American Association of Petroleum Geologists Bulletin, v. 82, p. 2270–2271, doi:10.1306/8626d379-173b-11d7-8645000102c1865d.

Overocker, Quintin M., 2006, Origin and classifi cation of Middle Wallace breccias, Mesoproterozoic Belt Supergroup, Montana and Idaho: Knoxville, University of Tennessee, M.S. thesis, 64 p., http://trace.tennessee.edu/utk_gradthes/1759

Palin, R.M., Searle, M.P., Waters, D.J., Parrish, R.R., Roberts, N.M.W., Horstwood, M.S.A., Yeh, M.W., Chung, S.L., and Anh, T.T., 2013, A geochronological and petrological study of anatectic paragneiss and associated granite dykes from the Day Nui Con Voi metamorphic core complex, North Vietnam: Constraints on the timing of metamorphism within the Red River shear zone: Journal of Metamorphic Geology, v. 31, p. 359–387, doi:10.1111/jmg.12025.

Park, Y., Swanson-Hysell, N.L., Xian, H., Zhang, S., Condon, D.J., Fu, H., and Macdonald, F.A., 2021, A Consistently High-Latitude South China From 820 to 780 Ma: Implications for Exclusion From Rodinia and the Feasibility of Large-Scale True Polar Wander: Journal of Geophysical Research: Solid Earth, v. 126, p. 1–29, doi:10.1029/2020JB021541.

Parrish, R.R., 1990, U–Pb dating of monazite and its application to geological problems: Canadian Journal of Earth Sciences, v. 27, p. 1431–1450, doi:10.1139/e90-152.

Paton, C., Hellstrom, J., Paul, B., Woodhead, J., and Hergt, J., 2011, Iolite: Freeware for the visualisation and processing of mass spectrometric data: Journal of Analytical Atomic Spectrometry, v. 26, p. 2508–2518, doi:10.1039/c1ja10172b.

Pattison, D.R.M., and Seitz, J.L.D., 2012, Stabilization of garnet in metamorphosed altered turbidites near the St. Eugene lead-zinc deposit, southeastern British Columbia: Equilibrium and kinetic controls: Lithos, v. 134–135, p. 221–235, doi:10.1016/j.lithos.2011.12.007.

Pattison, D.R.M., and Spear, F.S., 2018, Kinetic control of staurolite–Al2SiO5 mineral assemblages: Implications for Barrovian and Buchan metamorphism: Journal of Metamorphic Geology, v. 36, p. 667–690, doi:10.1111/jmg.12302.

Pattison, D.R.M., and Goldsmith, S.A., 2022, Metamorphism of the Buchan type-area, NE Scotland and its relation to the adjacent Barrovian domain: v. 179, doi:10.1144/jgs2021-040.

Pearson, D.M., and Link, P.K., 2021, Post-Belt Supergroup Mesoproterozoic to Cambrian rocks of the Leaton Gulch area, east of Challis, Idaho: Northwest Geology, v. 50, p. 11–21.

Paton, C., Hellstrom, J., Paul, B., Woodhead, J., and Hergt, J., 2011, Iolite: Freeware for the visualisation and processing of mass spectrometric data: Journal of Analytical Atomic Spectrometry, v. 26, p. 2508–2518, doi:10.1039/c1ja10172b.

Pisarevsky, S.A., Elming, S.Å., Pesonen, L.J., and Li, Z.X., 2014, Mesoproterozoic paleogeography: Supercontinent and beyond: Precambrian Research, v. 244, p. 207–225, doi:10.1016/j.precamres.2013.05.014.

Rainbird, R.H., Rooney, A.D., Creaser, R.A., and Skulski, T., 2020, Shale and pyrite Re-Os ages from the Hornby Bay and Amundsen basins provide new chronological markers for Mesoproterozoic stratigraphic successions of northern Canada: Earth and Planetary Science Letters, v. 548, p. 116492, doi:10.1016/j.epsl.2020.116492.

Ross, G.M., and Villeneuve, M., 2003, Provenance of the Mesoproterozoic (1.45 Ga) Belt basin (western North America): Another piece in the pre-Rodinia paleogeographic puzzle: Bulletin of the Geological Society of America, v. 115, p. 1191–1217, doi:10.1130/B25209.1.

Ruppel, C., 1995, Extensional processes in continental lithosphere: Journal of Geophysical Research, v. 100, doi:10.1029/95jb02955.

Schoene, B., and Bowring, S.A., 2006, U-Pb systematics of the McClure Mountain syenite: Thermochronological constraints on the age of the 40Ar/39Ar standard MMhb: Contributions to Mineralogy and Petrology, v. 151, p. 615–630, doi:10.1007/s00410-006-0077-4.

Sears, J.W., 2007, Belt-Purcell Basin : Keystone of the Rocky Mountain fold-and-thrust belt, United States and Canada: Geological Society of America Special Paper, v. 433, p. 147–166, doi:10.1130/2007.2433(07).

Slack, J.F., Neymark, L.A., Moscati, R.J., Lowers, H.A., Ransom, P.W., Hauser, R.L., and Adams, D.T., 2020, Origin of Tin Mineralization in the Sullivan Pb-Zn-Ag Deposit, British Columbia: Constraints from Textures, Geochemistry, and LA-ICP-MS U-Pb Geochronology of Cassiterite: Economic Geology, v. 115, p. 1699–1724, doi:10.5382/econgeo.4761.

Sims, P.K., 2009, The Trans-Rocky Mountain Fault System: A Fundamental Precambrian Strike-Slip System: USGS Circular 1334, p. 13, http://pubs.usgs.gov/circ/1334/pdf/C1334.pdf.

Smit, M.A., Scherer, E.E., and Mezger, K., 2013, Peak metamorphic temperatures from cation diffusion zoning in garnet: Journal of Metamorphic Geology, v. 31, p. 339–358, doi:10.1111/jmg.12024.

Sobolev, S. V., and Brown, M., 2019, Surface erosion events controlled the evolution of plate tectonics on Earth: Nature, v. 570, p. 52–57, doi:10.1038/s41586-019-1258-4.

Spencer, C.J., Kirkland, C.L., and Taylor, R.J.M., 2016, Strategies towards statistically robust interpretations of in situ U-Pb zircon geochronology: Geoscience Frontiers, v. 7, p. 581–589, doi:10.1016/j.gsf.2015.11.006.

Spencer, C.J., Mitchell, R.N., and Brown, M., 2021, Enigmatic Mid-Proterozoic Orogens: Hot, Thin, and Low: Geophysical Research Letters, v. 48, p. 1–12, doi:10.1029/2021gl093312.

Stein, C.A., Kley, J., Stein, S., Hindle, D., and Randy Keller, G., 2015, North America's Midcontinent Rift: When rift met LIP: Geosphere, v. 11, p. 1607–1616, doi:10.1130/GES01183.1.

Stevens, L.M., Baldwin, J.A., Cottle, J.M., and Kylander-Clark, A.R.C., 2015, Phase equilibria modelling and LASS monazite petrochronology: *P–T*-t constraints on the evolution of the Priest River core complex, northern Idaho: Journal of Metamorphic Geology, v. 33, p. 385–411, doi:10.1111/jmg.12125.

Swanson-Hysell, N.L., Ramezani, J., Fairchild, L.M., and Rose, I.R., 2018, Failed rifting and fast drifting : Midcontinent Rift development , Laurentia ' s rapid motion and the driver of Grenvillian orogenesis: Geological Society of America Bulletin, p. 1–28, doi:10.1130/B31944.1/4630143/b31944.pdf.

Swanson-Hysell, N. L., 2021, The Precambrian paleogeography of Laurentia. In: Pesonen, L.J., Salminen, J., Evans, D.A.D., Elming, S.-Å., Veikkolainen, T. (eds.) Ancient Supercontinents and the Paleogeography of the Earth, doi:10.1016/B978-0-12- 818533-9.00009-6.

Tang, M., Chu, X., Hao, J., and Shen, B., 2021, Orogenic quiescence in Earth's middle age: Science, v. 731, p. 728–731.

Thomson, S.N., Gehrels, G.E., Ruiz, J., and Buchwaldt, R., 2012, Routine low-damage apatite U-Pb dating using laser ablation-multicollector- ICPMS: Geochemistry, Geophysics, Geosystems, v. 13, p. 1–23, doi:10.1029/2011GC003928.

Timmons, J.M., Karlstrom, K.E., Dehler, C.M., Geissman, J.W., and Heizler, M.T., 2001, Proterozoic multistage (ca. 1.1 and 0.8 Ga) extension recorded in the Grand Canyon Supergroup and establishment of northwest- and north-trending tectonic grains in the southwestern United States: Bulletin of the Geological Society of America, v. 113, p. 163–180, doi:10.1130/0016-7606(2001)113<0163:PMCAGE>2.0.CO;2.

Tucker, N.M., Hand, M., and Payne, J.L., 2015, A rift-related origin for regional medium-pressure, high-temperature metamorphism: Earth and Planetary Science Letters, v. 421, p. 75–88, doi:10.1016/j.epsl.2015.04.003.

Turnbull, R.E., Schwartz, J.J., Fiorentini, M.L., Jongens, R., Evans, N.J., Ludwig, T., McDonald, B.J., and Klepeis, K.A., 2021, A hidden Rodinian lithospheric keel beneath Zealandia, Earth's newly recognized continent: Geology, v. 49, p. 1009–1014, doi:10.1130/G48711.1.

Van Schmus, W.R., Bickford, M.E., and Turek, E., 1996, Proterozoic geology of the east-central mid-continent basement, in van der Pluijm, B.A., and Catacosinos, P.A., eds., Basement and basins of eastern North Amer-ica: Geological Society of America Special Paper 308, p. 7–32.

Vermeesch, P., 2018, IsoplotR: A free and open toolbox for geochronology: Geoscience Frontiers, v. 9, p. 1479–1493, doi:10.1016/j.gsf.2018.04.001.

Verbaas, J., Thorkelson, D.J., Milidragovic, D., Crowley, J.L., Foster, D., Daniel Gibson, H., and Marshall, D.D., 2018, Rifting of western Laurentia at 1.38 Ga: The Hart River sills of Yukon, Canada: Lithos, v. 316–317, p. 243–260, doi:10.1016/j.lithos.2018.06.018.

Wen, B., Evans, D.A.D., and Li, Y.X., 2017, Neoproterozoic paleogeography of the Tarim Block: An extended or alternative "missing-link" model for Rodinia? Earth and Planetary Science Letters, v. 458, p. 92–106, doi:10.1016/j.epsl.2016.10.030.

Wen, B., Evans, D.A.D., Wang, C., Li, Y.X., and Jing, X., 2018, A positive test for the Greater Tarim Block at the heart of Rodinia: Mega-dextral suturing of supercontinent assembly: Geology, v. 46, p. 687–690, doi:10.1130/G40254.1.

Wernicke, B., 1981, Low-angle normal faults in the Basin and Range Province: nappe tectonics in an extending orogen: Nature, v. 291, p. 25–28.

White, R.W., Powell, R., Holland, T.J.B., Johnson, T.E., and Green, E.C.R., 2014a, New mineral activity-composition relations for thermodynamic calculations in metapelitic systems: Journal of Metamorphic Geology, v. 32, p. 261–286, doi:10.1111/jmg.12071.

White, R.W., Powell, R., and Johnson, T.E., 2014b, The effect of Mn on mineral stability in metapelites revisited: New a-x relations for manganese-bearing minerals: Journal of Metamorphic Geology, v. 32, p. 809–828, doi:10.1111/jmg.12095.

Whitmeyer, S.J., and Karlstrom, K.E., 2007, Tectonic model for the Proterozoic growth of North America: Geosphere, v. 3, p. 220–259, doi:10.1130/GES00055.1.

Whitney, D.L., and Evans, B.W., 2010, Abbreviations for names of rock-forming minerals: American Mineralogist, v. 95, p. 185–187, doi:10.2138/am.2010.3371.

Winston, D., 1986, Sedimentation and tectonics of the Middle Proterozoic Belt Basin and their influence on Phanerozoic compression and extension in western Montana and northern Idaho, in Peterson, J.A., ed., Sedimentation and tectonics: American Association of Petroleum Geologists Memoir 41, p. 87–118.

Yakymchuk, C., Clark, C., and White, R.W., 2017, Phase Relations, Reaction Sequences and Petrochronology: Reviews in Mineralogy and Geochemistry, v. 83, p. 13–53, doi:10.2138/rmg.2017.83.2.

Zhu, Z., Campbell, I.H., Allen, C.M., Brocks, J.J., and Chen, B., 2022, The temporal distribution of Earth's supermountains and their potential link to the rise of atmospheric oxygen and biological evolution: Earth and Planetary Science Letters, v. 580, p. 117391, doi:10.1016/j.epsl.2022.117391.

Zirakparvar, N.A., Vervoort, J.D., McClelland, W., and Lewis, R.S., 2010, Insights into the metamorphic evolution of the Belt–Purcell basin; evidence from Lu–Hf garnet geochronology: Canadian Journal of Earth Sciences, v. 47, p. 161–179, doi:10.1139/E10-001.

Chapter 5: Recalibrating Rodinian rifting in the northwestern United States

Abstract

A lack of precise age constraints for Neoproterozoic strata in the northwestern United States (Washington State), including the Buffalo Hump Formation (BHF), has resulted in conflicting interpretations of Rodinia amalgamation and breakup processes. Previous detrital zircon (DZ) studies identified a youngest ca. 1.1 Ga DZ age population in the BHF, interpreted to reflect mostly first-cycle sourcing of unidentified but proximal magmatic rocks intruded during the amalgamation of Rodinia at ca. 1.0 Ga. Alternatively, the ca. 1.1 Ga DZ population has been suggested to represent a distal source with deposition occurring during the early phases of Rodinia rifting, more than 250 m.y. after zircon crystallization. We combined conventional laser-ablation split-stream analyses of U-Pb/Lu-Hf isotopes in zircon with a method of rapid (8 s per spot) U-Pb analysis to evaluate these opposing models. Our study of ~2000 DZ grains from the BHF identified for the first time a minor (~1%) yet significant ca. 760 Ma population, which constrains the maximum depositional age. This new geochronology implies that the BHF records early rift deposition during the breakup of Rodinia and correlates with sedimentary rocks found in other late Tonian basins of southwestern Laurentia.

5.1. Introduction

Correlation of pre-rift and rift strata across purportedly paired margins, such as Neoproterozoic strata of the Adelaide rift complex (southeastern Australia) and the Windermere Supergroup (western Laurentia), has long been used to define key piercing points for reconstructing supercontinents (e.g., Bell and Jefferson, 1987; Dalziel, 1991; Brookfield, 1993). In the northwestern United States, strata of the ca. 1.47–1.38 Ga Belt Supergroup, the ca. 1.3 Ga Deer Trail Group, the <1.1 Ga Buffalo Hump Formation (BHF), and the ca. <720 Ma Windermere Supergroup provide key constraints in the reconstructions of the supercontinents Nuna (ca. 1.6–1.3 Ga) and Rodinia (ca. 900–700 Ma; Fig. 5.1A; Ross et al., 1992; Ross and Villeneuve, 2003; Li et al., 2008; Kirscher et al., 2020). However, uncertain provenance and depositional ages of these key strata have resulted in varying proposed configurations, timings, and identities of alleged Laurentian conjugates such as Australia, Antarctica, and/or South China during the Proterozoic (e.g., Li et al., 2008; Box et al., 2020).

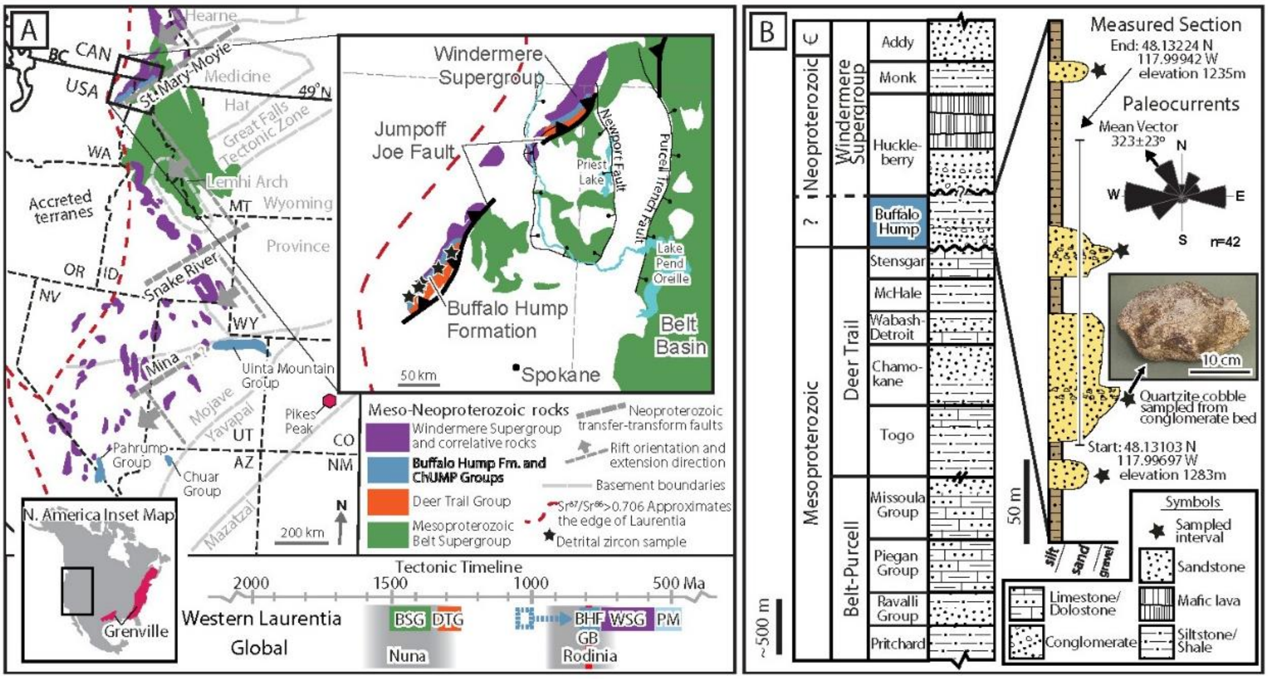

Fig 5.1: (A) Geologic map and time line of the North American Cordillera, and the northwestern United States study area, where Proterozoic rocks of the Belt Supergroup, Deer Trail Group, Buffalo Hump Formation, and Windermere Supergroup outcrop adjacent to the edge of Lau- rentia. Extent of the Grenville Province is shown on the inset map. Neoproterozoic rift geometry and structures are indicated (after Lund et al., 2010). (B) Stratigraphy of the study region (after Box et al., 2020) and photo of the cobble analyzed. Paleocurrent measurements indicate a mean vector to the northwest, roughly perpendicular to the Jumpoff Joe thrust fault. Abbreviations: ChUMP—Chuar–Uinta Mountain–middle Pahrump Group; BSG—Belt Supergroup, DTG—Deer Trail Group, BHF—Buffalo Hump Formation; GB—Gun Barrel, WSG—Windermere Super- group, PM—passive margin; Є—Cambrian. State/province abbreviations: BC—British Columbia, Canada; WA—Washington; MT—Montana; OR—Oregon; ID—Idaho; NV—Nevada; WY—Wyoming; UT—Utah; CO—Colorado; AZ—Arizona; NM—New Mexico

Approximately 10 km west of the westernmost Belt Supergroup in northeastern Washington State, coarse-grained quartzite and locally feldspathic siltite of the BHF and finer-grained argillite and carbonate rocks of the underlying Deer Trail Group crop out. An initial study suggested these rocks comprise a relatively continuous sequence that was correlative to the Piegan and Missoula Groups of the Belt Supergroup (Miller and Whipple, 1989). Ross et al. (1992) dated six detrital zircon (DZ) grains from the BHF and found four ca. 1.2–1.0 Ga grains and two older ca. 1.8 Ga grains. Because the BHF is coarser than Belt Supergroup rocks to the east, Ross et al. (1992) advocated a western source of ca. 1.1 Ga detritus into the BHF basin. More recent geochronology and field work have demonstrated that the Belt Supergroup and Deer Trail Group are characterized by DZ populations ca. 1.3 Ga and older, signifying deposition before the onset of the Grenville orogeny and Rodinia amalgamation (Ross and Villeneuve, 2003; Box et al., 2020). West of the Mesozoic Jumpoff Joe thrust fault (Fig. 5.1A), Deer Trail Group rocks are unconformably overlain by BHF strata containing abundant ca. 1.1 Ga (Grenvillian) DZs (Box et al., 2020).

Despite these developments, the original interpretation of a western ca. 1.1 Ga DZ source for the BHF (Ross et al., 1992) remained an important constraint for the reconstruction of Rodinia during its assembly (e.g., Li et al., 2008; Yao et al., 2017). However, others have argued that the youngest ca. 1.1 Ga DZ population does not represent the age of deposition, and instead the BHF may be the basal unit of the overlying Windermere Supergroup that constrains early Rodinia breakup (Box et al., 2020).

We adopted an integrated approach combining a rapid laser-ablation–inductively coupled plasma–mass spectrometry (LA-ICP-MS) U-Pb technique with standard split-stream ICP-MS U-Pb and Lu-Hf analyses of DZ from the BHF. Our approach identified a minor and previously unrecognized DZ age population that permits recalibration of a key piercing point for Rodinia reconstructions.

5.2. Geologic setting and methodology

The >350-m-thick BHF is characterized by alternating mudstone and sandstone strata that experienced regional lower-greenschist-facies metamorphism. Locally, the sandstone intervals include monolithic quartzite conglomerate beds containing cobbles >20 cm in diameter. The sandstone intervals decrease in thickness and grain size up section, recording an overall fining-upward trend at the formation scale (Fig. 1B).

To reassess the depositional age and evaluate conflicting sources for the BHF detritus, DZ grains separated from four sandstone intervals and one quartzite cobble were mounted and imaged. Approximately 120 grains from each sample were analyzed by conventional laser-ablation split-stream ICP-MS (LA-SS-ICP-MS) methods for U-Pb and Lu-Hf isotopes at the GeoHistory Facility in the John de Laeter Centre at Curtin University (Perth, Australia) using a 38 μm spot. This approach identified a single concordant 756 ± 30 Ma ($\varepsilon Hf_t = 3.4 \pm 1.5$; all uncertainties reported at 2σ) zircon grain. An additional U-Pb session (~400 unknowns), utilizing a 20 μm spot, identified two additional ca. 760 Ma grains. To further characterize this age, the remaining DZ grains from all four sandstone sample mounts (∼1200 unknowns) were analyzed using a technique involving rapid (8 s each) LA-ICP-MS analysis. This analysis rate was achieved by bypassing the aerosol homogenization device tubing, omitting "cleaning pulses," and reducing ablation and washout times (Chew et al., 2019). Rapid analysis identified additional ca. 760 Ma DZ grains in all four samples. Reanalysis of these grains via conventional U-Pb LA-ICP-MS methods provided robust age constraints. Age-population plots and maximum depositional age calculations only include zircon analyses with discordance less than 10% (Fig. 5.2).

5.3. Detrital zircon U-Pb and Lu-Hf isotope data

The U-Pb/Lu-Hf LA-SS-ICP-MS analysis of DZ grains from all four BHF sandstone samples showed older components at ca. 2.8–2.4 Ga and ca. 1.9–1.6 Ga, along with two broad younger age peaks at ca. 1450 Ma and 1105 Ma that had mostly juvenile Lu-Hf (εHf_t = +5 to +10) values (Fig. 2). Laurentian sources such as the Grenville Province (Fig. 1A, inset), the midcontinent (A-type) Granite-Rhyolite Province, the Yavapai-Mazatzal-Mojave Province, and Archean provinces to the east/southeast (e.g., Wyoming craton) are consistent with these age components (Whitmeyer and Karlstrom, 2007).

A juvenile (εHf_t = +5 to +10) ca. 1380 Ma component may represent detritus derived from plutonic rocks that intrude the Belt Supergroup (Brennan et al., 2020). A minor ca. 1.1 Ga component with an evolved (εHf_t = 0 to –5) signature indicates an additional source inconsistent with juvenile Grenville sources in southeastern Laurentia (Howard et al., 2015; Thomas et al., 2017). The 1.07 Ga Pike's Peak batholith of central Colorado is of similar age and isotopic composition (εHf$_t$ of 2 to −3; Howard et al., 2015) and was also undergoing rapid exhumation during the late Tonian (Flowers et al., 2020), indicating it could be a first-cycle source for this DZ component.

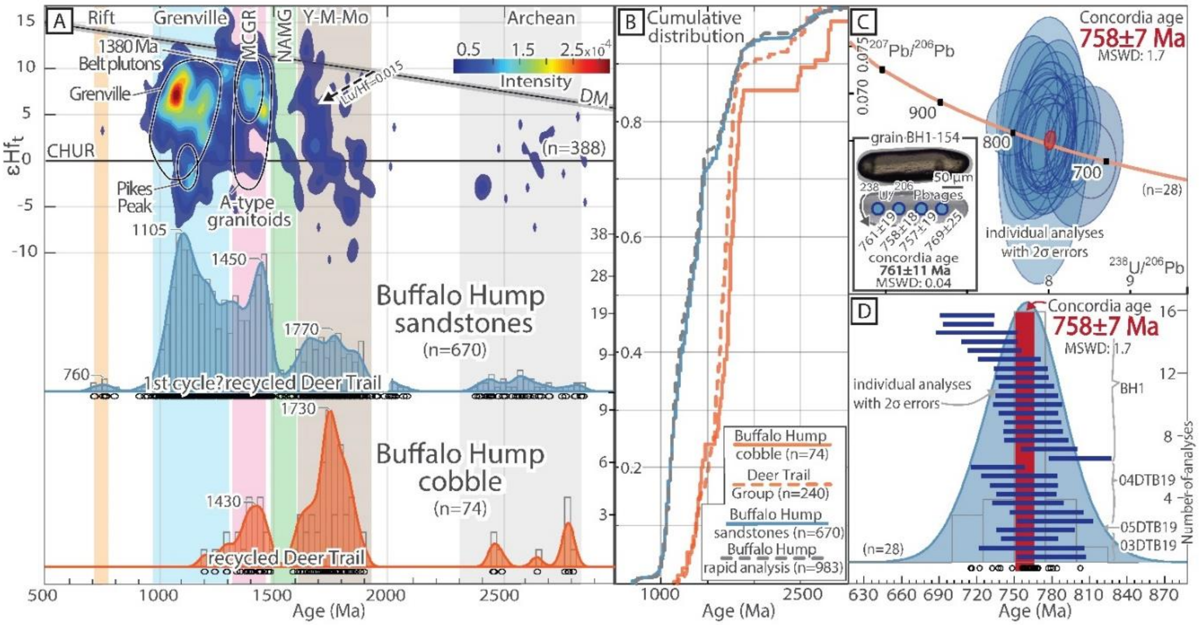

Fig 5.2: (A) Detrital zircon (DZ) U-Pb/Lu-Hf results for the Buffalo Hump Formation (BHF; Washington State, USA) sandstones and the BHF cobble. Age spectra are kernel density estimates (KDEs) with 25 m.y. bandwidths, which are also used for the histograms, and exclude repeated measurements on the targeted young grains. Lu-Hf data shown in the bivariate KDE plot also have 25 m.y. and 1 εHf bandwidths. Average crustal evolution (Lu/Hf = 0.015) is indicated. The εHf and age fields are from Thomas et al. (2017) and Brennan et al. (2020). CHUR—chondritic uniform reservoir; DM—depleted mantle; MCGR—Midcontinent Granite-Rhyolite; NAMG—North American magmatic gap; Y-M-Mo—Yavapai-Mazatzal-Mojave. (B) Cumulative distribution function highlights the similarity between the BHF cobble sample (orange) and the Deer Trail Group (dashed orange; Box et al., 2020), and BHF conventional sandstone (blue) and rapid sandstone (dashed gray) analyses (see the Supplemental Material). (C) Terra-Wasserberg concordia plot of ca. 760 Ma DZ grains, which yielded a Concordia age of 758 ± 7 Ma (2σ). Images (cathodoluminescence and reflected light) of grain BH1-154 in inset. Four analyses of this grain yielded similar (238U/206Pb) ages and a Concordia age of 760 ± 12 Ma (2σ), indicating this grain experienced minimal Pb loss. MSWD—mean square weighted deviation. (D) KDE plot of young analyses with individual analysis bars (2σ) and preferred 758 ± 7 Ma maximum depositional age shown.

Twenty-eight (28) conventional U-Pb spot analyses on 21 ca. 760 Ma grains yielded a Concordia age of 758 ± 7 Ma (mean square weighted deviation [MSWD] = 1.7, all given as a measure of concordance plus equivalence; Figs. 5.2C and 5.2D). All analyses overlapped with concordia at 2σ and yielded alpha-doses and calculated densities (conservatively assuming damage accumulation initiated at crystallization) indicative of closed-system behavior of U-Pb (Murakami et al., 1991). Multiple robust analyses of single DZ grains allows better evaluation of potential Pb loss. Five individual zircon grains were large enough for multiple robust analyses. Four had similar concordia ages of 762 ± 10 Ma (n = 4; MSWD = 0.25; Fig. 2C), 762 ± 17 Ma (n = 2, MSWD = 0.16), 766 ± 16 Ma (n = 2, MSWD = 0.19), and 770 ± 12 Ma (n = 3, MSWD = 0.34). The fifth multi-analysis grain gave a Concordia age of 736 ± 14 Ma (n = 2, MSWD = 0.28).

The DZ ages from the quartzite cobble from the BHF conglomerate contain ca. 1.7 Ga and ca. 1.4 Ga components, with no grains younger than ca. 1.2 Ga (Figs. 2A and 2B).

5.4. Recalibrating rifting of Rodinia in western Laurentia

5.4.1 New constraints from the Buffalo Hump Formation

Based on the Concordia age of the young (ca. 760 Ma, *n* = 28) analyses, we favor a 758 ± 7 Ma (MSWD = 1.7) maximum depositional age for the BHF. This age is a purely descriptive measure of the youngest ages present (Figs. 2C and 2D). The single 736 ± 14 Ma multi-analysis grain was found in the stratigraphically highest sampled interval (BH1) and may support a maximum depositional age that decreases up section from ca. 760 to 735 Ma, and a continued connection to the source of these ca. 760 Ma grains throughout BHF deposition. While ca. 760 Ma magmatic sources were present in eastern Laurentia (e.g., MacLennan et al., 2020), similar-aged source rocks are unknown from western Laurentia. Non-Laurentian source rocks with ca. 760 Ma ages occur in Tasmania (760 ± 12 Ma; Turner et al., 1998), Western Australia (755 ± 3 Ma; Wingate and Giddings, 2000), and the Yangtze block of South China (768 ± 7 Ma to 751 ± 10 Ma; Li et al., 2003).

The large size of the BHF cobble (Fig. 1B) and the ages of the DZ it contains (Fig. 2A) suggest it was sourced from the underlying Deer Trail Group. To the east of the Mesozoic Jumpoff Joe thrust fault, BHF rocks are absent, and Deer Trail Group strata are ∼3 km thinner than they are west of the fault (Box et al., 2020). However, Cambrian rocks are continuous across the fault (Lindsey and Gaylord, 1992). These relationships suggest that the Mesozoic Jumpoff Joe thrust fault may have been an ancestral down-to-the-northwest Neoproterozoic normal fault during BHF deposition. The fault is parallel to the Paleoproterozoic boundary between the Archean Hearne and Medicine Hat blocks (Fig. 1A), and likely exhumed Deer Trail Group rocks on the footwall to its east, interpreted as a rift shoulder, providing a proximal source for the cobbles that were recycled into the adjacent hanging-wall BHF rift basin.

5.4.2 A "ChUMP-B" Correlation and Implications

Detrital zircon grains with ca. 760 Ma ages are rare in western Laurentia and only known to occur in the Uinta Mountain Group (Fig. 1A). The Uinta Mountain Group has the same maximum depositional age (766 ± 5 Ma; Dehler et al., 2010) as the BHF and is also unconformably overlain by younger than 720 Ma Windermere Supergroup strata. A south-dipping, syndepositional fault is inferred to have bounded the Uinta Mountain Group basin to the north. The fault is parallel to, and likely related to, the east-west–trending Paleoproterozoic suture zone along the southern margin of the Archean Wyoming craton (Fig. 1A; Dehler et al., 2010). The orientations of the BHF and Uinta Mountain Group syndepositional faults suggest north-south to northwest-southeast extension along preexisting boundaries.

The Uinta Mountain Group is correlative to the Chuar and middle Pahrump Groups in southwestern Laurentia (Fig. 5.1A). These three coeval (Chuar–Uinta Mountain–middle Pahrump) groups comprise the "ChUMP" correlation (Dehler et al., 2017, and references therein). Similar to the BHF, ChUMP strata contain significant ca. 1.90–1.65 Ga, ca. 1.45 Ga, and ca. 1.3–1.0 Ga DZ age components (Fig. 3). A few late Tonian (ca. 800–720 Ma) DZ grains in ChUMP rocks constitute a comparable (<1.5%) component of the total DZ population. Basal rocks of the more southern Chuar and middle Pahrump Groups have ca. 780 Ma maximum depositional ages (<782 ± 7 Ma and <775 ± 18 Ma, respectively; Dehler et al., 2017; Mahon et al., 2014). Upper Chuar Group strata contain a 742 ± 6 Ma interbedded tuff and are unconformably overlain by Cambrian rocks (Karlstrom et al., 2000, 2018). Middle Pahrump Group strata are overlain by younger than 720 Ma Sturtian diamictites (Mahon et al., 2014; Dehler et al., 2017).

ChUMP strata record an interval of intracratonic rift-basin formation that occurred after intrusion of the ca. 780 Ma Gunbarrel dike swarms (Harlan et al., 2003) but prior to widespread Laurentian rifting at ca. 720 Ma (Yonkee et al., 2014). The stratigraphic position, DZ ages, and tectonic setting of the BHF indicate that it is likely a correlative to ChUMP group strata in an expanded "ChUMP-B" (Chuar, Uinta Mountain, middle Pahrump Groups–Buffalo Hump Formation) correlation. The absence of ca. 900–800 Ma DZ grains in ChUMP-B strata (Fig. 5.3) likely reflects tectono-magmatic quiescence in western Laurentia during that interval due to its central location within Rodinia (e.g., Li et al., 2008).

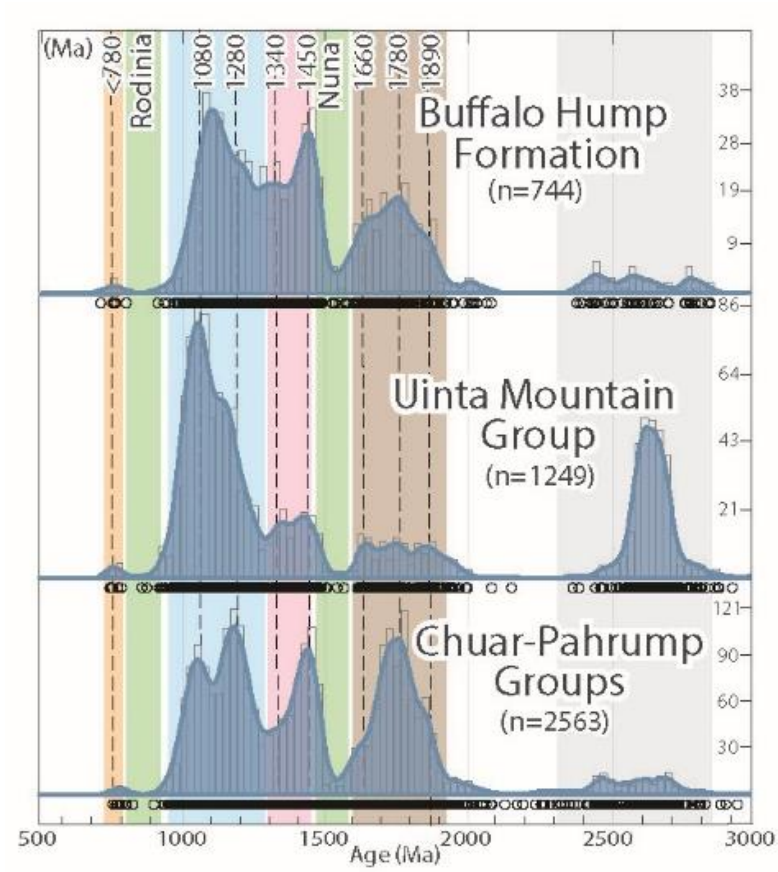

Fig. 5.3: Normalized U-Pb detrital zircon kernel density estimate (KDE) plots and main age components for late Tonian strata in western Laurentia.

The proposed ChUMP-B correlation extends the <780 to ca. 720 Ma interval of rift-basin development northward to the Belt segment (central Idaho to southeastern British Columbia) of the Cordilleran margin. In this region, intermittent Cryogenian–Cambrian Windermere Supergroup deposition and magmatism record predominately northeast-southwest extension, recurrent margin-parallel exhumation (e.g., the Lemhi arch; Fig. 1A), and accompanying breakup in the late Ediacaran–early Cambrian (Lund et al., 2010; Lund and Cheney, 2016; Brennan et al., 2020). Thus, it appears that the orientations of the BHF and Uinta Mountain Group syndepositional faults require earlier extension oblique to the main extension direction during deposition of the Windermere Supergroup. Southwestern Laurentia also likely experienced similar complex multiphase extension during this time (Timmons et al., 2001).

This history of rifting is difficult to reconcile with a single event between southeastern Australia (the Gawler craton) and western Laurentia (e.g., Yonkee et al., 2014). Southeastern Australia contains ca. 830–790 Ma synrift magmatism (Preiss, 2000), of which there is no record in the Belt region. Additionally, high-quality paleomagnetic constraints indicate Australia was widely separated or significantly offset from western Laurentia at ca. 750 Ma (Eyster et al., 2020). Thus, our proposed ChUMP-B correlation and the younger Windermere Supergroup strata support a scenario with multiple rifting events west of Laurentia during Rodinia breakup (see Fig. 4). Intervening blocks, likely including western Tasmania, occupied the region between western Laurentia and Australia within Rodinia.

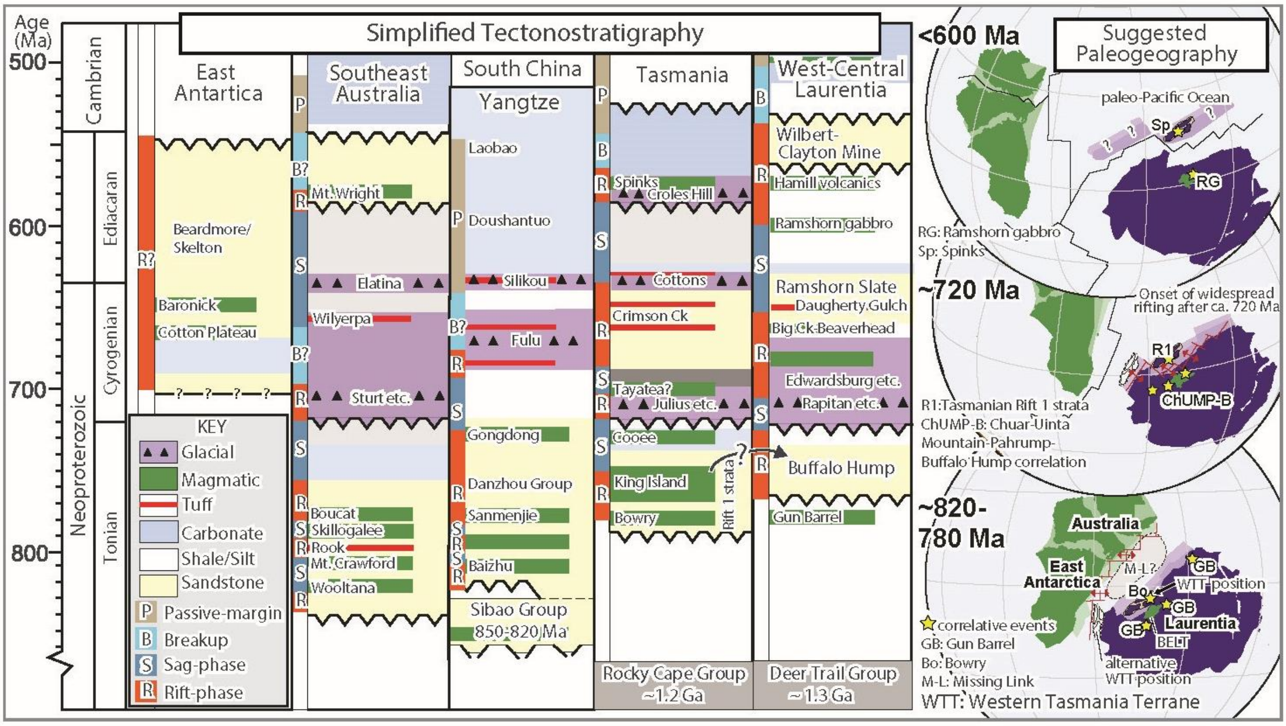

Fig 5.4: Simplified Neoproterozoic tectono-stratigraphy (and inferred rift/faulting, sag/thermal subsidence, lithospheric breakup, and passive margin phases) for west-central Laurentia (Belt segment) and suggested conjugate margins, and proposed paleographic cartoon (adapted from Preiss, 2000; Li et al., 2003; Mulder et al., 2020; Brennan et al., 2020, and references therein). In addition to being a magmatic source of ca. 780–720 Ma zircon, western Tasmania also contains a Neoproterozoic history (Mulder et al., 2020) similar to the Belt region (Lund et al., 2010; Brennan et al., 2020). This correlation is consistent with a multiple-rift scenario. Chuar, Uinta Mountain, middle Pahrump Groups–Buffalo Hump Formation (ChUMP-B) strata may have formed in localized inboard rift basins generated from the breakup of Australia-Antarctica and Laurentia. Younger Windermere Supergroup records the rifting of additional intervening blocks, likely including western Tasmania, into an already open paleo–Pacific Ocean.

5.5. References

Geological Society of America reference style

Bell, R.T., and Jefferson, C.W., 1987, An hypothesis for an Australian-Canadian connection in the late Proterozoic and the birth of the Pacific Ocean, in Proceedings of the Pacific Rim Congress 87: Parkville, Victoria, Australia, Australian Institute of Mining and Metallurgy, p. 39–50.

Box, S.E., Pritchard, C., Stephens, T.S., and O’Sullivan, P.B., 2020, Between the supercontinents—Mesoproterozoic Deer Trail Group, an intermediate age unit between the Mesoproterozoic Belt-Purcell Supergroup and the Neoproterozoic Windermere Supergroup in northeastern Washington, U.S.A.: Canadian Journal of Earth Sciences, v. 17, p. 1–17, https://doi.org/10.1139/ cjes-2019-0188.

Brennan, D.T., Pearson, D.M., Link, P.K., and Chamberlain, K.R., 2020, Neoproterozoic Windermere Supergroup near Bayhorse, Idaho: Late-stage Rodinian rifting was deflected west around the Belt basin: Tectonics, v. 39, e2020TC006145, https:// doi.org/10.1029/2020TC006145.

Brookfield, M.E., 1993, Neoproterozoic Laurentia-Australia fit: Geology, v. 21, p. 683–686, https:// doi.org/10.1130/0091-7613(1993)021<0683:NL AF>2.3.CO;2.

Chew, D., Drost, K., and Petrus, J.A., 2019, Ultra- fast, >50 Hz LA-ICP-MS spot analysis applied to U-Pb dating of zircon and other U-bearing minerals: Geostandards and Geoanalytical Research, v. 43, p. 39–60, https://doi.org/10.1111/ggr.12257.

Dalziel, I.W.D., 1991, Pacific margins of Laurentia and East Antarctica–Australia as a conjugate rift pair: Evidence and implications for an Eocambrian supercontinent: Geology, v. 19, p. 598–601, https:// doi.org/10.1130/0091-7613(1991)019<0598:PM OLAE>2.3.CO;2.

Dehler, C.M., Fanning, C.M., Link, P.K., Kingsbury, E.M., and Rybczynski, D., 2010, Maximum depositional age and provenance of the Uinta Mountain Group and Big Cottonwood Formation, northern Utah: Paleogeography of rifting western Laurentia: Geological Society of America Bulle- tin, v. 122, p. 1686–1699, https://doi .org/10.1130/ B30094.1.

Dehler, C., Gehrels, G., Porter, S., Heizler, M., Karl- strom, K., Cox, G., Crossey, L., and Timmons, M., 2017, Synthesis of the 780–740 Ma Chuar, Uinta Mountain, and Pahrump (ChUMP) groups, western USA: Implications for Laurentia-wide cratonic marine basins: Geological Society of America Bulletin, v. 129, p. 607–624, https:// doi.org/10.1130/B31532.1.

Eyster, A., Weiss, B.P., Karlstrom, K., and Macdonald, F.A., 2020, Paleomagnetism of the Chuar Group and evaluation of the late Tonian Laurentian apparent polar wander path with implications for the makeup and breakup of Rodinia: Geological Society of America Bulletin, v. 132, p. 710–738, https://doi.org/10.1130/B32012.1.

Flowers, R.M., Macdonald, F.A., Siddoway, C.S., and Havranek, R., 2020, Diachronous develop- ment of Great Unconformities before Neoproterozoic snowball Earth: Proceedings of the National Academy of Sciences of the United States of America, v. 117, p. 10172–10180, https://doi .org/10.1073/pnas.201913131117.

Harlan, S.S., Heaman, L., LeCheminant, A.N., and Premo, W.R., 2003, Gunbarrel mafic magmatic event: A key 780 Ma time marker for Rodinia plate reconstructions: Geology, v. 31, p. 1053– 1056, https://doi.org/10.1130/G19944.1.

Howard, A.L., Farmer, G.L., Amato, J.M., and Fedo, C.M., 2015, Zircon U-Pb ages and Hf isoto- pic compositions indicate multiple sources for Grenvillian detrital zircon deposited in western Laurentia: Earth and Planetary Science Letters, v. 432, p. 300–310, https://doi.org/10.1016/ j.epsl.2015.10.018.

Karlstrom, K.E., et al., 2000, Chuar Group of the Grand Canyon: Record of breakup of Rodinia, associated change in the global carbon cycle, and ecosystem expansion by

740 Ma: Geology, v. 28, p. 619–622, https://doi.org/10.1130/0091-7613(2000)28<619:CGOTGC>2.0.CO;2.

Karlstrom, K., Hagadorn, J., Gehrels, G., Matthews, W., Schmitz, M., Madronich, L., Mulder, J., Pecha, M., Geisler, D., and Crossey, L., 2018, Cambrian Sauk transgression in the Grand Canyon region redefined by detrital zircons: Nature Geoscience, v. 11, p. 438–443, https:// doi .org/10.1038/s41561-018-0131-7.

Kirscher, U., et al., 2020, Paleomagnetic constraints on the duration of the Australia-Laurentia connection in the core of the Nuna supercontinent: Geology, v. 49, p. 174–179, https://doi.org/10.1130/ G47823.1.

Li, Z.X., Li, X.H., Kinny, P.D., Wang, J., Zhang, S., and Zhou, H., 2003, Geochronology of Neoproterozoic syn-rift magmatism in the Yangtze craton, South China, and correlations with other continents: Evidence for a mantle superplume that broke up Rodinia: Precambrian Research, v. 122, p. 85–109, https://doi.org/10.1016/S0301- 9268(02)00208-5.

Li, Z.X., et al., 2008, Assembly, configuration, and break-up history of Rodinia: A synthesis: Precambrian Research, v. 160, p. 179–210, https:// doi.org/10.1016/j.precamres.2007.04.021.

Lindsey, K.A., and Gaylord, D.R., 1992, Fluvial, coastal, nearshore, and shelf deposition in the Upper Proterozoic (?) to Lower Cambrian Addy Quartzite, northeastern Washington: Sedimentary Geology, v. 77, p. 15–35, https://doi. org/10.1016/0037-0738(92)90101-V.

Lund, K., and Cheney, E.R., 2016, Correlation of unconformity-bounded sequences of the Neo- proterozoic Windermere Supergroup in Idaho, Washington, and southern British Columbia, in Cheney, E.R., ed., The Geology of Washington and Beyond: From Laurentia to Cascadia: Seattle, Washington, University of Washington Press, p. 28–42.

MacLennan, S.A., Eddy, M.P., Merschat, A.J., Meh- ra, A.K., Crockford, P.W., Maloof, A.C., South- worth, C.S., and Schoene, B., 2020, Geologic evidence for an icehouse Earth before the Sturtian global glaciation: Science Advances, v. 6, p. 1–6, https://doi.org/10.1126/sciadv.aay6647.

Mahon, R.C., Dehler, C.M., Link, P.K., Karlstrom, K.E., and Gehrels, G.E., 2014, Geochronologic and stratigraphic constraints on the Mesopro- terozoic and Neoproterozoic Pahrump Group, Death Valley, California: A record of the assem- bly, stability, and breakup of Rodinia: Geological Society of America Bulletin, v. 126, p. 652–664, https://doi.org/10.1130/B30956.1.

Miller, F.K., and Whipple, J.W., 1989, The Deer Trail Group—Is it part of the Belt Supergroup, in Joseph, N.L., ed., Geologic Guidebook for Washington and Adjacent Areas: Washington Division of Geology and Earth Resources Information Circular 86, p. 1–21.

Mulder, J.A., Everard, J.L., Cumming, G., Meffre, S., Bottrill, R.S., Merdith, A.S., Halpin, J.A., Mc- Neill, A.W., and Cawood, P.A., 2020, Neoproterozoic opening of the Pacific Ocean recorded by multi-stage rifting in Tasmania, Australia: Earth-Science Reviews, v. 201, 103041, https:// doi.org/10.1016/j.earscirev.2019.103041.

Murakami, T., Chakoumakos, B.C., Ewing, R.C., Lumpkin, G.R., and Weber, W.J., 1991, Alpha- decay event damage in zircon: The American Mineralogist, v. 76, p. 1510–1532.

Preiss, W.V., 2000, The Adelaide geosyncline of South Australia and its significance in Neoproterozoic continental reconstruction: Precambrian Research, v. 100, p. 21–63, https://doi.org/10.1016/ S0301-9268(99)00068-6. Ross, G.M., and Villeneuve, M., 2003, Provenance of the Mesoproterozoic (1.45 Ga) Belt basin (western North America): Another piece in the pre-Rodinia paleogeographic puzzle: Geological Society of America Bulletin, v. 115, p. 1191–1217, https://doi.org/10.1130/B25209.1.

Ross, G.M., Parrish, R.R., and Winston, D., 1992, Provenance and U-Pb geochronology of the Mesoproterozoic Belt Supergroup (northwestern United States): Implications for age of deposition and pre-Panthalassa plate reconstructions: Earth and Planetary Science Letters, v. 113, p. 57–76, https://doi.org/10.1016/0012-821X(92)90211-D.

Thomas, W.A., Gehrels, G.E., Greb, S.F., Nadon, G.C., Satkoski, A.M., and Romero, M.C., 2017, Detrital zircons and sediment dispersal in the Appalachian foreland: Geosphere, v. 13, no. 6, p. 2206–2230, https://doi.org/10.1130/GES01525.1.

Timmons, J.M., Karlstrom, K.E., Dehler, C.M., Geissman, J.W., and Heizler, M.T., 2001, Pro- terozoic multistage (ca. 1.1 and 0.8 Ga) extension recorded in the Grand Canyon Supergroup and establishment of northwest- and north-trending tectonic grains in the southwestern United States: Geological Society of America Bulletin, v. 113, p. 163–180.

Turner, N.J., Black, L.P., and Kamperman, M., 1998, Dating of Neoproterozoic and Cambrian orogenies in Tasmania: Australian Journal of Earth Sciences, v. 45, p. 789–806, https://doi .org/10.1080/08120099808728433.

Whitmeyer, S.J., and Karlstrom, K.E., 2007, Tectonic model for the Proterozoic growth of North America: Geosphere, v. 3, p. 220–259, https:// doi.org/10.1130/GES00055.1.

Wingate, M.T.D., and Giddings, J.W., 2000, Age and palaeomagnetism of the Mundine Well dyke swarm, Western Australia: Implications for an Australia-Laurentia connection at 755 Ma: Precambrian Research, v. 100, p. 335–357, https:// doi.org/10.1016/S0301-9268(99)00080-7.

Yao, W., Li, Z.X., Li, W.X., and Li, X.H., 2017, Pro- terozoic tectonics of Hainan Island in supercontinent cycles: New insights from geochronological and isotopic results: Precambrian Research, v. 290, p. 86–100, https://doi.org/10.1016/ j.precamres.2017.01.001.

Yonkee, W.A., Dehler, C.D., Link, P.K., Balgord, E.A., Keeley, J.A., Hayes, D.S., Wells, M.L., Fanning, C.M., and Johnston, S.M., 2014, Tectono-stratigraphic framework of Neoproterozoic to Cambrian strata, west-central U.S.: Protracted rifting, glaciation, and evolution of the North American Cordilleran margin: Earth Science Reviews, v. 136, p. 59–95, https://doi .org/10.1016/ j.earscirev.2014.05.004

Chapter 6: A tectonic model for the Transcontinental Arch: Progressive migration of a Laurentian drainage divide during the Neoproterozoic–Cambrian Sauk Transgression

Abstract

A widespread provenance shift recorded by passive margin strata of western Laurentia, from predominant Stenian (1.2–1.0 Ga) detrital zircon age components to their absence, occurred during the Neoproterozoic–Cambrian Sauk transgression and is commonly used as a ca. 540 Ma chronostratigraphic marker throughout the west/south-western United States. However, in Neoproterozoic–Cambrian strata of this region, we identify a probable shift from distal to more proximal Stenian-age zircon sources before a diachronous loss of Stenian detrital zircon age components. We suggest these provenance patterns reflect progressive subsidence of the passive margins surrounding Laurentia and concomitant relative uplift of the Transcontinental Arch, a broad and segmented northeast–southwest trending topographic high across the Laurentian midcontinent possibly due to lithospheric flexure. The Transcontinental Arch segments align with transverse rift structures of the Neoproterozoic–Cambrian Iapetan margin and the Mesoproterozoic Midcontinent Rift, perhaps reflecting rejuvenation of midcontinent lithospheric weaknesses during the Sauk transgression and final Rodinia breakup.

6.1. Introduction

Many detrital zircon datasets from extensional (rift, post-rift passive margin and intracratonic) basins show provenance shifts which are commonly interpreted to represent the effects of far-field tectonics that result in reorganization of continental drainage divides (Cawood et al., 2012; Gehrels & Pecha, 2014). Several detrital zircon provenance studies of western Laurentian Neoproterozoic and early Palaeozoic strata deposited during the Sauk transgressions (Sloss, 1963) propose that uplift of a northeast to southwest (all directions in modern coordinates) continental drainage divide across the midcontinent of Laurentia (the Transcontinental Arch; TCA; Fig. 6.1) resulted in the transition from Stenian (ca. 1.2–1.0 Ga) source terranes east of the TCA (Llano Uplift/Wichita province and/or Grenville) for Neoproterozoic strata, to more proximal, predominantly late Palaeoproterozoic source terranes west of the TCA for middle Cambrian through pre-Carboniferous strata (e.g. Amato & Mack, 2012; Gehrels & Pecha, 2014; Linde et al., 2014; Matthews et al., 2018; Mueller et al., 2007; Rainbird et al., 2017; Yonkee et al., 2014). The proposed timing of the initial uplift of the TCA varies from early Neoproterozoic (Craddock et al., 2017), late Neoproterozoic (Gehrels & Pecha, 2014), Cambrian (Linde et al., 2014; Saylor & Sundell, 2021), to Devonian (Myrow et al., 2003). Others (e.g. Howard et al., 2015; Karlstrom et al., 2018) have advocated that a combination of localized factors, predominately (Neoproterozoic–Cambrian) rift-related exhumation and reworking of underlying strata during the Sauk Transgression, require further consideration as potential mechanisms for this provenance shift. Here, we evaluate these competing models with a two-dimensional (U-Pb/Lu-Hf) quantitative comparison (Saylor & Sundell, 2021; Sundell & Saylor, 2021) of ca. 1.3–1.0 Ga detrital zircon components in Neoproterozoic to Cambrian strata of south-western Laurentia and Stenian-age sources to the east (e.g. Llano Uplift/Wichita province, Pikes Peak Batholith and/or Grenville province). We also revisit the timing of the provenance shift in question considering revision of the depositional ages of Cambrian strata in south-western Laurentia (Karlstrom et al., 2018, 2020; Spencer et al., 2014). Collectively, the results suggest a probable progressive shift in Stenian-age sources during the Cryogenian–Ediacaran, prior to a diachronous transition to predominantly late Palaeoproterozoic detrital zircon age components during the Cambrian. We suggest this provenance pattern reflects progressive northeast to southwest uplift (or relative uplift) of a segmented TCA, which correlates with the geometry and timing of the Neoproterozoic–Cambrian rift-drift transition along the Iapetan margin.

6.2. Laurentian Rifting and the Sauk Transgression

Sloss (1963) recognized that an extensive latest Precambrian to early Ordovician, unconformity-bounded stratigraphic "Sauk" transgressive mega-sequence occurred across most of Laurentia. The Neoproterozoic to early Ordovician Sauk mega-sequence has been further subdivided into three Sauk sub-sequences (or super-sequences; Keller et al., 2012; Palmer, 1981). These three sub-sequences (Sauk I, Sauk II and Sauk III) progressively onlap the cratonic platform and are separated by two regional unconformities, likely relating to relatively short-lived eustatic events at ca. 515 and 495 Ma respectively (Fig. 6.2; Burgess, 2019; Karlstrom et al., 2020; Keller et al., 2012; Palmer, 1981). However, a young and rapid ca. 505 to 501 Ma Sauk II transgression proposed for south-western Laurentia (Karlstrom et al., 2018) implies diachroneity both in the onset times of Sauk sequence transgressions and in drift-phase subsidence of the Laurentian rift margin, which may indicate important local tectonic influences in addition to global eustasy.

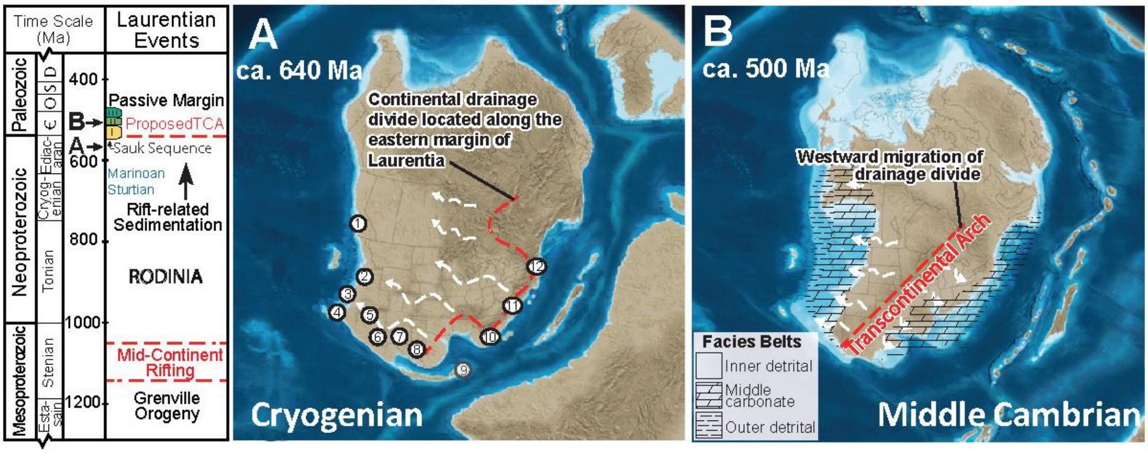

Fig. 6.1: Timeline for the Proterozoic and Early Palaeozoic major tectonic events for Laurentia with suggested palaeogeographic reconstructions at (a) ca. 640 Ma, showing the continental divide following the Grenville Belt along eastern Laurentia inferred from detrital zircon populations in Cryogenian–Ediacaran strata along the western margin and (b) at ca. 500 Ma, after relative uplift of the Transcontinental Arch and resulting westward migration of the continental divide resulting in a switch to more proximal source terranes for western Laurentia strata. Cambrian regional facies belts of the Sauk sequence are from Myrow et al., (2012). Numbered locations refer to locality of stratigraphic time–space diagrams in Fig. 6.2. The position of Sonora is restored along the Mojave mega-shear as per Stewart (2005) and Precordillera restored within the Ouachita embayment of per Martin, Collins, et al., (2020). Palaeogeographic reconstructions are modified from Gehrels and Pecha (2014) and Ron Blakey (http://jan.ucc.nau.edu/rcb7/nam.html), which are artistically rendered.

It is now recognized that the Sauk transgressive mega-sequence is likely related to the final breakup of Rodinia (Bond et al., 1984; Dalziel, 2014; Valentine & Moores, 1970). Palaeogeographic models of supercontinent Rodinia (e.g. Li et al., 2008) indicate a diachronous breakup, beginning along the western Laurentian margin with the emplacement of the ca. 780 Ma Gunbarrel magmatic event (Harlan et al., 2003). Related localized sedimentation occurred shortly after (Brennan et al., 2021; Dehler et al., 2017; Lund et al., 2003; Karlstrom et al., 2000) and along most of the western margin by ca. 720 Ma (e.g. Yonkee et al., 2014), coeval with the emplacement of the Franklin large igneous province (Macdonald et al., 2010). The western margin of Laurentia also records a younger (Ediacaran–Cambrian) phase of extension, breakup and syn-to post-breakup magmatism (Beranek, 2017; Bond et al., 1985; Prave, 1999; Ross, 1991).

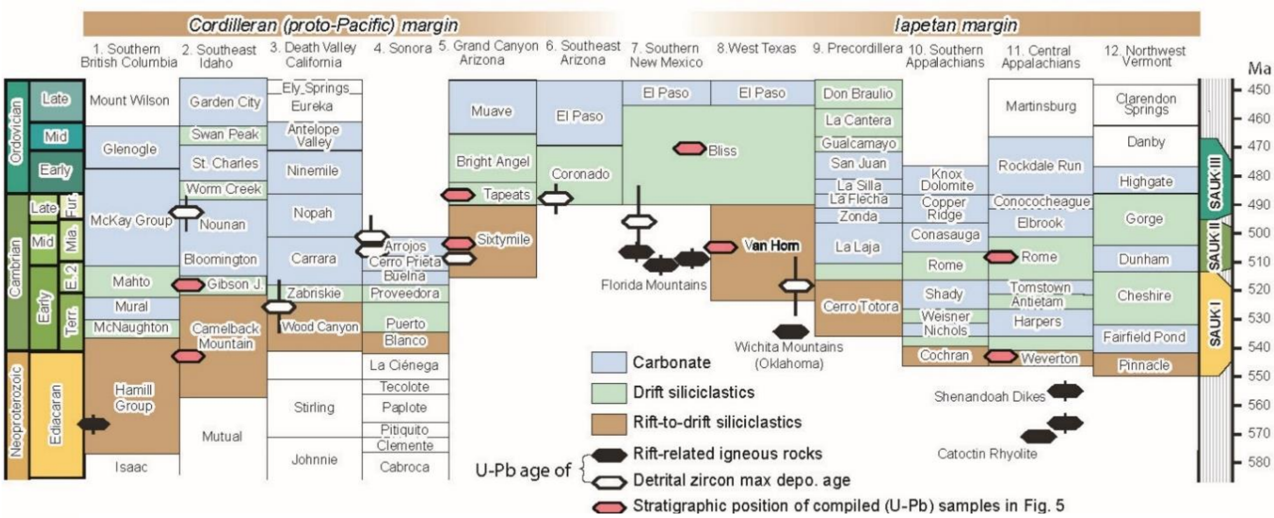

Fig. 6.2: Generalized stratigraphic time–space diagram representative of the Neoproterozoic to Ordovician sedimentary units along the Laurentian margin adapted from Spencer et al., (2014). The ages of the reported maximum depositional ages (in Ma) are plotted as additional depositional constraints. Uncertainties are 2σ. See Fig. 6.1 for generalized stratigraphic section locations. Red zircon symbols indicate the stratigraphic positions of compiled samples in Fig. 6.5. Various rock types, general depositional settings and indicated rift-drift intervals are per the following references: Southern British Columbia and Southeast Idaho (Colpron et al., 2002; Link et al., 1987; Yonkee et al., 2014); rift-related igneous rock age (Colpron et al., 2002); Worm Creek Quartzite detrital zircons (Link et al., 2017); Death Valley stratigraphy (Corsetti & Kaufman, 2003; Heaman & Grotzinger, 1992; Hogan et al., 2011; Prave, 1999); Death Valley detrital zircons (Stewart et al., 2001); Sonora stratigraphy (Farmer et al., 2005; Sour-Tovar et al., 2007; Stewart, 2005; Stewart et al., 2002); Grand Canyon stratigraphy (Karlstrom et al., 2000, 2018, and references therein); southeast Arizona stratigraphy (Hayes, 1972); south-central and southeast Arizona detrital zircons (Stewart et al., 2001); southern New Mexico stratigraphy (Hayes, 1972); southern New Mexico detrital/igneous zircons (Amato & Mack, 2012); west Texas stratigraphy (Hayes, 1972; LeMone, 1969); west Texas detrital zircons (Spencer et al., 2014); Precordillera stratigraphy (Finney et al., 2005); southern Appalachians stratigraphy (Chakraborty et al., 2012; Tull et al., 2010); central Appalachians stratigraphy (Astini, 1995; Burton & Southworth, 2010; Southworth et al., 2009; Tollo 2010); central Appalachians rift-related zircons (Aleinikoff et al., 1995, recalculated by Burton & Southworth, 2010; Southworth et al., 2009) and northwest Vermont stratigraphy (Brink et al., 2019; Landing et al., 2009; Shaw, 1958). Sauk sequence after Palmer (1981). Geologic time scale is after Peng et al., (2020) with Early, Middle and Late Cambrian divisions from the United State Geologic Survey time-scale (U.S. Geological Survey Geologic Names Committee, 2010).

Neoproterozoic to lower Palaeozoic strata preserved along the Laurentian margins were likely deposited within the proximal margin domain (e.g. Brennan et al., 2020; Yonkee et al., 2014). While precise timing is often difficult to determine, in proximal margin domains, the lithospheric breakup surface (i.e. rift-drift transition) is typically recorded as an unconformity (Soares et al., 2012). Evidence for a rift-drift transition at ca. 540 Ma in south-eastern Idaho (Linde et al., 2014; Yonkee et al., 2014) is recognized as an unconformity within the upper Brigham Group, where the feldspathic Ediacaran–Cambrian Camelback Mountain Quartzite disconformably overlies the quartzose Ediacaran Mutual Formation, delineating the base of the Sauk I super-sequence (Link et al., 1987). Further south, an interpreted rift-drift transition in the Grand Canyon region occurred at ca. 505 Ma, recorded as an unconformably between the coarse Cambrian Tapeats Sandstone and the underlying cherty siltstone and sandstone of the Ediacaran–Cambrian Sixtymile Formation. This unconformity is interpreted to coincide with the Sauk I/Sauk II boundary (Amato & Mack, 2012; Karlstrom et al., 2018; Spencer et al., 2014).

Provenance studies document an abundance of distal Stenian detrital zircons in Neoproterozoic strata and a provenance shift to more proximal, predominantly older sources in Cambrian strata (Linde et al., 2014; Matthews et al., 2018; Yonkee et al., 2014). The loss of Stenian detrital zircon populations in Cambrian strata has been interpreted as ca. 540–530 Ma chronostratigraphic indicator in Nevada, Utah, Idaho and Montana (Brennan et al., 2020; Gehrels & Pecha, 2014; Linde et al., 2014; Matthews et al., 2018; Yonkee et al., 2014), generally coinciding with initiation of the Sauk I transgression. However, the absence of biostratigraphic markers, and relatively limited radiometric age control due to the scarcity of syn-depositional volcanism, implies that the depositional ages of these clastic rocks may be poorly constrained and so the inferred synchroneity of the provenance changes remains an open question.

6.2.1 Evaluating the Stenian sources

Until recently, quantitative assessment of detrital zircon distributions and potential source similarities/dissimilarities was limited to one-dimension, often (U-Pb) age-only, statistical comparison methods (e.g. Nordsvan et al., 2020; Saylor & Sundell, 2016; Vermeesch, 2012, 2013, 2018). However, it is difficult to differentiate between separate source regions with similar magmatic histories using these methods. Consequently, we compiled bivariate (U-Pb and Lu-Hf) datasets (Gehrels & Pecha, 2014; Howard et al., 2015; Martin, Spencer, et al., 2020; Spencer et al., 2012; Wooden et al., 2013 and references therein) of ca. 1,300 to 900 Ma detrital zircon components in late Tonian (<760 Ma) to Cambrian strata of western/south-western Laurentia. These strata are compared to potential source regions in eastern Laurentia (Grenville province), south-eastern Laurentian (Llano and Wichita province) and central Laurentia (Pikes Peak Batholith; Fig. 6.3) utilizing recent two-dimensional quantitative comparison methods (DZstats2D MATLAB code; Sundell & Saylor, 2021). Cross-correlation coefficient results (Fig. 6.4) indicate that north-eastern Stenian-age sources (Grenville) show the strongest statistical correlation with the detrital zircon components in the oldest Tonian–Cryogenian strata, and generally show decreasing similarity with younger Ediacaran and Cambrian strata. Conversely, the similarity of south-western Laurentian strata with south-eastern Stenian-age sources (Llano and Wichita province) increases up-section and is strongest in Cambrian strata. Both the Ediacaran and Cambrian strata show a second strongest similarity with their immediately underlying (older) Tonian–Cryogenian or Ediacaran strata respectively. Additional comparison metrics (Similarity, Likeness, K-S Test D and Kuiper Test V) all show the same trend as the Cross-correlation metric (see supplementary information).

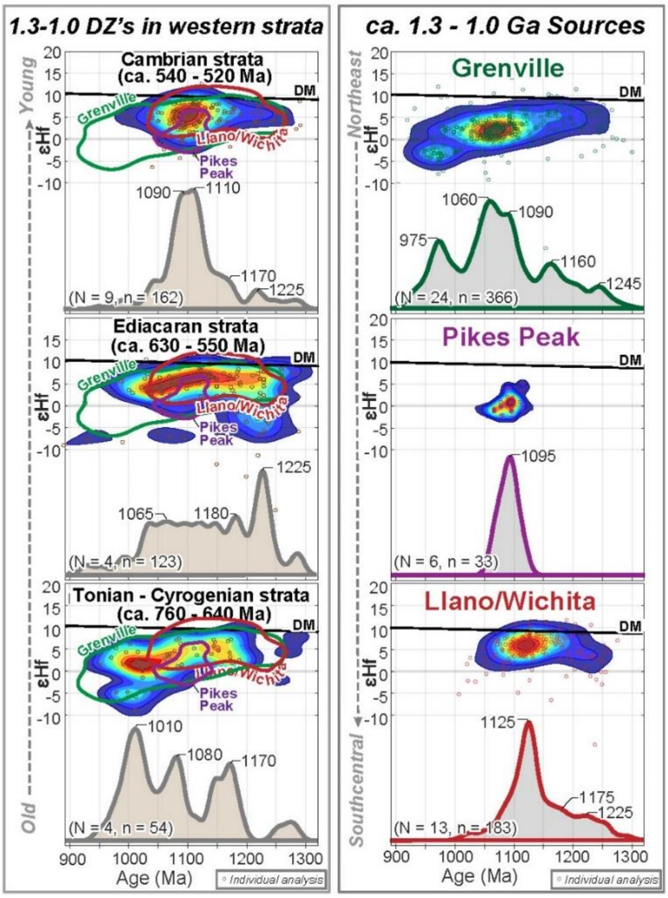

Fig. 6.3: Approximately 1.3–0.9 Ga detrital zircon U-Pb/ Lu-Hf values from (ca. 760–640 Ma) Tonian–Cyrogenian, (ca. 630–550 Ma), Ediacaran (ca. 540–530 Ma) and Cambrian strata in south-western Laurentia and potential ca. 1.3–0.9 Ga eastern source provinces including the Grenville (eastern Laurentia), Pikes Peak (central Laurentia) and Llano/Wichita province (south-eastern Laurentia; see Fig. 6.6). Age (U-Pb) data are shown in kernel density estimation plots with 10 m.y. bandwidths generated with DensityPlotter (Vermeesch, 2012). Lu-Hf data are shown in with individual analysis scatter plots, and bivariate kernel density estimation plots with 25 million-year bin-and 1.5 εHf band-widths generated with the MATLAB code of Spencer et al., (2020). Abbreviations: DM, depleted mantle; N, number of samples; n, number of analyses.

6.2.2 A diachronous loss of Stenian zircon grains?

In south-eastern Idaho and northern Utah (location 2 in Figs. 6.1, 6.2, 6.5 and 6.6), the provenance shift from Stenian sources to predominantly older sources occurs within the Camelback Mountain Quartzite that spans the Ediacaran–Cambrian boundary (Link et al., 1987; Yonkee et al., 2014). Approximately 2,500 meters stratigraphically above where this provenance shift occurs, feldspathic sandstones deposited within a predominately carbonate sequence mark the Sauk II/Sauk III sequence boundary (Armstrong & Oriel, 1965). These feldspathic sandstones (Worm Creek Quartzite Member of the St. Charles Formation) have a late Cambrian (Furongian) age of ca. 495 Ma (detrital zircon maximum depositional age of ca. 497 Ma and Dunderbergia and Elvinia trilobite zones from 495.2 to 493 Ma; Link et al., 2017).

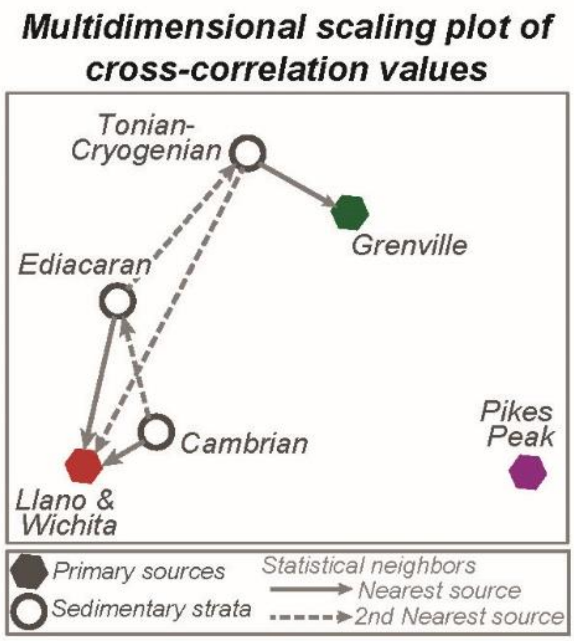

Fig. 6.4: Multi-dimensional scaling (MDS) plot of two-dimensional (U-Pb and Lu-Hf) cross-correlation comparison results for ca. 1.3 to 0.9 Ga zircon components. MDS plots are used to visualize the similarity of datasets, where similar datasets plot closer together in Cartesian space, and less similar datasets plot further apart (see Nordsvan et al., 2020; Saylor & Sundell, 2021; Vermeesch, 2013, for further discussion of MDS plots as applied to zircon datasets). Statistically nearest (or most similar) sources (solid arrow) and second nearest (dashed arrow) geologically feasible sources are indicated. Geologically feasible indicating that it is available as a source at the time of the units' deposition (e.g. Ediacaran strata cannot be sourced from recycling of younger Cambrian strata). Note that Tonian–Cryogenian strata show the greatest similarity to a Grenville source, while Ediacaran and Cambrian strata show a greatest similarity to a Llano and Wichita source, with a second greatest similarity to Tonian–Cryogenian and Ediacaran strata respectively. Similarity, Likeness, Kolmogorov–Smirnov Test D and Kuiper Text V comparison metrics were also calculated and all show the same statistically nearest and second nearest sources indicating reliability of the results. Comparison matrices for all metrics were generated with the DZstats2D MATLAB script of Saylor and Sundell (2021).

In Arizona and west of the TCA (location 5 in Figs. 6.1, 6.2, 6.5 and 6.6) within similar-age strata (Spencer et al., 2014), deposition of the ca. 540–512 Ma Sixtymile Formation spans the Sauk I transgression and contains significant Stenian detrital zircon age components throughout its various stratigraphic intervals (Karlstrom et al., 2018). The provenance shift from dominantly Stenian detrital zircon sources to proximal, dominantly older, sources is not observed in this sequence until the younger (<508 Ma) Tapeats Sandstone, which was deposited during the second major Sauk II transgression (Karlstrom et al., 2018, 2020). The recognition of Cambrian-age detrital zircon in these rocks allowed precise maximum depositional age constraints via tandem dating: laser ablation–inductively coupled plasma–mass spectrometry (LA-ICP-MS) of a large number of grains, followed by chemical abrasion–isotope dilution–thermal ionization mass spectrometry (CA-TIMS) of the youngest grains (Karlstrom et al., 2018, 2020).

East of the TCA in south-eastern New Mexico and western Texas (location 7 in Figs. 6.1, 6.2, 6.5 and 6.6), rocks coeval with the Sixtymile Formation and Tapeats Sandstone that are also interpreted to span the Sauk I/Sauk II boundary contain significant Stenian detrital zircon populations (Amato & Mack, 2012; Spencer et al., 2014). Also east of the TCA, in the central Appalachian region (location 11 in Figs. 6.1, 6.2, 6.5 and 6.6), the Weverton Formation and the overlying Rome Sandstone also contain significant Stenian detrital zircon components. These rocks are interpreted to record the basal Sauk I transgression, suggesting they are mostly similar in age to the upper Brigham Group of southeast Idaho, i.e. Camelback Mountain Quartzite and Gibson Jack Formation (Fig. 6.2). The lower Cambrian Weverton Formation is generally interpreted to record provenance from proximal Grenvillian basement. The overlying Rome Sandstone contains Stenian detrital zircon in addition to older ages typical of the Laurentian craton (including the Granite-Rhyolite, Trans-Hudson, Penokean and Superior provinces), consistent with an Early–Middle Cambrian drainage system that originated in central Laurentia and flowed eastward (Thomas et al., 2004). Similar detrital zircon patterns are found further north in strata of comparable age along the rifted margin of Laurentia in Newfoundland (Cawood & Nemchin, 2001).

Although prolonged rifting started at ca. 750 Ma, continental break-up along the eastern Laurentian margin occurred later than along the western margin (Li et al., 2008; Merdith et al., 2021). Rift-to-drift magmatism indicates continental separation along a north-to-south propagating rift, or distributed rift system, from ca. 615 to 510 Ma, resulting in the opening of the Iapetus Ocean and/or removal of further blocks into an already open Iapetus Ocean (Bond et al., 1984; Cawood et al., 2001; Dalziel, 2014; Mitchell et al., 2011). The rift-drift transition initiated in the central Appalachians at ca. 545 Ma and propagated southward to West Texas by ca. 510 Ma (Fig. 2.2; Martin et al., 2020; Spencer et al., 2014). Iapetan-associated rifting propagated far into the craton, forming intra-continental rift basins (or aulacogens), including the Reelfoot Rift and the Southern Oklahoma aulacogen (Fig. 6.6; Thomas, 2011).

6.2.3 The Transcontinental Arch

Initial isopach maps suggested that the Transcontinental Arch (TCA) was a southwest-trending elevated linear feature during Cambrian time (Sloss, 1988). However, stratigraphic compilations and further isopach mapping (Carlson, 1999; Poole et al., 1992) indicate that the TCA was likely a composite, broad and discontinuous plateau dissected by several smaller northwest-striking, laterally persistent, basement-controlled structures of the Mazatzal-Yavapai province highs that served as local sources of detritus for small intervening basins, resulting in a broad, yet segmented TCA (Carlson, 1999).

6.3. Tectonic Model: Progressive uplift of an arch between two young passive margins

Bond et al., (1989) advocate that flexural bending of the Laurentian margin and long-term eustasy is responsible for the retreat of the siliciclastic shoreline during the Sauk transgression and have calculated broad flexural uplifts of 100–200 m located over 600 km inboard from the Cordilleran continental margin. These results suggest that sediment loading, thermal densification and post-rifting lithospheric rigidity increase along the craton margin could result in broad uplift of the midcontinent region. Widespread denudation occurred during the Neoproterozoic associated with the formation of the “Great Unconformity” (Flowers et al., 2020; Keller et al., 2018). This denudation, along with the lateral continuity in sedimentary thickness and facies of the Sauk sequence (Sloss, 1963), suggests that the sub-Sauk depositional surface across Laurentia exhibited rather low relief. For example, the Cambrian basal transgressive unit in Wyoming and Montana (the Flathead Quartzite) shows a remarkably uniform average thickness of approximately 35 meters over a region in excess of 90,000 square kilometres (Deiss, 1935). Thus, we propose that a regionally extensive uplift (or relative uplift) of any significant magnitude would have had a notable influence on sedimentary transport systems.

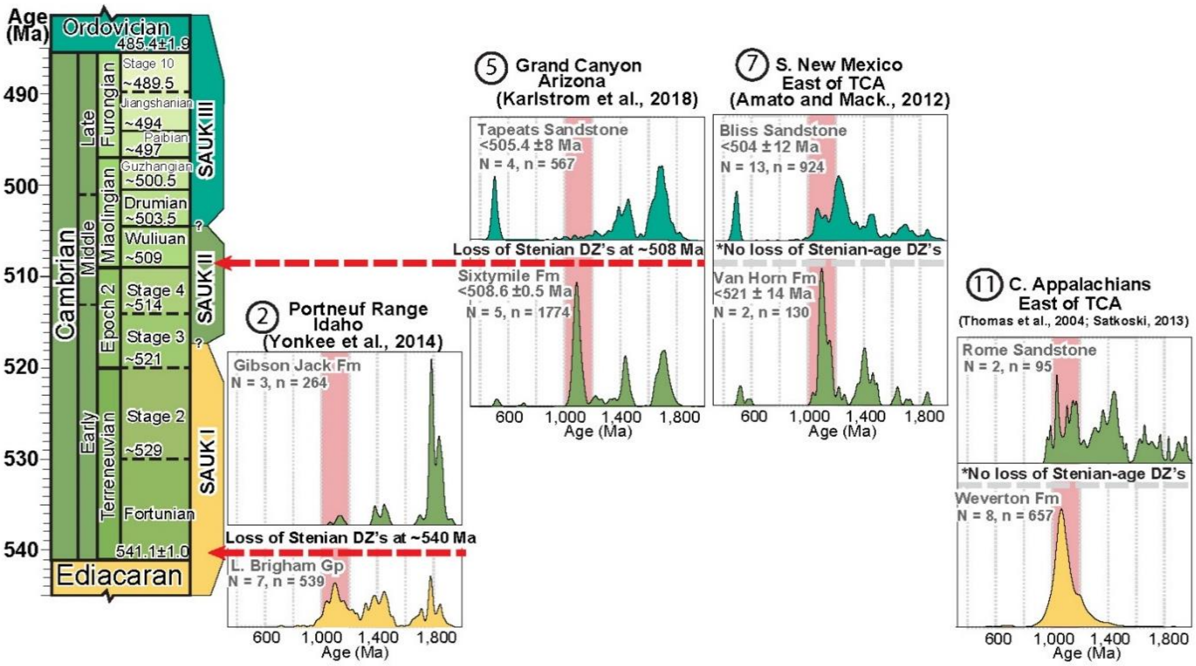

Fig. 6.5: Proposed timeline for the widespread provenance shift from dominant Stenian (ca. 1.2–1.0 Ga) detrital grains to older dominantly Palaeoproterozoic detrital grains. In Idaho, northern Utah and Nevada (location 2), this shift has been previously stratigraphically recognized to take place during the Sauk I transgression at ~540–530 Ma (Linde et al., 2014; Yonkee et al., 2014). To the south in the Grand Canyon region (location 5), this shift is precisely placed (by 508.6 ± 0.8 TIMS max depositional age on youngest detrital zircon in Sixtymile Formation) to the Sauk II transgression at ~508 Ma (Karlstrom et al., 2018). Red dashed lines indicate the approximate timing of the provenance shift. East of the Transcontinental Arch at location 7 (Amato & Mack, 2012; Spencer et al., 2014), in a stratigraphic section similar in age to the Grand Canyon section, no loss of Grenville detritus is observed. Also east of the Transcontinental Arch at location 11 (Thomas et al., 2004; Satkoski, 2013), in a stratigraphic section generally similar in age to the Idaho section, no loss of Stenian detrital zircons and possibly a shift to Laurentian midcontinent sources is observed. Data are shown in normalized kernel density estimation plots with 10 m.y. bandwidths. Full sample list can be found in supplementary material A. DZ, detrital zircon; *N*, number of samples; *n*, number of analyses.

At first order, comparison of bivariate (U-Pb and Lu-Hf) datasets suggests that Neoproterozoic–Cambrian strata in south-western Laurentia record a decrease in the contribution of Stenian zircon from north-eastern sources (Grenville) with time and a corresponding increase in the contribution of south-eastern Stenian sources (Llano and Wichita provinces), with recycling from proximal underlying strata being a secondary contributor. Furthermore, the stratigraphic interval that contains the switch from predominantly Stenian zircon components to older Palaeoproterozoic components is variable. In south-eastern Idaho/northern Utah, the shift occurred during the Sauk I transgression at ca. 540 Ma, whereas in south-eastern New Mexico/western Texas Stenian zircon components are present throughout Sauk I strata, and the shift does not occur until ca. 510 Ma within Sauk II transgressive strata. These trends appear to be consistent with progressive (northeast to southwest) west-stepping migration of a significant continental drainage divide resulting from Ediacaran to Cambrian uplift of the TCA. This drainage divide migration probably cut off westward transport of distal Grenville sourced zircon to western/south-western Laurentia at ca. 540 Ma, while northern/north-western transport of more proximal Llano and Wichita sourced zircon appears to have persisted until ca. 510 Ma. This provenance pattern likely reflects progressive (northeast to southwest) formation of the TCA during the Ediacaran–Cambrian resulting from the subsidence of passive margins (and perhaps intra-continental rift basins such as the Reelfoot Rift) surrounding Laurentia, and the resulting lithospheric flexure during the breakup of Rodinia.

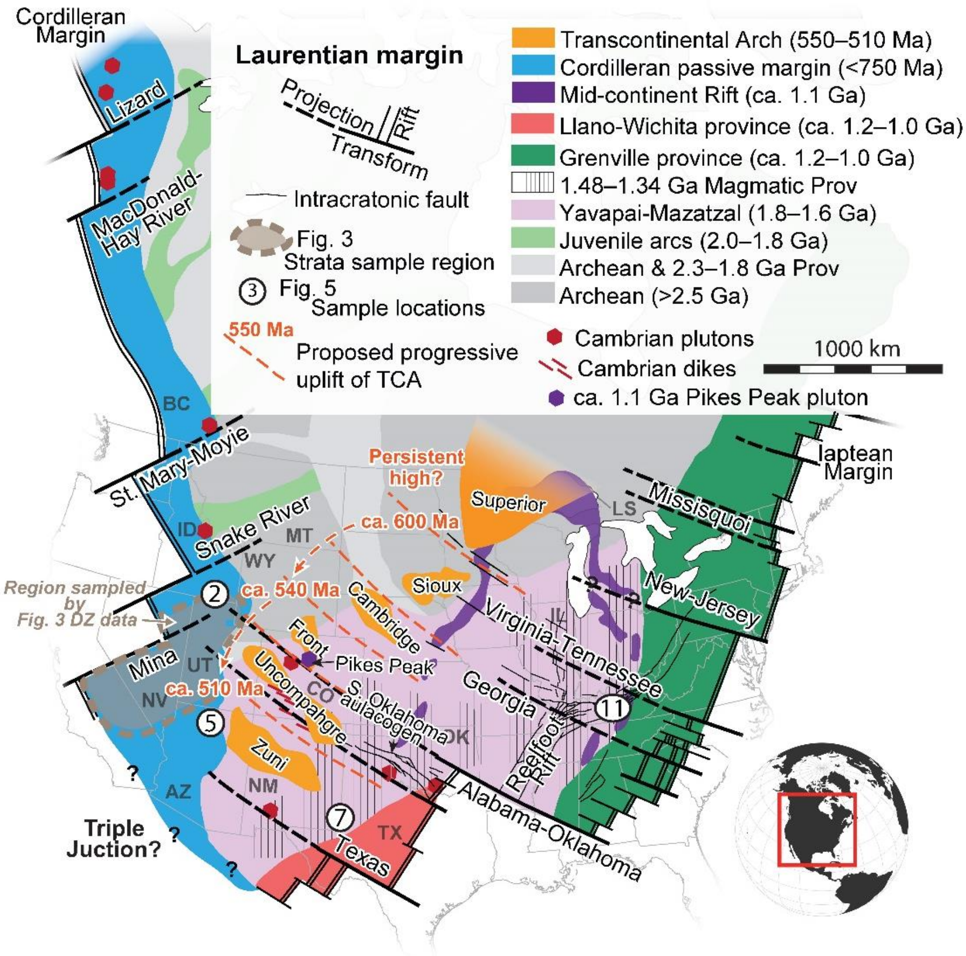

(Previous page) **Fig. 6.6:** Map of the tectonic structures suggested to be interrelated and have influenced the uplift of the Transcontinental Arch (TCA). Laurentian basement provinces and structures adapted from Whitmeyer and Karlstrom (2007), Gehrels and Pecha (2014), Marshak et al., (2017) and Stein et al., (2018). The ca. 1.1 Ga Midcontinent Rift (Stein et al., 2018), the Iapetus rift margin (Thomas, 2014), the western Laurentian margin (Lund, 2008) and uplifted regions of the TCA (Carlson, 1999) all show geometric affinities with each other. Cambrian plutons/dikes/localized detrital zircon age components from Lund (2008); Amato and Mack (2012); Hanson et al., (2013); Link et al., (2017) and references within. Iapetan transform faults bisect segments of the Midcontinent rift and the TCA. Although precise timing of the rift-drift transition along the Iapetan margin is difficult to determine, generally it is thought to have progressively opened from north to south at ca. 615 to 500 Ma (Dalziel, 2014); with rift-drift transitions in the central Appalachians at ca. 545 Ma, and west Texas at ca. 510 Ma (Spencer et al., 2014), consistent with our proposed timing of northwest to southeast progressive uplift of the Transcontinental Arch. The proposed geometry of the Laurentian margin is consistent with an oceanic triple-junction located off south-western Laurentia. AZ, Arizona; BC, British Columbia; IL, Illinois; OK, Oklahoma; NV, Nevada; NM, New Mexico; MT, Montana; ID, Idaho; UT, Utah; WY, Wyoming; TX, Texas; LS, Lake Superior.

The major transverse faults and fault zones of the Iapetan margin (New Jersey, Virginia-Tennessee, Georgia, Alabama-Oklahoma and Texas; Thomas, 2014) align with segments of the Midcontinent Rift and the proposed north-eastward-trending tectonic units of the TCA (Fig. 6.6). Localized Cambrian deformation, dike swarms and associated magmatism are identified more than 800–1400 km inwards from the continental margin, adjacent to these major transverse fault zones in Colorado, northern New Mexico and perhaps central Illinois (Fig. 6.6; Brueseke et al., 2016; Freiburg et al., 2020; Hanson et al., 2013; Thomas, 2014). These observations lead us to link these Laurentian structures and suggest that the segmented geometry of the Mesoproterozoic Midcontinent Rift acted as a genetic control of the segmentation of the Neoproterozoic Iapetan rifted margin and influenced the geometry of alternating broad highs and intervening lows of the TCA. These transverse fault zone/transverse fault zone-parallel structures initially formed during Midcontinent rifting ca. 1.1 Ga, and we suggest were rejuvenated during Neoproterozoic–Cambrian opening of the Iapetus Ocean and (relative) uplift of the Transcontinental Arch, prior to probable reactivation during Ordovician closure of the Iapetus and subsequent late Palaeozoic closure of the Rheic Ocean (e.g. Craddock et al., 2017). Our analysis suggests that intra-continental transverse rift-structures are long-lived regions of lithospheric weakness.

6.4. References

Terra Nova reference style

Aleinikoff, J. N., Zartman, R. E., Walter, M., Rankin, D. W., Lyttle, P. T., & Burton, W. C. (1995). U-Pb ages of metarhyolites of the Catoctin and Mount Rogers formations, central and southern Appalachians: Evidence for two pulses of Iapetan rifting. *American Journal of Science.*, *295*, 428–454. https://doi.org/10.2475/ajs.295.4.428

Amato, J. M., & Mack, G. H. (2012). Detrital zircon geochronology from the Cambrian-Ordovician Bliss Sandstone, New Mexico: Evidence for contrasting Grenville-age and Cambrian sources on opposite sides of the Transcontinental Arch. *Geological Society of America Bulletin*, *124*, 1826–1840. https://doi.org/10.1130/B30657.1

Armstrong, F. C., & Oriel, S. S. (1965). Tectonic development of the Idaho-Wyoming thrust belt. *American Association of Petroleum Geologists Bulletin*, *49*, 1847–1866.

Astini, R. (1995). The early Paleozoic evolution of the Argentine Precordillera as a Laurentian rifted, drifted, and collided terrane: A geodynamic model. *Geological Society of America Bulletin*, *107*, 253–273.https://doi.org/10.1130/0016-7606(1995)107<0253:TEPEO T>2.3.CO;2

Beranek, L. P. (2017). A magma-poor rift model for the Cordilleran margin of western North America. *Geology*, *45*, 1115–1118. https://doi.org/10.1130/G39265.1

Bond, G. C., Christie-Blick, N., Kominz, M. A., & Devlin, W. J. (1985). An early Cambrian rift to post-rift transition in the Cordillera of western North America. *Nature*, *315*, 742–746. https://doi.org/10.1038/315742a0

Bond, G. C., Kominz, M. A., Steckler, M. S., & Grotzinger, J. P. (1989). Role of thermal subsidence, flexure, and eustasy in the evolution of early Paleozoic passive-margin carbonate platforms. In: *Controls on carbonate platform and basin development*. *SEPM Special Publication*, **44**, 39–61. https://doi.org/10.2110/pec.89.44.0039

Bond, G. C., Nickeson, P. A., & Kominz, M. A. (1984). Breakup of a supercontinent between 625 Ma and 555 Ma: New evidence and implications for continental histories. *Earth and Planetary Science Letters*, *70*, 325–345. https://doi.org/10.1016/0012-821X(84)90017-7

Brennan, D. T., Li, Z., Rankenburg, K., Evans, N., Link, P. K., Nordsvan, A. R., Kirkland, C. L., Mahoney, J. B., Johnson, T., & McDonald, B. J. (2021). Recalibrating Rodinian Rifting in the Northwestern United States. *Geology*. https://doi.org/10.1130/G48435.1/5230844/g48435.pdf

Brennan, D. T., Pearson, D. M., Link, P. K., & Chamberlain, K. R. (2020). Neoproterozoic Windermere Supergroup near Bayhorse, Idaho: Late-stage Rodinian rifting was deflected west around the Belt basin. *Tectonics*, *39*, e2020TC006145. https://doi.org/10.1029/2020T C006145

Brink, R., Mehrtens, C., & Maguire, H. (2019). Sedimentology and petrography of a lower Cambrian transgressive sequence: Altona formation (Potsdam group) in Northeastern New York. *Bulletin of Geosciences*, *94*, 369–388. https://doi.org/10.3140/bull.geosci.1728

Brueseke, M. E., Hobbs, J. M., Bulen, C. L., Mertzman, S. A., Puckett, R. E., Walker, J. D., & Feldman, J. (2016). Cambrian intermediate-mafic magmatism along the Laurentian margin: Evidence for flood basalt volcanism from well cuttings in the Southern Oklahoma Aulacogen (U.S.A.). *Lithos*, *260*, 164–177. https://doi.org/10.1016/j.lithos.2016.05.016

Burgess, P. M. (2019). Phanerozoic evolution of the sedimentary cover of the North American Craton. In: A. Miall (Ed.), *The Sedimentary Basins of the United States and Canada* (pp. 39–75). Elsevier B.V. https://doi.org/10.1016/b978-0-444-63895-3.00002-4

Burton, W. & Southworth, S. (2010). A model for Iapetan rifting of Laurentia based on Neoproterozoic dikes and related rocks. In: R.P. Tollo, M. J. Bartholomew, J. P. Hibbard, & P. M. Karabinos (Eds.), *From Rodinia to Pangea: The Lithotectonic Record of the Appalachian Region*. *Geological Society of America Memoir*, 206, 455–476. https://doi.org/10.1130/2010.1206(20)

Carlson, M. P. (1999). Transcontinental Arch—A pattern formed by rejuvenation of local features across central North America. *Tectonophysics*, *305*, 225–233. https://doi.org/10.1016/S0040-1951(99)00005-0

Cawood, P. A., Hawkesworth, C. J., & Dhuime, B. (2012). Detrital zircon record and tectonic setting. *Geology*, *40*, 875–878. https://doi.org/10.1130/G32945.1

Cawood, P. A., McCausland, P. J. A., & Dunning, G. R. (2001). Opening Iapetus: Constraints from the Laurentian margin in Newfoundland. *Geological Society of America Bulletin*, *113*, 443–453. https://doi.org/10.1130/0016-606(2001)113<0443:OICFT L>2.0.CO;2

Cawood, P. A., & Nemchin, A. A. (2001). Paleogeographic development of the East Laurentian margin: Constraints from U-Pb dating of detrital zircons in the Newfoundland Appalachians. *Geological Society of America Bulletin*, *113*, 1234–1246. https://doi.org/10.1130/0016-7606(2001)113<1234:PDOTE L>2.0.CO;2

Chakraborty, S., Moecher, D. P., & Samson, S. D. (2012). Provenance of the Lower Ocoee Supergroup, eastern Great Smoky Mountains. *Geological Society of America Bulletin*, *124*, 1278–1292. https://doi.org/10.1130/B30578.1

Colpron, M., Logan, J. M., & Mortensen, J. K. (2002). U-Pb zircon age constraint for late Neoproterozoic rifting and initiation of the lower Paleozoic passive margin of western Laurentia. *Canadian Journal of Earth Sciences*, *39*, 133–143. https://doi.org/10.1139/e01-069

Corsetti, F. A., & Kaufman, A. J. (2003). Stratigraphic investigations of carbon isotope anomalies and Neoproterozoic ice ages in Death Valley, California. *Geological Society of America Bulletin*, *115*, 916–932. https://doi.org/10.1130/B25066.1

Craddock, J. P., Malone, D. H., Porter, R., Compton, J., Luczaj, J., Konstantinou, A., Day, J. E., & Johnston, S. T. (2017). Paleozoic reactivation structures in the Appalachian-Ouachita-Marathon foreland: Far-field deformation across Pangea. *Earth-Science Reviews, 169*, 1–34. https://doi.org/10.1016/j.earsc irev.2017.04.002

Dalziel, I. W. D. (2014). Cambrian transgression and radiation linked to an Iapetus-Pacific oceanic connection? *Geology*, *42*, 979–982. https://doi.org/10.1130/G35886.1

Dehler, C., Gehrels, G., Porter, S., Heizler, M., Karlstrom, K., Cox, G., Crossey, L., & Timmons, M. (2017). Synthesis of the 780–740 Ma Chuar, Uinta Mountain, and Pahrump (ChUMP) groups, western USA: Implications for Laurentia-wide cratonic marine basins. *Geological Society of America Bulletin*, *129*, 607–624. https://doi.org/10.1130/B31532.1

Deiss, C. F. (1935). Cambrian-Algonkian unconformity in western Montana. *Geological Society of America Bulletin*, *46*, 95–124. https://doi.org/10.1130/GSAB-46-95

Farmer, G., Bowring, S., Matzel, J., Maldanado, G., Fedo, C., & Wooden, J. (2005). Paleoproterozoic Mojave province in northwestern Mexico? Isotopic and U-Pb Isotopic and U-Pb zircon geochronologic studies of Precambrian and sedimentary rocks, Caborca, Sonora. In: T. H. Anderson, J. A. Nourse, J. W. McKee, & M. B. Steiner (Eds.), *The Mohave-Sonora Mega-Sonora hypothesis: Development, assessment, and alternatives*. *Geological Society of America Special Paper*, 393, 183–198. https://doi.org/10.1130/0-8137-2393-0

Finney, S., Peralta, S., Gehrels, G., & Marsaglia, K. (2005). The Early Paleozoic history of the Cuyania (greater Precordillera) terrane of western Argentina: Evidence from geochronology of detrital zircons from Middle Cambrian. *Geologica Acta*, *3*, 339–354.

Flowers, R. M., Macdonald, F. A., Siddoway, C. S., & Havranek, R. (2020). Diachronous development of Great Unconformities before Neoproterozoic Snowball Earth. *Proceedings of the National Academy of Sciences*, *117*(19), 201913131. https://doi.org/10.1073/pnas.19131 31117

Freiburg, J. T., Holland, M. E., Malone, D. H., & Malone, S. J. (2020). Detrital Zircon Geochronology of Basal Cambrian Strata in the Deep Illinois Basin, USA: Evidence for the Paleoproterozoic-Cambrian Tectonic and Sedimentary Evolution of Central Laurentia. *The Journal of Geology*, *123*(3), 303–317. https://doi.org/10.1086/708432

Gehrels, G., & Pecha, M. (2014). Detrital zircon U-Pb geochronology and Hf isotope geochemistry of Paleozoic and Triassic passive margin strata of western North America. *Geosphere*, *10*, 49–65. https://doi.org/10.1130/GES00 889.1

Hanson, R. E., Puckett, R. E., Keller, G. R., Brueseke, M. E., Bulen, C. L., Mertzman, S. A., Finegan, S. A., & McCleery, D. A. (2013). Intraplate magmatism related to opening of the southern Iapetus Ocean: Cambrian Wichita igneous province in the Southern Oklahoma rift zone. *Lithos*, *174*, 57–70. https://doi.org/10.1016/j.lithos.2012.06.003

Harlan, S. S., Heaman, L., LeCheminant, A. N., & Premo, W. R. (2003). Gunbarrel mafic magmatic event: A key 780 Ma time marker for Rodinia plate reconstructions. *Geology*, *31*, 1053–1056. https://doi.org/10.1130/G19944.1

Hayes, P. (1972). Stratigraphic nomenclature of Cambrian and Lower Ordovician Rocks of easternmost southern Arizona and adjacent westernmost New Mexico. *U.S. Geological Survey Bulletin*, *1372-B*, 32.

Heaman, L., & Grotzinger, J. (1992). 1.08 Ga diabase sills in the Pahrump Group, California: Implications for development of the Cordilleran miogeocline. *Geology*, *20*, 637–640. https://doi.org/10.1130/0091-7613(1992)020<0637:GDSIT P>2.3.CO;2

Hogan, E. G., Fedo, C. M., & Cooper, J. D. (2011). Reassessment of the basal Sauk supersequence boundary across the Laurentian craton-margin hinge zone, southeastern California. *The Journal of Geology*, *119*, 661–685. https://doi.org/10.1086/661990

Howard, A. L., Farmer, G. L., Amato, J. M., & Fedo, C. M. (2015). Zircon U-Pb ages and Hf isotopic compositions indicate multiple sources for Grenvillian detrital zircon deposited in western Laurentia. *Earth and Planetary Science Letters*, *432*, 300–310. https://doi.org/10.1016/j.epsl.2015.10.018

Karlstrom, K. E., Bowring, S. A., Dehler, C. M., Knoll, A. H., Porter, S. M., Des Marais, D. J., Weil, A. B., Sharp, Z. D., Geissman, J. W., Elrick, M. B., Timmons, J. M., Crossey, L. J., & Davidek, K. L. (2000). Chuar Group of the Grand Canyon: Record of breakup of Rodinia, associated change in the global carbon cycle, and ecosystem expansion by 740 Ma. *Geology*, *28*, 619–622. https://doi.org/10.1130/0091-7613(2000)28<619:CGOTG C>2.0.CO;2

Karlstrom, K., Hagadorn, J., Gehrels, G., Matthews, W., Schmitz, M., Madronich, L., Mulder, J., Pecha, M., Giesler, D., & Crossey, L. (2018). Cambrian Sauk transgression in the Grand Canyon region redefined by detrital zircons. *Nature Geoscience*, *11*, 438–443. https://doi.org/10.1038/s41561-018-0131-7

Karlstrom, K. E., Mohr, M. T., Schmitz, M. D., Sundberg, F. A., Rowland, S. M., Blakey, R., Foster, J. R., & Crossey, L. J. (2020). Redefining the Tonto Group of Grand Canyon and recalibrating the Cambrian time scale. *Geology*, *48*, 1–6. https://doi.org/10.1130/G46755.1/4944753/g46755.pdf

Keller, C. B., Husson, J. M., Mitchell, R. N., Bottke, W. F., Gernon, T. M., Boehnke, P., Bell, E. A., Swanson-Hysell, N. L., & Peters, S. E. (2018). Neoproterozoic glacial origin of the Great Unconformity. *Proceedings of the National Academy of Sciences*, *116*(4), 1136–1145. https://doi.org/10.1073/pnas.18043 50116

Keller, M., Lehnert, O., & Cooper, J. D. (2012). Sauk Megasequence Supersequences, Southern Great Basin: Second-order Accommodation Events on the Southwestern Cordilleran Margin Platform. In J. R. Derby, R. D. Fritz, S. A. Longacre, W. A. Morgan, & C. A. Sternbach (Eds.), *The great American carbonate bank: The geology and economic resources of the Cambrian –Ordovician Sauk megasequence of Laurentia, AAPG Memoir*, 98, 873–896. https://doi.org/10.1306/13331519M983514

Landing, E., Amati, L., & Franzi, D. A. (2009). Epeirogenic transgression near a triple junction: The oldest (latest early –Middle Cambrian) marine onlap of cratonic New York and Quebec. *Geological Magazine*, *146*, 552–566.https://doi.org/10.1017/S0016 75680 9006013

LeMone, D. (1969). Lower Paleozoic rocks in the El Paso area. *New Mexico Geological Society Guidebook*, *20th Field Conference*, 145–162.

Li, Z. X., Bogdanova, S. V., Collins, A. S., Davidson, A., De Waele, B., Ernst, R. E., Fitzsimons, I. C. W., Fuck, R. A., Gladkochub, D. P., Jacobs, J., Karlstrom, K. E., Lu, S., Natapov, L. M., Pease, V., Pisarevsky, S. A., Thrane, K., & Vernikovsky, V. (2008). Assembly, configuration, and break-up history of Rodinia: A synthesis. *Precambrian Research*, *160*, 179–210. https://doi.org/10.1016/j.preca mres.2007.04.021

Linde, G. M., Cashman, P. H., Trexler, J. H., & Dickinson, W. R. (2014). Stratigraphic trends in detrital zircon geochronology of upper Neoproterozoic and Cambrian strata, Osgood Mountains, Nevada, and elsewhere in the Cordilleran miogeocline: Evidence for early Cambrian uplift of the Transcontinental Arch. *Geosphere*, *10*, 1402–1410. https://doi.org/10.1130/GES01 048.1

Link, P., Jansen, S., Halimdihardja, P., Lande, A., & Zahn, P. (1987). Stratigraphy of the Brigham Group (Late Proterozoic-Cambrian), Bannock, Portneuf, and Bear River Ranges, southeastern Idaho. *The Thrust Belt Revisited; 38th Annual Field Conference Guidebook*, 133–148.

Link, P. K., Todt, M. K., Pearson, D. M., & Thomas, R. C. (2017). 500–490 Ma detrital zircons in Upper Cambrian Worm Creek and correlative sandstones, Idaho, Montana, and Wyoming: Magmatism and tectonism within the passive margin. *Lithosphere*, *9*, 1–17. https://doi.org/10.1130/L671.1

Lund, K. (2008). Geometry of the Neoproterozoic and Paleozoic rift margin of western Laurentia: Implications for mineral depositsettings. *Geosphere*, *4*, 429–444. https://doi.org/10.1130/GES00121.1

Lund, K., Aleinikoff, J. N., Evans, K. V., & Fanning, C. M. (2003). SHRIMP U-Pb geochronology of Neoproterozoic Windermere Supergroup, central Idaho: Implications for rifting of western Laurentia and synchroneity of Sturtian glacial deposits. *Bulletin of the Geological Society of America*, *115*, 349–372. https://doi.org/10.1130/0016-7606(2003)115

Macdonald, F. A., Schmitz, M. D., Crowley, J. L., Roots, C. F., Jones, D. S., Maloof, A. C., Strauss, J. V., Cohen, P. A., Johnston, D. T., & Schrag, D. P. (2010). Calibrating the Cryogenian. *Science*, *327*, 1241–1244. https://doi.org/10.1126/scien ce.1183325

Marshak, S., Domrois, S., Abert, C., Larson, T., Pavlis, G., Hamburger, M., Xiaotao, Y., Gilbert, H., & Chen, C. (2017). The basement revealed: Tectonic insight from a digital elevation model of the Great Unconformity. *USA Cratonic Platform. Geology*, *45*(5), 391–394. https://doi.org/10.1130/G38875.1

Martin, E. L., Collins, W. J., & Spencer, C. J. (2020). Laurentian origin of the Cuyania suspect terrane, western Argentina, confirmed by Hf isotopes in zircon. *Geological Society of America Bulletin*, *132*, 273–290. https://doi.org/10.1130/b35150.1

Martin, E. L., Spencer, C. J., Collins, W. J., Thomas, R. J., Macey, P. H., & Roberts, N. M. W. (2020). The core of Rodinia formed by the juxtaposition of opposed retreating and advancing accretionary orogens. *Earth-Science Reviews, 211*, https://doi.org/10.1016/j.earscirev.2020.103413

Matthews, W., Guest, B., & Madronich, L. (2018). Latest Neoproterozoic to Cambrian detrital zircon facies of western Laurentia. *Geosphere*, *14*, 243–264. https://doi.org/10.1130/GES01 544.1

Merdith, A. S., Williams, S. E., Collins, A. S., Tetley, M. G., Mulder, J.A., Blades, M. L., Young, A., Armistead, S. E., Cannon, J., Zahirovic, S., & Müller, R. D. (2021). Extending full-plate tectonic models into deep time: Linking the Neoproterozoic and the Phanerozoic. *Earth-Science Reviews, 214*, https://doi.org/10.1016/j.earscirev.2020.103477

Mitchell, R. N., Kilian, T. M., Raub, T. D., Evans, D. A. D., Bleeker, W., & Maloof, A. C. (2011). Sutton hotspot: Resolving Ediacaran-Cambrian tectonics and true polar wander for Laurentia. *American Journal of Science*, *311*(8), 651–663. https://doi.org/10.2475/08.2011.01

Mueller, P. A., Foster, D. A., Mogk, D. W., Wooden, J. L., Kamenov, G. D., & Vogl, J. J. (2007). Detrital mineral chronology of the Uinta Mountain Group: Implications for the Grenville flood in southwestern Laurentia. *Geology*, *35*, 431–434. https://doi.org/10.1130/G23148A.1

Myrow, P. M., Taylor, J. F., Miller, J. F., Ethington, R. L., Ripperdan, R. L., & Allen, J. (2003). Fallen arches: Dispelling myths concerning Cambrian and Ordovician paleogeography of the Rocky Mountain region. *Geological Society of America Bulletin*, *115*, 695–713. https://doi.org/10.1130/0016-7606(2003)115<0695:FADMCC>2.0.CO;2

Myrow, P. M., Taylor, J. F., Runkel, A. C., & Ripperdan, R. L. (2012). Mixed siliciclastic-carbonate upward-deepening cycles of the upper Cambrian inner detrital belt of Laurentia. *Journal of Sedimentary Research*, *82*, 216–231. https://doi.org/10.2110/jsr.2012.20

Nordsvan, A. R., Kirscher, U., Kirkland, C. L., Barham, M., & Brennan, D. T. (2020). Resampling (detrital) zircon age distributions for accurate multidimensional scaling solutions. *Earth-Science Reviews, 204*, https://doi.org/10.1016/j.earscirev.2020.103149

Palmer, A. R. (1981). Subdivision of the Sauk sequence. In M. E. Taylor (Ed.), *Short Papers for the Second International Symposium on the Cambrian System, U.S. Geological Survey*, *Open-File Report*, 81–743, 160–162.

Peng, S. C., Babcock, L. E., & Ahlberg, P. (2020). The Cambrian Period. In F. M. Gradstein, J. G. Ogg, M. D. Schmitz, & G. M. Ogg (Eds.), *Geologic Time Scale 2020*. Elsevier.

Poole, F. G., Stewart, J. H., Palmer, A. R., Sandberg, C. A., Madrid, R. J., Ross, R. J. Jr, Hintze, L. F., Miller, M. M., & Wrucke, C. T. (1992). Latest Precambrian to latest Devonian time; Development of a continental margin. In B. C. Burchfiel, P. W. Lipman, & M. L. Zoback (Ed.), *The Cordilleran Orogen: Conterminous U.S., The Geology of North America*, V. G-3. Geological Society of America.

Prave, A. (1999). Two diamictites, two cap carbonates, two δ13 C excursions, two rifts: The Neoproterozoic Kingston Peak Formation, Death Valley, California. *Geology*, *27*, 339–342. https://doi.org/10.1130/0091-76137613(1999)027<0339:TDTCC T>2.3.CO;2

Rainbird, R. H., Rayner, N. M., Hadlari, T., Heaman, L. M., Ielpi, A., Turner, E. C., & MacNaughton, R. B. (2017). Zircon provenance data record the lateral extent of pancontinental, early Neoproterozoic rivers and erosional unroofing history of the Grenville Orogen. *Geological Society of America Bulletin*, *129*(11–12), 1408–1423. https://doi.org/10.1130/B31695.1

Ross, G. M. (1991). Tectonic setting of the Windermere Supergroup revisited. *Geology*, *19*, 1125–1128. https://doi.org/10.1130/0091-7613(1991)019<1125:TSOTW S>2.3.CO;2

Satkoski, A. (2013). Sr-Nd-Hf isotope geochemistry of 3.5 Ga gneisses of the Minnesota River Valley and U-Pb geochronology of detrital zircon for Cambrian sedimentary rocks of the Laurentian rifted margin. PhD thesis Syracuse, New York, Syracuse University, 215 pp.

Saylor, J. E., & Sundell, K. E. (2016). Quantifying comparison of large detrital geochronology data sets. *Geosphere*, *12*(6), 1881. https://doi.org/10.1130/GES01 237.1

Saylor, J. E., & Sundell, K. E. (2021). Tracking proterozoic-triassic sediment routing to western Laurentia via bivariate non-negative matrix factorization of detrital provenance data. *Journal of the Geological Society*, 97–195, https://doi.org/10.1144/jgs20 20-215

Shaw, A. B. (1958). Stratigraphy and structure of the Saint Albans area, northwestern Vermont. *Geological Society of America Bulletin*, *69*, 519–567. https://doi.org/10.1130/0016-606(1958)69[519:SASOTS]2.0.CO;2

Sloss, L. L. (1963). Sequences in the cratonic interior of North America. *Geological Society of America Bulletin*, *74*, 93–114. https://doi.org/10.1130/0016-7606(1963)74[93:SITCI O]2.0.CO;2

Sloss, L. L. (1988). Tectonic evolution of the craton in Phanerozoic time. In L. L. Sloss (Ed.), *Sedimentary cover–North American craton: The Geology of North America D-2*. Geological Society of America. https://doi.org/10.1130/DNAG-GNA-D2.25

Soares, D. M., Alves, T. M., & Terrinha, P. (2012). The breakup sequence and associated lithospheric breakup surface: Their significance in the context of rifted continental margins (West Iberia and Newfoundland margins, North Atlantic). *Earth and Planetary Science Letters*, *355–356*, 311–326. https://doi.org/10.1016/j.epsl.2012.08.036

Sour-Tovar, F., Hagadorn, J., & Huitron-Rubio, T. (2007). Ediacaran and Cambrian index fossils from Sonora, Mexico. *Paleontology*, *50*, 169–175. https://doi.org/10.1111/j.1475-983.2006.00619.x

Southworth, S., Bailey, C. M., Eaton, L. S., Hancock, G., Lamoreaux, M.H., Litwin, R. J., Burton, W. C., & Whitten, J. (2009). Geology of the Shenandoah National Park Region: *Guidebook for 39th Annual Virginia Geological Field Conference* (October 2–3, 2009), 40.

Spencer, C. J., Hoiland, C. W., Harris, R. A., Link, P. K., & Balgord, E. A. (2012). Constraining the timing and provenance of the Neoproterozoic Little Willow and Big Cottonwood Formations, Utah: Expanding the sedimentary record for early rifting of Rodinia. *Precambrian Research*, *204–205*, 57–65. https://doi.org/10.1016/j.precamres.2012.02.009

Spencer, C. J., Kirkland, C. L., Roberts, N. M. W., Evans, N. J., & Liebmann, J. (2020). Strategies towards robust interpretations of in situ zircon Lu–Hf isotope analyses. *Geoscience Frontiers, 11*, 843–853. https://doi.org/10.1016/j.gsf.2019.09.004

Spencer, C. J., Prave, A. R., Cawood, P. A., & Roberts, N. M. W. (2014). Detrital zircon geochronology of the Grenville/Llano forelandand basal Sauk Sequence in west Texas, USA. *Geological Society of America Bulletin*, *126*, 1117–1128. https://doi.org/10.1130/B30884.1

Stein, S., Stein, C. A., Elling, R., Kley, J., Keller, G. R., Wysession, M., Rooney, T., Frederiksen, A., & Moucha, R. (2018). Insights from North America's failed Midcontinent Rift into the evolution of continental rifts and passive continental margins. *Tectonophysics*, *744*, 403–421. https://doi.org/10.1016/j.tecto.2018.07.021

Stewart, J. (2005). Evidence for Mojave-Sonora megashear—Systematic left-lateral offset of Neoproterozoic to Lower Jurassic strata and facies, western United States and northwestern Mexico. In T. H. Anderson, J. A. Nourse, J. W. McKee, & M. B. Steiner (Eds.), *The Mohave-Sonora Megashear hypothesis: Development, assessment, and alternatives*. *Geological Society of America Special Paper*, *393*, 209–231. https://doi.org/10.1130/0-8137-2393-0.209

Stewart, J. H., Amaya-Martínez, R., & Palmer, A. R. (2002). Neoproterozoic and Cambrian strata of Sonora, Mexico: Rodinian supercontinent to Laurentian Cordilleran margin. In A. Barth (Ed.), *Contributions to crustal evolution of the Southwestern United States*. *Geological Society of America Special Paper*, **365**, 5–20. https://doi.org/10.1130/0-137-2365-5.5

Stewart, J. H., Gehrels, G. E., Barth, A. P., Link, P. K., Christie-Blick, N., & Wrucke, C. T. (2001). Detrital zircon provenance of Mesoproterozoic to Cambrian arenites in the Western United States and Northwestern Mexico. *Geological Society of America*

Bulletin, *113*, 1343–1356. https://doi.org/10.1130/0016-7606(2001)113<1343:DZPOM T>2.0.CO;2

Sundell, K. E., & Saylor, J. E. (2021). Two-Dimensional quantitative comparison of density distributions in detrital geochronology and geochemistry. *Geochemistry Geophysics Geosystems*, https://doi.org/10.1029/2020GC009559

Thomas, W. A. (2011). The Iapetan rifted margin of southern Laurentia. *Geosphere, 7*, 97–120. https://doi.org/10.1130/GES00 574.1

Thomas, W. A. (2014). A Mechanism for Tectonic Inheritance at Transform Faults of the Iapetan Margin of Laurentia. *Geoscience Canada*, *41*, 321–344. https://doi.org/10.12789/ geoca nj.2013.40.022

Thomas, W. A., Astini, R. A., Mueller, P. A., Gehrels, G. E., & Wooden, J. L. (2004). Transfer of the Argentine Precordillera terrane from Laurentia: Constraints from detrital-zircon geochronology. *Geology*, *32*, 965–968. https://doi.org/10.1130/G20727.1

Tollo, R. P., Aleinikoff, J. N., Wooden, J. L., Mazdab, F. K., Southworth, S., & Fanning, C. M. (2010). Thermomagmatic evolution of Mesoproterozoic crust in the Blue Ridge of SW Virginia and NW North Carolina: Evidence from U-Pb geochronology and zircon geothermometry. In R. P. Tollo, M. J. Bartholomew, J. P. Hibbard, & P. M. Karabinos (Eds.), *From Rodinia to Pangea: The Lithotectonic Record of the Appalachian Region: Geological Society of America Memoir* 206, 859–896. https://doi.org/10.1130/2010.1206(33)

Tull, J. F., Allison, D. T., Whiting, S. E., & John, N. L. (2010). Southern Appalachian Laurentian margin initial drift-facies sequences. In R. P. Tollo, M. J. Bartholomew, J. P. Hibbard, & P. M. Karabinos (Eds.), *From Rodinia to Pangea: The Lithotectonic Record of the Appalachian Region: Implications for margin evolution*. *Geological Society of America Memoir*, 206, 935–956. https://doi.org/10.1130/2010.1206

U.S. Geological Survey Geologic Names Committee. (2010). Divisions of geologic time–Major chronostratigraphic and geochronologic units: U.S. Geologic Survey Fact Sheet 2010-3059.2. https://doi.org/10.3133/fs201 03059

Valentine, J. W., & Moores, E. M. (1970). Plate-tectonic regulation of faunal diversity and sea level: A model. *Nature*, *228*, 657–659. https://doi.org/10.1038/228657a0

Vermeesch, P. (2012). On the Visualisation of Detrital Age Distributions. *Chemical Geology*, *312–313*, 190–194. https://doi.org/10.1016/j. chemg eo.2012.04.021

Vermeesch, P. (2013). Multi-sample comparison of detrital age distributions. *Chemical Geology*, *341*, 140–146. https://doi.org/10.1016/j.chemg eo.2013.01.010

Vermeesch, P. (2018). Dissimilarity measures in detrital geochronology. *Earth-Science Reviews*, *178*, 310–321. https://doi.org/10.1016/j.earscirev.2017.11.027

Whitmeyer, S. J., & Karlstrom, K. E. (2007). Tectonic model for the Proterozoic growth of North America. *Geosphere*, *3*, 220–259. https://doi.org/10.1130/GES00 055.1

Wooden, J. L., Barth, A. P., & Mueller, P. A. (2013). Crustal growth and tectonic evolution of the Mojave crustal province: Insights from hafnium isotope systematics in zircons. *Lithosphere*, *5*, 17–28. https://doi.org/10.1130/L218.1

Yonkee, W. A., Dehler, C. D., Link, P. K., Balgord, E. A., Keeley, J. A., Hayes, D. S., Wells, M. L., Fanning, C. M., & Johnston, S. M. (2014).Tectono-stratigraphic framework of Neoproterozoic to Cambrian strata, west-central U.S.: Protracted rifting, glaciation, and evolution of the North American Cordilleran margin. *Earth-Science Reviews*, *136*, 59–95. https://doi.org/10.1016/j.earsc irev.2014.05.004

Chapter 7: Synthesis and Conclusions

7.1 Introduction

The geologic focus of this thesis spans over 2,000 million years, from the Neoarchean Era to the Cambrian Period. During this time span, Earth underwent numerous cyclical, secular and stepwise modifications. To espouse the preamble quote of this thesis, there are many "horizons" during these 2,000 million years where the geological evidence, and consequently our knowledge of these Earth modifications is missing or incomplete. This work aimed to reduce the extent and uncertainty of several key tectonic/geologic horizons within the key piercing point of the Belt Basin region of western Laurentia, and thus increase the completeness of the Paleoproterozoic to early Paleozoic knowledge of this critical area in many tectonic reconstructions. In doing so, this work provides a more robust regional geologic history against which inherently more speculative larger scale global Nuna and Rodinia tectonic models must be compared, evaluated and redefined.

In the following chapter, the work of this thesis is synthesized and discussed within the context of three general time intervals that correspond to significant global plate-tectonic reorganization events. These time intervals include: ca. 2000–1350 Ma (section 7.2.1) during which supercontinent Nuna assembled, ca. 1350–900 Ma (section 7.2.2) during which supercontinent Nuna broke apart and subsequent supercontinent Rodinia assembled, and finally from ca. 800–500 Ma (section 7.2.3) during which Rodinia broke apart. In a way, these three delineations are a Belt Basin regionally focused update to the unconformity bounded successions A (~1700–1200 Ma), B (1200–800 Ma), and C (800–570 Ma) defined by Young et al., (1979) in northern Laurentia, and subsequently applied southward to most of the western Laurentian margin (Link et al., 1993).

7.2 Summary and significant findings

7.2.1 Paleoproterozoic Laurentia and Nuna assembly

As introduced in Chapter 1, a main controversy surrounding global Paleoproterozoic paleogeography is whether the final assembly of supercontinent Nuna was primarily a ca. 1800 Ma process coeval with the main assembly of Laurentia (e.g. Zhao et al., 2002), or if final Nuna assembly was primarily a later, ca. 1600 Ma process (e.g. Kirscher et al., 2021). In northwestern Laurentia and northeastern Australia, ca. 1750–1550 Ma strata record final Nuna assembly at ca. 1600 Ma

(Furlanetto et al., 2016; Nordsvan et al., 2018). However, ~1500 km further south in the Belt Basin region, the focus area of this study, previous provenance studies have primarily focused on the ca. 1470–1380 Ma Belt Supergroup (e.g. Ross and Villenaeuve, 2003; Lewis et al., 2007) and neglected the significance of potential pre-Belt Supergroup units, such as the Gold Cup and likely correlative Neihart quartzites (Doughty and Chamberlain, 2008) to constrain the tectonostratigraphic record of this region prior to ca. 1470 Ma.

As discussed in Chapter 3 (section 3.2.1) the Mesoproterozoic Belt Basin traverses at least two significant Paleoproterozoic sutures associated with the assembly of Laurentia, which include the Great Falls Tectonic Zone and the Vulcan Structure. The better exposed, and thus better studied of these structures is the Great Falls Tectonic Zone which records ca. 1860–1730 Ma convergent events associated with northwest dipping subduction and amalgamation of the Medicine Hat and likely Clearwater block(s) to the Wyoming province (e.g. Mueller et al., 2002; Foster et al., 2006; Gifford et al., 2020). In Chapter 2, existing (Vervoort et al., 2016) and new zircon geochronology from the Clearwater Block indicates that crustal growth in this region occurred primarily at ca. 2670 and ca. 1880–1840 Ma, with localized magmatism at ca. 1581 Ma. New zircon Lu/Hf and O- isotope data, also suggest that the younger interval of Paleoproterozoic crustal growth primarily records remelting of older lithosphere, as opposed to significant juvenile mantle contributions. However, additional constraints on this period of ca. 1880–1840 Ma crustal growth in the Clearwater block have been published (Wang et al., 2022) following the publication of Chapters 2 and 3. Thus, we include these new results here (Fig. 7.1).

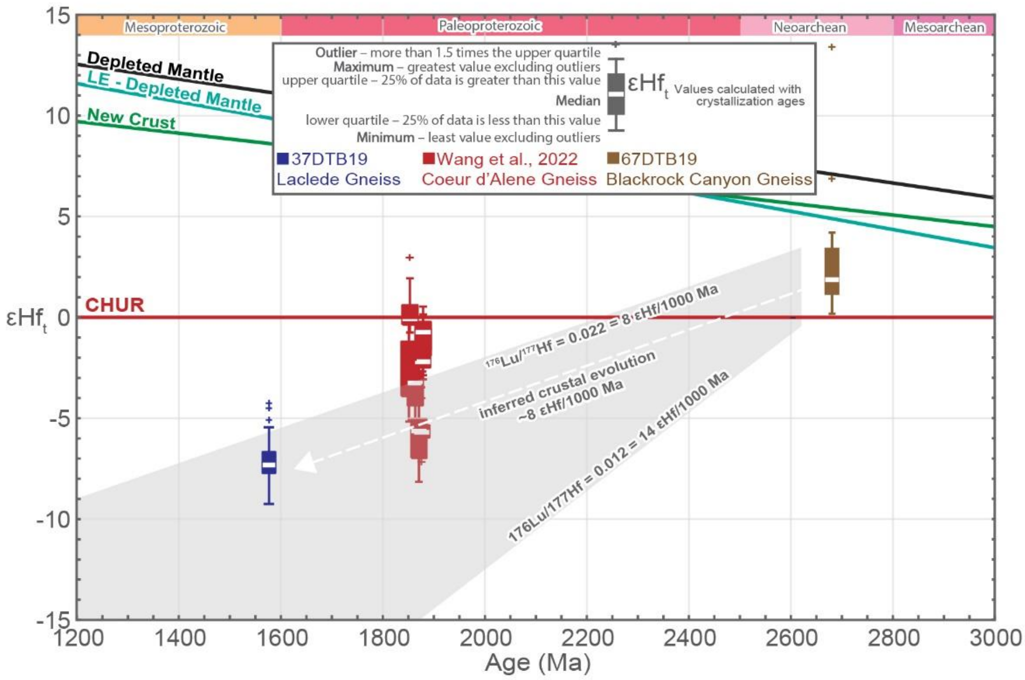

Fig. 7.1: εHf_t values vs. ($^{207}Pb/^{206}Pb$) Age plot for the Clearwater Block (Chapter 2; Wang et al., 2022). The colored box plots indicate the range of εHf_t values calculated for each gneiss based on the measured Lu/Hf, and the interpreted crystallization age of the sample. See Fig. 2.7 for explanation of Mantle evolution curves. The red boxes are from the Coeur d'Alene Gneiss in the Priest River complex near the Laclede Gneiss outcrop (Wang et al., 2022). Wang et al., (2022) also reports Lu/Hf data from ca. 1900–1830 Ma orthogneiss located further south in the Clearwater complex, which show a slightly wider range of εHf_t values from approximately –8 to +8 (Wang et al., 2022). CHUR–Chondritic Uniform Reservoir (Bouiver et al., 2008).

In Chapter 3, additional U/Pb (prior limited n-analyses presented by Ross and Villeneuve, 2003; Doughty and Chamberlain, 2008; Mueller et al., 2016) and the first Lu/Hf detrital zircon results from the oldest, younger than ca. 1750 Ma strata that unconformably overlie the Clearwater and Medicine Hat/Great Falls Tectonic Zone basement terranes, the Gold Cup Quartzite and Neihart Quartzite, was presented. The objective of this data was to evaluate whether these likely pre-Belt Supergroup units require non-Laurentia sources or not, and thus assess competing models on the timing of Nuna assembly. The detrital zircon components of both the Gold Cup and Neihart quartzites consist of primarily two age distributions at ca. 2670 Ma and ca. 1860–1780 Ma. The Neoarchean grains contain CHUR-like Lu/Hf values, and consequently are similar in age and Hf composition to the nearby Clearwater Block basement. However, the Paleoproterozoic grains contain a wider range of Lu/Hf values that are generally concentrated around three εHf ranges, +8 to +4, -3 to -7, and -14 to -18 (Neihart Quartzite only), suggesting perhaps mixing of at least three possible sources. Suitable sources for these grains are found within ca. 1800 Ma (εHf_t = -10 to -20) rocks of the

Medicine Hat block (Gifford et al., 2020), ca. 1880–1840 Ma (εHf_t = +8 to -8) rocks of the Clearwater complex (Vervoort et al., 2016; Wang et al., 2022), the extensive ca. 1860-1780 Ma Trans-Hudson orogen, and perhaps ca. 1880–1740 Ma (εHf_t = +10 to -5) rocks of the Mojave-Yavapai-Mazatzal provinces (Whitmeyer and Karlstrom, 2007; Holland et al., 2018 and references within). Consequently, the tectonostratigraphic record of the Belt region does not require any non-Laurentian sources during Laurentian assembly, and thus is broadly consistent with the ca. 1800 Ma assembly of the main Archean blocks (Wyoming, Medicine Hat, Clearwater, Hearne) of western Laurentia prior to a later ca. 1650–1600 Ma assembly of Nuna. In western/southwestern Laurentia, a record of this later assembly may be associated with ca. 1670 Ma metamorphism in the Farmington Zone (Mueller et al., 2011), and the ca. 1650–1600 Ma Mazatzal Orogeny (Gibson and Champion, 2019; Holland et al., 2020).

In Chapter 2, the 1581 ± 3 Ma Laclede Gneiss within the Priest River complex contains evolved Lu–Hf (εHf = -6 to -10) and mantle-like δ18O zircon values, suggesting remelting of a Neoarchean lower continental lithosphere source. The evolved values of this gneiss makes it a poor direct match for coeval, mostly juvenile, magmatism in the Gawler Craton of southeastern Australia (Reid and Payne, 2017). Thus, I advocated that the Laclede Gneiss is not a stranded fragment of Australian crust. However, as Wang et al., (2022) note, Antarctica and southeastern Australia do have similar age (ca. 1580 Ma) evolved (negative εHf_t) magmatism that could be a non-Laurentian source for the Laclede Gneiss. Nevertheless, the evolved (negative εHf_t) values for the Laclede Gneiss importantly demonstrate that a non-Laurentian source for the similar-age evolved (positive εHf) detrital zircon grains within the surrounding Belt Supergroup is required. This zircon source is likely the Gawler Craton of southeastern Australia, as it contains magmatic rocks with the same age and Hf values as the juvenile ca. 1600 Ma detrital zircon grains within the overlying Belt Supergroup (Fig. 7.2). Ca. 1630–1580 Ma St. Peters Suite and Gawler Range Volcanics in southeastern Australia have plume and/or back-arc genesis models (e.g. Reid and Payne 2017; Chapman et al., 2019). Consequently, as discussed in Chapter 2 (section 2.5.4), the Laclede Gneiss may be a crustal-derived, distal manifestation of a ca. 1580 Ma mantle up-welling (perhaps plume) event beneath southeastern Australia. Therefore, the Belt Basin regional geologic record does not require the assembly of Australia/East Antarctica with western Laurentia within Nuna at ca. 1800

Ma, and rather the first indirect evidence of this association may be recorded in the 1581 Ma Laclede Gneiss.

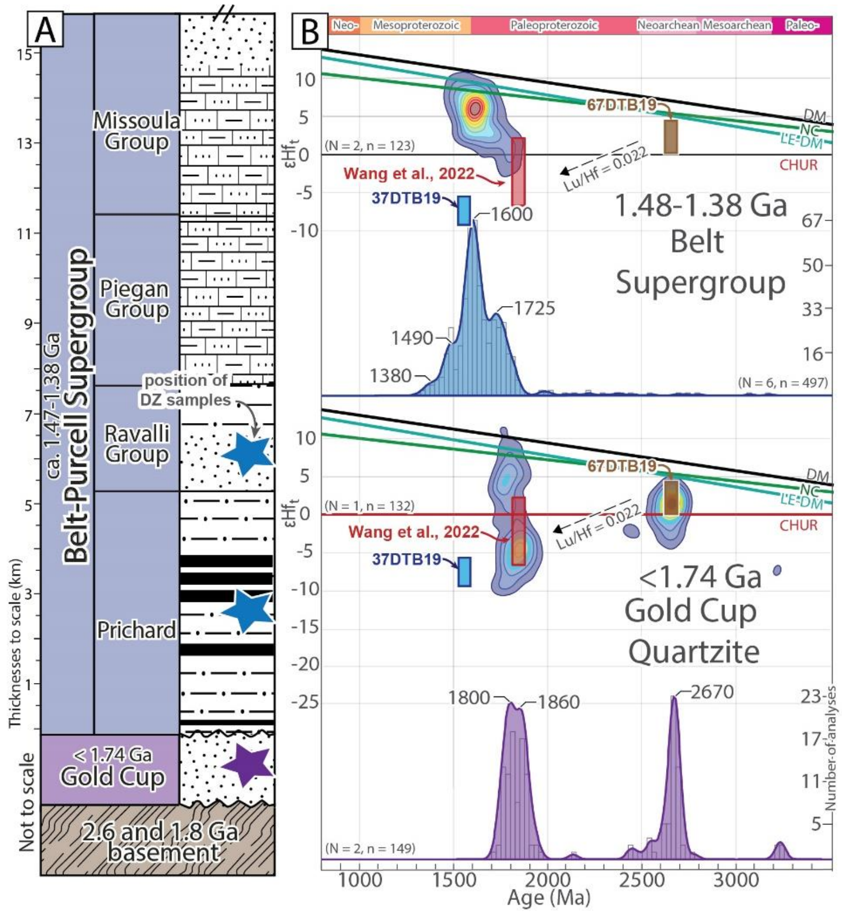

Fig. 7.2: Paleo–Mesoproterozoic stratigraphy and U–Pb/Lu–Hf detrital zircon results from the Priest River Region (Doughty and Chamberlain, 2008; Box et al., 2020; Lewis et al., 2020; Brennan et al., 2021) and the range of robust εHf_t values (samples 67DTB19 and 37DTB19) from the underlying ca. 2670 and 1580 Ma igneous basement. The red box indicates the age and εHf_t range (ca. 1.88-1.83 Ga) of Paleoproterozoic magmatism in the northern extent of the Clearwater Block (Vervoort et al., 2016) and the Lu–Hf values of Wang et al., (2022) for the Coeur d'Alene Gneiss. Wang et al., (2022) also reports Lu/Hf data from ca. 1900–1830 Ma orthogneiss located further south in the Clearwater complex, which show a slightly wider range of εHf_t values from approximately –8 to +8, which could be the source of the more juvenile ca. 1860–1830 Ma grains in the Gold Cup Quartzite. (Wang et al., 2022). Inferred crustal evolution line (Lu/Hf = 0.022) for the Clearwater Block indicated. LE–Late Extraction, NC–New Crust, CHUR–Chondritic Uniform Reservoir. See Fig. 2.7 for explanation of mantle evolution lines.

7.2.2 Mesoproterozoic Laurentia and the Nuna to Rodinia transition

In Chapters 2 and 4, it was demonstrated that the ca. 1600 Ma detrital zircon grains within Belt Basin strata were not sourced from the Laurentian ca. 1581 Ma Laclede Gneiss, as its evolved (negative εHf_t) values could not have supplied the juvenile (positive εHf_t) detrital grains. Other workers (e.g. Yao et al., 2017; Xu et al., 2019; Goodge et al., 2017) have suggested that ca. 1570–1510 Ma magmatic rocks in Hainan Island (south China) or East Antarctica could have contributed detritus to the

Belt Basin. However, zircon grains from these magmatic rocks also exhibit evolved (negative εHf_t) values (see Fig. 2.10), and thus are also poor matches for the grains in Belt Basin strata. Consequently, the mostly juvenile ca. 1630–1580 Ma magmatism within the Gawler craton of southeastern Australia is the best match for these detrital grains, adding further support to long-standing correlations between these two regions during the Mesoproterozoic (Ross et., 1992; Ross and Villeneuve, 2003).

A long-standing controversy in Belt Supergroup geology, is whether the ca. 1470–1380 Ma Belt Basin is a rift to passive margin sequence that records Nuna breakup at ca. 1400 Ma, or whether the Belt Basin was completely intracratonic and preceded Nuna breakup (e.g. Evans et al., 2000; Ross and Villeneuve, 2003; Lonn et al., 2020 and references within). In fact, paleomagnetic data indicates that Australia and western Laurentia were likely in a stable configuration from ca. 1600–1300 Ma suggesting that the Belt Basin may have been completely intracratonic and preceded ca. 1300–1200 Ma Nuna breakup (Kirscher et al., 2021). Limited (n = 29 within their applied -5 to 20% discordant filter) U/Pb detrital zircon results from upper Belt Supergroup strata in northeastern Washington reported by Box et al., (2020) also suggests that the exotic, likely Australian, ca. 1630–1580 Ma source terrane shared sediments with Laurentia until ca. 1390 Ma. The limited geochronology results (of Box et al., 2020) from upper Belt Supergroup, Missoula Group strata (Snowslip Formation) in the Priest River region require substantiating, particularly due to the notable Pb-loss in this sample. It is worth noting that I analyzed a similar upper Belt Supergroup, Missoula Group (Snowslip Formation) sample (14DTB19; see Chapter 3), which yielded almost entirely discordant ages consistent with ca. 95 Ma Pb-loss. Nevertheless, the Missoula Group results of Box et al., (2020) do suggest an Australian-Laurentian connection within Nuna until at least ca. 1390 Ma. However, until recently (Chapter 3; Box et al., 2020), no strata between the ca. 1380 Ma upper Belt Supergroup and ca. 720 Ma basal Windermere Supergroup, were identified in the Belt Basin region. Consequently, there was a limited regional geologic record to compare against paleomagnetically constrained models of ca. 1300–1200 Ma Nuna breakup.

Early work on the Deer Trail Group in northeastern Washington State (Miller and Whipple, 1989) correlated these rocks with ca. 1450–1380 Ma Belt Supergroup strata, suggesting they were the western-most exposures of Belt strata. In Chapter 3 new detrital zircon U–Pb results from the Deer Trail Group were presented. These results support interpretations like those recently presented by Box et al., (2020), and indicate that the Deer Trail Group is mostly younger than 1300 Ma, and thus not correlative to older Belt Supergroup strata further east. The ages and Lu/Hf values of the detrital zircon components in the Deer Trail Group indicate a mixed Laurentian provenance. Notably, Deer Trail Group strata do not record any non-Laurentian sources, and thus indicate a provenance shift from the sources recorded in the underlying Belt Supergroup. The fine-grained siliciclastic and carbonate lithology, and lack of significant syn-depositional magmatic detrital zircon components in Deer Trail Group strata are consistent with their deposition during a period of regional subsidence within the Priest River region that coincides with purported Nuna breakup at ca. 1300–1200 Ma (Kirscher et al., 2020). These stratigraphic and provenance observations suggest the Deer Trail Group may have been deposited during final rifting and passive margin subsidence associated with Nuna breakup. While the only minimum depositional age constraint on the Deer Trail Group is the maximum depositional age of the overlying, < 760 Ma, Buffalo Hump Formation, it is possible that the Deer Trail Group is much younger than ca. 1200 Ma. For example, it is possible that the Deer Trail Group was instead deposited during the assembly and/or early tenure of Rodinia. However, given the absence of ca. 1200–1000 Ma "Grenville-age" zircon grains in the Deer Trail Group, despite their prevalence in Neoproterozoic strata in the region lends credence to a likely ca. 1300–1200 Ma age for the Deer Trail Group.

During this same general time interval, prior workers identified a tectono-magmatic event that may have terminated deposition of the Belt Supergroup. McMechan and Price (1982) delineated the East Kooteny orogeny as a ca. 1350 Ma period of regional folding, metamorphism, and magmatism within the northern extent (southeastern British Columbia) of the Belt Basin. However, in the more southern extent of the Belt Basin (north central Idaho) Doughty and Chamberlain (1996) instead assert that the East Kooteny "orogeny" was not an orogen but rather a ca. 1380–1330 Ma pulse of bimodal magmatism, basin rifting, and renewed subsidence and sedimentation that shortly preceded the end of the deposition in the Belt Basin.

New results from ca. 1400–1350 Ma metamorphic zircon from a mafic sill within the Clearwater complex (presented in Chapter 2) contain δ18O values consistent with hydrothermal zircon growth. In Chapter 4, metapelitic rocks from the western portion of the Clearwater complex are also shown to contain ca. 1350 Ma and younger ca. 1070 Ma monazite U/Pb ages. Interestingly, within the three studied samples from the western Clearwater complex, all three-record garnet growth associated within the younger ca. 1070 Ma monazite ages. However, only one sample recorded garnet growth (Zirakparvar et al., 2010; Neishem et al., 2012) associated within the older ca. 1350 Ma monazite ages, suggesting lower pressure (below approximately 6 kbar) metamorphism for this older event. Consequently, the occurrence of hydrothermal zircon growth and apparently high temperature, lower pressure metamorphism, as well as the absence of any coarse-grained strata possibly associated with this event, suggests that the “East Kootenay Orogeny” is more consistent with a period of bimodal magmatism and basin rifting within the Clearwater complex, then tectonic thickening.

7.2.3 Neoproterozoic Laurentia and Rodinia breakup.

The correlation of ca. 1200–1000 Ma “Grenville-age” orogens have been critical in the construction of various Rodinia models (e.g. Dalziel et al., 1991; Karlstrom et al., 2000; Li et al., 1995). Consequently, the absence, or presence of a poorly preserved/recognized, Grenville-age orogen in western Laurentia is a significant constraint that accurate paleogeographic models must account for. Within this work, the metamorphic (Chapter 4) and tectonostratigraphic (Chapters 3 and 5) record of a potential Grenville-age orogen in the Belt Basin region was investigated. We note that no direct record of ca. 1250–800 Ma magmatism in the Belt Basin region was found by this, or any previous studies.

In Chapter 4, existing Lu/Hf garnet geochronology (Zirakparvar et al., 2010; Neishem et al., 2012) and new monazite and apatite U-Pb results and Thermocalc (pressure-temperature) constraints from ca. 1450 Ma Belt Supergroup metapelitic strata within the western portion of Clearwater complex (notably within the Piegan Group of the Belt Supergroup) indicate that Phanerozoic Cordilleran conditions did not exceed ~550–450°C in this region. Consequently, the mineral assemblages within these rocks likely reflect a high-grade, Grenville-age, metamorphic event recorded by ca. 1100–1060 Ma garnet Lu/Hf and monazite U/Pb ages. Thermodynamic modeling of these mineral assemblages indicate they are consistent with pressures of 7.5–5 Kbar, and temperatures of 670–620°C, suggesting burial to a depth of ~22–17 km or greater around along a moderately-high average geothermal gradient of ~36–23°C/km. Elsewhere in the Belt Basin, and I suggest spatially associated with inherited lithospheric-scale faults, similar ca. 1100–1070 Ma metamorphic events are noted

(McFarlane and Pattison, 2000; Aleinikoff et al., 2012; Pattison and Seitz, 2012; Bookstrom et al., 2016).

At ca. 1100 Ma Laurentia was undergoing a period of widespread extension and thermal upwelling. Manifestations of this event are found in the 1110–1085 Ma Midcontinent Rift (e.g. Swanson-Hysell et al., 2019), 1115–1078 Ma Pikes Peak batholith (Guitreau et al., 2016), 1094–1080 Ma Southwestern Laurentian Large Igneous Province (Timmons et al., 2001; Bright et al., 2014), and 1090–1040 Ma Bylot and correlative basins in northern Laurentia (Greenman et al., 2021). Despite the evidence for Laurentian-wide extension and thermal upwelling at this time, it is indeed difficult to account for pure depositional burial of the Piegan Group (of the Belt Supergroup) to a depth ~22–17 km, when the preserved thicknesses of overlying Belt strata are >10 km, and Deer Trail Group strata are ~3.5 km thick. Therefore, the ca. 1110–1060 Ma period of continent-wide thermal upwelling and reactivation of crustal weaknesses, may have indeed combined with localized inversion of the Belt Basin to produce the metamorphism present in the Clearwater complex.

Importantly, as demonstrated in Chapter 5, if there was indeed any Grenville-age localized inversion of the Belt Basin, and the stratigraphic record of this event was preserved, it must be reflected in the Deer Trail Group, whose fine-grained lithology and recycled detrital zircon provenance signature is a better match for an extensional basin than typical convergent or collisional sequences (Fig. 7.3). Alternatively, no strata was deposited during local inversion of the Belt Basin, or it was subsequently eroded, likely prior to Cryogenian rifting.

Previously, the only possibly suspected Grenville-age (ca. 1000 Ma) strata in western Laurentia was the Buffalo Hump Formation. Prior workers had suggested it required a western Grenville-age source based in part on its erroneous correlation to finer-grained Belt Supergroup strata further east (Miller and Whipple, 1989), and that the Buffalo Hump Formation contained ca. 1100 Ma detrital zircon grains (Ross et al., 1992). However, in Chapter 5, the identification of a small, yet significant, ca. 760 Ma detrital zircon population in the Buffalo Hump Formation indicates that it was deposited during Rodinia breakup, not assembly. The presence of large (20+ cm) reworked Deer Trail Group cobbles in the Buffalo Hump Formation, and the absence of the Buffalo Hump strata along with thinned to absent Deer Trail Group strata east of a regional thrust fault (the Jumpoff Joe Fault) suggests that the thrust is a reactivated Neoproterozoic normal fault. Consequently, the Buffalo Hump Formation records early ca. 760–720 Ma Rodinia fault-controlled rift-basin formation similar to coeval deposits further south in the Uinta, Chuar and Pahrump basins. These results constrain the onset of rifting in the Belt Basin region to after ca. 760 Ma and thus about 70 Myrs later then in the Adelaide Superbasin of the Gawler craton in southeastern Australia (Preiss, 2000; Lloyd et al., 2020). This time difference makes it difficult for the Belt Basin region (western Laurentia) and the Adelaide Superbasin region (Gawler craton) to be direct conjugate margins as is suggested by Rodina SWEAT models (e.g. Moores et al., 1991).

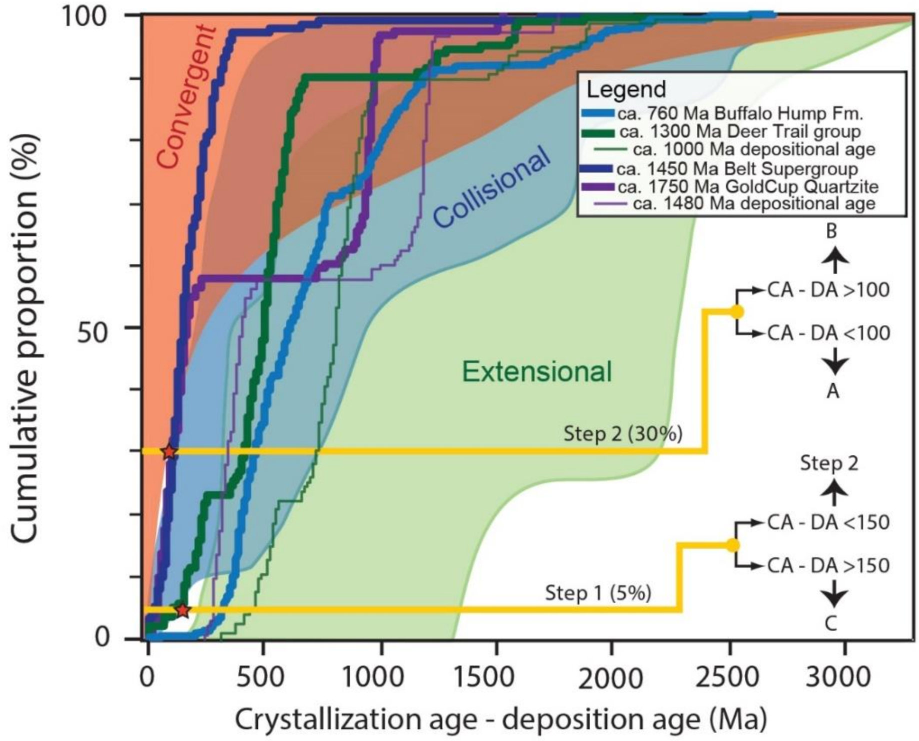

Fig. 7.3: Cumulative proportion curves of the general fields the variation of the difference between the measured crystallization age for a detrital zircon grain, and the depositional age of the succession in which it occurs for convergent, collisional, and extensional basins (from Cawood et al., 2012). Plotted curves show the strata investigated in this work, with the Gold Cup Quartzite in purple, Belt Supergroup in dark blue, Deer Trail Group in green, and Buffalo Hump Formation in light blue. For the Gold Cup Quartzite and Deer Trail Group, whose depositional ages are only broadly constrained, the maximum depositional age approximated by the youngest detrital zircon population is the thicker line, and potential younger minimum depositional ages are plotted as the same color but thinner lines.

Importantly, deposition of the Buffalo Hump Formation during Rodinia rifting, not assembly, along with the accompanying detrital zircon populations in the Buffalo Hump Formation indicates that its detrital zircon components came from eastern/southeastern Laurentia including the Grenville and intervening provinces. This detritus was likely carried via pancontinental fluvial systems that drained the Grenville orogeny as is suggested for other Neoproterozoic western, and northern Laurentia strata that contain similar detrital zircon age-components (e.g. Rainbird et al., 1992;

2017, Yonkee et al., 2014). During the Neoproterozoic–Cambrian Sauk transgression, many stratigraphic sections along the western U.S. Laurentian margin, record a provenance shift (often roughly correlated with the Neoproterozoic/Cambrian boundary, e.g. Linde et al., 2014) involving abundant ca. 1200–1000 Ma detrital zircon grains to their absence. Despite the widespread nature of this provenance shift, a tectonic mechanism and an understanding of how these Laurentian-wide provenance trends relate to Rodinia breakup processes was lacking.

In Chapter 6, a compilation of Stenian (ca. 1200–1000 Ma) zircon (detrital and igneous) U/Pb and Lu/Hf values were compiled and statistically compared. The results indicated that while eastern Laurentian Grenville province sources are the most likely source for Stenian detrital zircon grains in Tonian and Cyrogenian strata (like the Buffalo Hump Formation), more southern Llano Inlier and Wichita province sources are a better match for Stenian detrital zircon grains in Ediacaran strata. The trends also suggest that the eventual loss of far-travelled Stenian detrital zircon age-components progressed from north to south (Idaho to Arizona) from ca. 540 to 510 Ma. Consequently, these new results suggest that the generally north to south opening of the Iapetus Ocean along the eastern margin of Laurentia (near the center of Rodinia) results in the migration of a drainage divide from eastern to southern to the midcontinent of Laurentia, known as the Transcontinental Arch (e.g. Sloss, 1988). Importantly, this tectonic model provides a mechanism for the signification continent-scale shifts in Laurentian sedimentary systems during Rodinia breakup, and further emphasizes that the eastern and western margins of Laurentia not only differed in character during the assembly of Rodinia (see Chapter 5) but that these margins also differed (perhaps influenced by inheritance of older assembly related features) in character during the breakup of Rodinia.

7.3 From Laurentia assembly to Rodina breakup: A revised early tectonic evolution of the Belt Basin region and its importance for global models

This work provides several important updates to the timing, importance, and correlation of Proterozoic geologic events in the Belt Basin region, some of which were foundational in the proposal of various Precambrian paleographic models and thus have importance that ranges well beyond western Laurentia.

Almost thirty years ago, Link et al., (1993) wrote:

> *"First, the Neihart Quartzite at the base of the Belt (Schieber, 1989a) may be part of a supermature discontinuous quartz sand body (Freeman and Winston,*

1987) that blanketed the craton after the Early Proterozoic assembly of Laurentia (about 1,900 to 1,700 Ma; Hoffman, 1989) and before faulting and subsidence of the Belt Basin (about 1,450 Ma). If the Neihart is a genetically distinct unit, it should be removed from the Belt."

In 1998, Doughty et al., suggested that the Gold Cup Quartzite in the Priest River complex is a western equivalent to the Neihart Quartzite based on similarity in detrital zircon U/Pb ages. Mueller et al., (2016) presented further arguments for an approximately 200 m.y. "pre-Belt" age for the Neihart Quartzite based on additional detrital zircon age result differences between the Neihart Quartzite and the Prichard Formation (lower Belt Supergroup). In the simplest stratigraphic sense, Walter's Law of stratigraphic succession (i.e. any vertical progression of facies is the result of a succession of depositional environments that are laterally juxtaposed to each other; Middleton, 1973) dictates a disconformity between the coarse, pebbly fluvial to nearshore Goldcup Quartzite and the overlying lower slope deposits of the basal (member A) Prichard Formation (Cressman, 1985). This relationship is consistent with the tectonized unconformity contact identified by Doughty and Chamberlain (1998) in the field. The additional detrital zircon U/Pb and Lu/Hf data presented in Chapter 3 further support both these findings, and thus I tend to support the suggestion that the Neihart and Gold Cup quartzites both be "removed from the Belt" indicating that the unconformity between lower Belt strata and these pre-Belt quartzites may represent a significant ~300–200 Myr duration. I encourage further work on the physical, temporal and tectonostratigraphic relationships of the allegedly lower Belt equivalents within the Helena embayment (see Mueller et al., 2016). None of the detrital zircon components within these units suggest a non-Laurentian provenance, and consequently the strata in the Belt Basin region do not require Nuna assembly prior to ca. 1750 Ma, and are permissible with models (e.g. Nordsvan et al., 2018) of a later 1650–1600 Ma final Nuna assembly.

It has been long recognized that the source region of the western Belt Basin lay to the west of the basin and was removed by subsequent rifting (Ross et al., 1992). Detrital zircon studies of western Belt Basin strata revealed that this source terrane was primarily comprised of ca. 1700–1500 Ma rocks, including ca. 1610–1490 Ma "North American Magmatic Gap" ages, which are rare in Laurentia, but abundant in southeastern Australia, establishing early ties between these two regions during the Mesoproterozoic (Ross and Villeneuve, 2003). However, identification of other ca.

1590–1550 Ma "North American Magmatic Gap" granitoids in East Antarctica (Goodge et al., 2017), south China (Xu et al., 2019), and within the Belt Basin region itself (e.g. Evans and Fischer, 1986) brought into doubt the uniqueness of the western Belt Basin, southeastern Australia provenance tie. However, currently only the Gawler Craton of southeastern Australia contains ca. 1590–1550 Ma granitoid sources (Reid and Payne, 2017) that match the juvenile Lu/Hf values of the similar-age zircon grains found within the western Belt Basin (Fig. 7.2; see Chapters 2 and 3). Further testing of this relationship by other detrital phases (e.g. rutile, monazite) may yield interesting results into the tectonic setting of this relationship (e.g. Pereira et al., 2020). The similar timing, and proposed genetic relationship between ca. 1580 Ma magmatism in the Priest River region, and coeval magmatism in southeastern Australia, suggest that these two regions may have been adjacent to each other within Nuna by ca. 1580 Ma, consistent with paleomagnetic constraints (see Fig. 7.5; Kirscher et al., 2019).

The absence of juvenile (εHf > +5) ca. 1700–1500 Ma detrital zircon grains within ca. 1450 Ma successions on Hainan Island of south China, means that the detrital zircon provenance rationalization for featuring Hainan Island (Xu et al., 2019), and sometimes the entire Cathasia block (e.g. Yao et al., 2017) between the Belt Basin and SE Australia within Nuna is not strongly justified. However, the sample size (21 zircon grains, Xu et al., 2019) from ca. 1450 Ma Hainan Island strata that include Lu/Hf data is relatively small and additional analysis may refine this assertion. Other evidence commonly used to justify the central location of Hainan Island and the Cathaysia block in Nuna, such as correlating ca. 1450 Ma felsic magmatism on Hainan Island with the ca. 1500–1350 Ma Granite-Rhyolite province of southern Laurentia (Li et al., 2008b) is permissible. Magmatism at this time was generally widespread along the margin of Nuna, with coeval magmatism recognized in other cratons like Baltica, Amazonia, and India (e.g. Johansson et al., 2022; Sequeira et al., 2022).

Many of the Paleoproterozoic to early Mesoproterozoic correlations discussed above and in prior chapters of this work were incorporated into early reconstructions of supercontinent Rodinia (e.g. Bell and Jefferson, 1987; Moores et al., 1991; Dalziel, 1991; Hoffman, 1991). Thus, at least some of the evidence for a Neoproterozoic SWEAT-like **Rodinia** connection was, in fact, evidence of a Mesoproterozoic (proto-) SWEAT-like **Nuna** connection. In part, the apparent absence of Young et al.'s (1979) "succession B" or Grenville-age (ca. 1200–1000 Ma) strata between ca. 1480–1380 Ma Belt and < 720 Ma Windermere Supergroup strata in the Belt Basin region (see

Link et al., 1993), led many of these early models to advocate a long-lived relative tectonic relationship between Australia and western Laurentia during the Mesoproterozoic to Neoproterozoic. However, other subsequent models (such as the missing-Link; Li et al., 1995; 2002; 2013) rather advocated for a complete Wilson cycle (e.g. opening and closing of an ocean basin) along western Laurentia during Grenville-time. One line of reasoning to support this model was the alleged presence of "succession B" or Grenville-age (ca. 1200–1000 Ma) orogenesis and foreland basin strata recorded within the Buffalo Hump Formation along the western edge of the Belt Basin. Consequently, this thesis took a critical look at the geologic record of a potential western Grenville-age orogen within the Belt Basin region, which until this work (Chapter 3, 4, and 5) was not vigorously tested.

In Chapter 5, the speculated South China-derived ca. 1100–1000 Ma foreland basin deposit within the Buffalo Hump Formation (Li et al., 1995; 2002; Yao et al., 2017) was investigated. While, the Buffalo Hump Formations' coarse nature, and conglomeratic horizons did indeed suggest proximal uplift during its deposition, the small yet significant ca. 760 Ma detrital zircon population, and regional stratigraphic relations, indicated that the Buffalo Hump Formation was not an exotically derived Grenville-age orogenic deposit. Instead, the Buffalo Hump Formation is a Laurentian sourced ca. 760–720 Ma rift basin deposit. The unconformably underlying Deer Trail Group strata (see Chapter 3), could possibly be ca. 1200–1000 Ma in age, given that they contain a ca. 1300 Ma youngest detrital zircon population. However, Deer Trail strata lack Grenville-age detritus but otherwise exhibit a clear Laurentian provenance signature. Additionally, their fine-grained siliciclastic and carbonate nature precludes adjacent significant uplift. Thus, if the Deer Trail Group is Grenville in age, they are also inconsistent with a proximal orogen and rather suggest a period of extension within the region.

In Chapter 4, the ca. 1400–1000 Ma garnets reported from the Clearwater complex (Zirakparvar et al., 2010; Neishem et al., 2012) and their potential record of a Grenville-age orogen was also investigated. The new monazite U/Pb results support the occurrence of two main metamorphic events, an older ca. 1380–1330 Ma event, and younger ca. 1100–1060 Ma event. The older event was widely recorded in monazite U/Pb ages but only locally resulted in garnet growth, consistent with a lower pressure, higher temperature event. This event likely relates to similar-age hydrothermal zircon growth (see section 2.5.6) and magmatism within the Belt Basin.

These results are consistent with previous interpretations of ca. 1380–1330 Ma being a period of magmatism and renewed rifting within the Belt Basin (Doughty and Chamberlain, 1996) and do not require orogenic thickening. However, the Pressure-Temperature-time constraints suggest that the younger ca. 1100–1060 Ma event recorded burial of middle Belt Supergroup strata (Piegan Group) to depths of at least ~17–22 km along a moderately-high average geothermal gradient. Elsewhere in Laurentia at this time, similar age geology records mantle/thermal upwelling, intraplate volcanism, reactivation of crustal weaknesses and extension such as within the 1110–1085 Ma Midcontinent Rift (e.g. Swanson-Hysell et al., 2018), 1115–1078 Ma Pikes Peak batholith (Guitreau et al., 2016), 1094–1080 Ma Southwestern Laurentian Large Igneous Province (Timmons et al., 2001; Bright et al., 2014), and 1090–1040 Ma Bylot and correlative basins in northern Laurentia (Greenman et al., 2021; see Fig. 4.2).

Consequently, thermal upwelling and reactivation of crustal weaknesses within the Belt Basin likely contributed to the ca. 1100–1060 Ma metamorphism. However, there is an approximately 6 km discrepancy between the calculated burial depth, and the preserved thickness of overlying units, suggesting either A) a component of tectonic burial, likely through localized inversion of the Belt Basin, and related burial of Belt strata in the Clearwater region or B) miscalculation of Belt Supergroup and perhaps Deer Trail Group stratigraphic thickness and/or subsequent erosion. However, if calculated pressures do reflect tectonic burial, this tectonism was amagmatic, localized, associated with syndepositional Belt Basin structures, and produced very little (to no) preserved sedimentation. Thus, of the multiple working models presented in Chapter 4, transpressional/transtensional mechanism, rather than subduction-driven continent-continent collisional orogenic tectonic mechanism may be more likely. Importantly, after the termination of this metamorphic event around ca. 1060 Ma, there is no record of any magmatism and/or tectonism in the Belt Basin region until the intrusion of the Gun Barrel dyke swarm around 780 Ma (Harlan et al., 2003). In the Belt Basin region, recalibration of the Buffalo Hump Formation (see Chapter 5) indicates that ca. 780 Ma dyke intrusion was followed by widespread but localized rift-basin development from ca. 760–720 that correlates to other localized Laurentian basins. Collectively, these "CHUMP-B" basins reflect early Rodinia breakup (e.g. Dehler et al., 2017; Chapter 5). As discussed in Chapters 5 and 6, in the Belt Basin region, intermittent Cryogenian–Cambrian sedimentation was likely influenced by local rift structure/timing as well as Laurentian-scale drainage divide migrations associated with circum-Laurentia rifting. Importantly, Neoproterozoic–Cambrian strata in the Belt Basin region record final rifting and breakup in the late Ediacaran–early Cambrian (Lund et al., 2010; Lund and Cheney, 2016; Brennan et al., 2020; 2022).

This revised geologic record (Fig. 7.4) is difficult to reconcile with a SWEAT-like (e.g. Moores, 1991; Merdith et al., 2017) configuration which places southeastern Australia, and its record of mantle plume and rifting activity as early as 830 Ma, as a direction conjugate to Belt region within Rodinia. A Missing-Link configuration (Li et al., 1995; 2013) which was initially proposed to alleviate some of the same discrepancies with a SWEAT configured Rodinia, highlighted above, instead places South China, and its significant ca. 1300–900 Ma Grenville-age orogenesis (Li et al., 1995; 2007), widespread ca. 950–830 Ma volcanism (Yao et al., 2019), and record of rifting as early as 850 Ma (Li et al., 2008) directly conjugate to the Belt region within Rodinia. Thus, a Missing-Link configuration, with South China adjacent to the Belt Basin region of Laurentia near the center of Rodinia, is also not a perfect fit for allegedly adjacent regional geologic histories. Recently, an external or peripheral location of South China within Rodinia is often advocated due to South China's Neoproterozoic tectonostratigraphic similarity with India (e.g. Cawood et al., 2013) and some paleomagnetic constraints (Park et al., 2021; Chang et al., 2022).

As a result, the regional geologic constraints discussed and redefined throughout this thesis highlights issues with both of the most commonly applied Rodinia models, and echos the ethos of recent paleomagnetic reconstructions that also indicate a tight-fitting SWEAT or Missing-Link configuration may be untenable within Rodinia (Eyster et al., 2020; Park et al., 2021; Swanson-Hysell, 2021; Chang et al., 2022). Consequently, perhaps neither southeastern Australia, nor South China were directly adjacent to the Belt Basin region within Rodinia. As speculated in Chapter 5, widespread, perhaps multiphase ca. 760–540 Ma rifting and passive margin sequences along most of western Laurentia may instead reflect the rifting of other smaller blocks (recent work suggests Tasmania or Tarim may be suitable candidates) or yet-to-be identified ribbon continents (e.g. Mulder et al., 2020; Jing et al., 2021), rather than a single protracted rifting event between Laurentia and eastern Australia or Laurentia and South China (see Fig. 7.5).

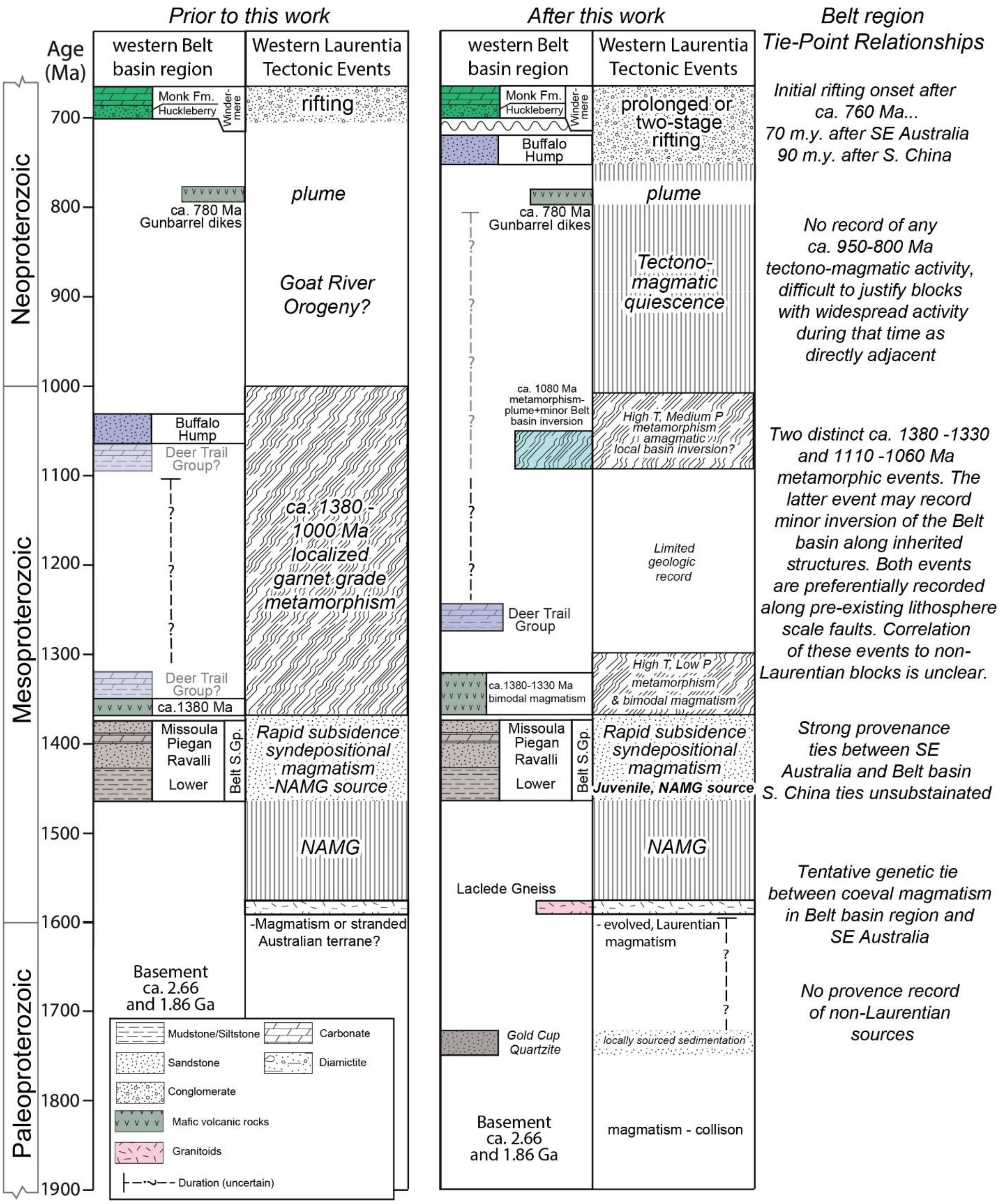

Fig. 7.4: Left: Time-space diagram for the Paleo–Neoproterozoic geology and corresponding tectonic events of the western Belt basin region (northeastern Washington and northern Idaho, USA), and major western Laurentian tectonic events (ca. 2018) prior to the onset of this work. Center: The revised Time-space diagram for the western Belt basin region resulting from the data and conclusions presented in this work. Right: Summary of the tie-point relationships of the Belt basin region and their importance for paleogeographic tectonic reconstructions.

Although hardly proven, reconsidering the "Missing-Link" model (Li et al., 1995) for a more a peripheral location of South China within Rodinia does imply significant geodynamic implications for Rodinia breakup. Importantly, Li et al., (1999; 2008) speculate that Rodinia breakup began around ca. 825 Ma via a superplume centered beneath the supercontinent. In this model, the superplume event was best recorded in the ca. 830–820 Ma plume and rifting record of a centrally placed South China block. Thus, alternative models that argue for a peripheral location of South China within Rodinia (e.g. Park et al., 2021; Chang et al., 2022; Wang et al., 2020) instead suggest that supercontinent breakup initiated mostly along the margins of the supercontinent landmass. Consequently, these later models instead imply that circum-supercontinent subduction processes, such as subduction retreat and more localized mantle upwelling were more key drivers of Rodinia breakup than a proposed central superplume event (c.f. Cawood et al., 2016; Li et al., 2008).

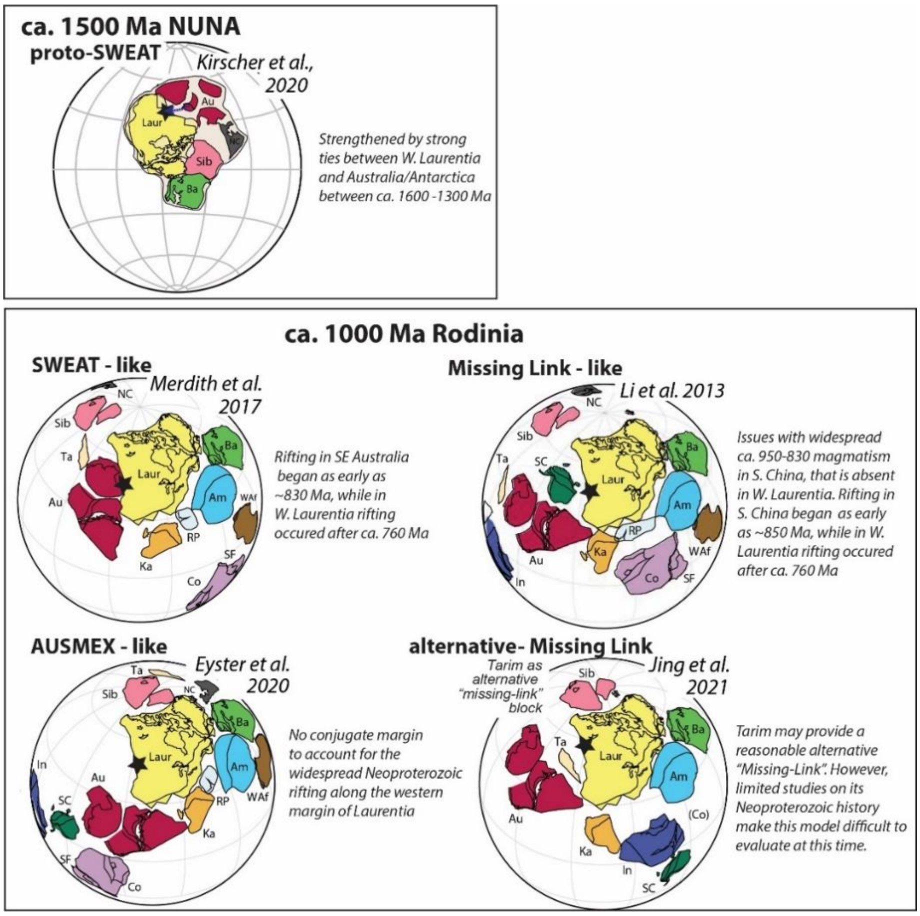

Fig. 7.5: Growing consensus Nuna and debated Rodinia models. The location of the Belt basin region is indicated by the black star in each reconstruction. Figure adapted from Evans (2021 and references within). Abbreviations include: Am, Amazonia; Au, Australian cratons including Antarctic Mawsonland; Ba, Baltica; Co, Congo; In, India; Ka, Kalahari; Laur, Laurentia; NC, North China; RP, Rio Plata; SC, South China; SF, Sao Francisco; Sib, Siberia; Ta, Tarim; WAf, West African craton.

Collectively, the redefined tectonic history of the Belt Basin region strengthens models of a (proto-) SWEAT configured Nuna supercontinent from ca. 1600–1300 Ma (Kirscher et al., 2020) but identified tectonostratigraphic issues with these same regions as directly conjugate rift margins within subsequent supercontinent Rodinia (Fig. 7.5). I also emphasize that some of the original SWEAT correlations made in support of early Rodinia models (Moores, 1991; Dalziel, 1991; Hoffman, 1991), such as western derived detritus in the Mesoproterozoic Belt Basin, instead support a (proto) SWEAT-like relationship during Nuna-time. On the other hand, several of the foundational assertions that the Missing-Link model relied upon, such as the shared provenance between Hainan Island and the Belt Basin and Buffalo Hump Formation, (Li et al., 1995; 2008; Yao et al., 2017), considering new data are worth re-evaluating. However, it is worth noting that a Missing-Link configuration, notably the significant ca. 1300–900 Ma Grenville-age orogenesis and Neoproterozoic plume record in South China (e.g. Li et al., 1995; 2008), does perhaps provide the most compatible geologic record to reconcile the aforementioned differences with a SWEAT-like configured Rodinia.

Consequently, while the value and importance of global tectonic models for understanding and predicting fundamental earth processes is undeniable, it is clear that after more than 30 years of focused research, a clear consensus on Proterozoic paleogeography is still lacking. Thus, I respectfully submit that the work of this thesis espouses the foundational tenet that scientific progress requires that all viable models remain open to observation-driven modification and refinement. With anticipation, openness, and humility, I look forward to new observations testing, refining and perhaps refuting the interpretations I present here.

7.4 References

Geological Society of American reference style

Aleinikoff, J.N., Slack, J.F., Lund, K., Evans, K. V., Fanning, C.M., Mazdab, F.K., Wooden, J.L., and Pillers, R.M., 2012, Constraints on the Timing of Co-Cu Au Mineralization in the Blackbird District, Idaho, Using SHRIMP U-Pb Ages of Monazite and Xenotime Plus Zircon Ages of Related Mesoproterozoic Orthogneisses and Metasedimentary Rocks: Economic Geology, v. 107, p. 1143–1175, doi:10.2113/econgeo.107.6.1143.

Bookstrom, A.A., Box, S.E., Cossette, P.M., Frost, T.P., Gillerman, V.S., King, G.R., and Zirakparvar, N.A., 2016, Geologic history of the Blackbird Co-Cu district in the

Lemhi subbasin of the Belt-Purcell Basin: Geological Society of American Special Paper, v. 522, p. 185–219, doi:10.1130/2016.2522(08).

Bouvier, A., Vervoort, J.D., and Patchett, P.J., 2008, The Lu-Hf and Sm-Nd isotopic composition of CHUR: Constraints from unequilibrated chondrites and implications for the bulk composition of terrestrial planets: Earth and Planetary Science Letters, v. 273, p. 48–57, doi:10.1016/j.epsl.2008.06.010.

Box, S.E., Pritchard, C., Stephens, T.S., and O’Sullivan, P.B., 2020, Between the supercontinents -- Mesoproterozoic Deer Trail Group, an intermediate age unit between the Mesoproterozoic Belt-Purcell Supergroup and the Neoproterozoic Windermere Supergroup in northeastern Washington, U.S.A.: Canadian Journal of Earth Sciences, v. 17, p. 1–17, doi:10.1139/cjes-2019-0188.

Brennan, D.T., Pearson, D.M., Link, P.K., and Chamberlain, K.R., 2020, Neoproterozoic Windermere Supergroup near Bayhorse, Idaho: late-stage Rodinian rifting was deflected west around the Belt basin: Tectonics, doi:10.1029/2020tc006145.

Brennan, D.T., Brian Mahoney, J., Li, Z.X., Link, P.K., Evans, N.J., and Johnson, T.E., 2021, Detrital zircon U–Pb and Hf signatures of Paleo-Mesoproterozoic strata in the Priest River region, northwestern USA: A record of Laurentia assembly and Nuna tenure: Precambrian Research, v. 367, p. 106445, doi:10.1016/j.precamres.2021. 106445.

Bright, R.M., Amato, J.M., Denyszyn, S.W., and Ernst, R.E., 2014, U-Pb geochronology of 1.1 Ga diabase in the southwestern United States: Testing models for the origin of a post-Grenville large igneous province: Lithosphere, v. 6, p. 135–156, doi:10.1130/L335.1.

Cawood, P.A., Hawkesworth, C.J., and Dhuime, B., 2012, Detrital zircon record and tectonic setting: Geology, v. 40, p. 875–878, doi:10.1130/G32945.1.

Cawood, P. A., Wang, Y., Xu, Y., and Zhao, G., 2013, Locating South China in Rodinia and Gondwana: A fragment of greater India lithosphere? Geology, v. 41, no. 8, p. 903–906. https://doi.org/10.1130/G34395.1

Cawood, P. A., Strachan, R. A., Pisarevsky, S. A., Gladkochub, D. P., & Murphy, J. B., 2016, Linking collisional and accretionary orogens during Rodinia assembly and breakup: Implications for models of supercontinent cycles: Earth and Planetary Science Letters, no. 449, p. 118–126. https://doi.org/10.1016/j.epsl.2016.05.049

Chapman, N.D., Ferguson, M., Meffre, S.J., Stepanov, A., Maas, R., and Ehrig, K.J., 2019, Pb-isotopic constraints on the source of A-type Suites: Insights from the Hiltaba Suite - Gawler Range Volcanics Magmatic Event, Gawler Craton, South Australia: Lithos, v. 346–347, p. 105156, doi:10.1016/j.lithos.2019.105156.

Chang, L., Zhang, S., Li, H., Xian, H., and Wu, H., 2022, New Paleomagnetic Insights Into the Neoproterozoic Connection Between South China and India and Their Position in Rodinia: Geophysical Research Letters, vol. 49 p. 1–11, doi:10.1029/ 2022GL098348.

Cressman, E.R., 1985, The Prichard Formation of the lowest part of the Belt Supergroup (middle Proterozoic) near Plains, Sanders County, Montana: US Geological Survey Bulletin, v. 1553.

Dalziel, I.W.D., 1991, Pacific margins of Laurentia and East Antarctica-Australia as a conjugate rift pair: evidence and implications for an Eocambrian supercontinent: Geology, v. 19, p. 598–601, doi:10.1130/0091-7613(1991) 019<0598:PMOLAE>2.3.CO;2.

Dehler, C., Gehrels, G., Porter, S., Heizler, M., Karlstrom, K., Cox, G., Crossey, L., and Timmons, M., 2017, Synthesis of the 780-740 ma chuar, Uinta Mountain, and Pahrump (ChUMP) groups, western USA: Implications for laurentia-wide cratonic marine basins: Bulletin of the Geological Society of America, v. 129, p. 607–624, doi:10.1130/B31532.1.

Doughty, P.T., and Chamberlain, K.R., 2008, Protolith age and timing of Precambrian magmatic and metamorphic events in the Priest River complex, northern Rockies: Canadian Journal of Earth Sciences, v. 45, p. 99–116, doi:10.1139/e07-067.

Evans, K. V., and Fischer, L.B., 1986, U-Pb geochronology of two augen gneiss terranes, Idaho-new data and tectonic implications two augen gneiss terranes, Idaho-new data and tectonic implications: Canadian Journal of Earth Sciences, v. 23, p. 1919–1927, doi:10.1016/0148-9062(76)90561-1.

Evans, K. V, Aleinikoff, J.N., Obradovich, J.D., and Fanning, C.M., 2000, SHRIMP U-Pb geochronology of volcanic rocks, Belt Supergroup, western Montana: evidence for rapid deposition of sedimentary strata: Canadian Journal of Earth Sciences, v. 37, p. 1287–1300, doi:10.1139/e00-036.

Eyster, A., Weiss, B.P., Karlstrom, K., and Macdonald, F.A., 2020, Paleomagnetism of the Chuar Group and evaluation of the late Tonian Laurentian apparent polar wander path with implications for the makeup and breakup of Rodinia: Bulletin of the Geological Society of America, v. 132, p. 710–738, doi:10.1130/B32012.1.

Foster, D.A., Mueller, P.A., Mogk, D.W., Wooden, J.L., and Vogl, J.J., 2006, Proterozoic evolution of the western margin of the Wyoming craton: Implications for the tectonic and magmatic evolution of the northern Rocky Mountains: Canadian Journal of Earth Sciences, v. 43, p. 1601–1619, doi:10.1139/E06-052.

Furlanetto, F., Thorkelson, D.J., Rainbird, R.H., Davis, W.J., Gibson, H.D., and Marshall, D.D., 2016, The Paleoproterozoic Wernecke Supergroup of Yukon, Canada: Relationships to orogeny in northwestern Laurentia and basins in North America, East Australia, and China: Gondwana Research, v. 39, p. 14–40, doi:10.1016/j.gr.2016.06.007.

Gibson, G.M., and Champion, D.C., 2019, Antipodean fugitive terranes in southern Laurentia: How Proterozoic Australia built the American West: Lithosphere, v. 11, p. 551–559, doi:10.1130/L1072.

Gifford, J., Malone, S., and Mueller, P., 2020, The Medicine Hat Block and the Early Paleoproterozoic Assembly of Western Laurentia: Geosciences, v. 10, p. 271, doi:10.3390/geosciences10070271.

Goodge, J.W., Fanning, C.M., Fisher, C.M., Vervoort, J.D., and Fisher, C.M., 2017, Proterozoic crustal evolution of central East Antarctica: Age and isotopic evidence from glacial igneous clasts, and links with Australia and Laurentia: Precambrian Research, v. 299, p. 151–176, doi:10.1016/j.precamres.2017.07.026.

Greenman, J.W., Rooney, A.D., Patzke, M., Ielpi, A., and Halverson, G.P., 2021, Re-Os geochronology highlights widespread latest Mesoproterozoic (ca. 1090–1050 Ma) cratonic basin development on northern Laurentia: Geology, v. 49, p. 779–783, doi:10.1130/g48521.1.

Guitreau, M., Mukasa, S.B., Blichert-Toft, J., and Fahnestock, M.F., 2016, Pikes Peak batholith (Colorado, USA) revisited: A SIMS and LA-ICP-MS study of zircon U-Pb ages combined with solution Hf isotopic compositions: Precambrian Research, v. 280, p. 179–194, doi:10.1016/j.precamres.2016.05.001.

Harlan, S.S., Heaman, L., LeCheminant, A.N., and Premo, W.R., 2003, Gunbarrel mafic magmatic event: A key 780 Ma time marker for Rodinia plate reconstructions: Geology, v. 31, p. 1053–1056, doi:10.1130/G19944.1.

Hoffman, P.F., 1991, Did the breakup of Laurentia turn Gondwanaland inside out? Science, v. 252, p. 1409–1411.

Holland, M.E., Grambling, T.A., Karlstrom, K.E., Jones, J. V., Nagotko, K.N., and Daniel, C.G., 2020, Geochronologic and Hf-isotope framework of Proterozoic rocks from central New Mexico, USA: Formation of the Mazatzal crustal province in an extended continental margin arc: Precambrian Research, v. 347, p. 105820, doi:10.1016/j.precamres.2020.105820.

Johansson, Å. et al., 2022, A geochronological review of magmatism along the external margin of Columbia and in the Grenville-age orogens forming the core of Rodinia: Precambrian Research, v. 371, doi:10.1016/j.precamres.2021.106463.

Karlstrom, K.E., Harlan, S.S., Williams, M.L., McLelland, J., Geissman, J.W., and Ahall, K., 1999, Refining Rodinia: Geological evidence for the Australia–Western U.S. connection in the Proterozoic: GSA Today, v. 9, no. 10, p. 1–7.

Kirscher, U., Liu, Y., Li, Z.X., Mitchell, R.N., Pisarevsky, S.A., Denyszyn, S.W., and Nordsvan, A., 2019, Paleomagnetism of the Hart Dolerite (Kimberley, Western Australia) – A two-stage assembly of the supercontinent Nuna? Precambrian Research, doi:10.1016/j.precamres.2018.12.026.

Kirscher, U., Mitchell, R.N., Liu, Y., Nordsvan, A.R., Cox, G.M., Pisarevsky, S.A., Wang, C., Wu, L., Murphy, J.B., and Li, Z.-X., 2021, Paleomagnetic constraints on the duration of the Australia-Laurentia connection in the core of the Nuna supercontinent: Geology, v. 49, p. 1–6, doi:10.1130/g47823.1.

Lewis, R.S., Vervoort, J.D., Burmester, R.F., McClelland, W.C., and Chang, Z., 2007, Geochronological constraints on Mesoproterozoic and Neoproterozoic (?) high-grade metasedimentary rocks of north-central Idaho, U.S.A.: SEPM, v. 86, p. 37–53.

Lewis, R.S., Burmester, R.F., Breckenridge, R.M., Mcfaddan, M.D., and Phillips, W.M., 2020, Geologic Map of the Sandpoint 30´ x 60´ Quadrangle, Idaho and Montana, and the Idaho Part of the Chewelah 30´ x 60´ Quadrangle: Idaho Geological Survey, Digital Web Map 183.

Li, Z.X., Li, X.H., Kinny, P.D., and Wang, J., 1999, The breakup of Rodinia: Did it start with a mantle plume beneath South China? Earth and Planetary Science Letters, v. 173, p. 171–181, doi:10.1016/S0012-821X(99)00240-X.

Li, Z.X., Li, X.H., Zhou, H., and Kinny, P.D., 2002, Grenvillian continental collision in South China: New SHRIMP U-Pb zircon results and implications for the configuration of Rodinia: Geology, v. 30, p. 163–166, doi:10.1130/0091-7613(2002)030<0163:GCCISC>2.0.CO;2.

Li, Z.X., Wartho, J.A., Occhipinti, S., Zhang, C.L., Li, X.H., Wang, J., and Bao, C., 2007, Early history of the eastern Sibao Orogen (South China) during the assembly of Rodinia: New mica 40Ar/39Ar dating and SHRIMP U-Pb detrital zircon provenance constraints: Precambrian Research, v. 159, p. 79–94, doi:10.1016/j.precamres.2007.05.003.

Li, Z.X. et al., 2008, Assembly, configuration, and break-up history of Rodinia: A synthesis: Precambrian Research, v. 160, p. 179–210, doi:10.1016/j.precamres.2007.04.021.

Li, Z.X., Li, X.H., Li, W.X., and Ding, S., 2008b, Was Cathaysia part of Proterozoic Laurentia? - New data from Hainan Island, South China: Terra Nova, v. 20, p. 154–164, doi:10.1111/j.1365-3121.2008.00802.x.

Li, Z.X., Evans, D.A.D., and Halverson, G.P., 2013, Neoproterozoic glaciations in a revised global palaeogeography from the breakup of Rodinia to the assembly of Gondwanaland: Sedimentary Geology, v. 294, p. 219–232, doi:10.1016/j.sedgeo.2013.05.016.

Linde, G.M., Cashman, P.H., Trexler, J.H., and Dickinson, W.R., 2014, Stratigraphic trends in detrital zircon geochronology of upper Neoproterozoic and Cambrian strata, Osgood Mountains, Nevada, and elsewhere in the Cordilleran miogeocline: Evidence for early Cambrian uplift of the Transcontinental Arch: Geosphere, v. 10, p. 1402–1410, doi:10.1130/GES01048.1.

Link, P.K., Christie-Blick, N., Devlin, W.J., Elston, D.P., Horodyski, R.J., Levy, M., Miller, J.M.G., Pearson, R.C., Prave, A., Stewart, J.H., Winston, D., Wright, L.A., and Wrucke, C.T., 1993, Middle and Late Proterozoic stratified rocks of the western U.S. Cordillera, Colorado Plateau, and Basin and Range Province, in Reed, J.C., Bickford, M.E., Houston, R.S., Link, P.K., Rankin, D.W., Sims, P.K., and Van Schmus, W.R., eds., Precambrian: Conterminous U.S.: Boulder, Geological Society of America, The Geology of North America, v. C-2, p. 463–595.

Lonn, J.D., Burmester, R.F., Lewis, R.S. and McFaddan, M.D., 2020, The Mesoproterozoic Belt Supergroup, in Barth, S., ed., Geology of Montana: Montana Bureau of Mines and Geology Special Publication 122, v. 1, Chapter 1, p 1-38.

Lund, K., and Cheney, E.R., 2016, Correlation of unconformity-bounded sequences of the Neoproterozoic Windermere Supergroup in Idaho, Washington, and southern British Columbia, in Cheney, E.R., ed., The Geology of Washing- ton and Beyond: From Laurentia to Cascadia: Seattle, Washington, University of Washington Press, p. 28–42.

Lund, K., Aleinikoff, J.N., Evans, K. V., duBray, E.A., Dewitt, E.H., and Unruh, D.M., 2010, SHRIMP U-Pb dating of recurrent Cryogenian and Late Cambrian–Early Ordovician alkalic magmatism in central Idaho: Implications for Rodinian rift tectonics: v. 122, 430–453 p., doi:10.1130/B26565.1.

McFarlane, C.R., and Pattison, D.R., 2000, Geology of the Matthew Creek metamorphic zone, southeast British Columbia: a window into Middle Proterozoic metamorphism in the Purcell Basin: Canadian Journal of Earth Sciences, v. 37, p. 1073–1092, doi:10.1139/e00-018.

McMechan, M.E., Price, R.A., 1982. Superimposed low-grade metamorphism in the Mount Fisher area, southeastern British Columbia—implications for the East Kootenay orogeny. Canadian Journal of Earth Sciences, no. 19, p. 476–489. https://doi. org/10.1139/e82-039.

Middleton, G. V., 1973, Johannes Walther's Law of the Correlation of Facies: Geological Society of America Bulletin, v. 84, p. 979–988, doi:10.1130/0016-7606(1973)84<979:JWLOTC>2.0.CO;2.

Miller, F.K., Whipple, J.W., 1989, The Deer Trail Group—Is it part of the Belt Supergroup, in Joseph, N.L., ed., Geologic guidebook for Washington and adjacent areas: Washington Division of Geology and Earth Resources Information Circular 86, p. 1–21.

Moores, E. M., 1991, Southwest U.S.–East Antarctic (SWEAT) connection: A hypothesis: Geology, v. 19, p. 425–428.

Mueller, P.A., Heatherington, A.L., Kelly, D.M., Wooden, J.L., and Mogk, D.W., 2002, Paleoproterozoic crust within the Great Falls tectonic zone: Implications for the assembly of southern Laurentia: Geology, v. 30, p. 127–130, doi:10.1136/jclinpath-2017-204981.

Mueller, P.A., Wooden, J.L., Mogk, D.W., and Foster, D.A., 2011, Paleoproterozoic evolution of the Farmington zone: Implications for terrane accretion in southwestern Laurentia: Lithosphere, v. 3, p. 401–408, doi:10.1130/L161.1.

Mueller, P., Mogk, D., Wooden, J., and Spake, D., 2016, U-Pb ages of zircons from the Lower Belt Supergroup and proximal crystalline basement: Implications for the early evolution of the Belt Basin: Geological Society of America Special Paper, v. 522, p. 1–21, doi:10.1130/2016.2522(11).

Mulder, J.A., Everard, J.L., Cumming, G., Meffre, S., Bottrill, R.S., Merdith, A.S., Halpin, J.A., McNeill, A.W., and Cawood, P.A., 2020, Neoproterozoic opening of the

Pacific Ocean recorded by multi-stage rifting in Tasmania, Australia: Earth-Science Reviews, v. 201, doi:10.1016/j.earscirev.2019.103041.

Nesheim, T.O., Vervoort, J.D., McClelland, W.C., Gilotti, J.A., and Lang, H.M., 2012, Mesoproterozoic syntectonic garnet within Belt Supergroup metamorphic tectonites: Evidence of Grenville-age metamorphism and deformation along northwest Laurentia: Lithos, v. 134–135, p. 91–107, doi:10.1016/j.lithos.2011.12.008.

Nordsvan, A.R., Collins, W.J., Li, Z., Spencer, C.J., Pourteau, A., Withnall, I.W., Betts, P.G., and Volante, S., 2018, Laurentian crust in northeast Australia: Implications for the assembly of the supercontinent Nuna: Geology, v. 46, p. 251–254, https://doi.org/10.1130/G39980.1.

Park, Y., Swanson-Hysell, N.L., Xian, H., Zhang, S., Condon, D.J., Fu, H., and Macdonald, F.A., 2021, A Consistently High-Latitude South China From 820 to 780 Ma: Implications for Exclusion From Rodinia and the Feasibility of Large-Scale True Polar Wander: Journal of Geophysical Research: Solid Earth, v. 126, p. 1–29, doi:10.1029/2020JB021541.

Pattison, D.R.M., and Seitz, J.L.D., 2012, Stabilization of garnet in metamorphosed altered turbidites near the St. Eugene lead-zinc deposit, southeastern British Columbia: Equilibrium and kinetic controls: Lithos, v. 134–135, p. 221–235, doi:10.1016/j.lithos.2011.12.007.

Pereira, I., Storey, C.D., Strachan, R.A., Bento dos Santos, T., and Darling, J.R., 2020, Detrital rutile ages can deduce the tectonic setting of sedimentary basins: Earth and Planetary Science Letters, v. 537, p. 116193, doi:10.1016/j.epsl.2020.116193.

Rainbird, R. H., Heaman, L. M., and Young, G., 1992, Sampling Laurentia: detrital zircon geochronology offers evidence for an extensive Neoproterozoic river system originating from the Grenville orogen. Geology, v. 20, no. 4, p.351–354. https://doi.org/10.1130/0091-7613(1992)020<0351:SLDZGO>2.3.CO;2

Rainbird, R. H., Rayner, N. M., Hadlari, T., Heaman, L. M., Ielpi, A., Turner, E. C., and MacNaughton, R. B., 2017, Zircon provenance data record the lateral extent of pancontinental, early Neoproterozoic rivers and erosional unroofing history of the Grenville orogen. Geological Society of America Bulletin, v. 129, no. 11–12, p. 1408–1423. https://doi.org/10.1130/B31695.1

Reid, A.J., and Payne, J.L., 2017, Magmatic zircon Lu–Hf isotopic record of juvenile addition and crustal reworking in the Gawler Craton, Australia: Lithos, v. 292–293, p. 294–306, doi:10.1016/j.lithos.2017.08.010.

Ross, G.M., and Villeneuve, M., 2003, Provenance of the Mesoproterozoic (1.45 Ga) Belt basin (western North America): Another piece in the pre-Rodinia paleogeographic puzzle: Bulletin of the Geological Society of America, v. 115, p. 1191–1217, doi:10.1130/B25209.1.

Ross, G.M., Parrish, R.R., and Winston, D., 1992, Provenance and UPb geochronology of the Mesoproterozoic Belt Supergroup (northwestern United States): implications for age of deposition and pre-Panthalassa plate reconstructions: Earth and Planetary Science Letters, v. 113, p. 57–76, doi:10.1016/0012-821X(92)90211-D.

Sequeira, N., Bhattacharya, A., and Bell, E., 2022, The ~1.4 Ga A-type granitoids in the "Chottanagpur crustal block" (India), and its relocation from Columbia to Rodinia? Geoscience Frontiers, v. 13, p. 101138, doi:10.1016/j.gsf.2020.12.017.

Swanson-Hysell, N.L., Ramezani, J., Fairchild, L.M., and Rose, I.R., 2018, Failed rifting and fast drifting : Midcontinent Rift development, Laurentia's rapid motion and the driver of Grenvillian orogenesis: Geological Society of America Bulletin, p. 1–28, doi:10.1130/B31944.1/4630143/b31944.pdf.

Swanson-Hysell, N.L., 2021, The Precambrian paleogeography of Laurentia: 109–153 p., doi:10.1016/b978-0-12-818533-9.00009-6.

Timmons, J.M., Karlstrom, K.E., Dehler, C.M., Geissman, J.W., and Heizler, M.T., 2001, Proterozoic multistage (ca. 1.1 and 0.8 Ga) extension recorded in the Grand Canyon Supergroup and establishment of northwest- and north-trending tectonic grains in the southwestern United States: Bulletin of the Geological Society of America, v. 113, p. 163–180, doi:10.1130/0016-7606(2001)113<0163:PMCAGE>2.0.CO;2.

Vervoort, J.D., Lewis, R.S., Fisher, C., Gaschnig, R.M., Jansen, A.C., and Brewer, R., 2016, Neoarchean and Paleoproterozoic crystalline basement rocks of north-central Idaho: Constraints on the formation of western Laurentia: Bulletin of the Geological Society of America, v. 128, p. 94–109, doi:10.1130/B31150.1.

Wang, W., Cawood, P.A., Pandit, M.K., Xia, X., Raveggi, M., Zhao, J., Zheng, J., and Qi, L., 2020, Fragmentation of South China from greater India during the Rodinia-Gondwana transition: Geology, v. 49, p. 228–232, doi:10.1130/g48308.1.

Wang, D., Vervoort, J.D., Fisher, C.M., Lewis, R.S., and Buddington, A., 2022, The Neoarchean and Paleoproterozoic crustal evolution of the Clearwater block, northwestern Laurentia: Implications for the assembly of supercontinents: Precambrian Research, v. 379, p. 106780, doi:10.1016/j.precamres.2022.106780.

Whitmeyer, S.J., and Karlstrom, K.E., 2007, Tectonic model for the Proterozoic growth of North America: Geosphere, v. 3, p. 220–259, doi:10.1130/GES00055.1.

Xu, Y.-J., Cawood, P.A., Zhang, H.-C., Zi, J.-W., Zhou, J.-B., Li, L.-X., and Du, Y.-S., 2019, The Mesoproterozoic Baoban Complex, South China: A missing fragment of western Laurentian lithosphere: GSA Bulletin, p. 1–15, doi:10.1130/b35380.1.

Yao, W., Li, Z.X., Li, W.X., and Li, X.H., 2017, Proterozoic tectonics of Hainan Island in supercontinent cycles: New insights from geochronological and isotopic results: Precambrian Research, v. 290, p. 86–100, doi:10.1016/j.precamres.2017.01.001.

Yao, J., Cawood, P.A., Shu, L., and Zhao, G., 2019, Jiangnan Orogen, South China: A ~970–820 Ma Rodinia margin accretionary belt: Earth-Science Reviews, v. 196, p. 102872, doi:10.1016/j.earscirev.2019.05.016.

Yonkee, W.A., Dehler, C.D., Link, P.K., Balgord, E.A., Keeley, J.A., Hayes, D.S., Wells, M.L., Fanning, C.M., and Johnston, S.M., 2014, Tectono-stratigraphic framework of Neoproterozoic to Cambrian strata, west-central U.S.: Protracted rifting, glaciation, and evolution of the North American Cordilleran margin: Earth-Science Reviews, v. 136, p. 59–95, doi:10.1016/j.earscirev.2014.05.004.

Young, G.M., Jefferson, C.W., Delaney, G.D., and Yeo, G.M., 1979, Middle and late Proterozoic evolution of the northern Canadian Cordillera and Shield: Geology, v. 7, p. 329–330, doi:10.1130/0091-7613(1979)7<329b:CAROMA>2.0.CO;2.

Zirakparvar, N.A., Vervoort, J.D., McClelland, W., and Lewis, R.S., 2010, Insights into the metamorphic evolution of the Belt–Purcell basin; evidence from Lu–Hf garnet geochronology: Canadian Journal of Earth Sciences, v. 47, p. 161–179, doi:10.1139/E10-001.

Zhao, G., Sun, M., Wilde, S.A., and Li, S., 2004, A Paleo-Mesoproterozoic supercontinent: Assembly, growth and breakup: Earth-Science Reviews, v. 67, p. 91–123, doi:10.1016/j.earscirev.2004.02.003.

Appendix A: Statements of Co-Authorship and Copyright Permissions

Appendix A1: Statement of Co-Authorship for Chapter 2

Chapter 2: Closing the "North American Magmatic" Gap: Crustal evolution of the Clearwater Block from multi-isotope and trace element zircon data *published in Precambrian Research*

<table>
<tr><th></th><th>Conceptualization and Design</th><th>Data Acquisition and Method</th><th>Data processing and Visualization</th><th>Interpretation and discussion</th><th>Total contribution (%)</th></tr>
<tr><td>Co-author 1
Daniel T. Brennan</td><td>75</td><td>75</td><td>80</td><td>70</td><td>75</td></tr>
<tr><td colspan="3">Co-author 1 acknowledgement:
I acknowledge that these represent my contribution to the above research output.</td><td colspan="3">Signed:</td></tr>
<tr><td>Co-author 2
Paul K. Link</td><td>15</td><td>-</td><td>5</td><td>10</td><td>7.5</td></tr>
<tr><td colspan="3">Co-author 2 acknowledgement:
I acknowledge that these represent my contribution to the above research output.</td><td colspan="3">Signed:</td></tr>
<tr><td>Co-author 3
Zheng-Xiang Li</td><td>10</td><td>-</td><td>5</td><td>10</td><td>6.25</td></tr>
<tr><td colspan="3">Co-author 3 acknowledgement:
I acknowledge that these represent my contribution to the above research output.</td><td colspan="3">Signed:</td></tr>
<tr><td>Co-author 4
Laure Martin</td><td>-</td><td>15</td><td>5</td><td>-</td><td>5</td></tr>
<tr><td colspan="3">Co-author 4 acknowledgement:
I acknowledge that these represent my contribution to the above research output.</td><td colspan="3">Signed:</td></tr>
<tr><td>Co-author 5
Tim E. Johnson</td><td>-</td><td>-</td><td>-</td><td>10</td><td>2.5</td></tr>
<tr><td colspan="3">Co-author 5 acknowledgement:
I acknowledge that these represent my contribution to the above research output.</td><td colspan="3">Signed:</td></tr>
<tr><td>Co-author 6
Noreen J. Evans</td><td>-</td><td>5</td><td>5</td><td>-</td><td>2.5</td></tr>
<tr><td colspan="3">Co-author 6 acknowledgement:
I acknowledge that these represent my contribution to the above research output.</td><td colspan="3">Signed:</td></tr>
<tr><td>Co-author 7
Jiangyu Li</td><td>-</td><td>5</td><td>-</td><td>-</td><td>1.25</td></tr>
<tr><td colspan="3">Co-author 7 acknowledgement:
I acknowledge that these represent my contribution to the above research output.</td><td colspan="3">Signed:</td></tr>
<tr><td>Total%</td><td>100</td><td>100</td><td>100</td><td>100</td><td>100</td></tr>
</table>

Appendix A2: Statement of Co-Authorship for Chapter 3

Chapter 3: Detrital zircon U-Pb and Hf signatures of Paleo-Mesoproterozoic strata in the Priest River region, northwestern USA: A record of Laurentia assembly and Nuna Tenure *published in Precambrian Research*

	Conceptualization and Design	**Data Acquisition and Method**	**Data processing and Visualization**	**Interpretation and discussion**	**Total contribution (%)**
Co-author 1 Daniel T. Brennan	50	85	85	60	70
Co-author 1 acknowledgement: I acknowledge that these represent my contribution to the above research output.			Signed:		
Co-author 2 J. Brian Mahoney	20	10	10	10	12.5
Co-author 2 acknowledgement: I acknowledge that these represent my contribution to the above research output.			Signed:		
Co-author 3 Zheng-Xiang Li	20	-	-	15	8.75
Co-author 3 acknowledgement: I acknowledge that these represent my contribution to the above research output.			Signed:		
Co-author 4 Paul K. Link	10	-	-	10	5
Co-author 4 acknowledgement: I acknowledge that these represent my contribution to the above research output.			Signed:		
Co-author 5 Noreen J. Evans	-	5	5	-	2.5
Co-author 5 acknowledgement: I acknowledge that these represent my contribution to the above research output.			Signed:		
Co-author 6 Tim E. Johnson	-	-	-	5	1.25
Co-author 6 acknowledgement: I acknowledge that these represent my contribution to the above research output.			Signed:		
Total%	**100**	**100**	**100**	**100**	**100**

Appendix A3: Statement of Co-Authorship for Chapter 5

Chapter 5: Recalibrating Rodinian rifting in the northwestern United States *published in Geology*

	Conceptualization and Design	Data Acquisition and Method	Data processing and Visualization	Interpretation and discussion	Total contribution (%)
Co-author 1 Daniel T. Brennan	70	60	70	60	65
Co-author 1 acknowledgement: I acknowledge that these represent my contribution to the above research output.			Signed:		
Co-author 2 Zheng-Xiang Li	20	-	-	15	8.75
Co-author 2 acknowledgement: I acknowledge that these represent my contribution to the above research output.			Signed:		
Co-author 3 Kai Rankenburg	5	15	10	-	7.5
Co-author 3 acknowledgement: I acknowledge that these represent my contribution to the above research output.			Signed:		
Co-author 4 Noreen Evans	-	15	10	-	6.25
Co-author 4 acknowledgement: I acknowledge that these represent my contribution to the above research output.			Signed:		
Co-author 5 Paul K. Link	5	-	-	10	3.75
Co-author 5 acknowledgement: I acknowledge that these represent my contribution to the above research output.			Signed:		
Co-author 6 Adam Nordsvan	-	-	5	5	2.5
Co-author 6 acknowledgement: I acknowledge that these represent my contribution to the above research output.			Signed:		
Co-author 7 Christopher L. Kirkland	-	5	5	-	2.5
Co-author 7 acknowledgement: I acknowledge that these represent my contribution to the above research output.			Signed:		
Co-author 8 J. Brian Mahoney	-	-	-	5	1.25
Co-author 8 acknowledgement: I acknowledge that these represent my contribution to the above research output.			Signed:		
Co-author 9 Tim Johnson	-	-	-	5	1.25
Co-author 9 acknowledgement: I acknowledge that these represent my contribution to the above research output.			Signed:		
Co-author 10 Bradley J. McDonald	-	5	-	-	1.25
Co-author 10 acknowledgement: I acknowledge that these represent my contribution to the above research output.			Signed:		
Total%	**100**	**100**	**100**	**100**	**100**

Appendix A4: Statement of Co-Authorship for Chapter 6

Chapter 6: A tectonic model for the Transcontinental Arch: Progressive migration of a Laurentian drainage divide during the Neoproterozoic–Cambrian Sauk Transgression *published in Terra Nova*

	Conceptualization and Design	**Data Acquisition and Method**	**Data processing and Visualization**	**Interpretation and discussion**	**Total contribution (%)**
Co-author 1 Daniel T. Brennan	50	80	80	50	65
Co-author 1 acknowledgement: I acknowledge that these represent my contribution to the above research output.			Signed:		
Co-author 2 Ross N. Mitchell	30	10	15	15	17.5
Co-author 2 acknowledgement: I acknowledge that these represent my contribution to the above research output.			Signed:		
Co-author 3 Christopher J. Spencer	10	10	5	15	10
Co-author 3 acknowledgement: I acknowledge that these represent my contribution to the above research output.			Signed:		
Co-author 4 J. Brendan Murphy	10	-	10	10	7.5
Co-author 4 acknowledgement: I acknowledge that these represent my contribution to the above research output.			Signed:		
Co-author 5 Zheng-Xiang Li	-	-	-	10	2.5
Co-author 5 acknowledgement: I acknowledge that these represent my contribution to the above research output.			Signed:		
Total%	**100**	**100** **100**	**100**	**100**	**100**

Appendix A5: Elsevier Copyright Permission

From:	Permissions Helpdesk
To:	Daniel Brennan
Subject:	Re: PhD thesis request to include 2 published papers [220627-004558]
Date:	Tuesday, 28 June 2022 3:49:34 PM

Dear Daniel Brennan

Thank you for your e-mail.

As the author of the articles in the question, you are allowed to include the formatted text in the body and appendix of your thesis. Formal permission is not required. Kindly ensure to credit the original source.

Please go ahead and use them.

Kind regards,

Roopa Lingayath
Senior Copyrights Coordinator
ELSEVIER | HCM - Health Content Management

Visit Elsevier Permissions

From: Administrator
Date: Monday, June 27, 2022 03:38 AM GMT

Dear Customer

Thank you for contacting Elsevier's Permissions Helpdesk.

This is an automated acknowledgement to confirm we have received your query. Ticket number 220627-004558 has been opened on your behalf and we aim to respond within two business days.

Regards,

Permissions Helpdesk

From: Daniel Brennan
Date: Monday, June 27, 2022 03:38 AM GMT

I have two published two chapters of my Ph.D. thesis in Precambrian Research as first author. I reformatted the papers to include them in the body of my thesis. Can I also include the formatted elsevier publications within an appendix of my thesis?

The publications are:
https://doi.org/10.1016/j.precamres.2021.106533
https://doi.org/10.1016/j.precamres.2021.106445

Appendix A6: Geological Society of America Copyright Permission

Author Guidelines

Copyright Information

- "Fair Use" Permission
- Permission Granting and Payment
- License Fees
- Additional Information for Authors
- Open Access Content

GSA obtains copyright ownership from authors of all articles and books. (See "Open Access Content" below, for exceptions.) Works prepared by U.S. government employees in the course of their work are in the public domain, however, and are not copyrighted. It is the responsibility of those requesting permission(s) to determine if an article meets this test and is in the public domain.

Special "Fair Use" permission

If you want to use a single figure, a brief paragraph, or a single table from a GSA publication, GSA considers this to be fair usage, and you need no formal permission and no fees are assessed unless you or your publisher require a formal permission letter. In that case, you should print a copy of this document and present it to your publisher.

An author has the right to use his or her article or a portion of the article in a thesis or dissertation without requesting permission from GSA, provided the bibliographic citation and the GSA copyright credit line are given on the appropriate pages.

Check the permission statement in each publication

Each publication includes a statement of copyright policy for that publication that permits and describes limited usages. These statements are found on the front or back of the title page or the table-of-contents page in the masthead statement. In most cases, these statements grant to individual scientists the right to reproduce a limited number of copies for purposes that further education and/or science, including classroom use. If your usage falls within the statement appearing in the publication in which you are interested, you need no further permission from that usage.

Other usages are also allowed by these statements, with instructions to remit a minimum fee to the Copyright Clearance Center (CCC), along with the ISSN or ISBN number of the publication. Within the U.S., the CCC collects and remits payments to GSA. Other organizations throughout the world are authorized by GSA to collect and remit payments for copyright usage in various countries. If your usage falls within the scope of these usages, please follow our instructions or observe the lawful practice within your country if you are outside the U.S. Please **do not write for permission**.

See also GSA's Open Access Policy .

Permission Granting and Payment

-

Appendix A7: John Wiley & Sons Copyright Permission

From: no-reply@copyright.com
To: Daniel Brennan
Subject: RESPONSE REQUIRED for Your Request to John Wiley & Sons - Books
Date: Wednesday, 6 July 2022 12:05:09 AM

Dear Daniel Brennan,

John Wiley & Sons - Books has approved your recent request. Before you can use this content, you must accept the license fee and terms set by the publisher.

Use this link to accept (or decline) the publisher's fee and terms for this order.

Request Summary:
Submit date: 27-Jun-2022
Request ID: 600085799
Publication: Terra nova
Title: A tectonic model for the Transcontinental Arch: Progressive migration of a Laurentian drainage divide during the Neoproterozoic–Cambrian Sauk Transgression
Type of Use: Republish in a thesis/dissertation

Please do not reply to this message.

To speak with a Customer Service Representative, call +1-855-239-3415 toll free or +1-978-646-2600 (24 hours a day), or email your questions and comments to support@copyright.com.

Sincerely,

Copyright Clearance Center

Tel: 1-855-239-3415 / +1-978-646-2600
support@copyright.com
Manage Account

CCC | Marketplace™

Special Requests > Special Request Details

Add To Cart | Decline Offer

Terra nova

Article: A tectonic model for the Transcontinental Arch: Progressive migration of a Laurentian draina...

GENERAL INFORMATION

Request ID

600085799

Request Date

27 Jun 2022

Request Status

Accepted

Price

0.00 AUD ?

ALL DETAILS

COMMENTS

Add Comment / Attachment

27 Jun 2022 12:12:16 PM, by Daniel Brennan

I published a chapter of my Ph.D. thesis with Terra Nova. I have reformatted the chapter to include it within the main body of the thesis but I would like permission to include the Terra Nova for View More

Add To Cart | Decline Offer

Appendix B: Conference Abstracts presented during this Doctoral Thesis

Appendix B1: 2022 Geological Society of Australia Earth Science Student Symposium Abstract

An ancient Australian-American Alliance: a multi-isotope investigation of western N. America relations within Proterozoic supercontinents

Daniel T. Brennan[1], Zheng-Xiang Li[1], Paul K. Link[2], Tim Johnson[3], Noreen Evans[4]

[1]Earth Dynamics Research Group, School of Earth and Planetary Sciences, Curtin University, GPO Box U1987, WA 6845, Australia

[2]Department of Geosciences, Idaho State University, Pocatello, Idaho, USA

[3]School of Earth and Planetary Science, John de Laeter Centre, Curtin University, GPO Box U1987, Perth WA 6845, Australia

[4]School of Earth and Planetary Sciences, The Institute for Geoscience Research (TIGeR), Curtin University, GPO Box U1987, Perth WA 6845, Australia

Email address: daniel.brennan1@postgrad.curtin.edu.au

Along the west-central margin of Laurentia (North America), within the Priest River and Clearwater metamorphic complexes, rare exposures of “North American Magmatic Gap” (NAMG, ca. 1.61-1.49 Ga) crystalline basement rocks of the Clearwater Block are present. Overlying these crystalline basement rocks are ca. 1.47–1.38 Ga Belt Supergroup strata that also contain NAMG-age detrital zircon grains. This unique igneous and detrital record of NAMG-magmatism stands in contrast to other regions of North America that generally lack a record of any ca. 1.61-1.49 Ga tectono-magmatic activity. These differences led some early researchers to speculate that Proterozoic supercontinent events may have stranded exotic, perhaps Australia associated basement terranes within the Clearwater Block and that Australia (or perhaps Antarctica or South China) may have supplied the NAMG zircon grains within the overlying Belt Supergroup. If true, the rocks that now constitute some of the most scenic mountains in the northwestern United States were actually once part of Australia. Here, we report new U-Pb, Lu-Hf and O isotope data from Neoarchean and Proterozoic igneous and sedimentary rocks within the Priest River and Clearwater regions of western N. America. Our isotopic results indicate that ca. 1.58 Ga “NAMG” magmatism within the Clearwater block records mantle-like δ18O values but subchondritic (−5.5 to −9.7) εHf_t values in zircon, suggesting (perhaps plume-driven) reworking of the Neoarchean country rock. The overlying Belt Supergroup strata contain similar-age detrital zircon grains but with more juvenile suprachondritic (positive) εHf_t values that are similar to igneous sources in southeastern Australia. Collectively, these zircon results suggest that the Clearwater Block does have a North American origin, and that detrital zircon grains in the overlying sedimentary rocks of the Belt Supergroup record non-North American sources consistent with rocks in southeastern Australia. Consequently, these new results lend further support for an ancient Australian-American geological alliance.

which point to a global increase in thermal gradients that intersected granite genesis. We suggest these changes occurred as the secular cooling of the mantle and crust was reversed by a net increase in the spatial extent of continental crust between 2–1.8 Ga, resulting in thermal insulation of the mantle. The following 1.2 billion years on Earth was dominated by a warm, insulated mantle and crust, maintained by stable continental volumes, which eventually cooled to allow the second emergence and widespread preservation of eclogites from *ca* 0.8 Ga until present. While novel, this idea combines unrelated global petrological and geochemical datasets to explore the sensitivity of switches in the thermal evolution of the solid Earth.

When did Australia's Cratons come together?

Gorczyk, Weronika, Tyler, Ian, Aitken, Alan, & Kohanpour, Fariba

Centre of Exploration Targeting, School of Earth Science, University of Western Australia, Perth, Australia

Assembly of Australian cratons as part of Nuna assembly has been a subject of debates for decades. Especially within Australian geoscience community the timing and style of Western Australia Craton (WAC) with Norther Australian Craton (NAC) collision causes a lot of controversy. The dispute arises mostly due to sparsity of data available. As the Proterozoic knowledge of Australian cratons, as well as others grew new models for Nunan assembly were proposed, and the literature become overcrowded with variable models, based on localised and limited data.

Here, without presenting any new data, an attempt is made to analyse existing models in an unbiased style, questioning and correlating all the tectonic and sedimentation events across WAC, NAC and SAC (Southern Australia Craton). The position and inter-actions with Laurentia and North China – which are believed to be proximal to Australia at the time of paleo–meso Proterozoic, as also considered.

To achieve this task, plate reconstruction software (GPlates) is used. Publicly available geological data that describe tectonic and sedimentary events affecting WAC, NAC and SAC, as well as paleomagnetic data to are taken into account to support or contradict conceptual models. The immense advantage of this approach is continuous space and time visual representation of the plate interactions and occurrence of events.

Three (with variations) time models of WAC and NAC collision are shown with different subduction polarity: (1) 1800–1765 Ma, (2) 1590–1550 Ma, (3) *ca* 1300 Ma. Essentially, in the first model one can correlate all the tectonic events across WAC an NAC and SAC with one another post-collision, but spatial problem arises between the cratons and events that follow. In the second model the collision of WAC and NAC can be correlated with metamorphic and magmatic events in Arunta region, as well as in Mt Isa, but does not allow for correlation of previous events across WAC and NAC. The third model with subduction under WAC combines the tectonic evolution of Paterson region, Wankanki Arc and Stage I of Albany Fraser in a very elegant way, but again keeps WAC on a separate palate prior 1300 Ma and does not allow for correlation of events across the cratons of with similar styles and timings. Pros and cons for all models will be presented, and the verdict will be left to you.

Detrital zircon record of Proterozoic strata in the Priest River region of western Laurentia: Evaluating "SWEAT" relationships for supercontinents Nuna and Rodinia

Brennan, Daniel T.[1], Li, Zheng-Xiang[1], Link, Paul K.[2], & Johnson, Tim[3]

[1]Earth Dynamics Research Group, School of Earth and Planetary Sciences, Curtin University, WA, Australia; [2]Department of Geosciences, Idaho State University, Pocatello, ID, USA; [3]School of Earth and Planetary Sciences, The Institute for Geoscience Research (TIGeR), Curtin University, WA, Australia

Correlation of rocks across purportedly paired margins, such as Proterozoic strata (notably the Belt-Purcell and Windermere Supergroups) of western Laurentia with coeval rocks and/or magmatic sources in and around the Gawler Craton, have long been used as a key piercing point for SWEAT-like reconstructions of supercontinents Nuna and Rodinia. Here we evaluate the nature and timing of the proposed correlations through U–Pb and Lu–Hf analysis of detrital zircon (DZ) from the Proterozoic Gold Cup Quartzite, Belt-Purcell Supergroup, Deer Trail Group, and Buffalo Hump Formation of the Priest River region, northwestern USA.

The <1.7 Ga Gold Cup quartzite contains mostly *ca* 2.6 and 1.8 Ga DZ grains, indicating it is likely a western equivalent of the Neihart Formation. Lu–Hf values from these grains suggest that the younger *ca* 1.8 Ga population (εHf_t = –9 to –3) resulted from a reworking event on the *ca* 2.6 Ga crust involving juvenile mantle input (εHf_t = –2 to 4). This is consistent with the sediments being sourced from proximal Neoarchean Laurentian terranes such as the Clearwater/Medicine Hat block, that were intruded by Paleoproterozoic magmatism associated with the collision of the Wyoming and Medicine Hat blocks. Thus, these units do not require a SWEAT configuration (or the existence of Nuna) at *ca* 1.7 Ga. In the overlying western (*ca* 1.48–1.37 Ga) Belt Supergroup units, significant juvenile (εHf_t = 2 to 8) *ca* 1.6 Ga DZ grains are present. These grains fall within the North American Magmatic Gap and likely indicate provenance from the Gawler Craton, supporting a proto-SWEAT configuration for Nuna during *ca* 1.5–1.4 Ga as in most Nuna reconstructions. The overlying <1.3 Ga, fine-grained and carbonate Deer Trail Group is interpreted as a passive margin succession and contains mostly *ca* 1.9–1.65 Ga DZ grains with a wide range of Lu–Hf values (εHf_t = –6 to 9), notably *ca* 1.6 Ga DZ grains are absent. This provenance shift could be indicative of Nuna breakup, removal of the Gawler Craton from its Nuna position along western Laurentia, and a southwestern Laurentia provenance or recycling from underlying rocks of the Lemhi group of the Belt-Purcell Supergroup.

Coarse, locally conglomeratic, rocks of the Buffalo Hump Formation unconformably overly Deer Trail group strata. Prior small-n DZ study of the Buffalo Hump Formation identified a *ca* 1.1 Ga youngest DZ population, which was suggested to record deposition at *ca* 1.0 Ga during Rodinia amalgamation. However, our large-n study of the Buffalo Hump Formation identified for the first time a minor (~1%) yet significant *ca* 760 Ma DZ population, which constrains the maximum age of deposition. These geochronology results redefine the onset of Rodinia rift-related sedimentation to after *ca* 760 Ma in this region. Additionally, the Buffalo Hump Formation lacks any *ca* 900–790 Ma DZ grains. Such a DZ age-spectrum, and inferred rift history, is difficult to reconcile with an immediate neighbourhood between Laurentia and Australia in Rodinia as the latter had an earlier start of continental rifting (with *ca* 830–750 Ma rifting and syn-rift magmatism).

Review of SHRIMP zircon ages for the Eastern Succession of the Mount Isa and Etheridge Provinces and their provenances

Withnall, Ian

Geological Survey of Queensland, Brisbane, Australia

The migration of zircon geochronology data collected by Geoscience Australia (GA) and Geological Survey of Queensland (GSQ) from the Mount Isa Province into the Online Geochron Delivery System, an important repository maintained by GA, provided an opportunity to review the data and replot it using a consistent approach. This included data for which only preliminary plots of had been available to GSQ and never published.

The review highlighted that the main magmatic events that would have contributed zircon to the Eastern Succession sedimentary rocks occurred at 1850–1870 Ma, 1790–1800 Ma, 1780 Ma, 1760 Ma, 1735–1745 Ma, 1725 Ma, 1705–1715 Ma and 1670–1680 Ma and volumetrically smaller events at 1770 Ma, 1755 Ma, 1655–1660 Ma and 1650 Ma.

The Soldiers Cap Group in the easternmost part of the Mount Isa Province and extending under cover to the east is younger than most of the eastern succession. It consists of Llewellyn Formation, Mount Norna Quartzite and Toole Creek Volcanics in ascending stratigraphic order. The Kuridala Group comprises the Starcross Formation and Hampden Slate.

Samples of the two lowermost units of the Soldiers Cap Group and Starcross Formation have similar maximum depositional ages. A closer comparison has been made of their respective provenances by pooling analyses for units in each group. These provenances are similar, indicating a minor, very old source around the Archean–Proterozoic boundary and then almost none up to *ca* 1900 Ma (the Barramundi Orogeny). Except for minor components from the Kalkadoon–Leichhardt basement (1850–1870 Ma) and Argylla Formation (1780 Ma), by far the major sources appear to be the Wonga–Burstall–Gin Creek plutonic suites at *ca* 1740 Ma and Fiery Creek Volcanics or Weberra Granite at *ca* 1710 Ma. They also both have a significant younger component (slightly older in the Soldiers Cap Group at *ca* 1685 Ma, and *ca* 1675 Ma in the Starcross Formation). Pooling analyses from the Hampden Slate indicates that apart from the youngest component being *ca* 1655 Ma, other components are almost identical to those in the Starcross Formation.

By contrast the provenance of the Toole Creek Volcanics is dissimilar to the other units. It shows an *ca* 1795 Ma, *ca* 1850 Ma, and *ca* 2680 Ma.

Comparing the provenance spectra of the lower part of the Soldiers Cap and Kuridala Groups with those of the lower part of the Etheridge Group in the Etheridge Province (Georgetown region) suggests that they were probably deposited at about the same time, but the provenance patterns are strikingly different. The Etheridge Group shows a large Archean component as well as almost continuous spread of data points throughout the Paleoproterozoic including peaks around 1900–2000 Ma. This dissimilarity has been cited as evidence that the Georgetown rocks were not distal to Mount Isa and were part of Laurentia until welded to the Australian craton during the assembly of Nuna. The provenance of the upper part of the Etheridge Group, however, is like that of the Toole Creek Volcanics.

Partial melting, granulites, retrogression and their control on late orogenic exhumation processes

Cenki-Tok, Bénédicte[1,2], Rey, Patrice F.[2], & Arcay, Diane[1]

[1]Géosciences Montpellier, Université de Montpellier, CNRS, 34095 Montpellier Cedex 5, France; [2]Earthbyte Research Group, School of Geosciences, University of Sydney, NSW 2006, Sydney, Australia

Orogenesis drives the differentiation of the continental crust through metamorphic and magmatic processes, the exhumation of deep metamorphic terranes and the concomitant formation of sedimentary basins. A major consequence of prograde metamorphism following a typical orogenic thermal gradient is the dehydration and partial melting of buried rocks leading to the formation of migmatites and granulites. Partial melting and granulitisation are often intertwined and primarily linked to the availability of fluids. Here, we consider the thermal and mechanical consequences of coupled partial melting, granulitisation and strain-rate dependent retrogression during the orogenic cycle, in particular during the recovery phase when the crust's thickness and geotherm re-equilibrate. We explore through 2D thermo-mechanical modelling how the interplay between mechanical weakening due to partial melting and mechanical strengthening due to granulitisation impacts the formation and preservation of crustal roots, the exhumation of the partially molten crust in gneiss domes, the formation of HT/UHT terranes and the partitioning of deformation through the crust.

Our results show that the survival of granulites, which strengthen the lower crust and decrease its capacity to flow under gravitational stresses, impedes the formation of migmatite-cored gneiss domes, and controls the formation and preservation of thick and strong granulitic roots. These are strong enough to stay immune to gravitational stresses and persist over hundreds of million years. These can be actually compared with stable intracontinental regions where the presence of localized crustal roots explains the remarkable variability – from 25 to 65 km – of crustal thickness. Finally, our results highlight the importance of an elevated radiogenic heat production in the upper crust in order to form the long-lived HT/UHT terranes often resulting from supercontinents amalgamation. Our experimental results explain as well why some ancient orogenic domains expose at the Earth's surface dominantly granulitic terranes (e.g., South India, Sri

Appendix B3: International Geoscience Programme 648 Virtual Seminar Series Abstract

SUPERCONTINENT CYCLES & GLOBAL GEODYNAMICS

Home | IGCP 648 | Group members | Research | News | Contact Us | Links | PhD Opportunities | Australian palaeo-/rock-magnetism workshop

IGCP 648 VIRTUAL SEMINAR SERIES

- Series 1
- Series 2
- **Series 3**
- Series 4

Home > IGCP 648 Virtual Seminar Series > Series 3

Series 3

Series 3, Seminar 1 - Daniel Brennan

Reconciling paleographic reconstructions with the record of Rodinian rifting in the northwestern United States

Speaker bio

Daniel Brennan is a PhD student with the Earth Dynamics Research Group at Curtin University in Perth (Australia). Dan's current focus is on the Neoarchean-Neoproterozoic regional geologic record of the northwestern U.S., and its implications for global paleogeographic tectonic models. While Dan's published research has consisted primarily of geologic mapping and tectonostratigraphic (U–Pb, Lu–Hf) provenance studies, his current research is branching into more diverse isotope geochemistry and phase equilibrium modeling. Dan also enjoys teaching and filled a temporary (1 semester) associate lecturer position during his PhD where he taught Physical Geology and Geologic Mapping. Prior to undertaking the PhD, Dan completed a B.Sc. at University of Wisconsin–Eau Claire (2016), and an M.Sc. at Idaho State University (2018). At Idaho State, Dan's award-winning geologic mapping (2019 USGS Student Geologic Map 1st place winner) redefined a sequence of Neoproterozoic and lower Paleozoic strata. Dan is scheduled to finish his PhD in January 2022.

Abstract

Supercontinent Rodinia assembled through widespread (Grenvillian) orogenic events between 1300 Ma and 900 Ma, and much like its assembly experienced a diachronous break up, perhaps recorded by localized rifting as early as 825 Ma. The western margin of Laurentia (North America) occupied a critical, central location within Rodinia. Despite its important location and its relatively well-studied nature, the evolution of these processes in western Laurentia and the identity of its conjugate margins is a subject of long-standing debate. Here, we present results from the northwestern United States (Washington State), including the Buffalo Hump Formation. The Buffalo Hump Formation unconformably overlies ca. 1.3 Ga strata, and was previously interpreted by some to be a ca. 1.0 Ga "Grenvillian" deposit formed during Rodinia assembly. Our study of ~2000 detrital zircon grains from the Buffalo Hump Formation identified for the first time a minor (~1%) yet significant ca. 760 Ma population, which constrains the maximum age of deposition. This indicates an absence of Grenville-age sedimentation and a ca. 760 Ma earliest onset of Neoproterozoic rifting in this region which must be accounted for in paleographic tectonic reconstructions.

Appendix B4: 2019 Geological Society of America Annual Meeting

GSA 2019
22-25 September
Phoenix, Arizona, USA

Start |Grid View | Author Index | View Uploaded Presentations | Meeting Information

GSA Annual Meeting in Phoenix, Arizona, USA - 2019

Paper No. 127-4
Presentation Time: 9:00 AM-6:30 PM

DETRITAL ZIRCON U/PB AND LU/HF ANALYSES OF THE BUFFALO HUMP FORMATION AND UNDERLYING DEER TRAIL GROUP: INSIGHTS INTO THE PROTEROZOIC TECTONOSTRATIGR

BRENNAN, Daniel T.[1], LI, Zheng-Xiang[2], NORDSVAN, Adam[2], LINK, Paul K.[3], MAHONEY, J. Brian[4], YAO, Weihau[2] and PARKER, Stuart D.[5], (1)Department of A Australia; Geology, University of Wisconsin - Eau Claire, Eau Claire, WI 54703, (2)Department of Applied Geology, Curtin University of Techology, Department 6845, Australia, (3)Geosciences, Idaho State University, Pocatello, ID 83209, (4)Geology, University of Wisconsin - Eau Claire, Eau Claire, WI 54703, (5)Idaho St

Significant uncertainties regarding the Proterozoic tectonic history of the western margin of Laurentia hampers our understanding of the timing, geometry, the occurrence of a complete Wilson cycle along the western margin of Laurentia during the Nuna to Rodinia transition has been suggested, substantiating the sedimentary, metamorphic, and structural record of the region.
The Deer Trail Group and the overlying Buffalo Hump Formation constitute a ~3km thick siliciclastic and dolomitic sequence that are typically thought to be Belt Supergroup. Early work suggested a possible exotic western provenance for some of the units. Here we present new detrital zircon data that revise the predominantly argillaceous and dolomitic Deer Trail Group (Togo Fm.) has a maximum depositional age (MDA) of ~1365 Ma, but consist mostly of a ~1.6 to 1 younger than, but shares similar sources with, the upper Belt Supergroup equivalent strata in the Lemhi sub-basin. Up-section, detrital zircon spectra from Ga and a dominant Stenian (1.2–1.0 Ga) population that shows juvenile Lu-Hf isotopic values (εHf of +2 to +12). Several tectonic models propose the existen western margin of Laurentia, offering a proximal, non-Laurentian source for this detritus at ca. 1.0 Ga. However, nearby (<780 Ma) Windermere Supergroup zircon populations that are interpreted to have been sourced from distal Laurentian Grenville provinces.
This new data corroborates Box et al.'s (2019; GSA Cordillera abstract) that the Buffalo Hump Formation likely unconformably overlies the Deer Trail Group, including paleocurrent analysis, is required to evaluate their potential for constraining the late Proterozoic tectonic evolution of western Laurentia and its p

Session No. 127--Booth# 324
T50. Structure and Tectonic Studies, from Outcrop to Supercontinent (Posters): In Honor of Ian Dalziel
Monday, 23 September 2019: 9:00 AM-6:30 PM

Hall AB, North Building (Phoenix Convention Center)
Geological Society of America *Abstracts with Programs.* Vol. 51, No. 5
doi: 10.1130/abs/2019AM-338099

Back to: T50. Structure and Tectonic Studies, from Outcrop to Supercontinent (Posters): In Honor of

<< Previous Abstract | Next Abstract >>

Appendix C: Non Peer-Reviewed Science Outreach Articles

Appendix C1: A Short Hike on the Edge of Ancient North America: Out There Outdoors Magazine, 2021

HIKING

Quartzite Mountain

A Short Hike on the Edge of Ancient North America

By Daniel T. Brennan

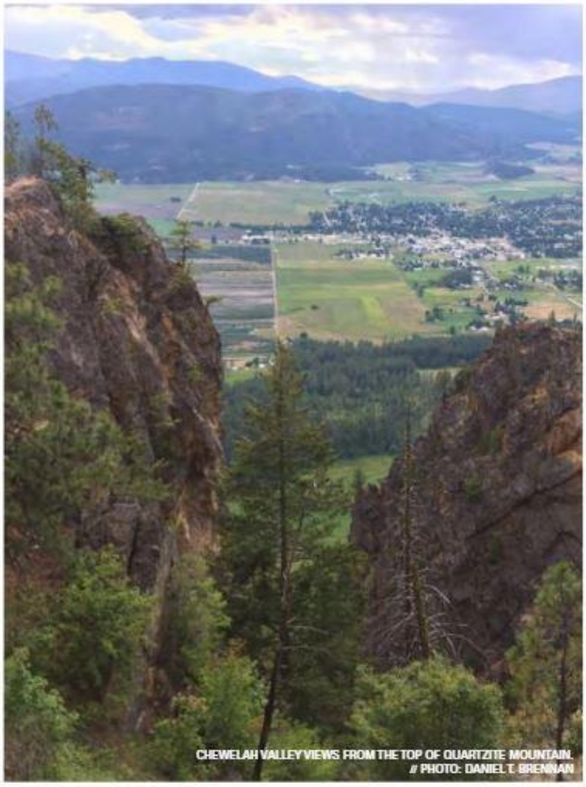

CHEWELAH VALLEY VIEWS FROM THE TOP OF QUARTZITE MOUNTAIN. // PHOTO: DANIEL T. BRENNAN

THE CHEWELAH VALLEY, like any good valley, is flanked on both sides by mountain ranges. To the east is the Selkirk Range and to the west are the Huckleberry Mountains. However, these mountains are relatively young geologically—we are talking only tens of millions of years.

GEOLOGIC HISTORY OF THE CHEWELAH VALLEY

Long before the rocks that make up the Selkirks and Huckleberry Range were uplifted into mountains, geologists have suggested western North America was connected to an unidentified continent, perhaps Australia, around 1 billion years ago. Scientists consider ancient configurations such as this one as a "supercontinent," this one being called "Rodinia," which comes from the Russian word "to give birth" since geologists once thought all subsequent continents spawned from the breakup of Rodinia. You may be more familiar with the most recent supercontinent called Pangea that existed approximately 300 million years ago.

Around 780 million years ago, tectonic forces broke apart supercontinent Rodinia, and a new pre-Pacific Ocean formed. Since the rocks that make up the western portions of Washington State and Oregon are significantly younger than 780 million years old, this suggests that the ancient edge of North America, that formed during breakup of supercontinent Rodinia, lies unidentified somewhere in the mountains of eastern Washington.

Research, by myself and other colleagues that was recently published in the peer-reviewed scientific journal "Geology," suggests that this supercontinent breakup process occurred directly beneath the Chewelah Valley about 760 million years ago. All it takes is a short but steep hike up Quartzite

The Edge of Ancient N. America ~760 Million Years Ago

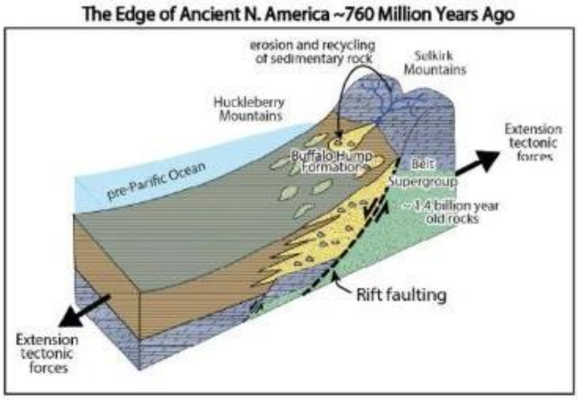

Mountain, just east of Chewelah, to get an awesome view from what was once the edge of this ancient world.

SOLVING AN ANCIENT GEOLOGIC MYSTERY

On Quartzite Mountain, the oldest sedimentary rocks are called the Belt Supergroup and are made of silt, sand, and limestone that were deposited approximately 1.4 billion years ago, likely within a huge ancient lake in the center of supercontinent Rodinia. As you start the steep incline near the Quartzite Mountain trailhead, these are the poorly exposed rocks you are hiking over. However, at the top of Quartzite Mountain, orange blocky outcrops of hard quartzite rocks create a striking cliff. These rocks are only about 540 million years old, indicating a complete absence of the approximately 780-600 million year-old rocks that are thought to have been deposited when supercontinent Rodinia was breaking apart.

However, west across the valley in the Huckleberry Mountains, beneath the same approximately 540-million-year-old quartzite rocks, very different rock layers, or stratigraphy, is present. These different rock layers include small quartzite boulders in a unit called the Buffalo Hump Formation. The nature of the sand and silt layers in the Buffalo Hump indicated to us that it was likely deposited in ancient river channels, deltas, or a shallow basin. By measuring uranium and lead isotopes of certain minerals in these different rock layers, our geologic study revealed that an ancient river deposited these small boulders approximately 760 million years ago, and the boulders were sourced from the approximately 1.3-billion-year-old rocks exposed across the valley, near the top of Quartzite Mountain.

This suggests uplift and erosion of the eastern side of the modern Chewelah valley, and subsidence of the western side sometime around 760 million years ago. We proposed that the simplest way to explain the ancient topography suggested by these rocks is the existence of an ancient fault, or fracture in the earth's crust, underneath the Chewelah Valley. This fault likely lowered the western portion of the valley and uplifted the eastern portion. Such faults commonly form when continents are pulled apart in a process known as rifting. All of this suggests that the edge of ancient North America was forming directly below Chewelah about 760 million years ago.

HIKING QUARTZITE MOUNTAIN

There you go. Take a hike up Quartzite Mountain and contemplate that. You are a human living on a 4.6 billion-year-old planet currently standing on the 760 million-year-old edge of ancient North America. If you are fortunate, you may live for 100 years—an infinitesimally small quantity in comparison. Don't waste it. Go for a hike. Get out there! This moderate hike is 3 miles roundtrip with 800 feet of elevation gain.

To get there from Chewelah, Wash., take Flowery Trail road east, then turn south onto Mud Lake Road. About 2.5 miles up Mud Lake Road, you will spot the Quartzite Mountain trailhead on the west (right) side of the road.

Daniel T. Brennan is a PhD student at Curtin University in Perth, Australia. This is his first article in Out There.

Appendix C2: When the Mountains Were Made: A New Geological Discovery, Idaho Magazine, 2020

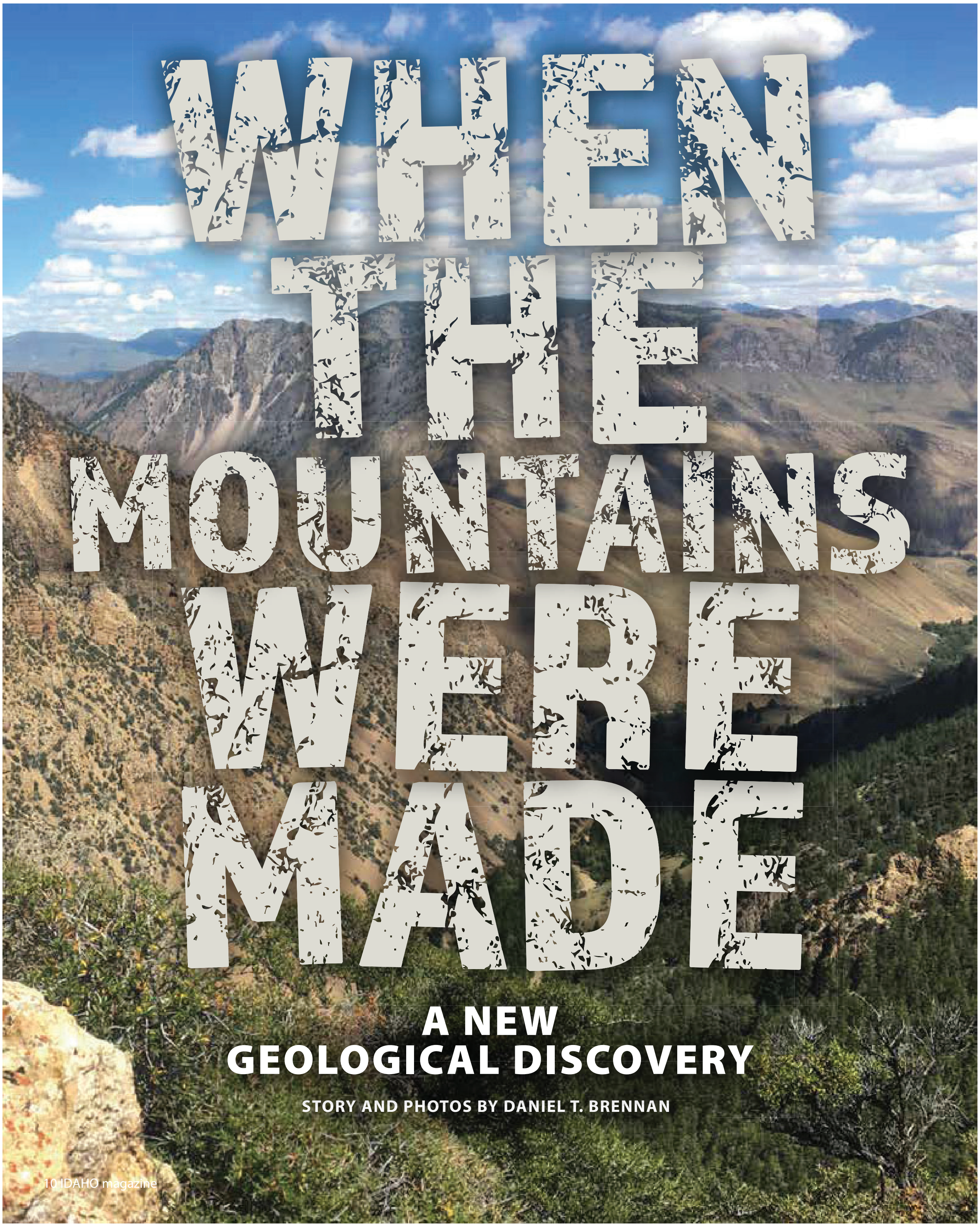

Being footloose has always exhilarated us. It is associated in our minds with escape from history and oppression and law and irksome obligations, with absolute freedom, and the road has always led west.

— *Wallace Stegner,* The American West as Living Space

LEFT: Dolomite cliffs near Bayhorse in the Salmon River Mountains.

ABOVE: Dan Brennan in the mountains with Blue.

On Easter of 2016, I sat in the living room with my grandfather, whom we all called Papa, when he unknowingly echoed Stegner's phrase "the road has always led west." I had just shared my plan to leave our home in Wisconsin and head to Idaho for graduate school, which had spurred his comment. "If you move west, you won't move back," Papa said nonchalantly, and quickly delved into to his own story of adventures out West on a road trip as a much younger man. He was that kind of guy, one with a story for every situation—a quality I now realize is likely the hard-earned result of a life well-lived. Between the chaos of family gatherings, Papa would share his stories to those who would listen, usually sitting in his recliner, the one with armrests worn thin from his signature way of slapping his hands when he reached a particularly exciting part, or was upset with the current politics on TV. But Papa (and Wallace Stegner) were right: the West was calling me. The day after I graduated with a bachelor's degree, my prone-to-overheating little truck was loaded down with gear and the rising sun glinted off the rearview mirror as I headed out to start the first chapter of my own western story.

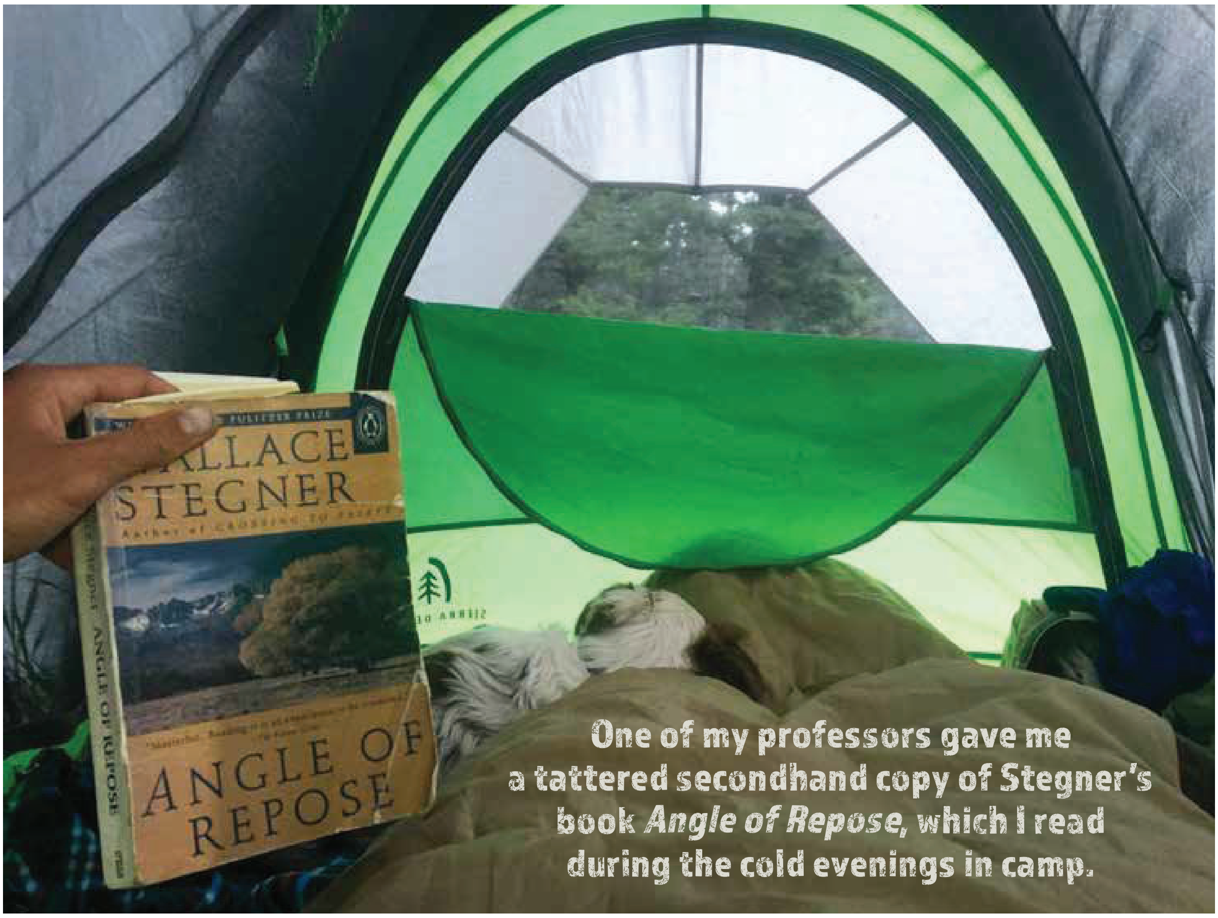

ABOVE: Dan shows off his battered copy of the novel.

Actually, I had been a full year in Idaho before I was introduced to the writing of the author that Papa had unknowingly echoed. On a visit to my field area in the Salmon River Mountains, one of my professors gave me a tattered secondhand copy of Stegner's book *Angle of Repose*, which I read during the cold evenings in camp. To be honest, I spent most of that first year unsure of what I was doing . . . with both my research project and my life. I'm a geologist, and although there is no better place for young geologists to gain experience than Idaho, the billions of years of Earth's history recorded in the rocks can be daunting to a green scientist. But I knew one thing: I liked to make geologic maps, and under the tutelage of my professors, Idaho was the place to learn. Eventually, as I had hoped, map-making became the main task of my master's research project, thanks to a bit of funding from the United States Geologic Survey (USGS). I had one summer to complete a geologic map of about a thirty-five-square-mile region in the Salmon River Mountains just west of Challis.

Short of actual hunting or gathering, I think geologic mapping is as close to the activities of our hunter-gather ancestors as a scientist can get. Maybe that's why most field geologists find something primordially satisfying about it. If you're not familiar with the premise of geologic mapping, it's relatively straightforward. Before you begin, you must lace up your hopefully broken-in boots, equip yourself with a topographic map, a rock hammer, a hand lens (which is small magnifying glass for identifying minerals), a notebook, a good compass, and as much food and water as necessary. If you have a trusty field dog, let it out of the truck. (I didn't have a dog at first, but that changed after a few weeks of isolated hikes, cold toes at night, and one trip "just to look" at dogs for adoption.) With your pack loaded—and the dog you just adopted eagerly leading the way—you start walking. The joke goes that geologic mapping is ninety percent intentional walking, but I don't think that's far from the truth.

All joking aside, geologic mapping is a scientifically rigorous activity. As I traverse any mapping area, I constantly develop, test, and alter a 3D conceptual model of the rocks beneath my feet. This geologic model is visualized in my head, sketched in my notebook, and drawn on my map.

In preparation for my Idaho field season, I poured through the literature and found I was far from the first young person who had aimed to find fame and fortune in the craggy peaks and glaciated meadows of the Salmon River Mountains. I uncovered the labor of souls kindred to mine in reading about 18th Century Shoshoni hunters who drove buffalo off the steep cliffs south of Challis, in photos of the still-standing but dilapidated late 19th-Century ruins of failed gold and silver mines at the Bayhorse ghost town, and in several late-1980s publications by a USGS geologist named Warren Hobbs. Although I was fortunate to collaborate with current Idaho Geological Survey mappers, I never got the chance to meet Warren, who died before my time. Luckily, if you're a young person driving a truck with a university logo in Challis, you open yourself up to some good-natured questioning by the locals. On a particularly warm late-summer afternoon, one provider of such questioning happened to be an old friend of Warren's. Unfortunately, I did not catch the oldtimer's name, but with a sparkle in his eye, he made sure the university was not paying for the burger and cold drink I was scarfing down. He said Warren would have been happy to know that young geologists were still out scampering around the Salmon River Mountains, just as he had spent many a summer doing.

As I traversed the field area with my supervisors, we began to decipher something that I'm sure Warren knew all too well. In those mountains, as with most other central Idaho ranges, the original layer-cake stratigraphy of sedimentary rocks that formed in ancient lakes, rivers, and oceans was long gone. The orderly

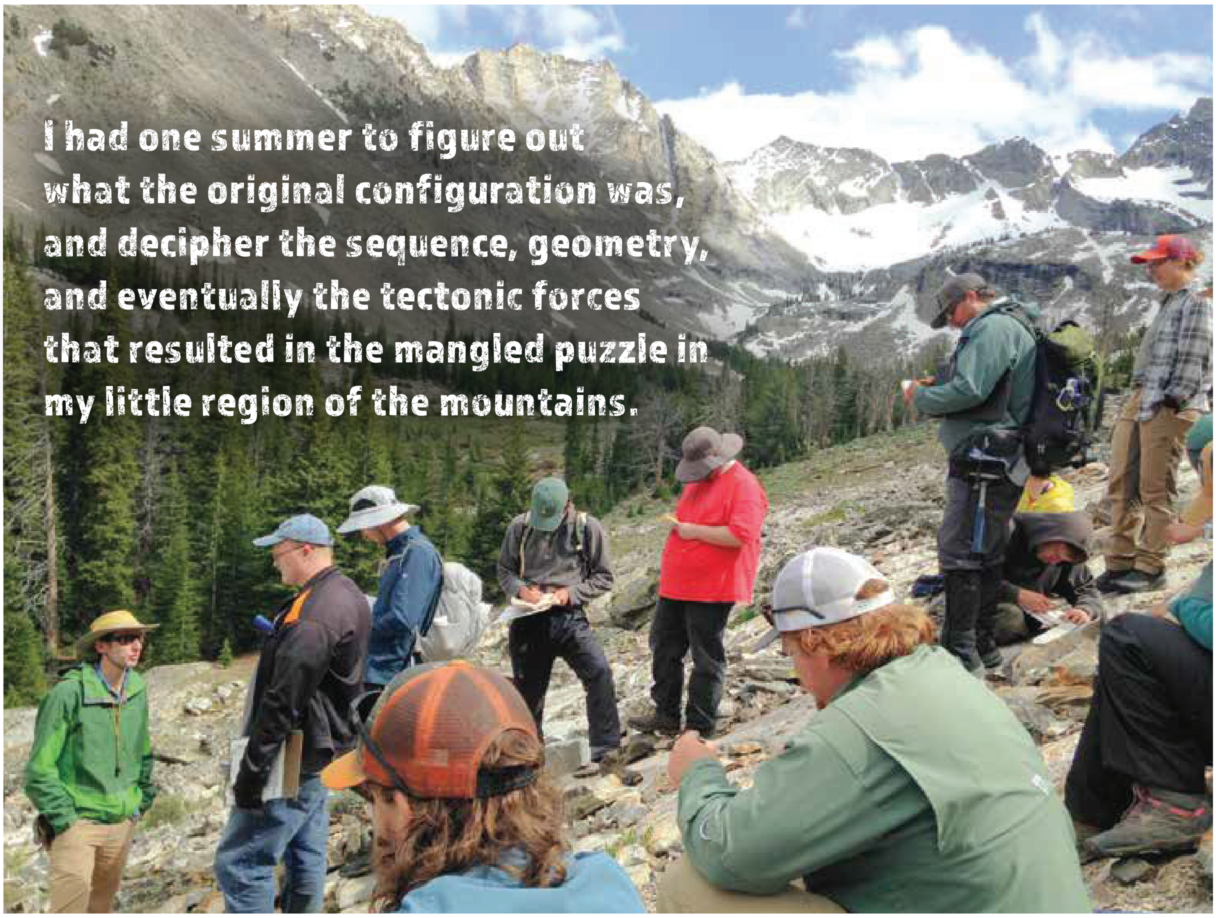

configuration of the sedimentary rocks had been erased and deformed by younger igneous rocks, crystallized from molten material. Adjacent to where these igneous melts had intruded, the pressures and temperatures were great enough to alter the minerals in the rocks that didn't melt, a process called metamorphism. To muddy the story even more, the rocks had been displaced across a series of faults or fractures, which created a complex three-dimensional pattern. As I have learned in my travels since then, these complexities are not unique to the Salmon River Mountains, but rather are a paradox of many mountain ranges. In such cases, exposure of the ancient earth record comes at a cost: the same processes that can make the rocks available for geologic study can mask their original identity.

I had one summer to figure out what the original configuration was, and decipher the sequence, geometry, and eventually the tectonic forces that resulted in the mangled puzzle in my little region of the mountains. I would have to piece it together one rock description at a time, and I quickly found that the secrets of ancient geologic processes entrusted to these mountains would not be shared easily. After about ten weeks of camping, hiking, eating more hot dogs than I'd like to admit, and of Blue (my newly adopted dog) terrorizing every chipmunk in Custer County, our team arrived at a hypothesis. Our geologic mapping suggested that the original geologic mapping

ABOVE: Idaho State geology class in the Pioneer Mountains.

OPPOSITE, CLOCKWISE FROM TOP LEFT: Blue in the Salmon River Mountains; the author and his dog in the Pioneers; Dan in the Pioneers; Lost River Valley sunset.

done by Warren and his colleagues had incorporated a slight misunderstanding in how the rocks were configured. They had postulated a large thrust fault or fracture across which rocks were displaced. This supposed structure required that the rocks on top be older and shoved above the allegedly younger rocks they now overlaid. However, our geologic mapping suggested that instead, the rocks on top were indeed younger than those beneath, and there was very little evidence for a thrust fault.

Armed with this hypothesis, we took several kilograms of specifically chosen rock samples to the lab. We prepared the samples in our lab at Idaho State University in Pocatello but for additional analysis, we then traveled to the University of Arizona and shipped other samples off to collaborators in Wyoming, California, and

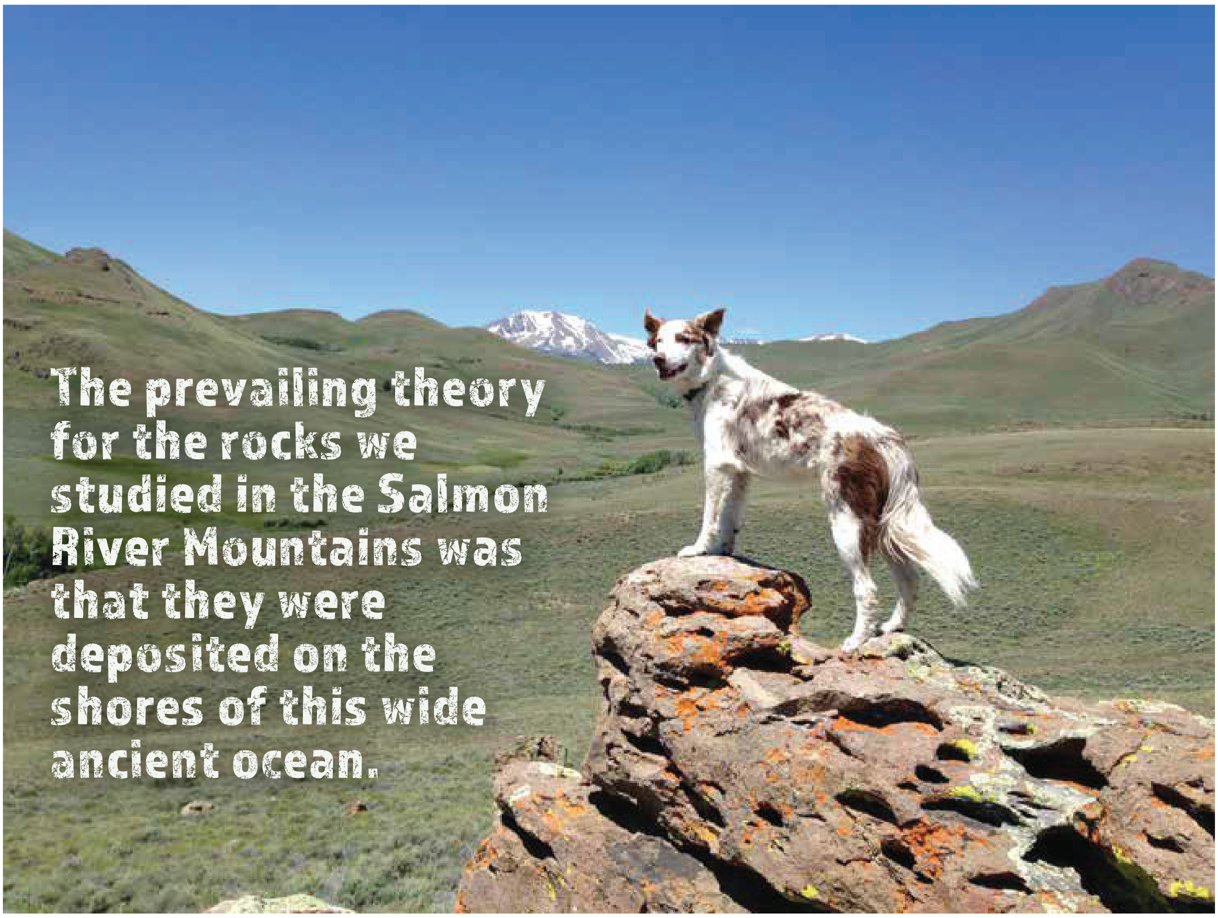

ABOVE: Hamming it up.

Australia. This analysis consisted of measuring particular isotopes of elements such as uranium and lead in the carefully chosen minerals zircon and baddeleyite. Our results indicated that the majority of rocks thought to be about 450 million years old were actually millions of years older, and had formed mostly between 660 and 600 million years ago. As you can imagine, this was quite an exciting discovery.

The data suggested a new origin for rocks in the Salmon River Mountains. Geologists had already proposed that the shores of an ancient pre-Pacific ocean once ran through what is now Idaho. During that time, Idaho was at the edge of North America, and the majority of rocks that make up Oregon and Washington had not yet formed. The prevailing theory for the rocks we studied in the Salmon River Mountains was that they were deposited on the shores of this wide ancient ocean. However, our data indicated that instead these rocks were deposited when the ocean was just beginning to open. Back then, other continents that were connected to the western margin of North America were in the process of slowly moving, or being rifted, away, which created an ocean. Our discovery showed that this rifting process was taking place in central Idaho more than six hundred million years ago, and this ancient ocean formed in a fashion similar to the creation of better-understood modern oceans such as the North Atlantic. Much later in geological terms, a series of processes deformed the rocks of this ancient ocean shoreline into the Salmon River Mountains we see today. Warren and his colleagues had gotten in some good punches early, and had set us up for the knockout. At last, the mystery of at least some of the rocks in the Salmon River Mountains was solved.

Our uncovering of these geologic secrets would soon give me another reason to continue my westward movement. Papa seemed to have known a thing or two when he predicted that my ticket west would not be a round trip. After two years in Idaho, another geologic challenge led me across an ocean to begin a PhD program in Perth, Australia. Other geologists have suggested that Australia was one of the continents originally west of North America, whose removal might be recorded in the rocks of the Salmon River Mountains. So, I'm now doing research into that question, and although I am now on the other side of the world, geologically, it feels like home.

Unfortunately, Papa is not around anymore to let me know if my westward trajectory is destined to continue after I finish my PhD in a couple of years. But as a good mate of mine likes to say, "Life is all about stories." Wherever I go, I hope to make a few of my own and find more rocks that reveal stories of Earth's ancient past. One thing I know: at this point, if I go any farther west, I'll be headed towards home. ■

The author encourages anyone interested in studying geosciences to visit Idaho State University at **isu.edu/geosciences/undergrad**, or get a book on geology from the local library. He recommends *Timefulness: How Thinking Like a Geologist Can Help Save the World*, by Marcia Bjornerud.

To learn more about the research Daniel and colleagues conducted, their geologic map can be downloaded at **idahogeology.org/product/t-20-01**

For their recent scientific paper, visit **agupubs.onlinelibrary.wiley.com/doi/abs/10.1029/2020TC006145**

Appendix D: Supplementary Datatables

Appendix D2.1: SHRIMP U/Pb Results

Spot Fundamentals		SQUID OUTPUTS 27.01.2021										ISOPLOT R AGE CALCS								DTB Calcs
Fraction	Date/Time	U (ppm)	Th (ppm)	232Th /238U	+/-1sigma	4-corr 208* /232	+/-1sigma	4-corr 238 /206*	+/-1sigma %	4-corr 207* /206*	+/-1sigma	207/235	1sigma Ma	206/238	1sigma Ma	207/206	1sigma Ma	Concordia Age	1sigma Ma	Discordance
36DB-1	2/12/2020 13:15	565.5598	343.0617	0.626853	0.205623	0.078952	5.421301	3.26006	5.226450083	0.185327	1.651189	2212.2	49.4	1724.7	79.1	2700.4	27.3	2646.5	17.7	36.13
36DB-10	2/12/2020 18:25	1095.304	10.57142	0.009974	0.698257	0.084385	12.08252	4.178825	4.988562229	0.113849	0.702957	1583.1	40.4	1383.1	62.1	1860.9	12.7	1849.44	9.26	25.68
36DB-11	2/12/2020 19:16	447.532	157.3846	0.363421	0.448084	0.099173	5.076978	3.726518	4.560969582	0.174226	0.429122	2038.2	40.3	1532.4	62.2	2597.91	7.15	2592.59	3.91	41.01
36DB-12	2/12/2020 19:40	648.4096	99.10715	0.157953	4.731734	0.106829	7.82059	4.095438	4.488499221	0.153573	0.813343	1847.4	38.8	1408.4	56.8	2385.3	13.9	2362.98	7.89	40.96
36DB-13	2/12/2020 20:05	1122.702	31.69806	0.029177	4.361709	0.035316	15.58424	6.451223	4.49077178	0.128779	1.169421	1342.4	38.2	929	43.2	2080.6	20.6	126.2	18.3	55.35
36DB-14	2/12/2020 20:29	1012.067	26.49559	0.027054	0.843339	0.036368	14.80102	5.332994	4.799380855	0.112864	0.469114	1386.2	36.5	1107.9	48.9	1845.22	8.49	1836.66	4.89	39.96
36DB-15	2/12/2020 21:41	1554.344	14.46448	0.009617	0.564892	0.056772	24.41126	7.919583	4.523285841	0.15347	0.804088	1320.4	33.9	766.5	32.7	2384.2	13.7	50.44	9.23	67.85
36DB-16	2/12/2020 22:05	1623.908	62.30459	0.039649	0.993335	0.002313	62.53068	37.02228	7.103949844	0.11658	2.07416	366	22.7	171.8	12	1903.6	37.3	33.57	5.47	90.97
36DB-17	2/12/2020 22:28	942.99	309.2797	0.338935	2.248068	0.065934	6.065685	4.665889	4.519636333	0.161676	0.346316	1780.6	38.1	1251.8	51.4	2472.5	5.85	15.79	6.69	49.37
36DB-18	2/12/2020 22:51	1359.535	11.10534	0.008441	0.672572	0.02827	37.20921	6.459103	4.480721669	0.125497	0.96616	1322.3	33.9	927.9	38.7	2035	17.1	111.1	15.4	54.40
36DB-19	2/12/2020 23:48	331.905	29.29865	0.091223	5.857506	0.117791	11.14903	2.977206	4.498198886	0.162512	1.074375	2175.7	41.4	1866.8	72.9	2481.2	18.1	2458.5	13.4	24.76
36DB-2	2/12/2020 13:47	537.0556	159.7283	0.307351	0.496542	0.12228	4.672815	2.311236	4.587721731	0.182376	1.733992	2512.5	45.6	2317.7	89.3	2673.9	28.7	2646.1	24.7	13.32
36DB-20	3/12/2020 0:12	264.5509	291.1166	1.137181	0.403984	0.13818	4.546927	2.018498	4.500491713	0.199835	0.376815	2725.3	42.7	2594.1	96.1	2824.12	6.15	2823.31	5.54	8.14
36DB-3	2/12/2020 14:17	2101.508	13.84426	0.006808	1.008327	0.020077	82.4959	10.84803	6.392827842	0.101411	1.114272	840.6	37.1	568.4	34.8	1649.3	20.7	57.9	12.1	65.54
36DB-4	2/12/2020 15:30	2320.623	23.74115	0.010572	0.88547	0.054379	35.54229	10.25757	4.928608451	0.100584	0.864882	868.2	29.2	599.7	28.2	1634.1	16.1	63.2	10.1	63.30
36DB-5	2/12/2020 15:53	982.9611	7.898468	0.008304	0.774796	0.034148	29.56924	5.10963	4.775584996	0.11279	0.41944	1418.3	36.6	1152.2	50.4	1844.03	7.59	1837.54	4.55	37.52
36DB-6	2/12/2020 16:25	1274.335	16.94421	0.013741	0.522273	0.02518	52.47443	7.027994	4.602684775	0.139257	0.493973	1336.9	34.4	857.6	37	2217.21	8.56	23.29	6.76	61.32
36DB-7	2/12/2020 17:14	1995.923	23.38719	0.012109	0.450077	0.035919	29.53344	9.891748	4.506307013	0.105985	0.766487	920.9	27.7	620.8	26.7	1730.6	14.1	56.7	8.84	64.13
36DB-8	2/12/2020 17:37	804.4948	97.86889	0.125717	4.626751	0.133027	8.336318	3.57489	5.164520521	0.154353	1.462755	1968.6	46.7	1590	72.8	2394	24.9	2347.9	16.8	33.58
36DB-9	2/12/2020 18:01	2338.375	15.82643	0.006994	0.536074	0.024691	54.95312	9.247654	4.543529281	0.105013	0.489822	956.5	28.3	661.9	28.6	1713.72	9.01	25.35	6.1	61.38
37DB-10	3/12/2020 4:54	1181.736	770.3403	0.673649	0.350263	0.080938	4.510497	3.673563	4.47965956	0.097498	0.3261	1562.2	35.8	1552	61.8	1575.96	6.1	1575.74	5.98	1.52
37DB-11	3/12/2020 5:17	379.7817	271.6599	0.739202	0.398131	0.078464	4.56852	3.711891	4.492954361	0.098036	0.618495	1558.3	36.1	1537.8	61.5	1586.3	11.6	1584.7	11	3.06
37DB-12	3/12/2020 5:39	515.7931	193.9921	0.388669	0.202776	0.071504	4.721745	4.015264	4.488701285	0.097515	0.573793	1492.1	35.4	1433.6	57.7	1576.3	10.7	1572.23	9.63	9.05
37DB-13	3/12/2020 6:02	682.8437	357.9954	0.541786	0.468089	0.079163	4.543286	3.636832	4.484133033	0.09774	0.414077	1572.2	36	1566	62.3	1580.6	7.75	1580.38	7.61	0.92
37DB-14	3/12/2020 6:26	222.8164	68.77476	0.318973	1.09442	0.07897	4.970092	3.753136	4.508022518	0.098161	0.862068	1550.5	36.5	1522.7	61.1	1588.6	16.1	1584.6	15.1	4.15
37DB-15	3/12/2020 6:48	1164.219	557.24	0.494629	0.338542	0.080372	4.517951	3.668401	4.480233469	0.098387	0.334844	1570.6	35.9	1554	61.9	1592.94	6.25	1592.56	6.06	2.44
37DB-16	3/12/2020 7:40	792.8298	370.1856	0.482515	0.162915	0.076156	4.581816	3.734862	4.483176358	0.098481	0.405957	1557	35.8	1529.4	61	1594.72	7.58	1593.8	7.2	4.10
37DB-17	3/12/2020 8:04	1064.285	301.6876	0.292935	2.280893	0.069427	5.431522	4.148861	4.560787014	0.097901	0.346818	1469.7	35.5	1392	57.1	1583.68	6.49	1581.75	5.62	12.10
37DB-18	3/12/2020 8:31	1839.119	678.4218	0.381208	0.364722	0.079408	4.510999	3.620998	4.477821118	0.097567	0.257513	1574.3	35.9	1572	62.5	1577.29	4.82	1577.26	4.79	0.34
37DB-19	3/12/2020 9:04	1043.48	319.341	0.316259	0.26404	0.081176	4.542231	3.61991	4.483772468	0.097546	0.590159	1574.3	36.2	1572.4	62.6	1576.9	11	1576.8	10.8	0.29
37DB-2	3/12/2020 0:36	2095.712	1033.705	0.509726	0.47158	0.084541	4.514265	3.472564	4.477427728	0.0977	0.240156	1609	36.2	1631.4	64.5	1579.84	4.49	1631.39	4	-3.26
37DB-20	3/12/2020 9:32	339.4567	166.8197	0.507849	1.442636	0.068738	5.269801	4.603948	4.649055605	0.097738	1.893847	1388.6	38	1267.1	53.5	1580.6	35.4	1495.4	30.3	19.83
37DB-21	3/12/2020 10:43	458.8063	384.9033	0.86695	0.53999	0.076893	4.565413	4.035325	4.491758214	0.097695	0.58184	1489.7	35.4	1427.2	57.5	1579.7	10.9	1575.31	9.7	9.65
37DB-22	3/12/2020 11:08	2799.094	1349.131	0.498091	0.614912	0.086196	4.770723	3.520802	4.524540959	0.097811	0.205747	1598.8	36.5	1611.6	64.5	1581.96	3.85	1611.61	3.59	-1.87
37DB-23	3/12/2020 11:56	318.9183	298.1252	0.966031	2.108519	0.070451	5.366321	3.873448	4.501028913	0.097003	0.904434	1516.2	36.1	1480.5	59.5	1566.4	17	1560.5	15.6	5.48
37DB-24	3/12/2020 12:23	1184.69	309.6275	0.270089	0.163278	0.083717	4.580189	3.801025	4.492945235	0.097324	0.317187	1533.7	35.6	1505.6	60.3	1572.62	5.94	1572.03	5.64	4.26
37DB-3	3/12/2020 1:00	645.5069	376.0411	0.602013	1.213404	0.077627	4.689923	3.725024	4.486856851	0.097404	0.480346	1550.4	35.9	1533	61.2	1574.16	8.99	1573.33	8.66	2.61
37DB-4	3/12/2020 1:45	1359.09	1124.593	0.855104	0.304009	0.08304	4.65024	3.594009	4.493093872	0.097869	0.312623	1582.7	36.1	1582.5	63	1583.07	5.85	1583.07	5.82	0.04
37DB-5	3/12/2020 2:09	1389.05	422.6928	0.31447	0.406602	0.077989	4.686731	4.371237	4.637840659	0.09742	0.330692	1425.6	35.6	1328	55.7	1574.47	6.19	1572.26	5.13	15.65
37DB-6	3/12/2020 2:31	1657.799	694.2526	0.43277	0.302863	0.080772	4.507358	3.672802	4.478209135	0.09759	0.476419	1563.1	35.9	1552.3	61.8	1577.73	8.92	1577.23	8.68	1.61
37DB-7	3/12/2020 2:55	798.0581	511.8584	0.662807	0.832571	0.082351	4.651937	3.564775	4.482824413	0.097741	0.383781	1588.2	36.1	1594	63.3	1580.62	7.18	1593.99	6.91	-0.85
37DB-8	3/12/2020 3:18	366.9846	85.45325	0.240631	0.460027	0.075797	4.710276	3.887583	4.495978104	0.098128	0.606831	1522.4	35.8	1475.7	59.3	1588	11.3	1584.5	10.4	7.07
37DB-9	3/12/2020 3:41	788.795	252.0717	0.330241	0.850471	0.080097	4.740358	3.64188	4.523163937	0.09816	0.416527	1574.5	36.3	1564	62.8	1588.62	7.78	1588.26	7.6	1.55
37DT-1	2/12/2020 12:02	148.3967	0.234376	0.001632	6.625215	0.134285	24.05571	110.0595	5.362190765	0.062005	9.610531	75.93	8.05	58.31	3.11	673	206	57.37	3.09	91.34
46DB-1	4/12/2020 2:06	1844.319	85.39201	0.047847	0.252532	0.088947	5.64358	3.400075	4.478882795	0.11252	0.247144	1742.1	37.4	1662	65.6	1839.7	4.47	1839.02	3.98	9.66
46DTB-16	9/12/2020 4:27	2054.138	90.72429	0.045642	0.674909	0.090546	3.361025	3.197225	2.333761334	0.113369	0.593145	1800	20.3	1754.3	35.8	1853.3	10.7	1845.76	9.87	5.34
46DTB-20	9/12/2020 6:17	2268.106	85.86225	0.039121	0.711808	0.085525	5.389913	4.493789	2.451165882	0.111451	0.387866	1508.6	19.5	1295.2	28.8	1822.4	7.04	1805.63	4.94	28.93
46DB-12	4/12/2020 8:02	2318.336	43.57549	0.019424	0.364942	0.088086	10.50418	8.860194	4.724638058	0.109252	0.515628	1008.3	30.4	689.4	30.9	1786.16	9.4	25.54	6.5	61.40
46DB-11	4/12/2020 7:40	2373.205	108.9272	0.047432	0.748602	0.083261	4.770792	3.508209	4.47651974	0.111264	0.22607	1706.9	37	1616.7	64	1819.35	4.1	1818.68	3.59	11.14
46DTB-18	9/12/2020 5:33	2418.746	110.9657	0.04741	0.370816	0.091915	3.066897	3.038671	2.197003032	0.113116	0.57639	1841.1	19.3	1834	35.1	1849.3	10.4	1848.03	9.93	0.83
46DB-7	4/12/2020 5:18	2573.923	108.36	0.043506	0.878165	0.073623	4.822237	3.699499	4.528250859	0.112451	0.360927	1671.9	37.2	1542.4	62.1	1838.59	6.54	1836.23	5.37	16.11
46DB-8	4/12/2020 5:40	2725.278	134.7398	0.051092	0.769071	0.090412	4.793778	3.126653	4.485945834	0.113711	0.208413	1821.4	38	1788.9	70.1	1858.74	3.76	1858.55	3.6	3.76
46DTB-14	9/12/2020 3:43	2768.126	129.6287	0.048394	1.057864	0.083315	3.358161	3.416568	2.282372155	0.111139	0.472838	1727.9	19.4	1655	33.3	1817.31	8.58	1808.55	7.69	8.93
46DB-5	4/12/2020 4:34	2774.996	92.94719	0.034614	0.266621	0.068043	4.726703	5.641138	4.508519084	0.10844	0.507462	1314.4	33.4	1052	43.8	1772.55	9.26	1760.37	5.33	40.65
46DTB-15	9/12/2020 4:05	2802.311	112.148	0.041357	0.673067	0.079378	3.25672	4.187859	2.195150699	0.111512	0.335006	1564.8	17.7	1380.4	27.3	1823.39	6.08	1810.31	4.54	24.29
46DB-9	4/12/2020 6:49	2915.003	157.9671	0.056001	0.882672	0.081301	4.695901	3.477712	4.515754937	0.111941	0.204847	1719.1	37.5	1629.3	65	1830.35	3.71	1829.82	3.25	10.98
46DTB-19	9/12/2020 5:55	3088.718	117.7191	0.039386	0.709458	0.051766	5.015316	6.121164	2.552458222	0.103892	0.399111	1224.3	18.4	975.5	23.1	1693.95	7.36	1667.54	4.24	42.41
46DTB-17	9/12/2020 5:12	3261.847	145.7118	0.046164	1.956519	0.062218	5.85413	5.274943	4.555043946	0.109619	0.362719	1372.5	34.4	1119.1	46.8	1792.27	6.61	1786.74	3.95	37.56
46DB-3	4/12/2020 2:58	3622.022	168.17	0.047981	1.028491	0.083218	4.688376	3.258724	4.475487731	0.112543	0.172346	1777.8	37.6	1725.3	67.7	1840.07	3.12	1839.85	2.9	6.24
46DTB-13	9/12/2020 3:20	3638.352	206.9486	0.05878	0.288719	0.096914	2.676071	2.94667	2.402539371	0.113883	0.248157	1873.1	20.6	1883.6	39.2	1861.47	4.48	1883.62	4.24	-1.19
46DB-6	4/12/2020 4:56	3641.74	120.7523	0.034266	2.732131	0.065176	6.257218	6.796978	5.541904137	0.108133	0.801068	1178.7	39	884.8	45.8	1767.4	14.6	59.4	13.4	49.94
46DB-10	4/12/2020 7:18	3680.654	153.3389	0.043053	2.241077	0.067841	6.929215	4.949814	5.58474745	0.108718	0.251576	1414.5	42.7	1186.2	60.5	1777.22	4.59	1775.64	2.93	33.26
46DB-2	4/12/2020 2:35	3690.679	226.4007	0.063393	0.402034	0.095987	4.548678	2.952485	4.475596531	0.11334	0.174287	1867.3	38.2	1880.4	73	1852.83	3.15	1880.4	2.97	-1.49
46DB-4	4/12/2020 3:21	4471.553	174.627	0.040358	0.579845	0.097212	4.666487	2.98163	4.561424487	0.113771	0.34602	1862.2	39	1864.4	73.9	1859.69	6.25	1864.44	6.16	-0.25
52DB-26	9/12/2020 1:47	37.20119	1.419309	0.039427	5.456007	-0.17467	-97.7968	7.00703	4.09413988	0.051864	36.34414	714	188	860	33	278	832	857.5	32.8	-209.35
52DB-5	8/12/2020 13:46	209.4101	0.549115	0.00271	4.533339	-0.54271	-61.715	4.214277	2.381697477	0.085441	2.108428	1354	23.8	1372.6	29.4	1324.7	40.8	1355.9	23.4	-3.62
52DB-11	8/12/2020 17:23	768.2108	5.29546	0.007124	4.972174	0.053501	32.1107	3.86363	2.230460679	0.090395	0.631803	1463.1	18	1483.8	29.6	1433	12.1	1440.5	11.3	-3.55
52DB-24	9/12/2020 0:39	708.8787	2.556835	0.003727	2.289909	-0.12205	-90.6671	4.169126	2.255702318	0.087384	1.076555	1378.9	18.9	1386	28.1	1368.1	20.7	1374.4	16.6	-1.31
52DB-9	8/12/2020 16:37	571.3648	124.192	0.224622	0.404615	0.081857	3.503273	3.64543	2.246415648	0.095937	0.916434	1555.5	19.3	1562.7	31.2	1545.7	17.2	1549.7	15.1	-1.10
52DB-1	8/12/2020 11:52	312.7339	0.918071	0.003034	3.511912	-0.32993	-61.0133	4.239708	2.306560096	0.087052	1.526051	1363.5	20.7	1365.2	28.4	1360.8	29.4	1363	20.4	-0.32
52DB-2	8/12/2020 12:16	384.8222	2.127013	0.005712	5.530937	-0.05384	-124.224	4.360624	2.28463463	0.085922	1.198355	1332.7	19.1	1331	27.5	1335.6	23.2	1333.6	17.7	0.34
52DB-10	8/12/2020 16:58	399.5279	11.67228	0.030191	19.74394	0.069305	22.81742	4.28878	2.277191115	0.087061	0.920515	1354.9	18.4	1351.1	27.8	1361	17.7	1358.1	15	0.73
52DB-16	8/12/2020 20:28	157.9184	0.390748	0.002557	5.339353	-0.61044	-70.1143	4.403034	2.418050631	0.085904	3.285052	1325.4	30.2	1319.4	28.9	1335.2	63.5	1322	26.4	1.18
52DB-23	9/12/2020 0:17	1089.843	3.767556	0.003572	3.664115	0.001114	3925.351	4.217767	2.697486995	0.08884	1.741093	1382.7	24.2	1371.6	33.3	1399.9	33.4	1385.6	23.8	2.02
52DB-14	8/12/2020 18:54	645.2352	1.8962	0.003037	2.291333	-0.05381	-129.997	4.192292	2.22817667	0.089404	0.77918	1392	17.9	1379.1	27.7	1412	14.9	1404.7	13.1	2.33
52DB-22	8/12/2020 23:52	421.0677	1.970128	0.004835	2.003936	0.087722	48.30641	4.424819	2.241626564	0.087143	0.882211	1332.4	17.9	1313.5	26.6	1362.8	17	1348.8	14.4	3.62
52DB-3	8/12/2020 12:38	288.4589	0.586933	0.002103	4.34218	-0.03396	-412.146	4.341068	2.310496003	0.088345	1.168443	1356.8	19.4	1336.4	27.9	1389.1	22.4	1368.5	17.7	3.79
52DB-13	8/12/2020 18:32	292.7173	2.205973	0.007788	8.595669	0.1321	26.44721	4.190819	2.30591972	0.090931	1.079043	1405.2	19.4	1379.5	28.6	1444.3	20.6	1422.6	16.9	4.49
52DB-6	8/12/2020 14:30	496.5893	1.763365	0.00367	2.466938	0.101096	34.34994	4.297903	2.254706515	0.089454	1.374106	1373.7	19.9	1348.5	27.4	1413	26.3	1382	19.5	4.56
52DB-25	9/12/2020 1:24	573.593	47.91262	0.086321	2.821867	0.067378	6.339391	4.386676	2.239963738	0.088718	0.776218	1352.1	17.7	1323.8	26.8	1397.2	14.9	1380.6	12.9	5.25
52DB-4	8/12/2020 13:23	267.9808	1.001847	0.003863	3.66833	0.205059	41.90041	4.327806	2.315876704	0.089687	1.241598	1370.4	19.8	1340.1	28	1418	23.7	1385.5	18.6	5.49
52DB-12	8/12/2020 18:07	451.6426	1.2132	0.002776	3.05699	0.118377	23.21546	4.463232	2.426019123	0.088378	0.841157	1336.4	19.1	1303.3	28.6	1389.9	16.1	1369.9	14	6.23
52DB-20	8/12/2020 22:21	417.8825	4.84927	0.011992	8.602561	0.075798	30.19348	4.438131	2.563764725	0.089425	1.003664	1349.4	20.6	1309.9	30.4	1412.4	19.2	1384.3	16.3	7.26
52DB-7	8/12/2020 14:54	122.648	0.247554	0.002086	7.045035	0.258013	19.1938	4.495719	2.469442599	0.088957	1.612933	1335.8	21.9	1294.7	29	1402.4	30.9	1344.1	22.2	7.68
52DB-21	8/12/2020 23:28	181.4178	0.440016	0.002506	5.23243	-0.14027	-233.044	4.872265	2.41543082	0.08481	2.328507	1242.3	24	1203.4	26.5	1310.3	45.2	1228.5	24	8.16
52DB-15	8/12/2020 20:07	251.0212	0.798856	0.003289	3.845756	0.071735	198.8932	4.647919	2.342889221	0.088152	1.548334	1304.5	20.6	1256.2	26.7	1384.9	29.7	1312.1	21.2	9.29
52DB-19	8/12/2020 21:59	224.7205	0.375114	0.001725	5.400835	1.09478	31.3335	4.474447	2.339002305	0.092212	1.595866	1366.2	21.3	1300.3	27.5	1470.9	30.3	1374.4	22.2	11.60
52DB-18	8/12/2020 21:13	214.9164	0.476748	0.002292	4.801917	0.065095	196.5111	4.657227	2.349536699	0.089958	1.382618	1318	20.1	1253.9	26.8	1423.8	26.4	1338.5	20.3	11.93
52DB-8	8/12/2020 15:28	168.0152	0.449523	0.002765	5.25009	1.028206	17.50767	4.66793	2.405572895	0.090304	1.609213	1319.1	21.4	1251.3	27.4	1431.1	30.7	1327.1	22.4	12.56
52DB-17	8/12/2020 20:50	231.6701	44.08737	0.19666	14.07474	0.069934	22.73261	5.121795	2.703578743	0.085436	2.05806	1212	24	1149.7	28.5	1324.6	39.9	1202.9	25.5	13.20
52DB-27	9/12/2020 2:08	242.0126	1.12952	0.004823	3.203218	-0.15399	-88.9872	5.949805	2.35542373	0.082453	2.301534	1084.5	21.9	1001.5	21.8	1255.4	45	1035.1	21.8	20.22
67DB-15	3/12/2020 21:37	642.1959	250.3499	0.402858	0.190425	0.134583	4.533157	2.048708	4.484698999	0.178804	0.281643	2606.6	42.1	2562.5	94.8	2641.06	4.68	2640.88	4.5	2.97
67DB-16	3/12/2020 21:59	604.1588	304.4647	0.520784	1.15354	0.130398	4.895947	2.167543	4.485531278	0.180569	0.296882	2563	42	2445.5	91.3	2657.36	4.92	2656.83	4.45	7.97
~~67DT-1~~	~~2/12/2020 11:37~~	~~8.469227~~	~~0.08521~~	~~0.010397~~	~~12.7425~~	~~3.461981~~	~~61.46524~~	~~37.28196~~	~~33.89979066~~	~~0.598249~~	~~14.30594~~	~~1185~~	~~257~~	~~170.6~~	~~57.1~~	~~4503~~	~~208~~	~~29.9~~	~~24.3~~	~~96.21~~
67DT-10	3/12/2020 17:45	526.7952	189.0574	0.370872	0.426326	0.10454	4.562263	2.657475	4.488020756	0.176242	0.336241	2352.1	41.2	2059	79.1	2617.07	5.6	2615.27	4.22	21.32
67DT-11	3/12/2020 19:20	833.8978	280.3102	0.347374	0.179104	0.138441	4.57092	1.958099	4.531594848	0.181539	0.236419	2663.4	42.7	2659.6	98.8	2666.24	3.92	2666.23	3.9	0.25
67DT-12	3/12/2020 19:43	694.2542	183.464	0.273089	0.209839	0.141103	4.53636	2.035884	4.487191571	0.17948	0.519001	2616	42.4	2575.8	95.3	2647.33	8.61	2646.77	8.31	2.70
67DT-13	3/12/2020 20:12	539.0461	233.5866	0.44781	0.324534	0.140733	4.570809	1.970398	4.521813191	0.18223	0.284812	2661.1	42.7	2646	98.1	2672.53	4.71	2672.47	4.65	0.99
67DT-14	3/12/2020 20:49	836.1217	290.5135	0.359061	0.176711	0.138064	4.514917	1.959639	4.481876778	0.181867	0.232399	2664.3	42.3	2657.9	97.6	2669.22	3.85	2669.21	3.83	0.42
67DT-17	3/12/2020 22:22	259.493	103.0268	0.410295	0.27054	0.138248	4.588678	1.980408	4.499898723	0.182121	0.409792	2655.7	42.5	2635	97.3	2671.54	6.78	2671.36	6.66	1.37
67DT-18	3/12/2020 22:45	496.1401	188.9795	0.393624	0.211081	0.133529	4.567471	2.038536	4.51818226	0.18048	0.308027	2620	42.5	2573	95.9	2656.54	5.11	2656.32	4.91	3.14
67DT-19	4/12/2020 0:01	346.7186	118.4038	0.352907	0.263552	0.118312	4.631405	2.496965	4.496893196	0.171496	0.454656	2384.2	41.5	2171.3	82.9	2571.55	7.6	2569.08	6.23	15.56
67DT-2	3/12/2020 13:33	749.6213	338.3699	0.466468	0.868271	0.130972	4.755691	2.159261	4.647844213	0.175542	0.657023	2540.3	43.8	2453.3	94.8	2610.4	10.9	2608.6	10.1	6.02
67DT-20	4/12/2020 0:24	391.9087	159.6022	0.420849	0.228816	0.134746	4.558368	1.992971	4.491781241	0.183276	0.341291	2655.7	42.4	2621.4	96.7	2682	5.64	2681.8	5.48	2.26
67DT-21	4/12/2020 0:47	479.8055	252.7952	0.544472	0.762452	0.132654	4.650992	2.102577	4.551975995	0.181048	0.315101	2594	42.7	2508.1	94.6	2661.75	5.22	2661.33	4.86	5.77
67DT-3	3/12/2020 13:56	309.9531	87.81868	0.292794	0.284901	0.133894	4.612929	2.091237	4.496560491	0.181416	0.390178	2600.9	42.3	2519.4	93.8	2665.11	6.46	2664.49	6.03	5.47
67DT-4	3/12/2020 14:19	239.5415	125.8072	0.542746	0.266184	0.136374	4.583914	1.982257	4.504476108	0.183988	0.438874	2664.4	42.6	2633	97.4	2688.41	7.25	2688.11	7.06	2.06
67DT-5	3/12/2020 15:28	616.5366	188.978	0.316755	0.20855	0.133	4.547179	2.05161	4.485341902	0.180365	0.277132	2613.4	42.2	2559.5	94.8	2655.48	4.59	2655.27	4.39	3.61
67DT-6	3/12/2020 15:50	612.9384	269.3411	0.454106	0.191377	0.130067	4.561666	2.162194	4.522302945	0.179258	0.292773	2558.5	42.3	2450.6	92.2	2645.27	4.86	2644.8	4.43	7.36
67DT-7	3/12/2020 16:14	636.1915	198.8545	0.323013	0.848712	0.119255	4.776571	2.716658	4.619475307	0.152586	0.38386	2201.4	41.7	2020.5	80.1	2374.34	6.54	2372.59	5.42	14.90
67DT-8	3/12/2020 17:00	297.2827	117.909	0.409873	0.250482	0.131856	4.576745	1.996345	4.495623336	0.183837	0.603986	2657	42.7	2617.7	96.7	2687.05	9.98	2686.35	9.64	2.58
67DT-9	3/12/2020 17:22	297.4659	79.25224	0.275325	0.718815	0.126988	4.803695	2.189923	4.61313541	0.177309	0.41374	2536.5	43.2	2424.7	93.2	2627.11	6.88	2626.16	6.24	7.70

Appendix D2.2: SHRIMP U/Pb Standards

Spot Fundamentals		SQUID OUTPUTS 27.01.2021										ISOPLOT R AGE CALCS								DTB Calcs
Fraction	Date/Time	U (ppm)	Th (ppm)	232Th /238U	+/-1sigma	4-corr 208* /232	+/-1sigma	4-corr 238 /206*	+/-1sigma %	4-corr 207* /206*	+/-1sigma	207/235	1sigma Ma	206/238	1sigma Ma	207/206	1sigma Ma	Concordia Age	1sigma Ma	Discordance
OGC-1	2/12/2020 12:49	116.8504	77.20861	0.682821	0.336222	0.185055	4.622232	1.354281	4.529620718	0.298228	0.418792	3498.2	44.7	3565	124	3460.35	6.49	3564.64	5.44	-3.02
OGC-1	8/12/2020 10:46	282.21	170.2833	0.62355	0.363085	0.190776	2.470346	1.412668	2.289737609	0.299881	0.406531	3462.1	22.8	3450.5	61.2	3468.91	6.3	3468.72	6.22	0.53
OGC-10	4/12/2020 1:47	161.1597	52.86415	0.338982	0.372119	0.188421	4.725698	1.382113	4.600009636	0.296913	0.373977	3473.9	45.3	3509	124	3453.49	5.8	3509.26	5.26	-1.61
OGC-11	4/12/2020 6:25	187.4651	154.7243	0.852922	0.278761	0.171291	4.587918	1.496572	4.517312592	0.301396	0.396712	3410.5	44.4	3299	117	3476.72	6.14	3476.27	5.74	5.11
OGC-2	2/12/2020 15:06	93.42488	60.90468	0.67369	0.889841	0.194051	4.728354	1.355634	4.539503293	0.300368	0.446708	3504.2	44.8	3562	124	3471.43	6.92	3561.91	5.93	-2.61
OGC-2	8/12/2020 11:07	257.6634	211.3093	0.847496	0.35187	0.182231	2.455159	1.407638	2.301618265	0.300919	0.427754	3469	23	3460	61.6	3474.26	6.62	3474.1	6.55	0.41
OGC-3	2/12/2020 21:17	56.1525	27.76209	0.510922	0.897618	0.187714	4.874294	1.355972	4.581727262	0.298531	0.57389	3498	45.4	3561	125	3461.92	8.89	3561.22	7.51	-2.86
OGC-3	8/12/2020 15:50	256.5092	219.6716	0.884998	0.351146	0.174733	2.477691	1.430895	2.306966564	0.298726	0.4372	3445.8	23	3416.3	61.2	3462.93	6.78	3462.38	6.63	1.35
OGC-4	3/12/2020 4:26	101.2382	52.86829	0.539663	0.390102	0.183882	4.689806	1.397894	4.540390371	0.302165	0.458757	3479.9	44.8	3479	122	3480.66	7.1	3480.65	7.08	0.05
OGC-4	8/12/2020 19:38	154.1068	134.7953	0.903909	0.428992	0.179552	2.6587	1.459878	2.387311615	0.297813	0.584039	3423.1	24.1	3363.5	62.6	3458.19	9.05	3456.33	8.68	2.74
OGC-5	3/12/2020 10:21	197.3397	155.0681	0.812044	0.253155	0.182014	4.555753	1.419381	4.507728419	0.299151	0.329236	3455.1	44.4	3438	120	3465.14	5.1	3465.09	5.05	0.78
OGC-5	8/12/2020 23:05	148.2808	84.3386	0.587778	0.473387	0.180363	2.832832	1.407987	2.379002542	0.299736	0.562848	3464.9	24	3459.3	63.7	3468.16	8.72	3468	8.61	0.26
OGC-6	3/12/2020 13:10	287.0915	245.0727	0.882158	0.2069	0.176792	4.611336	1.44555	4.536751368	0.298829	0.268484	3436.1	44.6	3389	120	3463.47	4.16	3463.38	4.04	2.15
OGC-6	9/12/2020 2:57	199.1519	92.10318	0.477927	1.224248	0.180312	3.10704	1.407321	2.342282411	0.29672	0.528268	3455.5	23.6	3460.6	62.7	3452.49	8.19	3460.61	8.01	-0.23
OGC-7	3/12/2020 15:04	171.0295	139.1057	0.840516	0.266356	0.178174	4.568067	1.444334	4.512676078	0.299662	0.703653	3439.7	44.8	3392	119	3467.8	10.9	3467.2	10.6	2.19
OGC-7	9/12/2020 7:01	88.31484	45.40984	0.531359	0.622478	0.191301	3.21373	1.416842	2.513854176	0.304488	0.71615	3474.2	25.7	3442.6	67.1	3492.5	11.1	3491.2	10.8	1.43
OGC-8	3/12/2020 18:51	161.6706	84.26102	0.538601	0.31652	0.183565	4.61469	1.376344	4.516208737	0.300984	0.375268	3491.3	44.5	3521	123	3474.6	5.81	3520.6	5.36	-1.34
OGC-9	3/12/2020 23:36	90.48369	60.67674	0.692985	0.719676	0.186127	4.736919	1.394378	4.560978392	0.297796	0.538906	3468.1	45.1	3485	123	3458.1	8.35	3485.42	7.94	-0.78

Appendix D2.3: SIMS O- Results

Analysis session 1 20 µm diameter, 2.5 nA, Cs^{+} ion-beam

Sample #	Analysis #	*Raw Data from CIPS*			SIMS corrected			Drift corrected		***Notes***
		18O/16O	1sigma error		d18O	± per mil		OH/O	± rel (%)	
37DTB19	OH-DB_09-DB20_37DTB19@01	0.002016266	3.06086E-07		5.51884379	0.151808103		0.000857162	0.3608533	
37DTB19	OH-DB_09-37DB19@02	0.002016441	3.32346E-07		5.606012346	0.164818147		0.000759828	0.1151747	
37DTB19	OH-DB_09-37DB19@03	0.002015946	2.81726E-07		5.359034772	0.139748723		0.000745774	0.1942408	
37DTB19	OH-DB_09-37DB19@04	0.00201548	2.88722E-07		5.126585291	0.143252387		0.000795772	0.4011484	
37DTB19	OH-DB_09-37DB19@05	0.002015897	3.39436E-07		5.334487305	0.168379672		0.00076661	0.2437459	
37DTB19	OH-DB_09-37DB19@06	0.002015423	2.99935E-07		5.098030075	0.148819812		0.000986084	0.2392039	
37DTB19	OH-DB_09-37DB19@07	0.002015292	2.84799E-07		5.032904143	0.141319191		0.000808253	0.567568	
37DTB19	OH-DB_09-37DB19@08	0.002016017	3.16431E-07		5.394603551	0.156958348		0.000861948	0.5737716	
37DTB19	OH-DB_09-37DB19@09	0.002015448	3.18059E-07		5.110554292	0.15781074		0.000858881	0.4914057	
37DTB19	OH-DB_09-37DB19@10	0.002014307	2.91251E-07		4.541453839	0.144591377		0.000766662	0.1029989	
37DTB19	OH-DB_09-37DB19@11	0.002014643	2.69003E-07		4.709278356	0.133524047		0.000820311	0.5304983	
37DTB19	OH-DB_09-37DB19@12	0.00201529	3.03855E-07		5.031902205	0.150774969		0.000748316	0.1278924	
37DTB19	OH-DB_09-37DB19@13	0.002015458	2.85052E-07		5.11556398	0.14143272		0.000792465	0.2259297	
37DTB19	OH-DB_09-37DB19@14	0.002015777	3.22489E-07		5.274872029	0.159982353		0.000753895	0.4566869	
37DTB19	OH-DB_09-37DB19@15	0.002016066	3.42332E-07		5.419151017	0.169801831		0.000716048	0.2629586	
37DTB19	OH-DB_09-37DB19@16	0.002016213	2.81178E-07		5.492292449	0.139458705		0.000804882	0.363914	
37DTB19	OH-DB_09-37DB19@17	0.002015205	3.00356E-07		4.989319865	0.149044993		0.000792993	0.2558843	
37DTB19	OH-DB_09-37DB19@18	0.002015534	2.81848E-07		5.153637601	0.139837888		0.000799125	0.1219552	
37DTB19	OH-DB_09-37DB19@19	0.002014837	3.21374E-07		4.805965317	0.159503905		0.000902445	0.2574412	
37DTB19	OH-DB_09-37DB19@20	0.002015767	4.09255E-07		5.269862342	0.203027147		0.000745844	0.1927767	
46DTB19	OH-DB_09-46DB19@01	0.002015749	3.12402E-07		5.260844905	0.154980417		0.000791339	0.4824054	
46DTB19	OH-DB_09-46DB19@02	0.002016283	3.83631E-07		5.527360259	0.190266324		0.000756203	0.3999153	
46DTB19	OH-DB_09-46DB19@03	0.002016438	2.90515E-07		5.60450944	0.144073574		0.000774367	0.5494097	
46DTB19	OH-DB_09-46DB19@04	0.002016929	3.08165E-07		5.849483139	0.152788979		0.000770785	0.1987718	
46DTB19	OH-DB_09-46DB19@05	0.002017005	3.17804E-07		5.887055792	0.157562422		0.000821509	0.5677005	
46DTB19	OH-DB_09-46DB19@06	0.002016197	2.98799E-07		5.48427695	0.148199406		0.000786919	0.2243366	
46DTB19	OH-DB_09-46DB19@07	0.002015497	3.05506E-07		5.135101759	0.151578558		0.000867206	0.4198946	
46DTB19	OH-DB_09-46DB19@08	0.002015671	2.90978E-07		5.221769346	0.144358029		0.001003019	0.9196111	
~~46DTB19~~	~~OH-DB_09-46DB19@09~~	~~0.002017~~	~~2.71523E-07~~		~~5.884550948~~	~~0.134617258~~		~~0.001395404~~	~~1.015526~~	omitted high OH/O-
46DTB19	OH-DB_09-46DB19@10	0.002016567	3.27575E-07		5.668633435	0.162441742		0.000872832	0.1851135	
46DTB19	OH-DB_09-46DB19@11	0.002016368	2.9277E-07		5.56944163	0.145196642		0.000921191	0.5056991	
~~46DTB19~~	~~OH-DB_09-46DB19@12~~	~~0.002017166~~	~~2.95829E-07~~		~~5.967711754~~	~~0.146655891~~		~~0.002378079~~	~~2.745597~~	omitted high OH/O-
46DTB19	OH-DB_09-46DB19@13	0.002016505	2.66461E-07		5.638074343	0.132140071		0.001005206	0.217211	
~~46DTB19~~	~~OH-DB_09-46DB19@14~~	~~0.002016386~~	~~2.58765E-07~~		~~5.578459067~~	~~0.128331081~~		~~0.001186586~~	~~0.6217962~~	omitted high OH/O-
46DTB19	OH-DB_09-46DB19@15	0.002015347	3.72267E-07		5.060457422	0.184716174		0.000943951	0.7896001	
46DTB19	OH-DB_09-46DB19@16	0.002015323	3.03353E-07		5.048434173	0.150523469		0.001043421	0.4183532	
46DTB19	OH-DB_09-46DB19@17	0.002015864	2.98742E-07		5.317955338	0.148195591		0.000856083	0.2268726	
46DTB19	OH-DB_09-46DB19@18	0.002015603	3.30695E-07		5.188204442	0.164067722		0.000910641	0.2741711	
46DTB19	OH-DB_09-46DB19@19	0.002016272	2.71938E-07		5.521849603	0.134871544		0.000886009	0.1250535	
46DTB19	OH-DB_09-46DB19@20	0.002016962	3.23785E-07		5.865514137	0.16053106		0.000882343	0.2237801	
~~67DTB19~~	~~OH-DB_09-67DB19@01~~	~~0.002020957~~	~~3.92151E-07~~		~~7.857866694~~	~~0.194042027~~		~~0.001780457~~	~~4.975086~~	omitted high OH/O-
67DTB19	OH-DB_09-67DB19@02	0.002016982	2.74882E-07		5.875533511	0.136283737		0.00071295	0.5009309	
~~67DTB19~~	~~OH-DB_09-67DB19@03~~	~~0.002018159~~	~~2.84159E-07~~		~~6.462668839~~	~~0.14080088~~		~~0.001694431~~	~~4.486829~~	omitted high OH/O-
67DTB19	OH-DB_09-67DB19@04	0.002016811	2.87526E-07		5.790368831	0.142564532		0.000914548	1.120014	
67DTB19	OH-DB_09-67DB19@05	0.002012857	2.90348E-07		3.818555991	0.144246603		0.000710549	5.998934	
67DTB19	OH-DB_09-67DB19@06	0.002016481	3.16902E-07		5.626051094	0.157155752		0.000679686	0.1958074	
67DTB19	OH-DB_09-67DB19@07	0.002016347	2.98094E-07		5.558921287	0.14783864		0.000711895	0.4390393	
67DTB19	OH-DB_09-67DB19@08	0.002016024	3.17266E-07		5.398110332	0.157372094		0.000706171	3.334309	
67DTB19	OH-DB_09-67DB19@09	0.002016131	3.8142E-07		5.451213015	0.189184371		0.000808887	1.802832	
67DTB19	OH-DB_09-67DB19@10	0.002015924	2.80113E-07		5.348013461	0.138950289		0.000725139	0.3149293	
67DTB19	OH-DB_09-67DB19@11	0.002015411	3.24853E-07		5.09201845	0.161184488		0.000703479	0.218183	
67DTB19	OH-DB_09-67DB19@12	0.002016514	3.24684E-07		5.642082093	0.161012678		0.000762307	0.2272872	
67DTB19	OH-DB_09-67DB19@13	0.002016064	3.34509E-07		5.41814908	0.165921817		0.000672457	0.3035271	
67DTB19	OH-DB_09-67DB19@14	0.002016162	2.81184E-07		5.466743045	0.139465173		0.00069224	0.2536313	
67DTB19	OH-DB_09-67DB19@15	0.0020153	3.536E-07		5.036911892	0.175457584		0.000701259	0.2124638	
67DTB19	OH-DB_09-67DB19@16	0.002015918	2.75734E-07		5.345007648	0.136778464		0.000690229	0.3118861	
67DTB19	OH-DB_09-67DB19@17	0.002012996	3.23452E-07		3.887689673	0.160681932		0.000759254	0.7287932	
67DTB19	OH-DB_09-67DB19@18	0.002015898	3.4336E-07		5.334988274	0.170326268		0.000774998	1.460556	
67DTB19	OH-DB_09-67DB19@19	0.0020153	2.66571E-07		5.036911892	0.132273386		0.000783027	0.1887783	
67DTB19	OH-DB_09-67DB19@20	0.002015229	3.4611E-07		5.001343114	0.171747071		0.000790339	0.5659688	

Analysis session 2 10 µm diameter, 1.0 nA, Cs^{+} ion-beam

Sample #	Analysis #	*Raw Data from CIPS*			SIMS corrected			Drift corrected		***Notes***
		18O/16O	1sigma error		d18O	± per mil		OH/O	± rel (%)	
52DTB19	OH-DB_52DTB19@1	0.00201456	3.65128E-07		4.667697953	0.181244599		0.000951835	0.187781	
52DTB19	OH-DB_52DTB19@2	0.002013571	3.23901E-07		4.174744744	0.160859222		0.001172443	0.5562904	
52DTB19	OH-DB_52DTB19@3	0.002014413	3.05061E-07		4.594556522	0.151439222		0.000997259	0.2089095	
52DTB19	OH-DB_52DTB19@4	0.00201449	3.20391E-07		4.633131113	0.15904311		0.000952211	0.2070688	
52DTB19	OH-DB_52DTB19@5	0.002012897	2.97348E-07		3.83859474	0.147721254		0.000975512	0.1273858	
52DTB19	OH-DB_52DTB19@6	0.002014484	3.00463E-07		4.6301253	0.14915154		0.000943785	0.1370374	
52DTB19	OH-DB_52DTB19@7	0.00201525	2.9129E-07		5.011863457	0.144542949		0.001173869	0.6260424	
52DTB19	OH-DB_52DTB19@8	0.002014478	3.40544E-07		4.627119488	0.169048024		0.001013108	0.2638681	

Appendix D2.4: SIMS O- Standards

Analysis session 1 20 µm diameter, 2.5 nA, Cs[+] ion-beam

Sample #	Analysis #	Raw Data from CIPS			SIMS corrected			Drift corrected		Notes
		18O/16O	1sigma error		d18O	± per mil		OH/O	± rel (%)	
91500	OH-DB_09-DB20_91500@4	0.002025401	2.73962E-07		10.07415226	0.135263313		0.000687249	0.5323319	
91500	OH-DB_09-DB20_91500@3	0.002025391	3.3901E-07		10.06914258	0.16738018		0.000656006	0.2116581	
91500	OH-DB_09-DB20_91500@2	0.00202526	2.84147E-07		10.00401664	0.140301653		0.000661941	0.4074392	
91500	OH-DB_09-DB20_91500@14	0.002025039	2.95929E-07		9.893803528	0.14613504		0.000670406	0.1463796	
91500	OH-DB_09-DB20_91500@13	0.002025428	3.43505E-07		10.08767842	0.169596216		0.000652035	0.1458913	
91500	OH-DB_09-DB20_91500@12	0.002024792	3.19069E-07		9.770565226	0.157580972		0.000670077	0.3364866	
91500	OH-DB_09-DB20_91500@11	0.002025348	2.71902E-07		10.04810189	0.134249664		0.000676422	0.5313374	
91500	OH-DB_09-DB20_91500@09	0.002025177	3.48236E-07		9.962436241	0.171953366		0.000692961	0.5174865	
91500	OH-DB_09-DB20_91500@08	0.002024948	2.77273E-07		9.848215376	0.136928478		0.000662578	0.1474669	
91500	OH-DB_09-DB20_91500@07	0.0020252	2.81412E-07		9.973958522	0.138955236		0.000677362	0.1864196	
91500	OH-DB_09-DB20_91500@06	0.002025184	2.94617E-07		9.965943022	0.145476677		0.000664564	0.3690465	
91500	OH-DB_09-DB20_91500@05	0.002024706	2.79989E-07		9.727481917	0.138286387		0.000694405	0.5311041	
91500	OH-DB_09-DB20_91500@010	0.002025113	3.50732E-07		9.930875213	0.173191217		0.000658301	0.1500499	
91500	OH-DB_09-DB20_91500@01	0.002024858	3.06937E-07		9.803629161	0.151584245		0.000665258	0.3946493	
OGC	OH-DB_09-DB20_OGC@13	0.002016687	3.08647E-07		5.72874968	0.153046334		0.001089232	0.140743	
OGC	OH-DB_09-DB20_OGC@12	0.002016559	3.1645E-07		5.664625685	0.156925875		0.001043832	0.1129922	
OGC	OH-DB_09-DB20_OGC@11	0.00201674	3.98285E-07		5.754800053	0.197489386		0.000948023	0.3038348	
OGC	OH-DB_09-DB20_OGC@10	0.002016268	2.86055E-07		5.519845728	0.141873554		0.000981907	0.1130113	
OGC	OH-DB_09-DB20_OGC@09	0.002016035	3.18542E-07		5.403620987	0.158003934		0.000957154	0.2112503	
OGC	OH-DB_09-DB20_OGC@08	0.002015189	2.91543E-07		4.981304365	0.144672793		0.000915684	0.1470667	
OGC	OH-DB_09-DB20_OGC@07	0.002016805	3.18388E-07		5.787363019	0.1578676		0.00100767	0.209695	
OGC	OH-DB_09-DB20_OGC@06	0.002016358	2.90876E-07		5.564431943	0.144257908		0.000893493	0.1580112	
OGC	OH-DB_09-DB20_OGC@05	0.002016569	3.54759E-07		5.669635372	0.175921933		0.00083367	0.2175937	
OGC	OH-DB_09-DB20_OGC@04	0.002016356	3.43124E-07		5.563430006	0.170170348		0.000856599	0.2124317	
OGC	OH-DB_09-DB20_OGC@03	0.0020179	2.6318E-07		6.333418912	0.13042275		0.000925105	0.3843214	
OGC	OH-DB_09-DB20_OGC@02	0.002016758	3.14937E-07		5.763817489	0.156160053		0.000819279	0.4766153	
OGC	OH-DB_09-DB20_OGC@01	0.002017293	3.10541E-07		6.030833811	0.153939654		0.000986657	0.2255265	
M257	OH-DB_09-DB20_M257@4	0.002033391	2.98287E-07		14.05885738	0.146694184		0.000643488	0.2676096	
M257	OH-DB_09-DB20_M257@30	0.002033596	3.25667E-07		14.16105499	0.16014357		0.000654028	0.195474	
M257	OH-DB_09-DB20_M257@3	0.002033235	2.78309E-07		13.98120723	0.136879808		0.000650297	0.1625557	
M257	OH-DB_09-DB20_M257@29	0.002033071	2.99631E-07		13.89954933	0.147378253		0.000662105	0.1113873	
M257	OH-DB_09-DB20_M257@28	0.002032616	3.08013E-07		13.6726105	0.151535136		0.0006703	0.3621382	
M257	OH-DB_09-DB20_M257@27	0.002033152	3.02482E-07		13.93962682	0.148774856		0.000638871	0.1699941	
M257	OH-DB_09-DB20_M257@26	0.002032675	3.33561E-07		13.70166669	0.164099626		0.000670975	0.398922	
M257	OH-DB_09-DB20_M257@25	0.002033107	3.07945E-07		13.91708323	0.151465412		0.000641157	0.1556723	
M257	OH-DB_09-DB20_M257@24	0.002032869	2.88182E-07		13.79885462	0.141761172		0.000642864	0.3452287	
M257	OH-DB_09-DB20_M257@23	0.002033209	3.02998E-07		13.96818204	0.149024494		0.000646363	0.2559461	
M257	OH-DB_09-DB20_M257@22	0.002033046	3.24747E-07		13.88702511	0.15973423		0.00067389	0.3661834	
M257	OH-DB_09-DB20_M257@21	0.002032833	3.28822E-07		13.78081974	0.161755516		0.000675872	0.255695	
M257	OH-DB_09-DB20_M257@20	0.002033173	3.3958E-07		13.95014717	0.167019848		0.000658617	0.2600312	
M257	OH-DB_09-DB20_M257@2	0.00203327	2.98378E-07		13.99874113	0.14674806		0.000648604	0.1942788	
M257	OH-DB_09-DB20_M257@19	0.002033451	3.32724E-07		14.0889155	0.163625035		0.000651835	0.1603915	
M257	OH-DB_09-DB20_M257@18	0.00203246	2.72836E-07		13.59445938	0.134239145		0.000680224	0.2829176	
M257	OH-DB_09-DB20_M257@17	0.00203294	2.60471E-07		13.83392243	0.128125275		0.000667519	0.3641615	
M257	OH-DB_09-DB20_M257@16	0.002033281	2.77544E-07		14.00425179	0.136500688		0.000658583	0.2886507	
M257	OH-DB_09-DB20_M257@15	0.002033245	3.22523E-07		13.98621691	0.158624509		0.000642591	0.1161775	
M257	OH-DB_09-DB20_M257@14	0.002033524	3.00555E-07		14.12548622	0.147800214		0.000645779	0.2443702	
M257	OH-DB_09-DB20_M257@13	0.00203345	3.36534E-07		14.08841453	0.165498782		0.000650669	0.1970071	
M257	OH-DB_09-DB20_M257@12	0.002034067	3.23027E-07		14.39600932	0.158808488		0.000647806	0.2153644	
M257	OH-DB_09-DB20_M257@11	0.002033583	3.03471E-07		14.1545424	0.1492296		0.000648651	0.2560871	
M257	OH-DB_09-DB20_M257@10	0.002033712	3.83584E-07		14.21916736	0.188612903		0.000667922	0.2456096	
M257	OH-DB_09-DB20_M257@09	0.002033519	3.1474E-07		14.12298137	0.154776226		0.000659663	0.2778733	
M257	OH-DB_09-DB20_M257@08	0.002033513	2.77601E-07		14.11997556	0.136512877		0.000667268	0.2093164	
M257	OH-DB_09-DB20_M257@07	0.002033864	3.65642E-07		14.29481364	0.179777259		0.00064654	0.2257004	
M257	OH-DB_09-DB20_M257@06	0.002033357	3.57767E-07		14.04182444	0.175948953		0.000660983	0.2102762	
M257	OH-DB_09-DB20_M257@05	0.002033608	3.22347E-07		14.16706662	0.158509873		0.000624511	0.41315	
M257	OH-DB_09-DB20_M257@02	0.002033185	3.24303E-07		13.95615879	0.159504744		0.000643087	0.231571	
M257	OH-DB_09-DB20_M257@01	0.002033329	3.22878E-07		14.02779732	0.15879291		0.000660593	0.3742145	
M257	OH-DB_09-DB20_M257@01	0.002033259	3.25413E-07		13.99323048	0.160045095		0.000655022	0.2275834	

Analysis session 2 10 µm diameter, 1.0 nA, Cs[+] ion-beam

Sample #	Analysis #	Raw Data from CIPS			SIMS corrected			Drift corrected		Notes
		18O/16O	1sigma error		d18O	± per mil		OH/O	± rel (%)	
M257	OH-DB_52DTB19_M257@7	0.002033513	3.46641E-07		14.11997556	0.170464127		0.0008626	0.2054075	
M258	OH-DB_52DTB19_M257@6	0.002033424	3.18243E-07		14.07538934	0.156505899		0.000900419	0.1926557	
M259	OH-DB_52DTB19_M257@5	0.00203344	3.04378E-07		14.08340484	0.149686074		0.000975826	0.4281997	
M260	OH-DB_52DTB19_M257@4	0.002033133	2.98886E-07		13.93010842	0.147007435		0.000949523	0.3940813	
M261	OH-DB_52DTB19_M257@2	0.002033196	2.88108E-07		13.96166945	0.141702169		0.000946904	0.1929651	
M262	OH-DB_52DTB19_M257@01	0.002032816	3.45779E-07		13.77230328	0.170098706		0.000957122	0.1667874	
~~91500~~	~~OH-DB_52DTB19_91500@01~~	~~0.002025602~~	~~3.24555E-07~~		~~10.17434601~~	~~0.160226595~~		~~0.001010495~~	~~0.4473895~~	omitted sample topology
~~91500~~	~~OH-DB_52DTB19_91500@2~~	~~0.002025449~~	~~3.35421E-07~~		~~10.09819876~~	~~0.165603069~~		~~0.001012409~~	~~0.5280014~~	omitted sample topology
~~91500~~	~~OH-DB_52DTB19_91500@3~~	~~0.002025547~~	~~3.19891E-07~~		~~10.1472937~~	~~0.157928369~~		~~0.000988545~~	~~0.3153125~~	omitted sample topology
~~91500~~	~~OH-DB_52DTB19_91500@4~~	~~0.002025569~~	~~2.8907E-07~~		~~10.15831501~~	~~0.142710472~~		~~0.000825623~~	~~0.1556147~~	omitted sample topology
~~91500~~	~~OH-DB_52DTB19_91500@5~~	~~0.002025503~~	~~2.9946E-07~~		~~10.12525107~~	~~0.147844556~~		~~0.000823978~~	~~0.3675927~~	omitted sample topology
OGC	OH-DB_52DTB19_OGC@01	0.002017058	2.9771E-07		5.913607133	0.147596137		0.001304474	0.2429095	
OGC	OH-DB_52DTB19_OGC@03	0.002017023	3.38173E-07		5.896073229	0.167659562		0.001092478	0.1834291	
OGC	OH-DB_52DTB19_OGC@2	0.002016708	3.38891E-07		5.739270023	0.168041624		0.001308865	0.5039747	

Appendix D2.5: LA-ICPMS U/Pb-Lu/Hf Results

Curtin University Ge	Analysis date-time	Spot ID	238U conc.	±2σ INT	232Th conc.	±2σ INT	LA-ICP-MS Isotopic Ratios					Apparent Ages - Calculated in Isoplot R (Ma)				Discordance	Lu-Hf Isotopic Ratios from Iolite							εHf Calculations						
Sample ID			ppm		ppm		238U/206Pb	±2σ PROP	207Pb/206Pb	±2σ PROP	rho	238U/206Pb	±2σ PROP	207Pb/206Pb	±2σ PROP	(7/6-6/8)/7/6 *100	176Hf/177Hf 0.282785 0.283250	±2σ INT	(2% External ±)	176Lu/177Hf 0.03360 Bouvier et al., 2008 EPSL-273 0.03840 Griffin et al., 2002, Lithos-237	±2σ INT	176Yb/177Hf	±2σ INT	Hfi	εHf Lu decay	±2σ 0.02	TDM(Ga) Scherer et al., 2001, Science-293	TDMCrustal (Ga)	HfCHUR(t)	HfDM(t)
37DTB19	17/03/2021 (4)	37DTB-L - 1	1120	100	879	61	3.937008	0.22394448	0.09832	0.0025164	0.35039	1459.1	31.5	1591.66	5.33	8.33	0.281694	0.000037	0.005671	0.001913	0.000052	0.066	0.0018	0.28164	-5.51	1.30	2.24	2.630	0.281791501	0.28209403
37DTB19	17/03/2021 (4)	37DTB-L - 10	426	16	353	17	4.051864	0.21743469	0.09677	0.0025954	0.30431	1422	29	1561.92	6.52	8.96	0.281609	0.000032	0.005664	0.0008345	0.0000049	0.02392	0.00023	0.28158	-7.35	1.12	2.29	2.766	0.281791501	0.282115964
37DTB19	17/03/2021 (4)	37DTB-L - 11	2340	100	643	38	5.094244	0.29370665	0.09574	0.0023948	-0.39109	1155.4	25.8	1541.83	4.81	25.06	0.281639	0.000031	0.005664	0.0021	0.00014	0.0499	0.003	0.28158	-7.59	1.09	2.33	2.794	0.281791501	0.282130774
37DTB19	17/03/2021 (4)	37DTB-L - 12	702	44	430	20	3.812429	0.20999602	0.09701	0.0024902	0.20395	1501.6	31.3	1566.57	5.42	4.15	0.281593	0.000036	0.005668	0.001138	0.000031	0.03323	0.00098	0.28156	-8.24	1.26	2.33	2.820	0.281791501	0.282112535
37DTB19	17/03/2021 (4)	37DTB-L - 13	385	7.5	369	30	4.012841	0.21326669	0.09754	0.0026508	0.16999	1434.3	29	1576.77	6.85	9.04	0.2816	0.00003	0.005662	0.00098	0.0001	0.035	0.0042	0.28157	-7.83	1.05	2.31	2.787	0.281791501	0.282105013
37DTB19	17/03/2021 (4)	37DTB-L - 14	1123	33	733	18	4.224757	0.2363865	0.09722	0.0024444	0.17208	1369.5	29.2	1570.62	4.91	12.81	0.28156	0.000029	0.00566	0.00099	0.000026	0.02981	0.00082	0.28153	-9.26	1.02	2.37	2.881	0.281791501	0.282109549
37DTB19	17/03/2021 (4)	37DTB-L - 15	1416	64	1032	45	3.837299	0.21274475	0.09701	0.0023902	0.29269	1492.9	31.3	1566.57	4.43	4.70	0.281615	0.000031	0.005663	0.001773	0.000014	0.05852	0.00076	0.28156	-8.13	1.09	2.34	2.812	0.281791501	0.282112535
37DTB19	17/03/2021 (4)	37DTB-L - 16	1715	65	1037	19	4.257131	0.24002318	0.09668	0.0023536	0.10872	1360.1	29.3	1560.18	4.16	12.82	0.281675	0.000031	0.005665	0.001623	0.000051	0.0538	0.0019	0.28163	-5.83	1.09	2.25	2.672	0.281791501	0.282117247
37DTB19	17/03/2021 (4)	37DTB-L - 17	1063	36	369.2	8.6	4.610207	0.2533393	0.09679	0.0024958	0.21143	1265.5	26.7	1562.31	5.53	19.00	0.281679	0.00003	0.005664	0.0006223	0.0000062	0.01808	0.00023	0.28166	-4.65	1.05	2.18	2.595	0.281791501	0.282115676
37DTB19	17/03/2021 (4)	37DTB-L - 18	245	24	194	16	4.014452	0.21343802	0.0992	0.003184	0.46775	1433.8	29	1608.3	11.5	10.85	0.281694	0.000035	0.005669	0.001359	0.00001	0.04792	0.0004	0.28165	-4.93	1.23	2.21	2.583	0.281791501	0.282081752
37DTB19	17/03/2021 (4)	37DTB-L - 19	1957	53	1411	39	4.764173	0.27327609	0.09598	0.0023896	-0.1543	1228.3	27.2	1546.54	4.69	20.58	0.281601	0.00003	0.005662	0.001275	0.000012	0.03795	0.00028	0.28156	-8.08	1.05	2.33	2.823	0.281791501	0.282127302
37DTB19	17/03/2021 (4)	37DTB-L - 2	844	25	669	11	3.90625	0.22045902	0.09774	0.0025148	-0.053689	1469.3	31.4	1580.6	5.47	7.04	0.281584	0.000032	0.005664	0.001208	0.000016	0.03734	0.00068	0.28155	-8.65	1.12	2.35	2.836	0.281791501	0.282102188
37DTB19	17/03/2021 (4)	37DTB-L - 20	645	20	491	21	3.883495	0.21789799	0.09738	0.0025376	0.091151	1477	31.4	1573.7	5.79	6.14	0.281629	0.000029	0.005662	0.001224	0.000067	0.0426	0.0027	0.28159	-7.06	1.02	2.29	2.740	0.281791501	0.282107277
37DTB19	17/03/2021 (4)	37DTB-L - 3	519	25	232	28	4.251701	0.23941119	0.09856	0.0026512	-0.016695	1361.7	29.3	1596.22	6.57	14.69	0.281588	0.000029	0.005661	0.000627	0.000039	0.0208	0.0017	0.28157	-7.89	1.02	2.31	2.778	0.281791501	0.282090665
37DTB19	17/03/2021 (4)	37DTB-L - 4	299	13	158.6	5.7	5.38503	0.31073675	0.09745	0.002769	0.16016	1098	24.7	1575.04	8.03	30.29	0.281591	0.000033	0.005665	0.000851	0.00003	0.0256	0.001	0.28157	-8.02	1.16	2.32	2.800	0.281791501	0.282106289
37DTB19	17/03/2021 (4)	37DTB-L - 5	1174	43	921	70	3.898635	0.21960033	0.09755	0.002441	0.13002	1471.9	31.4	1576.96	4.79	6.66	0.281567	0.000031	0.005662	0.001612	0.000011	0.05085	0.00074	0.28152	-9.67	1.09	2.40	2.903	0.281791501	0.282104873
37DTB19	17/03/2021 (4)	37DTB-L - 6	1378	86	517	28	4.222973	0.23618687	0.09724	0.0023948	0.23958	1370	29.2	1571	4.42	12.79	0.281596	0.00003	0.005662	0.000935	0.000034	0.0272	0.0011	0.28157	-7.92	1.05	2.32	2.797	0.281791501	0.282109268
37DTB19	17/03/2021 (4)	37DTB-L - 7	1727	72	593	28	5.035247	0.28083794	0.09576	0.0023952	0.1761	1167.8	25.2	1542.22	4.81	24.28	0.281625	0.000032	0.005665	0.001253	0.000018	0.03478	0.00067	0.28159	-7.21	1.12	2.30	2.770	0.281791501	0.282130487
37DTB19	17/03/2021 (4)	37DTB-L - 8	1025	45	710	14	3.85505	0.21471763	0.09747	0.0024694	0.26197	1486.8	31.3	1575.43	5.09	5.63	0.281636	0.000031	0.005664	0.001507	0.00003	0.04534	0.00094	0.28159	-7.11	1.09	2.30	2.743	0.281791501	0.282106001
37DTB19	17/03/2021 (4)	37DTB-L - 9	451	26	255	12	3.536068	0.19570912	0.0971	0.002552	0.083883	1605.4	33.3	1568.3	6	-2.37	0.281606	0.000028	0.00566	0.0009672	0.000008	0.03206	0.00054	0.28158	-7.89	0.98	2.30	2.778	0.281799599	0.28211126
46DTB19	17/03/2021 (4)	46DTB-L - 10	2055	91	99.5	4.8	3.859514	0.1823252	0.11262	0.0005508	0.2211	1485.2	31.3	1841.3	4.43	19.34	0.28149	0.000026	0.005656	0.0004846	0.0000088	0.01747	0.0004	0.28147	-5.05	0.91	2.43	2.822	0.28161504	0.281897793
46DTB19	17/03/2021 (4)	46DTB-L - 8	3910	100	221.5	3	4.589261	0.21482546	0.10643	0.0005202	0.14562	1270.8	27	1738.33	4.48	26.90	0.281463	0.000021	0.00565	0.000913	0.000039	0.0344	0.0014	0.28143	-6.54	0.74	2.50	2.916	0.28161504	0.281897793
46DTB19	17/03/2021 (4)	46DTB-L - 12	3970	210	198	13	4.777831	0.22585697	0.10793	0.000459	-0.0086911	1225.1	26.4	1763.94	3.89	30.55	0.281517	0.000023	0.005653	0.000809	0.000033	0.03	0.0014	0.28149	-4.49	0.81	2.42	2.787	0.28161504	0.281897793
46DTB19	17/03/2021 (4)	46DTB-L - 6	3530	160	184	11	4.90918	0.24582051	0.10894	0.0005202	-0.27712	1195.2	27.3	1780.95	4.35	32.89	0.281614	0.000026	0.005658	0.0005949	0.0000089	0.02285	0.00036	0.28159	-0.78	0.91	2.27	2.551	0.28161504	0.281897793
46DTB19	17/03/2021 (4)	46DTB-L - 1	2109	86	79	3.5	4.743833	0.22265407	0.11239	0.0004998	-0.09462	1233.1	26.3	1837.6	4.03	32.90	0.282065	0.000046	0.005687	0.0003788	0.0000049	0.01354	0.00022	0.28205	15.50	1.61	1.65	1.503	0.28161504	0.281897793
46DTB19	17/03/2021 (4)	46DTB-L - 15	3320	130	156.9	7.5	4.975124	0.25246897	0.10949	0.0004488	0.14437	1180.7	27.4	1790.12	3.73	34.04	0.281794	0.00004	0.005676	0.000902	0.000012	0.03111	0.00045	0.28176	5.23	1.40	2.04	2.167	0.28161504	0.281897793
46DTB19	17/03/2021 (4)	46DTB-L - 13	3970	200	270	13	5.714286	0.53289798	0.10792	0.0005814	0.060123	1039.6	44.8	1763.77	4.92	41.06	0.281542	0.000027	0.005658	0.000815	0.000013	0.02755	0.00024	0.28151	-3.61	0.95	2.38	2.731	0.28161504	0.281897793
46DTB19	17/03/2021 (4)	46DTB-L - 11	2600	120	89.2	4.7	5.583473	0.29890753	0.11041	0.0005202	0.044635	1062.1	26.2	1805.35	4.28	41.17	0.281937	0.000033	0.005672	0.000505	0.000011	0.0189	0.00062	0.28192	10.80	1.16	1.83	1.808	0.28161504	0.281897793
46DTB19	17/03/2021 (4)	46DTB-L - 4	3407	72	132.1	4.2	5.988024	0.35476355	0.10873	0.0005304	-0.073122	995.6	27.3	1777.43	4.45	43.99	0.28162	0.000022	0.005654	0.0005883	0.0000086	0.02184	0.00038	0.28160	-0.56	0.77	2.26	2.537	0.28161504	0.281897793
46DTB19	17/03/2021 (4)	46DTB-L - 17	3550	220	498	30	6.101281	0.37590448	0.10904	0.0005406	-0.35497	978.4	28	1782.62	4.52	45.11	0.281657	0.000024	0.005657	0.000834	0.000013	0.02862	0.00072	0.28163	0.45	0.84	2.23	2.473	0.28161504	0.281897793
46DTB19	17/03/2021 (4)	46DTB-L - 19	2700	100	113.4	3.9	6.002401	0.2866453	0.11083	0.0006018	0.079299	993.4	22	1812.25	4.93	45.18	0.28277	0.00022	0.005875	0.000965	0.000015	0.03233	0.0004	0.28274	39.80	7.70	0.68	-0.099	0.28161504	0.281897793
46DTB19	17/03/2021 (4)	46DTB-L - 18	1840	190	62.7	6.2	6.079027	0.2902412	0.11175	0.0007038	-0.11213	981.7	21.7	1827.25	5.71	46.27	0.282055	0.000051	0.005692	0.000833	0.000028	0.0264	0.0013	0.28203	14.58	1.79	1.68	1.563	0.28161504	0.281897793
46DTB19	17/03/2021 (4)	46DTB-L - 16	1759	97	69.8	2.2	6.422608	0.30714668	0.11129	0.0005304	-0.15406	932.8	20.8	1819.77	4.32	48.74	0.28291	0.000052	0.00571	0.0005083	0.0000018	0.01625	0.00016	0.28289	45.35	1.82	0.48	-0.471	0.28161504	0.281897793
46DTB19	17/03/2021 (4)	46DTB-L - 3	2920	130	114.9	5.4	8.912656	0.50234969	0.1125	0.0007854	0.32739	685.5	18.3	1839.37	6.32	62.73	0.283023	0.000099	0.005759	0.000635	0.000015	0.02087	0.00053	0.28300	49.20	3.47	0.32	-0.732	0.28161504	0.281897793
46DTB19	17/03/2021 (4)	46DTB-L - 9	9160	720	546	55	11.83432	1.01425016	0.09861	0.0009078	-0.7383	522.9	21.5	1597.16	8.59	67.26	0.281644	0.000041	0.005674	0.000985	0.000026	0.03338	0.00091	0.28161	-0.20	1.44	2.25	2.514	0.28161504	0.281897793
46DTB19	17/03/2021 (4)	46DTB-L - 14	6630	750	187	18	11.08647	0.91518725	0.1076	0.000816	-0.63735	556.7	22	1758.34	6.93	68.34	0.281997	0.000029	0.005669	0.000798	0.000013	0.02619	0.0004	0.28197	12.56	1.02	1.76	1.694	0.28161504	0.281897793
46DTB19	17/03/2021 (4)	46DTB-L - 7	3660	380	129	13	11.60093	0.87854824	0.10717	0.0008466	-0.82959	533	19.4	1751.02	7.23	69.56	0.283318	0.000042	0.005708	0.000572	0.00001	0.02042	0.0005	0.28330	59.76	1.47	-0.10	-1.451	0.28161504	0.281897793
46DTB19	17/03/2021 (4)	46DTB-L - 20	9690	550	720	120	18.05054	1.39582206	0.099	0.000816	0.4016	347.6	13.1	1604.53	7.69	78.34	0.281562	0.000021	0.005652	0.000949	0.000011	0.03238	0.00036	0.28153	-3.07	0.74	2.36	2.696	0.28161504	0.281897793
46DTB19	17/03/2021 (4)	46DTB-L - 5	1.30E+04	1.10E+03	568	70	20.70393	1.31167818	0.09761	0.00102	-0.52576	304.08	9.41	1578.11	9.78	80.73	0.28363	0.00014	0.005813	0.000903	0.000025	0.0321	0.0011	0.28360	70.42	4.90	-0.55	-2.188	0.28161504	0.281897793
46DTB19	17/03/2021 (4)	46DTB-L - 2	1.68E+04	1.70E+03	1017	99	20.87683	2.40061692	0.09817	0.0009894	-0.62731	301.6	16.9	1588.81	9.42	81.02	0.281549	0.000025	0.005656	0.00103	0.000024	0.0394	0.0013	0.28151	-3.63	0.88	2.39	2.732	0.28161504	0.281897793
67DTB19	17/03/2021 (4)	67DTB-L - 8	340	16	159.4	7.4	2.087683	0.09780292	0.18008	0.0009996	0.25756	2522.9	48.9	2652.86	4.6	4.90	0.281147	0.000025	0.005648	0.0008821	0.0000075	0.03149	0.00037	0.28110	0.04	0.88	2.92	3.112	0.281101089	0.281303344
67DTB19	17/03/2021 (4)	67DTB-L - 14	368	15	215.5	7.6	2.154244	0.09940522	0.17578	0.00102	-0.29201	2458.1	47.2	2612.7	4.83	5.92	0.281184	0.000036	0.00566	0.001174	0.000023	0.04296	0.00078	0.28113	-0.07	1.26	2.90	3.088	0.281127207	0.281333553
67DTB19	17/03/2021 (4)	67DTB-L - 7	471	12	230.7	9.5	2.118195	0.09610622	0.18149	0.0008262	0.14182	2492.8	46.9	2665.79	3.77	6.49	0.28118	0.000036	0.00566	0.001071	0.000024	0.0369	0.0011	0.28113	1.16	1.26	2.89	3.050	0.281092676	0.281293613
67DTB19	17/03/2021 (4)	67DTB-L - 16	327	12	147	12	2.154708	0.10418372	0.1779	0.001326	-0.6472	2457.6	49.4	2632.64	6.19	6.65	0.28115	0.000031	0.005654	0.0006	0.00003	0.0216	0.0011	0.28112	0.20	1.09	2.90	3.086	0.281114242	0.281318556
67DTB19	17/03/2021 (4)	67DTB-L - 17	433	16	177	4.3	2.266546	0.11003944	0.17679	0.00102	-0.48568	2356	47.9	2622.24	4.8	10.15	0.281205	0.000028	0.005652	0.0009014	0.0000079	0.03041	0.00029	0.28116	1.38	0.98	2.85	3.003	0.281121004	0.281326379
67DTB19	17/03/2021 (4)	67DTB-L - 12	646	24	300.6	6.8	2.274795	0.10556378	0.17596	0.0008262	0.45454	2348.8	45.7	2614.41	3.91	10.16	0.28121	0.000031	0.005655	0.0011557	0.0000043	0.039367	0.000055	0.28115	0.93	1.09	2.86	3.025	0.281126095	0.281332267
67DTB19	17/03/2021 (4)	67DTB-L - 20	673	23	246.5	8.4	2.256318	0.10385579	0.17814	0.0008262	0.25583	2364.9	45.6	2634.88	3.85	10.25	0.281128	0.000027	0.00565	0.0009714	0.0000046	0.03635	0.00028	0.28108	-1.20	0.95	2.96	3.177	0.281112785	0.281316872
67DTB19	17/03/2021 (4)	67DTB-L - 15	727	11	284.2	3	2.247191	0.10301725	0.18015	0.0008466	0.14468	2373	45.5	2653.51	3.9	10.57	0.281153	0.000032	0.005655	0.001236	0.000012	0.04294	0.00064	0.28109	-0.37	1.12	2.94	3.138	0.281100666	0.281302855
67DTB19	17/03/2021 (4)	67DTB-L - 10	816	25	286.3	8.2	2.250731	0.10334212	0.18087	0.0007956	0.18655	2369.9	45.5	2660.12	3.65	10.91	0.281148	0.000036	0.005659	0.001085	0.000011	0.03761	0.00028	0.28109	-0.13	1.26	2.94	3.128	0.281096366	0.281297881
67DTB19	17/03/2021 (4)	67DTB-L - 11	635	20	269.2	8.9	2.303617	0.10825566	0.17751	0.0008772	-0.3597	2324.2	45.8	2629	4.11	11.59	0.28125	0.000037	0.005662	0.0011511	0.0000049	0.03911	0.00033	0.28119	2.69	1.30	2.80	2.924	0.281116609	0.281321294
67DTB19	17/03/2021 (4)	67DTB-L - 19	491.7	8.2	177.5	3.7	2.363507	0.11395777	0.17567	0.0007956	-0.16158	2274.5	46.2	2611.66	3.77	12.91	0.281229	0.000041	0.005666	0.0009639	0.0000061	0.03512	0.00035	0.28118	1.89	1.44	2.82	2.962	0.281127883	0.281334335
67DTB19	17/03/2021 (4)	67DTB-L - 6	589	19	299.9	8.4	2.392344	0.11091776	0.1754	0.001122	-0.47106	2251.4	44.1	2609.1	5.33	13.71	0.281332	0.00005	0.005677	0.001289	0.000025	0.04387	0.00092	0.28127	4.92	1.75	2.70	2.766	0.281129547	0.281336259
67DTB19	17/03/2021 (4)	67DTB-L - 4	882	12	480.9	5.6	2.416626	0.11318083	0.17419	0.0007548	0.17465	2232.3	44.2	2597.56	3.61	14.06	0.281229	0.000032	0.005657	0.001782	0.00003	0.06505	0.00093	0.28114	0.12	1.12	2.88	3.064	0.281137048	0.281344935
67DTB19	17/03/2021 (4)	67DTB-L - 2	649	23	283	11	2.445586	0.11590964	0.17264	0.0007752	0.26271	2209.9	44.3	2582.65	3.75	14.43	0.281202	0.000035	0.005659	0.0011047	0.0000095	0.03912	0.00056	0.28115	0.03	1.23	2.87	3.059	0.281146737	0.281356141
67DTB19	17/03/2021 (4)	67DTB-L - 5	899	19	257.6	6.1	2.529084	0.11743546	0.16804	0.0007344	-0.27887	2147.8	42.4	2537.46	3.66	15.36	0.281166	0.00003	0.005653	0.0009603	0.0000063	0.03558	0.00039	0.28112	-2.01	1.05	2.90	3.154	0.281176086	0.281390087
67DTB19	17/03/2021 (4)	67DTB-L - 18	312.5	5	104.9	2.1	2.603489	0.11753317	0.1707	0.001122	0.28569	2095.4	40.4	2563.77	5.5	18.27	0.281488	0.000032	0.005662	0.000758	0.00001	0.02643	0.00039	0.28145	10.38	1.12	2.45	2.379	0.281159002	0.281370327
67DTB19	17/03/2021 (4)	67DTB-L - 13	1122	25	353.9	7.7	2.701243	0.12652498	0.1647	0.000816	-0.48056	2030.3	40.8	2503.74	4.17	18.91	0.281186	0.000028	0.005652	0.0011698	0.0000034	0.04345	0.00029	0.28113	-2.41	0.98	2.89	3.154	0.28119797	0.281415399
67DTB19	17/03/2021 (4)	67DTB-L - 1	967	50	442	26	2.730748	0.12930418	0.16606	0.0009486	-0.40395	2011.5	40.9	2517.56	4.8	20.10	0.281178	0.000038	0.005662	0.001443	0.000067	0.0506	0.0025	0.28111	-2.86	1.33	2.92	3.192	0.281189002	0.281405027
67DTB19	17/03/2021 (4)	67DTB-L - 9	563	12	245.5	2.2	2.777778	0.12592594	0.17541	0.0009078	0.064084	1982.2	38.7	2609.19	4.31	24.03	0.281159	0.000033	0.005656	0.001033	0.0000045	0.03539	0.00016	0.28111	-0.78	1.16	2.92	3.131	0.281129489	0.281336192
67DTB19	17/03/2021 (4)	67DTB-L - 3	767	11	193	8.7	3.011141	0.13872469	0.16217	0.0008976	-0.26449	1848.6	37	2477.65	4.67	25.39	0.281243	0.000029	0.005654	0.001062	0.000011	0.0361	0.00062	0.28119	-0.79	1.02	2.81	3.030	0.281214892	0.281434972

Appendix D2.6: LA-ICPMS Trace Element Results

Curtin University Ge Sample ID	Analysis date-time	Spot ID	Si_ppm_m29	Si_ppm_m29_Int2SE	Si_ppm_m29_LOD	P_ppm_m31	P_ppm_m31_Int2SE	P_ppm_m31_LOD	Ca_ppm_m43	Ca_ppm_m43_Int2SE	Ca_ppm_m43_LOD	Ca_ppm_m44	Ca_ppm_m44_Int2SE	Ca_ppm_m44_LOD	Ti_ppm_m49	Ti_ppm_m49_Int2SE	Ti_ppm_m49_LOD	Y_ppm_m89
37DTB19	17/03/2021 (4)	37DTB-L - 1	1.44E+05	3.10E+03	780	1.48E+04	3.60E+03	59	3.21E+04	7.60E+03	320	3.16E+04	7.80E+03	64	6.9	1.3	0.95	2224
37DTB19	17/03/2021 (4)	37DTB-L - 10	1.48E+05	3.60E+03	840	78	22	55	Below LOD	Below LOD	290	Below LOD	Below LOD	58	6.9	1.8	0.75	425.9
37DTB19	17/03/2021 (4)	37DTB-L - 11	1.51E+05	4.50E+03	730	Below LOD	Below LOD	52	Below LOD	Below LOD	300	Below LOD	Below LOD	52	3.3	1.2	0.84	478.5
37DTB19	17/03/2021 (4)	37DTB-L - 12	1.48E+05	3.40E+03	840	72	27	57	Below LOD	Below LOD	300	Below LOD	Below LOD	53	3.8	1.2	0.86	608
37DTB19	17/03/2021 (4)	37DTB-L - 13	1.45E+05	2.90E+03	750	102	29	64	Below LOD	Below LOD	250	Below LOD	Below LOD	60	6.3	1.6	1.1	752
37DTB19	17/03/2021 (4)	37DTB-L - 14	1.43E+05	3.20E+03	710	115	27	64	Below LOD	Below LOD	330	Below LOD	Below LOD	59	5.7	1.6	0.59	630
37DTB19	17/03/2021 (4)	37DTB-L - 15	1.46E+05	3.60E+03	740	71	29	57	Below LOD	Below LOD	300	Below LOD	Below LOD	54	4.7	1.5	1.2	698
37DTB19	17/03/2021 (4)	37DTB-L - 16	1.51E+05	4.20E+03	890	203	47	63	Below LOD	Below LOD	300	154	61	52	8.1	1.8	0.62	733
37DTB19	17/03/2021 (4)	37DTB-L - 17	1.48E+05	3.70E+03	860	Below LOD	Below LOD	59	Below LOD	Below LOD	270	Below LOD	Below LOD	54	3	1.1	0.98	365
37DTB19	17/03/2021 (4)	37DTB-L - 18	1.47E+05	3.10E+03	860	244	55	57	Below LOD	Below LOD	290	91	57	54	13.8	2.5	1.1	1054
37DTB19	17/03/2021 (4)	37DTB-L - 19	1.54E+05	3.60E+03	800	293	51	55	Below LOD	Below LOD	300	348	87	54	18.7	2.7	1	615
37DTB19	17/03/2021 (4)	37DTB-L - 2	1.50E+05	3.30E+03	750	262	63	57	390	190	300	300	130	53	8.9	1.9	0.82	1228
37DTB19	17/03/2021 (4)	37DTB-L - 20	1.48E+05	4.60E+03	820	Below LOD	Below LOD	65	Below LOD	Below LOD	300	Below LOD	Below LOD	65	4.5	1.3	1.1	243.5
37DTB19	17/03/2021 (4)	37DTB-L - 3	1.52E+05	3.90E+03	720	338	33	62	Below LOD	Below LOD	280	Below LOD	Below LOD	58	14.3	2.2	0.61	2750
37DTB19	17/03/2021 (4)	37DTB-L - 4	1.49E+05	3.30E+03	910	71	26	54	Below LOD	Below LOD	260	Below LOD	Below LOD	62	5.1	1.6	1	605
37DTB19	17/03/2021 (4)	37DTB-L - 5	1.54E+05	3.30E+03	850	59	23	49	Below LOD	Below LOD	280	Below LOD	Below LOD	46	4.1	1.2	0.58	802
37DTB19	17/03/2021 (4)	37DTB-L - 6	1.49E+05	3.30E+03	680	96	25	54	Below LOD	Below LOD	250	Below LOD	Below LOD	58	1.49	0.94	1	865
37DTB19	17/03/2021 (4)	37DTB-L - 7	1.50E+05	3.50E+03	670	195	35	48	Below LOD	Below LOD	270	Below LOD	Below LOD	57	5.9	1.3	0.88	749
37DTB19	17/03/2021 (4)	37DTB-L - 8	1.53E+05	3.90E+03	800	87	30	55	Below LOD	Below LOD	270	Below LOD	Below LOD	53	4.6	1.4	0.31	583.4
37DTB19	17/03/2021 (4)	37DTB-L - 9	1.50E+05	4.00E+03	780	164	27	54	Below LOD	Below LOD	300	Below LOD	Below LOD	64	8.7	1.9	0.85	1065
46DTB19	17/03/2021 (4)	46DTB-L - 10	1.55E+05	3.40E+03	790	563	39	53	Below LOD	Below LOD	320	158	42	64	7.5	1.6	0.88	1640
46DTB19	17/03/2021 (4)	46DTB-L - 8	1.47E+05	3.30E+03	700	816	84	58	Below LOD	Below LOD	260	Below LOD	Below LOD	65	7.2	1.5	0.6	2130
46DTB19	17/03/2021 (4)	46DTB-L - 12	1.55E+05	3.30E+03	830	974	57	53	Below LOD	Below LOD	270	108	35	60	12.9	1.9	0.68	2690
46DTB19	17/03/2021 (4)	46DTB-L - 6	1.66E+05	4.90E+03	930	544	30	66	Below LOD	Below LOD	290	Below LOD	Below LOD	68	4.2	1.4	0.96	1326
46DTB19	17/03/2021 (4)	46DTB-L - 1	1.50E+05	3.60E+03	700	208	34	58	Below LOD	Below LOD	320	Below LOD	Below LOD	58	202	68	0.9	676
46DTB19	17/03/2021 (4)	46DTB-L - 15	1.57E+05	3.10E+03	910	1830	320	54	510	230	290	550	190	75	14	2.2	1	4610
46DTB19	17/03/2021 (4)	46DTB-L - 13	1.56E+05	4.10E+03	790	1114	58	54	Below LOD	Below LOD	240	Below LOD	Below LOD	67	14.4	2.1	1.4	2990
46DTB19	17/03/2021 (4)	46DTB-L - 11	1.55E+05	3.40E+03	820	527	43	50	Below LOD	Below LOD	270	Below LOD	Below LOD	51	4.6	1.2	1.1	2204
46DTB19	17/03/2021 (4)	46DTB-L - 4	1.55E+05	3.80E+03	760	881	42	60	Below LOD	Below LOD	210	Below LOD	Below LOD	64	9.3	2	0.87	2208
46DTB19	17/03/2021 (4)	46DTB-L - 17	1.63E+05	4.90E+03	880	1043	47	55	Below LOD	Below LOD	240	Below LOD	Below LOD	60	7	1.6	1	3179
46DTB19	17/03/2021 (4)	46DTB-L - 19	1.60E+05	4.10E+03	800	970	140	56	3110	540	300	3340	560	54	18.2	2.3	0.46	4070
46DTB19	17/03/2021 (4)	46DTB-L - 18	1.44E+05	3.10E+03	860	654	38	54	Below LOD	Below LOD	290	Below LOD	Below LOD	66	5.9	1.6	1.3	1813
46DTB19	17/03/2021 (4)	46DTB-L - 16	1.50E+05	2.90E+03	860	504	36	53	Below LOD	Below LOD	300	Below LOD	Below LOD	56	8.8	1.7	0.93	2410
46DTB19	17/03/2021 (4)	46DTB-L - 3	1.51E+05	3.60E+03	820	672	83	66	550	190	290	570	170	62	33.4	7.8	0.31	3190
46DTB19	17/03/2021 (4)	46DTB-L - 9	1.68E+05	3.60E+03	1100	2.33E+04	2.60E+03	65	Below LOD	Below LOD	340	269	58	78	81.2	9.5	0.87	6.14E+04
46DTB19	17/03/2021 (4)	46DTB-L - 14	1.57E+05	4.10E+03	880	1060	110	57	1030	260	270	920	240	62	22.4	3	0.68	4870
46DTB19	17/03/2021 (4)	46DTB-L - 7	1.55E+05	3.50E+03	850	1340	220	58	Below LOD	Below LOD	280	102	48	52	10.2	1.9	0.99	4390
46DTB19	17/03/2021 (4)	46DTB-L - 20	1.50E+05	4.40E+03	1000	1550	180	58	460	220	320	456	89	85	6.5	1.4	0.86	2920
46DTB19	17/03/2021 (4)	46DTB-L - 5	1.57E+05	3.10E+03	760	466	31	55	Below LOD	Below LOD	240	125	33	53	43	12	0.89	1381
46DTB19	17/03/2021 (4)	46DTB-L - 2	1.52E+05	3.40E+03	770	398	30	54	Below LOD	Below LOD	270	Below LOD	Below LOD	62	4.2	1.2	0.73	1031
67DTB19	17/03/2021 (4)	67DTB-L - 8	1.51E+05	4.80E+03	1400	1.91E+05	2.90E+04	88	3.66E+05	5.10E+04	600	3.80E+05	5.40E+04	110	11.9	3.1	1.9	4360
67DTB19	17/03/2021 (4)	67DTB-L - 14	1.43E+05	3.20E+03	740	202	30	56	Below LOD	Below LOD	280	Below LOD	Below LOD	73	4.1	1.3	0.66	753
67DTB19	17/03/2021 (4)	67DTB-L - 7	1.46E+05	3.40E+03	760	241	27	57	Below LOD	Below LOD	290	Below LOD	Below LOD	62	4.7	1.2	0.72	719
67DTB19	17/03/2021 (4)	67DTB-L - 16	1.46E+05	3.60E+03	750	256	24	59	Below LOD	Below LOD	270	Below LOD	Below LOD	66	4.7	1.2	1	1058
67DTB19	17/03/2021 (4)	67DTB-L - 17	1.45E+05	3.40E+03	840	201	20	60	Below LOD	Below LOD	320	Below LOD	Below LOD	67	4.8	1.4	1.1	806
67DTB19	17/03/2021 (4)	67DTB-L - 12	1.50E+05	3.20E+03	900	264	24	55	Below LOD	Below LOD	240	119	33	59	26.2	4.9	0.72	1338
67DTB19	17/03/2021 (4)	67DTB-L - 20	1.45E+05	3.20E+03	740	287	31	53	Below LOD	Below LOD	280	Below LOD	Below LOD	56	7.2	1.4	1	980
67DTB19	17/03/2021 (4)	67DTB-L - 15	1.45E+05	3.10E+03	710	250	26	57	Below LOD	Below LOD	270	Below LOD	Below LOD	70	4.2	1.2	0.66	1049
67DTB19	17/03/2021 (4)	67DTB-L - 10	1.49E+05	3.20E+03	810	168	26	49	Below LOD	Below LOD	260	Below LOD	Below LOD	57	8.1	1.7	1.1	637
67DTB19	17/03/2021 (4)	67DTB-L - 11	1.54E+05	2.90E+03	810	2070	700	56	4.50E+03	1.80E+03	310	4.30E+03	1.70E+03	56	792	82	0.97	1133
67DTB19	17/03/2021 (4)	67DTB-L - 19	1.41E+05	2.60E+03	830	287	41	60	Below LOD	Below LOD	320	69	58	62	8.3	1.6	1	1138
67DTB19	17/03/2021 (4)	67DTB-L - 6	1.50E+05	3.10E+03	800	284	26	50	Below LOD	Below LOD	240	55	26	50	15.1	2.4	0.77	633
67DTB19	17/03/2021 (4)	67DTB-L - 4	1.45E+05	3.50E+03	760	129	21	50	Below LOD	Below LOD	260	Below LOD	Below LOD	53	3.2	1.1	1	315.4
67DTB19	17/03/2021 (4)	67DTB-L - 2	1.49E+05	3.20E+03	720	1120	290	53	1020	480	260	1230	520	56	8.9	1.7	1.1	1644
67DTB19	17/03/2021 (4)	67DTB-L - 5	1.49E+05	4.00E+03	880	274	30	54	Below LOD	Below LOD	270	Below LOD	Below LOD	77	8.2	1.7	1.1	1089
67DTB19	17/03/2021 (4)	67DTB-L - 18	1.44E+05	4.40E+03	850	235	28	55	Below LOD	Below LOD	290	67	35	65	6.2	1.6	1	873
67DTB19	17/03/2021 (4)	67DTB-L - 13	1.50E+05	3.50E+03	880	227	28	47	Below LOD	Below LOD	290	Below LOD	Below LOD	56	5.2	1.4	0.73	820
67DTB19	17/03/2021 (4)	67DTB-L - 1	1.44E+05	2.60E+03	790	5.40E+03	1.50E+03	52	1.18E+04	3.50E+03	290	1.16E+04	3.50E+03	60	3.6	1.3	0.71	1059
67DTB19	17/03/2021 (4)	67DTB-L - 9	1.43E+05	3.30E+03	840	156	24	52	Below LOD	Below LOD	290	Below LOD	Below LOD	55	6.1	1.7	1.1	386.3
67DTB19	17/03/2021 (4)	67DTB-L - 3	1.47E+05	3.60E+03	700	367	27	44	Below LOD	Below LOD	310	Below LOD	Below LOD	58	9.1	1.5	0.77	1430

Spot ID	Y_ppm_m89_Int2SE	Y_ppm_m89_LOD	La_ppm_m139	La_ppm_m139_Int2SE	La_ppm_m139_LOD	Ce_ppm_m140	Ce_ppm_m140_Int2SE	Ce_ppm_m140_LOD	Pr_ppm_m141	Pr_ppm_m141_Int2SE	Pr_ppm_m141_LOD	Nd_ppm_m146	Nd_ppm_m146_Int2SE	Nd_ppm_m146_LOD	Sm_ppm_m147	Sm_ppm_m147_Int2SE	Sm_ppm_m147_LOD	Eu_ppm_m153	Eu_ppm_m153_Int2SE	Eu_ppm_m153_LOD	Gd_ppm_m157	Gd_ppm_m157_Int2SE	Gd_ppm_m157_LOD
37DTB-L - 1	92	NaN	Below LOD	Below LOD	NaN	317	63	NaN	52	13	NaN	162	39	NaN	45.4	7.8	NaN	6.74	0.88	NaN	78	6.6	0.038
37DTB-L - 10	6.6	NaN	0	1	NaN	69.4	1.6	0.017	0.091	0.028	NaN	1.21	0.25	NaN	1.73	0.31	NaN	0.72	0.094	NaN	6.11	0.49	NaN
37DTB-L - 11	8.1	NaN	0	1	NaN	18.56	0.49	NaN	0.026	0.014	NaN	0.411	0.098	NaN	1.41	0.25	NaN	0.39	0.076	0.017	6.55	0.47	NaN
37DTB-L - 12	48	0.033	0	1	NaN	30.6	1.7	0.0073	0.06	0.021	NaN	1.09	0.25	NaN	2.19	0.45	NaN	0.73	0.12	NaN	8.7	1.1	0.035
37DTB-L - 13	62	0.056	0.00634	0.00024	NaN	56.6	3.9	NaN	0.033	0.017	NaN	1.16	0.24	NaN	1.89	0.38	NaN	0.65	0.11	0.012	9.8	1	NaN
37DTB-L - 14	22	NaN	0	1	NaN	44.24	0.99	NaN	0.161	0.034	NaN	2.08	0.36	NaN	3.56	0.51	NaN	0.99	0.12	NaN	11.8	1.1	NaN
37DTB-L - 15	19	NaN	0	1	NaN	47.13	0.96	NaN	0.061	0.02	NaN	0.66	0.15	NaN	2.12	0.32	NaN	0.586	0.097	0.012	9.86	0.73	0.036
37DTB-L - 16	15	NaN	Below LOD	Below LOD	NaN	47.6	4.1	NaN	0.255	0.049	NaN	2	0.37	NaN	3.32	0.48	NaN	0.85	0.14	NaN	14.32	0.86	NaN
37DTB-L - 17	19	NaN	0	1	NaN	17.2	1.5	NaN	0.023	0.013	NaN	0.12	0.082	NaN	0.89	0.26	NaN	0.216	0.056	NaN	3.91	0.43	NaN
37DTB-L - 18	46	0.028	Below LOD	Below LOD	NaN	46.8	1.3	NaN	0.662	0.079	NaN	8.58	0.93	NaN	10.12	0.82	NaN	2.82	0.3	NaN	33.1	2.4	NaN
37DTB-L - 19	34	NaN	Below LOD	Below LOD	NaN	48.2	3.1	NaN	0.437	0.094	NaN	2.36	0.46	NaN	2.19	0.4	NaN	0.76	0.13	NaN	7.78	0.93	NaN
37DTB-L - 2	45	0.0098	Below LOD	Below LOD	NaN	84	4.4	0.015	1.02	0.17	NaN	7.23	0.67	NaN	10.23	0.8	NaN	2.91	0.22	NaN	31.7	1.7	NaN
37DTB-L - 20	9.8	NaN	Below LOD	Below LOD	NaN	25.19	0.94	NaN	0.025	0.014	NaN	0.45	0.13	NaN	0.67	0.18	NaN	0.207	0.049	NaN	3.77	0.38	NaN
37DTB-L - 3	120	NaN	Below LOD	Below LOD	NaN	135	4.3	0.011	1.42	0.11	NaN	13.46	0.85	NaN	22.1	1.4	NaN	5.4	0.32	NaN	75.7	2.9	NaN
37DTB-L - 4	22	0.0095	Below LOD	Below LOD	NaN	43.7	1.4	NaN	0.203	0.036	NaN	2.29	0.33	NaN	3.34	0.47	NaN	1.26	0.13	0.012	13.53	0.86	NaN
37DTB-L - 5	12	0.02	0	1	NaN	37.3	2.1	NaN	0.049	0.02	NaN	1.03	0.21	NaN	2.27	0.34	NaN	0.63	0.1	NaN	11.01	0.64	0.035
37DTB-L - 6	52	0.092	0.00643	0.00025	NaN	31.4	0.94	0.0075	0.107	0.036	NaN	2.06	0.31	NaN	3.59	0.46	NaN	1.13	0.14	0.017	15	1.4	0.072
37DTB-L - 7	26	NaN	Below LOD	Below LOD	NaN	32.9	1.3	0.0074	0.128	0.038	NaN	0.7	0.18	NaN	1.18	0.26	NaN	0.463	0.093	NaN	7.06	0.61	NaN
37DTB-L - 8	7.8	0.0068	-0.036	0.036	NaN	31.71	0.93	NaN	0.03	0.016	NaN	0.59	0.15	NaN	2.31	0.37	NaN	0.621	0.095	0.012	10.34	0.72	NaN
37DTB-L - 9	56	NaN	Below LOD	Below LOD	NaN	70.7	2.9	0.0076	0.52	0.074	NaN	5.55	0.57	NaN	8.96	0.99	0.046	2.55	0.21	NaN	29.5	2.4	NaN
46DTB-L - 10	120	NaN	Below LOD	Below LOD	NaN	63	12	NaN	15.2	3.2	NaN	79	16	NaN	46.9	9.8	NaN	0.048	0.022	NaN	66	12	NaN
46DTB-L - 8	200	0.0096	Below LOD	Below LOD	NaN	4.36	0.35	NaN	1.22	0.25	NaN	10.9	2.1	NaN	22.9	4.4	NaN	0.091	0.038	NaN	79	14	NaN
46DTB-L - 12	99	0.022	Below LOD	Below LOD	NaN	5.26	0.2	NaN	0.584	0.095	NaN	4.18	0.52	NaN	6.97	0.84	NaN	0	1	NaN	41.9	2.9	NaN
46DTB-L - 6	26	0.57	Below LOD	Below LOD	NaN	3.68	0.21	NaN	0.328	0.073	NaN	2.37	0.55	NaN	6.5	1.1	NaN	0.007	0.01	NaN	26.7	2.6	NaN
46DTB-L - 1	11	NaN	Below LOD	Below LOD	NaN	1.76	0.12	NaN	0.019	0.012	NaN	0.111	0.068	NaN	0.41	0.14	NaN	0	1	NaN	3.83	0.43	NaN
46DTB-L - 15	740	0.14	Below LOD	Below LOD	NaN	17.4	2	NaN	3.69	0.85	NaN	23.9	5.5	0.13	32.3	7.2	NaN	0.149	0.054	NaN	119	25	NaN
46DTB-L - 13	170	0.0098	Below LOD	Below LOD	NaN	21.6	3.1	NaN	2.18	0.45	NaN	10.6	2.1	NaN	9.5	1.3	NaN	0.014	0.013	NaN	43.2	3.9	0.053
46DTB-L - 11	30	0.0067	Below LOD	Below LOD	NaN	4.38	0.2	NaN	0.042	0.018	NaN	0.6	0.15	NaN	1.8	0.32	0.035	0	1	NaN	17.9	1.2	NaN
46DTB-L - 4	43	0.0069	Below LOD	Below LOD	NaN	13.6	1.8	NaN	0.74	0.17	NaN	5.6	1.2	NaN	8.67	0.99	NaN	0	1	NaN	41	1.8	NaN
46DTB-L - 17	76	0.44	Below LOD	Below LOD	NaN	20.2	7.6	0.0081	6	3.5	NaN	41	24	NaN	19.8	8.1	NaN	0.036	0.022	0.012	69	11	NaN
46DTB-L - 19	630	0.01	Below LOD	Below LOD	NaN	155	46	NaN	46	13	NaN	167	47	NaN	98	24	NaN	0.129	0.044	NaN	220	57	0.04
46DTB-L - 18	64	NaN	Below LOD	Below LOD	NaN	4.46	0.24	0.0086	0.153	0.049	NaN	0.95	0.22	NaN	2.54	0.35	NaN	Below LOD	Below LOD	0.013	20.1	1.8	0.042
46DTB-L - 16	190	NaN	Below LOD	Below LOD	NaN	10.8	2.5	0.015	2.38	0.73	NaN	16.3	4.2	NaN	25.1	4.9	NaN	0.104	0.038	NaN	73	11	NaN
46DTB-L - 3	260	0.0098	Below LOD	Below LOD	NaN	253	84	NaN	75	27	NaN	420	140	NaN	292	92	NaN	0.211	0.077	NaN	370	100	NaN
46DTB-L - 9	7.10E+03	NaN	Below LOD	Below LOD	NaN	35.5	6.2	NaN	22.1	6.3	NaN	234	34	NaN	623	38	NaN	1.92	0.31	NaN	3050	170	NaN
46DTB-L - 14	660	NaN	Below LOD	Below LOD	NaN	326	82	NaN	85	21	0.088	293	69	NaN	160	35	NaN	0.24	0.056	NaN	330	73	0.053
46DTB-L - 7	670	0.0068	Below LOD	Below LOD	NaN	7.22	0.88	NaN	1.35	0.3	NaN	14.2	3	NaN	29.2	6.4	NaN	0.081	0.033	NaN	128	28	NaN
46DTB-L - 20	280	NaN	Below LOD	Below LOD	NaN	3.75	0.31	NaN	0.56	0.11	0.01	4.16	0.57	NaN	10.4	1	NaN	0.055	0.028	NaN	59.3	7.5	0.038
46DTB-L - 5	23	0.1	Below LOD	Below LOD	NaN	1.63	0.12	NaN	0.474	0.082	NaN	3.87	0.57	NaN	6.7	0.73	NaN	0.0031	0.0062	NaN	21.4	1.8	NaN
46DTB-L - 2	18	0.27	Below LOD	Below LOD	NaN	2.64	0.15	NaN	0.067	0.025	NaN	0.48	0.14	NaN	0.96	0.2	NaN	0	1	NaN	7.28	0.64	NaN
67DTB-L - 8	670	0.087	Below LOD	Below LOD	NaN	1970	320	NaN	511	82	NaN	1840	300	NaN	501	80	NaN	30.4	4.9	NaN	650	110	0.068
67DTB-L - 14	25	NaN	0	1	NaN	16.73	0.65	NaN	0.046	0.021	NaN	0.82	0.19	NaN	2.14	0.33	NaN	0.214	0.043	0.012	10.71	0.74	NaN
67DTB-L - 7	13	0.0068	0	1	NaN	19.39	0.43	0.0077	0.088	0.031	NaN	1.03	0.26	NaN	2.27	0.38	NaN	0.2	0.047	NaN	14.05	0.68	NaN
67DTB-L - 16	14	0.089	0	1	NaN	21.42	0.62	NaN	0.063	0.021	NaN	1.62	0.32	NaN	3.28	0.4	NaN	0.112	0.033	NaN	19.18	0.96	0.037
67DTB-L - 17	14	NaN	Below LOD	Below LOD	NaN	16.35	0.7	0.015	0.06	0.025	NaN	0.99	0.24	NaN	1.86	0.28	NaN	0.165	0.044	NaN	11.35	0.62	NaN
67DTB-L - 12	53	0.021	Below LOD	Below LOD	NaN	24.91	0.79	NaN	0.265	0.044	NaN	2.22	0.31	NaN	4.41	0.58	NaN	0.6	0.14	NaN	21.9	2.1	NaN
67DTB-L - 20	17	0.0068	Below LOD	Below LOD	NaN	19.81	0.5	NaN	0.079	0.022	NaN	1.43	0.27	NaN	3.63	0.36	NaN	0.097	0.032	NaN	18.74	0.82	NaN
67DTB-L - 15	30	0.0068	0	1	NaN	25.29	0.6	NaN	0.083	0.031	NaN	1.7	0.29	NaN	3.53	0.46	NaN	0.377	0.057	NaN	16.85	0.87	NaN
67DTB-L - 10	11	0.0068	Below LOD	Below LOD	NaN	16.51	0.46	NaN	0.085	0.028	NaN	0.93	0.21	NaN	1.4	0.21	NaN	0.147	0.045	NaN	8.37	0.59	NaN
67DTB-L - 11	21	0.017	Below LOD	Below LOD	NaN	26.2	3.2	NaN	2.56	0.87	NaN	12.1	3.9	NaN	5.5	1.1	NaN	0.51	0.12	NaN	17.7	1.4	0.041
67DTB-L - 19	21	NaN	Below LOD	Below LOD	NaN	16.56	0.47	0.0079	0.123	0.042	NaN	1.04	0.29	NaN	2.62	0.4	NaN	0.103	0.035	NaN	16.5	0.81	NaN
67DTB-L - 6	34	NaN	Below LOD	Below LOD	NaN	4.01	0.69	NaN	0.173	0.059	NaN	1.07	0.28	0.042	0.94	0.28	NaN	0.201	0.06	0.02	4.6	1.2	NaN
67DTB-L - 4	5.3	NaN	0.00533	0.00019	NaN	5.9	0.3	0.0077	0.026	0.017	NaN	0.22	0.1	0.041	0.41	0.13	NaN	0.055	0.027	NaN	2.93	0.35	NaN
67DTB-L - 2	35	0.098	Below LOD	Below LOD	NaN	26	2.1	0.0079	1.87	0.49	NaN	10.3	1.9	NaN	9.15	0.86	NaN	0.432	0.075	NaN	41	1.3	0.053
67DTB-L - 5	17	0.0073	Below LOD	Below LOD	NaN	17.88	0.51	0.0082	0.071	0.028	NaN	1.03	0.22	0.044	2.34	0.37	NaN	0.104	0.036	NaN	15.73	0.85	NaN
67DTB-L - 18	13	NaN	Below LOD	Below LOD	NaN	19.7	0.54	0.011	0.083	0.029	NaN	1.38	0.28	NaN	2.46	0.33	NaN	0.26	0.057	NaN	12.23	0.71	0.038
67DTB-L - 13	23	0.0069	0.00512	0.00017	NaN	13.39	0.51	NaN	0.036	0.017	NaN	0.66	0.16	NaN	1.67	0.29	NaN	0.052	0.023	NaN	11.52	0.89	0.037
67DTB-L - 1	16	NaN	Below LOD	Below LOD	NaN	52.8	8.8	NaN	8.5	2.4	NaN	32.3	8.9	NaN	9.7	2.3	0.035	1.33	0.31	NaN	25.8	3.6	0.037
67DTB-L - 9	7.8	NaN	Below LOD	Below LOD	NaN	11.26	0.35	0.0076	0.048	0.021	NaN	0.46	0.15	NaN	0.69	0.17	NaN	0.134	0.038	NaN	4.83	0.45	0.063
67DTB-L - 3	23	NaN	0	1	NaN	30.64	0.69	NaN	0.198	0.049	NaN	2.91	0.45	NaN	4.99	0.48	NaN	0.311	0.07	NaN	29	1.3	NaN

Appendix D2.6 continued.

Curtin University Ge

Sample ID	Analysis date-time	Spot ID	Tb_ppm_m159	Tb_ppm_m159_Int2SE	Tb_ppm_m159_LOD	Dy_ppm_m163	Dy_ppm_m163_Int2SE	Dy_ppm_m163_LOD	Ho_ppm_m165	Ho_ppm_m165_Int2SE	Ho_ppm_m165_LOD	Er_ppm_m166	Er_ppm_m166_Int2SE	Er_ppm_m166_LOD	Tm_ppm_m169	Tm_ppm_m169_Int2SE	Tm_ppm_m169_LOD	Yb_ppm_m173	Yb_ppm_m173_Int2SE	Yb_ppm_m173_LOD
37DTB19	17/03/2021 (4)	37DTB-L - 1	19.6	1.2	NaN	195.5	9.4	NaN	68.5	2.7	NaN	309	12	0.047	66.2	1.9	0.01	676	22	NaN
37DTB19	17/03/2021 (4)	37DTB-L - 10	2.32	0.14	NaN	27.4	1	NaN	11.57	0.36	NaN	67.8	1.6	NaN	17.56	0.37	NaN	211.2	4.8	NaN
37DTB19	17/03/2021 (4)	37DTB-L - 11	2.36	0.12	0.0053	31.6	1.1	NaN	13	0.31	NaN	74.1	1.5	0.045	20.27	0.46	NaN	241.8	5.5	NaN
37DTB19	17/03/2021 (4)	37DTB-L - 12	3.19	0.36	0.011	37.7	3.6	NaN	16.7	1.5	NaN	94.9	7.9	NaN	24	1.8	0.0046	295	20	NaN
37DTB19	17/03/2021 (4)	37DTB-L - 13	3.47	0.32	NaN	46	3.9	NaN	20.6	1.8	NaN	117	10	NaN	30.7	2.6	NaN	373	32	NaN
37DTB19	17/03/2021 (4)	37DTB-L - 14	3.72	0.26	NaN	44.2	2.3	NaN	17.96	0.76	NaN	97.6	3.5	NaN	24.2	0.71	0.0047	284.6	7.4	0.031
37DTB19	17/03/2021 (4)	37DTB-L - 15	3.52	0.17	0.0053	44	1.4	0.046	19.27	0.6	NaN	113.4	3.4	NaN	28.51	0.85	NaN	348.5	9.4	NaN
37DTB19	17/03/2021 (4)	37DTB-L - 16	4.79	0.21	0.0055	55.5	2.1	NaN	22.02	0.69	NaN	113.7	2.8	NaN	27.83	0.57	NaN	313.1	6.6	NaN
37DTB19	17/03/2021 (4)	37DTB-L - 17	1.43	0.11	NaN	20	1.3	NaN	9.24	0.55	NaN	57.2	3.2	0.015	15.83	0.8	NaN	200.9	8.8	NaN
37DTB19	17/03/2021 (4)	37DTB-L - 18	9.27	0.52	0.0052	98.2	5	NaN	35.5	1.8	NaN	162.8	7.2	NaN	34.5	1.3	NaN	343.4	9.4	NaN
37DTB19	17/03/2021 (4)	37DTB-L - 19	2.82	0.24	0.0054	34.6	2.4	NaN	16.5	1.1	NaN	101.7	5.1	NaN	27.4	1.3	NaN	348	17	NaN
37DTB19	17/03/2021 (4)	37DTB-L - 2	9.19	0.44	NaN	100.6	4.1	NaN	37.5	1.5	NaN	190.8	7.1	NaN	42.8	1.6	NaN	459	16	NaN
37DTB19	17/03/2021 (4)	37DTB-L - 20	1.33	0.13	0.0055	14.9	1.1	NaN	6.97	0.37	NaN	39.9	2	0.016	10.3	0.4	NaN	119.3	4.2	NaN
37DTB19	17/03/2021 (4)	37DTB-L - 3	23.77	0.94	NaN	250	10	NaN	86.9	4	0.01	404	16	NaN	85.8	3.1	0.0048	851	23	NaN
37DTB19	17/03/2021 (4)	37DTB-L - 4	3.79	0.2	NaN	46.6	2.4	NaN	18.45	0.83	0.01	95	3.5	NaN	23.35	0.83	NaN	261.8	9.5	NaN
37DTB19	17/03/2021 (4)	37DTB-L - 5	4.06	0.17	0.0051	52.8	1.1	NaN	22.47	0.45	NaN	128.8	2.5	0.014	32.8	0.67	0.0046	402.4	5.9	NaN
37DTB19	17/03/2021 (4)	37DTB-L - 6	4.92	0.43	NaN	57.4	4.4	NaN	23.9	1.7	NaN	132.6	7.6	NaN	31.7	1.6	NaN	395	20	NaN
37DTB19	17/03/2021 (4)	37DTB-L - 7	2.66	0.16	NaN	38.9	1.8	NaN	19.11	0.82	NaN	127.6	5.7	NaN	37.5	1.6	NaN	487	23	NaN
37DTB19	17/03/2021 (4)	37DTB-L - 8	3.53	0.16	NaN	42.3	1.3	NaN	17.15	0.34	NaN	89.2	1.8	NaN	22.07	0.52	NaN	257.7	4.3	NaN
37DTB19	17/03/2021 (4)	37DTB-L - 9	8.74	0.73	NaN	94.9	7	NaN	34.3	2.2	NaN	161.2	8	NaN	36.3	1.2	0.024	369	10	NaN
46DTB19	17/03/2021 (4)	46DTB-L - 10	15.9	2.3	NaN	145	16	0.021	47.1	3.3	NaN	209.7	9.8	NaN	48.8	1.4	NaN	491	10	NaN
46DTB19	17/03/2021 (4)	46DTB-L - 8	26.7	4.5	0.0074	233	33	0.041	66.4	7.7	NaN	252	19	NaN	52.5	2.6	0.0048	490	21	NaN
46DTB19	17/03/2021 (4)	46DTB-L - 12	17.15	0.8	0.0093	206.5	7.5	NaN	76.5	2.9	0.0054	375	12	NaN	94.2	2.8	NaN	1045	33	NaN
46DTB19	17/03/2021 (4)	46DTB-L - 6	11.54	0.64	NaN	130.3	4.6	NaN	43.8	1.3	NaN	192.7	4.5	NaN	42.1	1.1	NaN	407.4	9.2	NaN
46DTB19	17/03/2021 (4)	46DTB-L - 1	2.25	0.15	NaN	33.8	1.1	NaN	15.9	0.38	NaN	93.8	2	0.015	25.53	0.51	NaN	293.9	5.7	NaN
46DTB19	17/03/2021 (4)	46DTB-L - 15	41.8	9.1	NaN	414	88	0.022	122	21	NaN	487	65	NaN	107.8	9.6	NaN	1062	47	NaN
46DTB19	17/03/2021 (4)	46DTB-L - 13	17.6	1.4	NaN	217	16	NaN	85.7	5.9	NaN	432	25	NaN	107.2	6.3	NaN	1182	72	NaN
46DTB19	17/03/2021 (4)	46DTB-L - 11	9.67	0.64	NaN	136.7	6.5	NaN	54.5	1.7	NaN	271.9	5.9	NaN	64.5	1.5	NaN	651	11	NaN
46DTB19	17/03/2021 (4)	46DTB-L - 4	18.5	0.55	NaN	220.7	4.3	NaN	73.9	1.3	NaN	319.8	5.6	NaN	68	1.3	NaN	630	10	NaN
46DTB19	17/03/2021 (4)	46DTB-L - 17	34.6	1.2	NaN	426	13	NaN	143.5	4.6	NaN	589	22	NaN	125.1	4.6	NaN	1133	37	NaN
46DTB19	17/03/2021 (4)	46DTB-L - 19	52	11	NaN	416	76	0.032	114	16	0.0057	435	34	0.016	99.5	5.6	NaN	1045	41	NaN
46DTB19	17/03/2021 (4)	46DTB-L - 18	9.58	0.59	0.012	139.1	7.2	NaN	56.1	2.7	NaN	281	13	NaN	69	3	NaN	711	34	NaN
46DTB19	17/03/2021 (4)	46DTB-L - 16	26.3	3.8	NaN	252	29	NaN	76.9	7.2	NaN	311	23	NaN	65.1	3.4	NaN	638	25	NaN
46DTB19	17/03/2021 (4)	46DTB-L - 3	70	15	0.0076	432	61	NaN	98.8	7.9	NaN	387	20	NaN	83.2	2.7	NaN	845	26	NaN
46DTB19	17/03/2021 (4)	46DTB-L - 9	838	61	0.0069	6610	620	NaN	1690	200	0.0068	4920	660	0.17	669	89	NaN	4270	550	0.042
46DTB19	17/03/2021 (4)	46DTB-L - 14	71	15	0.0054	550	100	NaN	128	19	NaN	479	43	NaN	102.1	3.9	NaN	1092	28	NaN
46DTB19	17/03/2021 (4)	46DTB-L - 7	42.3	8.2	NaN	405	67	NaN	125	18	NaN	501	61	NaN	107	11	NaN	1024	93	NaN
46DTB19	17/03/2021 (4)	46DTB-L - 20	23.6	3	0.0055	256	30	NaN	78.6	7.3	NaN	296	21	NaN	60.8	2.7	0.02	576	14	0.033
46DTB19	17/03/2021 (4)	46DTB-L - 5	7.83	0.47	NaN	88.9	3.1	NaN	35.61	0.98	NaN	197.2	4.5	NaN	53	1.3	NaN	596	20	0.13
46DTB19	17/03/2021 (4)	46DTB-L - 2	3.88	0.16	NaN	59.8	2	NaN	25.54	0.65	NaN	139	2.6	0.03	34.66	0.9	NaN	376.1	7.7	0.15
67DTB19	17/03/2021 (4)	67DTB-L - 8	125	20	NaN	830	130	NaN	169	26	NaN	495	71	NaN	82	11	NaN	683	78	0.058
67DTB19	17/03/2021 (4)	67DTB-L - 14	4.06	0.23	NaN	55.9	2.3	NaN	23.83	0.88	NaN	123.1	4.5	NaN	29.42	0.93	NaN	309	10	NaN
67DTB19	17/03/2021 (4)	67DTB-L - 7	4.96	0.17	0.0053	62.1	1.5	NaN	24.14	0.53	NaN	112.3	2.7	NaN	24.46	0.71	NaN	239.2	5.9	0.032
67DTB19	17/03/2021 (4)	67DTB-L - 16	7.01	0.2	0.0053	92.5	1.8	NaN	36.34	0.65	NaN	169.2	3	0.029	36.2	0.62	NaN	343.6	7	NaN
67DTB19	17/03/2021 (4)	67DTB-L - 17	4.15	0.2	NaN	58.1	1.6	NaN	25.1	0.57	0.0051	131.3	2.5	0.029	32.46	0.63	NaN	340	6.6	NaN
67DTB19	17/03/2021 (4)	67DTB-L - 12	7.75	0.55	NaN	99.9	5.2	NaN	42.2	1.6	NaN	213.9	6.6	NaN	48.8	1	NaN	505.4	7.6	0.064
67DTB19	17/03/2021 (4)	67DTB-L - 20	7.02	0.21	NaN	87.8	1.8	0.021	34.32	0.67	0.016	159.3	3.2	NaN	32.72	0.65	NaN	308.4	6.6	NaN
67DTB19	17/03/2021 (4)	67DTB-L - 15	6.28	0.26	NaN	80.8	3	NaN	33.5	1.1	NaN	164.7	4.7	NaN	40.1	1.3	NaN	407.4	9.7	NaN
67DTB19	17/03/2021 (4)	67DTB-L - 10	3.21	0.13	0.0053	45.4	1.3	NaN	19.44	0.49	NaN	102.5	1.7	NaN	25.04	0.63	NaN	265.9	5.8	NaN
67DTB19	17/03/2021 (4)	67DTB-L - 11	6.31	0.29	NaN	82.2	2.1	NaN	35.37	0.64	NaN	183.8	3.4	NaN	44.92	0.74	0.0052	488	8.8	NaN
67DTB19	17/03/2021 (4)	67DTB-L - 19	6.8	0.27	NaN	92.3	2	0.043	38.43	0.86	NaN	188.1	3.9	0.015	40.58	0.92	NaN	400.6	7.5	0.066
67DTB19	17/03/2021 (4)	67DTB-L - 6	1.81	0.29	NaN	30.6	3.3	NaN	17.4	1.1	NaN	120.9	4.1	NaN	38	1.1	NaN	495	13	0.13
67DTB19	17/03/2021 (4)	67DTB-L - 4	1.34	0.095	0.0053	19.8	0.8	0.041	9.65	0.34	NaN	53.4	1.2	0.014	14.01	0.32	NaN	162	4.5	NaN
67DTB19	17/03/2021 (4)	67DTB-L - 2	13.1	0.36	NaN	149.1	3.1	NaN	55	1.2	NaN	241.8	5.3	NaN	48.5	1	NaN	441	9	0.033
67DTB19	17/03/2021 (4)	67DTB-L - 5	6.35	0.2	NaN	86.4	2	NaN	36.95	0.73	NaN	175.6	3.7	NaN	39.13	0.81	NaN	376.8	5.4	0.034
67DTB19	17/03/2021 (4)	67DTB-L - 18	4.56	0.17	NaN	63.3	1.5	NaN	27.22	0.59	NaN	142.1	2.7	NaN	34.03	0.61	0.014	364.2	7	NaN
67DTB19	17/03/2021 (4)	67DTB-L - 13	4.85	0.27	NaN	66.2	2.9	NaN	27.8	1.2	NaN	133.3	3.6	0.073	29.49	0.96	NaN	278.6	6.1	NaN
67DTB19	17/03/2021 (4)	67DTB-L - 1	7.42	0.5	0.0053	83.5	3.3	NaN	33.21	0.72	NaN	165.6	2.8	NaN	40.1	0.78	NaN	409.9	8.2	NaN
67DTB19	17/03/2021 (4)	67DTB-L - 9	1.91	0.12	NaN	25.34	0.89	NaN	11.62	0.37	NaN	64.5	1.7	NaN	16.13	0.41	NaN	175.4	4.2	NaN
67DTB19	17/03/2021 (4)	67DTB-L - 3	10.29	0.33	NaN	124.8	2.9	NaN	49.27	0.99	0.02	224.5	4.8	NaN	46.8	0.91	NaN	425.4	7.1	NaN

Sample ID	Spot ID	Lu_ppm_m175	Lu_ppm_m175_Int2SE	Lu_ppm_m175_LOD	Hf_ppm_m178	Hf_ppm_m178_Int2SE	Hf_ppm_m178_LOD	Pb_ppm_m204	Pb_ppm_m204_Int2SE	Pb_ppm_m204_LOD	Pb_ppm_m206	Pb_ppm_m206_Int2SE	Pb_ppm_m206_LOD	Pb_ppm_m207	Pb_ppm_m207_Int2SE	Pb_ppm_m207_LOD	Pb_ppm_m208	Pb_ppm_m208_Int2SE	Pb_ppm_m208_LOD	Th_ppm_m232	Th_ppm_m232_Int2SE	Th_ppm_m232_LOD	U_ppm_m238	U_ppm_m238_Int2SE	U_ppm_m238_LOD
37DTB19	37DTB-L - 1	135.6	4.9	0.005	10480	130	NaN	Below LOD	Below LOD	NaN	338.8	7.8	0.02	535	12	0.28	7720	300	3.4	1182	32	0.018	1536	26	NaN
37DTB19	37DTB-L - 10	50.29	0.92	0.011	10060	150	NaN	-240	190	NaN	91.1	3.1	0.017	142.9	5.3	0.26	3060	160	4.4	447	20	NaN	413	12	NaN
37DTB19	37DTB-L - 11	59	1.3	NaN	13140	240	0.11	-190	230	NaN	247.5	4.6	0.075	394.6	9	0.21	2700	110	3.3	426	14	NaN	1214	18	NaN
37DTB19	37DTB-L - 12	70.5	4.5	NaN	11250	140	0.015	Below LOD	Below LOD	NaN	144.6	7.8	0.03	235	15	0.3	2800	190	3.6	414	41	NaN	654	44	NaN
37DTB19	37DTB-L - 13	83.8	6.7	0.034	10680	160	NaN	Below LOD	Below LOD	NaN	179.2	9.9	0.018	281	18	0.24	4130	310	3.5	614	58	NaN	811	62	NaN
37DTB19	37DTB-L - 14	63.6	1.4	0.0047	10260	140	0.74	Below LOD	Below LOD	NaN	102.3	2.3	0.025	164.6	5.2	0.32	2377	77	3.6	336	11	NaN	462	12	0.094
37DTB19	37DTB-L - 15	80.5	2.2	0.0047	10710	170	NaN	-240	230	NaN	159	3.7	0.02	249.3	6.8	0.27	3146	80	3.4	458	14	NaN	717	25	NaN
37DTB19	37DTB-L - 16	68.2	1.5	0.0049	11270	160	NaN	-340	300	NaN	299	13	0.024	482	22	0.27	6510	730	3.5	1080	100	0.095	1382	33	NaN
37DTB19	37DTB-L - 17	49.5	2.1	NaN	12130	210	NaN	Below LOD	Below LOD	NaN	145.3	5.4	0.02	234.8	9	0.25	1540	140	4	219	17	0.041	652	17	0.12
37DTB19	37DTB-L - 18	67.8	1.6	NaN	9590	210	NaN	Below LOD	Below LOD	NaN	50.2	1.6	0.019	82.2	4	0.31	1557	45	4.5	227.6	4	NaN	240	10	NaN
37DTB19	37DTB-L - 19	84.1	3.2	NaN	10260	160	0.098	-120	260	NaN	239.8	5.3	0.026	375	11	0.24	5800	200	4.4	888	32	NaN	1563	52	NaN
37DTB19	37DTB-L - 2	95.4	3.1	NaN	9830	120	NaN	Below LOD	Below LOD	NaN	123.2	3.5	0.021	192.5	8.2	0.27	4570	190	4.1	714	28	NaN	611	18	NaN
37DTB19	37DTB-L - 20	28.45	0.87	NaN	10630	180	NaN	Below LOD	Below LOD	NaN	40.4	1.6	0.019	67.9	3.8	0.35	832	80	3.7	105.3	5.6	NaN	178.2	5.4	NaN
37DTB19	37DTB-L - 3	154.6	4.9	NaN	8710	160	NaN	Below LOD	Below LOD	NaN	167.3	8.6	0.016	272	13	0.32	6780	330	3.3	1040	42	NaN	960	33	0.036
37DTB19	37DTB-L - 4	58.2	2.3	NaN	10340	130	NaN	Below LOD	Below LOD	NaN	64.3	4.5	0.023	104.5	7.8	0.29	1810	130	4.8	281	20	NaN	315	25	NaN
37DTB19	37DTB-L - 5	92.9	1.6	NaN	11300	220	NaN	Below LOD	Below LOD	NaN	255	7.1	0.021	405	12	0.25	4113	73	3.4	595	9.4	0.0081	1120	57	0.1
37DTB19	37DTB-L - 6	89.8	4	NaN	11310	180	0.17	-170	140	NaN	198	14	0.019	323	24	0.17	3570	220	2.8	518	36	NaN	883	76	NaN
37DTB19	37DTB-L - 7	121.7	7.6	NaN	11780	230	0.62	Below LOD	Below LOD	NaN	393	23	0.04	627	38	0.22	4540	240	3.2	714	39	0.033	2000	150	NaN
37DTB19	37DTB-L - 8	58.4	1	NaN	11610	150	NaN	Below LOD	Below LOD	NaN	278.6	6.3	0.016	442	13	0.28	4900	220	3	784	25	0.23	1329	23	NaN
37DTB19	37DTB-L - 9	71.9	1.5	NaN	9570	160	NaN	-240	170	NaN	63.2	1.1	0.022	101.9	3.9	0.38	2261	70	2.8	349.8	5.4	NaN	305.5	6.2	0.018
46DTB19	46DTB-L - 10	91.2	2.2	0.015	26790	360	NaN	-700	1400	NaN	434	6.9	0.022	805	14	0.23	931	39	3.9	117.5	5.3	0.026	2451	44	NaN
46DTB19	46DTB-L - 8	83.8	2.4	0.019	27950	460	NaN	-1.30E+03	1.20E+03	NaN	423.4	7.3	0.019	781	17	0.27	1040	40	2.8	151.8	8.7	NaN	2407	63	NaN
46DTB19	46DTB-L - 12	208.3	6.6	NaN	26780	320	0.41	5.40E+03	3.10E+03	1200	514	22	0.024	949	49	0.23	1196	48	2.9	191	7.7	NaN	4150	130	NaN
46DTB19	46DTB-L - 6	69.3	1.5	0.0054	27730	430	NaN	Below LOD	Below LOD	NaN	448	10	0.02	856	24	0.31	1202	94	3.6	112.9	2.4	NaN	2117	43	NaN
46DTB19	46DTB-L - 1	57.5	1.3	NaN	31820	370	NaN	Below LOD	Below LOD	NaN	323.9	7.6	0.019	598	15	0.21	691	26	4.1	76.2	3.1	NaN	1361	31	0.019
46DTB19	46DTB-L - 15	212.3	7	NaN	24780	350	NaN	6.50E+03	1.60E+03	760	463	14	0.043	762	17	0.38	1630	110	3.4	610	150	NaN	1.02E+04	1.80E+03	1.9
46DTB19	46DTB-L - 13	231	15	NaN	29770	580	0.79	2.80E+03	2.20E+03	1100	737	31	0.018	1332	51	0.13	1753	91	4	201.7	8	NaN	4090	150	NaN
46DTB19	46DTB-L - 11	116.3	2.3	0.0047	27490	420	NaN	4.00E+03	7.30E+03	1800	837	14	0.021	1558	28	0.3	2400	64	3.8	251.3	7.3	NaN	3695	55	NaN
46DTB19	46DTB-L - 4	104.3	2	0.033	28170	310	0.096	-600	550	NaN	767	14	0.02	1399	28	0.23	1597	49	4.9	266	40	NaN	3741	80	2.4
46DTB19	46DTB-L - 17	175.3	6.2	0.005	6.23E+04	1.90E+03	4.8	Below LOD	Below LOD	650	977	43	0.022	1846	82	0.4	2190	110	4.6	229.3	6.3	NaN	4068	87	NaN
46DTB19	46DTB-L - 19	201.6	5	NaN	22180	330	1.1	760	660	610	328	11	0.027	569	17	0.34	1101	62	3.9	309	54	NaN	8.20E+03	1.10E+03	1.2
46DTB19	46DTB-L - 18	133.9	6.4	NaN	24600	320	NaN	2560	910	610	627	18	0.026	1160	38	0.32	1308	61	4.4	158.9	5.9	NaN	3555	75	NaN
46DTB19	46DTB-L - 16	116.8	3.6	NaN	23850	330	NaN	1.40E+03	1.10E+03	780	491	79	0.024	830	120	0.26	1540	290	2.5	482	92	NaN	1.09E+04	1.80E+03	0.12
46DTB19	46DTB-L - 3	168.7	5	0.0097	24850	390	0.016	Below LOD	Below LOD	NaN	519	42	0.018	838	68	0.2	4610	980	4	4.00E+03	1.40E+03	NaN	1.10E+04	1.10E+03	0.11
46DTB19	46DTB-L - 9	568	71	0.0062	28750	330	NaN	-5.60E+03	2.00E+03	NaN	404	37	0.066	631	42	0.49	1630	230	4.5	2190	500	NaN	2.00E+04	4.50E+03	0.78
46DTB19	46DTB-L - 14	221.3	6.9	0.0049	24090	370	NaN	5.40E+03	1.80E+03	940	557	23	0.026	967	42	0.2	1880	170	3.5	429	55	0.0086	4820	500	NaN
46DTB19	46DTB-L - 7	191	16	0.0047	37250	480	0.016	-1500	790	NaN	611	29	0.018	1108	54	0.32	1560	110	3.8	710	150	NaN	9.50E+03	1.20E+03	NaN
46DTB19	46DTB-L - 20	105.6	1.9	0.0049	26860	340	NaN	2050	570	410	397	13	0.032	673	21	0.13	1132	81	3.3	162	11	NaN	9760	940	NaN
46DTB19	46DTB-L - 5	121.9	5	NaN	25640	350	NaN	Below LOD	Below LOD	NaN	180	17	0.033	309	32	0.23	530	110	3.9	58.9	2.3	0.017	2680	78	0.059
46DTB19	46DTB-L - 2	73.4	2.1	NaN	26290	330	NaN	Below LOD	Below LOD	NaN	214.4	5.2	0.022	394	12	0.27	550	23	5	62.7	2.3	0.0085	1933	35	NaN
67DTB19	67DTB-L - 8	109	11	NaN	9710	250	NaN	1550	530	490	199	15	0.036	615	53	0.35	5130	700	4.8	308	36	NaN	559	39	0.011
67DTB19	67DTB-L - 14	59	1.6	NaN	10350	170	NaN	Below LOD	Below LOD	190	132	2.5	0.023	401	10	0.29	2166	55	3.2	168.1	5.4	NaN	333.7	9.9	NaN
67DTB19	67DTB-L - 7	44.1	1	NaN	9550	120	NaN	Below LOD	Below LOD	290	84.5	1.4	0.018	263.4	6.7	0.12	1837	54	4.5	130.2	3.7	NaN	206.1	7	NaN
67DTB19	67DTB-L - 16	61.2	1.2	NaN	10680	160	0.48	Below LOD	Below LOD	180	184.6	4.8	0.018	561	16	0.43	3370	100	2.7	262.4	5	NaN	451.7	7.6	NaN
67DTB19	67DTB-L - 17	65.9	1.2	NaN	10610	140	0.016	290	180	180	202.4	9.8	0.017	615	29	0.3	3130	180	3.2	250	12	NaN	501	16	NaN
67DTB19	67DTB-L - 12	94.8	2.2	NaN	10350	180	NaN	350	180	190	230	15	0.023	592	28	0.34	5750	540	3.6	546	59	NaN	778	70	NaN
67DTB19	67DTB-L - 20	54.3	1.1	0.0047	10220	150	NaN	310	130	130	144.8	2.3	0.018	429.3	7	0.3	2470	64	3.6	200.7	3.5	0.017	376.5	8.1	0.047
67DTB19	67DTB-L - 15	74.8	1.9	NaN	9730	160	NaN	Below LOD	Below LOD	190	192.3	6.2	0.024	586	20	0.19	3920	110	3.3	297	5.5	0.017	466.5	9.2	NaN
67DTB19	67DTB-L - 10	53.02	0.94	NaN	10710	150	NaN	Below LOD	Below LOD	220	146.8	2.7	0.016	419.2	7.8	0.21	2459	66	4.6	169.4	3.2	NaN	423.3	7.9	NaN
67DTB19	67DTB-L - 11	92.7	1.2	NaN	11190	150	NaN	Below LOD	Below LOD	200	293.3	8.2	0.026	779	30	0.24	5390	170	2.8	465	9.9	NaN	919	19	0.051
67DTB19	67DTB-L - 19	70.3	1.3	NaN	11430	220	NaN	Below LOD	Below LOD	170	194.2	5	0.017	568	13	0.21	2638	72	4.1	229.3	4.6	0.012	528	12	NaN
67DTB19	67DTB-L - 6	120.5	1.9	NaN	7680	130	0.37	250	240	250	257	11	0.016	566	24	0.27	1140	160	4.2	90	13	NaN	939	18	0.48
67DTB19	67DTB-L - 4	34.04	0.7	NaN	12140	190	1.5	830	280	280	134.3	2.6	0.041	410	10	0.31	916	52	4.3	63.7	2.5	0.0084	345	13	NaN
67DTB19	67DTB-L - 2	77.4	1.3	NaN	9010	160	NaN	Below LOD	Below LOD	410	130.3	3.2	0.023	385	11	0.27	3960	130	4	296.6	6.9	NaN	335.6	6.5	NaN
67DTB19	67DTB-L - 5	66.3	1.2	NaN	11230	150	NaN	600	290	310	251	8.4	0.019	736	26	0.23	3490	130	2.5	240.2	4.2	NaN	624	11	NaN
67DTB19	67DTB-L - 18	70.2	1	NaN	10160	140	NaN	Below LOD	Below LOD	150	201.7	4.8	0.024	610	14	0.28	3446	85	3.9	284.3	4.2	0.05	523.1	7.9	NaN
67DTB19	67DTB-L - 13	50.5	1.4	NaN	11100	140	0.81	480	190	180	124.3	3.1	0.018	372.5	8.7	0.27	1595	62	2.3	119.1	4.8	NaN	326	10	NaN
67DTB19	67DTB-L - 1	77.1	1.5	NaN	9960	170	0.76	1170	270	280	254.1	8.4	0.024	783	32	0.22	5420	200	3.9	381	9.9	NaN	640	14	NaN
67DTB19	67DTB-L - 9	34.44	0.88	NaN	10550	150	0.36	480	220	310	72.7	2.3	0.02	202.1	5.8	0.21	1095	42	3.9	103.2	3.2	NaN	246.3	7.2	0.076
67DTB19	67DTB-L - 3	73.3	1.3	0.015	9650	130	0.12	800	290	260	182.2	5.3	0.017	541	15	0.28	4490	170	3.7	312.9	6	NaN	438.9	7.6	0.012

Appendix D2.6 continued.

Sample Info		Preferred Age		LA-ICPMS Results	Lu-Hf	
Analysis date	Spot ID	Ma	2 sig	Discord	eHf	2sig
17/03/2021 (4)	37DTB-L - 1	1591.66	5.33	8.328411847	-5.264	1.295
17/03/2021 (4)	37DTB-L - 2	1580.6	5.47	7.041629761	-8.655	1.12
17/03/2021 (4)	37DTB-L - 3	1596.22	6.57	14.69221035	-7.550	1.015
17/03/2021 (4)	37DTB-L - 4	1575.04	8.03	30.28748476	-8.150	1.155
17/03/2021 (4)	37DTB-L - 5	1576.96	4.79	6.662185471	-9.766	1.085
17/03/2021 (4)	37DTB-L - 6	1571	4.42	12.79439847	-8.150	1.05
17/03/2021 (4)	37DTB-L - 7	1542.22	4.81	24.27798887	-8.083	1.12
17/03/2021 (4)	37DTB-L - 8	1575.43	5.09	5.625765664	-7.239	1.085
17/03/2021 (4)	37DTB-L - 9	1568.3	6	-2.365618823	-7.889	0.98
17/03/2021 (4)	37DTB-L - 10	1561.92	6.52	8.958205286	-7.783	1.12
17/03/2021 (4)	37DTB-L - 11	1541.83	4.81	25.0630744	-8.471	1.085
17/03/2021 (4)	37DTB-L - 12	1566.57	5.42	4.147277172	-8.568	1.26
17/03/2021 (4)	37DTB-L - 13	1576.77	6.85	9.035560037	-7.929	1.05
17/03/2021 (4)	37DTB-L - 14	1570.62	4.91	12.80513428	-9.494	1.015
17/03/2021 (4)	37DTB-L - 15	1566.57	4.43	4.702630588	-8.455	1.085
17/03/2021 (4)	37DTB-L - 16	1560.18	4.16	12.82416131	-6.306	1.085
17/03/2021 (4)	37DTB-L - 17	1562.31	5.53	18.99815018	-5.068	1.05
17/03/2021 (4)	37DTB-L - 18	1608.3	11.5	10.8499658	-4.311	1.225
17/03/2021 (4)	37DTB-L - 19	1546.54	4.69	20.5775473	-8.863	1.05
17/03/2021 (4)	37DTB-L - 20	1573.7	5.79	6.1447544	-7.226	1.015
17/03/2021 (4)	46DTB-L - 2	1588.81	9.42	67.26063763	-9.528	0.875
17/03/2021 (4)	46DTB-L - 8	1738	4.48	19.33959702	-9.163	0.735
17/03/2021 (4)	46DTB-L - 20	1605	7.69	69.56059897	-8.635	0.735
17/03/2021 (4)	46DTB-L - 12	1764	3.89	41.16930235	-6.557	0.805
17/03/2021 (4)	46DTB-L - 9	1597	8.59	43.98654237	-5.926	1.435
17/03/2021 (4)	46DTB-L - 13	1764	4.92	34.04352781	-5.680	0.945
17/03/2021 (4)	46DTB-L - 10	1841	4.43	32.89616892	-5.398	0.91
17/03/2021 (4)	46DTB-L - 6	1781	4.35	30.54752429	-2.480	0.91
17/03/2021 (4)	46DTB-L - 4	1777	4.45	45.1144944	-2.337	0.77
17/03/2021 (4)	46DTB-L - 17	1783	4.52	46.27445615	-1.203	0.84
17/03/2021 (4)	46DTB-L - 15	1790	3.73	68.33945653	3.745	1.4
17/03/2021 (4)	46DTB-L - 11	1805	4.28	48.74077493	9.642	1.155
17/03/2021 (4)	46DTB-L - 14	1758	6.93	80.73138121	10.373	1.015
17/03/2021 (4)	46DTB-L - 18	1827	5.71	81.01723932	13.919	1.785
17/03/2021 (4)	46DTB-L - 1	1838	4.03	41.05807447	15.067	1.61
17/03/2021 (4)	46DTB-L - 19	1812	4.93	45.18416333	38.812	7.7
17/03/2021 (4)	46DTB-L - 16	1820	4.32	78.33633525	44.509	1.82
17/03/2021 (4)	46DTB-L - 3	1839	6.32	62.73180491	48.806	3.465
17/03/2021 (4)	46DTB-L - 7	1751	7.23	32.88974985	57.373	1.47
17/03/2021 (4)	46DTB-L - 5	1578	9.78	26.89535359	64.220	4.9
17/03/2021 (4)	67DTB-L - 1	2518	4.8	20.10120911	-2.858	1.33
17/03/2021 (4)	67DTB-L - 2	2583	3.75	14.43284998	0.027	1.225
17/03/2021 (4)	67DTB-L - 3	2478	4.67	25.38897746	-0.786	1.015
17/03/2021 (4)	67DTB-L - 4	2598	3.61	14.06165786	0.124	1.12
17/03/2021 (4)	67DTB-L - 5	2537.46	3.66	15.35630118	-2.014	1.05
17/03/2021 (4)	67DTB-L - 6	2609	5.33	13.70970833	4.915	1.75
17/03/2021 (4)	67DTB-L - 7	2666	3.77	6.489258344	1.164	1.26
17/03/2021 (4)	67DTB-L - 8	2653	4.6	4.898863868	0.042	0.875
17/03/2021 (4)	67DTB-L - 9	2609	4.31	24.03006297	-0.783	1.155
17/03/2021 (4)	67DTB-L - 10	2660	3.65	10.91003413	-0.126	1.26
17/03/2021 (4)	67DTB-L - 11	2629	4.11	11.59376189	2.687	1.295
17/03/2021 (4)	67DTB-L - 12	2614.41	3.91	10.15946236	0.930	1.085
17/03/2021 (4)	67DTB-L - 13	2503.74	4.17	18.90931167	-2.414	0.98
17/03/2021 (4)	67DTB-L - 14	2612.7	4.83	5.917250354	-0.065	1.26
17/03/2021 (4)	67DTB-L - 15	2653.51	3.9	10.57128106	-0.369	1.12
17/03/2021 (4)	67DTB-L - 16	2632.64	6.19	6.648839188	0.198	1.085
17/03/2021 (4)	67DTB-L - 17	2622.24	4.8	10.1531515	1.381	0.98
17/03/2021 (4)	67DTB-L - 18	2563.77	5.5	18.26879946	10.381	1.12
17/03/2021 (4)	67DTB-L - 19	2611.66	3.77	12.90979683	1.885	1.435
17/03/2021 (4)	67DTB-L - 20	2634.88	3.85	10.24638693	-1.199	0.945

Sample #/Spot #	Ti	Nb	La	Ce	Pr	Nd	Sm	Eu	Gd	Tb	Dy	Ho	Er	Tm	Yb	Lu	Hf	Pb	Th	U	Y
MC and Sun (1995) PM	1205	0.658	0.648	1.675	0.254	1.25	0.406	0.154	0.544	0.099	0.674	0.149	0.438	0.068	0.441	0.0675	0.283	0.15	0.0795	0.0203	4.3
CI Anders 89			0.446	1.136	0.1669	0.8279	0.2582	0.0973	0.33	0.0603	0.3942	0.0889	0.2508	0.0378	0.2479	0.0367				0.009	
37DTB-L - 1	6.9		Below LOD	317	52	162	45.4	6.74	78	19.6	195.5	68.5	309	66.2	676	135.6	10480	338.8	1182	1536	2224
37DTB-L - 2	8.9		Below LOD	84	1.02	7.23	10.23	2.91	31.7	9.19	100.6	37.5	190.8	42.8	459	95.4	9830	123.2	714	611	1228
37DTB-L - 3	14.3		Below LOD	135	1.42	13.46	22.1	5.4	75.7	23.77	250	86.9	404	85.8	851	154.6	8710	167.3	1040	960	2750
37DTB-L - 4	5.1		Below LOD	43.7	0.203	2.29	3.34	1.26	13.53	3.79	46.6	18.45	95	23.35	261.8	58.2	10340	64.3	281	315	605
37DTB-L - 5	4.1		0	37.3	0.049	1.03	2.27	0.63	11.01	4.06	52.8	22.47	128.8	32.8	402.4	92.9	11300	255	595	1120	802
37DTB-L - 6	1.49		0.00643	31.4	0.107	2.06	3.59	1.13	15	4.92	57.4	23.9	132.6	31.7	395	89.8	11310	198	518	883	865
37DTB-L - 7	5.9		Below LOD	32.9	0.128	0.7	1.18	0.463	7.06	2.66	38.9	19.11	127.6	37.5	487	121.7	11780	393	714	2000	749
37DTB-L - 8	4.6		-0.036	31.71	0.03	0.59	2.31	0.621	10.34	3.53	42.3	17.15	89.2	22.07	257.7	58.4	11610	278.6	784	1329	583.4
37DTB-L - 9	8.7		Below LOD	70.7	0.52	5.55	8.96	2.55	29.5	8.74	94.9	34.3	161.2	36.3	369	71.9	9570	63.2	349.8	305.5	1065
37DTB-L - 10	6.9		0	69.4	0.091	1.21	1.73	0.72	6.11	2.32	27.4	11.57	67.8	17.56	211.2	50.29	10060	91.1	447	413	425.9
37DTB-L - 11	3.3		0	18.56	0.026	0.411	1.41	0.39	6.55	2.36	31.6	13	74.1	20.27	241.8	59	13140	247.5	426	1214	478.5
37DTB-L - 12	3.8		0	30.6	0.06	1.09	2.19	0.73	8.7	3.19	37.7	16.7	94.9	24	295	70.5	11250	144.6	414	654	608
37DTB-L - 13	6.3		0.00634	56.6	0.033	1.16	1.89	0.65	9.8	3.47	46	20.6	117	30.7	373	83.8	10680	179.2	614	811	752
37DTB-L - 14	5.7		0	44.24	0.161	2.08	3.56	0.99	11.8	3.72	44.2	17.96	97.6	24.2	284.6	63.6	10260	102.3	336	462	630
37DTB-L - 15	4.7		0	47.13	0.061	0.66	2.12	0.586	9.86	3.52	44	19.27	113.4	28.51	348.5	80.5	10710	159	458	717	698
37DTB-L - 16	8.1		Below LOD	47.6	0.255	2	3.32	0.85	14.32	4.79	55.5	22.02	113.7	27.83	313.1	68.2	11270	299	1080	1382	733
37DTB-L - 17	3		0	17.2	0.023	0.12	0.89	0.216	3.91	1.43	20	9.24	57.2	15.83	200.9	49.5	12130	145.3	219	652	365
37DTB-L - 18	13.8		Below LOD	46.8	0.662	8.58	10.12	2.82	33.1	9.27	98.2	35.5	162.8	34.5	343.4	67.8	9590	50.2	227.6	240	1054
37DTB-L - 19	18.7		Below LOD	48.2	0.437	2.36	2.19	0.76	7.78	2.82	34.6	16.5	101.7	27.4	348	84.1	10260	239.8	888	1563	615
37DTB-L - 20	4.5		Below LOD	25.19	0.025	0.45	0.67	0.207	3.77	1.33	14.9	6.97	39.9	10.3	119.3	28.45	10630	40.4	105.3	178.2	243.5
46DTB-L - 2	81.2		Below LOD	35.5	22.1	234	623	1.92	3050	838	6610	1690	4920	68	4270	568	28750	404	2190	2.00E+04	6.14E+04
46DTB-L - 8	7.5		Below LOD	63	15.2	79	46.9	0.048	66	15.9	145	47.1	209.7	25.53	491	91.2	26790	434	117.5	2451	1640
46DTB-L - 20	10.2		Below LOD	7.22	1.35	14.2	29.2	0.081	128	42.3	405	125	501	42.1	1024	191	37250	611	710	9.50E+03	4390
46DTB-L - 12	4.6		Below LOD	4.38	0.042	0.6	1.8	0	17.9	9.67	136.7	54.5	271.9	65.1	651	116.3	27490	837	251.3	3695	2204
46DTB-L - 9	9.3		Below LOD	13.6	0.74	5.6	8.67	0	41	18.5	220.7	73.9	319.8	125.1	630	104.3	28170	767	266	3741	2208
46DTB-L - 13	14		Below LOD	17.4	3.69	23.9	32.3	0.149	119	41.8	414	122	487	102.1	1062	212.3	24780	463	610	1.02E+04	4610
46DTB-L - 10	202		Below LOD	1.76	0.019	0.111	0.41	0	3.83	2.25	33.8	15.9	93.8	107.2	293.9	57.5	31820	323.9	76.2	1361	676
46DTB-L - 6	12.9		Below LOD	5.26	0.584	4.18	6.97	0	41.9	17.15	206.5	76.5	375	64.5	1045	208.3	26780	514	191	4150	2690
46DTB-L - 4	7		Below LOD	20.2	6	41	19.8	0.036	69	34.6	426	143.5	589	69	1133	175.3	6.23E+04	977	229.3	4068	3179
46DTB-L - 17	5.9		Below LOD	4.46	0.153	0.95	2.54	Below LOD	20.1	9.58	139.1	56.1	281	34.66	711	133.9	24600	627	158.9	3555	1813
46DTB-L - 15	22.4		Below LOD	326	85	293	160	0.24	330	71	550	128	479	53	1092	221.3	24090	557	429	4820	4870
46DTB-L - 11	8.8		Below LOD	10.8	2.38	16.3	25.1	0.104	73	26.3	252	76.9	311	60.8	638	116.8	23850	491	482	1.09E+04	2410
46DTB-L - 14	43		Below LOD	1.63	0.474	3.87	6.7	0.0031	21.4	7.83	88.9	35.61	197.2	52.5	596	121.9	25640	180	58.9	2680	1381
46DTB-L - 18	4.2		Below LOD	2.64	0.067	0.48	0.96	0	7.28	3.88	59.8	25.54	139	669	376.1	73.4	26290	214.4	62.7	1933	1031
46DTB-L - 1	14.4		Below LOD	21.6	2.18	10.6	9.5	0.014	43.2	17.6	217	85.7	432	107.8	1182	231	29770	737	201.7	4090	2990
46DTB-L - 19	18.2		Below LOD	155	46	167	98	0.129	220	52	416	114	435	99.5	1045	201.6	22180	328	309	8.20E+03	4070
46DTB-L - 16	6.5		Below LOD	3.75	0.56	4.16	10.4	0.055	59.3	23.6	256	78.6	296	107	576	105.6	26860	397	162	9760	2920
46DTB-L - 3	33.4		Below LOD	253	75	420	292	0.211	370	70	432	98.8	387	83.2	845	168.7	24850	519	4.00E+03	1.10E+04	3190
46DTB-L - 7	4.2		Below LOD	3.68	0.328	2.37	6.5	0.007	26.7	11.54	130.3	43.8	192.7	94.2	407.4	69.3	27730	448	112.9	2117	1326
46DTB-L - 5	7.2		Below LOD	4.36	1.22	10.9	22.9	0.091	79	26.7	233	66.4	252	48.8	490	83.8	27950	423.4	151.8	2407	2130
67DTB-L - 1	3.6		Below LOD	52.8	8.5	32.3	9.7	1.33	25.8	7.42	83.5	33.21	165.6	40.1	409.9	77.1	9960	254.1	381	640	1059
67DTB-L - 2	8.9		Below LOD	26	1.87	10.3	9.15	0.432	41	13.1	149.1	55	241.8	48.5	441	77.4	9010	130.3	296.6	335.6	1644
67DTB-L - 3	9.1		0	30.64	0.198	2.91	4.99	0.311	29	10.29	124.8	49.27	224.5	46.8	425.4	73.3	9650	182.2	312.9	438.9	1430
67DTB-L - 4	3.2		0.00533	5.9	0.026	0.22	0.41	0.055	2.93	1.34	19.8	9.65	53.4	14.01	162	34.04	12140	134.3	63.7	345	315.4
67DTB-L - 5	8.2		Below LOD	17.88	0.071	1.03	2.34	0.104	15.73	6.35	86.4	36.95	175.6	39.13	376.8	66.3	11230	251	240.2	624	1089
67DTB-L - 6	15.1		Below LOD	4.01	0.173	1.07	0.94	0.201	4.6	1.81	30.6	17.4	120.9	38	495	120.5	7680	257	90	939	633
67DTB-L - 7	4.7		0	19.39	0.088	1.03	2.27	0.2	14.05	4.96	62.1	24.14	112.3	24.46	239.2	44.1	9550	84.5	130.2	206.1	719
67DTB-L - 8	11.9		Below LOD	1970	511	1840	501	30.4	650	125	830	169	495	82	683	109	9710	199	308	559	4360
67DTB-L - 9	6.1		Below LOD	11.26	0.048	0.46	0.69	0.134	4.83	1.91	25.34	11.62	64.5	16.13	175.4	34.44	10550	72.7	103.2	246.3	386.3
67DTB-L - 10	8.1		Below LOD	16.51	0.085	0.93	1.4	0.147	8.37	3.21	45.4	19.44	102.5	25.04	265.9	53.02	10710	146.8	169.4	423.3	637
67DTB-L - 11	792		Below LOD	26.2	2.56	12.1	5.5	0.51	17.7	6.31	82.2	35.37	183.8	44.92	488	92.7	11190	293.3	465	919	1133
67DTB-L - 12	26.2		Below LOD	24.91	0.265	2.22	4.41	0.6	21.9	7.75	99.9	42.2	213.9	48.8	505.4	94.8	10350	230	546	778	1338
67DTB-L - 13	5.2		0.00512	13.39	0.036	0.66	1.67	0.052	11.52	4.85	66.2	27.8	133.3	29.49	278.6	50.5	11100	124.3	119.1	326	820
67DTB-L - 14	4.1		0	16.73	0.046	0.82	2.14	0.214	10.71	4.06	55.9	23.83	123.1	29.42	309	59	10350	132	168.1	333.7	753
67DTB-L - 15	4.2		0	25.29	0.083	1.7	3.53	0.377	16.85	6.28	80.8	33.5	164.7	40.1	407.4	74.8	9730	192.3	297	466.5	1049
67DTB-L - 16	4.7		0	21.42	0.063	1.62	3.28	0.112	19.18	7.01	92.5	36.34	169.2	36.2	343.6	61.2	10680	184.6	262.4	451.7	1058
67DTB-L - 17	4.8		Below LOD	16.35	0.06	0.99	1.86	0.165	11.35	4.15	58.1	25.1	131.3	32.46	340	65.9	10610	202.4	250	501	806
67DTB-L - 18	6.2		Below LOD	19.7	0.083	1.38	2.46	0.26	12.23	4.56	63.3	27.22	142.1	34.03	364.2	70.2	10160	201.7	284.3	523.1	873
67DTB-L - 19	8.3		Below LOD	16.56	0.123	1.04	2.62	0.103	16.5	6.8	92.3	38.43	188.1	40.58	400.6	70.3	11430	194.2	229.3	528	1138
67DTB-L - 20	7.2		Below LOD	19.81	0.079	1.43	3.63	0.097	18.74	7.02	87.8	34.32	159.3	32.72	308.4	54.3	10220	144.8	200.7	376.5	980

CI normalized	1	2	3	4	5	6	7	8	9	10	11	12	13	14		
Spot ID	La	Ce	Pr	Nd	Sm	Eu	Gd	Tb	Dy	Ho	Er	Tm	Yb	Lu	Eu/Eu*	
37DTB-L - 1		279.05	311.56	195.68	175.83	69.27	236.36	325.04	495.94	770.53	1232.06	1751.32	2726.91	3694.82	0.34	
37DTB-L - 2		73.94	6.11	8.73	39.62	29.91	96.06	152.40	255.20	421.82	760.77	1132.28	1851.55	2599.46	0.48	
37DTB-L - 3		118.84	8.51	16.26	85.59	55.50	229.39	394.20	634.20	977.50	1610.85	2269.84	3432.84	4212.53	0.40	
37DTB-L - 4		38.47	1.22	2.77	12.94	12.95	41.00	62.85	118.21	207.54	378.79	617.72	1056.07	1585.83	0.56	
37DTB-L - 5		32.83	0.29	1.24	8.79	6.47	33.36	67.33	133.94	252.76	513.56	867.72	1623.24	2531.34	0.38	
37DTB-L - 6		27.64	0.64	2.49	13.90	11.61	45.45	81.59	145.61	268.84	528.71	838.62	1593.38	2446.87	0.46	
37DTB-L - 7		28.96	0.77	0.85	4.57	4.76	21.39	44.11	98.68	214.96	508.77	992.06	1964.50	3316.08	0.48	
37DTB-L - 8		27.91	0.18	0.71	8.95	6.38	31.33	58.54	107.31	192.91	355.66	583.86	1039.53	1591.28	0.38	
37DTB-L - 9		62.24	3.12	6.70	34.70	26.21	89.39	144.94	240.74	385.83	642.74	960.32	1488.50	1959.13	0.47	
37DTB-L - 10		61.09	0.55	1.46	6.70	7.40	18.52	38.47	69.51	130.15	270.33	464.55	851.96	1370.30	0.66	
37DTB-L - 11		16.34	0.16	0.50	5.46	4.01	19.85	39.14	80.16	146.23	295.45	536.24	975.39	1607.63	0.38	
37DTB-L - 12		26.94	0.36	1.32	8.48	7.50	26.36	52.90	95.64	187.85	378.39	634.92	1190.00	1920.98	0.50	
37DTB-L - 13		49.82	0.20	1.40	7.32	6.68	29.70	57.55	116.69	231.72	466.51	812.17	1504.64	2283.38	0.45	
37DTB-L - 14		38.94	0.96	2.51	13.79	10.17	35.76	61.69	112.13	202.02	389.15	640.21	1148.04	1732.97	0.46	
37DTB-L - 15		41.49	0.37	0.80	8.21	6.02	29.88	58.37	111.62	216.76	452.15	754.23	1405.81	2193.46	0.38	
37DTB-L - 16		41.90	1.53	2.42	12.86	8.74	43.39	79.44	140.79	247.69	453.35	736.24	1263.01	1858.31	0.37	
37DTB-L - 17		15.14	0.14	0.14	3.45	2.22	11.85	23.71	50.74	103.94	228.07	418.78	810.41	1348.77	0.35	
37DTB-L - 18		41.20	3.97	10.36	39.19	28.98	100.30	153.73	249.11	399.33	649.12	912.70	1385.24	1847.41	0.46	
37DTB-L - 19		42.43	2.62	2.85	8.48	7.81	23.58	46.77	87.77	185.60	405.50	724.87	1403.79	2291.55	0.55	
37DTB-L - 20		22.17	0.15	0.54	2.59	2.13	11.42	22.06	37.80	78.40	159.09	272.49	481.24	775.20	0.39	
46DTB-L - 2		31.25	132.41	282.64	2412.86	19.73	9242.42	13897.18	16768.14	19010.12	19617.22	1798.94	17224.69	15476.84	0.00	
46DTB-L - 8		55.46	91.07	95.42	181.64	0.49	200.00	263.68	367.83	529.81	836.12	675.40	1980.64	2485.01	0.00	
46DTB-L - 20		6.36	8.09	17.15	113.09	0.83	387.88	701.49	1027.40	1406.07	1997.61	1113.76	4130.70	5204.36	0.00	
46DTB-L - 12		3.86	0.25	0.72	6.97	0.00	54.24	160.36	346.78	613.05	1084.13	1722.22	2626.06	3168.94	0.00	
46DTB-L - 9		11.97	4.43	6.76	33.58	0.00	124.24	306.80	559.87	831.27	1275.12	3309.52	2541.35	2841.96	0.00	
46DTB-L - 13		15.32	22.11	28.87	125.10	1.53	360.61	693.20	1050.23	1372.33	1941.79	2701.06	4283.99	5784.74	0.01	
46DTB-L - 10		1.55	0.11	0.13	1.59	0.00	11.61	37.31	85.74	178.85	374.00	2835.98	1185.56	1566.76	0.00	
46DTB-L - 6		4.63	3.50	5.05	26.99	0.00	126.97	284.41	523.85	860.52	1495.22	1706.35	4215.41	5675.75	0.00	
46DTB-L - 4		17.78	35.95	49.52	76.68	0.37	209.09	573.80	1080.67	1614.17	2348.48	1825.40	4570.39	4776.57	0.00	
46DTB-L - 17		3.93	0.92	1.15	9.84	#VALUE!	60.91	158.87	352.87	631.05	1120.41	916.93	2868.09	3648.50	#VALUE!	
46DTB-L - 15		286.97	509.29	353.91	619.67	2.47	1000.00	1177.45	1395.23	1439.82	1909.89	1402.12	4405.00	6029.97	0.00	
46DTB-L - 11		9.51	14.26	19.69	97.21	1.07	221.21	436.15	639.27	865.02	1240.03	1608.47	2573.62	3182.56	0.01	
46DTB-L - 14		1.43	2.84	4.67	25.95	0.03	64.85	129.85	225.52	400.56	786.28	1388.89	2404.20	3321.53	0.00	
46DTB-L - 18		2.32	0.40	0.58	3.72	0.00	22.06	64.34	151.70	287.29	554.23	17698.41	1517.14	2000.00	0.00	
46DTB-L - 1		19.01	13.06	12.80	36.79	0.14	130.91	291.87	550.48	964.00	1722.49	2851.85	4768.05	6294.28	0.00	
46DTB-L - 19		136.44	275.61	201.72	379.55	1.33	666.67	862.35	1055.30	1282.34	1734.45	2632.28	4215.41	5493.19	0.00	
46DTB-L - 16		3.30	3.36	5.02	40.28	0.57	179.70	391.38	649.42	884.14	1180.22	2830.69	2323.52	2877.38	0.01	
46DTB-L - 3		222.71	449.37	507.31	1130.91	2.17	1121.21	1160.86	1095.89	1111.36	1543.06	2201.06	3408.63	4596.73	0.00	
46DTB-L - 7		3.24	1.97	2.86	25.17	0.07	80.91	191.38	330.54	492.69	768.34	2492.06	1643.40	1888.28	0.00	
46DTB-L - 5		3.84	7.31	13.17	88.69	0.94	239.39	442.79	591.07	746.91	1004.78	1291.01	1976.60	2283.38	0.01	
67DTB-L - 1		46.48	50.93	39.01	37.57	13.67	78.18	123.05	211.82	373.57	660.29	1060.85	1653.49	2100.82	0.25	
67DTB-L - 2		22.89	11.20	12.44	35.44	4.44	124.24	217.25	378.23	618.67	964.11	1283.07	1778.94	2108.99	0.07	
67DTB-L - 3		26.97	1.19	3.51	19.33	3.20	87.88	170.65	316.59	554.22	895.14	1238.10	1716.01	1997.28	0.08	
67DTB-L - 4		5.19	0.16	0.27	1.59	0.57	8.88	22.22	50.23	108.55	212.92	370.63	653.49	927.52	0.15	
67DTB-L - 5		15.74	0.43	1.24	9.06	1.07	47.67	105.31	219.18	415.64	700.16	1035.19	1519.97	1806.54	0.05	
67DTB-L - 6		3.53	1.04	1.29	3.64	2.07	13.94	30.02	77.63	195.73	482.06	1005.29	1996.77	3283.38	0.29	
67DTB-L - 7		17.07	0.53	1.24	8.79	2.06	42.58	82.26	157.53	271.54	447.77	647.09	964.91	1201.63	0.11	
67DTB-L - 8		1734.15	3061.71	2222.49	1940.36	312.44	1969.70	2072.97	2105.53	1901.01	1973.68	2169.31	2755.14	2970.03	0.16	Omitted from Fig. 8, TE inclusion?, hig
67DTB-L - 9		9.91	0.29	0.56	2.67	1.38	14.64	31.67	64.28	130.71	257.18	426.72	707.54	938.42	0.22	
67DTB-L - 10		14.53	0.51	1.12	5.42	1.51	25.36	53.23	115.17	218.67	408.69	662.43	1072.61	1444.69	0.13	
67DTB-L - 11		23.06	15.34	14.62	21.30	5.24	53.64	104.64	208.52	397.86	732.85	1188.36	1968.54	2525.89	0.16	
67DTB-L - 12		21.93	1.59	2.68	17.08	6.17	66.36	128.52	253.42	474.69	852.87	1291.01	2038.73	2583.11	0.18	
67DTB-L - 13		11.79	0.22	0.80	6.47	0.53	34.91	80.43	167.94	312.71	531.50	780.16	1123.84	1376.02	0.04	
67DTB-L - 14		14.73	0.28	0.99	8.29	2.20	32.45	67.33	141.81	268.05	490.83	778.31	1246.47	1607.63	0.13	
67DTB-L - 15		22.26	0.50	2.05	13.67	3.87	51.06	104.15	204.97	376.83	656.70	1060.85	1643.40	2038.15	0.15	
67DTB-L - 16		18.86	0.38	1.96	12.70	1.15	58.12	116.25	234.65	408.77	674.64	957.67	1386.04	1667.57	0.04	
67DTB-L - 17		14.39	0.36	1.20	7.20	1.70	34.39	68.82	147.39	282.34	523.52	858.73	1371.52	1795.64	0.11	
67DTB-L - 18		17.34	0.50	1.67	9.53	2.67	37.06	75.62	160.58	306.19	566.59	900.26	1469.14	1912.81	0.14	
67DTB-L - 19		14.58	0.74	1.26	10.15	1.06	50.00	112.77	234.15	432.28	750.00	1073.54	1615.97	1915.53	0.05	
67DTB-L - 20		17.44	0.47	1.73	14.06	1.00	56.79	116.42	222.73	386.05	635.17	865.61	1244.05	1479.56	0.04	

Appendix D2.7: LA-ICPMS Standards

Curtin University Geohistory center							LA-ICP-MS Isotopic Ratios					Apparent Ages - Calculated in Isoplot R (Ma)				Discord
Sample ID	Analysis date-time	Spot ID	238U conc. ppm	±2σ INT	232Th conc. ppm	±2σ INT	238U/206Pb	±2σ PROP	207Pb/206Pb	±2σ PROP	rho	238U/206Pb	±2σ PROP	207Pb/206Pb	±2σ PROP	(7/6-6/8)/7/6 *100
Standard Results - U/Pb on 8900																
Z_91500_1	17/03/2021 (4)	91500 - 1	80.2	2.2	30.02	0.830000	5.589715	0.04999186	0.0744	0.0022	0.2059	1060.96	8.75	1051.4	59.6	-0.91
Z_91500_2	17/03/2021 (4)	91500 - 2	80.5	2.2	30.13	0.850000	5.567929	0.04960293	0.075	0.0023	0.31127	1064.79	8.74	1067.6	61.6	0.26
Z_91500_3	17/03/2021 (4)	91500 - 3	80.3	2.4	30.38	0.900000	5.583473	0.04988027	0.0746	0.0023	0.10934	1062.06	8.75	1056.8	62.1	-0.50
Z_91500_4	17/03/2021 (4)	91500 - 4	78.8	2.2	29.58	0.840000	5.586592	0.04993602	0.0762	0.0023	0.32915	1061.51	8.75	1099.4	60.4	3.45
Z_91500_5	17/03/2021 (4)	91500 - 5	79.4	2.2	29.66	0.800000	5.577245	0.04976906	0.0748	0.0022	0.2862	1063.15	8.75	1062.2	59.2	-0.09
Z_91500_6	17/03/2021 (4)	91500 - 6	80.6	2.2	30.23	0.830000	5.589715	0.04686737	0.0752	0.0022	0.26414	1060.96	8.2	1072.9	58.8	1.11
Z_91500_7	17/03/2021 (4)	91500 - 7	79.4	2.2	29.77	0.830000	5.561735	0.04949264	0.0743	0.0022	0.23573	1065.88	8.74	1048.7	59.7	-1.64
Z_91500_8	17/03/2021 (4)	91500 - 8	80.6	2.3	30.11	0.840000	5.592841	0.04691981	0.0745	0.0024	0.13085	1060.42	8.2	1054.1	64.9	-0.60
Z_91500_9	17/03/2021 (4)	91500 - 9	81.6	2.2	30.66	0.830000	5.56483	0.04954774	0.0744	0.0022	0.076848	1065.34	8.74	1051.4	59.6	-1.33
Z_91500_10	17/03/2021 (4)	91500 - 10	78	2.3	29.39	0.900000	5.599104	0.05015995	0.0754	0.0023	0.17689	1059.32	8.75	1078.3	61.2	1.76
Z_91500_11	17/03/2021 (4)	91500 - 11	80.6	2.2	30.2	0.830000	5.583473	0.04988027	0.0756	0.0022	0.26446	1062.06	8.75	1083.6	58.4	1.99
Z_91500_12	17/03/2021 (4)	91500 - 12	79.5	2.1	29.78	0.750000	5.574136	0.04971359	0.0738	0.0022	0.13229	1063.7	8.75	1035.1	60.2	-2.76
Z_91500_13	17/03/2021 (4)	91500 - 14	80.2	2.1	30.02	0.770000	5.580357	0.04982462	0.076	0.0024	0.24936	1062.6	8.75	1094.2	63.2	2.89
Z_91500_14	18/03/2021 (5)	91500 - 16	80.9	2.1	30.36	0.780000	5.586592	0.04681502	0.0761	0.0023	0.2684	1061.51	8.2	1096.8	60.5	3.22
Z_91500_15	18/03/2021 (5)	91500 - 17	79.4	2	29.76	0.750000	5.577245	0.05287962	0.0731	0.0023	0.30092	1063.15	9.29	1015.8	63.7	-4.66
Z_OG1_1	17/03/2021 (4)	ogc - 1	174.4	5.1	157.2	5.300000	1.429593	0.06539952	0.299	0.0014	0.37891	3419	121	3464.35	7.26	1.31
Z_OG1_2	17/03/2021 (4)	ogc - 2	203	12	253	17.000000	1.398797	0.06261226	0.2992	0.0014	0.44315	3477	120	3465.39	7.25	-0.34
Z_OG1_3	17/03/2021 (4)	ogc - 4	195	14	239	22.000000	1.47232	0.06719955	0.2992	0.0014	0.13639	3341	119	3465.39	7.25	3.59
Z_OG1_4	17/03/2021 (4)	ogc - 5	118.9	4.3	86.4	3.200000	1.4041	0.0630879	0.2987	0.0015	0.2732	3467	120	3462.8	7.78	-0.12
Z_OG1_5	17/03/2021 (4)	ogc - 6	186.9	2.9	148.5	1.700000	1.43246	0.06566209	0.2992	0.0016	0.39773	3413	121	3465.39	8.29	1.51
Z_OG1_6	17/03/2021 (4)	ogc - 7	180.7	6.5	234.9	8.300000	1.381979	0.06302558	0.2989	0.0015	0.27171	3510	123	3463.84	7.78	-1.33
Z_OG1_7	17/03/2021 (4)	ogc - 8	108.6	3.5	119.7	4.700000	1.466061	0.06662935	0.2992	0.0018	0.42007	3352	119	3465.39	9.32	3.27
Z_OG1_8	17/03/2021 (4)	ogc - 9	142.1	4.5	141.3	4.200000	1.431025	0.06553061	0.2997	0.0016	0.35637	3416	121	3467.98	8.27	1.50
Z_OG1_9	17/03/2021 (4)	ogc - 10	125.3	5.1	113.3	6.500000	1.417434	0.06429185	0.2985	0.0015	0.35322	3441	121	3461.76	7.79	0.60
Z_OG1_10	17/03/2021 (4)	ogc - 11	146.2	4	105.3	2.900000	1.392758	0.06401254	0.2994	0.0017	0.35595	3489	124	3466.43	8.8	-0.65
Z_OG1_11	17/03/2021 (4)	ogc - 12	209.5	4.1	225.5	5.200000	1.446969	0.06699898	0.2988	0.0014	0.2986	3387	122	3463.32	7.26	2.20
Z_OG1_12	17/03/2021 (4)	ogc - 14	158.1	3.4	145.7	4.000000	1.407261	0.06337231	0.2994	0.0016	0.47642	3461	121	3466.43	8.28	0.16
Z_OG1_13	18/03/2021 (5)	ogc - 15	163	3.7	164.9	3.900000	1.465631	0.0665903	0.2989	0.0017	0.20247	3353	119	3463.84	8.81	3.20
Z_OG1_14	18/03/2021 (5)	ogc - 17	174.5	6.4	185.3	8.200000	1.405679	0.06322987	0.2991	0.0015	0.3223	3464	121	3464.87	7.77	0.03
Z_GJ1_1	17/03/2021 (4)	gj1 - 1	369	11	9.18	0.270000	10.18745	0.07783809	0.06019	0.0016	0.23293	603.62	4.4	609.4	57.5	0.95
Z_GJ1_2	17/03/2021 (4)	gj1 - 2	372	11	9.1	0.270000	10.11941	0.07884988	0.05991	0.0015	0.15607	607.49	4.52	599.4	54.2	-1.35
Z_GJ1_3	17/03/2021 (4)	gj1 - 3	367	10	9.02	0.260000	10.1916	0.07790157	0.06036	0.0016	0.129	603.38	4.4	615.5	57.2	1.97
Z_GJ1_4	17/03/2021 (4)	gj1 - 4	365	11	8.94	0.270000	10.15435	0.07836417	0.06058	0.0016	0.24131	605.49	4.46	623.4	57	2.87
Z_GJ1_5	17/03/2021 (4)	gj1 - 5	368	9.9	9.08	0.240000	10.14199	0.07611634	0.06022	0.0016	0.0098388	606.2	4.34	610.5	57.4	0.70
Z_GJ1_6	17/03/2021 (4)	gj1 - 6	374	10	9.21	0.270000	10.202	0.0791014	0.05977	0.0016	0.2102	602.79	4.46	594.3	58	-1.43
Z_GJ1_7	17/03/2021 (4)	gj1 - 7	369	11	8.94	0.260000	10.25326	0.07674435	0.06068	0.0016	0.21895	599.92	4.29	626.9	56.8	4.30
Z_GJ1_8	17/03/2021 (4)	gj1 - 8	370	10	9.03	0.250000	10.16467	0.07955676	0.05975	0.0016	0.15796	604.91	4.52	593.6	58	-1.91
Z_GJ1_9	17/03/2021 (4)	gj1 - 9	369	10	9.02	0.250000	10.15332	0.07731735	0.06042	0.0017	0.2035	605.55	4.4	617.7	60.7	1.97
Z_GJ1_10	17/03/2021 (4)	gj1 - 10	362	10	8.89	0.270000	10.11736	0.07984158	0.0594	0.0016	0.053297	607.61	4.58	580.8	58.5	-4.62
Z_GJ1_11	17/03/2021 (4)	gj1 - 11	356	10	8.69	0.250000	10.0898	0.08246128	0.06104	0.0017	0.40729	609.19	4.75	639.7	59.9	4.77
Z_GJ1_12	17/03/2021 (4)	gj1 - 12	350.6	9.9	8.55	0.250000	10.18953	0.08098461	0.06059	0.0016	0.28001	603.5	4.58	623.7	56.9	3.24
Z_GJ1_13	17/03/2021 (4)	gj1 - 13	367	11	8.98	0.270000	10.12248	0.07992242	0.06032	0.0016	0.18597	607.31	4.58	614.1	57.3	1.11
Z_GJ1_14	17/03/2021 (4)	gj1 - 14	368	10	8.84	0.250000	10.09285	0.07639928	0.06059	0.0017	0.28056	609.02	4.4	623.7	60.5	2.35
Z_GJ1_15	18/03/2021 (5)	gj1 - 15	349	11	8.37	0.250000	10.11122	0.0777	0.0598	0.0016	0.17034	607.96	4.46	595.4	58	-2.11
Z_GJ1_16	18/03/2021 (5)	gj1 - 16	352	10	8.46	0.250000	10.09999	0.07956764	0.06086	0.0017	0.13646	608.6	4.58	633.3	60.1	3.90
Z_GJ1_17	18/03/2021 (5)	gj1 - 17	352.4	9.5	8.37	0.230000	10.09591	0.07542629	0.06018	0.0017	0.36568	608.84	4.34	609.1	61.1	0.04
Z_Plesovice_1	17/03/2021 (4)	ples - 2	595	12	52.57	0.950000	18.71608	0.1541283	0.05295	0.0015	0.12496	335.55	2.69	325.6	64.3	-3.06
Z_Plesovice_2	17/03/2021 (4)	ples - 3	601	22	58.5	2.000000	18.6428	0.1563994	0.05237	0.0014	0.10069	336.83	2.75	300.6	61	-12.05
Z_Plesovice_3	17/03/2021 (4)	ples - 4	1637	69	166	7.500000	18.71257	0.1435658	0.05253	0.0013	0.24899	335.61	2.51	307.5	56.4	-9.14
Z_Plesovice_4	17/03/2021 (4)	ples - 5	1790	67	189	7.400000	18.53912	0.1409165	0.0535	0.0013	0.087974	338.67	2.51	349	54.9	2.96
Z_Plesovice_5	17/03/2021 (4)	ples - 7	842	32	114.1	4.200000	18.5701	0.1620789	0.05397	0.0015	0.10724	338.12	2.87	368.8	62.6	8.32
Z_Plesovice_6	17/03/2021 (4)	ples - 8	820	28	90.2	3.200000	18.72309	0.1612548	0.05407	0.0014	0.055979	335.42	2.81	373	58.3	10.08
Z_Plesovice_7	17/03/2021 (4)	ples - 10	983	35	145.4	5.300000	18.86081	0.1494066	0.05413	0.0014	0.2191	333.04	2.57	375.5	58.2	11.31

Curtin University Geohistory center			Lu-Hf Isotopic Ratios from Iolite								
Sample ID	Analysis date-time	Spot ID	178Hf/177Hf	±2σ INT	176Hf/177Hf 0.282785 0.283250	±2σ INT	(2% External ±)	176Lu/177Hfm	±2σ INT	176Yb/177Hf	±2σ INT
								0.03360 Bouvier et al., 2008 EPSL-273			
								0.03840 Griffin et al., 2002, Lithos-237			
Standard Results - Lu/Hf on Nu Plasma II											
Z_MT_1	17/03/2021 (4)	mud - 1	1.46713	0.00012	0.282472	0.000078	0.00572744	0.00002428	0.00000046	0.001084	0.000013
Z_MT_2	17/03/2021 (4)	mud - 2	1.467261	0.000097	0.282489	0.000076	0.00572578	0.00002402	0.00000037	0.001095	0.000012
Z_MT_3	17/03/2021 (4)	mud - 3	1.467139	0.000095	0.282512	0.000075	0.00572524	0.00002426	0.00000045	0.001062	0.000012
Z_MT_4	17/03/2021 (4)	mud - 4	1.46728	0.00011	0.28251	0.000077	0.0057272	0.0000269	0.00000043	0.001183	0.000014
Z_MT_5	17/03/2021 (4)	mud - 5	1.46713	0.00012	0.28255	0.000077	0.005728	0.00002464	0.00000043	0.001088	0.000013
Z_MT_6	17/03/2021 (4)	mud - 6	1.46719	0.00012	0.282517	0.000078	0.00572834	0.00002278	0.00000037	0.001014	0.000014
Z_MT_7	17/03/2021 (4)	mud - 7	1.4672	0.00012	0.282491	0.000079	0.00572882	0.00002179	0.00000046	0.00098	0.000012
Z_MT_8	17/03/2021 (4)	mud - 8	1.46722	0.00012	0.282552	0.000079	0.00573004	0.00002654	0.00000041	0.001141	0.000012
Z_MT_9	17/03/2021 (4)	mud - 9	1.4672	0.00012	0.28256	0.000077	0.0057282	0.00002319	0.00000046	0.00102	0.000013
Z_MT_10	17/03/2021 (4)	mud - 10	1.46721	0.00012	0.282469	0.000077	0.00572638	0.00002271	0.00000048	0.000996	0.000012
Z_MT_11	17/03/2021 (4)	mud - 11	1.46732	0.00012	0.282466	0.000077	0.00572632	0.00002266	0.00000045	0.000998	0.000012
Z_GJ1_1	17/03/2021 (4)	gj1 - 1	1.46716	0.00013	0.282017	0.000077	0.00571734	0.00031031	0.00000065	0.010799	0.000045
Z_GJ1_2	17/03/2021 (4)	gj1 - 2	1.4671	0.00013	0.282035	0.000080	0.0057207	0.00030966	0.00000053	0.010822	0.000043
Z_GJ1_3	17/03/2021 (4)	gj1 - 3	1.46712	0.000096	0.282028	0.000082	0.00572256	0.00030214	0.00000066	0.010434	0.000036
Z_GJ1_4	17/03/2021 (4)	gj1 - 4	1.46716	0.00013	0.28199	0.000077	0.0057168	0.00030063	0.00000079	0.010307	0.000037
Z_GJ1_5	17/03/2021 (4)	gj1 - 5	1.46712	0.00011	0.282033	0.000079	0.00571966	0.00029996	0.00000068	0.010256	0.000036
Z_GJ1_6	17/03/2021 (4)	gj1 - 6	1.46718	0.00014	0.282049	0.000081	0.00572198	0.00030274	0.00000067	0.010404	0.000038
Z_GJ1_7	17/03/2021 (4)	gj1 - 7	1.46717	0.00013	0.282032	0.000086	0.00572664	0.00029801	0.00000069	0.010142	0.000045
Z_GJ1_8	17/03/2021 (4)	gj1 - 8	1.46719	0.00011	0.282056	0.000081	0.00572212	0.00029566	0.00000058	0.010077	0.000045
Z_GJ1_9	17/03/2021 (4)	gj1 - 9	1.46707	0.00012	0.282003	0.000081	0.00572106	0.00029492	0.00000077	0.010011	0.000038
Z_GJ1_10	17/03/2021 (4)	gj1 - 10	1.46729	0.00012	0.282034	0.000079	0.00571968	0.00029247	0.0000008	0.009977	0.000037
Z_Plesovice_1	17/03/2021 (4)	ples - 2	1.467117	0.000094	0.282475	0.000075	0.0057245	0.00007974	0.00000079	0.004174	0.000028
Z_Plesovice_2	17/03/2021 (4)	ples - 3	1.467082	0.000099	0.282499	0.000074	0.00572398	0.0000873	0.00000064	0.004572	0.000046
Z_Plesovice_3	17/03/2021 (4)	ples - 4	1.46703	0.00011	0.282508	0.000076	0.00572616	0.0001422	0.000001	0.007537	0.000089
Z_Plesovice_4	17/03/2021 (4)	ples - 5	1.46705	0.00012	0.282482	0.000075	0.00572464	0.00014895	0.00000048	0.007966	0.000045
Z_Plesovice_5	17/03/2021 (4)	ples - 7	1.46715	0.00011	0.2825	0.000078	0.005728	0.00014695	0.00000054	0.007515	0.000039
Z_91500_1	17/03/2021 (4)	91500 - 1	1.46709	0.00012	0.28228	0.000085	0.0057306	0.00034562	0.00000084	0.012494	0.000051
Z_91500_2	17/03/2021 (4)	91500 - 2	1.46718	0.00013	0.282295	0.000084	0.0057299	0.00034699	0.00000065	0.012551	0.000053
Z_91500_3	17/03/2021 (4)	91500 - 3	1.46729	0.00013	0.282283	0.000087	0.00573266	0.00034267	0.00000094	0.012301	0.000051
Z_91500_4	17/03/2021 (4)	91500 - 4	1.46713	0.00015	0.282263	0.000087	0.00573226	0.00033783	0.00000076	0.011996	0.000045
Z_91500_5	17/03/2021 (4)	91500 - 5	1.4671	0.00013	0.282264	0.000092	0.00573728	0.00033553	0.00000092	0.011886	0.000046
Z_91500_6	17/03/2021 (4)	91500 - 6	1.46709	0.00014	0.282299	0.000087	0.00573298	0.00033601	0.00000088	0.011963	0.000047
Z_91500_7	17/03/2021 (4)	91500 - 7	1.46707	0.00012	0.282323	0.000086	0.00573246	0.00033273	0.00000091	0.011778	0.000045
Z_91500_8	17/03/2021 (4)	91500 - 8	1.46726	0.00012	0.282355	0.000087	0.0057341	0.00033496	0.00000085	0.011755	0.00005
Z_91500_9	17/03/2021 (4)	91500 - 9	1.4671	0.00013	0.282331	0.000087	0.00573362	0.00033408	0.00000072	0.011768	0.000047
Z_R33_1	17/03/2021 (4)	r33 - 1	1.46706	0.0001	0.282801	0.000080	0.00573602	0.003074	0.000033	0.1171	0.0017
Z_R33_2	17/03/2021 (4)	r33 - 2	1.46714	0.00011	0.282731	0.000077	0.00573162	0.0017338	0.0000038	0.06453	0.00037
Z_R33_3	17/03/2021 (4)	r33 - 3	1.467117	0.000099	0.282742	0.000076	0.00573084	0.0011505	0.000002	0.04146	0.00015
Z_R33_4	17/03/2021 (4)	r33 - 4	1.46716	0.00011	0.282765	0.000078	0.0057333	0.0017315	0.000002	0.06291	0.00018
Z_R33_5	17/03/2021 (4)	r33 - 5	1.46711	0.00011	0.282774	0.000078	0.00573348	0.001168	0.000019	0.04314	0.00085
Z_R33_6	17/03/2021 (4)	r33 - 6	1.4671	0.00011	0.282805	0.000081	0.0057371	0.001941	0.000019	0.0747	0.0012
Z_R33_7	17/03/2021 (4)	r33 - 8	1.4671	0.00012	0.28275	0.000079	0.005734	0.002784	0.000011	0.10504	0.00082
Z_R33_8	17/03/2021 (4)	r33 - 9	1.46722	0.0001	0.282768	0.000078	0.00573336	0.0012671	0.000003	0.045802	0.000076

Appendix D2.8: Detrital Zircon Trace Element Results

Sample Info		LA-ICPMS Results: Preferred Age			Lu-Hf	
Analysis date	Spot ID	Ma	2 sig	Discord	eHf	2sig
16/07/2020 (5) 18:56:11.00	X38DT_62	2600.5	78.2	8.6	-1.3	1.4
16/07/2020 (5) 19:24:38.00	X38DT_68	2605	138	2.5	-0.2	1.2
14/07/2020 (3) 17:27:06.00	38DTB19 - 55	2610	82.6	8.2	2.3	1.2
14/07/2020 (3) 18:19:38.00	38DTB19 - 74	2612	101	7.6	-0.4	1.3
14/07/2020 (3) 19:06:38.00	38DTB19 - 92	2622.3	81.2	5.8	-0.2	1.2
16/07/2020 (5) 17:52:19.00	X38DT_35	2635.4	74.2	7.1	-3.4	1.4
14/07/2020 (3) 17:15:58.00	38DTB19 - 49	2638.2	72.3	8.8	0.9	1.5
14/07/2020 (3) 17:41:57.00	38DTB19 - 63	2642.9	71.2	6.8	-1.5	1.5
16/07/2020 (5) 22:06:16.00	X38DT_127	2647.5	60	7.4	1.2	1.5
14/07/2020 (3) 16:08:07.00	38DTB19 - 24	2647.5	72	5.9	3.0	1.2
16/07/2020 (5) 19:19:01.00	X38DT_65	2654	67.2	7.4	0.9	1.8
14/07/2020 (3) 17:12:15.00	38DTB19 - 47	2654	78.3	7.0	-2.5	1.4
14/07/2020 (3) 18:32:35.00	38DTB19 - 81	2655.8	75.4	4.7	0.1	1.3
16/07/2020 (5) 20:50:57.00	X38DT_103	2656.7	76.3	7.7	1.0	1.4
16/07/2020 (5) 16:55:53.00	X38DT_34	2657.6	72.6	9.6	1.9	1.2
16/07/2020 (5) 17:57:55.00	X38DT_38	2659.5	92.7	-3.9	1.2	1.4
14/07/2020 (3) 18:01:03.00	38DTB19 - 64	2661.3	60.6	8.9	2.3	1.1
16/07/2020 (5) 21:35:56.00	X38DT_122	2662.2	73.4	1.4	4.6	1.3
16/07/2020 (5) 19:30:10.00	X38DT_71	2663.1	75.2	5.7	2.6	1.5
16/07/2020 (5) 21:21:04.00	X38DT_114	2665	76.1	6.4	1.1	1.6
16/07/2020 (5) 16:52:08.00	X38DT_12	2665	67.8	3.2	3.8	1.6
14/07/2020 (3) 16:13:38.00	38DTB19 - 27	2665.9	81.5	8.8	1.8	1.3
14/07/2020 (3) 19:21:39.00	38DTB19 - 96	2666.8	73.3	2.7	-1.8	1.4
16/07/2020 (5) 22:13:45.00	X38DT_131	2667.7	54.1	8.8	-0.2	1.4
14/07/2020 (3) 16:09:56.00	38DTB19 - 25	2667.7	69.6	6.0	1.0	1.2
14/07/2020 (3) 15:52:51.00	38DTB19 - 21	2668.6	63.2	5.6	1.7	1.5
16/07/2020 (5) 18:45:01.00	X38DT_56	2668.6	79.6	5.1	-2.9	1.6
16/07/2020 (5) 21:09:55.00	X38DT_108	2669.5	63.2	6.9	1.5	1.4
16/07/2020 (5) 16:33:34.00	X38DT_2	2674.1	75.8	8.6	2.4	1.4
14/07/2020 (3) 18:30:47.00	38DTB19 - 80	2674.1	72.1	4.9	-4.9	1.5
14/07/2020 (3) 16:11:49.00	38DTB19 - 26	2678.6	79.2	7.8	2.0	1.5
16/07/2020 (5) 22:11:51.00	X38DT_130	2679.5	73.8	6.4	2.7	1.5
14/07/2020 (3) 18:06:37.00	38DTB19 - 67	2681.3	80.5	5.6	1.1	1.3
14/07/2020 (3) 16:30:44.00	38DTB19 - 32	2683.1	97.1	0.2	-0.8	1.6
16/07/2020 (5) 17:20:27.00	X38DT_22	2683.1	73.7	0.2	0.9	1.3
14/07/2020 (3) 18:36:18.00	38DTB19 - 83	2683.9	68.2	4.9	1.5	1.5
14/07/2020 (3) 17:10:22.00	38DTB19 - 46	2686.7	71.7	9.6	0.7	1.4
16/07/2020 (5) 22:08:09.00	X38DT_128	2688.5	69	7.7	0.2	2.0
16/07/2020 (5) 21:34:02.00	X38DT_121	2690.3	89.6	8.6	2.8	1.4
16/07/2020 (5) 16:31:42.00	X38DT_1	2693.9	66.2	4.0	2.6	1.2
16/07/2020 (5) 16:59:36.00	X38DT_16	2694.8	83.1	4.4	0.5	1.1
16/07/2020 (5) 17:31:38.00	X38DT_28	2695.7	75.9	6.3	1.9	1.5
16/07/2020 (5) 16:50:19.00	X38DT_11	2697.5	91.1	8.7	2.0	1.2
14/07/2020 (3) 18:34:30.00	38DTB19 - 82	2702.8	67.7	4.1	-0.5	1.5
16/07/2020 (5) 16:37:16.00	X38DT_4	2706.4	81.8	6.4	-2.6	1.3
09/04/2020 (5) 00:21:03.00	10DTB19 - 44	1489	101	-0.5	7.1	1.4
08/04/2020 (4) 22:25:37.00	10DTB19 - 1	1491	105	1.9	9.8	1.3
09/04/2020 (5) 04:25:53.00	10DTB19 - 134	1497	111	6.4	9.8	1.1
09/04/2020 (5) 02:50:06.00	10DTB19 - 101	1517	122	5.6	6.6	1.5
09/04/2020 (5) 01:02:40.00	10DTB19 - 60	1521.3	91.5	1.7	8.6	1.2
08/04/2020 (4) 19:58:22.00	12DTB19 - 77	1523	123	7.6	2.8	1.1
08/04/2020 (4) 21:21:53.00	12DTB19 - 109	1539	105	2.0	8.8	1.4
08/04/2020 (4) 20:40:08.00	12DTB19 - 93	1547	100	8.2	7.1	1.5
08/04/2020 (4) 19:10:31.00	12DTB19 - 63	1550.8	76.6	8.5	2.5	1.3
09/04/2020 (5) 02:32:23.00	10DTB19 - 92	1552.8	64.8	-2.4	8.5	1.5
08/04/2020 (4) 23:57:02.00	10DTB19 - 37	1561	109	9.3	10.6	1.5
09/04/2020 (5) 00:24:59.00	10DTB19 - 46	1562.5	84	9.6	8.2	1.7
08/04/2020 (4) 21:31:42.00	12DTB19 - 114	1563	111	3.0	5.8	1.2
08/04/2020 (4) 16:47:40.00	12DTB19 - 6	1564.4	97.5	2.3	3.0	1.4
09/04/2020 (5) 02:20:35.00	10DTB19 - 86	1566.4	68.4	5.1	5.5	1.2
09/04/2020 (5) 00:38:45.00	10DTB19 - 53	1568.3	79.9	5.4	7.5	1.3
08/04/2020 (4) 22:33:31.00	10DTB19 - 5	1572.2	79.8	3.1	5.5	1.1
08/04/2020 (4) 21:59:37.00	12DTB19 - 123	1576	114	-0.8	4.6	1.4
08/04/2020 (4) 22:37:27.00	10DTB19 - 7	1577.9	93	-0.5	5.4	1.2
09/04/2020 (5) 00:42:42.00	10DTB19 - 55	1577.9	71.9	2.4	2.3	1.4
08/04/2020 (4) 18:16:57.00	12DTB19 - 41	1577.9	85.4	9.4	5.0	1.7
09/04/2020 (5) 04:06:08.00	10DTB19 - 124	1579.8	70	8.5	5.0	1.3
09/04/2020 (5) 03:32:09.99	10DTB19 - 112	1580	114	4.4	3.1	1.8
08/04/2020 (4) 23:13:17.00	10DTB19 - 20	1584	114	3.2	3.0	1.6
08/04/2020 (4) 17:11:20.00	12DTB19 - 18	1585.6	87	1.6	7.3	1.6
09/04/2020 (5) 01:38:35.00	10DTB19 - 70	1585.6	96.5	6.7	2.9	1.3
09/04/2020 (5) 00:34:48.00	10DTB19 - 51	1591	102	4.7	5.8	1.2
08/04/2020 (4) 17:15:18.00	12DTB19 - 20	1593.2	100	8.1	10.2	1.5
08/04/2020 (4) 17:17:13.00	12DTB19 - 21	1595	106	8.1	7.0	1.6
08/04/2020 (4) 22:55:10.00	10DTB19 - 16	1595	143	9.4	6.5	1.6
09/04/2020 (5) 00:40:45.00	10DTB19 - 54	1595.1	92.3	0.2	5.9	1.4
08/04/2020 (4) 23:15:13.00	10DTB19 - 21	1598.9	94	4.4	4.5	1.1
08/04/2020 (4) 23:51:05.00	10DTB19 - 34	1600.8	97.7	3.8	6.9	1.3
08/04/2020 (4) 18:56:39.00	12DTB19 - 56	1601	103	5.3	4.6	1.2
09/04/2020 (5) 01:54:24.00	10DTB19 - 78	1603	135	0.0	2.9	1.3
09/04/2020 (5) 02:18:34.00	10DTB19 - 85	1606.4	84.3	3.4	3.9	1.4
08/04/2020 (4) 21:23:49.00	12DTB19 - 110	1606.4	76.8	9.0	5.5	1.2
09/04/2020 (5) 04:35:47.00	10DTB19 - 139	1608.3	95.5	4.9	8.2	1.4
08/04/2020 (4) 22:35:27.00	10DTB19 - 6	1610.2	76.7	-3.7	5.3	1.3
08/04/2020 (4) 20:10:19.00	12DTB19 - 83	1612	118	5.4	4.2	1.2
09/04/2020 (5) 01:56:25.00	10DTB19 - 79	1612	86	9.7	5.1	1.2
09/04/2020 (5) 00:17:05.00	10DTB19 - 42	1613.9	70.9	7.9	6.4	2.0
08/04/2020 (4) 16:45:39.00	12DTB19 - 5	1613.9	85.9	8.0	6.1	1.2
09/04/2020 (5) 04:27:53.00	10DTB19 - 135	1615.8	95.2	3.3	6.2	1.2
08/04/2020 (4) 22:43:20.00	10DTB19 - 10	1617.7	82	2.8	7.2	1.5
09/04/2020 (5) 01:52:27.00	10DTB19 - 77	1617.7	89.5	3.8	8.2	1.2
09/04/2020 (5) 01:26:45.00	10DTB19 - 64	1619.5	96.9	2.5	4.0	1.1
09/04/2020 (5) 01:24:48.00	10DTB19 - 63	1621.4	96.8	3.3	5.4	1.1
08/04/2020 (4) 23:35:16.00	10DTB19 - 26	1621.4	67	5.4	7.8	1.5
09/04/2020 (5) 02:28:27.00	10DTB19 - 90	1623.2	80	5.7	5.9	1.1
08/04/2020 (4) 23:58:57.00	10DTB19 - 38	1623.2	76.3	9.7	8.4	1.3
09/04/2020 (5) 04:23:56.00	10DTB19 - 133	1627	79.9	4.2	6.4	1.2
09/04/2020 (5) 01:28:46.00	10DTB19 - 65	1629	122	4.1	7.3	1.1
09/04/2020 (5) 02:22:30.00	10DTB19 - 87	1630.7	85.3	-4.5	6.4	1.1
08/04/2020 (4) 19:00:36.00	12DTB19 - 58	1630.7	72.3	3.7	4.2	1.2
08/04/2020 (4) 23:39:14.00	10DTB19 - 28	1630.7	85.3	5.7	2.1	1.4
08/04/2020 (4) 20:34:15.00	12DTB19 - 90	1631	100	4.0	5.9	1.2
09/04/2020 (5) 03:22:16.00	10DTB19 - 107	1633	106	6.9	6.4	1.6
08/04/2020 (4) 19:08:30.00	12DTB19 - 62	1634	102	8.1	2.8	1.3
09/04/2020 (5) 03:34:06.00	10DTB19 - 113	1634	109	9.5	7.9	1.4
09/04/2020 (5) 01:40:36.00	10DTB19 - 71	1636	115	8.4	8.6	1.3
08/04/2020 (4) 23:31:19.00	10DTB19 - 24	1638	109	7.3	7.2	1.3
09/04/2020 (5) 03:47:56.00	10DTB19 - 120	1639.9	83.1	2.0	5.1	1.2
08/04/2020 (4) 20:51:58.00	12DTB19 - 99	1642	107	8.9	7.0	1.5
09/04/2020 (5) 03:38:01.00	10DTB19 - 115	1643.6	84.8	1.4	4.5	1.1
08/04/2020 (4) 17:41:11.00	12DTB19 - 28	1643.6	86.7	4.5	3.6	1.3
08/04/2020 (4) 20:48:02.00	12DTB19 - 97	1643.6	83	9.2	0.0	1.2
08/04/2020 (4) 19:06:35.00	12DTB19 - 61	1644	118	5.9	6.4	1.7
09/04/2020 (5) 00:19:01.00	10DTB19 - 43	1645.4	95.8	-3.0	6.6	1.0
09/04/2020 (5) 01:30:42.00	10DTB19 - 66	1651.3	50.9	9.3	7.3	1.5
09/04/2020 (5) 03:12:20.00	10DTB19 - 102	1652.7	66.3	9.4	-1.1	1.4
08/04/2020 (4) 19:30:33.00	12DTB19 - 68	1656.4	98.9	5.1	5.4	1.2
09/04/2020 (5) 01:36:39.00	10DTB19 - 69	1660	77	4.6	6.0	1.1
08/04/2020 (4) 17:53:00.00	12DTB19 - 34	1663.6	73.2	4.4	2.1	1.4
09/04/2020 (5) 04:10:05.00	10DTB19 - 126	1665	118	7.1	6.9	1.2
08/04/2020 (4) 22:57:11.00	10DTB19 - 17	1674.5	99.9	6.3	7.0	1.3
09/04/2020 (5) 03:16:23.00	10DTB19 - 104	1676	121	5.3	5.7	1.3
09/04/2020 (5) 01:22:48.00	10DTB19 - 62	1680	103	5.8	3.8	1.2
09/04/2020 (5) 03:24:16.00	10DTB19 - 108	1696	133	7.8	9.3	1.5

Sample #/Spot #	Ti	Nb	La	Ce	Pr	Nd	Sm	Eu	Gd	Tb	Dy	Ho	Er	Tm	Yb	Lu	Hf	Pb	Th	U	Y
MC and Sun (1995) PM	1205	0.658	0.648	1.675	0.254	1.25	0.406	0.154	0.544	0.099	0.674	0.149	0.438	0.068	0.441	0.0675	0.283	0.15	0.0795	0.0203	4.3
CI Anders 89			0.446	1.136	0.1669	0.8279	0.2582	0.0973	0.33	0.0603	0.3942	0.0889	0.2508	0.0378	0.2479	0.0367					
X38DT_62	Below LOD		-0.012	15.69	Below LOD	0.67	1.62	0.193	11.3		40.5				151.7	28.13	8870			124.8	
X38DT_68	Below LOD		-0.01	9.56	Below LOD	0.89	1.7	0.55	6.84		19.9				64.7	12.46	8960			21.42	
38DTB19 - 55	200		Below LOD	44.94	0.108	2.27	5.9	1.5	18.3		55.9				192.2	36.42	8010			102.1	
38DTB19 - 74	Below LOD		169	570	48	284	52.8	2.29	46.8		72.5				162.8	27.92	9180			85.3	
38DTB19 - 92	14.3		Below LOD	16.92	Below LOD	0.38	1.11	0.253	7.54		32.1				128.6	24.2	8440			84.5	
X38DT_35	4.8		-0.019	7.12	0.171	3.66	7.09	1.61	33.2		113.4				337.8	59.3	8400			172.1	
38DTB19 - 49	10		Below LOD	21.65	0.118	2.01	3.84	0.36	16.5		63.6				206.3	37.08	8710			189.9	
38DTB19 - 63	Below LOD		0.038	14.65	Below LOD	0.99	2.58	0.198	11.5		50.8				187.5	33.24	8700			140.7	
X38DT_127	3.9		Below LOD	23.4	0.33	3.87	4.96	0.95	20.5		78.5				292.7	55.6	7992			229.9	
38DTB19 - 24	13		Below LOD	1100	82	430	74	10.3	35		51.9				172.3	31.55	8550			151.7	
X38DT_65	5.4		-0.014	18.78	Below LOD	1.07	2.61	0.291	15.7		65.3				255.8	47.21	9520			256.4	
38DTB19 - 47	Below LOD		Below LOD	8.34	0.034	0.51	1.22	0.37	7.66		33.1				178	35.37	8440			125	
38DTB19 - 81	Below LOD		0.017	17.6	0.044	0.71	1.71	0.279	7.2		34.6				178.5	35	9100			152.9	
X38DT_103	4.1		Below LOD	32.11	0.33	2.45	3.43	0.399	13.3		58.8				216.1	40.3	9020			181.9	
X38DT_34	6.8		Below LOD	12.7	0.39	1.64	2	0.43	10.2		46.6				191.2	33.52	9470			171.8	
X38DT_38	5.3		Below LOD	20.4	1.07	7.3	7.4	0.94	22.8		68.9				197	35.7	7417			74	
38DTB19 - 64	Below LOD		0.122	41.12	0.056	1.27	5.5	1.96	20.4		37.3				122.9	24.79	9250			281.8	
X38DT_122	3.4		Below LOD	36.5	0.55	5.9	9.5	1.45	36.4		102.9				272.5	46.8	9100			166	
X38DT_71	3.2		-0.011	16.05	0.055	1.39	3.62	0.34	16.7		61.5				209.1	39.04	8900			127	
X38DT_114	Below LOD		-0.015	21.47	0.26	2.86	5.02	1.06	22.1		81.4				306	56.9	8031			128.9	
X38DT_12	13.4		Below LOD	34.7	1.08	8.77	16.3	3.84	69.4		185.6				489	85.5	7518			155.8	
38DTB19 - 27	7.8		Below LOD	15.86	Below LOD	0.48	1.19	0.183	6.43		27.6				124.7	23.31	8940			113.2	
38DTB19 - 96	12		3.4	31	1.79	13.1	10.9	0.98	33.4		111.4				291.3	50.2	8420			128.7	
X38DT_131	4.7		-0.034	18.07	0.082	0.95	1.79	0.192	10.8		59.1				332	64.7	10460			613	
38DTB19 - 25	Below LOD		Below LOD	13.7	0.21	3	4.84	1.03	22.6		95.5				322	56.5	8930			187.9	
38DTB19 - 21	12.8		Below LOD	23.3	0.45	4.3	5.37	0.414	22.5		96.4				331.4	58.9	8840			288.5	
X38DT_56	5.1		-0.018	13.19	0.163	2.51	3.83	1.52	12.3		41.9				175.5	35.5	7510			119.3	
X38DT_108	4.1		Below LOD	132	18.9	51	10.8	0.89	19.3		64.5				250.9	46.24	9360			272.1	
X38DT_2	18.1		Below LOD	139	14	41	14.8	1.8	27.6		75.9				239.5	44.05	8320			139.4	
38DTB19 - 80	16.9		0.08	48.4	0.68	10.94	15.5	3.85	55.4		177.9				521	93.9	7361			139	
38DTB19 - 26	Below LOD		-0.0104	46.1	0.155	3.39	6.44	1.03	27.1		100.1				329.3	59	8360			144.3	
X38DT_130	3.5		0.019	17.61	0.078	1.25	2.68	0.161	13.4		55.5				197.1	36.02	9100			161	
38DTB19 - 67	10		0.028	26.38	0.045	2.02	4.08	0.52	17.8		66.2				234.9	42.55	8420			128.8	
38DTB19 - 32	21.6		-0.0022	3.27	0.175	3.84	5.32	2.88	21.2		58.9				158.3	29.3	6211			46.37	
X38DT_22	Below LOD		Below LOD	22.4	2.29	13.1	6.2	0.51	17.9		63.4				246.9	43.9	9540			144.8	
38DTB19 - 83	Below LOD		0.024	15.22	0.182	3.79	8.02	0.89	37.4		119.8				325	56	8170			167	
38DTB19 - 46	Below LOD		Below LOD	17.26	0.038	0.5	1.09	0.171	4.87		27.8				143.7	27.14	9170			157.4	
X38DT_128	Below LOD		-0.01	30.66	0.085	1.51	2.86	0.398	14.6		51.1				189.8	35.22	8840			114.1	
X38DT_121	5.6		Below LOD	18.3	1	3	4.04	0.58	18.5		61.6				199.5	36.54	8209			114.3	
X38DT_1	6.4		Below LOD	11.67	0.45	4.7	9.8	1.18	48.8		173				475	81	8050			212.4	
X38DT_16	8.4		-0.0076	14.45	0.128	0.88	2.8	0.295	14.3		52.8				183.5	32.1	8660			100.7	
X38DT_28	Below LOD		-0.029	5.82	0.044	0.28	1.02	0.1	6.63		30.8				128.2	22.61	9660			110.7	
X38DT_11	8.2		-0.009	15.83	0.135	0.7	2.38	0.36	11.3		42.5				156.6	27.86	8510			88.5	
38DTB19 - 82	Below LOD		Below LOD	8.65	0.083	1.97	4.83	0.53	25.1		95.4				282	50.1	8320			148.1	
X38DT_4	5.5		-0.0023	13.28	Below LOD	0.36	0.8	0.306	6.43		25.4				106.7	20.18	8910			77.5	
10DTB19 - 44	6		Below LOD	28.8	0.113	2.32	3.79	1.34	20.9		91.7				442	87.7	9120			161.4	
10DTB19 - 1	450		Below LOD	29.8	1.88	14.2	9.1	0.75	33.9		131.5				424.6	75.7	9693			184.5	
10DTB19 - 134	6		Below LOD	25.36	0.372	5.91	10	2.66	47		192				675	123	9390			160	
10DTB19 - 101	770		3.9	75	2.9	22	8.5	2.6	40		101				316.1	58.2	8750			134.4	
10DTB19 - 60	8.2		0.076	24.92	0.113	2.89	4.2	1.01	18.46		69.8				269.5	51.3	9475			315.8	
12DTB19 - 77	8.6		Below LOD	14.9	0.069	2.39	4.2	1.11	24.2		109.9				472	90.9	10500			127.2	
12DTB19 - 109	7		46	30.5	1	8.8	4.61	0.474	21.5		96.1				380	69.9	10130			183.4	
12DTB19 - 93	14.3		0.085	29.27	0.213	4.43	6.83	1.35	30.4		115.4				397	74.6	9670			139.2	
12DTB19 - 63	259		18.7	50	4.9	32	11	1.22	35.4		162.2				850	159.6	11480			406	
10DTB19 - 92	12		4.1	54	4.9	39	17.1	2.06	80		274				747	128.2	10980			613	
10DTB19 - 37	9.9		1.18	19.08	0.251	3.26	5.25	1.16	27.1		107.4				364	67.7	8363			104.2	
10DTB19 - 46	55		186	360	34	185	219	101	1130		2590				1170	137	13300			499	
12DTB19 - 114	11.7		Below LOD	12.85	0.087	3.42	5.05	0.77	28.3		115.7				379.2	68.5	9530			95.2	
12DTB19 - 6	12		0.083	20.58	0.056	0.89	2.1	0.358	13.03		64.8				236.4	43.5	9920			144.5	
10DTB19 - 86	Below LOD		Below LOD	5.98	0.095	1.6	3.67	0.284	30.6		185				798	144.4	11730			790	
10DTB19 - 53	5.3		16.6	90	5.7	31.5	9.9	1.83	24.7		86.1				444.2	90.4	10700			482	
10DTB19 - 5	6.4		Below LOD	11.8	0.88	4.6	4.98	0.282	32.9		228.2				1207	222.3	11840			353	
12DTB19 - 123	10.4		Below LOD	32	0.48	5.6	5.58	0.71	30		137.5				535	99.5	10930			86.7	
10DTB19 - 7	8.3		-0.041	56.5	0.141	2.25	5.16	0.91	28.2		122.1				482	90.3	9940			149.5	
10DTB19 - 55	7.3		Below LOD	11.09	0.152	2.97	4.4	0.62	29.7		182.9				1015	189.9	11490			399.7	
12DTB19 - 41	11		Below LOD	269.8	1.89	33.5	40.5	15.65	152.1		420				1025	187.8	6930			172	
10DTB19 - 124	5.5		0.025	15.9	0.105	0.81	1.95	0.313	11.65		68.4				380	73.7	12390			641	
10DTB19 - 112	37		0.86	63.8	1.32	15.8	29.2	11.8	156		460				673	112.1	8220			142	
10DTB19 - 20	Below LOD		Below LOD	26.4	0.477	7.44	15.7	2.85	76.2		274				699	123.9	6830			100.9	
12DTB19 - 18	5.5		41	23.4	0.62	8.1	8.93	0.381	44.1		155.1				408.5	73.9	8170			157.3	
10DTB19 - 70	21		2.7	54	2.3	16	4.6	1.23	17.2		56.5				267.5	55	10430			263.9	
10DTB19 - 51	9.2		0.062	7.52	0.085	1.75	4.69	0.53	36.5		177.6				674.1	121.8	10520			181.2	
12DTB19 - 20	Below LOD		2.9	34.1	0.205	5.5	9.06	2.21	48		190.5				637	118.5	9150			196	
12DTB19 - 21	11.5		0.061	16.67	0.083	1.97	3.96	0.91	21.7		95				370	69.7	8851			116.6	
10DTB19 - 16	15.6		Below LOD	84.6	0.635	10.24	19.2	8.59	80.3		254				719	130.6	7015			108.4	
10DTB19 - 54	10.9		Below LOD	107.1	0.326	5.53	10.63	1.62	52.5		196.4				623	112.5	8776			227.1	
10DTB19 - 21	Below LOD		-0.048	25.2	0.083	1.21	2.41	0.79	13.5		58.7				281	57.3	9790			139	
10DTB19 - 34	9.6		2.6	32.4	0.113	1.96	4.26	2.22	26.5		109.9				420	77.1	9600			178	
12DTB19 - 56	6.1		Below LOD	27.12	0.091	1.62	3.34	0.9	14.59		62.3				331.7	67.7	10000			175.4	
10DTB19 - 78	12.5		Below LOD	7.1	0.068	1.39	1.98	0.326	11.17		46.3				159.7	29.29	8396			55.54	
10DTB19 - 85	7		4.8	135	3.1	24.7	10.1	2.11	49.2		205.8				717	128.9	9270			249.5	
12DTB19 - 110	Below LOD		3.3	6.54	0.101	2.3	4.91	0.7	35.4		261				1413	258.7	11980			403	
10DTB19 - 139	9.8		22.2	219	16.9	87	29.2	5.68	93.8		344				935	161.3	9720			197.8	
10DTB19 - 6	25.2		Below LOD	131	8.2	40	16.9	1.92	57.5		199.9				686	124.1	9290			429	
12DTB19 - 83	9.8		Below LOD	20.91	0.061	1.53	3.13	0.95	17		76.2				322.7	61.8	9610			98.5	
10DTB19 - 79	102		0.138	41.9	0.41	5.79	6.46	1.93	34.8		137.1				556	105.3	8960			253.6	
10DTB19 - 42	24.5		0.4	25.4	0.58	7.8	19.5	2.34	122		612				2180	374	10390			560	
12DTB19 - 5	6.4		0.056	44.9	0.085	1.94	3.12	1.1	20.7		99.1				455.2	89	9979			207	
10DTB19 - 135	8.5		0.04	30.2	0.176	2.47	4.12	1.29	25		109.9				453.4	85.5	10590			238	
10DTB19 - 10	9.7		Below LOD	25.61	0.125	2.3	5.78	0.72	30.7		136.8				450	81.6	9840			211	
10DTB19 - 77	5.4		0.069	26.2	0.61	16.1	23.2	5.6	119		376				669	111.9	9280			268	
10DTB19 - 64	6.3		0.03	31.7	0.133	3.3	4.94	1.41	27.7		132.3				640	122.4	9770			136.4	
10DTB19 - 63	21.3		49	340	36	200	41	3.03	61		166				557	102	10640			209.4	
10DTB19 - 26	9.2		Below LOD	42.3	0.215	2.54	6.87	0.97	41.3		233				1237	226.7	12680			830	
10DTB19 - 90	14.9		1.36	18.9	0.76	7	4.7	1.06	33.2		187.3				967	178.8	11340			292.3	
10DTB19 - 38	5.8		0.22	16.47	0.064	1.51	3.86	0.59	19.8		104.9				424	80	10630			229	
10DTB19 - 133	17.3		0.57	56.9	0.41	5.3	7.9	1.83	47.8		230.2				931	168.7	10630			394	
10DTB19 - 65	Below LOD		16.1	113	10.4	62	12.4	0.86	24.2		88.1				396	74	10280			112.8	
10DTB19 - 87	12.2		0.097	22.2	0.56	10	10.6	1.24	56.9		274				910	154	10630			240	
12DTB19 - 58	Below LOD		Below LOD	24.2	0.079	1.61	4.23	0.37	28.6		150.9				719	133.2	11560			404.4	
10DTB19 - 28	Below LOD		-0.5	68.9	0.266	3.65	6.76	2.07	27.3		87.5				336	67.7	9920			372.4	
12DTB19 - 90	7.7		32	106	4	23	8.7	3.41	45.1		163.7				508	91.8	9780			148.3	
10DTB19 - 107	16.5		Below LOD	36.36	0.558	7.56	10.7	3.2	53.4		182.3				499	88.6	7967			114.4	
12DTB19 - 62	7.5		23	56	2.8	20.1	8.5	1.44	31.2		125.6				424	76.9	9110			172	
10DTB19 - 113	29.1		0.031	8.91	0.16	2.03	3.34	0.342	20.2		93.5				343.9	63	9680			113.1	
10DTB19 - 71	43		Below LOD	11.26	0.083	2.19	3.33	0.356	19.6		79.2				290.9	55.4	9104			106.2	
10DTB19 - 24	59		Below LOD	36.9	0.3	4.1	7.7	1.93	38.5		148				535	98.7	10200			166	
10DTB19 - 120	26		Below LOD	18.1	0.073	1.72	3.06	0.94	19.4		88.4				397	76	10220			279	
12DTB19 - 99	19.9		0.88	44.8	0.238	4.71	6.41	2	31.4		126.1				522	100.2	9130			142.7	
10DTB19 - 115	10.6		0.035	53.1	0.193	3.64	6.23	2.13	41.9		192.6				776	143.7	10320			305.5	
12DTB19 - 28	12.9		-0.23	7.04	0.164	3.54	4.85	0.303	25.3		97.5				262.9	45.59	8658			147.3	
12DTB19 - 97	7.5		0.098	75.6	0.11	2.96	4.8	0.98	24.9		107.7				455	84.8	10142			379	
12DTB19 - 61	9.6		84	113	11	79	28.6	2.57	68		221				724	131.9	10530			105.7	
10DTB19 - 43	7.1		1.06	13.2	0.358	4.93	8.04	0.97	45.3		169				476	82.6	9118			189	
10DTB19 - 66	36.1		3.2	77	2.79	20.5	12.5	0.325	54.2		261.9				1020	176	11148			3230	
10DTB19 - 102	Below LOD		63	450	53	276	64	9.3	159		370				455	72	10890			600	
12DTB19 - 68	6.2		2.39	37.3	0.398	5.16	5.65	1.21	25		87.2				315	59.9	9115			176.1	
10DTB19 - 69	230		1.7	25.8	1.21	11.2	8.6	0.83	39.3		161.4				590	105.9	9920			363	
12DTB19 - 34	10.2		Below LOD	78.5	4.4	29.1	8.6	1.14	26.9		101.5				338.5	62.5	9842			264.8	
10DTB19 - 126	18.8		0.11	23	0.17	1.52	2.22	0.489	14.7		71.7				313.6	58.8	10257			91.5	
10DTB19 - 17	30		Below LOD	93	7.5	25	9.3	0.39	19.2		63.6				226.8	41.44	9950			148.7	
10DTB19 - 104	Below LOD		Below LOD	46.8	0.117	2.11	3.49	1.09	23.6		100.2				391	72.4	9400			84.8	
10DTB19 - 62	11		0.133	59.6	0.198	3.07	4.24	0.83	22.3		90.2				347.5	64.5	9880			141.8	
10DTB19 - 108	10.8		1.62	22.4	2.09	12	4.85	0.7	23		85.4				262.1	47.07	8567			62.43	

Spot ID	CI normalized La	Ce	Pr	Nd	Sm	Eu	Gd	Tb	Dy	Ho	Er	Tm	Yb	Lu	Eu/Eu*
X38DT_62	-0.03	13.81	#VALUE!	0.81	6.27	1.98	34.24		102.74				611.94	766.49	0.135326
X38DT_68	-0.02	8.42	#VALUE!	1.08	6.58	5.65	20.73		50.48				260.99	339.51	0.483874
38DTB19 - 55	#VALUE!	39.56	0.65	2.74	22.85	15.42	55.45		141.81				775.31	992.37	0.433074
38DTB19 - 74	378.92	501.76	287.60	343.04	204.49	23.54	141.82		183.92				656.72	760.76	0.138203
38DTB19 - 92	#VALUE!	14.89	#VALUE!	0.46	4.30	2.60	22.85		81.43				518.76	659.40	0.262359
X38DT_35	-0.04	6.27	1.02	4.42	27.46	16.55	100.61		287.67				1362.65	1615.80	0.314815
38DTB19 - 49	#VALUE!	19.06	0.71	2.43	14.87	3.70	50.00		161.34				832.19	1010.35	0.13568
38DTB19 - 63	0.09	12.90	#VALUE!	1.20	9.99	2.03	34.85		128.87				756.35	905.72	0.109051
X38DT_127	#VALUE!	20.60	1.98	4.67	19.21	9.76	62.12		199.14				1180.72	1514.99	0.282636
38DTB19 - 24	#VALUE!	968.31	491.31	519.39	286.60	105.86	106.06		131.66				695.04	859.67	0.607169
X38DT_65	-0.03	16.53	#VALUE!	1.29	10.11	2.99	47.58		165.65				1031.87	1286.38	0.136378
38DTB19 - 47	#VALUE!	7.34	0.20	0.62	4.73	3.80	23.21		83.97				718.03	963.76	0.363103
38DTB19 - 81	0.04	15.49	0.26	0.86	6.62	2.87	21.82		87.77				720.05	953.68	0.238541
X38DT_103	#VALUE!	28.27	1.98	2.96	13.28	4.10	40.30		149.16				871.72	1098.09	0.177224
X38DT_34	#VALUE!	11.18	2.34	1.98	7.75	4.42	30.91		118.21				771.28	913.35	0.285611
X38DT_38	#VALUE!	17.96	6.41	8.82	28.66	9.66	69.09		174.78				794.68	972.75	0.217103
38DTB19 - 64	0.27	36.20	0.34	1.53	21.30	20.14	61.82		94.62				495.76	675.48	0.555114
X38DT_122	#VALUE!	32.13	3.30	7.13	36.79	14.90	110.30		261.04				1099.23	1275.20	0.233926
X38DT_71	-0.02	14.13	0.33	1.68	14.02	3.49	50.61		156.01				843.49	1063.76	0.131186
X38DT_114	-0.03	18.90	1.56	3.45	19.44	10.89	66.97		206.49				1234.37	1550.41	0.301912
X38DT_12	#VALUE!	30.55	6.47	10.59	63.13	39.47	210.30		470.83				1972.57	2329.70	0.342515
38DTB19 - 27	#VALUE!	13.96	#VALUE!	0.58	4.61	1.88	19.48		70.02				503.03	635.15	0.19847
38DTB19 - 96	7.62	27.29	10.72	15.82	42.22	10.07	101.21		282.60				1175.07	1367.85	0.154086
X38DT_131	-0.08	15.91	0.49	1.15	6.93	1.97	32.73		149.92				1339.25	1762.94	0.131004
38DTB19 - 25	#VALUE!	12.06	1.26	3.62	18.75	10.59	68.48		242.26				1298.91	1539.51	0.295449
38DTB19 - 21	#VALUE!	20.51	2.70	5.19	20.80	4.25	68.18		244.55				1336.83	1604.90	0.112991
X38DT_56	-0.04	11.61	0.98	3.03	14.83	15.62	37.27		106.29				707.95	967.30	0.664376
X38DT_108	#VALUE!	116.20	113.24	61.60	41.83	9.15	58.48		163.62				1012.10	1259.95	0.184936
X38DT_2	#VALUE!	122.36	83.88	49.52	57.32	18.50	83.64		192.54				966.12	1200.27	0.267183
38DTB19 - 80	0.18	42.61	4.07	13.21	60.03	39.57	167.88		451.29				2101.65	2558.58	0.394151
38DTB19 - 26	-0.02	40.58	0.93	4.09	24.94	10.59	82.12		253.93				1328.36	1607.63	0.233901
X38DT_130	0.04	15.50	0.47	1.51	10.38	1.65	40.61		140.79				795.08	981.47	0.080599
38DTB19 - 67	0.06	23.22	0.27	2.44	15.80	5.34	53.94		167.94				947.56	1159.40	0.183057
38DTB19 - 32	0.00	2.88	1.05	4.64	20.60	29.60	64.24		149.42				638.56	798.37	0.813563
X38DT_22	#VALUE!	19.72	13.72	15.82	24.01	5.24	54.24		160.83				995.97	1196.19	0.145235
38DTB19 - 83	0.05	13.40	1.09	4.58	31.06	9.15	113.33		303.91				1311.01	1525.89	0.154166
38DTB19 - 46	#VALUE!	15.19	0.23	0.60	4.22	1.76	14.76		70.52				579.67	739.51	0.222659
X38DT_128	-0.02	26.99	0.51	1.82	11.08	4.09	44.24		129.63				765.63	959.67	0.184776
X38DT_121	#VALUE!	16.11	5.99	3.62	15.65	5.96	56.06		156.27				804.76	995.64	0.201268
X38DT_1	#VALUE!	10.27	2.70	5.68	37.96	12.13	147.88		438.86				1916.10	2207.08	0.161876
X38DT_16	-0.02	12.72	0.77	1.06	10.84	3.03	43.33		133.94				740.22	874.66	0.139861
X38DT_28	-0.07	5.12	0.26	0.34	3.95	1.03	20.09		78.13				517.14	616.08	0.115363
X38DT_11	-0.02	13.93	0.81	0.85	9.22	3.70	34.24		107.81				631.71	759.13	0.208256
38DTB19 - 82	#VALUE!	7.61	0.50	2.38	18.71	5.45	76.06		242.01				1137.56	1365.12	0.144407
X38DT_4	-0.01	11.69	#VALUE!	0.43	3.10	3.14	19.48		64.43				430.42	549.86	0.404756
10DTB19 - 44	#VALUE!	25.3521	0.6770521	2.80227	14.6785	13.7718	63.3333		232.623				1782.977	2389.6458	0.451684
10DTB19 - 1	#VALUE!	26.2324	11.26423	17.1518	35.244	7.70812	102.727		333.587				1712.7874	2062.6703	0.128104
10DTB19 - 134	#VALUE!	22.3239	2.2288796	7.13854	38.7297	27.3381	142.424		487.062				2722.8721	3351.4986	0.368091
10DTB19 - 101	8.744394619	66.0211	17.375674	26.5733	32.9202	26.7215	121.212		256.215				1275.1109	1585.8311	0.423015
10DTB19 - 60	0.170403587	21.9366	0.6770521	3.49076	16.2665	10.3803	55.9394		177.067				1087.1319	1397.8202	0.344115
12DTB19 - 77	#VALUE!	13.1162	0.4134212	2.88682	16.2665	11.408	73.3333		278.792				1903.9935	2476.8392	0.330303
12DTB19 - 109	103.1390135	26.8486	5.9916117	10.6293	17.8544	4.87153	65.1515		243.785				1532.8762	1904.6322	0.142834
12DTB19 - 93	0.19058296	25.7658	1.2762133	5.35089	26.4524	13.8746	92.1212		292.745				1601.4522	2032.6975	0.281066
12DTB19 - 63	41.92825112	44.0141	29.358898	38.652	42.6026	12.5385	107.273		411.466				3428.8019	4348.7738	0.185474
10DTB19 - 92	9.192825112	47.5352	29.358898	47.1071	66.2277	21.1716	242.424		695.079				3013.3118	3493.188	0.167088
10DTB19 - 37	2.64573991	16.7958	1.5038945	3.93767	20.3331	11.9219	82.1212		272.451				1468.334	1844.6866	0.291753
10DTB19 - 46	417.0403587	316.901	203.7148	223.457	848.18	1038.03	3424.24		6570.27				4719.645	3732.97	0.609091
12DTB19 - 114	#VALUE!	11.3116	0.5212702	4.13093	19.5585	7.91367	85.7576		293.506				1529.6491	1866.485	0.19323
12DTB19 - 6	0.186098655	18.1162	0.3355303	1.07501	8.13323	3.67934	39.4848		164.384				953.61033	1185.2861	0.205316
10DTB19 - 86	#VALUE!	5.26408	0.5692031	1.9326	14.2138	2.91881	92.7273		469.305				3219.0399	3934.6049	0.080398
10DTB19 - 53	37.21973094	79.2254	34.152187	38.0481	38.3424	18.8078	74.8485		218.417				1791.8516	2463.2153	0.351081
10DTB19 - 5	#VALUE!	10.3873	5.2726183	5.55623	19.2874	2.89825	99.697		578.894				4868.8987	6057.2207	0.066093
12DTB19 - 123	#VALUE!	28.169	2.8759736	6.7641	21.6112	7.29702	90.9091		348.808				2158.1283	2711.1717	0.164628
10DTB19 - 7	-0.091928251	49.7359	0.8448173	2.71772	19.9845	9.35252	85.4545		309.741				1944.3324	2460.4905	0.226315
10DTB19 - 55	#VALUE!	9.76232	0.910725	3.58739	17.0411	6.37205	90		463.978				4094.3929	5174.3869	0.162708
12DTB19 - 41	#VALUE!	237.5	11.324146	40.4638	156.855	160.843	460.909		1065.45				4134.7317	5117.1662	0.598197
10DTB19 - 124	0.056053812	13.9965	0.6291192	0.97838	7.55229	3.21686	35.303		173.516				1532.8762	2008.1744	0.197009
10DTB19 - 112	1.928251121	56.162	7.9089275	19.0844	113.091	121.274	472.727		1166.92				2714.8044	3054.4959	0.524506
10DTB19 - 20	#VALUE!	23.2394	2.8579988	8.98659	60.8056	29.2909	230.909		695.079				2819.6854	3376.0218	0.247195
12DTB19 - 18	91.92825112	20.5986	3.7147993	9.78379	34.5856	3.91572	133.636		393.455				1647.8419	2013.624	0.057597
10DTB19 - 70	6.053811659	47.5352	13.780707	19.326	17.8156	12.6413	52.1212		143.328				1079.0641	1498.6376	0.414843
10DTB19 - 51	0.139013453	6.61972	0.509287	2.11378	18.1642	5.44707	110.606		450.533				2719.2416	3318.8011	0.121525
12DTB19 - 20	6.502242152	30.0176	1.2282804	6.64331	35.0891	22.7133	145.455		483.257				2569.5845	3228.8828	0.317929
12DTB19 - 21	0.1367713	14.6743	0.4973038	2.37951	15.3369	9.35252	65.7576		240.994				1492.5373	1899.1826	0.294501
10DTB19 - 16	#VALUE!	74.4718	3.8046735	12.3686	74.361	88.2837	243.333		644.343				2900.363	3558.5831	0.656307
10DTB19 - 54	#VALUE!	94.2782	1.9532654	6.67955	41.1696	16.6495	159.091		498.224				2513.1101	3065.3951	0.205727
10DTB19 - 21	-0.107623318	22.1831	0.4973038	1.46153	9.33385	8.11922	40.9091		148.909				1133.5216	1561.3079	0.415503
10DTB19 - 34	5.829596413	28.5211	0.6770521	2.36744	16.4988	22.816	80.303		278.792				1694.2315	2100.8174	0.626827
12DTB19 - 56	#VALUE!	23.8732	0.5452367	1.95676	12.9357	9.24974	44.2121		158.042				1338.0395	1844.6866	0.38678
10DTB19 - 78	#VALUE!	6.25	0.4074296	1.67895	7.66847	3.35046	33.8485		117.453				644.21138	798.09264	0.20796
10DTB19 - 85	10.76233184	118.838	18.573996	29.8345	39.117	21.6855	149.091		522.07				2892.2953	3512.2616	0.283963
12DTB19 - 110	7.399103139	5.75704	0.6051528	2.77811	19.0163	7.19424	107.273		662.1				5699.879	7049.0463	0.159286
10DTB19 - 139	49.77578475	192.782	101.25824	105.085	113.091	58.3762	284.242		872.653				3771.6821	4395.0954	0.325595
10DTB19 - 6	#VALUE!	115.317	49.131216	48.315	65.4531	19.7328	174.242		507.103				2767.2449	3381.4714	0.184776
12DTB19 - 83	#VALUE!	18.4067	0.3654883	1.84805	12.1224	9.76362	51.5152		193.303				1301.7346	1683.9237	0.390705
10DTB19 - 79	0.30941704	36.8838	2.4565608	6.9936	25.0194	19.8356	105.455		347.793				2242.8399	2869.2098	0.386166
10DTB19 - 42	0.896860987	22.3592	3.4751348	9.42143	75.5229	24.0493	369.697		1552.51				8793.8685	10190.736	0.143927
12DTB19 - 5	0.125560538	39.5246	0.509287	2.34328	12.0837	11.3052	62.7273		251.395				1836.2243	2425.0681	0.410632
10DTB19 - 135	0.089686099	26.5845	1.0545237	2.98345	15.9566	13.258	75.7576		278.792				1828.9633	2329.7003	0.381323
10DTB19 - 10	#VALUE!	22.544	0.7489515	2.77811	22.3857	7.39979	93.0303		347.032				1815.2481	2223.4332	0.162152
10DTB19 - 77	0.15470852	23.0634	3.6548832	19.4468	89.8528	57.554	360.606		953.831				2698.6688	3049.0463	0.319737
10DTB19 - 64	0.067264574	27.9049	0.7968844	3.98599	19.1325	14.4913	83.9394		335.616				2581.6862	3335.1499	0.361608
10DTB19 - 63	109.8654709	299.296	215.69802	241.575	158.792	31.1408	184.848		421.106				2246.8737	2779.2916	0.181764
10DTB19 - 26	#VALUE!	37.2359	1.2881965	3.068	26.6073	9.96917	125.152		591.071				4989.9153	6177.1117	0.172759
10DTB19 - 90	3.049327354	16.6373	4.5536249	8.45513	18.2029	10.8941	100.606		475.14				3900.7664	4871.9346	0.254572
10DTB19 - 38	0.493273543	14.4982	0.3834632	1.82389	14.9497	6.06372	60		266.109				1710.3671	2179.8365	0.202464
10DTB19 - 133	1.278026906	50.088	2.4565608	6.40174	30.5964	18.8078	144.848		583.968				3755.5466	4596.7302	0.282518
10DTB19 - 65	36.09865471	99.4718	62.312762	74.8883	48.0248	8.83864	73.3333		223.491				1597.4183	2016.3488	0.148937
10DTB19 - 87	0.217488789	19.5423	3.3553026	12.0788	41.0534	12.7441	172.424		695.079				3670.835	4196.1853	0.151473
12DTB19 - 58	#VALUE!	21.3028	0.4733373	1.94468	16.3826	3.80267	86.6667		382.801				2900.363	3629.4278	0.100918
10DTB19 - 28	-1.121076233	60.6514	1.5937687	4.40875	26.1813	21.2744	82.7273		221.969				1355.3852	1844.6866	0.457128
12DTB19 - 90	71.74887892	93.3099	23.966447	27.7811	33.6948	35.0462	136.667		415.271				2049.2134	2501.3624	0.516451
10DTB19 - 107	#VALUE!	32.007	3.3433194	9.13154	41.4407	32.888	161.818		462.456				2012.9084	2414.1689	0.401615
12DTB19 - 62	51.56950673	49.2958	16.776513	24.2783	32.9202	14.7996	94.5455		318.62				1710.3671	2095.3678	0.265276
10DTB19 - 113	0.069506726	7.84331	0.9586579	2.45199	12.9357	3.5149	61.2121		237.189				1387.2529	1716.6213	0.124911
10DTB19 - 71	#VALUE!	9.91197	0.4973038	2.64525	12.897	3.65879	59.3939		200.913				1173.457	1509.5368	0.132197
10DTB19 - 24	#VALUE!	32.4824	1.7974835	4.95229	29.8218	19.8356	116.667		375.444				2158.1283	2689.3733	0.336282
10DTB19 - 120	#VALUE!	15.9331	0.4373877	2.07755	11.8513	9.66084	58.7879		224.252				1601.4522	2070.8447	0.366006
12DTB19 - 99	1.97309417	39.4366	1.4260036	5.68909	24.8257	20.555	95.1515		319.888				2105.6878	2730.2452	0.42292
10DTB19 - 115	0.078475336	46.743	1.1563811	4.39667	24.1286	21.8911	126.97		488.584				3130.2945	3915.5313	0.395504
12DTB19 - 28	-0.515695067	6.19718	0.9826243	4.27588	18.7839	3.11408	76.6667		247.336				1060.5083	1242.2343	0.08206
12DTB19 - 97	0.219730942	66.5493	0.6590773	3.57531	18.5902	10.0719	75.4545		273.212				1835.4175	2310.6267	0.268923
12DTB19 - 61	188.3408072	99.4718	65.907729	95.4222	110.767	26.4132	206.061		560.629				2920.5325	3594.0054	0.174831
10DTB19 - 43	2.376681614	11.6197	2.144997	5.95483	31.1387	9.96917	137.273		428.716				1920.1291	2250.6812	0.152481
10DTB19 - 66	7.174887892	67.7817	16.716597	24.7614	48.4121	3.34018	164.242		664.384				4114.5623	4795.6403	0.037459
10DTB19 - 102	141.2556054	396.127	317.55542	333.374	247.87	95.5807	481.818		938.61				1835.4175	1961.8529	0.276577
12DTB19 - 68	5.358744395	32.8345	2.3846615	6.23264	21.8823	12.4358	75.7576		221.208				1270.6737	1632.1526	0.305431
10DTB19 - 69	3.811659193	22.7113	7.2498502	13.5282	33.3075	8.53032	119.091		409.437				2379.9919	2885.5586	0.135442
12DTB19 - 34	#VALUE!	69.1021	26.363092	35.1492	33.3075	11.7163	81.5152		257.484				1365.4699	1702.9973	0.224855
10DTB19 - 126	0.246636771	20.2465	1.018574	1.83597	8.59799	5.02569	44.5455		181.887				1265.0262	1602.1798	0.256801
10DTB19 - 17	#VALUE!	81.8662	44.937088	30.1969	36.0186	4.00822	58.1818		161.339				914.88503	1129.1553	0.087558
10DTB19 - 104	#VALUE!	41.1972	0.7010186	2.54862	13.5167	11.2025	71.5152		254.186				1577.2489	1972.752	0.360313
10DTB19 - 62	0.298206278	52.4648	1.1863391	3.70818	16.4214	8.53032	67.5758		228.818				1401.7749	1757.4932	0.256074
10DTB19 - 108	3.632286996	19.7183	12.522469	14.4945	18.7839	7.19424	69.697		216.641				1057.2812	1282.5613	0.198832

Appendix D3.1: U/Pb-Lu/Hf Results

Curtin University Geohistory center — Sample ID	Analysis date-time	Spot ID	238U conc. (ppm)	±2σ INT	232Th conc. (ppm)	±2σ INT	Isotopic Ratios — 238U/206Pb	±2σ PROP	207Pb/206Pb	±2σ PROP	rho	Apparent Ages - Calculated in Isoplot R (Ma) — 238U/206Pb	±2σ PROP	207Pb/206Pb	±2σ PROP	Discord (7/6-6/8)/7/6*100	Perferred age *1500 Ma cutoff — Ma	2 σ	error %	Lu-Hf Isotopic Ratios from Iolite — 176Hf/177Hf (0.282785; 0.283250)	±2σ INT	(2% External ±)	176Lu/177Hfm (0.03360 Bouvier et al., 2008 EPSL-273; 0.03840 Griffin et al., 2002, Lithos-237)	±2σ INT	176Yb/177Hf	±2σ INT	εHf Calculations — Hfi	εHf Lu decay	±2σ (0.02)	TDM(Ga) (Scherer et al., 2001, Science-293)	TDMCrustal (Ga)	HfCHUR(t)	HfDM(t)	Analysis Notes
38DTB19 - Run 1	14/07/2020 (3) 18:04:48.00	38DTB19 - 66	81.9	3	42	0.071	1.443091	0.11006789	0.2443	0.012286	0.18258	3394	201	3147.5	79.9	-7.83	3147.5	79.9	2.54%	0.280593	0.000046	0.005612049	0.00048	0.000028	0.01522	0.00074	0.28056	-6.75	1.61	3.63	3.978391062	0.280753612	0.280929413	> 5% reverse discordant, excluded
38DTB19 - Run 1	14/07/2020 (3) 16:39:58.00	38DTB19 - 37	129.8	3.3	5.5	0.046	3.127932	0.10854326	0.108	0.00576	0.088722	1788.3	54.2	1765.1	97.4	-1.31	1765.1	97.4	5.52%	0.28143	0.00005	0.005628822	0.000761	0.000014	0.0264	0.0006	0.28140	-9.09	1.75	2.53	3.036176667	0.281660511	0.281965869	
38DTB19 - Run 1	14/07/2020 (3) 15:34:18.00	38DTB19 - 11	176	11	13	0.056	3.152585	0.10877015	0.108	0.00596	0.23288	1776	53.6	1765	101	-0.62	1765	101	5.72%	0.281859	0.00005	0.005637402	0.00127	0.0001	0.0391	0.0034	0.28182	5.54	1.75	1.97	2.106350448	0.281660575	0.281965943	
38DTB19 - Run 1	14/07/2020 (3) 16:30:44.00	38DTB19 - 32	46.37	0.77	1	0.055	1.941748	0.08784995	0.1834	0.010768	0.44865	2677.9	99.1	2683.1	97.1	0.19	2683.1	97.1	3.62%	0.281077	0.000047	0.005621736	0.000737	0.000016	0.02549	0.0008	0.28104	-0.77	1.65	3.01	3.233416343	0.281060885	0.281280583	
38DTB19 - Run 1	14/07/2020 (3) 15:39:50.00	38DTB19 - 14	80.3	1.3	1.4	0.043	3.153579	0.12572547	0.1098	0.007096	0.36052	1775.6	61.9	1795	118	1.08	1795	118	6.57%	0.281493	0.000044	0.005630032	0.0004761	0.000004	0.01657	0.00028	0.28148	-5.84	1.54	2.43	2.854424947	0.281641142	0.281943733	
38DTB19 - Run 1	14/07/2020 (3) 16:45:34.00	38DTB19 - 40	96.4	1.3	1.4	0.06	3.113325	0.11945398	0.1115	0.00723	0.29527	1795.6	60.1	1823	118	1.50	1823	118	6.47%	0.281443	0.00004	0.005629002	0.0004352	0.0000023	0.015186	0.000057	0.28143	-6.93	1.40	2.49	2.945521867	0.281622994	0.281922993	
38DTB19 - Run 1	14/07/2020 (3) 18:38:11.00	38DTB19 - 84	91.4	2.4	2.5	0.05	3.173596	0.12692369	0.1097	0.006894	0.35739	1765.8	61.8	1794	114	1.57	1794	114	6.35%	0.281486	0.000034	0.005629823	0.000777	0.000012	0.02698	0.00031	0.28146	-6.47	1.19	2.46	2.893779257	0.28164179	0.281944474	
38DTB19 - Run 1	14/07/2020 (3) 17:25:13.00	38DTB19 - 54	117.6	3.2	2.3	0.037	3.081664	0.1186132	0.1129	0.006558	0.15059	1811.7	60.8	1846	105	1.86	1846	105	5.69%	0.281533	0.000039	0.005630795	0.000784	0.000014	0.02791	0.00058	0.28151	-3.64	1.37	2.39	2.755745642	0.281608079	0.281905948	
38DTB19 - Run 1	14/07/2020 (3) 18:55:30.00	38DTB19 - 86	72.1	1.5	2.1	0.054	3.149606	0.12747225	0.1109	0.008218	0.21769	1777.5	62.9	1813	135	1.96	1813	135	7.45%	0.281482	0.000045	0.00562982	0.001422	0.000015	0.05188	0.00037	0.28143	-6.97	1.58	2.50	2.940595763	0.281629476	0.281930401	
38DTB19 - Run 1	14/07/2020 (3) 18:25:11.00	38DTB19 - 77	54.8	1.9	1.9	0.048	3.115265	0.13606235	0.1126	0.009252	0.060841	1794.6	68.4	1841	149	2.52	1841	149	8.09%	0.281504	0.000059	0.005630389	0.0002593	0.0000058	0.00839	0.00025	0.28149	-4.13	2.07	2.40	2.782956896	0.281611322	0.281909654	
38DTB19 - Run 1	14/07/2020 (3) 19:21:39.00	38DTB19 - 96	128.7	4.1	3.9	0.055	2.018978	0.08032704	0.1816	0.008032	0.4235	2593.6	85	2666.8	73.3	2.74	2666.8	73.3	2.75%	0.281068	0.000041	0.00562151	0.000925	0.000017	0.03352	0.00039	0.28102	-1.81	1.44	3.03	3.286522422	0.281071621	0.281292853	
38DTB19 - Run 1	14/07/2020 (3) 17:38:15.00	38DTB19 - 61	103.9	1.8	1.3	0.059	3.292723	0.11789618	0.1087	0.007574	0.035127	1709.6	53.8	1777	127	3.79	1777	127	7.15%	0.28175	0.000045	0.005635518	0.0004824	0.0000037	0.016823	0.000024	0.28173	2.87	1.58	2.08	2.286285078	0.281652803	0.281957061	
38DTB19 - Run 1	14/07/2020 (3) 16:17:21.00	38DTB19 - 29	236	14	8.8	0.06	3.118179	0.10125574	0.1143	0.005486	0.3338	1793.1	50.8	1868.1	86.6	4.01	1868.1	86.6	4.64%	0.281541	0.00004	0.005630962	0.001103	0.000032	0.0397	0.0014	0.28150	-3.26	1.40	2.40	2.74913519	0.281593743	0.281889563	
38DTB19 - Run 1	14/07/2020 (3) 17:28:55.00	38DTB19 - 56	60.5	1.1	1.1	0.058	3.133814	0.15302754	0.1138	0.007876	0.32955	1785.3	76.1	1860	125	4.02	1860	125	6.72%	0.281484	0.000052	0.00562992	0.0004755	0.0000038	0.01615	0.00025	0.28147	-4.68	1.82	2.44	2.8326625	0.281598998	0.281895569	
38DTB19 - Run 1	14/07/2020 (3) 18:34:30.00	38DTB19 - 82	148.1	3.3	3.5	0.044	2.02061	0.07429999	0.1856	0.007612	0.19102	2591.8	78.5	2702.8	67.7	4.11	2702.8	67.7	2.50%	0.281081	0.000044	0.005621792	0.000927	0.000024	0.0333	0.0011	0.28103	-0.53	1.54	3.02	3.233318652	0.281047904	0.281265748	
38DTB19 - Run 1	14/07/2020 (3) 15:38:00.00	38DTB19 - 13	301	10	6	0.059	3.12989	0.08904758	0.1143	0.005486	0.27622	1787.3	44.4	1868.1	86.6	4.33	1868.1	86.6	4.64%	0.281543	0.000044	0.005631032	0.001336	0.000016	0.05039	0.00039	0.28150	-3.48	1.54	2.41	2.763245683	0.281593743	0.281889563	
38DTB19 - Run 1	14/07/2020 (3) 18:32:35.00	38DTB19 - 81	152.9	3.2	4.9	0.069	2.0803	0.06713911	0.1804	0.008208	0.34651	2530.3	67.5	2655.8	75.4	4.73	2655.8	75.4	2.84%	0.28111	0.000036	0.005622315	0.0055	0.000017	0.01759	0.00065	0.28108	0.11	1.26	2.95	3.155423147	0.281078865	0.281301132	
38DTB19 - Run 1	14/07/2020 (3) 18:36:18.00	38DTB19 - 83	167	14	13	0.065	2.056344	0.07495528	0.1836	0.007572	-0.017571	2554.6	76.9	2684.9	68.2	4.85	2684.9	68.2	2.54%	0.281155	0.000043	0.005623264	0.001036	0.000037	0.0376	0.0016	0.28110	1.50	1.51	2.93	3.089920176	0.281059699	0.281279227	
38DTB19 - Run 1	14/07/2020 (3) 18:30:47.00	38DTB19 - 80	139	2.4	11	0.056	2.06868	0.06405462	0.1824	0.007948	0.11191	2542.1	65	2674.1	72.1	4.94	2674.1	72.1	2.70%	0.281031	0.000044	0.005620792	0.002009	0.000045	0.0708	0.0015	0.28093	-4.93	1.54	3.17	3.490680797	0.281066813	0.281287358	
38DTB19 - Run 1	14/07/2020 (3) 16:19:15.00	38DTB19 - 30	183	3.1	2.8	0.039	3.243594	0.11221594	0.1115	0.00613	0.12007	1732.3	52.6	1823.2	99.7	4.99	1823.2	99.7	5.47%	0.281417	0.000048	0.005628545	0.000664	0.0000016	0.02435	0.00015	0.28139	-8.13	1.68	2.54	3.02144006	0.281622864	0.281922845	
38DTB19 - Run 1	14/07/2020 (3) 17:32:38.00	38DTB19 - 58	64	2.4	2.5	0.047	3.07031	0.13587795	0.1173	0.008746	0.30851	1817.5	70.1	1915	134	5.09	1915	134	7.00%	0.281504	0.000056	0.005630358	0.000952	0.000045	0.0338	0.0018	0.28147	-3.34	1.96	2.44	2.790884562	0.281563298	0.281854769	
38DTB19 - Run 1	14/07/2020 (3) 15:15:40.00	38DTB19 - 1	235.2	3.3	2.7	0.05	3.17864	0.10297742	0.1137	0.005974	0.10186	1763.3	50	1858.6	94.9	5.13	1858.6	94.9	5.11%	0.281923	0.000044	0.005638632	0.0018926	0.0000045	0.0643	0.00068	0.28186	9.10	1.54	1.91	1.951002809	0.281599906	0.281896607	
38DTB19 - Run 1	14/07/2020 (3) 18:15:56.00	38DTB19 - 72	372	5.3	3.5	0.046	3.166561	0.09240984	0.1144	0.004988	0.50137	1769.2	45.2	1869.6	78.7	5.37	1869.6	78.7	4.21%	0.281671	0.000037	0.005633542	0.0005832	0.0000051	0.02069	0.00032	0.28165	2.04	1.30	2.19	2.412531333	0.281592769	0.281888451	
38DTB19 - Run 1	14/07/2020 (3) 18:06:37.00	38DTB19 - 67	128.8	2.1	2.2	0.047	2.07857	0.07181457	0.1832	0.008964	0.43187	2532.1	72.3	2681.3	80.9	5.56	2681.3	80.9	3.02%	0.281133	0.000038	0.005622788	0.000753	0.000012	0.02611	0.00064	0.28109	1.15	1.33	2.93	3.109343044	0.281062071	0.281281938	
38DTB19 - Run 1	14/07/2020 (3) 17:06:40.00	38DTB19 - 44	330	5	3.4	0.059	3.210273	0.10130653	0.1133	0.005066	0.32887	1748.1	48.3	1852.2	80.8	5.62	1852.2	80.8	4.36%	0.281539	0.000046	0.005630968	0.001067	0.000005	0.03853	0.00011	0.28150	-3.64	1.61	2.40	2.760694098	0.281604058	0.281901352	
38DTB19 - Run 1	14/07/2020 (3) 15:52:51.00	38DTB19 - 21	288.5	5.7	6.2	0.064	2.09205	0.06547504	0.1818	0.006936	0.47992	2518.5	65.2	2668.6	63.2	5.62	2668.6	63.2	2.37%	0.281166	0.000042	0.005623477	0.000961	0.0000072	0.0342	0.00054	0.28112	1.66	1.47	2.90	3.067053625	0.281070436	0.281291498	
38DTB19 - Run 1	14/07/2020 (3) 18:27:04.00	38DTB19 - 78	75.5	1.2	0.76	0.048	3.320053	0.14135578	0.1101	0.008602	0.14778	1697.3	63.5	1800	142	5.71	1800	142	7.89%	0.281928	0.000049	0.005638773	0.0011563	0.000004	0.04177	0.00049	0.28189	8.90	1.72	1.87	1.917893206	0.281637902	0.28194003	
38DTB19 - Run 1	14/07/2020 (3) 19:06:38.00	38DTB19 - 92	84.5	1.6	1.4	0.059	2.140411	0.07991723	0.1768	0.008636	0.48576	2471.3	76.6	2622.3	81.2	5.76	2622.3	81.2	3.10%	0.281117	0.000034	0.005622443	0.0004291	0.000002	0.014547	0.000066	0.28110	-0.19	1.19	2.93	3.148661502	0.281100917	0.281326333	
38DTB19 - Run 1	14/07/2020 (3) 18:02:55.00	38DTB19 - 65	181.7	3.9	2.3	0.053	3.376097	0.11995289	0.1087	0.006774	0.35703	1672.4	52.3	1777	114	5.89	1777	114	6.42%	0.281453	0.000044	0.005629232	0.0006603	0.000004	0.024944	0.000094	0.28143	-7.88	1.54	2.49	2.969637573	0.281652803	0.281957061	
38DTB19 - Run 1	14/07/2020 (3) 16:08:07.00	38DTB19 - 24	151.7	3.6	67	0.034	2.120441	0.07837898	0.1795	0.00779	0.28144	2490.6	76.4	2647.5	72	5.93	2647.5	72	2.72%	0.281197	0.000035	0.005624049	0.0005476	0.0000011	0.018852	0.000099	0.28117	3.02	1.23	2.83	2.96300196	0.28108433	0.281307377	
38DTB19 - Run 1	14/07/2020 (3) 16:09:56.00	38DTB19 - 25	187.9	8.1	6.6	0.035	2.101723	0.06632929	0.1817	0.007634	0.57565	2508.9	65.6	2667.7	69.6	5.95	2667.7	69.6	2.61%	0.281146	0.000035	0.005623029	0.000895	0.000018	0.03182	0.00079	0.28110	1.04	1.23	2.93	3.10547311	0.281071029	0.281292176	
38DTB19 - Run 1	14/07/2020 (3) 19:01:05.00	38DTB19 - 89	184.3	4.4	4.6	0.035	2.229157	0.06992577	0.1685	0.00647	0.039304	2389	62.6	2542	64.4	6.02	2542	64.4	2.53%	0.281078	0.000037	0.005621682	0.000738	0.000017	0.02627	0.0008	0.28104	-3.97	1.30	3.01	3.325659433	0.281153718	0.281386678	
38DTB19 - Run 1	14/07/2020 (3) 18:21:29.00	38DTB19 - 75	741	16	10	0.047	3.272251	0.09435562	0.1122	0.004444	0.42841	1719	43.5	1834.5	71.8	6.30	1834.5	71.8	3.91%	0.281466	0.000031	0.005629405	0.0012701	0.0000025	0.05026	0.00036	0.28142	-6.88	1.09	2.52	2.951712548	0.281615537	0.281914471	
38DTB19 - Run 1	14/07/2020 (3) 17:41:57.00	38DTB19 - 63	140.7	2.7	1.8	0.058	2.148689	0.07529184	0.179	0.00768	0.13991	2463.4	71.7	2642.9	71.2	6.79	2642.9	71.2	2.69%	0.281073	0.000044	0.005621632	0.0005612	0.000004	0.01958	0.0003	0.28104	-1.52	1.54	3.00	3.249417088	0.281087358	0.281310838	
38DTB19 - Run 1	14/07/2020 (3) 17:12:15.00	38DTB19 - 47	125	1.9	1.4	0.05	2.143163	0.07271873	0.1802	0.008504	-0.083316	2468.6	69.6	2654	78.3	6.99	2654	78.3	2.95%	0.281042	0.000039	0.005620975	0.0006341	0.0000071	0.01985	0.00016	0.28101	-2.50	1.37	3.05	3.320453756	0.28108005	0.281302486	
38DTB19 - Run 1	14/07/2020 (3) 15:45:27.00	38DTB19 - 17	204	10	2.3	0.046	3.463803	0.12326676	0.1078	0.005256	0.18608	1635	51.4	1761.7	89.1	7.19	1761.7	89.1	5.06%	0.281797	0.000034	0.005636043	0.000424	0.000018	0.01182	0.00074	0.28178	4.26	1.19	2.01	2.185191975	0.281662712	0.281968386	
38DTB19 - Run 1	14/07/2020 (3) 15:47:14.00	38DTB19 - 18	355	18	3.3	0.046	3.421143	0.10353551	0.1092	0.005284	0.35484	1653	44.1	1785.3	88.2	7.41	1785.3	88.2	4.94%	0.282029	0.000055	0.005640848	0.00187	0.0001	0.0679	0.0043	0.28197	11.30	1.93	1.76	1.751438902	0.281647426	0.281950916	
38DTB19 - Run 1	14/07/2020 (3) 18:28:53.00	38DTB19 - 79	64	1.3	1.7	0.052	3.393281	0.13925464	0.11	0.0081	0.21062	1665	60.2	1799	134	7.45	1799	134	7.45%	0.28155	0.000051	0.005631231	0.0003854	0.0000023	0.014348	0.000062	0.28154	-3.61	1.79	2.35	2.716656782	0.28163855	0.281940771	
38DTB19 - Run 1	14/07/2020 (3) 15:26:51.00	38DTB19 - 7	47.5	1.3	0.93	0.048	3.236246	0.17993112	0.1148	0.010396	0.1366	1735.8	84.6	1876	163	7.47	1876	163	8.69%	0.281573	0.000052	0.0056317	0.000623	0.000019	0.02106	0.00086	0.28155	-1.34	1.82	2.33	2.6334107	0.281588616	0.281883704	
38DTB19 - Run 1	14/07/2020 (3) 17:23:24.00	38DTB19 - 53	237.6	3.1	3.8	0.063	3.409478	0.11468773	0.1097	0.005594	0.45033	1658	49.2	1793.6	92.8	7.56	1793.6	92.8	5.17%	0.281821	0.000042	0.005636576	0.001111	0.000014	0.03993	0.00086	0.28178	5.01	1.47	2.02	2.162535505	0.281642049	0.28194477	
38DTB19 - Run 1	14/07/2020 (3) 18:19:38.00	38DTB19 - 74	85.3	2.4	3.5	0.053	2.201673	0.09008343	0.1757	0.010614	0.17675	2413.9	82.4	2612	101	7.58	2612	101	3.87%	0.281119	0.000037	0.005622502	0.0004716	0.0000022	0.01719	0.00015	0.28110	-0.44	1.30	2.93	3.156012774	0.281107694	0.281334079	
38DTB19 - Run 1	14/07/2020 (3) 16:11:49.00	38DTB19 - 26	144.3	3	5.8	0.056	2.143163	0.07271873	0.1829	0.008758	0.45676	2468.6	69.6	2678.6	79.2	7.84	2678.6	79.2	2.96%	0.281173	0.000043	0.005623624	0.001059	0.000025	0.03751	0.0008	0.28112	1.95	1.51	2.90	3.05585292	0.281063849	0.281283971	
38DTB19 - Run 1	14/07/2020 (3) 15:32:24.00	38DTB19 - 10	163.3	2.7	3.2	0.072	3.281917	0.11841613	0.114	0.00598	0.067789	1714.6	54.3	1863.3	94.7	7.98	1863.3	94.7	5.08%	0.281474	0.000043	0.005629644	0.0005372	0.000007	0.0189	0.00011	0.28146	-5.04	1.51	2.46	2.857932122	0.281596857	0.281893122	
38DTB19 - Run 1	14/07/2020 (3) 15:50:57.00	38DTB19 - 20	158.5	2.5	1.8	0.062	3.473428	0.12375973	0.1085	0.00607	0.48699	1631	51.3	1774	102	8.06	1774	102	5.75%	0.281801	0.000037	0.005636141	0.0006514	0.0000024	0.02349	0.00028	0.28178	4.41	1.30	2.02	2.185318557	0.281654746	0.281959282	
38DTB19 - Run 1	14/07/2020 (3) 16:41:51.00	38DTB19 - 38	210.1	3.7	1.4	0.038	3.424658	0.10836931	0.11	0.0057	0.32009	1651.5	46.1	1798.6	94.3	8.18	1798.6	94.3	5.24%	0.28172	0.000035	0.005634509	0.000944	0.000014	0.02928	0.00064	0.28169	1.74	1.23	2.15	2.375830172	0.281638809	0.281941067	
38DTB19 - Run 1	14/07/2020 (3) 15:30:34.00	38DTB19 - 9	498	31	32	0.058	3.220612	0.1059016	0.1163	0.004826	0.22223	1743.2	50.2	1899.3	74.6	8.22	1899.3	74.6	3.93%	0.281504	0.000037	0.005630202	0.000902	0.000029	0.0317	0.0014	0.28147	-3.62	1.30	2.44	2.796729384	0.281573492	0.28186642	
38DTB19 - Run 1	14/07/2020 (3) 17:27:06.00	38DTB19 - 55	102.1	2	1.6	0.054	2.222222	0.09876543	0.1755	0.00871	0.36448	2395.3	88.9	2610	82.6	8.23	2610	82.6	3.16%	0.281208	0.000033	0.005624257	0.0007157	0.0000045	0.02383	0.00022	0.28117	2.25	1.16	2.83	2.982849434	0.28110901	0.281335583	
38DTB19 - Run 1	14/07/2020 (3) 15:49:08.00	38DTB19 - 19	151.2	3	2.1	0.045	3.412969	0.12766601	0.1104	0.006608	0.29221	1656.5	54.6	1805	109	8.23	1805	109	6.04%	0.281849	0.000042	0.005637136	0.0004024	0.0000043	0.01345	0.00011	0.28184	7.12	1.47	1.94	2.036172871	0.281634661	0.281936327	
38DTB19 - Run 1	14/07/2020 (3) 15:23:09.00	38DTB19 - 5	609.1	7.1	5.5	0.046	2.414293	0.07334974	0.1588	0.005376	-0.0039969	2234.1	57.4	2442.2	57.3	8.52	2442.2	57.3	2.35%	0.281206	0.000043	0.005624284	0.0008591	0.0000046	0.03075	0.00019	0.28117	-1.89	1.51	2.84	3.115269559	0.281219232	0.281461551	
38DTB19 - Run 1	14/07/2020 (3) 18:17:45.00	38DTB19 - 73	196.5	2.8	2	0.053	3.267974	0.11021402	0.1154	0.006008	0.15775	1721	50.9	1885.3	93.7	8.71	1885.3	93.7	4.97%	0.281457	0.000043	0.005629304	0.0007225	0.0000057	0.02499	0.00021	0.28143	-5.38	1.51	2.49	2.896896992	0.28158258	0.281876806	
38DTB19 - Run 1	14/07/2020 (3) 17:15:58.00	38DTB19 - 49	189.9	3.6	3.2	0.095	2.209456	0.08226636	0.1785	0.00777	0.2285	2406.8	74.8	2638.2	72.3	8.77	2638.2	72.3	2.74%	0.281147	0.000042	0.005623097	0.0006408	0.0000055	0.02264	0.00029	0.28111	0.86	1.47	2.91	3.093836241	0.281090452	0.281314374	
38DTB19 - Run 1	14/07/2020 (3) 16:13:38.00	38DTB19 - 27	113.2	1.5	1.2	0.049	2.183406	0.07322515	0.1815	0.00893	0.20012	2430.7	67.9	2665.9	81.5	8.82	2665.9	81.5	3.06%	0.281143	0.000037	0.005622982	0.000371	0.0000029	0.012459	0.0003	0.28112	1.85	1.30	2.89	3.052765576	0.281072214	0.281293531	
38DTB19 - Run 1	14/07/2020 (3) 18:01:03.00	38DTB19 - 64	281.8	7.1	5.9	0.051	2.191541	0.06880564	0.181	0.00662	0.28666	2423.2	63.4	2661.3	60.6	8.95	2661.3	60.6	2.28%	0.28116	0.00003	0.005622328	0.000369	0.000013	0.01181	0.00044	0.28114	2.35	1.05	2.87	3.017050927	0.281075244	0.281296993	
38DTB19 - Run 1	14/07/2020 (3) 19:02:56.00	38DTB19 - 90	643.1	7	4.2	0.045	3.472222	0.09717399	0.1101	0.004102	0.34281	1631.5	40.3	1800.2	67.8	9.37	1800.2	67.8	3.77%	0.281877	0.000045	0.00563772	0.0015829	0.0000074	0.05921	0.0077	0.28182	6.58	1.58	1.96	2.067465278	0.281637772	0.281939882	
38DTB19 - Run 1	14/07/2020 (3) 17:21:30.00	38DTB19 - 52	120.6	1.8	1.6	0.047	3.49895	0.13486506	0.1094	0.007388	0.25587	1620.5	55.2	1789	123	9.42	1789	123	6.88%	0.281758	0.000036	0.005635275	0.0002932	0.0000043	0.010241	0.0008	0.28175	3.66	1.26	2.06	2.245618888	0.281645029	0.281948176	
38DTB19 - Run 1	14/07/2020 (3) 18:57:24.00	38DTB19 - 87	241.1	6.5	4.4	0.049	3.344482	0.10268342	0.1139	0.005478	0.12108	1686.3	45.6	1861.7	86.8	9.42	1861.7	86.8	4.66%	0.281551	0.000045	0.0056312	0.000669	0.000012	0.02397	0.0056	0.28153	-2.50	1.58	2.36	2.69600103	0.281597895	0.281894309	
38DTB19 - Run 1	14/07/2020 (3) 17:10:22.00	38DTB19 - 46	157.4	2.7	1.5	0.043	2.185792	0.07572635	0.1838	0.007976	0.25082	2428.5	70.1	2686.7	71.7	9.61	2686.7	71.7	2.67%	0.281099	0.00004	0.005622122	0.0004113	0.0000056	0.01345	0.0032	0.28108	0.69	1.40	2.95	3.143051045	0.281058513	0.281277872	
38DTB19 - Run 1	14/07/2020 (3) 17:34:31.00	38DTB19 - 59	189.3	2.1	1.3	0.051	3.547357	0.12379886	0.1085	0.00577	0.39641	1600.9	49.5	1773.6	97.1	9.74	1773.6	97.1	5.47%	0.281567	0.000036	0.005631455	0.0005119	0.0000025	0.0184	0.00025	0.28155	-3.74	1.26	2.33	2.704482565	0.281655006	0.281959578	
38DTB19 - Run 1	14/07/2020 (3) 15:28:39.00	38DTB19 - 8	269	5.6	2.4	0.05	1.745201	0.06536127	0.2584	0.008868	-0.0035773	2920.1	87.9	3236.3	54.1	9.77	3236.3	54.1	1.67%	0.280519	0.000042	0.005610537	0.0004593	0.000006	0.01563	0.00032	0.28049	-7.27	1.47	3.73	4.0808621	0.280694553	0.280861918	
38DTB19 - Run 1	14/07/2020 (3) 19:04:49.00	38DTB19 - 91	92	1.6	0.93	0.062	2.202158	0.08865856	0.1849	0.010298	0.49782	2413.5	81	2696.6	92	10.50	2696.6	92	3.41%	0.281174	0.000037	0.005623602	0.0007171	0.0000026	0.024701	0.000087	0.28114	3.03	1.30	2.88	3.001415585	0.28105199	0.281270417	> 10% Discordant, excluded
38DTB19 - Run 1	14/07/2020 (3) 17:30:49.00	38DTB19 - 57	305	30	27	0.053	3.384095	0.13066844	0.1142	0.005884	0.10985	1669	56.8	1866.5	99	10.58	1866.5	99	4.98%	0.281445	0.000037	0.005628022	0.000893	0.000044	0.0297	0.0016	0.28141	-6.44	1.30	2.52	2.949376229	0.281594781	0.281890749	> 10% Discordant, excluded
38DTB19 - Run 1	14/07/2020 (3) 16:04:21.00	38DTB19 - 22	487	22	23	0.068	2.793627	0.11472987	0.1042	0.004084	0.38615	1508.2	40.7	1699.4	72.2	11.25	1699.4	72.2	4.25%	0.281966	0.00004	0.005639462	0.000562	0.000029	0.01847	0.00097	0.28195	8.69	1.40	1.79	1.851707836	0.281703033	0.282014466	> 10% Discordant, excluded
38DTB19 - Run 1	14/07/2020 (3) 18:12:13.00	38DTB19 - 70	144.3	3.3	1.1	0.051	2.459011	0.12661104	0.1129	0.006758	0.29492	1637	52.9	1846	108	11.32	1846	108	5.85%	0.28188	0.000044	0.005637772	0.0006654	0.0000041	0.022894	0.000063	0.28186	8.83	1.54	1.91	1.958745578	0.281608079	0.281905948	> 10% Discordant, excluded
38DTB19 - Run 1	14/07/2020 (3) 18:14:02.00	38DTB19 - 71	183.6	6.6	4.3	0.044	2.008032	0.08048257	0.2152	0.009004	0.5676	2605.2	85.9	2944.4	67.6	11.52	2944.4	67.6	2.30%	0.281005	0.000042	0.005620257	0.00089	0.000052	0.03	0.0016	0.28095	2.35	1.47	3.12	3.239443724	0.280888322	0.281083367	> 10% Discordant, excluded
38DTB19 - Run 1	14/07/2020 (3) 19:27:24.00	38DTB19 - 99	465.5	7.8	6.1	0.043	2.295684	0.06541329	0.1803	0.006306	0.17479	2330.9	55.7	2654.9	58	12.20	2654.9	58	2.18%	no value														discordant, no Hf data
38DTB19 - Run 1	14/07/2020 (3) 19:12:14.00	38DTB19 - 95	294.5	4.5	3.9	0.043	3.637686	0.11509856	0.1091	0.005682	0.39074	1565.6	44	1783.6	94.9	12.22	1783.6	94.9	5.32%	0.28179	0.000045	0.005635598	0.001064	0.000027	0.03244	0.00083	0.28175	3.75	1.58	2.06	2.235763223	0.281648528	0.281952175	> 10% Discordant, excluded
38DTB19 - Run 1	14/07/2020 (3) 17:36:21.00	38DTB19 - 60	181.7	4.4	5.1	0.07	3.427005	0.12608747	0.1162	0.006324	0.22798	1650.5	53.6	1897.8	97.8	13.03	1897.8	97.8	5.15%	0.281723	0.000038	0.005624788	0.000696	0.000015	0.02558	0.00042	0.28171	4.74	1.33	2.12	2.262288097	0.281574466	0.281867533	> 10% Discordant, excluded
38DTB19 - Run 1	14/07/2020 (3) 15:42:32.00	38DTB19 - 16	114.4	3.9	3.7	0.04	3.342246	0.1215809	0.1194	0.006888	0.26948	1687.3	54	1946	109	13.29	1946	109	5.29%	0.281466	0.000044	0.005629492	0.0009433	0.0000084	0.03381	0.00035	0.28143	-3.98	1.54	2.49	2.856215936	0.28154316	0.281831754	> 10% Discordant, excluded
38DTB19 - Run 1	14/07/2020 (3) 16:06:14.00	38DTB19 - 23	332	13	5.3	0.049	2.350729	0.07740717	0.1785	0.00617	0.041671	2284.9	63.4	2638.2	57.4	13.39	2638.2	57.4	2.18%	0.281162	0.000035	0.005623349	0.0006233	0.0000025	0.0206	0.00018	0.28113	1.43	1.23	2.88	3.057738237	0.281090452	0.281314274	> 10% Discordant, excluded
38DTB19 - Run 1	14/07/2020 (3) 17:40:04.00	38DTB19 - 62	564	25	22	0.058	3.49162	0.1710211	0.1149	0.004598	0.068323	1623.5	70.3	1877.5	72.1	13.53	1877.5	72.1	3.84%	0.281833	0.000034	0.005636763	0.00177	0.000037	0.0616	0.0017	0.28177	6.47	1.19	2.04	2.135047838	0.281587643	0.281882592	> 10% Discordant, excluded
38DTB19 - Run 1	14/07/2020 (3) 19:23:42.00	38DTB19 - 97	304.8	6.8	14	0.045	3.582945	0.13841388	0.1126	0.005052	0.027996	1586.8	54.3	1841	81.2	13.81	1841	81.2	4.41%	no value														discordant, no Hf data
38DTB19 - Run 1	14/07/2020 (3) 15:21:16.00	38DTB19 - 4	514.2	7.2	9	0.048	2.41838	0.07059213	0.1753	0.006206	0.14524	2230.9	55	2608.2	59	14.47	2608.2	59	2.26%	0.281253	0.000038	0.005625188	0.001295	0.000019	0.04181	0.00089	0.28119	2.78	1.33	2.81	2.947368968	0.281110194	0.281336936	> 10% Discordant, excluded
38DTB19 - Run 1	14/07/2020 (3) 19:10:21.00	38DTB19 - 94	637	19	8.1	0.054	2.267574	0.10191228	0.194	0.00628	0.21187	2355.1	88.7	2775.6	53.9	15.15	2775.6	53.9	1.94%	0.281031	0.000046	0.005620808	0.0003968	0.0000093	0.01465	0.00031	0.28101	0.36	1.61	3.04	3.234117681	0.280999894	0.281210878	> 10% Discordant, excluded
38DTB19 - Run 1	14/07/2020 (3) 15:24:56.00	38DTB19 - 6	339	20	3.6	0.046	2.392917	0.09996541	0.1806	0.006412	-0.051237	2250.9	79.4	2657.6	58.9	15.30	2657.6	58.9	2.22%	0.281146	0.000037	0.005622042	0.00074	0.000039	0.0249	0.0012	0.28111	1.09	1.30	2.91	3.094346423	0.28107768	0.281299777	> 10% Discordant, excluded
38DTB19 - Run 1	14/07/2020 (3) 15:19:26.00	38DTB19 - 3	147	13	5.5	0.053	3.690037	0.23719724	0.112	0.00684	0.11231	1545.9	88.4	1831	111	15.57	1831	111	6.06%	0.281455	0.000036	0.005629215	0.000762	0.000027	0.02706	0.00077	0.28143	-6.72	1.26	2.50	2.938915493	0.281617807	0.281917065	> 10% Discordant, excluded
38DTB19 - Run 1	14/07/2020 (3) 15:41:43.00	38DTB19 - 15	224.8	8	2.4	0.058	2.456399	0.07990085	0.1771	0.007342	0.24454	2201.6	60.7	2625.2	68.9	16.14	2625.2	68.9	2.62%	0.281189	0.000037	0.005623902	0.0002287	0.0000087	0.00735	0.0004	0.28118	2.79	1.30	2.82	2.960139022	0.281099008	0.281324152	> 10% Discordant, excluded
38DTB19 - Run 1	14/07/2020 (3) 16:15:32.00	38DTB19 - 28	296	18	3.9	0.061	3.825555	0.1321236	0.1092	0.005584	0.2436	1497	46.1	1785.3	92.2	16.15	1785.3	92.2	5.22%	0.281795	0.00004	0.005636042	0.000701	0.00004	0.0218	0.0011	0.28177	4.40	1.40	2.03	2.19538034	0.281647426	0.281950916	> 10% Discordant, excluded
38DTB19 - Run 1	14/07/2020 (3) 17:14:04.00	38DTB19 - 48	409	22	0.61	0.056	3.667033	0.13250805	0.1139	0.004578	-0.012924	1554.5	49.9	1861.7	72.6	16.50	1861.7	72.6	3.90%	0.281456	0.000043	0.005629284	0.000314	0.0000014	0.005364	0.000079	0.28145	-5.21	1.51	2.46	2.873763553	0.281597895	0.281894209	> 10% Discordant, excluded
38DTB19 - Run 1	14/07/2020 (3) 15:17:31.00	38DTB19 - 2	680	14	11	0.028	2.646209	0.09353791	0.1659	0.005618	0.14052	2066.5	62.5	2515.9	56.9	17.86	2515.9	56.9	2.26%	0.281132	0.000036	0.005622755	0.000799	0.000016	0.02754	0.00081	0.28109	-2.74	1.26	2.94	3.226932683	0.281170864	0.281406273	> 10% Discordant, excluded
38DTB19 - Run 1	14/07/2020 (3) 16:53:18.00	38DTB19 - 42	87.7	3.1	2.1	0.05	2.506894	0.09915712	0.1783	0.011766	0.43227	2164	72.7	2636	110	17.91	2636	110	4.17%	0.281115	0.00005	0.005622522	0.000935	0.00004	0.0317	0.001	0.28107	-0.85	1.75	2.97	3.20160812	0.2810919	0.281316029	> 10% Discordant, excluded
38DTB19 - Run 1	14/07/2020 (3) 16:28:44.00	38DTB19 - 31	122.2	4.9	6.2	0.054	3.921569	0.24759708	0.1108	0.006816	0.19945	1464.2	82.7	1812	112	19.19	1812	112	6.18%	0.281529	0.000061	0.005636091	0.000614	0.000035	0.0229	0.002	0.28151	-4.34	2.14	2.39	2.773169487	0.281630124	0.281931142	> 10% Discordant, excluded
38DTB19 - Run 1	14/07/2020 (3) 19:25:31.00	38DTB19 - 98	154.1	8.3	1.2	0.061	2.565418	0.10330119	0.1795	0.00789	0.23529	2121.9	72.8	2647.5	72.9	19.85	2647.5	72.9	2.75%	no value														discordant, no Hf data
38DTB19 - Run 1	14/07/2020 (3) 16:42:40.00	38DTB19 - 30	298	11	4.9	0.056	2.724796	0.15101457	0.1666	0.007332	0.18769	2015.3	95.9	2523	73.9	20.12	2523	73.9	2.93%	0.281171	0.000042	0.005623577	0.00067	0.000016	0.02082	0.00052	0.28114	-0.98	1.47	2.88	3.120522254	0.2811662	0.281400943	> 10% Discordant, excluded
38DTB19 - Run 1	14/07/2020 (3) 17:08:34.00	38DTB19 - 45	128.4	14	9.8	0.04	4.022526	0.14031917	0.1122	0.003844	-0.068036	1421.3	44.8	1834.5	62.1	21.98	1834.5	62.1	3.39%	0.281503	0.000039	0.005620195	0.001436	0.000037	0.0525	0.0011	0.28145	-5.77	1.37	2.48	2.881590667	0.281615537	0.281914471	> 10% Discordant, excluded
38DTB19 - Run 1	14/07/2020 (3) 17:19:41.00	38DTB19 - 51	298.8	4.1	3.6	0.064	2.745744	0.11296603	0.173	0.00706	0.019253	2002.1	70.8	2586.1	68.1	22.58	2586.1	68.1	2.63%	0.28118	0.000043	0.005623764	0.00111	0.00004	0.0387	0.001	0.28113	0.02	1.51	2.90	3.106916275	0.28112473	0.281353549	> 10% Discordant, excluded
38DTB19 - Run 1	14/07/2020 (3) 18:59:12.00	38DTB19 - 88	601	11	4.9	0.039	4.070004	0.13109488	0.1119	0.004338	0.059191	1416.3	41	1829.7	70.3	22.59	1829.7	70.3	3.84%	0.281751	0.000031	0.005635105	0.000884	0.000038	0.0315	0.0015	0.28172	3.61	1.09	2.10	2.288441131	0.281644865	0.281918828	> 10% Discordant, excluded
38DTB19 - Run 1	14/07/2020 (3) 18:53:38.00	38DTB19 - 85	275.1	4.5	3.3	0.049	2.758621	0.10539834	0.1754	0.006608	0.18237	1994	65.5	2609.1	62.7	23.58	2609.1	62.7	2.40%	0.280799	0.000027	0.005616045	0.000537	0.0000071	0.01773	0.00022	0.28077	-12.00	0.95	3.36	3.886214023	0.281109602	0.281336259	> 10% Discordant, excluded
38DTB19 - Run 1	14/07/2020 (3) 15:36:07.00	38DTB19 - 12	267.5	4.3	5.2	0.059	3.114295	0.1253283	0.1569	0.007438	-0.42849	1795.1	63.1	2421.8	80.4	25.88	2421.8	80.4	3.32%	0.281362	0.000046	0.005625428	0.001577	0.00003	0.055	0.0015	0.28119	-1.55	1.61	2.82	3.077021941	0.281232609	0.281476839	> 10% Discordant, excluded
38DTB19 - Run 1	14/07/2020 (3) 19:29:13.00	38DTB19 - 100	159.8	7.8	7.3	2.1	2.849003	0.33295186	0.181	0.04262	0.15336	1939	196	2661	390	27.13	2661	390	14.66%															discordant, no Hf data, propogated uncertainty >10%
38DTB19 - Run 1	14/07/2020 (3) 17:04:48.00	38DTB19 - 43	480	41	170	0.046	4.784689	0.41619928	0.1052	0.005004	0.058147	1223.5	96.9	1717	87.4	28.74	1717	87.4	5.09%	0.281669	0.000053	0.005633629	0.001069	0.000076	0.0386	0.0031	0.28163	-2.04	1.86	2.22	2.551965202	0.281691647	0.282001454	> 10% Discordant, excluded
38DTB19 - Run 1	14/07/2020 (3) 16:34:26.00	38DTB19 - 34	330	12	6.8	0.07	3.030303	0.16161616	0.1758	0.007016	-0.13033	1838.4	85.3	2612.9	66.4	29.64	2612.9	66.4	2.54%	0.281303	0.000058	0.005626239	0.00119	0.000034	0.0384	0.0013	0.28125	4.95	2.03	2.73	2.812352829	0.281107102	0.281333402	> 10% Discordant, excluded
38DTB19 - Run 1	14/07/2020 (3) 16:51:14.00	38DTB19 - 41	226.8	5.3	3.3	0.065	3.142678	0.11421096	0.1768	0.007636	0.14691	1780.9	56.6	2622.3	71.8	32.09	2622.3	71.8	2.74%	0.281187	0.000037	0.005623862	0.00032093	0.0000075	0.009794	0.000067	0.28117	2.49	1.30	2.83	2.97725215	0.281100917	0.281326333	> 10% Discordant, excluded
38DTB19 - Run 1	14/07/2020 (3) 19:08:31.00	38DTB19 - 93	360.7	7.2	5.9	0.049	4.950495	0.2460543	0.1071	0.004942	0.12713	1186.1	53.8	1749.8	84.5	32.22	1749.8	84.5	4.83%	0.281882	0.000046	0.005637828	0.001554	0.000034	0.0538	0.0011	0.28183	5.68	1.61	1.95	2.084996103	0.281670418	0.281977192	> 10% Discordant, excluded
38DTB19 - Run 1	14/07/2020 (3) 17:17:48.00	38DTB19 - 50	323	20	5.6	0.051	3.378378	0.29583636	0.165	0.0078	0.18063	1671	129	2506.8	79.5	33.34	2506.8	79.5	3.17%	0.281106	0.000043	0.005622284	0.000831	0.000034	0.0283	0.001	0.28107	-3.93	1.51	2.98	3.295805105	0.28117684	0.281413102	> 10% Discordant, excluded
38DTB19 - Run 1	14/07/2020 (3) 18:08:31.00	38DTB19 - 68	149.8	6.5	6.4	0.047	3.205128	0.31065086	0.1842	0.010584	-0.090621	1751	149	2690.3	95	34.91	2690.3	95	3.53%	0.281064	0.000042	0.005621437	0.0004551	0.0000027	0.01484	0.00029	0.28104	0.55	1.47	3.00	3.225141244	0.281056141	0.281275161	> 10% Discordant, excluded
38DTB19 - Run 1	14/07/2020 (3) 16:38:08.00	38DTB19 - 36	289.7	8.9	3.7	0.048	3.410641	0.14033416	0.1702	0.007904	-0.14678	1657.5	60.1	2558.9	77.7	35.23	2558.9	77.7	3.04%	0.280655	0.000044	0.005613272	0.001309	0.000024	0.0472	0.0011	0.28059	-19.61	1.54	3.63	4.222003324	0.281142612	0.281373986	> 10% Discordant, excluded
38DTB19 - Run 1	14/07/2020 (3) 18:10:19.00	38DTB19 - 69	353	16	5.4	0.056	4.950495	0.4666209	0.1128	0.005356	0.017971	1186	102	1844.2	85.9	35.69	1844.2	85.9	4.66%	0.281574	0.000038	0.005631608	0.0006082	0.0000086	0.02078	0.00024	0.28155	-2.01	1.33	2.33	2.650563681	0.281609247	0.281907282	> 10% Discordant, excluded
38DTB19 - Run 1	14/07/2020 (3) 16:32:22.00	38DTB19 - 33	1072	36	210	0.078	5.211047	0.28344404	0.1077	0.004154	0.019233	1131.7	56.5	1760	70.5	35.70	1760	70.5	4.01%	0.281676	0.000044	0.005633692	0.0018948	0.0000072	0.06793	0.00061	0.28161	-1.81	1.54	2.26	2.571568944	0.281662813	0.281968644	> 10% Discordant, excluded
38DTB19 - Run 1	14/07/2020 (3) 18:22:22.00	38DTB19 - 76	696	83	370	0.067	3.311258	0.29647826	0.1891	0.006782	-0.23904	1701	134	2733.6	59	37.77	2733.6	59	2.16%	0.280832	0.000049	0.005616854	0.001536	0.000062	0.0537	0.0025	0.28075	-9.82	1.72	3.41	3.84678067	0.2810276	0.281242543	> 10% Discordant, excluded
38DTB19 - Run 1	14/07/2020 (3) 16:36:15.00	38DTB19 - 35	621.9	9.3	8.6	0.047	5.9988	0.3682767	0.1108	0.005616	-0.13271	993.9	56.5	1811.8	92.1	45.14	1811.8	92.1	5.08%	0.281742	0.00003	0.00563492	0.000874	0.000022	0.02912	0.00081	0.28171	2.90	1.05	2.11	2.312031389	0.281630254	0.281931129	> 10% Discordant, excluded

Appendix D3.1 continued.

Curtin University Geohistory center

Sample ID	Analysis date-time	Spot ID	238U conc. (ppm)	±2σ INT	232Th conc. (ppm)	±2σ INT	238U/206Pb	±2σ PROP	207Pb/206Pb	±2σ PROP	rho	238U/206Pb (Ma)	±2σ PROP	207Pb/206Pb (Ma)	±2σ PROP	Discord (7/6-6/8)/7/6*100	Perferred age *1500 Ma cutoff (Ma)
38DTB19 - Run 2	16/07/2020 (5) 17:57:55.00	X38DT_38	74	3.7	57.5	3.6	1.869159	0.13520832	0.1808	0.010116	0.26996	2762	163	2659.5	92.7	-3.85	2659.5
38DTB19 - Run 2	16/07/2020 (5) 19:50:37.00	X38DT_82	51.23	0.96	85.3	1.5	2.966479	0.21772948	0.1114	0.009328	0.26699	1873	119	1822	152	-2.80	1822
38DTB19 - Run 2	16/07/2020 (5) 16:44:42.00	X38DT_8	1.02E+02	1.40E+00	48.2	1	3.14169	0.2207573	0.1079	0.006858	0.1252	1781	109	1763	116	-1.02	1763
38DTB19 - Run 2	16/07/2020 (5) 20:26:28.00	X38DT_94	46.1	2.5	35	2.5	3.036745	0.2267276	0.1115	0.00973	0.28927	1835	119	1823	158	-0.66	1823
38DTB19 - Run 2	16/07/2020 (5) 17:48:37.00	X38DT_33	76.7	2.6	64.3	2.1	3.182686	0.22572562	0.1075	0.00755	0.2115	1761	109	1757	128	-0.23	1757
38DTB19 - Run 2	16/07/2020 (5) 21:15:28.00	X38DT_111	60.5	3	83.9	5.4	3.232062	0.24222704	0.1065	0.00753	0.24085	1738	114	1740	130	0.11	1740
38DTB19 - Run 2	16/07/2020 (5) 17:20:27.00	X38DT_22	144.8	1.9	77.1	1.5	1.941371	0.13681934	0.1834	0.008168	0.27867	2678	154	2683.1	73.7	0.19	2683.1
38DTB19 - Run 2	16/07/2020 (5) 20:28:22.00	X38DT_95	105.8	4	83.9	5.6	3.209243	0.22897066	0.1073	0.007346	0.49688	1749	109	1753	125	0.23	1753
38DTB19 - Run 2	16/07/2020 (5) 19:22:44.00	X38DT_67	237	19	95.7	7.5	3.191829	0.21665318	0.1081	0.005262	-0.083679	1757	104	1766.8	88.9	0.55	1766.8
38DTB19 - Run 2	16/07/2020 (5) 17:46:47.00	X38DT_32	392	14	395	43	3.033981	0.21710122	0.1132	0.004764	0.19748	1836	114	1850.6	76.1	0.79	1850.6
38DTB19 - Run 2	16/07/2020 (5) 19:37:37.00	X38DT_75	55.53	0.86	19.9	0.59	3.286231	0.23851362	0.1059	0.008518	0.26765	1713	109	1729	148	0.93	1729
38DTB19 - Run 2	16/07/2020 (5) 18:50:38.00	X38DT_59	143.5	1.9	75.2	1.4	3.305785	0.2300389	0.1055	0.00661	0.20062	1711	104	1722	115	1.05	1722
38DTB19 - Run 2	16/07/2020 (5) 16:46:36.00	X38DT_9	122.2	7.5	305	25	3.083565	0.2138052	0.112	0.00604	0.24649	1811	109	1831.3	97.7	1.11	1831.3
38DTB19 - Run 2	16/07/2020 (5) 21:35:56.00	X38DT_122	166	16	204	10	1.99005	0.13880845	0.1811	0.00822	0.27239	2625	150	2662.2	73.4	1.40	2662.2
38DTB19 - Run 2	16/07/2020 (5) 19:28:20.00	X38DT_70	277.7	3.4	284	3.4	3.249919	0.22342798	0.1074	0.005048	0.24187	1729	104	1754.9	86	1.48	1754.9
38DTB19 - Run 2	16/07/2020 (5) 18:24:38.00	X38DT_45	326.2	7.9	110	3.4	3.25839	0.2350415	0.1079	0.005058	-0.040708	1725	109	1763.4	85.7	2.18	1763.4
38DTB19 - Run 2	16/07/2020 (5) 20:20:56.00	X38DT_91	105.3	2.9	72.6	1.4	3.055301	0.22913352	0.1142	0.006784	0.23628	1825	119	1866	107	2.20	1866
38DTB19 - Run 2	16/07/2020 (5) 21:11:44.00	X38DT_109	76.8	3.6	194	10	1.574803	0.11085622	0.2592	0.011584	0.28439	3169	176	3241.1	70.4	2.22	3241.1
38DTB19 - Run 2	16/07/2020 (5) 19:24:38.00	X38DT_68	21.42	0.69	24.1	2.1	2.070393	0.16143066	0.175	0.0145	0.064751	2540	164	2605	138	2.50	2605
38DTB19 - Run 2	16/07/2020 (5) 18:46:55.00	X38DT_57	133.6	3.5	68.7	2.5	3.03306	0.2078525	0.1155	0.00651	0.14413	1837	110	1887	101	2.65	1887
38DTB19 - Run 2	16/07/2020 (5) 16:52:08.00	X38DT_12	155.8	5.2	209.4	8.6	2.030869	0.13960369	0.1814	0.007428	0.28889	2581	146	2665	67.8	3.15	2665
38DTB19 - Run 2	16/07/2020 (5) 18:58:04.00	X38DT_63	264	3.7	179.3	3	3.126954	0.21898458	0.113	0.00536	0.050633	1789	109	1847.4	85.8	3.16	1847.4
38DTB19 - Run 2	16/07/2020 (5) 17:33:27.00	X38DT_29	131.3	5.2	88.1	2.1	3.08642	0.3951379	0.1145	0.00909	-0.29978	1809	202	1871	143	3.31	1871
38DTB19 - Run 2	16/07/2020 (5) 19:54:20.00	X38DT_84	194.1	2.8	132.9	2.4	3.134796	0.21992712	0.1134	0.006768	0.20944	1785	109	1854	108	3.72	1854
38DTB19 - Run 2	16/07/2020 (5) 18:48:44.00	X38DT_58	388.1	6.4	183.8	3	3.328895	0.232801	0.1077	0.004854	0.35668	1693	104	1760	82.4	3.81	1760
38DTB19 - Run 2	16/07/2020 (5) 17:22:17.00	X38DT_23	2.27E+02	3.00E+00	226.4	3.4	3.092146	0.21482482	0.1149	0.005498	0.37277	1806	109	1877.5	86.2	3.81	1877.5
38DTB19 - Run 2	16/07/2020 (5) 16:31:42.00	X38DT_1	212.4	4.4	191.4	5.6	2.027575	0.13921695	0.1846	0.007392	0.20912	2585	146	2693.9	66.2	4.04	2693.9
38DTB19 - Run 2	16/07/2020 (5) 20:22:45.00	X38DT_92	112.6	3.5	139.2	7	3.07787	0.21313	0.1158	0.006716	0.52878	1814	109	1892	104	4.12	1892
38DTB19 - Run 2	16/07/2020 (5) 22:15:34.00	X38DT_132	75	1.3	113.7	1.9	1.633987	0.11811696	0.2555	0.01191	0.21533	3078	177	3218.5	73.6	4.37	3218.5
38DTB19 - Run 2	16/07/2020 (5) 16:59:36.00	X38DT_16	1.01E+02	2.20E+00	69.7	2.6	2.03666	0.1444328	0.1847	0.009294	0.3751	2575	151	2694.8	83.1	4.45	2694.8
38DTB19 - Run 2	16/07/2020 (5) 17:59:45.00	X38DT_39	112.8	2	39.08	0.68	3.361345	0.2367065	0.1078	0.007556	0.28486	1679	104	1762	128	4.71	1762
38DTB19 - Run 2	16/07/2020 (5) 21:08:02.00	X38DT_107	278	12	186	15	3.275467	0.22643954	0.1104	0.004908	0.22	1718	104	1805.2	80.8	4.83	1805.2
38DTB19 - Run 2	16/07/2020 (5) 20:19:03.00	X38DT_90	169.8	3.5	129.5	3.7	3.286231	0.22771432	0.1102	0.006004	0.30513	1713	104	1801.9	99.1	4.93	1801.9
38DTB19 - Run 2	16/07/2020 (5) 16:42:53.00	X38DT_7	127.7	1.7	69	1.2	3.189793	0.22659226	0.1132	0.007264	0.31161	1758	109	1851	116	5.02	1851
38DTB19 - Run 2	16/07/2020 (5) 18:45:01.00	X38DT_56	119.3	6.8	122.3	9.2	2.077706	0.14515882	0.1818	0.008736	0.3096	2533	146	2668.6	79.6	5.08	2668.6
38DTB19 - Run 2	16/07/2020 (5) 17:54:12.00	X38DT_36	257.5	4.3	270	7.1	3.284072	0.22745844	0.1107	0.005514	0.26561	1714	104	1810.1	90.5	5.31	1810.1
38DTB19 - Run 2	16/07/2020 (5) 19:17:09.00	X38DT_64	235.6	3	238	3.7	3.271181	0.22593302	0.1111	0.004922	-0.019824	1720	104	1816.7	80.4	5.32	1816.7
38DTB19 - Run 2	16/07/2020 (5) 19:26:27.00	X38DT_69	117.7	1.6	171.3	3.2	3.186743	0.22622016	0.1137	0.006274	0.6517	1759	109	1858.6	99.7	5.36	1858.6
38DTB19 - Run 2	16/07/2020 (5) 22:10:02.00	X38DT_129	296.5	5.1	243.7	6.6	3.211304	0.21891318	0.1131	0.004862	0.09143	1748	104	1849	77.7	5.46	1849
38DTB19 - Run 2	16/07/2020 (5) 18:52:26.00	X38DT_60	75.9	1.2	91.4	1.8	3.020236	0.21547572	0.1197	0.009194	0.22259	1844	114	1951	137	5.48	1951
38DTB19 - Run 2	16/07/2020 (5) 19:30:10.00	X38DT_71	127	3	86.6	2.2	2.099076	0.14772842	0.1812	0.008224	0.14339	2512	146	2663.1	75.2	5.67	2663.1
38DTB19 - Run 2	16/07/2020 (5) 16:39:10.00	X38DT_5	355.4	4.3	296.7	4.9	2.01005	0.13716825	0.1938	0.007176	0.1354	2603	146	2773.9	60.7	6.16	2773.9
38DTB19 - Run 2	16/07/2020 (5) 21:41:26.00	X38DT_125	245.3	3.5	113.5	2.1	3.388682	0.24002114	0.1088	0.005576	0.096371	1667	104	1778.6	93.5	6.27	1778.6
38DTB19 - Run 2	16/07/2020 (5) 17:31:38.00	X38DT_28	110.7	2.4	38.6	1.1	2.085071	0.14604192	0.1848	0.008496	0.48493	2526	146	2695.7	75.9	6.30	2695.7
38DTB19 - Run 2	16/07/2020 (5) 18:22:44.00	X38DT_44	123	1.9	68.1	1.8	2.306805	0.1632058	0.1622	0.008444	0.1233	2321	138	2478	87.8	6.34	2478
38DTB19 - Run 2	16/07/2020 (5) 19:43:12.00	X38DT_78	655.6	7.6	323.6	4.2	3.332223	0.23320006	0.1105	0.00411	0.14338	1692	104	1806.8	67.6	6.35	1806.8
38DTB19 - Run 2	16/07/2020 (5) 22:11:51.00	X38DT_130	161	2.5	105.1	2.2	2.101282	0.14799484	0.183	0.00816	0.30378	2509	146	2679.5	73.8	6.36	2679.5
38DTB19 - Run 2	16/07/2020 (5) 21:21:04.00	X38DT_114	128.9	2.1	101.9	2.1	2.115954	0.14977338	0.1814	0.008328	0.226	2495	146	2665	76.1	6.38	2665
38DTB19 - Run 2	16/07/2020 (5) 16:37:16.00	X38DT_4	77.5	2	56.7	2	2.077706	0.14947572	0.186	0.00922	0.2705	2533	151	2706.4	81.8	6.41	2706.4
38DTB19 - Run 2	16/07/2020 (5) 19:20:55.00	X38DT_66	52.19	0.83	32.92	0.73	3.25839	0.2350415	0.113	0.00976	0.27929	1725	109	1847	156	6.61	1847
38DTB19 - Run 2	16/07/2020 (5) 20:54:40.00	X38DT_105	179.9	5	76.3	2.6	3.194888	0.22721476	0.1153	0.006606	0.15883	1755	109	1884	103	6.85	1884
38DTB19 - Run 2	16/07/2020 (5) 21:09:55.00	X38DT_108	272.1	3.6	187	4.5	2.127207	0.14661934	0.1819	0.006938	0.1266	2484	142	2669.5	63.2	6.95	2669.5
38DTB19 - Run 2	16/07/2020 (5) 17:52:19.00	X38DT_35	172.1	2.9	164.5	2.2	2.163566	0.15093472	0.1782	0.007964	0.41409	2449	142	2635.4	74.2	7.07	2635.4
38DTB19 - Run 2	16/07/2020 (5) 19:19:01.00	X38DT_65	256.4	3.1	156.4	2.5	2.154708	0.14987776	0.1802	0.007304	0.21809	2458	142	2654	67.2	7.39	2654
38DTB19 - Run 2	16/07/2020 (5) 22:06:16.00	X38DT_127	229.9	3.8	174.9	3.5	2.162162	0.15076694	0.1795	0.00649	0.24968	2451	142	2647.5	60	7.42	2647.5
38DTB19 - Run 2	16/07/2020 (5) 18:09:22.00	X38DT_42	193.9	6.7	121.7	3.4	2.394063	0.16824356	0.1579	0.007458	0.097367	2250	133	2432.5	80	7.50	2432.5
38DTB19 - Run 2	16/07/2020 (5) 18:01:39.00	X38DT_40	228	13	164.4	9.4	2.267574	0.16875688	0.169	0.00708	0.31362	2355	147	2547	70.2	7.54	2547
38DTB19 - Run 2	16/07/2020 (5) 22:08:09.00	X38DT_128	114.1	1.7	99.6	1.8	2.129019	0.14683298	0.184	0.00768	0.35735	2482	142	2688.5	69	7.68	2688.5
38DTB19 - Run 2	16/07/2020 (5) 20:50:57.00	X38DT_103	181.9	2.5	142.3	2.3	2.160294	0.15054388	0.1805	0.00831	0.16485	2452	142	2656.7	76.3	7.71	2656.7
38DTB19 - Run 2	16/07/2020 (5) 20:49:03.00	X38DT_102	150.1	2.4	96.9	1.9	3.213368	0.22947906	0.1163	0.006926	0.38032	1747	109	1899	107	8.00	1899
38DTB19 - Run 2	16/07/2020 (5) 20:41:37.00	X38DT_98	615.6	7.2	469	5	3.405995	0.2421319	0.1103	0.004406	0.024116	1659	104	1803.5	72.6	8.01	1803.5
38DTB19 - Run 2	16/07/2020 (5) 16:48:26.00	X38DT_10	134.2	2.4	86.7	2.4	2.277386	0.15965042	0.1701	0.007702	0.40951	2347	138	2557.9	75.8	8.25	2557.9
38DTB19 - Run 2	16/07/2020 (5) 19:35:47.00	X38DT_74	51	0.85	48.8	0.97	3.144654	0.23100348	0.1192	0.009084	0.17984	1780	114	1943	136	8.39	1943
38DTB19 - Run 2	16/07/2020 (5) 18:56:11.00	X38DT_62	124.8	6.7	69.3	1.8	2.242152	0.17052424	0.1745	0.00819	-0.056589	2377	151	2600.5	78.2	8.59	2600.5
38DTB19 - Run 2	16/07/2020 (5) 21:34:02.00	X38DT_121	114.3	2.6	83.6	2.3	2.15378	0.154406	0.1842	0.009984	0.2851	2459	147	2690.3	89.6	8.60	2690.3
38DTB19 - Run 2	16/07/2020 (5) 16:33:34.00	X38DT_2	139.4	2.1	189.9	3.3	2.17061	0.1517778	0.1824	0.008348	0.10696	2443	142	2674.1	75.8	8.64	2674.1
38DTB19 - Run 2	16/07/2020 (5) 16:50:19.00	X38DT_11	88.5	2	58.5	1.6	2.148228	0.15372176	0.185	0.0102	0.32291	2464	147	2697.5	91.1	8.66	2697.5
38DTB19 - Run 2	16/07/2020 (5) 22:13:45.00	X38DT_131	613	25	254	14	2.180074	0.14816138	0.1817	0.005934	0.19821	2434	138	2667.7	54.1	8.76	2667.7
38DTB19 - Run 2	16/07/2020 (5) 18:28:19.00	X38DT_47	359	20	160.3	8	3.49406	0.253008	0.109	0.00498	0.019456	1623	104	1781.9	83.3	8.92	1781.9
38DTB19 - Run 2	16/07/2020 (5) 21:06:10.00	X38DT_106	253.4	4.9	206.7	5.2	1.742464	0.11986233	0.2554	0.009408	0.29331	2924	162	3217.8	58.2	9.13	3217.8
38DTB19 - Run 2	16/07/2020 (5) 16:55:53.00	X38DT_14	171.8	4.8	94.4	2.4	2.214349	0.15706388	0.1806	0.007912	0.25433	2402	142	2657.6	72.6	9.62	2657.6
38DTB19 - Run 2	16/07/2020 (5) 18:33:53.00	X38DT_50	377.4	5.5	133.2	1.9	3.518649	0.24370548	0.1093	0.004986	0.20652	1612.5	98.8	1787	83.1	9.76	1787
38DTB19 - Run 2	16/07/2020 (5) 18:26:27.00	X38DT_46	79.7	1.4	66.2	1.4	3.242542	0.24359024	0.1178	0.008356	0.14011	1733	114	1922	127	9.83	1922
38DTB19 - Run 2	16/07/2020 (5) 18:07:20.00	X38DT_41	266.9	2.9	121.3	1.9	3.304693	0.22990876	0.1158	0.005816	0.26596	1704	104	1891.6	90.4	9.92	1891.6
~~38DTB19 - Run 2~~	~~16/07/2020 (5) 17:07:02.00~~	~~X38DT_20~~	~~149.5~~	~~2.5~~	~~154.5~~	~~6.6~~	~~3.449465~~	~~0.2474715~~	~~0.112~~	~~0.00614~~	~~0.31791~~	~~1641~~	~~104~~	~~1831.3~~	~~99.4~~	~~10.39~~	~~1831.3~~
~~38DTB19 - Run 2~~	~~16/07/2020 (5) 17:35:20.00~~	~~X38DT_30~~	~~139.9~~	~~6.1~~	~~83.2~~	~~2.9~~	~~3.278689~~	~~0.23757058~~	~~0.1173~~	~~0.007446~~	~~0.29473~~	~~1716~~	~~109~~	~~1915~~	~~114~~	~~10.39~~	~~1915~~
~~38DTB19 - Run 2~~	~~16/07/2020 (5) 21:17:21.00~~	~~X38DT_112~~	~~406~~	~~18~~	~~200~~	~~11~~	~~2.376991~~	~~0.16619162~~	~~0.1676~~	~~0.006652~~	~~0.099954~~	~~2264~~	~~133~~	~~2533.1~~	~~66.6~~	~~10.62~~	~~2533.1~~
~~38DTB19 - Run 2~~	~~16/07/2020 (5) 21:26:36.00~~	~~X38DT_117~~	~~219.4~~	~~3.5~~	~~181.4~~	~~5.4~~	~~3.377237~~	~~0.23863074~~	~~0.1146~~	~~0.005992~~	~~0.11977~~	~~1672~~	~~104~~	~~1872.8~~	~~94.3~~	~~10.72~~	~~1872.8~~
~~38DTB19 - Run 2~~	~~16/07/2020 (5) 20:37:46.00~~	~~X38DT_96~~	~~951~~	~~10~~	~~297.6~~	~~3.9~~	~~3.692762~~	~~0.25112964~~	~~0.106~~	~~0.00362~~	~~0.45305~~	~~1544.9~~	~~93.4~~	~~1730.9~~	~~62.7~~	~~10.75~~	~~1730.9~~
~~38DTB19 - Run 2~~	~~16/07/2020 (5) 17:50:32.00~~	~~X38DT_34~~	~~142~~	~~5.2~~	~~112.7~~	~~7.1~~	~~3.363606~~	~~0.23697982~~	~~0.1151~~	~~0.007802~~	~~0.54977~~	~~1678~~	~~104~~	~~1881~~	~~122~~	~~10.79~~	~~1881~~
~~38DTB19 - Run 2~~	~~16/07/2020 (5) 18:30:10.00~~	~~X38DT_48~~	~~92.1~~	~~1.8~~	~~61.5~~	~~1.3~~	~~2.194426~~	~~0.15464512~~	~~0.1877~~	~~0.009754~~	~~0.4088~~	~~2421~~	~~142~~	~~2721.4~~	~~85.6~~	~~11.04~~	~~2721.4~~
~~38DTB19 - Run 2~~	~~16/07/2020 (5) 18:41:18.00~~	~~X38DT_54~~	~~1073~~	~~11~~	~~397.6~~	~~4.6~~	~~3.586801~~	~~0.25184792~~	~~0.1093~~	~~0.003686~~	~~0.14358~~	~~1585.3~~	~~98.7~~	~~1787~~	~~61.5~~	~~11.29~~	~~1787~~
~~38DTB19 - Run 2~~	~~16/07/2020 (5) 16:35:27.00~~	~~X38DT_3~~	~~233.4~~	~~8.3~~	~~117~~	~~4.5~~	~~2.2553~~	~~0.1570063~~	~~0.1826~~	~~0.007652~~	~~0.41277~~	~~2366~~	~~138~~	~~2675.9~~	~~69.3~~	~~11.58~~	~~2675.9~~
~~38DTB19 - Run 2~~	~~16/07/2020 (5) 17:08:56.00~~	~~X38DT_21~~	~~133.1~~	~~3.9~~	~~183.1~~	~~6.9~~	~~3.575259~~	~~0.25045988~~	~~0.11~~	~~0.0071~~	~~0.27229~~	~~1589.9~~	~~98.7~~	~~1799~~	~~117~~	~~11.62~~	~~1799~~
~~38DTB19 - Run 2~~	~~16/07/2020 (5) 20:13:33.00~~	~~X38DT_87~~	~~400.7~~	~~4.6~~	~~431~~	~~12~~	~~2.233639~~	~~0.15443388~~	~~0.1859~~	~~0.006718~~	~~-0.12236~~	~~2385~~	~~138~~	~~2705.5~~	~~59.6~~	~~11.85~~	~~2705.5~~
~~38DTB19 - Run 2~~	~~16/07/2020 (5) 16:54:03.00~~	~~X38DT_13~~	~~175.1~~	~~4.2~~	~~83~~	~~1.5~~	~~3.475843~~	~~0.25073916~~	~~0.1133~~	~~0.006766~~	~~0.17063~~	~~1630~~	~~104~~	~~1852~~	~~108~~	~~11.99~~	~~1852~~
~~38DTB19 - Run 2~~	~~16/07/2020 (5) 19:45:01.00~~	~~X38DT_79~~	~~131.7~~	~~2.7~~	~~65.1~~	~~1.3~~	~~2.277904~~	~~0.17009048~~	~~0.1823~~	~~0.008146~~	~~0.2117~~	~~2346~~	~~147~~	~~2673.2~~	~~74~~	~~12.24~~	~~2673.2~~
~~38DTB19 - Run 2~~	~~16/07/2020 (5) 20:39:48.00~~	~~X38DT_97~~	~~191.4~~	~~5.2~~	~~160~~	~~8~~	~~2.312139~~	~~0.15850848~~	~~0.1815~~	~~0.00753~~	~~0.1729~~	~~2317~~	~~133~~	~~2665.9~~	~~68.7~~	~~13.09~~	~~2665.9~~
~~38DTB19 - Run 2~~	~~16/07/2020 (5) 17:05:13.00~~	~~X38DT_19~~	~~3.33E+02~~	~~5.70E+00~~	~~327~~	~~11~~	~~2.436647~~	~~0.17341514~~	~~0.1695~~	~~0.00669~~	~~0.057882~~	~~2217~~	~~133~~	~~2552~~	~~66.1~~	~~13.13~~	~~2552~~
~~38DTB19 - Run 2~~	~~16/07/2020 (5) 17:56:01.00~~	~~X38DT_37~~	~~142.7~~	~~3.9~~	~~71.8~~	~~2.5~~	~~3.541076~~	~~0.25890982~~	~~0.113~~	~~0.00736~~	~~0.41349~~	~~1603~~	~~104~~	~~1847~~	~~118~~	~~13.21~~	~~1847~~
~~38DTB19 - Run 2~~	~~16/07/2020 (5) 19:39:30.00~~	~~X38DT_76~~	~~312~~	~~10~~	~~194.3~~	~~4.7~~	~~2.321263~~	~~0.16496696~~	~~0.1824~~	~~0.005848~~	~~0.25458~~	~~2309~~	~~138~~	~~2674.1~~	~~53.1~~	~~13.65~~	~~2674.1~~
~~38DTB19 - Run 2~~	~~16/07/2020 (5) 18:39:28.00~~	~~X38DT_53~~	~~589~~	~~15~~	~~22.6~~	~~3.3~~	~~3.561254~~	~~0.24878048~~	~~0.1141~~	~~0.004082~~	~~0.22583~~	~~1595.4~~	~~98.7~~	~~1864.9~~	~~64.6~~	~~14.45~~	~~1864.9~~
~~38DTB19 - Run 2~~	~~16/07/2020 (5) 16:57:47.00~~	~~X38DT_15~~	~~935~~	~~33~~	~~261~~	~~22~~	~~3.878976~~	~~0.27318342~~	~~0.106~~	~~0.00372~~	~~0.24679~~	~~1478.6~~	~~93.1~~	~~1730.9~~	~~64.4~~	~~14.58~~	~~1730.9~~
~~38DTB19 - Run 2~~	~~16/07/2020 (5) 21:30:19.00~~	~~X38DT_119~~	~~238.4~~	~~3.6~~	~~92.6~~	~~2.2~~	~~3.759398~~	~~0.27305106~~	~~0.1097~~	~~0.005694~~	~~0.0041428~~	~~1520.5~~	~~98.4~~	~~1793.6~~	~~94.5~~	~~15.23~~	~~1793.6~~
~~38DTB19 - Run 2~~	~~16/07/2020 (5) 20:09:46.00~~	~~X38DT_85~~	~~324.8~~	~~4.5~~	~~99.6~~	~~3.2~~	~~1.733102~~	~~0.11876406~~	~~0.2993~~	~~0.009386~~	~~0.34825~~	~~2936~~	~~162~~	~~3465.9~~	~~48.6~~	~~15.29~~	~~3465.9~~
~~38DTB19 - Run 2~~	~~16/07/2020 (5) 21:32:12.00~~	~~X38DT_120~~	~~484~~	~~7~~	~~443.1~~	~~8.9~~	~~2.376991~~	~~0.16619162~~	~~0.1839~~	~~0.006478~~	~~0.099407~~	~~2264~~	~~133~~	~~2687.6~~	~~58.2~~	~~15.76~~	~~2687.6~~
~~38DTB19 - Run 2~~	~~16/07/2020 (5) 19:48:44.00~~	~~X38DT_81~~	~~410.4~~	~~5.4~~	~~69.9~~	~~1.4~~	~~3.653635~~	~~0.2466104~~	~~0.1149~~	~~0.004598~~	~~0.21~~	~~1559.6~~	~~93.5~~	~~1877.5~~	~~72.1~~	~~16.93~~	~~1877.5~~
~~38DTB19 - Run 2~~	~~16/07/2020 (5) 18:32:04.00~~	~~X38DT_49~~	~~460~~	~~11~~	~~62.9~~	~~1.7~~	~~3.780718~~	~~0.27572796~~	~~0.1114~~	~~0.005228~~	~~-0.073206~~	~~1512.8~~	~~98.3~~	~~1821.6~~	~~85.2~~	~~16.95~~	~~1821.6~~
~~38DTB19 - Run 2~~	~~16/07/2020 (5) 17:03:20.00~~	~~X38DT_18~~	~~3.71E+02~~	~~1.70E+01~~	~~3.45E+02~~	~~6.40E+00~~	~~2.452784~~	~~0.16937868~~	~~0.1836~~	~~0.006472~~	~~0.35511~~	~~2204~~	~~129~~	~~2684.9~~	~~58.3~~	~~17.91~~	~~2684.9~~
~~38DTB19 - Run 2~~	~~16/07/2020 (5) 17:01:30.00~~	~~X38DT_17~~	~~296.2~~	~~5.4~~	~~166~~	~~5.4~~	~~2.506266~~	~~0.18831542~~	~~0.1788~~	~~0.007476~~	~~0.087954~~	~~2164~~	~~138~~	~~2641~~	~~69.4~~	~~18.06~~	~~2641~~
~~38DTB19 - Run 2~~	~~16/07/2020 (5) 20:24:39.00~~	~~X38DT_93~~	~~128.1~~	~~2.3~~	~~95.7~~	~~2.5~~	~~2.644104~~	~~0.18571648~~	~~0.1669~~	~~0.008438~~	~~0.18947~~	~~2068~~	~~124~~	~~2526~~	~~84.9~~	~~18.13~~	~~2526~~
~~38DTB19 - Run 2~~	~~16/07/2020 (5) 20:52:46.00~~	~~X38DT_104~~	~~189~~	~~3.6~~	~~201.1~~	~~3.1~~	~~2.696872~~	~~0.19212664~~	~~0.1634~~	~~0.007468~~	~~0.12993~~	~~2033~~	~~124~~	~~2490.4~~	~~77~~	~~18.37~~	~~2490.4~~
~~38DTB19 - Run 2~~	~~16/07/2020 (5) 20:45:20.00~~	~~X38DT_100~~	~~353.7~~	~~8.8~~	~~212.6~~	~~4.5~~	~~2.590674~~	~~0.19275688~~	~~0.1743~~	~~0.006486~~	~~-0.16938~~	~~2104~~	~~134~~	~~2598.6~~	~~62~~	~~19.03~~	~~2598.6~~
~~38DTB19 - Run 2~~	~~16/07/2020 (5) 17:24:12.00~~	~~X38DT_24~~	~~103~~	~~4.3~~	~~122.4~~	~~3.8~~	~~2.44978~~	~~0.1750254~~	~~0.1917~~	~~0.010734~~	~~0.25502~~	~~2207~~	~~134~~	~~2756.1~~	~~92~~	~~19.92~~	~~2756.1~~
~~38DTB19 - Run 2~~	~~16/07/2020 (5) 20:47:14.00~~	~~X38DT_101~~	~~494.8~~	~~9.2~~	~~183.8~~	~~5.3~~	~~3.675119~~	~~0.26259338~~	~~0.1195~~	~~0.00519~~	~~0.20817~~	~~1551.5~~	~~98.5~~	~~1948~~	~~77.6~~	~~20.35~~	~~1948~~
~~38DTB19 - Run 2~~	~~16/07/2020 (5) 20:11:38.00~~	~~X38DT_86~~	~~72.8~~	~~2.1~~	~~119~~	~~4.4~~	~~4.13736~~	~~0.3223957~~	~~0.1088~~	~~0.009076~~	~~0.23198~~	~~1395.5~~	~~97.8~~	~~1779~~	~~152~~	~~21.56~~	~~1779~~
~~38DTB19 - Run 2~~	~~16/07/2020 (5) 17:29:44.00~~	~~X38DT_27~~	~~5.84E+02~~	~~1.90E+01~~	~~237.5~~	~~7.5~~	~~2.73224~~	~~0.2039476~~	~~0.1709~~	~~0.005818~~	~~-0.294~~	~~2011~~	~~129~~	~~2565.7~~	~~56.9~~	~~21.62~~	~~2565.7~~
~~38DTB19 - Run 2~~	~~16/07/2020 (5) 21:24:47.00~~	~~X38DT_116~~	~~722~~	~~36~~	~~674~~	~~64~~	~~2.858776~~	~~0.21245502~~	~~0.1639~~	~~0.006078~~	~~-0.13739~~	~~1934~~	~~124~~	~~2495.5~~	~~62.5~~	~~22.50~~	~~2495.5~~
~~38DTB19 - Run 2~~	~~16/07/2020 (5) 21:39:38.00~~	~~X38DT_124~~	~~89~~	~~3.6~~	~~280~~	~~93~~	~~2.739726~~	~~0.21992872~~	~~0.1782~~	~~0.010864~~	~~0.057533~~	~~2006~~	~~138~~	~~2635~~	~~101~~	~~23.87~~	~~2635~~
~~38DTB19 - Run 2~~	~~16/07/2020 (5) 18:54:20.00~~	~~X38DT_61~~	~~99.5~~	~~2.8~~	~~95~~	~~1.7~~	~~2.816901~~	~~0.21503672~~	~~0.1786~~	~~0.010072~~	~~0.20704~~	~~1958~~	~~129~~	~~2639.2~~	~~93.6~~	~~25.81~~	~~2639.2~~
~~38DTB19 - Run 2~~	~~16/07/2020 (5) 18:35:45.00~~	~~X38DT_51~~	~~719.4~~	~~9.9~~	~~338~~	~~16~~	~~2.787845~~	~~0.1956543~~	~~0.1814~~	~~0.005528~~	~~0.14046~~	~~1976~~	~~119~~	~~2665~~	~~50.5~~	~~25.85~~	~~2665~~
~~38DTB19 - Run 2~~	~~16/07/2020 (5) 17:44:44.00~~	~~X38DT_31~~	~~335.8~~	~~7.6~~	~~231~~	~~15~~	~~2.169197~~	~~0.16101934~~	~~0.2698~~	~~0.009896~~	~~0.19933~~	~~2444~~	~~151~~	~~3304.2~~	~~57.5~~	~~26.03~~	~~3304.2~~
~~38DTB19 - Run 2~~	~~16/07/2020 (5) 21:22:53.00~~	~~X38DT_115~~	~~561.5~~	~~8.7~~	~~188.5~~	~~4.6~~	~~3.183699~~	~~0.21571308~~	~~0.16~~	~~0.006~~	~~0.3595~~	~~1761~~	~~104~~	~~2454.9~~	~~63.4~~	~~28.27~~	~~2454.9~~
~~38DTB19 - Run 2~~	~~16/07/2020 (5) 20:17:14.00~~	~~X38DT_89~~	~~1080~~	~~260~~	~~5000~~	~~1900~~	~~4.545455~~	~~0.6694215~~	~~0.1126~~	~~0.005552~~	~~-0.6605~~	~~1282~~	~~171~~	~~1841~~	~~89.3~~	~~30.36~~	~~1841~~
~~38DTB19 - Run 2~~	~~16/07/2020 (5) 20:43:30.00~~	~~X38DT_99~~	~~630~~	~~8.7~~	~~136~~	~~22~~	~~3.444712~~	~~0.25875094~~	~~0.1578~~	~~0.005756~~	~~-0.11623~~	~~1643~~	~~109~~	~~2431.5~~	~~61.8~~	~~32.43~~	~~2431.5~~
~~38DTB19 - Run 2~~	~~16/07/2020 (5) 19:46:54.00~~	~~X38DT_80~~	~~2530~~	~~110~~	~~1520~~	~~400~~	~~3.257329~~	~~0.29857078~~	~~0.172~~	~~0.00474~~	~~0.066919~~	~~1726~~	~~139~~	~~2576.4~~	~~46~~	~~33.01~~	~~2576.4~~
~~38DTB19 - Run 2~~	~~16/07/2020 (5) 19:52:27.00~~	~~X38DT_83~~	~~158.5~~	~~3.2~~	~~77.3~~	~~1.5~~	~~3.163556~~	~~0.23340862~~	~~0.1809~~	~~0.009718~~	~~0.31251~~	~~1771~~	~~114~~	~~2660.4~~	~~89~~	~~33.43~~	~~2660.4~~
~~38DTB19 - Run 2~~	~~16/07/2020 (5) 18:43:12.00~~	~~X38DT_55~~	~~394~~	~~11~~	~~222.2~~	~~8.5~~	~~4.901961~~	~~0.43444832~~	~~0.112~~	~~0.00524~~	~~0.029652~~	~~1196.8~~	~~96.8~~	~~1831.3~~	~~84.8~~	~~34.65~~	~~1831.3~~
~~38DTB19 - Run 2~~	~~16/07/2020 (5) 21:37:44.00~~	~~X38DT_123~~	~~567~~	~~30~~	~~630~~	~~110~~	~~3.289474~~	~~0.34712608~~	~~0.1766~~	~~0.006532~~	~~-0.068253~~	~~1711~~	~~159~~	~~2620.4~~	~~61.5~~	~~34.70~~	~~2620.4~~
~~38DTB19 - Run 2~~	~~16/07/2020 (5) 16:40:59.00~~	~~X38DT_6~~	~~392~~	~~33~~	~~578~~	~~70~~	~~4.916421~~	~~0.36421152~~	~~0.1128~~	~~0.005556~~	~~0.28641~~	~~1193.6~~	~~80.7~~	~~1844.2~~	~~89.1~~	~~35.28~~	~~1844.2~~
~~38DTB19 - Run 2~~	~~16/07/2020 (5) 18:20:52.00~~	~~X38DT_43~~	~~330.5~~	~~8.7~~	~~89.8~~	~~3.8~~	~~5.602241~~	~~0.42589582~~	~~0.105~~	~~0.0062~~	~~0.13285~~	~~1058.8~~	~~74.2~~	~~1713~~	~~109~~	~~38.19~~	~~1713~~
~~38DTB19 - Run 2~~	~~16/07/2020 (5) 17:26:00.00~~	~~X38DT_25~~	~~327~~	~~29~~	~~233~~	~~49~~	~~6.093845~~	~~0.5674963~~	~~0.1022~~	~~0.005444~~	~~-0.41553~~	~~979.5~~	~~84.6~~	~~1663.6~~	~~98.6~~	~~41.12~~	~~1663.6~~
~~38DTB19 - Run 2~~	~~16/07/2020 (5) 21:19:10.00~~	~~X38DT_113~~	~~194~~	~~13~~	~~53.6~~	~~2.4~~	~~3.787879~~	~~0.53489438~~	~~0.1793~~	~~0.008486~~	~~0.15923~~	~~1510~~	~~190~~	~~2645.7~~	~~78.5~~	~~42.93~~	~~2645.7~~
~~38DTB19 - Run 2~~	~~16/07/2020 (5) 19:41:18.00~~	~~X38DT_77~~	~~221.1~~	~~6.3~~	~~48.7~~	~~3.5~~	~~6.329114~~	~~0.72744748~~	~~0.1072~~	~~0.006344~~	~~-0.010344~~	~~946~~	~~101~~	~~1752~~	~~108~~	~~46.00~~	~~1752~~
~~38DTB19 - Run 2~~	~~16/07/2020 (5) 17:27:54.00~~	~~X38DT_26~~	~~123.5~~	~~3.2~~	~~32.7~~	~~1.2~~	~~7.662835~~	~~0.7991662~~	~~0.103~~	~~0.00916~~	~~-0.0042117~~	~~790.7~~	~~77.6~~	~~1678~~	~~164~~	~~52.88~~	~~1678~~
~~38DTB19 - Run 2~~	~~16/07/2020 (5) 19:33:54.00~~	~~X38DT_73~~	~~470~~	~~51~~	~~158~~	~~15~~	~~7.8125~~	~~1.987305~~	~~0.1033~~	~~0.007066~~	~~-0.36024~~	~~776~~	~~186~~	~~1683~~	~~126~~	~~53.89~~	~~1683~~
~~38DTB19 - Run 2~~	~~16/07/2020 (5) 21:43:20.00~~	~~X38DT_126~~	~~1256~~	~~21~~	~~346~~	~~30~~	~~10.89325~~	~~0.7755802~~	~~0.0891~~	~~0.004082~~	~~0.11113~~	~~566.2~~	~~38.6~~	~~1405.4~~	~~87.7~~	~~59.71~~	~~566.2~~
~~38DTB19 - Run 2~~	~~16/07/2020 (5) 20:15:21.00~~	~~X38DT_88~~	~~785~~	~~16~~	~~70.1~~	~~6.4~~	~~6.775068~~	~~0.68631986~~	~~0.1581~~	~~0.006362~~	~~0.066692~~	~~887.5~~	~~84~~	~~2434.7~~	~~68.2~~	~~63.55~~	~~2434.7~~
~~38DTB19 - Run 2~~	~~16/07/2020 (5) 19:32:04.00~~	~~X38DT_72~~	~~753~~	~~10~~	~~421~~	~~56~~	~~10.13171~~	~~0.8390741~~	~~0.1095~~	~~0.00739~~	~~-0.63289~~	~~606.8~~	~~48~~	~~1790~~	~~123~~	~~66.10~~	~~1790~~
~~38DTB19 - Run 2~~	~~16/07/2020 (5) 21:28:30.00~~	~~X38DT_118~~	~~321~~	~~3.6~~	~~75.3~~	~~2~~	~~8.305648~~	~~0.65589786~~	~~0.1706~~	~~0.008312~~	~~0.23187~~	~~732.9~~	~~54.7~~	~~2562.8~~	~~81.5~~	~~71.40~~	~~2562.8~~
~~38DTB19 - Run 2~~	~~16/07/2020 (5) 21:13:39.00~~	~~X38DT_110~~	~~193~~	~~11~~	~~34.7~~	~~1.2~~	~~9.259259~~	~~1.29972518~~	~~0.1555~~	~~0.01181~~	~~-0.169~~	~~661.1~~	~~88.2~~	~~2407~~	~~129~~	~~72.53~~	~~2407~~
~~38DTB19 - Run 2~~	~~16/07/2020 (5) 18:37:35.00~~	~~X38DT_52~~	~~1183~~	~~25~~	~~217~~	~~25~~	~~40.98361~~	~~4.6828812~~	~~0.1017~~	~~0.008934~~	~~-0.30098~~	~~155.4~~	~~17.5~~	~~1655~~	~~163~~	~~90.61~~	~~1655~~

Appendix D3.1 continued.

Curtin University Geohistory center Sample ID	Analysis date-time	Spot ID	238U conc. (ppm)	±2σ INT	232Th conc. (ppm)	±2σ INT	Isotopic Ratios 238U/206Pb	±2σ PROP	207Pb/206Pb	±2σ PROP	rho	Apparent Ages - Calculated in Isoplot R (Ma) 238U/206Pb	±2σ PROP	207Pb/206Pb	±2σ PROP	Discord (7/6-6/8)/7/6 *100	Perferred age *1500 Ma cutoff (Ma)
82DTB19	16/07/2020 (5) 22:41:40.00	82DTB19 - 14	28.58	0.62	19.19	0.62	3.058104	0.22949808	0.1066	0.011732	-0.0019313	1824	119	1741	202	-4.77	1741
82DTB19	17/07/2020 (6) 00:53:28.00	82DTB19 - 59	104.1	2	168.9	2.9	2.996704	0.21259808	0.1098	0.006596	0.30304	1856	114	1795	109	-3.40	1795
82DTB19	16/07/2020 (5) 22:26:50.00	82DTB19 - 6	114.7	5.3	42.8	1.5	3.04971	0.2191067	0.109	0.00688	0.29711	1828	114	1782	115	-2.58	1782
82DTB19	17/07/2020 (6) 00:13:50.00	82DTB19 - 47	130	2.1	74.5	1.5	3.106555	0.216542	0.1077	0.006454	0.38355	1799	109	1760	110	-2.22	1760
82DTB19	16/07/2020 (5) 23:39:55.00	82DTB19 - 36	90.5	2.2	83.8	2.8	3.137747	0.22028224	0.1068	0.006836	0.42789	1783	109	1745	117	-2.18	1745
82DTB19	16/07/2020 (5) 23:57:05.00	82DTB19 - 38	149.9	2.2	48.5	1.4	3.039514	0.21784718	0.1101	0.006902	0.18363	1834	114	1800	114	-1.89	1800
82DTB19	17/07/2020 (6) 00:08:14.00	82DTB19 - 44	95.9	1.8	68.4	2.8	3.035823	0.21739216	0.1105	0.00681	0.45028	1835	114	1807	112	-1.55	1807
82DTB19	16/07/2020 (5) 23:08:05.00	82DTB19 - 23	128.2	2.7	88.1	2.1	3.196931	0.22746452	0.1059	0.006618	0.34356	1754	109	1729	115	-1.45	1729
82DTB19	17/07/2020 (6) 01:57:13.00	82DTB19 - 82	109.1	1.9	35.5	1.2	3.147624	0.22147298	0.1073	0.007246	0.49897	1778	109	1753	124	-1.43	1753
82DTB19	17/07/2020 (6) 02:04:39.00	82DTB19 - 86	89.6	1.4	24.25	0.71	3.047851	0.21887682	0.1107	0.007314	0.11597	1829	114	1810	120	-1.05	1810
82DTB19	17/07/2020 (6) 01:17:41.00	82DTB19 - 72	104.1	2.5	66.2	1.5	2.993116	0.21216092	0.1126	0.006752	0.08519	1858	114	1841	109	-0.92	1841
82DTB19	16/07/2020 (5) 23:36:14.00	82DTB19 - 34	110.8	2.3	91.1	2.1	2.960332	0.20818724	0.1138	0.006676	0.086554	1876	114	1860	106	-0.86	1860
82DTB19	17/07/2020 (6) 02:29:05.00	82DTB19 - 95	113	16	70.8	6.2	1.912412	0.13699582	0.1842	0.009584	0.22088	2711	159	2690.3	86	-0.77	2690.3
82DTB19	17/07/2020 (6) 00:32:24.00	82DTB19 - 57	71.6	1	53.5	1	3.072197	0.22189664	0.111	0.00832	0.099695	1817	114	1815	136	-0.11	1815
82DTB19	17/07/2020 (6) 02:34:36.00	82DTB19 - 98	125.9	1.6	94.5	1.5	3.104626	0.21631172	0.11	0.0059	0.3526	1800	109	1798.6	97.6	-0.08	1798.6
82DTB19	16/07/2020 (5) 22:32:25.00	82DTB19 - 9	148.6	3.5	99.6	4.2	1.479728	0.10404076	0.2757	0.010614	0.1679	3328	183	3338	60.2	0.30	3338
82DTB19	17/07/2020 (6) 03:15:55.00	82DTB19 - 115	23.23	0.55	37.4	0.74	3.154574	0.26211828	0.109	0.01218	0.3077	1775	129	1782	204	0.39	1782
82DTB19	16/07/2020 (5) 22:21:17.00	82DTB19 - 3	113.7	2.8	148.2	5.9	1.52207	0.10689241	0.2638	0.010576	0.24237	3255	180	3268.8	63.1	0.42	3268.8
82DTB19	17/07/2020 (6) 03:10:22.00	82DTB19 - 112	164.5	3.9	74.7	2.6	3.076923	0.21301776	0.1115	0.00633	0.412	1814	109	1823	103	0.49	1823
82DTB19	16/07/2020 (5) 23:38:02.00	82DTB19 - 35	167.2	2.6	147.1	2.7	1.952744	0.13819828	0.1836	0.007772	0.30384	2666	155	2684.9	70	0.70	2684.9
82DTB19	17/07/2020 (6) 01:08:20.00	82DTB19 - 67	72.3	3.5	48.2	3.2	3.082614	0.22319498	0.1116	0.007832	0.16209	1811	114	1825	127	0.77	1825
82DTB19	17/07/2020 (6) 00:28:41.00	82DTB19 - 55	93.7	1.7	59.2	0.98	3.147624	0.23138058	0.1098	0.007196	0.11872	1778	114	1795	119	0.95	1795
82DTB19	17/07/2020 (6) 02:13:58.00	82DTB19 - 91	131.5	4.6	76.7	3.9	3.096934	0.21539468	0.1114	0.006228	0.17544	1804	109	1822	101	0.99	1822
82DTB19	17/07/2020 (6) 03:06:38.00	82DTB19 - 110	245.3	3.4	186.3	3.4	3.246753	0.22305616	0.1072	0.005244	0.20172	1731	104	1751.5	89.5	1.17	1751.5
82DTB19	17/07/2020 (6) 03:17:49.00	82DTB19 - 116	147.5	2	62.1	1.1	3.045067	0.20926024	0.1135	0.00587	0.013228	1831	110	1855.4	93.5	1.32	1855.4
82DTB19	17/07/2020 (6) 01:25:06.00	82DTB19 - 76r - 1	55.5	1.2	91.4	1.3	3.046923	0.22804576	0.1135	0.00967	0.30497	1830	119	1855	154	1.35	1855
82DTB19	17/07/2020 (6) 01:23:14.00	82DTB19 - 75	29.4	1.1	67.2	2.9	3.154574	0.26211828	0.1101	0.012002	0.15144	1775	129	1800	198	1.39	1800
82DTB19	17/07/2020 (6) 00:15:38.00	82DTB19 - 48	180.4	2.7	76	1.8	3.138732	0.22040084	0.1106	0.005912	0.40378	1783	109	1808.5	97.1	1.41	1808.5
82DTB19	17/07/2020 (6) 00:23:04.00	82DTB19 - 52	86.1	1.1	43.01	0.89	2.95858	0.2079759	0.1169	0.007938	0.26859	1877	114	1909	122	1.68	1909
82DTB19	16/07/2020 (5) 23:55:12.00	82DTB19 - 37	94.1	9.7	66	17	3.033981	0.22637032	0.1143	0.007686	0.29495	1836	119	1868	121	1.71	1868
82DTB19	17/07/2020 (6) 02:12:05.00	82DTB19 - 90	79.9	3.6	238	12	1.989258	0.14267096	0.1827	0.009554	0.40786	2625	155	2676.8	86.5	1.94	2676.8
82DTB19	17/07/2020 (6) 02:00:56.00	82DTB19 - 84	197.2	3.6	71.5	1.6	2.948113	0.20671556	0.1177	0.006954	0.21863	1883	114	1921	106	1.98	1921
82DTB19	17/07/2020 (6) 02:10:15.00	82DTB19 - 89	153.9	2.2	60	1.2	3.060912	0.21112514	0.1138	0.006076	0.36454	1822	109	1860.2	96.4	2.05	1860.2
82DTB19	16/07/2020 (5) 22:30:32.00	82DTB19 - 8	169.5	3.5	73.2	2	3.134796	0.21992712	0.1116	0.005532	0.081634	1785	109	1824.8	89.9	2.18	1824.8
82DTB19	16/07/2020 (5) 22:43:33.00	82DTB19 - 15	60.3	2	36.2	1.4	1.808318	0.13099679	0.21	0.0122	-0.012724	2838	166	2904.8	94.2	2.30	2904.8
82DTB19	17/07/2020 (6) 01:19:30.00	82DTB19 - 73	120.8	1.5	81.7	1.3	3.040438	0.21796126	0.1149	0.005898	0.2298	1833	114	1877.5	92.5	2.37	1877.5
82DTB19	17/07/2020 (6) 00:10:07.00	82DTB19 - 45	249	17	18.8	3.2	3.100775	0.2158524	0.1129	0.005858	0.14882	1802	109	1845.8	93.9	2.37	1845.8
82DTB19	17/07/2020 (6) 02:27:12.00	82DTB19 - 94	67.7	2.2	103.3	3.6	1.872659	0.13915188	0.2	0.011	0.13039	2758	167	2825.5	89.8	2.39	2825.5
82DTB19	17/07/2020 (6) 02:15:47.00	82DTB19 - 92	261.8	3.9	153.9	2.7	3.096934	0.21539468	0.1131	0.005462	0.074636	1804	109	1849	87.3	2.43	1849
82DTB19	17/07/2020 (6) 03:19:37.00	82DTB19 - 117	88.7	2.3	43.8	2.2	3.079766	0.21335462	0.1137	0.006674	0.26178	1813	109	1859	106	2.47	1859
82DTB19	17/07/2020 (6) 01:15:48.00	82DTB19 - 71	59.6	4.1	34.4	2.2	3.106555	0.2261927	0.113	0.00916	0.39331	1799	114	1847	147	2.60	1847
82DTB19	17/07/2020 (6) 02:06:32.00	82DTB19 - 87	125.7	1.5	114.9	1.9	3.021148	0.21558766	0.116	0.00712	0.49076	1843	114	1895	110	2.74	1895
82DTB19	17/07/2020 (6) 02:59:12.00	82DTB19 - 106	157.6	1.8	117.9	1.7	3.087373	0.21425736	0.1139	0.005578	0.05124	1809	109	1861.7	88.4	2.83	1861.7
82DTB19	17/07/2020 (6) 00:30:30.00	82DTB19 - 56	46.43	0.84	42.05	0.88	3.17965	0.235466	0.111	0.01062	0.27229	1763	114	1815	174	2.87	1815
82DTB19	17/07/2020 (6) 01:06:31.00	82DTB19 - 66	62.1	2.9	105.8	4.2	2.925688	0.21258746	0.1197	0.009594	0.11897	1895	119	1951	143	2.87	1951
82DTB19	17/07/2020 (6) 01:51:41.00	82DTB19 - 79	55.89	0.97	79.7	1.3	2.024291	0.14702752	0.1815	0.01083	-0.28981	2588	155	2665.9	98.8	2.92	2665.9
82DTB19	17/07/2020 (6) 03:04:44.00	82DTB19 - 109	193.7	2.8	46.9	1.1	3.165559	0.22364338	0.1117	0.006234	0.39851	1770	109	1826	101	3.07	1826
82DTB19	17/07/2020 (6) 01:55:24.00	82DTB19 - 81	58.4	4.8	68.2	1.7	3.145643	0.23112906	0.1125	0.00945	0.2238	1779	114	1839	152	3.26	1839
82DTB19	17/07/2020 (6) 02:30:54.00	82DTB19 - 96	81.4	1.5	32.08	0.71	3.15856	0.2327717	0.1121	0.008142	0.46512	1773	114	1833	132	3.27	1833
82DTB19	16/07/2020 (5) 23:02:34.00	82DTB19 - 20	266	7.4	219	12	3.139717	0.22051954	0.1127	0.005954	0.34003	1782	109	1842.6	95.6	3.29	1842.6
82DTB19	16/07/2020 (5) 23:30:36.00	82DTB19 - 31	36.15	0.69	14.49	0.41	3.014772	0.22389474	0.1171	0.010642	-0.035876	1847	119	1912	163	3.40	1912
82DTB19	16/07/2020 (5) 22:34:15.00	82DTB19 - 10	113.7	1.7	98	1.9	3.140704	0.22063838	0.1131	0.006362	0.36507	1782	109	1849	102	3.62	1849
82DTB19	17/07/2020 (6) 00:04:30.00	82DTB19 - 42	126.1	3.7	67.7	5	2.398082	0.17447914	0.1489	0.007378	-0.0034168	2247	138	2332.6	84.8	3.67	2332.6
82DTB19	16/07/2020 (5) 22:37:57.00	82DTB19 - 12	337.9	3.9	523	17	1.970832	0.13652108	0.1907	0.007014	0.29755	2646	150	2747.5	60.5	3.69	2747.5
82DTB19	16/07/2020 (5) 23:15:31.00	82DTB19 - 27	34.7	1.2	32.5	1.1	3.030303	0.23507806	0.117	0.01234	0.41211	1838	124	1910	189	3.77	1910
82DTB19	17/07/2020 (6) 00:24:58.00	82DTB19 - 53	79	1.8	233	82	1.485884	0.10478463	0.296	0.01692	0.20954	3317	183	3448.7	88.7	3.82	3448.7
82DTB19	17/07/2020 (6) 03:08:28.00	82DTB19 - 111	91.4	2.1	69.3	1.5	2.073398	0.14894246	0.1786	0.009772	0.13643	2537	151	2639.2	90.9	3.87	2639.2
82DTB19	17/07/2020 (6) 02:57:18.00	82DTB19 - 105	79	2.8	76.5	4.2	3.067485	0.2213106	0.1164	0.007328	0.40293	1819	114	1901	113	4.31	1901
82DTB19	17/07/2020 (6) 02:08:22.00	82DTB19 - 88	41.19	0.92	22.23	0.57	3.124024	0.22839238	0.1147	0.010594	0.037996	1790	114	1874	167	4.48	1874
82DTB19	16/07/2020 (5) 23:28:48.00	82DTB19 - 30	280.2	4.9	148.4	5	3.065604	0.21167888	0.1168	0.005536	0.28923	1820	109	1907	85.1	4.56	1907
82DTB19	17/07/2020 (6) 01:26:56.00	82DTB19 - 76_1	300.7	5.7	286.5	8.6	2.051282	0.14201184	0.1839	0.006878	0.42129	2560	146	2687.6	61.8	4.75	2687.6
82DTB19	16/07/2020 (5) 23:13:42.00	82DTB19 - 26	186.3	4.7	199.7	5.8	3.058104	0.21079408	0.1179	0.005858	0.064925	1824	109	1923.8	89.1	5.19	1923.8
82DTB19	17/07/2020 (6) 02:25:21.00	82DTB19 - 93	72.8	2	115.8	3.7	1.972387	0.14059574	0.1961	0.010922	0.33831	2644	155	2793.3	91.2	5.34	2793.3
82DTB19	17/07/2020 (6) 01:21:24.00	82DTB19 - 74	391.9	4.4	265.8	3.5	2.383222	0.16693914	0.1549	0.005398	0.25105	2259	133	2400	59.3	5.88	2400
82DTB19	17/07/2020 (6) 02:48:05.00	82DTB19 - 100	75.8	3.3	53.8	3.6	3.145643	0.22123396	0.1161	0.008222	-0.00072865	1779	109	1896	127	6.17	1896
82DTB19	17/07/2020 (6) 03:14:05.00	82DTB19 - 114	315	5.8	149.6	2.1	3.168568	0.21396866	0.1156	0.005212	0.35363	1768	104	1888.4	81.2	6.38	1888.4
82DTB19	17/07/2020 (6) 02:02:50.00	82DTB19 - 85	222.4	4.5	216.2	8.1	2.222716	0.15314462	0.1709	0.007018	0.24097	2395	138	2565.7	68.7	6.65	2565.7
82DTB19	17/07/2020 (6) 01:10:15.00	82DTB19 - 68	158.8	2.9	144.9	6.1	3.022061	0.20656682	0.1217	0.006434	0.17811	1843	110	1980.5	94.1	6.94	1980.5
82DTB19	17/07/2020 (6) 03:38:39.00	82DTB19 - 120	246.3	4.7	181.6	3.5	3.124024	0.21863288	0.1204	0.005108	0.27793	1790	109	1961.4	75.7	8.74	1961.4
~~82DTB19~~	~~17/07/2020 (6) 00:55:23.00~~	~~82DTB19 - 60~~	~~155.5~~	~~4.2~~	~~136~~	~~23~~	~~3.217503~~	~~0.22998726~~	~~0.1194~~	~~0.006788~~	~~0.42575~~	~~1745~~	~~109~~	~~1946~~	~~102~~	~~10.33~~	~~1946~~

Appendix D3.1 continued.

Sample ID (Curtin University Geohistory center)	Analysis date-time	Spot ID	238U conc. (ppm)	±2σ INT	232Th conc. (ppm)	±2σ INT	Isotopic Ratios 238U/206Pb	±2σ PROP	207Pb/206Pb	±2σ PROP	rho	Apparent Ages (Isoplot R, Ma) 238U/206Pb	±2σ PROP	207Pb/206Pb	±2σ PROP	Discord (7/6-6/8)/7/6 *100	Perferred age *1500 Ma cutoff: Ma	2σ	error %	176Hf/177Hf (0.282785, 0.283250)	±2σ INT	(2% External ε)	176Lu/177Hf (0.03360 Bouvier et al., 2008 EPSL-273)	±2σ INT	176Yb/177Hf (0.03840 Griffin et al., 2002, Lithos-237)	±2σ INT	Hfi	εHf (Lu decay, Scherer et al., 2001, Science-293)	±2σ (0.02)	TDM(Ga)	TDMcrustal (Ga)	HfCHUR(t)	HfDM(t)	Analysis Notes
10DTB30	09/04/2020 (5) 04:21:56.00	10DTB19 - 132	780	170	213	76	2.325581	1.50676062	0.121	0.07742	-0.014281	2306	1256	1970	1141	-17.06	1970	[illegible]	[illegible]	[illegible]	[illegible]	[illegible]	[illegible]	[illegible]	[illegible]	[illegible]	[illegible]	[illegible]	[illegible]	[illegible]	[illegible]	[illegible]	[illegible]	> 5% reverse discordant, spurious Hf, inclusion?, excluded
10DTB19	09/04/2020 (5) 02:10:34.00	10DTB19 - 81	128	10	87	8	3.202049	0.20758468	0.0954	0.004908	0.25251	1752	99.5	1535.1	96.8	-14.13	1535.1	[illegible]	[illegible]	[illegible]	[illegible]	[illegible]	[illegible]	[illegible]	[illegible]	[illegible]	[illegible]	[illegible]	[illegible]	[illegible]	[illegible]	[illegible]	[illegible]	> 5% reverse discordant, excluded
10DTB19	09/04/2020 (5) 02:22:30.00	10DTB19 - 87	240	34	174	16	3.305785	0.2300389	0.1004	0.004608	-0.31135	1704	104	1630.7	85.3	-4.50	1630.7	[illegible]	[illegible]	[illegible]	[illegible]	[illegible]	[illegible]	[illegible]	[illegible]	[illegible]	[illegible]	[illegible]	[illegible]	[illegible]	[illegible]	[illegible]	[illegible]	[illegible]
10DTB19	08/04/2020 (4) 22:35:27.00	10DTB19 - 6	429	15	650	57	3.384095	0.2165592	0.0993	0.004086	0.36763	1669	94.1	1610.2	76.7	-3.65	1610.2	[illegible]	[illegible]	[illegible]	[illegible]	[illegible]	[illegible]	[illegible]	[illegible]	[illegible]	[illegible]	[illegible]	[illegible]	[illegible]	[illegible]	[illegible]	[illegible]	[illegible]
10DTB19	08/04/2020 (4) 22:41:24.00	10DTB19 - 9	156	11	133	7	2.639916	0.16430482	0.1234	0.005368	0.1691	2071	110	2005.2	77.2	-3.28	2005.2	[illegible]	[illegible]	[illegible]	[illegible]	[illegible]	[illegible]	[illegible]	[illegible]	[illegible]	[illegible]	[illegible]	[illegible]	[illegible]	[illegible]	[illegible]	[illegible]	[illegible]
10DTB19	09/04/2020 (5) 00:19:01.00	10DTB19 - 43	189	24	175	25	3.32668	0.2325356	0.1012	0.005224	0.33169	1694	104	1645.4	95.8	-2.95	1645.4	[illegible]	[illegible]	[illegible]	[illegible]	[illegible]	[illegible]	[illegible]	[illegible]	[illegible]	[illegible]	[illegible]	[illegible]	[illegible]	[illegible]	[illegible]	[illegible]	[illegible]
10DTB19	09/04/2020 (5) 02:32:23.00	10DTB19 - 92	613	45	384	30	3.573981	0.22475972	0.0963	0.003326	0.064369	1590.4	88.6	1552.8	64.8	-2.42	1552.8	[illegible]	[illegible]	[illegible]	[illegible]	[illegible]	[illegible]	[illegible]	[illegible]	[illegible]	[illegible]	[illegible]	[illegible]	[illegible]	[illegible]	[illegible]	[illegible]	[illegible]
10DTB19	08/04/2020 (4) 23:17:14.00	10DTB19 - 22	208	3	139	2	3.236246	0.19040442	0.1051	0.004402	0.26072	1735.8	89.5	1715.2	77	-1.20	1715.2	[illegible]	[illegible]	[illegible]	[illegible]	[illegible]	[illegible]	[illegible]	[illegible]	[illegible]	[illegible]	[illegible]	[illegible]	[illegible]	[illegible]	[illegible]	[illegible]	[illegible]
10DTB19	08/04/2020 (4) 22:47:17.00	10DTB19 - 12	208	25	146	23	3.298153	0.21825246	0.1041	0.005582	0.11767	1707.2	99.2	1697.6	98.8	-0.57	1697.6	[illegible]	[illegible]	[illegible]	[illegible]	[illegible]	[illegible]	[illegible]	[illegible]	[illegible]	[illegible]	[illegible]	[illegible]	[illegible]	[illegible]	[illegible]	[illegible]	[illegible]
10DTB19	08/04/2020 (4) 22:37:27.00	10DTB19 - 7	150	2	246	6	3.585515	0.2131254	0.0976	0.004852	0.027809	1585.8	83.6	1577.9	93	-0.50	1577.9	[illegible]	[illegible]	[illegible]	[illegible]	[illegible]	[illegible]	[illegible]	[illegible]	[illegible]	[illegible]	[illegible]	[illegible]	[illegible]	[illegible]	[illegible]	[illegible]	[illegible]
10DTB19	09/04/2020 (5) 00:21:03.00	10DTB19 - 44	161	7	177	10	3.828484	0.12054155	0.0931	0.004962	0.13201	1496	42	1489	101	-0.47	1489	[illegible]	[illegible]	[illegible]	[illegible]	[illegible]	[illegible]	[illegible]	[illegible]	[illegible]	[illegible]	[illegible]	[illegible]	[illegible]	[illegible]	[illegible]	[illegible]	[illegible]
10DTB19	09/04/2020 (5) 03:14:21.00	10DTB19 - 103	179	4	258	17	3.850597	0.12594136	0.0929	0.004658	0.11988	1488.3	43.5	1485	95	-0.22	1485	[illegible]	[illegible]	[illegible]	[illegible]	[illegible]	[illegible]	[illegible]	[illegible]	[illegible]	[illegible]	[illegible]	[illegible]	[illegible]	[illegible]	[illegible]	[illegible]	[illegible]
10DTB19	09/04/2020 (5) 01:54:24.00	10DTB19 - 78	56	1	42	1	3.542331	0.22142392	0.0989	0.007178	0.29708	1602.9	88.7	1603	135	0.01	1603	[illegible]	[illegible]	[illegible]	[illegible]	[illegible]	[illegible]	[illegible]	[illegible]	[illegible]	[illegible]	[illegible]	[illegible]	[illegible]	[illegible]	[illegible]	[illegible]	[illegible]
10DTB19	09/04/2020 (5) 00:40:45.00	10DTB19 - 54	227	5	512	14	3.571429	0.21173468	0.0985	0.00487	0.12169	1591.4	83.6	1595.1	92.3	0.23	1595.1	[illegible]	[illegible]	[illegible]	[illegible]	[illegible]	[illegible]	[illegible]	[illegible]	[illegible]	[illegible]	[illegible]	[illegible]	[illegible]	[illegible]	[illegible]	[illegible]	[illegible]
10DTB19	09/04/2020 (5) 03:38:01.00	10DTB19 - 115	306	10	383	27	3.497726	0.20452952	0.1011	0.004622	-0.086932	1621	83.8	1643.6	84.8	1.38	1643.6	[illegible]	[illegible]	[illegible]	[illegible]	[illegible]	[illegible]	[illegible]	[illegible]	[illegible]	[illegible]	[illegible]	[illegible]	[illegible]	[illegible]	[illegible]	[illegible]	[illegible]
10DTB19	09/04/2020 (5) 04:04:06.00	10DTB19 - 123	247	14	117.4	8.8	3.220612	0.18888034	0.1084	0.004468	0.031396	1743.2	89.6	1771.9	75.2	1.62	1771.9	[illegible]	[illegible]	[illegible]	[illegible]	[illegible]	[illegible]	[illegible]	[illegible]	[illegible]	[illegible]	[illegible]	[illegible]	[illegible]	[illegible]	[illegible]	[illegible]	[illegible]
10DTB19	09/04/2020 (5) 00:30:52.00	10DTB19 - 49	28	1	47	2	3.658983	0.26061386	0.0979	0.010358	0.25188	1557.5	98.6	1584	198	1.67	1584	[illegible]	[illegible]	[illegible]	[illegible]	[illegible]	[illegible]	[illegible]	[illegible]	[illegible]	[illegible]	[illegible]	[illegible]	[illegible]	[illegible]	[illegible]	[illegible]	[illegible]
10DTB19	09/04/2020 (5) 01:02:40.00	10DTB19 - 60	316	5	335	6	3.82995	0.11180344	0.0947	0.004594	0.3733	1495.5	39	1521.3	91.5	1.70	1521.3	[illegible]	[illegible]	[illegible]	[illegible]	[illegible]	[illegible]	[illegible]	[illegible]	[illegible]	[illegible]	[illegible]	[illegible]	[illegible]	[illegible]	[illegible]	[illegible]	[illegible]
10DTB19	08/04/2020 (4) 22:25:37.00	10DTB19 - 1	185	5	142	6	3.924647	0.23252144	0.0932	0.005164	0.053036	1463.2	77.6	1491	105	1.86	1491	[illegible]	[illegible]	[illegible]	[illegible]	[illegible]	[illegible]	[illegible]	[illegible]	[illegible]	[illegible]	[illegible]	[illegible]	[illegible]	[illegible]	[illegible]	[illegible]	[illegible]
10DTB19	09/04/2020 (5) 03:47:56.00	10DTB19 - 120	279	18	68	3	3.531073	0.22024326	0.1009	0.004518	0.051819	1607.5	88.7	1639.9	83.1	1.98	1639.9	[illegible]	[illegible]	[illegible]	[illegible]	[illegible]	[illegible]	[illegible]	[illegible]	[illegible]	[illegible]	[illegible]	[illegible]	[illegible]	[illegible]	[illegible]	[illegible]	[illegible]
10DTB19	09/04/2020 (5) 01:44:34.00	10DTB19 - 73	761	12	585	12	3.340013	0.20066856	0.1057	0.003714	0.15364	1688.3	89.2	1725.7	64.5	2.17	1725.7	[illegible]	[illegible]	[illegible]	[illegible]	[illegible]	[illegible]	[illegible]	[illegible]	[illegible]	[illegible]	[illegible]	[illegible]	[illegible]	[illegible]	[illegible]	[illegible]	[illegible]
10DTB19	09/04/2020 (5) 00:42:42.00	10DTB19 - 55	400	5	160	10	3.705076	0.22510502	0.0976	0.003752	0.25056	1540.3	83.2	1577.9	71.9	2.38	1577.9	[illegible]	[illegible]	[illegible]	[illegible]	[illegible]	[illegible]	[illegible]	[illegible]	[illegible]	[illegible]	[illegible]	[illegible]	[illegible]	[illegible]	[illegible]	[illegible]	[illegible]
10DTB19	09/04/2020 (5) 01:26:45.00	10DTB19 - 64	136	8	120	4	3.602305	0.2147888	0.0998	0.005196	0.46224	1579.3	83.5	1619.5	96.9	2.48	1619.5	96.9	5.98%	0.281938	0.000032	0.00564	0.002279	0.000065	0.0866	0.003	0.28187	4.03	1.12	1.91	2.088036546	0.281754675	0.282073486	
10DTB19	08/04/2020 (4) 23:47:08.00	10DTB19 - 32	477	21	467	25	3.120125	0.1792246	0.1127	0.004154	0.27437	1792.2	89.9	1842.6	66.7	2.74	1842.6	66.7	3.62%	0.281612	0.000035	0.00563	0.001513	0.000035	0.0592	0.0018	0.28156	-1.82	1.23	2.33	2.637226115	0.281610284	0.281908468	
10DTB19	08/04/2020 (4) 22:43:20.00	10DTB19 - 10	211	17	220	15	3.620565	0.2166047	0.0997	0.004394	0.28597	1572.2	83.5	1617.7	82	2.81	1617.7	82	5.07%	0.282005	0.000042	0.00564	0.001515	0.000055	0.0602	0.0026	0.28196	7.20	1.47	1.78	1.88334677	0.281755838	0.282074814	
10DTB19	08/04/2020 (4) 22:33:31.00	10DTB19 - 5	353	14	92	5	3.749531	0.22963942	0.0973	0.004146	0.092672	1524	83.1	1572.2	79.8	3.07	1572.2	79.8	5.08%	0.282043	0.000031	0.00564	0.003413	0.000079	0.1342	0.0043	0.28194	5.54	1.09	1.82	1.953370924	0.281785211	0.282108383	
10DTB19	09/04/2020 (5) 00:15:04.00	10DTB19 - 41	188	23	216	24	3.227889	0.18958898	0.1098	0.005296	0.091402	1739.7	89.6	1795.3	87.8	3.10	1795.3	87.8	4.89%	0.281694	0.000035	0.00563	0.000908	0.000012	0.03682	0.0004	0.28166	0.79	1.23	2.18	2.434059041	0.281640947	0.281943511	
10DTB19	08/04/2020 (4) 23:13:17.00	10DTB19 - 20	101	6	129	10	3.724395	0.2270702	0.0979	0.005958	0.28393	1533.2	83.2	1584	114	3.21	1584	114	7.20%	0.281961	0.000045	0.00564	0.00334	0.00021	0.1343	0.0076	0.28186	2.95	1.58	1.94	2.128466715	0.281777595	0.28209968	
10DTB19	09/04/2020 (5) 04:27:53.00	10DTB19 - 135	238	22	166.5	8.3	3.644315	0.2189776	0.0996	0.005092	0.20851	1563.1	83.4	1615.8	95.2	3.26	1615.8	95.2	5.89%	0.281978	0.000034	0.00564	0.001487	0.000044	0.0558	0.0015	0.28193	6.23	1.19	1.82	1.94409103	0.281757065	0.282076217	
10DTB19	09/04/2020 (5) 01:24:48.00	10DTB19 - 63	209	5	263	11	3.633721	0.21791762	0.0999	0.005198	0.3503	1567.1	83.4	1621.4	96.8	3.35	1621.4	96.8	5.97%	0.281959	0.000031	0.00564	0.001774	0.000057	0.0678	0.0018	0.28190	5.36	1.09	1.86	2.003952709	0.281753448	0.282072083	
10DTB19	09/04/2020 (5) 02:18:34.00	10DTB19 - 85	250	9	500	34	3.675119	0.22207388	0.0991	0.004482	0.23676	1551.5	83.3	1606.4	84.3	3.42	1606.4	84.3	5.25%	0.281949	0.000039	0.00564	0.002544	0.000072	0.0994	0.0025	0.28187	3.85	1.37	1.91	2.088912904	0.281763135	0.282083154	
10DTB19	09/04/2020 (5) 00:28:55.00	10DTB19 - 48	907	69	843	55	3.958828	0.11992459	0.094	0.00348	0.27841	1451.9	39.4	1507.3	69.9	3.68	1507.3	69.9	4.64%	0.282081	0.000042	0.00564	0.00166	0.00023	0.075	0.013	0.28203	7.33	1.47	1.68	1.787364952	0.281827064	0.282156216	Used for MDA calculation
10DTB19	09/04/2020 (5) 01:52:27.00	10DTB19 - 77	268	17	323	24	3.663004	0.24768878	0.0997	0.004794	0.00095179	1556	93.5	1617.7	89.5	3.81	1617.7	89.5	5.53%	0.282053	0.000035	0.00564	0.00218	0.0001	0.0926	0.0056	0.28199	8.18	1.23	1.74	1.820307951	0.281755838	0.282074814	
10DTB19	08/04/2020 (4) 23:51:05.00	10DTB19 - 34	178	20	158	19	3.707824	0.22538398	0.0988	0.005176	-0.14078	1539.3	83.2	1600.8	97.7	3.84	1600.8	97.7	6.10%	0.282004	0.000036	0.00564	0.001444	0.000055	0.0561	0.0026	0.28196	6.87	1.26	1.78	1.891130323	0.28176675	0.282087286	
10DTB19	09/04/2020 (5) 01:28:46.00	10DTB19 - 65	113	5	94	10	3.646973	0.21924396	0.1003	0.006606	0.31527	1562.1	83.4	1629	122	4.11	1629	122	7.49%	0.281996	0.000031	0.00564	0.001349	0.000074	0.0506	0.0027	0.28195	7.31	1.09	1.78	1.885222565	0.281748539	0.282066473	
10DTB19	09/04/2020 (5) 03:26:12.00	10DTB19 - 109	434	28	181	20	3.33667	0.2003338	0.1079	0.004158	-0.048087	1689.8	89.2	1763.4	70.4	4.17	1763.4	70.4	3.99%	0.281643	0.000037	0.00563	0.00128	0.00014	0.052	0.0053	0.28160	-2.18	1.30	2.27	2.597652781	0.281661612	0.281967128	
10DTB19	09/04/2020 (5) 04:23:56.00	10DTB19 - 133	394	20	208	14	3.656307	0.23354914	0.1002	0.004304	0.083831	1558.5	88.4	1627	79.9	4.21	1627	79.9	4.91%	0.282018	0.000035	0.00564	0.002895	0.000054	0.1127	0.0023	0.28193	6.35	1.23	1.83	1.944885359	0.281749831	0.282067949	
10DTB19	09/04/2020 (5) 02:12:39.00	10DTB19 - 82	1285	17	1273	53	3.257329	0.19246888	0.1102	0.003304	0.019326	1725.9	89.5	1801.9	54.5	4.22	1801.9	54.5	3.02%	0.281769	0.000039	0.00564	0.002335	0.000099	0.0974	0.0037	0.28169	1.87	1.37	2.16	2.3704145	0.28163667	0.281938623	
10DTB19	08/04/2020 (4) 23:15:13.00	10DTB19 - 21	139	12	179	21	3.736921	0.22834872	0.0987	0.004974	0.25003	1528.6	83.2	1598.9	94	4.40	1598.9	94	5.88%	0.281928	0.00003	0.00564	0.001073	0.000055	0.0375	0.0017	0.28190	4.53	1.05	1.87	2.039708742	0.281767977	0.282088688	
10DTB19	09/04/2020 (5) 03:32:09.99	10DTB19 - 112	142	14	260	33	3.789314	0.24809308	0.0977	0.005954	0.34	1509.8	88.1	1580	114	4.44	1580	114	7.22%	0.28194	0.000051	0.00564	0.00242	0.00017	0.0985	0.0091	0.28187	3.10	1.79	1.92	2.115802984	0.281780177	0.282102631	
10DTB19	09/04/2020 (5) 01:36:39.00	10DTB19 - 69	363	30	189	8	3.589375	0.2135073	0.102	0.00424	-0.021966	1584.3	83.6	1660	77	4.56	1660	[illegible]	[illegible]	[illegible]	[illegible]	[illegible]	[illegible]	[illegible]	[illegible]	[illegible]	[illegible]	[illegible]	[illegible]	[illegible]	[illegible]	[illegible]	[illegible]	[illegible]
[illegible]	[illegible]	[illegible]	[illegible]	[illegible]	[illegible]	[illegible]	[illegible]	[illegible]	[illegible]	[illegible]	[illegible]	[illegible]	[illegible]	[illegible]	77	4.56	1660	77	4.64%	0.281958	0.00003	0.00564	0.001953	0.00005	0.076	0.0021	0.28190	5.97	1.05	1.87	1.995760973	0.281728508	0.282043581	
10DTB19	09/04/2020 (5) 00:34:48.00	10DTB19 - 51	181	7	114	12	3.769318	0.24587946	0.0983	0.005366	-0.051382	1516.9	88.2	1591	102	4.66	1591	102	6.41%	0.282001	0.000034	0.00564	0.002116	0.000021	0.0827	0.0014	0.28194	5.83	1.19	1.81	1.950106573	0.281773077	0.282094517	
10DTB19	09/04/2020 (5) 00:44:42.00	10DTB19 - 56	187	17	236	35	3.275467	0.20498224	0.1104	0.004908	-0.10716	1717.5	94.4	1805.2	80.8	4.86	1805.2	80.8	4.48%	0.281713	0.000045	0.00563	0.0015	0.00012	0.0601	0.0045	0.28166	0.96	1.58	2.19	2.430624031	0.281634532	0.281936179	
10DTB19	09/04/2020 (5) 04:35:47.00	10DTB19 - 139	197.8	8.2	323	13	3.732736	0.22792122	0.0992	0.005084	0.10226	1530.1	83.2	1608.3	95.5	4.86	1608.3	95.5	5.94%	0.282086	0.00004	0.00564	0.003038	0.000047	0.1223	0.0021	0.28199	8.22	1.40	1.74	1.810152423	0.281761908	0.282081752	
[illegible]	[illegible]	[illegible]	[illegible]	[illegible]	[illegible]	[illegible]	[illegible]	[illegible]	[illegible]	[illegible]	[illegible]	[illegible]	[illegible]	[illegible]	83.3	5.01	1687	83.3	4.94%	0.28184	0.000046	0.00564	0.000625	0.000013	0.02421	0.00071	0.28182	3.87	1.61	1.96	2.15153391	0.281711052	0.282023631	
[illegible]	[illegible]	[illegible]	[illegible]	[illegible]	[illegible]	[illegible]	[illegible]	[illegible]	[illegible]	[illegible]	[illegible]	[illegible]	[illegible]	[illegible]	109	5.03	1810	109	6.02%	0.281672	0.000033	0.00563	0.001176	0.000019	0.04723	0.00062	0.28163	0.01	1.16	2.23	2.49531774	0.281631421	0.281932624	
[illegible]	[illegible]	[illegible]	[illegible]	[illegible]	[illegible]	[illegible]	[illegible]	[illegible]	[illegible]	[illegible]	[illegible]	[illegible]	[illegible]	[illegible]	68.4	5.08	1566.4	68.4	4.37%	0.28201	0.000033	0.00564	0.002262	0.000029	0.0884	0.0016	0.28194	5.46	1.16	1.81	1.953887408	0.281788953	0.282112661	
[illegible]	[illegible]	[illegible]	[illegible]	[illegible]	[illegible]	[illegible]	[illegible]	[illegible]	[illegible]	[illegible]	[illegible]	[illegible]	[illegible]	[illegible]	60.8	5.11	1737.8	60.8	3.50%	0.281583	0.000035	0.00563	0.001241	0.00003	0.0489	0.00095	0.28154	-4.83	1.23	2.35	2.745546199	0.281678186	0.28198607	
[illegible]	[illegible]	[illegible]	[illegible]	[illegible]	[illegible]	[illegible]	[illegible]	[illegible]	[illegible]	[illegible]	[illegible]	[illegible]	[illegible]	[illegible]	121	5.29	1676	121	7.22%	0.281923	0.000038	0.00564	0.00143	0.000045	0.0537	0.0015	0.28188	5.66	1.33	1.89	2.028096307	0.281718165	0.28203176	
[illegible]	[illegible]	[illegible]	[illegible]	[illegible]	[illegible]	[illegible]	[illegible]	[illegible]	[illegible]	[illegible]	[illegible]	[illegible]	[illegible]	[illegible]	74.8	5.34	1672.7	74.8	4.47%	0.281961	0.000032	0.00564	0.002314	0.00002	0.08466	0.00048	0.28189	5.94	1.12	1.88	2.007399954	0.281720298	0.282034198	
[illegible]	[illegible]	[illegible]	[illegible]	[illegible]	[illegible]	[illegible]	[illegible]	[illegible]	[illegible]	[illegible]	[illegible]	[illegible]	[illegible]	[illegible]	50.2	5.36	3172	50.2	1.58%	0.280884	0.000043	0.00562	0.000691	0.000049	0.0274	0.0022	0.28084	3.72	1.51	3.26	3.329678671	0.280737327	0.280910802	
[illegible]	[illegible]	[illegible]	[illegible]	[illegible]	[illegible]	[illegible]	[illegible]	[illegible]	[illegible]	[illegible]	[illegible]	[illegible]	[illegible]	[illegible]	79.9	5.36	1568.3	79.9	5.09%	0.282044	0.000036	0.00564	0.00155	0.000017	0.0538	0.00065	0.28200	7.46	1.26	1.73	1.827211153	0.281787727	0.28211126	
[illegible]	[illegible]	[illegible]	[illegible]	[illegible]	[illegible]	[illegible]	[illegible]	[illegible]	[illegible]	[illegible]	[illegible]	[illegible]	[illegible]	[illegible]	71.5	5.42	1842.6	71.5	3.88%	0.281722	0.000047	0.00563	0.001587	0.00005	0.0636	0.0021	0.28167	2.00	1.65	2.18	2.394168476	0.281610284	0.281908468	
[illegible]	[illegible]	[illegible]	[illegible]	[illegible]	[illegible]	[illegible]	[illegible]	[illegible]	[illegible]	[illegible]	[illegible]	[illegible]	[illegible]	[illegible]	74.9	5.43	1667.2	74.9	4.49%	0.281813	0.000045	0.00564	0.001473	0.000017	0.0583	0.001	0.28177	1.51	1.58	2.05	2.286377898	0.281723854	0.282038262	
[illegible]	[illegible]	[illegible]	[illegible]	[illegible]	[illegible]	[illegible]	[illegible]	[illegible]	[illegible]	[illegible]	[illegible]	[illegible]	[illegible]	[illegible]	67	5.44	1621.4	67	4.13%	0.282078	0.000044	0.00564	0.00339	0.00011	0.1302	0.005	0.28197	7.83	1.54	1.77	1.845854625	0.281753448	0.282072083	
[illegible]	[illegible]	[illegible]	[illegible]	[illegible]	[illegible]	[illegible]	[illegible]	[illegible]	[illegible]	[illegible]	[illegible]	[illegible]	[illegible]	[illegible]	122	5.58	1517	122	8.04%	0.282041	0.000043	0.00564	0.001202	0.000012	0.04504	0.00032	0.28201	6.59	1.51	1.71	1.842682309	0.281820812	0.282149071	Used for MDA calculation
[illegible]	[illegible]	[illegible]	[illegible]	[illegible]	[illegible]	[illegible]	[illegible]	[illegible]	[illegible]	[illegible]	[illegible]	[illegible]	[illegible]	[illegible]	85.3	5.67	1630.7	85.3	5.23%	0.281844	0.00004	0.00564	0.001252	0.000046	0.0444	0.0021	0.28181	2.05	1.40	1.99	2.222911177	0.281747441	0.282065218	
[illegible]	[illegible]	[illegible]	[illegible]	[illegible]	[illegible]	[illegible]	[illegible]	[illegible]	[illegible]	[illegible]	[illegible]	[illegible]	[illegible]	[illegible]	80	5.74	1623.2	80	4.93%	0.282007	0.000031	0.00564	0.00288	0.000036	0.111	0.0019	0.28192	5.90	1.09	1.84	1.970991567	0.281752285	0.282070755	
[illegible]	[illegible]	[illegible]	[illegible]	[illegible]	[illegible]	[illegible]	[illegible]	[illegible]	[illegible]	[illegible]	[illegible]	[illegible]	[illegible]	[illegible]	93.6	5.78	1695.9	93.6	5.52%	0.281943	0.000036	0.00564	0.001798	0.000058	0.0685	0.0025	0.28189	6.39	1.26	1.88	1.997130916	0.281705297	0.282017053	
[illegible]	[illegible]	[illegible]	[illegible]	[illegible]	[illegible]	[illegible]	[illegible]	[illegible]	[illegible]	[illegible]	[illegible]	[illegible]	[illegible]	[illegible]	103	5.79	1680	103	6.13%	0.28186	0.000035	0.00564	0.001174	0.000024	0.0449	0.0012	0.28182	3.80	1.23	1.97	2.150354485	0.281715579	0.282028804	
[illegible]	[illegible]	[illegible]	[illegible]	[illegible]	[illegible]	[illegible]	[illegible]	[illegible]	[illegible]	[illegible]	[illegible]	[illegible]	[illegible]	[illegible]	84.2	5.96	1758.3	84.2	4.79%	0.281601	0.000039	0.00563	0.0008	0.000019	0.0274	0.0006	0.28157	-3.22	1.37	2.30	2.659396841	0.281664914	0.281970902	
[illegible]	[illegible]	[illegible]	[illegible]	[illegible]	[illegible]	[illegible]	[illegible]	[illegible]	[illegible]	[illegible]	[illegible]	[illegible]	[illegible]	[illegible]	85.4	6.09	1724	85.4	4.95%	0.281794	0.000038	0.00564	0.001015	0.00003	0.04012	0.0007	0.28176	2.62	1.33	2.05	2.260801569	0.281687117	0.281996277	
[illegible]	[illegible]	[illegible]	[illegible]	[illegible]	[illegible]	[illegible]	[illegible]	[illegible]	[illegible]	[illegible]	[illegible]	[illegible]	[illegible]	[illegible]	99.9	6.32	1674.5	99.9	5.97%	0.281941	0.000038	0.00564	0.000769	0.000015	0.02963	0.00038	0.28192	7.01	1.33	1.83	1.94024732	0.281719135	0.282032868	
[illegible]	[illegible]	[illegible]	[illegible]	[illegible]	[illegible]	[illegible]	[illegible]	[illegible]	[illegible]	[illegible]	[illegible]	[illegible]	[illegible]	[illegible]	111	6.43	1497	111	7.41%	0.282179	0.000032	0.00564	0.002447	0.000079	0.0947	0.0037	0.28211	9.79	1.12	1.57	1.620783763	0.281833702	0.282163802	Used for MDA calculation
[illegible]	[illegible]	[illegible]	[illegible]	[illegible]	[illegible]	[illegible]	[illegible]	[illegible]	[illegible]	[illegible]	[illegible]	[illegible]	[illegible]	[illegible]	96.5	6.69	1585.6	96.5	6.09%	0.281888	0.000037	0.00564	0.00096	0.000022	0.0331	0.0011	0.28186	2.93	1.30	1.92	2.131181437	0.281776563	0.2820985	
[illegible]	[illegible]	[illegible]	[illegible]	[illegible]	[illegible]	[illegible]	[illegible]	[illegible]	[illegible]	[illegible]	[illegible]	[illegible]	[illegible]	[illegible]	87.8	6.70	1837.8	87.8	4.78%	0.281708	0.000033	0.00563	0.00111	0.000037	0.0438	0.0013	0.28167	1.98	1.16	2.17	2.391132908	0.281613397	0.281912026	
[illegible]	[illegible]	[illegible]	[illegible]	[illegible]	[illegible]	[illegible]	[illegible]	[illegible]	[illegible]	[illegible]	[illegible]	[illegible]	[illegible]	[illegible]	106	6.86	1633	106	6.49%	0.281989	0.000047	0.00564	0.002012	0.000035	0.0799	0.0015	0.28193	6.42	1.65	1.83	1.945414756	0.281745955	0.28206352	
[illegible]	[illegible]	[illegible]	[illegible]	[illegible]	[illegible]	[illegible]	[illegible]	[illegible]	[illegible]	[illegible]	[illegible]	[illegible]	[illegible]	[illegible]	118	7.09	1665	118	7.09%	0.281952	0.000035	0.00564	0.001048	0.000017	0.0387	0.00088	0.28192	6.87	1.23	1.83	1.941411758	0.281725276	0.282039887	
[illegible]	[illegible]	[illegible]	[illegible]	[illegible]	[illegible]	[illegible]	[illegible]	[illegible]	[illegible]	[illegible]	[illegible]	[illegible]	[illegible]	[illegible]	109	7.30	1638	109	6.65%	0.282	0.000036	0.00564	0.00178	0.00011	0.0684	0.005	0.28194	7.17	1.26	1.80	1.900968489	0.281742725	0.282059828	
[illegible]	[illegible]	[illegible]	[illegible]	[illegible]	[illegible]	[illegible]	[illegible]	[illegible]	[illegible]	[illegible]	[illegible]	[illegible]	[illegible]	[illegible]	68.9	7.61	1819.9	68.9	3.79%	0.281664	0.000042	0.00563	0.000925	0.000022	0.0369	0.001	0.28163	0.25	1.47	2.22	2.487625469	0.281625003	0.28192529	
[illegible]	[illegible]	[illegible]	[illegible]	[illegible]	[illegible]	[illegible]	[illegible]	[illegible]	[illegible]	[illegible]	[illegible]	[illegible]	[illegible]	[illegible]	107	7.71	2219	107	4.82%	0.281278	0.000048	0.00563	0.000387	0.000046	0.0139	0.0014	0.28126	-3.68	1.68	2.71	3.053090161	0.281365312	0.281628499	
[illegible]	[illegible]	[illegible]	[illegible]	[illegible]	[illegible]	[illegible]	[illegible]	[illegible]	[illegible]	[illegible]	[illegible]	[illegible]	[illegible]	[illegible]	133	7.78	1696	133	7.84%	0.282	0.000042	0.00564	0.0009941	0.0000044	0.03898	0.0002	0.28197	9.33	1.47	1.76	1.807992201	0.281705232	0.282016979	
[illegible]	[illegible]	[illegible]	[illegible]	[illegible]	[illegible]	[illegible]	[illegible]	[illegible]	[illegible]	[illegible]	[illegible]	[illegible]	[illegible]	[illegible]	91.1	7.86	1834.5	91.1	4.97%	0.281508	0.000043	0.00563	0.000531	0.000011	0.0215	0.00058	0.28149	-4.47	1.51	2.41	2.799510793	0.281615537	0.281914471	
[illegible]	[illegible]	[illegible]	[illegible]	[illegible]	[illegible]	[illegible]	[illegible]	[illegible]	[illegible]	[illegible]	[illegible]	[illegible]	[illegible]	[illegible]	70.9	7.88	1613.9	70.9	4.39%	0.282147	0.000057	0.00564	0.00685	0.00048	0.279	0.021	0.28194	6.37	2.00	1.84	1.933590974	0.281758292	0.282077619	
[illegible]	[illegible]	[illegible]	[illegible]	[illegible]	[illegible]	[illegible]	[illegible]	[illegible]	[illegible]	[illegible]	[illegible]	[illegible]	[illegible]	[illegible]	115	8.40	1636	115	7.03%	0.282021	0.000036	0.00564	0.001106	0.000032	0.0409	0.0012	0.28199	8.61	1.26	1.74	1.806601112	0.281744017	0.282061305	
[illegible]	[illegible]	[illegible]	[illegible]	[illegible]	[illegible]	[illegible]	[illegible]	[illegible]	[illegible]	[illegible]	[illegible]	[illegible]	[illegible]	[illegible]	70	8.46	1579.8	70	4.43%	0.281954	0.000037	0.00564	0.001075	0.000035	0.0395	0.0014	0.28192	5.02	1.30	1.83	1.992775642	0.281780306	0.282102778	
[illegible]	[illegible]	[illegible]	[illegible]	[illegible]	[illegible]	[illegible]	[illegible]	[illegible]	[illegible]	[illegible]	[illegible]	[illegible]	[illegible]	[illegible]	59.7	8.59	1792	59.7	3.33%	0.281671	0.000036	0.00563	0.001467	0.00004	0.0551	0.0021	0.28162	-0.78	1.26	2.24	2.531162809	0.281643086	0.281945955	
[illegible]	[illegible]	[illegible]	[illegible]	[illegible]	[illegible]	[illegible]	[illegible]	[illegible]	[illegible]	[illegible]	[illegible]	[illegible]	[illegible]	[illegible]	92.9	8.60	1487	92.9	6.25%	0.282062	0.00004	0.00564	0.00254	0.00027	0.096	0.011	0.28199	5.34	1.40	1.75	1.899225253	0.281840145	0.282171166	Omitted from MDA calculation
[illegible]	[illegible]	[illegible]	[illegible]	[illegible]	[illegible]	[illegible]	[illegible]	[illegible]	[illegible]	[illegible]	[illegible]	[illegible]	[illegible]	[illegible]	82.5	8.92	1756.6	82.5	4.70%	0.281876	0.000045	0.00564	0.001474	0.000036	0.04996	0.00044	0.28183	5.71	1.58	1.96	2.088397649	0.281666015	0.28197216	
[illegible]	[illegible]	[illegible]	[illegible]	[illegible]	[illegible]	[illegible]	[illegible]	[illegible]	[illegible]	[illegible]	[illegible]	[illegible]	[illegible]	[illegible]	50.9	9.25	1651.3	50.9	3.08%	0.282032	0.000042	0.00564	0.002922	0.000041	0.1176	0.0012	0.28194	7.33	1.47	1.81	1.90138535	0.281734131	0.282050007	
[illegible]	[illegible]	[illegible]	[illegible]	[illegible]	[illegible]	[illegible]	[illegible]	[illegible]	[illegible]	[illegible]	[illegible]	[illegible]	[illegible]	[illegible]	109	9.34	1561	109	6.98%	0.282134	0.000042	0.00564	0.001479	0.000035	0.0566	0.0016	0.28209	10.57	1.47	1.60	1.621305604	0.281792437	0.282116642	
[illegible]	[illegible]	[illegible]	[illegible]	[illegible]	[illegible]	[illegible]	[illegible]	[illegible]	[illegible]	[illegible]	[illegible]	[illegible]	[illegible]	[illegible]	66.3	9.36	1652.7	66.3	4.01%	0.281743	0.000041	0.00564	0.00129	0.00023	0.056	0.011	0.28170	-1.09	1.44	2.13	2.440525528	0.281733226	0.282048973	
[illegible]	[illegible]	[illegible]	[illegible]	[illegible]	[illegible]	[illegible]	[illegible]	[illegible]	[illegible]	[illegible]	[illegible]	[illegible]	[illegible]	[illegible]	143	9.42	1595	143	8.97%	0.282057	0.000046	0.00564	0.003396	0.000067	0.135	0.0026	0.28195	6.53	1.61	1.80	1.908244388	0.281770495	0.282091566	
[illegible]	[illegible]	[illegible]	[illegible]	[illegible]	[illegible]	[illegible]	[illegible]	[illegible]	[illegible]	[illegible]	[illegible]	[illegible]	[illegible]	[illegible]	88.7	9.43	1729.2	88.7	5.13%	0.281793	0.00004	0.00564	0.000798	0.000019	0.03044	0.00084	0.28177	2.95	1.40	2.04	2.24363654	0.281683752	0.281992431	
[illegible]	[illegible]	[illegible]	[illegible]	[illegible]	[illegible]	[illegible]	[illegible]	[illegible]	[illegible]	[illegible]	[illegible]	[illegible]	[illegible]	[illegible]	109	9.51	1634	109	6.67%	0.282005	0.00004	0.00564	0.0011764	0.0000098	0.045	0.00057	0.28197	7.93	1.40	1.76	1.849380271	0.281745309	0.282062782	
[illegible]	[illegible]	[illegible]	[illegible]	[illegible]	[illegible]	[illegible]	[illegible]	[illegible]	[illegible]	[illegible]	[illegible]	[illegible]	[illegible]	[illegible]	84	9.59	1562.5	84	5.38%	0.282081	0.000049	0.00564	0.00195	0.00044	0.104	0.027	0.28202	8.23	1.72	1.69	1.773346228	0.281791469	0.282115536	
[illegible]	[illegible]	[illegible]	[illegible]	[illegible]	[illegible]	[illegible]	[illegible]	[illegible]	[illegible]	[illegible]	[illegible]	[illegible]	[illegible]	[illegible]	76.3	9.67	1623.2	76.3	4.70%	0.282032	0.000037	0.00564	0.001413	0.000055	0.053	0.002	0.28199	8.39	1.30	1.74	1.811188323	0.281752285	0.282070755	
[illegible]	[illegible]	[illegible]	[illegible]	[illegible]	[illegible]	[illegible]	[illegible]	[illegible]	[illegible]	[illegible]	[illegible]	[illegible]	[illegible]	[illegible]	86	9.74	1612	86	5.33%	0.28197	0.000034	0.00564	0.002155	0.00003	0.0789	0.0012	0.28190	5.14	1.19	1.86	2.011035057	0.281759519	0.282079021	
[illegible]	[illegible]	[illegible]	[illegible]	[illegible]	[illegible]	[illegible]	[illegible]	[illegible]	[illegible]	[illegible]	[illegible]	[illegible]	[illegible]	[illegible]	77.3	10.38	1650.9	77.3	4.68%	0.282023	0.00004	0.00564	0.001755	0.000021	0.07064	0.00085	0.28197	8.30	1.40	1.77	1.83887388	0.281734389	0.282050302	> 10% Discordant, excluded
[illegible]	[illegible]	[illegible]	[illegible]	[illegible]	[illegible]	[illegible]	[illegible]	[illegible]	[illegible]	[illegible]	[illegible]	[illegible]	[illegible]	[illegible]	70.9	10.64	1808.5	70.9	3.92%	0.281633	0.000053	0.00563	0.0027	0.00047	0.14	0.03	0.28154	-3.27	1.86	2.38	2.702350854	0.281632393	0.281933735	> 10% Discordant, excluded
[illegible]	[illegible]	[illegible]	[illegible]	[illegible]	[illegible]	[illegible]	[illegible]	[illegible]	[illegible]	[illegible]	[illegible]	[illegible]	[illegible]	[illegible]	106	11.01	1578	106	6.72%	0.282026	0.000032	0.00564	0.001654	0.000055	0.0644	0.002	0.28198	6.92	1.12	1.76	1.869377062	0.281781468	0.282104106	> 10% Discordant, excluded
[illegible]	[illegible]	[illegible]	[illegible]	[illegible]	[illegible]	[illegible]	[illegible]	[illegible]	[illegible]	[illegible]	[illegible]	[illegible]	[illegible]	[illegible]	86.9	11.04	1537.1	86.9	5.65%	0.28213	0.000048	0.00564	0.002141	0.000055	0.0781	0.0019	0.28207	9.22	1.68	1.63	1.689318958	0.281807853	0.28213426	> 10% Discordant, excluded
[illegible]	[illegible]	[illegible]	[illegible]	[illegible]	[illegible]	[illegible]	[illegible]	[illegible]	[illegible]	[illegible]	[illegible]	[illegible]	[illegible]	[illegible]	85.2	11.10	1634.4	85.2	5.21%	0.281999	0.000032	0.00564	0.00266	0.00011	0.1002	0.0058	0.28192	6.09	1.12	1.84	1.967488467	0.28174505	0.282062486	> 10% Discordant, excluded
[illegible]	[illegible]	[illegible]	[illegible]	[illegible]	[illegible]	[illegible]	[illegible]	[illegible]	[illegible]	[illegible]	[illegible]	[illegible]	[illegible]	[illegible]	77.4	11.13	1645.4	77.4	4.70%	0.282082	0.000041	0.00564	0.00334	0.00014	0.1391	0.0055	0.28198	8.52	1.44	1.76	1.820285178	0.281737943	0.282054364	> 10% Discordant, excluded
[illegible]	[illegible]	[illegible]	[illegible]	[illegible]	[illegible]	[illegible]	[illegible]	[illegible]	[illegible]	[illegible]	[illegible]	[illegible]	[illegible]	[illegible]	66.6	11.25	1849	66.6	3.60%	0.281764	0.000037	0.00564	0.000798	0.000036	0.0312	0.0015	0.28174	4.61	1.30	2.08	2.23195155	0.281606134	0.281903724	> 10% Discordant, excluded
[illegible]	[illegible]	[illegible]	[illegible]	[illegible]	[illegible]	[illegible]	[illegible]	[illegible]	[illegible]	[illegible]	[illegible]	[illegible]	[illegible]	[illegible]	72.1	11.28	1639.9	72.1	4.40%	0.282065	0.000039	0.00564	0.00358	0.00015	0.1431	0.0065	0.28195	7.54	1.37	1.79	1.879066988	0.281741497	0.282058425	> 10% Discordant, excluded
[illegible]	[illegible]	[illegible]	[illegible]	[illegible]	[illegible]	[illegible]	[illegible]	[illegible]	[illegible]	[illegible]	[illegible]	[illegible]	[illegible]	[illegible]	112	11.29	1691	112	6.62%	0.28197	0.000042	0.00564	0.001601	0.000016	0.06258	0.00096	0.28192	7.46	1.47	1.83	1.924149987	0.281708466	0.282020675	> 10% Discordant, excluded
[illegible]	[illegible]	[illegible]	[illegible]	[illegible]	[illegible]	[illegible]	[illegible]	[illegible]	[illegible]	[illegible]	[illegible]	[illegible]	[illegible]	[illegible]	78.2	11.40	1783.6	78.2	4.38%	0.281639	0.000037	0.00563	0.00096	0.000019	0.043	0.01	0.28161	-1.49	1.30	2.26	2.569827025	0.281648528	0.281952175	> 10% Discordant, excluded
[illegible]	[illegible]	[illegible]	[illegible]	[illegible]	[illegible]	[illegible]	[illegible]	[illegible]	[illegible]	[illegible]	[illegible]	[illegible]	[illegible]	[illegible]	74.2	11.93	1692.3	74.2	4.38%	0.281874	0.000034	0.00564	0.001607	0.000066	0.0565	0.0023	0.28182	4.08	1.19	1.97	2.14237097	0.281707625	0.282019714	> 10% Discordant, excluded
[illegible]	[illegible]	[illegible]	[illegible]	[illegible]	[illegible]	[illegible]	[illegible]	[illegible]	[illegible]	[illegible]	[illegible]	[illegible]	[illegible]	[illegible]	75.6	11.95	1645.4	75.6	4.59%	0.281946	0.000037	0.00564	0.001302	0.000028	0.044	0.0018	0.28191	5.94	1.30	1.85	1.985596811	0.281737943	0.282054364	> 10% Discordant, excluded
[illegible]	[illegible]	[illegible]	[illegible]	[illegible]	[illegible]	[illegible]	[illegible]	[illegible]	[illegible]	[illegible]	[illegible]	[illegible]	[illegible]	[illegible]	91.9	11.96	1604.5	91.9	5.73%	0.281943	0.000038	0.00564	0.001918	0.000038	0.0738	0.0013	0.28188	4.27	1.33	1.89	2.060422547	0.281764362	0.282084556	> 10% Discordant, excluded
[illegible]	[illegible]	[illegible]	[illegible]	[illegible]	[illegible]	[illegible]	[illegible]	[illegible]	[illegible]	[illegible]	[illegible]	[illegible]	[illegible]	[illegible]	107	12.02	1642	107	6.52%	0.281994	0.000034	0.00564	0.00144	0.00013	0.055	0.0045	0.28195	7.42	1.19	1.79	1.888115787	0.28174014	0.282056875	> 10% Discordant, excluded
[illegible]	[illegible]	[illegible]	[illegible]	[illegible]	[illegible]	[illegible]	[illegible]	[illegible]	[illegible]	[illegible]	[illegible]	[illegible]	[illegible]	[illegible]	82	12.59	1670.9	82	4.91%	0.282124	0.000046	0.00564	0.00357	0.00011	0.1438	0.004	0.28201	10.28	1.61	1.71	1.727077045	0.281721462	0.282035528	> 10% Discordant, excluded
[illegible]	[illegible]	[illegible]	[illegible]	[illegible]	[illegible]	[illegible]	[illegible]	[illegible]	[illegible]	[illegible]	[illegible]	[illegible]	[illegible]	[illegible]	119	12.60	1660	119	7.17%	0.282007	0.000038	0.00564	0.001396	0.000049	0.0533	0.0024	0.28196	8.33	1.33	1.77	1.844086637	0.281728508	0.282043581	> 10% Discordant, excluded
[illegible]	[illegible]	[illegible]	[illegible]	[illegible]	[illegible]	[illegible]	[illegible]	[illegible]	[illegible]	[illegible]	[illegible]	[illegible]	[illegible]	[illegible]	121	12.64	1713	121	7.06%	0.281967	0.00004	0.00564	0.001095	0.000019	0.04284	0.00062	0.28193	8.42	1.40	1.81	1.8799188	0.281694235	0.282004411	> 10% Discordant, excluded
[illegible]	[illegible]	[illegible]	[illegible]	[illegible]	[illegible]	[illegible]	[illegible]	[illegible]	[illegible]	[illegible]	[illegible]	[illegible]	[illegible]	[illegible]	139	13.11	1843	139	7.54%	0.282019	0.000043	0.00564	0.000967	0.000017	0.03734	0.00072	0.28199	13.32	1.51	1.73	1.666239602	0.281610025	0.281908172	> 10% Discordant, excluded
[illegible]	[illegible]	[illegible]	[illegible]	[illegible]	[illegible]	[illegible]	[illegible]	[illegible]	[illegible]	[illegible]	[illegible]	[illegible]	[illegible]	[illegible]	80.7	13.22	1656.4	80.7	4.87%	0.282017	0.000038	0.00564	0.002155	0.000046	0.0824	0.0021	0.28195	7.76	1.33	1.79	1.877867791	0.281730835	0.28204624	> 10% Discordant, excluded
[illegible]	[illegible]	[illegible]	[illegible]	[illegible]	[illegible]	[illegible]	[illegible]	[illegible]	[illegible]	[illegible]	[illegible]	[illegible]	[illegible]	[illegible]	101	13.39	1680	101	6.01%	0.282143	0.000037	0.00564	0.00267	0.00013	0.1117	0.0055	0.28206	12.16	1.30	1.64	1.61301439	0.281715579	0.282028804	> 10% Discordant, excluded
[illegible]	[illegible]	[illegible]	[illegible]	[illegible]	[illegible]	[illegible]	[illegible]	[illegible]	[illegible]	[illegible]	[illegible]	[illegible]	[illegible]	[illegible]	71.1	13.49	1798.6	71.1	3.95%	0.281746	0.000034	0.00564	0.001547	0.000025	0.0574	0.0022	0.28169	1.93	1.19	2.14	2.363519642	0.281638809	0.281941067	> 10% Discordant, excluded
[illegible]	[illegible]	[illegible]	[illegible]	[illegible]	[illegible]	[illegible]	[illegible]	[illegible]	[illegible]	[illegible]	[illegible]	[illegible]	[illegible]	[illegible]	46.6	13.53	3253.3	46.6	1.43%	0.280709	0.000039	0.00561	0.002348	0.000036	0.1014	0.0023	0.28056	-4.31	1.37	3.65	3.906613992	0.280683236	0.280848983	> 10% Discordant, excluded
[illegible]	[illegible]	[illegible]	[illegible]	[illegible]	[illegible]	[illegible]	[illegible]	[illegible]	[illegible]	[illegible]	[illegible]	[illegible]	[illegible]	[illegible]	72.4	13.91	1627	72.4	4.45%	0.282132	0.000032	0.00564	0.00134	0.00014	0.0474	0.005	0.28209	12.10	1.12	1.59	1.574805793	0.281749831	0.282067949	> 10% Discordant, excluded
[illegible]	[illegible]	[illegible]	[illegible]	[illegible]	[illegible]	[illegible]	[illegible]	[illegible]	[illegible]	[illegible]	[illegible]	[illegible]	[illegible]	[illegible]	87.4	13.94	1806.8	87.4	4.84%	0.28165	0.000045	0.00563	0.000785	0.000027	0.0307	0.0013	0.28162	-0.37	1.58	2.23	2.516766354	0.281633495	0.281934994	> 10% Discordant, excluded
[illegible]	[illegible]	[illegible]	[illegible]	[illegible]	[illegible]	[illegible]	[illegible]	[illegible]	[illegible]	[illegible]	[illegible]	[illegible]	[illegible]	[illegible]	97.4	13.95	1907	97.4	5.11%	0.281428	0.000043	0.00563	0.000829	0.000064	0.0341	0.0034	0.28140	-6.06	1.51	2.54	2.956941535	0.281568493	0.281860706	> 10% Discordant, excluded
[illegible]	[illegible]	[illegible]	[illegible]	[illegible]	[illegible]	[illegible]	[illegible]	[illegible]	[illegible]	[illegible]	[illegible]	[illegible]	[illegible]	[illegible]	115	14.00	1758	115	6.54%	0.28196	0.000045	0.00564	0.001512	0.00004	0.0581	0.0018	0.28191	8.68	1.58	1.84	1.898781166	0.281665108	0.281971124	> 10% Discordant, excluded
[illegible]	[illegible]	[illegible]	[illegible]	[illegible]	[illegible]	[illegible]	[illegible]	[illegible]	[illegible]	[illegible]	[illegible]	[illegible]	[illegible]	[illegible]	101	14.36	1618	101	6.24%	0.282152	0.000048	0.00564	0.003912	0.000081	0.1594	0.0034	0.28203	9.81	1.68	1.68	1.715158552	0.281755644	0.282074593	> 10% Discordant, excluded
[illegible]	[illegible]	[illegible]	[illegible]	[illegible]	[illegible]	[illegible]	[illegible]	[illegible]	[illegible]	[illegible]	[illegible]	[illegible]	[illegible]	[illegible]	89.9	14.52	1654.5	89.9	5.43%	0.281741	0.00004	0.00563	0.000902	0.000036	0.0357	0.0018	0.28171	-0.69	1.40	2.12	2.416479364	0.281732063	0.282047643	> 10% Discordant, excluded
[illegible]	[illegible]	[illegible]	[illegible]	[illegible]	[illegible]	[illegible]	[illegible]	[illegible]	[illegible]	[illegible]	[illegible]	[illegible]	[illegible]	[illegible]	89.4	14.81	1754.9	89.4	5.09%	0.281666	0.000046	0.00563	0.002039	0.000095	0.0787	0.002	0.28160	-2.45	1.61	2.29	2.607948938	0.281667116	0.281973418	> 10% Discordant, excluded
[illegible]	[illegible]	[illegible]	[illegible]	[illegible]	[illegible]	[illegible]	[illegible]	[illegible]	[illegible]	[illegible]	[illegible]	[illegible]	[illegible]	[illegible]	123	15.74	1703	123	7.22%	0.281993	0.000037	0.00564	0.001556	0.00005	0.0604	0.0021	0.28194	8.59	1.30	1.80	1.860916459	0.281700704	0.282011805	> 10% Discordant, excluded
[illegible]	[illegible]	[illegible]	[illegible]	[illegible]	[illegible]	[illegible]	[illegible]	[illegible]	[illegible]	[illegible]	[illegible]	[illegible]	[illegible]	[illegible]	62.8	16.99	2387.8	62.8	2.63%	0.281234	0.000031	0.00562	0.001152	0.000028	0.0468	0.0012	0.28118	-2.61	1.09	2.83	3.117818772	0.281254892	0.281502305	> 10% Discordant, excluded
[illegible]	[illegible]	[illegible]	[illegible]	[illegible]	[illegible]	[illegible]	[illegible]	[illegible]	[illegible]	[illegible]	[illegible]	[illegible]	[illegible]	[illegible]	70.3	18.29	2233.8	70.3	3.15%	0.281467	0.000034	0.00563	0.00156	0.00014	0.063	0.0062	0.28140	1.60	1.19	2.53	2.728324788	0.281355645	0.281617451	> 10% Discordant, excluded
[illegible]	[illegible]	[illegible]	[illegible]	[illegible]	[illegible]	[illegible]	[illegible]	[illegible]	[illegible]	[illegible]	[illegible]	[illegible]	[illegible]	[illegible]	55.1	18.37	1768.5	55.1	3.12%	0.281732	0.000039	0.00563	0.00178	0.00016	0.0699	0.0072	0.28167	0.50	1.37	2.18	2.431284061	0.281658309	0.281963353	> 10% Discordant, excluded
[illegible]	[illegible]	[illegible]	[illegible]	[illegible]	[illegible]	[illegible]	[illegible]	[illegible]	[illegible]	[illegible]	[illegible]	[illegible]	[illegible]	[illegible]	58.2	18.49	1783.6	58.2	3.26%	0.281765	0.000037	0.00564	0.001411	0.000019	0.0553	0.001	0.28172	2.44	1.30	2.11	2.319170942	0.281648528	0.281952175	> 10% Discordant, excluded
[illegible]	[illegible]	[illegible]	[illegible]	[illegible]	[illegible]	[illegible]	[illegible]	[illegible]	[illegible]	[illegible]	[illegible]	[illegible]	[illegible]	[illegible]	175	18.78	1787	175	9.79%	0.282087	0.000032	0.00564	0.00348	0.00012	0.1339	0.0054	0.28197	11.46	1.12	1.76	1.742508309	0.281646325	0.281949657	> 10% Discordant, excluded
[illegible]	[illegible]	[illegible]	[illegible]	[illegible]	[illegible]	[illegible]	[illegible]	[illegible]	[illegible]	[illegible]	[illegible]	[illegible]	[illegible]	[illegible]	86.8	20.23	1639.9	86.8	5.29%	0.28208	0.00011	0.00564	0.00583	0.00083	0.251	0.044	0.28190	5.59	3.85	1.89	2.004108841	0.281741497	0.282058425	> 10% Discordant, excluded
[illegible]	[illegible]	[illegible]	[illegible]	[illegible]	[illegible]	[illegible]	[illegible]	[illegible]	[illegible]	[illegible]	[illegible]	[illegible]	[illegible]	[illegible]	67.1	20.30	1617.7	67.1	4.15%	0.282073	0.00005	0.00564	0.00241	0.00025	0.1	0.013	0.28200	8.64	1.75	1.73	1.790726048	0.281755838	0.282074814	> 10% Discordant, excluded
[illegible]	[illegible]	[illegible]	[illegible]	[illegible]	[illegible]	[illegible]	[illegible]	[illegible]	[illegible]	[illegible]	[illegible]	[illegible]	[illegible]	[illegible]	108	20.63	1655	108	6.53%	0.28215	0.000053	0.00564	0.00328	0.00017	0.1248	0.0043	0.28205	11.20	1.86	1.65	1.655211009	0.28173174	0.282047274	> 10% Discordant, excluded
[illegible]	[illegible]	[illegible]	[illegible]	[illegible]	[illegible]	[illegible]	[illegible]	[illegible]	[illegible]	[illegible]	[illegible]	[illegible]	[illegible]	[illegible]	75.3	21.28	1656.4	75.3	4.55%	0.282062	0.000048	0.00564	0.00269	0.00015	0.1005	0.0062	0.28198	8.76	1.68	1.75	1.813443249	0.281730835	0.28204624	> 10% Discordant, excluded
[illegible]	[illegible]	[illegible]	[illegible]	[illegible]	[illegible]	[illegible]	[illegible]	[illegible]	[illegible]	[illegible]	[illegible]	[illegible]	[illegible]	[illegible]	58.1	21.47	1602.6	58.1	3.63%	0.282086	0.000035	0.00564	0.002238	0.000051	0.07634	0.00099	0.28202	8.96	1.23	1.70	1.757866699	0.281765588	0.282085958	> 10% Discordant, excluded
[illegible]	[illegible]	[illegible]	[illegible]	[illegible]	[illegible]	[illegible]	[illegible]	[illegible]	[illegible]	[illegible]	[illegible]	[illegible]	[illegible]	[illegible]	96.9	22.36	1661.8	96.9	5.83%	0.281755	0.000042	0.00564	0.001066	0.000026	0.0411	0.0011	0.28172	-0.21	1.47	2.11	2.391909627	0.281727345	0.282042251	> 10% Discordant, excluded
[illegible]	[illegible]	[illegible]	[illegible]	[illegible]	[illegible]	[illegible]	[illegible]	[illegible]	[illegible]	[illegible]	[illegible]	[illegible]	[illegible]	[illegible]	81.4	23.05	1834.5	81.4	4.44%	0.281595	0.000038	0.00563	0.00172	0.00012	0.0795	0.0053	0.28154	-2.86	1.33	2.37	2.696750437	0.281615537	0.281914471	> 10% Discordant, excluded
[illegible]	[illegible]	[illegible]	[illegible]	[illegible]	[illegible]	[illegible]	[illegible]	[illegible]	[illegible]	[illegible]	[illegible]	[illegible]	[illegible]	[illegible]	123	24.70	1533	123	8.02%	0.282048	0.000052	0.00564	0.00274	0.00029	0.104	0.011	0.28197	5.61	1.82	1.78	1.918290446	0.281810497	0.282137282	> 10% Discordant, excluded
[illegible]	[illegible]	[illegible]	[illegible]	[illegible]	[illegible]	[illegible]	[illegible]	[illegible]	[illegible]	[illegible]	[illegible]	[illegible]	[illegible]	[illegible]	58.8	28.07	1753.2	58.8	3.35%	0.281846	0.000033	0.00564	0.002177	0.00008	0.0643	0.0022	0.28177	3.74	1.16	2.04	2.211886828	0.281668216	0.281974676	> 10% Discordant, excluded
[illegible]	[illegible]	[illegible]	[illegible]	[illegible]	[illegible]	[illegible]	[illegible]	[illegible]	[illegible]	[illegible]	[illegible]	[illegible]	[illegible]	[illegible]	347	29.50	2322	347	14.94%	0.282011	0.000043	0.00564	0.002354	0.000056	0.0889	0.0026	0.28191	21.64	1.51	1.81	1.501670215	0.281297976	0.281551544	> 10% Discordant, excluded
[illegible]	[illegible]	[illegible]	[illegible]	[illegible]	[illegible]	[illegible]	[illegible]	[illegible]	[illegible]	[illegible]	[illegible]	[illegible]	[illegible]	[illegible]	119	30.34	1712	119	6.95%	0.281897	0.000032	0.00564	0.000969	0.000031	0.0388	0.0011	0.28187	6.06	1.12	1.90	2.030907016	0.281694882	0.282005151	> 10% Discordant, excluded
[illegible]	[illegible]	[illegible]	[illegible]	[illegible]	[illegible]	[illegible]	[illegible]	[illegible]	[illegible]	[illegible]	[illegible]	[illegible]	[illegible]	[illegible]	61.9	30.80	1765.1	61.9	3.51%	0.281786	0.000046	0.00564	0.003126	0.000076	0.1254	0.0024	0.28168	0.74	1.61	2.18	2.413049351	0.281660511	0.281965869	> 10% Discordant, excluded
[illegible]	[illegible]	[illegible]	[illegible]	[illegible]	[illegible]	[illegible]	[illegible]	[illegible]	[illegible]	[illegible]	[illegible]	[illegible]	[illegible]	[illegible]	105	31.46	1998	105	5.26%	0.282013	0.000042	0.00564	0.001095	0.000092	0.0453	0.0053	0.28197	16.41	1.47	1.75	1.587854207	0.281509354	0.281793119	> 10% Discordant, excluded
[illegible]	[illegible]	[illegible]	[illegible]	[illegible]	[illegible]	[illegible]	[illegible]	[illegible]	[illegible]	[illegible]	[illegible]	[illegible]	[illegible]	[illegible]	61.1	32.56	1636.2	61.1	3.73%	0.281632	0.000036	0.00563	0.001882	0.000097	0.0745	0.0059	0.28157	-6.04	1.26	2.32	2.741728782	0.281743888	0.282061157	> 10% Discordant, excluded
[illegible]	[illegible]	[illegible]	[illegible]	[illegible]	[illegible]	[illegible]	[illegible]	[illegible]	[illegible]	[illegible]	[illegible]	[illegible]	[illegible]	[illegible]	132	39.51	1726	132	7.65%	0.282218	0.00005	0.00564	0.00294	0.00012	0.116	0.0055	0.28212	15.48	1.75	1.54	1.434140873	0.281685823	0.281994798	> 10% Discordant, excluded
[illegible]	[illegible]	[illegible]	[illegible]	[illegible]	[illegible]	[illegible]	[illegible]	[illegible]	[illegible]	[illegible]	[illegible]	[illegible]	[illegible]	[illegible]	84.9	41.05	1480.9	84.9	5.73%	0.2861	0.0014	0.00589	0.0212	0.0055	1.31	0.34	0.28551	129.94	49.00	-9.71	-6.751965571	0.281844075	0.282175657	> 10% Discordant, excluded
[illegible]	[illegible]	[illegible]	[illegible]	[illegible]	[illegible]	[illegible]	[illegible]	[illegible]	[illegible]	[illegible]	[illegible]	[illegible]	[illegible]	[illegible]	125	50.15	1733	125	7.21%	0.282032	0.000044	0.00564	0.0013	0.00019	0.0538	0.0095	0.28199	10.93	1.54	1.73	1.733740813	0.281681293	0.28198962	> 10% Discordant, excluded

Appendix D3.1 continued.

Curtin University Geohistory center							Isotopic Ratios					Apparent Ages - Calculated in Isoplot R (Ma)				Discord	Perferred age *1500 Ma cutoff		error %	Lu-Hf Isotopic Ratios from Iolite							εHf Calculations							Analysis Notes
Sample ID	Analysis date-time	Spot ID	238U conc. (ppm)	±2σ INT	232Th conc. (ppm)	±2σ INT	238U/206Pb	±2σ PROP	207Pb/206Pb	±2σ PROP	rho	238U/206Pb	±2σ PROP	207Pb/206Pb	±2σ PROP	(7/6-6/8)/7/6 *100	Ma	2σ		176Hf/177Hf (0.282785, 0.283250)	±2σ INT	(2% External ε)	176Lu/177Hf (0.03360 Bouvier et al., 2008 EPSL-273)	±2σ INT	176Yb/177Hf (0.03840 Griffin et al., 2002, Lithos-237)	±2σ INT	Hf(i)	εHf (Lu decay)	±2σ (0.02)	TDM(Ga) (Scherer et al., 2001, Science-293)	TDMCrustal (Ga)	HfCHUR(t)	HfDM(t)	
12DTB19	08/04/2020 (4) 21:59:37.00	12DTB19 - 123	86.7	1.2	3.3	0.039	3.576538	0.22223866	0.0975	0.00595	0.051865	1589.3	83.6	1576	114	-0.84	1576	114	7.23%	0.281975	0.000039	0.005639635	0.001682	0.000029	0.06463	0.00066	0.28192	5.04	1.37	1.83	1.98858953	0.281782758	0.282105581	
12DTB19	08/04/2020 (4) 17:35:20.00	12DTB19 - 25	582	12	19	0.041	3.04878	0.274762	0.1114	0.004728	-0.34226	1829	143	1821.6	77	-0.41	1821.6	77	4.23%	0.281674	0.00005	0.005633702	0.001969	0.000098	0.0776	0.0059	0.28161	-0.64	1.75	2.27	2.545528215	0.281623901	0.28192403	
12DTB19	08/04/2020 (4) 18:44:49.00	12DTB19 - 50	123.6	1.6	1.6	0.046	3.292723	0.19595876	0.1047	0.005294	0.093776	1709.6	89.4	1708.2	93	-0.08	1708.2	93	5.44%	0.281803	0.000035	0.005636169	0.0007548	0.0000027	0.03024	0.00029	0.28178	2.88	1.23	2.02	2.231278495	0.28169734	0.28200796	
12DTB19	08/04/2020 (4) 19:40:23.00	12DTB19 - 73	124	18	3.3	0.056	3.332223	0.23099266	0.1042	0.005984	0.02903	1691.8	94.2	1699	106	0.42	1699	106	6.24%	0.281833	0.000036	0.005636775	0.00257	0.00003	0.1016	0.0057	0.28175	1.67	1.26	2.08	2.301680457	0.281703291	0.282014762	
12DTB19	08/04/2020 (4) 20:26:22.00	12DTB19 - 86	212.2	9.9	2.9	0.026	3.320053	0.19867406	0.1055	0.00501	0.18013	1697.3	89.3	1722.2	87.2	1.45	1722.2	87.2	5.06%	0.281781	0.000037	0.005635741	0.001215	0.000014	0.051	0.00035	0.28174	1.88	1.30	2.08	2.306222231	0.281688282	0.281997608	
12DTB19	08/04/2020 (4) 17:11:20.00	12DTB19 - 18	157.3	3	5.6	0.037	3.653635	0.2195123	0.098	0.00456	0.21615	1559.6	83.4	1585.6	87	1.64	1585.6	87	5.49%	0.282044	0.000045	0.005641059	0.001655	0.000015	0.06868	0.00088	0.28199	7.73	1.58	1.73	1.823771679	0.281779163	0.2820985	
12DTB19	08/04/2020 (4) 21:21:53.00	12DTB19 - 109	183.4	8	8.6	0.03	3.792188	0.23403136	0.0956	0.005312	0.11737	1508.7	83	1539	105	1.97	1539	105	6.82%	0.282104	0.000039	0.005642215	0.00216	0.00002	0.06891	0.00093	0.28207	9.25	1.37	1.63	1.688990219	0.281806627	0.28213286	
12DTB19	08/04/2020 (4) 16:47:40.00	12DTB19 - 6	144.5	2.7	2.8	0.045	3.738318	0.22849156	0.0969	0.00508	-0.023709	1528.1	83.2	1564.4	97.5	2.32	1564.4	97.5	6.23%	0.281911	0.000041	0.005638369	0.000823	0.000012	0.0334	0.00072	0.28189	3.42	1.44	1.88	2.083183126	0.281790243	0.282114135	
12DTB19	08/04/2020 (4) 16:41:40.00	12DTB19 - 3	123.9	5.7	8.7	0.034	4.135649	0.25374898	0.0903	0.005906	0.075724	1396	77	1431	125	2.45	1396	77	5.52%	0.282065	0.000035	0.005641409	0.00133	0.000053	0.05	0.002	0.28203	4.65	1.23	1.69	1.87095121	0.281898723	0.282238112	
12DTB19	08/04/2020 (4) 22:01:37.00	12DTB19 - 124	218	20	35	0.035	3.273322	0.20875674	0.1078	0.004756	-0.21463	1718.5	94.4	1761.7	80.6	2.45	1761.7	80.6	4.58%	0.281767	0.000045	0.005633552	0.00063	0.000036	0.02815	0.0099	0.28175	2.96	1.58	2.07	2.268970925	0.281662712	0.281968386	
12DTB19	08/04/2020 (4) 21:31:42.00	12DTB19 - 114	95.2	2.4	2	0.048	3.773585	0.2321111	0.0968	0.005736	0.13009	1515.4	83.1	1563	111	3.05	1563	111	7.10%	0.282006	0.000034	0.005640222	0.001327	0.000018	0.0524	0.0011	0.28197	6.23	1.19	1.77	1.902016528	0.281791147	0.282115168	
12DTB19	08/04/2020 (4) 21:47:47.00	12DTB19 - 117	248	27	10	0.03	3.193868	0.19648766	0.111	0.00432	0.063682	1755.9	94.6	1815	70.7	3.26	1815	70.7	3.90%	0.281797	0.000047	0.005636136	0.001623	0.000033	0.0609	0.0015	0.28174	4.01	1.65	2.08	2.243607851	0.28162813	0.28192892	
12DTB19	08/04/2020 (4) 20:32:14.00	12DTB19 - 89	133.8	5.9	9.1	0.039	3.471017	0.21099584	0.1039	0.005878	0.26959	1632	88.9	1694	104	3.66	1694	104	6.14%	0.281822	0.000041	0.005636589	0.000717	0.000053	0.0287	0.0025	0.28180	3.28	1.44	1.99	2.196558199	0.281706625	0.282018458	
12DTB19	08/04/2020 (4) 20:34:15.00	12DTB19 - 90	148.3	2.7	6.2	0.034	3.63901	0.2184465	0.1004	0.005408	0.28717	1565.1	83.4	1631	100	4.04	1631	100	6.13%	0.28198	0.000035	0.005639709	0.001741	0.000031	0.0701	0.0018	0.28193	6.35	1.23	1.83	1.948037404	0.281747247	0.282064996	
12DTB19	08/04/2020 (4) 17:53:00.00	12DTB19 - 34	264.8	5.3	6.4	0.031	3.573981	0.21338642	0.1022	0.004044	0.13283	1590.4	83.6	1663.6	73.2	4.40	1663.6	73.2	4.40%	0.281835	0.000039	0.005636835	0.0011859	0.0000098	0.04741	0.0005	0.28180	2.54	1.37	2.00	2.228206509	0.281726181	0.282040921	
12DTB19	08/04/2020 (4) 17:41:11.00	12DTB19 - 28	147.3	2.5	3	0.039	3.627131	0.21725952	0.1011	0.004722	0.43358	1569.7	83.4	1643.6	86.7	4.50	1643.6	86.7	5.28%	0.281885	0.000038	0.005637828	0.00099	0.000013	0.04231	0.00088	0.28185	4.08	1.33	1.92	2.103366883	0.281739106	0.282055693	
12DTB19	08/04/2020 (4) 19:30:33.00	12DTB19 - 68	176.1	9.2	19	0.026	3.619254	0.22957308	0.1018	0.005436	0.46169	1572.7	88.5	1656.4	98.9	5.05	1656.4	98.9	5.97%	0.281934	0.000035	0.005638789	0.001208	0.000043	0.0463	0.0021	0.28190	5.87	1.23	1.86	1.999334116	0.281730805	0.28204624	
12DTB19	08/04/2020 (4) 16:56:39.00	12DTB19 - 10	175.4	2.5	7.5	0.033	3.769318	0.23167166	0.0988	0.005476	0.036956	1516.9	83.1	1601	103	5.25	1601	103	6.43%	0.281948	0.000035	0.005638983	0.001271	0.000015	0.04508	0.00068	0.28191	5.07	1.23	1.85	2.006559456	0.281766823	0.282087139	
12DTB19	08/04/2020 (4) 20:10:19.00	12DTB19 - 83	98.5	1.9	1.8	0.032	3.745318	0.22920786	0.0994	0.006288	0.32034	1525.6	83.1	1612	118	5.36	1612	118	7.32%	0.281926	0.000033	0.005638617	0.001138	0.000019	0.04495	0.00085	0.28189	4.61	1.16	1.88	2.046668142	0.281759519	0.282079021	
12DTB19	08/04/2020 (4) 19:06:35.00	12DTB19 - 61	105.7	7.9	14	0.041	3.685957	0.22316814	0.1011	0.00642	0.23916	1547.4	83.3	1644	118	5.88	1644	118	7.18%	0.282004	0.000041	0.005640093	0.000828	0.000077	0.0324	0.003	0.28175	6.84	1.72	1.82	1.926973264	0.281728869	0.282043778	
12DTB19	08/04/2020 (4) 17:09:19.00	12DTB19 - 17	218	11	9.6	0.025	3.422313	0.23241746	0.1081	0.004662	-0.012303	1652.5	99	1766.8	78.8	6.47	1766.8	78.8	4.46%	0.281729	0.000032	0.005634671	0.00242	0.00012	0.1024	0.0051	0.28165	-0.41	1.12	2.22	2.487582482	0.28165941	0.281964611	
12DTB19	08/04/2020 (4) 21:29:46.00	12DTB19 - 113	51.8	2.6	2.3	0.036	4.096682	0.30011004	0.0945	0.0079	0.3641	1408	92.7	1517	155	7.19	1517	155	10.22%	0.282078	0.000033	0.005641557	0.001375	0.000055	0.0543	0.0016	0.28204	7.73	1.16	1.67	1.789670073	0.281822812	0.282149071	High uncertainty ~10%, included
12DTB19	08/04/2020 (4) 17:56:58.00	12DTB19 - 36	118.3	1.3	2.6	0.037	3.443526	0.21116502	0.1084	0.005668	0.21157	1643.5	89	1771.9	95.5	7.25	1771.9	95.5	5.39%	0.281842	0.000038	0.005636968	0.0007821	0.0000081	0.0325	0.00037	0.28182	5.67	1.33	1.97	2.103388907	0.281650107	0.28196083	
12DTB19	08/04/2020 (4) 19:38:22.00	12DTB19 - 77	127.2	7.2	6.9	0.033	4.098361	0.28052592	0.0968	0.006196	-0.047979	1407.5	87.5	1523	123	7.58	1523	123	8.08%	0.28191	0.000033	0.00563898	0.001032	0.000032	0.0612	0.0014	0.28191	3.21	1.05	1.86	2.066117954	0.28181694	0.28214465	
12DTB19	08/04/2020 (4) 16:45:39.00	12DTB19 - 5	207	10	14	0.029	3.862495	0.2562763	0.0995	0.00459	0.23853	1484.2	88	1613.9	85.9	8.04	1613.9	85.9	5.32%	0.281995	0.000033	0.005639664	0.00168	0.000015	0.0644	0.00066	0.28194	6.58	1.16	1.80	1.939971095	0.281758292	0.282077619	
12DTB19	08/04/2020 (4) 17:13:13.00	12DTB19 - 21	116.6	1.9	2.7	0.04	3.91547	0.24036474	0.0985	0.00557	0.16748	1466.3	82.7	1595	106	8.07	1595	106	6.65%	0.282025	0.000033	0.005640068	0.001471	0.000035	0.0585	0.0019	0.28198	7.46	1.16	1.75	1.848701878	0.281770935	0.282091566	
12DTB19	08/04/2020 (4) 17:15:18.00	12DTB19 - 20	196	9.9	13	0.027	3.921569	0.23221838	0.0984	0.005268	0.30523	1464.2	77.6	1593.2	100	8.10	1593.2	100	6.28%	0.282143	0.000042	0.005643016	0.002411	0.000077	0.0965	0.0028	0.28207	10.60	1.47	1.62	1.644977151	0.281771657	0.282092894	
12DTB19	08/04/2020 (4) 19:08:30.00	12DTB19 - 62	172	6.7	15	0.034	3.813883	0.2362836	0.1006	0.005512	0.46131	1501.1	83	1634	102	8.13	1634	102	6.24%	0.281885	0.000038	0.005637815	0.001558	0.000038	0.0637	0.0015	0.28184	3.22	1.26	1.95	2.155041941	0.281745309	0.282062782	
12DTB19	08/04/2020 (4) 20:40:08.00	12DTB19 - 93	139.2	6.3	8.7	0.041	4.056795	0.2621694	0.096	0.00512	0.32581	1420.4	82.4	1547	100	8.18	1547	100	6.46%	0.282056	0.000044	0.005641292	0.001422	0.000052	0.0545	0.0023	0.28201	7.56	1.54	1.70	1.804367713	0.281801468	0.282128963	
12DTB19	08/04/2020 (4) 19:10:31.00	12DTB19 - 63	406	17	20	0.029	4.061738	0.26270966	0.0962	0.003924	-0.29102	1418.8	82.4	1550.8	76.6	8.51	1550.8	76.6	4.94%	0.281956	0.000036	0.005639235	0.00257	0.00018	0.0997	0.0049	0.28188	2.89	1.26	1.90	2.106055698	0.281799017	0.282124162	
12DTB19	08/04/2020 (4) 20:51:58.00	12DTB19 - 99	142.7	1.5	14	0.027	3.82995	0.2232842	0.101	0.00582	0.19773	1495.5	77.8	1642	107	8.92	1642	107	6.52%	0.282014	0.000042	0.005640436	0.00205	0.00014	0.0761	0.005	0.28195	7.46	1.47	1.79	1.885764507	0.28174014	0.282056875	
12DTB19	08/04/2020 (4) 21:23:49.00	12DTB19 - 110	403	14	4.4	0.046	3.92773	0.2482523	0.0991	0.004082	-0.076547	1462.2	82.7	1606.4	76.8	8.98	1606.4	76.8	4.78%	0.282055	0.000034	0.005641202	0.004117	0.000075	0.1587	0.0053	0.28193	5.91	1.19	1.84	1.956672663	0.281763135	0.282083154	
12DTB19	08/04/2020 (4) 20:48:02.00	12DTB19 - 97	379	14	21	0.025	3.840246	0.23902732	0.1011	0.004522	0.11962	1491.9	82.9	1643.6	83	9.23	1643.6	83	5.05%	0.281799	0.000035	0.005636089	0.001559	0.000053	0.0601	0.0024	0.28175	0.40	1.23	2.07	2.338469093	0.281739106	0.282055693	
12DTB19	08/04/2020 (4) 20:46:06.00	12DTB19 - 96	240	13	45	0.028	2.840909	0.20209198	0.1336	0.009472	-0.82693	1944	119	2145	124	9.37	2145	124	5.78%	0.281461	0.000057	0.005629509	0.001438	0.000063	0.0592	0.0028	0.28140	-0.40	2.00	2.53	2.785934523	0.281413609	0.281683696	
12DTB19	08/04/2020 (4) 18:16:57.00	12DTB19 - 41	172	6.6	21	0.03	4.027386	0.24274612	0.0976	0.004452	0.34101	1429.7	77.3	1577.9	85.4	9.39	1577.9	85.4	5.41%	0.282085	0.000048	0.005641904	0.00509	0.00012	0.2017	0.0038	0.28193	5.37	1.68	1.84	1.968747868	0.281781532	0.28210418	Yb outside range of Standards, included
12DTB19	08/04/2020 (4) 16:43:41.00	12DTB19 - 4	106.7	3.6	6.5	0.03	3.692762	0.22385664	0.1047	0.005794	0.23668	1544.9	83.3	1708	102	9.55	1708	102	5.97%	0.282052	0.000036	0.005641155	0.002793	0.000056	0.1094	0.0032	0.28196	9.38	1.26	1.77	1.814466291	0.28169747	0.282008108	
12DTB19	08/04/2020 (4) 21:53:44.00	12DTB19 - 120	196.7	6.7	12	0.031	3.871467	0.24230014	0.1013	0.005226	0.18328	1481.1	82.8	1647.2	95.7	10.08	1647.2	95.7	5.81%	0.281976	0.00004	0.005639662	0.001205	0.000017	0.04458	0.00078	0.28194	7.16	1.40	1.81	1.909217614	0.28173678	0.282053035	> 10% Discordant, excluded
12DTB19	08/04/2020 (4) 20:50:02.00	12DTB19 - 98	57.1	2	1.1	0.033	2.463054	0.16452718	0.1594	0.008288	-0.06452	2197	124	2448.5	88	10.27	2448.5	88	3.59%	0.281351	0.000038	0.005627148	0.000926	0.000026	0.03509	0.00083	0.28131	3.29	1.33	2.65	2.789055282	0.2812151	0.281456829	> 10% Discordant, excluded
12DTB19	08/04/2020 (4) 22:17:38.00	12DTB19 - 127	150	22	23	0.041	3.912363	0.24661966	0.1007	0.005714	-0.11465	1467.3	82.7	1636	105	10.31	1636	105	6.42%	0.282051	0.000042	0.005641176	0.001398	0.000093	0.0576	0.0044	0.28201	9.36	1.47	1.71	1.758719244	0.281744017	0.282061305	> 10% Discordant, excluded
12DTB19	08/04/2020 (4) 20:28:18.00	12DTB19 - 87	195	14	5	0.033	4.144219	0.30615348	0.0964	0.005228	0.013497	1393.5	92.6	1555	102	10.39	1555	102	6.56%	0.281956	0.000039	0.005639255	0.002169	0.000018	0.08453	0.00053	0.28189	3.40	1.37	1.88	2.076934278	0.281796308	0.282121066	> 10% Discordant, excluded
12DTB19	08/04/2020 (4) 18:12:57.00	12DTB19 - 39	246.7	7.4	3.6	0.033	3.676471	0.27627592	0.1069	0.004838	-0.15685	1551	104	1746.4	82.9	11.19	1746.4	82.9	4.75%	0.281702	0.000041	0.005634189	0.001755	0.000042	0.0727	0.0023	0.28164	-1.02	1.44	2.22	2.510412313	0.281672619	0.281979707	> 10% Discordant, excluded
12DTB19	08/04/2020 (4) 17:47:09.00	12DTB19 - 31	106.4	3.3	4.6	0.045	3.473428	0.21424496	0.1124	0.007148	0.36364	1631	88.9	1838	115	11.26	1838	115	6.26%	0.281731	0.000041	0.005634769	0.000828	0.00003	0.0341	0.0015	0.28170	3.16	1.44	2.13	2.316489674	0.281613268	0.281911877	> 10% Discordant, excluded
12DTB19	08/04/2020 (4) 16:53:31.00	12DTB19 - 9	264.3	6.3	7.8	0.043	4.140787	0.24913304	0.0978	0.004156	0.1979	1394.5	75.4	1581.8	79.5	11.84	1581.8	79.5	5.03%	0.281956	0.000037	0.005639241	0.001555	0.000029	0.06169	0.00077	0.28191	4.63	1.30	1.85	2.019639646	0.281779015	0.282101303	> 10% Discordant, excluded
12DTB19	08/04/2020 (4) 21:49:48.00	12DTB19 - 118	232.2	8	7.7	0.036	4.163197	0.27391824	0.0974	0.004948	0.26915	1387.7	82.1	1574.1	95.1	11.84	1574.1	95.1	6.04%	0.282119	0.000051	0.00564261	0.002463	0.000066	0.0996	0.003	0.28205	9.29	1.79	1.66	1.714518331	0.281783984	0.282106982	> 10% Discordant, excluded
12DTB19	08/04/2020 (4) 19:32:29.00	12DTB19 - 69	228	10	17	0.032	4.125413	0.25269856	0.0982	0.004264	0.26844	1399.2	77	1589.4	81.1	11.97	1589.4	81.1	5.10%	0.281938	0.000036	0.005638875	0.001643	0.000036	0.0617	0.0021	0.28189	4.06	1.26	1.88	2.061930305	0.28177411	0.282095697	> 10% Discordant, excluded
12DTB19	08/04/2020 (4) 18:52:43.00	12DTB19 - 54	486	9.9	2.9	0.042	3.812429	0.23612928	0.1053	0.004306	0.25991	1501.6	83	1718.7	75.2	12.63	1718.7	75.2	4.38%	0.281722	0.000037	0.005634561	0.001373	0.000079	0.0583	0.0037	0.28168	-0.47	1.30	2.17	2.453585359	0.281690547	0.282000196	> 10% Discordant, excluded
12DTB19	08/04/2020 (4) 18:54:43.00	12DTB19 - 55	178	6.3	5.6	0.046	4.132231	0.27047332	0.0988	0.004976	0.4407	1397.1	82.2	1600.8	94	12.72	1600.8	94	5.87%	0.282032	0.000035	0.005640749	0.001288	0.000039	0.0527	0.0014	0.28199	8.03	1.23	1.73	1.816490607	0.28176675	0.282087286	> 10% Discordant, excluded
12DTB19	08/04/2020 (4) 17:31:22.00	12DTB19 - 23	457	16	10	0.044	3.725782	0.22721164	0.1079	0.003958	0.038356	1532.7	83.2	1763.4	67	13.08	1763.4	67	3.80%	0.281676	0.000041	0.005633669	0.000871	0.00003	0.0357	0.0011	0.28165	-0.52	1.44	2.20	2.492249192	0.281661612	0.281967128	> 10% Discordant, excluded
12DTB19	08/04/2020 (4) 18:36:56.00	12DTB19 - 46	256	16	11	0.035	3.584229	0.26438508	0.1117	0.005234	0.21883	1586	104	1826.4	85	13.16	1826.4	85	4.65%	0.281621	0.000037	0.005632542	0.000918	0.000028	0.0372	0.0013	0.28159	-1.12	1.30	2.28	2.580182797	0.281620789	0.281920474	> 10% Discordant, excluded
12DTB19	08/04/2020 (4) 21:15:53.00	12DTB19 - 106	214.6	3.2	2.5	0.035	3.992016	0.23920222	0.1025	0.00505	0.2024	1441.1	77.4	1669	91.1	13.65	1669	91.1	5.46%	0.281835	0.000042	0.005636856	0.000929	0.000016	0.03597	0.00082	0.28181	2.94	1.47	1.99	2.196411854	0.28172269	0.282036932	> 10% Discordant, excluded
12DTB19	08/04/2020 (4) 19:26:35.00	12DTB19 - 66	295.9	8.8	8.1	0.033	3.980892	0.25394034	0.1028	0.004356	0.16064	1444.7	82.6	1674.5	78.3	13.72	1674.5	78.3	4.68%	0.281875	0.000038	0.005637628	0.001682	0.000023	0.06753	0.00091	0.28182	3.64	1.33	1.97	2.156334455	0.281719135	0.282032868	> 10% Discordant, excluded
12DTB19	08/04/2020 (4) 16:59:29.00	12DTB19 - 12	209.6	6.3	4	0.038	4.1841	0.253497	0.0994	0.004788	0.38348	1381.5	75.3	1612	89.7	14.30	1612	89.7	5.56%	0.281929	0.000036	0.005638695	0.002124	0.000022	0.0855	0.001	0.28186	3.71	1.26	1.92	2.102057631	0.281759519	0.282079021	> 10% Discordant, excluded
12DTB19	08/04/2020 (4) 20:00:24.00	12DTB19 - 78	262.7	5.4	3.9	0.039	3.881988	0.24340786	0.1069	0.004838	0.21034	1477.6	82.8	1746.4	82.9	15.39	1746.4	82.9	4.75%	0.281802	0.000034	0.005636143	0.0010471	0.0000094	0.04336	0.00038	0.28177	3.36	1.19	2.04	2.230841911	0.281672619	0.281979707	> 10% Discordant, excluded
12DTB19	08/04/2020 (4) 20:53:59.00	12DTB19 - 100	71.5	8	5.7	0.031	4.255319	0.39293798	0.0995	0.00769	-0.0018883	1361	113	1614	144	15.68	1614	144	8.92%	0.281995	0.000047	0.005640096	0.00103	0.000058	0.0389	0.002	0.28196	7.29	1.65	1.77	1.8746352	0.281758227	0.282077545	> 10% Discordant, excluded
12DTB19	08/04/2020 (4) 17:07:23.00	12DTB19 - 16	251	14	6.5	0.035	4.027386	0.29140562	0.1045	0.00489	-0.23968	1429.7	92.8	1704.7	86.2	16.13	1704.7	86.2	5.06%	0.281672	0.000033	0.005633537	0.001027	0.000046	0.0424	0.0019	0.28164	-2.16	1.16	2.22	2.549781236	0.281699604	0.282010548	> 10% Discordant, excluded
12DTB19	08/04/2020 (4) 17:45:08.00	12DTB19 - 30	363	52	7.4	0.04	4.43459	0.3443444	0.0974	0.004348	-0.13964	1310.9	92.1	1574.1	83.6	16.72	1574.1	83.6	5.31%	0.281941	0.000038	0.005638948	0.00392	0.00048	0.151	0.016	0.28182	1.43	1.33	2.00	2.218156171	0.281783984	0.282106982	> 10% Discordant, excluded
12DTB19	08/04/2020 (4) 21:03:49.00	12DTB19 - 105	62.2	1.9	1.4	0.031	4.2123	0.3149111	0.1015	0.00713	0.0103	1373.2	92.5	1651	130	16.83	1651	130	7.87%	0.28182	0.000038	0.005636528	0.000586	0.000036	0.0233	0.0016	0.28180	2.39	1.33	1.99	2.217535229	0.281734325	0.282050228	> 10% Discordant, excluded
12DTB19	08/04/2020 (4) 21:19:52.00	12DTB19 - 108	300	18	41	0.029	4.97265	0.3467255	0.0899	0.004698	0.048145	1181.2	75.3	1422.5	99.8	16.96	1181.2	75.3	6.37%	0.282107	0.000041	0.005642289	0.002051	0.000067	0.0811	0.0027	0.28206	0.88	1.44	1.66	1.941958336	0.2820366	0.282395685	> 10% Discordant, excluded
12DTB19	08/04/2020 (4) 20:57:57.00	12DTB19 - 102	439	60	26	0.041	4.065041	0.46136562	0.1067	0.004434	-0.11523	1418	144	1743	76.1	18.65	1743	76.1	4.37%	0.281715	0.000041	0.005634449	0.00248	0.00039	0.105	0.017	0.28163	-1.48	1.44	2.24	2.537173489	0.28167482	0.281982223	> 10% Discordant, excluded
12DTB19	08/04/2020 (4) 18:48:46.00	12DTB19 - 52	346	73	3.6	0.031	4.032258	0.50338186	0.1094	0.005688	-0.54664	1428	160	1788.6	94.7	20.16	1788.6	94.7	5.29%	0.281608	0.00004	0.005632302	0.000763	0.000013	0.02937	0.0005	0.28158	-2.24	1.40	2.29	2.62156725	0.281645288	0.281948473	> 10% Discordant, excluded
12DTB19	08/04/2020 (4) 19:44:19.00	12DTB19 - 75	186.9	6.3	12	0.034	4.86618	0.3578004	0.0952	0.005904	0.29094	1204.8	80.8	1531	117	21.31	1531	117	7.64%	0.282021	0.000038	0.005640548	0.001541	0.000051	0.06	0.002	0.28198	5.84	1.33	1.76	1.901819378	0.281811786	0.282138756	> 10% Discordant, excluded
12DTB19	08/04/2020 (4) 18:50:46.00	12DTB19 - 53	540	12	58	0.03	4.892368	0.30129706	0.0951	0.004002	0.079014	1198.9	67.4	1529.2	79.3	21.60	1529.2	79.3	5.19%	0.282096	0.000046	0.005642108	0.004378	0.000087	0.1721	0.0036	0.28197	5.55	1.61	1.79	1.91901305	0.281812947	0.282140082	> 10% Discordant, excluded
12DTB19	08/04/2020 (4) 19:24:34.00	12DTB19 - 65	119	12	2.5	0.04	5.208333	0.61957466	0.0925	0.00755	-0.11339	1132	124	1477	155	23.36	1477	155	10.95%	0.282025	0.000045	0.00564068	0.001039	0.00007	0.0381	0.0017	0.28200	-2.31	1.58	1.73	2.105796595	0.282068103	0.282431689	> 10% Discordant, excluded
12DTB19	08/04/2020 (4) 20:12:14.00	12DTB19 - 84	642	24	4.4	0.041	4.878049	0.29268298	0.0972	0.003644	0.053318	1202.1	65.8	1570.2	70.2	23.44	1570.2	70.2	4.47%	0.282068	0.000039	0.005641495	0.00452	0.00011	0.1811	0.0055	0.28193	5.22	1.37	1.84	1.972391382	0.281786501	0.282109858	> 10% Discordant, excluded
12DTB19	08/04/2020 (4) 18:38:56.00	12DTB19 - 47	293	11	8.1	0.043	4.302926	0.26195262	0.1082	0.004664	0.082268	1347.1	74	1768.5	78.7	23.83	1768.5	78.7	4.45%	0.281609	0.000038	0.005632308	0.001225	0.000033	0.0513	0.0021	0.28157	-3.21	1.33	2.32	2.667026991	0.281658309	0.281963353	> 10% Discordant, excluded
12DTB19	08/04/2020 (4) 17:33:18.00	12DTB19 - 24	294	23	17	0.047	4.852014	0.29950178	0.098	0.00536	0.42955	1208	68	1586	102	23.83	1586	102	6.43%	0.282084	0.00003	0.00564176	0.001852	0.000089	0.0718	0.0039	0.28203	8.95	1.05	1.68	1.745711089	0.281776304	0.282098205	> 10% Discordant, excluded
12DTB19	08/04/2020 (4) 19:02:37.00	12DTB19 - 59	319	8.3	4	0.046	4.636069	0.28186098	0.1017	0.004534	0.025099	1259.1	69.5	1654.5	82.6	23.90	1654.5	82.6	4.99%	0.281899	0.000028	0.00563805	0.0006026	0.0000053	0.02123	0.00024	0.28188	5.26	0.98	1.88	2.037007735	0.281732063	0.282047643	> 10% Discordant, excluded
12DTB19	08/04/2020 (4) 17:05:22.00	12DTB19 - 15	440.6	7.3	26	0.033	4.833253	0.28354776	0.0984	0.004268	0.29696	1212.3	64.8	1593.2	81	23.91	1593.2	81	5.08%	0.282068	0.000049	0.005641573	0.0033	0.00016	0.149	0.012	0.28197	6.99	1.72	1.78	1.877539842	0.281771657	0.282092894	> 10% Discordant, excluded
12DTB19	08/04/2020 (4) 20:24:19.00	12DTB19 - 85	553	18	27	0.035	5.434783	0.39520326	0.0905	0.00351	0.12403	1088.8	72.8	1435.2	74	24.14	1088.8	72.8	6.69%	0.282174	0.000041	0.005643629	0.001499	0.00004	0.0539	0.0018	0.28214	1.68	1.44	1.54	1.81714179	0.28209574	0.282463274	> 10% Discordant, excluded
12DTB19	08/04/2020 (4) 20:30:18.00	12DTB19 - 88	232	13	21	0.043	5.512679	0.39287718	0.091	0.00512	0.14499	1074.6	70.5	1446	107	25.68	1074.6	70.5	6.56%	0.282182	0.000036	0.005643755	0.002788	0.000073	0.1085	0.0034	0.28213	0.74	1.26	1.58	1.866346499	0.28210482	0.282473651	> 10% Discordant, excluded
12DTB19	08/04/2020 (4) 16:51:35.00	12DTB19 - 8	395.6	9.4	33	0.034	5.24109	0.3190802	0.0951	0.004502	0.079164	1125.7	62.9	1529.2	89.2	26.39	1529.2	89.2	5.83%	0.282003	0.000036	0.005640175	0.002012	0.000039	0.0823	0.0024	0.28194	4.68	1.26	1.81	1.974833775	0.281812947	0.282140082	> 10% Discordant, excluded
12DTB19	08/04/2020 (4) 22:19:37.00	12DTB19 - 128	391	16	20	0.041	5.08647	0.357864	0.0973	0.004846	0.0049438	1157	74.5	1572.2	93.3	26.41	1572.2	93.3	5.93%	0.281866	0.000042	0.005637476	0.00139	0.00018	0.061	0.012	0.28182	1.40	1.47	1.97	2.218466783	0.281785211	0.282108383	> 10% Discordant, excluded
12DTB19	08/04/2020 (4) 20:38:12.00	12DTB19 - 92	410	72	2.6	0.048	5.747126	0.80856122	0.0909	0.004918	-0.39607	1034	134	1444	103	28.39	1034	134	12.96%	0.282145	0.000043	0.005643064	0.002234	0.000051	0.0912	0.0014	0.28210	-1.04	1.51	1.61	1.946885711	0.282130766	0.282503304	> 10% Discordant, excluded
12DTB19	08/04/2020 (4) 18:42:53.00	12DTB19 - 49	625	41	9.8	0.037	5.633803	0.43007336	0.0928	0.004256	0.11942	1053.3	74.2	1483	86.9	28.98	1053.3	74.2	7.04%	0.282043	0.000038	0.005640988	0.00363	0.00014	0.1436	0.0071	0.28197	-5.23	1.33	1.83	2.227811825	0.282118435	0.282489211	> 10% Discordant, excluded
12DTB19	08/04/2020 (4) 19:28:31.00	12DTB19 - 67	549	20	6.3	0.033	4.840271	0.29594532	0.1052	0.003904	0.071407	1210.7	67.5	1717	68.2	29.49	1717	68.2	3.97%	0.281689	0.000033	0.005633877	0.00225	0.00012	0.09	0.0048	0.28162	-2.69	1.16	2.27	2.593527628	0.281691647	0.282001454	> 10% Discordant, excluded
12DTB19	08/04/2020 (4) 18:15:01.00	12DTB19 - 40	392	26	73	0.037	5.509642	0.37429134	0.096	0.00422	-0.19094	1075.2	67.3	1546.9	82.6	30.49	1546.9	82.6	5.34%	0.282	0.000052	0.00564024	0.00206	0.00011	0.0804	0.0053	0.28194	4.90	1.82	1.81	1.974450023	0.281801532	0.282127037	> 10% Discordant, excluded
12DTB19	08/04/2020 (4) 17:58:58.00	12DTB19 - 37	269	28	17	0.035	5.230126	0.36446752	0.1004	0.005008	0.021928	1127.9	72.1	1630.7	92.7	30.83	1630.7	92.7	5.68%	0.282028	0.000051	0.005640791	0.001933	0.000045	0.0745	0.0024	0.28197	7.84	1.79	1.77	1.852299816	0.281747441	0.282065218	> 10% Discordant, excluded
12DTB19	08/04/2020 (4) 22:03:34.00	12DTB19 - 125	663.9	7.1	12	0.05	5.107252	0.30560044	0.1045	0.00409	0.11657	1152.7	63.2	1704.7	72.1	32.38	1704.7	72.1	4.23%	0.281813	0.000035	0.005636369	0.002242	0.000072	0.0885	0.0025	0.28174	1.45	1.23	2.09	2.319779203	0.281699604	0.282010548	> 10% Discordant, excluded
12DTB19	08/04/2020 (4) 16:39:45.00	12DTB19 - 2	258	11	7.6	0.028	5.580357	0.35450214	0.0973	0.004446	0.026216	1062.6	62.2	1572.2	85.6	32.41	1572.2	85.6	5.44%	0.282063	0.000039	0.005641395	0.002327	0.000049	0.0969	0.0024	0.28199	7.40	1.37	1.74	1.834212828	0.281785211	0.282108383	> 10% Discordant, excluded
12DTB19	08/04/2020 (4) 22:21:38.00	12DTB19 - 129	307	29	2.6	0.043	5.387931	0.39515362	0.1004	0.005308	0.14984	1097.5	74	1630.7	98.3	32.70	1630.7	98.3	6.03%	0.281766	0.000033	0.005635417	0.0006259	0.0000097	0.0249	0.0005	0.28175	-0.03	1.16	2.07	2.35569913	0.281747441	0.282065218	> 10% Discordant, excluded
12DTB19	08/04/2020 (4) 20:44:05.00	12DTB19 - 95	301.3	9.4	8.4	0.033	5.047956	0.31245852	0.1078	0.005156	0.021739	1165.1	66	1761.7	87.4	33.87	1761.7	87.4	4.96%	0.281688	0.000041	0.005633909	0.001165	0.000043	0.0455	0.0021	0.28165	-0.48	1.44	2.20	2.488400862	0.281662712	0.281968386	> 10% Discordant, excluded
12DTB19	08/04/2020 (4) 17:37:14.00	12DTB19 - 26	271	13	5.3	0.055	5.151984	0.31538318	0.1065	0.00503	0.41018	1143.5	64.1	1739.5	86.6	34.26	1739.5	86.6	4.98%	0.281662	0.000038	0.005633368	0.00084	0.000016	0.03352	0.00067	0.28163	-1.52	1.33	2.22	2.536710721	0.281677086	0.281984812	> 10% Discordant, excluded
12DTB19	08/04/2020 (4) 19:34:29.00	12DTB19 - 70	660	75	110	0.037	5.94884	0.5436412	0.0953	0.004106	-0.25258	1001.6	84.8	1533.2	81.1	34.67	1533.2	81.1	5.29%	0.282025	0.000035	0.005640609	0.00321	0.00027	0.132	0.011	0.28193	4.31	1.23	1.83	2.001456109	0.281810368	0.282137134	> 10% Discordant, excluded
12DTB19	08/04/2020 (4) 21:17:56.00	12DTB19 - 107	590	18	23	0.035	5.333333	0.35982226	0.1042	0.003884	-0.051019	1107.8	68.7	1699.4	68.7	34.81	1699.4	68.7	4.04%	0.281741	0.000034	0.005634923	0.002159	0.00003	0.0887	0.0016	0.28167	-1.12	1.19	2.19	2.479628216	0.281703033	0.282014466	> 10% Discordant, excluded
12DTB19	08/04/2020 (4) 20:08:18.00	12DTB19 - 82	857	85	100	0.044	5.617978	0.52266126	0.1005	0.00391	0.061782	1056	90.6	1632.5	72.3	35.31	1632.5	72.3	4.43%	0.281981	0.000041	0.005639769	0.00206	0.00021	0.0895	0.0093	0.28192	6.07	1.44	1.84	1.967312333	0.281746278	0.282063889	> 10% Discordant, excluded
12DTB19	08/04/2020 (4) 18:00:54.00	12DTB19 - 38	695	11	11	0.042	5.656109	0.35305888	0.1007	0.003814	0.078661	1049.5	60.5	1636.2	70.3	35.86	1636.2	70.3	4.30%	0.281757	0.000035	0.005635249	0.0011918	0.0000087	0.0467	0.00049	0.28172	-0.85	1.23	2.11	2.412130311	0.281743888	0.282061157	> 10% Discordant, excluded
12DTB19	08/04/2020 (4) 16:49:35.00	12DTB19 - 7	610	36	66	0.042	6.161429	0.44591588	0.0959	0.004218	-0.10367	969.5	65.1	1545	82.7	37.25	1545	82.7	5.35%	0.281983	0.000039	0.005639795	0.00296	0.00013	0.1187	0.0052	0.28190	3.33	1.37	1.88	2.073920497	0.281802758	0.282128438	> 10% Discordant, excluded
12DTB19	08/04/2020 (4) 18:40:53.00	12DTB19 - 48	840	110	56	0.036	7.194245	0.8684851	0.0873	0.003846	-0.60511	839	95	1366.3	84.8	38.59	839	95	11.32%	0.282089	0.000039	0.005641915	0.001305	0.000081	0.0491	0.0025	0.28207	-6.61	1.37	1.65	2.145105835	0.282255114	0.282645416	> 10% Discordant, excluded
12DTB19	08/04/2020 (4) 19:46:18.00	12DTB19 - 76	576	23	73	0.024	7.052186	0.53891032	0.0896	0.004092	-0.051839	854.8	61.2	1416.2	87.3	39.64	854.8	61.2	7.16%	0.282001	0.000037	0.005640141	0.001091	0.00003	0.0457	0.0016	0.28198	-9.27	1.30	1.77	2.324923575	0.282245056	0.282633921	> 10% Discordant, excluded
12DTB19	08/04/2020 (4) 17:51:04.00	12DTB19 - 33	522	36	45	0.037	6.188119	0.54498338	0.0993	0.004386	-0.2099	965.7	79	1610.2	82.3	40.03	1610.2	82.3	5.11%	0.281861	0.000048	0.005637424	0.00236	0.00022	0.1	0.013	0.28179	1.01	1.68	2.03	2.273561777	0.281760681	0.28208035	> 10% Discordant, excluded
12DTB19	08/04/2020 (4) 16:57:28.00	12DTB19 - 11	607	20	20	0.034	6.184292	0.45642144	0.1013	0.004226	0.07321	966.2	66.2	1647.2	77.4	41.34	1647.2	77.4	4.70%	0.281772	0.000033	0.005635537	0.001401	0.000056	0.0575	0.0025	0.28173	-0.30	1.16	2.10	2.386204241	0.28173678	0.282053035	> 10% Discordant, excluded
12DTB19	08/04/2020 (4) 21:01:53.00	12DTB19 - 104	479	12	32	0.035	6.644518	0.46842746	0.0969	0.004338	-0.096221	903.8	59.4	1564.4	83.9	42.23	1564.4	83.9	5.36%	0.281899	0.000035	0.005638089	0.001928	0.000074	0.0788	0.0029	0.28184	1.83	1.23	1.95	2.184560443	0.281790243	0.282114135	> 10% Discordant, excluded
12DTB19	08/04/2020 (4) 17:03:26.00	12DTB19 - 14	638	47	15	0.029	6.325111	0.52657252	0.1035	0.00417	-0.25967	946.2	73.3	1687	74.3	43.91	1687	74.3	4.40%	0.281623	0.000035	0.005632569	0.001164	0.000029	0.0456	0.0012	0.28159	-4.45	1.23	2.29	2.680996689	0.281711052	0.282023631	> 10% Discordant, excluded
12DTB19	08/04/2020 (4) 19:38:26.00	12DTB19 - 72	379	15	18	0.047	8.438819	0.61030108	0.0884	0.004668	-0.15543	721.9	49.4	1390	101	48.06	721.9	49.4	6.84%	0.282093	0.00004	0.005642002	0.002053	0.000065	0.0901	0.0043	0.28207	-9.36	1.40	1.68	2.22519337	0.28232957	0.282730508	> 10% Discordant, excluded
12DTB19	08/04/2020 (4) 18:34:59.00	12DTB19 - 45	1080	120	31	0.044	7.352941	1.01211072	0.0986	0.004672	-0.63941	822	106	1597	88.4	48.53	1597	88.4	5.54%	0.281689	0.000039	0.005633915	0.002157	0.000023	0.0805	0.0031	0.28162	-5.16	1.37	2.26	2.654984996	0.281769204	0.28209009	> 10% Discordant, excluded
12DTB19	08/04/2020 (4) 21:43:45.00	12DTB19 - 115	838	11	37	0.038	7.062147	0.42552424	0.1026	0.003752	0.051264	853.7	48.2	1670.9	67.6	48.91	1670.9	67.6	4.05%	0.281717	0.000035	0.005634449	0.00251	0.00014	0.0983	0.0053	0.28164	-2.98	1.23	2.24	2.575165634	0.281721462	0.282035528	> 10% Discordant, excluded
12DTB19	08/04/2020 (4) 17:39:15.00	12DTB19 - 27	1251	38	8.8	0.032	8.992806	0.58420892	0.0891	0.003182	-0.27444	679.7	41.9	1405.4	68.4	51.64	679.7	41.9	6.16%	0.282009	0.000034	0.005640282	0.002521	0.000014	0.10062	0.00095	0.28198	-13.44	1.19	1.82	2.447375988	0.282356362	0.282761128	> 10% Discordant, excluded
12DTB19	08/04/2020 (4) 18:58:40.00	12DTB19 - 57	823	69	9	0.029	8.849558	1.03845256	0.0911	0.004022	-0.2179	690.1	76.8	1447.8	84.1	52.33	690.1	76.8	11.13%	0.281889	0.000038	0.005637908	0.001769	0.000063	0.0666	0.0027	0.28187	-17.13	1.33	1.96	2.686118183	0.282349761	0.282753584	> 10% Discordant, excluded
12DTB19	08/04/2020 (4) 17:43:11.00	12DTB19 - 29	850	13	18	0.036	8.064516	0.49297602	0.0988	0.004276	0.053461	753.5	43.5	1600.8	80.7	52.93	1600.8	80.7	5.04%	0.281866	0.000038	0.005637448	0.001639	0.000056	0.0639	0.0017	0.28182	1.76	1.33	1.98	2.218108147	0.28176675	0.282087286	> 10% Discordant, excluded
12DTB19	08/04/2020 (4) 18:32:59.00	12DTB19 - 44	275	38	14	0.034	9.259259	1.72839518	0.0897	0.006994	-0.29252	661	117	1418	149	53.39	661	117	17.70%	0.282036	0.000052	0.00564096	0.001756	0.000027	0.0704	0.0021	0.28201	-12.54	1.82	1.75	2.37584139	0.282368227	0.282774688	> 10% Discordant, excluded
12DTB19	08/04/2020 (4) 20:06:22.00	12DTB19 - 81	1024	16	21	0.043	8.984726	0.55910342	0.0928	0.003356	-0.24982	680.3	40.2	1483	68.5	54.13	680.3	40.2	5.91%	0.281973	0.000032	0.005639551	0.001871	0.000034	0.0768	0.002	0.28195	-14.41	1.12	1.84	2.508455562	0.282355981	0.282760693	> 10% Discordant, excluded
12DTB19	08/04/2020 (4) 18:46:50.00	12DTB19 - 51	1.50E+05	1.40E+04	600	120	8.643042	0.91988264	0.099	0.01398	0.28244	705.8	71.1	1605	263	56.02	1605	263	16.39%	0.289	0.027	0.027611744	0.00003	0.00056	0.007	0.017	0.28900	256.78	945.00	-8.71	-17.17672451	0.281764039	0.282084187	> 10% Discordant, excluded
12DTB19	08/04/2020 (4) 20:36:11.00	12DTB19 - 91	1296	95	39	0.061	9.416196	0.75577832	0.0933	0.003966	-0.64781	650.6	49.7	1493.1	80.4	56.43	650.6	49.7	7.64%	0.281807	0.000038	0.005636268	0.001533	0.000035	0.06	0.0011	0.28179	-20.77	1.33	2.06	2.881099435	0.282374825	0.282782228	> 10% Discordant, excluded
12DTB19	08/04/2020 (4) 21:27:45.00	12DTB19 - 112	840	20	20	0.034	6.706908	0.44901646	0.13	0.0053	-0.26727	895.9	56	2097.2	71.6	57.28	2097.2	71.6	3.41%	0.281575	0.000035	0.005631609	0.001808	0.000036	0.0676	0.0012	0.28150	2.06	1.23	2.40	2.590847043	0.281444771	0.28171931	> 10% Discordant, excluded
12DTB19	08/04/2020 (4) 20:42:08.00	12DTB19 - 94	1068	41	57	0.045	11.7096	0.7963626	0.0874	0.004148	-0.09237	528.3	34.5	1368.5	91.4	61.40	528.3	34.5	6.53%	0.282157	0.000038	0.005643268	0.00159	0.00011	0.0605	0.0052	0.28214	-11.01	1.33	1.57	2.174424094	0.28245231	0.282870783	> 10% Discordant, excluded
12DTB19	08/04/2020 (4) 20:59:53.00	12DTB19 - 103	1469	66	64	0.039	13.03781	0.9576926	0.0822	0.003544	-0.20261	476.4	33.7	1249.4	84.4	61.87	476.4	33.7	7.07%	0.282179	0.000037	0.005643701	0.00259	0.00017	0.1046	0.0094	0.28216	-11.66	1.30	1.58	2.173363799	0.282485139	0.282908301	> 10% Discordant, excluded
12DTB19	08/04/2020 (4) 21:45:52.00	12DTB19 - 116	1347	90	24	0.029	11.13586	0.9295589	0.0923	0.003946	-0.34962	554.4	44.3	1472.7	81.1	62.35	554.4	44.3	7.99%	0.28187	0.000034	0.005637503	0.00121	0.0001	0.0463	0.0034	0.28186	-20.48	1.19	1.95	2.78607456	0.282435789	0.282851901	> 10% Discordant, excluded
12DTB19	08/04/2020 (4) 20:04:21.00	12DTB19 - 80	1302	85	63	0.028	12.0048	0.8021455	0.0898	0.003896	-0.42409	515.8	33.1	1420.4	82.9	63.69	515.8	33.1	6.42%	0.281866	0.000041	0.005637469	0.001501	0.000032	0.0585	0.0019	0.28185	-21.55	1.44	1.97	2.821834535	0.282460219	0.282879822	> 10% Discordant, excluded
12DTB19	08/04/2020 (4) 17:49:04.00	12DTB19 - 32	897	21	19	0.033	12.46883	0.7624331	0.0885	0.00407	0.19449	497.3	29.3	1392.5	88.2	64.29	497.3	29.3	5.89%	0.282025	0.000032	0.005640591	0.001783	0.000064	0.0628	0.0021	0.28201	-16.41	1.12	1.76	2.487383264	0.282471922	0.282893197	> 10% Discordant, excluded
12DTB19	08/04/2020 (4) 19:36:25.00	12DTB19 - 71	1668	89	69	0.034	14.51379	0.9854209	0.0848	0.003896	-0.22849	429.5	28.2	1310.1	89.2	67.22	429.5	28.2	6.57%	0.281889	0.000028	0.00563785	0.001325	0.00006	0.0492	0.0027	0.28188	-22.53	0.98	1.93	2.813397284	0.282514777	0.282942174	> 10% Discordant, excluded
12DTB19	08/04/2020 (4) 16:55:32.00	12DTB19 - 10	1576	99	230	0.035	17.15266	1.1962729	0.0818	0.003736	-0.47179	365.3	24.8	1239.9	89.5	70.54	365.3	24.8	6.79%	0.282208	0.000052	0.0056444	0.00559	0.00033	0.231	0.015	0.28217	-13.64	1.82	1.68	2.209232692	0.282555307	0.282988494	> 10% Discordant, excluded
12DTB19	08/04/2020 (4) 19:42:22.00	12DTB19 - 74	2855	90	31	0.036	20.03205	1.2433355	0.0754	0.003608	-0.12725	314	19	1078.3	96	70.88	314	19	6.05%	0.282004	0.000042	0.005640236	0.00433	0.00011	0.1536	0.0041	0.28198	-21.55	1.47	1.93	2.660771427	0.282587658	0.283025466	> 10% Discordant, excluded
12DTB19	08/04/2020 (4) 16:37:42.00	12DTB19 - 1	3.56E+04	1.60E+03	27	30	44.44444	4.4444448	0.06	0.0182	0.35966	143.4	14.2	603	656	76.22	143.4	14.2	9.90%	0.295	0.013	0.014276204	-0.00009	0.0002	-0.0089	0.007	0.29500	435.28	455.00	-19.53	-37.72417778	0.28269502	0.283148165	> 10% Discordant, excluded
12DTB19	08/04/2020 (4) 19:04:34.00	12DTB19 - 60	5.09E+04	2.30E+03	360	34	11.28668	1.0282855	0.224	0.01748	0.060654	547.3	47.8	3009	125	81.81	3009	125	4.15%	0.2799	0.008	0.009764098	0.00047	0.00018	0.0088	0.0054	0.27987	-34.63	280.00	4.54	5.606742745	0.28084553	0.281034463	> 10% Discordant, excluded
12DTB19	08/04/2020 (4) 21:51:43.00	12DTB19 - 119	7.90E+03	2.50E+03	490	74	10	4.9	0.32	0.5564	0.88642	614	287	3569	2674	82.80	3569	2674	74.92%	0.15	0.11	0.110040901	0.0036	0.0028	0.45	0.37	0.14975	-4660.71	3850.00	84.43	104.6883757	0.28047241	0.280608041	> 10% Discordant, excluded from all plots
12DTB19	08/04/2020 (4) 19:22:35.00	12DTB19 - 64	4053	71	96	0.04	24.42002	1.5021744	0.0966	0.005732	-0.15916	258.7	15.6	1559	111	83.41	1559	111	7.12%	0.282005	0.000029	0.005640175	0.003951	0.000053	0.144	0.0023	0.28189	3.36	1.02	1.90	2.082727819	0.281793727	0.282118117	> 10% Discordant, excluded
12DTB19	08/04/2020 (4) 20:55:56.00	12DTB19 - 101	5.86E+04	2.50E+03	400	38	17.09402	1.5691434	0.162	0.02224	0.1236	366.5	32.7	2476	232	85.20	2476	232	9.37%	0.285	0.013	0.014194717	0.00026	0.00029	0.0094	0.0089	0.28499	134.80	455.00	-2.52	-6.350152618	0.281197058	0.281436209	> 10% Discordant, excluded
12DTB19	08/04/2020 (4) 22:23:36.00	12DTB19 - 130	5.50E+04	3.30E+03	510	38	17.92115	1.546743	0.153	0.02406	0.22226	350	29.4	2379	268	85.29	2379	268	11.27%	0.2724	0.0084	0.010012028	0.00073	0.00025	0.0216	0.0077	0.27237	-316.21	294.00	13.57	20.06242695	0.281260657	0.281508894	> 10% Discordant, excluded
12DTB19	08/04/2020 (4) 21:25:49.00	12DTB19 - 111	5.01E+04	2.10E+03	250	33	24.75248	2.1492996	0.108	0.02016	0.12383	255.3	21.7	1765	341	85.54	1765	341	19.32%	0.2866	0.0082	0.01000479	0.00019	0.00023	0.0098	0.0045	0.28659	175.14	287.00	-4.92	-10.05020384	0.281660575	0.281965943	> 10% Discordant, excluded
12DTB19	08/04/2020 (4) 20:02:25.00	12DTB19 - 79	4.50E+04	1.70E+04	4400	390	11.23596	3.1283932	0.4	0.148	0.52728	550	147	3908	556	85.93	3908	556	14.23%	0.247	0.085	0.08514343	-0.0008	0.0019	0.15	0.1	0.24706	-1184.11	2975.00	35.11	51.35106816	0.280244639	0.280347731	> 10% Discordant, excluded
12DTB19	08/04/2020 (4) 22:05:35.00	12DTB19 - 126	5.22E+04	3.80E+03	170	33	29.67359	3.2350378	0.102	0.02404	0.22897	213.7	22.9	1660	436	87.13	1660	436	26.27%	0.2834	0.0096	0.011148373	0.00034	0.0002	0.0103	0.0066	0.28339	58.95	336.00	-0.21	-1.515856855	0.281728508	0.282043581	> 10% Discordant, excluded
12DTB19	08/04/2020 (4) 21:55:40.00	12DTB19 - 121	6.92E+04	4.60E+03	20000	33	12.42236	1.2669262	0.454	0.04108	0.064314	499.1	49	4098	134	87.82	4098	134	3.27%	0.2851	0.0091	0.010738846	0.00255	0.00037	0.093	0.018	0.28490	170.68	318.50	-2.84	-7.913669168	0.280116349	0.280201113	> 10% Discordant, excluded
12DTB19	08/04/2020 (4) 17:01:25.00	12DTB19 - 13	5.05E+04	2.90E+03	410	29	25.12563	2.2701446	0.133	0.02166	0.23154	251.6	22.3	2137	285	88.23	2137	285	13.34%	0.2703	0.0087	0.010242794	0.00036	0.00018	0.013	0.006	0.27029	-395.62	304.50	15.71	23.42412193	0.281418827	0.281689659	> 10% Discordant, excluded
12DTB19	08/04/2020 (4) 17:29:18.00	12DTB19 - 22	5.19E+04	2.40E+03	340	35	22.77904	2.3754548	0.157	0.02314	-0.078481	277	28.3	2423	250	88.57	2423	250	10.32%	0.286	0.01	0.011520347	0.0003	0.0002	0.0079	0.0062	0.28599	169.05	350.00	-4.02	-9.057618376	0.281231822	0.28147594	> 10% Discordant, excluded
12DTB19	08/04/2020 (4) 18:18:59.00	12DTB19 - 42	4.55E+04	2.40E+03	4600	29	23.25581	2.2498652	0.155	0.0241	-0.075751	271.4	25.7	2401	264	88.70	2401	264	11.00%	0.275	0.011	0.012298374	0.0047	0.0014	0.215	0.065	0.27478	-229.74	385.00	11.74	15.91540777	0.281246243	0.28149242	> 10% Discordant, excluded
12DTB19	08/04/2020 (4) 21:57:41.00	12DTB19 - 122	6.44E+04	3.30E+03	580	55	26.10966	2.7036792	0.137	0.02474	0.48642	242.3	24.6	2189	314	88.93	2189	314	14.34%	0.279	0.01	0.01145148	0.00064	0.00027	0.0138	0.0071	0.27897	-85.70	350.00	5.72	7.998058199	0.2813849	0.281650886	> 10% Discordant, excluded
12DTB19	08/04/2020 (4) 17:55:02.00	12DTB19 - 35	3.32E+04	2.90E+03	410	20	27.47253	2.1344046	0.17	0.0254	0.45368	230.5	17.6	2557	250	90.99	2557	250	9.78%	0.2818	0.0071	0.009065015	0.00398	0.00037	0.137	0.014	0.28161	16.42	248.50	2.21	2.026924777	0.281143861	0.281375413	> 10% Discordant, excluded
12DTB19	08/04/2020 (4) 18:31:00.00	12DTB19 - 43	5.52E+04	2.80E+03	580	39	17.57469	1.6487468	0.414	0.03528	-0.19676	356.7	32.6	3960	128	90.99	3960	128	3.23%	0.2904	0.0082	0.010048525	0.00075	0.00065	0.044	0.029	0.29034	361.62	287.00	-11.29	-26.07142172	0.280209573	0.280307655	> 10% Discordant, excluded
12DTB19	08/04/2020 (4) 17:13:16.00	12DTB19 - 19	7.10E+04	1.10E+04	700	41	46.08295	7.08021	0.133	0.10066	0.32202	138.4	21	2137	1324	93.52	2137	1324	61.96%	0.237	0.078	0.07814389	0.0027	0.0014	0.121	0.085	0.23689	-1582.29	2730.00	44.56	59.49358681	0.281418827	0.281689659	> 10% Discordant, excluded

Appendix D3.1 continued.

Sample ID	Analysis date-time	Spot ID	238U conc. (ppm)	±2σ INT	232Th conc. (ppm)	±2σ INT	238U/206Pb	±2σ PROP	207Pb/206Pb	±2σ PROP	rho	238U/206Pb age (Ma)	±2σ PROP	207Pb/206Pb age (Ma)	±2σ PROP	Discord (7/6-6/8)/7/6 *100	Perferred age *1500 Ma cutoff (Ma)	2σ	error %
01DTB19	17/03/2020 (3) 23:59:55.00	01DTB19 - 72	199	3	118	1	3.943218	0.13639553	0.0898	0.002996	0.012956	1457	44.3	1420.4	62.5	-2.6	1457	44	3.04%
01DTB19	18/03/2020 (4) 01:49:14.00	01DTB19 - 109	109	8	79	1	2.9274	0.1699538	0.1148	0.004696	0.087231	1894.4	93.3	1875.9	72.3	-1.0	1876	72	3.86%
01DTB19	17/03/2020 (3) 23:12:17.00	01DTB19 - 53	128	2	134	2	3.260515	0.1927818	0.1052	0.003904	0.18373	1724.4	87.6	1717	66.8	-0.4	1717	67	3.89%
01DTB19	18/03/2020 (4) 01:17:27.00	01DTB19 - 98	159	3	135	10	3.309067	0.19758044	0.1042	0.003684	0.14111	1702.2	87.6	1699.4	63.9	-0.2	1699	64	3.76%
01DTB19	18/03/2020 (4) 00:39:54.00	01DTB19 - 79	124	2	99	6	3.282994	0.19499648	0.1052	0.004304	0.40612	1714.1	87.6	1717	73.7	0.2	1717	74	4.29%
01DTB19	18/03/2020 (4) 01:45:18.00	01DTB19 - 107	157	3	197	10	3.439972	0.19896694	0.1016	0.003532	0.32621	1645	82.3	1652.7	63.1	0.5	1653	63	3.82%
01DTB19	17/03/2020 (3) 20:59:13.00	01DTB19 - 1	137	1	105	3	3.278689	0.19457138	0.1057	0.004114	0.32118	1716.1	87.6	1725.7	70.0	0.6	1726	70	4.05%
01DTB19	18/03/2020 (4) 01:35:26.00	01DTB19 - 102	146	4	133	4	3.483107	0.21524654	0.1012	0.003824	0.20385	1627	87.0	1645.4	68.6	1.1	1645	69	4.17%
01DTB19	18/03/2020 (4) 01:33:26.00	01DTB19 - 101	276	2	314	7	3.537319	0.20838528	0.1002	0.003104	0.15186	1604.9	81.9	1627	56.4	1.4	1627	56	3.47%
01DTB19	18/03/2020 (4) 00:43:53.00	01DTB19 - 81	90	2	69	3	3.501401	0.20488592	0.1012	0.004624	0.32372	1619.5	82.1	1645.4	83.1	1.6	1645	83	5.05%
01DTB19	18/03/2020 (4) 01:07:36.00	01DTB19 - 93	190	6	93	6	3.37952	0.1932231	0.1043	0.003386	0.19432	1670.9	82.5	1701.2	58.6	1.8	1701	59	3.44%
01DTB19	18/03/2020 (4) 00:01:52.00	01DTB19 - 73	149	4	125	2	3.980892	0.13983834	0.0923	0.003746	0.13947	1444.7	44.5	1472.7	75.5	1.9	1445	44	3.08%
01DTB19	18/03/2020 (4) 02:35:09.00	01DTB19 - 122	167	10	129	5	3.233107	0.19009794	0.1086	0.003872	0.37257	1737.3	87.8	1775.2	63.7	2.1	1775	64	3.59%
01DTB19	18/03/2020 (4) 01:13:30.00	01DTB19 - 96	170	5	226	13	3.374958	0.20418326	0.1048	0.003896	0.21945	1672.9	87.4	1710	67.0	2.2	1710	67	3.92%
01DTB19	18/03/2020 (4) 02:52:54.00	01DTB19 - 131	141	2	107	1	3.926188	0.12939309	0.0934	0.003968	0.032713	1462.7	42.3	1495.2	78.8	2.2	1463	42	2.89%
01DTB19	17/03/2020 (3) 22:12:35.00	01DTB19 - 33	95	5	83	1	3.709199	0.22552368	0.0974	0.004348	-0.10746	1538.8	81.5	1574.1	81.9	2.2	1574	82	5.20%
01DTB19	17/03/2020 (3) 21:52:49.00	01DTB19 - 23	33	2	60	2	3.167564	0.20381978	0.111	0.00692	0.37945	1768.7	97.6	1815	110.9	2.6	1815	111	6.11%
01DTB19	18/03/2020 (4) 01:53:12.00	01DTB19 - 111	133	4	73	5	2.272211	0.13321424	0.1565	0.00503	0.26374	2351.1	113.1	2417.4	53.5	2.7	2417	54	2.21%
01DTB19	17/03/2020 (3) 22:42:36.00	01DTB19 - 38	99	2	54	1	3.430532	0.19806464	0.104	0.00408	0.20638	1649	82.3	1695.9	71.0	2.8	1696	71	4.18%
01DTB19	18/03/2020 (4) 02:33:06.00	01DTB19 - 121	245	4	189	4	3.334445	0.2001112	0.1065	0.00343	0.2037	1690.8	87.4	1739.5	57.8	2.8	1740	58	3.32%
01DTB19	17/03/2020 (3) 21:21:03.00	01DTB19 - 12	123	4	77	3	3.474635	0.2143698	0.103	0.00356	0.026386	1630.5	87.0	1678	62.5	2.8	1678	63	3.73%
01DTB19	18/03/2020 (4) 02:09:01.00	01DTB19 - 119	59	1	67	1	3.582945	0.2128714	0.1006	0.004912	0.20317	1586.8	81.9	1634.4	89.0	2.9	1634	89	5.44%
01DTB19	17/03/2020 (3) 22:02:39.00	01DTB19 - 28	356	7	253	6	3.930818	0.13424114	0.0939	0.002978	-0.26863	1461.1	43.7	1505.3	58.8	2.9	1461	44	2.99%
01DTB19	17/03/2020 (3) 22:40:37.00	01DTB19 - 37	127	1	154	3	3.951008	0.23356376	0.0937	0.003674	0.38372	1454.4	75.5	1501.2	72.7	3.1	1454	75	5.19%
01DTB19	18/03/2020 (4) 00:53:44.00	01DTB19 - 86	181	3	119	3	3.228931	0.18969062	0.1098	0.003796	0.36025	1739.2	87.8	1795.3	61.7	3.1	1795	62	3.44%
01DTB19	18/03/2020 (4) 00:59:41.00	01DTB19 - 89	158	4	157	5	3.051572	0.18208864	0.1155	0.00391	0.25653	1827.2	93.1	1886.9	59.8	3.2	1887	60	3.17%
01DTB19	18/03/2020 (4) 02:48:56.00	01DTB19 - 129	82	12	78	9	3.10752	0.1876873	0.1137	0.006074	-0.20077	1798.5	92.9	1858.6	94.5	3.2	1859	94	5.08%
01DTB19	18/03/2020 (4) 02:44:58.00	01DTB19 - 127	119	3	142	6	3.15557	0.1826028	0.1124	0.004448	0.33436	1774.6	88.0	1837.8	70.2	3.4	1838	70	3.82%
01DTB19	17/03/2020 (3) 23:10:17.00	01DTB19 - 52	179	5	89	6	3.558719	0.21048368	0.1019	0.003838	0.2653	1596.4	81.9	1658.2	68.4	3.7	1658	68	4.13%
01DTB19	18/03/2020 (4) 01:41:21.00	01DTB19 - 105	117	2	106	3	3.335557	0.20022244	0.1077	0.003754	0.2147	1690.3	87.4	1760	62.5	4.0	1760	63	3.55%
01DTB19	17/03/2020 (3) 21:01:17.00	01DTB19 - 2	159	3	292	4	4.18235	0.14137078	0.0907	0.003214	0.10152	1382	41.2	1439.5	66.2	4.0	1382	41	2.98%
01DTB19	18/03/2020 (4) 01:31:27.00	01DTB19 - 100	183	4	207	8	3.644315	0.2189776	0.1005	0.00361	0.12479	1563.1	81.7	1632.5	65.5	4.3	1633	65	4.01%
01DTB19	18/03/2020 (4) 02:11:02.00	01DTB19 - 120	95	5	240	14	3.612717	0.21582324	0.1013	0.004726	0.11693	1575.2	81.7	1647.2	84.9	4.4	1647	85	5.15%
01DTB19	18/03/2020 (4) 00:45:49.00	01DTB19 - 82	133	4	142	5	3.343363	0.20100416	0.1083	0.004266	0.088584	1686.8	87.4	1770.2	70.6	4.7	1770	71	3.99%
01DTB19	18/03/2020 (4) 02:01:06.00	01DTB19 - 115	82	8	70	8	2.310536	0.13696653	0.158	0.00566	0.15902	2318.3	113.1	2433.6	59.6	4.7	2434	60	2.45%
01DTB19	18/03/2020 (4) 00:07:49.00	01DTB19 - 76	129	3	59	1	4.739336	0.16217065	0.0844	0.003488	0.074006	1234.1	37.6	1300.9	78.8	5.1	1234	38	3.05%
01DTB19	17/03/2020 (3) 21:11:07.00	01DTB19 - 7	122	4	110	5	3.810976	0.23597842	0.0981	0.003762	0.28368	1502.1	81.3	1587.5	70.2	5.4	1588	70	4.42%
01DTB19	18/03/2020 (4) 00:57:41.00	01DTB19 - 88	205	2	123	1	3.629764	0.21752238	0.1019	0.003538	0.13011	1568.7	81.7	1658.2	63.1	5.4	1658	63	3.81%
01DTB19	17/03/2020 (3) 21:22:59.00	01DTB19 - 13	77	2	97	3	3.664346	0.22098862	0.1016	0.005032	0.50833	1555.5	81.7	1652.7	90.0	5.9	1653	90	5.44%
01DTB19	17/03/2020 (3) 23:44:07.00	01DTB19 - 64	75	2	64	2	3.907776	0.14534667	0.0967	0.004234	0.38237	1468.8	47.8	1560.6	80.6	5.9	1469	48	3.26%
01DTB19	18/03/2020 (4) 02:47:00.00	01DTB19 - 128	123	7	88	2	3.49406	0.2041742	0.1058	0.004616	-0.031921	1622.5	82.1	1727.4	78.4	6.1	1727	78	4.54%
01DTB19	17/03/2020 (3) 22:56:29.00	01DTB19 - 45	144	1	81	1	2.416043	0.14171704	0.1533	0.004766	0.097278	2232.7	108.4	2382.3	51.9	6.3	2382	52	2.18%
01DTB19	17/03/2020 (3) 21:44:55.00	01DTB19 - 19	168	20	85	3	3.710575	0.2256635	0.1013	0.003826	0.11422	1538.3	81.5	1647.2	68.6	6.6	1647	69	4.16%
01DTB19	17/03/2020 (3) 23:57:54.00	01DTB19 - 71	257	10	198	8	3.183699	0.20557718	0.1159	0.003618	-0.038283	1760.9	97.4	1893.1	55.1	7.0	1893	55	2.91%
01DTB19	18/03/2020 (4) 00:51:48.00	01DTB19 - 85	105	5	85	5	3.620565	0.2297132	0.1037	0.003974	0.029984	1572.2	86.8	1690.5	69.2	7.0	1691	69	4.09%
01DTB19	17/03/2020 (3) 23:14:14.00	01DTB19 - 54	263	7	164	6	3.411805	0.1962806	0.1091	0.003282	0.15957	1657	82.3	1783.6	53.7	7.1	1784	54	3.01%
01DTB19	17/03/2020 (3) 21:13:09.00	01DTB19 - 8	111	4	139	3	4.029009	0.16499132	0.0959	0.004418	0.14339	1429.2	51.4	1545	84.9	7.5	1429	51	3.59%
01DTB19	17/03/2020 (3) 23:16:15.00	01DTB19 - 55	193	5	130	6	3.49895	0.2046482	0.1075	0.00345	0.079063	1620.5	82.1	1756.6	57.6	7.7	1757	58	3.28%
01DTB19	17/03/2020 (3) 22:46:33.00	01DTB19 - 40	162	3	129	2	3.952569	0.25090218	0.0978	0.004056	-0.1594	1453.9	80.9	1581.8	76.0	8.1	1454	81	5.57%
01DTB19	17/03/2020 (3) 21:56:45.00	01DTB19 - 25	367	9	126	3	3.507541	0.21778492	0.1077	0.003554	0.083179	1617	87.0	1760	59.2	8.1	1760	59	3.36%
01DTB19	17/03/2020 (3) 21:15:05.00	01DTB19 - 9	341	10	245	13	3.729952	0.24154954	0.1027	0.003054	-0.048369	1531.2	86.4	1672.7	53.9	8.5	1673	54	3.22%
01DTB19	17/03/2020 (3) 23:36:11.00	01DTB19 - 60	81	2	67	3	3.658983	0.22044936	0.1045	0.00489	0.28886	1557.5	81.7	1704.7	84.5	8.6	1705	84	4.96%
01DTB19	17/03/2020 (3) 21:25:00.00	01DTB19 - 14	349	11	438	19	4.173623	0.12876219	0.0945	0.00299	0.085584	1384.6	37.6	1517.3	58.4	8.7	1385	38	2.72%
01DTB19	17/03/2020 (3) 21:42:54.00	01DTB19 - 18	222	5	81	1	3.42818	0.2095926	0.1107	0.003714	0.090453	1650	87.2	1810.1	59.8	8.8	1810	60	3.30%
01DTB19	17/03/2020 (3) 22:18:29.00	01DTB19 - 36	326	4	148	5	3.367003	0.20338056	0.1125	0.00435	-0.49261	1676.4	87.4	1839.4	68.6	8.9	1839	69	3.73%
01DTB19	17/03/2020 (3) 21:09:11.00	01DTB19 - 6	255	7	139	8	3.595829	0.21414638	0.1065	0.00353	-0.046094	1581.8	81.9	1739.5	59.6	9.1	1740	60	3.43%
01DTB19	17/03/2020 (3) 22:52:31.00	01DTB19 - 43	103	5	104	4	4.389816	0.15331596	0.0915	0.00423	0.28266	1323	41.0	1456.2	86.2	9.1	1323	41	3.10%
01DTB19	17/03/2020 (3) 23:04:23.00	01DTB19 - 49	405	5	239	6	4.189359	0.13994951	0.0946	0.002992	0.35276	1379.9	40.6	1519.3	58.4	9.2	1380	41	2.94%
01DTB19	18/03/2020 (4) 01:11:33.00	01DTB19 - 95	338	13	237	7	3.462604	0.21312758	0.1103	0.003506	-0.13827	1635.5	87.2	1803.5	56.6	9.3	1804	57	3.14%
01DTB19	17/03/2020 (3) 21:38:53.00	01DTB19 - 16	182	2	65	2	3.522367	0.21933214	0.1087	0.003674	0.10846	1611	87.0	1776.9	60.4	9.3	1777	60	3.40%
01DTB19	18/03/2020 (4) 01:05:35.00	01DTB19 - 92	93	2	65	1	3.969829	0.23541608	0.0987	0.004974	-0.23523	1448.3	75.5	1598.9	92.1	9.4	1448	75	5.21%
01DTB19	18/03/2020 (4) 01:57:08.00	01DTB19 - 113	314	14	135	19	3.434066	0.21019502	0.1113	0.003226	-0.010651	1647.5	87.2	1819.9	51.5	9.5	1820	52	2.83%
01DTB19	17/03/2020 (3) 22:58:26.00	01DTB19 - 46	181	3	160	2	3.454231	0.21226522	0.1108	0.003716	0.39919	1639	87.2	1811.8	59.8	9.5	1812	60	3.30%
01DTB19	17/03/2020 (3) 22:10:34.00	01DTB19 - 32	139	5	141	3	3.886514	0.16684972	0.1011	0.004222	-0.093161	1476	55.5	1643.6	75.9	10.2	1476	55	3.76%
01DTB19	17/03/2020 (3) 21:03:13.00	01DTB19 - 3	262	4	127	6	4.462294	0.14898207	0.0914	0.003228	0.11685	1303.5	38.6	1454.1	65.9	10.4	1304	39	2.96%
01DTB19	17/03/2020 (3) 22:44:36.00	01DTB19 - 39	109	1	97	1	3.880481	0.22819092	0.1014	0.004428	0.10269	1478.1	76.0	1649.1	79.4	10.4	1478	76	5.14%
01DTB19	17/03/2020 (3) 23:00:26.00	01DTB19 - 47	466	10	377	15	3.695492	0.23778974	0.1057	0.003214	-0.25701	1543.8	86.6	1725.7	54.7	10.5	1726	55	3.17%
01DTB19	18/03/2020 (4) 00:49:47.00	01DTB19 - 84	232	3	121	2	3.716091	0.22622442	0.1055	0.00371	0.25255	1536.2	81.5	1722.2	63.3	10.8	1722	63	3.68%
01DTB19	18/03/2020 (4) 01:39:25.00	01DTB19 - 104	200	3	114	3	3.777862	0.23255184	0.1041	0.003782	0.098736	1513.8	81.3	1697.6	65.7	10.8	1698	66	3.87%
01DTB19	18/03/2020 (4) 00:41:53.00	01DTB19 - 80	276	5	78	5	3.570154	0.21160908	0.1092	0.003284	0.053062	1591.9	81.9	1785.3	53.7	10.8	1785	54	3.01%
01DTB19	18/03/2020 (4) 02:43:03.00	01DTB19 - 126	325	6	127	4	3.508772	0.21791324	0.1111	0.003422	0.018373	1616.5	87.0	1816.7	54.9	11.0	1817	55	3.02%
01DTB19	17/03/2020 (3) 22:14:31.00	01DTB19 - 34	85	1	70	2	3.743916	0.22906432	0.1051	0.004702	0.20156	1526.1	81.5	1715.2	80.6	11.0	1715	81	4.70%
01DTB19	17/03/2020 (3) 23:48:04.00	01DTB19 - 66	140	2	94	2	3.656307	0.22018054	0.1073	0.004346	0.27289	1558.5	81.7	1753.2	72.7	11.1	1753	73	4.15%
01DTB19	18/03/2020 (4) 00:03:51.00	01DTB19 - 74	175	11	146	5	3.559986	0.22328172	0.1098	0.004096	0.29485	1595.9	86.8	1795.3	66.6	11.1	1795	67	3.71%
01DTB19	17/03/2020 (3) 21:46:51.00	01DTB19 - 20	221	4	102	1	3.785011	0.23328962	0.1043	0.003486	0.095589	1511.3	81.3	1701.2	60.4	11.2	1701	60	3.55%
01DTB19	17/03/2020 (3) 21:26:56.00	01DTB19 - 15	245	14	276	26	4.108463	0.23408446	0.0978	0.003956	0.095107	1404.3	70.4	1581.8	74.1	11.2	1404	70	5.01%
01DTB19	18/03/2020 (4) 01:15:31.00	01DTB19 - 97	99	2	84	3	3.881988	0.22833806	0.1028	0.003756	0.30533	1477.6	76.0	1674.5	66.2	11.8	1478	76	5.15%
01DTB19	17/03/2020 (3) 23:08:20.00	01DTB19 - 51	229	12	251	17	4.50045	0.2641938	0.092	0.00314	0.29338	1293.5	67.4	1466.5	63.5	11.8	1294	67	5.21%
01DTB19	17/03/2020 (3) 23:18:11.00	01DTB19 - 56	242	2	100	1	3.661662	0.22071874	0.1083	0.003566	0.2063	1556.5	81.7	1770.2	59.0	12.1	1770	59	3.33%
01DTB19	18/03/2020 (4) 01:59:10.00	01DTB19 - 114	153	4	106	4	3.793627	0.23418014	0.1052	0.004104	0.19445	1508.2	81.3	1717	70.4	12.2	1717	70	4.10%
01DTB19	18/03/2020 (4) 02:05:05.00	01DTB19 - 117	171	5	186	7	3.880481	0.22819092	0.1033	0.003766	0.22367	1478.1	76.0	1683.4	66.1	12.2	1478	76	5.14%
01DTB19	18/03/2020 (4) 02:03:07.00	01DTB19 - 116	176	3	134	7	2.592017	0.15261854	0.1549	0.005698	-0.20111	2103.3	103.5	2400	61.3	12.4	2400	61	2.56%
01DTB19	17/03/2020 (3) 22:04:40.00	01DTB19 - 29	366	23	200	12	3.844675	0.2542718	0.10438	0.0030776	-0.13665	1490.4	86.2	1702.6	53.1	12.5	1490	86	5.79%
01DTB19	17/03/2020 (3) 21:07:10.00	01DTB19 - 5	113	4	179	6	3.960396	0.23605532	0.1019	0.004038	0.1615	1451.4	75.9	1658.2	71.9	12.5	1451	76	5.23%
01DTB19	17/03/2020 (3) 21:58:43.00	01DTB19 - 26	303	5	118	3	3.875969	0.24277388	0.1037	0.003374	-0.038835	1479.6	81.1	1690.5	58.8	12.5	1480	81	5.48%
01DTB19	18/03/2020 (4) 01:51:16.00	01DTB19 - 110	285	5	193	13	2.67666	0.1610008	0.1495	0.00469	-0.064671	2046.3	103.3	2339.4	52.5	12.5	2339	53	2.25%
01DTB19	17/03/2020 (3) 22:50:30.00	01DTB19 - 42	83	3	57	3	3.755163	0.23021706	0.1071	0.004142	0.31366	1522	81.5	1749.8	69.4	13.0	1750	69	3.97%
01DTB19	17/03/2020 (3) 23:55:59.00	01DTB19 - 70	317	11	330	26	3.695492	0.22413304	0.109	0.00328	-0.11876	1543.8	81.5	1781.9	53.7	13.4	1782	54	3.01%
01DTB19	18/03/2020 (4) 02:41:02.00	01DTB19 - 125	174	3	203	8	2.704164	0.17108338	0.1497	0.005194	-0.59168	2028.5	108.0	2341.7	58.2	13.4	2342	58	2.49%
01DTB19	18/03/2020 (4) 00:09:46.00	01DTB19 - 77	281	4	154	6	3.963535	0.2520764	0.1028	0.003456	0.37149	1450.3	80.9	1674.5	61.0	13.4	1450	81	5.58%
01DTB19	17/03/2020 (3) 23:06:19.00	01DTB19 - 50	268	3	168	11	3.731343	0.21385606	0.1082	0.003664	0.05773	1530.6	76.4	1768.5	60.6	13.5	1769	61	3.42%
01DTB19	18/03/2020 (4) 01:03:39.00	01DTB19 - 91	259	19	222	10	3.782148	0.26160336	0.1071	0.003942	-0.32178	1512.3	91.3	1749.8	66.1	13.6	1750	66	3.77%
01DTB19	17/03/2020 (3) 23:02:22.00	01DTB19 - 48	193	3	138	4	3.698225	0.22441	0.1094	0.003788	0.23294	1542.8	81.5	1788.6	61.7	13.7	1789	62	3.45%
01DTB19	17/03/2020 (3) 22:16:32.00	01DTB19 - 35	210	13	110	6	3.813883	0.25082606	0.1066	0.004132	0.13491	1501.1	86.2	1741.3	69.6	13.8	1741	70	4.00%
01DTB19	17/03/2020 (3) 23:46:03.00	01DTB19 - 65	288	8	255	5	3.702332	0.23853384	0.1096	0.003192	0.085637	1541.3	86.6	1792	51.9	14.0	1792	52	2.90%
01DTB19	17/03/2020 (3) 21:17:06.00	01DTB19 - 10	205	3	169	8	2.747253	0.19079826	0.1493	0.005286	-0.47845	2001.1	117.0	2337.2	59.4	14.4	2337	59	2.54%
01DTB19	17/03/2020 (3) 22:54:28.00	01DTB19 - 44	132	2	104	2	3.992016	0.22804692	0.1033	0.004066	0.22968	1441.1	72.3	1683.4	71.1	14.4	1441	72	5.02%
01DTB19	18/03/2020 (4) 02:39:06.00	01DTB19 - 124	333	12	189	16	3.918495	0.2303805	0.105	0.0037	-0.12468	1465.2	75.5	1713.5	63.5	14.5	1465	75	5.15%
01DTB19	17/03/2020 (3) 21:54:44.00	01DTB19 - 24	440	30	275	19	4.027386	0.20544052	0.1028	0.003156	-0.41598	1429.7	64.1	1674.5	55.7	14.6	1430	64	4.48%
01DTB19	18/03/2020 (4) 00:11:46.00	01DTB19 - 78	306	14	268	23	3.773585	0.2321111	0.1086	0.003472	-0.064507	1515.4	81.3	1775.2	57.2	14.6	1775	57	3.22%
01DTB19	18/03/2020 (4) 00:05:48.00	01DTB19 - 75	165	4	131	12	3.872967	0.27245764	0.1065	0.00353	0.26711	1480.6	91.1	1739.5	59.6	14.9	1481	91	6.16%
01DTB19	18/03/2020 (4) 01:01:38.00	01DTB19 - 90	74	1	66	2	3.507541	0.21778492	0.1169	0.005138	0.35071	1617	87.0	1908.5	77.4	15.3	1909	77	4.06%
01DTB19	18/03/2020 (4) 00:47:51.00	01DTB19 - 83	152	10	192	20	4.029009	0.16661462	0.1035	0.00357	0.10753	1429.2	51.9	1687	62.3	15.3	1429	52	3.63%
01DTB19	18/03/2020 (4) 02:50:57.00	01DTB19 - 130	264	6	178	10	3.926188	0.23267326	0.106	0.00352	0.042851	1462.7	76.0	1730.9	59.8	15.5	1463	76	5.20%
01DTB19	17/03/2020 (3) 22:06:36.00	01DTB19 - 30	744	7	258	10	4.302926	0.19714952	0.09854	0.0028908	-0.089315	1347.1	54.5	1595.8	53.7	15.6	1347	54	4.04%
01DTB19	17/03/2020 (3) 23:52:00.00	01DTB19 - 68	392	9	190	4	4.050223	0.14005996	0.105	0.0032	0.15639	1422.5	43.3	1713.5	54.9	17.0	1423	43	3.05%
01DTB19	18/03/2020 (4) 02:54:55.00	01DTB19 - 132	366	15	163	11	3.924647	0.16320863	0.1079	0.003458	-0.051787	1463.2	53.3	1763.4	57.4	17.0	1463	53	3.64%
01DTB19	18/03/2020 (4) 01:19:28.00	01DTB19 - 99	439	9	468	16	3.795066	0.23432912	0.1116	0.003632	-0.42519	1507.7	81.3	1824.8	57.8	17.4	1825	58	3.17%
01DTB19	17/03/2020 (3) 23:42:06.00	01DTB19 - 63	197	32	210	14	3.776435	0.2466662	0.1125	0.00435	-0.31173	1514.4	86.4	1839.4	68.6	17.7	1839	69	3.73%
01DTB19	18/03/2020 (4) 01:37:23.00	01DTB19 - 103	65	4	84	2	3.412969	0.27792988	0.1239	0.007478	-0.69991	1656.5	116.6	2012.3	104.9	17.7	2012	105	5.21%
01DTB19	18/03/2020 (4) 00:55:45.00	01DTB19 - 87	89	1	68	4	4.030633	0.16509186	0.1067	0.004434	0.03598	1428.7	51.4	1743	74.7	18.0	1429	51	3.59%
01DTB19	18/03/2020 (4) 01:43:22.00	01DTB19 - 106	134	4	104	3	3.958828	0.25157206	0.1092	0.004784	0.22786	1451.9	80.9	1785.3	78.2	18.7	1452	81	5.58%
01DTB19	17/03/2020 (3) 21:40:58.00	01DTB19 - 17	122	6	103	2	3.985652	0.16867139	0.1086	0.004272	0.35826	1443.1	53.7	1775.2	70.4	18.7	1443	54	3.72%
01DTB19	17/03/2020 (3) 22:08:36.00	01DTB19 - 31	292	5	225	13	3.85505	0.1811309	0.1121	0.008442	-0.82144	1486.8	61.2	1832.9	133.7	18.9	1487	61	4.11%
01DTB19	17/03/2020 (3) 23:50:00.00	01DTB19 - 67	122	2	125	2	4.291845	0.15030668	0.1026	0.004752	0.053258	1350.2	41.7	1670.9	83.9	19.2	1350	42	3.09%
01DTB19	18/03/2020 (4) 01:09:32.00	01DTB19 - 94	210	7	142	7	3.846154	0.13461539	0.1131	0.004062	0.10878	1489.8	45.7	1849	63.7	19.4	1490	46	3.07%
01DTB19	17/03/2020 (3) 21:19:02.00	01DTB19 - 11	332	3	303	29	4.171882	0.1495751	0.1064	0.003228	-0.024	1385.1	43.7	1737.8	54.5	20.3	1385	44	3.16%
01DTB19	18/03/2020 (4) 01:47:20.00	01DTB19 - 108	237	9	164	9	3.76506	0.259585	0.1169	0.003938	-0.082681	1518.4	91.3	1908.5	59.2	20.4	1909	59	3.10%
01DTB19	18/03/2020 (4) 01:55:12.00	01DTB19 - 112	116	3	96	5	3.951008	0.15238932	0.1124	0.004948	0.29715	1454.4	49.2	1837.8	78.2	20.9	1454	49	3.38%
01DTB19	17/03/2020 (3) 23:20:13.00	01DTB19 - 57	268	4	373	19	3.958828	0.23589976	0.1126	0.006552	0.073196	1451.9	75.9	1841	103.3	21.1	1452	76	5.22%
01DTB19	17/03/2020 (3) 21:05:14.00	01DTB19 - 4	363	12	218	13	3.816794	0.23658298	0.1191	0.003982	0.25336	1500.1	81.3	1942	58.6	22.8	1942	59	3.02%
01DTB19	17/03/2020 (3) 22:00:44.00	01DTB19 - 27	454	36	463	10	5.333333	0.19768888	0.0923	0.003446	0.028558	1107.8	37.0	1472.7	69.4	24.8	1108	37	3.34%
01DTB19	17/03/2020 (3) 23:40:09.00	01DTB19 - 62	282	9	214	9	4.686036	0.22986612	0.1022	0.003344	-0.28545	1246.9	54.5	1663.6	59.4	25.0	1247	54	4.37%
01DTB19	17/03/2020 (3) 21:50:48.00	01DTB19 - 22	26	1	39	3	6.079027	0.42091254	0.0861	0.006722	0.050857	981.7	61.7	1339.6	147.8	26.7	982	62	6.29%
01DTB19	17/03/2020 (3) 21:48:52.00	01DTB19 - 21	70	5	129	11	4.833253	0.22981896	0.1018	0.004536	0.19662	1212.3	51.5	1656.4	80.9	26.8	1212	52	4.25%
01DTB19	17/03/2020 (3) 23:32:11.00	01DTB19 - 58	386	14	252	17	3.259452	0.20330144	0.1541	0.005982	-0.62034	1724.9	92.5	2391.2	64.7	27.9	2391	65	2.70%
01DTB19	17/03/2020 (3) 23:53:58.00	01DTB19 - 69	176	3	94	2	4.777831	0.24621922	0.1043	0.003786	-0.0031321	1225.1	56.3	1701.2	65.5	28.0	1225	56	4.59%
01DTB19	17/03/2020 (3) 23:34:10.00	01DTB19 - 59	290	5	192	8	4.516712	0.29434114	0.1101	0.004102	0.082333	1289.3	74.7	1800.2	66.4	28.4	1289	75	5.79%
01DTB19	17/03/2020 (3) 23:38:08.00	01DTB19 - 61	316	6	267	32	4.892368	0.18162078	0.1047	0.003594	0.10791	1198.9	39.8	1708.2	61.9	29.8	1199	40	3.32%
01DTB19	18/03/2020 (4) 02:37:06.00	01DTB19 - 123	136	7	130	14	2.785515	0.2884832	0.211	0.02122	-0.8532	1977.4	172.9	2912.5	159.5	32.1	2913	160	5.48%
01DTB19	18/03/2020 (4) 02:07:05.00	01DTB19 - 118	212	6	321	56	5.136107	0.27418954	0.1079	0.003958	0.048625	1146.8	54.9	1763.4	65.7	35.0	1147	55	4.79%
01DTB19	17/03/2020 (3) 22:48:34.00	01DTB19 - 41	156	7	241	35	3.557453	0.24832566	0.1631	0.005962	0.27719	1596.9	96.8	2487.3	60.4	35.8	2487	60	2.43%

Spot ID	176Hf/177Hf	±2σ INT	(2% External ±)	176Lu/177Hf m	±2σ INT	176Yb/177Hf	±2σ INT	Hfi	εHf	±2σ	TDM(Ga)	TDMCrustal (Ga)	HfCHUR(t)	HfDM(t)	Analysis Notes
01DTB19 - 72	0.282054	0.000018	0.005641109	0.0009159	0.0000081	0.03391	0.00021	0.2820288	6.01	0.63	1.68	4.187	0.281859468	0.283251	
01DTB19 - 109	0.281432	0.000027	0.005628705	0.000583	0.00002	0.02104	0.00072	0.2814112	-6.30	0.95	2.52	3.639	0.281588681	0.282193249	
01DTB19 - 53	0.281591	0.000028	0.00563189	0.0003341	0.0000027	0.011771	0.000062	0.2815801	-3.96	0.98	2.29	2.408	0.281691647	0.281883778	
01DTB19 - 98	0.281821	0.000024	0.005636471	0.001141	0.000049	0.0436	0.0022	0.2817843	2.88	0.84	2.02	2.195	0.281703033	0.282001454	
01DTB19 - 79	0.281836	0.000027	0.005636785	0.000565	0.000034	0.0205	0.0013	0.2818176	4.47	0.95	1.97	2.166	0.281691647	0.282014466	
01DTB19 - 107	0.282054	0.000033	0.005641177	0.002733	0.000029	0.1001	0.0011	0.2819684	8.35	1.16	1.77	1.728	0.281733226	0.282001454	
01DTB19 - 1	0.281907	0.000022	0.005638183	0.000647	0.000027	0.0243	0.001	0.2818858	7.09	0.77	1.87	2.098	0.281686017	0.282048973	
01DTB19 - 102	0.281947	0.000024	0.005638991	0.001011	0.000028	0.0372	0.0011	0.2819155	6.30	0.84	1.84	1.827	0.281737943	0.28199502	
01DTB19 - 101	0.281985	0.000024	0.005639751	0.001862	0.000061	0.0655	0.0024	0.2819276	6.31	0.84	1.82	1.917	0.281749831	0.282054364	
01DTB19 - 81	0.281972	0.000025	0.005639495	0.000992	0.000022	0.037	0.001	0.2819411	7.21	0.88	1.80	1.935	0.281737943	0.282067949	
01DTB19 - 93	0.281789	0.000024	0.005635831	0.001404	0.00004	0.0525	0.0016	0.2817437	1.49	0.84	2.08	2.408	0.281701868	0.282054364	
01DTB19 - 73	0.282034	0.000021	0.005640719	0.001007	0.000027	0.03642	0.00088	0.2820065	4.94	0.74	1.72	1.460	0.281867387	0.282013135	
01DTB19 - 122	0.281627	0.000025	0.005632595	0.000564	0.000019	0.02053	0.00068	0.2816080	-1.63	0.88	2.25	3.120	0.281653969	0.282202299	
01DTB19 - 96	0.281762	0.000026	0.0056353	0.000657	0.000032	0.0241	0.0013	0.2817407	1.58	0.91	2.07	2.206	0.281696176	0.281958393	
01DTB19 - 131	0.282039	0.000029	0.005640855	0.0003984	0.0000074	0.01439	0.00027	0.2820280	6.11	1.02	1.68	1.414	0.281855797	0.282006629	
01DTB19 - 33	0.281711	0.000022	0.005634263	0.0004219	0.0000083	0.01574	0.00031	0.2816984	-3.04	0.77	2.13	2.687	0.281783984	0.282189054	
01DTB19 - 23	0.28153	0.000023	0.005630647	0.000657	0.000021	0.02497	0.00082	0.2815074	-4.29	0.81	2.39	3.172	0.28162818	0.282106982	
01DTB19 - 111	0.28118	0.000029	0.005623675	0.000636	0.00001	0.02357	0.00037	0.2811507	-3.02	1.02	2.86	4.172	0.281235494	0.28192892	
01DTB19 - 38	0.281862	0.000026	0.0056373	0.000622	0.000013	0.02312	0.00044	0.2818420	4.85	0.91	1.93	0.860	0.281705297	0.281480135	
01DTB19 - 121	0.28197	0.000023	0.005639447	0.000736	0.000017	0.0241	0.00052	0.2819457	9.54	0.81	1.79	1.903	0.281677086	0.282017053	
01DTB19 - 12	0.281859	0.000026	0.00563173	0.000797	0.000012	0.02959	0.00046	0.2818337	4.15	0.91	1.95	2.023	0.281716872	0.281984812	
01DTB19 - 119	0.28201	0.000031	0.005640285	0.001508	0.000016	0.05329	0.00042	0.2819633	7.75	1.09	1.77	1.788	0.28174505	0.282030282	
01DTB19 - 28	0.281583	0.000028	0.00563173	0.000708	0.000015	0.02685	0.00059	0.2815634	-10.41	0.98	2.32	2.593	0.281856828	0.282062486	
01DTB19 - 37	0.282106	0.000025	0.005642175	0.001214	0.000015	0.04077	0.00053	0.2820726	7.50	0.88	1.62	1.723	0.281861142	0.282190232	
01DTB19 - 86	0.281772	0.000022	0.005635483	0.000873	0.000016	0.03249	0.00058	0.2817423	3.60	0.77	2.07	2.823	0.281640947	0.282195162	
01DTB19 - 89	0.281436	0.000027	0.005628785	0.0007684	0.0000083	0.02837	0.00027	0.2814085	-6.15	0.95	2.52	3.099	0.281581542	0.281943511	
01DTB19 - 129	0.281632	0.000017	0.005632666	0.00045	0.00002	0.01626	0.0007	0.2816161	0.58	0.60	2.24	2.450	0.281599906	0.281875619	
01DTB19 - 127	0.281611	0.000018	0.005632249	0.0004623	0.0000097	0.01683	0.00045	0.2815949	-0.66	0.63	2.27	2.525	0.281613397	0.281896607	
01DTB19 - 52	0.281843	0.000024	0.005636911	0.001489	0.000089	0.0549	0.0032	0.2817962	2.36	0.84	2.01	1.923	0.281729671	0.281912026	
01DTB19 - 105	0.281802	0.000025	0.005636095	0.00059	0.000048	0.025	0.0034	0.2817823	4.21	0.88	2.02	2.358	0.281663813	0.28204491	
01DTB19 - 2	0.282171	0.000023	0.005643467	0.002623	0.000029	0.1002	0.001	0.2821025	6.91	0.81	1.59	1.077	0.281907727	0.281969644	
01DTB19 - 100	0.282033	0.000026	0.00564072	0.001717	0.000014	0.05785	0.00045	0.2819799	8.29	0.91	1.75	2.244	0.281746278	0.282248402	
01DTB19 - 120	0.281897	0.000022	0.005637983	0.001385	0.000067	0.053	0.0026	0.2818538	4.15	0.77	1.92	2.126	0.28173678	0.282063889	
01DTB19 - 82	0.281677	0.000022	0.005633583	0.001069	0.000036	0.0394	0.0011	0.2816411	-0.57	0.77	2.21	2.706	0.281657208	0.282053035	
01DTB19 - 115	0.281176	0.000024	0.005623571	0.000839	0.000047	0.0319	0.0021	0.2811370	-3.12	0.84	2.88	4.292	0.281224872	0.281962095	
01DTB19 - 76	0.282174	0.000021	0.005643519	0.002124	0.000032	0.0801	0.0011	0.2821245	4.32	0.74	1.57	-0.292	0.282002695	0.281467997	
01DTB19 - 7	0.28199	0.000023	0.005639847	0.001276	0.000015	0.04651	0.00064	0.2819517	6.26	0.81	1.79	2.508	0.281775336	0.282356938	
01DTB19 - 88	0.282032	0.000022	0.005640683	0.001165	0.0000059	0.04368	0.00031	0.2819954	9.43	0.77	1.73	1.891	0.281729671	0.282097099	
01DTB19 - 13	0.28198	0.00003	0.00563968	0.001572	0.000059	0.0578	0.0024	0.2819308	7.01	1.05	1.82	1.914	0.281733226	0.28204491	
01DTB19 - 64	0.282019	0.00002	0.005640415	0.001097	0.000012	0.04033	0.00055	0.2819885	4.85	0.70	1.74	1.607	0.281851869	0.282048973	
01DTB19 - 128	0.281872	0.000021	0.005637479	0.0003978	0.0000043	0.0145	0.0002	0.2818590	6.18	0.74	1.91	2.468	0.281684917	0.282184564	
01DTB19 - 45	0.281171	0.000021	0.005623459	0.000655	0.0000081	0.0248	0.00017	0.2811412	-4.17	0.74	2.87	4.301	0.281258495	0.281993762	
01DTB19 - 19	0.281967	0.000024	0.005639391	0.001036	0.000068	0.0377	0.0022	0.2819347	7.02	0.84	1.81	0.657	0.28173678	0.281506423	
01DTB19 - 71	0.281567	0.000023	0.005631387	0.0001772	0.0000085	0.00815	0.00034	0.2815606	-0.60	0.81	2.31	3.010	0.281577517	0.282053035	
01DTB19 - 85	0.281913	0.00002	0.005638295	0.001264	0.000034	0.0462	0.001	0.2818725	5.81	0.70	1.90	1.687	0.281708789	0.28187102	
01DTB19 - 54	0.281785	0.00002	0.005635735	0.00067	0.000014	0.02604	0.00063	0.2817623	4.04	0.70	2.04	2.373	0.281648528	0.282021044	
01DTB19 - 8	0.281711	0.000022	0.005634263	0.000925	0.000012	0.0355	0.00034	0.2816860	-6.79	0.77	2.16	2.036	0.281877364	0.281952175	
01DTB19 - 55	0.281547	0.000024	0.005630991	0.0002843	0.0000027	0.01046	0.0001	0.2815375	-4.56	0.84	2.34	3.284	0.281666015	0.282213701	
01DTB19 - 40	0.281992	0.000026	0.0056399	0.001412	0.000017	0.0537	0.00082	0.2819532	3.25	0.91	1.79	1.497	0.281861464	0.28197216	
01DTB19 - 25	0.281616	0.000017	0.005632346	0.000498	0.000011	0.01764	0.00037	0.2815994	-2.29	0.60	2.26	3.109	0.281663813	0.28219553	
01DTB19 - 9	0.28196	0.000029	0.005639275	0.00074	0.000013	0.0257	0.00072	0.2819366	7.68	1.02	1.81	1.748	0.281720298	0.281969644	
01DTB19 - 60	0.281902	0.000021	0.005638079	0.001031	0.00003	0.0394	0.0012	0.2818687	6.00	0.74	1.90	2.083	0.281699604	0.282034198	
01DTB19 - 14	0.282065	0.000022	0.005641343	0.00096	0.000026	0.0312	0.001	0.2820399	4.75	0.77	1.67	1.317	0.281906055	0.282010548	
01DTB19 - 18	0.281674	0.000022	0.005633523	0.001159	0.000012	0.04411	0.00068	0.2816342	0.10	0.77	2.22	3.195	0.281631356	0.282246491	
01DTB19 - 36	0.281619	0.000021	0.005632419	0.000995	0.000014	0.03616	0.0002	0.2815843	-1.00	0.74	2.29	2.632	0.28161236	0.28193255	
01DTB19 - 6	0.281671	0.000021	0.005633459	0.001272	0.000056	0.0485	0.0023	0.2816291	-1.71	0.74	2.23	2.381	0.281677086	0.28191084	
01DTB19 - 43	0.282094	0.000024	0.005641931	0.000789	0.000024	0.02867	0.00079	0.2820743	4.56	0.84	1.62	1.118	0.281945643	0.281984812	
01DTB19 - 49	0.281568	0.000024	0.005631411	0.000697	0.000014	0.02545	0.00056	0.2815498	-12.74	0.84	2.34	3.054	0.281909077	0.282291735	
01DTB19 - 95	0.281784	0.000024	0.005635731	0.001346	0.00002	0.0461	0.0011	0.2817380	3.63	0.84	2.08	2.964	0.281635633	0.282249945	
01DTB19 - 16	0.281637	0.000018	0.005632769	0.00095	0.000033	0.0364	0.0013	0.2816050	-1.70	0.63	2.26	2.533	0.281652868	0.281937438	
01DTB19 - 92	0.281963	0.000019	0.005639292	0.0007129	0.0000084	0.02646	0.00049	0.2819435	2.78	0.67	1.80	1.480	0.281865069	0.281957135	
01DTB19 - 113	0.281697	0.000023	0.005633987	0.001339	0.000055	0.0506	0.0022	0.2816508	0.92	0.81	2.20	3.063	0.281625003	0.28219965	
01DTB19 - 46	0.281588	0.000014	0.005631777	0.000916	0.000018	0.03513	0.0008	0.2815565	-2.62	0.49	2.33	2.650	0.281630254	0.28192529	
01DTB19 - 32	0.281948	0.000026	0.00563902	0.001682	0.000023	0.0622	0.0014	0.2819011	1.91	0.91	1.87	1.545	0.281847231	0.28193129	>10% Discordant, excluded
01DTB19 - 3	0.28218	0.000026	0.00564366	0.002215	0.000049	0.0798	0.0024	0.2821255	5.93	0.91	1.56	1.427	0.281958165	0.282179264	>10% Discordant, excluded
01DTB19 - 39	0.282001	0.000024	0.005640071	0.0013661	0.0000041	0.05257	0.00019	0.2819628	4.15	0.84	1.78	2.259	0.281845879	0.282306046	>10% Discordant, excluded
01DTB19 - 47	0.281628	0.00002	0.005632596	0.000861	0.00005	0.0336	0.0018	0.2815998	-3.06	0.70	2.27	3.034	0.281686017	0.282177719	>10% Discordant, excluded
01DTB19 - 84	0.281788	0.000019	0.005635792	0.001383	0.000018	0.05255	0.00042	0.2817429	1.94	0.67	2.08	2.297	0.281688282	0.28199502	>10% Discordant, excluded
01DTB19 - 104	0.281843	0.000021	0.005636899	0.000486	0.000019	0.01736	0.0007	0.2818274	4.37	0.74	1.95	2.086	0.281704197	0.281997608	>10% Discordant, excluded
01DTB19 - 80	0.281636	0.000021	0.005632759	0.001589	0.000044	0.0569	0.0015	0.2815822	-2.32	0.74	2.30	2.770	0.281647426	0.282015797	>10% Discordant, excluded
01DTB19 - 126	0.281603	0.000026	0.00563212	0.001263	0.000058	0.0435	0.0018	0.2815595	-2.40	0.91	2.33	2.706	0.281627078	0.281950916	>10% Discordant, excluded
01DTB19 - 34	0.281662	0.000032	0.005633331	0.0006337	0.0000081	0.02238	0.00013	0.2816414	-1.83	1.12	2.21	2.367	0.281692811	0.28192766	>10% Discordant, excluded
01DTB19 - 66	0.281789	0.000025	0.005635835	0.000767	0.000022	0.02828	0.00051	0.2817635	3.38	0.88	2.04	2.299	0.281668216	0.282002785	>10% Discordant, excluded
01DTB19 - 74	0.281741	0.000024	0.005634871	0.001739	0.000038	0.0656	0.0017	0.2816818	1.45	0.84	2.16	2.462	0.281640947	0.281974676	>10% Discordant, excluded
01DTB19 - 20	0.281883	0.00002	0.005637695	0.001309	0.000019	0.04899	0.00087	0.2818408	4.93	0.70	1.94	1.936	0.281701868	0.281943511	>10% Discordant, excluded
01DTB19 - 15	0.282039	0.000025	0.005640835	0.001087	0.000075	0.0357	0.0022	0.2820102	4.14	0.88	1.71	1.411	0.281893385	0.282013135	>10% Discordant, excluded
01DTB19 - 97	0.281958	0.000025	0.005639215	0.002041	0.00002	0.07611	0.0008	0.2819010	1.94	0.88	1.87	2.231	0.281846201	0.282232011	>10% Discordant, excluded
01DTB19 - 51	0.282093	0.000029	0.005641935	0.001859	0.000011	0.06443	0.00044	0.2820476	2.94	1.02	1.67	1.592	0.281964585	0.282178087	>10% Discordant, excluded
01DTB19 - 56	0.281645	0.000021	0.005632939	0.0003892	0.0000058	0.01432	0.00023	0.2816319	-0.90	0.74	2.22	3.309	0.281657208	0.282313383	>10% Discordant, excluded
01DTB19 - 114	0.281925	0.000031	0.005638585	0.001571	0.000053	0.0601	0.002	0.2818739	6.47	1.09	1.90	1.919	0.281691647	0.281962095	>10% Discordant, excluded
01DTB19 - 117	0.281875	0.000026	0.00563756	0.001434	0.00005	0.053	0.0018	0.2818349	-0.39	0.91	1.96	1.858	0.281845879	0.282001454	>10% Discordant, excluded
01DTB19 - 116	0.281202	0.000023	0.005624087	0.0006294	0.0000063	0.02309	0.00021	0.2811732	-2.62	0.81	2.83	4.654	0.281246898	0.282177719	>10% Discordant, excluded
01DTB19 - 29	0.28164	0.000025	0.005632855	0.001614	0.000044	0.0628	0.002	0.2815945	-8.64	0.88	2.30	1.258	0.281837955	0.281493169	>10% Discordant, excluded
01DTB19 - 5	0.281711	0.00002	0.005634255	0.000764	0.000017	0.02919	0.00056	0.2816900	-6.14	0.70	2.15	2.537	0.281863073	0.282168663	>10% Discordant, excluded
01DTB19 - 26	0.281699	0.000025	0.005634035	0.0004982	0.0000037	0.01833	0.000095	0.2816851	-5.67	0.88	2.15	2.641	0.281844912	0.28219737	>10% Discordant, excluded
01DTB19 - 110	0.281217	0.000026	0.0056244	0.000845	0.000015	0.03168	0.00048	0.2811793	-3.81	0.91	2.83	4.577	0.281286588	0.282176614	>10% Discordant, excluded
01DTB19 - 42	0.281885	0.000022	0.005637743	0.0004739	0.000007	0.0172	0.00029	0.2818693	7.06	0.77	1.90	0.987	0.281670418	0.28153853	>10% Discordant, excluded
01DTB19 - 70	0.281258	0.000024	0.005625211	0.000792	0.00003	0.02902	0.00096	0.2812312	-14.86	0.84	2.77	3.465	0.281649629	0.281977192	>10% Discordant, excluded
01DTB19 - 125	0.281163	0.000026	0.00562332	0.000522	0.00001	0.02001	0.00044	0.2811397	-5.17	0.91	2.88	4.175	0.281285083	0.281953433	>10% Discordant, excluded
01DTB19 - 77	0.281936	0.000025	0.005638775	0.000886	0.000025	0.03495	0.00092	0.2819117	1.70	0.88	1.85	0.584	0.281863782	0.281536809	>10% Discordant, excluded
01DTB19 - 50	0.28168	0.000023	0.005633647	0.001627	0.000049	0.0626	0.0016	0.2816254	-1.17	0.81	2.24	3.065	0.281658309	0.282198179	>10% Discordant, excluded
01DTB19 - 91	0.281611	0.000023	0.005632267	0.000494	0.00002	0.01996	0.00086	0.2815946	-2.69	0.81	2.27	2.588	0.281670418	0.281963353	>10% Discordant, excluded
01DTB19 - 48	0.281648	0.000022	0.005633003	0.001075	0.000012	0.0412	0.00052	0.2816115	-1.20	0.77	2.25	2.620	0.281645288	0.281977192	>10% Discordant, excluded
01DTB19 - 35	0.281739	0.000032	0.005634871	0.0016	0.00012	0.0564	0.0036	0.2816862	0.36	1.12	2.16	2.339	0.28167592	0.281948473	>10% Discordant, excluded
01DTB19 - 65	0.281713	0.000022	0.005634303	0.0007877	0.0000099	0.03014	0.00052	0.2816862	1.53	0.77	2.15	2.469	0.281643086	0.28198348	>10% Discordant, excluded
01DTB19 - 10	0.281254	0.00003	0.00562516	0.00071	0.000034	0.0253	0.00095	0.2812224	-2.33	1.05	2.77	3.970	0.281288028	0.281945955	>10% Discordant, excluded
01DTB19 - 44	0.281872	0.000024	0.005637491	0.001478	0.00003	0.05508	0.00049	0.2818317	-1.35	0.84	1.96	0.769	0.281869704	0.281540175	>10% Discordant, excluded
01DTB19 - 124	0.281815	0.00003	0.00563638	0.001449	0.000078	0.0513	0.0037	0.2817749	-2.81	1.05	2.04	2.442	0.281854187	0.282204948	>10% Discordant, excluded
01DTB19 - 24	0.281739	0.000014	0.005634797	0.001418	0.000093	0.0541	0.0036	0.2817007	-6.26	0.49	2.15	2.533	0.281877042	0.282187214	>10% Discordant, excluded
01DTB19 - 78	0.281627	0.000023	0.005632587	0.001082	0.000019	0.03985	0.00077	0.2815906	-2.25	0.81	2.28	3.184	0.281653969	0.282213333	>10% Discordant, excluded
01DTB19 - 75	0.281871	0.00002	0.005637455	0.001528	0.000053	0.0565	0.0019	0.2818282	-0.57	0.70	1.97	1.778	0.281844268	0.281958393	>10% Discordant, excluded
01DTB19 - 90	0.281619	0.000019	0.005632412	0.00066	0.000025	0.0254	0.001	0.2815951	0.98	0.67	2.27	3.223	0.281567519	0.282175878	>10% Discordant, excluded
01DTB19 - 83	0.281904	0.000021	0.005638119	0.000984	0.00005	0.0361	0.0019	0.2818774	0.00	0.74	1.90	1.388	0.281877364	0.281859593	>10% Discordant, excluded
01DTB19 - 130	0.281917	0.000039	0.005638475	0.0024	0.00015	0.0816	0.0043	0.2818506	-0.18	1.37	1.95	2.288	0.281855797	0.282213701	>10% Discordant, excluded
01DTB19 - 30	0.281622	0.000024	0.005632491	0.000308	0.000016	0.01512	0.00043	0.2816142	-11.21	0.84	2.24	2.648	0.28193016	0.282189054	>10% Discordant, excluded
01DTB19 - 68	0.281864	0.000025	0.005637335	0.000982	0.000019	0.03889	0.00046	0.2818376	-1.56	0.88	1.95	2.413	0.281881675	0.28227404	>10% Discordant, excluded
01DTB19 - 132	0.281696	0.000025	0.005633975	0.001232	0.000044	0.0505	0.0024	0.2816619	-6.87	0.88	2.20	2.724	0.281855475	0.282218629	>10% Discordant, excluded
01DTB19 - 99	0.281443	0.000022	0.005628903	0.001021	0.000047	0.0394	0.0021	0.2814077	-7.60	0.77	2.53	3.585	0.281621827	0.282188686	>10% Discordant, excluded
01DTB19 - 63	0.281613	0.000031	0.005632345	0.00095	0.00012	0.0364	0.0044	0.2815798	-1.15	1.09	2.29	2.617	0.28161236	0.281921659	>10% Discordant, excluded
01DTB19 - 103	0.281183	0.00002	0.005623696	0.0006062	0.0000078	0.02251	0.0003	0.2811598	-12.09	0.70	2.86	3.706	0.281500051	0.28191084	>10% Discordant, excluded
01DTB19 - 87	0.281953	0.000021	0.005639099	0.00083	0.000015	0.03118	0.00062	0.2819306	1.88	0.74	1.82	1.088	0.281877685	0.281782487	>10% Discordant, excluded
01DTB19 - 106	0.281849	0.000029	0.005637055	0.000931	0.00007	0.0308	0.0018	0.2818234	-1.39	1.02	1.97	2.340	0.281862751	0.282214069	>10% Discordant, excluded
01DTB19 - 17	0.281564	0.000023	0.005631327	0.000454	0.000011	0.018	0.00056	0.2815516	-11.24	0.81	2.33	2.902	0.281868417	0.282197002	>10% Discordant, excluded
01DTB19 - 31	0.281918	0.000025	0.005638415	0.001057	0.000036	0.0385	0.0015	0.2818883	1.70	0.88	1.88	2.204	0.281840274	0.282203476	>10% Discordant, excluded
01DTB19 - 67	0.282018	0.000026	0.00564042	0.001531	0.000021	0.05497	0.00036	0.2819790	1.80	0.91	1.76	1.789	0.281928168	0.282171313	>10% Discordant, excluded
01DTB19 - 94	0.281697	0.000028	0.00563401	0.000967	0.00009	0.0328	0.0026	0.2816698	-5.98	0.98	2.18	2.852	0.281838341	0.282271763	>10% Discordant, excluded
01DTB19 - 11	0.281506	0.000021	0.005630159	0.000709	0.000021	0.02565	0.00072	0.2814874	-14.84	0.74	2.43	2.925	0.281905733	0.282169104	>10% Discordant, excluded
01DTB19 - 108	0.281614	0.000031	0.005632365	0.001796	0.00007	0.0682	0.0021	0.2815489	-0.66	1.09	2.34	3.483	0.281567519	0.282246124	>10% Discordant, excluded
01DTB19 - 112	0.282033	0.000025	0.005640715	0.002244	0.00005	0.0827	0.0019	0.2819713	3.91	0.88	1.78	1.198	0.281861142	0.281859593	>10% Discordant, excluded
01DTB19 - 57	0.281835	0.000023	0.005636747	0.001287	0.000023	0.0493	0.0007	0.2817997	-2.24	0.81	2.01	2.351	0.281862751	0.282195162	>10% Discordant, excluded
01DTB19 - 4	0.281573	0.000025	0.005631515	0.001115	0.000099	0.0426	0.0032	0.2815319	-0.49	0.88	2.36	3.445	0.281545759	0.282197002	>10% Discordant, excluded
01DTB19 - 27	0.281696	0.000026	0.00563398	0.001524	0.000025	0.0581	0.0011	0.2816642	-14.87	0.91	2.21	1.497	0.282083587	0.281834725	>10% Discordant, excluded
01DTB19 - 62	0.281621	0.000021	0.005632459	0.001076	0.000028	0.0427	0.0013	0.2815957	-14.14	0.74	2.29	3.168	0.281994487	0.282449386	>10% Discordant, excluded
01DTB19 - 22	0.282108	0.00002	0.005642195	0.0008025	0.000008	0.03002	0.00028	0.2820932	-2.52	0.70	1.60	1.561	0.282164161	0.282347556	>10% Discordant, excluded
01DTB19 - 21	0.281712	0.000018	0.005634269	0.001232	0.000035	0.0496	0.0012	0.2816838	-11.80	0.63	2.17	3.142	0.282016671	0.28254147	>10% Discordant, excluded
01DTB19 - 58	0.281211	0.000022	0.005624263	0.000742	0.000053	0.0275	0.0015	0.2811772	-2.68	0.77	2.83	5.063	0.281252664	0.28237291	>10% Discordant, excluded
01DTB19 - 69	0.281976	0.000022	0.005639563	0.001667	0.000051	0.0608	0.0021	0.2819375	-2.52	0.77	1.83	0.213	0.282008466	0.281499759	>10% Discordant, excluded
01DTB19 - 59	0.281739	0.000033	0.005634877	0.001615	0.000048	0.0613	0.0014	0.2816997	-9.49	1.16	2.16	2.789	0.281967281	0.282363533	>10% Discordant, excluded
01DTB19 - 61	0.281676	0.000026	0.00563358	0.000752	0.000014	0.02953	0.00084	0.2816590	-12.99	0.91	2.20	2.685	0.282025259	0.282316464	>10% Discordant, excluded
01DTB19 - 123	0.28108	0.00014	0.005623343	0.000797	0.000072	0.0285	0.0036	0.2810355	4.49	4.90	3.01	5.914	0.280909433	0.282382725	>10% Discordant, excluded
01DTB19 - 118	0.281895	0.000047	0.005638096	0.001955	0.00005	0.0704	0.0017	0.2818527	-7.30	1.65	1.96	-0.589	0.282058629	0.281107495	>10% Discordant, excluded
01DTB19 - 41	0.28106	0.000021	0.005621239	0.00076	0.000026	0.02633	0.00085	0.2810239	-5.89	0.74	3.03	5.596	0.281189642	0.282420862	>10% Discordant, excluded

Appendix D3.1 continued.

Sample ID	Analysis date-time	Spot ID	238U conc. ppm	±2σ INT	232Th conc. ppm	±2σ INT	238U/206Pb	±2σ PROP	207Pb/206Pb	±2σ PROP	rho	238U/206Pb age	±2σ PROP	207Pb/206Pb age	±2σ PROP	Discord (7/6-6/8)/7/6*100	Preferred age Ma	2σ	error %	176Hf/177Hf	±2σ INT	(2% External ±)	176Lu/177Hf	±2σ INT	176Yb/177Hf	±2σ INT	Hfi	εHf	±2σ	TDM(Ga)	TDMCrustal (Ga)	HfCHUR(t)	HfDM(t)	Analysis Notes
34DTB19 (U-Pb from Brennan et al., 2021)	[illegible]	[illegible]	[illegible]	[illegible]	[illegible]	[illegible]	[illegible]	0.154959	0.080400	0.002808	0.428380	1188	34.0	1206	68.8	1.5	1188	34	2.86%	0.282054	0.000022	0.005641123	0.0006818	0.0000069	0.03132	0.0004	0.28204	0.23	0.77	1.67	1.988407794	0.282032115	0.28239056	
34DTB19 (U-Pb from Brennan et al., 2021)	[illegible]	[illegible]	[illegible]	[illegible]	[illegible]	[illegible]	[illegible]	0.164306	0.084400	0.002888	0.275000	1235	39.0	1301	66.5	5.1	1235	39	3.16%	0.282172	0.000024	0.005643491	0.000748	0.000013	0.02343	0.00047	0.28215	5.40	0.84	1.51	1.695416534	0.282002323	0.282356513	
34DTB19 (U-Pb from Brennan et al., 2021)	[illegible]	[illegible]	[illegible]	[illegible]	[illegible]	[illegible]	[illegible]	0.170575	0.088800	0.003476	0.419220	1286	43.9	1399	75.0	8.1	1286	44	3.41%	0.282220	0.000018	0.005644429	0.0013	0.000016	0.04838	0.0008	0.28219	7.77	0.63	1.47	1.584004085	0.281969335	0.282318812	
34DTB19 (U-Pb from Brennan et al., 2021)	[illegible]	[illegible]	[illegible]	[illegible]	[illegible]	[illegible]	[illegible]	0.166144	0.084400	0.004388	0.423270	1288	42.9	1301	101.0	1.0	1288	43	3.33%	0.282197	0.000025	0.005643995	0.00078	0.000011	0.0284	0.00034	0.28218	7.44	0.88	1.48	1.606637993	0.281968321	0.282317653	
34DTB19 (U-Pb from Brennan et al., 2021)	[illegible]	[illegible]	[illegible]	[illegible]	[illegible]	[illegible]	[illegible]	0.142120	0.085400	0.003508	0.079229	1332	39.3	1324	79.6	-0.6	1332	39	2.95%	0.282304	0.00003	0.00564616	0.00255	0.00011	0.1058	0.004	0.28224	10.65	1.05	1.40	1.435399801	0.281939605	0.282284834	
34DTB19 (U-Pb from Brennan et al., 2021)	[illegible]	[illegible]	[illegible]	[illegible]	[illegible]	[illegible]	[illegible]	0.183946	0.089700	0.004594	-0.063333	1348	52.0	1418	97.9	4.9	1348	52	3.86%	0.282194	0.000025	0.005643935	0.000727	0.00006	0.0269	0.0024	0.28218	8.72	0.88	1.48	1.571769712	0.281929517	0.282273306	
34DTB19 (U-Pb from Brennan et al., 2021)	[illegible]	[illegible]	[illegible]	[illegible]	[illegible]	[illegible]	[illegible]	0.146700	0.088200	0.003864	0.330870	1371	42.9	1386	84.1	1.1	1371	43	3.13%	0.282223	0.000032	0.005644551	0.001124	0.000019	0.04032	0.00042	0.28219	9.90	1.12	1.46	1.514188978	0.281914747	0.282256426	
34DTB19 (U-Pb from Brennan et al., 2021)	[illegible]	[illegible]	[illegible]	[illegible]	[illegible]	[illegible]	[illegible]	0.132777	0.088500	0.003570	0.218840	1381	39.4	1393	77.4	0.8	1381	39	2.85%	0.282179	0.000023	0.005643627	0.0006587	0.000005	0.023768	0.000072	0.28216	8.99	0.81	1.50	1.58073269	0.281908382	0.282249151	
34DTB19 (U-Pb from Brennan et al., 2021)	[illegible]	[illegible]	[illegible]	[illegible]	[illegible]	[illegible]	[illegible]	0.141776	0.095400	0.003808	0.011862	1390	42.7	1535	75.1	9.4	1390	43	3.07%	0.282049	0.000023	0.005641027	0.00075	0.000015	0.02801	0.00045	0.28203	4.50	0.81	1.68	1.876146724	0.281902363	0.282242273	
34DTB19 (U-Pb from Brennan et al., 2021)	[illegible]	[illegible]	[illegible]	[illegible]	[illegible]	[illegible]	[illegible]	0.142827	0.090800	0.004316	0.263930	1394	43.3	1442	90.6	3.3	1394	43	3.11%	0.282219	0.000024	0.005644431	0.001643	0.000076	0.0648	0.0036	0.28218	9.79	0.84	1.48	1.539827284	0.281899695	0.282239222	
34DTB19 (U-Pb from Brennan et al., 2021)	[illegible]	[illegible]	[illegible]	[illegible]	[illegible]	[illegible]	[illegible]	0.148971	0.091100	0.003122	-0.014691	1399	45.4	1448	65.3	3.4	1399	45	3.25%	0.282109	0.000029	0.005642255	0.00124	0.0001	0.0473	0.0037	0.28208	6.36	1.02	1.62	1.763913409	0.281897051	0.282236201	
34DTB19 (U-Pb from Brennan et al., 2021)	[illegible]	[illegible]	[illegible]	[illegible]	[illegible]	[illegible]	[illegible]	0.124954	0.091600	0.003532	0.313740	1425	39.5	1458	73.3	2.3	1425	40	2.77%	0.281952	0.000027	0.005639105	0.0006851	0.000008	0.02529	0.00038	0.28193	1.90	0.95	1.81	2.070098113	0.281880034	0.282216753	
34DTB19 (U-Pb from Brennan et al., 2021)	[illegible]	[illegible]	[illegible]	[illegible]	[illegible]	[illegible]	[illegible]	0.142101	0.092000	0.003940	0.343650	1430	45.3	1467	81.3	2.5	1430	45	3.17%	0.282231	0.000021	0.005644659	0.001453	0.000017	0.05945	0.0007	0.28219	11.18	0.74	1.46	1.478843025	0.281876707	0.282212951	
34DTB19 (U-Pb from Brennan et al., 2021)	[illegible]	[illegible]	[illegible]	[illegible]	[illegible]	[illegible]	[illegible]	0.149324	0.095000	0.005200	0.428410	1435	47.9	1527	103.0	6.0	1435	48	3.34%	0.282142	0.000025	0.005642895	0.001102	0.000021	0.0446	0.0087	0.28211	8.47	0.88	1.57	1.6572998	0.281873373	0.28220914	
34DTB19 (U-Pb from Brennan et al., 2021)	[illegible]	[illegible]	[illegible]	[illegible]	[illegible]	[illegible]	[illegible]	0.145939	0.097800	0.003656	0.248960	1436	46.9	1582	69.9	9.2	1436	47	3.27%	0.281975	0.000022	0.005639543	0.001156	0.0002	0.0431	0.0081	0.28194	2.51	0.77	1.80	2.039742369	0.2818727	0.282208405	
34DTB19 (U-Pb from Brennan et al., 2021)	[illegible]	[illegible]	[illegible]	[illegible]	[illegible]	[illegible]	[illegible]	0.130679	0.093900	0.003678	0.028249	1453	43.0	1505	74.0	3.4	1453	43	2.96%	0.282084	0.000031	0.005641765	0.0010198	0.0000086	0.0385	0.00046	0.28206	6.89	1.09	1.65	1.773051582	0.281861779	0.282195891	
34DTB19 (U-Pb from Brennan et al., 2021)	[illegible]	[illegible]	[illegible]	[illegible]	[illegible]	[illegible]	[illegible]	0.143656	0.100100	0.004602	0.204530	1470	48.4	1625	85.5	9.6	1470	48	3.29%	0.281700	0.000018	0.005634029	0.000546	0.000027	0.0214	0.0011	0.28168	-5.90	0.63	2.15	2.601141253	0.28185116	0.282183755	
34DTB19 (U-Pb from Brennan et al., 2021)	[illegible]	[illegible]	[illegible]	[illegible]	[illegible]	[illegible]	[illegible]	0.242932	0.098500	0.004070	-0.002632	1479	82.8	1595	77.1	7.3	1479	83	5.60%	0.281921	0.000033	0.005638517	0.001084	0.000012	0.04052	0.00053	0.28189	1.61	1.16	1.88	2.131155788	0.281845235	0.282176982	
34DTB19 (U-Pb from Brennan et al., 2021)	[illegible]	[illegible]	[illegible]	[illegible]	[illegible]	[illegible]	[illegible]	0.216083	0.097700	0.004254	0.373490	1574	83.5	1580	81.5	0.4	1580	82	5.16%	0.281708	0.000022	0.005634203	0.0007271	0.0000089	0.02821	0.0044	0.28169	-3.34	0.77	2.15	2.525828175	0.281780306	0.282102778	
34DTB19 (U-Pb from Brennan et al., 2021)	[illegible]	[illegible]	[illegible]	[illegible]	[illegible]	[illegible]	[illegible]	0.208385	0.098800	0.004076	0.281040	1605	83.7	1601	77.0	-0.3	1601	77	4.81%	0.281744	0.000022	0.005634923	0.0006354	0.0000026	0.02401	0.0019	0.28172	-1.49	0.77	2.10	2.425167546	0.28176675	0.282087286	
34DTB19 (U-Pb from Brennan et al., 2021)	[illegible]	[illegible]	[illegible]	[illegible]	[illegible]	[illegible]	[illegible]	0.215581	0.099300	0.003886	0.286380	1524	78.0	1610	72.9	5.4	1610	73	4.53%	0.281728	0.00002	0.005634595	0.0004796	0.0000029	0.01778	0.0014	0.28171	-1.68	0.70	2.11	2.444559555	0.281760681	0.28208035	
34DTB19 (U-Pb from Brennan et al., 2021)	[illegible]	[illegible]	[illegible]	[illegible]	[illegible]	[illegible]	[illegible]	0.211358	0.099900	0.003998	0.336890	1593	83.6	1621	74.5	1.8	1621	75	4.59%	0.281784	0.000022	0.005635723	0.000868	0.000012	0.03127	0.0003	0.28176	0.14	0.77	2.05	2.337776684	0.281753448	0.282072083	
34DTB19 (U-Pb from Brennan et al., 2021)	[illegible]	[illegible]	[illegible]	[illegible]	[illegible]	[illegible]	[illegible]	0.227921	0.100100	0.004302	0.000043	1530	83.2	1625	79.9	5.8	1625	80	4.92%	0.281959	0.000032	0.005639271	0.000812	0.000011	0.03116	0.00071	0.28193	6.49	1.12	1.81	1.93432556	0.281751058	0.282069352	
34DTB19 (U-Pb from Brennan et al., 2021)	[illegible]	[illegible]	[illegible]	[illegible]	[illegible]	[illegible]	[illegible]	0.225664	0.100900	0.004418	0.455670	1538	83.2	1640	81.3	6.2	1640	81	4.96%	0.281977	0.000026	0.0056396	0.000888	0.000021	0.03156	0.0087	0.28195	7.38	0.91	1.79	1.889093268	0.281741497	0.282058425	
34DTB19 (U-Pb from Brennan et al., 2021)	[illegible]	[illegible]	[illegible]	[illegible]	[illegible]	[illegible]	[illegible]	0.228492	0.101800	0.003936	-0.322350	1528	83.2	1656	71.6	7.7	1656	72	4.32%	0.282006	0.000022	0.005640163	0.000754	0.000021	0.02865	0.00086	0.28198	8.93	0.77	1.74	1.802612582	0.281730835	0.28204624	
34DTB19 (U-Pb from Brennan et al., 2021)	[illegible]	[illegible]	[illegible]	[illegible]	[illegible]	[illegible]	[illegible]	0.202880	0.102000	0.003640	-0.139090	1628	83.9	1660	66.1	1.9	1660	66	3.98%	0.281635	0.00002	0.005632736	0.00044323	0.0000061	0.016972	0.000052	0.28162	-3.81	0.70	2.23	2.619528706	0.281728508	0.282043581	
34DTB19 (U-Pb from Brennan et al., 2021)	[illegible]	[illegible]	[illegible]	[illegible]	[illegible]	[illegible]	[illegible]	0.224271	0.102600	0.004152	0.347460	1543	83.3	1671	74.8	7.6	1671	75	4.48%	0.281950	0.000023	0.005639047	0.000991	0.000038	0.0357	0.013	0.28192	7.00	0.81	1.83	1.938091858	0.281721462	0.282035528	
34DTB19 (U-Pb from Brennan et al., 2021)	[illegible]	[illegible]	[illegible]	[illegible]	[illegible]	[illegible]	[illegible]	0.210679	0.102900	0.003958	0.173100	1646	89.0	1676	71.1	1.8	1676	71	4.24%	0.281856	0.000027	0.005637185	0.0005274	0.0000099	0.01976	0.00032	0.28184	4.30	0.95	1.94	2.115175688	0.281718036	0.282031612	
34DTB19 (U-Pb from Brennan et al., 2021)	[illegible]	[illegible]	[illegible]	[illegible]	[illegible]	[illegible]	[illegible]	0.219645	0.103400	0.004668	0.208840	1561	83.4	1685	83.3	7.4	1685	83	4.94%	0.281783	0.000031	0.005635745	0.000717	0.000064	0.0284	0.0025	0.28176	1.70	1.09	2.05	2.28683627	0.281712216	0.282024962	
34DTB19 (U-Pb from Brennan et al., 2021)	[illegible]	[illegible]	[illegible]	[illegible]	[illegible]	[illegible]	[illegible]	0.205005	0.104600	0.003592	0.193570	1619	83.8	1707	63.2	5.1	1707	63	3.70%	0.281620	0.000019	0.005632432	0.00029924	0.0000077	0.012389	0.000036	0.28161	-3.13	0.67	2.25	2.612831717	0.28169844	0.282009217	
34DTB19 (U-Pb from Brennan et al., 2021)	[illegible]	[illegible]	[illegible]	[illegible]	[illegible]	[illegible]	[illegible]	0.197689	0.104900	0.004198	0.271890	1702	89.3	1712	73.6	0.6	1712	74	4.30%	0.281681	0.000018	0.005633649	0.0016	0.000011	0.00607	0.0045	0.28168	-0.68	0.63	2.16	2.461598988	0.281695076	0.282005372	
34DTB19 (U-Pb from Brennan et al., 2021)	[illegible]	[illegible]	[illegible]	[illegible]	[illegible]	[illegible]	[illegible]	0.187676	0.105300	0.003206	0.258750	1749	89.6	1719	56.0	-1.8	1719	56	3.26%	0.281894	0.000024	0.005637931	0.0006625	0.0000083	0.02642	0.00021	0.28187	6.46	0.84	1.89	2.010672814	0.281690527	0.282000174	
34DTB19 (U-Pb from Brennan et al., 2021)	[illegible]	[illegible]	[illegible]	[illegible]	[illegible]	[illegible]	[illegible]	0.202924	0.105400	0.004208	0.352240	1678	89.2	1721	73.4	2.4	1721	73	4.27%	0.281641	0.000023	0.005632867	0.0004114	0.0000041	0.014738	0.000095	0.28163	-2.19	0.81	2.22	2.564581076	0.281689382	0.281998865	
34DTB19 (U-Pb from Brennan et al., 2021)	[illegible]	[illegible]	[illegible]	[illegible]	[illegible]	[illegible]	[illegible]	0.199534	0.105500	0.003710	0.191490	1643	84.0	1722	64.6	4.6	1722	65	3.75%	0.281863	0.000019	0.005637292	0.0004956	0.0000087	0.01668	0.0029	0.28185	5.63	0.67	1.93	2.066603169	0.281688282	0.281997608	
34DTB19 (U-Pb from Brennan et al., 2021)	[illegible]	34DTB19-D-20	40	1	113	2	[illegible]	0.186484	0.105600	0.005312	0.332620	1755	89.6	1724	92.4	-1.8	1724	92	5.36%	0.281866	0.000026	0.00563738	0.000493	0.00001	0.01873	0.00044	0.28185	5.78	0.91	1.92	2.058386888	0.281687117	0.281996277	
34DTB19 (U-Pb from Brennan et al., 2021)	17/03/2020 (3) 19:32:43.12	34DTB19-D-105	139	4	108	6	3.345601	0.201229	0.105900	0.003818	0.111380	1686	89.2	1729	66.2	2.5	1729	66	3.83%	0.281827	0.000029	0.005636615	0.00059935	0.0000089	0.021978	0.000078	0.28181	4.39	1.02	1.98	2.151616587	0.281683752	0.281992431	
34DTB19 (U-Pb from Brennan et al., 2021)	17/03/2020 (3) 19:09:00.97	34DTB19-D-93	156	1	475	34	3.328895	0.199556	0.106300	0.003726	0.205110	1693	89.3	1736	64.3	2.5	1736	64	3.70%	0.281854	0.000021	0.005637119	0.000582	0.000021	0.02183	0.0011	0.28183	5.52	0.74	1.94	2.084362289	0.281679286	0.281987327	
34DTB19 (U-Pb from Brennan et al., 2021)	17/03/2020 (3) 20:12:23.68	34DTB19-D-120	226	2	75	3	3.585515	0.213125	0.106300	0.003626	0.025066	1586	83.6	1736	62.6	8.7	1736	63	3.61%	0.281859	0.000023	0.005637227	0.0006306	0.000021	0.02604	0.00029	0.28184	5.64	0.81	1.94	2.076619817	0.281679286	0.281987327	
34DTB19 (U-Pb from Brennan et al., 2021)	17/03/2020 (3) 18:13:19.09	34DTB19-D-75	146	7	93	1	3.479471	0.214870	0.106500	0.003930	0.120810	1629	88.9	1740	67.6	6.4	1740	68	3.89%	0.281893	0.000023	0.005637907	0.0004493	0.000005	0.01658	0.0023	0.28188	7.14	0.81	1.88	1.983272965	0.281677086	0.281984812	
34DTB19 (U-Pb from Brennan et al., 2021)	17/03/2020 (3) 19:56:35.72	34DTB19-D-112	143	9	76	1	3.511236	0.205841	0.106600	0.003932	0.369190	1616	83.8	1741	67.6	7.2	1741	68	3.88%	0.281641	0.00002	0.005632856	0.0006734	0.000022	0.024434	0.000079	0.28162	-2.03	0.70	2.24	2.570555376	0.2816759	0.28198348	
34DTB19 (U-Pb from Brennan et al., 2021)	17/03/2020 (3) 19:30:44.58	34DTB19-D-104	106	2	158	7	3.220612	0.188880	0.106700	0.004134	0.007022	1743	89.6	1743	71.0	0.0	1743	71	4.07%	0.281823	0.000026	0.00563652	0.0005156	0.0000062	0.019507	0.000029	0.28181	4.66	0.91	1.98	2.14536995	0.28167482	0.281982223	
34DTB19 (U-Pb from Brennan et al., 2021)	17/03/2020 (3) 15:22:34.31	34DTB19-D-9	378	17	285	6	3.138732	0.180994	0.106900	0.003738	0.289200	1783	89.8	1746	64.0	-2.1	1746	64	3.66%	0.281582	0.00002	0.005631676	0.0005174	0.000016	0.020456	0.000032	0.28156	-3.83	0.70	2.31	2.688638807	0.281672619	0.281979707	
34DTB19 (U-Pb from Brennan et al., 2021)	17/03/2020 (3) 15:32:27.01	34DTB19-D-14	188	4	340	8	3.486750	0.203467	0.106900	0.003638	0.146790	1626	83.8	1746	62.3	6.9	1746	62	3.57%	0.281726	0.000024	0.005634571	0.000276	0.000013	0.01232	0.00073	0.28172	1.57	0.84	2.10	2.34533101	0.281672619	0.281979707	
34DTB19 (U-Pb from Brennan et al., 2021)	17/03/2020 (3) 16:00:15.96	34DTB19-D-23	154	3	118	3	3.590664	0.213635	0.106900	0.005038	0.311770	1584	83.5	1746	86.3	9.3	1746	86	4.94%	0.281899	0.00003	0.00563806	0.000604	0.0001	0.02267	0.0031	0.28188	7.33	1.05	1.88	1.976659688	0.281672619	0.281979707	
34DTB19 (U-Pb from Brennan et al., 2021)	17/03/2020 (3) 16:31:52.18	34DTB19-D-39	319	11	148	2	3.355705	0.202243	0.107500	0.003850	0.104480	1681	89.2	1757	65.5	4.3	1757	66	3.73%	[illegible]	[illegible]	[illegible]	[illegible]	[illegible]	[illegible]	[illegible]	[illegible]	[illegible]	[illegible]	[illegible]	[illegible]	[illegible]	[illegible]	
34DTB19 (U-Pb from Brennan et al., 2021)	17/03/2020 (3) 15:18:37.08	34DTB19-D-7	86	1	357	23	3.418803	0.208635	0.108100	0.003962	0.093569	1654	89.0	1767	67.0	6.4	1767	67	3.79%	[illegible]	[illegible]	[illegible]	[illegible]	[illegible]	[illegible]	[illegible]	[illegible]	[illegible]	[illegible]	[illegible]	[illegible]	[illegible]	[illegible]	
34DTB19 (U-Pb from Brennan et al., 2021)	17/03/2020 (3) 18:17:16.09	34DTB19-D-77	132	2	187	6	3.483107	0.215247	0.108100	0.005262	0.348480	1627	88.9	1767	88.9	7.9	1767	89	5.03%	[illegible]	[illegible]	[illegible]	[illegible]	[illegible]	[illegible]	[illegible]	[illegible]	[illegible]	[illegible]	[illegible]	[illegible]	[illegible]	[illegible]	
34DTB19 (U-Pb from Brennan et al., 2021)	17/03/2020 (3) 16:33:50.85	34DTB19-D-40	152	3	44	5	3.404835	0.195619	0.108700	0.003574	0.276750	1660	84.1	1777	60.0	6.6	1777	60	3.38%	[illegible]	[illegible]	[illegible]	[illegible]	[illegible]	[illegible]	[illegible]	[illegible]	[illegible]	[illegible]	[illegible]	[illegible]	[illegible]	[illegible]	
34DTB19 (U-Pb from Brennan et al., 2021)	17/03/2020 (3) 15:08:44.27	34DTB19-D-2	87	5	49	1	3.145643	0.181654	0.108700	0.003174	0.184110	1780	89.8	1777	53.3	-0.1	1777	53	3.00%	[illegible]	[illegible]	[illegible]	[illegible]	[illegible]	[illegible]	[illegible]	[illegible]	[illegible]	[illegible]	[illegible]	[illegible]	[illegible]	[illegible]	
34DTB19 (U-Pb from Brennan et al., 2021)	17/03/2020 (3) 17:21:43.83	34DTB19-D-54	68	1	177	4	3.258390	0.192573	0.108800	0.003576	0.352160	1725	89.5	1779	60.0	3.0	1779	60	3.37%	[illegible]	[illegible]	[illegible]	[illegible]	[illegible]	[illegible]	[illegible]	[illegible]	[illegible]	[illegible]	[illegible]	[illegible]	[illegible]	[illegible]	
34DTB19 (U-Pb from Brennan et al., 2021)	17/03/2020 (3) 19:28:46.42	34DTB19-D-103	131	2	409	6	3.216468	0.188477	0.108900	0.004078	0.302340	1745	89.6	1780	68.3	2.0	1780	68	3.84%	[illegible]	[illegible]	[illegible]	[illegible]	[illegible]	[illegible]	[illegible]	[illegible]	[illegible]	[illegible]	[illegible]	[illegible]	[illegible]	[illegible]	
34DTB19 (U-Pb from Brennan et al., 2021)	17/03/2020 (3) 15:30:29.17	34DTB19-D-13	250	9	161	1	3.156566	0.182698	0.109800	0.003696	0.052161	1774	89.8	1795	61.3	1.2	1795	61	3.41%	[illegible]	[illegible]	[illegible]	[illegible]	[illegible]	[illegible]	[illegible]	[illegible]	[illegible]	[illegible]	[illegible]	[illegible]	[illegible]	[illegible]	
34DTB19 (U-Pb from Brennan et al., 2021)	17/03/2020 (3) 18:21:12.73	34DTB19-D-79	264	4	219	5	3.174603	0.184429	0.110000	0.003700	0.227830	1765	89.7	1799	61.2	1.9	1799	61	3.40%	[illegible]	[illegible]	[illegible]	[illegible]	[illegible]	[illegible]	[illegible]	[illegible]	[illegible]	[illegible]	[illegible]	[illegible]	[illegible]	[illegible]	
34DTB19 (U-Pb from Brennan et al., 2021)	17/03/2020 (3) 15:24:32.91	34DTB19-D-10	59	1	274	5	3.280840	0.194784	0.110000	0.004400	0.054274	1715	89.4	1799	72.8	4.6	1799	73	4.05%	[illegible]	[illegible]	[illegible]	[illegible]	[illegible]	[illegible]	[illegible]	[illegible]	[illegible]	[illegible]	[illegible]	[illegible]	[illegible]	[illegible]	
34DTB19 (U-Pb from Brennan et al., 2021)	17/03/2020 (3) 15:58:17.24	34DTB19-D-22	112	2	71	5	3.379520	0.193223	0.110500	0.003910	0.216710	1671	84.2	1807	64.3	7.5	1807	64	3.56%	[illegible]	[illegible]	[illegible]	[illegible]	[illegible]	[illegible]	[illegible]	[illegible]	[illegible]	[illegible]	[illegible]	[illegible]	[illegible]	[illegible]	
34DTB19 (U-Pb from Brennan et al., 2021)	17/03/2020 (3) 18:07:22.41	34DTB19-D-72	92	10	369	6	3.204101	0.187277	0.111300	0.003826	0.040722	1751	89.6	1820	62.4	3.8	1820	62	3.43%	[illegible]	[illegible]	[illegible]	[illegible]	[illegible]	[illegible]	[illegible]	[illegible]	[illegible]	[illegible]	[illegible]	[illegible]	[illegible]	[illegible]	
34DTB19 (U-Pb from Brennan et al., 2021)	17/03/2020 (3) 18:23:11.34	34DTB19-D-80	157	4	147	5	3.415301	0.196613	0.111300	0.003626	0.078847	1656	84.1	1820	59.1	9.0	1820	59	3.25%	[illegible]	[illegible]	[illegible]	[illegible]	[illegible]	[illegible]	[illegible]	[illegible]	[illegible]	[illegible]	[illegible]	[illegible]	[illegible]	[illegible]	
34DTB19 (U-Pb from Brennan et al., 2021)	17/03/2020 (3) 18:55:12.40	34DTB19-D-86	128	2	143	4	3.254149	0.192157	0.111800	0.003736	-0.026213	1727	89.5	1828	60.6	5.5	1828	61	3.31%	[illegible]	[illegible]	[illegible]	[illegible]	[illegible]	[illegible]	[illegible]	[illegible]	[illegible]	[illegible]	[illegible]	[illegible]	[illegible]	[illegible]	
34DTB19 (U-Pb from Brennan et al., 2021)	17/03/2020 (3) 17:01:56.91	34DTB19-D-44	184	2	133	20	3.417635	0.220196	0.112000	0.006840	-0.298140	1655	94.0	1831	111.0	9.7	1831	111	6.06%	[illegible]	[illegible]	[illegible]	[illegible]	[illegible]	[illegible]	[illegible]	[illegible]	[illegible]	[illegible]	[illegible]	[illegible]	[illegible]	[illegible]	
34DTB19 (U-Pb from Brennan et al., 2021)	17/03/2020 (3) 17:13:49.52	34DTB19-D-50	78	3	108	1	3.299241	0.196605	0.112200	0.004144	0.241940	1707	89.4	1835	66.9	7.0	1835	67	3.65%	[illegible]	[illegible]	[illegible]	[illegible]	[illegible]	[illegible]	[illegible]	[illegible]	[illegible]	[illegible]	[illegible]	[illegible]	[illegible]	[illegible]	
34DTB19 (U-Pb from Brennan et al., 2021)	17/03/2020 (3) 15:06:45.98	34DTB19-D-1	587	16	101	2	3.224766	0.189285	0.112600	0.004952	0.182320	1741	89.6	1841	79.6	5.4	1841	80	4.32%	[illegible]	[illegible]	[illegible]	[illegible]	[illegible]	[illegible]	[illegible]	[illegible]	[illegible]	[illegible]	[illegible]	[illegible]	[illegible]	[illegible]	
34DTB19 (U-Pb from Brennan et al., 2021)	17/03/2020 (3) 16:23:58.66	34DTB19-D-35	66	3	74	1	3.148615	0.181938	0.113400	0.004068	0.081029	1778	89.8	1854	64.8	4.1	1854	65	3.50%	[illegible]	[illegible]	[illegible]	[illegible]	[illegible]	[illegible]	[illegible]	[illegible]	[illegible]	[illegible]	[illegible]	[illegible]	[illegible]	[illegible]	
34DTB19 (U-Pb from Brennan et al., 2021)	17/03/2020 (3) 20:14:22.33	34DTB19-D-121	123	6	118	2	3.262643	0.192991	0.114800	0.004496	-0.132080	1724	89.5	1876	70.6	8.1	1876	71	3.76%	[illegible]	[illegible]	[illegible]	[illegible]	[illegible]	[illegible]	[illegible]	[illegible]	[illegible]	[illegible]	[illegible]	[illegible]	[illegible]	[illegible]	
34DTB19 (U-Pb from Brennan et al., 2021)	17/03/2020 (3) 18:05:24.08	[illegible]	74	1	245	7	3.115265	0.188496	0.115700	0.003614	0.358100	1795	94.8	1890	56.2	5.0	1890	56	2.97%	[illegible]	[illegible]	[illegible]	[illegible]	[illegible]	[illegible]	[illegible]	[illegible]	[illegible]	[illegible]	[illegible]	[illegible]	[illegible]	[illegible]	
34DTB19 (U-Pb from Brennan et al., 2021)	17/03/2020 (3) 17:59:28.03	34DTB19-D-68	112	5	192	14	2.376426	0.143534	0.160500	0.004610	-0.098127	2264	115.0	2460	48.5	8.0	2460	49	1.97%	[illegible]	[illegible]	[illegible]	[illegible]	[illegible]	[illegible]	[illegible]	[illegible]	[illegible]	[illegible]	[illegible]	[illegible]	[illegible]	[illegible]	
34DTB19 (U-Pb from Brennan et al., 2021)	17/03/2020 (3) 18:11:20.27	34DTB19-D-74	175	2	192	3	2.153316	0.126528	0.160900	0.005218	-0.025219	2459	120.0	2464	54.8	0.2	2464	55	2.22%	[illegible]	[illegible]	[illegible]	[illegible]	[illegible]	[illegible]	[illegible]	[illegible]	[illegible]	[illegible]	[illegible]	[illegible]	[illegible]	[illegible]	
34DTB19 (U-Pb from Brennan et al., 2021)	17/03/2020 (3) 15:20:35.42	34DTB19-D-8	72	3	147	4	2.115059	0.122824	0.164200	0.005584	0.070079	2496	120.0	2499	57.3	0.1	2499	57	2.29%	[illegible]	[illegible]	[illegible]	[illegible]	[illegible]	[illegible]	[illegible]	[illegible]	[illegible]	[illegible]	[illegible]	[illegible]	[illegible]	[illegible]	
34DTB19 (U-Pb from Brennan et al., 2021)	17/03/2020 (3) 15:12:41.22	34DTB19-D-4	456	5	80	2	1.968117	0.116832	0.180200	0.005204	0.260800	2649	129.0	2654	47.9	0.2	2654	48	1.80%	[illegible]	[illegible]	[illegible]	[illegible]	[illegible]	[illegible]	[illegible]	[illegible]	[illegible]	[illegible]	[illegible]	[illegible]	[illegible]	[illegible]	
34DTB19 (U-Pb from Brennan et al., 2021)	17/03/2020 (3) 16:14:06.36	34DTB19-D-30	127	4	130	3	2.018163	0.125896	0.194000	0.007880	0.159540	2594	133.0	2776	66.6	6.5	2776	67	2.40%	[illegible]	[illegible]	[illegible]	[illegible]	[illegible]	[illegible]	[illegible]	[illegible]	[illegible]	[illegible]	[illegible]	[illegible]	[illegible]	[illegible]	
34DTB19 (U-Pb from Brennan et al., 2021)	17/03/2020 (3) 15:14:39.94	34DTB19-D-5	408	8	86	3	1.900418	0.110240	0.195800	0.005316	0.074372	2725	129.0	2791	44.5	2.3	2791	45	1.59%	[illegible]	[illegible]	[illegible]	[illegible]	[illegible]	[illegible]	[illegible]	[illegible]	[illegible]	[illegible]	[illegible]	[illegible]	[illegible]	[illegible]	
34DTB19 (U-Pb from Brennan et al., 2021)	17/03/2020 (3) 19:44:44.01	34DTB19-D-106	202	3	70	2	1.866716	0.110512	0.196000	0.006220	0.221770	2765	133.0	2792	52.0	1.0	2792	52	1.86%	[illegible]	[illegible]	[illegible]	[illegible]	[illegible]	[illegible]	[illegible]	[illegible]	[illegible]	[illegible]	[illegible]	[illegible]	[illegible]	[illegible]	
34DTB19 (U-Pb from Brennan et al., 2021)	17/03/2020 (3) 15:34:25.47	34DTB19-D-15	302	8	23	1	1.970055	0.117023	0.196200	0.005924	-0.148360	2646	129.0	2794	49.4	5.3	2794	49	1.77%	[illegible]	[illegible]	[illegible]	[illegible]	[illegible]	[illegible]	[illegible]	[illegible]	[illegible]	[illegible]	[illegible]	[illegible]	[illegible]	[illegible]	
34DTB19 (U-Pb from Brennan et al., 2021)	17/03/2020 (3) 17:29:38.23	34DTB19-D-58	344	7	277	19	1.950458	0.115095	0.198200	0.005964	0.256330	2668	129.0	2811	49.2	5.1	2811	49	1.75%	[illegible]	[illegible]	[illegible]	[illegible]	[illegible]	[illegible]	[illegible]	[illegible]	[illegible]	[illegible]	[illegible]	[illegible]	[illegible]	[illegible]	
34DTB19 (U-Pb from Brennan et al., 2021)	17/03/2020 (3) 16:04:13.02	34DTB19-D-25	182	3	48	0	1.612383	0.094642	0.236600	0.006432	0.445320	3111	145.0	3097	43.3	-0.5	3097	43	1.40%	[illegible]	[illegible]	[illegible]	[illegible]	[illegible]	[illegible]	[illegible]	[illegible]	[illegible]	[illegible]	[illegible]	[illegible]	[illegible]	[illegible]	
34DTB19 (U-Pb from Brennan et al., 2021)	17/03/2020 (3) 19:46:42.31	34DTB19-D-107	148	3	424	47	1.451589	0.085924	0.306600	0.009032	0.303660	3378	156.0	3503	45.5	3.6	3503	46	1.30%	[illegible]	[illegible]	[illegible]	[illegible]	[illegible]	[illegible]	[illegible]	[illegible]	[illegible]	[illegible]	[illegible]	[illegible]	[illegible]	[illegible]	

Appendix D3.1 continued.

Curtin University Geohistory center

Sample ID	Analysis date-time	Spot ID	238U conc. (ppm)	±2σ INT	232Th conc. (ppm)	±2σ INT	Isotopic Ratios: 238U/206Pb	±2σ PROP	207Pb/206Pb	±2σ PROP	rho	Apparent Ages - Calculated in Isoplot R (Ma): 238U/206Pb	±2σ PROP	207Pb/206Pb	±2σ PROP	Discord (7/6-6/8)/7/6*100	Perferred age *1500 Ma cutoff: Ma	2 σ	error %	Analysis Notes
12DTB19	23/04/2020 (5) 17:00:26.00	12DTB19 - 47	152.8	7.2	117.8	4.5	3.320053	0.10167387	0.099	0.00428	0.18812	1697.3	45.7	1604.5	80.6	-5.78	1604.5	80.6	5.02%	No Hf data collected - > 5% reverse discordant, excluded
12DTB19	23/04/2020 (5) 17:59:52.00	12DTB19 - 64	316	12	276	16	3.435246	0.14777103	0.0978	0.003756	0.076517	1647	62.5	1581.8	71.8	-4.12	1581.8	71.8	4.54%	No Hf data collected
12DTB19	23/04/2020 (5) 14:13:37.00	12DTB19 - 1	128.7	1.3	122.6	2.1	3.528582	0.11290466	0.0968	0.004636	0.019935	1608.5	45.5	1562.5	89.8	-2.94	1562.5	89.8	5.75%	No Hf data collected
12DTB19	23/04/2020 (5) 17:02:19.00	12DTB19 - 48	201.7	3.7	123.7	1.3	3.082614	0.09111006	0.108	0.00426	0.33759	1811.2	46.7	1765.1	72.1	-2.61	1765.1	72.1	4.08%	No Hf data collected
12DTB19	23/04/2020 (5) 15:14:59.00	12DTB19 - 19	212	5	121	1.5	3.183699	0.10016337	0.1057	0.004214	0.21723	1760.9	48.5	1725.7	73.2	-2.04	1725.7	73.2	4.24%	No Hf data collected
12DTB19	23/04/2020 (5) 14:55:48.00	12DTB19 - 14	172.8	1.8	172.5	6.4	3.582945	0.11273889	0.0967	0.003934	0.097932	1586.8	44.3	1560.6	76.3	-1.68	1560.6	76.3	4.89%	No Hf data collected
12DTB19	23/04/2020 (5) 17:19:35.00	12DTB19 - 52	309.4	7.9	144.6	3.5	3.126954	0.08796147	0.1078	0.003956	0.33641	1788.8	43.9	1761.7	67.1	-1.54	1761.7	67.1	3.81%	No Hf data collected
12DTB19	23/04/2020 (5) 14:52:03.00	12DTB19 - 12	147.5	2.9	92.8	1.7	3.692762	0.11340107	0.0949	0.003998	0.000667	1544.9	42.2	1525.2	79.4	-1.29	1525.2	79.4	5.21%	No Hf data collected
12DTB19	23/04/2020 (5) 14:40:30.00	12DTB19 - 10	90.6	1.5	76.1	1.6	3.667033	0.13250805	0.0955	0.00491	0.28832	1554.5	49.9	1537.1	96.7	-1.13	1537.1	96.7	6.29%	No Hf data collected
12DTB19	23/04/2020 (5) 17:06:05.00	12DTB19 - 50	112.3	1.5	80.2	1.9	3.585515	0.116706	0.0971	0.004342	0.22335	1585.8	45.8	1568.3	83.8	-1.12	1568.3	83.8	5.34%	No Hf data collected
12DTB19	23/04/2020 (5) 14:21:14.00	12DTB19 - 5	216.8	4.9	125.5	2.3	3.131851	0.09304334	0.1086	0.004072	0.16396	1786.3	46.4	1775.2	68.4	-0.63	1775.2	68.4	3.85%	No Hf data collected
12DTB19	23/04/2020 (5) 17:25:15.00	12DTB19 - 55	391.3	4.1	187.5	1.7	3.266906	0.09415435	0.105	0.0037	0.097273	1721.5	43.5	1713.5	64.8	-0.47	1713.5	64.8	3.78%	No Hf data collected
12DTB19	23/04/2020 (5) 18:01:47.00	12DTB19 - 65	403.5	4.8	505.5	5.8	3.554924	0.10142844	0.0992	0.003384	0.02986	1597.9	40.4	1608.3	63.6	0.65	1608.3	63.6	3.95%	No Hf data collected
12DTB19	23/04/2020 (5) 14:15:33.00	12DTB19 - 2	90.8	1.5	60.9	1.4	3.745318	0.11698859	0.0955	0.00511	0.26496	1525.6	42.4	1537	101	0.74	1537	101	6.57%	No Hf data collected
12DTB19	23/04/2020 (5) 14:32:48.00	12DTB19 - 7	185.5	5.9	106.2	2.6	3.617945	0.10508272	0.0983	0.004166	0.15217	1573.2	40.5	1591.3	79.2	1.14	1591.3	79.2	4.98%	No Hf data collected
12DTB19	23/04/2020 (5) 16:41:18.00	12DTB19 - 41	76	2.1	73	1.5	1.384658	0.04207274	0.3168	0.011236	0.51619	3504.3	82.1	3553.7	54.6	1.39	3553.7	54.6	1.54%	No Hf data collected
12DTB19	23/04/2020 (5) 16:25:58.00	12DTB19 - 38	372.5	5.9	164.5	2.6	3.355705	0.09751814	0.1058	0.003816	0.20232	1681.4	43	1727.4	66.2	2.66	1727.4	66.2	3.83%	No Hf data collected
12DTB19	23/04/2020 (5) 14:19:20.00	12DTB19 - 4	165.3	3	111.1	1.3	3.654971	0.11584762	0.0991	0.004182	0.15277	1559	43.9	1606.4	78.7	2.95	1606.4	78.7	4.90%	No Hf data collected
12DTB19	23/04/2020 (5) 14:17:29.00	12DTB19 - 3	250.7	6	280.2	8.3	3.511236	0.10844393	0.1025	0.00365	0.26947	1615.5	44.1	1669	65.9	3.21	1669	65.9	3.95%	No Hf data collected
12DTB19	23/04/2020 (5) 16:27:52.00	12DTB19 - 39	73.4	1.9	100.1	1.7	3.932363	0.13431579	0.0947	0.005294	0.22	1460.6	44.6	1521	105	3.97	1521	105	6.90%	No Hf data collected
12DTB19	23/04/2020 (5) 15:49:31.00	12DTB19 - 28	84.8	4.8	74.7	4.9	3.579098	0.12154074	0.1019	0.005638	0.176	1588.3	47.8	1658	102	4.20	1658	102	6.15%	No Hf data collected
12DTB19	23/04/2020 (5) 14:57:43.00	12DTB19 - 15	306.1	5.8	115.7	2.7	3.356831	0.09305375	0.1074	0.003948	-0.097126	1680.9	41	1754.9	67.3	4.22	1754.9	67.3	3.83%	No Hf data collected
12DTB19	23/04/2020 (5) 14:53:54.00	12DTB19 - 13	700	25	1414	45	3.968254	0.11085916	0.0953	0.003006	0.25327	1448.8	36.2	1533.2	59.4	5.50	1533.2	59.4	3.87%	No Hf data collected
12DTB19	23/04/2020 (5) 17:36:51.00	12DTB19 - 57	481.9	8.9	343	12	3.531073	0.1055332	0.1046	0.003492	0.12254	1607.5	42.5	1706.5	61.4	5.80	1706.5	61.4	3.60%	No Hf data collected
12DTB19	23/04/2020 (5) 15:26:31.00	12DTB19 - 21	71.3	1.3	101.6	2.2	3.937008	0.13764028	0.0963	0.005126	0.21376	1459.1	45.6	1552.8	99.9	6.03	1552.8	99.9	6.43%	No Hf data collected
12DTB19	23/04/2020 (5) 15:34:06.00	12DTB19 - 25	383	10	287.5	5.4	3.481894	0.10479628	0.1067	0.003934	-0.10884	1627.5	43.3	1743	67.6	6.63	1743	67.6	3.88%	No Hf data collected
12DTB19	23/04/2020 (5) 17:56:06.00	12DTB19 - 62	452	13	504	17	4.088307	0.12355178	0.0944	0.003588	0.27095	1410.6	38.3	1515.3	71.7	6.91	1515.3	71.7	4.73%	No Hf data collected
12DTB19	23/04/2020 (5) 15:16:50.00	12DTB19 - 20	624	24	44.11	0.72	3.548616	0.11630595	0.1055	0.00351	0.053915	1600.4	46.4	1722.2	61.1	7.07	1722.2	61.1	3.55%	No Hf data collected
12DTB19	23/04/2020 (5) 15:32:15.00	12DTB19 - 24	90.4	1	59.63	0.69	3.556188	0.11285712	0.1056	0.005612	0.29584	1597.4	44.9	1724	97.6	7.34	1724	97.6	5.66%	No Hf data collected
12DTB19	23/04/2020 (5) 16:58:32.00	12DTB19 - 46	178.5	2.4	120	1.7	3.883495	0.1198982	0.0986	0.004272	0.14832	1477	40.8	1597	80.9	7.51	1597	80.9	5.07%	No Hf data collected
12DTB19	23/04/2020 (5) 16:43:12.00	12DTB19 - 42	334.8	3.3	66.5	1.6	3.878976	0.1167003	0.0995	0.00379	0.17135	1478.6	39.8	1613.9	70.9	8.38	1613.9	70.9	4.39%	No Hf data collected
12DTB19	23/04/2020 (5) 16:22:08.00	12DTB19 - 36	326	11	419	15	3.729952	0.11077164	0.1028	0.003756	0.17691	1531.2	40.5	1674.5	67.5	8.56	1674.5	67.5	4.03%	No Hf data collected
12DTB19	23/04/2020 (5) 16:10:36.00	12DTB19 - 34	165.8	1.9	107.6	1.1	3.543586	0.11230983	0.1078	0.004556	0.35432	1602.4	45	1761.7	77.3	9.04	1761.7	77.3	4.39%	No Hf data collected
12DTB19	23/04/2020 (5) 17:42:36.00	12DTB19 - 59	264	13	248	14	4.046945	0.14317439	0.097	0.00374	-0.0098134	1423.5	45.2	1566.4	72.3	9.12	1566.4	72.3	4.62%	No Hf data collected
12DTB19	23/04/2020 (5) 15:09:16.00	12DTB19 - 16	230	24	160.7	4.6	4.385965	0.2993229	0.0921	0.004042	-0.18868	1324	81.7	1468.6	83.3	9.85	1468.6	83.3	5.67%	No Hf data collected
12DTB19	23/04/2020 (5) 16:12:32.00	12DTB19 - 35	541.7	7.1	664.9	7.5	3.937008	0.11904024	0.1022	0.003544	0.33829	1459.1	39.5	1663.6	64.2	12.29	1663.6	64.2	3.86%	No Hf data collected, > 10% Discordant, excluded
12DTB19	23/04/2020 (5) 16:24:06.00	12DTB19 - 37	115.3	2.6	127.4	2	3.930818	0.13424114	0.1028	0.004856	0.2024	1461.1	44.6	1674.5	87.3	12.74	1674.5	87.3	5.21%	No Hf data collected, > 10% Discordant, excluded
12DTB19	23/04/2020 (5) 18:19:04.00	12DTB19 - 69	289.3	5.5	338.9	8.5	4.353505	0.17046331	0.0952	0.004104	0.10768	1332.9	47.1	1531.2	81.2	12.95	1531.2	81.2	5.30%	No Hf data collected, > 10% Discordant, excluded
12DTB19	23/04/2020 (5) 17:44:31.00	12DTB19 - 60	553	29	651	47	4.185852	0.12927256	0.0981	0.003462	0.19304	1381	38.4	1587.5	66	13.01	1587.5	66	4.16%	No Hf data collected, > 10% Discordant, excluded
12DTB19	23/04/2020 (5) 17:57:58.00	12DTB19 - 63	569.3	5	155.4	1.9	3.930818	0.12651547	0.1033	0.003566	0.27354	1461.1	42.1	1683.4	63.7	13.21	1683.4	63.7	3.78%	No Hf data collected, > 10% Discordant, excluded
12DTB19	23/04/2020 (5) 17:04:14.00	12DTB19 - 49	263	22	100.8	8.4	4.149378	0.23966526	0.1004	0.004108	-0.028769	1391.9	72.3	1630.7	76	14.64	1630.7	76	4.66%	No Hf data collected, > 10% Discordant, excluded
12DTB19	23/04/2020 (5) 15:30:18.00	12DTB19 - 23	402	13	532	35	4.1841	0.1939742	0.1006	0.003612	-0.17913	1381.5	57.6	1634.4	66.7	15.47	1634.4	66.7	4.08%	No Hf data collected, > 10% Discordant, excluded
12DTB19	23/04/2020 (5) 14:36:38.00	12DTB19 - 8	311	11	59.7	1.6	4.424779	0.16681025	0.0974	0.003848	0.054624	1313.5	44.8	1574.1	74	16.56	1574.1	74	4.70%	No Hf data collected, > 10% Discordant, excluded
12DTB19	23/04/2020 (5) 17:21:31.00	12DTB19 - 53	523	16	193.1	4.9	4.198153	0.12097448	0.1033	0.003766	0.25742	1377.3	35.7	1683.4	67.3	18.18	1683.4	67.3	4.00%	No Hf data collected, > 10% Discordant, excluded
12DTB19	23/04/2020 (5) 15:53:15.00	12DTB19 - 30	445	35	443	15	4.640371	0.27583832	0.0957	0.004014	-0.15283	1258.1	67.9	1541	78.9	18.36	1541	78.9	5.12%	No Hf data collected, > 10% Discordant, excluded
12DTB19	23/04/2020 (5) 15:45:39.00	12DTB19 - 26	230.1	3.3	70.3	1.6	4.13394	0.14590979	0.1051	0.004002	0.096954	1396.6	44.3	1715.2	70	18.58	1715.2	70	4.08%	No Hf data collected, > 10% Discordant, excluded
12DTB19	23/04/2020 (5) 17:54:08.00	12DTB19 - 61	186.5	7.2	171	3.8	4.688233	0.18607866	0.0978	0.004456	0.12231	1246.4	45	1581.8	85.2	21.20	1581.8	85.2	5.39%	No Hf data collected, > 10% Discordant, excluded
12DTB19	23/04/2020 (5) 16:02:56.00	12DTB19 - 31	493.3	8.8	338	18	4.438526	0.14393197	0.1053	0.003606	0.19389	1309.8	38.4	1718.7	62.9	23.79	1718.7	62.9	3.66%	No Hf data collected, > 10% Discordant, excluded
12DTB19	23/04/2020 (5) 16:47:00.00	12DTB19 - 44	1260	210	337.1	7.7	5.649718	0.49602606	0.0887	0.003174	-0.4902	1050.6	85.1	1396.8	68.6	24.79	1050.6	85.1	8.10%	No Hf data collected, > 10% Discordant, excluded
12DTB19	23/04/2020 (5) 17:17:39.00	12DTB19 - 51	903	83	615	53	5.387931	0.36902682	0.0934	0.003068	-0.28547	1097.5	69.1	1495.2	62.1	26.60	1495.2	62.1	4.15%	No Hf data collected, > 10% Discordant, excluded
12DTB19	23/04/2020 (5) 15:11:10.00	12DTB19 - 17	593	24	319	14	5.257624	0.20743008	0.0957	0.003414	0.2061	1122.5	40.6	1541	67.1	27.16	1541	67.1	4.35%	No Hf data collected, > 10% Discordant, excluded
12DTB19	23/04/2020 (5) 15:47:35.00	12DTB19 - 27	461.7	8.2	668	18	4.987531	0.17437702	0.1015	0.00353	0.22801	1178	37.6	1650.9	64.5	28.64	1650.9	64.5	3.91%	No Hf data collected, > 10% Discordant, excluded
12DTB19	23/04/2020 (5) 16:48:51.00	12DTB19 - 45	99	4.9	0.0274	0.0069	32.89474	1.8481648	0.0517	0.007734	0.39561	193.1	10.7	271	343	28.75	193.1	10.7	5.54%	No Hf data collected, > 10% Discordant, excluded
12DTB19	23/04/2020 (5) 15:28:25.00	12DTB19 - 22	258	21	193	23	5.22466	0.3201401	0.0989	0.004378	-0.11254	1129	63.5	1602.6	82.6	29.55	1602.6	82.6	5.15%	No Hf data collected, > 10% Discordant, excluded
12DTB19	23/04/2020 (5) 18:15:14.00	12DTB19 - 67	802	12	241.4	2.3	5.995204	0.18460052	0.0942	0.003184	0.21281	994.5	28.4	1511.3	63.8	34.20	1511.3	63.8	4.22%	No Hf data collected, > 10% Discordant, excluded
12DTB19	23/04/2020 (5) 14:50:05.00	12DTB19 - 11	919.2	7.1	697	13	6.644518	0.21677464	0.0891	0.003082	0.0079991	903.8	27.5	1405.4	66.2	35.69	903.8	27.5	3.04%	No Hf data collected, > 10% Discordant, excluded
12DTB19	23/04/2020 (5) 16:29:47.00	12DTB19 - 40	9.27	0.33	17.74	0.78	1.615509	0.08189769	0.798	0.03896	0.41403	3106	125	4917.5	69.5	36.84	4917.5	69.5	1.41%	No Hf data collected, > 10% Discordant, excluded
12DTB19	23/04/2020 (5) 17:34:54.00	12DTB19 - 56	906	29	1910	100	6.69344	0.326518	0.0919	0.003038	0.005145	897.6	40.9	1464.5	62.8	38.71	1464.5	62.8	4.29%	No Hf data collected, > 10% Discordant, excluded
12DTB19	23/04/2020 (5) 17:40:41.00	12DTB19 - 58	926	36	369.3	3	5.624297	0.19156773	0.1061	0.003422	0.038753	1054.9	33.1	1732.6	59.2	39.11	1732.6	59.2	3.42%	No Hf data collected, > 10% Discordant, excluded
12DTB19	23/04/2020 (5) 16:08:40.00	12DTB19 - 33	1173	42	544	15	6.91085	0.5393997	0.0964	0.003328	-0.33684	871.2	63.6	1554.7	64.8	43.96	1554.7	64.8	4.17%	No Hf data collected, > 10% Discordant, excluded
12DTB19	23/04/2020 (5) 14:38:31.74	12DTB19 - 9	144	4.7	45.1	1.8	8.077544	0.31161838	0.0906	0.004912	0.18092	752.4	27.4	1437	103	47.64	752.4	27.4	3.64%	No Hf data collected, > 10% Discordant, excluded
12DTB19	23/04/2020 (5) 18:17:07.00	12DTB19 - 68	1448	60	1087	60	8.873114	0.50813738	0.0855	0.00311	-0.24858	688.4	37.4	1326	70.4	48.08	688.4	37.4	5.43%	No Hf data collected, > 10% Discordant, excluded
12DTB19	23/04/2020 (5) 14:30:51.00	12DTB19 - 6	152.9	4	35.9	2.5	7.886435	0.3256575	0.0938	0.004676	-0.08161	769.6	30	1503.2	94.2	48.80	1503.2	94.2	6.27%	No Hf data collected, > 10% Discordant, excluded
12DTB19	23/04/2020 (5) 15:13:03.00	12DTB19 - 18	645	77	129.2	2.9	10.72961	1.0550019	0.0805	0.00401	-0.3442	574.4	54	1208.4	98.1	52.47	574.4	54	9.40%	No Hf data collected, > 10% Discordant, excluded
12DTB19	23/04/2020 (5) 16:45:05.00	12DTB19 - 43	1230	49	421.4	8.6	6.082725	0.2622528	0.1318	0.004036	-0.24444	981.2	39.2	2121.3	53.7	53.75	2121.3	53.7	2.53%	No Hf data collected, > 10% Discordant, excluded
12DTB19	23/04/2020 (5) 16:04:52.00	12DTB19 - 32	1214	25	521	11	8.361204	0.30704358	0.101	0.00362	0.11647	728.3	25.3	1641.7	66.5	55.64	1641.7	66.5	4.05%	No Hf data collected, > 10% Discordant, excluded
12DTB19	23/04/2020 (5) 15:51:22.00	12DTB19 - 29	2010	160	2240	190	10	0.93	0.0903	0.003606	-0.64465	614.4	54.5	1431	76.2	57.06	614.4	54.5	8.87%	No Hf data collected, > 10% Discordant, excluded
12DTB19	23/04/2020 (5) 18:13:20.00	12DTB19 - 66	51.9	2.8	0.0111	0.0049	36.49635	2.594704	0.055	0.0131	0.2123	174.3	12.2	411	533	57.59	174.3	12.2	7.00%	No Hf data collected, > 10% Discordant, excluded
12DTB19	23/04/2020 (5) 18:20:55.00	12DTB19 - 70	62.2	3.4	0.0586	0.0095	28.49003	1.7873236	0.0624	0.009148	0.091075	222.4	13.7	687	313	67.63	222.4	13.7	6.16%	No Hf data collected, > 10% Discordant, excluded
12DTB19	23/04/2020 (5) 17:23:22.00	12DTB19 - 54	77.2	3.4	0.518	0.049	33.09067	1.6801564	0.088	0.01176	0.28454	191.93	9.6	1382	257	86.11	191.93	9.6	5.00%	No Hf data collected, > 10% Discordant, excluded

Lu-Hf Isotopic Ratios from Iolite: 176Hf/177Hf	±2σ INT	(2% External ±)	176Lu/177Hfm	±2σ INT	176Yb/177Hf	±2σ INT	εHf Calculations: Hfi	εHf	±2σ	TDM(Ga)	TDMCrustal (Ga)	HfCHUR(t)	HfDM(t)
0.282785			0.00360 Bouvier et al., 2008 EPSL-273					Lu decay	0.02	Scherer et al., 2001, Science-293			
0.283250			0.03840 Griffin et al., 2002, Lithos-237										

Appendix D3.1 continued.

Table 21JBM18. U-Pb geochronologic analyses. University of Arizona Laserchron center				Measured ratios					Apparent ages (Ma)						Preferred ages		Discord	Analysis Notes
Analysis	U (ppm)	206Pb 204Pb	U/Th	207Pb 235U	± 2 sig	206Pb* 238U	± 2 sig	error corr.	207Pb 235U	± (Ma) 2 sig	206Pb 238U	± (Ma) 2 sig	206Pb 207Pb	± (Ma) 2 sig	Best age (Ma)	± (Ma) 2 sig	(7/6-6/8)/7/6 *100	
Note black text analyses were included, red are excluded, see analysis note column "S" for further description.																		
-21JBM18 Spot 3	174.54	83934.63	2.14	2.567	0.067	0.2229	0.0049	0.86	1291.3	18.7	1297.2	25.3	1281.5	36.6	1281.5	25.284	-0.76%	Used for MDA calculation
-21JBM18 Spot 97	63.16	150092.50	2.01	2.5627	0.072	0.221	0.0049	0.81	1290.1	20.2	1287.2	25.3	1294.9	39.6	1294.9	25.284	0.37%	Used for MDA calculation
-21JBM18 Spot 20	203.67	94535.71	1.67	2.6681	0.075	0.2273	0.0055	0.84	1319.7	20.4	1320.3	28.2	1318.6	40.0	1318.6	28.224	-0.08%	Used for MDA calculation
-21JBM18 Spot 188	481.84	106470.62	4.21	2.7948	0.13	0.2267	0.0095	0.9	1354.1	34.1	1317.2	49.0	1413.0	66.8	1413	49	4.17%	
-21JBM18 Spot 99	195.10	77456.48	1.58	3.0753	0.086	0.2493	0.006	0.84	1426.6	21.0	1434.9	30.4	1414.2	41.1	1414.2	30.38	-0.88%	
-21JBM18 Spot 39	99.76	19554.94	1.63	3.1549	0.082	0.2555	0.0051	0.75	1446.2	19.6	1466.8	25.7	1416.1	38.4	1416.1	25.676	-2.13%	
-21JBM18 Spot 163	104.29	74946.63	1.96	3.2018	0.096	0.2586	0.0062	0.81	1457.6	22.7	1482.7	31.2	1421.2	44.6	1421.2	31.164	-2.56%	
-21JBM18 Spot 40	324.12	266324.70	1.67	2.762	0.072	0.2229	0.0045	0.8	1345.3	19.1	1297.2	23.3	1422.8	37.3	1422.8	23.324	5.44%	
-21JBM18 Spot 9	189.64	138309.45	3.59	3.0848	0.086	0.2487	0.006	0.83	1428.9	21.0	1431.8	30.4	1424.7	41.1	1424.7	30.38	-0.29%	
-21JBM18 Spot 117	464.98	366707.31	3.71	2.9741	0.089	0.2397	0.0062	0.88	1401.0	22.3	1385.1	31.6	1425.3	43.8	1425.3	31.556	1.70%	
-21JBM18 Spot 185	250.82	79777.47	30.77	3.1428	0.075	0.2527	0.0045	0.72	1443.2	18.0	1452.4	22.7	1429.8	35.3	1429.8	22.736	-0.94%	
-21JBM18 Spot 128	69.49	34741.17	4.95	3.1562	0.082	0.2531	0.0056	0.82	1446.5	19.6	1454.4	28.2	1434.9	38.4	1434.9	28.224	-0.81%	
-21JBM18 Spot 53	285.28	62673.02	2.24	3.086	0.086	0.2472	0.0059	0.83	1429.2	21.0	1424.0	29.8	1437.0	41.1	1437	29.792	0.54%	
-21JBM18 Spot 100	63.10	94428.74	1.32	3.1331	0.11	0.2508	0.007	0.8	1440.9	26.5	1442.6	35.3	1438.3	51.9	1438.3	35.28	-0.18%	
-21JBM18 Spot 141	242.49	77154.74	2.15	3.0119	0.078	0.241	0.0053	0.85	1410.6	19.3	1391.9	27.0	1439.1	37.9	1439.1	27.048	1.98%	
-21JBM18 Spot 27	307.06	906891.88	2.38	3.1177	0.075	0.2494	0.0045	0.77	1437.1	18.1	1435.4	22.7	1439.6	35.5	1439.6	22.736	0.18%	
-21JBM18 Spot 140	221.89	624404.51	1.16	3.1306	0.094	0.2503	0.0055	0.72	1440.2	22.7	1440.0	27.8	1440.6	44.6	1440.6	27.832	0.03%	
-21JBM18 Spot 120	115.43	41127.06	1.93	3.031	0.085	0.2421	0.0053	0.78	1415.5	21.0	1397.6	27.0	1442.4	41.1	1442.4	27.048	1.86%	
-21JBM18 Spot 143	103.20	72460.99	2.14	3.2048	0.083	0.2559	0.0051	0.73	1458.3	19.6	1468.8	25.7	1443.0	38.4	1443	25.676	-1.06%	
-21JBM18 Spot 103	69.65	18174.32	2.14	3.1717	0.089	0.2532	0.0051	0.7	1450.3	21.2	1455.0	25.7	1443.5	41.5	1443.5	25.676	-0.47%	
-21JBM18 Spot 158	47.05	28572.40	1.31	3.2344	0.11	0.258	0.0062	0.74	1465.4	25.9	1479.6	31.2	1445.0	50.7	1445	31.164	-1.41%	
-21JBM18 Spot 172	195.37	66487.11	2.08	3.2354	0.078	0.2577	0.0052	0.83	1465.7	18.3	1478.1	26.1	1447.8	35.9	1447.8	26.068	-1.23%	
-21JBM18 Spot 18	205.34	279959.13	3.13	3.1079	0.099	0.2475	0.0054	0.73	1434.6	23.9	1425.6	27.4	1448.1	46.9	1448.1	27.44	0.93%	
-21JBM18 Spot 98	215.50	3902493.84	3.36	3.03	0.091	0.2412	0.0058	0.84	1415.2	22.5	1392.9	29.6	1448.9	44.2	1448.9	29.596	2.33%	
-21JBM18 Spot 60	68.59	3481623.57	1.36	3.1181	0.081	0.2482	0.0055	0.82	1437.2	19.6	1429.2	27.8	1449.0	38.4	1449	27.832	0.82%	
-21JBM18 Spot 127	129.57	79170.72	1.74	3.203	0.083	0.2541	0.0051	0.74	1457.9	19.6	1459.6	25.7	1455.4	38.4	1455.4	25.676	-0.17%	
-21JBM18 Spot 182	358.46	196509.78	1.54	2.8678	0.1	0.2271	0.0077	0.91	1373.5	25.7	1319.3	39.6	1458.8	50.3	1458.8	39.592	5.85%	
-21JBM18 Spot 167	157.50	395356.36	3.79	3.204	0.083	0.2535	0.0051	0.75	1458.1	19.6	1456.5	25.7	1460.5	38.4	1460.5	25.676	0.16%	
-21JBM18 Spot 42	137.98	108649.95	1.48	3.1552	0.088	0.2496	0.0055	0.81	1446.3	21.2	1436.4	27.8	1460.8	41.5	1460.8	27.832	0.99%	
-21JBM18 Spot 102	164.64	853430.63	0.81	3.1657	0.095	0.25	0.0055	0.75	1448.8	22.7	1438.5	27.8	1464.1	44.6	1464.1	27.832	1.05%	
-21JBM18 Spot 82	250.27	102521.44	4.03	3.2069	0.09	0.2532	0.0056	0.83	1458.8	21.4	1455.0	28.2	1464.5	41.9	1464.5	28.224	0.39%	
-21JBM18 Spot 79	485.22	111635.12	4.65	3.1637	0.11	0.2494	0.0075	0.87	1448.3	26.3	1435.4	37.8	1467.4	51.5	1467.4	37.828	1.30%	
-21JBM18 Spot 164	134.42	2018745.93	1.34	3.3137	0.086	0.261	0.0057	0.79	1484.3	19.8	1495.0	28.6	1469.1	38.8	1469.1	28.616	-1.03%	
-21JBM18 Spot 72	215.11	62100.44	4.31	3.2484	0.091	0.2548	0.0066	0.91	1468.8	21.4	1463.2	33.3	1476.9	41.9	1476.9	33.32	0.55%	
-21JBM18 Spot 66	123.79	104775.96	2.22	3.2663	0.072	0.2559	0.0046	0.8	1473.1	16.8	1468.8	23.1	1479.2	32.9	1479.2	23.128	0.42%	
-21JBM18 Spot 134	57.19	131572.09	1.42	3.2767	0.092	0.2559	0.0056	0.76	1475.5	21.4	1468.8	28.2	1485.2	41.9	1485.2	28.224	0.65%	
-21JBM18 Spot 77	267.41	23728.64	1.72	3.2906	0.47	0.2567	0.036	0.98	1478.8	109.0	1472.9	180.9	1487.3	213.6	1487.3	180.908	0.57%	
-21JBM18 Spot 48	235.97	64833.78	1.08	3.0899	0.099	0.2405	0.0063	0.86	1430.2	24.1	1389.3	32.1	1491.6	47.3	1491.6	32.144	4.12%	
-21JBM18 Spot 149	201.77	96788.45	0.68	3.2019	0.077	0.2484	0.0045	0.78	1457.6	18.2	1430.2	22.7	1497.8	35.7	1497.8	22.736	2.68%	
-21JBM18 Spot 22	78.96	78592.85	1.64	3.3274	0.087	0.258	0.0052	0.73	1487.5	20.0	1479.6	26.1	1498.8	39.2	1498.8	26.068	0.75%	
-21JBM18 Spot 21	174.92	51157.50	3.06	3.2836	0.092	0.2544	0.0056	0.79	1477.2	21.4	1461.1	28.2	1500.3	41.9	1500.3	28.224	1.54%	
-21JBM18 Spot 33	97.56	59794.31	1.45	3.3342	0.12	0.2623	0.0079	0.83	1489.1	27.6	1501.6	39.6	1471.3	54.2	1501.6	54.16656	-1.21%	
-21JBM18 Spot 116	259.77	72902.45	4.18	3.7868	0.11	0.2625	0.0053	0.73	1589.9	22.9	1502.6	26.5	1707.8	44.9	1502.6	44.94672	6.90%	
-21JBM18 Spot 16	224.24	135710.56	2.52	3.8575	0.1	0.2668	0.0059	0.81	1604.8	20.6	1524.5	29.4	1711.9	40.3	1524.5	40.3368	6.26%	
-21JBM18 Spot 197	223.32	196820.32	2.77	4.012	0.11	0.2771	0.0067	0.84	1636.6	21.8	1576.7	33.1	1714.5	42.6	1576.7	42.64176	4.54%	
-21JBM18 Spot 122	360.82	313918.35	3.33	4.0169	0.11	0.2802	0.0062	0.8	1637.6	21.8	1592.4	30.6	1696.2	42.6	1592.4	42.64176	3.45%	
-21JBM18 Spot 6	384.21	71466.10	1.87	4.2775	0.14	0.2806	0.0079	0.86	1689.0	26.5	1594.4	39.0	1808.6	51.9	1594.4	51.8616	6.61%	
-21JBM18 Spot 61	154.39	85341.50	1.26	4.0557	0.11	0.281	0.0067	0.85	1645.4	21.6	1596.4	33.1	1708.7	42.3	1596.4	42.2576	3.70%	
-21JBM18 Spot 121	244.85	79573.11	3.32	4.0553	0.12	0.2819	0.0073	0.85	1645.4	23.7	1600.9	36.1	1702.6	46.5	1600.9	46.48336	3.36%	
-21JBM18 Spot 108	389.76	191299.13	3.00	4.1	0.18	0.2823	0.011	0.91	1654.3	35.1	1602.9	54.1	1720.2	68.8	1602.9	68.76464	3.83%	
-21JBM18 Spot 175	473.47	101048.77	1.80	4.1319	0.18	0.2842	0.011	0.92	1660.6	34.9	1612.5	54.1	1722.1	68.4	1612.5	68.38048	3.57%	
-21JBM18 Spot 171	338.51	134763.49	3.88	4.409	0.15	0.285	0.008	0.83	1714.0	27.6	1616.5	39.4	1835.4	54.2	1616.5	54.16656	6.61%	
-21JBM18 Spot 196	325.29	873708.13	2.37	4.0387	0.18	0.2863	0.011	0.92	1642.0	35.5	1623.0	54.1	1666.5	69.5	1623	69.53296	1.47%	
-21JBM18 Spot 90	71.11	47892.83	1.03	3.9572	0.12	0.2866	0.0069	0.84	1625.5	24.1	1624.5	33.9	1626.7	47.3	1624.5	47.25168	0.07%	
-21JBM18 Spot 64	253.05	190278.10	1.48	3.5794	0.11	0.2592	0.0062	0.84	1545.0	23.9	1485.7	31.2	1627.0	46.9	1627	31.164	5.04%	
-21JBM18 Spot 28	451.24	689133.95	1.18	4.1913	0.16	0.2892	0.01	0.92	1672.3	30.6	1637.5	49.0	1716.3	59.9	1637.5	59.92896	2.56%	
-21JBM18 Spot 126	623.88	160784.12	6.14	3.5097	0.15	0.2522	0.0096	0.9	1529.4	33.1	1449.8	48.4	1641.3	64.9	1641.3	48.412	6.82%	
-21JBM18 Spot 37	185.02	28491.68	1.34	4.1927	0.44	0.2902	0.03	0.97	1672.6	84.3	1642.5	146.8	1710.5	165.2	1642.5	165.1888	2.22%	
-21JBM18 Spot 74	165.94	85680.47	1.29	4.3474	0.14	0.2923	0.0076	0.8	1702.4	26.1	1653.0	37.2	1763.7	51.1	1653	51.09328	3.48%	
-21JBM18 Spot 68	83.27	863772.69	1.77	4.1065	0.11	0.2924	0.0064	0.81	1655.6	21.4	1653.6	31.4	1658.2	41.9	1653.5	41.87344	0.16%	
-21JBM18 Spot 124	154.30	68282.65	6.37	4.2149	0.11	0.2947	0.0065	0.84	1676.9	21.0	1665.0	31.8	1691.9	41.1	1665	41.10512	0.89%	
-21JBM18 Spot 191	71.54	76684.47	1.54	4.2416	0.16	0.2949	0.0094	0.85	1682.1	30.4	1666.0	45.9	1702.3	59.5	1666	59.5448	1.19%	
-21JBM18 Spot 51	377.69	146870.79	3.67	4.3935	0.12	0.2957	0.0071	0.84	1711.1	22.1	1670.0	34.7	1761.9	43.4	1670	43.41008	2.88%	
-21JBM18 Spot 8	165.90	88192.69	1.96	4.4687	0.11	0.2958	0.0059	0.85	1725.2	20.0	1670.4	28.8	1792.2	39.2	1670.4	39.18432	3.74%	
-21JBM18 Spot 46	129.07	36336.83	2.53	4.2418	0.1	0.297	0.0053	0.77	1682.2	19.0	1676.4	25.9	1689.3	37.2	1676.4	37.225104	0.42%	
-21JBM18 Spot 105	593.25	43607.27	6.18	3.6367	0.15	0.256	0.0097	0.94	1557.6	32.1	1469.3	48.8	1679.4	63.0	1679.4	48.804	7.25%	
-21JBM18 Spot 56	275.72	219234.37	2.45	4.2415	0.1	0.2981	0.0054	0.74	1682.1	19.0	1681.9	26.3	1682.4	37.2	1681.9	37.225104	0.02%	
-21JBM18 Spot 29	181.85	75270.07	1.58	4.3573	0.15	0.2986	0.009	0.86	1704.3	27.8	1684.4	43.7	1728.9	54.6	1684.4	54.55072	1.42%	
-21JBM18 Spot 136	125.68	78594.34	2.73	4.3104	0.095	0.299	0.0054	0.83	1695.4	17.8	1686.3	26.3	1706.5	34.9	1686.3	34.881728	0.65%	
-21JBM18 Spot 145	208.86	7873954.06	3.75	4.4032	0.11	0.2991	0.0054	0.77	1712.9	20.2	1686.8	26.3	1745.0	39.6	1686.8	39.56848	1.84%	
-21JBM18 Spot 78	200.85	62904.71	3.05	4.2392	0.12	0.2994	0.006	0.8	1681.6	22.7	1688.3	32.1	1673.3	44.6	1688.3	44.56256	-0.50%	
-21JBM18 Spot 67	247.90	117595.87	2.28	4.3782	0.12	0.2997	0.0078	0.88	1708.2	22.1	1689.8	37.8	1730.9	43.4	1689.8	43.41008	1.31%	
-21JBM18 Spot 15	192.62	235880.62	1.98	4.1708	0.1	0.3003	0.0054	0.79	1668.3	19.2	1692.8	26.3	1637.6	37.7	1692.8	37.724512	-1.87%	
-21JBM18 Spot 25	202.46	95117.75	2.77	3.7085	0.096	0.259	0.0057	0.8	1573.2	20.4	1484.7	28.6	1694.0	40.0	1694	28.616	7.13%	
-21JBM18 Spot 114	346.25	498869.67	4.12	4.2939	0.14	0.3006	0.0078	0.82	1692.2	26.3	1694.3	37.8	1689.6	51.5	1694.3	51.47744	-0.15%	
-21JBM18 Spot 144	101.16	99071.48	2.11	4.3577	0.11	0.3008	0.0066	0.84	1704.4	20.4	1695.3	32.1	1715.5	40.0	1695.3	39.95264	0.65%	
-21JBM18 Spot 150	158.59	130304.85	1.09	4.3947	0.097	0.301	0.0048	0.74	1711.3	17.9	1696.3	23.3	1729.8	35.1	1696.3	35.073808	1.07%	
-21JBM18 Spot 62	467.50	478619.78	2.04	3.7443	0.13	0.261	0.0084	0.9	1580.9	27.2	1495.0	42.1	1697.5	53.4	1697.5	42.14	6.87%	
-21JBM18 Spot 43	353.61	67212.66	1.14	3.7583	0.11	0.2619	0.0063	0.84	1583.9	22.9	1499.6	31.6	1698.1	44.9	1698.1	31.556	6.73%	
-21JBM18 Spot 189	296.36	963373158.42	2.07	4.3986	0.13	0.3022	0.0079	0.83	1712.1	23.9	1702.2	38.4	1724.2	46.9	1702.2	46.86752	0.70%	
-21JBM18 Spot 71	116.49	60824.47	2.12	4.3365	0.11	0.3023	0.006	0.81	1700.3	20.6	1702.7	29.2	1697.4	40.3	1702.7	40.3368	-0.17%	
-21JBM18 Spot 70	108.97	807773.25	3.17	4.477	0.13	0.3024	0.0073	0.8	1726.7	23.7	1703.2	35.5	1755.3	46.5	1703.2	46.48336	1.63%	
-21JBM18 Spot 174	165.04	105961.94	3.24	4.3604	0.11	0.303	0.0073	0.88	1704.9	20.4	1706.2	35.5	1703.3	40.0	1706.2	39.95264	-0.09%	
-21JBM18 Spot 47	184.75	93583.29	3.89	4.4557	0.13	0.303	0.0079	0.88	1722.8	23.7	1706.2	38.2	1743.0	46.5	1706.2	46.48336	1.16%	
-21JBM18 Spot 11	240.17	65029.82	3.25	4.34	0.11	0.3035	0.0061	0.82	1701.0	20.6	1708.6	30.1	1691.6	40.3	1708.6	40.3368	-0.56%	
-21JBM18 Spot 199	216.20	114360.60	4.03	4.4832	0.13	0.3041	0.0067	0.79	1727.9	23.5	1711.6	32.5	1747.6	46.1	1711.6	46.0992	1.13%	
-21JBM18 Spot 83	620.04	29854.86	1.90	3.5973	0.12	0.2485	0.0075	0.91	1548.9	26.1	1430.7	38.0	1714.1	51.1	1714.1	38.024	9.64%	
-21JBM18 Spot 87	234.00	1218997.11	1.13	4.3753	0.11	0.3048	0.0061	0.74	1707.7	20.4	1715.1	29.6	1698.6	40.0	1715.1	39.95264	-0.54%	
-21JBM18 Spot 162	171.95	63673.30	5.82	4.4298	0.12	0.3048	0.0073	0.83	1717.9	22.0	1715.1	35.3	1721.4	43.0	1715.1	43.02592	0.20%	
-21JBM18 Spot 160	106.59	25687.58	3.06	4.4323	0.12	0.3048	0.0067	0.77	1718.4	22.0	1715.1	32.5	1722.5	43.0	1715.1	43.02592	0.24%	
-21JBM18 Spot 148	553.42	196273.28	4.75	4.5364	0.18	0.305	0.011	0.89	1737.7	32.3	1716.1	53.3	1763.8	63.4	1716.1	63.3864	1.48%	
-21JBM18 Spot 34	151.84	119059.60	3.03	4.3905	0.14	0.3051	0.0079	0.83	1710.6	25.9	1716.5	38.2	1703.2	50.7	1716.5	50.70912	-0.43%	
-21JBM18 Spot 113	102.30	155971.37	1.80	4.4652	0.13	0.3051	0.0061	0.74	1724.5	23.7	1716.5	29.6	1734.2	46.5	1716.5	46.48336	0.56%	
-21JBM18 Spot 190	107.04	62874.91	2.33	4.3322	0.12	0.3056	0.0067	0.8	1699.5	22.3	1719.0	32.3	1675.5	43.8	1719	43.79424	-1.43%	
-21JBM18 Spot 187	54.30	28200.57	2.07	4.3399	0.12	0.306	0.0061	0.73	1701.0	22.3	1721.0	29.6	1676.4	43.8	1721	43.79424	-1.47%	
-21JBM18 Spot 36	140.81	116491.88	1.74	4.3823	0.11	0.3071	0.0061	0.75	1709.0	20.4	1726.4	30.1	1687.7	40.0	1726.4	39.95264	-1.26%	
-21JBM18 Spot 89	107.51	63790.85	3.00	4.3979	0.13	0.3074	0.0074	0.81	1711.9	23.9	1727.9	35.7	1692.5	46.9	1727.9	46.86752	-1.15%	
-21JBM18 Spot 133	307.92	514200.61	2.24	4.9524	0.15	0.3084	0.0074	0.84	1811.2	25.1	1732.8	35.7	1902.7	49.2	1732.8	49.17248	4.81%	
-21JBM18 Spot 94	68.35	63873.73	3.27	4.5251	0.14	0.3086	0.008	0.81	1735.6	25.3	1733.8	38.6	1737.7	49.6	1733.8	49.55664	0.12%	
-21JBM18 Spot 52	163.31	88750.32	0.96	4.9805	0.16	0.3087	0.008	0.79	1816.0	26.7	1734.3	38.6	1911.1	52.2	1734.3	52.24576	4.98%	
-21JBM18 Spot 110	124.69	281981.32	3.69	4.5225	0.13	0.3092	0.0068	0.77	1735.1	23.5	1736.8	33.5	1733.1	46.1	1736.8	46.0992	-0.12%	
-21JBM18 Spot 50	296.05	74365.71	2.92	4.5605	0.12	0.3092	0.0056	0.74	1742.1	21.6	1736.8	27.0	1748.5	42.3	1736.8	42.2576	0.37%	
-21JBM18 Spot 179	105.11	80195.09	1.61	4.563	0.14	0.3102	0.0068	0.79	1742.5	25.1	1741.7	33.5	1743.6	49.2	1741.7	49.17248	0.06%	
-21JBM18 Spot 150	129.50	74151.85	4.00	4.4738	0.13	0.3103	0.0074	0.86	1726.1	23.7	1742.2	35.7	1706.7	46.5	1742.2	46.48336	-1.14%	
-21JBM18 Spot 118	458.32	373753.17	2.55	4.6256	0.16	0.3106	0.0087	0.86	1753.9	28.2	1743.7	41.9	1766.1	55.3	1743.7	55.31904	0.69%	
-21JBM18 Spot 126	215.24	105624.66	3.15	4.4463	0.13	0.3108	0.0075	0.82	1721.0	23.7	1744.6	36.7	1692.4	46.5	1744.6	46.48336	-1.69%	
-21JBM18 Spot 44	230.14	9923542.89	2.71	4.5894	0.12	0.3109	0.0068	0.84	1747.3	21.4	1745.1	32.7	1750.0	41.9	1745.1	41.87344	0.15%	
-21JBM18 Spot 54	103.08	154220.58	2.50	4.6175	0.14	0.3109	0.0075	0.76	1752.4	24.9	1745.1	36.1	1761.2	48.8	1745.1	48.78832	0.50%	
-21JBM18 Spot 161	356.71	127739.89	6.59	4.6243	0.12	0.3109	0.0062	0.76	1753.7	21.2	1745.1	29.8	1763.8	41.5	1745.1	41.48928	0.57%	
-21JBM18 Spot 186	244.87	76421.49	4.62	4.7761	0.13	0.3129	0.0075	0.86	1780.7	22.3	1755.0	36.1	1811.0	43.8	1755	43.79424	1.67%	
-21JBM18 Spot 45	342.31	107429.76	3.95	4.667	0.15	0.313	0.0081	0.82	1761.3	26.3	1755.5	39.0	1768.3	51.5	1755.5	51.47744	0.40%	
-21JBM18 Spot 82	157.97	79493.06	2.37	4.6855	0.094	0.3135	0.005	0.77	1764.7	16.4	1757.9	24.1	1772.6	32.2	1757.9	32.231024	0.45%	
-21JBM18 Spot 91	405.87	101967.64	19.10	5.1452	0.16	0.3139	0.0094	0.89	1843.6	25.9	1759.9	45.3	1939.5	50.7	1759.9	50.70912	4.94%	
-21JBM18 Spot 198	199.98	160538.96	1.76	4.7399	0.12	0.3143	0.0063	0.78	1774.3	20.8	1761.8	30.4	1789.1	40.7	1761.8	40.72096	0.83%	
-21JBM18 Spot 192	117.41	38730.69	5.89	4.6528	0.15	0.3147	0.0082	0.82	1758.8	26.5	1763.8	39.4	1752.9	51.9	1763.8	51.8616	-0.34%	
-21JBM18 Spot 73	193.40	257243.86	2.72	4.857	0.18	0.3152	0.01	0.85	1794.8	30.6	1766.2	48.0	1828.2	59.9	1766.2	59.92896	1.83%	
-21JBM18 Spot 107	169.91	93364.47	7.53	4.732	0.14	0.317	0.0076	0.82	1772.9	24.3	1775.1	36.5	1770.4	47.6	1775.1	47.63584	-0.14%	
-21JBM18 Spot 129	120.62	119777.53	4.98	4.7714	0.14	0.3182	0.0076	0.8	1779.9	24.1	1780.9	36.5	1778.6	47.3	1780.9	47.25168	-0.07%	
-21JBM18 Spot 24	102.38	509305.62	3.13	4.8351	0.14	0.3187	0.0064	0.75	1791.0	23.9	1783.4	30.6	1799.9	46.9	1783.4	46.86752	0.49%	
-21JBM18 Spot 131	85.02	7949647.45	5.28	4.812	0.13	0.3192	0.0064	0.75	1787.0	22.3	1785.8	30.6	1788.4	43.8	1785.8	43.79424	0.08%	
-21JBM18 Spot 176	94.87	68586.70	2.99	4.8212	0.13	0.3206	0.0077	0.82	1788.6	22.1	1792.7	36.8	1783.9	43.4	1792.7	43.41008	-0.26%	
-21JBM18 Spot 111	92.89	30810.94	2.84	4.8544	0.16	0.3218	0.0084	0.81	1794.4	27.2	1798.5	40.2	1789.6	53.4	1798.5	53.39824	-0.27%	
-21JBM18 Spot 132	55.25	17831.26	3.63	4.8298	0.14	0.3221	0.0064	0.73	1790.1	23.9	1800.0	30.6	1778.6	46.9	1800	46.86752	-0.65%	
-21JBM18 Spot 137	139.29	101687.86	4.19	4.8393	0.14	0.3232	0.0071	0.77	1791.8	23.9	1805.3	33.9	1776.0	46.9	1805.3	46.86752	-0.89%	
-21JBM18 Spot 49	149.39	1721170.64	5.39	4.8193	0.13	0.3234	0.0071	0.84	1788.3	22.1	1806.3	33.9	1767.3	43.4	1806.3	43.41008	-1.19%	
-21JBM18 Spot 181	108.25	68539.56	1.50	4.754	0.14	0.3239	0.0078	0.81	1776.8	24.3	1808.7	37.2	1739.5	47.6	1808.7	47.63584	-2.14%	
-21JBM18 Spot 104	150.16	187513.50	3.58	5.0366	0.13	0.3269	0.0065	0.75	1825.5	21.4	1823.3	31.0	1828.0	41.9	1823.3	41.87344	0.14%	
-21JBM18 Spot 201	155.87	46810.34	2.64	5.1156	0.14	0.3292	0.0079	0.81	1838.7	22.7	1834.5	37.6	1843.5	44.6	1834.5	44.56256	0.26%	
-21JBM18 Spot 95	71.17	31933.99	3.01	5.1293	0.14	0.3298	0.0079	0.8	1841.0	22.7	1837.4	37.4	1845.0	44.6	1837.4	44.56256	0.22%	
-21JBM18 Spot 26	146.01	23422.54	2.20	5.185	0.15	0.33	0.0059	0.69	1850.2	24.1	1838.4	28.0	1863.4	47.3	1838.4	47.25168	0.71%	
-21JBM18 Spot 166	91.80	78699.98	3.37	5.0996	0.1	0.3304	0.0059	0.86	1836.0	16.3	1840.3	28.0	1831.2	32.0	1840.3	31.962112	-0.26%	
-21JBM18 Spot 155	86.75	47032.63	1.83	5.0566	0.12	0.3317	0.006	0.76	1828.9	19.8	1846.6	28.4	1808.7	38.8	1846.6	38.80016	-1.12%	
-21JBM18 Spot 58	125.59	77826.13	4.59	5.3602	0.13	0.3358	0.0067	0.8	1878.5	20.4	1866.4	31.8	1891.9	40.0	1866.4	39.95264	0.71%	
-21JBM18 Spot 204	289.82	65602.70	5.77	5.3451	0.12	0.3382	0.0054	0.76	1876.1	18.8	1878.0	25.5	1874.0	36.9	1878	36.87936	-0.11%	
-21JBM18 Spot 55	209.40	1509852.64	1.37	5.3285	0.15	0.3393	0.0081	0.83	1873.4	23.5	1883.3	38.2	1862.5	46.1	1883.3	46.0992	-0.59%	
-21JBM18 Spot 10	53.78	21724.70	4.03	5.437	0.18	0.3446	0.0096	0.81	1890.7	27.8	1908.8	45.1	1870.9	54.6	1908.8	54.55072	-1.06%	
-21JBM18 Spot 130	163.40	820532.09	1.46	10.0477	0.3	0.4589	0.012	0.86	2439.2	27.0	2434.7	51.9	2442.9	53.0	2434.7	53.01408	0.15%	
-21JBM18 Spot 85	121.10	56191.13	2.84	10.2773	0.31	0.4618	0.011	0.81	2460.1	27.4	2447.5	47.6	2470.5	53.8	2447.5	53.7824	0.42%	
-21JBM18 Spot 76	141.72	3386916.91	2.39	10.4896	0.27	0.4669	0.0093	0.77	2479.0	23.3	2470.0	40.0	2486.4	45.7	2470	45.71504	0.30%	
-21JBM18 Spot 88	148.43	318702.01	2.85	10.4526	0.31	0.4697	0.011	0.8	2475.7	26.9	2482.2	47.2	2470.4	52.6	2482.2	52.62992	-0.21%	
-21JBM18 Spot 159	163.60	18455121.61	2.73	10.5729	0.27	0.4733	0.01	0.84	2486.3	23.1	2498.0	42.9	2476.8	45.3	2498	45.33088	-0.38%	
-21JBM18 Spot 5	125.46	3015969.90	1.72	10.774	0.34	0.4738	0.011	0.78	2503.8	28.8	2500.2	47.2	2506.8	56.5	2500.2	56.47152	0.12%	
-21JBM18 Spot 75	166.09	149703.95	1.88	10.4799	0.27	0.4745	0.0085	0.75	2478.1	23.3	2503.3	36.5	2457.6	45.7	2503.3	45.71504	-0.83%	
-21JBM18 Spot 115	174.64	195409.97	1.47	11.0657	0.38	0.4824	0.014	0.82	2528.7	31.4	2537.7	59.6	2521.4	61.5	2537.7	61.4656	-0.29%	
-21JBM18 Spot 200	308.77	721832.69	1.10	11.994	0.34	0.4888	0.011	0.84	2603.9	26.1	2565.5	46.6	2634.0	51.1	2565.5	51.09328	1.14%	
-21JBM18 Spot 2	111.59	107924.03	1.81	11.3072	0.29	0.4893	0.011	0.82	2548.8	23.5	2567.6	46.6	2533.8	46.1	2567.6	46.0992	-0.59%	
-21JBM18 Spot 173	295.62	136831.81	1.42	11.63	0.33	0.4911	0.012	0.87	2575.1	26.1	2575.4	50.8	2574.8	51.1	2575.4	51.09328	-0.01%	
-21JBM18 Spot 109	129.87	150411.76	2.07	11.8431	0.33	0.4931	0.0089	0.66	2592.1	25.5	2584.1	37.6	2598.3	49.9	2584.1	49.9408	0.24%	
-21JBM18 Spot 96	100.91	66657.32	1.92	11.8535	0.31	0.5	0.009	0.72	2592.9	23.9	2613.8	37.8	2576.6	46.9	2613.8	46.86752	-0.63%	
-21JBM18 Spot 154	86.74	94538.14	1.38	12.4441	0.3	0.5034	0.01	0.79	2638.5	22.1	2628.4	41.9	2646.3	43.4	2628.4	43.41008	0.29%	
-21JBM18 Spot 184	87.09	65659.99	2.12	12.7152	0.41	0.5053	0.014	0.85	2658.8	29.8	2636.5	58.8	2675.8	58.4	2636.5	58.39232	0.64%	
-21JBM18 Spot 156	311.33	119381.30	2.71	12.2555	0.37	0.5056	0.013	0.9	2624.2	27.8	2637.8	54.5	2613.7	54.6	2637.8	54.55072	-0.40%	
-21JBM18 Spot 138	148.23	4654025.77	1.68	12.8556	0.39	0.5116	0.013	0.83	2669.1	28.0	2663.5	54.3	2673.4	54.9	2663.5	54.93488	0.16%	
-21JBM18 Spot 123	11.20	76020.61	2.80	13.4609	0.46	0.5171	0.013	0.76	2712.5	31.6	2686.9	54.1	2731.7	61.8	2686.9	61.84976	0.70%	
-21JBM18 Spot 12	147.42	238106.94	1.07	17.1381	0.41	0.569	0.01	0.79	2942.6	22.5	2903.7	40.2	2969.3	44.2	2903.7	44.1784	0.90%	
-21JBM18 Spot 112	78.07	76085.48	1.11	18.469	0.44	0.6004	0.012	0.84	3014.5	22.5	3031.4	47.4	3003.2	44.2	3031.4	44.1784	-0.38%	
-21JBM18 Spot 0	109.14	1919768.90	4.08	35.4041	1.2	0.7632	0.021	0.83	3650.0	32.7	3656.0	75.3	3646.7	64.2	3656	64.15472	-0.09%	
-21JBM18 Spot 203	318.58	150281.34	4.05	2.7217	0.098	0.21	0.0063	0.84	1334.4	26.3	1228.8	32.9	1508.1	51.5	1508.1	32.928	11.52%	> 10% Discordant, not plotted
-21JBM18 Spot 86	178.93	105549.33	1.95	3.3329	0.15	0.2339	0.0094	0.94	1488.8	34.5	1354.9	48.2	1685.1	67.6	1685.1	48.216	11.65%	> 10% Discordant, not plotted
-21JBM18 Spot 202	610.68	18219.27	1.86	3.2591	0.29	0.231	0.015	0.75	1471.3	67.8	1339.7	77.0	1666.7	132.9	1666.7	77.028	11.72%	> 10% Discordant, not plotted
-21JBM18 Spot 125	63.74	71646.24	1.26	7.4539	0.3	0.3296	0.011	0.85	2167.5	35.3	1836.4	52.3	2497.5	69.1	1836.4	69.1488	13.21%	> 10% Discordant, not plotted
-21JBM18 Spot 165	331.37	188538.79	1.18	8.194	0.33	0.3407	0.013	0.95	2252.7	35.7	1890.0	61.3	2600.6	69.9	1890	69.91712	13.38%	> 10% Discordant, not plotted
-21JBM18 Spot 63	465.05	18796.83	1.93	2.6308	0.1	0.2024	0.0073	0.91	1309.3	27.4	1188.2	38.4	1513.5	53.8	1513.5	38.416	13.49%	> 10% Discordant, not plotted
-21JBM18 Spot 135	159.68	81448.12	1.35	3.2653	0.098	0.2269	0.0059	0.83	1472.8	22.9	1318.2	30.4	1703.3	44.9	1703.3	30.38	13.53%	> 10% Discordant, not plotted
-21JBM18 Spot 169	558.95	50927.10	2.63	3.0926	0.11	0.2192	0.0075	0.9	1430.9	26.7	1277.6	38.8	1666.7	52.2	1666.7	38.808	14.15%	> 10% Discordant, not plotted
-21JBM18 Spot 32	488.42	38274.69	1.31	2.3292	0.079	0.1879	0.0056	0.88	1221.2	23.5	1110.0	29.8	1423.5	46.1	1423.5	29.792	14.21%	> 10% Discordant, not plotted
-21JBM18 Spot 84	344.31	114121.38	1.99	2.8808	0.12	0.2103	0.0072	0.88	1376.9	30.8	1230.4	37.6	1612.0	60.3	1612	37.632	14.58%	> 10% Discordant, not plotted
-21JBM18 Spot 92	218.83	48560.14	1.64	9.7501	0.47	0.3465	0.016	0.95	2411.4	43.5	1917.9	75.1	2859.1	85.3	1917.9	85.28352	15.66%	> 10% Discordant, not plotted
-21JBM18 Spot 65	502.88	71956.25	1.71	3.1287	0.12	0.2165	0.0074	0.89	1439.8	29.0	1263.4	38.4	1711.0	56.9	1711	38.416	15.85%	> 10% Discordant, not plotted
-21JBM18 Spot 168	399.45	35163.51	3.03	3.0153	0.13	0.2119	0.0081	0.91	1411.5	32.1	1238.9	42.1	1682.5	63.0	1682.5	42.14	16.11%	> 10% Discordant, not plotted
-21JBM18 Spot 81	722.59	88549.60	2.26	2.8687	0.1	0.2054	0.007	0.91	1373.7	25.7	1204.3	36.7	1648.0	50.3	1648	36.652	16.64%	> 10% Discordant, not plotted
-21JBM18 Spot 101	626.03	71408.47	3.25	3.6372	0.12	0.2282	0.0068	0.88	1557.7	25.7	1325.1	34.9	1889.2	50.3	1889.2	34.888	17.55%	> 10% Discordant, not plotted
-21JBM18 Spot 59	378.25	12143.83	1.54	3.0442	0.097	0.2094	0.005	0.76	1418.8	23.9	1225.6	26.1	1722.0	46.9	1722	26.068	17.61%	> 10% Discordant, not plotted
-21JBM18 Spot 157	183.23	36915.68	1.18	1.6902	0.047	0.1514	0.0033	0.75	1004.8	17.4	908.8	18.1	1220.7	34.1	1220.7	18.1104	17.68%	> 10% Discordant, not plotted
-21JBM18 Spot 14	756.29	4990.48	2.02	2.7507	0.12	0.193	0.0077	0.93	1342.3	31.8	1137.6	40.8	1685.5	62.2	1685.5	40.768	20.36%	> 10% Discordant, not plotted
-21JBM18 Spot 41	410.39	7425.49	0.94	3.9921	0.26	0.2277	0.0096	0.64	1632.6	51.7	1322.4	49.4	2059.0	101.4	2059	49.392	20.71%	> 10% Discordant, not plotted
-21JBM18 Spot 13	462.42	66641.98	1.56	3.1758	0.11	0.2044	0.0061	0.88	1451.3	26.3	1198.9	31.9	1843.2	51.5	1843.2	31.948	21.26%	> 10% Discordant, not plotted
-21JBM18 Spot 4	621.34	79887.23	1.70	1.9173	0.069	0.1576	0.005	0.91	1087.1	23.5	943.4	27.2	1387.6	46.1	1387.6	27.244	21.66%	> 10% Discordant, not plotted
-21JBM18 Spot 139	648.36	16006.97	1.55	5.3772	0.24	0.2504	0.01	0.9	1881.2	37.4	1440.5	50.6	2410.0	73.4	2410	50.568	21.94%	> 10% Discordant, not plotted
-21JBM18 Spot 153	1022.21	21444.36	2.12	2.6071	0.083	0.1828	0.0051	0.91	1302.6	22.9	1082.3	27.2	1686.7	44.9	1686.7	27.244	22.77%	> 10% Discordant, not plotted
-21JBM18 Spot 170	720.75	26397.71	2.67	2.4644	0.089	0.1775	0.0057	0.88	1261.7	25.5	1053.3	30.6	1637.0	49.9	1637	30.576	22.93%	> 10% Discordant, not plotted
-21JBM18 Spot 17	672.47	9421.07	1.35	2.0275	0.26	0.1601	0.018	0.86	1124.8	85.5	957.3	98.0	1464.2	167.5	1464.2	98	23.18%	> 10% Discordant, not plotted
-21JBM18 Spot 19	577.22	8993.16	1.28	8.9321	0.43	0.281	0.013	0.95	2331.1	43.1	1596.4	64.1	3055.8	84.5	1596.4	84.5152	23.72%	> 10% Discordant, not plotted
-21JBM18 Spot 57	576.61	39213.77	1.30	5.5522	0.2	0.2411	0.0077	0.88	1908.7	30.4	1392.4	39.2	2528.0	59.5	2528	39.2	24.50%	> 10% Discordant, not plotted
-21JBM18 Spot 180	575.27	31557.57	3.13	2.2348	0.076	0.1644	0.0049	0.88	1192.0	23.3	981.2	26.7	1597.6	45.7	1597.6	26.656	25.39%	> 10% Discordant, not plotted
-21JBM18 Spot 1	773.53	44960.40	2.01	2.3477	0.099	0.1677	0.0064	0.93	1226.9	29.4	999.4	34.7	1652.3	57.6	1652.3	34.692	25.75%	> 10% Discordant, not plotted
-21JBM18 Spot 193	848.03	3512.99	2.88	5.8454	0.21	0.2387	0.0076	0.87	1953.2	30.6	1379.9	38.8	2630.7	59.9	2630.7	38.808	25.75%	> 10% Discordant, not plotted
-21JBM18 Spot 30	1016.38	33416.88	1.13	2.0674	0.095	0.1567	0.0069	0.92	1138.1	30.8	938.4	37.6	1541.6	60.3	1541.6	37.632	26.17%	> 10% Discordant, not plotted
-21JBM18 Spot 38	658.71	17740.83	1.00	4.3901	0.16	0.2018	0.0065	0.88	1710.5	29.6	1185.0	34.1	2432.0	58.0	2432	34.104	29.67%	> 10% Discordant, not plotted
-21JBM18 Spot 69	1050.55	8162.56	1.76	1.82	0.084	0.1397	0.0059	0.89	1052.7	29.6	843.0	32.7	1517.9	58.0	1517.9	32.732	30.65%	> 10% Discordant, not plotted
-21JBM18 Spot 35	951.87	3242.35	0.95	2.8419	0.18	0.1683	0.0098	0.9	1366.7	46.6	1002.7	52.9	1992.5	91.4	1992.5	52.92	31.41%	> 10% Discordant, not plotted
-21JBM18 Spot 147	810.49	24068.81	1.57	3.0356	0.11	0.1724	0.0052	0.83	1416.6	27.0	1025.3	28.0	2066.6	53.0	2066.6	28.028	31.45%	> 10% Discordant, not plotted
-21JBM18 Spot 119	1045.43	3945.63	1.08	2.5703	0.11	0.1609	0.0064	0.91	1292.2	30.6	961.8	34.9	1893.3	59.9	1893.3	34.888	31.75%	> 10% Discordant, not plotted
-21JBM18 Spot 80	720.76	19400.11	1.05	4.1577	0.15	0.19	0.0065	0.91	1665.7	29.0	1121.4	34.5	2441.9	56.9	2441.9	34.496	31.79%	> 10% Discordant, not plotted
-21JBM18 Spot 152	1209.71	20758.61	2.50	1.7596	0.074	0.134	0.0054	0.94	1030.7	26.7	810.6	30.0	1532.8	52.2	1532.8	29.988	32.76%	> 10% Discordant, not plotted
-21JBM18 Spot 151	1253.96	23997.79	1.23	1.3669	0.055	0.1165	0.004	0.87	874.8	23.1	710.4	22.5	1317.7	45.3	1317.7	22.54	33.61%	> 10% Discordant, not plotted
-21JBM18 Spot 183	992.21	3473.07	0.82	2.326	0.084	0.1492	0.0042	0.79	1220.3	25.1	896.5	23.1	1849.3	49.2	1849.3	23.128	34.01%	> 10% Discordant, not plotted
-21JBM18 Spot 7	1034.76	19797.13	1.70	2.0001	0.088	0.1388	0.0053	0.9	1115.5	29.2	837.9	29.4	1705.7	57.2	1705.7	29.4	34.60%	> 10% Discordant, not plotted
-21JBM18 Spot 23	1103.52	11511.80	2.25	1.8238	0.088	0.1319	0.0053	0.81	1054.1	31.0	798.7	29.6	1629.4	60.7	1629.4	29.596	35.31%	> 10% Discordant, not plotted
-21JBM18 Spot 177	968.23	16655.01	2.04	1.7711	0.064	0.1293	0.0039	0.87	1034.9	22.9	783.9	21.8	1611.8	44.9	1611.8	21.756	35.79%	> 10% Discordant, not plotted
-21JBM18 Spot 178	666.23	1829.33	3.46	3.081	0.48	0.1543	0.013	0.54	1428.0	117.0	925.0	71.1	2286.0	229.3	2286	71.148	37.53%	> 10% Discordant, not plotted
-21JBM18 Spot 106	1234.48	14612.96	7.88	1.4681	0.056	0.1148	0.0039	0.9	917.3	22.5	700.6	22.1	1482.8	44.2	1482.8	22.148	38.14%	> 10% Discordant, not plotted
-21JBM18 Spot 195	501.41	27874.89	2.00	1.6288	0.16	0.1179	0.012	0.98	981.4	60.6	718.5	67.8	1627.7	118.7	1627.7	67.816	39.71%	> 10% Discordant, not plotted
-21JBM18 Spot 31	2340.74	7221.21	0.91	1.4383	0.055	0.078	0.0027	0.91	905.0	22.5	484.2	15.8	2147.6	44.2	2147.6	15.8172	57.86%	> 10% Discordant, not plotted

Appendix D3.2: U/Pb-Lu/Hf Standards

Curtin University Geohistory center						LA-ICP-MS Isotopic Ratios					Apparent Ages - Calculated in Isoplot R (Ma)			
Sample ID	Spot ID	238U conc. ppm	±2σ INT	232Th conc. ppm	±2σ INT	238U/206Pb	±2σ PROP	207Pb/206Pb	±2σ PROP	rho	238U/206Pb	±2σ PROP	207Pb/206Pb	±2σ PROP
Standard Results - U/Pb on 7700 - Samples 10DTB19, 12DTB19, 14DTB19 - OGC primary standard for unknowns > 1500 Ma, 91500 primary standard for unknowns > 1500 Ma, errors propogated within run and are the same as long term running averages (Spencer et al., 2016)														
	91500 - 1	80.1	3.6	30.5	1.4	5.56483	0.1145791	0.0774	0.0066	0.34234	1065.3	20.2	1131	170
	91500 - 2	79.9	3.4	29.4	1.2	5.617978	0.1262467	0.0728	0.0064	0.051334	1056	21.9	1007	178
	91500 - 3	79.5	3.4	29.8	1.3	5.595971	0.1221281	0.0762	0.0066	0.25605	1059.9	21.3	1099	173
	91500 - 4	81.6	3.8	31.9	1.7	5.571031	0.1210419	0.0724	0.0055	0.31987	1064.2	21.3	996	154
	91500 - 5	78.3	3.8	28.6	1.4	5.56483	0.1145791	0.0703	0.0057	0.087615	1065.3	20.2	936	166
	91500 - 6	80.4	3.7	30.7	1.5	5.56483	0.1486432	0.0807	0.0065	0.37629	1065.3	26.2	1213	158
	91500 - 7	81	3.6	31.8	1.6	5.567929	0.1271075	0.078	0.0072	0.41012	1064.8	22.4	1146	183
	91500 - 8	79.4	3.7	28.5	1.4	5.574136	0.1304982	0.0727	0.0061	0.10247	1063.7	23	1005	170
	91500 - 9	80.6	3.9	30.8	1.7	5.580357	0.1307896	0.0751	0.0069	0.13871	1062.6	23	1070	185
	91500 - 10	78.1	3.5	28.7	1.2	5.605381	0.1288232	0.077	0.0074	0.3151	1058.2	22.4	1120	192
	91500 - 11	82.8	4.1	32	1.5	5.643341	0.1305739	0.0752	0.0058	0.012171	1051.7	22.5	1073	155
	91500 - 12	80.3	3.8	30.5	1.6	5.543237	0.1044734	0.074	0.0057	0.16447	1069.2	18.6	1041	155
	91500 - 13	78.8	3.7	29.7	1.5	5.592841	0.1219915	0.0755	0.0062	0.23186	1060.4	21.3	1081	165
	91500 - 14	81.1	3.8	30.4	1.5	5.574136	0.1087485	0.0786	0.0065	0.18703	1063.7	19.1	1161	164
	91500 - 15	79.3	3.6	29.4	1.4	5.54939	0.1016259	0.0739	0.0065	0.2662	1068.1	18	1038	178
	91500 - 16	80	3.6	30	1.4	5.599104	0.1159949	0.0739	0.006	0.19696	1059.3	20.2	1038	164
	91500 - 17	79.7	3.7	29.8	1.4	5.567929	0.1271075	0.0747	0.0059	0.30706	1064.8	22.4	1060	159
	91500 - 18	80.9	3.3	30.1	1.3	5.69152	0.1295736	0.0797	0.0067	0.36598	1043.4	21.9	1189	166
	91500 - 19	79.1	3.8	30.4	1.4	5.51572	0.124735	0.0778	0.0062	-0.008731	1074.1	22.4	1141	158
	91500 - 20	80.2	3.8	29.8	1.4	5.571031	0.1179383	0.0696	0.0053	0.18841	1064.2	20.8	916	157
	OGC - 1	146.4	4.5	96.2	1.9	1.446341	0.05857324	0.2992	0.0053	0.41659	3388	107	3465.4	27.4
	OGC - 2	193	11	141.9	9.3	1.42288	0.05668844	0.3002	0.004	0.33181	3431	106	3470.6	20.6
	OGC - 3	210	12	219	17	1.426127	0.05694744	0.2979	0.0039	0.26773	3425	106	3458.6	20.3
	OGC - 4	169.1	9.5	181	12	1.409841	0.05565422	0.3	0.0045	0.39067	3456	106	3469.5	23.2
	OGC - 5	232	17	267	24	1.410238	0.05568562	0.2976	0.0036	0.30544	3455	106	3457.1	18.8
	OGC - 6	239	20	297	29	1.406866	0.05541958	0.2993	0.0038	0.35718	3461	106	3465.9	19.7
	OGC - 7	236.6	5.3	292.1	3.1	1.424704	0.05683391	0.2998	0.0041	0.48448	3428	106	3468.5	21.2
	OGC - 8	211.7	6	208.8	6	1.355014	0.05508185	0.2988	0.0036	0.32582	3563	111	3463.3	18.7
	OGC - 9	138.6	5.3	134.3	4.7	1.414227	0.05600107	0.2979	0.0048	0.41434	3448	106	3458.6	25
	OGC - 10	198.7	7.9	192	7.8	1.445922	0.05853937	0.3027	0.0045	0.21833	3389	107	3483.4	23
	OGC - 11	98.3	4.3	85.9	4.7	1.37798	0.05506603	0.2972	0.0054	0.22496	3517	108	3455	28.2
	OGC - 13	184.9	6.9	175	14	1.474926	0.06526222	0.2994	0.0044	-0.26036	3337	115	3466.4	22.8
	OGC - 14	208	15	215	18	1.427144	0.05702874	0.2972	0.0034	0.33197	3423	106	3455	17.7
	OGC - 15	170.4	9.7	158.6	9.3	1.440715	0.05811844	0.3	0.0046	0.23619	3398	107	3469.5	23.8
	OGC - 16	132.8	5.7	141	5.6	1.417033	0.05622349	0.3004	0.0049	0.46143	3442	106	3471.6	25.3
	OGC - 17	115.9	5	117.2	5.6	1.381406	0.05534022	0.3	0.0051	0.35659	3511	108	3469.5	26.3
	OGC - 18	151.8	4	121.3	2.1	1.398406	0.05671063	0.2973	0.0041	0.62843	3478	109	3455.5	21.4
	OGC - 19	211	15	205	19	1.409443	0.05562285	0.3004	0.0031	0.28378	3457	106	3471.6	16
	OGC - 20	242	17	251	18	1.4403	0.0560105	0.2984	0.0035	0.24044	3399	103	3461.2	18.2
	GJ1 - 1	498	23	10.78	0.61	10.13171	0.1129168	0.0645	0.0038	0.2615	606.79	6.45	757	124
	GJ1 - 2	503	24	11.04	0.62	10.04016	0.1512072	0.0635	0.0039	0.1332	612.06	8.79	724	130
	GJ1 - 3	490	24	10.67	0.55	10.1626	0.1445899	0.0622	0.004	0.27069	605.03	8.22	680	137
	GJ1 - 4	478	23	10.87	0.49	10.17294	0.1552331	0.0645	0.004	0.33994	604.44	8.8	757	131
	GJ1 - 5	482	23	10.81	0.62	10.19368	0.1246933	0.061	0.0043	0.073006	603.26	7.04	638	152
	GJ1 - 6	500	23	11.32	0.71	10.19056	0.09865521	0.0646	0.004	0.43291	603.44	5.58	760	131
	GJ1 - 7	486	24	10.72	0.58	10.25641	0.1262327	0.0592	0.003	0.2364	599.74	7.05	573	110
	GJ1 - 8	511	25	11.58	0.58	10.17294	0.1138376	0.0613	0.0037	0.32445	604.44	6.46	649	130
	GJ1 - 9	497	23	10.75	0.6	10.26694	0.1159511	0.0632	0.004	0.31828	599.15	6.46	714	134
	GJ1 - 10	457	23	9.5	0.58	10.10101	0.1224365	0.0607	0.0038	0.20378	608.55	7.04	628	135
	GJ1 - 11	387	18	8.58	0.48	10.14199	0.1440039	0.0617	0.0039	0.13563	606.2	8.21	663	135
	GJ1 - 12	366	18	8.06	0.46	10.11122	0.1226842	0.0624	0.0036	0.14225	607.96	7.04	687	123
	GJ1 - 13	377	18	8.02	0.43	10.2459	0.1364721	0.06	0.0035	0.25924	600.33	7.64	603	126
	GJ1 - 14	393	17	8.44	0.47	10.26694	0.1264921	0.0634	0.004	0.26342	599.15	7.05	721	134
	GJ1 - 15	379	19	8.17	0.46	10.34126	0.1390242	0.0608	0.0039	0.19769	595.04	7.64	631	138
	GJ1 - 16	392	19	8.25	0.47	10.30928	0.1062812	0.0619	0.0042	0.11144	596.8	5.88	670	145
	GJ1 - 17	383	19	8.46	0.41	10.2145	0.1356369	0.0605	0.0037	0.34857	602.09	7.63	621	132
	GJ1 - 18	382	17	8.57	0.47	10.27749	0.1267522	0.0602	0.0038	-0.033923	598.57	7.05	610	136
	GJ1 - 19	387	18	8.18	0.47	10.26694	0.1370331	0.0588	0.0038	-0.026626	599.15	7.64	559	141
	GJ1 - 20	389	18	8.25	0.52	10.29866	0.1378811	0.0622	0.0034	-0.12909	597.39	7.64	680	117
	PLES - 1	941	46	105	5.9	18.21494	0.2355666	0.0551	0.0032	0.042565	344.53	4.34	415	130
	PLES - 2	1183	56	193.8	9.2	18.27485	0.2571571	0.0552	0.0031	0.26554	343.43	4.71	419	125
	PLES - 3	1204	54	195	8.8	18.28822	0.2307768	0.0544	0.0032	0.24536	343.19	4.22	387	132
	PLES - 4	1168	54	188.6	9.1	18.48429	0.2050013	0.0535	0.0031	0.35998	339.64	3.67	349	131
	PLES - 5	1234	58	206.7	9.6	18.60119	0.1730021	0.0533	0.003	0.084025	337.56	3.06	341	127
	PLES - 6	1022	48	158.5	7	18.34526	0.228853	0.0534	0.0034	0.22416	342.15	4.16	345	144
	PLES - 7	565	24	56.9	2.3	18.52881	0.243755	0.056	0.0038	0.19282	338.85	4.34	451	151
	PLES - 8	631	25	60.7	2.5	18.457	0.2452757	0.0531	0.0035	0.084908	340.13	4.4	332	149
	PLES - 9	645	28	61	2.4	18.50481	0.2396996	0.0556	0.0038	0.11576	339.28	4.28	435	152
	PLES - 10	661	28	65.8	2.9	18.63933	0.2466715	0.053	0.0033	0.24665	336.89	4.34	328	141
	PLES - 11	561	22	53	2.1	19.02226	0.2496739	0.0565	0.0041	0.26707	330.28	4.23	471	161
	PLES - 12	672	29	64.8	2.8	18.97533	0.2520443	0.0539	0.0036	0.26124	331.08	4.29	366	151
Standard Results - U/Pb on 7700 - samples 38DTB19, 84DTB19 - OGC primary standard for unknowns > 1500 Ma, 91500 primary standard for unknowns > 1500 Ma, errors propogated within run and are the same as long term running averages (Spencer et al., 2016)														
	91500 - 1	81.4	3.3	30.8	1.3	5.586592	0.1654131	0.075	0.0066	0.17574	1061.5	29	1068	177
	91500 - 2	78.2	3.1	29.2	1.3	5.497526	0.1601808	0.0742	0.0074	-0.08054	1077.3	28.9	1046	201
	91500 - 3	79.1	3.3	29.4	1.3	5.555556	0.1604938	0.076	0.0065	0.0066541	1067	28.4	1094	171
	91500 - 4	81.6	3	31.6	1.3	5.611672	0.1669016	0.075	0.0061	0.28143	1057.1	29	1068	163
	91500 - 5	80.1	3.7	30.7	1.4	5.561735	0.191784	0.0717	0.0077	0.077942	1065.9	33.9	977	219
	91500 - 6	83.5	3.3	30.9	1.3	5.69152	0.1975997	0.0865	0.0088	0.05089	1043.4	33.4	1349	196
	91500 - 7	77.3	2.8	27.8	1.3	5.567929	0.1736102	0.0717	0.007	0.21444	1064.8	30.6	977	199
	91500 - 8	79.5	3.1	30.2	1.2	5.583473	0.1371707	0.0777	0.0077	0.14931	1062.1	24.1	1138	197
	91500 - 9	80.6	3	29.7	1.4	5.530973	0.1376625	0.0662	0.0065	0.14928	1071.3	24.6	812	205
	91500 - 10	80.5	3.1	30.5	1.4	5.611672	0.1637525	0.0724	0.0076	0.34636	1057.1	28.5	996	213
	91500 - 11	79	3.3	29.6	1.2	5.717553	0.1765282	0.077	0.0074	0.3848	1039.1	29.6	1120	192
	91500 - 12	79.3	2.9	29.4	1.4	5.571031	0.1396637	0.076	0.0073	0.021016	1064.2	24.6	1094	192
	91500 - 13	78	3.5	28.4	1.3	5.583473	0.187051	0.0747	0.0076	0.075288	1062.1	32.8	1060	205
	91500 - 14	83.6	3.5	32.7	1.5	5.555556	0.1635802	0.0753	0.0079	0.27677	1067	29	1076	211
	91500 - 15	80.2	3.1	30.1	1.5	5.577245	0.1773023	0.0808	0.0077	0.21478	1063.1	31.2	1216	187
	91500 - 16	78.9	3.2	29.6	1.4	5.675369	0.1385022	0.0851	0.0077	0.16169	1046.2	23.6	1317	175
	91500 - 17	78.7	3.2	29.2	1.3	5.503577	0.1605336	0.0688	0.0078	0.37626	1076.3	28.9	892	234
	91500 - 18	79.8	3.5	31	1.3	5.479452	0.1741415	0.075	0.0081	0.17376	1080.6	31.6	1068	217
	91500 - 19	82	3.3	30.5	1.4	5.577245	0.1461966	0.0705	0.0069	0.18823	1063.1	25.7	942	201
	91500 - 20	81.3	3.1	29.2	1.4	5.646527	0.1243448	0.0721	0.0069	0.24333	1051.1	21.4	988	195
	OGC - 1	238.5	7	96.2	1.9	1.446341	0.05857324	0.2992	0.0054	0.41659	3388	107	3465.4	28
	OGC - 2	141.4	6.7	141.9	9.3	1.42288	0.05668844	0.3002	0.0042	0.33181	3431	106	3470.6	21.7
	OGC - 3	204	9.6	219	17	1.426127	0.05694744	0.2979	0.0041	0.26773	3425	106	3458.6	21.3
	OGC - 4	130.6	4.7	181	12	1.409841	0.05565422	0.3	0.0046	0.39067	3456	106	3469.5	23.8
	OGC - 5	365	25	267	24	1.410238	0.05568562	0.2976	0.0038	0.30544	3455	106	3457.1	19.8
	OGC - 6	210.8	4.7	297	29	1.406866	0.05541958	0.2993	0.004	0.35718	3461	106	3465.9	20.7
	OGC - 7	238	13	292.1	3.1	1.424704	0.05683391	0.2998	0.0043	0.48448	3428	106	3468.5	22.2
	OGC - 8	143	6.4	208.8	6	1.355014	0.05508185	0.2988	0.0038	0.32582	3563	111	3463.3	19.7
	OGC - 9	194.4	9.9	134.3	4.7	1.414227	0.05600107	0.2979	0.005	0.41434	3448	106	3458.6	26
	OGC - 10	174.8	2.4	192	7.8	1.445922	0.05853937	0.3027	0.0046	0.21833	3389	107	3483.4	23.5
	OGC - 11	176	11	85.9	4.7	1.37798	0.05506603	0.2972	0.0056	0.22496	3517	108	3455	29.2
	OGC - 13	223	11	175	14	1.474926	0.06526222	0.2994	0.0045	-0.26036	3337	115	3466.4	23.3
	OGC - 14	183.4	9.5	215	18	1.427144	0.05702874	0.2972	0.0036	0.33197	3423	106	3455	18.8
	OGC - 15	219	12	158.6	9.3	1.440715	0.05811844	0.3	0.0047	0.23619	3398	107	3469.5	24.3
	OGC - 16	162.2	6.1	141	5.6	1.417033	0.05622349	0.3004	0.0051	0.46143	3442	106	3471.6	26.3
	OGC - 17	157.9	8	117.2	5.6	1.381406	0.05534022	0.3	0.0052	0.35659	3511	108	3469.5	26.9
	OGC - 18	214	11	121.3	2.1	1.398406	0.05671063	0.2973	0.0042	0.62843	3478	109	3455.5	21.9
	GJ1 - 1	432	17	10.97	0.57	10.35197	0.1607448	0.0571	0.0038	0.24938	594.45	8.82	494	147
	GJ1 - 2	431	16	11.01	0.59	10.2459	0.1784635	0.0579	0.0036	0.35719	600.33	9.98	525	136
	GJ1 - 3	426	16	10.86	0.56	10.29866	0.1696999	0.0603	0.0035	0.22206	597.39	9.4	613	125
	GJ1 - 4	430	17	10.93	0.62	10.1833	0.1762893	0.0618	0.0037	0.41822	603.85	9.98	666	128
	GJ1 - 5	426	16	10.82	0.51	10.14199	0.1542899	0.057	0.0034	0.26273	606.2	8.8	491	132
	GJ1 - 6	418	15	10.08	0.51	10.26694	0.1264921	0.0619	0.004	0.097553	599.15	7.05	670	138
	GJ1 - 7	412	16	10.28	0.55	10.03009	0.1609643	0.0625	0.0045	0.12478	612.65	9.38	690	154
	GJ1 - 8	412	15	10.41	0.6	10.30928	0.1594218	0.0593	0.0037	-0.077725	596.8	8.81	577	136
	GJ1 - 9	437	17	10.71	0.5	10.17294	0.1966285	0.0602	0.0033	0.34775	604.4	11.2	610	118
	GJ1 - 10	422	17	10.67	0.58	10.40583	0.1515937	0.0612	0.0037	0.32155	591.51	8.23	645	130
	GJ1 - 11	431	16	10.81	0.52	10.10101	0.1326395	0.0617	0.0042	0.24259	608.55	7.63	663	146
	GJ1 - 12	435	16	11.1	0.56	10.26694	0.1475741	0.0596	0.0035	0.28827	599.15	8.22	588	127
	GJ1 - 13	434	16	10.99	0.51	10.13171	0.1539774	0.0611	0.0037	0.094735	606.79	8.8	642	130
	GJ1 - 14	446	16	11.57	0.58	10.36269	0.1718167	0.0609	0.003	0.38423	593.87	9.41	635	106
	GJ1 - 15	441	17	11.26	0.54	10.17294	0.1759308	0.0614	0.0044	0.16948	604.44	9.98	652	154
	GJ1 - 16	429	16	10.81	0.52	10.28807	0.1799353	0.0614	0.0041	0.20122	597.98	9.99	652	143
	GJ1 - 17	443	16	11.28	0.54	10.1833	0.1555494	0.0608	0.0044	0.051194	603.85	8.8	631	145
	GJ1 - 18	437	18	11.04	0.59	10.35197	0.1714611	0.0619	0.0032	0.20265	594.45	9.41	670	111
	GJ1 - 19	435	16	11.29	0.55	10.14199	0.1542899	0.0608	0.0037	0.28389	606.2	8.8	734	123
	GJ1 - 20	440	15	11	0.6	10.06036	0.1720585	0.0579	0.0032	0.1858	610.89	9.97	525	121
	PLES - 1	636	24	56.8	2.1	18.62544	0.3052783	0.0581	0.0035	0.10485	337.14	5.38	533	132
	PLES - 2	697	22	63.5	2.1	18.90002	0.3107753	0.0522	0.0036	0.29556	332.36	5.33	293	157
	PLES - 3	1151	46	146.8	5.9	18.62544	0.2567113	0.0518	0.0028	0.15585	337.14	4.53	276	124
	PLES - 4	1202	46	151.5	6.2	18.62197	0.2462123	0.0514	0.0029	0.30858	337.2	4.34	258	130
	PLES - 5	1235	49	150.6	6	18.60119	0.238743	0.0514	0.0024	0.15486	337.56	4.22	258	107
	PLES - 6	1220	45	149.3	5.9	18.30161	0.2076683	0.0541	0.003	0.49974	342.95	3.79	374	125
	PLES - 7	1166	38	151.4	4.8	18.36547	0.249595	0.0547	0.0025	0.21797	341.78	4.52	399	102
	PLES - 8	1136	42	179.7	5.7	18.43998	0.2142207	0.0544	0.0031	0.30657	340.44	3.85	387	128
	PLES - 9	1148	44	197.7	7.4	18.34526	0.2187565	0.0549	0.0033	0.33754	342.15	3.97	407	135
	PLES - 10	1238	50	156.4	6.3	18.35536	0.2122591	0.0541	0.0035	0.14456	341.97	3.85	374	125
	PLES - 11	1275	51	157.9	6.2	18.57355	0.2138856	0.055	0.0028	0.27905	338.05	3.79	411	114
	PLES - 12	1264	50	158	6.4	18.64976	0.2295569	0.0543	0.0028	0.1833	336.71	4.04	383	116
Standard Results - U/Pb on 7700 - Samples 01DTB19, 34DTB19 - OGC primary standard for unknowns > 1500 Ma, 91500 primary standard for unknowns > 1500 Ma, errors were propogated within the run and are similar to long term running averages (Spencer et al., 2016)														
	91500 - 1	80	3.4	30.1	1.4	5.512679	0.07597408	0.0749	0.0024	0.25032	1074.62	13.64	1064.9	64.4
	91500 - 2	80.4	3.3	30	1.4	5.605381	0.07226669	0.0748	0.0027	0.29811	1058.23	12.58	1062.2	72.6
	91500 - 3	79.7	3.2	30	1.4	5.546312	0.07382778	0.0747	0.0025	0.20576	1068.61	13.1	1059.5	67.4
	91500 - 4	79.6	3.2	29.7	1.4	5.646527	0.07970818	0.0754	0.0029	0.30112	1051.11	13.7	1078.3	77.2
	91500 - 5	80	3.1	30	1.3	5.546312	0.07690393	0.0742	0.0026	0.14999	1068.61	13.66	1046	70.6
	91500 - 6	80	3.3	29.9	1.2	5.617978	0.08206035	0.0755	0.0025	0.16575	1056.04	14.22	1080.9	66.4
	91500 - 7	80.3	2.9	30.2	1.2	5.592841	0.09071163	0.0741	0.0031	0.34494	1060.42	15.86	1043.3	84.4
	91500 - 8	81.2	2.9	30.5	1.1	5.627462	0.07917082	0.0752	0.0031	0.36115	1054.4	13.88	1072.9	82.8
	91500 - 9	78	3	29.2	1.2	5.537099	0.08584649	0.0749	0.0026	0.24556	1070.25	15.28	1064.9	69.8
	91500 - 10	80.3	2.7	30.1	1	5.552471	0.07399184	0.0751	0.0029	0.45888	1067.52	13.12	1070.3	77.6
	91500 - 11	80.5	3	30.1	1.2	5.621135	0.07899291	0.0748	0.003	0.17413	1055.49	13.88	1062.2	80.6
	91500 - 12	79.8	3.4	30	1.4	5.630631	0.0887712	0.0749	0.0024	0.047825	1053.85	15.32	1064.9	64.4
	91500 - 13	80.6	3.3	30.4	1.4	5.592841	0.08132767	0.0741	0.0032	0.44728	1060.42	14.22	1043.3	87.2
	91500 - 14	79.6	3	29.8	1.2	5.586592	0.09675104	0.0753	0.0025	-0.12148	1061.51	16.94	1075.6	66.6
	91500 - 15	80.7	3	30	1.1	5.537099	0.0797146	0.0749	0.0031	0.39444	1070.25	14.2	1064.9	83.2
	91500 - 16	78.5	3	29.5	1.3	5.56483	0.08361181	0.0751	0.0033	0.11805	1065.34	14.76	1070.3	88.2
	91500 - 17	81.7	3.3	30.9	1.4	5.605381	0.09740292	0.0743	0.003	0.3268	1058.23	16.96	1048.7	81.4
	91500 - 18	81.1	3.1	29.3	1.2	5.592841	0.1000916	0.0748	0.0031	0.41433	1060.42	17.5	1062.2	83.4
	91500 - 19	79.7	3	30.3	1.2	5.540166	0.09514867	0.0759	0.0029	0.37701	1069.71	16.92	1091.5	76.6
	91500 - 20	80.4	3.2	30	1.2	5.577245	0.08398528	0.0743	0.0028	0.35316	1063.15	14.76	1048.7	76
	OGC - 1	129.3	9.2	122	11	1.37779	0.05315255	0.2993	0.0022	0.28076	3517.7	104.6	3465.91	11.38
	OGC - 2	127.7	3.6	106.8	1.8	1.454757	0.05502427	0.2987	0.0024	0.43206	3372.7	99.4	3462.8	12.46
	OGC - 3	121	8.3	106.5	7.4	1.40056	0.05492393	0.2991	0.0026	0.01014	3473.5	105.4	3464.87	13.48
	OGC - 4	113.6	7.1	88.6	4.2	1.408848	0.05359099	0.299	0.0022	0.35032	3457.7	101.8	3464.35	11.4
	OGC - 5	151.3	5	118.9	4.5	1.462202	0.05986498	0.299	0.0021	0.27923	3359.3	107.2	3464.35	10.88
	OGC - 6	115.9	3.5	79.9	2.6	1.386386	0.05381783	0.2997	0.0022	0.2295	3500.9	104.8	3467.98	11.38
	OGC - 7	126.1	5.5	126.7	6.1	1.414627	0.0540316	0.299	0.0028	0.32254	3446.8	102	3464.35	14.52
	OGC - 8	215.8	5.7	259.4	8.3	1.42898	0.05513354	0.2989	0.0019	0.013834	3419.9	102.4	3463.84	9.86
	OGC - 9	208.8	5.7	167.1	3.6	1.437815	0.05581739	0.299	0.0018	0.24009	3403.6	102.6	3464.35	9.32
	OGC - 10	136.2	3.6	114.3	3.1	1.414227	0.05400104	0.298	0.0021	0.13944	3447.5	102	3459.16	10.92
	OGC - 11	131.5	4.4	131.8	3.6	1.397233	0.05466332	0.3004	0.0018	0.28814	3479.9	105.2	3471.59	9.28
	OGC - 12	130.4	7.7	90.3	6.3	1.435338	0.05562527	0.2985	0.0021	0.064126	3408.1	102.6	3461.76	10.9
	OGC - 13	125.6	5.9	118.9	5.8	1.403706	0.05320053	0.2987	0.0022	0.16678	3467.5	101.6	3462.8	11.42
	OGC - 14	153.5	4.9	135.5	8.8	1.425517	0.05689874	0.2992	0.002	0.1491	3426.3	106	3465.39	10.36
	GJ1 - 1	372	15	8.28	0.36	10.01703	0.110375	0.0551	0.0016	0.2758	613.41	6.44	64.8	32.4
	GJ1 - 2	356	15	7.67	0.4	10.17915	0.1139767	0.0573	0.0016	0.12911	604.09	6.46	61.4	30.7
	GJ1 - 3	361	15	7.69	0.36	10.30397	0.1274061	0.0595	0.0019	0.15822	597.1	7.06	69.4	34.7
	GJ1 - 4	356	15	7.4	0.36	10.14199	0.1234319	0.0614	0.0018	-0.023094	606.2	7.04	63	31.5
	GJ1 - 5	356	15	7.41	0.32	10.20825	0.12505	0.0601	0.0016	0.03992	602.44	7.04	57.6	28.8
	GJ1 - 6	349	13	7.6	0.36	10.25641	0.1262327	0.0609	0.0021	0.18391	599.74	7.04	74.2	37.1
	GJ1 - 7	348	13	7.5	0.33	10.1688	0.1240854	0.0599	0.0016	0.14701	604.67	7.04	57.8	28.9
	GJ1 - 8	363	13	7.74	0.32	10.11839	0.1330962	0.0607	0.0019	0.11075	607.55	7.62	67.4	33.7
	GJ1 - 9	367	16	7.81	0.38	10.14816	0.1132837	0.0583	0.0018	0.13976	605.85	6.46	67.6	33.8
	GJ1 - 10	353	14	7.62	0.35	10.14199	0.1440039	0.058	0.0019	0.29093	606.2	8.22	71.8	35.9
	GJ1 - 11	355	15	7.74	0.35	10.25641	0.1472715	0.0606	0.0019	0.38571	599.74	8.22	67.6	33.8
	GJ1 - 12	347	13	7.73	0.35	10.24066	0.1258452	0.063	0.0017	0.071369	600.62	7.04	57.4	28.7
	GJ1 - 13	345	13	7.6	0.35	10.22913	0.1360257	0.0627	0.0019	0.2467	601.27	7.64	64.6	32.3
	GJ1 - 14	361	14	7.98	0.33	10.20096	0.1352774	0.0596	0.0019	0.281	602.85	7.64	69.2	34.6
	GJ1 - 15	363	12	8.16	0.34	10.07252	0.1217468	0.0602	0.0018	0.25241	610.19	7.04	64.6	32.3
	GJ1 - 16	377	13	8.48	0.37	10.1968	0.1247696	0.06	0.0019	0.12616	603.09	7.04	68.6	34.3
	GJ1 - 17	364	12	8.2	0.33	10.27116	0.126596	0.0594	0.0019	0.18527	598.92	7.04	69.4	34.7
	GJ1 - 18	359	14	7.93	0.36	10.28807	0.1587664	0.0586	0.0018	-0.017609	597.98	8.82	67	33.5
	GJ1 - 19	364	15	8.01	0.38	10.23541	0.1466692	0.0599	0.0019	0.45323	600.92	8.22	68.6	34.3
	GJ1 - 20	371	13	7.9	0.3	10.39825	0.1297484	0.064	0.0019	0.16155	591.92	7.06	62.8	31.4
	PLES - 2	512.7	7.2	44.48	0.83	18.62544	0.2254896	0.0524	0.0018	0.065441	337.14	3.98	78.4	39.2
	PLES - 3	608	24	58.9	1.3	18.72659	0.2314523	0.0535	0.0017	0.41663	335.36	4.04	71.8	35.9
	PLES - 4	501.3	7.3	45.09	0.63	18.47063	0.2422266	0.0522	0.0017	0.044401	339.89	4.34	74.4	37.2
	PLES - 5	585	19	56.5	1.5	18.71257	0.2311059	0.0509	0.0016	-0.020645	335.61	4.04	72.6	36.3
	PLES - 6	389	11	31.6	1	18.31837	0.2483165	0.0542	0.0019	0.2683	342.64	4.52	78.8	39.4
	PLES - 7	466.4	5.5	41.8	0.78	18.43318	0.2310518	0.0551	0.0019	0.14634	340.56	4.16	77	38.5
	PLES - 10	706	24	78.2	4.1	18.02776	0.2340002	0.0515	0.0014	0.15773	348.02	4.4	62.4	31.2
Standard Results - U/Pb on 7700 - Sample 38DTB19 - OGC primary standard for unknowns > 1500 Ma, errors propogated based on long term running averages (see Spencer et al., 2016).														
	91500 - 1	81.3	3.1	29.2	1.4	5.646527	0.1243448	0.0721	0.0069	0.24333	1051.1	21.4	988	195
	91500 - 2	81.5	3.1	31.8	1.4	5.552471	0.1572327	0.0739	0.0065	0.22006	1067.5	27.9	1038	178
	91500 - 3	80.2	2.9	31.3	1.3	5.586592	0.1466871	0.0801	0.0075	0.25355	1061.5	25.7	1199	185
	91500 - 4	79	2.9	29.1	1.1	5.611672	0.1543052	0.0734	0.0085	0.084126	1057.1	26.8	1024	234
	91500 - 5	78.1	2.6	28.6	1.2	5.509642	0.1487452	0.0749	0.007	0.42305	1075.2	26.7	1065	188
	OGC - 1	160.6	4.5	150	2.6	1.424096	0.05466606	0.2996	0.0057	-0.068711	3429	102	3467.5	29.5
	OGC - 2	196	11	190	10	1.407856	0.05184569	0.2979	0.0052	0.30078	3459.6	98.6	3458.6	27.1
	OGC - 3	358	18	527	29	1.424096	0.0524352	0.2997	0.0038	0.24198	3429	97.9	3468	19.6
	OGC - 4	186.9	6.1	203.5	6.3	1.416431	0.055473535	0.2987	0.0044	0.18414	3443	104	3462.8	22.8
	GJ1 - 1	440	15	11	0.6	10.06036	0.1720585	0.0579	0.0032	0.1858	610.89	9.97	525	121
	GJ1 - 2	429	15	10.77	0.55	10.15228	0.1546033	0.058	0.0035	0.37525	605.61	8.8	529	132
	GJ1 - 3	425	15	10.79	0.46	10.2459	0.1574678	0.0582	0.0033	0.35197	600.33	8.81	536	124
	GJ1 - 4	418	14	10.61	0.49	9.940358	0.138335	0.056	0.0038	0.21629	617.92	8.2	451	151
	GJ1 - 5	411	14	10.22	0.51	10.11122	0.1533553	0.0595	0.0034	0.10575	607.96	8.8	584	124
	PLES - 1	1169	41	201.7	7.4	18.78287	0.2257896	0.0536	0.0023	0.14463	336.59	7.04	353.3	96.9
	PLES - 2	1133	40	196.6	7.5	18.98614	0.2487267	0.0535	0.0027	0.077448	335.97	8.26	349	114
	PLES - 3	1103	39	192.2	6.8	18.87861	0.2494814	0.0507	0.0029	0.36211	318.82	8.9	226	132
	PLES - 4	1080	39	186	6.6	18.96094	0.2624476	0.0557	0.0026	0.26414	349.42	7.94	439	104

Appendix D3.2 continued.

Curtin University Geohistory center	Lu-Hf Isotopic Ratios from Iolite								
Spot ID	178Hf/177Hf	±2σ INT	176Hf/177Hf 0.282785 0.283250	±2σ INT	(2% External ±)	176Lu/177Hfm	±2σ INT	176Yb/177Hf	±2σ INT
						0.03360 Bouvier et al., 2008 EPSL-273 0.03840 Griffin et al., 2002, Lithos-237			
Run 1: Standard Results - Lu/Hf on Nu Plasma II - samples 10DTB19, 12DTB19, 14DTB19 - MudTank Primary Standard - errors propogated within run and are similar to long term running averages (see Spencer et al., 2020).									
FC - 1	1.4675	0.00014	0.282202	0.000045	0.00568904	0.001822	0.000031	0.0775	0.0012
FC - 2	1.46752	0.00013	0.28222	0.000043	0.0056874	0.0015052	0.0000017	0.06502	0.0004
FC - 3	1.46762	0.00013	0.282169	0.000044	0.00568738	0.0010627	0.0000046	0.04379	0.00015
FC - 4	1.46753	0.00015	0.282286	0.000036	0.00568172	0.001807	0.000031	0.07137	0.00068
FC - 5	1.46747	0.00013	0.28227	0.000033	0.0056784	0.001857	0.000037	0.07218	0.00087
FC - 6	1.46751	0.00015	0.282185	0.000036	0.0056797	0.0016159	0.000003	0.06984	0.00049
FC - 7	1.46741	0.00014	0.282195	0.000033	0.0056769	0.001255	0.000015	0.05191	0.00034
FC - 8	1.46733	0.00014	0.282146	0.000036	0.00567892	0.00085855	0.00000059	0.03471	0.00026
FC - 9	1.46744	0.00016	0.28219	0.000044	0.0056878	0.00141074	0.00000059	0.05874	0.00036
FC - 10	1.46738	0.00014	0.282257	0.00003	0.00567514	0.0016104	0.0000063	0.06621	0.00067
FC - 11	1.46729	0.00017	0.282203	0.000041	0.00568506	0.001545	0.0000065	0.06521	0.00056
FC - 12	1.46735	0.00015	0.282252	0.000037	0.00568204	0.001637	0.000019	0.06753	0.00068
GJ1 - 1	1.46762	0.00015	0.281992	0.000054	0.00569384	0.00034026	0.00000096	0.013194	0.000081
GJ1 - 2	1.46768	0.00013	0.281963	0.000051	0.00569026	0.00033693	0.00000066	0.012847	0.000078
GJ1 - 3	1.46768	0.00015	0.282029	0.000049	0.00568958	0.00033294	0.00000084	0.012669	0.000074
GJ1 - 4	1.46763	0.00015	0.281994	0.000049	0.00568888	0.00032519	0.0000007	0.012306	0.000077
GJ1 - 5	1.46753	0.00015	0.282006	0.000049	0.00568912	0.00032549	0.00000081	0.012247	0.000068
GJ1 - 6	1.46751	0.00015	0.281969	0.000052	0.00569138	0.00033002	0.00000072	0.012347	0.000082
GJ1 - 7	1.46751	0.00012	0.282029	0.000046	0.00568658	0.00032936	0.00000074	0.012266	0.000079
GJ1 - 8	1.46749	0.00014	0.282079	0.000052	0.00569358	0.00032847	0.00000064	0.012166	0.000074
GJ1 - 9	1.46754	0.00015	0.28205	0.000045	0.005686	0.00032275	0.00000065	0.011949	0.000068
GJ1 - 10	1.46742	0.00012	0.282006	0.00005	0.00569012	0.00032044	0.00000085	0.011804	0.000062
GJ1 - 11	1.46752	0.00015	0.282021	0.000041	0.00568142	0.00032666	0.00000074	0.011931	0.000066
GJ1 - 12	1.46747	0.00016	0.282	0.000043	0.005683	0.0003219	0.0000007	0.011817	0.000066
GJ1 - 13	1.46752	0.00017	0.281998	0.00004	0.00567996	0.00032491	0.00000073	0.011934	0.000063
GJ1 - 14	1.46742	0.00014	0.282034	0.000055	0.00569568	0.00032222	0.0000008	0.011824	0.000065
GJ1 - 15	1.46749	0.00017	0.281995	0.000043	0.0056829	0.00031295	0.00000071	0.011472	0.000069
GJ1 - 16	1.46743	0.00013	0.282057	0.000056	0.00569714	0.0003197	0.00000063	0.011659	0.00007
GJ1 - 17	1.46752	0.00015	0.282026	0.000047	0.00568752	0.00031975	0.00000064	0.011692	0.000078
GJ1 - 18	1.46748	0.00017	0.282015	0.000043	0.0056833	0.00032387	0.00000073	0.011796	0.000071
GJ1 - 19	1.4674	0.00016	0.281985	0.000045	0.0056847	0.00032148	0.00000075	0.011776	0.000069
GJ1 - 20	1.46747	0.00016	0.282003	0.000039	0.00567906	0.00031987	0.00000079	0.011697	0.00008
MUD - 1	1.4676	0.00013	0.282529	0.000038	0.00568858	0.00002452	0.00000039	0.001217	0.000015
MUD - 2	1.46754	0.00015	0.282497	0.000044	0.00569394	0.00002601	0.00000051	0.001252	0.000024
MUD - 3	1.46759	0.00015	0.282482	0.000046	0.00569564	0.00002451	0.00000043	0.001205	0.000016
MUD - 4	1.46765	0.00014	0.282521	0.000035	0.00568542	0.00002353	0.00000045	0.001148	0.000015
MUD - 5	1.4676	0.00013	0.282495	0.000035	0.0056849	0.0000246	0.00000035	0.001171	0.000019
MUD - 6	1.46754	0.00012	0.282504	0.000042	0.00569208	0.00002843	0.00000044	0.001364	0.000016
MUD - 7	1.46759	0.00011	0.282492	0.000041	0.00569084	0.00002497	0.00000055	0.001194	0.000023
MUD - 8	1.46751	0.00014	0.282495	0.000029	0.0056789	0.00002584	0.00000046	0.001203	0.000013
MUD - 9	1.46749	0.00013	0.282524	0.000035	0.00568548	0.00002834	0.00000047	0.001374	0.000014
MUD - 10	1.46752	0.00015	0.282522	0.000027	0.00567744	0.00002445	0.00000057	0.001158	0.000015
MUD - 11	1.4675	0.00018	0.282487	0.000042	0.00569174	0.00002426	0.0000005	0.001153	0.000014
MUD - 12	1.46749	0.00016	0.282508	0.00003	0.00568016	0.00002417	0.0000004	0.001147	0.000013
MUD - 14	1.4674	0.00015	0.282494	0.000037	0.00568688	0.00002309	0.00000044	0.001115	0.00002
MUD - 15	1.46743	0.00016	0.282528	0.000034	0.00568456	0.00002751	0.00000041	0.001283	0.000014
MUD - 16	1.46753	0.00013	0.28251	0.000037	0.0056872	0.00002586	0.00000057	0.001195	0.000023
MUD - 17	1.46747	0.00016	0.282502	0.000042	0.00569204	0.00002524	0.00000049	0.001166	0.000015
MUD - 18	1.46748	0.00015	0.282485	0.000036	0.0056857	0.00002692	0.0000005	0.001234	0.000017
MUD - 19	1.46735	0.00012	0.282514	0.000038	0.00568828	0.00002109	0.00000047	0.000979	0.000012
MUD - 20	1.46736	0.00015	0.282514	0.000037	0.00568728	0.00002282	0.00000039	0.001053	0.00001
PLES - 1	1.46762	0.00018	0.282458	0.000034	0.00568316	0.0001439	0.00000046	0.008489	0.000054
PLES - 2	1.46762	0.00014	0.282465	0.000033	0.0056823	0.00013141	0.00000038	0.007894	0.000054
PLES - 3	1.4676	0.00016	0.282458	0.000042	0.00569116	0.00013048	0.00000031	0.007741	0.000056
PLES - 4	1.46758	0.00016	0.282489	0.000039	0.00568878	0.00012936	0.00000044	0.007611	0.000053
PLES - 5	1.46748	0.00016	0.282503	0.000037	0.00568706	0.00013587	0.00000039	0.007861	0.000043
PLES - 6	1.46742	0.00018	0.282475	0.000036	0.0056855	0.00013753	0.00000045	0.007855	0.000045
PLES - 7	1.46745	0.00013	0.282482	0.000032	0.00568164	0.00011909	0.00000077	0.006543	0.000024
PLES - 8	1.46743	0.00015	0.282468	0.000033	0.00568236	0.00012871	0.00000086	0.00704	0.000018
PLES - 9	1.46748	0.00014	0.282462	0.000034	0.00568324	0.00012964	0.00000085	0.007123	0.000027
PLES - 10	1.46743	0.00014	0.282493	0.000042	0.00569186	0.00013199	0.00000047	0.007285	0.000037
PLES - 11	1.46739	0.00011	0.282464	0.000039	0.00568828	0.00011219	0.00000058	0.006106	0.000026
R33 - 1	1.46768	0.00013	0.282741	0.000042	0.00569682	0.0013344	0.0000085	0.05549	0.00079
R33 - 2	1.46768	0.00016	0.282729	0.000037	0.00569158	0.0013444	0.0000073	0.05253	0.00056
R33 - 3	1.4676	0.00015	0.282805	0.000034	0.0056901	0.001936	0.000021	0.0764	0.0018
R33 - 4	1.46764	0.00014	0.282743	0.000033	0.00568786	0.001235	0.000018	0.04544	0.00053
R33 - 5	1.4676	0.00017	0.282795	0.000046	0.0057019	0.003598	0.000033	0.15253	0.00055
R33 - 6	1.4676	0.00015	0.282755	0.000038	0.0056931	0.001788	0.000016	0.0727	0.0011
R33 - 7	1.46754	0.00015	0.282806	0.000031	0.00568712	0.00209363	0.00000082	0.08579	0.00053
R33 - 8	1.46746	0.00013	0.282772	0.000039	0.00569444	0.002142	0.000046	0.0895	0.0025
R33 - 11	1.4675	0.00015	0.282779	0.000043	0.00569858	0.001098	0.000089	0.0427	0.0033
R33 - 12	1.46747	0.00014	0.282737	0.000039	0.00569374	0.0010988	0.0000054	0.04337	0.00043
R33 - 13	1.46741	0.00016	0.28276	0.000038	0.0056932	0.002432	0.000026	0.0979	0.0016
R33 - 14	1.46745	0.00014	0.282773	0.000045	0.00570046	0.001081	0.000016	0.04231	0.00093
R33 - 15	1.46748	0.00011	0.282757	0.000042	0.00569714	0.001535	0.000091	0.0626	0.0043
R33 - 16	1.46749	0.00011	0.282742	0.000053	0.00570784	0.002291	0.000044	0.0943	0.0013
R33 - 17	1.46744	0.00014	0.282707	0.000038	0.00569214	0.00132	0.00004	0.0508	0.0015
R33 - 18	1.46743	0.00017	0.282732	0.000038	0.00569264	0.0011112	0.0000059	0.04263	0.00017
R33 - 19	1.46747	0.00017	0.282753	0.00004	0.00569506	0.002054	0.000011	0.08185	0.00029
R33 - 20	1.46739	0.00013	0.282744	0.000031	0.00568588	0.00135	0.000034	0.0511	0.0012
91500 - 1	1.46751	0.00015	0.282294	0.000055	0.00570088	0.00031298	0.00000078	0.012524	0.000078
91500 - 2	1.46756	0.00015	0.282271	0.000043	0.00568842	0.00030758	0.00000073	0.012144	0.000073
91500 - 3	1.46762	0.00014	0.282258	0.000052	0.00569716	0.0003064	0.0000011	0.011946	0.000079
91500 - 4	1.46764	0.00014	0.282304	0.000058	0.00570408	0.00031624	0.00000082	0.012322	0.000059
91500 - 5	1.46774	0.00017	0.282276	0.000046	0.00569152	0.00030084	0.00000086	0.011515	0.000084
91500 - 6	1.46759	0.00016	0.282335	0.000044	0.0056907	0.00030118	0.00000091	0.011583	0.000066
91500 - 7	1.4676	0.00014	0.282326	0.000054	0.00570052	0.00030039	0.0000008	0.011477	0.000073
91500 - 8	1.46753	0.00017	0.282331	0.000056	0.00570262	0.00029342	0.0000009	0.011097	0.000086
91500 - 10	1.46752	0.00018	0.282304	0.000053	0.00569908	0.00030244	0.00000084	0.011497	0.000072
91500 - 12	1.46753	0.00013	0.282316	0.000058	0.00570432	0.00037716	0.00000073	0.014322	0.000085
91500 - 13	1.46754	0.00015	0.282294	0.000069	0.00571488	0.00037391	0.00000078	0.01413	0.0001
91500 - 14	1.46745	0.00013	0.282295	0.000057	0.0057029	0.00037119	0.0000009	0.014034	0.000098
91500 - 15	1.46744	0.00018	0.282281	0.000058	0.00570362	0.00036531	0.00000085	0.013822	0.000085
91500 - 16	1.46743	0.00017	0.282286	0.000057	0.00570272	0.00036507	0.00000089	0.013691	0.00008
91500 - 17	1.46749	0.00016	0.282294	0.000048	0.00569388	0.00036571	0.00000087	0.013735	0.000077
91500 - 18	1.46737	0.00018	0.282292	0.000055	0.00570084	0.0003683	0.0000012	0.013873	0.000078
91500 - 19	1.46741	0.00014	0.282296	0.000057	0.00570292	0.00036967	0.00000078	0.01393	0.000092
91500 - 20	1.46741	0.00019	0.282329	0.000055	0.00570158	0.00036813	0.00000085	0.01388	0.0001

Appendix D3.2 continued.

Curtin University Geohistory center	Lu-Hf Isotopic Ratios from Iolite								
Spot ID	178Hf/177Hf	±2σ INT	176Hf/177Hf 0.282785 0.283250	±2σ INT	(2% External ±)	176Lu/177Hfm	±2σ INT	176Yb/177Hf	±2σ INT
						0.03360 Bouvier et al., 2008 EPSL-273; 0.03840 Griffin et al., 2002, Lithos-237			
Run 2: Standard Results - Lu/Hf on Nu Plasma II - samples 38DTB19, 84DTB19 - MudTank Primary Standard - errors propogated within run and are similar to long term running averages (see Spencer et al., 2020).									
FC1_1	1.4675	0.00013	0.282156	0.000038	0.001276	0.001276	0.000015	0.05064	0.00032
FC1_2	1.46731	0.00012	0.282196	0.000039	0.000847	0.000847	0.000014	0.03236	0.00034
FC1_3	1.46722	0.00016	0.282156	0.000043	0.000903	0.000903	0.000023	0.03438	0.00074
FC1_4	1.46726	0.00012	0.282194	0.000045	0.001273	0.001273	0.000016	0.04913	0.00043
FC1_5	1.46722	0.00015	0.282186	0.000048	0.001272	0.001272	0.000012	0.04971	0.0002
FC1_6	1.46727	0.00015	0.282137	0.000045	0.001191	0.001191	0.0000018	0.04701	0.00037
FC1_7	1.46753	0.00014	0.282152	0.00004	0.001154	0.001154	0.000011	0.04459	0.00077
FC1_8	1.46751	0.000099	0.282195	0.00004	0.0011722	0.0011722	0.0000048	0.04499	0.00041
FC1_9	1.46723	0.00012	0.282145	0.000038	0.00074055	0.00074055	0.00000051	0.0276	0.00019
FC1_10	1.46716	0.00013	0.282175	0.000038	0.001176	0.001176	0.000015	0.04558	0.00031
FC1_11	1.46748	0.00014	0.282202	0.000043	0.00568704	0.001242	0.00005	0.0457	0.0016
FC1_12	1.46752	0.00015	0.282199	0.000046	0.00568998	0.001058	0.00001	0.03982	0.00014
FC1_13	1.46759	0.00012	0.282174	0.000044	0.00568748	0.000758	0.0000018	0.02708	0.00029
FC1_14	1.46749	0.00013	0.282156	0.00004	0.00568312	0.0008106	0.0000018	0.02957	0.00033
Z_GJ1_1	1.4675	0.00014	0.281998	0.000054	0.00028407	0.00028407	0.00000079	0.009863	0.000052
Z_GJ1_2	1.46735	0.00016	0.282066	0.00005	0.00028781	0.00028781	0.00000076	0.009947	0.000055
Z_GJ1_3	1.46726	0.00014	0.282013	0.000054	0.00028533	0.00028533	0.00000085	0.009889	0.000063
Z_GJ1_4	1.46733	0.00015	0.282042	0.000055	0.00028712	0.00028712	0.00000075	0.010002	0.000069
Z_GJ1_5	1.46739	0.00015	0.282041	0.000048	0.0002856	0.0002856	0.00000068	0.009961	0.000057
Z_GJ1_6	1.46734	0.00016	0.282026	0.000055	0.00028051	0.00028051	0.00000078	0.009715	0.000062
Z_GJ1_7	1.46752	0.00017	0.281949	0.000043	0.0002832	0.0002832	0.00000056	0.009875	0.000064
Z_GJ1_8	1.46754	0.00015	0.281972	0.00005	0.00028436	0.00028436	0.00000058	0.009819	0.000059
Z_GJ1_9	1.46762	0.00014	0.282026	0.000043	0.00028626	0.00028626	0.0000006	0.009904	0.000062
Z_GJ1_10	1.46745	0.00014	0.282064	0.000064	0.0002902	0.0002902	0.00000068	0.010024	0.000051
Z_GJ1_11	1.46745	0.00013	0.282093	0.000049	0.00028669	0.00028669	0.00000082	0.009916	0.000055
Z_GJ1_12	1.46716	0.00014	0.281996	0.000049	0.00028022	0.00028022	0.00000079	0.009679	0.00005
Z_GJ1_13	1.46715	0.00012	0.282008	0.000048	0.00028738	0.00028738	0.00000077	0.00996	0.000054
Z_GJ1_14	1.46729	0.00015	0.281979	0.000054	0.00028492	0.00028492	0.0000006	0.009885	0.000057
Z_GJ1_15	1.4672	0.00017	0.282006	0.000044	0.00028281	0.00028281	0.00000052	0.009801	0.000063
Z_MT_1	1.46751	0.00016	0.282511	0.000043	0.00002161	0.00002161	0.0000004	0.000949	0.000017
Z_MT_2	1.46736	0.00014	0.2825	0.000035	0.00002158	0.00002158	0.00000059	0.000961	0.000013
Z_MT_3	1.46733	0.00012	0.282514	0.000035	0.00001843	0.00001843	0.00000041	0.000813	0.000014
Z_MT_4	1.46733	0.00013	0.282504	0.000039	0.00001925	0.00001925	0.00000041	0.000868	0.000015
Z_MT_5	1.46726	0.00017	0.282506	0.000038	0.00002006	0.00002006	0.00000044	0.000868	0.000018
Z_MT_6	1.46732	0.00015	0.282507	0.000047	0.00002054	0.00002054	0.00000047	0.000906	0.000016
Z_MT_7	1.46725	0.00013	0.282508	0.000041	0.00002444	0.00002444	0.00000058	0.001076	0.000018
Z_MT_8	1.46726	0.00014	0.282506	0.000043	0.00002033	0.00002033	0.00000051	0.00092	0.000013
Z_MT_9	1.46735	0.00012	0.282509	0.000042	0.00002409	0.00002409	0.00000033	0.001041	0.00002
Z_MT_10	1.46756	0.00014	0.282503	0.000033	0.00002157	0.00002157	0.0000005	0.000932	0.00002
Z_MT_11	1.46759	0.0001	0.282515	0.000038	0.00002395	0.00002395	0.00000048	0.001047	0.000017
Z_MT_12	1.46737	0.00012	0.282502	0.000039	0.00002245	0.00002245	0.00000041	0.000944	0.000015
Z_MT_13	1.4674	0.00015	0.282505	0.000035	0.00002218	0.00002218	0.00000042	0.000945	0.00002
Z_MT_14	1.46725	0.00016	0.282511	0.00003	0.00002532	0.00002532	0.00000039	0.001081	0.000016
Z_MT_15	1.46723	0.00013	0.282505	0.000041	0.00002663	0.00002663	0.00000042	0.001161	0.000017
Z_MT_16	1.46733	0.00016	0.282507	0.000048	0.00002774	0.00002774	0.00000042	0.001212	0.000013
Z_MT_17	1.46723	0.00016	0.282507	0.000038	0.00003086	0.00003086	0.00000042	0.001349	0.000014
PLES_1	1.46733	0.0001	0.282503	0.000031	0.00006283	0.00006283	0.00000056	0.003264	0.000014
PLES_2	1.46732	0.00014	0.282474	0.000039	0.00019877	0.00019877	0.00000099	0.01037	0.00013
PLES_3	1.46756	0.00013	0.282474	0.000044	0.0002083	0.0002083	0.0000011	0.01094	0.00012
PLES_4	1.46727	0.0001	0.282485	0.000036	0.00021616	0.00021616	0.00000052	0.011238	0.000066
PLES_5	1.46726	0.00017	0.282502	0.000038	0.0002133	0.0002133	0.0000012	0.011044	0.00002
PLES_6	1.46738	0.00014	0.282484	0.000043	0.0001979	0.0001979	0.0000019	0.01028	0.000041
PLES_7	1.46745	0.00012	0.28247	0.000029	0.00017293	0.00017293	0.00000037	0.008842	0.000058
PLES_8	1.46757	0.00011	0.282457	0.000033	0.00016275	0.00016275	0.00000056	0.008246	0.000045
PLES_9	1.46746	0.00014	0.282471	0.000039	0.00020945	0.00020945	0.00000098	0.010899	0.000069
PLES_10	1.46725	0.00015	0.282499	0.000044	0.000214	0.000214	0.0000014	0.011142	0.000062
PLES_11	1.46721	0.00011	0.282483	0.000032	0.0002137	0.0002137	0.0000016	0.011141	0.000074
Z_R33_1	1.46742	0.00015	0.282744	0.000043	0.0011121	0.0011121	0.000003	0.03892	0.00017
Z_R33_2	1.4674	0.00013	0.282804	0.000046	0.0017781	0.0017781	0.0000079	0.06848	0.00078
Z_R33_3	1.46726	0.00015	0.282777	0.000049	0.0015899	0.0015899	0.0000099	0.05576	0.00021
Z_R33_4	1.4674	0.00017	0.282805	0.000045	0.0010866	0.0010866	0.0000091	0.03777	0.00013
Z_R33_5	1.46733	0.00017	0.282779	0.000042	0.0017139	0.0017139	0.0000078	0.06405	0.00091
Z_R33_6	1.46726	0.0001	0.282768	0.000039	0.0017211	0.0017211	0.0000093	0.05775	0.00065
Z_R33_7	1.46741	0.00012	0.282782	0.000034	0.001513	0.001513	0.000016	0.05853	0.00088
Z_R33_8	1.46721	0.00012	0.282768	0.000045	0.0013796	0.0013796	0.0000081	0.05169	0.0006
Z_R33_9	1.46729	0.00014	0.282724	0.000042	0.001171	0.001171	0.000011	0.042192	0.000063
Z_R33_10	1.46747	0.00013	0.282799	0.000041	0.00275	0.00275	0.000028	0.1083	0.0011
Z_R33_11	1.46746	0.00015	0.282715	0.000044	0.0023244	0.0023244	0.0000021	0.08921	0.00066
Z_R33_12	1.46735	0.00011	0.28277	0.000033	0.001321	0.001321	0.000018	0.04911	0.00035
Z_R33_13	1.46742	0.00015	0.282802	0.00003	0.0013815	0.0013815	0.000003	0.05045	0.00044
Z_R33_14	1.46723	0.00015	0.282787	0.000046	0.001739	0.001739	0.000014	0.06491	0.00098
Z_R33_15	1.46712	0.00014	0.282781	0.000043	0.00206	0.00206	0.00015	0.0783	0.0054
Z_R33_16	1.46722	0.00013	0.282736	0.000041	0.001342	0.001342	0.000028	0.051	0.0014
Z_R33_17	1.46727	0.00015	0.282789	0.000045	0.0009841	0.0009841	0.0000027	0.03562	0.00019
Z_91500_1	1.46755	0.00015	0.282272	0.000049	0.00027618	0.00027618	0.00000075	0.009809	0.000072
Z_91500_2	1.46732	0.00018	0.282269	0.000063	0.00027121	0.00027121	0.00000085	0.009692	0.000064
Z_91500_3	1.46741	0.00016	0.282268	0.000049	0.00026224	0.00026224	0.00000081	0.009252	0.000075
Z_91500_4	1.46727	0.00013	0.282357	0.000057	0.000281	0.000281	0.00000076	0.009951	0.000063
Z_91500_5	1.46727	0.0002	0.282267	0.000067	0.00027693	0.00027693	0.00000093	0.009828	0.000051
Z_91500_6	1.4672	0.00019	0.282278	0.000046	0.0002841	0.0002841	0.000001	0.010127	0.000055
Z_91500_7	1.4673	0.00017	0.282289	0.000058	0.0002654	0.0002654	0.00000081	0.009372	0.00006
Z_91500_8	1.46733	0.0002	0.282334	0.000061	0.00027633	0.00027633	0.00000065	0.009835	0.000073
Z_91500_9	1.46741	0.00014	0.282272	0.000056	0.0002625	0.0002625	0.0000011	0.00929	0.000053
Z_91500_10	1.46745	0.00014	0.282264	0.000057	0.00027529	0.00027529	0.00000095	0.009737	0.000052
Z_91500_11	1.46752	0.00017	0.282267	0.000069	0.00025405	0.00025405	0.00000096	0.008983	0.000083
Z_91500_12	1.46753	0.00015	0.282307	0.000049	0.00028603	0.00028603	0.00000069	0.010192	0.000079
Z_91500_13	1.4673	0.00015	0.282344	0.000043	0.00026143	0.00026143	0.00000089	0.009211	0.000083
Z_91500_14	1.46722	0.00015	0.282258	0.000043	0.0002551	0.0002551	0.0000011	0.009096	0.000032
Z_91500_15	1.46728	0.00014	0.28227	0.000051	0.00026297	0.00026297	0.00000084	0.009292	0.000064
Z_91500_16	1.46714	0.0002	0.282277	0.00004	0.00027668	0.00027668	0.00000052	0.009844	0.00007
Z_91500_17	1.46714	0.00015	0.282294	0.000051	0.00027364	0.00027364	0.00000099	0.009714	0.000079

Appendix D3.2 continued.

Curtin University Geohistory center	Lu-Hf Isotopic Ratios from Iolite								
Spot ID	178Hf/177Hf	±2σ INT	176Hf/177Hf	±2σ INT	(2% External ±)	176Lu/177Hfm	±2σ INT	176Yb/177Hf	±2σ INT
			0.282785			0.03360 Bouvier et al., 2008 EPSL-273			
			0.283250			0.03840 Griffin et al., 2002, Lithos-237			
Run 3: Standard Results - Lu/Hf on Nu Plasma II - samples 01DTB19, 34DTB19 - MudTank Primary Standard - errors propogated within run and are similar to long term running averages (see Spencer et al., 2020).									
Z_FC1_1	1.467254	0.000068	0.282218	0.000031	0.00567536	0.0011009	0.0000076	0.04489	0.00022
Z_FC1_2	1.46732	0.000082	0.282185	0.00002	0.0056637	0.0007049	0.0000026	0.02746	0.00017
Z_FC1_3	1.467301	0.000073	0.282203	0.000021	0.00566506	0.0012061	0.0000024	0.04894	0.0001
Z_FC1_4	1.467315	0.000081	0.282172	0.000026	0.00566944	0.000695	0.000023	0.02683	0.00087
Z_FC1_5	1.467227	0.000099	0.282356	0.000022	0.00566912	0.0030858	0.0000043	0.12093	0.00021
Z_FC1_6	1.46718	0.000094	0.282323	0.000025	0.00567146	0.0033308	0.0000057	0.13137	0.00019
Z_FC1_7	1.467162	0.000084	0.282262	0.000018	0.00566324	0.00222	0.00016	0.0875	0.0063
Z_FC1_8	1.4672	0.000089	0.282265	0.000031	0.0056763	0.002	0.00012	0.0779	0.0045
Z_FC1_9	1.467191	0.000078	0.282256	0.000028	0.00567312	0.00194	0.0001	0.0755	0.004
Z_FC1_10	1.467243	0.00007	0.282406	0.000027	0.00567512	0.004539	0.000021	0.17949	0.00069
Z_GJ1_1	1.467397	0.000092	0.28201	0.000031	0.0056712	0.00035847	0.0000007	0.013153	0.000028
Z_GJ1_2	1.467297	0.000078	0.282024	0.000024	0.00566448	0.00033509	0.00000036	0.012197	0.000038
Z_GJ1_3	1.46741	0.00011	0.28203	0.000024	0.0056646	0.00032499	0.0000005	0.011779	0.000034
Z_GJ1_4	1.46737	0.000092	0.282	0.000027	0.005667	0.00032552	0.00000057	0.011649	0.000027
Z_GJ1_5	1.46727	0.00011	0.282015	0.000029	0.0056693	0.00031846	0.00000043	0.01143	0.000023
Z_GJ1_6	1.467389	0.000094	0.282025	0.000022	0.0056625	0.00032197	0.00000053	0.011541	0.000049
Z_GJ1_7	1.467301	0.000081	0.281991	0.000034	0.00567382	0.00031978	0.00000055	0.011363	0.000028
Z_GJ1_8	1.467242	0.000077	0.282005	0.000036	0.0056761	0.00031952	0.00000047	0.011319	0.000023
Z_GJ1_9	1.46725	0.0001	0.282017	0.000027	0.00566734	0.00031515	0.00000044	0.011095	0.000037
Z_GJ1_10	1.467345	0.000083	0.282015	0.000021	0.0056613	0.00031233	0.00000055	0.010985	0.000029
Z_GJ1_11	1.46727	0.00012	0.282021	0.000024	0.00566442	0.00031723	0.0000005	0.011202	0.000042
Z_GJ1_12	1.46724	0.00011	0.282014	0.000027	0.00566728	0.00031306	0.00000045	0.011021	0.000029
Z_GJ1_13	1.467245	0.000096	0.28202	0.000028	0.0056684	0.00031188	0.00000054	0.010993	0.000021
Z_GJ1_14	1.467295	0.000086	0.282012	0.000025	0.00566524	0.00032024	0.00000057	0.011242	0.000027
Z_GJ1_15	1.467276	0.00009	0.282021	0.00003	0.00567042	0.00032266	0.00000043	0.011297	0.000024
Z_GJ1_16	1.467168	0.000092	0.282023	0.000026	0.00566646	0.00032254	0.00000055	0.011315	0.000023
Z_GJ1_17	1.467268	0.000081	0.281987	0.000029	0.00566874	0.00031169	0.00000062	0.011018	0.000017
Z_GJ1_18	1.467242	0.000076	0.282008	0.00002	0.00566016	0.0003323	0.000001	0.011743	0.000032
Z_GJ1_19	1.4673	0.000089	0.282008	0.000025	0.00566516	0.00034473	0.00000057	0.012138	0.000028
Z_MT_1	1.46734	0.0001	0.282512	0.00002	0.00567024	0.00002986	0.00000023	0.0013993	0.0000071
Z_MT_2	1.467462	0.000079	0.2825	0.000031	0.005681	0.00002819	0.00000026	0.0013011	0.0000051
Z_MT_3	1.46731	0.00011	0.282489	0.000023	0.00567278	0.0000264	0.00000017	0.0012255	0.0000069
Z_MT_4	1.467287	0.000076	0.282522	0.000023	0.00567344	0.00002742	0.00000015	0.0012433	0.0000064
Z_MT_5	1.467339	0.000068	0.282511	0.000023	0.00567322	0.00002822	0.00000019	0.0012875	0.0000064
Z_MT_6	1.467273	0.000086	0.282519	0.000027	0.00567738	0.0000224	0.000001	0.000991	0.000045
Z_MT_7	1.467316	0.000071	0.28249	0.000021	0.0056708	0.00001198	0.00000048	0.000475	0.000017
Z_MT_8	1.467319	0.000088	0.282507	0.000022	0.00567214	0.000025	0.00000018	0.0011341	0.0000049
Z_MT_9	1.467303	0.000079	0.282504	0.000023	0.00567308	0.00002507	0.00000022	0.0011255	0.0000054
Z_MT_10	1.467322	0.000076	0.282519	0.00002	0.00567038	0.00002534	0.00000023	0.0011267	0.0000049
Z_MT_11	1.467284	0.000092	0.282514	0.000017	0.00566728	0.0000147	0.0000012	0.00062	0.000053
Z_MT_12	1.467265	0.000075	0.282502	0.000013	0.00566304	0.00001442	0.00000029	0.000566	0.000012
Z_MT_13	1.46723	0.0001	0.282517	0.000023	0.00567334	0.00002297	0.00000019	0.0010103	0.0000058
Z_MT_14	1.467213	0.000086	0.282504	0.000024	0.00567408	0.00002398	0.00000022	0.0010762	0.0000072
Z_MT_15	1.467306	0.000081	0.282481	0.000023	0.00567262	0.00001626	0.00000035	0.000649	0.000015
Z_MT_16	1.467232	0.000075	0.282535	0.000027	0.0056777	0.00002797	0.00000019	0.0012286	0.0000066
Z_MT_17	1.467221	0.000074	0.2825	0.000023	0.005673	0.00002552	0.00000018	0.0011409	0.0000059
Z_MT_18	1.467268	0.000074	0.282511	0.000025	0.00567522	0.00001299	0.00000048	0.000508	0.000018
Z_MT_19	1.467266	0.000095	0.282518	0.000025	0.00567536	0.00002109	0.00000074	0.000887	0.000044
Z_Plesovice_1	1.467387	0.000097	0.282495	0.000024	0.0056739	0.0001091	0.0000012	0.00595	0.00005
Z_Plesovice_2	1.467278	0.000088	0.282467	0.000026	0.00567534	0.0000812	0.0000032	0.00437	0.00017
Z_Plesovice_3	1.467249	0.000067	0.282464	0.000021	0.00567028	0.0000838	0.0000031	0.00447	0.00016
Z_Plesovice_4	1.467273	0.000063	0.282464	0.000024	0.00567328	0.0001002	0.0000024	0.00533	0.00013
Z_Plesovice_5	1.46731	0.00011	0.282471	0.000018	0.00566742	0.0000571	0.00000072	0.003024	0.000045
Z_Plesovice_6	1.467245	0.000094	0.282489	0.000025	0.00567478	0.0000731	0.0000042	0.00385	0.00021
Z_Plesovice_7	1.467275	0.000084	0.282502	0.000023	0.00567304	0.0001849	0.0000039	0.00974	0.00019
Z_Plesovice_8	1.467275	0.000068	0.282472	0.000029	0.00567844	0.0001867	0.0000042	0.00981	0.00023
Z_Plesovice_9	1.46725	0.000085	0.282472	0.000024	0.00567344	0.0001792	0.0000039	0.00945	0.00023
Z_R33_1	1.467374	0.000085	0.282826	0.000025	0.00568152	0.0024426	0.0000094	0.09872	0.00015
Z_R33_2	1.46732	0.00011	0.282838	0.000024	0.00568076	0.002598	0.000071	0.1002	0.0024
Z_R33_3	1.46734	0.00011	0.282777	0.000028	0.00568354	0.0012962	0.0000012	0.04448	0.00014
Z_R33_4	1.46733	0.00011	0.282795	0.00002	0.0056759	0.0019994	0.0000058	0.07938	0.00039
Z_R33_5	1.467386	0.000072	0.282804	0.000026	0.00568208	0.002551	0.000029	0.10173	0.0009
Z_R33_6	1.467265	0.00008	0.282776	0.000024	0.00567952	0.002188	0.000046	0.0865	0.0021
Z_R33_7	1.467311	0.000088	0.282756	0.000031	0.00568612	0.000659	0.000012	0.02396	0.00053
Z_R33_8	1.46732	0.0001	0.282753	0.000025	0.00568006	0.001596	0.000041	0.0613	0.0014
Z_R33_9	1.467287	0.000087	0.282729	0.000021	0.00567558	0.00088	0.000011	0.0306	0.00043
Z_R33_10	1.467431	0.000099	0.282703	0.000027	0.00568106	0.001	0.000017	0.03758	0.00059
Z_R33_11	1.4673	0.000094	0.282744	0.000025	0.00567988	0.001056	0.000034	0.0376	0.0012
Z_R33_12	1.467251	0.000094	0.282739	0.000034	0.00568878	0.0010007	0.0000082	0.03604	0.00042
Z_R33_13	1.467281	0.000098	0.282795	0.00002	0.0056759	0.002017	0.000076	0.078	0.0032
Z_R33_14	1.467324	0.000066	0.282777	0.000023	0.00567854	0.001965	0.00002	0.07705	0.00091
Z_R33_15	1.46719	0.0001	0.282789	0.000027	0.00568278	0.001623	0.000038	0.0584	0.0014
Z_R33_16	1.467291	0.000086	0.282803	0.000027	0.00568306	0.001764	0.000017	0.06417	0.00098
Z_R33_17	1.467269	0.000087	0.282846	0.000026	0.00568292	0.0034368	0.0000074	0.13439	0.00072
Z_R33_18	1.467273	0.000099	0.282813	0.000026	0.00568226	0.002386	0.000034	0.09017	0.00099
Z_R33_19	1.46725	0.000086	0.282743	0.000025	0.00567986	0.001514	0.000013	0.0538	0.00063
Z_R33_20	1.46729	0.0001	0.282763	0.000027	0.00568226	0.00237	0.00017	0.0919	0.0066
Z_91500_1	1.467361	0.000092	0.282317	0.000031	0.00567734	0.0003918	0.00000064	0.014902	0.000046
Z_91500_2	1.467384	0.000099	0.282302	0.000033	0.00567904	0.0003771	0.00000068	0.014198	0.000037
Z_91500_3	1.46729	0.00011	0.282321	0.000037	0.00568342	0.00037321	0.00000091	0.013837	0.000032
Z_91500_4	1.46728	0.00012	0.282281	0.000034	0.00567962	0.00036631	0.00000062	0.013556	0.000027
Z_91500_5	1.467355	0.000087	0.282297	0.000038	0.00568394	0.00036535	0.00000048	0.013472	0.000023
Z_91500_6	1.467337	0.000091	0.282301	0.00003	0.00567602	0.00036181	0.00000042	0.013352	0.000044
Z_91500_7	1.46735	0.0001	0.282324	0.000027	0.00567348	0.00036676	0.00000047	0.013362	0.000028
Z_91500_8	1.467356	0.000097	0.282272	0.000032	0.00567744	0.00036352	0.00000056	0.013194	0.000026
Z_91500_9	1.467259	0.000076	0.282297	0.000031	0.00567694	0.0003571	0.0000018	0.012878	0.00003
Z_91500_10	1.46733	0.0001	0.2823	0.000021	0.005667	0.00035975	0.00000067	0.012975	0.000023
Z_91500_11	1.467275	0.000074	0.282287	0.00003	0.00567574	0.00036395	0.00000048	0.013235	0.000041
Z_91500_12	1.467269	0.000075	0.282335	0.000029	0.0056757	0.00036043	0.00000053	0.013113	0.000026
Z_91500_13	1.467357	0.000095	0.282316	0.000029	0.00567532	0.0003519	0.0000018	0.012782	0.00003
Z_91500_14	1.467238	0.000086	0.282319	0.000037	0.00568338	0.00034322	0.00000057	0.012479	0.000023
Z_91500_15	1.4673	0.000085	0.282315	0.000028	0.0056743	0.00034878	0.00000043	0.012555	0.000035
Z_91500_16	1.467236	0.000092	0.282294	0.000025	0.00567088	0.00036077	0.00000058	0.013017	0.000028
Z_91500_17	1.467404	0.000098	0.282313	0.000038	0.00568426	0.00035423	0.00000053	0.012761	0.000034
Z_91500_18	1.467278	0.000097	0.28233	0.000032	0.0056786	0.00036813	0.00000083	0.013268	0.000042
Z_91500_19	1.46742	0.00011	0.282302	0.000033	0.00567904	0.00037954	0.00000036	0.013687	0.000051
fc - 1	1.4675	0.00013	0.282156	0.000038	0.00568112	0.001276	0.000015	0.05064	0.00032
fc - 2	1.46731	0.00012	0.282196	0.000039	0.00568292	0.000847	0.000014	0.03236	0.00034
fc - 3	1.46722	0.00016	0.282156	0.000043	0.00568612	0.000903	0.000023	0.03438	0.00074
fc - 5	1.46726	0.00012	0.282194	0.000045	0.00568888	0.001273	0.000016	0.04913	0.00043
fc - 6	1.46722	0.00015	0.282186	0.000048	0.00569172	0.001272	0.000012	0.04971	0.0002
fc - 7	1.46727	0.00015	0.282137	0.000045	0.00568774	0.001191	0.0000018	0.04701	0.00037
fc - 8	1.46753	0.00014	0.282152	0.00004	0.00568304	0.001154	0.000011	0.04459	0.00077
fc - 9	1.46751	0.000099	0.282195	0.00004	0.0056839	0.0011722	0.0000048	0.04499	0.00041
fc - 11	1.46723	0.00012	0.282145	0.000038	0.0056809	0.00074055	0.00000051	0.0276	0.00019
fc - 12	1.46716	0.00013	0.282175	0.000038	0.0056815	0.001176	0.000015	0.04558	0.00031

Appendix D3.2 continued.

Curtin University Geohistory center		Lu-Hf Isotopic Ratios from Iolite								
	Spot ID	178Hf/177Hf	±2σ INT	176Hf/177Hf	±2σ INT	(2% External ±)	176Lu/177Hfm	±2σ INT	176Yb/177Hf	±2σ INT
				0.282785			0.03360 Bouvier et al., 2008 EPSL-273			
				0.283250			0.03840 Griffin et al., 2002, Lithos-237			
Run 4: Standard Results - Lu/Hf on Nu Plasma II - sample 38DTB19 - MudTank Primary Standard, errors propogated based on long term running averages (see Spencer et al., 2020).										
	Z_FC1_1	1.46748	0.00014	0.282202	0.000043	0.00568704	0.001242	0.00005	0.0457	0.0016
	Z_FC1_2	1.46752	0.00015	0.282199	0.000046	0.00568998	0.001058	0.00001	0.03982	0.00014
	Z_FC1_3	1.46759	0.00012	0.282174	0.000044	0.00568748	0.000758	0.0000018	0.02708	0.00029
	Z_FC1_4	1.46749	0.00013	0.282156	0.00004	0.00568312	0.0008106	0.0000018	0.02957	0.00033
	Z_GJ1_1	1.4675	0.00012	0.28198	0.00005	0.0056896	0.00028214	0.00000076	0.009402	0.000061
	Z_GJ1_2	1.46755	0.00014	0.282079	0.000048	0.00568958	0.00028185	0.00000095	0.009389	0.000072
	Z_GJ1_3	1.46754	0.00012	0.28195	0.000055	0.005694	0.00028301	0.00000073	0.009457	0.000064
	Z_GJ1_4	1.46752	0.00014	0.282029	0.00005	0.00569058	0.0002831	0.00000061	0.00942	0.000076
	Z_GJ1_5	1.46753	0.00014	0.282049	0.000042	0.00568298	0.0002816	0.00000067	0.00929	0.000072
	Z_MT_1	1.4675	0.00013	0.282512	0.000035	0.00568524	0.00001927	0.00000053	0.000823	0.000022
	Z_MT_2	1.46753	0.00012	0.282496	0.000047	0.00569692	0.00002075	0.00000038	0.000912	0.000021
	Z_MT_3	1.46743	0.00012	0.282493	0.000049	0.00569886	0.00002006	0.00000054	0.000858	0.000016
	Z_MT_4	1.46752	0.00013	0.282531	0.000048	0.00569862	0.00002338	0.0000006	0.000993	0.000021
	Z_MT_5	1.46754	0.00013	0.2825	0.000045	0.005695	0.0000216	0.00000073	0.000919	0.00002
	Z_Plesovice_1	1.46751	0.00014	0.28253	0.000037	0.0056876	0.000162	0.000001	0.007983	0.000095
	Z_Plesovice_2	1.46751	0.00013	0.282534	0.000037	0.00568768	0.000156	0.0000012	0.007699	0.00003
	Z_Plesovice_3	1.4675	0.00012	0.28244	0.00005	0.0056988	0.00014762	0.00000086	0.007343	0.000034
	Z_Plesovice_4	1.46745	0.00011	0.282419	0.000038	0.00568638	0.0001333	0.0000011	0.006817	0.000024
	Z_R33_1	1.467431	0.000098	0.282768	0.000042	0.00569736	0.001047	0.000019	0.03616	0.00048
	Z_R33_2	1.46755	0.00014	0.282796	0.000055	0.00571092	0.00223	0.00013	0.0848	0.0057
	Z_R33_3	1.46754	0.00012	0.282771	0.000055	0.00571042	0.001826	0.000026	0.0642	0.0015
	Z_R33_4	1.46758	0.00014	0.282741	0.000043	0.00569782	0.0015573	0.0000035	0.05245	0.00018
	Z_R33_5	1.46752	0.00013	0.282732	0.000043	0.00569764	0.0011273	0.0000025	0.03945	0.00031
	Z_91500_1	1.46752	0.00014	0.282292	0.000058	0.00570384	0.00025983	0.00000082	0.008756	0.00007
	Z_91500_2	1.46767	0.00014	0.282339	0.000059	0.00570578	0.00028391	0.00000097	0.009675	0.000075
	Z_91500_3	1.46758	0.00015	0.282321	0.000065	0.00571142	0.0002791	0.000001	0.009504	0.000052
	Z_91500_4	1.46738	0.00015	0.282304	0.000058	0.00570408	0.0002601	0.0000011	0.008873	0.000088
	Z_91500_5	1.46752	0.00014	0.282323	0.000056	0.00570246	0.0002719	0.0000012	0.009287	0.000072

Appendix D3.2 continued.

Table 21JBM18. U-Pb geochronologic analyse
University of Arizona Laserchron center

Analysis	U (ppm)	206Pb/204Pb	U/Th	Measured ratios: 207Pb/235U	± 2 sig	206Pb/238U	± 2 sig	error corr.	Apparent ages (Ma): 207Pb/235U	± (Ma) 2 sig	206Pb/238U	± (Ma) 2 sig	206Pb/207Pb	± (Ma) 2 sig
Standard Results - U/Pb on 7700 - Samples 10DTB19, 12DTB19, 14DTB19 - OGC primary standard for unknowns > 1500 Ma, 91500 primary standard for unknowns > 1500 Ma, errors propogated within run and are the same as long term running averages (Spencer et al., 2016)														
FC -1	271	69015	2.21	1.98649	0.0572	0.18848	0.00422	0.78	1110.93	17.6904	1113.1	20.748	1106.6	32.76
FC -1	1139	1088577	1.50	1.93898	0.0671	0.18735	0.00596	0.92	1094.6	21.112	1107	29.484	1070.2	24.752
FC -1	501	58287	1.59	1.92926	0.0722	0.18461	0.00591	0.86	1091.3	22.75	1092.1	29.302	1089.6	34.762
FC -1	463	78941	1.76	1.91642	0.0567	0.18351	0.00484	0.89	1086.82	17.9634	1086.1	24.024	1088.2	24.57
FC -1	505	99066	1.44	1.93512	0.0716	0.18549	0.00612	0.90	1093.3	22.568	1096.9	30.212	1086.2	29.484
FC -1	543	154574	1.73	1.96775	0.0649	0.18805	0.00549	0.89	1104.5	20.202	1110.8	27.118	1092.2	27.482
FC -1	291	288927	1.95	1.97963	0.0641	0.18777	0.00511	0.84	1108.6	19.838	1109.3	25.298	1107.2	32.032
FC -1	681	795728	2.25	1.97407	0.0612	0.18674	0.00504	0.87	1106.7	18.928	1103.7	24.934	1112.6	27.846
FC -1	293	77021	1.74	1.94369	0.0439	0.18578	0.0031	0.74	1096.27	13.7774	1098.47	15.3426	1091.9	27.664
FC -1	244	72996	1.62	1.95376	0.0508	0.18621	0.00387	0.80	1099.74	15.8886	1100.8	19.11	1097.6	28.392
FC -1	416	289313	1.69	1.96965	0.0741	0.18807	0.00643	0.91	1105.2	23.114	1110.9	31.668	1093.9	28.392
FC -1	512	64822	1.71	1.93836	0.0663	0.18663	0.00582	0.91	1094.4	20.93	1103.1	28.756	1077.2	25.844
FC -1	469	125055	1.74	1.95096	0.0831	0.18704	0.00729	0.92	1098.8	26.026	1105.3	36.036	1085.8	30.394
FC -1	230	65053	2.38	1.97984	0.0598	0.18677	0.00437	0.77	1108.7	18.564	1103.9	21.658	1118.1	34.944
FC -1	387	96138	2.64	1.98232	0.0777	0.18834	0.00693	0.94	1109.5	24.024	1112.4	34.216	1103.9	24.388
FC -1	358	105418	1.74	1.95244	0.0539	0.18622	0.00406	0.79	1099.29	16.8714	1100.9	20.02	1096.2	30.758
FC -1	229	122516	1.63	1.9057	0.048	0.18305	0.0035	0.76	1083.08	15.2698	1083.62	17.3628	1082	29.848
FC -1	305	1113304	1.90	1.95529	0.0567	0.18664	0.00463	0.85	1100.27	17.7268	1103.1	22.932	1094.6	27.846
FC -1	505	1662322	1.41	1.94098	0.0703	0.18492	0.0061	0.91	1095.3	22.022	1093.8	30.212	1098.4	27.3
FC -1	239	91423	1.55	1.96907	0.048	0.18805	0.0035	0.76	1104.99	14.9422	1110.8	17.29	1093.6	28.938
FC -1	300	178604	1.82	1.94924	0.0569	0.18533	0.00393	0.72	1098.19	17.8178	1096	19.474	1102.5	36.946
FC -1	669	278180	1.68	1.93533	0.0716	0.18444	0.00605	0.89	1093.4	22.568	1091.2	30.03	1097.8	30.758
FC -1	168	52430	2.46	1.96506	0.0491	0.18721	0.0036	0.77	1103.62	15.3062	1106.24	17.7814	1098.4	29.12
FC -1	291	61211	1.51	1.98762	0.0529	0.18773	0.00402	0.80	1111.31	16.3618	1109.1	19.838	1115.7	28.938
FC -1	145	110592	2.23	1.92675	0.0478	0.18295	0.0033	0.73	1090.41	15.0878	1083.07	16.3618	1105.1	30.758
FC -1	672	143084	1.77	1.94379	0.0568	0.18577	0.00498	0.92	1096.31	17.836	1098.4	24.57	1092.1	20.93
FC -1	427	119544	1.85	1.94702	0.0794	0.1856	0.00709	0.93	1097.4	24.934	1097.5	35.126	1097.3	27.3
FC -1	247	42914	1.63	1.94462	0.0572	0.18555	0.00423	0.78	1096.59	17.9452	1097.2	20.93	1095.3	33.488
FC -1	236	79783	2.20	1.95554	0.0583	0.18543	0.00438	0.79	1100.4	18.2	1096.6	21.658	1107.8	33.306
FC -1	1171	267399	1.38	1.94149	0.0652	0.18546	0.00553	0.89	1095.5	20.566	1096.7	27.3	1093.1	27.846
FC -1	234	45271	1.52	1.94998	0.0577	0.18693	0.00422	0.76	1098.44	18.0726	1104.7	20.93	1086	35.126
FC -1	332	177902	1.98	1.99366	0.0447	0.19061	0.0034	0.80	1113.36	13.7956	1124.68	16.744	1091.3	24.57
FC -1	163	68111	1.85	1.99861	0.062	0.19113	0.0047	0.80	1115	19.11	1127.5	23.114	1090.8	33.852
FC -1	248	31892	1.56	1.95095	0.0511	0.18805	0.0035	0.71	1098.77	15.9978	1110.8	17.29	1075	33.67
FC -1	286	84360	1.72	1.96519	0.0542	0.1872	0.00393	0.76	1103.66	16.8896	1106.2	19.474	1098.7	32.578
FC -1	478	101852	2.06	1.95253	0.0703	0.18633	0.00626	0.93	1099.3	22.022	1101.5	30.94	1095.1	24.024
FC -1	180	69528	2.09	1.96703	0.0492	0.18624	0.0035	0.75	1104.29	15.3244	1100.97	17.3082	1110.8	30.03
FC -1	548	135063	1.74	1.9303	0.0683	0.18236	0.00558	0.86	1091.6	21.476	1079.9	27.664	1115.2	32.76
FC -1	295	106194	1.77	1.94821	0.0507	0.18452	0.00373	0.78	1097.83	15.8886	1091.6	18.382	1110.2	29.666
FC -1	496	1828515	1.73	1.93792	0.0651	0.18606	0.00554	0.89	1094.3	20.384	1100	27.482	1082.9	28.028
FC -1	1284	671896	1.84	1.93159	0.0761	0.18509	0.00655	0.90	1092.1	24.024	1094.7	32.396	1086.8	31.304
FC -1	136	70296	2.21	1.95987	0.0564	0.18372	0.00408	0.77	1101.84	17.5994	1087.3	20.202	1130.7	33.306
FC -1	452	61153	2.46	1.94648	0.067	0.18594	0.0055	0.86	1097.2	20.93	1099.3	27.118	1093.1	32.032
FC -1	1111	666076	1.32	1.99996	0.0704	0.18926	0.00575	0.87	1115.5	21.658	1117.4	28.392	1111.9	31.486
FC -1	233	1071825	1.61	1.95153	0.0492	0.18532	0.0035	0.75	1098.97	15.3972	1095.97	17.3264	1104.9	30.394
R33	49	6239	1.52	0.51266	0.0252	0.06754	0.00142	0.43	420.24	15.3972	421.32	7.8078	414.3	90.272
R33	45	52106	2.41	0.55665	0.0233	0.07188	0.00178	0.59	449.34	13.832	447.47	9.737	458.9	68.25
R33	204	22312	1.27	0.51004	0.0138	0.06686	0.0013	0.70	418.48	8.4448	417.21	7.1526	425.5	39.312
R33	184	22396	1.32	0.51274	0.0157	0.06618	0.00142	0.70	420.29	9.5914	413.1	7.8078	459.9	44.044
R33	304	41050	1.15	0.51409	0.0155	0.0662	0.00146	0.73	421.2	9.464	413.22	8.0262	465.1	41.496
R33	961	287889	1.53	0.50794	0.0194	0.06614	0.00216	0.85	417.06	11.8846	412.86	11.8846	440.4	40.768
R33	84	9361	1.44	0.5148	0.0192	0.06678	0.00174	0.70	421.67	11.7026	416.73	9.5732	448.8	53.872
R33	667	1186073	1.82	0.51598	0.0219	0.06762	0.00253	0.88	422.46	13.3406	421.8	13.9048	426.1	40.95
R33	197	42202	1.21	0.51054	0.0147	0.06696	0.0012	0.64	418.81	8.9908	417.81	6.6066	424.3	44.954
R33	149	789391	1.33	0.52358	0.0175	0.0681	0.00174	0.76	427.54	10.6106	424.7	9.555	442.9	44.044
R33	200	54154	1.26	0.50823	0.0168	0.06541	0.00161	0.75	417.26	10.3012	408.44	8.8634	466.3	44.044
R33	251	18866	1.12	0.50945	0.0199	0.06563	0.00165	0.65	418.08	12.1758	409.77	9.0818	464.2	59.878
R33	94	35561	1.30	0.52117	0.0144	0.06881	0.0013	0.69	425.93	8.7542	428.98	7.1344	409.5	40.768
R33	204	67829	1.26	0.52115	0.0181	0.06774	0.00183	0.78	425.92	10.9928	422.53	10.0464	444.3	44.044
R33	215	25283	1.23	0.51526	0.0165	0.06743	0.00169	0.78	421.98	10.0646	420.65	9.282	429.2	40.586
SL2	857	69909	6.13	0.72722	0.0241	0.08888	0.00272	0.92	554.92	12.8856	548.91	14.651	579.7	25.662
SL2	385	31192	5.48	0.72586	0.0289	0.08967	0.00321	0.90	554.12	15.47	553.59	17.29	556.3	34.398
SL2	394	169299	5.38	0.73928	0.0235	0.09055	0.00241	0.84	561.99	12.4852	558.79	12.9584	574.9	34.216
SL2	109	23762	13.15	0.75535	0.0269	0.09076	0.00252	0.78	571.32	14.1596	560.03	13.559	616.5	43.862
SL2	62	6358	9.15	0.74119	0.0283	0.0922	0.0021	0.59	563.1	15.015	568.54	11.284	541.2	61.334
SL2	572	88857	6.24	0.71753	0.0255	0.0887	0.00268	0.85	549.21	13.7228	547.84	14.4326	554.9	37.128
SL2	843	78553	6.18	0.72352	0.0243	0.08928	0.00264	0.88	552.74	13.0312	551.28	14.2142	558.8	31.668
SL2	733	73164	5.79	0.72529	0.0225	0.08936	0.00247	0.89	553.78	12.0484	551.75	13.3042	562.2	28.028
SL2	706	270556	5.86	0.71451	0.025	0.08811	0.00266	0.86	547.42	13.468	544.35	14.3416	560.2	35.49
SL2	343	105312	1.18	0.77059	0.0205	0.09395	0.00188	0.75	580.1	10.7016	578.86	10.0828	585	34.762
SL2	844	352706	6.13	0.72712	0.0227	0.0899	0.00236	0.84	554.86	12.1394	554.95	12.7036	554.5	33.67
SL2	150	53742	10.41	0.73382	0.0223	0.09093	0.00216	0.79	558.79	11.8846	561.03	11.6116	549.7	36.946
SL2	104	22060	13.24	0.73768	0.0243	0.09232	0.00209	0.68	561.05	12.922	569.24	11.2294	528	48.23
SL2	371	96604	5.35	0.73337	0.0167	0.09074	0.0015	0.73	558.53	8.8998	559.91	8.0626	552.9	30.94
SL2	64	23001	9.76	0.74293	0.0266	0.09031	0.00204	0.63	564.11	14.105	557.37	10.9746	591.4	54.782
SL2	558	61247	6.15	0.71216	0.0286	0.08819	0.00316	0.89	546.03	15.4336	544.82	17.0352	551.1	36.4
SL2	804	180015	6.18	0.73915	0.0222	0.08996	0.00227	0.84	561.91	11.7936	555.3	12.2122	588.8	32.214
SL2	722	79717	5.84	0.71802	0.0213	0.08989	0.00237	0.89	549.5	11.4478	554.89	12.7582	527.2	26.936
SL2	680	110048	5.77	0.72298	0.0243	0.08849	0.00265	0.89	552.42	13.0312	546.6	14.287	576.5	30.394
SL2	797	515728	6.46	0.7314	0.0221	0.09037	0.00233	0.86	557.37	11.7936	557.72	12.5398	555.9	30.576
SL2	105	17031	12.79	0.73591	0.024	0.0906	0.00212	0.72	560.02	12.7764	559.08	11.4114	563.8	44.954
SL2	399	81881	5.36	0.72901	0.0242	0.09046	0.00264	0.88	555.97	12.9402	558.26	14.196	546.6	31.304
SL2	54	9206	9.06	0.74255	0.0306	0.09193	0.00213	0.56	563.89	16.2344	566.94	11.4478	551.6	67.886
SL2	559	35539	6.20	0.7159	0.0245	0.0886	0.00276	0.91	548.24	13.195	547.25	14.8694	552.4	28.21
SL2	830	94929	6.13	0.7249	0.0268	0.08957	0.00296	0.89	553.56	14.3598	552.99	15.9432	555.9	33.488

Appendix D4.1: Sample locations

sample #	Lat	Long	Description
49DTB19	47.05626	-116.43749	staurolite gt mu qf schist
50DTB19	46.99916	-116.35958	gt mica qf schist
51DTB19	46.98515	-116.31361	gt mu qf schist
59DTB19	47.02315	-115.46378	gt ky schist
52DTB19	47.01509	-115.81738	gt amphibolite

Appendix D4.2: Bulk Rock Geochemistry

			49DTB19	50DTB19	51DTB19	59DTB19	52DTB19
Wt. %	TiO2	79.9	0.617	0.572	0.597	0.686	1.888
	Cr2O3	151.99	0.009	0.009	0.009	0.009	0.002
	SiO2	60.09	71.19	67.63	61.21	62.1	58.01
	Al2O3	101.96	15.02	17.68	21.47	16.57	13.53
	CaO	56.08	0.28	0.27	0.21	0.39	6.64
	MgO	40.31	1.73	1.72	1.59	3.49	3.24
	FeO	71.85					
	MnO	70.94	0.041	0.04	0.04	0.114	0.228
	Fe2O3	159.69	4.6	5.39	6.25	9.8	13.31
	K2O	94.2	3.57	3.85	5.06	4.14	0.262
	Na2O	61.98	0.89	0.69	0.89	0.57	2.53
	H2O (LOI)	18.015	1.8	1.96	2.5	1.86	-0.04
	Total		99.75	99.81	99.83	99.73	99.60
Moles	TiO2		0.008	0.007	0.007	0.009	0.024
	Cr2O3		0.000	0.000	0.000	0.000	0.000
	SiO2		1.185	1.125	1.019	1.033	0.965
	Al2O3		0.147	0.173	0.211	0.163	0.133
	CaO		0.005	0.005	0.004	0.007	0.118
	MgO		0.043	0.043	0.039	0.087	0.080
	FeO		0.006	0.008	0.009	0.014	0.019
	MnO		0.001	0.001	0.001	0.002	0.003
	Fe2O3		0.012	0.014	0.016	0.025	0.033
	K2O		0.038	0.041	0.054	0.044	0.003
	Na2O		0.014	0.011	0.014	0.009	0.041
	H2O		0.100	0.109	0.139	0.103	-0.002
	total		1.558	1.536	1.512	1.494	1.417
	NF		64.171	65.109	66.153	66.922	70.574
Normalized MOLAR %	TiO2		0.496	0.466	0.494	0.575	1.668
	Cr2O3		0.000	0.000	0.000	0.000	0.000
	SiO2		76.024	73.279	67.386	69.161	68.131
	Al2O3		9.453	11.290	13.930	10.876	9.365
	CaO		0.320	0.313	0.248	0.465	8.356
	MgO		2.754	2.778	2.609	5.794	5.673
	FeO		0.411	0.488	0.575	0.913	1.307
	MnO		0.037	0.037	0.037	0.108	0.227
	Fe2O3		0.739	0.879	1.036	1.643	2.353
	K2O		2.432	2.661	3.553	2.941	0.196
	Na2O		0.921	0.725	0.950	0.615	2.881
	H2O		6.412	7.084	9.180	6.910	-0.157
	total		100.000	100.000	100.000	100.000	100.000
MnNCKFMASHTO	TiO2		0.50	0.47	0.49	0.57	1.67
	SiO2		76.02	73.28	67.39	69.16	68.13
	Al2O3		9.45	11.29	13.93	10.88	9.37
	CaO		0.32	0.31	0.25	0.47	8.36
	MgO		2.75	2.78	2.61	5.79	5.67
	FeO		3.37	4.00	4.72	7.48	10.72
	MnO		0.04	0.04	0.04	0.11	0.23
	O		0.74	0.88	1.04	1.64	2.35
	K2O		2.43	2.66	3.55	2.94	0.20
	Na2O		0.92	0.72	0.95	0.62	2.88
	H2O		6.41	7.08	9.18	6.91	-0.16
	total		102.96	103.52	104.14	106.57	109.41

Appendix D4.3: EPMA Garnet Geochemistry

[illegible]

Appendix D4.4: Monazite U/Pb Results

Spot ID	238U conc.	232Th conc.		Isotopic Ratios					Apparent Ages - Calculated in Isoplot R (Ma)				Discord	error %	Concordia Age - Calcuated in Isoplot R		Concordant within uncertainties?
	ppm	ppm		238U/206Pb	±2σ PROP	207Pb/206Pb	±2σ PROP	rho	238U/206Pb	±2σ PROP	207Pb/206Pb	±2σ PROP	(7/6-6/8)/7/6 *100		Age	±2σ PROP	
49DTB19																	
49DTB19-MM - 2.d	2816.309331	33990.37231	0.08285609	5.474705387	0.2525755	0.074157141	0.002183278	0.28683644	1081.5	23	1044.8	29.7	-3.51	2.13%	1066.7	15.2	concordant
49DTB19-MM - 9.d	2267.561078	25819.78107	0.08782263	5.359452345	0.2479169	0.075347832	0.002729109	0.19815474	1102.9	23.4	1076.9	36.4	-2.41	2.12%	1094.3	17.6	concordant
49DTB19-MM - 20.d	1797.623773	31010.47406	0.057968278	5.618365495	0.2596695	0.07461643	0.002348951	-0.0073103	1056	22.5	1057.3	31.7	0.12	2.13%	1056.4	18.4	concordant
49DTB19-MM - 12.d	2469.30557	63515.55195	0.03887718	5.433171686	0.2555347	0.075867012	0.002749404	0.52877379	1089.1	23.6	1090.7	36.3	0.15	2.17%	1089.7	13.8	concordant
49DTB19-MM - 10.d	2154.371869	40445.09743	0.053266576	5.435789668	0.2436672	0.07612913	0.002202525	0.47081442	1088.6	22.5	1097.6	28.9	0.82	2.07%	1092.3	13	concordant
49DTB19-MM - 4.d	3941.956264	57416.59227	0.06865535	5.534090907	0.2473975	0.075547412	0.001940652	0.30627341	1070.8	22.1	1082.2	25.8	1.05	2.06%	1075.8	14	concordant
49DTB19-MM - 1.d	2665.20904	34889.95567	0.076389006	5.566212976	0.2366896	0.076510926	0.002382321	0.45674465	1065.1	20.9	1107.6	31.1	3.84	1.96%	1080.6	13.1	concordant
49DTB19-MM - 23.d	2176.286444	34968.54891	0.062235538	5.533001102	0.2438308	0.077665713	0.002082374	0.26018075	1071	21.7	1137.4	26.7	5.84	2.03%	1098.7	14.9	concordant
49DTB19-MM - 13.d	2615.925855	52807.65378	0.04953687	5.38058761	0.2498111	0.07885405	0.002165294	0.24152653	1098.9	23.5	1167.6	27.2	5.88	2.14%	1129	15.9	concordant
49DTB19-MM - 24.d	1862.727831	30214.60403	0.061649917	5.4787853	0.230253	0.079351268	0.002232746	0.40393893	1080.7	20.9	1180	27.8	8.42	1.93%	1120.2	13.4	concordant
49DTB19-MM - 11.d	1976.822148	34317.91275	0.057603216	5.704223625	0.2414385	0.080433684	0.002302697	0.21840758	1041.3	20.3	1206.8	28.2	13.71	1.95%	1100	15.8	discordant
49DTB19-MM - 6.d	1901.771406	34400.07998	0.055283924	5.500441981	0.2475753	0.083860146	0.002286488	0.04554753	1076.8	22.3	1288.4	26.5	16.42	2.07%	1159.9	18.7	discordant
49DTB19-MM - 3.d	1404.225099	22971.04751	0.061130216	5.40897315	0.2400045	0.085702302	0.003261234	0.19680268	1093.6	22.3	1330.6	36.8	17.81	2.04%	1157.7	19.1	discordant
49DTB19-MM - 21.d	679.2227238	2028.879201	0.334777311	5.192162215	0.2459797	0.118714979	0.003829892	0.1218633	1135.4	24.7	1936.2	28.9	41.36	2.18%	1295.4	36.8	discordant
49DTB19-MM - 19.d	606.2022249	10324.21105	0.058716567	5.150346938	0.2369061	0.132511114	0.004806338	-0.1924004	1143.9	24.1	2130.7	31.7	46.31	2.11%	893.6	26	discordant
49DTB19-MM - 15.d	810.3926068	7696.298279	0.105296414	3.014298623	0.1388112	0.408847213	0.010783579	0.17777804	1846.9	37	3941.3	19.8	53.14	2.00%	584.4	29.6	discordant
~~49DTB19-MM - 22.d with links~~	~~746.339626~~	~~5150.459906~~	0.144907375	~~3.538066707~~	~~0.1943381~~	~~0.494088908~~	~~0.023160381~~	~~0.19708434~~	~~1604.6~~	~~39~~	~~4223~~	~~34.6~~	~~62.00~~	~~2.43%~~	882.2	37	~~discordant~~
49DTB19-MM - 17.d	1037.941167	16738.06221	0.062010832	4.852891319	0.2265118	0.606108979	0.016197415	0.32892829	1207.8	25.7	4522.1	19.4	73.29	2.13%	251.3	18.3	discordant
50DTB19-MI - 1.d	508.5082855	13382.97134	0.037996666	4.146590598	0.1915089	0.088948197	0.002990278	0.16273922	1392.7	28.9	1402.2	32.2	0.68	2.08%	1397	19.8	concordant
50DTB19-MI - 2.d	1074.381297	25577.74912	0.042004529	4.208869389	0.1960854	0.084141858	0.002584784	0.33071445	1374.2	28.8	1295	29.9	-6.12	2.10%	1335.6	16.6	concordant
50DTB19-MIc - 3.d	939.9942544	62802.17472	0.014967543	4.074795478	0.1874002	0.088281276	0.002812004	-0.002093	1414.8	29.2	1387.7	30.6	-1.95	2.06%	1401.8	20.9	discordant
50DTB19-MIc - 4.d	1206.74968	42909.0351	0.02812344	4.308045822	0.1957678	0.086338214	0.002627124	0.0200513	1345.6	27.6	1344.9	29.4	-0.05	2.05%	1345.3	19.9	concordant
50DTB19-MIc - 5.d	1627.696309	46832.71601	0.034755539	5.072290157	0.2289621	0.082991223	0.002965691	0.52787073	1160	24	1268.1	34.9	8.52	2.07%	1200.8	14.2	concordant
50DTB19-MIc - 6.d	1542.833743	52065.14387	0.029632757	4.286547089	0.1906818	0.08788379	0.002395103	-0.0552735	1351.7	27.1	1379.1	26.2	1.99	2.00%	1365.9	19.6	concordant
50DTB19-MM - 1.d	1625.230947	15102.27994	0.10761494	4.466833474	0.2046655	0.087969903	0.00251169	0.27380329	1302.3	27	1381	27.4	5.70	2.07%	1341.1	16.8	concordant
50DTB19-MM - 10.d	2560.013692	32882.96686	0.077852272	4.460701732	0.2125691	0.087139459	0.002395151	0.32805786	1303.9	28.1	1362.7	26.5	4.31	2.16%	1334.7	16	concordant
50DTB19-MM - 11.d with links	3221.660428	32328.31965	0.099654435	5.484788338	0.3094314	0.08045656	0.002494653	-0.0157056	1079.6	28	1207.3	30.5	10.58	2.59%	1136.6	22.3	discordant
50DTB19-MM - 12.d	2888.362767	40658.27702	0.07103997	4.472476836	0.2021001	0.086153497	0.002475397	0.34705942	1300.8	26.6	1340.8	27.8	2.98	2.04%	1320.2	15.7	concordant
50DTB19-MM - 13.d	1853.923939	42064.72568	0.044073126	4.259817355	0.1793889	0.088014403	0.00273432	0.28361649	1359.4	25.8	1381.9	29.8	1.63	1.90%	1369.4	16.7	concordant
50DTB19-MM - 14.d	5449.197834	32754.74412	0.166363621	5.651493505	0.2691872	0.07674033	0.002020913	0.44611244	1050.3	23.1	1113.6	26.3	5.68	2.20%	1079.1	13.2	concordant
50DTB19-MM - 15.d	3942.822814	29356.61315	0.134307823	5.748599505	0.2543115	0.076150169	0.002117216	0.39149016	1033.9	21.1	1098.1	27.8	5.85	2.04%	1059.6	13.5	concordant
50DTB19-MM - 17.d	1546.298973	46543.60851	0.033222585	5.633788146	0.2585588	0.0860192	0.002491603	0.36940363	1053.3	22.3	1337.7	28	21.26	2.12%	1169.5	15.5	discordant
50DTB19-MM - 18.d	1281.177559	43193.0722	0.029661645	5.498165814	0.2675565	0.089812982	0.003807315	0.29905067	1077.2	24.1	1420.7	40.5	24.18	2.24%	1171.2	20.3	discordant
50DTB19-MM - 19.d	1191.869079	15496.49794	0.076912157	5.319709248	0.2573419	0.08148579	0.002534665	-0.2201752	1110.4	24.7	1232.3	30.5	9.89	2.22%	1150.8	23.1	discordant
50DTB19-MM - 20.d	1248.959723	27277.87893	0.045786541	4.392146134	0.203221	0.091627834	0.002622856	0.03202808	1322.3	27.7	1458.8	27.2	9.36	2.09%	1390.8	20.2	discordant
50DTB19-MM - 21.d	1256.722059	26135.00229	0.048085783	4.824178275	0.2787532	0.086493443	0.002812151	-0.024235	1214.4	32	1348.4	31.4	9.94	2.64%	1281.8	24.1	discordant
50DTB19-MM - 22.d	1113.14758	13400.91945	0.083065015	4.406054364	0.2018019	0.088835137	0.002792114	0.27743894	1318.5	27.3	1399.7	30.1	5.80	2.07%	1355.8	17.7	concordant
50DTB19-MM - 23.d	1086.575529	13465.13156	0.0806955	5.594291096	0.2519775	0.080517306	0.002742493	0.36660062	1060.2	22	1208.8	33.5	12.29	2.08%	1111	15.6	discordant
50DTB19-MM - 24.d	1667.494576	31288.05416	0.053294927	4.743239486	0.2451099	0.083331005	0.002602491	0.07820986	1233.2	29	1276.1	30.4	3.36	2.35%	1253.6	20.5	concordant
50DTB19-MM - 25.d	1646.347118	48710.15023	0.033798851	4.573412886	0.2096654	0.086968685	0.002650611	0.42746681	1274.8	26.5	1358.9	29.4	6.19	2.08%	1313.8	15.2	concordant
50DTB19-MM - 4.d	1453.589546	42248.0304	0.03440609	4.365755252	0.1877013	0.088497484	0.002773528	0.40302889	1329.5	25.8	1392.4	30.1	4.52	1.94%	1357.5	15.4	concordant
50DTB19-MM - 5.d	1136.065558	40981.17005	0.027721648	4.436742794	0.2097329	0.086108746	0.002706487	0.45897149	1310.3	28	1339.8	30.4	2.20	2.14%	1324.2	15.3	concordant
50DTB19-MM - 6.d	884.3966102	19128.41369	0.046234707	4.836414094	0.2276647	0.085715562	0.002761247	0.06032845	1211.6	26	1330.9	31.2	8.96	2.15%	1259.6	20.5	discordant
50DTB19-MM - 7.d	1465.712704	30187.77596	0.048553186	4.31276801	0.2013306	0.091173534	0.003122713	-0.180452	1344.3	28.3	1449.4	32.6	7.25	2.11%	1385.6	24.7	discordant
50DTB19-MM - 8.d	1702.587633	13143.45588	0.12953881	5.140958645	0.2316597	0.078900528	0.00267989	0.19734399	1145.8	23.7	1168.7	33.6	1.96	2.07%	1154	17.6	concordant
50DTB19_MM																	
51DTB19_MM																	
51DTB19-MI - 7.d	1280.851104	28551.74114	0.0448607	4.217895357	0.189018	0.084674502	0.002491848	0.28112403	1371.5	27.7	1307.2	28.6	-4.92	2.02%	1340.1	16.6	concordant
51DTB19-MI - 8.d	1150.017422	58804.29208	0.019556692	4.447949923	0.2057656	0.083642932	0.002807426	0.37098518	1307.3	27.4	1283.4	32.7	-1.86	2.10%	1296.9	16.6	concordant
51DTB19-MI - 1.d	1911.984162	24180.54686	0.079071171	4.436692096	0.2075336	0.08420216	0.002465183	-0.1411876	1310.3	27.7	1296.4	28.5	-1.07	2.11%	1303.5	21.1	concordant
51DTB19-MI - 6.d	771.4424008	68881.47006	0.011199564	4.214633743	0.1965736	0.086952243	0.002808762	-0.0393661	1372.5	28.8	1358.6	31.1	-1.02	2.10%	1366.1	21.4	concordant
51DTB19-MI - 9.d	1184.620448	30503.18391	0.038835961	4.230957044	0.1914568	0.087599506	0.00245129	0.12632067	1367.7	27.9	1372.9	26.9	0.38	2.04%	1370.4	18.1	concordant
51DTB19-MIc - 4.d	1892.132911	28363.62093	0.06670985	4.459123305	0.2053527	0.084879796	0.002349037	0.0144034	1304.3	27.2	1311.9	26.8	0.58	2.09%	1308.2	19	concordant
51DTB19-MIc - 10.d	2507.247867	21670.88877	0.115696587	4.53762172	0.2473718	0.084076426	0.002335137	0.0614161	1283.9	31.7	1293.4	27	0.73	2.47%	1289.4	20	concordant
51DTB19-MIc - 6.d	3740.247221	25081.83906	0.14912173	4.531062463	0.1969124	0.084291767	0.00217786	-0.0392977	1285.6	25.3	1298.4	25.1	0.99	1.97%	1292	18.3	concordant
51DTB19-MI - 4.d	3657.699839	26014.38968	0.140602946	4.643235131	0.2238578	0.083557706	0.002449412	0.09822512	1257.3	27.5	1281.4	28.6	1.88	2.19%	1269	19	concordant
51DTB19-MIr - 2.d	6732.378369	21806.44468	0.308733426	6.002433481	0.2762309	0.073570986	0.001958195	0.00240785	993.3	21.2	1028.8	26.9	3.45	2.13%	1006.8	16.9	concordant
51DTB19-MIc - 2.d	1275.016638	20907.80446	0.060982809	4.345427809	0.2079884	0.088121859	0.002595401	-0.2442849	1335.2	28.9	1384.3	28.3	3.55	2.16%	1360.1	23.2	concordant
51DTB19-MIc - 7.d with links	5865.881443	21488.38193	0.272979206	5.02571933	0.2370648	0.081507637	0.002184827	-0.0928056	1169.8	25.2	1232.8	26.3	5.11	2.15%	1199.5	19.7	concordant
51DTB19-MI - 5.d	1352.311006	57117.41999	0.023675982	4.610409964	0.2143991	0.085994331	0.002548066	0.27175722	1265.5	26.7	1337.2	28.6	5.36	2.11%	1299.3	17.1	concordant
51DTB19-MIc - 1.d	1706.477819	23206.99228	0.073532916	4.857756777	0.2617992	0.084372438	0.002996304	-0.2630748	1206.7	29.7	1300.3	34.5	7.20	2.46%	1241.6	27	concordant
51DTB19-MIc - 3.d	4904.560336	24355.66401	0.201372475	5.933732275	0.2965648	0.075643355	0.002308845	0.03630766	1004	23.2	1084.7	30.6	7.44	2.31%	1033	19	concordant
51DTB19-MM - 1.d	2496.902823	51744.27278	0.04825467	4.197546876	0.1905833	0.087273951	0.002431613	0.28180578	1377.5	28.2	1365.7	26.8	-0.86	2.05%	1371.4	16.4	concordant
51DTB19-MM - 10.d	1157.692472	66781.05302	0.017335643	4.207370108	0.193013	0.086952741	0.002725437	0.38379298	1374.6	28.4	1358.6	30.2	-1.18	2.07%	1367	16.2	concordant
51DTB19-MM - 11.d	1844.230665	36258.65764	0.050863181	4.421777515	0.2097176	0.086584729	0.002510861	0.36162503	1314.3	28.2	1350.4	28	2.67	2.15%	1332.5	16	concordant
51DTB19-MM - 13.d with links	5253.346235	28549.68922	0.184007125	4.593131752	0.2215054	0.084935542	0.002236151	-0.0493787	1269.8	27.8	1313.2	25.5	3.30	2.19%	1293.4	19.6	concordant
51DTB19-MM - 14.d	4932.239261	24545.81964	0.200940092	4.596690881	0.2122059	0.083927069	0.002093207	0.38226486	1268.9	26.6	1290	24.3	1.64	2.10%	1280.2	14.2	concordant
51DTB19-MM - 15.d	1816.920232	62059.94373	0.029276859	4.126960881	0.1877297	0.088196169	0.002423598	-0.0179777	1398.7	28.6	1385.9	26.4	-0.92	2.04%	1391.8	19.5	concordant
51DTB19-MM - 16.d	1074.957889	53692.87755	0.020020493	4.010598088	0.1878223	0.087017054	0.002563868	0.33255666	1435.1	30.1	1360	28.4	-5.52	2.10%	1395.9	16.6	concordant
51DTB19-MM - 18.d	3724.147682	48117.34302	0.077397201	4.560595662	0.2300733	0.086994939	0.002433717	0.57637608	1278	29.2	1359.5	27	5.99	2.28%	1321.1	13.1	concordant
51DTB19-MM - 19.d	966.8692601	46662.33707	0.020720549	4.163780842	0.1838324	0.087290697	0.002397271	-0.1791609	1387.6	27.6	1366.1	26.4	-1.57	1.99%	1376.2	20.5	concordant
51DTB19-MM - 2.d with links	1134.7832	80929.58961	0.014021858	4.353901404	0.2065861	0.087857762	0.002663551	-0.0466538	1332.8	28.6	1378.5	29.1	3.32	2.15%	1355	21.3	concordant
51DTB19-MM - 21.d	1982.788675	29985.03999	0.066125931	4.195576016	0.179599	0.086073356	0.002300885	0.19475469	1378.1	26.6	1339	25.8	-2.92	1.93%	1358.1	16.4	concordant
51DTB19-MM - 24.d	3118.428819	30919.63582	0.100855936	4.625682465	0.2169743	0.083141442	0.002176348	0.06930663	1261.7	26.9	1271.7	25.5	0.79	2.13%	1266.9	17.9	concordant
51DTB19-MM - 27.d	3602.351476	43621.98966	0.08258109	4.412011509	0.2220432	0.084892162	0.002759281	0.0575961	1316.9	30	1312.2	31.5	-0.36	2.28%	1314.7	21.1	concordant
51DTB19-MM - 28.d	2722.676529	32916.08715	0.08271568	4.877917404	0.2298939	0.082705824	0.002215152	0.05807296	1202.2	25.8	1261.4	26.2	4.69	2.15%	1231.3	18.3	concordant
51DTB19-MM - 29.d	1032.847277	51343.10692	0.020116571	4.211684369	0.1989507	0.088126323	0.002661048		1373.3	29.2	1384.4	29	0.80	2.13%	1378.9	20.7	concordant
51DTB19-MM - 3.d	2041.804882	55749.58815	0.036624573	4.387362957	0.2056458	0.087524244	0.002443996	0.49616469	1323.6	28	1371.2	26.9	3.47	2.12%	1348.2	13.9	concordant
51DTB19-MM - 30.d	1708.048744	24822.82848	0.068809594	4.14371428	0.1868522	0.086029696	0.002264873	0.28309414	1393.6	28.3	1338	25.4	-4.16	2.03%	1363.6	15.8	concordant
51DTB19-MM - 4.d with links	4018.176374	24241.64649	0.165755093	5.83022153	0.2713176	0.073696022	0.001919273	0.09924935	1020.5	22	1032.2	26.3	1.13	2.16%	1025.4	16.1	concordant
51DTB19-MM - 5.d	1324.660658	42594.44904	0.031099373	4.165834958	0.1884651	0.087885967	0.00258371	-0.1292374	1386.9	28.2	1379.1	28.3	-0.57	2.03%	1383	21.1	concordant
51DTB19-MM - 6.d	1344.770045	64128.27298	0.020970003	4.282036192	0.1973912	0.086568451	0.0025508	-0.002953	1353	28.1	1350	28.4	-0.22	2.08%	1351.5	20	concordant
51DTB19-MM - 7.d	1818.978654	72207.76505	0.025190901	4.689473983	0.2297429	0.084078095	0.002733896	-0.0736903	1246.1	27.8	1293.5	31.6	3.66	2.23%	1266.2	22.1	concordant
51DTB19-MM - 8.d	2152.110801	56250.61735	0.038259328	4.149328849	0.1963701	0.086179029	0.002429748	0.08542695	1391.9	29.6	1341.3	27.2	-3.77	2.13%	1364.6	18.9	concordant
51DTB19-MM - 9.d	1547.838499	42836.3971	0.036133723	4.194204358	0.203672	0.086140287	0.002360076	-0.2051485	1378.5	30.1	1340.5	26.5	-2.83	2.18%	1356.4	21.5	concordant
51DTB19-MI - 3.d	1257.8509	31131.21133	0.040404817	3.898101841	0.1847832	0.085635686	0.002384689	-0.126796	1472.1	31.2	1329.1	26.9	-10.76	2.12%	1388.6	20.6	discordant
51DTB19-MIr - 1.d	1122.161735	28322.10755	0.039621406	3.996746568	0.1888734	0.085255255	0.002464353	0.08037108	1439.5	30.5	1320.5	28	-9.01	2.12%	1375.2	19.1	discordant
51DTB19-MIc - 5.d	1321.533779	35753.52848	0.036962332	4.054067338	0.1841486	0.084947686	0.002383308	-0.1679886	1421.3	29	1313.5	27.2	-8.21	2.04%	1362.8	20.5	discordant
51DTB19-MI - 2.d	4099.206822	29754.1479	0.137769256	4.941806142	0.2200011	0.083798193	0.002094717	0.07515324	1188	24.1	1287	24.3	7.69	2.03%	1236.8	17.2	discordant
51DTB19-MM - 17.d with links	4742.719108	20423.51481	0.232218556	5.693543598	0.2632091	0.07775683	0.002126859	-0.1069501	1043.1	22.3	1139.8	27.2	8.48	2.14%	1079	19.3	discordant
51DTB19-MM - 20.d	2395.505639	8763.077393	0.273363515	6.282057731	0.3011351	0.075074599	0.002141651	-0.0072584	952.2	21.2	1069.6	28.7	10.98	2.23%	991.2	18.4	discordant
51DTB19-MM - 23.d	1925.16152	22704.97117	0.084790309	5.408332202	0.26041	0.081208279	0.002379313	0.04863146	1093.7	24.2	1225.6	28.8	10.76	2.21%	1147.1	19.3	discordant
51DTB19-MM - 25.d	1440.712916	22941.89088	0.062798351	5.389037894	0.2675691	0.086479281	0.002912519	0.44469717	1097.3	25	1348	32.5	18.60	2.28%	1198.9	16.2	discordant
59DTB19_MM																	
59DTB19-MI - 6.d	2484.180791	33880.19791	0.073322499	5.128918922	0.2321674	0.077280732	0.002305627	0.10398317	1148.3	23.8	1127.5	29.7	-1.84	2.07%	1139.9	17.5	concordant
59DTB19-MI - 4.d	2023.512188	32628.90473	0.06201594	5.121344424	0.2507564	0.078192134	0.002345858	0.00185867	1149.8	25.8	1150.9	29.8	0.10	2.24%	1150.3	19.5	concordant
59DTB19-MM - 2.d	764.490199	20009.42844	0.038206499	4.402873885	0.2105814	0.085507438	0.003756936	-0.1111375	1319.4	28.5	1326.2	42.5	0.51	2.16%	1321.4	24.9	concordant
59DTB19-MI - 2.d	2303.942419	28662.83071	0.08038084	5.289933418	0.239652	0.077770294	0.002238005	-0.0451755	1116.2	23.2	1140.1	28.6	2.10	2.08%	1125.5	18.7	concordant
59DTB19-MM - 1.d	2839.100394	30738.45859	0.092363135	5.603498191	0.2500553	0.076184182	0.002039504	0.03744231	1058.6	21.8	1099	26.8	3.68	2.06%	1074.6	16.9	concordant
59DTB19-MI - 5.d	1807.105302	41491.05454	0.043554094	4.410763501	0.2051479	0.087580481	0.002389291	0.08770338	1317.3	27.7	1372.4	26.2	4.01	2.10%	1346.2	18.5	concordant
59DTB19-MI - 3.d	1663.813151	9322.64991	0.178469981	5.013153856	0.2514519	0.085124186	0.002487585	-0.1347907	1172.5	26.9	1317.5	28.3	11.01	2.29%	1238	22.7	discordant
59DTB19-MM - 3.d	983.438299	25456.14626	0.038632646	5.425888002	0.2875774	0.101809905	0.003582696	0.34886193	1090.4	26.6	1656.5	32.6	34.17	2.44%	1312.4	21.4	discordant

Appendix D4.5: Monazite U/Pb Standards

Spot ID	238U conc.	232Th conc.	Isotopic Ratios					Apparent Ages - Calculated in Isoplot R (Ma)				Discord	error %	Concordia Age - Calcuated in Isoplot R		Concordant within uncertainties?
	ppm	ppm	238U/206Pb	±2σ PROP	207Pb/206Pb	±2σ PROP	rho	238U/206Pb	±2σ PROP	207Pb/206Pb	±2σ PROP	(7/6-6/8)/7/6 *100		Age	±2σ PROP	
MZ_44069new																
44069 - 1.d	3243.518804	24978.56992	14.76711698	0.6645592	0.05476356	0.002258687	0.16386281	422.39	9.2	401.6	46.2	-5.18	2.18%			
44069 - 2.d	3251.196098	24977.28417	14.72054635	0.6778399	0.056093504	0.001722317	0.33528169	423.69	9.44	455.1	34.1	6.90	2.23%			
44069 - 3.d	3251.690787	24976.95095	14.69413699	0.6410222	0.054589327	0.001722874	0.19579051	424.42	8.96	394.4	35.4	-7.61	2.11%			
44069 - 4.d	3250.187346	24974.03055	14.7118746	0.6719385	0.054584742	0.002207566	0.28975646	423.93	9.37	394.2	45.4	-7.54	2.21%			
44069 - 5.d	3254.043414	24983.68745	14.74280857	0.6516427	0.055735617	0.001832215	0.36292596	423.07	9.05	440.9	36.6	4.04	2.14%			
44069 - 6.d	3249.089667	24961.08752	14.68803477	0.6672523	0.056028678	0.001954879	0.23786607	424.59	9.33	452.5	38.7	6.17	2.20%			
44069 - 7.d	3253.159618	25016.10892	14.61787127	0.6362738	0.054302245	0.001748718	0.40278567	426.57	8.98	382.6	36.2	-11.49	2.11%			
44069 - 8.d	3251.326617	24966.28887	14.76587432	0.6729929	0.055400366	0.001812094	0.04533965	422.43	9.32	427.4	36.5	1.16	2.21%			
44069 - 9.d	3250.328844	24985.30308	14.66056393	0.6182894	0.056064741	0.001834884	0.45623385	425.36	8.68	453.9	36.3	6.29	2.04%			
44069 - 10.d	3251.170187	24973.18726	14.74671192	0.6853422	0.055151767	0.002010633	0.39557211	422.96	9.51	417.4	40.7	-1.33	2.25%			
44069 - 11.d	3250.487202	24977.77486	14.69312724	0.6621168	0.055642112	0.002070614	0.33869222	424.45	9.26	437.1	41.4	2.89	2.18%			
44069 - 12.d	3251.483473	24975.1621	14.76443967	0.6843693	0.054871708	0.001759531	0.10402454	422.47	9.48	406	35.9	-4.06	2.24%			
44069 - 13.d	3250.527148	24980.60205	14.73255617	0.6445546	0.055623415	0.001999831	0.29631053	423.35	8.96	436.4	40	2.99	2.12%			
44069 - 14.d	3251.520411	24978.71231	14.66556404	0.6814878	0.055161611	0.001947405	0.24097567	425.22	9.56	417.8	39.4	-1.78	2.25%			
44069 - 15.d	3250.624466	24972.66919	14.69709028	0.6494291	0.055146073	0.001884323	0.39321707	424.34	9.07	417.1	38.2	-1.74	2.14%			
44069 - 16.d	3251.079071	24978.82057	14.63180304	0.6489698	0.054626821	0.001927496	0.39673366	426.17	9.15	396	39.6	-7.62	2.15%			
44069 - 17.d	3250.971754	24974.27677	14.73968645	0.6530249	0.055849394	0.001802246	0.28691504	423.15	9.07	445.4	35.9	5.00	2.14%			
MZ_Managotry																
manangotry - 1.d	2445.312646	156050.9537	10.90078637	0.492967	0.056578176	0.002116638	0.35592706	565.8	12.2	474.1	41.4	-19.34	2.16%			
manangotry - 2.d	1166.417887	93821.71826	11.10473644	0.4987602	0.059845837	0.00229602	0.0744909	555.8	12	597	41.6	6.90	2.16%			
manangotry - 3.d	1131.701632	113970.2089	11.17939022	0.5366315	0.06125878	0.002942554	-0.0919098	552.3	12.7	647.4	51.6	14.69	2.30%			
manangotry - 4.d	1308.763436	100317.2888	10.97415886	0.4495898	0.059474873	0.002211065	0.22781197	562.2	11	583.5	40.4	3.65	1.96%			
manangotry - 5.d	1039.194201	95102.89381	10.84982796	0.5057053	0.060194409	0.002352375	0.19378394	568.3	12.7	609.6	42.2	6.77	2.23%			
manangotry - 6.d	1538.781399	97030.14176	10.71696787	0.4754001	0.057562647	0.002189983	0.26911434	575.1	12.2	512.2	41.8	-12.28	2.12%			
manangotry - 7.d	1415.802273	193833.1438	11.00542991	0.5013939	0.060754697	0.002237869	0.39214022	560.6	12.2	629.6	39.7	10.96	2.18%			
manangotry - 8.d	1286.34326	113460.9615	11.10733946	0.4862088	0.058595331	0.002180442	0.17325293	555.7	11.7	551.1	40.6	-0.83	2.11%			
manangotry - 9.d	1455.920712	98267.54296	10.95049834	0.4984727	0.058776721	0.002248044	-0.0335608	563.3	12.3	557.9	41.7	-0.97	2.18%			
manangotry - 10.d	1406.031681	114848.756	10.91794175	0.4906137	0.055993257	0.002033949	0.28595143	564.9	12.2	451.1	40.3	-25.23	2.16%			
MZ_Stern																
stern - 1.d	4716.046586	66468.49277	11.96981284	0.5357428	0.056965475	0.001837118	0.21543503	517.2	11.1	489.2	35.6	-5.72	2.15%			
stern - 2.d	2695.972093	45306.58894	12.14514133	0.5385654	0.056889079	0.00183533	0.36780162	510.1	10.9	486.2	35.6	-4.92	2.14%			
stern - 3.d	3099.608252	48193.68877	12.02859804	0.5252223	0.057185912	0.001854031	0.26784599	514.8	10.8	497.7	35.7	-3.44	2.10%			
stern - 4.d	4784.554034	58795.04501	12.51354096	0.5471657	0.059371715	0.001993613	0.35571988	495.6	10.4	579.8	36.5	14.52	2.10%			
stern - 5.d	2284.324366	55914.94354	12.24088752	0.5662068	0.057332485	0.001778314	0.3996708	506.2	11.3	503.4	34.1	-0.56	2.23%			
stern - 6.d	3922.771542	71201.66831	12.04932215	0.5560998	0.057977281	0.001847418	0.38769498	514	11.4	527.9	34.9	2.63	2.22%			
stern - 7.d	2264.310716	39018.8655	12.20889671	0.5471817	0.057798501	0.001732318	0.46948958	507.5	10.9	521.1	32.9	2.61	2.15%			
stern - 8.d	2276.055191	53268.36894	11.94280232	0.5559893	0.056848146	0.001742985	0.30553073	518.4	11.6	484.7	33.8	-6.95	2.24%			
stern - 9.d	3179.408078	40654.60829	12.20205657	0.5491742	0.056639385	0.001821438	0.14391386	507.8	11	476.5	35.6	-6.57	2.17%			
stern - 10.d	3490.870842	46554.55204	12.01037183	0.5504661	0.056924917	0.001766215	0.19372435	515.6	11.4	487.6	34.2	-5.74	2.21%			
stern - 11.d	4318.883506	58544.67977	11.97128549	0.546125	0.058113212	0.001946219	0.25752547	517.2	11.3	533	36.7	2.96	2.18%			
stern - 12.d	3071.227963	91315.0855	12.19984235	0.5754622	0.057421818	0.001913389	0.27396409	507.9	11.5	506.8	36.6	-0.22	2.26%			
stern - 13.d	4199.287745	64532.97244	12.37691231	0.5734718	0.058516	0.00181575	0.18724364	500.9	11.2	548.2	33.9	8.63	2.24%			
stern - 14.d	3293.235653	58119.96669	12.34411226	0.5587759	0.058570247	0.002039494	0.50838357	502.2	10.9	550.2	38	8.72	2.17%			
stern - 15.d	4037.241764	63071.78953	12.04590793	0.550722	0.057407196	0.001736523	0.24110713	514.1	11.3	506.2	33.3	-1.56	2.20%			
stern - 16.d	3463.582117	47747.9531	12.28313599	0.579812	0.056744284	0.001743046	-0.0269402	504.5	11.5	480.6	33.9	-4.97	2.28%			
stern - 17.d	3320.348842	55247.58251	11.95139021	0.5453493	0.05588305	0.001799791	0.25182869	518	11.4	446.7	35.8	-15.96	2.20%			

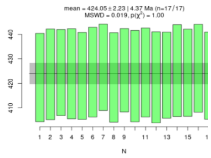

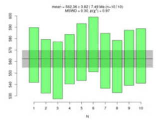

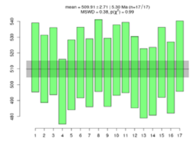

Appendix D4.6: Apatite U/Pb Results

Spot ID	238U conc.	±2σ INT	232Th conc.	±2σ INT	LA-ICP-MS Isotopic Ratios				
	ppm		ppm		238U/206Pb	±2σ PROP(2%)	207Pb/206Pb	±2σ PROP(2%)	rho
49DTB19-AM									
49DTB19-AM - 1.d	16.16910767	3.228772921	6.266060947	1.83720746	4.293569588	0.21663715	0.488298043	0.02127382	-0.167226571
49DTB19-AM - 3.d	0.028394951	0.037877737	0.002204098	0.011649757	0.058712115	0.011367308	0.874556964	0.042604669	0.006547696
49DTB19-AM - 4.d	35.1598577	7.146182393	37.5109583	7.157249245	4.950247987	0.224116394	0.412430588	0.015954654	-0.227660892
49DTB19-AM - 5.d	24.23391162	11.39616167	44.62092556	28.20789548	3.402707272	0.164162408	0.534504057	0.019654907	-0.236544666
49DTB19-AM - 6.d	24.86574051	5.69960188	17.43436269	3.145521581	4.161335316	0.179802944	0.48185622	0.017159251	0.380247864
49DTB19-AM - 7.d	3.313193842	1.310232909	0.535579031	0.421344579	0.812581735	0.048005138	0.810603114	0.033549295	0.173599725
49DTB19-AM - 8.d	41.5663909	5.399168233	62.71821622	10.36190696	4.953794319	0.207791613	0.405398136	0.01312726	0.206359263
49DTB19-AM - 9.d	30.87608627	5.824303489	17.38068957	5.087780567	4.838783016	0.205660979	0.447947609	0.014795148	0.337125431
49DTB19-AM - 10.d	17.34533631	12.84427607	30.8301396	20.66744351	3.264803664	0.187252048	0.572643098	0.021605858	-0.390443628
49DTB19-AM - 11.d	12.38677357	2.861355745	8.093189264	3.860958982	2.876571339	0.14481904	0.616686097	0.023248286	-0.111916185
49DTB19-AM - 16.d	4.422098035	4.958586231	0.789597818	1.482665242	1.192635159	0.101630077	0.742946516	0.032634135	-0.55514932
49DTB19-AM - 17.d	4.46554985	1.154423546	0.925480296	0.495292322	1.474176564	0.076262964	0.775376638	0.028424385	0.353871563
49DTB19-AM - 18.d	7.844615223	1.371272965	1.533876357	0.495189772	1.979072812	0.091506875	0.684435325	0.025028344	0.197917347
49DTB19-AM - 20.d	55.40247874	3.366806374	26.59298814	2.167576033	6.488591998	0.276501034	0.31068006	0.011427432	0.18238594
49DTB19-AM - 23.d	16.96791556	4.232193846	17.03223669	4.245602353	4.962218674	0.314781042	0.384645924	0.029005469	0.376476478
49DTB19-AM - 26.d	39.53071567	1.954011549	11.58922897	1.461058333	5.898956582	0.321502697	0.402990937	0.020328634	0.633787718
49DTB19-AM - 27.d	7.88623735	0.995867764	11.59720547	2.403037098	2.1919273	0.105474497	0.700490514	0.026869967	0.417499922
49DTB19-AM - 28.d	6.617566598	1.013370613	10.31899021	7.983077081	1.832010397	0.080841571	0.710425273	0.02441106	0.454407317
49DTB19-AM - 29.d	2.660713848	1.142757859	0.985311425	0.684239342	1.099711545	0.052809202	0.783077506	0.031129599	0.282704629
49DTB19-AM - 34.d	40.40172903	26.76539095	34.61111615	18.00930045	5.329109297	0.274842196	0.37270256	0.015044608	-0.538995655
49DTB19-AM - 35.d	97.54443104	27.82530835	89.90986547	17.28400687	7.531196467	0.317133765	0.255205325	0.009754442	0.012412085
49DTB19-AM - 37.d	2.320421023	0.495235113	0.36166923	0.583560738	0.738672212	0.037259502	0.797675041	0.028653981	0.237336767
49DTB19-AM - 38.d	5.20366824	1.615177416	9.566973263	3.875009661	1.405846019	0.071773112	0.741778976	0.026348777	0.14050001
49DTB19-AM - 39.d	4.134693337	1.69243573	0.435014242	0.251418593	1.00631578	0.08282848	0.76900225	0.037557042	0.224159471
49DTB19-AM - 40.d	3.977711821	0.970530998	1.669056205	0.376936679	1.579743305	0.087958993	0.709948434	0.042155589	0.363020091
49DTB19-AM - 42.d	2.759235582	0.569137949	0.40528838	0.196136214	0.884217743	0.041836714	0.797532582	0.029914831	0.404813914
49DTB19-AM - 43.d	3.024803457	1.101797385	0.475645798	0.332707673	0.899636334	0.043958646	0.778552831	0.029253909	0.334752933
49DTB19-AM - 44.d	2.189912805	0.331930743	0.202977389	0.117415242	0.711750247	0.032202278	0.825261038	0.029125107	0.466622987
49DTB19-AM - 45.d	0.759742772	1.533187956	0.192473296	0.133839369	0.358722727	0.033403995	0.877364134	0.033199385	-0.023345483
49DTB19-AM - 47.d	8.002808886	3.317626745	2.76381119	1.539251774	2.441126389	0.144055525	0.716564917	0.027652825	-0.192531677
49DTB19-AM - 48.d	8.009797223	2.306173947	2.192078268	0.877541029	2.157780902	0.099991452	0.684090695	0.025348241	0.382758257
49DTB19-AM - 49.d	2.21127492	0.490144441	0.188606164	0.112240316	0.708572015	0.033293332	0.813088479	0.02876897	0.458048492
49DTB19-AM - 51.d	5.650497929	3.531511664	2.286983497	1.879816372	1.618933328	0.098290714	0.710293608	0.026313466	-0.190383613
49DTB19-AM - 54.d	2.138071423	0.846693215	0.535140353	0.388933385	0.932605352	0.049256498	0.826568355	0.031603676	0.225986575
49DTB19-AM - 55.d	0.16250941	0.410881777	0.053935607	0.092214278	0.113915387	0.012375797	0.865993985	0.033137099	-0.114124128
49DTB19-AM - 57.d	4.596504364	1.071078561	0.41573973	0.158629467	1.185474173	0.054529918	0.758515044	0.027300229	0.379857184
49DTB19-AM - 59.d	1.448022703	1.190721116	0.171192939	0.146946523	0.74076446	0.148567505	0.789565486	0.052709707	0.252151135
49DTB19-AM - 60.d	2.859299225	1.576529035	1.563867619	1.309063077	0.696500915	0.043383845	0.826239706	0.028438251	-0.031278173
51DTB19-AM									
51DTB19-AM - 1.d	11.63337735	1.838209317	0.181500918	0.122528037	12.0360767	0.593185029	0.485117918	0.028135488	0.628914966
51DTB19-AM - 2.d	11.08094902	1.519430046	0.166653133	0.112339602	10.75361512	0.55723492	0.484503926	0.026266115	0.537198453
51DTB19-AM - 3.d	38.66091604	25.27232851	1.84309789	1.64265776	31.17923337	2.041284779	0.377177192	0.022447156	-0.290348763
51DTB19-AM - 4.d	12.6407077	1.468906989	0.186399311	0.121181734	12.79876451	0.63722049	0.473141703	0.027402197	0.666565283
51DTB19-AM - 5.d	12.38942254	1.749026887	0.188311922	0.136200604	12.40007895	0.665336755	0.468513512	0.026533946	0.648347781
51DTB19-AM - 6.d	26.38524325	8.312223494	1.142003183	0.627447792	20.31769523	1.07999912	0.398411968	0.023442412	0.609023037
51DTB19-AM - 8.d	12.39909607	1.947046842	0.203632665	0.129524166	13.45942058	0.669176784	0.488435155	0.029163031	0.643008786
51DTB19-AM - 9.d	18.38178909	2.61017016	2.283947606	2.586075828	7.883203441	0.418303792	0.333204513	0.018003047	0.531279462
51DTB19-AM - 10.d	14.20209589	9.539038898	0.543876731	0.888421203	8.63300039	0.543252475	0.342459628	0.027423568	0.843829799
51DTB19-AM - 11.d	53.07738374	12.68973276	3.000203205	0.89146889	37.57886428	1.901888	0.349380606	0.021186246	0.573507752
51DTB19-AM - 12.d	14.32441191	1.801157289	0.313722737	0.142087392	12.97940644	0.654577166	0.449755891	0.030135283	0.628143022
51DTB19-AM - 13.d	1.711416455	0.774491747	0.170134835	0.134644359	2.222645169	0.164614246	0.579811199	0.047098658	0.123485308
51DTB19-AM - 14.d	14.41994248	4.017609207	0.277769654	0.151655781	13.85686583	0.686315639	0.383897829	0.023009017	0.522138555
51DTB19-AM - 15.d	13.19935902	2.196970995	0.332629224	0.166748703	8.977825711	0.434530803	0.390441418	0.019247796	0.201013219
51DTB19-AM - 16.d	12.6866107	1.648231646	0.246843115	0.12818073	14.17486392	0.738086297	0.52007184	0.029089544	0.686642329
51DTB19-AM - 17.d	28.8411892	6.801183734	1.260383354	0.49938882	23.69730279	1.321194486	0.354471345	0.023700553	0.541465246
51DTB19-AM - 18.d	6.828717745	0.89552495	0.141315931	0.114727492	6.355256257	0.5156394	0.368161124	0.039177434	0.654620991
51DTB19-AM - 19.d	16.96177443	2.670647649	0.286778032	0.148782958	8.959948174	0.402016546	0.255308401	0.012967921	0.415605779
51DTB19-AM - 20.d	8.081757339	1.806223991	0.271490946	0.140842601	8.075619726	0.429905412	0.534254435	0.041101589	0.481412238
51DTB19-AM - 21.d	17.17863222	4.708266543	0.324602344	0.230763209	18.08338159	1.001917432	0.429315223	0.024508594	0.482138384
51DTB19-AM - 24.d	16.79203442	3.363584913	0.79767868	0.847637425	15.93427279	0.91476153	0.487302844	0.030709424	0.572430237
51DTB19-AM - 25.d	18.50754991	13.62317765	0.660555221	0.892218897	16.57044916	1.134779324	0.427088332	0.026877877	0.115155444
51DTB19-AM - 26.d	10.22652771	7.291678444	0.545941639	0.35214014	11.16766457	0.839485714	0.393858643	0.038657859	-0.151090845
51DTB19-AM - 28.d	16.33664943	6.905920978	0.440554824	0.479740606	16.36326173	0.993346494	0.422167628	0.029920958	0.4824416
51DTB19-AM - 29.d	13.74598607	1.21326282	0.198223237	0.109510322	12.75438979	0.670081852	0.449218785	0.030758927	0.681163106
51DTB19-AM - 31.d	16.62415615	4.755789044	0.806267775	0.854156591	10.40401002	0.557560817	0.40469445	0.036437574	0.170377467
51DTB19-AM - 33.d	13.72950283	2.140597483	0.217766906	0.132032192	13.02237063	0.656293837	0.454686058	0.02439631	0.356879079
51DTB19-AM - 34.d	36.05165866	11.67145678	1.692652205	0.601028385	30.94603359	1.798763087	0.326368788	0.028685367	0.127197221
51DTB19-AM - 36.d	15.03464115	1.672356717	0.261657893	0.137185027	11.66321496	0.551145457	0.363930142	0.019253875	0.455978741
51DTB19-AM - 37.d	1.265000302	1.358552664	0.021722665	0.067163283	3.040177231	0.815794597	0.381107432	0.086858799	0.026081922
51DTB19-AM - 38.d	47.12964903	15.25501588	2.433907133	1.003145982	35.16015939	2.115814178	0.365981891	0.030990955	0.298301448
51DTB19-AM - 39.d	12.81661358	2.751097721	0.228797743	0.144948778	12.82533136	0.621650548	0.452619924	0.025836297	0.570939897
51DTB19-AM - 40.d	16.22657722	2.885202138	0.471525076	0.218719914	9.5074641	0.445135982	0.439264721	0.020897542	0.398327835
51DTB19-AM - 41.d	13.60209683	1.144944532	0.221512102	0.116847447	12.62150377	0.678329886	0.489340136	0.027971801	0.565686273
51DTB19-AM - 42.d	13.03809892	5.284910361	0.29967095	0.296199856	11.0253274	0.594064809	0.406895751	0.02615181	0.677400475
51DTB19-AM - 44.d	4.814738	2.208980842	0.106305979	0.091792572	7.408920574	0.457338003	0.494023457	0.036473013	0.330710004
51DTB19-AM - 45.d	13.22461782	1.834851409	0.20115525	0.13249001	12.62244584	0.613214839	0.453976889	0.024803051	0.51486209
51DTB19-AM - 46.d	0.676049109	1.05514255	0.05136091	0.108584056	1.133825932	0.269581511	0.435483087	0.060411012	-0.25173157
51DTB19-AM - 47.d	12.26149109	4.711928402	0.226931774	0.256185495	10.79509505	0.677666891	0.430185313	0.031999288	0.744677358
51DTB19-AM - 48.d	11.2587776	2.012446058	0.193147292	0.181165804	11.15131982	0.582157978	0.474721271	0.027750062	0.616426628
51DTB19-AM - 49.d	13.97782694	2.07687475	0.281796315	0.249856205	11.917917	0.605264316	0.411505517	0.024624923	0.680593708
51DTB19-AM - 50.d	54.24670164	7.118104185	4.175505444	1.600073516	34.36735598	1.800224406	0.339190758	0.017111393	0.450993634

Appendix D4.6 continued.

Spot ID	238U conc.	±2σ INT	232Th conc.	±2σ INT	LA-ICP-MS Isotopic Ratios				
	ppm		ppm		238U/206Pb	±2σ PROP(2%)	207Pb/206Pb	±2σ PROP(2%)	rho
52DTB19-AM									
52DTB19-AM - 1.d	9.2334247	0.877672555	0.792702702	0.271824098	28.56222961	1.891494129	0.372533945	0.033636146	0.487984445
52DTB19-AM - 2.d	9.993455638	1.918500267	0.51598314	0.19512351	30.14502133	1.88309213	0.381247465	0.03412088	0.593188928
52DTB19-AM - 3.d	13.93637541	1.015543538	0.673978474	0.234163708	41.15623592	2.418169924	0.345263111	0.028519859	0.443112367
52DTB19-AM - 4.d	12.35049477	2.022687834	1.002805303	0.281178973	37.10959604	2.274322351	0.370636039	0.03348441	0.708552934
52DTB19-AM - 5.d	12.33143219	1.017884323	0.616436866	0.188158581	38.65534223	2.372692547	0.351526204	0.032998715	0.60962933
52DTB19-AM - 6.d	15.08364696	4.44601778	0.590215746	0.241874836	63.18714115	4.382742217	0.29137007	0.033451983	0.54818956
52DTB19-AM - 7.d	12.10759867	1.848668388	0.59590315	0.167905257	33.94833266	2.042095154	0.371998128	0.033047152	0.666770984
52DTB19-AM - 8.d	14.86676064	1.902687206	0.74638972	0.189995144	43.97959007	2.793216634	0.311339792	0.029839396	0.578663995
52DTB19-AM - 9.d	10.61557295	1.567492737	0.604603355	0.18413502	31.54609219	1.868025865	0.377399068	0.033699574	0.511051274
52DTB19-AM - 10.d	14.77397792	2.6329433	0.77531378	0.22618509	52.57551215	3.284210254	0.312842399	0.028295198	0.4820629
52DTB19-AM - 11.d	11.38246415	1.062490536	0.666640384	0.207821439	31.34534789	1.891810413	0.355057211	0.030325233	0.61021669
52DTB19-AM - 12.d	11.78630647	1.898152857	0.732657119	0.224117965	32.31999336	1.966385386	0.379015483	0.02995635	0.586915998
52DTB19-AM - 13.d	10.33095822	1.877235825	0.503698151	0.216191683	29.75042128	1.789469667	0.396884655	0.033239531	0.499715699
52DTB19-AM - 14.d	10.53886729	1.028214256	0.50045118	0.192279581	31.54048077	1.815306544	0.409267632	0.034414626	0.544709323
52DTB19-AM - 15.d	9.766312854	1.671508976	0.431542228	0.182301053	33.14414061	2.068221328	0.360092843	0.03545698	0.61200745
52DTB19-AM - 16.d	22.71020434	3.823799755	1.153081681	0.429563135	67.27967822	4.15251096	0.250761103	0.024919808	0.408741689
52DTB19-AM - 17.d	21.6160379	3.294941681	1.967737097	11.30919197	75.72675294	6.724085072	0.201252551	0.024479056	0.532627088
52DTB19-AM - 19.d	10.42081702	2.358135627	0.676253874	0.254850284	31.35578875	1.930267556	0.402219126	0.034251164	0.538273947
52DTB19-AM - 20.d	3.250940763	2.165263618	1.257872147	1.159142558	23.61923107	2.918436487	0.376046511	0.075356774	0.423140235
52DTB19-AM - 21.d	11.81324946	1.27338635	0.551763635	0.169724769	37.63949879	2.352847604	0.337490476	0.031741106	0.615039539
52DTB19-AM - 22.d	15.05766222	1.071620741	1.390489416	0.403789706	49.56656355	3.05571659	0.304171262	0.029041018	0.333552228
52DTB19-AM - 23.d	2.037003353	0.91322981	0.243866534	0.407286397	22.99177448	4.477221573	0.467679578	0.10771887	0.683108189
52DTB19-AM - 24.d	13.45639553	2.515449506	0.853053305	0.651174534	38.85321525	2.347498756	0.336359356	0.025842321	0.306472868
52DTB19-AM - 25.d	9.996475126	1.019726733	0.559204508	0.206412176	31.38682224	2.484960805	0.341739661	0.042139606	0.480937457
52DTB19-AM - 26.d	16.97091987	2.252321129	0.353157794	0.186910535	72.90228271	5.29615969	0.257268884	0.02992772	0.463712597
52DTB19-AM - 27.d	15.09203666	2.212345743	0.491982555	0.205491257	59.9515164	4.050876904	0.2818305	0.036481756	0.70518795
52DTB19-AM - 28.d	16.11843283	2.036075843	0.611740273	0.290152566	66.23714154	4.977305361	0.283194923	0.03847801	0.549941233
52DTB19-AM - 30.d	6.873751765	4.32970566	0.551310211	0.425882686	24.90241181	2.812278332	0.461450571	0.049325063	0.028137857
52DTB19-AM - 31.d	13.29875712	2.834915179	0.921643136	0.498893678	37.21654491	2.173865767	0.363560062	0.030835199	0.563116087
52DTB19-AM - 32.d	15.99974618	3.937639858	0.559892131	0.262968096	69.42649232	4.783253255	0.229616484	0.029853049	0.437737465
52DTB19-AM - 33.d	5.31283197	2.173215973	0.936256795	0.828975071	8.778095656	0.923337478	0.439543836	0.039872438	0.237761018
52DTB19-AM - 34.d	14.22112055	1.60076662	1.691191302	0.324619139	41.71554105	2.57813774	0.321358973	0.031296809	0.630468297
52DTB19-AM - 35.d	14.65550585	1.990457137	1.751759881	0.383932845	44.4459764	2.720113768	0.306967607	0.027590646	0.551919328
52DTB19-AM - 36.d	12.92414496	2.074602234	1.246647184	0.235069505	36.21619115	2.225823725	0.357404116	0.029971125	0.406062937
52DTB19-AM - 37.d	13.58231248	4.708640314	1.457616955	0.581775463	36.24408202	2.664398424	0.40376635	0.036916312	0.294656687
52DTB19-AM - 38.d	16.50824557	2.580938478	1.860994512	0.516558889	40.51516154	2.437109138	0.356102723	0.029073919	0.426034051
52DTB19-AM - 39.d	11.43173784	1.515963045	0.621018802	0.237231398	36.47648174	2.234239165	0.367933349	0.033830603	0.424044583
52DTB19-AM - 41.d	9.769051414	0.85063816	0.928468733	0.261901792	40.42978373	3.438982894	0.322718438	0.039908895	0.451941183
52DTB19-AM - 43.d	13.94849741	4.981209542	0.536458953	0.255273048	44.78650055	3.00201414	0.295084326	0.03198353	0.411103112
52DTB19-AM - 44.d	12.29070431	2.043867717	3.371491702	1.155508795	23.41699546	1.521902717	0.369527496	0.032044114	0.23753612
52DTB19-AM - 45.d	11.16760747	0.973639614	0.45354892	0.163900519	35.48652872	2.184742308	0.363018273	0.032297842	0.524240205
52DTB19-AM - 46.d	19.57774547	1.254771835	1.624554614	0.544969704	55.37813025	3.320886141	0.270192151	0.024593983	0.240811828
52DTB19-AM - 47.d	10.21794226	2.157953091	0.441090124	0.195666675	37.70317874	2.620903615	0.332875216	0.040867343	0.362896294
52DTB19-AM - 48.d	14.25186057	1.535510315	0.888762798	0.308569286	51.26960286	3.528139759	0.288196346	0.028494356	0.604940888
52DTB19-AM - 49.d	17.79443808	2.368519332	1.02765512	0.270691273	56.49326928	3.441404206	0.275507908	0.026101681	0.340148808
52DTB19-AM - 50.d	15.54046019	4.846240467	1.015891329	0.396568686	45.89161013	3.40351671	0.368426115	0.041168881	0.108707805
52DTB19-AM - 51.d	17.65688662	2.641501693	1.230820348	0.292054067	52.35879463	3.214668691	0.293008466	0.026082925	0.503653475
52DTB19-AM - 52.d	8.592927503	1.049887857	0.506676051	0.224783178	28.46390753	2.569757639	0.372487508	0.045660341	0.48310271
52DTB19-AM - 53.d	11.70700657	3.780244211	0.834429483	0.342509768	29.56566617	2.447415592	0.404927849	0.047199424	0.394574072
52DTB19-AM - 54.d	17.77184571	1.936083787	1.09258078	0.32943298	53.82578677	3.439884359	0.311383173	0.03157276	0.675388326
52DTB19-AM - 55.d	27.03414982	4.153987777	0.710411775	0.261585977	70.96164164	4.056771103	0.200552838	0.020839029	0.467750322
52DTB19-AM - 56.d	10.57833113	1.957805269	0.656808566	0.213612356	40.42674122	2.57704149	0.349661356	0.031905751	0.485855907
52DTB19-AM - 57.d	15.67661536	3.101112461	0.992890212	0.29977541	49.57589233	3.073135189	0.301964729	0.027310527	0.35812133
52DTB19-AM - 58.d	12.85315122	2.451671413	1.009589341	0.33805063	40.08013812	2.465532183	0.330694489	0.027850703	0.359367157
52DTB19-AM - 59.d	14.7368052	2.975581515	1.155568703	0.321494547	45.6030354	2.896924236	0.319911126	0.030920485	0.631322852
52DTB19-AM - 60.d	14.15638012	2.174116663	1.072508571	0.315390133	43.4860699	2.768737341	0.342919687	0.03211931	0.605530153
52DTB19-AM - 61.d	19.83750159	2.614094737	1.166120312	0.305894245	59.53454391	4.551549412	0.296425125	0.034220676	0.475684254
52DTB19-AM - 62.d	13.39706582	3.696262232	0.520062126	0.248361937	39.07629306	2.269167489	0.318871961	0.029446431	0.483817186
52DTB19-AM - 63.d	15.9313156	2.137048389	0.853633032	0.283253361	50.06113536	3.1704549	0.321522397	0.030841886	0.587715327
52DTB19-AM - 64.d	17.4124595	9.861731999	1.151592453	0.720766028	52.14572672	3.418028573	0.288818256	0.02696854	0.186193441
52DTB19-AM - 65.d	11.80242006	2.115277572	0.636690614	0.225748425	34.62721491	2.114724648	0.383104117	0.032514305	0.531057318
52DTB19-AM - 66.d	12.22406094	2.260556534	0.95706091	0.389496461	37.08876818	2.356237906	0.34166081	0.03009866	0.438915039
52DTB19-AM - 67.d	10.04370437	1.913464627	0.33837073	0.182373348	31.0194734	2.009651274	0.384283542	0.033178821	0.491394632
52DTB19-AM - 68.d	12.31201767	1.700886071	0.60934692	0.199932621	35.06126885	2.220489507	0.408504633	0.034337426	0.691679299
52DTB19-AM - 69.d	12.5638809	1.479453816	1.063066917	0.320349538	35.58955114	2.090402937	0.371929742	0.031183047	0.46599587
52DTB19-AM - 70.d	5.827220574	1.224022736	1.382032073	0.465458147	17.66395105	1.056744708	0.465025761	0.038692049	0.618481781
52DTB19-AM - 71.d	7.934749121	5.155961367	1.334500585	0.901886987	34.00394194	2.430178665	0.348049847	0.03823278	0.218868956
52DTB19-AM - 77.d	10.64089223	2.757628826	0.500351178	0.253993507	39.47245931	6.052836197	0.406509956	0.068205099	-0.21158126
52DTB19-AM - 78.d	21.93753409	7.134704803	3.27269755	2.096530938	61.37379597	4.339893666	0.273679735	0.050491233	0.423046731
52DTB19-AM - 79.d	14.12626035	1.136431569	8.625367951	5.242485838	37.61489864	3.167736955	0.30390216	0.036913555	0.455930434
52DTB19-AM - 80.d	23.90482362	3.168933173	0.995167923	0.271250137	63.46550104	3.681265604	0.261970492	0.022207133	0.4827701
52DTB19-AM - 81.d	13.43839409	3.959818333	0.631690297	0.20118973	41.82031549	2.694043752	0.344710647	0.029359258	0.515903423
52DTB19-AM - 82.d	10.72976581	1.469949115	0.554777925	0.223787349	32.36447125	2.003585523	0.341062523	0.028823437	0.471817465
52DTB19-AM - 83.d	10.28370104	1.582188246	0.837490985	0.251805118	29.55131238	1.785127131	0.382047738	0.029505231	0.545302249
52DTB19-AM - 84.d	10.85690483	1.665501714	0.825081752	0.233506877	29.02458146	1.624437218	0.40502342	0.030564226	0.583786991
52DTB19-AM - 85.d	10.01181902	1.611367754	0.750866516	0.212883416	28.67620273	1.678248343	0.402926012	0.032657918	0.470013746
52DTB19-AM - 86.d	11.22848694	1.819982572	0.947811856	0.279859757	31.25831413	1.838447563	0.36595696	0.029769755	0.649844787
52DTB19-AM - 87.d	10.53089858	1.605213971	0.584078007	0.20369662	31.44049065	1.960109361	0.382307682	0.033104646	0.542243403
52DTB19-AM - 88.d	9.938355436	1.913116819	0.64871938	0.231665877	26.01910893	1.602907981	0.400897445	0.030657475	0.409542897
52DTB19-AM - 89.d	9.007747073	1.39434909	0.572498309	0.210036857	22.68658491	1.312057857	0.443396646	0.03464436	0.522355768
52DTB19-AM - 90.d	8.971570661	1.393910632	0.65261358	0.443903977	21.61576053	1.300243038	0.481267503	0.038040899	0.652240265
52DTB19-AM - 91.d	8.522707452	1.60994921	0.746328176	0.410844649	23.20573804	1.373486506	0.420387096	0.032374321	0.505990129
52DTB19-AM - 92.d	9.3566715	1.406521153	0.638429274	0.217797173	27.33476578	1.676396168	0.411505028	0.037465005	0.577708135
52DTB19-AM - 93.d	9.853922442	1.53296751	1.001438925	0.449550738	26.90217351	1.585983567	0.36325356	0.030520512	0.496233776
52DTB19-AM - 95.d	16.67735518	1.710541892	0.998276996	0.266586235	46.69040132	2.632095301	0.310194219	0.028567676	0.462100995
52DTB19-AM - 96.d	13.6715593	1.616725007	0.975013406	0.282076254	39.24339604	2.297094731	0.355901169	0.031644555	0.495182874
52DTB19-AM - 97.d	1.865518561	0.806297889	0.535727533	0.342663555	2.702706163	0.219257858	0.480640649	0.053162498	0.439573901
52DTB19-AM - 98.d	21.53320033	2.258097755	0.256082663	0.126201071	76.46498198	5.000920462	0.226776066	0.025404803	0.37106181
52DTB19-AM - 99.d	20.27420168	2.702154089	0.432917653	0.181664561	76.16893603	4.783298102	0.239462829	0.027940744	0.337058698
52DTB19-AM - 100.d	16.68006645	3.529589471	1.976077239	0.379975364	60.11329772	4.962219	0.283315422	0.040031207	0.395098305
52DTB19-AM - 101.d	10.13235631	3.02905677	1.547425474	0.779384787	54.52775483	4.980253002	0.329053909	0.052375813	0.486798501

Appendix D4.6 continued.

Spot ID	238U conc.	±2σ INT	232Th conc.	±2σ INT	LA-ICP-MS Isotopic Ratios				
	ppm		ppm		238U/206Pb	±2σ PROP(2%)	207Pb/206Pb	±2σ PROP(2%)	rho
59DTB19-AM									
59DTB19-AM - 3.d	2.100375956	1.059529902	0.669529051	1.941849255	0.573109155	0.031526071	0.846897153	0.037097102	0.342477266
59DTB19-AM - 5.d	47.55065696	23.83707049	16.17172008	10.69673197	11.10887785	0.577823247	0.761665099	0.027568245	0.262346465
59DTB19-AM - 6.d	15.69484452	2.871855547	3.328329292	0.883944859	3.694394325	0.197600528	0.812970557	0.038330247	0.395519931
59DTB19-AM - 7.d	14.94387542	1.958715543	4.579852699	1.091711434	4.51954255	0.218487203	0.798803624	0.030008436	0.488083952
59DTB19-AM - 8.d	9.029009032	4.305511732	3.165728834	0.731312707	1.783958999	0.109571796	0.788350605	0.02775008	-0.089138318
59DTB19-AM - 11.d	6.666859786	0.697130932	0.665011951	0.251452377	1.778215063	0.080232357	0.82656627	0.028753458	0.267134285
59DTB19-AM - 12.d	3.830627176	0.631219296	0.584815702	0.460232909	1.002414639	0.044364812	0.820260009	0.028713714	0.488900482
59DTB19-AM - 13.d	2.545658497	0.595578444	0.380975309	0.178552553	0.513058147	0.024316728	0.864871706	0.02857143	0.277802176
59DTB19-AM - 14.d	78.29558571	10.41425199	19.25764845	3.378092123	19.5289289	1.094774562	0.689921668	0.030118442	-0.039623436
59DTB19-AM - 15.d	12.83630764	14.34720823	1.982765261	2.575798053	3.603793216	0.438060508	0.797624094	0.030178089	-0.041251072
59DTB19-AM - 16.d	46.03631377	7.393884575	9.992639294	1.741484201	9.743742614	0.448662398	0.752425001	0.027315773	0.212548216
59DTB19-AM - 17.d	4.298995316	0.553136325	0.254690086	0.140991066	1.049594983	0.047766427	0.833266643	0.028777177	0.549898747
59DTB19-AM - 18.d	0.511552	0.844226246	0.709297832	1.091979697	0.514400825	0.03913179	0.804013373	0.041280477	0.027553655
59DTB19-AM - 19.d	17.38700627	20.30129281	3.627053292	4.746371704	4.457879038	0.540470477	0.805392214	0.02903823	-0.194561471
59DTB19-AM - 20.d	4.464957326	0.64863078	1.187109923	1.241259423	1.150912866	0.051606481	0.820940169	0.028528637	0.495618119
59DTB19-AM - 21.d	4.397947328	0.97965997	1.349389922	0.581653537	1.076360913	0.049800528	0.837624853	0.02880475	0.603145481
59DTB19-AM - 22.d	4.041185783	0.586864661	0.293364875	0.151313877	1.143540304	0.05183013	0.826471737	0.029793766	0.534151675
59DTB19-AM - 23.d	0.25005604	0.287652444	0.60658225	0.601348799	0.185487016	0.015998377	0.825148301	0.030709649	0.280115199
59DTB19-AM - 24.d	0.140881417	0.115126337	0.308763203	0.174714698	0.548692384	0.051003792	0.867683466	0.05238088	0.306022853
59DTB19-AM - 25.d	8.270320497	9.511588758	2.757916272	3.23817105	1.580628785	0.170713893	0.811203757	0.028120355	-0.055955419
59DTB19-AM - 26.d	4.70004616	1.116060763	0.927339257	1.209617512	1.256732556	0.05806938	0.81521099	0.028118561	0.514076795
59DTB19-AM - 27.d	3.903283854	2.410472353	2.031855613	1.311597216	0.781287527	0.052448079	0.84226157	0.027716173	0.122227409
59DTB19-AM - 28.d	0.131286612	0.086395366	0.380625364	0.298682672	0.489951563	0.044494522	0.834389486	0.045139994	-0.053743422
59DTB19-AM - 29.d	4.196779027	0.931006125	1.482025228	0.403879699	0.948003064	0.044999791	0.818602528	0.027394478	0.385556599
59DTB19-AM - 30.d	0.25325408	0.298770623	1.447516222	2.439894533	0.425886064	0.035772299	0.802432189	0.038149568	0.311476695
59DTB19-AM - 31.d	3.220871208	0.436069104	0.42730885	0.193284591	1.228116646	0.062958494	0.844664426	0.038329103	0.683763642
59DTB19-AM - 32.d	38.91848368	8.4966695	9.420387672	1.887587974	12.1015058	0.560267077	0.750255768	0.032507869	0.477637411
59DTB19-AM - 33.d	5.091146474	0.980175184	0.494466319	0.221525539	1.272782099	0.058271157	0.846226006	0.029377784	0.557919349
59DTB19-AM - 34.d	0.137691971	0.095418681	0.336704008	0.1532724	0.475312623	0.040284676	0.827518569	0.043025197	0.069807996
59DTB19-AM - 35.d	0.146840053	0.097319341	0.376516113	0.207934338	0.482505705	0.0411005	0.860406536	0.04312096	0.088647212
59DTB19-AM - 36.d	4.24884379	0.897597861	0.300188462	0.156315654	1.235481119	0.05471758	0.847876471	0.030670716	0.476571727
59DTB19-AM - 37.d	12.68450787	3.595076342	2.669431605	0.866623493	3.164958866	0.157495997	0.811776436	0.029643987	0.292118023
59DTB19-AM - 38.d	0.180650755	0.124741281	0.272753959	0.203617272	0.985013968	0.17181587	0.830495729	0.048737807	0.133128098
59DTB19-AM - 39.d	13.28471129	13.64304071	2.129151559	3.002554293	3.462674263	0.399427293	0.825232171	0.029478126	-0.041045393
59DTB19-AM - 40.d	21.28075165	13.57485238	3.810550105	2.718002706	5.075429801	0.352033631	0.806111987	0.027506691	0.189254295
59DTB19-AM - 41.d	0.912220246	0.427250448	0.404320211	0.203466841	0.637893117	0.041937195	0.820481045	0.042801204	0.330419458
59DTB19-AM - 42.d	4.443705769	0.984843463	0.308603998	0.155502246	1.224172726	0.054959129	0.836579325	0.029520175	0.461686424
59DTB19-AM - 43.d	4.187447275	0.839757386	0.48005942	0.196109731	1.143278958	0.052232417	0.843791996	0.032175071	0.713764257
59DTB19-AM - 44.d	16.70765496	3.04767196	4.780379364	1.067062015	3.320918868	0.149182921	0.761976026	0.025179348	0.267852293
59DTB19-AM - 45.d	8.346940927	6.246589192	1.587926892	2.543656841	2.223735084	0.172908645	0.829767447	0.028122685	-0.028486738
59DTB19-AM - 46.d	3.40679711	1.870485595	0.664693028	0.93837602	0.828351697	0.055126988	0.837461763	0.029006884	0.073918256
59DTB19-AM - 47.d	42.86155954	22.17585773	7.964411177	4.429716497	10.04689499	0.713572496	0.778986717	0.027364663	-0.116631294
59DTB19-AM - 48.d	5.663204782	2.519378189	1.529699448	0.710044527	1.453803098	0.086736729	0.802419474	0.029746286	-0.216681604
59DTB19-AM - 49.d	1.824342521	0.687271157	13.77197937	7.47092854	0.333785088	0.016606679	0.749885544	0.025799964	0.151806811
59DTB19-AM - 54.d	16.02916805	1.857272506	2.109981097	0.429272258	3.83702986	0.173087067	0.825514581	0.031987656	0.597227244
59DTB19-AM - 55.d	4.152565259	0.823835252	0.70761448	0.369796444	1.100003443	0.048073681	0.837252807	0.029806763	0.456663359
59DTB19-AM - 59.d	9.441586807	2.788138642	1.086815875	0.71010919	2.639250886	0.153223972	0.813825368	0.029644948	0.075487651
59DTB19-AM - 60.d	9.031587385	1.063698181	3.730986639	3.078036028	2.397326039	0.111538626	0.815859523	0.030381305	0.450063581
59DTB19-AM - 61.d	0.180122057	0.178747804	0.875109757	0.93564961	0.473729912	0.038029883	0.856614913	0.042359269	0.207910285
59DTB19-AM - 62.d	22.45696436	4.64395039	5.140344682	0.974867758	5.429484402	0.295021973	0.804291602	0.02775778	0.211650786
59DTB19-AM - 63.d	3.132496615	1.001669717	1.083413207	0.454104891	0.961694909	0.047723435	0.825496677	0.030613505	0.458086856
59DTB19-AM - 64.d	7.250240959	0.985259747	2.058456985	0.573862866	2.226032242	0.142741155	0.835883441	0.052183323	0.625261069
59DTB19-AM - 65.d	13.42213805	6.742080065	7.820794347	1.707079138	3.393130008	0.19540635	0.802778309	0.027023535	0.246808798
59DTB19-AM - 68.d	1.530799876	0.711948921	0.709147829	0.347083513	0.633211985	0.034737188	0.836247647	0.032091257	0.289906286
59DTB19-AM - 69.d	0.129353205	0.0731417	0.347305765	0.225203359	0.336720426	0.027655718	0.836316963	0.037248555	0.261286855
59DTB19-AM - 70.d	10.20393032	13.30430846	1.513712533	1.52699247	2.480571777	0.277187636	0.815385857	0.028445951	-0.017090225
59DTB19-AM - 71.d	7.05764891	0.777176617	1.136987155	0.520161119	1.854814708	0.085942852	0.839645363	0.03116491	0.498295312
59DTB19-AM - 72.d	21.00667211	2.822012704	7.141012825	2.333753474	5.288156731	0.244434767	0.789301415	0.028710603	0.63923005
59DTB19-AM - 73.d	8.262478658	0.921417478	3.40385676	1.558953322	1.800278381	0.084128119	0.836752956	0.029637819	0.377866681
59DTB19-AM - 74.d	4.567096499	1.171361742	0.692787161	0.820825015	1.304007109	0.059286533	0.832726134	0.030947373	0.559769343
59DTB19-AM - 75.d	3.766132115	0.507597853	1.600273859	0.550885634	0.733018977	0.035700471	0.829443194	0.033827167	0.534867446
59DTB19-AM - 77.d	0.482762999	0.442586725	2.09475859	1.498632165	0.092844633	0.010011404	0.827590981	0.026929202	-0.089457054
59DTB19-AM - 78.d	0.15551436	0.098079999	1.461715474	0.543331732	0.083551379	0.00656122	0.826393652	0.025460355	0.183551709
59DTB19-AM - 79.d	4.342184283	0.848626988	0.296737319	0.140226597	1.22579776	0.055184194	0.843192739	0.032283529	0.621324337
59DTB19-AM - 81.d	35.82400608	23.25131137	7.26168649	5.712474063	8.0182694	0.620216046	0.765277993	0.02661592	-0.290235701
59DTB19-AM - 83.d	3.684772445	1.250184684	1.311966332	1.162156724	1.170203312	0.053507378	0.82345435	0.033448424	0.591449037
59DTB19-AM - 84.d	0.146038436	0.087902991	0.371434164	0.172279339	0.422108455	0.037449948	0.830268855	0.046706797	0.354765224
59DTB19-AM - 85.d	19.29268404	6.477102169	4.358867761	2.007442257	4.909754659	0.274881803	0.811952043	0.028226565	0.196100401
59DTB19-AM - 86.d	12.7308871	3.632438153	1.935936469	1.023260184	3.253705384	0.163589478	0.819201717	0.033814491	0.327196928
59DTB19-AM - 87.d	2.841353388	1.310787551	1.025455281	1.095038305	0.936493173	0.045651831	0.808053279	0.033082185	0.474274373
59DTB19-AM - 88.d	14.51052175	2.413174415	4.238683997	1.085192145	3.480396615	0.155614684	0.800257445	0.027702583	0.489158839
59DTB19-AM - 90.d	0.12784369	0.156698516	0.427215271	0.467265514	0.097061165	0.009540303	0.839957096	0.028657413	0.09099413
59DTB19-AM - 91.d	3.110633181	0.954633721	3.181104217	1.030515339	0.687778758	0.032350155	0.828687264	0.028630281	0.405807281
59DTB19-AM - 94.d	4.43985575	1.02471201	0.340918299	0.1809808	1.21546895	0.054582775	0.832802552	0.031866619	0.521427299
59DTB19-AM - 95.d	4.139260931	3.836975546	1.664372717	1.057826455	0.685256227	0.063517996	0.827135763	0.026333446	0.117455341
59DTB19-AM - 96.d	6.257231498	2.801581496	2.072982595	1.001806992	1.786250855	0.093878383	0.81523289	0.030958473	0.19672831
59DTB19-AM - 97.d	4.260430562	0.938270579	0.520444578	0.206287391	1.185726811	0.055448906	0.831078985	0.031737381	0.517221983
59DTB19-AM - 98.d	3.917890009	0.701868019	0.922389804	0.358481359	0.898743437	0.040681543	0.827525529	0.028205579	0.444790839
59DTB19-AM - 99.d	0.100985023	0.070849089	0.306952951	0.221346974	0.271570435	0.02485488	0.812193581	0.036933181	0.055613656
59DTB19-AM - 100.d	0.137960878	0.087887974	0.900915897	1.993791352	0.34871453	0.029252298	0.794626773	0.037306931	0.350965525

Appendix D4.7: Apatite U/Pb Standards

Spot ID	238U conc.	±2σ INT	232Th conc.	±2σ INT	LA-ICP-MS Isotopic Ratios				
	ppm		ppm		238U/206Pb	±2σ PROP(2%)	207Pb/206Pb	±2σ PROP(2%)	rho
A_MAD - Primary Standard									
mad - 1.d	22.19194504	3.300208787	798.6316479	121.4714414	13.25124456	0.634467819	0.0571961	0.001143922	0.060950228
mad - 2.d	22.2247748	3.41850828	799.8940407	138.3263063	13.13638824	0.613191313	0.0571961	0.001143922	-0.010117696
mad - 3.d	22.1629605	3.68275844	794.0417453	145.5407047	13.13507547	0.611170935	0.0571961	0.001143922	0.02281685
mad - 4.d	22.23225884	3.347274131	801.2371312	138.0209554	13.19399521	0.631346508	0.0571961	0.001143922	0.067057357
mad - 5.d	22.14658309	3.85450036	784.2336501	153.0709	13.20654303	0.622776513	0.0571961	0.001143922	0.034366938
mad - 6.d	22.23958998	3.329806283	809.6975798	137.8973705	13.10068376	0.620795013	0.0571961	0.001143922	0.034480607
mad - 7.d	22.17022334	3.533651126	793.5505745	149.3480518	13.17909901	0.641482198	0.0571961	0.001143922	0.05547993
mad - 8.d	22.22606432	3.225848452	796.4664249	137.9933459	13.15415974	0.623253233	0.0571961	0.001143922	-0.013557697
mad - 9.d	22.14382667	3.302072822	801.2086254	134.9880041	13.1011295	0.622711697	0.0571961	0.001143922	-0.01799102
mad - 10.d	22.32525677	4.158773631	802.8012868	155.3704129	13.08696766	0.620433947	0.0571961	0.001143922	0.027170444
mad - 11.d	22.13243755	3.829742527	795.5431653	153.4909703	13.18343031	0.653054003	0.0571961	0.001143922	0.039634266
mad - 12.d	22.22066759	4.062598965	792.1238543	159.9584331	13.09971908	0.620742212	0.0571961	0.001143922	0.046271264
mad - 14.d	22.19768723	3.360742921	797.4712336	142.9162994	13.26694991	0.629526419	0.0571961	0.001143922	0.014598319
mad - 15.d	22.20507379	3.463613098	801.9256361	145.5755386	13.03682552	0.612171978	0.0571961	0.001143922	0.093550078
mad - 16.d	22.20229604	3.295918668	797.9597034	131.5183577	13.13490411	0.637558491	0.0571961	0.001143922	0.018706154
mad - 17.d	22.17821758	3.653091279	794.4508213	138.555	13.05698558	0.60930642	0.0571961	0.001143922	0.0327634
mad - 18.d	22.23753478	3.656656065	804.2115283	142.6435058	13.22808379	0.616542344	0.0571961	0.001143922	0.037118298
mad - 19.d	22.17981889	3.587689378	794.3157041	142.2539654	12.98306448	0.615116828	0.0571961	0.001143922	0.041542782
A_MMC									
mmc - 1.d	15.86252134	2.132295456	55.92123559	7.735292905	10.44029668	0.483520706	0.176749879	0.011305296	0.367980901
mmc - 2.d	12.54691565	2.240722085	57.66612081	10.77288455	9.349098731	0.426272686	0.228263535	0.013675549	0.411942208
mmc - 3.d	12.45078639	1.085726125	49.07463184	6.029889968	9.973249064	0.461842866	0.236028493	0.014736952	0.412877209
mmc - 4.d	14.98104458	1.515636188	68.71848059	8.113396188	10.35814808	0.45169408	0.150593339	0.009361145	0.408247713
mmc - 5.d	10.68087378	1.821465106	33.72325445	5.267499467	9.731285723	0.45900297	0.213810491	0.013855389	0.408647091
mmc - 6.d	12.87155064	0.855142133	48.70721612	2.778937112	9.863815806	0.452719679	0.213312358	0.012927667	0.482870201
mmc - 7.d	15.27503811	1.682356271	55.96818461	6.816366713	10.25408776	0.464423211	0.178236808	0.011291495	0.486508887
mmc - 8.d	31.97149062	5.626542736	126.1041592	22.16616001	11.01743335	0.48529827	0.118650318	0.006520534	0.257409196
mmc - 9.d	18.76155584	2.656672255	77.1396034	8.845073582	10.13714756	0.46517429	0.151273977	0.008937537	0.40591861
mmc - 10.d	9.480452401	1.958560373	40.44370624	8.95945517	8.776325969	0.408014375	0.247913362	0.015442352	0.491565586
mmc - 11.d	13.399272	2.44830086	74.15288507	10.5841035	8.935220231	0.416645385	0.242400728	0.013615188	0.442519175
mmc - 12.d	16.84872619	6.214095435	72.33171998	25.0436049	9.902017437	0.456089648	0.193418464	0.013154159	0.084800551
mmc - 13.d	13.66566062	1.270173614	56.54799211	6.298243449	9.048580493	0.426341347	0.23949094	0.012246398	0.474587128
mmc - 14.d	13.89395303	1.668314163	60.88092861	6.149278524	9.779265612	0.4705829	0.200856764	0.012805423	0.400895802
mmc - 15.d	17.69380848	3.428135339	183.3670701	53.99054919	8.030373565	0.366091306	0.330247104	0.014707425	0.33895746
mmc - 16.d	14.12692902	2.392668229	66.08297137	10.67945114	9.140967319	0.425210546	0.231665164	0.013401575	0.351317961
mmc - 17.d	11.30695924	1.686794227	44.46761436	7.889541122	9.741614665	0.457257992	0.194113277	0.0133608	0.350314856
mmc - 18.d	14.26977511	1.767796092	61.01150557	9.251472687	8.49279578	0.396989857	0.280651665	0.017046135	0.548654447
mmc - 19.d	15.42743353	2.300834034	71.51070962	10.736103	9.926339735	0.460897372	0.175643776	0.011188533	0.421825253
A_FC									
fc1 - 1.d	5.976980877	0.883731516	20.65532198	3.477738928	4.038303239	0.195512616	0.297504351	0.017411374	0.553361129
fc1 - 2.d	6.454415956	0.98478724	24.45923208	2.708840404	3.001167228	0.138082175	0.450585279	0.020214944	0.515198761
fc1 - 3.d	4.467696284	0.544899469	15.35404313	1.386493898	3.665106424	0.193474887	0.364496338	0.022687694	0.538244239
fc1 - 4.d	5.077020482	0.783429799	15.91436854	2.250540405	2.581140639	0.118995035	0.534950345	0.023465536	0.477131705
fc1 - 5.d	4.718805914	0.972346451	16.0145826	2.69828954	3.838586675	0.183742156	0.331004223	0.018576238	0.446430338
fc1 - 6.d	5.065093018	0.793492481	16.50046447	2.612367349	4.33986582	0.210163232	0.267042589	0.016156256	0.489091962
fc1 - 7.d	2.108689173	0.452144209	6.763939362	1.19254217	3.095412384	0.177159154	0.445569375	0.029872158	0.522828392
fc1 - 8.d	5.027987124	1.286099091	22.54962493	5.607585409	4.392133687	0.213488395	0.236377041	0.014052861	0.403748033
fc1 - 9.d	2.778572546	0.506107449	8.527869147	1.169010241	3.717933188	0.196331907	0.343187391	0.020220793	0.316961209
fc1 - 10.d	3.214635268	0.393642053	10.09386633	0.82798166	3.802000022	0.215838123	0.332366704	0.024385749	0.496074941
fc1 - 11.d	3.53684539	0.598770978	10.81411816	1.612861255	3.681291366	0.183688493	0.366414731	0.020918062	0.457786569
fc1 - 12.d	5.373870286	0.950277158	17.08471625	2.581820308	4.335493296	0.211335485	0.268965855	0.016101641	0.491633517
fc1 - 13.d	7.833323253	1.32428718	30.32473335	4.644880512	4.534002951	0.211797904	0.212680539	0.011841225	0.39259671
fc1 - 14.d	5.598757015	1.161528709	21.4301717	4.17243638	4.089781839	0.19032162	0.27555278	0.015742369	0.303324824
fc1 - 15.d	5.693623763	0.739129971	22.53223108	3.072480682	4.359812672	0.214874005	0.229780384	0.013371667	0.347159658
fc1 - 16.d	6.718547939	0.877183137	26.0622378	2.518003987	4.295006935	0.201995542	0.273699841	0.014385078	0.424002937
fc1 - 17.d	7.433982935	1.449799397	30.79623511	6.037685669	4.161527089	0.187551151	0.25452063	0.013222714	0.344970522
fc1 - 18.d	5.811491747	1.03485646	19.03485391	2.934664406	4.159014917	0.194393421	0.264223956	0.015185366	0.464394443
fc1 - 19.d	6.815614616	0.964342659	22.89787482	3.482588556	4.149218586	0.194287968	0.264467243	0.014027905	0.493168094

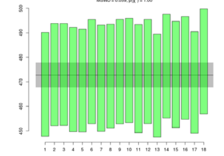

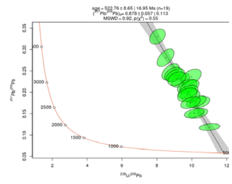

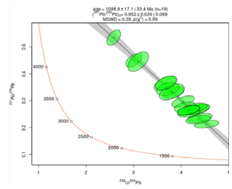

Appendix D5.1: Sample Locations

TABLE S1. LOCATIONS AND DESIGNATIONS FOR SAMPLES ANALYZED IN THIS PAPER

Sample number	Geologic Unit	Location		Elevation (m asl)	Analysis	Location Description
		Latitude (°N)	Longitude (°W)			
BH1	Buffalo Hump	48.1952	117.91376	1335	LA-SS-ICPMS	Ridge E/SE. of Klein Meadows. Upper Ybq
03DTB18	Buffalo Hump	48.18471	117.93345	1323	LA-SS-ICPMS	Lower Ybq near Double eagle Quarry
04DTB18	Buffalo Hump	48.18413	117.93176	1320	LA-SS-ICPMS	Along road cut N of Double eagle Quarry. Mid-lower Ybq
05DTB18	Buffalo Hump	48.20175	117.9069	1070	LA-SS-ICPMS	Duplication of Ross 1992 locality
34DTB19	Buffalo Hump conglomerate individual cobble sampled	48.13122	117.99775	1295	LA-SS-ICPMS	Conglomerate bed at 55.5-57m on measured section 1

Note: Locations are based on datum WGS84.

Appendix D5.2: U/Pb Results

Sample ID	Analysis date-time	Spot ID[1]	238U conc.		232Th conc.		Isotopic Ratios					Apparent Ages - Calculated in Isoplot R (Ma)				Discord	Perferred age 1500 Ma cutoff	
			ppm	±2σ INT	ppm	±2σ INT	238U/206Pb	±2σ PROP	207Pb/206Pb	±2σ PROP	rho	238U/206Pb	±2σ PROP	207Pb/206Pb	±2σ PROP	(7/6-6/8)/7/6 *100	Ma	2 σ
Analyses in blue font are from retargeted grains after rapid analysis identification																		
BH1	2020-07-30 16:07:02.000	BH1-154b - 1.d	306	7	340	7	8.022557	0.237716	0.063809	0.004110	0.118118	757	21	734	136	-3.11	757	21
BH1	2020-07-30 16:08:48.000	BH1-154c - 1.d	334	6	377	7	8.012350	0.233059	0.064696	0.004132	0.223823	758	21	764	135	0.70	758	21
BH1	2020-07-30 16:10:32.000	BH1-154d - 1.d	321	9	364	10	7.976002	0.240792	0.064390	0.004122	*0.017591*	761	22	754	135	-1.05	761	22
BH1	2020-07-30 16:12:11.000	BH1q - 709 - 1.d	246	4	5787	137	7.921050	0.243288	0.064355	0.004151	0.145446	766	22	752	136	-1.86	766	22
BH1	2020-07-30 16:13:52.000	BH1q - 709b - 1.d	257	4	2685	55	7.781355	0.234054	0.063674	0.004211	0.146663	779	22	730	140	-6.78	779	22
BH1	2020-07-30 16:15:35.000	BH1q - 709c - 1.d	219	5	2400	55	7.959874	0.257660	0.066166	0.004508	0.234983	763	23	811	143	5.90	763	23
BH1	2020-07-30 16:17:15.000	BH1q - 692 - 1.d	130	2	111	2	7.971016	0.270111	0.065862	0.004767	0.303211	762	24	801	152	4.88	762	24
BH1	2020-07-30 16:18:56.000	BH1q - 692b - 1.d	118	4	66	1	7.916348	0.255869	0.066167	0.005338	0.160344	767	23	811	169	5.41	767	23
BH1	2020-07-30 16:20:40.000	BH1q - 648 - 1.d	47	1	39	1	7.965560	0.300282	0.065553	0.006424	0.186646	762	27	791	206	3.64	762	27
BH1	2020-07-30 16:29:24.000	BH1q - 648b - 1.d	56	1	54	1	8.175774	0.318409	0.067506	0.006216	0.107191	744	27	853	191	12.74	744	27
BH1	2020-07-30 16:31:13.000	BH1q - 423b - 1.d	146	3	125	3	8.311182	0.265340	0.065977	0.004832	0.183944	732	22	805	153	8.98	732	22
BH1	2020-07-30 16:32:51.000	BH1q - 423 - 1.d	199	5	165	5	8.260927	0.251205	0.064184	0.004347	0.297804	737	21	747	143	1.36	737	21
BH1	2020-07-30 17:00:21.000	BH1q - 384 - 1.d	48	2	27	1	7.514458	0.384357	0.071371	0.007073	0.212671	805	39	967	202	16.72	805	39
BH1	2020-07-30 17:02:10.000	BH1q - 763 - 1.d	573	7	359	9	6.351496	0.270383	0.147526	0.016786	-0.828930	943	37	2317	195	59.31	943	37
BH1	2020-07-30 17:03:48.000	BH1q - 747 - 1.d	42	1	24	1	4.775377	0.181246	0.083440	0.006856	0.160520	1226	42	1279	160	4.14	1226	42
BH1	2020-07-30 17:05:30.000	BH1q - 655 - 1.d	1372	40	498	13	6.739803	0.227222	0.081847	0.004697	-0.001692	892	28	1241	112	28.14	892	28
BH1	2020-07-30 17:14:15.000	BH1q - 643 - 1.d	402	17	226	14	5.804436	0.194641	0.075485	0.004634	0.251428	1025	32	1081	123	5.17	1025	32
BH1	2020-07-30 17:16:02.000	BH1q - 60 - 1.d	25	1	20	1	5.393805	0.220218	0.074082	0.007499	0.228531	1096	41	1043	204	-5.14	1096	41
BH1	2020-07-30 17:17:46.000	BH1q - 505 - 1.d	129	2	45	1	4.669583	0.151220	0.087531	0.005718	0.072875	1251	37	1371	126	8.78	1251	37
BH1	2020-07-30 17:19:25.000	BH1q - 446 - 1.d	974	24	2144	69	7.577399	0.216055	0.081040	0.004749	0.391341	799	21	1222	115	34.58	799	21
BH1	2020-07-30 17:21:07.000	BH1q - 192 - 1.d	49	3	37	2	8.432193	0.393522	0.063251	0.006104	0.206552	722	32	716	205	-0.94	722	32
BH1	2020-07-30 17:22:51.000	BH1q - 178 - 1.d	791	10	45	1	5.429986	0.154281	0.075815	0.004409	0.250696	1090	29	1089	117	-0.03	1090	29
BH1	2020-07-30 17:24:29.000	BH1q - 172 - 1.d	255	4	118	2	2.942177	0.090668	0.128214	0.007470	0.259664	1886	50	2073	103	9.01	2073	103
BH1	2020-07-30 17:26:12.000	BH1q - 160 - 1.d	496	77	233	37	5.377492	0.361377	0.085000	0.005056	0.224969	1100	68	1315	115	16.37	1100	68
BH1	2020-07-30 17:27:55.000	BH1q - 152 - 1.d	98	4	98	5	8.125236	0.283560	0.066098	0.004943	0.326933	748	25	809	156	7.45	748	25
BH1	2020-07-30 17:36:35.000	BH1q - 111 - 1.d	252	7	75	2	4.623342	0.182250	0.089302	0.005455	0.202555	1262	45	1410	117	10.46	1262	45
BH1	03/12/2018 (2) 13:50:02.00	BH1 - 1	120	6	90	5	4.708098	0.173960	0.081900	0.006038	0.276460	1242	40	1242	139	0.03	1242	40
BH1	03/12/2018 (2) 13:52:08.00	BH1 - 2	272	16	118	5	4.405286	0.251121	0.080200	0.004604	-0.088564	1319	65	1201	110	-9.81	1319	65
BH1	03/12/2018 (2) 13:54:09.00	BH1 - 3	426	12	335	44	5.434783	0.197306	0.101400	0.009628	0.420240	1089	35	1649	167	33.97	1089	35
BH1	03/12/2018 (2) 13:56:14.00	BH1 - 4	205	10	101	10	4.159734	0.154139	0.091900	0.005638	0.216050	1389	45	1465	113	5.17	1389	45
BH1	03/12/2018 (2) 13:58:15.00	BH1 - 5	198	11	83	5	3.289474	0.107990	0.104800	0.005396	0.194190	1711	48	1710	93	-0.06	1710	93
BH1	03/12/2018 (2) 14:00:19.00	BH1 - 6	409	14	230	12	4.833253	0.159738	0.081900	0.004238	0.180900	1212	35	1242	99	2.41	1212	35
BH1	03/12/2018 (2) 14:02:20.00	BH1 - 7	76	2	34	1	5.515720	0.244176	0.101400	0.009028	0.256290	1074	42	1649	157	34.86	1074	42
BH1	03/12/2018 (2) 14:04:25.00	BH1 - 8	267	17	123	7	3.932363	0.128130	0.090500	0.005710	0.223500	1461	41	1435	117	-1.77	1461	41
BH1	03/12/2018 (2) 14:06:26.00	BH1 - 9	122	5	12	1	5.455537	0.219233	0.074900	0.007198	0.330940	1085	39	1065	183	-1.88	1085	39
BH1	03/12/2018 (2) 14:08:31.00	BH1 - 10	217	8	76	3	5.633803	0.182503	0.076100	0.004922	0.171300	1053	31	1097	125	3.97	1053	31
BH1	03/12/2018 (2) 14:10:31.00	BH1 - 11	106	4	66	2	5.521811	0.229349	0.076600	0.006132	0.256360	1073	40	1110	153	3.33	1073	40
BH1	03/12/2018 (2) 14:12:36.00	BH1 - 12	92	4	71	4	5.032713	0.204500	0.077200	0.007344	0.147400	1168	42	1125	180	-3.85	1168	42
BH1	03/12/2018 (2) 14:14:36.00	BH1 - 13	68	4	31	2	4.302926	0.193447	0.085100	0.008302	0.261400	1347	53	1317	179	-2.29	1347	53
BH1	03/12/2018 (2) 14:16:48.00	BH1 - 14	255	9	91	4	3.395586	0.158999	0.105500	0.005610	0.039335	1664	66	1722	95	3.38	1722	95
BH1	03/12/2018 (2) 14:18:50.00	BH1 - 15	822	37	266	11	5.614823	0.169044	0.074900	0.003098	0.163800	1057	29	1065	82	0.78	1057	29
BH1	03/12/2018 (2) 14:20:54.00	BH1 - 16	212	6	139	3	4.290004	0.139172	0.088100	0.004662	0.056209	1351	38	1384	99	2.39	1351	38
BH1	03/12/2018 (2) 14:22:54.00	BH1 - 17	151	8	73	5	6.060606	0.238751	0.075100	0.006302	0.190850	985	35	1070	161	7.99	985	35
BH1	03/12/2018 (2) 14:24:59.00	BH1 - 18	221	9	114	4	5.464481	0.195885	0.076300	0.005226	0.135610	1083	35	1102	132	1.71	1083	35
BH1	03/12/2018 (2) 14:26:59.00	BH1 - 19	103	4	99	4	3.003003	0.118677	0.112600	0.006752	0.093511	1853	62	1841	106	-0.65	1841	106
BH1	03/12/2018 (2) 14:29:06.00	BH1 - 20	220	10	121	5	4.955401	0.175232	0.078300	0.004966	0.287060	1185	37	1154	122	-2.72	1185	37
BH1	03/12/2018 (2) 14:31:07.00	BH1 - 21	414	4	130	2	4.807692	0.160873	0.079600	0.004092	0.081125	1218	36	1186	99	-2.70	1218	36
BH1	03/12/2018 (2) 14:43:41.00	BH1 - 22	155	7	71	3	4.191115	0.141788	0.086500	0.005630	0.040185	1379	41	1349	122	-2.29	1379	41
BH1	03/12/2018 (2) 14:45:46.99	BH1 - 23	84	12	92	31	7.092199	0.795735	0.085200	0.010704	0.335540	850	81	1319	227	35.53	850	81
BH1	03/12/2018 (2) 14:47:52.00	BH1 - 24	182	7	93	4	5.577245	0.214194	0.071400	0.005128	0.192100	1063	36	968	141	-9.82	1063	36
BH1	03/12/2018 (2) 14:49:57.00	BH1 - 25	189	18	83	10	4.073320	0.139538	0.088400	0.005268	-0.003210	1415	42	1390	111	-1.79	1415	42
BH1	03/12/2018 (2) 14:51:58.00	BH1 - 26	564	5	215	4	4.574565	0.137530	0.084600	0.003892	0.025697	1275	34	1306	88	2.37	1275	34
BH1	03/12/2018 (2) 14:54:05.00	BH1 - 27	350	7	97	4	4.321521	0.138722	0.087500	0.004850	-0.029183	1342	38	1371	104	2.11	1342	38
BH1	03/12/2018 (2) 14:56:06.00	BH1 - 28	353	15	69	5	3.667033	0.135197	0.096400	0.004228	0.101850	1555	49	1555	81	0.01	1555	81
BH1	03/12/2018 (2) 14:58:09.00	BH1 - 29	113	7	69	5	6.293266	0.288247	0.074000	0.006880	0.105980	951	39	1041	178	8.67	951	39
BH1	03/12/2018 (2) 15:00:11.00	BH1 - 30	257	17	169	32	3.628447	0.131814	0.101300	0.005326	0.121600	1569	49	1647	95	4.74	1647	95
BH1	03/12/2018 (2) 15:02:16.00	BH1 - 31	120	4	117	5	5.678592	0.236108	0.080600	0.006912	0.168780	1046	39	1211	161	13.66	1046	39
BH1	03/12/2018 (2) 15:04:17.00	BH1 - 32	77	4	57	3	5.202914	0.236703	0.080800	0.008316	0.186560	1133	45	1216	191	6.80	1133	45
BH1	03/12/2018 (2) 15:06:22.00	BH1 - 33	189	14	79	7	5.602241	0.218754	0.075200	0.005104	0.394950	1059	37	1073	132	1.31	1059	37
BH1	03/12/2018 (2) 15:08:23.00	BH1 - 34	208	12	112	7	4.543389	0.146602	0.081600	0.005232	0.358780	1282	36	1235	122	-3.83	1282	36
BH1	03/12/2018 (2) 15:10:27.00	BH1 - 35	153	3	325	11	5.205622	0.196247	0.079900	0.005598	0.326810	1133	38	1194	133	5.10	1133	38
BH1	03/12/2018 (2) 15:12:28.00	BH1 - 36	43	2	46	2	5.515720	0.295896	0.076000	0.011520	0.270300	1074	51	1094	278	1.82	1074	51
BH1	03/12/2018 (2) 15:14:33.00	BH1 - 37	64	2	58	1	5.194805	0.255018	0.074500	0.007990	-0.019879	1135	49	1054	203	-7.68	1135	49
BH1	03/12/2018 (2) 15:27:14.00	BH1 - 38	247	36	190	28	4.566210	0.529180	0.108400	0.006668	0.493800	1277	122	1772	109	27.93	1277	122
BH1	03/12/2018 (2) 15:29:19.00	BH1 - 39	397	13	140	5	5.333333	0.183467	0.077500	0.004050	-0.017650	1108	34	1133	102	2.24	1108	34
BH1	03/12/2018 (2) 15:31:24.00	BH1 - 40	165	7	78	4	3.053435	0.103024	0.113600	0.006272	0.220990	1826	52	1857	97	1.65	1857	97
BH1	03/12/2018 (2) 15:33:25.00	BH1 - 41	143	8	73	5	4.486317	0.172247	0.082600	0.006052	0.196630	1297	44	1259	138	-3.03	1297	44
BH1	03/12/2018 (2) 15:35:30.00	BH1 - 42	130	7	101	3	7.299270	0.891896	0.083100	0.006962	0.014692	828	85	1271	156	34.88	828	85
BH1	03/12/2018 (2) 15:48:08.00	BH1 - 43	84	3	60	2	5.652911	0.330355	0.084000	0.007180	0.159820	1050	54	1292	158	18.73	1050	54
BH1	03/12/2018 (2) 15:50:16.00	BH1 - 44	414	20	251	15	5.643341	0.230702	0.079400	0.003888	0.215990	1052	38	1181	95	10.96	1052	38
BH1	03/12/2018 (2) 15:52:22.00	BH1 - 45	413	11	142	3	4.793864	0.144138	0.081500	0.003930	-0.173430	1221	33	1233	93	0.91	1221	33
BH1	03/12/2018 (2) 15:54:22.00	BH1 - 46	117	2	137	4	3.297066	0.130078	0.107000	0.006340	0.060263	1708	57	1748	106	2.31	1748	106
BH1	03/12/2018 (2) 15:56:27.00	BH1 - 47	81	3	80	3	3.071253	0.131226	0.113700	0.008274	0.206620	1817	65	1859	127	2.24	1859	127
BH1	03/12/2018 (2) 15:58:29.00	BH1 - 48	103	6	41	3	5.157298	0.222836	0.077100	0.006642	0.267570	1143	44	1123	164	-1.74	1143	44
BH1	03/12/2018 (2) 16:00:33.00	BH1 - 49	1233	55	638	30	7.288630	0.246708	0.095900	0.006118	-0.415790	829	26	1545	116	46.36	829	26
BH1	03/12/2018 (2) 16:02:35.00	BH1 - 50	517	44	45	6	5.330490	0.163438	0.074700	0.003494	-0.046744	1108	30	1060	92	-4.62	1108	30
BH1	03/12/2018 (2) 16:04:40.00	BH1 - 51	156	5	71	2	2.223705	0.082550	0.155400	0.007108	0.246560	2394	72	2405	77	0.48	2405	77
BH1	03/12/2018 (2) 16:06:40.00	BH1 - 52	231	8	163	6	4.861449	0.156313	0.077200	0.004844	0.279470	1206	34	1126	121	-7.14	1206	34
BH1	03/12/2018 (2) 16:08:45.00	BH1 - 53	158	12	118	10	3.514938	0.124660	0.097800	0.004956	0.035174	1614	49	1582	93	-2.04	1582	93
BH1	03/12/2018 (2) 16:10:46.00	BH1 - 54	74	4	45	3	3.527337	0.147688	0.103000	0.008460	0.267550	1609	58	1678	145	4.11	1678	145
BH1	03/12/2018 (2) 16:12:51.00	BH1 - 55	231	14	151	9	3.427005	0.114343	0.101800	0.005336	0.116450	1651	47	1656	95	0.36	1656	95
BH1	03/12/2018 (2) 16:14:51.00	BH1 - 56	249	18	131	7	3.717472	0.135156	0.099300	0.005786	0.037848	1536	48	1610	106	4.63	1610	106
BH1	03/12/2018 (2) 16:16:57.00	BH1 - 57	144	6	100	4	5.144033	0.198141	0.074900	0.005598	0.287000	1145	39	1065	144	-7.53	1145	39
BH1	03/12/2018 (2) 16:18:58.00	BH1 - 58	158	4	107	8	5.339028	0.183745	0.077500	0.005350	0.220400	1107	34	1133	132	2.34	1107	34
BH1	03/12/2018 (2) 16:21:08.00	BH1 - 59	117	7	90	6	5.083884	0.207646	0.081000	0.006620	0.314410	1158	42	1221	153	5.19	1158	42
BH1	03/12/2018 (2) 16:23:09.00	BH1 - 60	161	7	85	4	3.921569	0.139946	0.088300	0.005466	0.195900	1464	45	1388	115	-5.47	1464	45
BH1	03/12/2018 (2) 16:25:15.00	BH1 - 61	185	19	92	9	4.875670	0.187848	0.079700	0.005494	-0.097252	1203	41	1189	131	-1.18	1203	41
BH1	03/12/2018 (2) 16:27:18.00	BH1 - 62	451	14	420	12	4.159734	0.126453	0.095500	0.004610	0.170800	1389	37	1537	89	9.65	1389	37
BH1	03/12/2018 (2) 16:29:22.00	BH1 - 63	233	5	114	2	5.614823	0.184807	0.074100	0.004782	0.339070	1057	31	1043	126	-1.27	1057	31
BH1	03/12/2018 (2) 16:41:58.00	BH1 - 64	127	8	54	3	5.411255	0.201926	0.071800	0.005236	0.050968	1093	36	979	143	-11.65	1093	36
BH1	03/12/2018 (2) 16:44:01.00	BH1 - 65	873	49	639	37	5.882353	0.498270	0.261000	0.031220	-0.945460	1012	74	3252	177	68.88	1012	74
BH1	03/12/2018 (2) 16:46:06.00	BH1 - 66	227	15	76	6	4.357298	0.151699	0.084700	0.005294	0.236100	1332	41	1308	118	-1.84	1332	41
BH1	03/12/2018 (2) 16:48:06.00	BH1 - 67	75	5	70	7	3.987241	0.168774	0.088000	0.007460	0.146830	1443	53	1382	155	-4.38	1443	53
BH1	03/12/2018 (2) 16:50:11.00	BH1 - 68	34	2	33	2	1.757469	0.084569	0.204600	0.010492	0.406200	2904	108	2863	82	-1.44	2863	82
BH1	03/12/2018 (2) 16:52:18.00	BH1 - 69	78	7	66	9	1.801153	0.065220	0.200500	0.009710	0.215450	2847	81	2830	78	-0.61	2830	78
BH1	03/12/2018 (2) 16:54:23.00	BH1 - 70	93	5	64	4	3.174603	0.517007	0.209000	0.054180	-0.953280	1765	220	2897	369	39.07	2897	369
BH1	03/12/2018 (2) 16:56:23.00	BH1 - 71	672	24	371	14	5.246590	0.228802	0.090200	0.003604	0.078484	1125	43	1429	75	21.30	1125	43
BH1	03/12/2018 (2) 16:58:28.00	BH1 - 72	112	5	38	2	5.319149	0.208239	0.077000	0.006740	0.155760	1111	39	1120	167	0.85	1111	39
BH1	03/12/2018 (2) 17:00:29.00	BH1 - 73	121	7	88	6	3.473428	0.135824	0.101700	0.006634	0.103100	1631	54	1655	117	1.42	1655	117
BH1	03/12/2018 (2) 17:02:34.00	BH1 - 74	363	59	243	41	5.730659	0.245975	0.077300	0.004946	0.229670	1037	40	1128	123	8.08	1037	40
BH1	03/12/2018 (2) 17:04:35.00	BH1 - 75	246	6	125	2	3.254149	0.107441	0.102800	0.004956	0.271670	1727	49	1675	87	-3.16	1675	87
BH1	03/12/2018 (2) 17:06:40.00	BH1 - 76	149	9	90	6	5.437738	0.218160	0.079000	0.006180	-0.139500	1088	39	1171	149	7.07	1088	39
BH1	03/12/2018 (2) 17:08:40.00	BH1 - 77	92	3	49	2	4.091653	0.185631	0.089900	0.006998	0.008848	1410	55	1423	142	0.95	1410	55
BH1	03/12/2018 (2) 17:10:45.00	BH1 - 78	93	6	51	3	4.116921	0.158609	0.087200	0.006544	0.233850	1402	47	1364	139	-2.77	1402	47
BH1	03/12/2018 (2) 17:12:46.00	BH1 - 79	190	9	207	11	4.844961	0.188446	0.080200	0.005504	0.282820	1210	41	1201	131	-0.72	1210	41
BH1	03/12/2018 (2) 17:25:29.00	BH1 - 80	118	12	31	4	5.376344	0.425483	0.084200	0.007184	-0.194490	1100	75	1296	159	15.15	1100	75
BH1	03/12/2018 (2) 17:27:38.00	BH1 - 81	137	7	54	3	4.926108	0.193162	0.075500	0.005810	0.285760	1191	41	1081	148	-10.21	1191	41
BH1	03/12/2018 (2) 17:29:37.00	BH1 - 82	485	23	260	8	5.476451	0.169512	0.072700	0.003854	0.334040	1081	30	1005	105	-7.61	1081	30
BH1	03/12/2018 (2) 17:31:44.00	BH1 - 83	96	6	50	1	1.501502	0.052575	0.267300	0.009946	0.251970	3290	88	3290	58	-0.03	3290	58
BH1	03/12/2018 (2) 17:33:45.00	BH1 - 84	151	7	108	5	3.971406	0.142516	0.092200	0.005544	0.151750	1448	45	1471	111	1.56	1448	45
BH1	03/12/2018 (2) 17:46:22.00	BH1 - 85	147	15	55	6	5.030181	0.199284	0.078900	0.006278	0.031098	1169	41	1169	151	0.01	1169	41
BH1	03/12/2018 (2) 17:48:29.00	BH1 - 86	493	31	191	12	4.514673	0.188128	0.085200	0.004204	0.319970	1290	47	1319	94	2.23	1290	47
BH1	03/12/2018 (2) 17:50:30.00	BH1 - 87	194	6	138	5	4.901961	0.179739	0.080000	0.005400	0.001498	1197	39	1196	129	-0.06	1197	39
BH1	03/12/2018 (2) 17:52:34.00	BH1 - 88	91	4	90	4	3.264773	0.135643	0.116100	0.007422	0.023686	1723	61	1896	112	9.16	1896	112
BH1	03/12/2018 (2) 17:54:41.00	BH1 - 89	225	11	157	9	3.188776	0.107499	0.109800	0.005396	0.289140	1758	50	1795	88	2.06	1795	88
BH1	03/12/2018 (2) 17:56:47.00	BH1 - 90	350	16	181	20	5.643341	0.310320	0.074600	0.004092	0.519760	1052	51	1057	108	0.48	1052	51
BH1	03/12/2018 (2) 17:58:48.00	BH1 - 91	65	2	47	2	5.437738	0.280255	0.075400	0.009008	0.089283	1088	49	1078	224	-0.95	1088	49
BH1	03/12/2018 (2) 18:00:53.00	BH1 - 92	448	8	121	2	5.411255	0.175573	0.073800	0.003776	0.150540	1093	32	1035	101	-5.60	1093	32
BH1	03/12/2018 (2) 18:02:53.00	BH1 - 93	170	6	223	7	4.812320	0.174985	0.080200	0.006040	0.132940	1217	39	1245	138	2.24	1217	39
BH1	03/12/2018 (2) 18:04:59.00	BH1 - 94	117	8	64	5	5.224660	0.194574	0.076700	0.006334	0.153700	1129	37	1113	157	-1.44	1129	37
BH1	03/12/2018 (2) 18:07:00.00	BH1 - 95	74	9	58	7	5.543237	0.227629	0.073600	0.007272	0.054029	1069	39	1030	188	-3.81	1069	39
BH1	03/12/2018 (2) 18:09:05.00	BH1 - 96	212	8	93	4	2.156567	0.069641	0.156000	0.006320	0.302780	2456	64	2412	68	-1.82	2412	68
BH1	03/12/2018 (2) 18:11:06.00	BH1 - 97	261	23	79	6	3.289474	0.101498	0.103500	0.004570	0.344400	1711	45	1687	80	-1.43	1687	80
BH1	03/12/2018 (2) 18:13:12.00	BH1 - 98	176	7	115	4	5.875441	0.200359	0.073100	0.005562	0.225570	1013	31	1016	148	0.28	1013	31
BH1	03/12/2018 (2) 18:15:12.00	BH1 - 99	93	4	61	3	3.966680	0.150139	0.092400	0.006248	-0.069289	1449	48	1475	124	1.73	1449	48
BH1	03/12/2018 (2) 18:17:17.00	BH1 - 100	220	22	3	0	4.775549	0.154806	0.080500	0.004310	0.053783	1226	35	1208	103	-1.42	1226	35
BH1	03/12/2018 (2) 18:19:17.00	BH1 - 101	105	4	167	6	1.917178	0.064808	0.181600	0.007832	0.303970	2706	73	2667	70	-1.47	2667	70
BH1	03/12/2018 (2) 18:21:23.00	BH1 - 102	67	4	43	2	5.081301	0.186831	0.078300	0.008466	0.128760	1158	38	1154	201	-0.36	1158	38
BH1	03/12/2018 (2) 18:23:24.00	BH1 - 103	165	9	84	5	3.985652	0.141666	0.091200	0.005324	0.375920	1443	45	1450	108	0.47	1443	45
BH1	03/12/2018 (2) 18:25:35.00	BH1 - 104	115	5	118	5	5.316321	0.213727	0.074500	0.005590	0.208200	1111	40	1054	145	-5.42	1111	40
BH1	03/12/2018 (2) 18:27:36.00	BH1 - 105	205	10	166	9	4.796163	0.167233	0.077900	0.005158	0.120800	1221	38	1143	127	-6.77	1221	38
BH1	03/12/2018 (2) 18:40:13.00	BH1 - 106	304	19	342	22	4.828585	0.164186	0.077100	0.003842	0.104150	1213	36	1123	97	-8.05	1213	36
BH1	03/12/2018 (2) 18:42:20.00	BH1 - 107	239	11	241	16	5.175983	0.183892	0.074900	0.004998	0.252320	1139	36	1065	130	-6.93	1139	36
BH1	03/12/2018 (2) 18:44:21.00	BH1 - 108	251	14	196	11	3.218539	0.101663	0.105800	0.004916	0.148960	1744	47	1727	84	-0.97	1727	84
BH1	03/12/2018 (2) 18:46:26.00	BH1 - 109	333	6	121	2	5.417118	0.196378	0.077100	0.004342	0.403950	1092	35	1123	109	2.74	1092	35
BH1	03/12/2018 (2) 18:48:28.00	BH1 - 110	199	5	129	2	5.810575	0.207371	0.076500	0.005430	0.189680	1024	33	1107	137	7.52	1024	33
BH1	03/12/2018 (2) 18:50:33.00	BH1 - 111	128	4	78	2	5.681818	0.565599	0.097400	0.008448	0.481710	1045	88	1574	155	33.60	1045	88
BH1	03/12/2018 (2) 18:52:34.00	BH1 - 112	190	4	89	3	5.249344	0.204187	0.078600	0.005372	0.428660	1124	39	1161	131	3.19	1124	39
BH1	03/12/2018 (2) 18:54:41.00	BH1 - 113	156	8	75	5	4.081633	0.153269	0.098900	0.005578	0.016688	1413	46	1603	103	11.86	1413	46
BH1	03/12/2018 (2) 18:56:48.00	BH1 - 114	458	22	193	3	4.024145	0.120967	0.090400	0.003808	0.092846	1431	38	1433	79	0.17	1431	38
BH1	03/12/2018 (2) 18:58:53.00	BH1 - 115	147	9	146	10	4.282655	0.201202	0.084100	0.005782	0.305960	1353	55	1294	129	-4.54	1353	55
BH1	03/12/2018 (2) 19:00:54.00	BH1 - 116	57	4	86	6	1.996008	0.083745	0.174900	0.009598	0.374550	2618	87	2604	89	-0.53	2604	89
BH1	03/12/2018 (2) 19:02:59.00	BH1 - 117	872	46	262	15	6.131208	0.179012	0.074600	0.003392	0.154100	974	26	1057	90	7.84	974	26
BH1	03/12/2018 (2) 19:04:59.00	BH1 - 118	562	20	207	10	4.657662	0.145218	0.090300	0.004306	0.275760	1254	35	1431	89	12.38	1254	35
BH1	03/12/2018 (2) 19:07:04.00	BH1 - 119	225	7	87	3	5.387931	0.183236	0.073200	0.004264	0.254050	1098	33	1019	115	-7.75	1098	33
BH1	03/12/2018 (2) 19:09:04.79	BH1 - 120	436	17	188	23	6.574622	0.295750	0.070600	0.003812	-0.036169	913	37	945	108	3.41	913	37
BH1	03/12/2018 (2) 19:11:11.00	BH1 - 121	622	21	317	9	5.030181	0.171451	0.080200	0.003304	0.135470	1169	35	1201	80	2.67	1169	35
BH1	03/12/2018 (2) 19:27:40.00	BH1 - 122	243	7	96	4	5.437738	0.188591	0.073200	0.004664	0.169010	1088	34	1019	125	-6.83	1088	34
BH1	03/12/2018 (2) 19:29:44.00	BH1 - 123	503	38	290	14	4.299226	0.171008	0.111200	0.004624	0.013329	1348	47	1818	74	25.86	1348	47
BH1	03/12/2018 (2) 19:31:50.00	BH1 - 124	200	9	110	4	4.334634	0.152454	0.083600	0.004772	0.166510	1338	41	1282	108	-4.35	1338	41
BH1	03/12/2018 (2) 19:33:51.00	BH1 - 125	276	16	266	14	4.444444	0.286420	0.098400	0.004768	-0.051157	1308	72	1593	89	17.89	1308	72
BH1	03/12/2018 (2) 19:35:57.00	BH1 - 126	190	7	152	7	1.826150	0.056532	0.193300	0.007166	0.278090	2815	69	2770	60	-1.64	2770	60
BH1	03/12/2018 (2) 19:48:31.00	BH1 - 127	217	17	164	9	5.122951	0.170695	0.079500	0.005390	0.199620	1150	34	1184	129	2.89	1150	34
BH1	03/12/2018 (2) 19:50:33.00	BH1 - 128	169	13	77	5	4.990020	0.184461	0.078200	0.005164	0.274140	1178	39	1151	127	-2.29	1178	39
BH1	03/12/2018 (2) 19:52:39.00	BH1 - 129	284	7	124	3	4.050223	0.136779	0.088400	0.004168	0.449520	1423	42	1390	89	-2.32	1423	42
BH1	03/12/2018 (2) 19:54:40.00	BH1 - 130	31	2	28	1	5.564830	0.328068	0.069000	0.012380	0.339400	1065	55	898	333	-18.63	1065	55
BH1	03/12/2018 (2) 19:56:45.00	BH1 - 131	299	21	113	7	3.920031	0.126037	0.087300	0.005046	0.053031	1465	41	1366	108	-7.20	1465	41
BH1	03/12/2018 (2) 19:58:51.00	BH1 - 132	186	12	267	17	2.933412	0.100832	0.114900	0.005998	0.094041	1891	55	1878	92	-0.72	1878	92
BH1	03/12/2018 (2) 20:00:56.00	BH1 - 133	335	18	96	4	3.891051	0.118700	0.089000	0.004680	0.296160	1475	39	1403	98	-5.07	1475	39
BH1	03/12/2018 (2) 20:02:57.00	BH1 - 134	303	7	183	3	5.202914	0.174441	0.076200	0.004724	0.326170	1133	34	1099	120	-3.08	1133	34
BH1	03/12/2018 (2) 20:05:02.00	BH1 - 135	186	9	239	21	3.947888	0.139742	0.092400	0.005448	0.060014	1456	45	1475	109	1.31	1456	45
BH1	03/12/2018 (2) 20:07:03.00	BH1 - 136	152	5	58	2	5.213764	0.183107	0.075400	0.005808	0.134860	1131	35	1078	148	-4.93	1131	35
BH1	03/12/2018 (2) 20:09:08.00	BH1 - 137	73	4	46	2	5.476451	0.265485	0.072600	0.007252	0.098269	1081	46	1002	191	-7.90	1081	46
BH1	03/12/2018 (2) 20:11:09.00	BH1 - 138	286	11	220	8	5.382131	0.261170	0.110000	0.009000	-0.465030	1099	47	1799	142	38.93	1099	47
~~BH1~~	~~03/12/2018 (2) 20:13:14.00~~	~~BH1 - 139~~	~~687~~	~~12~~	~~1027~~	~~71~~	~~8.510638~~	~~0.257130~~	~~0.063000~~	~~0.003360~~	~~-0.025889~~	~~716~~	~~20~~	~~707~~	~~110~~	-1.25	~~716~~	~~20~~
BH1	03/12/2018 (2) 20:15:15.00	BH1 - 140	147	3	97	3	7.122507	0.558437	0.089900	0.007198	0.268080	847	58	1423	146	40.48	847	58
BH1	03/12/2018 (2) 20:17:21.00	BH1 - 141	106	4	47	2	4.222973	0.164710	0.083800	0.007076	0.127060	1370	46	1287	157	-6.45	1370	46
BH1	03/12/2018 (2) 20:19:21.00	BH1 - 142	692	34	523	31	4.952947	0.148122	0.075800	0.003216	0.030876	1186	32	1089	84	-8.87	1186	32
BH1	03/12/2018 (2) 20:21:27.00	BH1 - 143	261	16	126	13	3.327787	0.137430	0.111300	0.005326	0.178960	1694	59	1820	85	6.93	1820	85
BH1	03/12/2018 (2) 20:23:28.00	BH1 - 144	227	11	70	4	3.206156	0.105241	0.105400	0.005608	-0.046367	1750	49	1721	95	-1.71	1721	95
BH1	03/12/2018 (2) 20:25:34.00	BH1 - 145	45	7	40	6	3.571429	1.040816	0.101000	0.027020	-0.337980	1591	326	1642	429	3.11	1642	429
BH1	03/12/2018 (2) 20:27:34.00	BH1 - 146	127	6	77	4	5.184033	0.203115	0.076300	0.007126	0.198370	1137	39	1102	177	-3.19	1137	39
BH1	03/12/2018 (2) 20:29:47.00	BH1 - 147	219	6	120	4	5.307856	0.182225	0.077100	0.005342	0.339370	1113	34	1123	133	0.91	1113	34
BH1	03/12/2018 (2) 20:42:23.00	BH1 - 148	82	2	66	2	5.359057	0.236419	0.077000	0.007740	0.322300	1103	43	1120	190	1.53	1103	43

Appendix D.2 continued.

Sample ID	Analysis date-time	Spot ID[1]	238U conc. ppm	±2σ INT	232Th conc. ppm	±2σ INT	Isotopic Ratios 238U/206Pb	±2σ PROP	207Pb/206Pb	±2σ PROP	rho	Apparent Ages - Calculated in Isoplot R (Ma) 238U/206Pb	±2σ PROP	207Pb/206Pb	±2σ PROP	Discord (7/6-6/8)/7/6 *100	Perferred age 1500 Ma cutoff Ma	2σ
BH1	03/12/2018 (2) 20:44:25.00	BH1 - 149	209	9	132	5	3.196931	0.104820	0.105600	0.005812	0.309820	1755	49	1724	99	-1.77	1724	99
BH1	03/12/2018 (2) 20:46:30.00	BH1 - 150	129	9	87	5	5.515720	0.256346	0.079000	0.005880	0.110850	1074	44	1171	142	8.27	1074	44
BH1	03/12/2018 (2) 20:48:32.00	BH1 - 151	240	22	101	9	2.884338	0.094292	0.115100	0.005602	0.407940	1919	53	1881	86	-2.03	1881	86
BH1	03/12/2018 (2) 20:50:37.00	BH1 - 152	39	1	29	1	4.933399	0.273905	0.085000	0.011700	0.340730	1190	57	1315	246	9.52	1190	57
BH1	03/12/2018 (2) 20:52:38.00	BH1 - 153	618	17	438	7	4.672897	0.182985	0.091000	0.003720	0.170270	1250	43	1446	77	13.53	1250	43
BH1	03/12/2018 (2) 20:54:44.00	BH1 - 154	229	13	171	14	3.193868	0.136303	0.111700	0.005134	0.180400	1756	63	1826	82	3.86	1826	82
BH1	03/12/2018 (2) 20:56:44.00	BH1 - 155	343	15	13	1	5.002501	0.160110	0.075500	0.004010	0.005345	1175	33	1081	104	-8.69	1175	33
BH1	03/12/2018 (2) 20:58:50.00	BH1 - 156	77	3	97	3	5.282620	0.245183	0.078000	0.008360	0.140520	1118	46	1146	200	2.48	1118	46
BH1	03/12/2018 (2) 21:00:56.00	BH1 - 157	68	4	12	2	2.092050	0.103114	0.179400	0.008788	0.101170	2519	99	2647	80	4.84	2647	80
BH1	03/12/2018 (2) 21:03:01.00	BH1 - 158	738	30	266	18	6.093845	0.177579	0.076600	0.003432	0.328530	980	26	1110	88	11.75	980	26
BH1	03/12/2018 (2) 21:05:01.00	BH1 - 159	598	52	589	61	5.356186	0.282125	0.087300	0.004546	0.524630	1104	51	1366	98	19.23	1104	51
BH1	03/12/2018 (2) 21:07:07.00	BH1 - 160	540	78	394	79	13.245030	1.633262	0.085500	0.006110	-0.072302	469	50	1326	133	64.62	469	50
BH1	03/12/2018 (2) 21:09:08.00	BH1 - 161	296	18	153	9	5.924171	0.244828	0.081700	0.006734	-0.374310	1006	37	1237	155	18.71	1006	37
BH1	03/12/2018 (2) 21:11:13.00	BH1 - 162	172	9	71	4	5.173306	0.197137	0.084500	0.005690	0.615900	1139	38	1303	126	12.58	1139	38
BH1	03/12/2018 (2) 21:13:13.00	BH1 - 163	92	11	81	14	10.309280	1.268998	0.115000	0.016300	0.427920	597	63	1879	236	68.24	597	63
BH1	03/12/2018 (2) 21:25:48.00	BH1 - 164	63	3	39	2	5.617978	0.342760	0.085300	0.009306	0.216820	1056	56	1321	199	20.06	1056	56
BH1	03/12/2018 (2) 21:27:57.00	BH1 - 165	172	8	53	3	5.858231	0.213257	0.074000	0.006080	0.264420	1016	33	1041	158	2.40	1016	33
BH1	03/12/2018 (2) 21:29:57.00	BH1 - 166	217	10	85	4	4.399472	0.155733	0.090400	0.005008	0.170770	1320	41	1433	103	7.87	1320	41
BH1	03/12/2018 (2) 21:32:08.00	BH1 - 167	164	6	83	3	4.496403	0.160690	0.084000	0.005980	0.292090	1295	41	1292	133	-0.22	1295	41
BH1	03/12/2018 (2) 21:34:10.00	BH1 - 168	117	7	40	3	5.561735	0.228780	0.075300	0.006606	-0.043739	1066	39	1076	167	0.94	1066	39
BH1	03/12/2018 (2) 21:46:47.00	BH1 - 169	156	6	158	6	4.746084	0.295397	0.089400	0.005788	0.159410	1233	66	1412	120	12.71	1233	66
BH1	03/12/2018 (2) 21:48:53.00	BH1 - 170	362	33	148	19	5.390836	0.189188	0.076400	0.004228	0.136550	1097	34	1105	108	0.70	1097	34
BH1	03/12/2018 (2) 21:50:54.00	BH1 - 171	309	47	213	45	9.551098	0.647139	0.100300	0.008806	0.309270	642	39	1629	156	60.60	642	39
BH1	03/12/2018 (2) 21:52:58.00	BH1 - 172	269	10	234	11	3.107520	0.111399	0.113800	0.005676	0.338850	1799	55	1860	88	3.32	1860	88
BH1	03/12/2018 (2) 21:55:00.00	BH1 - 173	98	9	72	5	6.013229	0.293827	0.074700	0.008294	-0.010710	992	43	1060	209	6.44	992	43
BH1	03/12/2018 (2) 21:57:05.00	BH1 - 174	433	29	204	15	5.192108	0.176629	0.078000	0.004060	0.123350	1135	34	1146	101	0.92	1135	34
BH1	03/12/2018 (2) 21:59:06.00	BH1 - 175	681	7	447	14	4.599816	0.178745	0.086700	0.003434	0.071783	1268	43	1353	75	6.27	1268	43
BH1	03/12/2018 (2) 22:01:13.00	BH1 - 176	1175	56	345	17	5.230126	0.142898	0.079000	0.003080	0.316450	1128	28	1171	76	3.70	1128	28
BH1	03/12/2018 (2) 22:03:19.00	BH1 - 177	253	19	114	11	4.892368	0.172047	0.080700	0.005014	0.259840	1199	37	1213	118	1.19	1199	37
BH1	03/12/2018 (2) 22:05:26.00	BH1 - 178	317	11	90	12	5.903188	0.330634	0.093500	0.005970	0.320110	1009	50	1497	117	32.62	1009	50
BH1	03/12/2018 (2) 22:07:26.00	BH1 - 179	251	10	7	0	1.828154	0.053608	0.203400	0.006968	0.181000	2813	65	2853	55	1.41	2853	55
BH1	03/12/2018 (2) 22:09:32.00	BH1 - 180	147	10	69	6	4.948046	0.292378	0.090900	0.007018	0.067903	1187	61	1444	141	17.83	1187	61
BH1	03/12/2018 (2) 22:11:31.00	BH1 - 181	86	7	53	6	5.688282	0.246428	0.073700	0.007574	0.171250	1044	40	1032	196	-1.16	1044	40
BH1	03/12/2018 (2) 22:13:39.00	BH1 - 182	745	25	502	18	5.767013	0.251700	0.122000	0.019440	-0.641230	1031	40	1985	260	48.07	1031	40
BH1	03/12/2018 (2) 22:15:39.00	BH1 - 183	213	7	88	4	7.122507	0.314933	0.109900	0.009498	-0.333060	847	34	1797	150	52.87	847	34
BH1	03/12/2018 (2) 22:17:43.00	BH1 - 184	155	10	90	7	3.272251	0.146823	0.109100	0.005182	-0.081119	1719	65	1784	85	3.62	1784	85
BH1	03/12/2018 (2) 22:19:44.00	BH1 - 185	73	2	36	2	4.280822	0.195569	0.097000	0.008440	0.094177	1353	54	1566	156	13.58	1353	54
BH1	03/12/2018 (2) 22:21:51.00	BH1 - 186	59	5	31	4	2.028398	0.098170	0.186700	0.010134	0.234300	2584	99	2713	88	4.76	2713	88
BH1	03/12/2018 (2) 22:23:51.00	BH1 - 187	426	33	208	21	4.239084	0.133300	0.087400	0.003748	0.250000	1365	38	1369	81	0.23	1365	38
BH1	03/12/2018 (2) 22:25:58.00	BH1 - 188	33	2	15	1	4.761905	0.247166	0.083000	0.011660	0.031825	1229	55	1268	253	3.09	1229	55
BH1	03/12/2018 (2) 22:28:00.00	BH1 - 189	494	25	359	20	4.187605	0.215272	0.167600	0.007052	-0.085892	1381	61	2533	70	45.50	1381	61
BH1	03/12/2018 (2) 22:40:40.00	BH1 - 190	108	5	129	8	5.157298	0.230815	0.090600	0.010312	-0.460380	1143	45	1437	204	20.49	1143	45
BH1	03/12/2018 (2) 22:42:47.00	BH1 - 191	181	10	122	9	5.015045	0.170723	0.084500	0.005990	0.236640	1172	35	1303	133	10.06	1172	35
BH1	03/12/2018 (2) 22:44:48.00	BH1 - 192	170	14	244	20	4.468275	0.169227	0.085100	0.006102	0.302450	1302	43	1317	134	1.15	1302	43
BH1	03/12/2018 (2) 22:46:53.00	BH1 - 193	610	10	409	13	7.942812	0.650945	0.092300	0.004746	-0.032167	764	55	1473	95	48.10	764	55
BH1	03/12/2018 (2) 22:48:54.00	BH1 - 194	38	3	97	17	5.494505	0.441976	0.097000	0.015940	0.112930	1078	74	1566	281	31.17	1078	74
BH1	03/12/2018 (2) 22:50:58.00	BH1 - 195	64	3	41	1	3.061849	0.124986	0.112000	0.008840	0.182030	1822	63	1831	138	0.50	1831	138
BH1	03/12/2018 (2) 22:52:59.00	BH1 - 196	71	3	78	4	3.411805	0.146227	0.103600	0.006872	0.273230	1657	60	1689	118	1.88	1689	118
BH1	03/12/2018 (2) 22:55:05.00	BH1 - 197	138	8	39	3	3.131851	0.119526	0.110900	0.006318	0.043171	1786	58	1813	101	1.49	1813	101
BH1	03/12/2018 (2) 22:57:05.00	BH1 - 198	123	10	45	3	4.230118	0.181229	0.089000	0.006880	-0.087547	1368	51	1403	142	2.49	1368	51
BH1	03/12/2018 (2) 22:59:11.00	BH1 - 199	202	7	40	2	5.420054	0.193594	0.077400	0.005748	0.283000	1092	35	1131	142	3.49	1092	35
BH1	03/12/2018 (2) 23:01:12.00	BH1 - 200	162	20	116	17	7.072136	0.551567	0.107400	0.009948	0.393890	853	58	1755	161	51.42	853	58
BH1	13/07/2020 (2) 12:49:08.00	BH1 - 139b	854	12	892	9	8.124797	0.261514	0.066600	0.002532	0.274600	748	22	824	78	9.23	748	22
BH1	13/07/2020 (2) 12:50:44.00	BH1 - 139c	1313	12	2673	17	9.174312	0.326572	0.073300	0.002766	-0.078192	667	22	1021	76	34.70	667	22
BH1	13/07/2020 (2) 12:52:10.00	BH1 - 139d	385	6	495	3	8.833922	0.309343	0.073700	0.003474	0.279760	691	22	1032	93	33.04	691	22
BH1	13/07/2020 (2) 12:53:40.00	BH1 - 2.4	503	12	625	20	7.535795	0.252935	0.066900	0.002838	0.128490	803	25	834	87	3.65	803	25
BH1	13/07/2020 (2) 12:55:08.00	BH1 - 2.5	233	7	105	5	4.553734	0.151211	0.087100	0.003842	0.307920	1280	37	1362	84	6.02	1280	37
BH1	13/07/2020 (2) 12:56:39.00	BH1 - 2.6	253	3	127	1	5.353319	0.190175	0.077600	0.003952	0.392710	1104	35	1136	99	2.80	1104	35
BH1	13/07/2020 (2) 12:58:05.00	BH1 - 2.7	180	4	85	2	4.372540	0.156280	0.089100	0.004282	0.313820	1328	42	1405	90	5.53	1328	42
BH1	13/07/2020 (2) 12:59:34.00	BH1 - 2.8	466	7	160	3	4.024145	0.130684	0.094800	0.003596	0.489130	1431	40	1523	71	6.08	1431	40
BH1	13/07/2020 (2) 13:01:03.00	BH1 - 2.9	488	37	387	59	6.365372	0.451451	0.078500	0.003470	-0.132240	941	58	1159	86	18.82	941	58
BH1	13/07/2020 (2) 13:02:34.00	BH1 - 2.10	321	9	180	5	3.866976	0.286689	0.101300	0.003826	0.191940	1483	92	1647	69	9.99	1483	92
BH1	13/07/2020 (2) 13:04:01.00	BH1 - 2.11	434	14	387	20	5.470460	0.294950	0.105500	0.004110	0.116590	1082	51	1722	71	37.16	1082	51
BH1	13/07/2020 (2) 13:05:31.00	BH1 - 2.12	256	16	93	5	3.927730	0.131007	0.095800	0.004116	0.295560	1462	42	1543	80	5.24	1462	42
BH1	13/07/2020 (2) 13:06:59.00	BH1 - 2.13	112	2	72	2	3.966680	0.142272	0.093100	0.004862	0.292290	1449	45	1489	97	2.67	1449	45
BH1	13/07/2020 (2) 13:08:31.00	BH1 - 2.14	563	10	322	9	4.935834	0.162059	0.089000	0.003480	0.406310	1189	35	1403	74	15.25	1189	35
BH1	13/07/2020 (2) 13:09:57.00	BH1 - 2.15	60	1	28	1	5.192108	0.208978	0.083700	0.006074	0.177690	1135	40	1285	136	11.62	1135	40
BH1	13/07/2020 (2) 13:11:26.00	BH1 - 2.16	406	7	128	2	5.359057	0.173236	0.078400	0.003268	0.324630	1103	32	1156	81	4.60	1103	32
BH1	13/07/2020 (2) 13:12:55.00	BH1 - 2.17	438	20	185	5	5.464481	0.177969	0.077000	0.003140	0.097225	1083	32	1120	80	3.30	1083	32
BH1	13/07/2020 (2) 13:14:26.00	BH1 - 2.18	237	7	115	3	4.732608	0.159605	0.081400	0.003728	0.239890	1236	37	1230	88	-0.45	1236	37
BH1	13/07/2020 (2) 13:15:53.00	BH1 - 2.19	638	8	421	5	5.291005	0.170208	0.081300	0.002926	0.353380	1116	32	1228	70	9.11	1116	32
BH1	13/07/2020 (2) 13:17:21.00	BH1 - 2.20	141	2	54	1	3.101737	0.215967	0.112800	0.004956	0.274150	1801	103	1844	78	2.32	1844	78
BH1	13/07/2020 (2) 13:18:50.00	BH1 - 2.21	132	2	40	0	5.279831	0.186439	0.078800	0.004476	0.087961	1118	35	1166	109	4.12	1118	35
BH1	13/07/2020 (2) 13:20:21.00	BH1 - 2.22	614	11	208	3	5.440696	0.179857	0.078700	0.002974	0.281610	1088	32	1164	74	6.53	1088	32
BH1	13/07/2020 (2) 13:26:24.00	BH1 - 2.23	738	13	373	6	4.088307	0.135252	0.094800	0.003296	0.227040	1411	41	1523	65	7.40	1411	41
BH1	13/07/2020 (2) 13:27:55.00	BH1 - 2.24	333	6	194	3	5.428882	0.182260	0.076600	0.003232	0.338080	1090	33	1110	83	1.80	1090	33
BH1	13/07/2020 (2) 13:29:24.00	BH1 - 2.25	108	2	52	1	4.351610	0.153310	0.086100	0.004522	0.316200	1333	41	1340	99	0.46	1333	41
BH1	13/07/2020 (2) 13:30:53.00	BH1 - 2.26	672	10	220	3	5.112474	0.167593	0.081700	0.002834	0.239590	1152	34	1238	67	6.94	1152	34
BH1	13/07/2020 (2) 13:32:25.00	BH1 - 2.27	148	5	86	3	4.079967	0.138196	0.091300	0.004026	0.079022	1413	42	1452	83	2.67	1413	42
BH1	13/07/2020 (2) 13:33:52.00	BH1 - 2.28	292	7	181	4	5.094244	0.166763	0.079800	0.003296	0.132380	1155	34	1191	80	3.00	1155	34
BH1	13/07/2020 (2) 13:35:20.00	BH1 - 2.29	142	3	106	2	5.402485	0.183936	0.080800	0.004516	0.165200	1095	33	1216	107	9.95	1095	33
BH1	13/07/2020 (2) 13:36:49.00	BH1 - 2.30	195	3	84	2	3.313453	0.230954	0.110200	0.004504	0.354800	1700	98	1802	73	5.64	1802	73
BH1	13/07/2020 (2) 13:38:20.00	BH1 - 2.31	109	2	69	2	4.737091	0.171038	0.086900	0.005138	0.200560	1235	39	1357	111	9.04	1235	39
BH1	13/07/2020 (2) 13:39:47.00	BH1 - 2.32	266	4	190	2	5.571031	0.189012	0.078700	0.003774	-0.002818	1064	32	1164	93	8.55	1064	32
BH1	13/07/2020 (2) 13:41:16.00	BH1 - 2.33	243	4	88	1	5.470460	0.181231	0.078900	0.003978	0.317540	1082	32	1169	98	7.40	1082	32
BH1	13/07/2020 (2) 13:42:44.00	BH1 - 2.34	80	2	46	1	3.918495	0.144395	0.093600	0.005172	0.160010	1465	47	1499	102	2.27	1465	47
BH1	13/07/2020 (2) 13:44:15.00	BH1 - 2.35	206	3	201	3	2.856327	0.203981	0.124600	0.004492	0.128660	1935	112	2022	63	4.31	2022	63
BH1	13/07/2020 (2) 13:45:42.00	BH1 - 2.36	675	12	383	6	6.082725	0.195654	0.077400	0.002748	0.227740	981	28	1131	70	13.22	981	28
BH1	13/07/2020 (2) 13:51:46.00	BH1 - 2.37	222	5	586	16	5.221932	0.180791	0.078900	0.003978	0.204750	1130	35	1169	98	3.35	1130	35
BH1	13/07/2020 (2) 13:53:21.00	BH1 - 2.38	243	6	94	2	5.205622	0.177278	0.078900	0.003478	0.239660	1133	34	1169	86	3.08	1133	34
BH1	13/07/2020 (2) 13:54:50.00	BH1 - 2.39	417	8	206	3	4.020909	0.133772	0.094600	0.003492	0.420860	1432	41	1519	69	5.76	1432	41
BH1	13/07/2020 (2) 13:56:21.00	BH1 - 2.40	572	18	241	10	4.436557	0.153685	0.110100	0.003702	0.034279	1310	40	1800	61	27.21	1310	40
BH1	13/07/2020 (2) 13:57:48.00	BH1 - 2.41	270	2	112	3	5.780347	0.202479	0.075000	0.003700	0.208550	1029	32	1068	97	3.65	1029	32
BH1	13/07/2020 (2) 13:59:17.00	BH1 - 2.42	148	5	173	5	3.918495	0.133646	0.093700	0.004474	0.238240	1465	43	1501	89	2.40	1465	43
BH1	13/07/2020 (2) 14:00:45.00	BH1 - 2.43	510	4	292	3	4.244482	0.138937	0.091400	0.003328	0.246450	1364	39	1454	69	6.21	1364	39
BH1	13/07/2020 (2) 14:02:16.00	BH1 - 2.44	180	11	155	13	2.446184	0.174584	0.172300	0.006046	0.225720	2209	126	2579	58	14.34	2579	58
BH1	13/07/2020 (2) 14:08:21.00	BH1 - 2.45	204	5	50	1	3.075031	0.222249	0.115400	0.004608	0.403980	1815	108	1885	71	3.72	1885	71
BH1	13/07/2020 (2) 14:09:51.00	BH1 - 2.46	576	4	347	4	5.577245	0.192420	0.093800	0.003676	0.437180	1063	33	1503	73	29.27	1063	33
BH1	13/07/2020 (2) 14:11:20.00	BH1 - 2.47	624	19	443	19	5.558644	0.182239	0.078500	0.002770	0.082129	1066	31	1159	69	7.96	1066	31
BH1	13/07/2020 (2) 14:12:48.00	BH1 - 2.48	122	4	60	2	3.309067	0.241380	0.107100	0.004842	0.002900	1702	103	1750	81	2.72	1750	81
BH1	13/07/2020 (2) 14:14:20.00	BH1 - 2.49	161	1	182	2	4.894763	0.172167	0.087200	0.004344	0.278570	1198	37	1364	94	12.15	1198	37
BH1	13/07/2020 (2) 14:15:47.00	BH1 - 2.50	233	3	237	3	5.125577	0.191835	0.090400	0.004008	0.329340	1149	38	1433	83	19.83	1149	38
BH1	13/07/2020 (2) 14:17:16.00	BH1 - 2.51	330	6	188	3	3.227889	0.231266	0.112900	0.003858	0.270790	1740	103	1846	61	5.75	1846	61
BH1	13/07/2020 (2) 14:18:45.00	BH1 - 2.52	427	4	174	2	6.501951	0.214590	0.073100	0.003362	0.393180	922	28	1016	91	9.21	922	28
BH1	13/07/2020 (2) 14:20:16.00	BH1 - 2.53	71	3	27	1	2.921414	0.212052	0.119800	0.006096	0.361990	1898	112	1952	89	2.80	1952	89
BH1	13/07/2020 (2) 14:21:42.00	BH1 - 2.54	390	14	168	7	5.530973	0.187099	0.078700	0.003374	0.295700	1071	32	1164	84	7.94	1071	32
BH1	13/07/2020 (2) 14:23:11.00	BH1 - 2.55	650	8	68	1	5.246590	0.176501	0.082400	0.003448	-0.293660	1125	34	1254	81	10.33	1125	34
BH1	13/07/2020 (2) 14:24:40.00	BH1 - 2.56	341	4	133	1	4.793864	0.160224	0.084100	0.003482	0.400200	1221	36	1294	79	5.61	1221	36
BH1	13/07/2020 (2) 14:26:11.00	BH1 - 2.57	329	4	395	5	3.772161	0.274652	0.095700	0.003514	0.226150	1516	92	1541	68	1.63	1541	68
BH1	13/07/2020 (2) 14:27:38.00	BH1 - 2.58	478	13	190	6	4.585053	0.205224	0.118800	0.004376	-0.037335	1272	50	1937	65	34.36	1272	50
BH1	13/07/2020 (2) 14:29:07.00	BH1 - 2.59	246	6	70	2	3.921569	0.133795	0.094200	0.003884	0.310470	1464	43	1511	77	3.12	1464	43
BH1	13/07/2020 (2) 14:30:36.00	BH1 - 2.60	228	4	202	4	3.186743	0.226220	0.107000	0.004140	0.351960	1759	103	1748	70	-0.65	1748	70
BH1	13/07/2020 (2) 14:32:08.00	BH1 - 2.61	99	3	58	2	5.307856	0.204764	0.084400	0.005288	0.181740	1113	38	1301	118	14.47	1113	38
BH1	13/07/2020 (2) 14:33:35.00	BH1 - 2.62	418	4	513	33	5.390836	0.221155	0.089500	0.003390	0.168330	1097	40	1414	72	22.42	1097	40
BH1	13/07/2020 (2) 14:35:03.00	BH1 - 2.63	209	5	161	4	4.332756	0.148605	0.089200	0.003884	0.269380	1339	40	1408	82	4.90	1339	40
BH1	13/07/2020 (2) 14:36:33.00	BH1 - 2.64	134	3	33	1	4.980080	0.178965	0.094100	0.005082	0.317590	1180	38	1509	99	21.84	1180	38
BH1	13/07/2020 (2) 14:38:03.00	BH1 - 2.65	73	1	24	0	4.723666	0.179263	0.078700	0.005074	0.359120	1238	41	1164	124	-6.38	1238	41
BH1	13/07/2020 (2) 14:39:30.00	BH1 - 2.66	129	2	56	1	5.373455	0.202753	0.075400	0.004708	0.304140	1100	37	1078	121	-2.03	1100	37
BH1	13/07/2020 (2) 14:45:34.00	BH1 - 2.67	68	1	39	1	5.783690	0.229407	0.076600	0.005632	0.128800	1028	36	1110	141	7.37	1028	36
BH1	13/07/2020 (2) 14:47:06.00	BH1 - 2.68	231	4	154	3	4.380201	0.147081	0.088600	0.003772	0.187760	1326	39	1395	80	4.96	1326	39
BH1	13/07/2020 (2) 14:48:35.00	BH1 - 2.69	144	4	67	2	5.633803	0.198373	0.073300	0.004466	0.336710	1053	33	1021	120	-3.13	1053	33
BH1	13/07/2020 (2) 14:50:06.00	BH1 - 2.70	86	3	53	2	5.122951	0.191691	0.075600	0.005212	0.298080	1149	38	1084	133	-6.08	1149	38
BH1	13/07/2020 (2) 14:51:32.00	BH1 - 2.71	149	3	123	2	4.849661	0.172255	0.083800	0.004276	0.418200	1209	38	1287	97	6.10	1209	38
BH1	13/07/2020 (2) 14:53:02.00	BH1 - 2.72	457	11	235	7	5.760369	0.194844	0.078200	0.003064	0.472090	1032	31	1151	77	10.35	1032	31
BH1	13/07/2020 (2) 14:59:04.00	BH1 - 2.73	823	13	342	3	4.271679	0.147474	0.095900	0.003218	0.260640	1356	41	1545	63	12.24	1356	41
BH1	13/07/2020 (2) 15:00:39.00	BH1 - 2.74	215	5	262	6	2.207506	0.156231	0.159000	0.005480	0.281380	2409	134	2444	58	1.46	2444	58
BH1	13/07/2020 (2) 15:02:10.00	BH1 - 2.75	289	9	215	4	4.460303	0.158836	0.110600	0.004812	0.438300	1304	41	1809	78	27.89	1304	41
BH1	13/07/2020 (2) 15:03:37.00	BH1 - 2.76	456	39	154	13	5.577245	0.220415	0.081500	0.003430	0.073918	1063	37	1233	81	13.75	1063	37
BH1	13/07/2020 (2) 15:05:05.00	BH1 - 2.77	261	9	106	4	4.284490	0.148103	0.087200	0.003644	0.129470	1352	41	1364	79	0.87	1352	41
BH1	13/07/2020 (2) 15:06:33.00	BH1 - 2.78	561	27	227	15	4.382121	0.172136	0.098200	0.004764	-0.000249	1325	45	1589	89	16.63	1325	45
BH1	13/07/2020 (2) 15:08:04.00	BH1 - 2.79	293	2	151	2	5.527916	0.183897	0.078100	0.003462	0.304470	1072	32	1149	87	6.67	1072	32
BH1	13/07/2020 (2) 15:09:31.00	BH1 - 2.80	782	50	343	17	5.917160	0.608522	0.099300	0.006386	-0.676930	1007	87	1610	116	37.49	1007	87
BH1	13/07/2020 (2) 15:11:00.00	BH1 - 2.81	134	5	74	2	3.888025	0.135204	0.091900	0.004738	0.249390	1476	44	1465	96	-0.75	1476	44
BH1	13/07/2020 (2) 15:12:29.00	BH1 - 2.82	240	3	76	1	5.130836	0.176328	0.079200	0.003784	0.239900	1148	35	1176	93	2.41	1148	35
BH1	13/07/2020 (2) 15:14:01.00	BH1 - 2.83	251	5	68	1	3.410641	0.242700	0.104500	0.003890	0.258550	1658	98	1705	68	2.77	1705	68
BH1	13/07/2020 (2) 15:15:27.00	BH1 - 2.84	252	2	104	1	4.032258	0.137552	0.093200	0.003864	0.296910	1428	42	1491	77	4.22	1428	42
BH1	13/07/2020 (2) 15:16:55.00	BH1 - 2.85	613	12	158	3	5.485464	0.178917	0.077900	0.002758	0.220400	1080	31	1143	70	5.59	1080	31
BH1	13/07/2020 (2) 15:18:24.00	BH1 - 2.86	201	5	506	16	4.780115	0.161866	0.080800	0.003716	0.161500	1225	37	1216	89	-0.73	1225	37
BH1	13/07/2020 (2) 15:19:56.00	BH1 - 2.87	215	7	222	10	3.734130	0.269895	0.102100	0.004342	0.271840	1530	92	1662	78	7.96	1662	78
BH1	13/07/2020 (2) 15:21:22.00	BH1 - 2.88	356	8	211	5	4.823927	0.196541	0.096700	0.003934	0.446160	1214	43	1561	75	22.18	1214	43
BH1	13/07/2020 (2) 15:27:26.00	BH1 - 2.89	157	3	93	2	3.264773	0.235835	0.109700	0.004594	0.239230	1723	103	1794	75	3.96	1794	75
BH1	13/07/2020 (2) 15:28:59.00	BH1 - 2.90	437	9	166	4	5.580357	0.189458	0.076300	0.003226	0.173770	1063	32	1102	83	3.58	1063	32
BH1	13/07/2020 (2) 15:30:27.00	BH1 - 2.91	536	8	638	6	3.909304	0.292143	0.111200	0.003724	0.268180	1468	92	1818	60	19.25	1468	92
BH1	13/07/2020 (2) 15:31:59.00	BH1 - 2.92	245	5	167	4	5.025126	0.168683	0.081900	0.003838	0.380430	1170	35	1242	90	5.82	1170	35
BH1	13/07/2020 (2) 15:33:27.00	BH1 - 2.93	311	19	119	6	3.980892	0.222245	0.108800	0.004176	0.062901	1445	69	1779	69	18.77	1445	69
BH1	13/07/2020 (2) 15:34:54.00	BH1 - 2.94	875	32	577	12	8.605852	0.453548	0.076800	0.003636	-0.214650	709	34	2453	-1245	71.11	709	34
BH1	13/07/2020 (2) 15:36:23.00	BH1 - 2.95	186	4	76	2	4.705882	0.160554	0.084400	0.003988	0.197580	1242	37	1301	90	4.52	1242	37
BH1	13/07/2020 (2) 15:37:56.00	BH1 - 2.96	484	6	437	5	4.504505	0.150962	0.090500	0.003010	0.294320	1292	38	1435	63	9.95	1292	38
BH1	13/07/2020 (2) 15:39:22.00	BH1 - 2.97	61	1	73	1	3.992016	0.145179	0.090800	0.006216	0.172030	1441	46	1442	126	0.03	1441	46
BH1	13/07/2020 (2) 15:40:51.00	BH1 - 2.98	259	3	104	2	4.807692	0.167807	0.087000	0.003540	0.111950	1218	38	1360	77	10.40	1218	38
BH1	13/07/2020 (2) 15:42:20.00	BH1 - 2.99	317	6	440	8	3.841721	0.125539	0.096000	0.003920	0.237780	1491	42	1547	76	3.59	1491	42
BH1	13/07/2020 (2) 15:43:51.00	BH1 - 2.100	355	12	160	7	5.296610	0.181678	0.079400	0.003488	0.352980	1115	34	1181	85	5.62	1115	34
BH1	13/07/2020 (2) 15:45:17.00	BH1 - 2.101	276	8	183	7	4.623209	0.152312	0.088300	0.003666	0.372000	1262	37	1388	78	9.07	1262	37
BH1	13/07/2020 (2) 15:46:47.00	BH1 - 2.102	451	8	185	4	5.917160	0.195371	0.078600	0.003272	0.235790	1007	30	1161	81	13.31	1007	30
BH1	13/07/2020 (2) 15:48:15.00	BH1 - 2.103	137	2	63	1	5.503577	0.194882	0.079000	0.004280	0.122640	1076	34	1171	105	8.11	1076	34
BH1	13/07/2020 (2) 15:49:46.00	BH1 - 2.104	152	4	85	2	3.353454	0.235754	0.107000	0.004340	0.513470	1682	98	1748	73	3.76	1748	73
BH1	13/07/2020 (2) 15:51:12.00	BH1 - 2.105	125	1	123	1	3.898635	0.134210	0.092900	0.004558	0.134630	1472	44	1485	91	0.88	1472	44
BH1	13/07/2020 (2) 15:52:41.00	BH1 - 2.106	261	6	204	5	3.109453	0.216888	0.115600	0.004312	0.351480	1798	103	1888	67	4.81	1888	67
BH1	13/07/2020 (2) 15:54:09.00	BH1 - 2.107	109	2	74	1	5.197505	0.184992	0.082500	0.005250	0.144030	1134	36	1257	121	9.72	1134	36
BH1	13/07/2020 (2) 15:55:42.00	BH1 - 2.108	145	2	108	2	5.197505	0.182291	0.080100	0.004002	0.358880	1134	35	1199	96	5.36	1134	35
BH1	13/07/2020 (2) 15:57:07.00	BH1 - 2.109	133	3	178	4	5.241090	0.184482	0.080500	0.004510	0.381600	1126	35	1208	107	6.84	1126	35
BH1	13/07/2020 (2) 15:58:37.00	BH1 - 2.110	532	9	367	7	16.835020	0.705144	0.193300	0.011266	-0.410070	372	15	2770	93	86.57	372	15
BH1	13/07/2020 (2) 16:09:15.00	BH1 - 2.111	597	22	270	11	6.644518	0.278584	0.074900	0.002998	-0.042243	904	34	1065	79	15.13	904	34
BH1	13/07/2020 (2) 16:10:47.00	BH1 - 2.112	302	7	169	5	5.109862	0.170085	0.081400	0.003528	0.235460	1152	34	1230	84	6.34	1152	34
BH1	13/07/2020 (2) 16:12:16.00	BH1 - 2.113	199	2	104	1	2.470966	0.177638	0.167000	0.005640	0.229260	2191	126	2527	56	13.31	2527	56
BH1	13/07/2020 (2) 16:13:47.00	BH1 - 2.114	96	4	43	2	4.359198	0.153693	0.084300	0.004886	0.052563	1331	41	1299	110	-2.52	1331	41
BH1	13/07/2020 (2) 16:15:14.00	BH1 - 2.115	389	8	376	6	4.048583	0.153092	0.188300	0.006166	0.212450	1423	47	2727	54	47.81	1423	47
BH1	13/07/2020 (2) 16:16:44.00	BH1 - 2.116	673	20	438	24	5.747126	0.204122	0.115500	0.004410	0.149700	1034	33	1887	68	45.20	1034	33
BH1	13/07/2020 (2) 16:18:14.00	BH1 - 2.117	383	7	130	3	3.957262	0.130823	0.092400	0.003748	0.277650	1452	42	1475	76	1.52	1452	42
BH1	13/07/2020 (2) 16:19:45.00	BH1 - 2.118	247	4	106	1	3.940110	0.134690	0.092800	0.003756	0.259330	1458	43	1483	76	1.68	1458	43
BH1	13/07/2020 (2) 16:21:12.00	BH1 - 2.119	41	2	32	2	5.643341	0.249810	0.074400	0.006588	0.384930	1052	41	1051	170	-0.03	1052	41
BH1	13/07/2020 (2) 16:22:41.00	BH1 - 2.120	93	2	43	1	3.921569	0.278354	0.093500	0.005270	0.450850	1464	87	1497	104	2.20	1464	87
BH1	13/07/2020 (2) 16:24:10.00	BH1 - 2.121	144	2	37	1	4.655493	0.162465	0.085200	0.004004	0.300480	1254	39	1319	89	4.92	1254	39
BH1	13/07/2020 (2) 16:25:40.00	BH1 - 2.122	127	2	60	1	4.110152	0.146398	0.093700	0.004674	0.196410	1404	44	1501	92	6.49	1404	44
BH1	13/07/2020 (2) 16:27:07.00	BH1 - 2.123	314	10	53	3	4.708098	0.160661	0.082700	0.003654	0.379730	1242	37	1261	85	1.56	1242	37
BH1	13/07/2020 (2) 16:28:35.00	BH1 - 2.124	298	4	116	2	5.022602	0.171086	0.096600	0.008132	-0.385310	1170	35	1559	151	24.90	1170	35
BH1	13/07/2020 (2) 16:30:04.00	BH1 - 2.125	612	9	497	5	3.480682	0.251341	0.108100	0.003462	0.429040	1628	98	1767	58	7.86	1767	58
BH1	13/07/2020 (2) 16:31:35.00	BH1 - 2.126	210	5	96	2	4.380201	0.154756	0.085500	0.004010	0.294060	1326	41	1326	89	0.03	1326	41

Appendix D.2 continued.

Sample ID	Analysis date-time	Spot ID[1]	238U conc. ppm	±2σ INT	232Th conc. ppm	±2σ INT	Isotopic Ratios 238U/206Pb	±2σ PROP	207Pb/206Pb	±2σ PROP	rho	Apparent Ages - Calculated in Isoplot R (Ma) 238U/206Pb	±2σ PROP	207Pb/206Pb	±2σ PROP	Discord (7/6-6/8)/7/6 *100	Perferred age 1500 Ma cutoff Ma	2σ
BH1	13/07/2020 (2) 16:33:01.00	BH1 - 2.127	141	3	106	3	3.544842	0.259385	0.099500	0.004390	0.311220	1602	97	1614	81	0.74	1614	81
BH1	13/07/2020 (2) 16:34:29.00	BH1 - 2.128	202	4	104	2	2.152853	0.154292	0.171000	0.005620	0.153340	2459	138	2567	55	4.18	2567	55
BH1	13/07/2020 (2) 16:36:00.00	BH1 - 2.129	390	8	359	8	5.464481	0.183941	0.077800	0.003456	0.347000	1083	33	1141	87	5.05	1083	33
BH1	13/07/2020 (2) 16:37:30.00	BH1 - 2.130	389	8	402	8	4.001601	0.134476	0.091400	0.003428	0.181760	1438	42	1454	71	1.11	1438	42
BH1	13/07/2020 (2) 16:38:57.00	BH1 - 2.131	99	3	73	2	4.701457	0.175813	0.082700	0.004454	0.298060	1243	41	1261	103	1.44	1243	41
BH1	13/07/2020 (2) 16:40:25.00	BH1 - 2.132	124	3	83	3	3.531073	0.257649	0.101800	0.004736	0.206530	1608	98	1656	85	2.95	1656	85
BH1	13/07/2020 (2) 16:46:29.00	BH1 - 2.133	126	2	80	1	5.205622	0.179988	0.077700	0.004654	0.161630	1133	35	1138	116	0.49	1133	35
BH1	13/07/2020 (2) 16:48:02.00	BH1 - 2.134	419	34	439	50	3.642987	0.271930	0.104400	0.003788	-0.060682	1564	97	1703	66	8.18	1703	66
BH1	13/07/2020 (2) 16:49:33.00	BH1 - 2.135	351	16	152	8	5.344735	0.181167	0.078900	0.003578	0.219770	1106	33	1169	88	5.39	1106	33
BH1	13/07/2020 (2) 16:51:00.00	BH1 - 2.136	301	3	412	4	2.145462	0.153381	0.160300	0.005106	0.265600	2466	138	2458	54	-0.34	2458	54
BH1	13/07/2020 (2) 16:52:30.00	BH1 - 2.137	799	8	171	2	5.434783	0.173677	0.083900	0.003778	-0.313720	1089	31	1289	86	15.56	1089	31
BH1	13/07/2020 (2) 16:53:58.00	BH1 - 2.138	84	4	102	4	3.298153	0.240008	0.108000	0.006060	0.416410	1707	103	1765	100	3.28	1765	100
BH1	13/07/2020 (2) 16:55:30.00	BH1 - 2.139	83	2	57	2	3.170577	0.224252	0.109300	0.004886	0.330940	1767	103	1787	80	1.11	1787	80
BH1	13/07/2020 (2) 16:56:56.00	BH1 - 2.140	165	4	89	2	3.438790	0.246155	0.101200	0.004424	0.244500	1646	98	1645	80	-0.01	1645	80
BH1	13/07/2020 (2) 16:58:25.00	BH1 - 2.141	287	7	262	10	2.405002	0.169565	0.186700	0.005734	0.254430	2241	126	2713	51	17.37	2713	51
BH1	13/07/2020 (2) 16:59:53.00	BH1 - 2.142	202	5	89	3	4.098361	0.137396	0.093100	0.003762	0.473300	1407	41	1489	75	5.48	1407	41
BH1	13/07/2020 (2) 17:01:25.00	BH1 - 2.143	119	4	55	2	5.681818	0.210486	0.075000	0.004600	0.345420	1045	35	1068	119	2.11	1045	35
BH1	13/07/2020 (2) 17:02:52.00	BH1 - 2.144	129	3	111	3	4.098361	0.139076	0.091800	0.004136	0.188140	1407	42	1462	84	3.76	1407	42
BH1	13/07/2020 (2) 17:04:20.00	BH1 - 2.145	852	7	470	5	7.092199	0.237413	0.079700	0.002994	0.029017	850	26	1189	73	28.47	850	26
BH1	13/07/2020 (2) 17:05:49.00	BH1 - 2.146	207	5	105	4	3.889537	0.138305	0.094900	0.004298	0.306570	1475	45	1525	84	3.29	1475	45
BH1	13/07/2020 (2) 17:07:20.00	BH1 - 2.147	379	8	526	23	5.534034	0.205620	0.112900	0.004558	0.301710	1071	35	1846	72	41.99	1071	35
BH1	13/07/2020 (2) 17:13:23.00	BH1 - 2.148	254	5	181	3	4.923683	0.171202	0.086400	0.003728	0.241510	1192	37	1346	82	11.46	1192	37
BH1	13/07/2020 (2) 17:14:56.00	BH1 - 2.149	126	1	68	1	5.497526	0.197597	0.077900	0.004758	0.340880	1077	35	1143	118	5.78	1077	35
BH1	13/07/2020 (2) 17:16:25.00	BH1 - 2.150	478	8	113	2	3.984064	0.130474	0.091500	0.003230	0.284900	1444	41	1456	67	0.86	1444	41
BH1	13/07/2020 (2) 17:17:53.00	BH1 - 2.151	123	3	39	1	4.008016	0.144417	0.091600	0.004432	0.295910	1436	45	1458	90	1.54	1436	45
BH1	13/07/2020 (2) 17:19:24.00	BH1 - 2.152	273	7	148	4	5.070994	0.168279	0.081700	0.003734	0.277160	1160	34	1238	88	6.24	1160	34
BH1	13/07/2020 (2) 17:20:51.00	BH1 - 2.153	49	1	67	1	4.037142	0.160606	0.093600	0.005972	0.353460	1427	49	1499	117	4.84	1427	49
BH1	13/07/2020 (2) 17:22:20.00	BH1 - 2.154	304	5	347	6	7.892660	0.282441	0.065800	0.003316	0.333320	769	25	799	103	3.77	769	25
BH1	13/07/2020 (2) 17:28:23.00	BH1 - 2.155	169	5	73	2	2.051703	0.146271	0.166600	0.005532	0.271700	2559	142	2523	55	-1.44	2523	55
BH1	13/07/2020 (2) 17:29:56.00	BH1 - 2.156	40	1	34	1	5.232862	0.214189	0.080400	0.007108	0.298570	1127	41	1206	166	6.52	1127	41
BH1	13/07/2020 (2) 17:31:27.00	BH1 - 2.157	373	21	96	7	5.356186	0.196059	0.077000	0.003640	0.148600	1103	36	1120	92	1.50	1103	36
BH1	13/07/2020 (2) 17:32:55.00	BH1 - 2.158	100	2	38	1	4.118616	0.141743	0.091800	0.004736	0.342860	1401	42	1462	96	4.18	1401	42
BH1	13/07/2020 (2) 17:34:23.00	BH1 - 2.159	741	12	411	7	5.025126	0.161107	0.091200	0.003224	0.208470	1170	33	1450	67	19.31	1170	33
BH1	13/07/2020 (2) 17:35:52.00	BH1 - 2.160	100	2	66	1	4.875670	0.175962	0.085900	0.004618	0.247650	1203	38	1335	101	9.92	1203	38
BH1	13/07/2020 (2) 17:37:23.00	BH1 - 2.161	425	8	243	3	3.915427	0.128899	0.093600	0.003472	0.103850	1466	42	1499	69	2.20	1466	42
BH1	13/07/2020 (2) 17:38:51.00	BH1 - 2.162	590	7	185	2	4.930966	0.161837	0.083500	0.003070	0.258100	1190	35	1280	71	7.01	1190	35
BH1	13/07/2020 (2) 17:40:20.00	BH1 - 2.163	195	5	101	3	4.147657	0.141444	0.089800	0.003996	0.282010	1392	41	1420	84	1.97	1392	41
BH1	13/07/2020 (2) 17:41:49.00	BH1 - 2.164	152	3	109	2	5.211047	0.182970	0.079300	0.004086	0.262450	1132	35	1179	100	3.99	1132	35
BH1	13/07/2020 (2) 17:43:20.00	BH1 - 2.165	294	4	269	4	5.546312	0.187830	0.079600	0.003692	0.212660	1069	32	1186	90	9.91	1069	32
BH1	13/07/2020 (2) 17:44:47.00	BH1 - 2.166	62	2	87	3	5.307856	0.204764	0.077000	0.005740	0.172920	1113	38	1120	143	0.68	1113	38
BH1	13/07/2020 (2) 17:46:16.00	BH1 - 2.167	110	2	95	2	3.606203	0.254190	0.102100	0.004942	0.408140	1578	93	1662	88	5.06	1662	88
BH1	13/07/2020 (2) 17:47:45.00	BH1 - 2.168	418	11	101	4	3.037667	0.217620	0.112400	0.003948	0.311250	1835	108	1838	63	0.18	1838	63
BH1	13/07/2020 (2) 17:49:16.00	BH1 - 2.169	166	3	56	1	4.422822	0.153009	0.087400	0.004148	0.225380	1314	40	1369	90	3.98	1314	40
BH1	13/07/2020 (2) 17:50:42.00	BH1 - 2.170	136	2	78	1	3.921569	0.130719	0.094400	0.004388	0.276350	1464	42	1515	86	3.37	1464	42
BH1	13/07/2020 (2) 17:52:10.00	BH1 - 2.171	340	6	226	4	4.770992	0.156878	0.083800	0.003576	0.475610	1227	36	1287	82	4.69	1227	36
BH1	13/07/2020 (2) 17:53:39.00	BH1 - 2.172	332	3	102	1	4.734848	0.157470	0.083900	0.003478	0.314580	1235	36	1289	79	4.20	1235	36
BH1	13/07/2020 (2) 17:55:11.00	BH1 - 2.173	727	7	109	3	5.350455	0.172852	0.076900	0.002738	0.311300	1105	32	1118	70	1.18	1105	32
BH1	13/07/2020 (2) 17:56:38.00	BH1 - 2.174	445	7	253	4	4.192872	0.138356	0.097700	0.004154	-0.098187	1379	40	1580	78	12.72	1379	40
BH1	13/07/2020 (2) 17:58:07.00	BH1 - 2.175	274	6	121	3	3.367003	0.237391	0.105200	0.003804	0.223630	1676	98	1717	66	2.36	1717	66
BH1	13/07/2020 (2) 17:59:35.00	BH1 - 2.176	314	6	134	2	5.479452	0.187652	0.074200	0.003384	0.379230	1081	33	1046	90	-3.31	1081	33
BH1	13/07/2020 (2) 18:05:39.00	BH1 - 2.177	95	2	56	1	2.726281	0.195745	0.123800	0.005276	0.280220	2014	117	2011	75	-0.17	2011	75
BH1	13/07/2020 (2) 18:07:13.00	BH1 - 2.178	896	28	886	32	5.482456	0.184792	0.085000	0.003000	0.486030	1080	33	1315	68	17.85	1080	33
BH1	13/07/2020 (2) 18:08:40.00	BH1 - 2.179	124	2	49	1	5.035247	0.184372	0.082600	0.004552	0.303270	1168	38	1259	105	7.24	1168	38
BH1	13/07/2020 (2) 18:10:09.00	BH1 - 2.180	250	11	192	10	2.117298	0.149937	0.176300	0.005826	0.324500	2494	138	2618	55	4.74	2618	55
BH1	13/07/2020 (2) 18:11:37.00	BH1 - 2.181	384	8	149	3	4.050223	0.133498	0.089900	0.003298	0.277280	1422	41	1423	69	0.00	1422	41
BH1	13/07/2020 (2) 18:13:10.00	BH1 - 2.182	65	2	74	1	2.805049	0.197730	0.120200	0.006604	0.187040	1966	113	1958	96	-0.37	1958	96
BH1	13/07/2020 (2) 18:14:36.00	BH1 - 2.183	171	9	70	5	5.265929	0.182963	0.077400	0.003848	0.332150	1121	35	1131	97	0.86	1121	35
BH1	13/07/2020 (2) 18:20:40.00	BH1 - 2.184	369	11	152	4	5.678592	0.187739	0.075400	0.003108	0.229630	1046	31	1078	81	3.03	1046	31
BH1	13/07/2020 (2) 18:22:14.00	BH1 - 2.185	117	3	150	3	5.243838	0.192870	0.077200	0.004044	0.085479	1125	37	1126	102	0.03	1125	37
BH1	13/07/2020 (2) 18:23:43.00	BH1 - 2.186	72	2	52	1	2.964720	0.217507	0.115900	0.005418	0.364440	1874	112	1893	83	1.02	1893	83
BH1	13/07/2020 (2) 18:25:13.00	BH1 - 2.187	170	2	77	1	4.498426	0.154723	0.087400	0.004048	0.263880	1294	39	1369	87	5.44	1294	39
BH1	13/07/2020 (2) 18:26:39.00	BH1 - 2.188	249	10	113	8	3.057169	0.220030	0.122400	0.004348	0.175630	1824	108	1991	63	8.36	1991	63
BH1	13/07/2020 (2) 18:28:08.00	BH1 - 2.189	459	8	302	7	10.090820	0.548020	0.220000	0.017400	-0.775280	609	30	2980	123	79.56	609	30
BH1	13/07/2020 (2) 18:29:38.00	BH1 - 2.190	242	10	128	6	5.711022	0.195760	0.074900	0.003698	0.269270	1040	32	1065	97	2.32	1040	32
BH1	13/07/2020 (2) 18:31:09.00	BH1 - 2.191	107	4	176	4	5.704507	0.234493	0.075100	0.004402	0.068727	1041	38	1070	114	2.72	1041	38
BH1	13/07/2020 (2) 18:32:36.00	BH1 - 2.192	456	12	91	1	4.291845	0.141097	0.092400	0.003148	0.155960	1350	39	1475	64	8.45	1350	39
BH1	13/07/2020 (2) 18:34:05.00	BH1 - 2.193	1185	26	341	9	5.882353	0.190311	0.077700	0.002494	0.118930	1012	29	1138	63	11.09	1012	29
BH1	13/07/2020 (2) 18:35:35.00	BH1 - 2.194	150	4	66	2	5.347594	0.192742	0.078100	0.004362	0.113120	1105	35	1149	108	3.78	1105	35
BH1	13/07/2020 (2) 18:37:04.00	BH1 - 2.195	351	6	92	2	5.068424	0.170729	0.078200	0.002964	0.100170	1161	35	1151	74	-0.84	1161	35
BH1	13/07/2020 (2) 18:38:32.00	BH1 - 2.196	252	4	168	4	5.263158	0.182825	0.079200	0.003784	0.297790	1121	35	1176	93	4.66	1121	35
BH1	13/07/2020 (2) 18:40:01.00	BH1 - 2.197	189	5	92	2	3.677823	0.262926	0.129100	0.011882	-0.611840	1550	93	2085	154	25.64	2085	154
BH1	13/07/2020 (2) 18:41:30.00	BH1 - 2.198	382	8	172	3	4.095004	0.133884	0.092500	0.003450	0.228880	1408	40	1477	70	4.63	1408	40
BH1	13/07/2020 (2) 18:47:34.00	BH1 - 2.199	427	5	56	1	5.279831	0.175288	0.077900	0.003358	0.170050	1118	33	1143	84	2.21	1118	33
BH1	13/07/2020 (2) 18:49:09.00	BH1 - 2.200	54	1	1893	22	8.136697	0.387834	0.099400	0.008888	0.063283	747	32	1612	159	53.65	747	32
BH1	13/07/2020 (2) 18:50:35.00	BH1 - 2.201	74	3	50	2	4.918839	0.195157	0.082400	0.005348	0.366140	1193	42	1254	123	4.88	1193	42
BH1	13/07/2020 (2) 18:52:04.00	BH1 - 2.202	156	4	237	6	3.422313	0.119980	0.105700	0.004914	0.264130	1653	50	1726	84	4.24	1726	84
BH1	13/07/2020 (2) 18:53:35.00	BH1 - 2.203	387	7	222	4	5.184033	0.176241	0.077700	0.003454	0.118170	1137	34	1138	87	0.11	1137	34
BH1	13/07/2020 (2) 18:55:05.00	BH1 - 2.204	252	4	104	2	4.972650	0.168689	0.082500	0.003450	0.176680	1181	36	1257	81	5.99	1181	36
BH1	13/07/2020 (2) 18:56:32.00	BH1 - 2.205	94	2	55	1	4.482295	0.163982	0.088300	0.004966	0.414340	1298	42	1388	105	6.48	1298	42
BH1	13/07/2020 (2) 18:58:01.00	BH1 - 2.206	62	1	75	1	5.546312	0.215516	0.080500	0.006110	0.221480	1069	37	1208	143	11.57	1069	37
BH1	13/07/2020 (2) 18:59:29.00	BH1 - 2.207	147	3	115	3	5.089059	0.179477	0.079500	0.004190	0.170270	1156	36	1184	102	2.30	1156	36
BH1	13/07/2020 (2) 19:01:01.00	BH1 - 2.208	306	15	370	40	3.588088	0.252003	0.103700	0.003874	0.111310	1585	93	1691	68	6.25	1691	68
BH1	13/07/2020 (2) 19:02:28.00	BH1 - 2.209	818	24	779	31	8.520791	0.279322	0.064800	0.002596	0.381990	715	22	767	83	6.72	715	22
BH1	13/07/2020 (2) 19:03:57.00	BH1 - 2.210	344	5	154	4	5.787037	0.202814	0.076000	0.003620	0.461780	1028	32	1094	93	6.09	1028	32
BH1	13/07/2020 (2) 19:05:26.00	BH1 - 2.211	210	3	136	2	3.957262	0.135521	0.094000	0.004180	0.389590	1452	43	1507	83	3.64	1452	43
BH1	13/07/2020 (2) 19:06:57.00	BH1 - 2.212	101	5	152	10	5.580357	0.205028	0.074600	0.004592	0.306440	1063	35	1057	120	-0.55	1063	35
BH1	13/07/2020 (2) 19:08:24.00	BH1 - 2.213	349	24	178	18	5.988024	0.550038	0.086600	0.003832	0.153020	996	78	1351	84	26.29	996	78
BH1	13/07/2020 (2) 19:09:53.00	BH1 - 2.214	230	4	252	4	4.123711	0.138591	0.090000	0.003900	0.327270	1400	41	1425	81	1.76	1400	41
BH1	13/07/2020 (2) 19:11:21.00	BH1 - 2.215	209	4	56	1	3.222688	0.230625	0.108700	0.004074	0.125190	1742	103	1777	68	1.95	1777	68
BH1	13/07/2020 (2) 19:12:52.00	BH1 - 2.216	238	6	176	4	2.126302	0.151034	0.172700	0.005254	0.263880	2485	138	2583	51	3.81	2583	51
BH1	13/07/2020 (2) 19:14:19.00	BH1 - 2.217	64	1	129	1	5.614823	0.225791	0.076700	0.005834	0.099535	1057	38	1113	146	5.03	1057	38
BH1	13/07/2020 (2) 19:15:49.00	BH1 - 2.218	257	3	144	2	4.407228	0.206629	0.092600	0.003952	-0.191580	1318	54	1479	80	10.87	1318	54
BH1	13/07/2020 (2) 19:17:16.00	BH1 - 2.219	164	3	137	3	3.472222	0.250289	0.102400	0.004248	0.379550	1632	98	1667	76	2.14	1667	76
BH1	13/07/2020 (2) 19:18:46.00	BH1 - 2.220	174	3	104	2	3.380663	0.239046	0.110900	0.004918	0.101780	1670	98	1813	79	7.89	1813	79
BH1	13/07/2020 (2) 19:29:24.00	BH1 - 2.221	485	10	220	5	5.422993	0.181982	0.076800	0.002936	-0.001435	1091	33	1115	75	2.16	1091	33
BH1	13/07/2020 (2) 19:30:58.00	BH1 - 2.222	1100	10	883	8	6.027728	0.215022	0.085000	0.002800	0.377830	989	32	1315	63	24.74	989	32
BH1	13/07/2020 (2) 19:32:25.00	BH1 - 2.223	124	3	46	1	4.182350	0.150117	0.087700	0.004054	0.214290	1382	43	1375	87	-0.50	1382	43
BH1	13/07/2020 (2) 19:33:55.00	BH1 - 2.224	544	6	287	3	4.199916	0.140444	0.093200	0.003264	0.291330	1377	40	1491	66	7.66	1377	40
BH1	13/07/2020 (2) 19:35:23.00	BH1 - 2.225	72	2	31	1	5.219207	0.188829	0.079400	0.005088	0.272840	1130	36	1181	123	4.33	1130	36
BH1	13/07/2020 (2) 19:36:55.00	BH1 - 2.226	249	3	551	6	5.803831	0.190182	0.075600	0.003712	0.299920	1025	30	1084	96	5.43	1025	30
BH1	13/07/2020 (2) 19:38:21.00	BH1 - 2.227	107	2	34	1	4.955401	0.177687	0.076800	0.004836	0.273500	1185	38	1115	122	-6.27	1185	38
BH1	13/07/2020 (2) 19:39:51.00	BH1 - 2.228	224	4	107	3	5.970149	0.208510	0.077800	0.003956	0.208180	998	31	1141	99	12.50	998	31
BH1	13/07/2020 (2) 19:41:20.00	BH1 - 2.229	73	2	66	2	7.052186	0.285270	0.086300	0.005926	0.191190	855	31	1344	128	36.40	855	31
BH1	13/07/2020 (2) 19:42:51.00	BH1 - 2.230	185	2	92	2	5.455537	0.189471	0.080300	0.004106	0.112220	1085	34	1204	98	9.85	1085	34
BH1	13/07/2020 (2) 19:44:17.00	BH1 - 2.231	333	4	157	2	5.356186	0.181714	0.082100	0.004142	0.000946	1103	33	1247	97	11.51	1103	33
BH1	13/07/2020 (2) 19:45:47.00	BH1 - 2.232	201	3	78	2	4.982561	0.171646	0.080400	0.003808	0.420960	1179	36	1206	91	2.22	1179	36
BH1	13/07/2020 (2) 19:47:15.00	BH1 - 2.233	102	3	76	2	3.043214	0.218304	0.112600	0.005052	0.222140	1832	108	1841	80	0.51	1841	80
BH1	13/07/2020 (2) 19:48:45.00	BH1 - 2.234	74	1	84	1	3.203075	0.228217	0.113600	0.005472	0.423680	1752	103	1857	85	5.68	1857	85
BH1	13/07/2020 (2) 19:50:12.00	BH1 - 2.235	146	3	86	2	5.138746	0.176714	0.078800	0.004376	0.133840	1146	35	1166	107	1.71	1146	35
BH1	13/07/2020 (2) 19:51:41.00	BH1 - 2.236	86	2	71	2	4.058442	0.145406	0.090100	0.005302	0.162420	1420	44	1427	109	0.48	1420	44
BH1	13/07/2020 (2) 19:53:10.00	BH1 - 2.237	117	5	72	3	4.997501	0.184865	0.083400	0.004368	0.374400	1176	38	1278	100	7.97	1176	38
BH1	13/07/2020 (2) 19:54:41.00	BH1 - 2.238	265	6	76	1	5.128205	0.170940	0.077900	0.003658	0.340170	1148	34	1143	92	-0.44	1148	34
BH1	13/07/2020 (2) 19:56:07.00	BH1 - 2.239	629	4	329	16	4.918839	0.187898	0.091700	0.003234	0.324270	1193	40	1460	66	18.30	1193	40
BH1	13/07/2020 (2) 19:57:37.00	BH1 - 2.240	1090	31	1030	35	5.102041	0.388380	0.321000	0.047420	-0.938870	1154	75	3574	211	67.72	1154	75
BH1	13/07/2020 (2) 19:59:05.00	BH1 - 2.241	674	24	373	16	4.368720	0.144632	0.087300	0.002946	0.052571	1329	39	1366	64	2.75	1329	39
BH1	13/07/2020 (2) 20:00:36.00	BH1 - 2.242	524	14	154	4	4.033885	0.129494	0.090900	0.003218	0.289920	1428	40	1444	67	1.11	1428	40
BH1	13/07/2020 (2) 20:06:41.00	BH1 - 2.243	149	4	84	2	3.393281	0.240581	0.104200	0.004784	0.200250	1665	98	1699	83	2.02	1699	83
BH1	13/07/2020 (2) 20:08:10.00	BH1 - 2.244	745	8	537	4	4.137360	0.135812	0.120500	0.004110	-0.060485	1396	40	1963	60	28.90	1396	40
BH1	13/07/2020 (2) 20:09:39.00	BH1 - 2.245	84	1	54	1	5.431831	0.203052	0.075300	0.005406	0.391130	1089	36	1076	139	-1.28	1089	36
BH1	13/07/2020 (2) 20:11:08.00	BH1 - 2.246	278	5	124	3	2.730748	0.196298	0.129400	0.004288	0.188930	2012	117	2089	58	3.71	2089	58
BH1	13/07/2020 (2) 20:12:40.00	BH1 - 2.247	138	4	136	5	3.835827	0.132628	0.094700	0.004694	0.302270	1493	45	1521	91	1.83	1493	45
BH1	13/07/2020 (2) 20:14:06.00	BH1 - 2.248	231	4	84	2	5.959476	0.211529	0.075000	0.003400	0.132510	1000	32	1068	89	6.33	1000	32
BH1	13/07/2020 (2) 20:15:34.00	BH1 - 2.249	791	17	426	25	5.081301	0.163593	0.084400	0.002988	0.273760	1158	33	1301	68	10.98	1158	33
BH1	13/07/2020 (2) 20:17:04.00	BH1 - 2.250	259	7	104	3	3.220612	0.230370	0.108600	0.004072	0.100590	1743	103	1775	68	1.80	1775	68
BH1	13/07/2020 (2) 20:18:35.00	BH1 - 2.251	232	5	180	4	5.546312	0.190906	0.076200	0.003924	0.337160	1069	33	1099	101	2.80	1069	33
BH1	13/07/2020 (2) 20:20:01.00	BH1 - 2.252	241	2	303	9	5.611672	0.194110	0.077400	0.003648	0.160210	1057	33	1131	92	6.50	1057	33
BH1	13/07/2020 (2) 20:21:31.00	BH1 - 2.253	133	3	52	1	4.786979	0.166777	0.084100	0.004182	0.330310	1223	38	1294	95	5.49	1223	38
BH1	13/07/2020 (2) 20:23:00.00	BH1 - 2.254	163	5	125	5	5.144033	0.221955	0.080100	0.003902	0.021471	1145	44	1199	94	4.46	1145	44
BH1	13/07/2020 (2) 20:24:31.00	BH1 - 2.255	205	5	96	2	4.327131	0.152077	0.086600	0.003932	0.281760	1340	41	1351	86	0.77	1340	41
BH1	13/07/2020 (2) 20:25:58.00	BH1 - 2.256	50	1	19	1	5.260389	0.213127	0.081700	0.006734	0.278220	1122	40	1238	154	9.34	1122	40
BH1	13/07/2020 (2) 20:27:27.00	BH1 - 2.257	72	2	76	2	1.996406	0.147540	0.225700	0.009514	-0.009169	2618	150	3021	67	13.35	3021	67
BH1	13/07/2020 (2) 20:28:55.00	BH1 - 2.258	587	14	334	12	4.649000	0.159981	0.092800	0.003156	0.102070	1256	38	1483	64	15.31	1256	38
BH1	13/07/2020 (2) 20:34:58.00	BH1 - 2.259	483	10	186	4	5.865103	0.192981	0.073300	0.002866	0.024617	1015	30	1021	78	0.63	1015	30
BH1	13/07/2020 (2) 20:36:33.00	BH1 - 2.260	247	5	115	3	4.830918	0.161964	0.082000	0.003740	0.283740	1213	36	1245	88	2.55	1213	36
BH1	13/07/2020 (2) 20:38:00.00	BH1 - 2.261	285	14	181	8	5.524862	0.189860	0.094800	0.003996	0.243830	1072	33	1523	78	29.60	1072	33
BH1	13/07/2020 (2) 20:39:30.00	BH1 - 2.262	1199	18	1231	19	6.009615	0.221316	0.163100	0.005162	-0.133760	992	33	2487	53	60.11	992	33
BH1	13/07/2020 (2) 20:40:59.00	BH1 - 2.263	188	4	84	2	4.945598	0.169843	0.085300	0.004306	-0.026926	1187	36	1322	96	10.17	1187	36
BH1	13/07/2020 (2) 20:42:31.00	BH1 - 2.264	80	2	23	1	3.330003	0.244023	0.104900	0.004998	0.347270	1693	102	1712	86	1.10	1712	86
BH1	13/07/2020 (2) 20:48:35.00	BH1 - 2.265	658	8	412	4	5.319149	0.196922	0.142600	0.008752	-0.703320	1111	37	2258	103	50.82	1111	37
BH1	13/07/2020 (2) 20:50:05.00	BH1 - 2.266	513	5	178	3	4.060089	0.132303	0.091100	0.003322	0.329210	1419	40	1448	69	1.96	1419	40
BH1	13/07/2020 (2) 20:51:33.00	BH1 - 2.267	397	9	302	8	4.889976	0.159970	0.084600	0.003492	0.296280	1199	35	1306	79	8.12	1199	35
BH1	13/07/2020 (2) 20:53:02.00	BH1 - 2.268	283	10	154	11	5.083884	0.205061	0.112000	0.005140	-0.073987	1158	41	1831	82	36.79	1158	41
BH1	13/07/2020 (2) 20:54:33.00	BH1 - 2.269	222	4	116	2	4.048583	0.141618	0.091600	0.003932	0.277830	1423	43	1458	80	2.42	1423	43
BH1	13/07/2020 (2) 20:56:00.00	BH1 - 2.270	211	4	124	2	4.413063	0.146687	0.092900	0.004158	0.284010	1317	38	1485	83	11.34	1317	38
BH1	13/07/2020 (2) 20:57:28.00	BH1 - 2.271	214	5	93	2	5.227392	0.189257	0.081800	0.003936	0.017121	1128	36	1240	92	8.99	1128	36
BH1	13/07/2020 (2) 20:58:58.00	BH1 - 2.272	133	3	46	1	2.666667	0.344889	0.114900	0.004998	0.316710	2053	205	1878	77	-9.34	1878	77
BH1	13/07/2020 (2) 21:00:29.00	BH1 - 2.273	239	6	77	2	4.975124	0.166333	0.079000	0.003780	0.321770	1181	35	1171	93	-0.81	1181	35
BH1	13/07/2020 (2) 21:01:56.00	BH1 - 2.274	374	25	291	30	6.493506	0.551526	0.083800	0.003776	-0.194560	923	68	1287	86	28.26	923	68
BH1	13/07/2020 (2) 21:03:25.00	BH1 - 2.275	217	4	178	3	4.374453	0.150637	0.088700	0.003774	-0.004794	1327	40	1397	80	4.99	1327	40
BH1	13/07/2020 (2) 21:06:25.00	BH1 - 2.277	876	20	254	6	5.032713	0.166508	0.107100	0.003742	0.283680	1168	34	1750	63	33.23	1168	34
BH1	13/07/2020 (2) 21:07:51.00	BH1 - 2.278	113	3	42	1	5.291005	0.189804	0.075200	0.004504	0.250320	1116	36	1073	117	-4.01	1116	36
BH1	13/07/2020 (2) 21:09:20.00	BH1 - 2.279	199	6	465	15	2.996704	0.212598	0.117100	0.004542	0.304570	1856	108	1912	69	2.89	1912	69
BH1	13/07/2020 (2) 21:10:49.00	BH1 - 2.280	153	1	128	1	4.266212	0.143566	0.090200	0.004604	0.210260	1358	40	1429	95	5.00	1358	40
BH1	13/07/2020 (2) 21:12:20.00	BH1 - 2.281	266	10	111	6	6.261741	0.293835	0.084100	0.004182	0.010128	955	40	1294	95	26.19	955	40
BH1	13/07/2020 (2) 21:13:46.00	BH1 - 2.282	642	8	615	6	2.354049	0.168995	0.160800	0.004916	0.303900	2282	130	2463	52	7.35	2463	52
BH1	13/07/2020 (2) 21:15:15.00	BH1 - 2.283	335	5	244	3	4.205214	0.140693	0.093100	0.003662	0.067446	1375	40	1489	74	7.65	1375	40
BH1	13/07/2020 (2) 21:16:44.00	BH1 - 2.284	210	1	116	1	4.885198	0.164526	0.082900	0.003958	0.110520	1201	36	1266	91	5.17	1201	36
BH1	13/07/2020 (2) 21:18:17.00	BH1 - 2.285	722	36	431	25	6.430868	0.343669	0.106100	0.003822	-0.120500	932	44	1733	66	46.23	932	44
BH1	13/07/2020 (2) 21:19:42.00	BH1 - 2.286	279	5	114	1	4.422822	0.149097	0.087500	0.003650	0.022695	1314	39	1371	79	4.13	1314	39
BH1	13/07/2020 (2) 21:25:48.00	BH1 - 2.287	196	4	86	2	8.257638	0.294711	0.080300	0.004906	0.092420	737	24	1204	117	38.77	737	24
BH1	13/07/2020 (2) 21:27:20.00	BH1 - 2.288	183	3	157	2	5.417118	0.184640	0.088100	0.004862	0.001224	1092	33	1384	103	21.08	1092	33
BH1	13/07/2020 (2) 21:28:48.00	BH1 - 2.289	120	4	177	3	3.685957	0.263927	0.101700	0.004634	0.229710	1547	93	1655	83	6.47	1655	83
BH1	13/07/2020 (2) 21:30:20.00	BH1 - 2.290	272	14	101	5	5.277045	0.177944	0.075700	0.003514	0.354700	1119	34	1086	91	-2.99	1119	34
BH1	13/07/2020 (2) 21:31:47.00	BH1 - 2.291	1075	35	163	12	5.858231	0.209826	0.076700	0.002734	0.286570	1016	33	1113	70	8.68	1016	33
BH1	13/07/2020 (2) 21:33:16.00	BH1 - 2.292	546	14	264	9	5.050505	0.174982	0.110000	0.007100	-0.038952	1165	36	1799	114	35.25	1165	36
BH1	13/07/2020 (2) 21:34:45.00	BH1 - 2.293	221	9	94	7	4.048583	0.139979	0.091800	0.003936	0.419060	1423	43	1462	80	2.69	1423	43
BH1	13/07/2020 (2) 21:36:17.00	BH1 - 2.294	112	3	60	2	4.418913	0.158675	0.087900	0.004858	0.351180	1315	41	1379	104	4.66	1315	41
BH1	13/07/2020 (2) 21:42:20.00	BH1 - 2.295	141	2	88	2	5.485464	0.199980	0.078000	0.004460	0.036960	1080	35	1146	110	5.80	1080	35
BH1	13/07/2020 (2) 21:43:52.00	BH1 - 2.296	104	2	49	1	4.516712	0.165817	0.088100	0.004762	0.234870	1289	42	1384	101	6.83	1289	42
BH1	13/07/2020 (2) 21:45:21.00	BH1 - 2.297	385	6	292	2	3.274394	0.237034	0.108500	0.003670	0.406350	1718	103	1774	61	3.13	1774	61
BH1	13/07/2020 (2) 21:46:50.00	BH1 - 2.298	1122	40	191	29	6.146281	0.258922	0.090900	0.005218	0.866120	972	37	1444	106	32.69	972	37
BH1	13/07/2020 (2) 21:48:21.00	BH1 - 2.299	216	4	237	5	4.042037	0.139658	0.100100	0.004002	0.209420	1425	43	1625	73	12.31	1425	43
BH1	13/07/2020 (2) 21:49:48.00	BH1 - 2.300	449	4	259	2	4.460303	0.144910	0.085100	0.003502	0.261500	1304	37	1317	79	0.98	1304	37

Appendix D.2 continued.

Sample ID	Analysis date-time	Spot ID[1]	238U conc.	±2σ INT	232Th conc.	±2σ INT	Isotopic Ratios					Apparent Ages - Calculated in Isoplot R (Ma)				Discord	Perferred age 1500 Ma cutoff	
			ppm		ppm		238U/206Pb	±2σ PROP	207Pb/206Pb	±2σ PROP	rho	238U/206Pb	±2σ PROP	207Pb/206Pb	±2σ PROP	(7/6-6/8)/7/6 *100	Ma	2 σ
Analyses in blue font are from retargeted grains after rapid analysis identification																		
34DTB19-D	17/03/2020 (3) 17:06:51.00	34DTB19-D - 46	139	1	96	1	7.745933	0.292917	0.120700	0.004214	-0.278220	783	28	1966	62	60.18	783	28
34DTB19-D	17/03/2020 (3) 16:09:06.00	34DTB19-D - 27	96	2	139	3	5.213764	0.185825	0.190700	0.005414	0.008824	1131	37	2747	47	58.83	1131	37
34DTB19-D	17/03/2020 (3) 17:40:26.00	34DTB19-D - 63	221	5	81	5	4.214075	0.213918	0.201100	0.005522	0.203960	1373	63	2834	45	51.57	1373	63
34DTB19-D	17/03/2020 (3) 20:09:23.00	34DTB19-D - 118	140	6	207	17	4.585053	0.165281	0.149900	0.005098	-0.142240	1272	42	2344	58	45.74	1272	42
34DTB19-D	17/03/2020 (3) 19:13:54.00	34DTB19-D - 95	167	2	107	2	5.313496	0.295433	0.120000	0.005400	0.532150	1112	57	1955	80	43.15	1112	57
34DTB19-D	17/03/2020 (3) 20:01:30.00	34DTB19-D - 114	184	8	139	9	4.484305	0.371212	0.140100	0.007502	0.742540	1298	97	2228	93	41.75	1298	97
34DTB19-D	17/03/2020 (3) 17:32:31.00	34DTB19-D - 59	156	1	55	1	4.659832	0.171367	0.129300	0.004786	-0.227030	1253	42	2088	65	39.97	1253	42
34DTB19-D	17/03/2020 (3) 20:11:19.00	34DTB19-D - 119	125	2	61	2	4.593477	0.260670	0.127300	0.004246	0.160260	1270	65	2060	59	38.37	1270	65
34DTB19-D	17/03/2020 (3) 19:11:53.00	34DTB19-D - 94	35	2	48	4	5.797101	0.220122	0.100590	0.002992	-0.091675	1026	36	1634	55	37.22	1026	36
34DTB19-D	17/03/2020 (3) 16:28:50.00	34DTB19-D - 37	134	5	112	5	5.659310	0.180445	0.102500	0.003850	0.312070	1049	31	1669	70	37.15	1049	31
34DTB19-D	17/03/2020 (3) 16:22:56.00	34DTB19-D - 34	378	17	498	49	4.775549	0.214101	0.112100	0.003742	0.155280	1226	50	1833	61	33.13	1226	50
34DTB19-D	17/03/2020 (3) 17:34:31.00	34DTB19-D - 60	51	1	60	2	6.093845	0.236995	0.091200	0.005024	0.224110	980	35	1450	105	32.44	980	35
34DTB19-D	17/03/2020 (3) 16:07:08.00	34DTB19-D - 26	214	2	309	3	5.913661	0.216193	0.092200	0.002844	0.165500	1007	34	1471	59	31.52	1007	34
34DTB19-D	17/03/2020 (3) 15:47:15.00	34DTB19-D - 21	170	2	84	2	4.130525	0.239574	0.122200	0.005644	0.882180	1398	73	1988	82	29.69	1398	73
34DTB19-D	17/03/2020 (3) 15:29:24.00	34DTB19-D - 12	128	2	141	7	3.933910	0.128200	0.127300	0.003846	0.414580	1460	43	2060	53	29.13	1460	43
34DTB19-D	17/03/2020 (3) 17:04:50.00	34DTB19-D - 45	74	2	85	4	3.903201	0.245649	0.127400	0.004048	0.516970	1470	83	2062	56	28.68	1470	83
34DTB19-D	17/03/2020 (3) 19:17:51.00	34DTB19-D - 97	126	1	98	2	4.168404	0.199784	0.117400	0.003748	0.480410	1386	60	1916	57	27.66	1386	60
34DTB19-D	17/03/2020 (3) 17:16:41.00	34DTB19-D - 51	163	2	121	1	4.081633	0.248230	0.118000	0.004660	0.462280	1413	77	1925	71	26.63	1413	77
34DTB19-D	17/03/2020 (3) 19:03:59.00	34DTB19-D - 90	181	2	203	2	5.420054	0.214158	0.092300	0.004946	0.108680	1092	40	1473	102	25.88	1092	40
34DTB19-D	17/03/2020 (3) 20:53:19.00	34DTB19-D - 130	83	1	111	1	4.210526	0.183490	0.113000	0.004060	0.271570	1374	54	1847	65	25.64	1374	54
34DTB19-D	17/03/2020 (3) 16:13:03.00	34DTB19-D - 29	157	4	182	6	3.898635	0.190448	0.121000	0.003820	0.632810	1472	64	1970	56	25.29	1472	64
34DTB19-D	17/03/2020 (3) 19:59:28.00	34DTB19-D - 113	72	3	69	3	4.098361	0.154192	0.114200	0.004184	0.312890	1408	48	1867	66	24.59	1408	48
34DTB19-D	17/03/2020 (3) 20:19:14.00	34DTB19-D - 123	264	4	168	3	3.971406	0.252921	0.117000	0.004340	0.589650	1448	83	1910	67	24.20	1448	83
34DTB19-D	17/03/2020 (3) 17:18:43.00	34DTB19-D - 52	85	1	105	2	4.282655	0.164520	0.109000	0.004380	-0.289810	1353	47	1782	73	24.08	1353	47
34DTB19-D	17/03/2020 (3) 18:30:03.00	34DTB19-D - 83	132	2	159	2	4.025765	0.177756	0.114000	0.004080	0.186450	1430	57	1863	65	23.24	1430	57
34DTB19-D	17/03/2020 (3) 19:27:41.00	34DTB19-D - 102	202	6	182	3	3.861004	0.330645	0.115300	0.004806	0.866030	1485	114	1884	75	21.19	1485	114
34DTB19-D	17/03/2020 (3) 20:25:12.00	34DTB19-D - 126	146	7	149	3	4.275331	0.187866	0.105100	0.003902	0.350580	1355	54	1715	68	21.01	1355	54
34DTB19-D	17/03/2020 (3) 20:47:17.00	34DTB19-D - 127	175	2	201	2	3.977725	0.228284	0.111800	0.004036	-0.353530	1446	74	1828	66	20.92	1446	74
34DTB19-D	17/03/2020 (3) 17:08:46.00	34DTB19-D - 47	63	1	44	1	3.759398	0.287184	0.117300	0.005646	-0.619190	1521	103	1915	86	20.59	1915	86
34DTB19-D	17/03/2020 (3) 19:25:45.00	34DTB19-D - 101	92	10	125	17	3.581662	0.212745	0.122900	0.004058	0.567290	1587	84	1998	59	20.55	1998	59
34DTB19-D	17/03/2020 (3) 17:00:48.00	34DTB19-D - 43	74	1	117	1	4.017678	0.141692	0.110200	0.004004	0.186070	1433	45	1802	66	20.48	1433	45
34DTB19-D	17/03/2020 (3) 19:51:34.00	34DTB19-D - 109	263	14	130	15	2.112825	0.131537	0.240500	0.006110	-0.147070	2498	129	3123	40	20.00	3123	40
34DTB19-D	17/03/2020 (3) 20:23:12.00	34DTB19-D - 125	86	1	158	4	2.724796	0.165864	0.166100	0.005422	0.132830	2015	105	2518	55	19.96	2518	55
34DTB19-D	17/03/2020 (3) 17:38:29.00	34DTB19-D - 62	87	3	115	5	4.198153	0.143886	0.104800	0.004596	0.214130	1377	43	1710	81	19.45	1377	43
34DTB19-D	17/03/2020 (3) 15:39:19.00	34DTB19-D - 17	112	5	132	12	3.636364	0.231405	0.119000	0.005980	0.737060	1566	89	1941	90	19.29	1941	90
34DTB19-D	17/03/2020 (3) 17:28:32.00	34DTB19-D - 57	64	1	69	1	5.336179	0.214928	0.087300	0.004346	0.303880	1107	41	1366	96	18.96	1107	41
34DTB19-D	17/03/2020 (3) 19:19:47.00	34DTB19-D - 98	135	4	88	3	5.420054	0.202407	0.086100	0.003122	-0.177010	1092	38	1340	70	18.52	1092	38
34DTB19-D	17/03/2020 (3) 16:38:44.00	34DTB19-D - 42	234	28	268	32	3.756574	0.230362	0.113300	0.003866	0.067569	1522	83	1852	62	17.85	1852	62
34DTB19-D	17/03/2020 (3) 19:53:35.00	34DTB19-D - 110	125	1	153	1	3.776435	0.218143	0.111800	0.004236	-0.065011	1514	78	1828	69	17.16	1828	69
34DTB19-D	17/03/2020 (3) 17:26:36.00	34DTB19-D - 56	313	4	298	6	3.795066	0.234329	0.110900	0.003618	0.293960	1508	83	1813	59	16.86	1813	59
34DTB19-D	17/03/2020 (3) 17:24:36.00	34DTB19-D - 55	82	2	69	3	4.649000	0.175110	0.093800	0.005676	0.481930	1256	43	1503	114	16.45	1256	43
34DTB19-D	17/03/2020 (3) 20:21:15.00	34DTB19-D - 124	298	11	384	9	3.773585	0.289071	0.110600	0.003812	0.114280	1515	103	1809	63	16.21	1809	63
34DTB19-D	17/03/2020 (3) 18:26:05.00	34DTB19-D - 81	167	18	86	17	3.829950	0.142607	0.107900	0.004458	0.396140	1496	50	1763	76	15.19	1496	50
34DTB19-D	17/03/2020 (3) 19:02:03.00	34DTB19-D - 89	220	5	500	8	5.246590	0.237060	0.085400	0.004308	0.406770	1125	47	1324	98	15.05	1125	47
34DTB19-D	17/03/2020 (3) 20:07:22.00	34DTB19-D - 117	140	4	92	3	1.819174	0.109190	0.266000	0.007020	0.223990	2824	137	3282	42	13.96	3282	42
34DTB19-D	17/03/2020 (3) 17:52:24.00	34DTB19-D - 64	344	7	236	3	3.916960	0.231765	0.104200	0.004684	-0.026379	1466	78	1699	83	13.75	1466	78
34DTB19-D	17/03/2020 (3) 17:36:29.31	34DTB19-D - 61	355	35	254	27	3.958828	0.204555	0.102700	0.004354	0.014187	1452	67	1673	78	13.20	1452	67
34DTB19-D	17/03/2020 (3) 17:58:25.00	34DTB19-D - 67	125	3	161	3	3.658983	0.233838	0.109700	0.004094	0.269450	1558	88	1794	68	13.16	1794	68
34DTB19-D	17/03/2020 (3) 18:54:06.00	34DTB19-D - 85	492	27	153	11	3.484321	0.203232	0.114100	0.003682	0.105120	1627	84	1865	58	12.78	1865	58
34DTB19-D	17/03/2020 (3) 19:21:48.00	34DTB19-D - 99	68	1	101	1	3.489184	0.203702	0.113600	0.004172	0.310160	1625	84	1857	66	12.52	1857	66
34DTB19-D	17/03/2020 (3) 18:04:18.00	34DTB19-D - 70	226	5	83	2	3.531073	0.207775	0.112300	0.004046	0.114320	1608	84	1836	65	12.46	1836	65
34DTB19-D	17/03/2020 (3) 18:58:07.00	34DTB19-D - 87	111	2	107	3	3.556188	0.210235	0.111300	0.004026	0.132500	1597	84	1820	66	12.23	1820	66
34DTB19-D	17/03/2020 (3) 18:28:02.00	34DTB19-D - 82	452	18	242	15	3.371544	0.203839	0.116800	0.006336	-0.729320	1674	89	1907	97	12.20	1907	97
34DTB19-D	17/03/2020 (3) 17:54:29.00	34DTB19-D - 65	78	3	100	4	3.763643	0.231088	0.105900	0.004218	0.187480	1519	83	1729	73	12.16	1729	73
34DTB19-D	17/03/2020 (3) 20:55:16.00	34DTB19-D - 131	408	8	430	22	4.411116	0.169946	0.093200	0.004364	0.199810	1317	46	1491	89	11.66	1317	46
34DTB19-D	17/03/2020 (3) 19:15:51.00	34DTB19-D - 96	444	2	600	4	3.571429	0.211735	0.109600	0.004192	0.216820	1591	84	1792	70	11.19	1792	70
34DTB19-D	17/03/2020 (3) 16:30:50.00	34DTB19-D - 38	112	1	115	1	4.170142	0.192960	0.096100	0.005722	-0.104660	1386	58	1549	112	10.54	1386	58
34DTB19-D	17/03/2020 (3) 17:02:53.00	34DTB19-D - 44	77	4	133	20	3.417635	0.220196	0.112000	0.006840	-0.298140	1655	94	1831	111	9.65	1831	111
34DTB19-D	17/03/2020 (3) 16:11:06.00	34DTB19-D - 28	206	8	120	3	3.904725	0.143656	0.100100	0.004602	0.204530	1470	48	1625	86	9.55	1470	48
34DTB19-D	17/03/2020 (3) 18:02:23.00	34DTB19-D - 69	107	2	134	3	4.154549	0.141776	0.095400	0.003808	0.011862	1390	43	1535	75	9.43	1390	43
34DTB19-D	17/03/2020 (3) 16:01:11.00	34DTB19-D - 23	184	2	118	3	3.590664	0.213635	0.106900	0.005038	0.311770	1584	84	1746	86	9.31	1746	86
34DTB19-D	17/03/2020 (3) 16:18:59.00	34DTB19-D - 32	50	1	37	1	4.006410	0.145939	0.097800	0.003656	0.248960	1436	47	1582	70	9.19	1436	47
34DTB19-D	17/03/2020 (3) 18:24:05.00	34DTB19-D - 80	199	6	147	5	3.415301	0.196613	0.111300	0.003626	0.078847	1656	84	1820	59	9.03	1820	59
34DTB19-D	17/03/2020 (3) 20:13:21.00	34DTB19-D - 120	88	4	75	3	3.585515	0.213125	0.106300	0.003626	0.025066	1586	84	1736	63	8.66	1736	63
34DTB19-D	17/03/2020 (3) 20:15:17.00	34DTB19-D - 121	152	3	118	2	3.262643	0.192991	0.114800	0.004496	-0.132080	1724	90	1876	71	8.12	1876	71
34DTB19-D	17/03/2020 (3) 17:20:38.00	34DTB19-D - 53	456	5	95	2	4.528986	0.170575	0.088800	0.003476	0.419220	1286	44	1399	75	8.07	1286	44
34DTB19-D	17/03/2020 (3) 18:00:23.00	34DTB19-D - 68	319	11	192	14	2.376426	0.143534	0.160500	0.004610	-0.098127	2264	115	2460	49	7.97	2460	49
34DTB19-D	17/03/2020 (3) 18:18:13.00	34DTB19-D - 77	127	2	187	6	3.483107	0.215247	0.108100	0.005262	0.348480	1627	89	1767	89	7.91	1767	89
34DTB19-D	17/03/2020 (3) 19:07:56.00	34DTB19-D - 92	150	10	231	20	3.738318	0.228492	0.101800	0.003936	-0.322350	1528	83	1656	72	7.75	1656	72
34DTB19-D	17/03/2020 (3) 19:49:38.00	34DTB19-D - 108	378	29	220	13	3.696858	0.224271	0.102600	0.004152	0.347460	1543	83	1671	75	7.64	1671	75
34DTB19-D	17/03/2020 (3) 15:59:11.00	34DTB19-D - 22	66	3	71	5	3.379520	0.193223	0.110500	0.003910	0.216710	1671	84	1807	64	7.52	1807	64
34DTB19-D	17/03/2020 (3) 20:17:18.00	34DTB19-D - 122	121	3	115	3	3.650968	0.219645	0.103400	0.004668	0.208840	1561	83	1685	83	7.39	1685	83
34DTB19-D	17/03/2020 (3) 16:20:56.00	34DTB19-D - 33	380	14	236	16	3.877472	0.242932	0.098500	0.004070	-0.002632	1479	83	1595	77	7.27	1479	83
34DTB19-D	17/03/2020 (3) 19:57:32.00	34DTB19-D - 112	57	1	76	1	3.511236	0.205841	0.106600	0.003932	0.369190	1616	84	1741	68	7.22	1741	68
34DTB19-D	17/03/2020 (3) 17:14:45.00	34DTB19-D - 50	128	2	108	1	3.299241	0.196605	0.112200	0.004144	0.241940	1707	89	1835	67	6.97	1835	67
34DTB19-D	17/03/2020 (3) 15:33:22.00	34DTB19-D - 14	127	4	340	8	3.486750	0.203467	0.106900	0.003638	0.146790	1626	84	1746	62	6.92	1746	62
34DTB19-D	17/03/2020 (3) 16:34:47.00	34DTB19-D - 40	406	7	44	5	3.404835	0.195619	0.108700	0.003574	0.276750	1660	84	1777	60	6.58	1777	60
34DTB19-D	17/03/2020 (3) 16:15:03.00	34DTB19-D - 30	145	3	130	3	2.018163	0.125896	0.194000	0.007880	0.159540	2594	133	2776	67	6.53	2776	67
34DTB19-D	17/03/2020 (3) 15:19:33.00	34DTB19-D - 7	397	17	357	23	3.418803	0.208635	0.108100	0.003962	0.093569	1654	89	1767	67	6.38	1767	67
34DTB19-D	17/03/2020 (3) 18:14:15.00	34DTB19-D - 75	92	1	93	1	3.479471	0.214870	0.106500	0.003930	0.120810	1629	89	1740	68	6.38	1740	68
34DTB19-D	17/03/2020 (3) 20:05:26.00	34DTB19-D - 116	235	6	195	6	3.710575	0.225664	0.100900	0.004418	0.455670	1538	83	1640	81	6.20	1640	81
34DTB19-D	17/03/2020 (3) 20:51:18.00	34DTB19-D - 129	182	3	235	5	4.009623	0.149324	0.095000	0.005200	0.428410	1435	48	1527	103	6.01	1435	48
34DTB19-D	17/03/2020 (3) 15:27:28.00	34DTB19-D - 11	59	6	50	5	3.732736	0.227921	0.100100	0.004302	0.000043	1530	83	1625	80	5.85	1625	80
34DTB19-D	17/03/2020 (3) 18:56:06.00	34DTB19-D - 86	154	3	143	4	3.254149	0.192157	0.111800	0.003736	-0.026213	1727	90	1828	61	5.51	1828	61
34DTB19-D	17/03/2020 (3) 15:07:39.00	34DTB19-D - 1	112	2	101	2	3.224766	0.189285	0.112600	0.004952	0.182320	1741	90	1841	80	5.42	1841	80
34DTB19-D	17/03/2020 (3) 18:10:18.00	34DTB19-D - 73	561	72	398	66	3.749531	0.215581	0.099300	0.003886	0.286380	1524	78	1610	73	5.35	1610	73
34DTB19-D	17/03/2020 (3) 15:35:22.00	34DTB19-D - 15	40	1	23	1	1.970055	0.117023	0.196200	0.005924	-0.148360	2646	129	2794	49	5.29	2794	49
34DTB19-D	17/03/2020 (3) 20:49:21.00	34DTB19-D - 128	87	5	316	50	3.502627	0.205005	0.104600	0.003592	0.193570	1619	84	1707	63	5.13	1707	63
34DTB19-D	17/03/2020 (3) 16:26:53.00	34DTB19-D - 36	200	16	171	6	4.737091	0.164306	0.084400	0.002888	0.275000	1235	39	1301	67	5.09	1235	39
34DTB19-D	17/03/2020 (3) 17:30:33.00	34DTB19-D - 58	505	27	277	19	1.950458	0.115095	0.198200	0.005964	0.256330	2668	129	2811	49	5.07	2811	49
34DTB19-D	17/03/2020 (3) 18:06:19.00	34DTB19-D - 71	634	13	245	7	3.115265	0.188469	0.115700	0.003614	0.358100	1795	95	1890	56	5.05	1890	56
34DTB19-D	17/03/2020 (3) 19:23:45.00	34DTB19-D - 100	40	0	39	1	4.299226	0.183946	0.089700	0.004594	-0.063333	1348	52	1418	98	4.95	1348	52
34DTB19-D	17/03/2020 (3) 15:25:27.00	34DTB19-D - 10	302	8	274	5	3.280840	0.194784	0.110000	0.004400	0.054274	1715	89	1799	73	4.64	1799	73
34DTB19-D	17/03/2020 (3) 19:55:32.00	34DTB19-D - 111	188	4	116	2	3.445899	0.199534	0.105500	0.003710	0.191490	1643	84	1722	65	4.63	1722	65
34DTB19-D	17/03/2020 (3) 16:32:47.00	34DTB19-D - 39	67	1	148	2	3.355705	0.202243	0.107500	0.003850	0.104480	1681	89	1757	66	4.28	1757	66
34DTB19-D	17/03/2020 (3) 16:24:53.00	34DTB19-D - 35	107	1	74	1	3.148615	0.181938	0.113400	0.004068	0.081029	1778	90	1854	65	4.09	1854	65
34DTB19-D	17/03/2020 (3) 18:08:16.00	34DTB19-D - 72	213	4	369	6	3.204101	0.187277	0.111300	0.003826	0.040722	1751	90	1820	62	3.79	1820	62
34DTB19-D	17/03/2020 (3) 19:47:37.00	34DTB19-D - 107	250	9	424	47	1.451589	0.085924	0.306600	0.009032	0.303660	3378	156	3503	46	3.56	3503	46
34DTB19-D	17/03/2020 (3) 17:12:44.00	34DTB19-D - 49	110	8	89	6	3.954132	0.130679	0.093900	0.003678	0.028249	1453	43	1505	74	3.45	1453	43
34DTB19-D	17/03/2020 (3) 15:43:16.00	34DTB19-D - 19	196	1	173	2	4.127115	0.148971	0.091100	0.003122	-0.014691	1399	45	1448	65	3.40	1399	45
34DTB19-D	17/03/2020 (3) 18:32:00.00	34DTB19-D - 84	122	5	87	3	4.140787	0.142827	0.090800	0.004316	0.263930	1394	43	1442	91	3.27	1394	43
34DTB19-D	17/03/2020 (3) 17:22:40.00	34DTB19-D - 54	112	3	177	4	3.258390	0.192573	0.108800	0.003576	0.352160	1725	90	1779	60	2.99	1779	60
34DTB19-D	17/03/2020 (3) 19:33:39.00	34DTB19-D - 105	131	6	108	6	3.345601	0.201229	0.105900	0.003818	0.111380	1686	89	1729	66	2.50	1729	66
34DTB19-D	17/03/2020 (3) 19:00:03.00	34DTB19-D - 88	34	4	44	2	4.025765	0.142101	0.092000	0.003940	0.343650	1430	45	1467	81	2.47	1430	45
34DTB19-D	17/03/2020 (3) 19:09:57.00	34DTB19-D - 93	330	12	475	34	3.328895	0.199556	0.106300	0.003726	0.205110	1693	89	1736	64	2.47	1736	64
34DTB19-D	17/03/2020 (3) 17:10:48.00	34DTB19-D - 48	80	1	72	2	3.362475	0.202924	0.105400	0.004208	0.352240	1678	89	1721	73	2.45	1721	73
34DTB19-D	17/03/2020 (3) 15:15:36.00	34DTB19-D - 5	123	6	86	3	1.900418	0.110240	0.195800	0.005316	0.074372	2725	129	2791	45	2.34	2791	45
34DTB19-D	17/03/2020 (3) 20:57:17.00	34DTB19-D - 132	226	2	223	6	4.042037	0.124954	0.091600	0.003532	0.313740	1425	40	1458	73	2.28	1425	40
34DTB19-D	17/03/2020 (3) 19:29:43.00	34DTB19-D - 103	270	4	409	6	3.216468	0.188477	0.108900	0.004078	0.302340	1745	90	1780	68	1.98	1780	68
34DTB19-D	17/03/2020 (3) 15:17:32.00	34DTB19-D - 6	157	3	122	4	3.480682	0.202880	0.102000	0.003640	-0.139090	1628	84	1660	66	1.93	1660	66
34DTB19-D	17/03/2020 (3) 18:22:08.00	34DTB19-D - 79	283	4	219	5	3.174603	0.184429	0.110000	0.003700	0.227830	1765	90	1799	61	1.85	1799	61
34DTB19-D	17/03/2020 (3) 16:03:12.00	34DTB19-D - 24	183	1	150	3	3.438790	0.210679	0.102900	0.003958	0.173100	1646	89	1676	71	1.83	1676	71
34DTB19-D	17/03/2020 (3) 20:03:26.00	34DTB19-D - 115	115	5	119	9	3.567606	0.211358	0.099900	0.003998	0.336890	1593	84	1621	75	1.76	1621	75
34DTB19-D	17/03/2020 (3) 16:36:43.00	34DTB19-D - 41	241	2	233	2	4.940711	0.154959	0.080400	0.002808	0.428380	1188	34	1206	69	1.47	1188	34
34DTB19-D	17/03/2020 (3) 15:31:25.00	34DTB19-D - 13	163	1	161	1	3.156566	0.182698	0.109800	0.003696	0.052161	1774	90	1795	61	1.18	1795	61
34DTB19-D	17/03/2020 (3) 18:16:12.00	34DTB19-D - 76	138	8	92	6	4.219409	0.146700	0.088200	0.003864	0.330870	1371	43	1386	84	1.08	1371	43
34DTB19-D	17/03/2020 (3) 15:41:16.00	34DTB19-D - 18	143	9	54	2	4.522840	0.166144	0.084400	0.004388	0.423270	1288	43	1301	101	1.02	1288	43
34DTB19-D	17/03/2020 (3) 19:45:37.00	34DTB19-D - 106	64	1	70	2	1.866716	0.110512	0.196000	0.006220	0.221770	2765	133	2792	52	0.97	2792	52
34DTB19-D	17/03/2020 (3) 19:06:00.00	34DTB19-D - 91	78	1	58	1	4.185852	0.132777	0.088500	0.003570	0.218840	1381	39	1393	77	0.83	1381	39
34DTB19-D	17/03/2020 (3) 17:56:24.00	34DTB19-D - 66	601	11	681	15	3.310162	0.197689	0.104900	0.004198	0.271890	1702	89	1712	74	0.58	1712	74
34DTB19-D	17/03/2020 (3) 15:11:39.00	34DTB19-D - 3	134	2	120	2	3.615329	0.216083	0.097700	0.004254	0.373490	1574	84	1580	82	0.35	1580	82
34DTB19-D	17/03/2020 (3) 18:12:14.00	34DTB19-D - 74	178	4	192	3	2.153316	0.126528	0.160900	0.005218	-0.025219	2459	120	2464	55	0.22	2464	55
34DTB19-D	17/03/2020 (3) 15:13:35.00	34DTB19-D - 4	148	3	80	2	1.968117	0.116832	0.180200	0.005204	0.260800	2649	129	2654	48	0.21	2654	48
34DTB19-D	17/03/2020 (3) 15:21:29.00	34DTB19-D - 8	202	3	147	4	2.115059	0.122824	0.164200	0.005584	0.070079	2496	120	2499	57	0.11	2499	57
34DTB19-D	17/03/2020 (3) 19:31:39.00	34DTB19-D - 104	139	4	158	7	3.220612	0.188880	0.106700	0.004134	0.007022	1743	90	1743	71	-0.01	1743	71
34DTB19-D	17/03/2020 (3) 15:09:38.00	34DTB19-D - 2	106	2	49	1	3.145643	0.181654	0.108700	0.003174	0.184110	1780	90	1777	53	-0.15	1777	53
34DTB19-D	17/03/2020 (3) 18:20:08.00	34DTB19-D - 78	131	2	176	3	3.537319	0.208385	0.098800	0.004076	0.281040	1605	84	1601	77	-0.26	1601	77
34DTB19-D	17/03/2020 (3) 16:05:06.00	34DTB19-D - 25	82	1	48	0	1.612383	0.094642	0.236600	0.006432	0.445320	3111	145	3097	43	-0.46	3097	43
34DTB19-D	17/03/2020 (3) 16:17:00.00	34DTB19-D - 31	143	6	88	8	4.355401	0.142120	0.085400	0.003508	0.079229	1332	39	1324	80	-0.65	1332	39
34DTB19-D	17/03/2020 (3) 15:37:18.00	34DTB19-D - 16	142	1	96	1	3.208213	0.187676	0.105300	0.003206	0.258750	1749	90	1719	56	-1.77	1719	56
34DTB19-D	17/03/2020 (3) 15:45:14.00	34DTB19-D - 20	59	1	115	2	3.195909	0.186484	0.105600	0.005312	0.332620	1755	90	1724	92	-1.80	1724	92
34DTB19-D	17/03/2020 (3) 15:23:30.00	34DTB19-D - 9	587	16	285	6	3.138732	0.180994	0.106900	0.003738	0.289200	1783	90	1746	64	-2.09	1746	64

Appendix D.2 continued.

Sample ID	Analysis date-time	Spot ID[1]	238U conc.		232Th conc.		Isotopic Ratios					Apparent Ages - Calculated in Isoplot R (Ma)				Discord	Perferred age 1500 Ma cutoff	
			ppm	±2σ INT	ppm	±2σ INT	238U/206Pb	±2σ PROP	207Pb/206Pb	±2σ PROP	rho	238U/206Pb	±2σ PROP	207Pb/206Pb	±2σ PROP	(7/6-6/8)/7/6 *100	Ma	2 σ
05DTB19	2020-07-30 17:46:53.000	05DTB19q - 34 - 1.d	52	1	58	1	7.900234	0.326350	0.071568	0.006914	0.381941	768	30	973	197	21.02	768	30
05DTB19	2020-07-30 16:56:57.000	05DTB19q - 3b - 1.d	67	2	66	2	8.254010	0.323560	0.068782	0.006133	0.263606	737	27	891	184	17.29	737	27
05DTB19	2020-07-30 16:58:40.000	05DTB19q - 3 - 1.d	44	1	36	1	7.899340	0.334711	0.065052	0.006816	0.267513	768	31	775	220	0.86	768	31
05DTB18	10/05/2019 (6) 07:17:05.69	05DTB18 - 100	49	3	49	4	5.299417	0.198665	0.165500	0.010110	0.080382	1114	37	2512	100	55.64	1114	37
05DTB18	10/05/2019 (6) 04:22:40.00	05DTB18 - 30	317	9	68	2	4.545455	0.380165	0.151000	0.032020	-0.901520	1282	90	2357	323	45.61	1282	90
05DTB18	10/05/2019 (6) 03:08:40.00	05DTB18 - 1	235	8	96	4	3.333333	0.255556	0.199900	0.012098	-0.121690	1691	107	2825	96	40.12	2825	96
05DTB18	10/05/2019 (6) 07:24:37.00	05DTB18 - 104	65	4	51	2	4.306632	0.199270	0.131100	0.010022	0.432390	1346	54	2112	129	36.27	1346	54
05DTB18	10/05/2019 (6) 04:07:38.00	05DTB18 - 22	53	2	30	2	3.669725	0.179783	0.153400	0.009968	0.574700	1554	65	2383	107	34.82	2383	107
05DTB18	10/05/2019 (6) 07:05:50.00	05DTB18 - 94	131	4	56	2	7.153076	0.270978	0.081600	0.005232	0.261190	844	29	1235	122	31.70	844	29
05DTB18	10/05/2019 (6) 05:17:52.00	05DTB18 - 51	499	53	50	2	5.701254	0.257044	0.092000	0.011840	0.218300	1042	42	1467	227	28.98	1042	42
05DTB18	10/05/2019 (6) 05:38:35.00	05DTB18 - 59	311	18	108	6	4.737091	0.188990	0.104800	0.008996	-0.141370	1235	43	1710	151	27.80	1235	43
05DTB18	10/05/2019 (6) 05:06:33.00	05DTB18 - 45	94	8	86	7	5.356186	0.213272	0.094100	0.008382	0.173600	1104	39	1509	160	26.89	1104	39
05DTB18	10/05/2019 (6) 05:08:27.00	05DTB18 - 46	216	9	112	5	5.200208	0.309525	0.093000	0.015860	0.319070	1134	59	1487	293	23.75	1134	59
05DTB18	10/05/2019 (6) 04:32:06.00	05DTB18 - 35	120	5	52	3	5.120328	0.304283	0.094000	0.013880	0.376100	1150	59	1507	257	23.69	1150	59
05DTB18	10/05/2019 (6) 05:12:12.00	05DTB18 - 48	236	9	219	8	4.208754	0.155030	0.107400	0.010048	0.202410	1374	44	1755	163	21.69	1374	44
05DTB18	10/05/2019 (6) 05:48:04.00	05DTB18 - 64	89	4	49	3	4.409171	0.265095	0.103000	0.015060	0.310250	1318	68	1678	249	21.47	1318	68
05DTB18	10/05/2019 (6) 07:47:19.00	05DTB18 - 113	137	6	70	4	3.736921	0.159922	0.118800	0.006576	0.285930	1529	56	1937	97	21.10	1937	97
05DTB18	10/05/2019 (6) 05:51:48.00	05DTB18 - 66	189	11	118	6	5.414185	0.210881	0.087700	0.007454	0.393970	1093	38	1375	156	20.54	1093	38
05DTB18	10/05/2019 (6) 05:46:07.96	05DTB18 - 63	240	9	146	6	5.512679	0.234851	0.086000	0.007620	0.074597	1075	41	1337	163	19.64	1075	41
05DTB18	10/05/2019 (6) 05:42:23.00	05DTB18 - 61	208	5	152	3	5.527916	0.260292	0.085400	0.011308	-0.124120	1072	45	1324	238	19.04	1072	45
05DTB18	10/05/2019 (6) 06:43:02.00	05DTB18 - 86	564	8	523	10	3.477051	0.148125	0.122500	0.007450	0.349260	1630	59	1992	105	18.21	1992	105
05DTB18	10/05/2019 (6) 05:15:57.00	05DTB18 - 50	216	8	88	4	5.656109	0.205898	0.083400	0.005868	0.131870	1049	34	1278	132	17.86	1049	34
05DTB18	10/05/2019 (6) 05:27:12.00	05DTB18 - 56	323	11	137	5	6.265664	0.309828	0.078400	0.009768	0.115780	955	42	1156	230	17.42	955	42
05DTB18	10/05/2019 (6) 06:03:20.00	05DTB18 - 68	707	29	208	8	3.259452	0.136370	0.129100	0.010682	-0.178230	1725	61	2085	140	17.27	2085	140
05DTB18	10/05/2019 (6) 05:02:43.00	05DTB18 - 44	85	6	62	6	3.849115	0.173284	0.107400	0.011448	0.349430	1489	58	1755	184	15.16	1489	58
05DTB18	10/05/2019 (6) 03:44:51.00	05DTB18 - 14	437	13	228	7	5.224660	0.221871	0.085600	0.010412	0.421900	1129	42	1328	220	15.00	1129	42
05DTB18	10/05/2019 (6) 05:40:33.00	05DTB18 - 60	960	63	612	50	3.680530	0.126441	0.111200	0.007724	0.070402	1549	46	1818	122	14.79	1818	122
05DTB18	10/05/2019 (6) 08:23:21.36	05DTB18 - 127	212	10	73	4	6.527415	0.266891	0.075400	0.006208	0.160230	919	34	1078	158	14.78	919	34
05DTB18	10/05/2019 (6) 08:36:30.00	05DTB18 - 134	78	2	49	2	5.070994	0.345712	0.086000	0.017720	0.256850	1160	68	1337	355	13.22	1160	68
05DTB18	10/05/2019 (6) 03:52:23.00	05DTB18 - 18	272	6	145	4	5.561735	0.367978	0.081000	0.015620	-0.012587	1066	61	1221	339	12.70	1066	61
05DTB18	10/05/2019 (6) 05:25:22.00	05DTB18 - 55	994	54	134	12	5.437738	0.392617	0.082000	0.018640	-0.072093	1088	68	1245	391	12.59	1088	68
05DTB18	10/05/2019 (6) 03:48:37.00	05DTB18 - 16	101	4	78	3	5.899705	0.292027	0.078100	0.010462	0.198300	1009	44	1149	246	12.15	1009	44
05DTB18	10/05/2019 (6) 08:15:52.00	05DTB18 - 123	258	20	370	22	5.411255	0.254634	0.081800	0.009436	0.131130	1093	45	1240	212	11.84	1093	45
05DTB18	10/05/2019 (6) 05:49:53.00	05DTB18 - 65	52	1	28	1	3.173596	0.124909	0.122800	0.009156	0.296400	1766	59	1997	128	11.56	1997	128
05DTB18	10/05/2019 (6) 05:00:43.00	05DTB18 - 43	92	6	63	4	5.112474	0.185889	0.084400	0.005988	0.061501	1152	37	1301	133	11.47	1152	37
05DTB18	10/05/2019 (6) 05:19:43.00	05DTB18 - 52	163	7	85	4	4.403347	0.188892	0.093000	0.009160	0.312250	1319	49	1487	177	11.28	1319	49
05DTB18	10/05/2019 (6) 05:14:04.59	05DTB18 - 49	100	4	39	2	2.232143	0.129345	0.184000	0.016680	-0.141060	2386	110	2689	143	11.24	2689	143
05DTB18	10/05/2019 (6) 08:08:21.00	05DTB18 - 119	290	12	104	6	5.073567	0.250770	0.084300	0.010786	0.318610	1160	50	1299	231	10.72	1160	50
05DTB18	10/05/2019 (6) 05:10:21.00	05DTB18 - 47	155	6	54	2	3.946330	0.189499	0.099600	0.011192	0.226950	1456	60	1616	197	9.89	1456	60
05DTB18	10/05/2019 (6) 06:22:25.00	05DTB18 - 75	765	41	113	8	5.455537	0.189471	0.080100	0.005502	0.211040	1085	34	1199	131	9.48	1085	34
05DTB18	10/05/2019 (6) 05:21:38.00	05DTB18 - 53	44	1	38	1	5.211047	0.291591	0.082000	0.013640	0.448520	1132	55	1245	296	9.10	1132	55
05DTB18	10/05/2019 (6) 05:29:07.00	05DTB18 - 57	332	20	214	9	2.999400	0.110368	0.125600	0.008212	0.031923	1855	57	2037	112	8.92	2037	112
05DTB18	10/05/2019 (6) 08:28:58.00	05DTB18 - 130	495	8	208	7	5.656109	0.381851	0.078000	0.014560	0.500720	1050	62	1146	333	8.42	1050	62
05DTB18	10/05/2019 (6) 04:47:26.00	05DTB18 - 40	274	12	93	4	5.787037	0.199465	0.076800	0.005536	0.115180	1028	32	1115	138	7.85	1028	32
05DTB18	10/05/2019 (6) 04:33:57.00	05DTB18 - 36	326	21	105	8	4.631774	0.182739	0.087100	0.006842	0.175410	1260	44	1362	145	7.46	1260	44
05DTB18	10/05/2019 (6) 08:34:39.00	05DTB18 - 133	399	42	152	17	5.913661	0.233679	0.075600	0.006812	0.195030	1007	36	1084	172	7.06	1007	36
05DTB18	10/05/2019 (6) 07:03:59.00	05DTB18 - 93	251	9	220	11	4.488330	0.210637	0.088100	0.008662	0.068023	1297	53	1384	179	6.29	1297	53
05DTB18	10/05/2019 (6) 05:23:27.00	05DTB18 - 54	87	10	23	2	1.547988	0.062111	0.285100	0.015302	0.305790	3213	98	3390	82	5.24	3390	82
05DTB18	10/05/2019 (6) 03:22:10.00	05DTB18 - 5	251	13	311	18	3.524850	0.127650	0.103600	0.006772	0.282200	1610	50	1689	117	4.67	1689	117
05DTB18	10/05/2019 (6) 07:00:08.00	05DTB18 - 91	77	1	90	3	3.607504	0.155440	0.101400	0.010728	0.430130	1577	58	1649	185	4.36	1649	185
05DTB18	10/05/2019 (6) 04:11:23.00	05DTB18 - 24	581	19	118	5	5.027652	0.292660	0.081000	0.011620	0.318430	1169	59	1221	259	4.23	1169	59
05DTB18	10/05/2019 (6) 05:30:58.00	05DTB18 - 58	63	3	38	1	5.652911	0.253662	0.076000	0.013520	-0.012621	1050	42	1094	321	4.02	1050	42
05DTB18	10/05/2019 (6) 03:24:03.96	05DTB18 - 6	211	3	116	2	3.076923	0.165680	0.115700	0.012214	0.397430	1814	81	1890	180	4.02	1890	180
05DTB18	10/05/2019 (6) 04:28:21.00	05DTB18 - 33	59	2	26	2	1.652893	0.065843	0.239600	0.013692	0.438260	3050	94	3117	89	2.14	3117	89
05DTB18	10/05/2019 (6) 06:26:11.00	05DTB18 - 77	72	4	88	7	4.502476	0.219792	0.085200	0.011004	0.405200	1293	55	1319	233	1.97	1293	55
05DTB18	10/05/2019 (6) 03:43:01.00	05DTB18 - 13	339	23	303	21	2.070393	0.084273	0.172900	0.012458	0.440290	2540	83	2585	116	1.74	2585	116
05DTB18	10/05/2019 (6) 04:26:26.00	05DTB18 - 32	83	3	50	3	5.265929	0.227331	0.077600	0.009152	0.157840	1121	43	1136	219	1.32	1121	43
05DTB18	10/05/2019 (6) 03:50:32.00	05DTB18 - 17	107	5	121	5	5.299417	0.204282	0.077300	0.006546	0.138120	1114	38	1128	161	1.21	1114	38
05DTB18	10/05/2019 (6) 06:33:41.00	05DTB18 - 81	187	6	129	5	5.497526	0.248975	0.075800	0.008716	0.296720	1077	43	1089	216	1.07	1077	43
05DTB18	10/05/2019 (6) 04:15:09.00	05DTB18 - 26	122	3	93	2	2.958580	0.164210	0.116000	0.013320	0.479220	1877	86	1895	194	0.93	1895	194
05DTB18	10/05/2019 (6) 08:00:46.00	05DTB18 - 115	47	5	31	1	5.336179	0.212080	0.076700	0.007434	0.347880	1107	39	1113	183	0.47	1107	39
05DTB18	10/05/2019 (6) 06:50:33.23	05DTB18 - 90	307	12	210	19	2.100840	0.094979	0.165400	0.009408	0.300880	2510	91	2511	93	0.04	2511	93
05DTB18	10/05/2019 (6) 06:44:57.00	05DTB18 - 87	190	6	68	2	3.838772	0.199086	0.093200	0.011664	0.172710	1492	66	1491	221	-0.09	1492	66
05DTB18	10/05/2019 (6) 04:30:11.00	05DTB18 - 34	106	7	83	6	4.081633	0.174927	0.089200	0.009284	0.285230	1413	52	1408	188	-0.36	1413	52
05DTB18	10/05/2019 (6) 04:17:04.00	05DTB18 - 27	138	3	64	2	4.870921	0.246891	0.080100	0.009902	0.290190	1204	53	1199	227	-0.39	1204	53
05DTB18	10/05/2019 (6) 04:24:35.00	05DTB18 - 31	359	12	305	9	5.379236	0.188606	0.076000	0.006520	0.241950	1099	34	1094	164	-0.45	1099	34
05DTB18	10/05/2019 (6) 08:06:26.00	05DTB18 - 118	91	7	30	2	3.060912	0.127739	0.110900	0.007918	0.250080	1822	64	1813	125	-0.50	1813	125
05DTB18	10/05/2019 (6) 04:35:52.00	05DTB18 - 37	92	9	71	9	4.585053	0.190508	0.082800	0.007356	0.139560	1272	46	1264	165	-0.65	1272	46
05DTB18	10/05/2019 (6) 04:18:55.00	05DTB18 - 28	266	15	118	7	5.078720	0.173796	0.078200	0.005564	0.219640	1159	35	1151	136	-0.66	1159	35
05DTB18	10/05/2019 (6) 03:10:35.00	05DTB18 - 2	177	10	70	6	4.101723	0.169520	0.088700	0.008274	0.169690	1406	50	1397	170	-0.69	1406	50
05DTB18	10/05/2019 (6) 04:03:54.00	05DTB18 - 20	246	13	119	7	5.476451	0.208501	0.075200	0.006704	0.324330	1081	37	1073	170	-0.77	1081	37
05DTB18	10/05/2019 (6) 04:49:17.00	05DTB18 - 41	116	6	50	3	4.861449	0.255575	0.080000	0.012600	0.017481	1206	55	1196	284	-0.83	1206	55
05DTB18	10/05/2019 (6) 04:20:50.00	05DTB18 - 29	112	3	71	3	3.943218	0.201701	0.090700	0.009814	0.161860	1457	64	1440	194	-1.22	1457	64
05DTB18	10/05/2019 (6) 08:30:54.00	05DTB18 - 131	309	10	93	4	3.000300	0.142823	0.112000	0.012240	0.462550	1854	74	1831	187	-1.26	1831	187
05DTB18	10/05/2019 (6) 04:09:32.99	05DTB18 - 23	53	1	42	1	2.087683	0.085338	0.163400	0.009968	0.281500	2523	83	2490	100	-1.31	2490	100
05DTB18	10/05/2019 (6) 03:39:13.00	05DTB18 - 11	353	19	527	28	5.151984	0.201249	0.077100	0.007142	0.298430	1144	40	1123	175	-1.84	1144	40
05DTB18	10/05/2019 (6) 08:10:11.00	05DTB18 - 120	126	5	42	3	4.796163	0.247744	0.080100	0.009502	-0.002972	1221	55	1199	218	-1.85	1221	55
05DTB18	10/05/2019 (6) 06:31:46.00	05DTB18 - 80	265	13	111	7	4.531038	0.195325	0.082700	0.007354	0.248180	1286	48	1261	165	-1.93	1286	48
05DTB18	10/05/2019 (6) 08:04:35.00	05DTB18 - 117	214	6	97	3	5.797101	0.203319	0.072700	0.004654	-0.174400	1026	32	1005	126	-2.11	1026	32
05DTB18	10/05/2019 (6) 07:09:35.00	05DTB18 - 96	123	7	57	4	2.114165	0.086980	0.158400	0.012768	0.311320	2497	82	2438	131	-2.41	2438	131
05DTB18	10/05/2019 (6) 07:20:52.00	05DTB18 - 102	496	21	234	10	4.342162	0.218824	0.084500	0.010890	0.098184	1336	58	1303	233	-2.54	1336	58
05DTB18	10/05/2019 (6) 07:30:17.00	05DTB18 - 107	81	3	57	3	2.907822	0.124954	0.113500	0.011770	0.302500	1905	68	1855	177	-2.69	1855	177
05DTB18	10/05/2019 (6) 04:01:57.00	05DTB18 - 19	345	16	348	23	3.401361	0.183720	0.099600	0.010592	0.153490	1662	76	1616	187	-2.83	1616	187
05DTB18	10/05/2019 (6) 06:46:48.00	05DTB18 - 88	431	13	131	5	4.854369	0.276181	0.079000	0.016580	0.298700	1208	60	1171	369	-3.12	1208	60
05DTB18	10/05/2019 (6) 07:41:43.00	05DTB18 - 110	182	8	32	2	3.197953	0.113048	0.104100	0.007082	0.277770	1754	53	1698	121	-3.32	1698	121
05DTB18	10/05/2019 (6) 08:38:25.00	05DTB18 - 135	110	4	59	2	4.083299	0.148359	0.087300	0.006046	0.199990	1412	45	1366	129	-3.35	1412	45
05DTB18	10/05/2019 (6) 08:12:06.00	05DTB18 - 121	168	5	70	3	4.355401	0.227482	0.083900	0.010378	0.065307	1332	60	1289	225	-3.37	1332	60
05DTB18	10/05/2019 (6) 08:19:37.00	05DTB18 - 125	71	4	50	3	5.120328	0.288553	0.076500	0.011330	0.328020	1150	56	1107	272	-3.88	1150	56
05DTB18	10/05/2019 (6) 07:37:54.00	05DTB18 - 108	227	10	62	3	5.293806	0.220776	0.075200	0.007404	0.344130	1115	41	1073	187	-3.96	1115	41
05DTB18	10/05/2019 (6) 06:24:15.00	05DTB18 - 76	109	5	52	2	3.355705	0.202243	0.099500	0.007990	-0.227800	1681	85	1614	143	-4.18	1614	143
05DTB18	10/05/2019 (6) 06:35:31.00	05DTB18 - 82	264	7	174	4	5.370569	0.208362	0.074500	0.006290	0.411850	1101	38	1054	162	-4.43	1101	38
05DTB18	10/05/2019 (6) 08:13:57.00	05DTB18 - 122	425	21	163	11	2.999400	0.105870	0.108600	0.007072	0.266290	1855	55	1775	115	-4.48	1775	115
05DTB18	10/05/2019 (6) 07:45:29.00	05DTB18 - 112	133	8	94	6	3.163556	0.113312	0.103900	0.007578	0.173210	1771	54	1694	130	-4.52	1694	130
05DTB18	10/05/2019 (6) 03:18:19.00	05DTB18 - 3	53	2	32	1	2.799552	0.111637	0.115000	0.010300	0.228070	1969	65	1879	154	-4.78	1879	154
05DTB18	10/05/2019 (6) 03:25:55.00	05DTB18 - 7	100	4	54	3	1.715266	0.087264	0.200000	0.019000	0.349010	2961	116	2826	148	-4.80	2826	148
05DTB18	10/05/2019 (6) 07:26:32.00	05DTB18 - 105	281	11	93	4	3.990423	0.164203	0.087600	0.008152	0.300890	1442	51	1373	170	-5.00	1442	51
05DTB18	10/05/2019 (6) 08:02:40.00	05DTB18 - 116	62	3	39	2	2.707826	0.098884	0.118200	0.007064	0.376920	2026	62	1928	104	-5.07	1928	104
05DTB18	10/05/2019 (6) 07:02:04.00	05DTB18 - 92	599	23	731	23	1.852538	0.065879	0.179400	0.010088	0.288970	2783	78	2647	91	-5.14	2647	91
05DTB18	10/05/2019 (6) 06:41:12.00	05DTB18 - 85	169	8	126	6	4.518753	0.192471	0.081200	0.008124	0.245940	1289	48	1225	186	-5.17	1289	48
05DTB18	10/05/2019 (6) 03:29:40.00	05DTB18 - 9	194	6	202	6	3.910833	0.177632	0.088600	0.006872	0.118570	1468	57	1395	143	-5.24	1468	57
05DTB18	10/05/2019 (6) 06:48:42.00	05DTB18 - 89	118	6	62	3	3.189793	0.119757	0.102000	0.008140	0.202880	1758	56	1660	142	-5.90	1660	142
05DTB18	10/05/2019 (6) 08:25:13.00	05DTB18 - 128	37	1	38	2	3.976143	0.139600	0.087200	0.006544	0.328250	1446	44	1364	139	-6.02	1446	44
05DTB18	10/05/2019 (6) 08:32:44.00	05DTB18 - 132	162	8	56	3	3.080715	0.117610	0.104600	0.006892	0.181030	1812	58	1707	117	-6.19	1707	117
05DTB18	10/05/2019 (6) 07:15:16.00	05DTB18 - 99	82	3	78	5	5.763689	0.258120	0.071300	0.007426	0.165340	1031	41	965	200	-6.87	1031	41
05DTB18	10/05/2019 (6) 04:05:48.00	05DTB18 - 21	274	14	96	5	3.891051	0.173205	0.087600	0.008752	0.255710	1475	56	1373	182	-7.40	1475	56
05DTB18	10/05/2019 (6) 06:18:39.00	05DTB18 - 73	125	9	69	5	5.482456	0.265947	0.072700	0.008154	0.121250	1080	46	1005	213	-7.50	1080	46
05DTB18	10/05/2019 (6) 03:46:47.00	05DTB18 - 15	56	2	20	1	4.482295	0.222246	0.080400	0.008908	-0.044879	1298	56	1206	205	-7.65	1298	56
05DTB18	10/05/2019 (6) 06:37:26.00	05DTB18 - 83	173	12	61	5	4.139073	0.199279	0.084100	0.009782	0.204200	1395	58	1294	212	-7.81	1395	58
05DTB18	10/05/2019 (6) 07:11:31.00	05DTB18 - 97	140	8	80	5	2.906977	0.113068	0.108100	0.008362	0.230690	1906	62	1767	136	-7.87	1767	136
05DTB18	10/05/2019 (6) 06:01:19.00	05DTB18 - 67	113	4	62	3	3.797949	0.172603	0.088000	0.010560	0.281010	1507	59	1382	215	-9.05	1382	215
05DTB18	10/05/2019 (6) 06:05:10.00	05DTB18 - 69	487	58	176	19	4.456328	0.148703	0.080000	0.005900	0.194740	1305	38	1196	140	-9.11	1305	38
05DTB18	10/05/2019 (6) 07:07:45.00	05DTB18 - 95	136	7	62	3	4.025765	0.148584	0.084700	0.007494	0.290040	1430	46	1308	164	-9.36	1430	46
05DTB18	10/05/2019 (6) 06:07:05.00	05DTB18 - 70	99	3	58	3	2.613013	0.107566	0.116900	0.009438	0.238720	2089	71	1909	139	-9.45	1909	139
05DTB18	10/05/2019 (6) 03:31:36.00	05DTB18 - 10	243	29	51	4	5.216484	0.226782	0.073700	0.007074	0.252660	1131	43	1032	184	-9.51	1131	43
05DTB18	10/05/2019 (6) 07:19:02.00	05DTB18 - 101	100	2	49	1	5.109862	0.177918	0.074400	0.005488	0.223190	1152	36	1051	143	-9.59	1152	36
05DTB18	10/05/2019 (6) 07:39:47.00	05DTB18 - 109	144	6	110	5	5.022602	0.163518	0.075000	0.004400	0.361050	1170	34	1068	115	-9.64	1170	34
05DTB18	10/05/2019 (6) 07:13:21.00	05DTB18 - 98	162	7	103	4	5.428882	0.211732	0.072200	0.007544	0.358080	1090	38	991	200	-10.01	1090	38
05DTB18	10/05/2019 (6) 07:28:22.00	05DTB18 - 106	150	9	118	6	4.017678	0.165905	0.084400	0.008988	0.072786	1433	51	1301	195	-10.14	1433	51
05DTB18	10/05/2019 (6) 06:20:30.00	05DTB18 - 74	470	13	250	11	3.787879	0.194846	0.086800	0.008536	0.088670	1510	66	1355	180	-11.44	1355	180
05DTB18	10/05/2019 (6) 03:41:07.00	05DTB18 - 12	157	10	59	4	5.115090	0.261903	0.073600	0.010172	0.191300	1151	52	1030	257	-11.76	1151	52
05DTB18	10/05/2019 (6) 03:20:19.00	05DTB18 - 4	181	8	162	7	5.260389	0.243566	0.072500	0.009550	0.207730	1122	46	999	248	-12.30	1122	46
05DTB18	10/05/2019 (6) 04:37:42.00	05DTB18 - 38	203	23	52	3	3.872967	0.215458	0.085000	0.012700	0.188070	1481	70	1315	266	-12.59	1481	70
05DTB18	10/05/2019 (6) 06:14:49.00	05DTB18 - 71	134	2	106	5	5.133470	0.345113	0.073000	0.016460	0.200780	1147	67	1013	401	-13.26	1147	67
05DTB18	10/05/2019 (6) 08:17:42.00	05DTB18 - 124	279	14	313	20	4.368720	0.173260	0.078600	0.006872	0.131430	1329	46	1161	165	-14.42	1329	46
05DTB18	10/05/2019 (6) 08:21:28.00	05DTB18 - 126	97	4	120	6	4.923683	0.176050	0.073800	0.005476	0.234300	1192	38	1035	144	-15.15	1192	38
05DTB18	10/05/2019 (6) 07:43:34.00	05DTB18 - 111	335	19	237	22	5.422993	0.196686	0.070600	0.005012	0.312200	1091	35	945	140	-15.46	1091	35
05DTB18	10/05/2019 (6) 06:28:01.00	05DTB18 - 78	157	7	53	2	5.347594	0.269953	0.070800	0.008216	0.316110	1105	49	951	222	-16.24	1105	49
05DTB18	10/05/2019 (6) 04:45:27.00	05DTB18 - 39	158	15	73	7	4.436557	0.206829	0.077200	0.010944	0.261750	1310	53	1125	261	-16.47	1310	53
05DTB18	10/05/2019 (6) 04:51:11.00	05DTB18 - 42	86	3	75	3	4.759638	0.183544	0.074500	0.006790	0.289450	1229	42	1054	174	-16.63	1229	42
05DTB18	10/05/2019 (6) 08:27:08.00	05DTB18 - 129	229	15	211	18	4.192872	0.198129	0.079200	0.008584	0.110110	1379	56	1176	202	-17.23	1379	56
05DTB18	10/05/2019 (6) 07:22:47.00	05DTB18 - 103	493	8	431	6	3.332223	0.162136	0.090600	0.011112	0.320890	1692	69	1437	218	-17.70	1437	218
05DTB18	10/05/2019 (6) 03:27:51.00	05DTB18 - 8	111	5	54	3	5.184033	0.289113	0.071000	0.012420	0.209750	1137	55	956	323	-18.94	1137	55
05DTB18	10/05/2019 (6) 06:16:44.00	05DTB18 - 72	530	11	199	10	5.205622	0.193537	0.070600	0.005812	0.184510	1133	37	945	161	-19.88	1133	37
05DTB18	10/05/2019 (6) 04:13:18.00	05DTB18 - 25	104	2	35	1	5.807201	0.244294	0.067200	0.007644	0.283140	1024	38	843	221	-21.49	1024	38
05DTB18	10/05/2019 (6) 06:29:56.00	05DTB18 - 79	286	16	117	6	4.472272	0.205453	0.072800	0.007556	0.261410	1301	52	1008	198	-29.12	1301	52
05DTB18	10/05/2019 (6) 07:51:08.00	05DTB18 - 114	451	22	170	7	5.434783	0.259334	0.062000	0.010140	0.094544	1089	46	673	317	-61.78	1089	46

Appendix D.2 continued.

Sample ID	Analysis date-time	Spot ID[1]	238U conc.	±2σ INT	232Th conc.	±2σ INT	Isotopic Ratios					Apparent Ages - Calculated in Isoplot R (Ma)				Discord	Perferred age 1500 Ma cutoff	
			ppm		ppm		238U/206Pb	±2σ PROP	207Pb/206Pb	±2σ PROP	rho	238U/206Pb	±2σ PROP	207Pb/206Pb	±2σ PROP	(7/6-6/8)/7/6 *100	Ma	2σ
04DTB19	2020-07-30 17:50:21.000	04DTB19q - 81 - 1.d	949	25	634	21	10.913784	0.338738	0.081224	0.004798	0.229592	565	17	1226	116	53.90	565	17
04DTB19	2020-07-30 18:00:51.000	04DTB19q - 105 - 1.d	91	3	120	5	7.916175	0.276437	0.073040	0.006074	0.135852	767	25	1014	169	24.39	767	25
04DTB19	2020-07-30 16:51:48.000	04DTB19q - 178 - 1.d	43	1	49	1	7.788034	0.317423	0.072134	0.007388	0.262568	779	30	989	208	21.24	779	30
04DTB19	2020-07-30 16:43:04.000	04DTB19q - 130 - 1.d	54	2	52	2	7.850665	0.307937	0.067890	0.006608	0.286459	773	29	864	202	10.58	773	29
04DTB19	2020-07-30 16:55:14.000	04DTB19q - 64 - 1.d	66	2	117	2	7.999056	0.296865	0.067140	0.005979	0.270946	759	27	841	185	9.73	759	27
04DTB19	2020-07-30 16:53:32.000	04DTB19q - 34 - 1.d	50	1	76	3	7.734419	0.309947	0.067967	0.006692	0.185005	784	30	867	204	9.55	784	30
04DTB19	2020-07-30 16:39:39.000	04DTB19q - 125 - 1.d	57	2	52	2	7.803501	0.306847	0.067398	0.006622	0.278938	777	29	849	204	8.47	777	29
04DTB19	2020-07-30 17:59:06.000	04DTB19q - 117 - 1.d	388	13	290	11	8.231249	0.246160	0.065752	0.004189	0.236775	739	21	798	134	7.33	739	21
04DTB19	2020-07-30 17:48:39.000	04DTB19q - 91 - 1.d	39	2	32	2	5.145563	0.192872	0.079809	0.007617	0.149369	1145	39	1191	188	3.91	1145	39
04DTB19	2020-07-30 16:41:25.000	04DTB19q - 130b - 1.d	60	1	58	1	7.962577	0.310366	0.064635	0.006098	0.119656	763	28	762	199	-0.15	763	28
04DTB18	14/07/2020 (3) 03:00:43.00	04DTB18 - 2.172	939	19	1043	28	7.434944	0.353229	0.227000	0.019540	-0.575630	814	35	3030	132	73.15	814	35
04DTB18	13/07/2020 (2) 23:01:38.00	04DTB18 - 2.39	710	13	283	7	9.765625	0.414658	0.090700	0.003514	0.059785	628	24	1440	73	56.34	628	24
04DTB18	14/07/2020 (3) 02:27:57.00	04DTB18 - 2.153	875	17	342	7	4.308488	0.173416	0.189900	0.005598	0.322420	1346	47	2741	48	50.90	1346	47
04DTB18	10/05/2019 (6) 00:48:05.51	04DTB18 - 11	135	6	138	9	7.272727	0.462810	0.103000	0.018060	0.316360	831	47	1678	294	50.51	831	47
04DTB18	13/07/2020 (2) 22:12:22.00	04DTB18 - 2.12	607	4	758	23	6.341154	0.347979	0.114100	0.005482	0.488490	944	46	1865	85	49.38	944	46
04DTB18	14/07/2020 (3) 01:17:47.00	04DTB18 - 2.115	492	17	967	24	3.821169	0.280842	0.204900	0.006398	0.081843	1499	92	2865	51	47.69	1499	92
04DTB18	14/07/2020 (3) 02:57:44.00	04DTB18 - 2.170	1331	56	893	21	6.807352	0.219559	0.102000	0.003240	0.412280	884	26	1660	59	46.77	884	26
04DTB18	14/07/2020 (3) 00:30:43.00	04DTB18 - 2.186	911	12	244	8	6.093845	0.211001	0.110500	0.003610	0.242260	980	30	1807	59	45.79	980	30
04DTB18	14/07/2020 (3) 03:06:39.00	04DTB18 - 2.176	537	6	468	6	3.496503	0.289990	0.189000	0.006080	-0.082621	1622	111	2733	53	40.66	2733	53
04DTB18	13/07/2020 (2) 21:52:49.00	04DTB18 - 2.2	69	5	152	8	7.824726	0.321806	0.084300	0.006786	0.358150	775	29	1299	150	40.30	775	29
04DTB18	14/07/2020 (3) 01:31:17.00	04DTB18 - 2.121	1088	28	284	11	4.187605	0.138114	0.146600	0.004332	0.080312	1380	40	2306	51	40.13	1380	40
04DTB18	13/07/2020 (2) 23:59:59.00	04DTB18 - 2.72	475	13	643	47	6.825939	0.271640	0.092000	0.003640	0.064468	881	32	1467	74	39.90	881	32
04DTB18	14/07/2020 (3) 02:50:20.00	04DTB18 - 2.165	474	4	168	1	4.230118	0.143652	0.141100	0.004722	0.219780	1368	41	2240	57	38.93	1368	41
04DTB18	13/07/2020 (2) 21:55:47.00	04DTB18 - 2.4	261	18	207	13	3.891051	0.211055	0.156000	0.006320	-0.185190	1475	68	2412	68	38.87	1475	68
04DTB18	13/07/2020 (2) 23:46:20.00	04DTB18 - 2.66	1047	17	171	3	4.230118	0.138284	0.139200	0.004284	-0.089296	1368	39	2217	53	38.28	1368	39
04DTB18	14/07/2020 (3) 02:20:31.00	04DTB18 - 2.148	1141	15	177	1	7.818608	0.260294	0.079300	0.002886	0.278830	776	24	1179	71	34.18	776	24
04DTB18	14/07/2020 (3) 01:43:09.00	04DTB18 - 2.129	259	3	194	2	5.428882	0.185207	0.101200	0.004224	0.377790	1090	33	1645	76	33.76	1090	33
04DTB18	13/07/2020 (2) 22:01:43.00	04DTB18 - 2.8	526	8	136	7	6.688963	0.254583	0.086400	0.003728	0.015698	898	31	1346	82	33.29	898	31
04DTB18	13/07/2020 (2) 22:19:45.00	04DTB18 - 2.17	525	16	38	2	4.904365	0.160625	0.106700	0.003934	0.496500	1196	35	1743	67	31.37	1196	35
04DTB18	14/07/2020 (3) 00:22:24.00	04DTB18 - 2.84	127	3	103	1	8.097166	0.299628	0.075800	0.004816	0.292440	751	25	1089	123	31.06	751	25
04DTB18	14/07/2020 (3) 02:59:15.00	04DTB18 - 2.171	1391	37	438	15	5.186722	0.165609	0.099870	0.002987	0.215030	1137	32	1621	55	29.88	1137	32
04DTB18	14/07/2020 (3) 01:35:45.00	04DTB18 - 2.124	474	3	834	13	6.226650	0.205952	0.086900	0.003838	0.146970	960	29	1357	84	29.27	960	29
04DTB18	13/07/2020 (2) 23:49:17.00	04DTB18 - 2.68	470	6	784	16	4.302926	0.141604	0.113900	0.004178	0.430680	1347	39	1862	66	27.64	1347	39
04DTB18	14/07/2020 (3) 03:32:12.00	04DTB18 - 2.187	1063	12	39	3	6.920415	0.229403	0.079700	0.002794	0.091172	870	26	1189	69	26.81	870	26
04DTB18	14/07/2020 (3) 01:29:50.00	04DTB18 - 2.120	808	34	819	40	5.073567	0.160676	0.097800	0.003256	0.303240	1160	33	1582	62	26.68	1160	33
04DTB18	10/05/2019 (6) 01:43:02.00	04DTB18 - 33	565	14	192	5	5.871991	0.351906	0.087300	0.008046	0.353950	1014	53	1366	169	25.80	1014	53
04DTB18	14/07/2020 (3) 00:10:34.00	04DTB18 - 2.76	94	1	148	2	3.310162	0.241518	0.145100	0.007202	0.058064	1702	103	2288	84	25.63	2288	84
04DTB18	14/07/2020 (3) 02:36:39.00	04DTB18 - 2.190	653	36	222	6	6.468305	0.221412	0.081900	0.003038	0.191420	927	29	1242	72	25.40	927	29
04DTB18	14/07/2020 (3) 02:23:31.00	04DTB18 - 2.150	257	8	618	49	4.405286	0.225892	0.107900	0.004358	0.110790	1319	58	1763	73	25.21	1319	58
04DTB18	14/07/2020 (3) 03:09:37.00	04DTB18 - 2.178	161	12	125	4	8.857396	0.530189	0.069700	0.004494	0.117220	690	37	919	128	24.93	690	37
04DTB18	14/07/2020 (3) 02:14:35.00	04DTB18 - 2.144	206	13	328	33	4.297379	0.213373	0.109000	0.006380	0.614480	1349	58	1782	104	24.32	1349	58
04DTB18	10/05/2019 (6) 03:03:00.00	04DTB18 - 63	187	7	100	2	4.950495	0.211744	0.096100	0.009122	0.196440	1186	45	1549	169	23.42	1186	45
04DTB18	10/05/2019 (6) 02:30:41.00	04DTB18 - 50	178	4	238	3	4.149378	0.181126	0.110500	0.009010	0.147880	1392	53	1807	142	22.96	1392	53
04DTB18	10/05/2019 (6) 02:36:17.00	04DTB18 - 53	280	15	121	4	5.643341	0.326244	0.087000	0.012740	0.021593	1052	53	1360	259	22.67	1052	53
04DTB18	14/07/2020 (3) 00:58:18.00	04DTB18 - 2.105	210	7	244	7	4.440497	0.153879	0.102900	0.004658	0.186260	1309	40	1676	82	21.89	1309	40
04DTB18	13/07/2020 (2) 21:58:45.00	04DTB18 - 2.6	256	7	230	8	4.918839	0.166123	0.095000	0.003800	0.218240	1193	36	1527	74	21.88	1193	36
04DTB18	13/07/2020 (2) 21:54:20.00	04DTB18 - 2.3	599	24	889	38	5.934718	0.196180	0.083300	0.003266	0.181460	1004	30	1275	75	21.29	1004	30
04DTB18	10/05/2019 (6) 02:13:34.79	04DTB18 - 42	142	5	125	7	3.831418	0.238106	0.116000	0.012320	0.524340	1495	79	1895	180	21.10	1495	79
04DTB18	10/05/2019 (6) 00:42:27.00	04DTB18 - 8	94	7	77	4	4.734848	0.242661	0.096200	0.011024	0.280710	1235	55	1551	202	20.35	1235	55
04DTB18	14/07/2020 (3) 03:08:08.00	04DTB18 - 2.177	141	6	414	56	5.440696	0.336743	0.087000	0.004640	0.006618	1088	59	1360	100	20.00	1088	59
04DTB18	10/05/2019 (6) 03:04:55.60	04DTB18 - 64	172	6	159	5	4.442470	0.221078	0.100400	0.006008	-0.071713	1309	56	1631	108	19.74	1309	56
04DTB18	14/07/2020 (3) 00:19:28.00	04DTB18 - 2.82	539	10	540	13	4.844961	0.153236	0.093800	0.003476	0.226670	1210	34	1503	69	19.53	1210	34
04DTB18	14/07/2020 (3) 02:47:23.00	04DTB18 - 2.163	540	23	1420	140	3.995206	0.135770	0.109300	0.003786	0.127180	1440	43	1787	63	19.42	1440	43
04DTB18	13/07/2020 (2) 22:49:38.61	04DTB18 - 2.31	651	12	149	19	3.901678	0.149582	0.111400	0.003728	0.441210	1471	49	1822	60	19.25	1471	49
04DTB18	10/05/2019 (6) 02:32:29.70	04DTB18 - 51	240	8	381	21	4.568296	0.235364	0.097600	0.011452	0.143620	1276	57	1578	206	19.13	1276	57
04DTB18	14/07/2020 (3) 03:29:15.00	04DTB18 - 2.185	197	7	70	2	4.531038	0.150159	0.097200	0.004244	0.317740	1286	37	1570	81	18.13	1286	37
04DTB18	14/07/2020 (3) 00:02:55.00	04DTB18 - 2.74	200	4	117	2	3.837299	0.268169	0.111100	0.004522	0.132150	1493	88	1817	73	17.82	1493	88
04DTB18	10/05/2019 (6) 02:08:00.00	04DTB18 - 39	96	3	62	3	5.691520	0.327627	0.083000	0.012660	0.282100	1043	53	1268	273	17.71	1043	53
04DTB18	13/07/2020 (2) 23:06:09.00	04DTB18 - 2.42	341	7	217	7	2.933412	0.213557	0.144300	0.005486	-0.133890	1891	112	2279	65	17.01	2279	65
04DTB18	13/07/2020 (2) 22:09:21.00	04DTB18 - 2.10	320	4	334	4	4.340278	0.145203	0.099000	0.003980	0.091895	1337	39	1605	74	16.70	1337	39
04DTB18	13/07/2020 (2) 23:18:01.00	04DTB18 - 2.50	754	6	402	4	6.049607	0.201507	0.079300	0.002986	0.329070	986	30	1179	74	16.33	986	30
04DTB18	13/07/2020 (2) 23:56:51.00	04DTB18 - 2.70	261	7	192	2	3.772161	0.274652	0.110800	0.004316	0.234780	1516	92	1812	70	16.33	1812	70
04DTB18	13/07/2020 (2) 22:52:44.00	04DTB18 - 2.33	552	20	338	22	4.506534	0.155119	0.095800	0.003516	0.160290	1292	39	1543	68	16.27	1292	39
04DTB18	10/05/2019 (6) 02:19:17.00	04DTB18 - 45	405	16	337	13	4.759638	0.172217	0.091300	0.005926	0.165870	1229	39	1452	120	15.33	1229	39
04DTB18	10/05/2019 (6) 02:17:22.47	04DTB18 - 44	191	7	92	4	3.862495	0.142893	0.107200	0.006044	0.434460	1484	47	1752	101	15.26	1484	47
04DTB18	14/07/2020 (3) 03:02:11.00	04DTB18 - 2.173	294	12	99	2	3.718855	0.267995	0.110200	0.004404	0.137260	1535	92	1802	72	14.80	1802	72
04DTB18	14/07/2020 (3) 02:56:15.00	04DTB18 - 2.169	827	20	1178	38	5.390836	0.177563	0.083700	0.002974	0.139430	1097	32	1285	69	14.61	1097	32
04DTB18	14/07/2020 (3) 01:38:42.00	04DTB18 - 2.126	369	10	115	3	4.149378	0.141527	0.099800	0.003596	0.246550	1392	41	1620	66	14.05	1392	41
04DTB18	13/07/2020 (2) 22:15:17.00	04DTB18 - 2.14	931	21	213	6	6.127451	0.197640	0.077500	0.002550	0.367470	975	28	1133	65	14.00	975	28
04DTB18	13/07/2020 (2) 23:14:59.00	04DTB18 - 2.48	149	2	153	3	4.321521	0.146192	0.096600	0.004732	0.082131	1342	40	1559	90	13.91	1342	40
04DTB18	14/07/2020 (3) 01:28:17.00	04DTB18 - 2.119	153	5	134	11	3.816794	0.280287	0.106500	0.004930	0.054232	1500	92	1740	83	13.76	1740	83
04DTB18	13/07/2020 (2) 22:18:18.00	04DTB18 - 2.16	746	26	518	11	4.975124	0.166333	0.087300	0.002946	0.086033	1181	35	1366	64	13.58	1181	35
04DTB18	14/07/2020 (3) 03:03:41.00	04DTB18 - 2.174	64	1	77	1	3.640335	0.131116	0.110500	0.004410	0.143870	1565	48	1807	72	13.40	1807	72
04DTB18	14/07/2020 (3) 02:41:18.00	04DTB18 - 2.162	180	5	172	6	2.677376	0.189746	0.151300	0.005626	0.192100	2046	117	2360	63	13.31	2360	63
04DTB18	14/07/2020 (3) 01:04:18.00	04DTB18 - 2.106	413	8	184	2	4.391744	0.143768	0.094800	0.003996	0.492410	1322	38	1523	78	13.19	1322	38
04DTB18	14/07/2020 (3) 01:10:20.00	04DTB18 - 2.110	611	17	312	9	3.946330	0.130319	0.102300	0.003546	0.087251	1456	42	1665	64	12.57	1456	42
04DTB18	13/07/2020 (2) 22:25:41.00	04DTB18 - 2.21	193	6	150	2	3.538570	0.258594	0.111900	0.004338	0.164320	1604	97	1830	69	12.31	1830	69
04DTB18	14/07/2020 (3) 01:52:02.00	04DTB18 - 2.135	774	13	516	7	5.431831	0.176498	0.081900	0.002738	-0.017580	1089	32	1242	65	12.31	1089	32
04DTB18	14/07/2020 (3) 01:59:28.00	04DTB18 - 2.140	341	9	209	7	2.541296	0.179990	0.157900	0.005158	0.069453	2139	121	2433	55	12.07	2433	55
04DTB18	14/07/2020 (3) 01:41:41.00	04DTB18 - 2.128	110	5	72	3	3.490401	0.252552	0.112700	0.005054	-0.076114	1624	98	1843	80	11.86	1843	80
04DTB18	13/07/2020 (2) 22:36:07.00	04DTB18 - 2.28	364	11	194	5	2.452182	0.175321	0.164300	0.005286	0.285620	2205	126	2500	54	11.79	2500	54
04DTB18	14/07/2020 (3) 00:15:01.00	04DTB18 - 2.79	375	11	118	2	3.853565	0.129046	0.103200	0.003764	0.232190	1487	43	1682	67	11.56	1487	43
04DTB18	13/07/2020 (2) 22:54:15.00	04DTB18 - 2.34	218	6	219	5	3.885004	0.133545	0.102400	0.004448	0.374250	1477	44	1667	79	11.44	1477	44
04DTB18	14/07/2020 (3) 01:19:14.00	04DTB18 - 2.116	151	4	112	3	2.311604	0.163789	0.175600	0.006012	0.351750	2317	130	2611	57	11.24	2611	57
04DTB18	10/05/2019 (6) 00:40:37.00	04DTB18 - 7	84	3	90	3	5.934718	0.231401	0.077200	0.004744	0.142040	1004	35	1126	119	10.81	1004	35
04DTB18	14/07/2020 (3) 03:23:10.00	04DTB18 - 2.184	87	2	139	1	3.868472	0.146209	0.101800	0.005536	0.360670	1482	48	1656	98	10.52	1482	48
04DTB18	13/07/2020 (2) 22:07:47.00	04DTB18 - 2.9	79	1	84	1	3.633721	0.257529	0.107000	0.005640	0.143750	1567	93	1748	94	10.35	1748	94
04DTB18	14/07/2020 (3) 03:12:34.00	04DTB18 - 2.180	318	6	286	5	3.723008	0.268511	0.103900	0.004078	0.151430	1534	92	1694	71	9.47	1694	71
04DTB18	13/07/2020 (2) 22:00:16.00	04DTB18 - 2.7	535	18	268	9	4.171882	0.133911	0.095100	0.003502	0.272640	1385	39	1529	69	9.42	1385	39
04DTB18	13/07/2020 (2) 23:30:04.00	04DTB18 - 2.55	349	3	169	3	4.222973	0.139743	0.094200	0.003884	0.293020	1370	40	1511	77	9.35	1370	40
04DTB18	13/07/2020 (2) 22:55:42.00	04DTB18 - 2.35	176	7	154	7	5.130836	0.171063	0.082900	0.004158	0.174580	1148	34	1266	96	9.33	1148	34
04DTB18	13/07/2020 (2) 23:50:46.00	04DTB18 - 2.69	122	5	49	2	3.016591	0.215029	0.125100	0.005702	0.113250	1846	108	2029	79	9.06	2029	79
04DTB18	14/07/2020 (3) 03:35:13.00	04DTB18 - 2.189	87	1	45	1	4.533092	0.162583	0.089300	0.005086	0.245720	1285	40	1410	106	8.84	1285	40
04DTB18	14/07/2020 (3) 03:05:12.00	04DTB18 - 2.175	89	3	50	1	3.985652	0.141666	0.097700	0.005454	0.277220	1443	45	1580	102	8.65	1443	45
04DTB18	13/07/2020 (2) 23:40:24.00	04DTB18 - 2.62	321	5	502	8	3.932363	0.131223	0.098500	0.003970	0.063114	1461	42	1595	74	8.43	1461	42
04DTB18	14/07/2020 (3) 01:47:38.00	04DTB18 - 2.132	298	9	106	2	4.347826	0.177694	0.091400	0.003928	0.166310	1335	48	1454	80	8.23	1335	48
04DTB18	14/07/2020 (3) 01:44:38.00	04DTB18 - 2.130	442	21	336	18	4.116921	0.167084	0.095000	0.003400	0.184110	1402	49	1527	67	8.21	1402	49
04DTB18	10/05/2019 (6) 00:31:07.50	04DTB18 - 2	183	5	161	5	8.038585	0.348166	0.066500	0.007530	0.208850	756	30	821	221	7.96	756	30
04DTB18	14/07/2020 (3) 00:26:52.00	04DTB18 - 2.87	67	2	52	2	4.666356	0.169539	0.087000	0.005240	0.227180	1252	40	1360	113	7.94	1252	40
04DTB18	10/05/2019 (6) 02:42:02.00	04DTB18 - 56	193	5	152	6	5.461496	0.306094	0.079200	0.010984	0.091176	1084	53	1176	253	7.83	1084	53
04DTB18	10/05/2019 (6) 02:40:06.00	04DTB18 - 55	222	7	503	32	4.201681	0.152885	0.093100	0.005862	0.274650	1376	44	1489	116	7.58	1376	44
04DTB18	10/05/2019 (6) 02:34:28.00	04DTB18 - 52	229	14	201	16	4.616805	0.190385	0.087300	0.008646	0.207770	1264	46	1366	180	7.49	1264	46
04DTB18	10/05/2019 (6) 01:44:58.00	04DTB18 - 34	169	5	156	4	2.969121	0.131671	0.124300	0.011886	0.344200	1871	69	2018	161	7.27	2018	161
04DTB18	14/07/2020 (3) 03:33:42.00	04DTB18 - 2.188	104	3	200	4	3.877472	0.137689	0.098500	0.004970	0.422100	1479	45	1595	92	7.27	1479	45
04DTB18	13/07/2020 (2) 23:58:28.00	04DTB18 - 2.71	105	2	54	1	4.370629	0.156181	0.090300	0.005306	0.303410	1328	42	1431	109	7.18	1328	42
04DTB18	14/07/2020 (3) 01:49:05.00	04DTB18 - 2.133	92	2	42	1	2.091613	0.151203	0.186600	0.006932	0.280220	2519	142	2712	61	7.11	2712	61
04DTB18	10/05/2019 (6) 01:22:14.00	04DTB18 - 25	490	15	243	12	4.987531	0.199252	0.082900	0.006758	0.236370	1178	41	1266	152	6.95	1178	41
04DTB18	14/07/2020 (3) 01:11:51.00	04DTB18 - 2.111	357	10	155	4	5.035247	0.166625	0.082400	0.003748	0.308360	1168	34	1254	87	6.89	1168	34
04DTB18	14/07/2020 (3) 01:37:12.00	04DTB18 - 2.125	272	11	222	8	5.035247	0.169160	0.082300	0.003346	0.192040	1168	35	1252	78	6.71	1168	35
04DTB18	13/07/2020 (2) 23:43:22.00	04DTB18 - 2.64	123	2	53	1	5.042864	0.182235	0.082200	0.004244	0.365530	1166	37	1249	99	6.66	1166	37
04DTB18	10/05/2019 (6) 02:43:52.00	04DTB18 - 57	120	4	72	7	4.275331	0.167760	0.091200	0.008024	0.260020	1355	46	1450	160	6.55	1355	46
04DTB18	10/05/2019 (6) 01:24:03.50	04DTB18 - 26	529	18	345	26	5.399568	0.274177	0.079000	0.009680	0.337490	1095	49	1171	226	6.46	1095	49
04DTB18	13/07/2020 (2) 23:13:30.00	04DTB18 - 2.47	133	3	104	1	3.667033	0.261601	0.102000	0.004540	0.172460	1555	93	1660	81	6.36	1660	81
04DTB18	10/05/2019 (6) 01:09:04.00	04DTB18 - 18	723	26	568	31	3.937008	0.191890	0.096500	0.011330	0.477480	1459	61	1557	206	6.27	1459	61
04DTB18	13/07/2020 (2) 22:22:44.00	04DTB18 - 2.19	328	4	309	4	3.156566	0.222554	0.115800	0.004216	0.251360	1774	103	1892	65	6.21	1892	65
04DTB18	14/07/2020 (3) 02:05:33.00	04DTB18 - 2.141	433	11	303	14	3.431709	0.245284	0.107500	0.003850	0.242820	1649	98	1757	65	6.15	1757	65
04DTB18	14/07/2020 (3) 02:35:23.00	04DTB18 - 2.158	393	4	123	1	3.264773	0.235835	0.112200	0.003944	0.308270	1723	103	1835	63	6.11	1835	63
04DTB18	14/07/2020 (3) 01:40:10.00	04DTB18 - 2.127	330	5	126	3	5.216484	0.169638	0.080300	0.003406	0.154980	1131	33	1204	82	6.06	1131	33
04DTB18	13/07/2020 (2) 21:57:15.00	04DTB18 - 2.5	278	5	249	5	3.855050	0.270299	0.097700	0.003754	0.374800	1487	88	1580	71	5.89	1487	88
04DTB18	13/07/2020 (2) 23:16:28.00	04DTB18 - 2.49	74	2	74	2	4.625347	0.169525	0.086100	0.005522	0.075457	1262	41	1340	120	5.81	1262	41
04DTB18	10/05/2019 (6) 02:45:47.00	04DTB18 - 58	375	8	404	13	5.241090	0.225686	0.079800	0.009096	0.103140	1126	43	1191	211	5.50	1126	43
04DTB18	13/07/2020 (2) 23:03:07.00	04DTB18 - 2.40	193	3	82	1	4.574565	0.158457	0.086500	0.004330	-0.008450	1274	39	1349	95	5.49	1274	39
04DTB18	14/07/2020 (3) 00:29:52.00	04DTB18 - 2.89	55	1	93	2	4.757374	0.178888	0.084400	0.005688	0.191640	1230	41	1301	126	5.46	1230	41
04DTB18	13/07/2020 (2) 22:33:06.00	04DTB18 - 2.26	215	9	98	7	3.331113	0.112117	0.109400	0.004288	0.246610	1692	49	1789	71	5.38	1789	71
04DTB18	14/07/2020 (3) 02:33:52.00	04DTB18 - 2.157	158	10	74	4	4.074980	0.149582	0.093300	0.004466	0.227010	1415	45	1493	89	5.25	1415	45
04DTB18	14/07/2020 (3) 00:25:23.00	04DTB18 - 2.86	215	2	189	5	4.248088	0.142710	0.090600	0.003612	0.200830	1363	40	1437	75	5.19	1363	40
04DTB18	13/07/2020 (2) 23:19:27.99	04DTB18 - 2.51	512	11	398	10	4.127115	0.137048	0.092300	0.003346	0.293670	1399	41	1473	68	5.03	1399	41
04DTB18	13/07/2020 (2) 22:27:10.00	04DTB18 - 2.22	271	3	95	1	3.343363	0.234538	0.108600	0.004272	0.461640	1687	98	1775	71	4.98	1775	71
04DTB18	14/07/2020 (3) 02:26:28.00	04DTB18 - 2.152	448	9	359	5	4.868549	0.161368	0.082900	0.003258	0.231420	1204	35	1266	76	4.88	1204	35
04DTB18	10/05/2019 (6) 02:15:31.00	04DTB18 - 43	122	4	70	3	3.485535	0.120736	0.104700	0.006794	0.298240	1626	48	1708	116	4.81	1708	116
04DTB18	14/07/2020 (3) 00:09:00.00	04DTB18 - 2.75	178	4	81	3	4.875670	0.180716	0.082600	0.004052	0.116480	1203	39	1259	94	4.47	1203	39
04DTB18	14/07/2020 (3) 00:32:48.00	04DTB18 - 2.91	698	25	217	8	3.299241	0.229260	0.109100	0.003382	0.367310	1707	98	1784	56	4.31	1784	56
04DTB18	14/07/2020 (3) 00:53:53.00	04DTB18 - 2.102	581	14	263	6	4.533092	0.146144	0.086200	0.003224	0.284740	1285	36	1342	71	4.23	1285	36
04DTB18	10/05/2019 (6) 02:57:16.00	04DTB18 - 60	175	6	60	3	4.918839	0.219352	0.082000	0.008440	0.197270	1193	47	1245	190	4.15	1193	47
04DTB18	14/07/2020 (3) 01:22:12.00	04DTB18 - 2.118	305	9	82	3	3.304693	0.229909	0.108500	0.003570	0.296280	1704	98	1774	60	3.91	1774	60
04DTB18	14/07/2020 (3) 02:51:49.00	04DTB18 - 2.166	230	4	120	2	4.627487	0.154649	0.084900	0.003698	0.177470	1261	37	1312	83	3.90	1261	37
04DTB18	10/05/2019 (6) 02:28:46.00	04DTB18 - 49	101	3	16	1	3.546099	0.150143	0.102300	0.007846	0.345060	1601	58	1665	136	3.84	1665	136
04DTB18	14/07/2020 (3) 00:38:44.00	04DTB18 - 2.95	282	6	176	5	5.299417	0.173390	0.078400	0.003668	0.060132	1114	33	1156	91	3.61	1114	33
04DTB18	13/07/2020 (2) 23:09:04.00	04DTB18 - 2.44	370	7	297	6	3.607504	0.254347	0.100700	0.003614	0.175910	1577	93	1636	66	3.61	1636	66
04DTB18	13/07/2020 (2) 22:37:34.00	04DTB18 - 2.29	436	13	295	10	4.430660	0.145542	0.087000	0.003240	0.230170	1312	38	1360	71	3.51	1312	38
04DTB18	10/05/2019 (6) 02:47:38.00	04DTB18 - 59	73	2	93	3	2.024291	0.081463	0.182900	0.013458	0.178190	2588	83	2679	118	3.38	2679	118
04DTB18	14/07/2020 (3) 00:01:26.00	04DTB18 - 2.73	232	5	173	2	3.591954	0.252469	0.100800	0.003916	0.283250	1583	93	1638	71	3.35	1638	71
04DTB18	14/07/2020 (3) 00:37:15.00	04DTB18 - 2.94	247	7	169	5	3.441156	0.246446	0.104300	0.004086	0.231950	1645	98	1701	71	3.33	1701	71
04DTB18	14/07/2020 (3) 03:11:08.00	04DTB18 - 2.179	354	7	345	6	3.718855	0.267995	0.098100	0.003862	0.055784	1535	92	1588	73	3.29	1588	73
04DTB18	14/07/2020 (3) 03:18:36.00	04DTB18 - 2.181	247	7	219	8	3.889537	0.132253	0.094900	0.003898	0.338840	1475	44	1525	76	3.29	1475	44
04DTB18	10/05/2019 (6) 02:38:12.00	04DTB18 - 54	263	11	136	6	4.308488	0.171560	0.088400	0.008668	0.211210	1346	47	1390	178	3.22	1346	47
04DTB18	14/07/2020 (3) 00:55:19.00	04DTB18 - 2.103	584	18	371	7	4.494382	0.156546	0.086000	0.003120	0.157030	1295	40	1337	69	3.16	1295	40
04DTB18	14/07/2020 (3) 01:55:00.00	04DTB18 - 2.137	161	5	88	3	4.703669	0.164872	0.083600	0.004572	0.224010	1243	38	1282	104	3.10	1243	38
04DTB18	10/05/2019 (6) 01:41:14.27	04DTB18 - 32	258	19	94	5	5.096840	0.182468	0.079800	0.005596	0.137630	1155	37	1191	133	3.05	1155	37
04DTB18	13/07/2020 (2) 22:57:11.00	04DTB18 - 2.36	275	7	348	3	4.752852	0.165085	0.083000	0.003560	0.241980	1231	38	1268	82	2.94	1231	38
04DTB18	14/07/2020 (3) 02:22:00.00	04DTB18 - 2.149	276	7	331	11	3.604903	0.254033	0.100000	0.003800	0.289800	1578	93	1623	70	2.77	1623	70
04DTB18	10/05/2019 (6) 02:23:02.00	04DTB18 - 47	85	5	106	7	4.541326	0.158885	0.085100	0.005702	0.187480	1283	39	1317	126	2.58	1283	39
04DTB18	14/07/2020 (3) 00:16:30.00	04DTB18 - 2.80	224	7	183	6	3.847634	0.130248	0.095000	0.004000	0.089795	1489	44	1527	78	2.48	1489	44
04DTB18	13/07/2020 (2) 22:51:15.00	04DTB18 - 2.32	176	6	126	5	3.926188	0.134018	0.093600	0.004572	0.286290	1463	43	1499	90	2.44	1463	43
04DTB18	13/07/2020 (2) 21:51:16.00	04DTB18 - 2.1	357	14	553	23	7.974482	0.267597	0.065200	0.003004	0.245160	762	23	780	95	2.35	762	23
04DTB18	14/07/2020 (3) 00:12:05.00	04DTB18 - 2.77	105	2	83	1	3.495281	0.253161	0.102000	0.004540	0.012871	1622	98	1660	81	2.29	1660	81
04DTB18	10/05/2019 (6) 02:09:50.05	04DTB18 - 40	1085	39	193	7	2.092050	0.094361	0.172000	0.015440	0.278190	2519	91	2576	143	2.25	2576	143
04DTB18	14/07/2020 (3) 02:39:47.00	04DTB18 - 2.161	250	4	763	12	3.028468	0.216487	0.115100	0.004402	0.201820	1839	108	1881	68	2.19	1881	68
04DTB18	13/07/2020 (2) 22:13:48.00	04DTB18 - 2.13	353	9	126	2	2.086811	0.146251	0.172000	0.005440	0.496950	2524	138	2576	53	2.04	2576	53
04DTB18	14/07/2020 (3) 02:24:59.00	04DTB18 - 2.151	110	3	49	1	4.012841	0.144668	0.091800	0.004836	0.117370	1434	45	1462	98	1.92	1434	45
04DTB18	14/07/2020 (3) 00:40:13.00	04DTB18 - 2.96	215	4	169	2	3.581662	0.251229	0.099700	0.003994	0.249240	1587	93	1618	74	1.88	1618	74
04DTB18	14/07/2020 (3) 02:19:02.00	04DTB18 - 2.147	342	10	191	7	4.260758	0.139677	0.088100	0.003662	0.251830	1359	39	1384	79	1.79	1359	39
04DTB18	14/07/2020 (3) 02:11:35.00	04DTB18 - 2.142	129	5	147	4	3.677823	0.262926	0.097600	0.004652	0.197720	1550	93	1578	87	1.74	1578	87
04DTB18	14/07/2020 (3) 02:48:52.00	04DTB18 - 2.164	192	3	179	2	5.022602	0.176132	0.079800	0.003896	0.311310	1170	36	1191	94	1.74	1170	36
04DTB18	14/07/2020 (3) 02:13:06.00	04DTB18 - 2.143	94	1	33	0	3.158560	0.222795	0.110200	0.005404	0.003526	1773	103	1802	87	1.60	1802	87
04DTB18	14/07/2020 (3) 01:14:46.00	04DTB18 - 2.113	126	2	54	1	4.768717	0.170419	0.082100	0.004442	0.462190	1227	39	1247	103	1.59	1227	39
04DTB18	14/07/2020 (3) 01:50:34.00	04DTB18 - 2.134	194	9	154	9	3.588088	0.252003	0.099300	0.004086	0.359550	1585	93	1610	76	1.58	1610	76
04DTB18	13/07/2020 (2) 22:10:50.00	04DTB18 - 2.11	219	5	242	3	3.772161	0.274652	0.095600	0.004012	0.293410	1516	92	1539	78	1.51	1539	78
04DTB18	13/07/2020 (2) 22:28:39.00	04DTB18 - 2.23	336	8	180	4	2.681684	0.190271	0.128300	0.003966	0.253220	2043	117	2074	54	1.50	2074	54
04DTB18	14/07/2020 (3) 02:53:21.00	04DTB18 - 2.167	273	4	256	4	3.582945	0.251384	0.099300	0.004086	0.395320	1587	93	1610	76	1.45	1610	76

Appendix D.2 continued.

Sample ID	Analysis date-time	Spot ID[1]	238U conc.	±2σ INT	232Th conc.	±2σ INT	Isotopic Ratios					Apparent Ages - Calculated in Isoplot R (Ma)				Discord	Perferred age 1500 Ma cutoff	
			ppm		ppm		238U/206Pb	±2σ PROP	207Pb/206Pb	±2σ PROP	rho	238U/206Pb	±2σ PROP	207Pb/206Pb	±2σ PROP	(7/6-6/8)/7/6 *100	Ma	2 σ
04DTB18	14/07/2020 (3) 00:56:48.00	04DTB18 - 2.104	335	7	301	7	4.273504	0.142085	0.087700	0.003354	0.391030	1355	39	1375	73	1.43	1355	39
04DTB18	14/07/2020 (3) 01:05:55.00	04DTB18 - 2.107	323	9	277	8	3.003003	0.213367	0.115000	0.004100	0.405490	1853	108	1879	64	1.39	1879	64
04DTB18	14/07/2020 (3) 01:57:57.00	04DTB18 - 2.139	284	7	192	4	3.475843	0.250739	0.101600	0.003632	0.245250	1630	98	1653	66	1.37	1653	66
04DTB18	13/07/2020 (2) 23:07:35.00	04DTB18 - 2.43	295	8	347	13	4.570384	0.149895	0.084000	0.003280	0.254510	1276	37	1292	75	1.25	1276	37
04DTB18	13/07/2020 (2) 23:28:33.00	04DTB18 - 2.54	391	8	677	14	3.173596	0.224619	0.109300	0.004086	0.178830	1766	103	1787	67	1.19	1787	67
04DTB18	13/07/2020 (2) 23:04:37.00	04DTB18 - 2.41	182	2	76	1	4.235493	0.143910	0.088000	0.004160	0.334680	1366	41	1382	89	1.10	1366	41
04DTB18	10/05/2019 (6) 02:06:06.00	04DTB18 - 38	96	5	85	3	4.789272	0.182947	0.081600	0.007332	0.085653	1222	41	1235	168	1.03	1222	41
04DTB18	13/07/2020 (2) 22:39:03.00	04DTB18 - 2.30	107	4	50	3	3.777862	0.275369	0.095100	0.004702	0.352190	1514	92	1529	91	1.01	1529	91
04DTB18	13/07/2020 (2) 23:10:32.00	04DTB18 - 2.45	440	4	438	3	3.832886	0.267641	0.094100	0.003482	0.453210	1494	88	1509	69	0.99	1494	88
04DTB18	13/07/2020 (2) 22:16:47.00	04DTB18 - 2.15	277	3	147	2	3.965107	0.131185	0.091800	0.003636	0.328780	1450	42	1462	74	0.86	1450	42
04DTB18	14/07/2020 (3) 00:28:21.00	04DTB18 - 2.88	128	1	104	1	5.678592	0.203862	0.074500	0.004490	0.236600	1046	34	1054	118	0.80	1046	34
04DTB18	10/05/2019 (6) 03:06:45.00	04DTB18 - 65	274	19	337	30	3.875969	0.193197	0.093200	0.009564	0.338770	1480	63	1491	184	0.77	1480	63
04DTB18	14/07/2020 (3) 00:50:49.00	04DTB18 - 2.100	211	3	221	1	3.113325	0.217351	0.110600	0.004012	0.219560	1796	103	1809	65	0.71	1809	65
04DTB18	13/07/2020 (2) 22:58:40.00	04DTB18 - 2.37	216	3	130	2	4.222973	0.148660	0.087900	0.003858	0.153270	1370	42	1379	83	0.68	1370	42
04DTB18	14/07/2020 (3) 02:17:35.00	04DTB18 - 2.146	444	12	301	10	4.006410	0.136308	0.091000	0.003520	0.267860	1436	43	1446	73	0.64	1436	43
04DTB18	14/07/2020 (3) 02:32:23.00	04DTB18 - 2.156	451	9	215	4	4.861449	0.158677	0.080700	0.003014	0.278360	1206	35	1213	73	0.61	1206	35
04DTB18	14/07/2020 (3) 01:16:16.00	04DTB18 - 2.114	324	7	159	4	3.998401	0.132726	0.091100	0.003622	0.464980	1439	42	1448	75	0.61	1439	42
04DTB18	14/07/2020 (3) 02:16:04.00	04DTB18 - 2.145	231	3	130	1	5.146680	0.174452	0.078200	0.003864	0.289500	1145	34	1151	96	0.56	1145	34
04DTB18	13/07/2020 (2) 23:37:27.00	04DTB18 - 2.60	90	1	45	1	4.490346	0.160378	0.084500	0.005290	0.184790	1296	41	1303	118	0.54	1296	41
04DTB18	14/07/2020 (3) 02:36:50.00	04DTB18 - 2.159	327	5	173	4	3.992016	0.129243	0.091100	0.003522	0.388310	1441	41	1448	73	0.47	1441	41
04DTB18	10/05/2019 (6) 00:33:05.00	04DTB18 - 3	427	7	421	5	4.553734	0.219641	0.083700	0.010674	0.062781	1280	54	1285	231	0.40	1280	54
04DTB18	14/07/2020 (3) 02:54:48.00	04DTB18 - 2.168	244	3	224	7	3.006615	0.213808	0.113600	0.004172	0.165670	1851	108	1857	66	0.32	1857	66
04DTB18	14/07/2020 (3) 00:18:02.00	04DTB18 - 2.81	381	8	502	10	3.591954	0.252469	0.098100	0.003462	0.212740	1583	93	1588	65	0.26	1588	65
04DTB18	14/07/2020 (3) 00:52:18.00	04DTB18 - 2.101	221	5	240	4	3.920031	0.130647	0.092100	0.003942	0.160660	1465	42	1469	80	0.26	1465	42
04DTB18	10/05/2019 (6) 01:39:09.75	04DTB18 - 31	160	3	84	3	2.021836	0.074774	0.173900	0.009678	0.293190	2591	76	2595	91	0.17	2595	91
04DTB18	13/07/2020 (2) 23:00:11.00	04DTB18 - 2.38	117	1	78	1	3.958828	0.138731	0.091400	0.004528	0.131740	1452	44	1454	92	0.15	1452	44
04DTB18	13/07/2020 (2) 23:20:56.00	04DTB18 - 2.52	257	5	57	1	3.122073	0.105330	0.109600	0.004092	0.170580	1791	51	1792	67	0.04	1792	67
04DTB18	13/07/2020 (2) 22:30:10.00	04DTB18 - 2.24	149	5	112	2	3.926188	0.135559	0.091800	0.004236	0.176980	1463	44	1462	86	-0.02	1463	44
04DTB18	14/07/2020 (3) 01:34:14.00	04DTB18 - 2.123	183	5	85	3	3.915427	0.128899	0.091900	0.004038	0.381950	1466	42	1465	82	-0.12	1466	42
04DTB18	10/05/2019 (6) 01:14:45.00	04DTB18 - 21	343	13	144	7	3.189793	0.123827	0.107400	0.007748	0.070608	1758	58	1755	127	-0.17	1755	127
04DTB18	14/07/2020 (3) 01:32:46.00	04DTB18 - 2.122	315	3	155	2	4.353505	0.143929	0.085700	0.003514	0.279390	1333	39	1331	78	-0.18	1333	39
04DTB18	14/07/2020 (3) 03:21:38.00	04DTB18 - 2.183	244	7	174	5	2.968240	0.209142	0.114300	0.004386	0.236090	1872	108	1868	68	-0.19	1868	68
04DTB18	14/07/2020 (3) 02:30:54.00	04DTB18 - 2.155	298	2	121	1	4.344049	0.145380	0.085800	0.003316	0.145540	1336	39	1333	74	-0.21	1336	39
04DTB18	10/05/2019 (6) 00:34:56.00	04DTB18 - 4	125	2	62	2	3.889537	0.144356	0.092200	0.006544	0.216540	1475	47	1471	130	-0.29	1475	47
04DTB18	13/07/2020 (2) 23:36:00.00	04DTB18 - 2.59	262	7	129	5	3.180662	0.105091	0.107500	0.004250	0.326340	1762	49	1757	71	-0.32	1757	71
04DTB18	13/07/2020 (2) 23:27:00.00	04DTB18 - 2.53	236	6	243	7	3.912363	0.133351	0.091800	0.003636	0.154280	1467	43	1462	74	-0.33	1467	43
04DTB18	13/07/2020 (2) 23:31:31.00	04DTB18 - 2.56	141	3	238	8	3.593245	0.122219	0.097500	0.004550	0.284990	1583	46	1576	86	-0.43	1576	86
04DTB18	14/07/2020 (3) 01:20:43.00	04DTB18 - 2.117	203	2	73	1	5.385030	0.183097	0.075900	0.003718	0.222090	1098	33	1092	96	-0.60	1098	33
04DTB18	14/07/2020 (3) 00:23:56.00	04DTB18 - 2.85	131	1	74	1	3.852080	0.269942	0.092600	0.004552	0.458720	1488	88	1479	91	-0.60	1488	88
04DTB18	14/07/2020 (3) 01:13:18.00	04DTB18 - 2.112	590	6	167	3	3.862495	0.123498	0.092400	0.003248	0.151690	1484	41	1475	66	-0.64	1484	41
04DTB18	14/07/2020 (3) 01:07:22.00	04DTB18 - 2.108	286	4	80	2	5.750431	0.194371	0.073500	0.003270	0.312770	1034	31	1027	88	-0.65	1034	31
04DTB18	13/07/2020 (2) 23:47:51.00	04DTB18 - 2.67	63	1	120	1	1.968892	0.140168	0.177200	0.007644	0.208820	2648	146	2626	71	-0.82	2626	71
04DTB18	13/07/2020 (2) 22:34:35.00	04DTB18 - 2.27	687	8	301	2	4.366812	0.142636	0.085100	0.003002	0.311470	1329	38	1317	68	-0.94	1329	38
04DTB18	13/07/2020 (2) 23:38:55.00	04DTB18 - 2.61	125	3	46	1	3.926188	0.135559	0.091100	0.004422	0.241760	1463	44	1448	91	-1.03	1463	44
04DTB18	14/07/2020 (3) 01:08:50.00	04DTB18 - 2.109	113	2	67	1	1.825817	0.129857	0.195200	0.006504	0.384150	2816	153	2786	54	-1.07	2786	54
04DTB18	14/07/2020 (3) 00:31:19.00	04DTB18 - 2.90	239	5	298	6	5.073567	0.168398	0.078000	0.003760	0.256520	1160	34	1146	94	-1.20	1160	34
04DTB18	13/07/2020 (2) 22:21:14.00	04DTB18 - 2.18	92	1	283	5	4.859086	0.175097	0.079700	0.004794	0.177690	1206	38	1189	115	-1.49	1206	38
04DTB18	10/05/2019 (6) 01:10:59.00	04DTB18 - 19	215	3	98	2	4.098361	0.147474	0.088200	0.006464	0.189440	1408	44	1386	135	-1.55	1408	44
04DTB18	14/07/2020 (3) 01:53:33.00	04DTB18 - 2.136	274	3	195	2	3.086420	0.223670	0.108900	0.004078	0.266970	1809	107	1780	68	-1.62	1780	68
04DTB18	10/05/2019 (6) 02:59:15.00	04DTB18 - 61	175	10	77	5	5.324814	0.217075	0.075900	0.006518	0.270900	1109	40	1092	164	-1.64	1109	40
04DTB18	14/07/2020 (3) 02:29:28.00	04DTB18 - 2.154	201	5	206	6	3.262643	0.235570	0.103900	0.004278	0.109280	1724	103	1694	75	-1.74	1694	75
04DTB18	10/05/2019 (6) 01:46:47.00	04DTB18 - 35	115	4	60	2	6.385696	0.205190	0.069800	0.003796	0.119780	938	27	922	109	-1.76	938	27
04DTB18	14/07/2020 (3) 00:13:32.00	04DTB18 - 2.78	174	7	204	10	3.403676	0.241849	0.100400	0.004308	0.249150	1661	98	1631	78	-1.83	1631	78
04DTB18	14/07/2020 (3) 00:34:17.00	04DTB18 - 2.92	482	20	183	10	5.691520	0.185096	0.073400	0.003068	0.058423	1043	30	1024	83	-1.89	1043	30
04DTB18	10/05/2019 (6) 01:20:20.00	04DTB18 - 24	348	19	177	7	3.533569	0.144339	0.097500	0.007550	0.260210	1607	56	1576	139	-1.94	1576	139
04DTB18	10/05/2019 (6) 00:36:50.00	04DTB18 - 5	260	6	268	9	3.969829	0.132979	0.089800	0.005896	0.153990	1448	42	1420	121	-1.96	1448	42
04DTB18	10/05/2019 (6) 02:04:16.00	04DTB18 - 37	314	16	110	2	3.988831	0.168877	0.089300	0.008386	0.087058	1442	53	1410	171	-2.30	1442	53
04DTB18	14/07/2020 (3) 00:49:21.00	04DTB18 - 2.99	43	1	57	2	3.084516	0.223432	0.108200	0.005864	0.261900	1810	107	1769	97	-2.36	1769	97
04DTB18	10/05/2019 (6) 00:38:42.00	04DTB18 - 6	382	21	161	6	4.975124	0.235638	0.078200	0.009164	0.154720	1181	49	1151	217	-2.57	1181	49
04DTB18	10/05/2019 (6) 02:11:44.96	04DTB18 - 41	150	8	63	3	4.887586	0.286471	0.078900	0.010278	-0.309020	1200	61	1169	239	-2.65	1200	61
04DTB18	10/05/2019 (6) 01:16:35.00	04DTB18 - 22	219	9	114	5	4.768717	0.168144	0.079900	0.006698	0.083228	1227	38	1194	158	-2.82	1227	38
04DTB18	14/07/2020 (3) 01:56:28.00	04DTB18 - 2.138	171	4	79	2	4.692633	0.159915	0.080600	0.004112	0.286450	1245	37	1211	98	-2.85	1245	37
04DTB18	14/07/2020 (3) 00:47:54.00	04DTB18 - 2.98	118	1	119	1	4.952947	0.182467	0.078200	0.004664	0.230880	1186	39	1151	115	-2.99	1186	39
04DTB18	10/05/2019 (6) 02:21:05.27	04DTB18 - 46	311	5	181	5	4.476276	0.231789	0.082700	0.011154	0.218340	1300	58	1261	244	-3.08	1300	58
04DTB18	10/05/2019 (6) 01:27:51.00	04DTB18 - 28	107	6	157	11	2.959455	0.112615	0.111300	0.007226	0.260060	1877	60	1820	114	-3.12	1820	114
04DTB18	10/05/2019 (6) 01:07:14.00	04DTB18 - 17	207	11	201	9	3.568879	0.147799	0.095700	0.007414	0.291980	1592	56	1541	140	-3.34	1541	140
04DTB18	13/07/2020 (2) 22:24:15.00	04DTB18 - 2.20	301	14	53	2	4.618938	0.158516	0.080900	0.003418	0.379290	1263	38	1218	82	-3.71	1263	38
04DTB18	13/07/2020 (2) 22:31:36.00	04DTB18 - 2.25	164	1	98	4	4.235493	0.149292	0.085100	0.004102	0.251330	1366	42	1317	92	-3.76	1366	42
04DTB18	10/05/2019 (6) 01:05:17.67	04DTB18 - 16	258	6	156	4	3.352330	0.143466	0.099600	0.006092	-0.081039	1683	61	1616	111	-4.15	1616	111
04DTB18	10/05/2019 (6) 00:44:23.00	04DTB18 - 9	220	12	154	10	4.184100	0.151958	0.085300	0.006006	0.304560	1382	44	1322	131	-4.54	1382	44
04DTB18	13/07/2020 (2) 23:44:51.00	04DTB18 - 2.65	154	4	155	4	4.580852	0.165062	0.080800	0.004416	0.441330	1273	40	1216	105	-4.70	1273	40
04DTB18	13/07/2020 (2) 23:34:29.00	04DTB18 - 2.58	284	5	245	5	4.612546	0.151823	0.080400	0.003208	0.353780	1265	37	1206	78	-4.90	1265	37
04DTB18	13/07/2020 (2) 23:41:56.00	04DTB18 - 2.63	135	4	59	2	4.995005	0.177245	0.076900	0.004338	0.173840	1176	37	1118	110	-5.25	1176	37
04DTB18	14/07/2020 (3) 03:20:09.00	04DTB18 - 2.182	112	1	122	1	3.746722	0.271465	0.091100	0.004322	0.300620	1525	92	1448	89	-5.33	1448	89
04DTB18	14/07/2020 (3) 01:46:07.00	04DTB18 - 2.131	131	5	148	6	3.610108	0.125637	0.093300	0.004366	0.206490	1576	47	1493	87	-5.57	1493	87
04DTB18	14/07/2020 (3) 00:35:49.00	04DTB18 - 2.93	201	10	101	5	3.868472	0.126754	0.088800	0.003776	0.392360	1482	42	1399	80	-5.94	1482	42
04DTB18	13/07/2020 (2) 23:33:00.00	04DTB18 - 2.57	169	5	78	2	5.482456	0.196815	0.073200	0.003964	0.344070	1080	35	1019	107	-6.03	1080	35
04DTB18	14/07/2020 (3) 02:38:18.00	04DTB18 - 2.160	265	6	88	2	5.299417	0.173390	0.074300	0.003286	0.342390	1114	33	1049	88	-6.26	1114	33
04DTB18	10/05/2019 (6) 01:03:29.00	04DTB18 - 15	184	12	174	15	3.259452	0.123621	0.099900	0.007898	0.364360	1725	56	1621	141	-6.38	1621	141
04DTB18	10/05/2019 (6) 02:02:14.00	04DTB18 - 36	146	8	82	6	3.856537	0.193139	0.088600	0.010972	0.490050	1486	64	1395	221	-6.57	1486	64
04DTB18	10/05/2019 (6) 00:59:44.00	04DTB18 - 13	116	2	85	2	4.327131	0.189525	0.082300	0.008946	0.118300	1340	51	1252	200	-7.07	1340	51
04DTB18	14/07/2020 (3) 00:46:18.00	04DTB18 - 2.97	170	3	101	3	4.761905	0.167800	0.078000	0.003660	0.181420	1229	38	1146	91	-7.23	1229	38
04DTB18	14/07/2020 (3) 00:20:56.00	04DTB18 - 2.83	233	8	78	3	4.712535	0.158654	0.078300	0.003466	0.250920	1241	37	1154	86	-7.54	1241	37
04DTB18	10/05/2019 (6) 01:01:34.00	04DTB18 - 14	63	3	59	3	3.125000	0.126953	0.102200	0.008144	0.083242	1790	61	1664	141	-7.58	1664	141
04DTB18	10/05/2019 (6) 00:46:12.99	04DTB18 - 10	177	3	86	3	2.940312	0.110679	0.106900	0.008138	0.213850	1887	60	1746	134	-8.06	1746	134
04DTB18	10/05/2019 (6) 00:29:18.00	04DTB18 - 1	432	15	203	8	3.787879	0.181933	0.088600	0.009772	0.211740	1510	62	1395	199	-8.29	1395	199
04DTB18	10/05/2019 (6) 01:29:47.00	04DTB18 - 29	101	4	43	2	3.806624	0.183361	0.088200	0.009464	0.007329	1504	62	1386	194	-8.48	1386	194
04DTB18	10/05/2019 (6) 02:26:52.00	04DTB18 - 48	898	63	162	9	4.782401	0.207718	0.076900	0.007038	0.158070	1224	47	1118	173	-9.51	1224	47
04DTB18	13/07/2020 (2) 23:12:03.00	04DTB18 - 2.46	74	2	52	2	5.561735	0.210220	0.071300	0.004926	0.282440	1066	36	965	136	-10.44	1066	36
04DTB18	10/05/2019 (6) 01:12:48.00	04DTB18 - 20	127	7	93	7	5.503577	0.213055	0.070900	0.007418	0.352420	1076	37	954	201	-12.86	1076	37
04DTB18	10/05/2019 (6) 01:26:02.00	04DTB18 - 27	415	15	421	13	5.181347	0.216382	0.071900	0.008038	-0.069527	1138	42	982	213	-15.82	1138	42
04DTB18	10/05/2019 (6) 01:31:38.00	04DTB18 - 30	268	10	228	7	5.055612	0.190569	0.072600	0.006352	0.249250	1163	39	1002	169	-16.13	1163	39
04DTB18	10/05/2019 (6) 01:18:29.00	04DTB18 - 23	96	4	58	3	5.327651	0.208735	0.070900	0.006618	0.356060	1109	39	954	181	-16.29	1109	39
04DTB18	10/05/2019 (6) 03:01:09.00	04DTB18 - 62	300	28	394	26	3.516174	0.143268	0.088200	0.008064	0.303390	1614	56	1386	167	-16.41	1386	167
04DTB18	10/05/2019 (6) 00:57:39.93	04DTB18 - 12	114	3	116	4	5.076142	0.253549	0.066300	0.008326	0.300960	1159	51	815	243	-42.23	1159	51

Appendix D5.2 continued.

Sample ID	Analysis date-time	Spot ID[1]	238U conc.	±2σ INT	232Th conc.	±2σ INT	Isotopic Ratios					Apparent Ages - Calculated in Isoplot R (Ma)				Discord	Perferred age 1500 Ma cutoff	
			ppm		ppm		238U/206Pb	±2σ PROP	207Pb/206Pb	±2σ PROP	rho	238U/206Pb	±2σ PROP	207Pb/206Pb	±2σ PROP	(7/6-6/8)/7/6 *100	Ma	2σ
03DTB19	2020-07-30 17:38:25.000	03DTB19q - 89 - 1.d	72	2	34	1	6.689858	0.270765	0.083013	0.006666	0.256375	898	34	1269	157	29.21	898	34
03DTB19	2020-07-30 17:45:11.000	03DTB19q - 14 - 1.d	235	20	117	8	5.924952	0.377252	0.081451	0.005155	0.004661	1005	59	1232	124	18.36	1005	59
03DTB19	2020-07-30 16:37:58.000	03DTB19q - 86 - 1.d	68	1	844	11	7.997036	0.303971	0.067944	0.006388	0.222079	760	27	866	195	12.28	760	27
03DTB19	2020-07-30 16:34:33.000	03DTB19q - 76 - 1.d	103	3	59	2	7.956399	0.263150	0.067552	0.005367	0.206280	763	24	854	165	10.62	763	24
03DTB19	2020-07-30 17:43:33.000	03DTB19q - 16 - 1.d	237	5	173	4	7.948072	0.246154	0.066868	0.004455	0.184724	764	22	833	139	8.26	764	22
03DTB19	2020-07-30 17:41:48.000	03DTB19q - 17 - 1.d	117	3	69	2	5.117896	0.162498	0.079613	0.005534	0.219639	1151	34	1187	137	3.03	1151	34
03DTB19	2020-07-30 17:40:08.000	03DTB19q - 8 - 1.d	13	0	1916	34	7.931832	0.452856	0.064000	0.011563	0.130006	765	41	741	382	-3.29	765	41
03DTB19	2020-07-30 16:36:19.000	03DTB19q - 86b - 1.d	65	1	1200	27	7.763663	0.284781	0.063708	0.005838	0.266352	781	27	731	194	-6.85	781	27
03DTB18	09/05/2019 (5) 22:58:05.00	03DTB18 - 64	386	16	252	8	3.783579	0.168722	0.168000	0.020360	-0.704310	1512	58	2537	191	40.41	2537	191
03DTB18	09/05/2019 (5) 23:13:09.75	03DTB18 - 72	28	1	26	1	5.847953	0.493143	0.102000	0.024040	0.335610	1018	74	1660	383	38.70	1018	74
03DTB18	09/05/2019 (5) 20:58:17.00	03DTB18 - 19	38	2	34	2	5.379236	0.356436	0.088000	0.021760	0.454780	1099	63	1382	413	20.47	1099	63
03DTB18	09/05/2019 (5) 22:40:42.00	03DTB18 - 62	57	3	50	3	5.889282	0.343229	0.083000	0.014660	0.001177	1011	52	1268	312	20.27	1011	52
03DTB18	09/05/2019 (5) 23:11:17.00	03DTB18 - 71	67	3	32	2	5.260389	0.321047	0.089000	0.015780	0.096044	1122	59	1403	307	20.04	1122	59
03DTB18	09/05/2019 (5) 23:20:43.00	03DTB18 - 76	43	3	48	4	5.714286	0.440816	0.084000	0.016680	0.254250	1040	69	1292	345	19.54	1040	69
03DTB18	09/05/2019 (5) 20:35:24.00	03DTB18 - 11	288	8	157	6	3.680530	0.145406	0.113000	0.007560	0.205480	1549	53	1847	117	16.13	1847	117
03DTB18	10/05/2019 (6) 00:12:01.00	03DTB18 - 95	80	3	42	2	4.911591	0.269510	0.087000	0.012740	0.226560	1195	57	1360	259	12.16	1195	57
03DTB18	09/05/2019 (5) 20:18:29.36	03DTB18 - 2	88	1	42	1	5.230126	0.290611	0.083000	0.012660	0.197130	1128	55	1268	273	11.05	1128	55
03DTB18	09/05/2019 (5) 23:07:31.00	03DTB18 - 69	64	3	49	2	4.446421	0.251048	0.089000	0.014780	0.321180	1308	64	1403	290	6.79	1308	64
03DTB18	09/05/2019 (5) 21:32:37.00	03DTB18 - 33	65	3	76	3	4.405286	0.264705	0.089000	0.011780	0.215410	1319	68	1403	236	6.00	1319	68
03DTB18	09/05/2019 (5) 23:16:57.00	03DTB18 - 74	87	2	123	4	5.917160	0.352929	0.075000	0.012500	0.247020	1007	53	1068	304	5.75	1007	53
03DTB18	09/05/2019 (5) 20:39:07.01	03DTB18 - 13	36	2	29	2	5.390836	0.380991	0.078000	0.018560	0.219300	1097	67	1146	413	4.28	1097	67
03DTB18	09/05/2019 (5) 21:49:41.00	03DTB18 - 39	212	8	70	3	4.374453	0.169773	0.088200	0.006764	-0.052460	1327	45	1386	141	4.24	1327	45
03DTB18	09/05/2019 (5) 22:05:02.00	03DTB18 - 43	167	7	117	5	3.325574	0.128444	0.108000	0.009960	0.340660	1695	56	1765	160	3.98	1765	160
03DTB18	09/05/2019 (5) 20:16:35.00	03DTB18 - 1	102	5	91	5	3.322259	0.166886	0.107900	0.011058	0.508560	1696	72	1763	177	3.81	1763	177
03DTB18	09/05/2019 (5) 22:31:21.00	03DTB18 - 57	95	7	91	6	5.112474	0.264301	0.080000	0.011600	0.094949	1152	52	1196	263	3.71	1152	52
03DTB18	10/05/2019 (6) 00:02:40.00	03DTB18 - 90	125	6	35	2	2.958580	0.131823	0.118500	0.009970	0.259300	1877	70	1933	144	2.89	1933	144
03DTB18	09/05/2019 (5) 21:17:19.66	03DTB18 - 28	311	41	208	30	2.111932	0.076137	0.169200	0.010084	0.214720	2499	72	2549	97	1.97	2549	97
03DTB18	09/05/2019 (5) 22:25:40.00	03DTB18 - 54	350	7	174	6	5.414185	0.222606	0.076600	0.005932	0.362030	1093	40	1110	148	1.56	1093	40
03DTB18	09/05/2019 (5) 22:42:37.00	03DTB18 - 63	268	10	114	4	4.694836	0.175450	0.082700	0.006554	0.276620	1245	41	1261	148	1.31	1245	41
03DTB18	09/05/2019 (5) 23:05:42.00	03DTB18 - 68	329	12	124	5	3.162555	0.107259	0.108600	0.007072	0.387580	1771	51	1775	115	0.23	1775	115
03DTB18	09/05/2019 (5) 21:11:39.43	03DTB18 - 25	41	2	23	2	3.194888	0.176178	0.107000	0.014140	0.173050	1756	81	1748	225	-0.43	1748	225
03DTB18	09/05/2019 (5) 21:07:52.00	03DTB18 - 23	121	5	94	4	4.757374	0.228680	0.081000	0.010220	0.196240	1230	52	1221	230	-0.73	1230	52
03DTB18	10/05/2019 (6) 00:00:45.00	03DTB18 - 89	365	9	192	3	5.359057	0.201955	0.076000	0.006820	0.130270	1103	37	1094	171	-0.80	1103	37
03DTB18	09/05/2019 (5) 21:04:07.00	03DTB18 - 21	83	4	50	3	2.079002	0.097769	0.165400	0.012608	0.425160	2532	95	2511	123	-0.82	2511	123
03DTB18	09/05/2019 (5) 21:47:46.00	03DTB18 - 38	165	16	75	8	4.847310	0.228526	0.080100	0.009102	0.373230	1209	50	1199	210	-0.88	1209	50
03DTB18	09/05/2019 (5) 22:18:09.00	03DTB18 - 50	131	3	98	4	4.559964	0.211800	0.082800	0.008556	0.412740	1278	52	1264	190	-1.16	1278	52
03DTB18	09/05/2019 (5) 23:18:47.19	03DTB18 - 75	58	2	35	1	1.600000	0.072960	0.236000	0.016720	0.393750	3130	109	3093	109	-1.21	3093	109
03DTB18	09/05/2019 (5) 23:30:05.00	03DTB18 - 81	667	39	120	8	5.385030	0.177297	0.075400	0.005108	0.348250	1098	32	1078	131	-1.83	1098	32
03DTB18	09/05/2019 (5) 20:31:38.00	03DTB18 - 9	150	7	56	3	2.162162	0.083915	0.154100	0.009882	0.156860	2451	77	2391	106	-2.48	2391	106
03DTB18	09/05/2019 (5) 23:49:09.00	03DTB18 - 87	498	14	105	4	2.086376	0.063057	0.160400	0.007008	0.102030	2524	62	2459	73	-2.65	2459	73
03DTB18	09/05/2019 (5) 22:21:55.00	03DTB18 - 52	102	4	67	4	4.201681	0.218205	0.086100	0.010322	0.390440	1376	61	1340	216	-2.74	1376	61
03DTB18	09/05/2019 (5) 22:12:33.00	03DTB18 - 47	281	9	158	5	3.935458	0.140660	0.089800	0.007196	0.273110	1460	45	1420	147	-2.76	1460	45
03DTB18	10/05/2019 (6) 00:19:33.00	03DTB18 - 99	184	10	72	5	3.880481	0.160429	0.090600	0.009112	0.342370	1478	53	1437	181	-2.83	1478	53
03DTB18	09/05/2019 (5) 20:24:07.00	03DTB18 - 5	72	3	31	1	4.601933	0.229694	0.081000	0.012620	0.106200	1268	55	1221	279	-3.82	1268	55
03DTB18	09/05/2019 (5) 21:40:11.50	03DTB18 - 34	49	3	28	2	1.897533	0.081158	0.175000	0.014500	0.150930	2729	92	2605	133	-4.74	2605	133
03DTB18	09/05/2019 (5) 23:43:24.00	03DTB18 - 85	131	6	54	3	3.907776	0.171307	0.088800	0.008976	0.557140	1469	55	1399	183	-4.99	1469	55
03DTB18	09/05/2019 (5) 22:33:12.00	03DTB18 - 58	296	12	122	5	3.087373	0.113220	0.105100	0.006302	0.223380	1809	56	1715	107	-5.45	1715	107
03DTB18	09/05/2019 (5) 22:27:35.00	03DTB18 - 55	131	7	140	9	3.219575	0.131768	0.101600	0.009432	0.157360	1744	60	1653	164	-5.51	1653	164
03DTB18	09/05/2019 (5) 21:15:24.00	03DTB18 - 27	91	3	121	5	4.125413	0.210151	0.085500	0.010210	0.360680	1399	61	1326	216	-5.52	1399	61
03DTB18	09/05/2019 (5) 22:23:50.00	03DTB18 - 53	206	5	201	6	5.017561	0.206090	0.076600	0.007132	0.290590	1172	42	1110	176	-5.56	1172	42
03DTB18	09/05/2019 (5) 22:06:52.00	03DTB18 - 44	215	8	124	5	4.987531	0.204228	0.076800	0.007436	0.289950	1178	42	1115	183	-5.64	1178	42
03DTB18	09/05/2019 (5) 23:26:19.00	03DTB18 - 79	114	4	92	3	4.020909	0.190359	0.086500	0.009530	0.179620	1432	58	1349	200	-6.18	1432	58
03DTB18	09/05/2019 (5) 21:19:10.00	03DTB18 - 29	208	6	142	4	3.088326	0.113270	0.104300	0.007186	0.540770	1808	56	1701	123	-6.30	1701	123
03DTB18	09/05/2019 (5) 21:44:01.00	03DTB18 - 36	238	6	135	3	3.016591	0.112201	0.106300	0.007726	0.270070	1846	58	1736	128	-6.31	1736	128
03DTB18	09/05/2019 (5) 20:33:33.00	03DTB18 - 10	194	9	200	12	5.068424	0.227244	0.075900	0.008318	0.061512	1161	46	1092	206	-6.35	1161	46
03DTB18	10/05/2019 (6) 00:13:56.00	03DTB18 - 96	366	11	346	11	4.476276	0.157651	0.080900	0.006718	0.260720	1300	40	1218	156	-6.71	1300	40
03DTB18	09/05/2019 (5) 21:42:11.00	03DTB18 - 35	75	4	32	2	3.944773	0.201829	0.087000	0.012740	0.303770	1457	64	1360	259	-7.10	1457	64
03DTB18	09/05/2019 (5) 23:28:14.00	03DTB18 - 80	227	7	170	6	5.467469	0.249847	0.072900	0.007358	0.263670	1083	44	1010	193	-7.18	1083	44
03DTB18	09/05/2019 (5) 20:52:33.00	03DTB18 - 16	64	3	74	3	5.288207	0.290334	0.074000	0.011480	0.036788	1117	54	1041	285	-7.25	1117	54
03DTB18	09/05/2019 (5) 21:22:55.00	03DTB18 - 31	109	4	165	5	3.408316	0.149483	0.095500	0.010010	0.251750	1659	62	1537	186	-7.90	1537	186
03DTB18	09/05/2019 (5) 23:15:02.00	03DTB18 - 73	50	5	93	11	4.844961	0.319899	0.077000	0.016540	0.201420	1210	69	1120	379	-8.00	1210	69
03DTB18	10/05/2019 (6) 00:27:18.00	03DTB18 - 100	156	3	129	6	4.739336	0.216078	0.077600	0.008952	0.243340	1234	49	1136	215	-8.65	1234	49
03DTB18	09/05/2019 (5) 20:41:04.00	03DTB18 - 14	72	3	26	1	5.170631	0.266499	0.074300	0.010686	0.227540	1140	51	1049	266	-8.66	1140	51
03DTB18	09/05/2019 (5) 23:00:01.00	03DTB18 - 65	93	4	35	2	1.949318	0.080785	0.159800	0.011796	0.390420	2669	88	2453	120	-8.83	2453	120
03DTB18	09/05/2019 (5) 23:39:36.00	03DTB18 - 83	403	19	343	16	3.958828	0.135597	0.085800	0.005916	0.102530	1452	43	1333	129	-8.93	1452	43
03DTB18	09/05/2019 (5) 22:20:04.00	03DTB18 - 51	257	5	188	4	3.958828	0.145000	0.085700	0.006814	0.139950	1452	46	1331	147	-9.12	1452	46
03DTB18	09/05/2019 (5) 20:26:02.00	03DTB18 - 6	507	9	288	5	6.079027	0.213967	0.069000	0.005880	0.244890	982	31	898	167	-9.35	982	31
03DTB18	09/05/2019 (5) 21:09:43.00	03DTB18 - 24	527	17	500	9	4.604052	0.157793	0.078500	0.005270	0.286590	1267	38	1159	129	-9.35	1267	38
03DTB18	09/05/2019 (5) 23:03:46.00	03DTB18 - 67	208	8	1	0	5.420054	0.231784	0.072400	0.007048	0.072746	1092	41	996	187	-9.56	1092	41
03DTB18	09/05/2019 (5) 22:10:38.00	03DTB18 - 46	109	3	67	3	5.824112	0.303044	0.070100	0.010802	0.150830	1022	47	930	289	-9.84	1022	47
03DTB18	09/05/2019 (5) 21:45:56.00	03DTB18 - 37	163	6	64	3	3.835827	0.153227	0.087000	0.007940	0.317470	1493	51	1360	167	-9.84	1493	51
03DTB18	09/05/2019 (5) 20:29:48.00	03DTB18 - 8	391	15	126	5	4.436557	0.157622	0.079800	0.005796	0.177250	1310	41	1191	138	-10.00	1310	41
03DTB18	09/05/2019 (5) 21:05:58.00	03DTB18 - 22	230	14	114	7	4.198153	0.161511	0.082300	0.006546	-0.009508	1377	46	1252	149	-10.03	1377	46
03DTB18	09/05/2019 (5) 22:01:14.53	03DTB18 - 41	21	1	25	1	3.039514	0.208609	0.102000	0.019040	0.187330	1834	103	1660	312	-10.45	1660	312
03DTB18	09/05/2019 (5) 22:08:47.00	03DTB18 - 45	74	3	31	2	4.291845	0.209251	0.081000	0.012620	0.150610	1350	57	1221	279	-10.58	1350	57
03DTB18	10/05/2019 (6) 00:04:31.00	03DTB18 - 91	138	8	29	2	5.827506	0.299933	0.069800	0.009296	0.237650	1021	46	922	253	-10.73	1021	46
03DTB18	10/05/2019 (6) 00:06:24.01	03DTB18 - 92	46	1	52	2	4.710316	0.293890	0.077000	0.013540	0.111870	1241	67	1120	317	-10.81	1241	67
03DTB18	09/05/2019 (5) 21:30:39.00	03DTB18 - 32	236	20	73	6	4.159734	0.169712	0.082300	0.006946	0.452800	1389	49	1252	158	-10.94	1389	49
03DTB18	09/05/2019 (5) 23:31:59.00	03DTB18 - 82	178	7	198	11	3.930818	0.168234	0.085100	0.008002	0.322760	1461	54	1317	173	-10.95	1461	54
03DTB18	09/05/2019 (5) 21:02:07.00	03DTB18 - 20	178	9	123	6	3.049710	0.121449	0.101000	0.007920	0.132140	1828	61	1642	140	-11.36	1642	140
03DTB18	09/05/2019 (5) 22:29:26.00	03DTB18 - 56	258	10	126	5	5.027652	0.189024	0.074300	0.007086	0.253230	1169	39	1049	182	-11.51	1169	39
03DTB18	09/05/2019 (5) 23:58:47.00	03DTB18 - 88	307	13	1	0	5.546312	0.212439	0.071000	0.006320	0.300350	1069	36	957	173	-11.72	1069	36
03DTB18	09/05/2019 (5) 21:21:00.00	03DTB18 - 30	272	10	105	4	5.636979	0.230309	0.070400	0.007108	0.359440	1053	38	939	195	-12.11	1053	38
03DTB18	09/05/2019 (5) 23:22:34.00	03DTB18 - 77	341	15	115	3	4.972650	0.188471	0.074400	0.006388	0.153110	1181	40	1051	165	-12.35	1181	40
03DTB18	09/05/2019 (5) 22:35:07.00	03DTB18 - 59	102	2	47	2	3.968254	0.176997	0.083700	0.009374	0.022113	1449	56	1285	205	-12.77	1449	56
03DTB18	10/05/2019 (6) 00:17:42.00	03DTB18 - 98	191	10	116	7	5.617978	0.260699	0.070300	0.007506	0.364170	1056	43	936	206	-12.80	1056	43
03DTB18	10/05/2019 (6) 00:15:47.00	03DTB18 - 97	247	12	138	7	4.960317	0.200086	0.074300	0.006886	0.172370	1184	42	1049	177	-12.89	1184	42
03DTB18	09/05/2019 (5) 20:56:25.0(	03DTB18 - 18	297	19	49	3	3.371544	0.123131	0.092800	0.006556	0.354120	1674	52	1483	129	-12.91	1483	129
03DTB18	09/05/2019 (5) 22:03:06.00	03DTB18 - 42	227	6	89	2	4.716981	0.192239	0.075800	0.007016	0.267000	1240	44	1089	176	-13.83	1240	44
03DTB18	10/05/2019 (6) 00:10:11.00	03DTB18 - 94	260	14	81	6	3.906250	0.136108	0.083700	0.006474	-0.125200	1469	44	1285	145	-14.37	1469	44
03DTB18	09/05/2019 (5) 23:24:29.00	03DTB18 - 78	208	12	139	10	5.012531	0.215828	0.073400	0.007368	0.229390	1173	44	1024	192	-14.50	1173	44
03DTB18	09/05/2019 (5) 22:38:52.00	03DTB18 - 61	230	13	68	4	5.277045	0.214145	0.071400	0.006428	0.183080	1119	40	968	174	-15.57	1119	40
03DTB18	09/05/2019 (5) 23:41:29.00	03DTB18 - 84	165	6	307	11	4.766444	0.213468	0.074800	0.007396	0.209850	1228	48	1062	188	-15.59	1228	48
03DTB18	09/05/2019 (5) 20:27:53.00	03DTB18 - 7	197	6	58	2	5.213764	0.207572	0.071700	0.007134	-0.041129	1131	40	977	191	-15.83	1131	40
03DTB18	09/05/2019 (5) 23:01:55.00	03DTB18 - 66	217	9	145	6	3.846154	0.146450	0.083600	0.007172	0.120850	1490	49	1282	159	-16.17	1490	49
03DTB18	09/05/2019 (5) 23:47:14.00	03DTB18 - 86	112	5	57	3	4.500450	0.215584	0.076600	0.009932	0.163610	1294	54	1110	240	-16.53	1294	54
03DTB18	09/05/2019 (5) 22:16:18.00	03DTB18 - 49	230	13	142	8	5.327651	0.220088	0.070800	0.006716	0.129270	1109	41	951	184	-16.64	1109	41
03DTB18	09/05/2019 (5) 20:22:17.00	03DTB18 - 4	141	15	43	6	3.961965	0.160865	0.081600	0.008932	0.194440	1451	51	1235	202	-17.46	1451	51
03DTB18	09/05/2019 (5) 22:36:57.00	03DTB18 - 60	151	7	75	4	3.952569	0.172788	0.081500	0.007630	0.194390	1454	55	1233	174	-17.95	1454	55
03DTB18	09/05/2019 (5) 20:37:19.00	03DTB18 - 12	90	5	120	8	4.606172	0.219424	0.075200	0.011104	0.165750	1267	52	1073	272	-18.03	1267	52
03DTB18	09/05/2019 (5) 20:20:22.00	03DTB18 - 3	114	5	64	3	4.967710	0.222745	0.071800	0.007936	-0.089709	1182	47	979	211	-20.72	1182	47
03DTB18	09/05/2019 (5) 22:14:23.00	03DTB18 - 48	645	28	40	2	5.344735	0.181167	0.069400	0.004988	0.392700	1106	33	910	142	-21.54	1106	33
03DTB18	09/05/2019 (5) 21:59:11.84	03DTB18 - 40	134	9	122	8	7.692308	0.414201	0.060400	0.008808	0.225810	788	38	617	288	-27.70	788	38
03DTB18	09/05/2019 (5) 20:42:55.00	03DTB18 - 15	323	13	116	4	5.470460	0.214150	0.067200	0.005744	0.188700	1082	38	843	169	-28.38	1082	38
03DTB18	09/05/2019 (5) 20:54:30.00	03DTB18 - 17	115	5	36	2	5.279831	0.250555	0.066000	0.009120	0.092248	1118	47	805	267	-38.89	1118	47
03DTB18	10/05/2019 (6) 00:08:16.00	03DTB18 - 93	58	1	25	2	5.068424	0.317155	0.066000	0.014320	0.267820	1161	63	805	400	-44.20	1161	63
03DTB18	09/05/2019 (5) 23:09:23.84	03DTB18 - 70	70	11	39	2	5.678592	0.368318	0.062000	0.014240	0.217400	1046	59	673	428	-55.36	1046	59

Appendix D5.3: Lu/Hf Results

Sample ID	Analysis date-time	Spot ID	Discord (7/6-6/8)/7/6 *100	Preferred age 1500 Ma cutoff Ma	2σ	error %	Lu-Hf Isotopic Ratios from Iolite 176Hf/177Hf (0.282785 / 0.283250)	t2σ INT	(2% External ±)	176Lu/177Hf (0.03360 Bouvier et al., 2008 EPSL-273)	t2σ INT	176Yb/177Hf (0.03840 Griffin et al., 2002, Lithos-237)	t2σ INT	Hfi	εHf Calculations εHf (Lu decay)	t2σ	TDM(Ga) (0.02 Scherer et al., 2001, Science-293)	TDMCrustal	HfCHUR(t)	HfDM(t)	Notes
[illegible]																					
BH1	03/12/2018 (2) 17:27:38.00	BH1 - 81	-10.21	1191	41	3.45%	0.282172	0.000031	0.00564	0.000793	0.000021	0.0377	0.0011	0.2821542	4.40	1.09	1.52	1.73	0.282030	0.282388	discordant, not plotted
05DTB18	10/05/2019 (6) 07:28:22.00	05DTB18 - 106	-10.14	1433	51	3.57%	0.28229	0.00012	0.00565	0.00109	0.00004	0.04170	0.00190	0.2822605	13.29	1.09	1.52	1.32	0.281886	0.282211	discordant, not plotted
03DTB18	09/05/2019 (5) 21:05:58.00	03DTB18 - 22	-10.03	1377	46	3.35%	0.28196	0.00003	0.00564	0.00095	0.00000	0.03736	0.00042	0.2819302	0.32	1.16	1.82	2.11	0.281921	0.282252	discordant, not plotted
05DTB18	10/05/2019 (6) 07:13:21.00	05DTB18 - 98	-10.01	1090	38	3.46%	0.28223	0.00006	0.00565	0.00143	0.00009	0.05380	0.00340	0.2822026	3.52	1.16	1.82	1.68	0.282103	0.282462	discordant, not plotted
03DTB18	09/05/2019 (5) 20:29:48.00	03DTB18 - 8	-10.00	1310	41	3.11%	0.28226	0.00004	0.00565	0.00218	0.00002	0.09084	0.00087	0.2822090	8.70	1.30	1.44	1.52	0.281964	0.282301	discordant, not plotted
03DTB18	09/05/2019 (5) 21:45:56.00	03DTB18 - 37	-9.84	1493	51	3.44%	0.28188	0.00004	0.00564	0.00062	0.00000	0.02530	0.00110	0.2818584	0.39	1.40	1.92	2.19	0.281847	0.282166	
03DTB18	09/05/2019 (5) 22:10:38.00	03DTB18 - 46	-9.84	1022	47	4.59%	0.28231	0.00004	0.00565	0.00086	0.00001	0.03102	0.00012	0.2822955	5.28	1.54	1.32	1.52	0.282146	0.282512	
BH1	03/12/2018 (2) 14:47:52.00	BH1 - 24	-9.82	1063	36	3.41%	0.282296	0.000023	0.00565	0.0009236	0.000008	0.05052	0.00025	0.2822775	5.86	0.81	1.35	1.53	0.282112	0.282482	
BH1	03/12/2018 (2) 13:52:08.00	BH1 - 2	-9.81	1319	65	4.90%	0.282259	0.000035	0.00565	0.001886	0.000031	0.1032	0.002	0.2822120	9.35	1.23	1.44	1.51	0.281948	0.282295	
05DTB18	10/05/2019 (6) 07:39:47.00	05DTB18 - 109	-9.64	1170	34	2.89%	0.28235	0.00008	0.00565	0.00199	0.00003	0.07970	0.00150	0.2823080	9.07	1.79	1.82	1.39	0.282052	0.282404	
05DTB18	10/05/2019 (6) 07:19:02.00	05DTB18 - 101	-9.59	1152	36	3.09%	0.28227	0.00005	0.00565	0.00306	0.00004	0.13322	0.00079	0.2821995	4.81	1.30	1.30	1.65	0.282064	0.282417	
03DTB18	09/05/2019 (5) 23:03:46.00	03DTB18 - 67	-9.56	1092	41	3.78%	0.28222	0.00004	0.00565	0.00002	0.00000	0.01899	0.00020	0.2822156	4.02	1.40	1.43	1.65	0.282102	0.282461	
05DTB18	10/05/2019 (6) 03:31:36.00	05DTB18 - 10	-9.51	1131	43	3.84%	0.28232	0.00004	0.00565	0.00060	0.00004	0.02230	0.00160	0.2823072	8.14	1.30	1.30	1.42	0.282078	0.282433	
04DTB18	10/05/2019 (6) 02:26:52.00	04DTB18 - 48	-9.51	1224	47	3.80%	0.28214	0.00004	0.00564	0.00140	0.00000	0.05149	0.00037	0.2821077	3.16	1.26	1.58	1.81	0.282018	0.282364	
05DTB18	10/05/2019 (6) 06:07:05.00	05DTB18 - 70	-9.45	1909	139	7.29%	0.28153	0.00008	0.00563	0.00053	0.00001	0.01959	0.00036	0.2815060	-2.70	2.73	2.39	2.71	0.281582	0.281860	
05DTB18	10/05/2019 (6) 07:07:45.00	05DTB18 - 95	-9.36	1430	46	3.20%	0.28214	0.00011	0.00564	0.00086	0.00002	0.03134	0.00041	0.2821169	8.14	2.21	1.53	1.65	0.281888	0.282213	
03DTB18	09/05/2019 (5) 21:09:43.00	03DTB18 - 24	-9.35	1267	38	3.02%	0.28225	0.00005	0.00565	0.00542	0.00009	0.20960	0.00300	0.2821174	4.48	1.58	1.61	1.76	0.281991	0.282333	
03DTB18	09/05/2019 (5) 20:26:02.00	03DTB18 - 6	-9.35	982	31	3.16%	0.28238	0.00004	0.00565	0.00412	0.00014	0.15930	0.00480	0.2822989	4.51	1.37	1.35	1.53	0.282172	0.282541	
03DTB18	09/05/2019 (5) 22:20:04.00	03DTB18 - 51	-9.12	1452	46	3.18%	0.28193	0.00005	0.00564	0.00097	0.00000	0.05410	0.00600	0.2819024	1.02	1.65	1.86	2.12	0.281874	0.282197	
05DTB18	10/05/2019 (6) 06:05:10.00	05DTB18 - 69	-9.11	1305	38	2.93%	0.28227	0.00005	0.00565	0.00270	0.00006	0.10160	0.00250	0.2822035	8.39	1.72	1.45	1.54	0.281967	0.282305	
05DTB18	10/05/2019 (6) 06:01:19.00	05DTB18 - 67	-9.05	1382	215	15.59%	0.28193	0.00009	0.00564	0.00066	0.00001	0.02386	0.00042	0.2819117	-0.24	3.29	1.84	2.15	0.281918	0.282249	
03DTB18	09/05/2019 (5) 23:39:36.00	03DTB18 - 83	-8.93	1452	43	2.98%	0.28217	0.00005	0.00564	0.00227	0.00001	0.00126	0.00011	0.2821078	8.30	1.58	1.58	1.66	0.281874	0.282197	
BH1	03/12/2018 (2) 20:19:21.00	BH1 - 142	-8.87	1186	32	2.66%	0.282226	0.000042	0.00564	0.002093	0.00006	0.1095	0.004	0.2821792	5.15	1.47	1.49	1.67	0.282034	0.282393	
03DTB18	09/05/2019 (5) 23:00:01.00	03DTB18 - 65	-8.83	2453	120	4.91%	0.28124	0.00003	0.00562	0.00038	0.00000	0.04247	0.00055	0.2812251	-0.21	1.09	2.76	2.97	0.281231	0.281454	
BH1	03/12/2018 (2) 20:56:44.00	BH1 - 155	-8.69	1175	33	2.84%	0.281835	0.000028	0.00564	0.00286	0.000014	0.1268	0.0016	0.2817716	-9.54	0.98	2.09	2.60	0.282041	0.282400	
03DTB18	09/05/2019 (5) 20:41:04.00	03DTB18 - 14	-8.66	1140	51	4.51%	0.28225	0.00004	0.00565	0.00085	0.00000	0.03111	0.00015	0.2822277	5.53	1.40	1.41	1.59	0.282072	0.282426	
03DTB18	10/05/2019 (6) 00:27:18.00	03DTB18 - 100	-8.65	1234	49	3.98%	0.28206	0.00003	0.00564	0.00110	0.00011	0.03957	0.00092	0.2820344	0.79	1.19	1.68	1.97	0.282012	0.282357	
04DTB18	10/05/2019 (6) 01:29:47.00	04DTB18 - 29	-8.48	1386	194	14.00%	0.28210	0.00005	0.00564	0.00090	0.00003	0.03322	0.00096	0.2820805	5.85	1.65	1.61	1.76	0.281916	0.282245	
04DTB18	10/05/2019 (6) 00:29:18.00	04DTB18 - 1	-8.29	1395	199	14.25%	0.28210	0.00004	0.00564	0.00194	0.00002	0.06713	0.00096	0.2820500	4.96	1.44	1.66	1.83	0.281910	0.282239	
04DTB18	10/05/2019 (6) 00:46:12.99	04DTB18 - 10	-8.06	1746	134	7.68%	0.28170	0.00005	0.00563	0.00100	0.00006	0.03450	0.00180	0.2816659	-0.71	1.65	2.18	2.46	0.281686	0.281980	
BH1	03/12/2018 (2) 18:40:13.00	BH1 - 106	-8.05	1213	36	3.00%	0.282097	0.00003	0.00564	0.0010867	0.0000064	0.05032	0.0006	0.2820721	1.99	1.05	1.63	1.90	0.282016	0.282372	
03DTB18	09/05/2019 (5) 23:15:02.00	03DTB18 - 73	-8.00	1210	69	5.68%	0.28198	0.00005	0.00564	0.00039	0.00004	0.02138	0.00060	0.2819711	-2.00	1.82	1.76	2.13	0.282028	0.282375	
BH1	03/12/2018 (2) 20:09:08.00	BH1 - 137	-7.90	1081	46	4.28%	0.282356	0.000028	0.00565	0.0009599	0.0000038	0.04975	0.00021	0.2823364	8.36	0.98	1.27	1.38	0.282101	0.282469	
03DTB18	09/05/2019 (5) 21:22:55.00	03DTB18 - 31	-7.90	1537	186	12.11%	0.28190	0.00004	0.00564	0.00101	0.00003	0.02413	0.00091	0.2818676	1.71	1.47	1.91	2.14	0.281820	0.282134	
05DTB18	10/05/2019 (6) 07:11:31.00	05DTB18 - 97	-7.87	1767	136	7.69%	0.28168	0.00006	0.00563	0.00066	0.00006	0.02320	0.00210	0.2816580	-0.53	1.86	2.83	2.46	0.281673	0.281965	
05DTB18	10/05/2019 (6) 06:37:26.00	05DTB18 - 83	-7.81	1395	58	4.15%	0.28223	0.00007	0.00565	0.00085	0.00000	0.03317	0.00013	0.2822105	10.66	2.28	1.43	1.46	0.281910	0.282239	
BH1	03/12/2018 (2) 19:07:04.00	BH1 - 119	-7.75	1098	33	3.03%	0.282455	0.000036	0.00565	0.001703	0.000035	0.0934	0.0013	0.2824198	11.68	1.26	1.15	1.18	0.282090	0.282457	
BH1	03/12/2018 (2) 15:14:33.00	BH1 - 37	-7.68	1135	49	4.31%	0.282011	0.000034	0.00564	0.000691	0.000033	0.0373	0.0016	0.2819962	-2.48	1.19	1.73	2.12	0.282066	0.282430	
05DTB18	10/05/2019 (6) 03:46:47.00	05DTB18 - 15	-7.65	1298	56	4.29%	0.28211	0.00005	0.00564	0.00080	0.00001	0.02879	0.00034	0.2820913	4.25	1.82	1.60	1.80	0.281971	0.282310	
BH1	03/12/2018 (2) 17:29:37.00	BH1 - 82	-7.61	1081	30	2.77%	0.282376	0.000024	0.00565	0.0013452	0.0000028	0.07392	0.00061	0.2823486	8.79	0.84	1.25	1.36	0.282101	0.282469	
04DTB18	10/05/2019 (6) 01:01:34.00	04DTB18 - 14	-7.58	1664	141	8.50%	0.28170	0.00004	0.00563	0.00097	0.00004	0.03390	0.00160	0.2816683	-2.50	1.26	2.18	2.51	0.281739	0.282041	
BH1	03/12/2018 (2) 16:16:57.00	BH1 - 57	-7.53	1145	39	3.41%	0.282087	0.000034	0.00564	0.001026	0.000035	0.0559	0.0018	0.2820649	0.18	1.19	1.64	1.96	0.282060	0.282422	
05DTB18	10/05/2019 (6) 06:18:39.00	05DTB18 - 73	-7.50	1080	46	4.28%	0.28233	0.00004	0.00565	0.00095	0.00001	0.03535	0.00054	0.2823147	7.27	1.51	1.30	1.43	0.282109	0.282470	
05DTB18	10/05/2019 (6) 04:05:48.00	05DTB18 - 21	-7.40	1475	56	3.83%	0.28217	0.00006	0.00564	0.00102	0.00005	0.03680	0.00200	0.2821445	10.12	1.93	1.52	1.56	0.281859	0.282180	
03DTB18	09/05/2019 (5) 20:52:33.00	03DTB18 - 16	-7.25	1117	54	4.80%	0.28227	0.00004	0.00565	0.00116	0.00001	0.04447	0.00029	0.2822436	5.57	1.30	1.40	1.57	0.282086	0.282443	
BH1	03/12/2018 (2) 19:56:45.00	BH1 - 131	-7.20	1465	41	2.79%	0.282032	0.00003	0.00564	0.0008995	0.0000093	0.04305	0.00044	0.2820071	5.41	1.05	1.71	1.88	0.281855	0.282188	
03DTB18	09/05/2019 (5) 23:28:14.00	03DTB18 - 80	-7.18	1083	44	4.04%	0.28225	0.00004	0.00565	0.00107	0.00001	0.02349	0.00015	0.2822232	4.09	1.33	1.42	1.64	0.282108	0.282468	
BH1	03/12/2018 (2) 16:06:40.00	BH1 - 52	-7.14	1206	34	2.85%	0.28212	0.00003	0.00564	0.0011709	0.0000025	0.05949	0.00064	0.2820934	2.57	1.05	1.60	1.85	0.282021	0.282378	
03DTB18	09/05/2019 (5) 21:42:11.00	03DTB18 - 35	-7.10	1457	64	4.38%	0.28199	0.00004	0.00564	0.00059	0.00001	0.04565	0.00067	0.2819688	3.48	1.44	1.76	1.97	0.281871	0.282194	
04DTB18	10/05/2019 (6) 00:59:44.00	04DTB18 - 13	-7.07	1340	51	3.81%	0.28221	0.00004	0.00564	0.00195	0.00003	0.06980	0.00170	0.2821646	7.80	1.26	1.50	1.60	0.281945	0.282279	
BH1	03/12/2018 (2) 18:42:20.00	BH1 - 107	-6.93	1139	36	3.15%	0.282412	0.000031	0.00565	0.001652	0.000073	0.0839	0.0027	0.2823765	11.09	1.09	1.21	1.25	0.282064	0.282427	
05DTB18	10/05/2019 (6) 07:15:16.00	05DTB18 - 99	-6.87	1031	41	3.98%	0.28232	0.00005	0.00565	0.00054	0.00001	0.02050	0.00063	0.2823085	5.97	2.07	2.19	1.48	0.282140	0.282505	
BH1	03/12/2018 (2) 19:27:40.00	BH1 - 122	-6.83	1088	34	3.09%	0.282322	0.00003	0.00565	0.0006351	0.0000048	0.03177	0.00043	0.2823090	7.55	1.05	1.30	1.44	0.282096	0.282464	
BH1	03/12/2018 (2) 18:27:36.00	BH1 - 105	-6.77	1221	38	3.08%	0.282112	0.000032	0.00564	0.00084	0.000011	0.04222	0.00079	0.2820927	2.89	1.12	1.60	1.85	0.282011	0.282367	
03DTB18	10/05/2019 (6) 00:13:56.00	03DTB18 - 96	-6.71	1300	40	3.09%	0.28216	0.00005	0.00564	0.00208	0.00001	0.03436	0.00029	0.2821080	4.88	1.79	1.59	1.76	0.281970	0.282309	
04DTB18	10/05/2019 (6) 02:02:14.00	04DTB18 - 36	-6.57	1486	64	4.28%	0.28202	0.00006	0.00564	0.00100	0.00001	0.03521	0.00033	0.2819930	5.01	2.10	1.73	1.89	0.281852	0.282172	
BH1	03/12/2018 (2) 20:17:21.00	BH1 - 141	-6.45	1370	46	3.39%	0.282175	0.00003	0.00564	0.0006299	0.0000071	0.02667	0.00038	0.2821587	8.63	1.05	1.50	1.60	0.281915	0.282257	
04DTB18	10/05/2019 (6) 01:03:29.00	04DTB18 - 15	-6.38	1621	141	8.70%	0.28199	0.00006	0.00564	0.00079	0.00002	0.02856	0.00097	0.2819648	7.06	1.93	1.77	1.87	0.281766	0.282072	
03DTB18	09/05/2019 (5) 20:33:33.00	03DTB18 - 10	-6.35	1161	46	3.94%	0.28200	0.00003	0.00564	0.00204	0.00003	0.07940	0.00170	0.2819555	-3.65	1.12	1.81	2.19	0.282058	0.282411	
03DTB18	09/05/2019 (5) 21:44:01.00	03DTB18 - 36	-6.31	1736	128	7.40%	0.28192	0.00005	0.00564	0.00076	0.00004	0.02119	0.00047	0.2818949	7.19	1.79	1.86	1.95	0.281692	0.281987	
03DTB18	09/05/2019 (5) 21:19:10.00	03DTB18 - 29	-6.30	1701	123	7.21%	0.28173	0.00004	0.00563	0.00127	0.00002	0.03900	0.00460	0.2816841	-1.09	1.47	2.16	2.45	0.281715	0.282013	
05DTB18	10/05/2019 (6) 08:32:44.00	05DTB18 - 132	-6.19	1707	117	6.88%	0.28179	0.00006	0.00564	0.00078	0.00002	0.02887	0.00059	0.2817657	1.93	2.77	2.45	2.26	0.281711	0.282009	
03DTB18	09/05/2019 (5) 23:26:19.00	03DTB18 - 79	-6.18	1432	58	4.07%	0.28206	0.00005	0.00564	0.00063	0.00000	0.04670	0.00220	0.2820470	5.69	1.72	1.66	1.81	0.281887	0.282212	
05DTB18	10/05/2019 (6) 08:25:13.00	05DTB18 - 128	-6.02	1446	44	3.05%	0.28215	0.00012	0.00564	0.00085	0.00001	0.03118	0.00015	0.2821267	8.84	1.47	1.72	1.62	0.281877	0.282201	
05DTB18	10/05/2019 (6) 06:48:42.00	05DTB18 - 89	-5.90	1660	142	8.54%	0.28200	0.00007	0.00564	0.00104	0.00001	0.03759	0.00036	0.2819704	8.14	2.66	1.46	1.83	0.281741	0.282044	
03DTB18	09/05/2019 (5) 22:06:52.00	03DTB18 - 44	-5.64	1178	42	3.61%	0.28206	0.00005	0.00564	0.00089	0.00001	0.02510	0.00150	0.2820362	-0.40	1.82	1.68	2.00	0.282048	0.282398	
BH1	03/12/2018 (2) 18:00:53.00	BH1 - 92	-5.60	1093	32	2.89%	0.2823	0.000034	0.00565	0.000455	0.000016	0.02388	0.0007	0.2822906	7.01	1.19	1.33	1.48	0.282093	0.282460	
03DTB18	09/05/2019 (5) 22:23:50.00	03DTB18 - 53	-5.56	1172	42	3.62%	0.28227	0.00005	0.00565	0.00133	0.00002	0.01216	0.00040	0.2822436	6.81	1.58	1.39	1.54	0.282052	0.282403	
03DTB18	09/05/2019 (5) 21:15:24.00	03DTB18 - 27	-5.52	1399	61	4.38%	0.28215	0.00003	0.00564	0.00146	0.00005	0.02154	0.00015	0.2821145	7.35	1.19	1.57	1.68	0.281907	0.282236	
03DTB18	09/05/2019 (5) 22:27:35.00	03DTB18 - 55	-5.51	1653	164	9.90%	0.28157	0.00004	0.00563	0.00045	0.00001	0.04120	0.00150	0.2815508	-6.91	1.37	2.33	2.78	0.281746	0.282049	
BH1	03/12/2018 (2) 16:23:09.00	BH1 - 60	-5.47	1464	45	3.09%	0.281978	0.000027	0.00564	0.0008014	0.0000031	0.04049	0.00024	0.2819558	3.58	0.95	1.78	1.99	0.281855	0.282188	
03DTB18	09/05/2019 (5) 22:33:12.00	03DTB18 - 58	-5.45	1715	107	6.25%	0.28175	0.00004	0.00564	0.00021	0.00000	0.03740	0.00430	0.2817390	1.18	1.40	2.07	2.32	0.281706	0.282003	
BH1	03/12/2018 (2) 18:25:35.00	BH1 - 104	-5.42	1111	40	3.56%	0.282039	0.000029	0.00564	0.0008271	0.0000073	0.04339	0.00029	0.2820217	-2.12	1.02	1.70	2.08	0.282081	0.282447	
05DTB18	10/05/2019 (6) 03:29:40.00	05DTB18 - 9	-5.24	1468	57	3.90%	0.28202	0.00004	0.00564	0.00075	0.00011	0.02780	0.00420	0.2819992	4.81	1.40	1.72	1.89	0.281864	0.282185	
05DTB18	10/05/2019 (6) 06:41:12.00	05DTB18 - 85	-5.17	1289	48	3.71%	0.28232	0.00006	0.00565	0.00217	0.00004	0.08200	0.00210	0.2822701	10.38	2.21	1.35	1.40	0.281977	0.282317	
05DTB18	10/05/2019 (6) 07:02:04.00	05DTB18 - 92	-5.14	2647	91	3.44%	0.28093	0.00004	0.00562	0.00059	0.00000	0.02099	0.00008	0.2808973	-7.40	2.45	2.00	3.58	0.281105	0.281308	
BH1	03/12/2018 (2) 20:00:56.00	BH1 - 133	-5.07	1475	39	2.66%	0.282112	0.00003	0.00564	0.0016	0.00004	0.0788	0.0026	0.2820674	7.78	1.05	1.63	1.73	0.281848	0.282180	
05DTB18	10/05/2019 (6) 08:02:40.00	05DTB18 - 116	-5.07	1928	104	5.40%	0.28149	0.00011	0.00563	0.00053	0.00000	0.01983	0.00010	0.2814706	-3.50	2.98	1.35	2.78	0.281569	0.281845	
05DTB18	10/05/2019 (6) 07:26:32.00	05DTB18 - 105	-5.00	1442	51	3.56%	0.28213	0.00006	0.00564	0.00104	0.00000	0.04046	0.00031	0.2821027	7.89	1.47	1.52	1.67	0.281880	0.282205	
03DTB18	09/05/2019 (5) 23:43:24.00	03DTB18 - 85	-4.99	1469	55	3.77%	0.28201	0.00005	0.00564	0.00069	0.00001	0.07947	0.00015	0.2819860	4.36	1.61	1.74	1.92	0.281863	0.282185	
BH1	03/12/2018 (2) 20:07:03.00	BH1 - 136	-4.93	1131	35	3.12%	0.282353	0.000031	0.00565	0.001122	0.000008	0.04991	0.00073	0.2823291	9.23	1.09	1.27	1.37	0.282069	0.282432	
05DTB18	10/05/2019 (6) 03:25:55.00	05DTB18 - 7	-4.80	2826	148	5.23%	0.28114	0.00007	0.00562	0.00039	0.00001	0.01387	0.00042	0.2811232	4.79	2.49	2.89	2.94	0.280989	0.281173	
05DTB18	10/05/2019 (6) 03:18:19.00	05DTB18 - 3	-4.78	1879	154	8.19%	0.28163	0.00009	0.00563	0.00047	0.00001	0.01701	0.00040	0.2816112	0.37	3.29	2.25	2.49	0.281601	0.281881	
03DTB18	09/05/2019 (5) 21:40:11.50	03DTB18 - 34	-4.74	2605	133	5.09%	0.28124	0.00005	0.00562	0.00127	0.00001	0.02748	0.00052	0.2811768	1.59	1.61	2.83	2.98	0.281132	0.281339	
BH1	03/12/2018 (2) 16:02:35.00	BH1 - 50	-4.62	1108	30	2.74%	0.282334	0.000028	0.00565	0.000639	0.000042	0.0367	0.0026	0.2823207	8.42	0.98	1.29	1.40	0.282083	0.282449	
BH1	03/12/2018 (2) 18:58:53.00	BH1 - 115	-4.54	1353	55	4.06%	0.281994	0.000029	0.00564	0.001315	0.000044	0.0694	0.0023	0.2819604	1.20	1.02	1.79	2.06	0.281926	0.282270	
04DTB18	10/05/2019 (6) 00:44:23.00	04DTB18 - 9	-4.54	1382	44	3.17%	0.28215	0.00004	0.00564	0.00232	0.00001	0.09229	0.00061	0.2820853	5.92	1.23	1.62	1.75	0.281918	0.282249	
05DTB18	10/05/2019 (6) 07:45:29.00	05DTB18 - 112	-4.52	1694	130	7.65%	0.28185	0.00004	0.00564	0.00045	0.00000	0.01479	0.00006	0.2818397	4.27	2.21	1.74	2.10	0.281719	0.282018	
05DTB18	10/05/2019 (6) 08:13:57.00	05DTB18 - 122	-4.48	1775	115	6.49%	0.28169	0.00008	0.00563	0.00124	0.00000	0.04446	0.00035	0.2816524	-0.53	2.94	1.38	2.47	0.281667	0.281958	
05DTB18	10/05/2019 (6) 06:35:31.00	05DTB18 - 82	-4.43	1101	38	3.44%	0.28236	0.00009	0.00565	0.00045	0.00001	0.01667	0.00062	0.2823537	9.12	3.01	1.24	1.33	0.282096	0.282455	
BH1	03/12/2018 (2) 16:48:06.00	BH1 - 67	-4.38	1443	53	3.65%	0.282139	0.000025	0.00564	0.000909	0.000033	0.0445	0.0021	0.2821142	8.71	0.88	1.57	1.65	0.281869	0.282204	
BH1	03/12/2018 (2) 19:31:50.00	BH1 - 124	-4.35	1338	41	3.08%	0.282251	0.000029	0.00565	0.0013287	0.0000033	0.07074	0.00059	0.2822174	9.99	1.02	1.43	1.48	0.281936	0.282281	
05DTB18	10/05/2019 (6) 06:24:15.00	05DTB18 - 76	-4.18	1614	143	8.89%	0.28170	0.00008	0.00563	0.00068	0.00003	0.02550	0.00130	0.2816793	-3.24	2.87	2.16	2.52	0.281771	0.282078	
[illegible]																					

Appendix D5.3 continued.

Sample ID	Analysis date-time	Spot ID	Discord (7/6-6/8)/7/6 *100	Preferred age 1500 Ma cutoff: Ma	2σ	error %	Lu-Hf Isotopic Ratios from Iolite: 176Hf/177Hf	±2σ INT	(2% External ±)	176Lu/177Hfm	±2σ INT	176Yb/177Hf	±2σ INT	Hfi	εHf Calculations: εHf Lu decay	±2σ	TDM(Ga)	TDMCrustal	HfCHUR(t)	HfDM(t)	Notes
							0.282785			0.03360	Bouvier et al., 2008 EPSL-273					0.02	Scherer et al., 2001, Science-293				
							0.283250			0.03840	Griffin et al., 2002, Lithos-237										
BH1	03/12/2018 (2) 18:21:23.00	BH1 - 102	-0.36	1158	38	3.26%	0.282012	0.000033	0.00564	0.0005473	0.0000053	0.02856	0.00017	0.2820001	-1.82	1.16	1.73	2.10	0.282051	0.282413	
05DTB18	10/05/2019 (6) 04:30:11.00	05DTB18 - 34	-0.36	1413	52	3.70%	0.28189	0.00004	0.00564	0.00071	0.00002	0.02487	0.00075	0.2818712	-0.98	1.37	1.90	2.22	0.281899	0.282226	
04DTB18	10/05/2019 (6) 00:34:56.00	04DTB18 - 4	-0.29	1475	47	3.21%	0.28213	0.00006	0.00564	0.00130	0.00003	0.04539	0.00099	0.2820927	8.29	2.03	1.60	1.67	0.281859	0.282180	
BH1	03/12/2018 (2) 21:32:08.00	BH1 - 167	-0.22	1295	41	3.13%	0.282387	0.000049	0.00565	0.0021413	0.0000092	0.1106	0.001	0.2823347	13.15	1.72	1.26	1.24	0.281964	0.282313	
04DTB18	10/05/2019 (6) 01:14:45.00	04DTB18 - 21	-0.17	1755	127	7.25%	0.28181	0.00003	0.00564	0.00092	0.00001	0.03455	0.00082	0.2817835	3.66	1.19	2.02	2.19	0.281680	0.281973	
05DTB18	10/05/2019 (6) 06:44:57.00	05DTB18 - 87	-0.09	1492	66	4.42%	0.28207	0.00005	0.00564	0.00132	0.00001	0.04811	0.00077	0.2820319	6.53	2.21	1.35	1.80	0.281848	0.282167	
BH1	03/12/2018 (2) 13:58:15.00	BH1 - 5	-0.06	1710	93	5.42%	0.281898	0.000024	0.00564	0.001169	0.000018	0.064	0.0013	0.2818601	5.82	0.84	1.91	2.04	0.281696	0.282007	
BH1	03/12/2018 (2) 17:50:30.00	BH1 - 87	-0.06	1197	39	3.24%	0.282137	0.000027	0.00564	0.0006349	0.0000039	0.03041	0.00023	0.2821227	3.41	0.95	1.56	1.79	0.282027	0.282384	
BH1	03/12/2018 (2) 17:31:44.00	BH1 - 83	-0.03	3290	58	1.76%	0.280737	0.00003	0.00561	0.00145	0.00017	0.0622	0.0067	0.2806453	-0.49	1.05	3.53	3.69	0.280659	0.280821	too old to be shown on Fig. 2
BH1	03/12/2018 (2) 17:46:22.00	BH1 - 85	0.01	1169	41	3.50%	0.281985	0.000043	0.00564	0.000642	0.000052	0.0327	0.003	0.2819709	-2.61	1.51	1.77	2.15	0.282044	0.282405	
BH1	03/12/2018 (2) 14:56:06.00	BH1 - 28	0.01	1555	81	5.21%	0.28183	0.000021	0.00564	0.00113	0.00014	0.0618	0.0071	0.2817968	0.01	0.74	2.00	2.29	0.281797	0.282121	
BH1	03/12/2018 (2) 13:50:02.00	BH1 - 1	0.03	1242	40	3.25%	0.282215	0.000026	0.00564	0.001077	0.000012	0.0595	0.001	0.2821898	6.80	0.91	1.47	1.61	0.281998	0.282351	
05DTB18	10/05/2019 (6) 06:50:33.23	05DTB18 - 90	0.04	2511	93	3.72%	0.28114	0.00006	0.00562	0.00138	0.00001	0.05058	0.00065	0.2810730	-4.28	2.00	2.97	3.28	0.281193	0.281410	
04DTB18	10/05/2019 (6) 01:39:09.75	04DTB18 - 31	0.17	2595	91	3.49%	0.28123	0.00004	0.00562	0.00097	0.00001	0.03567	0.00027	0.2811800	1.46	1.33	2.82	2.98	0.281139	0.281347	
BH1	03/12/2018 (2) 18:56:48.00	BH1 - 114	0.17	1431	38	2.62%	0.28268	0.00024	0.00566	0.002263	0.000036	0.1161	0.0024	0.2826188	26.34	8.40	0.84	0.49	0.281876	0.282213	outlier plotting off extent shown on Fig. 2 density map
03DTB18	09/05/2019 (5) 23:05:42.00	03DTB18 - 68	0.23	1775	115	6.49%	0.28193	0.00004	0.00564	0.00186	0.00000	0.00067	0.00002	0.2818683	7.13	1.51	1.90	1.98	0.281667	0.281958	
BH1	03/12/2018 (2) 22:23:51.00	BH1 - 187	0.23	1365	38	2.75%	0.28223	0.000024	0.00564	0.0016396	0.0000094	0.08441	0.00084	0.2821877	9.55	0.84	1.47	1.53	0.281918	0.282261	
BH1	03/12/2018 (2) 18:13:12.00	BH1 - 98	0.28	1013	31	3.06%	0.282324	0.00003	0.00565	0.001195	0.00001	0.05867	0.00072	0.2823012	5.57	1.05	1.32	1.51	0.282144	0.282518	
BH1	03/12/2018 (2) 16:12:51.00	BH1 - 55	0.36	1656	95	5.73%	0.28181	0.000025	0.00564	0.0006386	0.000001	0.03289	0.00026	0.2817900	2.10	0.88	2.01	2.24	0.281731	0.282046	
04DTB18	10/05/2019 (6) 00:33:05.00	04DTB18 - 3	0.40	1280	54	4.19%	0.28220	0.00008	0.00564	0.00092	0.00001	0.03507	0.00037	0.2821727	6.73	2.94	1.49	1.62	0.281983	0.282323	
05DTB18	10/05/2019 (6) 08:00:46.00	05DTB18 - 115	0.47	1107	39	3.53%	0.28231	0.00009	0.00565	0.00132	0.00001	0.05431	0.00073	0.2822795	6.64	1.37	1.94	1.50	0.282092	0.282450	
BH1	03/12/2018 (2) 18:23:24.00	BH1 - 103	0.47	1443	45	3.08%	0.281886	0.000032	0.00564	0.000765	0.000016	0.03801	0.00094	0.2818651	-0.12	1.12	1.91	2.21	0.281868	0.282203	
BH1	03/12/2018 (2) 16:04:40.00	BH1 - 51	0.48	2405	77	3.18%	0.281213	0.000032	0.00562	0.000728	0.000021	0.0376	0.00084	0.2811796	-2.27	1.12	2.82	3.11	0.281243	0.281489	
BH1	03/12/2018 (2) 17:56:47.00	BH1 - 90	0.48	1052	51	4.83%	0.282271	0.000029	0.00565	0.001074	0.00007	0.0524	0.0043	0.2822497	4.62	1.02	1.39	1.60	0.282119	0.282490	
BH1	03/12/2018 (2) 22:50:58.00	BH1 - 195	0.50	1831	138	7.52%	0.281502	0.000031	0.00563	0.0002634	0.0000012	0.012582	0.000056	0.2814929	-4.44	1.09	2.40	2.79	0.281618	0.281917	
BH1	03/12/2018 (2) 21:48:53.00	BH1 - 170	0.70	1097	34	3.13%	0.282385	0.000033	0.00565	0.001184	0.000027	0.0591	0.002	0.2823605	9.57	1.16	1.23	1.32	0.282090	0.282457	
04DTB18	10/05/2019 (6) 03:06:45.00	04DTB18 - 65	0.77	1480	63	4.26%	0.28210	0.00008	0.00564	0.00198	0.00006	0.07600	0.00260	0.2820405	6.54	2.70	1.67	1.79	0.281856	0.282177	
BH1	03/12/2018 (2) 14:18:50.00	BH1 - 15	0.78	1057	29	2.70%	0.282331	0.000028	0.00565	0.0009183	0.0000041	0.05281	0.00029	0.2823127	6.96	0.98	1.30	1.45	0.282116	0.282487	
BH1	03/12/2018 (2) 16:58:28.00	BH1 - 72	0.85	1111	39	3.47%	0.282139	0.000029	0.00564	0.0008923	0.0000049	0.04497	0.00023	0.2821203	1.36	1.02	1.57	1.85	0.282082	0.282447	
BH1	03/12/2018 (2) 20:29:47.00	BH1 - 147	0.91	1113	34	3.06%	0.282146	0.000032	0.00564	0.002401	0.000044	0.1387	0.0015	0.2820957	0.54	1.12	1.62	1.91	0.282080	0.282446	
BH1	03/12/2018 (2) 15:52:22.00	BH1 - 45	0.91	1221	33	2.67%	0.282312	0.000022	0.00565	0.00237	0.0001	0.1216	0.0041	0.2822574	8.74	0.77	1.38	1.47	0.282011	0.282366	
BH1	03/12/2018 (2) 21:57:05.00	BH1 - 174	0.92	1135	34	3.02%	0.282238	0.000027	0.00564	0.001051	0.000013	0.0512	0.0011	0.2822155	5.30	0.95	1.43	1.62	0.282066	0.282429	
05DTB18	10/05/2019 (6) 04:15:09.00	05DTB18 - 26	0.93	1895	194	10.24%	0.28186	0.00006	0.00564	0.00033	0.00000	0.01130	0.00006	0.2818433	8.96	2.17	1.93	1.96	0.281591	0.281870	
BH1	03/12/2018 (2) 21:34:10.00	BH1 - 168	0.94	1066	39	3.65%	0.282253	0.000026	0.00565	0.0005221	0.0000018	0.02594	0.00016	0.2822425	4.68	0.91	1.39	1.61	0.282110	0.282480	
BH1	03/12/2018 (2) 17:08:40.00	BH1 - 77	0.95	1410	55	3.91%	0.28215	0.00003	0.00564	0.00095	0.000042	0.0494	0.0019	0.2821247	8.32	1.05	1.55	1.65	0.281890	0.282228	
04DTB18	10/05/2019 (6) 02:06:06.00	04DTB18 - 38	1.03	1222	41	3.36%	0.28219	0.00004	0.00564	0.00099	0.00001	0.03780	0.00059	0.2821672	5.24	1.44	1.50	1.68	0.282019	0.282366	
05DTB18	10/05/2019 (6) 06:33:41.00	05DTB18 - 81	1.07	1077	43	4.00%	0.28236	0.00005	0.00565	0.00083	0.00000	0.03352	0.00036	0.2823441	8.25	1.61	1.25	1.37	0.282111	0.282472	
BH1	03/12/2018 (2) 22:44:48.00	BH1 - 192	1.15	1302	43	3.31%	0.282165	0.00004	0.00564	0.001833	0.000045	0.084	0.0024	0.2821199	5.70	1.40	1.57	1.73	0.281959	0.282307	
BH1	03/12/2018 (2) 22:03:19.00	BH1 - 177	1.19	1199	37	3.11%	0.282259	0.000036	0.00565	0.001333	0.000059	0.0658	0.0037	0.2822289	7.22	1.30	1.41	1.55	0.282025	0.282383	
05DTB18	10/05/2019 (6) 03:50:32.00	05DTB18 - 17	1.21	1114	38	3.42%	0.28235	0.00005	0.00565	0.00049	0.00001	0.01884	0.00035	0.2823398	8.93	1.68	1.26	1.35	0.282088	0.282445	
BH1	03/12/2018 (2) 20:05:02.00	BH1 - 135	1.31	1456	45	3.07%	0.282194	0.000031	0.00564	0.002019	0.000062	0.1003	0.0046	0.2821384	9.86	1.09	1.53	1.58	0.281860	0.282194	
03DTB18	09/05/2019 (5) 22:42:37.00	03DTB18 - 63	1.31	1245	41	3.29%	0.28232	0.00004	0.00565	0.00214	0.00007	0.04000	0.00160	0.2822678	9.31	1.26	1.36	1.43	0.282005	0.282349	
BH1	03/12/2018 (2) 15:06:22.00	BH1 - 33	1.31	1059	37	3.48%	0.282345	0.000031	0.00565	0.001125	0.000036	0.061	0.0024	0.2823226	7.36	1.09	1.29	1.43	0.282115	0.282485	
05DTB18	10/05/2019 (6) 04:26:26.00	05DTB18 - 32	1.32	1121	43	3.81%	0.28237	0.00007	0.00565	0.00027	0.00000	0.00929	0.00003	0.2823622	9.87	2.59	1.23	1.30	0.282084	0.282440	
BH1	03/12/2018 (2) 22:07:26.00	BH1 - 179	1.41	2853	55	1.94%	0.280978	0.000027	0.00562	0.0003653	0.0000003	0.01711	0.00015	0.2809580	0.33	0.95	3.11	3.30	0.280949	0.281153	
BH1	03/12/2018 (2) 17:00:29.00	BH1 - 73	1.42	1655	117	7.08%	0.282037	0.000039	0.00564	0.001584	0.000044	0.0779	0.0028	0.2819874	9.06	1.37	1.74	1.79	0.281732	0.282048	
BH1	03/12/2018 (2) 22:55:05.00	BH1 - 197	1.49	1813	101	5.56%	0.281833	0.000027	0.00564	0.001009	0.000019	0.0479	0.0015	0.2817983	6.00	0.95	1.99	2.11	0.281629	0.281930	
BH1	03/12/2018 (2) 20:42:23.00	BH1 - 148	1.53	1103	43	3.89%	0.282027	0.000029	0.00564	0.0006164	0.0000047	0.031026	0.000056	0.2820142	-2.57	1.02	1.71	2.10	0.282087	0.282453	
BH1	03/12/2018 (2) 17:33:45.00	BH1 - 84	1.56	1448	45	3.12%	0.282041	0.000031	0.00564	0.000738	0.000016	0.03631	0.00094	0.2820208	5.51	1.09	1.69	1.86	0.281865	0.282200	
03DTB18	09/05/2019 (5) 22:25:40.00	03DTB18 - 54	1.56	1093	40	3.64%	0.28224	0.00003	0.00564	0.00104	0.00004	0.05044	0.00093	0.2822196	4.18	1.09	1.43	1.64	0.282102	0.282460	
BH1	03/12/2018 (2) 15:31:24.00	BH1 - 40	1.65	1857	97	5.24%	0.281608	0.000035	0.00563	0.0006783	0.0000068	0.03587	0.00067	0.2815841	-0.60	1.23	2.28	2.57	0.281601	0.281898	
BH1	03/12/2018 (2) 14:24:59.00	BH1 - 18	1.71	1083	35	3.19%	0.28234	0.000025	0.00565	0.00084	0.0000064	0.04575	0.00033	0.2823229	7.93	0.88	1.28	1.41	0.282099	0.282467	
BH1	03/12/2018 (2) 18:15:12.00	BH1 - 99	1.73	1449	48	3.28%	0.282226	0.000032	0.00564	0.001379	0.000024	0.0692	0.00075	0.2821882	11.49	1.12	1.46	1.47	0.281864	0.282199	
05DTB18	10/05/2019 (6) 03:43:01.00	05DTB18 - 13	1.74	2585	116	4.50%	0.28128	0.00004	0.00563	0.00052	0.00001	0.01735	0.00031	0.2812576	4.00	1.23	2.71	2.81	0.281145	0.281354	
BH1	03/12/2018 (2) 15:12:28.00	BH1 - 36	1.82	1074	51	4.71%	0.282058	0.000025	0.00564	0.000864	0.000015	0.04763	0.00048	0.2820405	-2.29	0.88	1.68	2.06	0.282105	0.282474	
BH1	03/12/2018 (2) 22:52:59.00	BH1 - 196	1.88	1689	118	7.01%	0.2818	0.000039	0.00564	0.0017789	0.000002	0.09411	0.00091	0.2817431	1.18	1.37	2.08	2.32	0.281710	0.282022	
03DTB18	09/05/2019 (5) 21:17:19.66	03DTB18 - 28	1.97	2549	97	3.82%	0.28124	0.00004	0.00563	0.00102	0.00011	0.05400	0.00180	0.2811943	0.92	1.30	2.80	2.98	0.281169	0.281381	
05DTB18	10/05/2019 (6) 06:26:11.00	05DTB18 - 77	1.97	1293	55	4.24%	0.28226	0.00007	0.00565	0.00180	0.00004	0.06940	0.00110	0.2822171	8.60	2.59	1.43	1.51	0.281975	0.282314	
BH1	03/12/2018 (2) 17:54:41.00	BH1 - 89	2.06	1795	88	4.88%	0.281648	0.000037	0.00563	0.0003788	0.000004	0.0199	0.0004	0.2816351	-0.21	1.30	2.21	2.50	0.281641	0.281944	
BH1	03/12/2018 (2) 14:54:05.00	BH1 - 27	2.11	1342	38	2.81%	0.281831	0.000033	0.00564	0.00163	0.00012	0.0867	0.0057	0.2817897	-5.10	1.16	2.03	2.45	0.281934	0.282278	
05DTB18	10/05/2019 (6) 04:28:21.00	05DTB18 - 33	2.14	3117	89	2.85%	0.28073	0.00005	0.00561	0.00061	0.00001	0.02208	0.00032	0.2806883	-3.91	1.79	3.47	3.72	0.280798	0.280953	too old to be shown on Fig. 2
BH1	03/12/2018 (2) 17:48:29.00	BH1 - 86	2.23	1290	47	3.64%	0.282331	0.000027	0.00565	0.002466	0.000019	0.1412	0.0017	0.2822710	10.78	0.95	1.35	1.39	0.281967	0.282316	
BH1	03/12/2018 (2) 15:56:27.00	BH1 - 47	2.24	1859	127	6.82%	0.281379	0.00004	0.00563	0.00062	0.0000043	0.02861	0.00011	0.2813571	-8.62	1.40	2.59	3.08	0.281600	0.281897	
BH1	03/12/2018 (2) 18:02:53.00	BH1 - 93	2.24	1217	39	3.21%	0.281948	0.000021	0.00564	0.0007909	0.0000018	0.03906	0.00025	0.2819298	-2.97	0.74	1.82	2.21	0.282014	0.282369	
BH1	03/12/2018 (2) 15:29:19.00	BH1 - 39	2.24	1108	34	3.06%	0.282383	0.000027	0.00565	0.001386	0.000049	0.0657	0.0019	0.2823541	9.59	0.95	1.24	1.33	0.282084	0.282449	
04DTB18	10/05/2019 (6) 02:09:50.05	04DTB18 - 40	2.25	2576	143	5.57%	0.28145	0.00023	0.00563	0.00039	0.00010	0.01780	0.00460	0.2814306	9.95	8.05	2.48	2.42	0.281151	0.281361	
BH1	03/12/2018 (2) 15:54:22.00	BH1 - 46	2.31	1748	106	6.04%	0.281412	0.00003	0.00563	0.001086	0.000041	0.0513	0.0017	0.2813760	-10.49	1.05	2.58	3.11	0.281672	0.281978	
BH1	03/12/2018 (2) 16:18:58.00	BH1 - 58	2.34	1107	34	3.06%	0.282098	0.000063	0.00564	0.000582	0.000011	0.03156	0.00087	0.2820859	0.06	2.21	1.61	1.94	0.282084	0.282450	
BH1	03/12/2018 (2) 14:51:58.00	BH1 - 26	2.37	1275	34	2.66%	0.282026	0.000027	0.00564	0.0008101	0.0000033	0.04601	0.00024	0.2820065	1.05	0.95	1.72	2.00	0.281977	0.282327	
BH1	03/12/2018 (2) 14:20:54.00	BH1 - 16	2.39	1351	38	2.84%	0.282096	0.000021	0.00564	0.001095	0.000036	0.0589	0.0016	0.2820681	4.97	0.74	1.63	1.81	0.281928	0.282271	
BH1	03/12/2018 (2) 21:27:57.00	BH1 - 165	2.40	1016	33	3.26%	0.282365	0.00003	0.00565	0.0006534	0.0000067	0.0327	0.00035	0.2823525	7.45	1.05	1.24	1.39	0.282142	0.282516	
BH1	03/12/2018 (2) 14:00:19.00	BH1 - 6	2.41	1212	35	2.93%	0.282307	0.000024	0.00565	0.002319	0.000029	0.1283	0.0023	0.2822540	8.41	0.84	1.38	1.48	0.282017	0.282373	
BH1	03/12/2018 (2) 20:58:50.00	BH1 - 156	2.48	1118	46	4.09%	0.282114	0.000034	0.00564	0.001268	0.00003	0.066	0.0012	0.2820873	0.35	1.19	1.62	1.92	0.282077	0.282442	
BH1	03/12/2018 (2) 22:57:05.00	BH1 - 198	2.49	1368	51	3.72%	0.282195	0.000026	0.00564	0.001211	0.000013	0.06135	0.00012	0.2821637	8.76	0.91	1.50	1.59	0.281917	0.282259	
04DTB18	10/05/2019 (6) 02:23:02.00	04DTB18 - 47	2.58	1283	39	3.07%	0.28202	0.00003	0.00564	0.00097	0.00004	0.04150	0.00310	0.2819915	0.37	1.16	1.74	2.03	0.281981	0.282321	
BH1	03/12/2018 (2) 19:11:11.00	BH1 - 121	2.67	1169	35	3.03%	0.282337	0.000041	0.00565	0.002314	0.000043	0.1248	0.0026	0.2822860	8.56	1.44	1.34	1.44	0.282044	0.282405	
BH1	03/12/2018 (2) 18:46:26.00	BH1 - 109	2.74	1092	35	3.23%	0.282258	0.000029	0.00564	0.001299	0.000013	0.06649	0.00055	0.2822313	4.88	1.02	1.41	1.62	0.282094	0.282461	
BH1	03/12/2018 (2) 19:48:31.00	BH1 - 127	2.89	1150	34	2.96%	0.2822	0.000022	0.00564	0.001287	0.000022	0.0616	0.0013	0.2821721	4.08	0.67	1.50	1.71	0.282057	0.282419	
03DTB18	10/05/2019 (6) 00:02:40.00	03DTB18 - 90	2.89	1933	144	7.46%	0.28124	0.00004	0.00562	0.00035	0.00000	0.03243	0.00021	0.2812271	-12.05	1.47	2.76	3.32	0.281566	0.281841	
04DTB18	10/05/2019 (6) 01:41:14.27	04DTB18 - 32	3.05	1155	37	3.17%	0.28226	0.00003	0.00565	0.00254	0.00010	0.10270	0.00380	0.2822037	5.02	1.19	1.46	1.64	0.282062	0.282415	
BH1	03/12/2018 (2) 22:25:58.00	BH1 - 188	3.09	1229	55	4.51%	0.282251	0.000039	0.00565	0.00116	0.000071	0.0606	0.0036	0.2822241	7.73	1.37	1.42	1.54	0.282006	0.282361	
BH1	03/12/2018 (2) 20:25:34.00	BH1 - 145	3.11	1642	429	26.12%	0.282109	0.000053	0.00564	0.000926	0.000023	0.0476	0.0013	0.2820802	12.07	1.86	1.61	1.59	0.281740	0.282057	
BH1	03/12/2018 (2) 18:52:34.00	BH1 - 112	3.19	1124	39	3.45%	0.282275	0.000026	0.00565	0.001164	0.000031	0.0575	0.001	0.2822503	6.28	0.91	1.39	1.55	0.282073	0.282437	
04DTB18	10/05/2019 (6) 02:38:12.00	04DTB18 - 54	3.22	1346	47	3.47%	0.28228	0.00011	0.00565	0.00101	0.00000	0.03760	0.00035	0.2822543	11.10	3.85	1.37	1.39	0.281941	0.282275	
BH1	03/12/2018 (2) 21:52:58.00	BH1 - 172	3.32	1860	88	4.74%	0.281486	0.000024	0.00563	0.000982	0.000054	0.0498	0.0026	0.2814513	-5.24	0.84	2.47	2.87	0.281599	0.281895	
BH1	03/12/2018 (2) 14:10:31.00	BH1 - 11	3.33	1073	40	3.69%	0.282324	0.000035	0.00565	0.001147	0.00003	0.064	0.0014	0.2823008	6.91	1.23	1.32	1.47	0.282106	0.282475	
BH1	03/12/2018 (2) 14:16:48.00	BH1 - 14	3.38	1722	95	5.54%	0.281678	0.000027	0.00564	0.000834	0.000016	0.0454	0.0012	0.2816508	-1.33	0.95	2.20	2.51	0.281688	0.281998	
04DTB18	10/05/2019 (6) 02:47:38.00	04DTB18 - 59	3.38	2679	118	4.39%	0.28119	0.00005	0.00562	0.00079	0.00000	0.02968	0.00022	0.2811523	2.42	1.89	2.86	2.98	0.281084	0.281284	
BH1	03/12/2018 (2) 19:09:04.79	BH1 - 120	3.41	913	37	4.02%	0.28285	0.00037	0.00567	0.00101	0.00015	0.061	0.013	0.2828327	22.13	12.95	0.57	0.36	0.282208	0.282592	outlier plotting off extent shown on Fig. 2 density map
BH1	03/12/2018 (2) 22:59:11.00	BH1 - 199	3.49	1092	35	3.18%	0.2824	0.00003	0.00565	0.000655	0.000053	0.0329	0.0031	0.2823865	10.37	1.05	1.19	1.26	0.282094	0.282461	
BH1	03/12/2018 (2) 22:17:43.00	BH1 - 184	3.62	1784	85	4.77%	0.281568	0.000036	0.00563	0.0007885	0.0000092	0.03925	0.00042	0.2815413	-3.81	1.26	2.35	2.72	0.281649	0.281952	
BH1	03/12/2018 (2) 22:01:13.00	BH1 - 176	3.70	1128	28	2.44%	0.282395	0.000076	0.00565	0.003442	0.000045	0.1843	0.003	0.2823218	8.90	2.66	1.30	1.39	0.282071	0.282435	
03DTB18	09/05/2019 (5) 22:31:21.00	03DTB18 - 57	3.71	1152	52	4.52%	0.28203	0.00004	0.00564	0.00096	0.00011	0.06114	0.00029	0.2820122	-1.85	1.47	1.72	2.07	0.282064	0.282417	
03DTB18	09/05/2019 (5) 20:16:35.00	03DTB18 - 1	3.81	1763	177	10.05%	0.28157	0.00004	0.00563	0.00054	0.00001	0.01933	0.00034	0.2815499	-4.45	1.33	2.33	2.71	0.281675	0.281967	
04DTB18	10/05/2019 (6) 02:49:46.00	04DTB18 - 49	3.84	1665	136	8.19%	0.28192	0.00009	0.00564	0.00178	0.00007	0.06540	0.00290	0.2818588	4.30	1.51	1.92	2.08	0.281738	0.282040	
BH1	03/12/2018 (2) 20:54:44.00	BH1 - 154	3.86	1826	82	4.49%	0.281711	0.000034	0.00563	0.000551	0.000012	0.02255	0.00069	0.2816919	2.53	1.19	2.14	2.35	0.281621	0.281920	
BH1	03/12/2018 (2) 14:08:31.00	BH1 - 10	3.97	1053	31	2.90%	0.282304	0.000029	0.00565	0.000112	0.0000036	0.00553	0.00021	0.2823018	6.50	1.02	1.31	1.48	0.282118	0.282489	
03DTB18	09/05/2019 (5) 22:05:02.00	03DTB18 - 43	3.98	1765	160	9.09%	0.28156	0.00004	0.00563	0.00069	0.00004	0.04350	0.00160	0.2815389	-4.79	1.33	2.35	2.73	0.281674	0.281966	
05DTB18	10/05/2019 (6) 03:24:03.96	05DTB18 - 6	4.02	1890	180	9.50%	0.28196	0.00006	0.00564	0.00063	0.00002	0.02344	0.00091	0.2819413	12.34	1.93	1.80	1.73	0.281594	0.281873	
05DTB18	10/05/2019 (6) 05:30:58.00	05DTB18 - 58	4.02	1050	42	3.97%	0.28242	0.00010	0.00565	0.00069	0.00001	0.02562	0.00051	0.2824064	9.85	3.50	1.17	1.24	0.282128	0.282492	
BH1	03/12/2018 (2) 16:10:46.00	BH1 - 54	4.11	1678	145	8.66%	0.281806	0.000034	0.00564	0.0004343	0.0000022	0.02234	0.00013	0.2817922	2.67	1.19	2.00	2.22	0.281717	0.282030	
04DTB18	10/05/2019 (6) 02:57:16.00	04DTB18 - 60	4.15	1193	47	3.91%	0.28212	0.00004	0.00564	0.00065	0.00000	0.02417	0.00041	0.2821004	2.21	1.44	1.59	1.85	0.282038	0.282387	
05DTB18	10/05/2019 (6) 04:11:23.00	05DTB18 - 24	4.23	1169	59	5.05%	0.28223	0.00007	0.00565	0.00094	0.00005	0.03460	0.00200	0.2822103	5.58	2.49	1.44	1.61	0.282053	0.282404	
03DTB18	09/05/2019 (5) 21:49:41.00	03DTB18 - 39	4.24	1327	45	3.39%	0.28199	0.00005	0.00564	0.00051	0.00000	0.03350	0.00170	0.2819813	1.00	1.65	1.75	2.03	0.281953	0.282289	
03DTB18	09/05/2019 (5) 20:39:07.01	03DTB18 - 13	4.28	1097	67	6.11%	0.28226	0.00005	0.00565	0.00115	0.00001	0.04400	0.00067	0.2822382	4.94	1.72	1.40	1.60	0.282099	0.282457	
05DTB18	10/05/2019 (6) 07:00:08.00	05DTB18 - 91	4.36	1649	185	11.22%	0.28182	0.00007	0.00564	0.00064	0.00001	0.02372	0.00012	0.2817979	1.77	2.00	2.97	2.23	0.281748	0.282052	
BH1	03/12/2018 (2) 16:14:51.00	BH1 - 56	4.63	1610	106	6.56%	0.28178	0.000029	0.00564	0.001168	0.000095	0.0545	0.0043	0.2817444	-0.58	1.02	2.08	2.37	0.281761	0.282080	
05DTB18	10/05/2019 (6) 03:22:10.00	05DTB18 - 5	4.67	1689	117	6.91%	0.28190	0.00004	0.00564	0.00259	0.00003	0.09347	0.00093	0.2818191	3.42	1.44	1.98	2.15	0.281723	0.282022	
BH1	03/12/2018 (2) 15:00:11.00	BH1 - 30	4.74	1647	95	5.79%	0.28218	0.00013	0.00565	0.00131	0.000055	0.0699	0.0048	0.2821391	14.28	4.55	1.52	1.45	0.281737	0.282053	
BH1	03/12/2018 (2) 22:21:51.00	BH1 - 186	4.76	2713	88	3.23%	0.281206	0.000027	0.00562	0.000963	0.000026	0.0443	0.0019	0.2811560	4.08	0.95	2.85	2.95	0.281041	0.281258	
04DTB18	10/05/2019 (6) 02:15:31.00	04DTB18 - 43	4.81	1708	116	6.77%	0.28168	0.00004	0.00563	0.00145	0.00001	0.05450	0.00130	0.2816362	-2.63	1.51	2.23	2.55	0.281710	0.282008	
BH1	03/12/2018 (2) 21:00:56.00	BH1 - 157	4.84	2647	80	3.01%	0.281132	0.000025	0.00562	0.0005368	0.0000004	0.02284	0.00025	0.2811048	0.71	0.88	2.92	3.11	0.281085	0.281308	
BH1	03/12/2018 (2) 15:10:27.00	BH1 - 35	5.10	1133	38	3.34%	0.282198	0.000025	0.00564	0.001267	0.000089	0.0686	0.0046	0.2821710	3.66	0.88	1.50	1.73	0.282068	0.282431	
BH1	03/12/2018 (2) 13:56:14.00	BH1 - 4	5.17	1389	45	3.23%	0.28215	0.000025	0.00564	0.000915	0.000039	0.0481	0.0024	0.2821260	7.90	0.88	1.55	1.66	0.281903	0.282243	
BH1	03/12/2018 (2) 16:21:08.00	BH1 - 59	5.19	1158	42	3.61%	0.282011	0.000023	0.00564	0.000658	0.000016	0.0355	0.0013	0.2819966	-1.95	0.81	1.73	2.10	0.282052	0.282413	
05DTB18	10/05/2019 (6) 05:23:27.00	05DTB18 - 54	5.24	3390	82	2.42%	0.28077	0.00004	0.00562	0.00117	0.00000	0.04448	0.00037	0.2806935	2.69	1.44	3.46	3.51	0.280618	0.280745	too old to be shown on Fig. 2
04DTB18	10/05/2019 (6) 02:45:47.00	04DTB18 - 58	5.50	1126	43	3.80%	0.28220	0.00004	0.00564	0.00076	0.00002	0.02778	0.00067	0.2821838	3.66	1.33	1.48	1.70	0.282081	0.282436	
03DTB18	09/05/2019 (5) 23:16:57.00	03DTB18 - 74	5.75	1007	53	5.23%	0.28228	0.00005	0.00565	0.00168	0.00004	0.01370	0.00150	0.2822483	3.28	1.58	1.40	1.63	0.282156	0.282523	
03DTB18	09/05/2019 (5) 21:32:37.00	03DTB18 - 33	6.00	1319	68	5.16%	0.28222	0.00004	0.00564	0.00079	0.00001	0.06710	0.00200	0.2821954	8.41	1.37	1.46	1.55	0.281958	0.282295	
04DTB18	10/05/2019 (6) 01:09:04.00	04DTB18 - 18	6.27	1459	61	4.18%	0.28206	0.00004	0.00564	0.00123	0.00010	0.04660	0.00400	0.2820260	5.57	1.54	1.69	1.84	0.281869	0.282192	
BH1	03/12/2018 (2) 21:59:06.00	BH1 - 175	6.27	1268	43	3.41%	0.282191	0.000025	0.00564	0.001879	0.000029	0.0866	0.0024	0.2821460	5.86	0.88	1.53	1.69	0.281981	0.282332	
05DTB18	10/05/2019 (6) 07:03:59.00	05DTB18 - 93	6.29	1297	53	4.08%	0.28216	0.00006	0.00564	0.00083	0.00004	0.03120	0.00150	0.2821387	5.90	1.37	3.20	1.69	0.281972	0.282311	
BH1	03/12/2018 (2) 21:55:00.00	BH1 - 173	6.44	992	43	4.33%	0.282319	0.00003	0.00565	0.0004602	0.0000097	0.02163	0.00046	0.2823104	5.41	1.05	1.30	1.50	0.282158	0.282534	
04DTB18	10/05/2019 (6) 01:24:03.50	04DTB18 - 26	6.46	1095	49	4.46%	0.28232	0.00004	0.00565	0.00052	0.00002	0.02033	0.00053	0.2823094	7.43	1.30	1.30	1.44	0.282100	0.282459	
04DTB18	10/05/2019 (6) 02:43:52.00	04DTB18 - 57	6.55	1355	46	3.42%	0.28214	0.00004	0.00564	0.00085	0.00003	0.08750	0.00270	0.2820936	5.61	1.33	1.60	1.75	0.281935	0.282268	
03DTB18	09/05/2019 (5) 23:07:31.00	03DTB18 - 69	6.79	1308	64	4.86%	0.28222	0.00004	0.00564	0.00097	0.00001	0.07472	0.00040	0.2822000	8.32	1.30	1.45	1.54	0.281965	0.282303	
BH1	03/12/2018 (2) 15:04:17.00	BH1 - 32	6.80	1133	45	4.01%	0.281982	0.000028	0.00564	0.0005262	0.0000059	0.0282	0.00041	0.2819708	-3.42	0.98	1.77	2.18	0.282067	0.282431	
BH1	03/12/2018 (2) 20:21:27.00	BH1 - 143	6.93	1820	85	4.68%	0.281931	0.000034	0.00564	0.000936	0.00009	0.0431	0.0046	0.2818987	9.72	1.19	1.86	1.88	0.281625	0.281925	
04DTB18	10/05/2019 (6) 01:22:14.00	04DTB18 - 25	6.95	1178	41	3.50%	0.28230	0.00008	0.00565	0.00234	0.00011	0.08900	0.00390	0.2822460	7.04	2.63	1.40	1.53	0.282048	0.282398	
05DTB18	10/05/2019 (6) 08:34:39.00	05DTB18 - 133	7.06	1007	36	3.53%	0.28235	0.00007	0.00565	0.00061	0.00001	0.01760	0.00014	0.2823360	6.40	2.14	2.04	1.43	0.282155	0.282523	
BH1	03/12/2018 (2) 17:06:40.00	BH1 - 76	7.07	1088	39	3.56%	0.282235	0.000025	0.00564	0.0006765	0.0000094	0.0356	0.00085	0.2822211	4.43	0.88	1.42	1.64	0.282096	0.282464	
04DTB18	10/05/2019 (6) 01:44:58.00	04DTB18 - 34	7.27	2018	161	7.99%	0.28152	0.00003	0.00563	0.00069	0.00003	0.02534	0.00064	0.2814927	-0.67	1.09	2.41	2.67	0.281512	0.281778	
05DTB18	10/05/2019 (6) 04:33:57.00	05DTB18 - 36	7.46	1260	44	3.46%	0.28221	0.00008	0.00565	0.00076	0.00001	0.02659	0.00046	0.2821909	6.93	2.66	1.46	1.60	0.281995	0.282338	
04DTB18	10/05/2019 (6) 02:34:28.00	04DTB18 - 52	7.49	1264	46	3.61%	0.28208	0.00006	0.00564	0.00150	0.00003	0.05813	0.00046	0.2820411	1.70	2.03	1.68	1.93	0.281993	0.282335	
BH1	03/12/2018 (2) 18:48:28.00	BH1 - 110	7.52	1024	33	3.20%	0.282326	0.000028	0.00565	0.001302	0.000061	0.0637	0.0025	0.2823009	5.80	0.98	1.32	1.50	0.282137	0.282511	
04DTB18	10/05/2019 (6) 02:40:06.00	04DTB18 - 55	7.58	1376	44	3.17%	0.28204	0.00004	0.00564	0.00097	0.00002	0.03585	0.00094	0.2820108	3.16	1.23	1.71	1.93	0.281922	0.282253	
04DTB18	10/05/2019 (6) 02:42:02.00	04DTB18 - 56	7.83	1084	53	4.91%	0.28218	0.00003	0.00564	0.00066	0.00001	0.02387	0.00060	0.2821706	2.25	1.09	1.49	1.76	0.282107	0.282467	
BH1	03/12/2018 (2) 19:02:59.00	BH1 - 117	7.84	974	26	2.64%	0.282365	0.000025	0.00565	0.001006	0.000013	0.0538	0.0012	0.2823466	6.29	0.88	1.25	1.43	0.282169	0.282547	
05DTB18	10/05/2019 (6) 04:47:26.00	05DTB18 - 40	7.85	1028	32	3.09%	0.28239	0.00006	0.00565	0.00011	0.00000	0.00301	0.00005	0.2823829	8.52	1.93	1.20	1.31	0.282143	0.282508	
BH1	03/12/2018 (2) 21:29:57.00	BH1 - 166	7.87	1320	41	3.10%	0.28206	0.000028	0.00564	0.0008457	0.0000084	0.04254	0.00032	0.2820389	3.25	0.98	1.67	1.90	0.281947	0.282294	
04DTB18	10/05/2019 (6) 00:31:07.50	04DTB18 - 2	7.96	756	30	3.93%	0.28242	0.00004	0.00565	0.00096	0.00010	0.05320	0.00640	0.2824084	3.35	1.51	1.17	1.43	0.282314	0.282706	
BH1	03/12/2018 (2) 14:22:54.00	BH1 - 17	7.99	985	35	3.52%	0.282331	0.000027	0.00565	0.000477	0.000012	0.0274	0.00088	0.2823222	5.66	0.95	1.28	1.48	0.282162	0.282539	
BH1	03/12/2018 (2) 17:02:34.00	BH1 - 74	8.08	1037	40	3.82%	0.282302	0.000032	0.00565	0.00172	0.00014	0.0872	0.0076	0.2822684	4.94	1.12	1.37	1.57	0.282129	0.282501	
BH1	03/12/2018 (2) 20:46:30.00	BH1 - 150	8.27	1074	44	4.11%	0.282343	0.00003	0.00565	0.0003797	0.0000072	0.01914	0.00051	0.2823353	8.16	1.05	1.26	1.39	0.282105	0.282474	
05DTB18	10/05/2019 (6) 08:28:58.00	05DTB18 - 130	8.42	1050	62	5.87%	0.28241	0.00015	0.00565	0.00065	0.00001	0.02510	0.00068	0.2823972	9.52	1.23	2.71	1.27	0.282129	0.282492	
BH1	03/12/2018 (2) 14:58:09.00	BH1 - 29	8.67	951	39	4.09%	0.282447	0.000029	0.00565	0.001001	0.000025	0.058	0.0017	0.2824291	8.69	1.02	1.14	1.26	0.282184	0.282564	
05DTB18	10/05/2019 (6) 05:29:07.00	05DTB18 - 57	8.92	2037	112	5.50%	0.28165	0.00011	0.00563	0.00118	0.00006	0.04050	0.00190	0.2816044	3.72	3.85	2.26	2.40	0.281500	0.281764	
05DTB18	10/05/2019 (6) 05:21:38.00	05DTB18 - 53	9.10	1132	55	4.88%	0.28237	0.00004	0.00565	0.00055	0.00002	0.02028	0.00083	0.2823593	10.01	1.54	1.23	1.30	0.282077	0.282432	
[illegible]	[illegible]	[illegible]	[illegible]	[illegible]	[illegible]	[illegible]	[illegible]	[illegible]	[illegible]	[illegible]	[illegible]	[illegible]	[illegible]	[illegible]	[illegible]	[illegible]	[illegible]	[illegible]	[illegible]	[illegible]	[illegible]

Appendix D5.4: Maximum Depositional Age Calculations

Sample ID	Analysis date-time	Spot ID	U conc. (ppm)	±2σ INT	Th conc. (ppm)	±2σ INT	Isotopic Ratios: 238U/206Pb	±2σ PROP	207Pb/206Pb	±2σ PROP	rho	Apparent Ages - Calculated in Isoplot R (Ma): 238U/206Pb	±2σ PROP	207Pb/206Pb	±2σ PROP	Discord (7/6-6/8)/7/6 *100	Discord at closest approach (where null = concordant)	CONCORDIA Age	1sigm a priori err	MSWD	Probability	#alpha events/mg x 10^15	Metamict stage	Calc. density	Perferred age 1500 Ma cutoff: Ma	2 σ
	Blue text analyses are analyses following identification during "rapid" session																									
BH1	13/07/2020 (2) 19:02:28.0(	BH1 - 2.209	818	24	779	31	8.520791	0.279322	0.064800	0.002596	0.381990	715	22	767	83	6.72		718	22	0.35	0.55	2.66	I: crystalline	4.54	715	22
BH1	03/12/2018 (2) 20:13:14.00	BH1 - 139	687	12	1027	71	8.510638	0.257130	0.063000	0.003360	-0.025889	716	20	707	110	-1.25		716	20	0.00	0.95	2.26	I: crystalline	4.58	716	20
BH1	2020-07-30 17:21:07.000	BH1q - 192 - 1.d	49	3	37	2	8.432193	0.393522	0.063251	0.006104	0.206552	722	32	716	205	-0.94		722	16	0.00	0.96	0.14	I: crystalline	4.75	722	32
BH1	2020-07-30 16:31:13.000	BH1q - 423b - 1.d	146	3	125	3	8.311182	0.265340	0.065977	0.004832	0.183944	732	22	805	153	8.98		734	11	0.86	0.35	0.49	I: crystalline	4.73	732	22
BH1	2020-07-30 16:32:51.000	BH1q - 423 - 1.d	199	5	165	5	8.260927	0.251205	0.064184	0.004347	0.297804	737	21	747	143	1.36		737	10	0.02	0.88	0.62	I: crystalline	4.72	737	21
BH1	2020-07-30 17:27:55.000	BH1q - 152 - 1.d	98	4	98	5	8.125236	0.283560	0.066098	0.004943	0.326933	748	25	809	156	7.45		750	12	0.58	0.45	0.34	I: crystalline	4.74	748	25
BH1	*2020-07-30 16:07:02.000*	*BH1-154b - 1.d*	*306*	*7*	*340*	*7*	*8.022557*	*0.237716*	*0.063809*	*0.004110*	*0.118118*	*757*	*21*	*734*	*136*	*-3.11*		*757*	*10*	*0.10*	*0.75*	*0.98*	*I: crystalline*	*4.70*	*757*	*21*
BH1	*2020-07-30 16:08:48.000*	*BH1-154c - 1.d*	*334*	*6*	*377*	*7*	*8.012350*	*0.233059*	*0.064696*	*0.004132*	*0.223823*	*758*	*21*	*764*	*135*	*0.70*		*758*	*10*	*0.01*	*0.93*	*1.12*	*I: crystalline*	*4.69*	*758*	*21*
BH1	*2020-07-30 16:10:32.000*	*BH1-154d*	*321*	*9*	*364*	*10*	*7.976002*	*0.240792*	*0.064390*	*0.004122*	*0.017591*	*761*	*22*	*754*	*135*	*-1.05*		*761*	*11*	*0.01*	*0.92*	*1.06*	*I: crystalline*	*4.69*	*761*	*22*
BH1	2020-07-30 16:17:15.000	BH1q - 692	130	2	111	2	7.971016	0.270111	0.065862	0.004767	0.303211	762	24	801	152	4.88		763	12	0.27	0.61	0.44	I: crystalline	4.73	762	24
BH1	2020-07-30 16:20:40.000	BH1q - 648	47	1	39	1	7.965560	0.300282	0.065553	0.006424	0.186646	762	27	791	206	3.64		763	13	0.08	0.78	0.15	I: crystalline	4.75	762	27
BH1	2020-07-30 16:15:35.000	BH1q - 709c	219	5	2400	55	7.959874	0.257660	0.066166	0.004508	0.234983	763	23	811	143	5.90		764	12	0.44	0.51	2.15	I: crystalline	4.59	763	23
BH1	2020-07-30 16:12:11.000	BH1q - 709	246	4	5787	137	7.921050	0.243288	0.064355	0.004151	0.145446	766	22	752	136	-1.86		766	11	0.04	0.85	4.06	II: intermediate	4.40	766	22
BH1	2020-07-30 16:18:56.000	BH1q - 692b	118	4	66	1	7.916348	0.255869	0.066167	0.005338	0.160344	767	23	811	169	5.41		768	12	0.27	0.60	0.38	I: crystalline	4.74	767	23
BH1	*13/07/2020 (2) 17:22:20.0(*	*BH1 - 2.154*	*304*	*5*	*347*	*6*	*7.892660*	*0.282441*	*0.065800*	*0.003316*	*0.333320*	*769*	*25*	*799*	*103*	*3.77*		*771*	*25*	*0.08*	*0.78*	*1.07*	*I: crystalline*	*4.69*	*769*	*25*
BH1	2020-07-30 16:13:52.000	BH1q - 709b	257	4	2685	55	7.781355	0.234054	0.063674	0.004211	0.146663	779	22	730	140	-6.78		778	11	0.48	0.49	2.19	I: crystalline	4.59	779	22
BH1	13/07/2020 (2) 12:53:40.0(	BH1 - 2.4	503	12	625	20	7.535795	0.252935	0.066900	0.002838	0.128490	803	25	834	87	3.65		806	24	0.12	0.73	1.89	I: crystalline	4.62	803	25
04DTB19	2020-07-30 17:59:06.000	04DTB19q - 117	388	13	290	11	8.231249	0.246160	0.065752	0.004189	0.236775	739	21	798	134	7.33		740	10	0.75	0.39	1.27	I: crystalline	4.68	739	21
04DTB18	10/05/2019 (6) 00:31:07.50	04DTB18 - 2	183	5	161	5	8.038585	0.348166	0.066500	0.007530	0.208850	756	30	821	221	7.96		757	31	0.07	0.78	0.63	I: crystalline	4.72	756	30
04DTB19	2020-07-30 16:55:14.000	04DTB19q - 64	66	2	117	2	7.999056	0.296865	0.067140	0.005979	0.270946	759	27	841	185	9.73		761	13	0.75	0.39	0.27	I: crystalline	4.74	759	27
04DTB18	13/07/2020 (2) 21:51:16.00	04DTB18 - 2.1	357	14	553	23	7.974482	0.267597	0.065200	0.003004	0.245160	762	23	780	95	2.35		763	23	0.04	0.85	1.31	I: crystalline	4.67	762	23
04DTB19	2020-07-30 16:41:25.000	04DTB19q - 130b	60	1	58	1	7.962577	0.310366	0.064635	0.006098	0.119656	763	28	762	199	-0.15		763	14	0.00	1.00	0.19	I: crystalline	4.75	763	28
04DTB19	2020-07-30 16:39:39.000	04DTB19q - 125	57	2	52	2	7.803501	0.306847	0.067398	0.006622	0.278938	777	29	849	204	8.47		778	14	0.48	0.49	0.21	I: crystalline	4.75	777	29
04DTB19	2020-07-30 16:53:32.000	04DTB19q - 34	50	1	76	3	7.734419	0.309947	0.067967	0.006692	0.185005	784	30	867	204	9.55		785	15	0.63	0.43	0.21	I: crystalline	4.75	784	30
05DTB19	2020-07-30 16:58:40.000	05DTB19q - 3	44	1	36	1	7.899340	0.334711	0.065052	0.006816	0.267513	768	31	775	220	0.86		769	15	0.00	0.95	0.14	I: crystalline	4.75	768	31
03DTB19	2020-07-30 17:43:33.000	03DTB19q - 16	237	5	173	4	7.948072	0.246154	0.066868	0.004455	0.184724	764	22	833	139	8.26		765	11	0.95	0.33	0.81	I: crystalline	4.71	764	22
03DTB19	2020-07-30 17:40:08.000	03DTB19q - 8	13	0	1916	34	7.931832	0.452856	0.064000	0.011563	0.130006	765	41	741	382	-3.29		765	20	0.02	0.90	1.15	I: crystalline	4.69	765	41
03DTB19	2020-07-30 16:36:19.000	03DTB19q - 86b	65	1	1200	27	7.763663	0.284781	0.063708	0.005838	0.266352	781	27	731	194	-6.85		780	13	0.26	0.61	0.85	I: crystalline	4.71	781	27

Appendix D5.4 continued.

Metric	Method	Reference	BH1	03DTB19	04DTB19	05DTB19
Youngest analysis	single analysis	Ludwig and Mundil, 2002	715±22	764±22	739±21	768±31
Youngest single analysis with uncertainty	single analysis	Dickinson and Gehrels, 2009	715±22	764±22	739±21	768±31
Youngest single grain (multiple analysis)	Weighted mean	Spencer et al., 2016	735±11	N/A	759±18	N/A
Youngest analysis cluster 2 or more (1σ overlap)	Weighted mean	Dickinson and Gehrels, 2009	718±18	770±16	757±10	N/A
Youngest cluster 3 or more (1σ overlap)	Weighted mean	Dickinson and Gehrels, 2009	727±11	770±16	757±10	N/A
Youngest three grains	Weighted mean	Zhang et al., 2016	723±14	770±16	749±14	N/A
Youngest cluster 2+ (2σ overlap)	Weighted mean	Coutts et al., 2019	736±17	770±16	760±16	N/A
Concordia age of youngest cluster	Concordia Age	Dehler et al., 2010	758±8 (1 rej)	770±16	760±16	N/A
Youngest Unmix population (6+ grains needed)	Isoplot unmix function	Dehler et al., 2017	729±13	N/A	746±30	N/A
Youngest graphical peak (PDP, 2 grain minimum)	Probability density plot	Dickinson and Gehrels, 2009	759	769	759	N/A
Maximum Likelihood Age	IsoplotR radial plot minimum finite mixture	Vermeesch, 2020	726±7	771±7	760±5	N/A

Appendix D5.5: U/Pb-Lu/Hf Standards

Recommended $^{176}Hf/^{177}Hf$ value for zircon reference materials and weighted mean standard corrected ratio obtained in each analytical session (Mud Tank primary reference material).

Zircon standard	Recommended $^{176}Hf/^{177}Hf$	Weighted mean for session 1 (3/12/2018)	Weighted mean for session 2 (09/05/2019)	Weighted mean for session 3 (17/03/2020)
Mud Tank	0.282505 ± 0.000044 (Woodhead and Hergt, 2005)	0.282507 ± 0.000006 (MSWD = 0.47, n = 17)	0.282507 ± 0.000004 (MSWD = 0.89, n = 20)	0.282507 ± 0.00009 (MSWD = 0.11, n = 20)
GJ-1	0.282000 ± 0.00005, (Morel et al., 2008)	0.282027 ± 0.000008 (MSWD = 0.21, n = 16)	0.282011 ± 0.000005 (MSWD = 1.00, n = 19)	0.282013 ± 0.00005 (MSWD = 0.30, n = 19)
Plešovice	0.282482 ± 0.000013 (Sláma et al., 2008)	0.282485 ± 0.000009 (MSWD = 0.52, n = 10)	0.282473 ± 0.000006 (MSWD = 0.77, n = 8)	0.282477 ± 0.000006 (MSWD = 0.55, n = 9)
91500	0.282306 ± 0.000311 (Woodhead et al., 2004)	0.282300 ± 0.000009 (MSWD = 0.18, n = 15)	0.282303 ± 0.000006 (MSWD = 1.03, n = 18)	0.282306 ± 0.000005 (MSWD = 0.59, n = 19)

Recommended ages for zircon reference materials and weighted mean standard corrected ages obtained in each analytical session.

Zircon standard	Recommended age (Ma)	1st session (03/12/2018)	2nd session (9/05/2019)	3rd session (7/03/2020)
GJ-1	608.5 ± 1.5 Ma (Jackson et al., 2004) 601.5± 0.40 Ma (Horstwood et al., 2016)	603.6 ± 0.88 Ma (MSWD = 0.83, n = 20)	608.3± 1.4 Ma (MSWD = 5.0, n = 17)	602.2 ± 0.84 Ma (MSWD = 1.38, n = 19)
Plešovice	337.13 ± 0.37 Ma (Sláma et al., 2008)	338.4 ± 0.7 Ma (MSWD = 2.0, n = 9)	-	339.5 ± 1.79 Ma (MSWD = 4.5, n = 7)
91500	1062.4 ± 0.4 Ma (Wiedenbeck et al., 1995)	1062.0 ± 2.6 Ma (MSWD = 0.54, n = 20)	1061.4 ± 3.9 Ma (MSWD = 0.01, n = 20)	1062.3 ± 1.6 Ma (MSWD = 0.89, n = 20)
OGC	3467 ± 3 Ma (Stern et al., 2009)	3465.2 ± 2.2 Ma (MSWD = 0.54, n = 18)	-	3465.1 ± 4.0 Ma (MSWD = 1.69, n = 14)

Appendix D6.1: Compiled U/Pb Data Sources

U-Pb Detrital Zircon Data presented in Fig. 5

Sample Number	Area	Unit	Source
09JK08	Pocatello	Camelback Mountain Fm	Yonkee et al., 2014
20AY11	Pocatello	Geertsen Canyon Fm	Yonkee et al., 2014
66CD10	Pocatello	Geertsen Canyon Fm	Yonkee et al., 2014
05Z08	Pocatello	Camelback Mountain Fm	Yonkee et al., 2014
03Z08	Pocatello	Mutual Fm	Yonkee et al., 2014
04Z08	Pocatello	Mutual Fm	Yonkee et al., 2014
01JK08	Pocatello	Caddy Canyon Fm	Yonkee et al., 2014
65CD10	Pocatello	Browns Hole Fm	Yonkee et al., 2014
59CD10	Pocatello	Mutual Fm	Yonkee et al., 2014
57CD10	Pocatello	Caddy Canyon Fm	Yonkee et al., 2014
Sample E*	Grand Canyon	Sixtymile Fm	Karlstrom et al., 2018
Sample D*	Grand Canyon	Sixtymile Fm	Karlstrom et al., 2018
Sample C*	Grand Canyon	Sixtymile Fm	Karlstrom et al., 2018
Sample B*	Grand Canyon	Sixtymile Fm	Karlstrom et al., 2018
Sample A*	Grand Canyon	Sixtymile Fm	Karlstrom et al., 2018
Tapeats 1*	Grand Canyon	Tapeats Sandstone	Gehrels et al., 2011
Sample F*	Grand Canyon	Tapeats Sandstone	Karlstrom et al., 2018
Sample G*	Grand Canyon	Tapeats Sandstone	Karlstrom et al., 2018
Sample H*	Grand Canyon	Tapeats Sandstone	Karlstrom et al., 2018
06SA10*	New Mexico	Bliss Sandstone	Amato and Mack, 2012
04SASC2*	New Mexico	Bliss Sandstone	Amato and Mack, 2012
04SASC6*	New Mexico	Bliss Sandstone	Amato and Mack, 2012
07SD3c*	New Mexico	Bliss Sandstone	Amato and Mack, 2012
07SD3a*	New Mexico	Bliss Sandstone	Amato and Mack, 2012
09MS1*	New Mexico	Bliss Sandstone	Amato and Mack, 2012
08FM8b*	New Mexico	Bliss Sandstone	Amato and Mack, 2012
08FM9*	New Mexico	Bliss Sandstone	Amato and Mack, 2012
09SL1*	New Mexico	Bliss Sandstone	Amato and Mack, 2012
09SL2*	New Mexico	Bliss Sandstone	Amato and Mack, 2012
10BM216*	New Mexico	Bliss Sandstone	Amato and Mack, 2012
10BM215*	New Mexico	Bliss Sandstone	Amato and Mack, 2012
11LHM03*	New Mexico	Bliss Sandstone	Amato and Mack, 2012
CS12-5*	New Mexico	Van Horn Fm	Spencer et al., 2014
CS12-3*	New Mexico	Van Horn Fm	Spencer et al., 2014
MD09	C. Appalachians	Weverton Fm	Satoski, 2013
MD10	C. Appalachians	Weverton Fm	Satoski, 2013
MD11	C. Appalachians	Weverton Fm	Satoski, 2013
VA12	C. Appalachians	Weverton Fm	Satoski, 2013
VA13	C. Appalachians	Weverton Fm	Satoski, 2013
VA14	C. Appalachians	Weverton Fm	Satoski, 2013
VA15	C. Appalachians	Weverton Fm	Satoski, 2013
VA16	C. Appalachians	Weverton Fm	Satoski, 2013
Rome 1	C. Appalachians	Rome Sandstone	Thomas, 2004
Rome 2	C. Appalachians	Rome Sandstone	Thomas, 2004

*Presented max depositional age constraints (shown in Fig. 2) are from Karlstrom et al., 2018 and shown in Karlstrom et al., 2018 supplementary tables

Appendix D6.2: Compiled Lu/Hf Data Sources

Lu-Hf Detrital Zircon Data from late Tonian-Cambrian strata presented in Fig. 3 and 4

Sample Number	Group	Unit	Source
08LW6	Tonian-Cryogenian Strata	Little Willow Fm	Spencer et al., 2012
BCF-HF	Tonian-Cryogenian Strata	Middle Big Cottonwood Fm	Spencer et al., 2012
LW17-3	Tonian-Cryogenian Strata	Little Willow Fm	Spencer et al., 2012
Caddy	Tonian-Cryogenian Strata	Caddy Canyon Quartzite	Gehrels and Pecha, 2014
J39-A-9	Ediacaran Strata	Johnnie Fm	Howard et al., 2015
NR30	Ediacaran Strata	Stirling Quartzite	Howard et al., 2015
Mutual	Ediacaran Strata	Mutual Fm	Gehrels and Pecha, 2014
WQ	Ediacaran Strata	Wildhorse Meadows	Wooden et al., 2013
Geertsen	Cambrian Strata	Geertsen Canyon Fm	Gehrels and Pecha, 2014
Wood Canyon	Cambrian Strata	Wood Canyon Fm	Gehrels and Pecha, 2014
85NV_CL_3B	Cambrian Strata	Wood Canyon Fm	Howard et al., 2015
83WMAM_4	Cambrian Strata	Campito Fm	Howard et al., 2015
Zabriskie2	Cambrian Strata	Zabriskie Quartzite	Gehrels and Pecha, 2014
Proveedora	Cambrian Strata	Proveedora	Gehrels and Pecha, 2014
ZAB	Cambrian Strata	Zabriskie Quartzite	Wooden et al., 2013
ZBR	Cambrian Strata	Zabriskie Quartzite	Wooden et al., 2013
WC	Cambrian Strata	Wood Canyon Fm	Wooden et al., 2013
12COPP-03	Pikes Peak	Pikes Peak Syenogranite	Howard et al., 2015
12COPP-02	Pikes Peak	Pikes Peak Monzogranite	Howard et al., 2015
12COPP-05	Pikes Peak	Pikes Peak Quartz syenite	Howard et al., 2015
Yqs-10	Pikes Peak	Lake George quartz syenite	Guitreau et al., 2016
Ypm-9	Pikes Peak	Lake George monzogranite	Guitreau et al., 2016
Ypp-20	Pikes Peak	Pikes Peak granite	Guitreau et al., 2016
11LBM_01	Llano/Wichita	Little Hatchet Mountain Granite	Howard et al., 2015
12TXFM01	Llano/Wichita	Franklin Mountains, Stage 2	Howard et al., 2015
12TXFM02	Llano/Wichita	Franklin Mountains, Stage 4	Howard et al., 2015
12TXFM03	Llano/Wichita	Franklin Mountains, Stage 1	Howard et al., 2015
5/04 LL-1	Llano/Wichita	Escuadra Granite	Howard et al., 2015
GRLL-5	Llano/Wichita	Lone Grove pluton	Howard et al., 2015
GRLL-14	Llano/Wichita	Grape Creek pluton	Howard et al., 2015
CS12-4	Llano/Wichita	compiled in Martin et al., 2020	Mulder et al., 2018
CS12-5	Llano/Wichita	compiled in Martin et al., 2020	Mulder et al., 2019
CS12-1	Llano/Wichita	compiled in Martin et al., 2020	Mulder et al., 2020
CS12-3	Llano/Wichita	compiled in Martin et al., 2020	Mulder et al., 2021
OK-4-WL	Llano/Wichita	compiled in Martin et al., 2020	Thomas et al., 2016
OK-1-VN	Llano/Wichita	compiled in Martin et al., 2020	Thomas et al., 2016
BR-1	Grenville	Blowing Rock Gneiss	Howard et al., 2015
CG	Grenville	Corbin Gneiss	Howard et al., 2015
TX	Grenville	Toxaway Gneiss	Howard et al., 2015
WL	Grenville	Wiley Gneiss	Howard et al., 2015
WD	Grenville	Woodland Gneiss	Howard et al., 2015
13-AM-007	Grenville	compiled in Martin et al., 2020	Augland et al., 2016
13-FS-1029	Grenville	compiled in Martin et al., 2020	Augland et al., 2016
13-TC-5016	Grenville	compiled in Martin et al., 2020	Augland et al., 2016
n3422	Grenville	compiled in Martin et al., 2020	Spencer et al., 2015
n3423	Grenville	compiled in Martin et al., 2020	Spencer et al., 2015
n3427	Grenville	compiled in Martin et al., 2020	Spencer et al., 2015
CS11-1	Grenville	compiled in Martin et al., 2020	Spencer et al., 2015
CS11-13	Grenville	compiled in Martin et al., 2020	Spencer et al., 2015
CS11-18	Grenville	compiled in Martin et al., 2020	Spencer et al., 2015
CS11-20	Grenville	compiled in Martin et al., 2020	Spencer et al., 2015
CS11-3	Grenville	compiled in Martin et al., 2020	Spencer et al., 2015
CS11-6	Grenville	compiled in Martin et al., 2020	Spencer et al., 2015
CS11-9	Grenville	compiled in Martin et al., 2020	Spencer et al., 2015
KY-18-CB	Grenville	compiled in Martin et al., 2020	Thomas et al., 2017
KY-19-PR7	Grenville	compiled in Martin et al., 2020	Thomas et al., 2017
KY-21-SG	Grenville	compiled in Martin et al., 2020	Thomas et al., 2017
OH-1-SS	Grenville	compiled in Martin et al., 2020	Thomas et al., 2017
VA-1-GN	Grenville	compiled in Martin et al., 2020	Thomas et al., 2017
WV-1-PR	Grenville	compiled in Martin et al., 2020	Thomas et al., 2017

Abbreviations: FM - Formation

Appendix D6.3: Statistical Comparison Results

Statistical results generated from DZStats-2D (Sundell and Saylor, 2021)

Sundell, K.E., and Saylor, J.E., 2021, Two-dimensional Quantitative Comparison of Density Distributions in Detrital Geochronology and Geochemistry: Geochemistry Geophysics Geosystems, doi:10.1029/2020GC009559.

DZstats2D Results

MDS PLOTS

Cross-correlation

	Grenville	Pikes Peak	Llano/Wichita	Stentian-Cryogenian	Ediacaran	Cambrian
Grenville	1	0.426854753	0.274316864	0.770183729	0.474454264	0.462331331
Pikes Peak	0.426854753	1	0.062011811	0.187423138	0.078132217	0.19763872
Llano/Wichita	0.274316864	0.062011811	1	0.380173424	0.653479709	0.800640595
Stentian-Cryogenian	0.770183729	0.187423138	0.380173424	1	0.56196941	0.472054653
Ediacaran	0.474454264	0.078132217	0.653479709	0.56196941	1	0.692551412
Cambrian	0.462331331	0.19763872	0.800640595	0.472054653	0.692551412	1

See Fig. 4

Likeness

	Grenville	Pikes Peak	Llano/Wichita	Stentian-Cryogenian	Ediacaran	Cambrian
Grenville	1	0.424673852	0.468235074	0.742896371	0.568893514	0.581816995
Pikes Peak	0.424673852	1	0.244411589	0.336260072	0.219678172	0.346164282
Llano/Wichita	0.468235074	0.244411589	1	0.500314997	0.62121186	0.723636186
Stentian-Cryogenian	0.742896371	0.336260072	0.500314997	1	0.610730274	0.567177089
Ediacaran	0.568893514	0.219678172	0.62121186	0.610730274	1	0.637237657
Cambrian	0.581816995	0.346164282	0.723636186	0.567177089	0.637237657	1

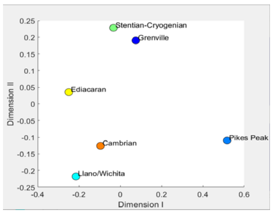

Similarity

	Grenville	Pikes Peak	Llano/Wichita	Stentian-Cryogenian	Ediacaran	Cambrian
Grenville	1	0.681305315	0.772454111	0.940079556	0.833254383	0.835563425
Pikes Peak	0.681305315	1	0.518008562	0.615254083	0.475171631	0.638635801
Llano/Wichita	0.772454111	0.518008562	1	0.790880589	0.862038612	0.927946867
Stentian-Cryogenian	0.940079556	0.615254083	0.790880589	1	0.837474096	0.831758658
Ediacaran	0.833254383	0.475171631	0.862038612	0.837474096	1	0.869925073
Cambrian	0.835563425	0.638635801	0.927946867	0.831758658	0.869925073	1

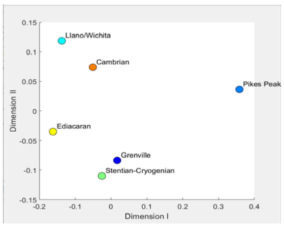

K-S Test D

	Grenville	Pikes Peak	Llano/Wichita	Stentian-Cryogenian	Ediacaran	Cambrian
Grenville	0	0.476731512	0.475021841	0.080312451	0.374636295	0.368292847
Pikes Peak	0.476731512	0	0.734338073	0.551847976	0.666269051	0.62988338
Llano/Wichita	0.475021841	0.734338073	0	0.429978063	0.298053989	0.216186869
Stentian-Cryogenian	0.080312451	0.551847976	0.429978063	0	0.313646632	0.340530273
Ediacaran	0.374636295	0.666269051	0.298053989	0.313646632	0	0.29685264
Cambrian	0.368292847	0.62988338	0.216186869	0.340530273	0.29685264	0

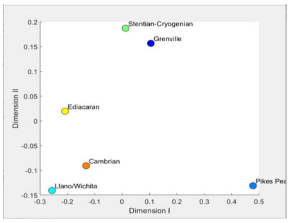

Kuiper Test V

	Grenville	Pikes Peak	Llano/Wichita	Stentian-Cryogenian	Ediacaran	Cambrian
Grenville	0	0.535770229	0.476568755	0.101301506	0.394890118	0.369835468
Pikes Peak	0.535770229	0	0.7394555	0.63232497	0.72219529	0.638849709
Llano/Wichita	0.476568755	0.7394555	0	0.438857807	0.34116225	0.219808536
Stentian-Cryogenian	0.101301506	0.63232497	0.438857807	0	0.327609597	0.340530273
Ediacaran	0.394890118	0.72219529	0.34116225	0.327609597	0	0.346740626
Cambrian	0.369835468	0.638849709	0.219808536	0.340530273	0.346740626	0